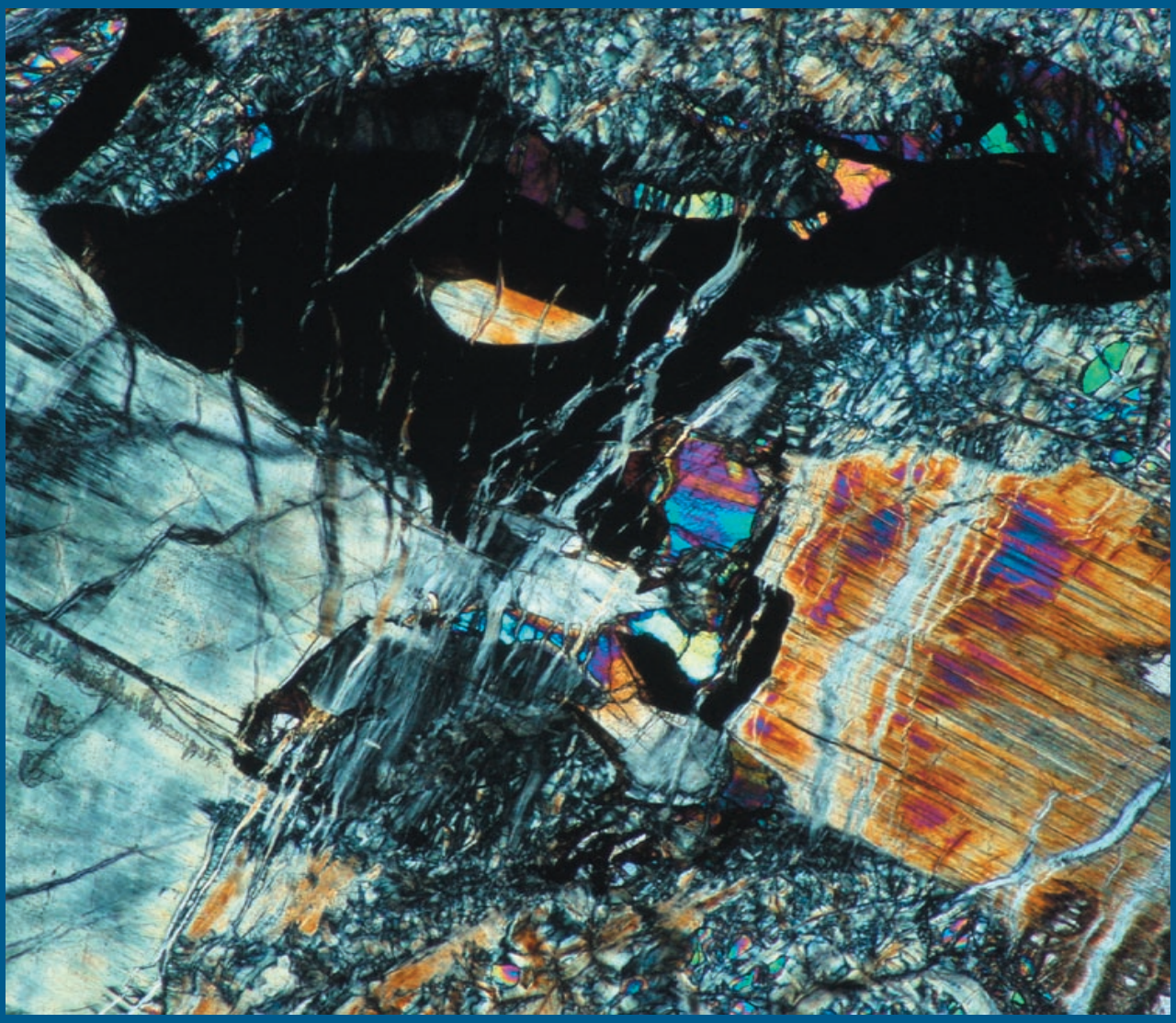
THE OCEANIC MANTLE AS AN IMPORTANT REPOSITORY FOR THE LIGHT ELEMENTS Li, Be AND B

Thèse présentée à la Faculté des Sciences
Institut de Géologie et d'Hydrogéologie
Université de Neuchâtel

pour l'obtention du grade de Docteur ès sciences par **Laure Pelletier**

soutenue le 22 janvier 2008



Acceptée par les membres du jury:
Prof. Angelika Kalt (Neuchâtel, CH, directrice de thèse)
Prof. Othmar Müntener (Lausanne, CH)
Dr. Tim Elliott (Bristol, UK)
Dr. Jean-Louis Bodinier (Montpellier, F)
Dr. Sonia Tonarini (Pisa, I)
Dr. Arjan Dijkstra (Neuchâtel, CH)

Université de Neuchâtel unine

A Martin Burkhard
(1957-2006)

Université de Neuchâtel

FACULTE DES SCIENCES
Secrétariat-Décanat de la faculté
- Rue Emile-Argand 11
- CP 158
- CH-2009 Neuchâtel

IMPRIMATUR POUR LA THESE

The oceanic mantle as an important repository for the light elements Li, Be and B

Laure PELLETIER

UNIVERSITE DE NEUCHATEL

FACULTE DES SCIENCES

La Faculté des sciences de l'Université de Neuchâtel,
sur le rapport des membres du jury

Mmes A. Kalt (directrice de thèse), S. Tonarini (Pise I)
et MM. O. Müntener (Université de Lausanne), A. Dijkstra,
J.-L. Bodinier (Montpellier F) et T. Elliott (Bristol UK)

autorise l'impression de la présente thèse.

Neuchâtel, le 7 février 2008

Le doyen :

F. Kessler

Felix Kessler

■ Téléphone : +41 32 718 21 00 ■ Fax : +41 32 718 21 03 ■ E-mail : secretariat.sciences@unine.ch ■ www.unine.ch/sciences

Table of contents

Imprimatur **I**

Table of contents **III**

Abstract **VII**

Acknowledgements / Remerciements **IX**

Chapter 1: Introduction **1**
- Li, Be and B geochemistry 1
- Rationale of the study 1
- Li, Be and B in the mantle 3
- Li, Be and B during serpentinization 4
- Organization of the thesis 5
- Studied localities 5
  - Mid-Atlantic Ridge ODP Leg 209 – Sites 1272 and 1274 5
  - The Pindos and Vourinos ophiolites (Greece) 6
  - The Geisspfad ultramafic massif (Alps) 8

Chapter 2: Li, B and Be contents of harzburgites from the Dramala Complex (Pindos ophiolite, Greece): a MOR-type mantle in a supra-subduction zone environment **14**
- Abstract 14
- Introduction 15
  - Ophiolites – supra-subduction zone versus ocean ridge origin 15
  - Li, B and Be as indicators of recent and ancient subduction setting 16
  - Rationale of the study 16
- General Geological framework 17
- The Pindos ophiolite 18
- Sample characteristics 19
- Interpretation of specific textures 23
  - Textures related to melt impregnation 23
  - Textures related to cooling and hydration 24
- Analytical techniques 25
- Major element composition of minerals 26
- Li, B and Be contents of rock-forming minerals 34
- Li, B and Be contents of whole rock samples 36
- Discussion 36
  - Compositional effects of melt impregnation 36
    - Major element composition of minerals 36
    - Impact on Li, B and Be systematics 40
  - High-temperature hydration – impact on Li, B and Be systematics 41
  - Low-temperature hydration – impact on Li, B and Be systematics 43
- Conclusion 45
  - The Dramala harzburgites: MOR- rather than SSZ-type mantle 45
  - Tectonic setting of formation of the Pindos ophiolite 47
- Acknowledgements 48

Chapter 3: N-MORB and ultra-depleted melt percolation in the Dramala harzburgites (Pindos ophiolite, Greece) and the famous spoon-shaped pattern **49**
Abstract 49
Introduction 50
General geological framework 52
The Pindos ophiolite 53
Selected samples and melt impregnation textures 54
Analytical techniques 56
Major element composition of minerals 57
Trace element composition of minerals 57
Trace element composition of whole rock samples 60
Melt impregnation model 60
Discussion 64
Melt impregnation in plagioclase-bearing harzburgite 64
Melt infiltration in spinel harzburgite and the famous spoon-shaped pattern 68
Evolution of the Dramala mantle over time 70
Conclusion 71
Acknowledgements 73

Chapter 4: Li, Be and B mobility during emplacement of ultramafic rocks into the continental crust: the example of the Geisspfad body (Swiss-Italian Alps) **74**
Abstract 74
Introduction 75
Geological setting 76
Analytical techniques 79
Sample description and mineralogy 80
Whole rock composition 83
Mineral composition – light elements (Li, Be and B) 88
Discussion 92
Nature of the protolith 92
Serpentinization of the protolith 93
Li, Be and B budgets of the protolith before Alpine metamorphism 94
Trace element behaviour related to retrograde metamorphism 95
Origin of the fluid 96
Implications for Li, Be and B studies in orogenic environments 98
Summary and conclusion 98
Acknowledgements 99

Chapter 5: Li and B variability in serpentine: intracrystalline or intercrystalline ? **100**
Abstract 100
Introduction 101
Sample characteristics 102
Serpentine textures 104
Analytical techniques 107
Identification of serpentine polymorphs 108
Discussion 111
Relation between texture and polymorphs 111
Major element composition of serpentine 111
Li and B content of serpentine 114
Grain boundary effect 119
Summary 119

Chapter 6: Summary, conclusions and outlook **121**
Summary and conclusions 121
Light element in fresh oceanic peridotites and Li enrichment during melt-related metasomatism 121
B enrichment during serpentinization of oceanic peridotites 121
Li, Be and B systematics during emplacement of oceanic peridotites into the continental crust 122
Contribution to the discussion on supra-subduction zone ophiolites 123
Outlook 123

Chapter 7: Analytical techniques **124**
Determination of texture and mineralogy 124
Secondary electron microscopy 124
Micro-Raman spectroscopy 124
In situ mineral analyses 124
Electron microprobe 124
Secondary Ion Mass Spectrometry (SIMS) 124
Laser Ablation – Inductively Coupled Plasma Mass Spectrometry (LA-ICPMS) 126
Whole rock analyses 128
Wavelength Dispersive X-Ray Fluorescence (WD-XRF) 128
Inductively Coupled Plasma Mass Spectrometry (ICPMS) 128
Prompt Gamma Neutron Activation Analysis (PGNAA) 129
Oxygen and Hydrogen Isotope Analyses 129

Appendix A: Supplement to chapter 4 **130**
Analytical techniques – Microprobe analyses 130
Mineral chemistry – major elements 130
Whole rock chemistry – rare earth elements (REE) 130

Appendix B: Thermobarometric study on Dramala harzburgites (Pindos ophiolite, Greece) **139**
Application of thermobarometers 139
P-T evolution of the Dramala harzburgites 142

Appendix C: Li zoning in orthopyroxene **144**

Appendix D: Bulk rock fusion using an iridium-strip heater: Preliminary results **146**
Introduction 146
Sample preparation and fusion technique 146
Results 146
Heterogeneous glass 146
Major element composition 147
Li and B composition 147

Appendix E: Mineralogical composition of the studied samples **152**

References **153**

Publications, manuscript and abstracts **176**
Complementary appendix (on enclosed CD-ROM)

Key words: Lithium; beryllium; boron; oceanic peridotite; serpentinite; melt percolation; melt impregnation; serpentinization; metamorphism; fluid; SIMS; ICP-MS; LA-ICP-MS; PGNAA.

Mots clés: Lithium; beryllium; bore; péridotite océanique; serpentinite; percolation de liquide; imprégnation de liquide; serpentinisation; métamorphisme; fluide; SIMS; ICP-MS; LA-ICP-MS; PGNAA.

Abstract

It is important to quantify the Li, Be and B content of oceanic peridotites, in order to evaluate their contributions to the light element input in subduction zones compared to the one related to the oceanic crust (mafic rocks and sediments), which is well constrained. In previous studies, the input related to the oceanic mantle was usually neglected, because no strong data are available for the light element contents of minerals and whole rock samples. The objective of this thesis is to provide a strong dataset of Li, Be and B contents of minerals and whole rock samples from the fresh and serpentinized oceanic mantle, and to determine the processes which can potentially modify the light element signature of the oceanic mantle.

The Li, Be and B content of the oceanic mantle can be modified during different processes acting at or close to mid-ocean ridges. The most important ones are mafic melt percolation and/or impregnation and serpentinization. The Li, Be and B content can also be changed during emplacement of oceanic mantle onto the continental crust. In order to constrain the importance of these processes, oceanic mantle from various tectonic settings was studied. Melt percolation and impregnation were studied in samples for the Pindos ophiolite (Greece), while serpentinization was studied in the same samples and in some additional samples for the Vourinos ophiolite (Greece), and compared to samples of the Mid-Atlantic ridge ODP Leg 209 (MAR sites 1272A and 1274A). The effect of the emplacement onto the continental crust was studied in samples from the Geisspfad ultramafic body (Swiss-Italian Alps), which mainly includes serpentinites equilibrated under amphibolite facies conditions. Secondary Ion Mass Spectrometry (SIMS) was used to determine in situ Li, Be and B contents of minerals. Inductively Coupled Plasma Mass Spectrometry was used to measure the Li and Be whole rock contents, while B whole rock contents were measured by Prompt Gamma Neutron Activation Analysis.

The study of the Dramala spinel and plagioclase-bearing harzburgites (Pindos ophiolite), which record high degree of partial melting (up to 22%) prior to melt percolation, shows that there is a Li enrichment of the depleted harzburgite during the crystallization of clinopyroxene cumulate related to percolation of N-MORB melt. Subsequent impregnation by ultra-depleted melt did not change the Li, Be and B content of the harzburgites. The Li, Be and B contents of the fresh Dramala harzburgite after these melt-related processes (before serpentinization) are low at about 0.9-1.0 μg/g, <0.003 μg/g and <0.03 μg/g, respectively. These low contents are certainly due to the high degree partial melting recorded in these rocks. In fresh harzburgite, clinopyroxene shows the highest Li content, with values up to 3.7 μg/g, while olivine and orthopyroxene show values up to 1.05 μg/g and 1.49 μg/g, respectively. This study of the Dramala harzburgites shows that Li, Be and B content of the oceanic mantle decreases during partial melting, leading to very low light element contents, and that melt impregnation and/or percolation does not strongly modify their light element content, except for the observed Li enrichment.

During serpentinization on the ocean floor, there is a B enrichment in whole rock samples, while no Li or Be enrichment is observed. Li, Be and B

contents of the primary mantle phases (olivine, clinopyroxene, orthopyroxene) stay constant during this process (e.g. Li: 0.5-1.1 μg/g, 0.4-3.7 μg/g and 0.1-1.5 μg/g, respectively). The major B carrier phase is serpentine, with B contents up to 28 μg/g. The quantity of B which can be incorporated into the serpentinized harzburgite seems to depend on the nature of serpentinization in terms of temperature, pH and water/rock ratio. This is shown by the very different B contents in serpentine and serpentinites from serpentinized harzburgites of Dramala compared to serpentinites from the MAR ODP Leg 209. Samples from Dramala show low whole rock B contents in highly serpentinized harzburgites (up to 1.1 μg/g) and highly heterogeneous B content in serpentine (0.1-28 μg/g). The latter probably reflects serpentinization occurring at high temperature and low water/rock ratio. In contrast, serpentinization in samples from the MAR led to high B content in serpentine (up to 200 μg/g) and serpentinites (10-65 μg/g), which could be related to low temperatures and high water/rock ratio.

Li and B contents in serpentine are heterogeneous at the micrometer scale in the samples from Pindos ophiolite and ODP Leg 209. This problem was investigated by a micro-Raman study on points previously measured by SIMS (spot size ~ 15 μm). The results show that the highest Li contents (> 1 μg/g) in serpentine are due to a mixture of serpentine with other phases such as tremolite, talc or enstatite. The major outcome of this study is that Li and B variability in serpentine is not related to the type of serpentine polymorph (antigorite, lizardite or chrysotile).

The study on the Geisspfad serpentinites showed that Li, Be and B contents of oceanic serpentinites can be modified during emplacement into the continental crust by fluids related to retrograde metamorphism. The effect of fluid metasomatism is evident from the Li, Be and B contents in minerals and whole rock samples. Retrograde fluids can penetrate ultramafic bodies on hundreds of meters or travel along the contact between the ultramafics and the surrounding crustal rocks. This result shows that studies on (ultra) high pressure orogenic peridotites, conducted in order to constrain the Li, Be and B budget and systematics of subducted oceanic lithosphere, should be treated with caution. As all of these rocks were emplaced into continental crust, their light element systematics and budget were probably modified, and only large ultramafic bodies (about 1 km width) can potentially maintain the subduction-related light element systematics in the core.

In conclusion, light element content of the fresh oceanic mantle is low, except for Li, which can be enriched in these rocks during N-MORB type melt impregnation. The oceanic mantle is enriched in B during serpentinization, but the quantity of B potentially introduced probably depends on temperature, pH and water/rock ratio related to the serpentinization process. Due to its big volume compared to the oceanic crust, the oceanic mantle could strongly contribute to the Li and B input into subduction zones. An outlook will be to evaluate the Li and B input related to the serpentinized oceanic mantle into subduction zones, and to compare it with the input related to the oceanic mafic crust and sediments.

Acknowledgements / Remerciements

Je souhaite premièrement remercier ma directrice de thèse **Angelika Kalt** pour son énergie, pour son soutien et pour ses nombreux conseils au fil de ces quatre années. Je remercie également **Othmar Müntener** pour sa collaboration et pour nos discussions toujours passionnantes. Il a su il y a quelques années me donner le virus de la pétrologie qui depuis ne m'a plus quittée.

Je tiens à remercier **Flurin Vils** mon binôme pour son humour et pour les moments sympas que nous avons passés sur le terrain. Je le remercie également d'avoir su rendre le SIMS plus vivable en y faisant entrer la musique et le cinéma!

Merci à **Benjamin Kaeser** qui a été mon collègue de bureau pendant ces quelques années et qui a su tous les jours mettre de l'ambiance et avoir le sourire. Je le remercie également pour tout ses conseils et ses «trucs» qui m'ont souvent permis de gagner du temps.

J'adresse un grand merci à **Erwan Bourdon** pour l'aide qu'il m'a apportée, mais aussi pour les nombreux moments drôles hors des murs de l'institut. Merci aussi à **Arjan Dijkstra** pour nos discussions. Au début de ma thèse je me plongeais dans ses articles, je suis contente à présent de mettre un visage sur ce nom qui m'était devenu familier.

I thank **Julien Allaz**, **Alfons Berger**, **Massoud Dadras**, **Edwin Gnos**, **Mireille Leboeuf**, **Thomas Ludwig**, **Hans Peter Meyer** and **Alexey Ulianov** for their help during measurement on complicated machines. I also thank **Katalin Gméling** (PGNAA), **Horst Marschall** (ICPMS), **Thomas Pettke** (LA-ICPMS), **Terry Plank** (ICPMS), **Benita Putlitz** (Isotopes) and **Torsten Venneman** (Isotopes) for the analyses they did for me. A particular thank to **Chiara Groppo** and **Roberto Compagnoni** for their very warm welcome in Torino and for the micro-Raman analyses.

Je remercie **André Villard** qui a préparé des centaines de lames minces de qualité en un temps record.

I also thank **Ilona Fin** and **Oliver Wienand** for the thin sections they prepared in Heidelberg.

Un grand merci à **Sabine Erb** et **Gianfranca Cerrito** qui font vivre le secrétariat de l'institut de géologie de Neuchâtel avec un «punch» inégalé. Merci mille fois à **Elisabeth Kuster**, notre bibliothécaire, qui a toujours su dégotter les articles introuvables que je lui demandais.

Merci à tous mes potes maître assistants, doctorants et étudiants de l'institut de géologie avec qui les soirées ont pris des tournures souvent hilarantes: **Mary-Alix**, **Erwan**, **les Stéphane de Strassbourg**, **Alex**, **Charles**, **Virginie**, **Cécile**, **Flurin**, **François**, **Nico**, **Laure**, **Pauline**, **Lucien**, **Mélody**, **Laurent**, **Anne** et **Guillaume**. Merci également à toutes les personnes qui font la vie de l'institut de géologie de Neuchâtel.

Finalement je souhaite remercier **ma famille** qui m'a toujours soutenue dans cette drôle d'entreprise qu'est l'élaboration d'une thèse de doctorat, sans même vraiment comprendre dans quel but!

Un énorme merci à **Laurent** pour son soutien inconditionnel et pour la possibilité qu'il m'a offert d'aller voir des cimes où la neige est plus blanche.

This research was supported by the Swiss National Science Foundation (SNF) grants 200021-103611 and 200020-112149. Financial support from the SNF (grants 21-26579.89 and 200021-103479/1) for the electron microprobe facility at the Institute of Geological Sciences, University of Bern (Switzerland) is acknowledged.

Introduction

Li, Be AND B GEOCHEMISTRY

Li, Be and B are powerful tracers of the geochemical processes occurring at the interface between the different Earth's reservoirs. Being incompatible and extremely mobile under a wide range of temperatures, they give information on the transfer of chemical components during fluid or melt metasomatism, but also during hydrothermal alteration. Experimentally determined mineral/fluid partition coefficients increase in the order $D_B < D_{Li} << D_{Be}$ (clinopyroxene; Brenan et al., 1998a), while mineral/melt partition coefficients increase in the order $D_B \leq D_{Be} << D_{Li}$ (olivine, orthopyroxene, clinopyroxene; Ryan & Langmuir, 1988; Brenan et al., 1998b; Blundy & Dalton, 2000).

The alkali metal Li has the atomic number 3 and an atomic mass of 6.941u. It is exclusively monovalent (Li^+). Lithium has two stable isotopes ^6Li and ^7Li, with natural abundances of 7.5 atom% and 92.5 atom%, respectively. Due to its ionic radius of 76 pm in 6-fold coordination (Shannon, 1976), Li^+ substitutes for octahedrally coordinated Mg and Fe^{2+} (72 and 78 pm) in ferro-magnesian silicates. In feldspar and amphiboles, Li^+ can substitute for Na^+ and K^+ on larger coordination sites (7, 8, 12). In hydrous fluids, Li is tetrahedrally coordinated to four H_2O molecules (Olsher et al., 1991).

The alkaline earth metal Be has the atomic number 4 and an atomic mass of 9.012182u. It is exclusively divalent (Be^{2+}). Beryllium has only one stable isotope ^9Be, and one cosmogenic isotope ^{10}Be. In nature, Be is tetrahedrally coordinated to oxygen in minerals (Hawthorne & Huminicki, 2002). Even if Be^{2+} and Si^{4+} have similar ionic radii (27 and 26 pm respectively), Be hardly substitutes for Si because of a large difference in charge. Be^{2+} generally substitutes for Al^{3+} (39 pm) or B^{3+} (11 pm) on the tetrahedral site. However, Be can also be incorporated into minerals in vacant tetrahedral sites (Hawthorne & Huminicki, 2002).

The nonmetal B has the atomic number 5 and an atomic mass of 10.811u. It is exclusively trivalent (B^{3+}). Boron has two stable isotopes ^{10}B and ^{11}B, with natural abundances of 19.9 atom% and 80.1 atom%, respectively. In minerals, melts and fluids, B can be trigonally or tetrahedrally coordinated to oxygen (Hawthorne et al., 1996). B is nearly always bonded to O, and forms $B(OH)_3$ or $B(OH)_4^-$ ions. In silicates, B can substitute for Si^{4+} or Al^{3+} on the tetrahedral site. However, the presence of B in the tetrahedral site generates a distortion of the TO_4 units, as B has a very small ionic radius in this coordination (11 pm). Coordination of B in fluids is highly dependent on pH. At low pH, B is trigonally coordinated to H_2O, while at high pH B is tetrahedrally coordinated to H_2O (Schmidt et al., 2005).

RATIONALE OF THE STUDY

The importance of the oceanic mantle as a repository for the light elements Li, Be and B is poorly constrained. This should be determined in order to complete the global geochemical cycle of these elements on Earth (Fig. 1.1), and their behaviour during some geodynamic processes. This thesis is part of a project, which includes two PhD students (L. Pelletier and F. Vils). This project focuses on Li, Be and B abundances, partitioning and mobility in rock-forming minerals from hydrothermally altered oceanic mantle in different geodynamic environments.

In order to constrain the important light element addition during serpentinization of the oceanic mantle, and to evaluate the potential input of light elements into subduction zones, two types of samples were studied (Fig. 1.2). (i) Samples from

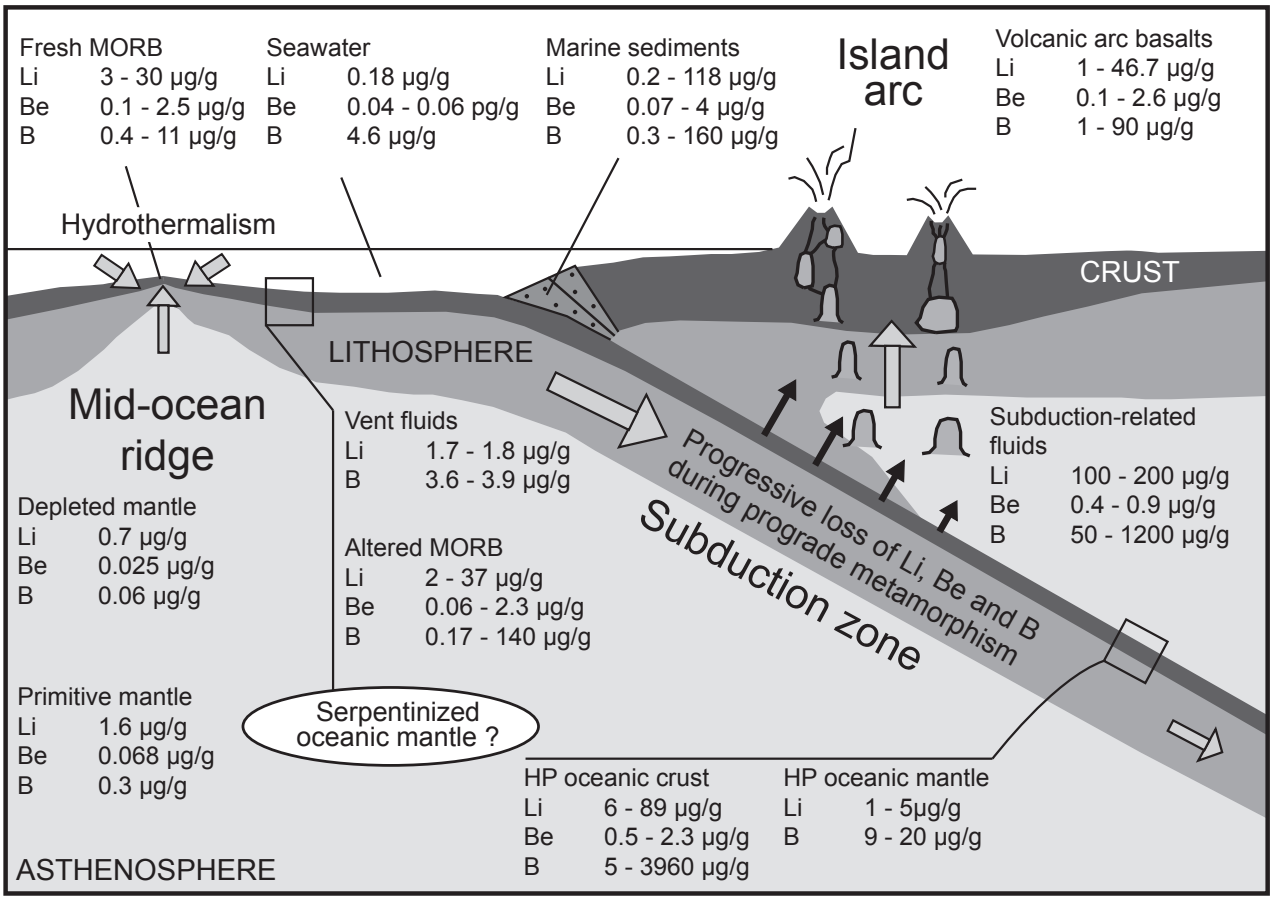


Fig. 1.1: Li, Be and B geochemical cycles on Earth. Primitive mantle after McDonough & Sun (1995). Depleted mantle after Salters & Stracke (2004). Fresh MORB after Ryan & Langmuir (1987, 1988, 1993), Chaussidon & Jambon (1994), Niu & Batiza (1997), Perfit et al. (1999), Regelous et al. (1999), Danyushevsky et al. (2000), Kamenetsky et al. (2000) and Bach et al. (2001). Altered MORB after Chan et al. (1992), Bach et al. (2001), Kelley et al. (2003) and Bouman et al. (2004). Seawater after Morozov (1968), Broeker & Peng (1982) and Measures & Edmond (1983). High pressure oceanic crust after Marschall et al. (2006). High pressure oceanic mantle after Scambelluri & Philippot (2004). Sediments after Ryan & Langmuir (1988), Ishikawa & Nakamura (1993), Hoefs & Sywall (1997), Spivack & You (1997), Gao et al. (1998), Chan & Kastner (2000), Ryan (2002), Bouman (2004) and Bouman et al. (2004). Island arc basalts (IAB) after Ryan & Langmuir (1988, 1993), Smith et al. (1997), Sano et al. (2001), Ryan (2002), Bouman et al. (2004), Leeman et al. (2004). Vent fluids after Schmidt et al. (2007). Subduction related fluids (calculated) after Marschall et al. (2007).

the Ocean Drilling Program along the Mid-Atlantic Ridge (ODP Leg 209 sites 1272A and 1274A). (ii) Samples from the non-metamorphic Pindos and Vourinos ophiolites (Greece). Moreover, we studied non-subducted oceanic mantle from the Geisspfad ultramafic body (Switzerland), which is imbricated in the continental crust and metamorphosed under crustal conditions, in order to evaluate the mobility of light elements during crustal tectonic and metamorphic processes. This latter study helps to understand the mobility of light elements during metamorphism and exhumation, and will improve our understanding on light element signatures found in high pressure metamorphic peridotite massifs.

In addition to field work, petrography and electron microprobe analyses, the project included the in situ measurement of Li, Be and B in minerals by SIMS (Secondary Ion Mass Spectrometry), accompanied by a laser ablation ICP-MS (Inductively Coupled Plasma Mass Spectrometry) study for other trace elements. Whole rock analyses of Li and Be were obtained by ICP-MS and B

by PGNAA (Prompt Gamma Neutron Activation Analysis). A micro-Raman study was done to characterize the nature of the serpentine polymorphs and their potential influence on the Li and B content of serpentine and serpentinites.

Li, Be AND B IN THE MANTLE

Unaltered mantle has extremely low Li, Be and B contents (Fig. 1.1). Estimated primitive mantle composition is 1.6 μg/g, 0.054-0.068 μg/g and 0.17-0.30 μg/g, respectively (Chaussidon & Jambon, 1994; McDonough & Sun, 1995; Lyubetskaya & Korenaga, 2007). Depleted mantle composition was estimated at 0.7 μg/g Li, 0.025 μg/g Be and 0.06 μg/g B by Salters & Stracke (2004). Ottolini et al. (2004) measured some unmetasomatized mantle xenoliths and showed that these peridotites have low Li (1.6–1.8 μg/g) and B (0.07-0.10 μg/g) contents.

In the unaltered and unmetasomatized mantle, the major Li-bearing phase is olivine, with contents between 1.3-1.9 μg/g, while other minerals show lower contents (orthopyroxene: 0.7-1.1 μg/g, clinopyroxene: 0.8-1.1 μg/g and spinel: 0.4-0.7 μg/g; Ottolini et al., 2004). According to Ottolini et al. (2004), B contents of all minerals are low (< 0.04 μg/g).

In subduction zones, there is a progressive release of Li and B from the subducted altered oceanic crust with depth during dehydration reactions (Moran et al., 1992; Bebout et al., 1993 and 1999; Domanik et al., 1993; You et al., 1994, 1995a and b; Peacock & Hervig, 1999; Chan & Kastner, 2000; Benton et al., 2001). Be can be released by melting (Johnson & Planck, 1999), but also by dehydration during high pressure and temperature metamorphism of the subducted altered oceanic crust (Marschall et al., 2007). Li, Be and B concentrations (and their isotopic signatures) in arc

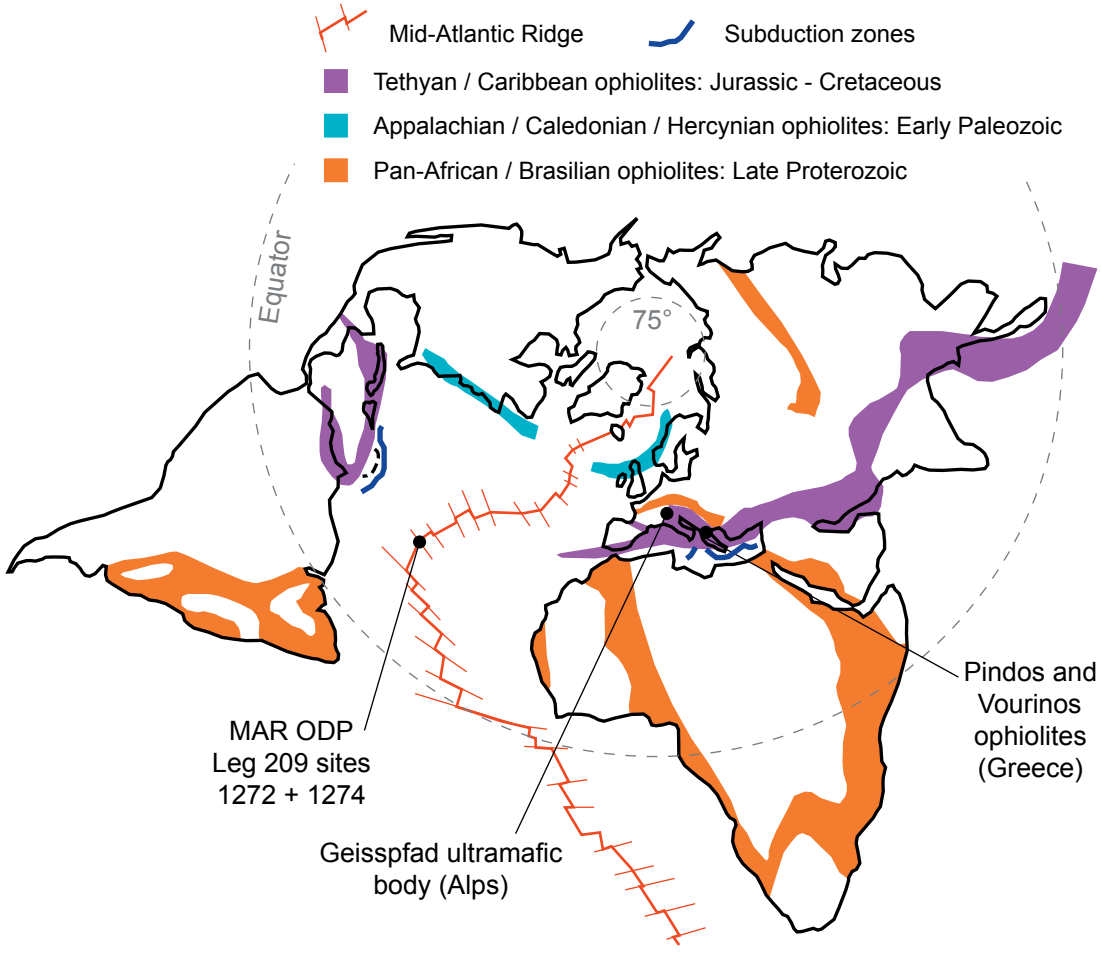


Fig. 1.2: Localization of the studied ultramafic body on a North polar projection map of ophiolite belts. Map modified after Dilek (2003). Abbreviations: MAR = Mid-Atlantic Ridge, ODP = Ocean Drilling Program.

lavas show that the mantle wedges (sources) are modified by slab-derived fluids or melts (Tatsumi, 1989; Ishikawa & Nakamura, 1994; Leeman, 1996; Chan et al., 1999, 2002; Rose et al., 2001; Tomascak et al., 2002; Ryan, 2002), because the calculated composition of the source is clearly enriched in Li, Be and B compared to the unmetasomatized mantle.

Due to the above interpretation that mantle wedges can react with subduction-related fluids or melts, the light element enrichment observed in orogenic high pressure peridotites is usually assumed to result from interaction of the peridotites with subduction-related fluid or melt in a similar type of setting (Paquin et al., 2004; Scambelluri et al., 2006).

Li, Be AND B DURING SERPENTINIZATION

Hydrothermally altered oceanic mantle can be enriched in light elements, due to the interaction of seawater or seawater-derived fluids during serpentinization on the ocean floor (Thompson & Melson, 1970; Bonatti et al., 1984; Spivack & Edmond, 1987; Decitre et al., 2002; Niu, 2004). Seawater contains 0.2 μg/g Li, 0.0002 ng/g Be and 4.44 μg/g B (Li, 1982; Measures & Edmond, 1982), and only represents an endmember. Previous light element studies on abyssal peridotites dealt with dredged samples. No light element study on drilled abyssal peridotites from mid-ocean ridges were performed, for this reason the present study will include serpentinized harzburgites from the Mid-Atlantic ridge ODP Leg 209. Previous studies show that serpentinized abyssal peridotites are highly enriched in B (up to 100 μg/g) and to a lesser extent in Li (up to 13.7 μg/g) compared to fresh mantle rocks (e.g. Thompson & Melson, 1970; Niu, 2004). Niu (2004) reported Be contents of dredged serpentinites between 0.001 and 0.212 μg/g.

Many parameters can influence the light element enrichment of peridotites during serpentinization. Fluid-rock ratio and fluid composition play an important role as described by Decitre et al. (2002), because low fluid-rock ratio can induce local differences in fluid composition and disequilibrium. This can happen if the fluid composition evolved during its interaction with the mantle or if the fluid interacted with a mafic crust before the serpentinization of the mantle (Smith et al., 1995; Decitre et al., 2002).

Temperature, pH and time could play an important role during serpentinization. Serpentinites are enriched in Li and B when they react with low-temperature fluids and under equilibrium conditions (Thompson & Melson, 1970; Seitz & Hart, 1973; Seyfried & Dibble, 1980; Bonatti et al., 1984; Decitre et al., 2002; Scambelluri et al., 2004; Paulick et al., 2006). This was also experimentally demonstrated by Seyfried & Dibble (1980). B coordination in a fluid depends on pH. At low pH, B is trigonally coordinated to H_2O, while at high pH B is tetrahedrally coordinated to H_2O (Spivack & Edmond, 1987; Schmidt et al., 2005). As B is preferentially incorporated in the tetrahedral site in serpentine (Page, 1968), high B contents should be expected for alkaline fluids.

Light element data on drilled serpentinites are documented from the Izu-Bonin-Mariana forearc (Parkinson & Pearce, 1998; Benton et al., 2001 and 2004; Savov et al., 2005; Wei et al., 2005; Zanetti et al., 2006). However, in this environment, a light element contribution from the subducting slab is to be expected (Benton et al., 2001).

Considering all the data mentioned above, studies combining light element content of minerals (primary mantle phases and serpentinization-related minerals) and whole rocks are rare. Decitre et al. (2002) reported data for Li only, in some samples from the South West Indian Ridge, and Bonatti et al. (1984) for B only in some serpentinites from the Vema and Romanche fracture zones from the Atlantic. One study deals with Li and B contents in minerals from ophiolitic serpentinites (Scambelluri et al., 2004). These studies show that serpentine is the major B-bearing phase in the serpentinized oceanic mantle, while Li is mainly concentrated in the pre-serpentinization phases like olivine or pyroxenes. In order to study the light element behaviour during serpentinization, hydrothermally altered samples from the Pindos and Vourinos ophiolites, and from the Mid-Atlantic ridge ODP Leg 209 will be used.

Studies on light element contents in high pressure peridotites can give us information about the fate of light elements during subduction. During antigorite breakdown at depth, the major quantity of water contained in the hydrous peridotite is released (Ulmer & Trommsdorff, 1995; Bromiley & Pawley, 2003). Because trace elements and

potentially light elements can be liberated with the fluids (e.g. Tatsumi, 1989; Scambelluri et al., 2001), subducted hydrous peridotites suffer a loss of light elements during dehydration at high pressure (Scambelluri et al., 2004). However, experiments and studies on high pressure oceanic mantle showed that major quantities of Li and B can be retained beyond the depths of arc magma sources (Scambelluri et al., 2004; Tenthorey & Hermann, 2004), and be introduced into the deep mantle. In this context, it would be important to evaluate the input of Li and B into subduction zones related to the hydrothermally altered oceanic mantle, which is the aim of this study.

ORGANIZATION OF THE THESIS

This study includes a detailed investigation of textures, mineralogy, major, light (Li, Be and B) and other trace elements in minerals and whole rocks, in different oceanic peridotites serpentinized to different degrees and from various tectonic settings. The objective of this thesis is (1) to study the Li, Be and B systematics during serpentinization of the oceanic mantle, and to determine which are the major-carrier phases of these light elements; (2) to define Li, Be and B behaviour during metasomatic processes commonly observed in the oceanic mantle, i.e. mafic melt metasomatism; (3) to study Li, Be and B systematics during emplacement of serpentinized mantle into the continental crust. These topics will help to evaluate the importance of the hydrothermally altered oceanic mantle in the Li, Be and B input in subduction zones.

Topics (1) and (2) will be addressed in **chapter 2**, which is a detailed study of Li, Be and B contents of minerals and whole rocks of the Dramala harzburgites (Pindos ophiolite, Greece). The paper corresponding to this chapter was *accepted by the Journal of Petrology* (with minor revisions). Issues (1) and (2) were also extensively studied in samples from ODP Leg 209 of the Mid-Atlantic ridge and will be part of the thesis of Flurin Vils (see «list of publications» at the end of this manuscript). **Chapter 3** is a complementary part to **chapter 2**, and consists of a detailed trace element study of minerals and whole rocks, in order to describe mafic melt metasomatism in the Dramala harzburgites. Issue number (3) will be addressed in **chapter 4**, which represents a complete study of major, light and other trace elements in minerals and whole rocks of the Geisspfad body (Swiss-Italian Alps). This chapter was *submitted to Chemical Geology*. **Chapter 5** is related to topic (1) and focuses on Li and B content in serpentine, in order to understand the heterogeneity usually observed in Li and B contents of this mineral. It includes a detailed micro-Raman study, where the different serpentine polymorphs were determined. This chapter was *submitted to the European Journal of Mineralogy*. **Chapter 6** mainly includes the conclusions and an outlook to further research which could solve remaining questions. **Chapter 7** presents a detailed description of all the analytical methods used. Work of the author, the different co-authors and collaborators can be found in Table 1.1.

STUDIED LOCALITIES

In order to define the enrichment of the oceanic mantle in light elements during serpentinization, samples from the Mid-Atlantic Ridge ODP Leg 209, and samples from the Pindos and Vourinos ophiolites from northern Greece were studied. The effect of metamorphism and crustal tectonic on the light element content of the oceanic mantle was studied in the Geisspfad ultramafic body (Alps). The localization of the different ultramafics can be found in Fig. 1.2.

Mid-Atlantic Ridge ODP Leg 209 – Sites 1272 and 1274

ODP Leg 209 was drilled along the slow spreading Mid-Atlantic ridge (Fig. 1.3), where the full spreading rate is estimated at 25 km/m.y (Fujiwara et al., 2003). Site 1274 is situated north of the 15°20' fracture zone (Fig. 1.4), while site 1272 is located to the south of it (Kelemen et al., 2004; Paulick et al, 2006). The halfspreading rates (E and W) show little long-term asymmetry, which could be related to shallow detachment faults (Escartin et al., 2003; Fujiwara et al., 2003). This model diverges from the previous hypothesis (amagmatic or melt-assisted extension; e.g. Tucholke et al., 1998; Dick et al., 2002), because the root of the detachment is situated in the shallow lithosphere, probably at the rheological boundary materialized by the alteration front. The area where the samples were drilled is covered by a thin sedimentary cover (Kelemen et al., 2004).

Samples studied in this thesis are serpentinized

spinel harzburgites recovered from sites 1272A and 1274A. These rocks have been extensively studied for melt impregnation (Seyler et al., 2007) and conditions of serpentinization (Bach et al., 2004 and 2006). These spinel harzburgites are highly refractory (Seyler et al., 2007) and represent residues after more than 20% partial melting, which later reacted with a percolating melt prior to cooling in the lithosphere (Seyler et al., 2007). Bach et al. (2004 and 2006) described a retrograde serpentinization sequence related to cooling. Serpentinization began at high temperature (≥ 350°C), where pyroxenes were replaced by talc and tremolite, while olivine was stable. At temperatures below 250°C, olivine was transformed to serpentine, magnetite and brucite.

The Pindos and Vourinos ophiolites (Greece)

The Pindos and Vourinos ophiolites belong to the Sub-Pelagonian ophiolites, which are aligned along two parallel NNW-SSE trends within the Hellenides (Fig. 1.5). Magnetic studies showed that the two ophiolites are linked under the Tertiary post-orogenic Mesohellenic Molasse (Rassios & Moores, 2006).

Their evolution is related to the tectonic history of the Neo-Tethys from the Triassic to the Tertiary. Sea-floor spreading began during the Triassic (Fig. 1.6a-b), where oceanic lithosphere was created (Jones & Robertson, 1991; Pe-Piper & Piper, 2002; Robertson, 2002). Later, during Mid-Jurassic, convergence began and ophiolites were moved towards the subduction zone (Jones & Robertson, 1991). When the trench collided with the Pelagonian passive margin, the ophiolites were emplaced onto the oceanic crust, and probably onto the accretionary prism. This intra-oceanic obduction led to the formation of the well-known metamorphic soles (Fig. 1.7 and 1.8), which are present at the base of the Pindos and Vourinos ophiolites (Robertson 2002 and references therein). These soles are mainly composed of metabasites and metasediments metamorphosed under greenschist to amphibolite facies conditions. They were dated using Ar/Ar or K/Ar on hornblende. The metamorphic sole of the Pindos ophiolite (Loumnitsa Unit) gives ages of 169±5, 165±3 and 176±5 Ma (Roddick et al., 1979;

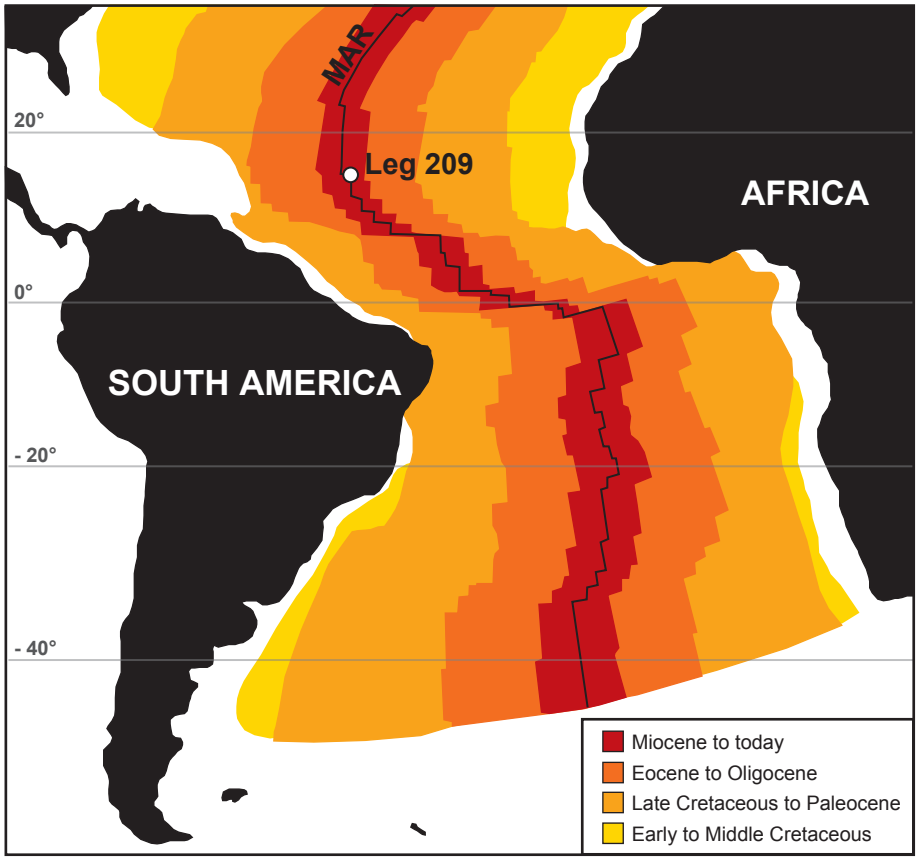


Fig. 1.3: Position of the ODP Leg 209 along the Mid-Atlantic Ridge. Modified after Scotese et al. (1988).

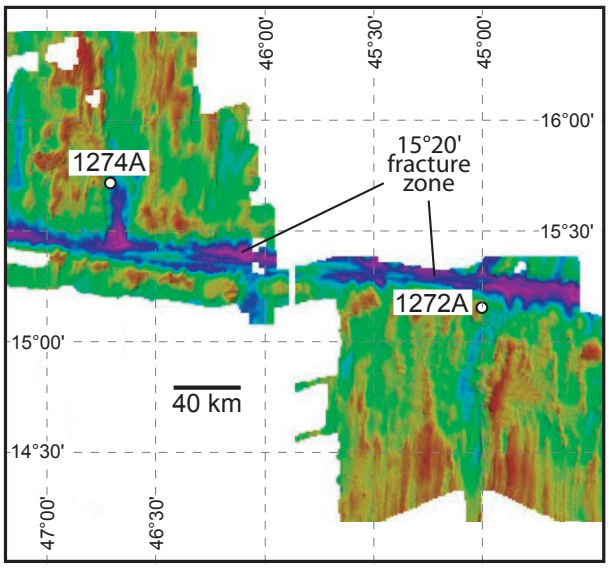


Fig. 1.4: Position of the studied sites 1272 and 1274 along the 15°20' fracture zone. Modified after Figure F2 of Kelemen et al. (2004).

Spray & Roddick, 1980; Thuizat et al., 1981), while the sole from the Vourinos ophiolite gives an age of 171±4 Ma (Spray & Roddick, 1980; Fig. 1.5 and 1.8). The sub-ophiolitic melange (Avdella) in the Pindos ophiolite represents the over-ridden trench accretionary complex, which was related to the ocean-ocean subduction (Pe-Piper & Piper, 2002). Finally, in the Late Jurassic, the ophiolites were obducted onto the continental crust of the Pelagonian margin (Pe-Piper & Piper, 2002).

The palaeogeography of the Neo-Tethys is still a matter of debate and two different scenarios were proposed for the sub-pelagonian ophiolites. (i) All the sub-pelagonian ophiolites were formed in a single and large ocean, the Vardar ocean, located to the east of the Pelagonian microcontinent. The present position of the ophiolites is due to post-obduction tectonics (Aubouin, 1959; Dercourt et al., 1986 and 1993; Jacobshagen, 1986). (ii) The actual regional distribution of the sub-pelagonian ophiolites aligned along two parallel trends (Fig. 1.5) reflects their formation in various small ocean basins (Fig. 1.6a-b). In this context, the Pindos and Vourinos ophiolites were formed in a small Pindos basin, located to the west of the Pelagonian micro-continent (Pe-Piper & Piper, 2002 and references therein). This last scenario is presented in Figure 1.6. The postulated model of Pe-Piper & Piper (2002 and references therein) for the evolution of the Pindos and Vourinos ophiolites from the Triassic to the Tertiary is presented in Figure 1.7. In this scenario, the Pindos and Vourinos ophiolites were formed in a supra-subduction zone environment during the Early to Mid Jurassic, and represent two pieces of the same oceanic lithosphere. They were emplaced simultaneously on the Pelagonian margin, and are today separated by the Tertiary Mesohellenic Trough (Molasse).

The Pindos and Vourinos ophiolites show many similarities, such as the presence of highly depleted harzburgites and the occurrence of podiform chromitite bodies. However, they also present some discrepancies. The mantle section from the Pindos ophiolite (Dramala mantle, Fig. 1.8) includes a MOR-type cumulate sequence (Kostopoulos, 1988), and is characterized by rare chromitite bodies with low-Cr MORB to high-Cr boninitic affinities (Economou-Eliopoulos et al., 1999). In the extrusive sequence (Aspropotamos complex; Fig. 1.8), lavas evolved with time from high-Ti MORB to N-MORB to island arc tholeiites and finally to boninites. In contrary, the Vourinos

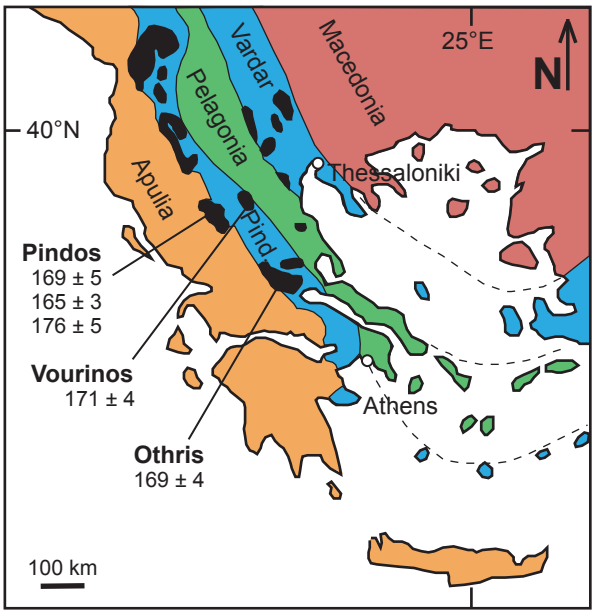


Fig. 1.5: Structural elements of the Hellenides. Black zones represent the sub-pelagonian ophiolites. Numbers are Ar/Ar and K/Ar ages (in Ma) of the different metamorphic soles and therefore record the timing of intra-oceanic obduction. The colours correspond to those of Figure 1.6. Modified after Channell & Kozur (1997).

mantle section shows many chromitite bodies, which are economically exploited, and is overlain by a cumulate sequence and some extrusives with island arc tholeiites to boninitic affinities. The Vourinos oceanic crust is characterized by the lack of MOR-type intrusives and extrusives. From these geochemical data, many authors regard the Pindos and Vourinos ophiolites as a unique supra-subduction zone ophiolite (Capedri et al., 1981; Beccaluva et al., 1984; Pearce et al., 1984; Jones et al., 1991). For more details about the Pindos ophiolite and its geochemistry, the reader is referred to chapter 2 and 3.

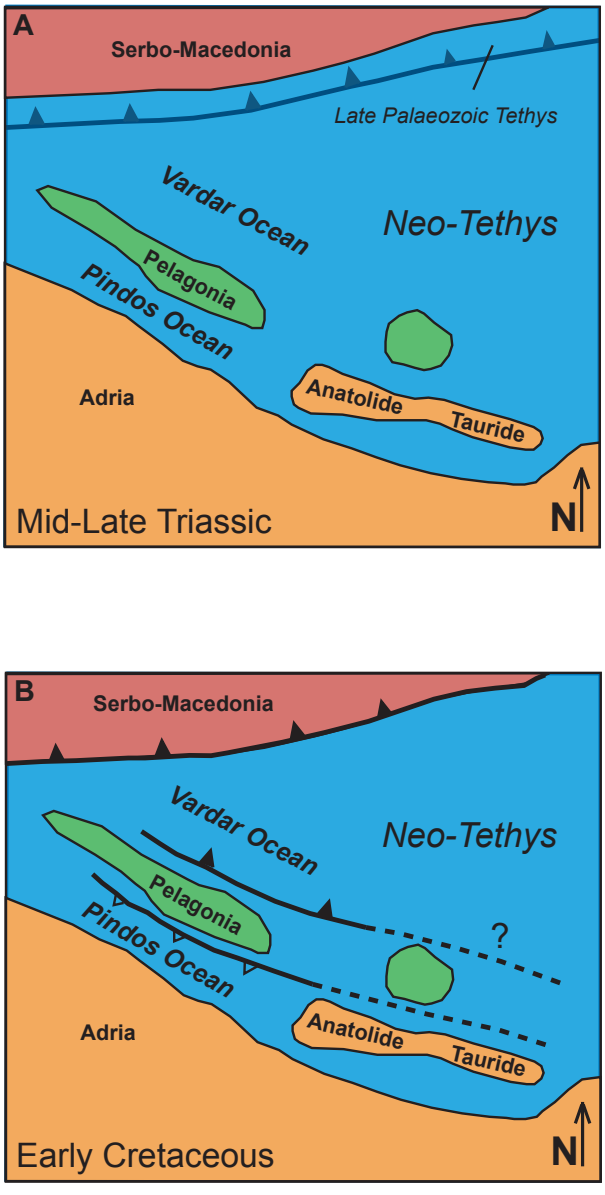


Fig. 1.6: Palaeogeography of the Neo-Tethys in the Eastern Mediterranean region. (a) Mid-Late Triassic and (b) Early Cretaceous. Modified from Robertson et al. (2004), Pe-Piper and & Piper (2002) and Channell & Kozur (1997).

The Geisspfad ultramafic massif (Alps)

The Geisspfad ultramafic massif (Swiss-Italian Alps) has not been extensively studied. Only two major studies have been realized, one in the seventies by Keusen (1972) and one in the nineties by Pastorelli (1994). The mineral preiswerkite, an Al-rich sodium mica, was discovered in rodingites from this locality by Keusen & Peters (1980). The Geisspfad ultramafic body is one of the largest ultramafic outcrops in the central Alps (Pastorelli et al., 1995). It is included in the lower penninic Monte Leone nappe (Fig. 1.9-1.10), which was part of the European margin before the alpine collision. The Monte Leone nappe mainly includes ortho- and paragneiss, and shows an overturned Mesozoic sedimentary sequence, including Triassic dolomitic marbles and some calcschists. It is not clear if the Geisspfad ultramafic body is directly related to the Monte Leone nappe, or if its position is due to emplacement tectonics because the contact between the two units is a shear zone.

The Geisspfad complex includes various mafic and ultramafic rocks, mainly serpentinite, ophicarbonate and metabasics (Keusen, 1972). Pastorelli (1994) and Pastorelli et al. (1995) mentioned the presence of fresh lherzolite in some loose blocks. Previous studies agree on the fact that the Geisspfad rocks were probably serpentinized on the ocean floor and later recrystallized under amphibolite facies conditions during alpine metamorphism (Keusen, 1972; Pastorelli et al., 1995). Pastorelli et al. (1995) postulated that the Geisspfad ultramafics represent a piece of subcontinental mantle which was exposed on the ocean floor due to Triassic rifting in an ocean-continent transition environment. The lherzolite could represent a piece of this fresh subcontinental mantle. For more details about the Geisspfad ultramafic massif, refer to chapter 4.

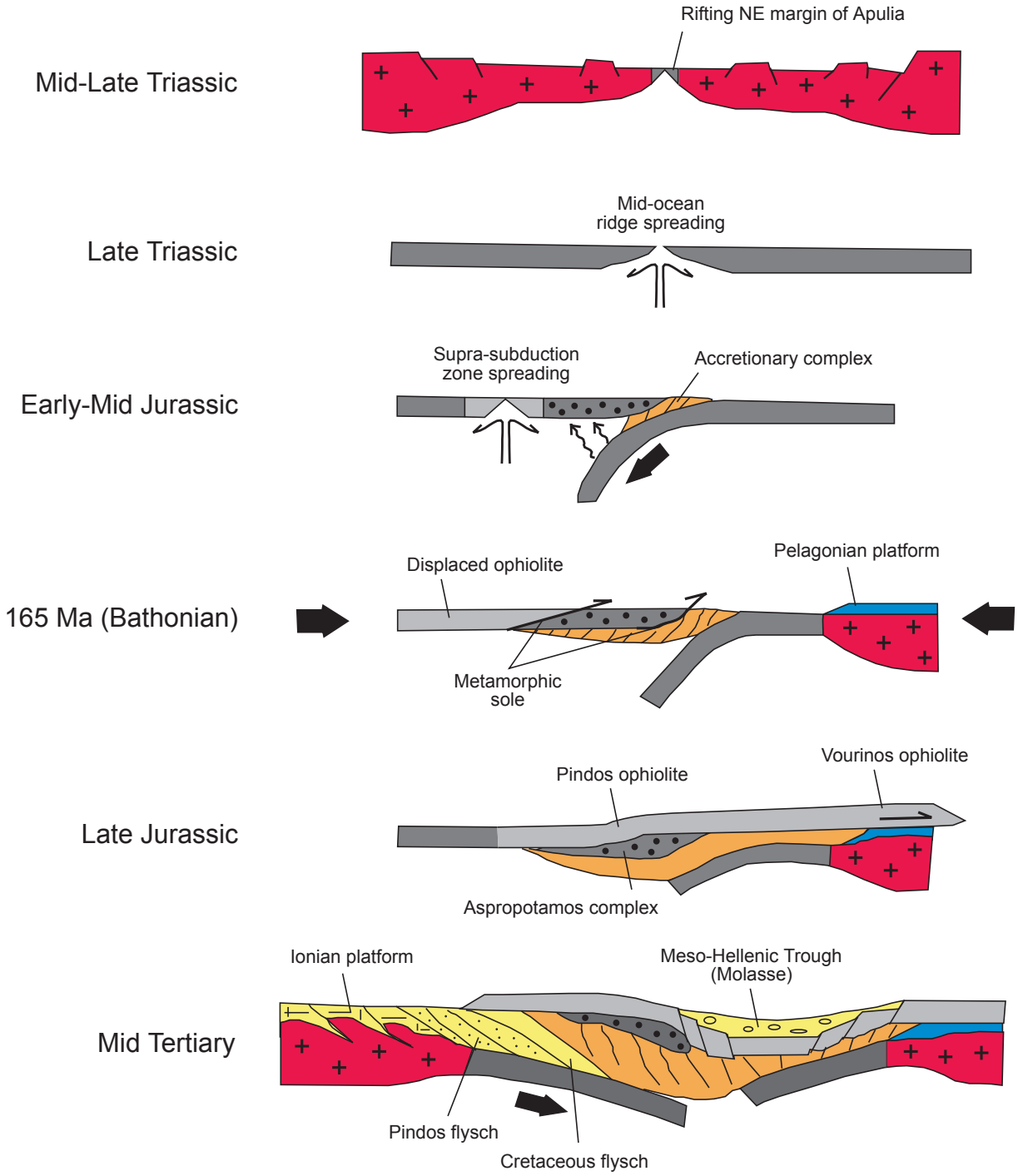


Fig. 1.7: Interpreted tectonic evolution of the Neo-Tethys from the Triassic to the Tertiary. Modified from Pe-Piper & Piper (2002).

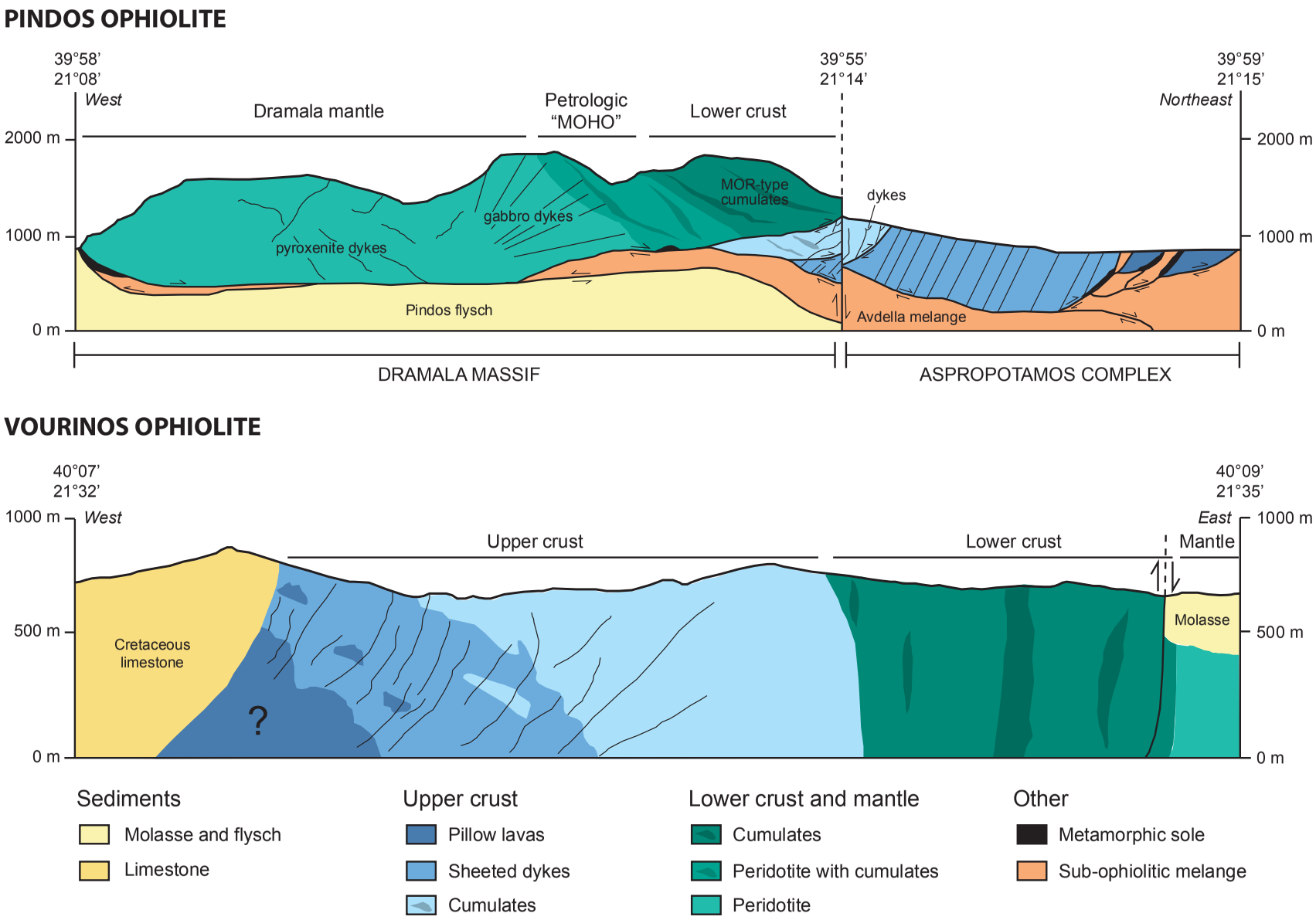


Fig. 1.8: Profile across the Pindos and Vourinos ophiolites. Modified after Rassios & Moores (2006).

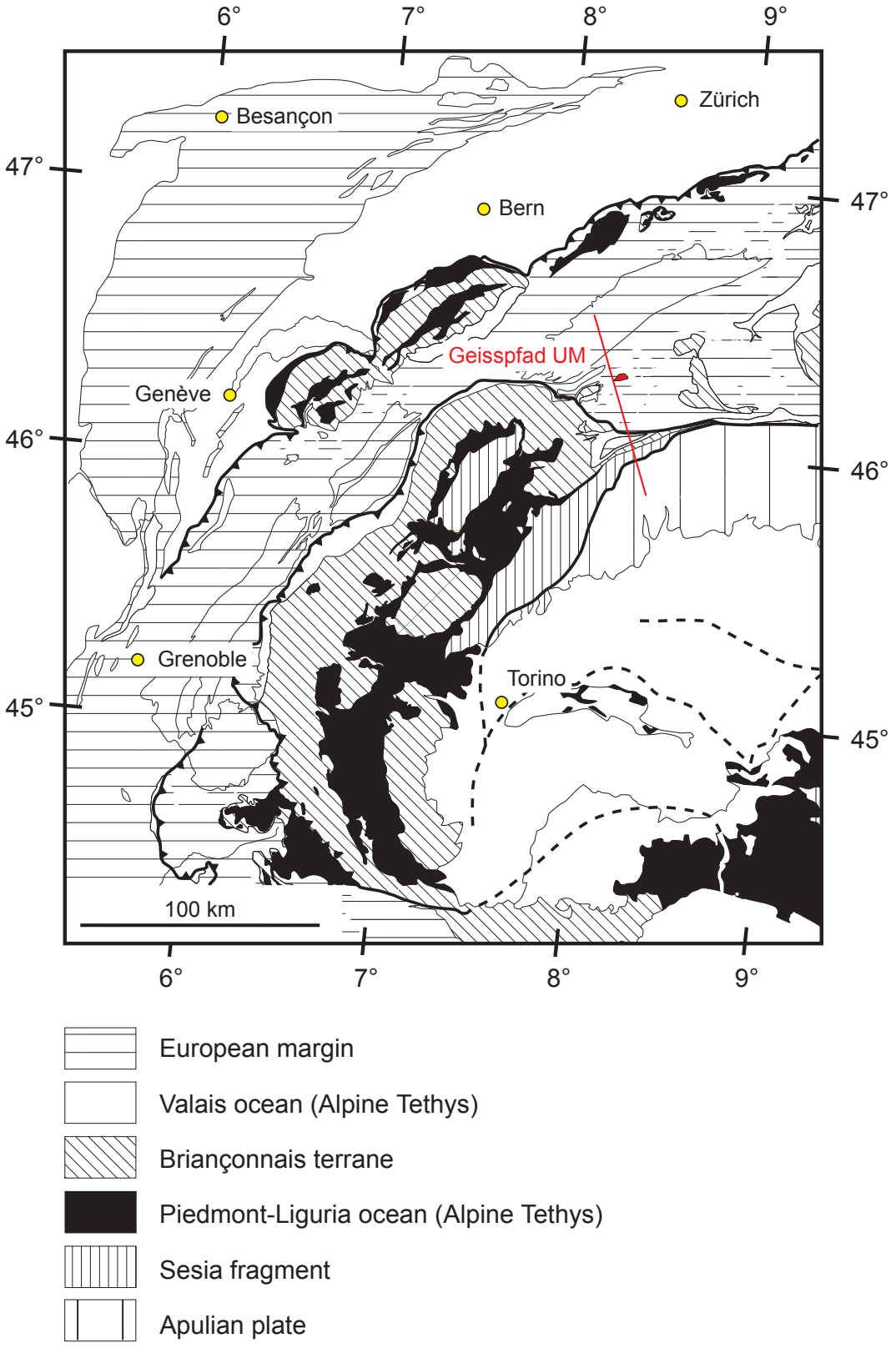


Fig. 1.9: Tectonic map of the Central and Western Alps showing the position of the Geisspfad ultramafic massif. Modified after Froitzheim et al. (1996) and Schmid et al. (2004).

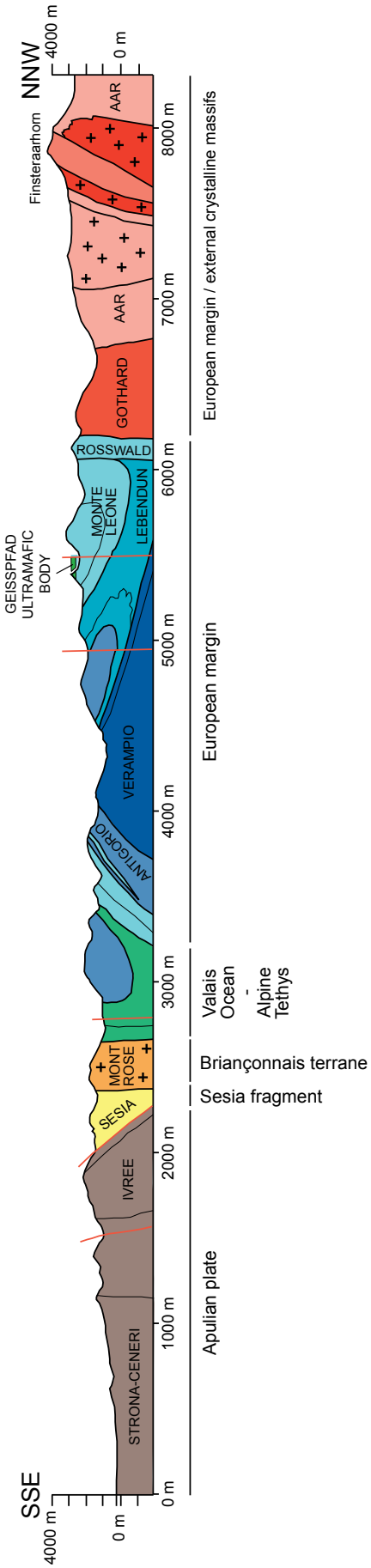


Fig. 1.10: Tectonic profile across the Central Alps. Position of the profile is shown in Figure 1.9. Modified after Steck et al. (1999).

Table 1.1: Contributions of the co-authors and collaborators to the different chapters

ANALYTICS		Pindos I	Pindos II	Geisspfad	Serpentine	
Collaboration	**University**	**Chapter 2**	**Chapter 3**	**Chapter 4**	**Chapter 5**	**Appendix**
Pelletier L.	University of Neuchâtel (CH)	80%	80%	85%	50%	100%
Vils F.	University of Neuchâtel (CH)	10%	-	-	35%	-
Vennemann T.	University of Lausanne (CH)	-	-	5%	-	-
Pettke T.	University of Bern (CH)	-	10%	-	-	-
Serneels V.	University of Fribourg (CH)	-	-	5%	-	-
Gméling K.	Hungarian Acad. of Sciences - Budapest (H)	10%	-	-	-	-
Belgya T.	Hungarian Acad. of Sciences - Budapest (H)	-	-	5%	-	-
Groppo C.	Universita degli studi di Torino (IT)	-	-	-	15%	-
Marschall H.	Bristol University (UK)	-	10%	-	-	-

WRITING		Intro	Pindos I	Pindos II	Geisspfad	Serpentine	Conclusion	Anal. tech	
Collaboration	**University**	**Chapter 1**	**Chapter 2**	**Chapter 3**	**Chapter 4**	**Chapter 5**	**Chapter 6**	**Chapter7**	**Appendix**
Pelletier L.	University of Neuchâtel (CH)	80%	60%	60%	65%	60%	80%	55%	80%
Kalt A.	University of Neuchâtel (CH)	20%	35%	15%	10%	35%	20%	10%	20%
Dijkstra A.	University of Neuchâtel (CH)	-	-	15%	-	-	-	-	-
Müntener O.	University of Lausanne (CH)	-	-	-	10%	-	-	-	-
Vennemann T.	University of Lausanne (CH)	-	-	-	5%	-	-	5%	-
Pettke T.	University of Bern (CH)	-	-	5%	-	-	-	10%	-
Serneels V.	University of Fribourg (CH)	-	-	-	5%	-	-	5%	-
Gméling K.	Hungarian Acad. of Sciences - Budapest (H)	-	5%	-	-	-	-	5%	-
Belgya T.	Hungarian Acad. of Sciences - Budapest (H)	-	-	-	5%	-	-	-	-
Groppo C.	Universita degli studi di Torino (IT)	-	-	-	-	5%	-	5%	-
Marschall H.	Bristol University (UK)	-	-	5%	-	-	-	5%	-

INTERPRETATION OF RESULTS		Pindos I	Pindos II	Geisspfad	Serpentine
Collaboration	**University**	**Chapter 2**	**Chapter 3**	**Chapter 4**	**Chapter 5**
Pelletier L.	University of Neuchâtel (CH)	50%	40%	60%	50%
Kalt A.	University of Neuchâtel (CH)	50%	20%	15%	40%
Dijkstra A.	University of Neuchâtel (CH)	-	40%	-	-
Müntener O.	University of Lausanne (CH)	-	-	15%	-
Vennemann T.	University of Lausanne (CH)	-	-	10%	-
Groppo C.	Universita degli studi di Torino (IT)	-	-	-	10%

Li, B and Be contents of harzburgites from the Dramala Complex (Pindos ophiolite, Greece): a MOR-type mantle in a supra-subduction zone environment

L. Pelletier[1], F. Vils[1], A. Kalt[1] and K. Gméling[2]

[1]Institute of Geology and Hydrogeology, University of Neuchâtel, Emile Argand 11, CP158, 2009 Neuchâtel, Switzerland

[2]Institute of isotopes, Hungarian Academy of Sciences, P.O. BOX 77, 1525 Budapest, Hungary

Manuscript accepted by the Journal of Petrology with minor revisions

Abstract

The Pindos ophiolite represents oceanic lithosphere obducted during the Jurassic. The Dramala mantle section mainly consists of highly depleted spinel harzburgite and minor plagioclase-bearing harzburgite. Textural observations and major element compositions of minerals indicate that the harzburgites experienced impregnation by a mafic, depleted melt and subsequent high-temperature hydration and cooling (> 750°C) forming pargasite and edenitic hornblende. During further cooling (≥ 350-400°C to < 100°C), talc + tremolite ± serpentine ± olivine, serpentine + magnetite, and finally plagioclase alteration phases formed. In order to test the hypothesis of a supra-subduction origin for the Dramala mantle, we measured Li, B and Be contents of minerals by SIMS (Secondary Ion Mass Spectrometry). Whole rock contents were measured using ICP-MS (Inductively Coupled Plasma – Mass Spectrometry) and PGNAA (Prompt Gamma Neutron Activation Analysis). We observe low Li and B contents of primary minerals (olivine, orthopyroxene, clinopyroxene) and whole rock samples consistent with values for unmetasomatized mantle minerals; only Li contents of clinopyroxene (up to 3.7 μg/g) and of the bulk (0.5-1.1 μg/g) are slightly elevated. Be abundances are generally very low or below detection limit (~ 0.005 μg/g). The selective addition of Li to clinopyroxene and the bulk can be explained by infiltration of a mafic, depleted melt. During high-temperature hydration and cooling, the fluid calculated to be in equilibrium with the pargasite or edenitic hornblende (based on B and Be) could have been reaction-modified seawater. Low-temperature hydration led at most to a very minor increase in B in most whole rock samples and to the formation of serpentine with highly variable B contents (0.1 - 28 μg/g). B and Li may even have been leached from some samples. The lack of correlation between degree of serpentinization and bulk B contents as well as the presence of high- and low-B serpentine can be explained by low fluid-rock ratios, decreasing temperature during

serpentinization and lack of equilibrium due to fast obduction/exhumation. The low light element contents in primary minerals and in whole rock samples clearly argue against a supra-subduction zone origin of the Dramala mantle section. We therefore conclude that the Dramala harzburgites represent a MOR-type mantle, and not an SSZ-type mantle, juxtaposed with MOR-type and SSZ-type oceanic crust, either in a back-arc or in an intra-oceanic subduction zone setting.

Key words: light elements; melt impregnation; peridotite; supra-subduction zone ophiolite; MOR-type mantle

INTRODUCTION

Ophiolites - supra-subduction zone versus ocean ridge origin

Many authors believe that most ophiolites formed in supra-subduction zone (SSZ) settings (Beccaluva et al., 1984; Pearce et al., 1984; Jones et al., 1991; Wallin & Metcalf, 1998; Bizimis et al., 2000; Metcalf et al., 2000; Saccani & Photiades, 2004; Beccaluva et al., 2004 and 2005). The interpretation is mainly based on the association of depleted peridotite with island arc tholeiite and boninite found in these ophiolites, corresponding to what is observed in present-day forearc environments (Natland & Tarney, 1982; Parkinson & Pearce, 1998). Many of the fossil ophiolites are attributed to pre-arc settings during early initiation of subduction zones (Pearce et al., 1984; Wallin & Metcalf, 1998; Metcalf et al., 2000). Rarely, SSZ ophiolites are assigned to the early stages of back-arc spreading, subsequent to the splitting of an arc (Pearce et al., 1984).

Ophiolites assigned to SSZ settings usually have structures comparable to those of ophiolites from mid-ocean ridge (MOR) settings. The arguments to assign an SSZ origin to ophiolites are (1) A depleted mantle sequence, mainly composed of harzburgite (80-90%), with < 1% modal clinopyroxene (Pearce et al., 1984), due to higher degrees of partial melting in the sub-arc mantle when compared to MOR. (2) Abundant podiform chromite deposits in dunites (Pearce et al., 1984; Filippidis, 1996; Economou-Eliopoulos et al., 1999), because of the involvement of subduction-derived water. (3) Chemical characteristics of the igneous crust that range from MORB via IAT (island arc tholeiite) to boninite (high magnesium andesite), notably an enrichment in Sr, K, Rb, Ba and Th and a lack of enrichment in Ta, Nb, Hf, Zr, Ti, Y and Yb, due to modification of the mantle source by subduction fluids and/or melts (Pearce et al., 1984 and references therein; Pe-Piper et al., 2004). (4) Crustal cumulate sequences with clinopyroxene crystallized before plagioclase because of the higher CaO/Al_2O_3 ratio compared to MORB or the presence of water (Pearce et al., 1984; Murton, 1989; Gaetani et al., 1994; Beccaluva et al., 2005).

Ti content and trace element composition of clinopyroxene in peridotites were also used to argue for an SSZ origin of ophiolites (Bizimis et al., 2000). These clinopyroxenes are characterized by extremely low contents in Ti and HREE (Heavy Rare Earth Elements). They show an enrichment in LREE (Light Rare Earth Elements), and to lesser extent in MREE (Middle Rare Earth Elements), Zr and Sr compared to clinopyroxene from abyssal peridotites. This signature is attributed to hydrous melting of a MORB-depleted peridotite above a subduction zone, giving the famous "spoon-shaped" trace-element pattern in clinopyroxene of peridotites from mantle wedges (Bizimis et al., 2000). This signature was described in the Izu-Bonin-Mariana forearc mantle by Parkinson & Pearce (1998) and Ohara et al. (2002), and in the Lihir sub-arc mantle (Papua New Guinea) by Grégoire et al. (2001). Very high Cr# in spinel (> 0.6) are also an argument used by many authors to attribute an SSZ-setting to ophiolitic peridotites (Pearce, 2003 and references therein), because this characteristic was described in present-day arc-related mantle (Parkinson & Pearce, 1998; McInnes et al., 2001).

Despite the above similarities, the model of an SSZ origin for most ophiolites is not undisputed. The presence of ultra-depleted harzburgites in the SSZ ophiolites is not conclusive because similar rocks were described from many present-day mid-ocean ridges: Mid-Atlantic ridge ODP Leg 209 (Kelemen et al., 2003; Paulick et al., 2006), East Pacific Rise (Hess Deep) ODP Leg 147 (Allan & Dick, 1996; Arai & Matsukage, 1996; Dick & Natland, 1996), Gakkel ridge (Hellebrand et al., 2002) and Macquarie Island in the South Tasmanian Ocean Basin (Dijkstra & Cawood, 2004). The

formation of podiform chromitite can be due to the involvement of water during melting of refractory peridotites (Edwards et al., 2000), but does not necessarily imply a SSZ origin. High Cr# in spinel (> 0.6) were also described in the Newfoundland margin spinel harzburgite by Müntener & Manatschal (2006), showing that high Cr# in spinel can be an inherited signature. Moreover, high Cr# in spinel were described at two mid-ocean ridges, East Pacific Rise Hess Deep ODP Leg 147 by Allan & Dick (1996) with a maximum of 0.57, and at the Mid-Atlantic ridge ODP Leg 209 by Seyler et al. (2007) with a maximum of 0.51.

Moreover, it is becoming more and more clear that lavas with island-arc chemical signature may also occur in other tectonic settings. Modern ridges can display lavas with a "subduction-component" in addition to "MORB-type" lavas, due to mantle heterogeneities (Moores et al., 2000). Klein & Karsten (1995) and Sturm et al. (2000) described basalts from the Chile ridge adjacent to the Chile trench with geochemical characteristics unlike MORB, but with affinities to arc volcanics, created by processes associated with subduction of a spreading-center. Moreover, boninite genesis is not restricted to subduction-related settings, but can also be related to spreading at a mid-ocean-ridge (Crawford et al., 1989). Nonnotte et al. (2005) showed that addition of seawater to a residual peridotite at shallow depth beneath a mid-ocean ridge (DSDP Site 334) can potentially lead to boninitic-andesitic magmas. Benoît et al. (1999) demonstrated that in a mid-ocean ridge setting, remelting of a hydrated residual peridotite (after MORB extraction) at low pressure by intruding mantle diapirs can yield depleted cumulates with arc signature, but with a MOR-type crystallization sequence. Haase et al. (2005) also mentioned the presence of Nb- and Ta-depleted andesites at the plume-influenced Pacific-Antarctic mid-ocean ridge, which were formed by crystallization of basalt and assimilation of melts from hydrothermally altered amphibolites. Caution is thus warranted in using the systematics of classical trace elements to identify the provenance of ophiolites (SSZ or MOR).

Li, B and Be as indicators of recent and ancient subduction settings

In the last decade, the light elements, particularly B, have proven to be powerful tracers of slab fluids and melts (Benton et al., 2004; Leeman et al., 2004; Paquin et al., 2004; Scambelluri & Philippot, 2004; Tenthorey & Hermann, 2004; Savov et al., 2005 and references therein; Scambelluri et al., 2006 and references therein). There is abundant evidence for a progressive release of Li and B from the oceanic slab during subduction. Fluids enriched in B and Li are liberated from subducting sediment and basaltic crust by dehydration reactions (You et al., 1994, 1995a, 1995b; Chan & Kastner, 2000; Benton et al., 2001; Moran et al., 1992; Bebout et al., 1993, 1999; Domanik et al., 1993; Peacock & Hervig, 1999). Be can be released by melting (Johnson & Planck, 1999), but also by dehydration during high pressure and temperature metamorphism of the subducted altered oceanic crust (Marschall et al., 2007). The abundances and isotopic compositions of Li, Be and B in arc lavas imply the presence of mantle sources that are considerably modified by slab-derived components (Tatsumi, 1989; Ishikawa & Nakamura, 1994; Leeman, 1996; Chan et al., 1999, 2002; Rose et al., 2001; Tomascak et al., 2002; Ryan, 2002). Slab signatures of arc lavas show considerable variations in light element contents and isotope composition (Ishikawa & Nakamura, 1994; Moriguti & Nakamura, 1998; Rosner et al., 2003; Leeman et al., 2004 and references therein), which have been attributed to differences in composition, age and tectonic environment of the subducting plate (Plank & Langmuir, 1993; Rüpke et al., 2002), to depth-controlled release of slab-derived components (Ishikawa & Nakamura, 1994; Moriguti & Nakamura, 1998), to sediment melting and to selective trapping of chemical components in the deep sub-arc mantle (slab-mantle interface) prior to reaching the zone of melt generation (Ayers, 1998; Tomascak et al., 2002; Paquin et al., 2004).

Rationale of the study

Although, to our knowledge, there are no systematic studies of light elements in mantle wedge xenoliths or mantle sections of modern SSZ ophiolite, the bottom line of the above cited studies is that SSZ mantle should be considerably enriched in Li, B, and Be compared to MOR mantle. An SSZ origin is postulated by many authors for the Pindos ophiolite (Pearce et al., 1984; Jones et al., 1991; Bizimis et al., 2000; Saccani & Photiades, 2004), because many petrographic and geochemical evidence are recorded in the crustal section of the

ophiolite. On the contrary, data on mantle rocks are sparse. The ophiolite is highly dismembered and consists of four units each containing either oceanic mantle or crust. The Dramala Complex (mantle) and the Aspropotamos Complex (crust) have been the subject of several geochemical, structural and petrogenetic studies. In the Aspropotamos Complex, lava affinities are diverse and evolved with time from N-MORB to IAT and finally to boninite (Kostopoulos, 1988; Pe-Piper et al., 2004; Beccaluva et al., 2005). Peridotites of the Dramala Complex are highly depleted and podiform chromite deposits are rare (Jones et al., 1991). The crustal cumulates which directly overlie the peridotites of the Dramala Complex show a typical MOR-type cumulate sequence, with the crystallization of plagioclase before clinopyroxene (Kostopoulos, 1988). However, clinopyroxene from the harzburgites shows the "spoon-shaped" trace-element pattern, interpreted as due to hydrous melting in a SSZ setting (Bizimis et al., 2000).

We carried out a detailed study on textures, major and light element (Li, Be, B) contents of minerals and whole rocks of fresh harzburgite and serpentinite from the Dramala Complex, in order to test the hypothesis of hydrous melting in a SSZ setting of the Pindos mantle rocks. The results show the investigated mantle rocks to be very similar to a MOR-type mantle modified by melt-rock reaction and impregnation.

GENERAL GEOLOGICAL FRAMEWORK

The Sub-Pelagonian ophiolites include the Pindos, Vourinos and Othris complexes (Greece) and the Albanian ophiolites (Fig. 2.1). The ophiolites are related to the evolution of the Neo-Tethys from the Triassic to the Tertiary. During the Triassic, sea-floor spreading began in the Eastern Mediterranean and led to the formation of oceanic lithosphere (Jones & Robertson, 1991; Pe-Piper & Piper, 2002; Robertson, 2002).

In the Mid-Jurassic, convergence began and ophiolites were moved towards a west- or east-dipping subduction zone (Jones & Robertson, 1991). Later, the subduction zone collided with the Pelagonian margin, leading to the emplacement of the ophiolites onto the oceanic crust and eventually onto the accretionary prism. During the emplacement, the well-known metamorphic soles present at the base of the ophiolites, mainly composed of metabasite and metasediment, were formed (Jones & Robertson, 1991; Ross & Zimmerman, 1996). Metamorphic soles generally recrystallized under greenschist to amphibolite facies conditions (Pe-Piper & Piper, 2002 and references therein). Finally, in the Late Jurassic, the neo-tethyan ophiolites were obducted onto the continental crust of the Pelagonian margin.

The Sub-Pelagonian ophiolitic remnants are

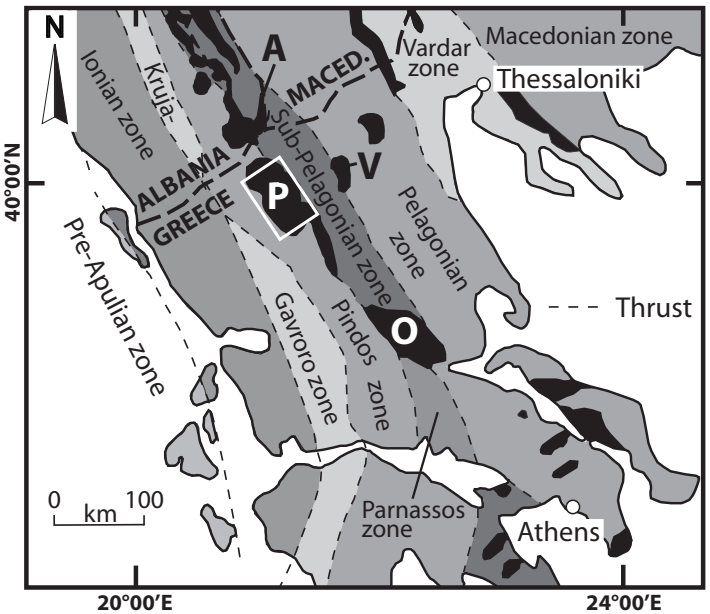


Fig. 2.1: The Pindos ophiolite within the Hellenides, modified after Robertson & Shallo (2000). The white box represents the area shown in Figure 2. P: Pindos ophiolite, V: Vourinos ophiolite, O: Othris ophiolite and A: Albanian ophiolites. Maced.: Macedonia.

actually aligned in NNW-SSE direction within the Hellenides (Fig. 2.1). Pindos and Vourinos ophiolites are thought to be connected beneath the Tertiary post-orogenic Mesohellenic Trough of the Sub-Pelagonian zone (Jones et al., 1991; Makris, 1977; Fig. 2.1), and Pindos could be related to Othris ultramafics along strike to the south (Smith, 1979).

Palaeogeography of the Neo-Tethys during the Jurassic is still a matter of debate, and two different models were proposed for the ophiolites in Greece. (i) All the Sub-Pelagonian ophiolites originate in a single and large Neo-Tethys ocean, the Vardar ocean, located to the east of the Pelagonian microcontinent. Their actual regional distribution is a consequence of post-obduction extensional tectonics (Aubouin, 1959; Dercourt et al., 1986, 1993; Jacobshagen, 1986). (ii) The actual regional distribution of the ophiolites reflects their origin in various small ocean basins. In this context, the Pindos, Vourinos and Othris ophiolites are assigned to the Pindos basin, located west of the Pelagonian microcontinent (Robertson et al., 1991; Smith & Woodcock, 1976). Another debated point is the origin of these small ocean basins. They could be related to a forearc environment (Dilek & Flower, 2003), to back-arc spreading (Stampfli et al., 1998) or to a Red Sea-type rifting (Robertson et al., 1991).

According to Robertson & Shallo (2000), the Sub-Pelagonian ophiolites can be subdivided into two groups. (i) The "Eastern-type" ophiolites, including the Eastern-Albanian and the Vourinos ophiolites are interpreted as SSZ-type ophiolites, which formed above an intra-oceanic subduction zone in the Late Jurassic. (ii) The "Western-type" ophiolites, including the Western-Albanian, the Othris and the Pindos ophiolites, were formed during the Early Jurassic at a slow-spreading ridge system (MOR-type ophiolite); at the onset of subduction, they evolved to SSZ-type ophiolites.

THE PINDOS OPHIOLITE

The northern Pindos mountains are made up of a series of imbricate Mesozoic and Tertiary thrust sheets, which include the Jurassic Pindos ophiolite (Capedri et al., 1980; Jones & Robertson, 1991). Five tectono-stratigraphic units were described by Jones & Robertson (1991). (i) The Pindos Ophiolite Group (Jurassic, Fig. 2.2) with three subunits, the Dramala Complex (dismembered ultramafics), the Loumnitsa Unit (metamorphic sole) and the Aspropotamos Complex (dismembered intrusives and extrusives). (ii) The shallow-water limestones of the Orliakas Group (Late Cretaceous). (iii) The Avdella Melange (Late Triassic – Late Jurassic) with volcanics and sediments of a subduction-accretion complex. (iv) The deep-water sediments of the Dio Dendra Group (Late Jurassic – Late Cretaceous). (v) The Pindos Flysch (Upper Cretaceous – Tertiary). The following description will focus on the Pindos Ophiolite Group and the Avdella Melange, which are relevant for this paper.

The Dramala Complex represents oceanic mantle and part of its crustal sequence. It includes tectonized spinel harzburgite and minor plagioclase-bearing harzburgite, websterite, pyroxenite and ultramafic cumulates (Jones & Robertson, 1991; Pe-Piper & Piper, 2002; Ross & Zimmerman, 1996). All these ultramafic rocks have slightly to highly serpentinized equivalents. Locally, breccias of harzburgite and chert are cemented by ophicalcite, showing that the Dramala mantle was once exposed on the Neo-Tethyan ocean floor (Jones et al., 1991). Comparison of harzburgite fabrics from the Pindos and Vourinos ophiolite complexes (Rassios, 1991; Rassios et al., 1994), and magnetic studies underneath the Mesohellenic Trough support the idea that they come from the same oceanic lithosphere (Rassios & Moores, 2006). Dramala ultramafics are overlain by crustal cumulates with plagioclase-bearing dunite, troctolite and anorthosite gabbro (Capedri et al., 1982; Rassios, 1991).

The Loumnitsa Unit is localized at the base of the Dramala Complex. This metamorphic sole consists of metasediments and metabasites, with MORB and WPB (Within Plate Basalt) affinities (Jones & Robertson, 1991). This unit was dated by the K-Ar and the Ar-Ar method on hornblende from different amphibolites, yielding ages between 165±5 and 176±5 Ma (Roddick et al., 1979; Spray & Roddick, 1980; Spray et al., 1984; Thuizat et al., 1981).

The Aspropotamos Complex (Lower to Middle Jurassic) preserves a crustal succession, including ultramafic and mafic cumulates, plagiogranite,

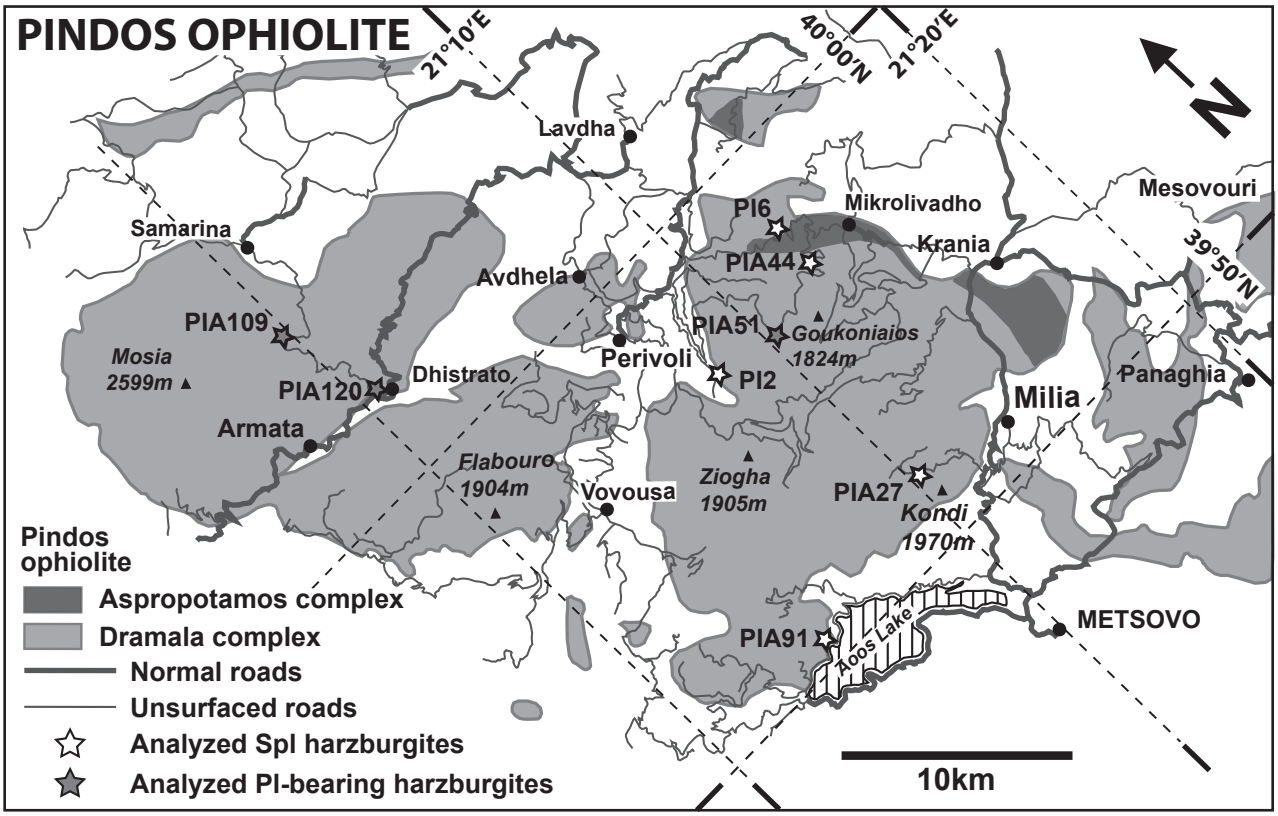


Fig. 2.2: Pindos ophiolite, including the Dramala complex (oceanic mantle) and the Aspropotamos complex (oceanic crust) and location of the analyzed samples. Simplified map modified after Jones & Robertson (1991) and Economou-Eliopoulos & Vacondios (1995).

sheeted dykes and pillow lavas. Successive phases of lava extrusion show a geochemical trend from high-Ti MORB to MORB/IAT (Island Arc Tholeiite) and finally to IAT-boninite-type for the youngest dykes (Capedri et al., 1980; Jones & Robertson, 1991; Jones et al., 1991; Kostopoulos, 1988; Pe-Piper et al., 2004; Saccani & Photiades, 2004; Beccaluva et al., 2005). Capedri et al. (1980) described lavas strongly depleted in incompatible elements, which are similar to some rocks of immature island arcs. These geochemical characteristics of intrusives and extrusives were used to define the Pindos ophiolite as a SSZ-type ophiolite.

The Avdella Melange represents a subduction-accretion complex and includes volcanics, sediments and metamorphic rocks of the Loumnitsa Unit. Basalts are Triassic and exhibit WPB (Within Plate Basalt), WPB to T-MORB and N-MORB signatures. These extrusives were formed at the initial stage of sea-floor spreading (Pe-Piper & Piper, 2002 and references therein).

SAMPLE CHARACTERISTICS

All samples described below were collected in the Dramala Complex, in order to study the Li, B and Be contents of the mantle and its minerals. The complex is essentially composed of spinel harzburgites. Plagioclase-bearing harzburgites are present in the northwestern and central part of the massif (Fig. 2.2). The harzburgites show various degrees of serpentinization and deformation. Eight clinopyroxene-bearing spinel harzburgite samples were chosen for this study (Fig. 2.2). Three of the samples additionally bear plagioclase and will be called plagioclase-bearing harzburgite (Fig. 2.2). Samples with different degrees of serpentinization were chosen in order to evaluate the impact of this process on the light element budget. Mineral nomenclature is used according to Kretz (1983), and serpentine terminology is applied according to Wicks & Whittaker (1977) and O'Hanley (1996).

Microstructures range from coarse

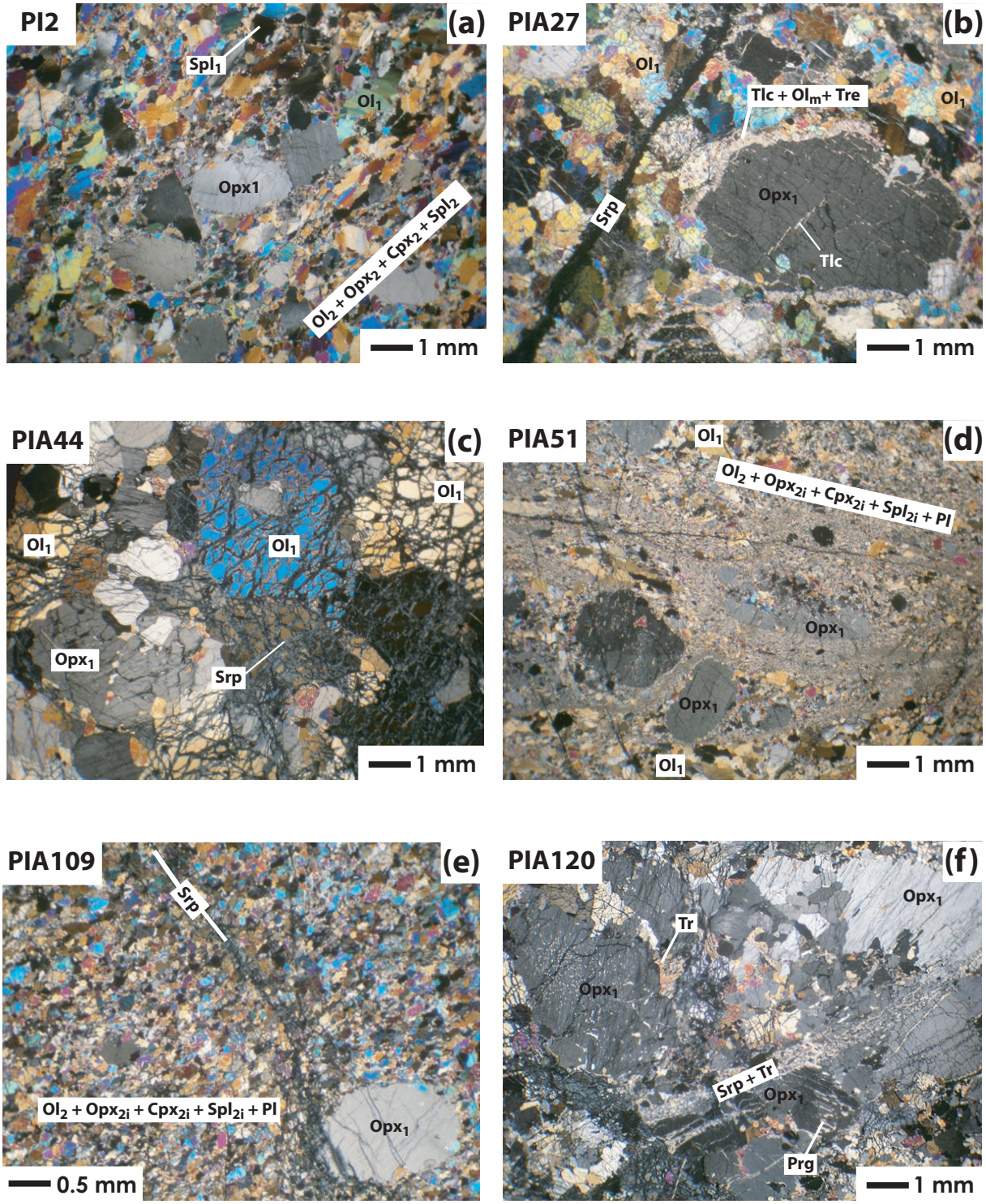


Fig. 2.3: Textures of the analyzed samples. PI2, PIA27 and PIA44 are spinel harzburgites and PIA51, PIA109 and PIA120 are plagioclase-bearing harzburgites. Mineral abbreviations after Kretz (1983). Suffixes after mineral names represent the different generations, 1: primary, 2: secondary and 2i: secondary related to melt infiltration.

porphyroclastic to mylonitic (Fig. 2.3a to f, nomenclature after Mercier & Nicolas, 1975). Most samples experienced high-temperature, low-stress plastic deformation leading to the formation of coarse-grained microstructures. Harzburgites preserve primary mantle porphyroclasts, including orthopyroxene with clinopyroxene exsolutions (Opx_1), rare clinopyroxene with orthopyroxene exsolutions (Cpx_1), olivine (Ol_1) and spinel (Spl_1) (Fig. 2.3a). Neoblasts include orthopyroxene, clinopyroxene, olivine and spinel (Opx_2 and Cpx_2 without exsolutions, Ol_2, Spl_2) crystallized during a deformation event at lower temperature (Fig. 2.3a). In the plagioclase-bearing harzburgite, plagioclase is generally associated with secondary orthopyroxene, clinopyroxene and spinel (Opx_{2i}, Cpx_{2i} and Spl_{2i}), related to melt impregnation (see section 'Interpretation of specific textures', Fig. 2.3d and e, Fig. 2.4e).

Some harzburgites record later cooling and hydration at fairly high temperatures (see section 'Interpretation of specific textures'), leading to post-kinematic crystallization of retrograde assemblages with anthophyllite, talc, tremolite, and rare metamorphic olivine, Ol_m (Fig. 2.3b and f, Fig. 2.4a and b). Finally, the rocks were serpentinized, with pseudomorphs of serpentine after orthopyroxene (bastite), olivine (mesh rim texture), and small serpentine veins (Fig. 2.3b, c , e and f, Fig. 2.4c and d).

Spinel harzburgites

Samples PI2 and PIA91 (Fig. 2.3a) are only weakly serpentinized (< 1.7 vol%), with serpentine crystallized in veins of 10-20 μm width. In thin sections, the rocks are deformed and exhibit a porphyroclastic texture (Fig. 2.3a), with bimodal grain size distributions for orthopyroxene, clinopyroxene, olivine and spinel. Ol_1 (with kink banding), Opx_1 and Spl_1 porphyroclasts have diameters up to 2 mm, while rare Cpx_1 has a maximum size of 1 mm. Neoblasts are smaller (< 0.5 mm). Spl_1 porphyroclasts are usually subhedral, but rare euhedral grains are also present. Rare tremolite (~20 μm) formed at the expense of Cpx_1.

Sample PIA27 has a porphyroclastic texture similar to samples PI2 and PIA91 (Fig. 2.3b), but contains more hydrated minerals. Embayed clinopyroxene grains (Cpx_1, Fig. 2.4b) crystallized at olivine – orthopyroxene joints (Fig. 2.4b) were replaced by edenitic hornblende pseudomorphs. This amphibole also partially or completely replaced clinopyroxene exsolution lamellae within orthopyroxene (Fig. 2.4a). Anthophyllite and tremolite crystallized at edenitic hornblende rims (Fig. 2.4b). Fine-grained aggregates of talc and olivine (Ol_m) form rims around orthopyroxene. Serpentine is mainly present as mesh-rim textures that contain rare magnetite (Fig. 2.4a and b), or in veins (maximum 500 μm width). More rarely, serpentine crystallized as bastite or is associated with talc at orthopyroxene rims. The total percentage of serpentine is 19 vol%.

PI6 and PIA44 are spinel harzburgites with 47 and 55 volume % of serpentine, respectively. These rocks show a granoblastic texture, with very rare Ol_1 grains (up to 4 mm, often kinked) and large Opx_1 porphyroclasts (Fig. 2.3c). Embayed interstitial grains of Cpx_1 at Opx_1 rims are similar to those in sample PIA27 (Fig. 2.4c). In some cases, accessory Spl_1 is intergrown with Cpx_1. Hydrous phases include tremolite which crystallized at clinopyroxene rims (Fig. 2.4c) and talc formed at orthopyroxene-olivine contacts. Serpentine forms mesh-rim texture, rare bastite after orthopyroxene and clinopyroxene, and some veins penetrating clinopyroxene and spinel. Magnetite is concentrated at the margins of the net formed by the mesh-rim texture (Fig. 2.4c).

Plagioclase-bearing harzburgites

PIA120 is a highly serpentinized (41 vol. %) plagioclase-bearing harzburgite (Fig. 2.3f). The earliest minerals are Ol_1 as well as large grains of Opx_1 (up to 4 mm) and Cpx_1 (up to 400 μm). Some Cpx_1 have corroded margins and present clusters of single grains which are in optical continuity (Fig. 2.4f). Rare, small Spl_{2i} grains are disseminated in the rock. Plagioclase (up to 1 mm) crystallized as single crystals or in polycrystalline lenses and small dykes with igneous textures along foliation planes (Fig. 2.4d and f). Opx_{2i}, Cpx_{2i} and Spl_{2i} are texturally related to plagioclase and crystallized at the rim of these lenses. Opx_{2i} rims crystallized at the contact between olivine lenses and plagioclase (Fig. 2.4d). Pargasite formed at Opx_1 rims, probably at the expense of clinopyroxene. Olivine (Ol_m) crystallized at Opx_1 rims in association with tremolite, diopside and serpentine. Serpentine forms mesh-rim textures and bastite after Opx_1. An association of natrolite ($Na_2Al_2Si_3O_{10}\cdot 2H_2O$), vuagnatite ($CaAlSiO_4(OH)$), pectolite ($NaCa_2(Si_3O_8)(OH)$) and chlorite

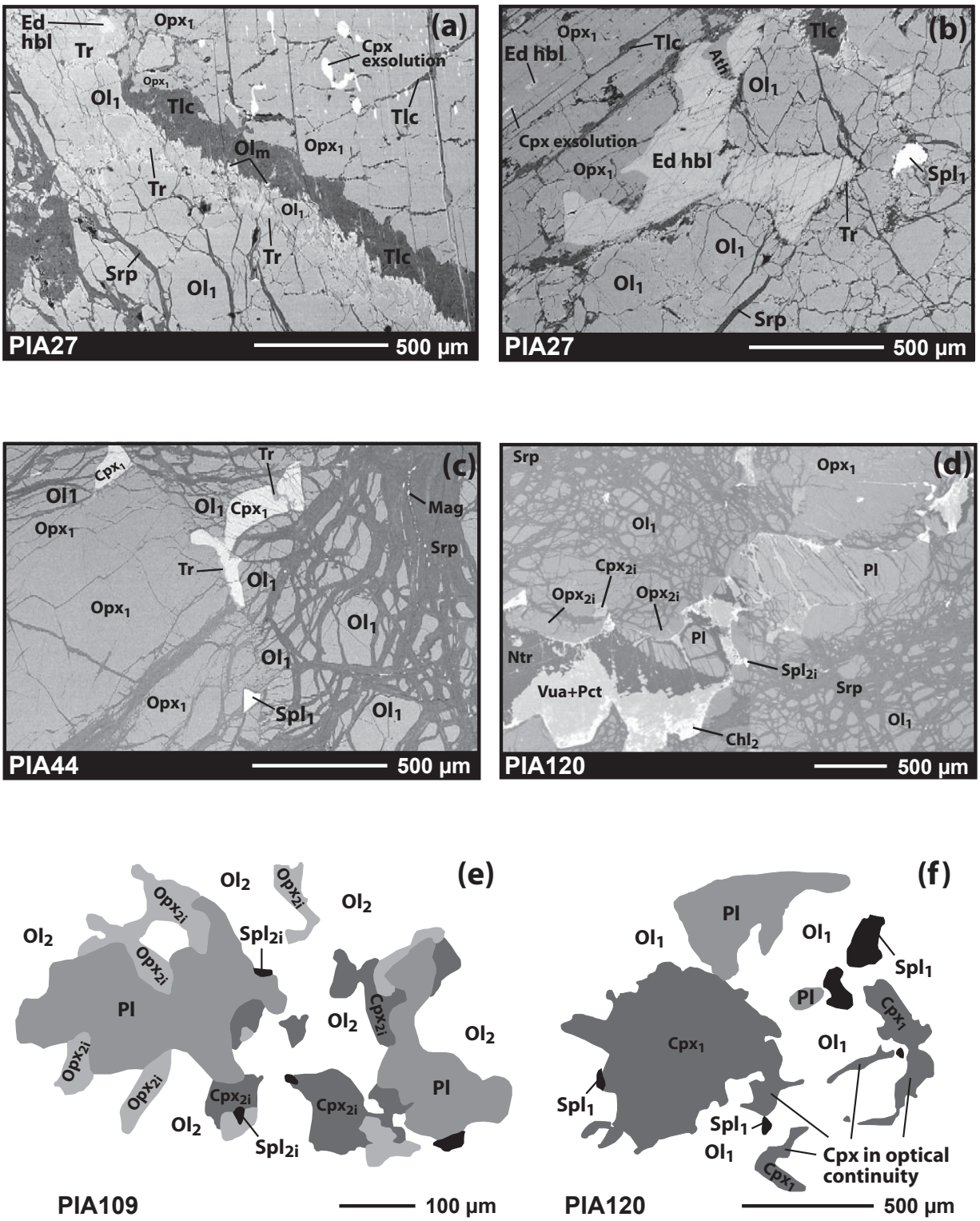


Fig. 2.4: (a) to (c) Microtextures related to serpentinization and cooling in the spinel harzburgites. (d) to (f) Microtextures related to melt infiltration in the plagioclase-bearing harzburgites. Mineral abbreviations after Kretz (1983), Ntr: natrolite, Pct: pectolite, Vua: vuagnatite. Suffixes after mineral names represent the different generations, 1: primary, 2: secondary, 2i: secondary related to melt infiltration and m: metamorphic.

crystallized as pseudomorphs after plagioclase (Fig. 2.4d). Two types of chlorite are present: chlorite (Chl_1) in association with tremolite and chlorite (Chl_2) crystallized in the plagioclase lenses.

PIA51 and PIA109 are weakly serpentinized plagioclase-bearing harzburgites (9 vol. % serpentine). PIA51 is a mylonitized peridotite, with ultrafine bands (~ 20 μm) of plagioclase and Ol_2, Opx_{2i}, Cpx_{2i} and Spl_{2i} (Fig. 2.3d). Primary mantle relics are Opx_1 and Ol_1 porphyroclasts (up to 3 mm), which are preserved in the less deformed zones. Apparently undeformed plagioclase is subhedral and preferentially concentrated at the margins of the mylonitized zones. PIA109 is a highly recrystallized sample (Fig. 2.3e and 2.4e). Opx_1 porphyroclasts (up to 4 mm) have corroded rims and float in a matrix of recrystallized Ol_2, Opx_{2i}, Cpx_{2i}, Spl_{2i} and plagioclase (grain size up to 100 μm). Cpx_1 is present as inclusions in the Opx_1 clasts. In sample PIA51, relic Spl_1 grains (up to 1 mm) are preserved. In PIA109, pargasite is present as inclusions in Opx_1 and probably formed at the expense of clinopyroxene. In PIA51, hornblende formed as subhedral grains in the less deformed zones. Tremolite crystallized after clinopyroxene at Opx_1 rims and talc is sometimes present at Opx_1 – Ol_1 grain boundaries. Serpentine forms veins with rare magnetite, texturally related to? the crystallization of vuagnatite and chlorite after plagioclase. Rare bastite after Opx_1 and mesh-rim texture are observed.

Nature of the serpentine minerals

The different serpentine polymorphs were determined by Chiara Groppo on a micro-Raman facility (HORIBA Jobin Yvon HR800) at the University of Torino (Italy), following the procedure published in Groppo et al. (2006). All details concerning these analyses will be published in another paper. For all serpentine points of samples PIA27, PIA44, PIA109 and PIA120 previously analyzed for Li, B and Be by Secondary Ion Mass Spectrometry (SIMS), the polymorphs were determined. Serpentine crystallized in veins is lizardite. In rare cases, when veins were larger, some chrysotile was observed in the center of the veins. Serpentine crystallized in bastite and after olivine is generally lizardite. Only in spinel harzburgite PIA27, serpentine formed after orthopyroxene (no bastite texture) is chrysotile. In spinel harzburgite PIA44, bastite is in places composed of a fine mixture of lizardite and talc.

INTERPRETATION OF SPECIFIC TEXTURES

Textures related to melt impregnation

In the samples from the Dramala Complex, no plagioclase corona around primary spinel was observed, indicating that feldspar was not formed by subsolidus decompression reactions (Piccardo et al., 2004b). Many plagioclase peridotites are commonly interpreted as resulting from impregnation of spinel peridotites by diffuse porous flow of melt, melt-rock reaction and fractional crystallization of plagioclase and pyroxenes (Dick, 1989; Rampone et al., 1997; Dijkstra et al., 2001 and 2003). The Dramala samples present textural evidence of these processes, which is presented below.

In plagioclase-bearing harzburgite, millimeter-scale plagioclase dykelets are aligned along the foliation plane defined by flattened olivine and orthopyroxene. In the Othris peridotite, where there is major and trace element evidence of melt impregnation (Dijkstra et al., 2001; Barth et al., 2007), this texture was interpreted as representing cumulate phases of a melt that impregnated harzburgites. There is also primary clinopyroxene grains (Cpx_1) with irregular outlines due to embayments of olivine (Fig. 2.4f), which are in optical continuity and associated with plagioclase. A similar texture was described from abyssal peridotites from the South West Indian Ridge (Seyler et al., 2001) and from the Othris peridotites (Dijkstra et al., 2003), and was interpreted as dissolution of primary clinopyroxene by pyroxene-undersaturated melt. Melt was not completely trapped into the harzburgites, but some batches of melt were left behind to crystallize after the melt flux. In the Dramala harzburgites, plagioclase is often associated with secondary clinopyroxene (Cpx_{2i} of Fig. 2.4d and 2.4e), a feature generally interpreted as originating from an infiltrating melt (Pearce et al. 2000; Dijkstra et al., 2001, 2003 and references therein). The ubiquitous presence of this texture in some plagioclase-bearing harzburgites indicates that melt migrated by diffuse porous flow.

In many places in plagioclase-bearing

harzburgite, secondary, undeformed orthopyroxene (Opx_{2i}) crystallized at the contact between primary olivine and plagioclase (Fig. 2.4d). This secondary orthopyroxene replaced olivine along the contact between olivine and plagioclase via the reaction olivine + melt = orthopyroxene + plagioclase, documented in melt-impregnated peridotites of the Lanzo massif (Piemontese Italian Alps) by Piccardo et al. (2004b) and in the Othris peridotites by Dijkstra et al. (2003).

The presence of corroded primary clinopyroxene (Cpx_1) in the sample with plagioclase lenses, where secondary clinopyroxene (Cpx_{2i}) crystallized at vein rims, may show that there was an evolution of melt composition over time or that the temperature was decreasing. The incoming melt probably evolved from pyroxene-undersaturated to pyroxene-saturated, as observed by Piccardo et al. (2004b) in some Alpine-Apennine peridotites and by Dijkstra et al. (2003) in the Othris harzburgites. According to Dijkstra et al. (2003), increasing saturation of the melt in clinopyroxene and plagioclase could be due to cooling.

Some spinel harzburgites also show evidence of melt impregnation in their textures. Figure 2.4c shows an interstitial clinopyroxene crystallized at a triple junction between olivine and primary orthopyroxene. These lobed grains show no exsolution lamellae of orthopyroxene. The shape and position of this clinopyroxene exclude a primary origin. A similar texture was described from abyssal spinel peridotites (plagioclase-free) by Seyler et al. (2001) and was interpreted as clinopyroxene crystallized from incompletely extracted melts. Piccardo et al. (2004b) also described a similar texture from Alpine-Apennine peridotites. In Figure 2.4b, the edenitic hornblende and the other associated retrograde amphiboles (anthophyllite and tremolite) are probably pseudomorphs after this type of clinopyroxene, as they present exactly the same texture.

Textures related to cooling and hydration

In the Dramala harzburgite, earliest cooling and hydration is documented by replacement of clinopyroxene by edenitic hornblende (sample PIA27), suggesting temperatures above 750°C (Lykins & Jenkins, 1992; Sharma & Jenkins, 1999). Edenitic hornblende was partially replaced during further cooling by anthophyllite and tremolite. Further cooling and hydration is also indicated by coronas of talc ± tremolite ± olivine around orthopyroxene (sample PIA27, PI6, PIA51). In sample PIA27 (Fig. 2.3b, 2.4a-b), this transformation was very penetrative and replaced entire grains. Experiments on peridotite-seawater interaction (Allen & Seyfried, 2003), petrographic studies (Mével, 2003), and observations on serpentinized peridotites of mid-Atlantic ridge ODP Leg 209 (Bach et al., 2004 and 2006) suggest that the transformation of pyroxenes to talc (and tremolite) is favoured at temperatures above 300-400°C, where pyroxenes react faster than olivine. In many Dramala samples, serpentine was formed with talc and may replace the latter, leading to bastite. This phenomenon can be explained by a decrease of silica activity in the fluid as pyroxene transforms to talc (and tremolite). Once the serpentine-talc silica buffer is reached, serpentine and talc co-precipitate (Frost & Beard, 2007). When olivine begins to hydrate, serpentine becomes the most important hydrous mineral.

Serpentine also crystallized in veins, at olivine-orthopyroxene grain boundaries and at the expense of olivine (mesh-rim texture). These textures are younger than the talc-bearing coronas and bastite texture. Mesh rims are composed of serpentine, while mesh centers show an association of serpentine with little magnetite. The pressure-temperature stabilities of the serpentine polymorphs are not well known and partially overlap. They thus give no precise indication of serpentinization temperatures (see discussion in Bach et al., 2004). However, it is commonly accepted that the direct transformation of olivine to serpentine preferentially takes place at temperatures below 250-300°C due to the fast reaction of olivine (Allen & Seyfried, 2003; Mével 2003; Bach et al., 2004).

In sample PIA120, bulk serpentinization was followed by the alteration of plagioclase (Fig. 2.4d) to natrolite ($Na_2Al_2Si_3O_{10}\cdot 2H_2O$), vuagnatite ($CaAlSiO_4(OH)$) and pectolite ($NaCa_2(Si_3O_8)(OH)$). Formation of natrolite after plagioclase during low temperature ($T < 100°C$) hydrothermal alteration was described in pillow basalts from the West Philippine Sea Basin (ODP Leg 195, site 1201; D'Antonio & Kristensen, 2005). A post-serpentine alteration is also visible in the mesh centers of some samples, which present a yellowish color under the microscope, probably due to the transformation of magnetite into limonite.

In conclusion, the Dramala harzburgites

record fluid-rock reaction during cooling from approximately > 750°C to < 100°C. Cooling must have proceeded quickly and the fluid-rock ratio was probably low because otherwise the rocks would display higher degrees of serpentinization and the higher-temperature hydrous phases (talc, pargasite and edenitic hornblende) would not be preserved.

ANALYTICAL TECHNIQUES

Major element compositions of minerals were determined by electron microprobe (Cameca SX-50 and Jeol JXA-8200 at the Institute of Geological Sciences of the University of Bern, Cameca SX-51 at the Institute of Mineralogy of the Ruprecht-Karls University of Heidelberg, and Jeol JXA-8200 at the ETH Zürich) equipped with four to five wavelength-dispersive spectrometers. Operating conditions comprise an accelerating voltage of 15 kV and a 20 nA beam current. The spot size was about 3 μm except for hydrous minerals where a defocused beam was used (amphiboles, talc: 5 μm, serpentine: 1-10 μm, natrolite: 5-10 μm). Natural and synthetic oxides and silicates were used as standards. Approximate detection limits (in wt. %) were: (i) For silicates and spinel, Si (0.02), Ti (0.01), Cr (0.01), Fe (0.07), Mn (0.01), Zn (0.07), Ni (0.02), Ca (0.01), Na (0.01) and K (0.01). (ii) For silicates, Al (0.01) and Mg (0.01). (iii) For spinel, Al (0.04) and Mg (0.03). Backscattered electron (BSE) images were obtained at the Centre Suisse d'Electronique et de Microtechnique (CSEM, Neuchâtel), with a Philips XL-30 Scanning Electron Microscope, operated at 25 kV.

Light element compositions were measured in situ in minerals by secondary ion mass spectrometry (SIMS) with a modified Cameca ims 3f ion microprobe (equipped with a primary beam mass filter) at the Institute of Mineralogy of the Ruprecht-Karls University of Heidelberg (Germany). The protocol established by Marschall and Ludwig (2004) was used for sample preparation and measurements to minimise boron surface contamination. SIMS measurements were performed on points previously measured at the electron microprobe. The primary $^{16}O^-$ ion beam was set to 14 keV/20 nA. Positive secondary ions were accelerated to 4.5 keV and the energy window was set to 40 eV. The energy filtering technique was applied with an offset of ~ 75 eV at a mass resolution m/Δm between 1018 to 1080. Quantitative results were obtained using relative sensitivity factors with ^{30}Si as reference isotope (Ottolini et al., 1993). Detection limits (the critical value; Currie, 1968) for sample PI2, were calculated at 2.0, 1.4 and 3.7 ng/g (ppb) for Li, Be and B respectively. For other samples, values were lower at 1.4 for Li, 1.0 for Be and 2.6 ng/g for B. All rock-forming minerals were analysed, except for spinel and other oxides (for which no standard was available). Backscattered electron images of the serpentine matrix showed that serpentine grains are extremely small and could potentially be intergrown with other phases like brucite, chlorite or magnetite at the micrometer scale, meaning that the SIMS analyses could represent multigrain analyses.

Li and Be whole rock contents were measured by inductively coupled plasma mass spectrometry (ICP-MS) at the Department of Earth Sciences, University of Bristol. Pindos harzburgites and two ultramafic rock standards (PCC-1; UB-N) were dissolved using a HF-HNO3 multi-acid method on a hotplate. After evaporating the HF, samples were taken up in 2 % HNO3 at a dilution of ~500:1 of the original rock. ICP-MS analyses were performed on a Thermo Electron Element sector field ICP-MS in pulse-counting mode. Mass calibration was completed by using a multi-element solution (10 μg/L of each Li, B, Na, Sc, Fe, Co, Ga, Y, Rh, In, Ba, Lu, Tl, U in 5 % HNO3). Precision and reproducibility of solution ICP-MS analyses were < 12 % for Li and < 25 % for Be. Detection limits were ~ 37 ng/g for Li and ~ 3 ng/g for Be. Measured intensities were normalised to solutions of USGS reference material PCC-1 (peridotite), except for Be, where ANRT reference material UB-N (serpentinite) was used. The published values for PCC-1 of 985 ng/g Li (Moriguti et al., 2004) was used to calculate the concentrations of Li. The accepted concentration of Be in UB-N is 200 ng/g (Govindaraju, 1994).

B whole rock contents were measured by PGNAA (Prompt Gamma Neutron Activation Analysis) at the prompt gamma activation analysis facility of the Budapest Research Reactor (BRR). This method has already been used to analyze B whole rock contents in geological samples (Gméling et al., 2005; Marschall et al., 2005). PGNAA is especially useful for analyzing whole rock boron concentrations. In contrast to other geoanalytical methods, sample preparation procedures are not

needed, and hence contamination problems are eliminated (Anderson & Kasztovszky, 2004). The principle of the PGNAA method is the detection of prompt γ-rays that originate from the (n,γ)-reactions during neutron irradiation (Révay & Belgya, 2004). The detection limit was different in each sample, depending on measurement time and the sample weight, but ranges from 0.01 to 0.03 μg/g. B has a small relative uncertainty (1 to 2 %), but is above 5 % only if the B content goes under 1 μg/g. Further information on this analytical technique can be found in Révay et al. (2004), Molnár (2004) and Marschall et al. (2005).

MAJOR ELEMENT COMPOSITION OF MINERALS

Microprobe analyses were normalized considering Fe as Fe^{2+} in all minerals, except for spinel where Fe^{2+} and Fe^{3+} were calculated, and plagioclase where Fe was considered as Fe^{3+}. Mg# was calculated as Mg / [Mg + Fe^{2+}] for all minerals, including spinel.

Olivine

Ol_1 and Ol_2 compositions are similar and coincide with the mantle olivine array (Takahashi et al., 1987). Mg# are between 0.89 and 0.92 and NiO contents are 0.18-0.53 wt.% (Table 2.1, Fig. 2.5). Olivine from plagioclase-bearing harzburgite shows a greater variation in Ni contents and lower Mg# compared to olivine from spinel harzburgite (Fig. 2.5). Metamorphic olivine (Ol_m) shows lower Mg# and Ni contents (Table 2.1, Fig. 2.5). Ol_1 and Ol_2 of sample PIA44 have Mg# within the mantle olivine array, but variable NiO contents from 0.05 to 0.45 wt.%. This variation can be due to the presence of pentlandite (Fe-Ni sulfide; Filippidis, 1982; Sovatzoglou-Skounakis and Economou-Eliopoulos, 1997; McInnes et al., 2001), which crystallized during serpentinization at olivine rims in sample PIA44.

Spinel

Cr# (= Cr / [Cr + Al]) of spinel is variable in spinel harzburgites (0.27-0.69; Table 2.2, Fig. 2.6a-b). The higher contents reflect the refractory origin of these rocks. Cr# of spinel from plagioclase-bearing harzburgites is more restricted with values between 0.20 and 0.38 (Fig. 2.6b). Moreover, spinel in plagioclase-bearing harzburgites is enriched in Ti compared to that in spinel harzburgites (except for

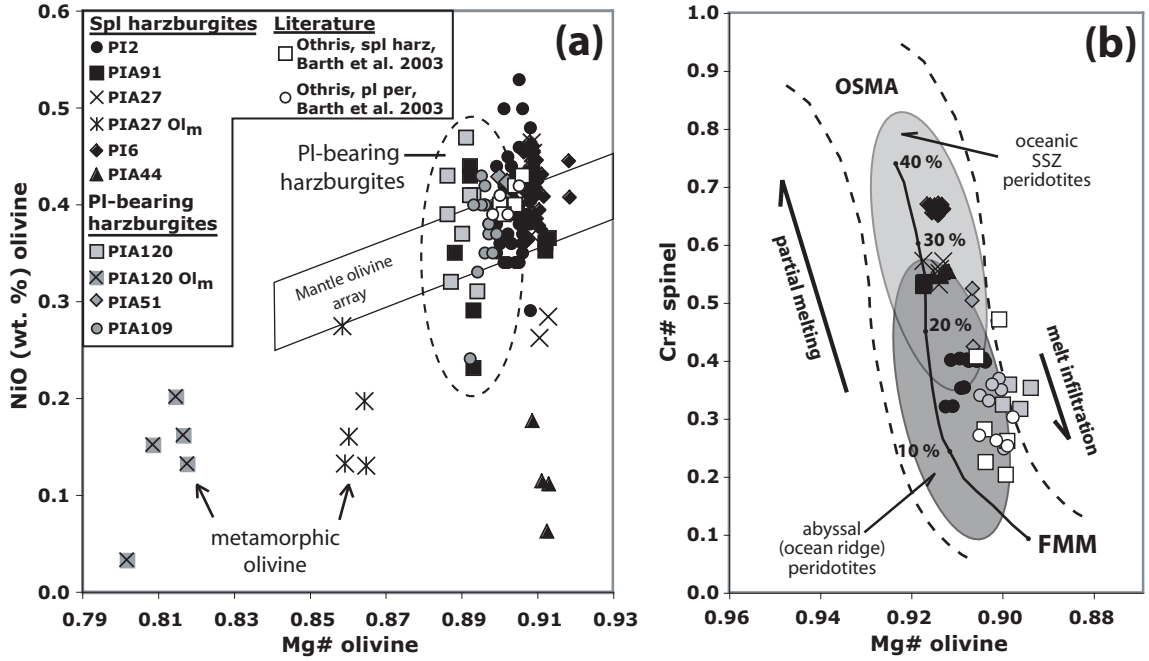


Fig. 2.5: (a) Mg# vs. NiO (wt. %) content of olivine. Mantle olivine array after Takahashi et al. (1987). Ol_m = metamorphic olivine. (b) Mg# in olivine vs. Cr# in spinel. Light grey field represents values for oceanic SSZ peridotites (Pearce et al., 2000) and dark grey field for abyssal ocean ridge peridotites (Dick & Bullen, 1984). OSMA = olivine-spinel mantle array and partial melting trend after Arai (1994) and FMM = fertile MORB mantle.

sample PIA51), and plots in the field of plagioclase-bearing abyssal peridotite defined by Dick & Bullen (1984) and Dick et al. (1984) (Fig. 2.6b). Spl_1 shows a systematic decrease in Cr_2O_3 (~ 2.50 wt.%) and an increase in Al_2O_3 (~ 2.50 wt.%) from core to rim. Spl_2 neoblasts have similar compositions as Spl_1 rims in spinel peridotites.

Orthopyroxene

Orthopyroxene porphyroclasts display large intragrain and intergrain compositional variations (Fig. 2.7a-b). Opx_1 porphyroclasts from spinel harzburgites and plagioclase-bearing harzburgites are zoned and show exsolution lamellae of clinopyroxene (Fig. 2.3b and f). They present a rimward decrease in Al_2O_3 and Cr_2O_3 and an increase in SiO_2 (Table 2.3, Fig. 2.7a-b). Zoning is more pronounced in plagioclase-bearing harzburgites than in spinel harzburgites (Fig. 2.7a-b). Al_2O_3 contents range from ~ 1.00 to 3.25 wt.% in the core and ~ 0.30 to 3.00 wt.% at the rim. Zoning is illustrated in Figure 2.7b, where the different samples are defined by their Al_2O_3 and Cr_2O_3 contents. Opx_2 neoblasts have the same composition as Opx_1 porphyroclast rims in both spinel and plagioclase-bearing harzburgites (Fig. 2.7a-b). Sample PIA44 (serpentinized spinel harzburgite) shows a peculiar pattern, with nearly no variation in its Al_2O_3 content, but a great variability in its Cr_2O_3 content (Fig. 2.7b). Mg# is between 0.90 and 0.92 in all samples.

Clinopyroxene

Cpx_1 porphyroclasts from spinel and plagioclase-bearing harzburgites are zoned and have exsolution lamellae of orthopyroxene. Zoning is more pronounced in the plagioclase-bearing harzburgites. The grains show a rimward decrease in Al_2O_3 and Cr_2O_3 and an increase of Mg# (Table 2.4, Fig. 2.7c-d). Clinopyroxenes (Cpx_1 and Cpx_{2i}) from plagioclase-bearing harzburgite are enriched in TiO_2 (~ 0.17 to 0.50 wt.%) and Al_2O_3, and show lower Mg# (~ 0.91-0.93) compared to spinel harzburgite (TiO_2 ~ 0.00 to 0.15 wt.% and Mg# ~ 0.92 to 0.95). Sample PIA51 (plagioclase-bearing harzburgite) shows intermediate values. In spinel harzburgite, Cpx_2 neoblasts show a higher Mg# and a depletion in TiO_2 and Al_2O_3 compared to Cpx_1 cores (Fig. 2.7c-d). Cpx_1 rims have the same composition as Cpx_2 neoblasts.

Plagioclase

Plagioclase shows An# (= Ca / [Ca + Na]) between 0.78 and 0.92 (Table 2.5). Profiles through

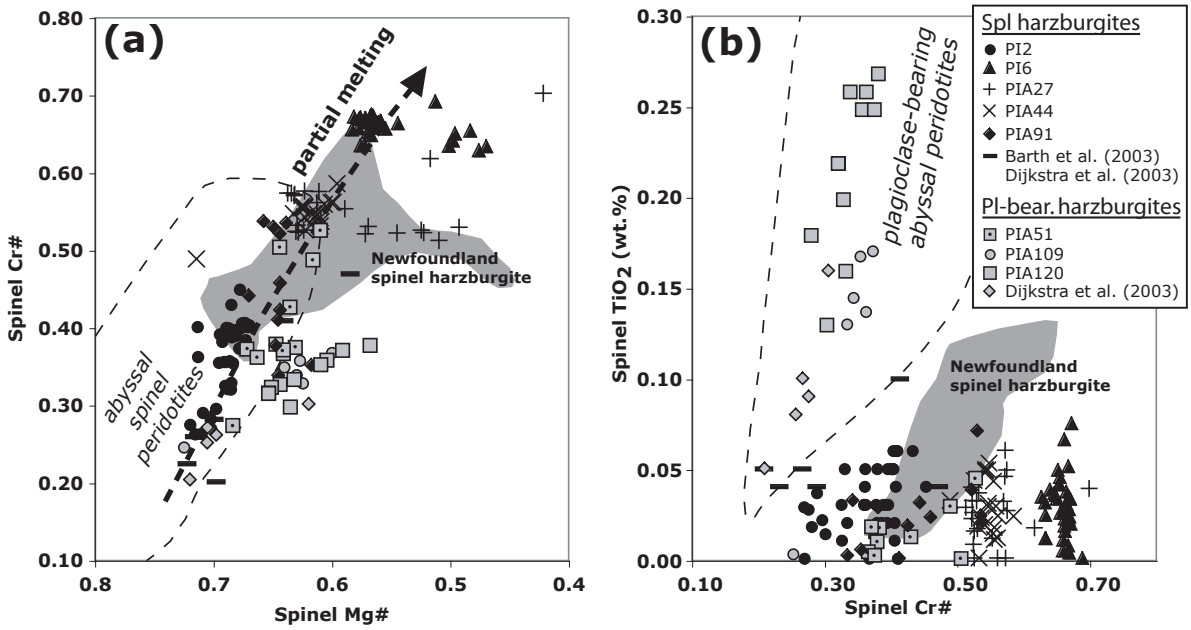


Fig. 2.6: Spinel composition. (a) Mg# vs. Cr#, partial melting trend and abyssal spinel peridotites field after Dick & Bullen (1984) and Dick et al. (1984). (b) Cr# vs. TiO_2 (wt. %). Abyssal plagioclase-bearing peridotites field after Dick & Bullen (1984) and Dick et al. (1984). Newfoundland spinel harzburgite field in grey after Müntener & Manatschal (2006).

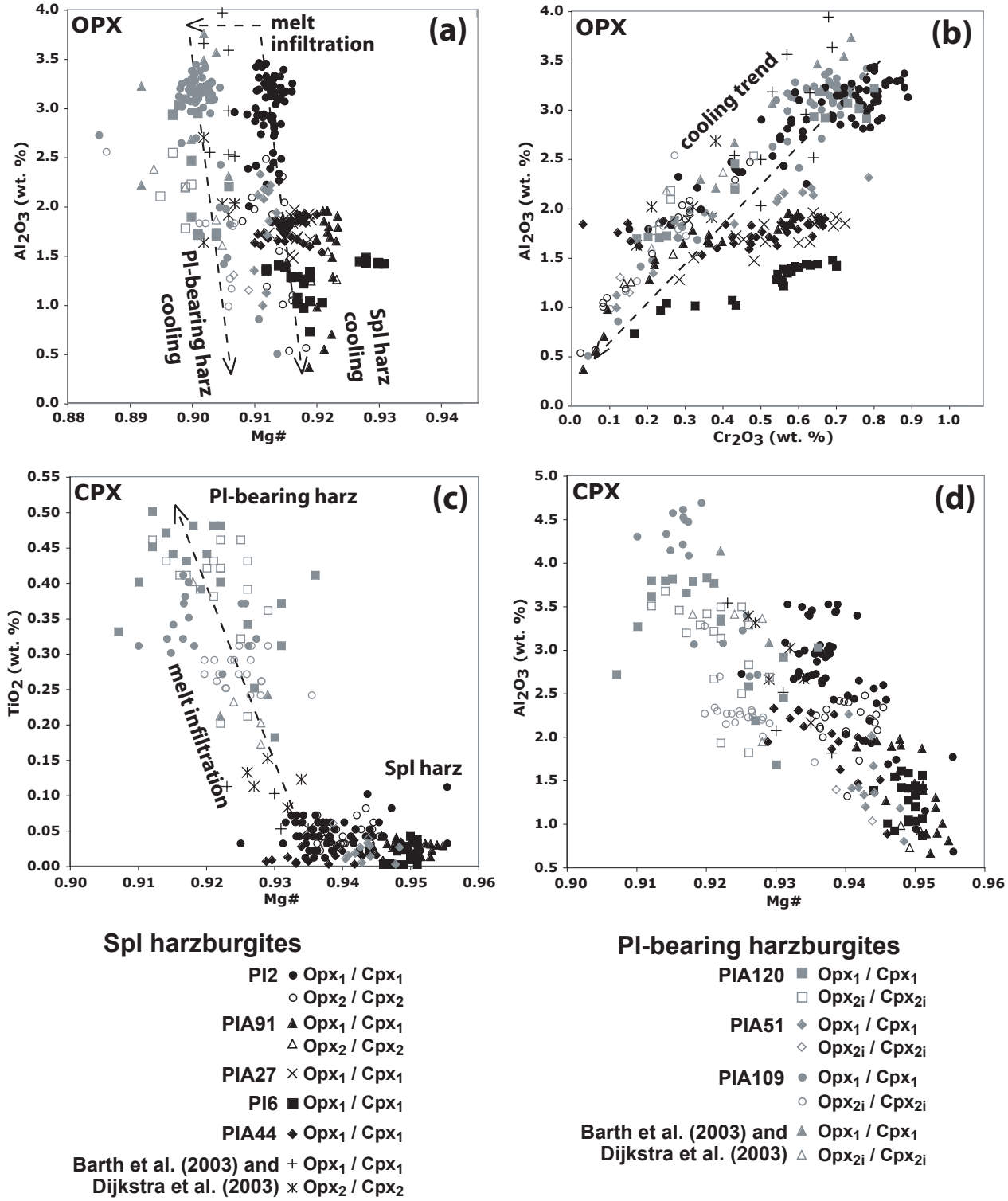


Fig. 2.7: Pyroxene composition. (a) Mg# vs. Al_2O_3 (wt. %) in orthopyroxene, showing the different cooling interpreted trends of spinel and plagioclase-bearing harzburgites and the shift in their Mg# due to melt infiltration. (b) Cr_2O_3 (wt. %) vs. Al_2O_3 (wt. %) in orthopyroxene, showing the cooling interpreted trend of spinel harzburgites. (c) Mg# vs. TiO_2 (wt. %) in clinopyroxene, showing the enrichment in TiO_2 of the plagioclase-bearing harzburgites due to melt infiltration. (d) Mg# vs. Al_2O_3 (wt. %) in clinopyroxene, showing the enrichment in Al_2O_3 and the lower Mg# of the plagioclase-bearing harzburgites due to melt infiltration.

plagioclase grains of sample PIA120 show a rimward increase of An#. Ba and Sr contents are below their respective detection limits.

Serpentine

Cr_2O_3 contents of serpentine are controlled by the composition of the mineral it replaces. Serpentine formed after olivine is low in Cr_2O_3, compared to crystals formed after orthopyroxene or clinopyroxene (Table 2.6). Al_2O_3 and FeO contents are variable, with values of ~ 0.00-2.40 and ~ 2.50-8.50 wt.%, respectively. Mg# ranges from ~ 0.88 to 0.97. In sample PIA27 (serpentinized spinel harzburgite), two types of serpentine are present (Table 2.6): i) Fe-rich, Cr- and Al-poor serpentine crystallized in veins and in mesh-rim textures after olivine (Srp_1), and, ii) Fe-poor, Cr- and Al-rich serpentine associated with talc at orthopyroxene rims (Srp_2).

Talc and chlorite

Talc is nearly stoechiometric, with Mg# between 0.95 and 0.98 (Table 2.6). It contains variable amounts of Al_2O_3 (0.35 to 2.06 wt.%). In sample PIA120 (plagioclase-bearing harzburgite) Mg# are ~ 0.91 and ~ 0.34 for Chl_1 and Chl_2 respectively. Chlorite in other samples is Mg-rich with Mg# between 0.94 and 0.97 (Table 2.6).

Amphiboles

Two types of amphibole are present, high temperature amphiboles (pargasite and edenitic hornblende) and lower temperature amphiboles (anthophyllite and tremolite). In pargasite, Mg# varies between 0.87 and 0.91, and (Na + K) on site A is between 0.75 and 0.94 c.p.f.u (Table 2.7).

Table 2.1: Major element composition of olivine (representative analyses)

	OLIVINE								
Rock	**spl harz**	**spl harz**	**spl harz**	**spl harz**	**spl harz**	**pl harz**	**pl harz**	**pl harz**	**pl harz**
	Ol 1	**Ol 1**	**Ol m**	**Ol 1**	**Ol 1**	**Ol 1**	**Ol m**	**Ol 1**	**Ol 1**
sample	PI2	PIA27	PIA27	PI6	PIA44	PIA120	PIA120	PIA109	PIA51
type	core	core	core	core	core	core	core	core	core
SiO_2	41.0	40.9	40.2	41.1	40.6	40.8	40.0	41.4	41.8
TiO_2	b.d.	b.d.	b.d.	b.d.	b.d.	b.d.	0.11	b.d.	0.01
Cr_2O_3	0.01	b.d.	0.03	0.01	0.05	0.01	0.02	b.d.	0.04
Al_2O_3	b.d.	b.d.	b.d.	0.01	b.d.	0.01	0.03	b.d.	b.d.
FeO	9.31	8.11	12.5	8.57	8.57	10.5	16.6	9.53	9.10
MnO	0.17	0.12	0.28	0.10	0.14	0.18	0.29	0.10	0.17
NiO	0.38	0.28	0.20	0.39	0.18	0.32	0.16	0.37	0.43
MgO	49.8	50.4	46.6	50.6	50.3	48.8	43.2	50.1	49.5
CaO	0.03	0.02	0.01	0.02	0.01	0.02	0.06	0.03	0.01
Na_2O	0.02	0.01	b.d.	0.02	0.02	0.01	0.01	b.d.	b.d.
K_2O	b.d.	b.d.	b.d.	b.d.	b.d.	0.01	0.02	0.02	b.d.
Total	**100.7**	**99.8**	**99.8**	**100.9**	**99.8**	**100.7**	**100.5**	**101.6**	**101.1**
Stoich.	**4O**	**4O**	**4O**	**4O**	**4O**	**4O**	**4O**	**4O**	**4O**
Si	0.995	0.997	1.000	0.992	0.992	0.996	1.009	0.999	1.010
Ti	b.d.	b.d.	b.d.	b.d.	b.d.	b.d.	0.002	b.d.	0.000
Cr	0.000	b.d.	0.001	0.000	0.001	0.000	0.000	b.d.	0.001
Al	b.d.	b.d.	b.d.	0.000	b.d.	0.000	0.001	b.d.	b.d.
Fe^{2+}	0.189	0.165	0.261	0.173	0.175	0.215	0.351	0.192	0.184
Mn	0.004	0.003	0.006	0.002	0.003	0.004	0.006	0.002	0.003
Ni	0.007	0.006	0.004	0.008	0.003	0.006	0.003	0.007	0.008
Mg	1.803	1.831	1.728	1.823	1.831	1.778	1.625	1.799	1.783
Ca	0.001	0.001	0.000	0.001	0.000	0.001	0.002	0.001	0.000
Na	0.001	0.000	b.d.	0.001	0.001	0.000	0.000	b.d.	b.d.
K	b.d.	b.d.	b.d.	b.d.	b.d.	0.000	0.001	0.001	b.d.
Total	**3.000**	**3.003**	**3.000**	**3.006**	**3.008**	**3.000**	**2.999**	**3.000**	**2.990**
Mg#	***0.905***	***0.917***	***0.869***	***0.913***	***0.913***	***0.892***	***0.822***	***0.904***	***0.907***

b.d.: below detection limit.

Table 2.2: Major element composition of spinel (representative analyses)

	SPINEL												
Rock	**spl harz**	**spl harz**	**spl harz**	**spl harz**	**spl harz**	**spl harz**	**spl harz**	**spl harz**	**spl harz**	**pl harz**	**pl harz**	**pl harz**	**pl harz**
	Spl 1	**Spl 1**	**Spl 2**	**Spl 1**	**Spl 1**	**Spl 1**	**Spl 1**	**Spl 1**	**Spl 1**	**Spl 2i**	**Spl 2i**	**Spl 1**	**Spl 2**
sample	PI2	PI2	PI2	PIA91	PIA91	PIA27	PIA27	PIA44	PIA44	PIA120	PIA109	PIA51	PIA51
type	clast core	clast rim	blast	clast core	clast rim	clast core	clast rim	clast core	clast rim	clast core	blast	clast core	blast
SiO_2	0.02	b.d.	0.08	b.d.	b.d.	0.06	0.10	0.02	0.05	0.03	0.06	0.03	0.04
TiO_2	b.d.	0.03	0.03	0.04	0.03	b.d.	0.03	0.01	0.04	0.26	0.15	0.01	0.02
Cr_2O_3	35.3	31.2	24.0	43.2	37.6	45.7	40.8	44.8	41.8	30.1	28.1	35.4	30.6
Al_2O_3	34.4	37.8	44.7	26.7	31.8	22.8	26.3	24.1	25.4	35.9	36.5	31.8	35.2
Fe_2O_3	0.80	0.53	1.10	1.61	1.55	2.52	1.74	2.69	4.00	3.22	3.89	3.21	3.43
FeO	13.5	12.7	12.3	13.9	13.2	14.1	18.6	14.50	14.6	16.3	15.0	14.5	14.3
MnO	0.08	0.04	0.49	0.80	0.76	0.86	0.87	0.86	0.82	0.05	0.56	0.70	0.65
NiO	0.16	0.13	0.16	0.07	0.08	0.02	b.d.	0.02	0.05	0.17	0.11	0.04	0.14
ZnO	0.18	0.19	0.04	0.17	0.30	b.d.	0.29	0.13	0.07	b.d.	0.20	0.12	0.42
MgO	15.4	16.1	17.2	14.1	15.0	13.4	10.7	13.4	13.5	14.0	14.3	14.2	14.3
CaO	0.01	b.d.	b.d.	0.01	b.d.	0.01	0.01	0.02	0.02	0.03	b.d.	0.01	0.01
Total	**99.7**	**98.8**	**100.0**	**100.6**	**100.4**	**99.6**	**99.5**	**100.6**	**100.3**	**100.1**	**98.8**	**100.0**	**99.1**
Stoich.	**4O**	**4O**	**4O**	**4O**	**4O**	**4O**	**4O**	**4O**	**4O**	**4O**	**4O**	**4O**	**4O**
	3 cations	**3 cations**	**3 cations**	**3 cations**	**3 cations**	**3 cations**	**3 cations**	**3 cations**	**3 cations**	**3 cations**	**3 cations**	**3 cations**	**3 cations**
Si	0.001	b.d.	0.002	b.d.	b.d.	0.002	0.002	0.001	0.001	0.001	0.002	0.001	0.001
Ti	b.d.	0.001	0.001	0.001	0.001	b.d.	0.001	0.000	0.001	0.006	0.003	0.000	0.000
Cr	0.807	0.708	0.523	1.021	0.867	1.111	0.997	1.075	1.000	0.690	0.649	0.824	0.707
Al	1.174	1.277	1.449	0.940	1.095	0.827	0.958	0.861	0.904	1.227	1.256	1.103	1.215
Fe^{3+}	0.017	0.012	0.023	0.036	0.034	0.058	0.040	0.062	0.091	0.070	0.085	0.071	0.075
Fe^{2+}	0.326	0.304	0.282	0.348	0.323	0.364	0.479	0.368	0.370	0.396	0.365	0.358	0.350
Mn	0.002	0.001	0.011	0.020	0.019	0.022	0.023	0.022	0.021	0.001	0.014	0.017	0.016
Ni	0.004	0.003	0.004	0.002	0.002	0.001	b.d.	0.000	0.001	0.004	0.003	0.001	0.003
Zn	0.004	0.004	0.001	0.004	0.007	b.d.	0.007	0.003	0.002	b.d.	0.004	0.003	0.009
Mg	0.665	0.690	0.705	0.628	0.652	0.615	0.493	0.607	0.608	0.604	0.619	0.622	0.623
Ca	0.000	b.d.	b.d.	0.000	b.d.	0.000	0.000	0.001	0.001	0.001	b.d.	0.000	0.000
Mg#	***0.671***	***0.695***	***0.714***	***0.643***	***0.669***	***0.628***	***0.507***	***0.623***	***0.621***	***0.604***	***0.629***	***0.635***	***0.640***
Cr#	***0.408***	***0.357***	***0.265***	***0.521***	***0.442***	***0.573***	***0.510***	***0.555***	***0.525***	***0.360***	***0.341***	***0.428***	***0.368***

Fe_2O_3 in spinel calculated assuming perfect stoichiometry. Cr# calculated as Cr / (Cr + Al). b.d.: below detection limit.

Table 2.3: Major element composition of orthopyroxene (representative analyses)

	ORTHOPYROXENE													
Rock	**spl harz**	**spl harz**	**spl harz**	**spl harz**	**spl harz**	**spl harz**	**spl harz**	**spl harz**	**spl harz**	**pl harz**	**pl harz**	**pl harz**	**pl harz**	**pl harz**
	Opx 1	**Opx 1**	**Opx 2**	**Opx 1**	**Opx 1**	**Opx 2**	**Opx 1**	**Opx 1**	**Opx 1**	**Opx 1**	**Opx 1**	**Opx 2i**	**Opx 1**	**Opx 2i**
sample	PI2	PI2	PI2	PIA91	PIA91	PIA91	PIA27	PIA44	PIA44	PIA120	PIA120	PIA120	PIA109	PIA109
type	clast core	clast rim	blast	clast core	clast rim	blast	clast core	clast core	clast rim	clast core	clast rim	blast vein	clast core	blast
SiO_2	56.2	56.4	57.1	57.0	57.9	57.9	56.3	56.4	58.0	55.5	56.0	55.6	55.6	57.3
TiO_2	0.04	b.d.	0.03	0.02	b.d.	0.01	0.01	b.d.	0.03	0.16	0.17	0.14	0.09	0.11
Cr_2O_3	0.79	0.20	0.26	0.39	0.03	0.14	0.70	0.63	0.43	0.69	0.43	0.48	0.71	0.24
Al_2O_3	3.03	1.80	1.85	1.69	0.37	1.26	1.92	1.84	1.65	2.59	2.20	2.54	4.02	1.83
FeO	5.76	5.68	6.25	5.45	5.56	5.45	5.40	5.84	5.84	6.30	6.26	6.80	6.49	6.41
MnO	0.16	0.10	0.13	0.19	0.17	0.15	0.07	0.03	0.11	0.12	0.21	0.11	0.15	0.14
NiO	0.06	0.11	0.07	0.13	0.16	0.08	b.d.	0.14	0.06	0.03	0.08	0.07	0.07	0.08
MgO	34.1	34.4	34.7	34.5	35.3	34.8	34.3	34.4	34.8	33.1	33.9	33.2	33.7	35.1
CaO	0.68	0.46	0.41	0.72	0.25	0.27	0.86	0.75	0.58	1.73	0.93	0.81	0.05	0.47
Na_2O	0.02	b.d.	b.d.	0.02	0.02	b.d.	0.01	b.d.	0.01	0.01	b.d.	0.01	0.04	b.d.
K_2O	0.02	0.01	b.d.	b.d.	b.d.	b.d.	0.01	b.d.	b.d.	b.d.	b.d.	0.02	b.d.	0.01
Total	**100.9**	**99.2**	**100.8**	**100.1**	**99.8**	**100.1**	**99.6**	**100.0**	**101.5**	**100.2**	**100.1**	**99.8**	**100.9**	**101.7**
Stoich.	**6O**	**6O**	**6O**	**6O**	**6O**	**6O**	**6O**	**6O**	**6O**	**6O**	**6O**	**6O**	**6O**	**6O**
Si	1.923	1.958	1.954	1.961	1.992	1.983	1.947	1.946	1.967	1.923	1.936	1.932	1.905	1.947
Ti	0.001	b.d.	0.001	0.001	b.d.	0.000	0.000	b.d.	0.001	0.004	0.004	0.004	0.002	0.003
Cr	0.021	0.006	0.007	0.011	0.001	0.004	0.019	0.017	0.011	0.019	0.012	0.013	0.019	0.006
Al	0.122	0.074	0.075	0.068	0.015	0.051	0.078	0.075	0.066	0.106	0.090	0.104	0.162	0.073
Fe^{2+}	0.165	0.165	0.179	0.157	0.160	0.156	0.156	0.169	0.166	0.183	0.181	0.197	0.186	0.182
Mn	0.005	0.003	0.004	0.005	0.005	0.004	0.002	0.001	0.003	0.004	0.006	0.003	0.004	0.004
Ni	0.002	0.003	0.002	0.003	0.004	0.002	b.d.	0.004	0.002	0.001	0.002	0.002	0.002	0.002
Mg	1.740	1.778	1.769	1.765	1.813	1.779	1.769	1.769	1.756	1.708	1.745	1.719	1.719	1.775
Ca	0.025	0.017	0.015	0.027	0.009	0.010	0.032	0.028	0.021	0.064	0.034	0.030	0.002	0.017
Na	0.001	b.d.	b.d.	0.001	0.001	b.d.	0.000	b.d.	0.001	0.001	b.d.	0.001	0.003	b.d.
K	0.001	0.001	b.d.	b.d.	b.d.	b.d.	0.000	b.d.	b.d.	b.d.	b.d.	0.001	b.d.	0.000
Total	**4.005**	**4.003**	**4.005**	**3.999**	**4.000**	**3.989**	**4.005**	**4.008**	**3.994**	**4.011**	**4.009**	**4.007**	**4.004**	**4.010**
Mg#	***0.913***	***0.915***	***0.908***	***0.918***	***0.919***	***0.919***	***0.919***	***0.913***	***0.914***	***0.903***	***0.906***	***0.897***	***0.902***	***0.907***
Cr#	***0.149***	***0.069***	***0.086***	***0.135***	***0.049***	***0.069***	***0.197***	***0.186***	***0.148***	***0.152***	***0.117***	***0.112***	***0.105***	***0.079***

Cr# calculated as Cr / (Cr + Al). b.d.: below detection limit.

Table 2.4: Major element composition of clinopyroxene (representative analyses)

	CLINOPYROXENE															
Rock	**spl harz**	**spl harz**	**spl harz**	**spl harz**	**spl harz**	**spl harz**	**spl harz**	**spl harz**	**spl harz**	**pl harz**	**pl harz**	**pl harz**	**pl harz**	**pl harz**	**pl harz**	**pl harz**
	Cpx 1	**Cpx 1**	**Cpx 2**	**Cpx 1**	**Cpx 1**	**Cpx 1**	**Cpx 1**	**Cpx 1**	**Cpx 1**	**Cpx 1**	**Cpx 1**	**Cpx 2i**	**Cpx 1**	**Cpx 1**	**Cpx 2i**	**Cpx 2**
sample	PI2	PI2	PI2	PIA91	PIA91	PIA27	PIA27	PIA44	PIA44	PIA120	PIA120	PIA120	PIA109	PIA109	PIA109	PIA51
type	clast core	clast rim	blast	clast core	clast rim	in opx exsol	in opx exsol	ass opx core	ass opx core	clast core	clast rim	blast vein	clast core	clast core	blast	blast
SiO_2	53.2	55.5	54.7	54.0	54.3	54.0	53.8	53.3	53.6	51.3	53.2	51.1	53.4	52.9	53.4	54.7
TiO_2	0.06	0.03	0.01	0.02	0.01	b.d.	b.d.	0.03	0.03	0.51	0.38	0.60	0.29	0.31	0.33	0.03
Cr_2O_3	1.22	0.29	0.18	0.68	0.21	1.23	1.40	0.76	0.67	1.36	0.67	1.54	0.45	0.83	0.52	0.52
Al_2O_3	3.53	0.68	0.92	1.85	0.88	2.11	2.24	1.99	1.59	4.07	2.77	4.45	2.16	2.67	2.43	1.63
FeO	2.20	1.49	1.90	1.79	1.62	1.96	1.99	1.93	1.71	2.68	2.55	2.52	2.51	2.44	2.64	1.80
MnO	0.01	0.09	0.07	0.04	0.05	0.08	b.d.	b.d.	0.02	0.09	0.15	0.05	0.05	0.09	0.12	0.09
NiO	0.06	0.05	0.03	0.10	0.08	0.07	0.11	0.07	0.07	0.02	0.03	0.03	0.06	0.02	b.d.	0.03
MgO	16.8	18.0	18.1	17.5	17.9	17.4	17.4	17.5	17.8	15.9	17.2	15.7	17.5	17.2	17.0	17.0
CaO	23.8	25.0	24.8	23.9	24.2	23.0	23.0	24.7	24.7	23.1	23.3	23.4	23.6	23.4	23.4	24.6
Na_2O	0.05	0.02	0.02	0.03	0.02	0.31	0.34	0.03	0.05	0.48	0.42	0.47	0.32	0.33	0.39	0.04
K_2O	0.01	b.d.	0.02	0.01	b.d.	0.01	b.d.	b.d.	b.d.	0.01	b.d.	b.d.	b.d.	0.01	b.d.	b.d.
Total	**100.9**	**101.1**	**100.8**	**99.9**	**99.3**	**100.1**	**100.3**	**100.2**	**100.3**	**99.4**	**100.7**	**99.8**	**100.3**	**100.2**	**100.2**	**100.4**
Stoich.	**6O**	**6O**	**6O**	**6O**	**6O**	**6O**	**6O**	**6O**	**6O**	**6O**	**6O**	**6O**	**6O**	**6O**	**6O**	**6O**
Si	1.915	1.987	1.971	1.958	1.981	1.956	1.946	1.935	1.945	1.883	1.924	1.871	1.937	1.922	1.937	1.973
Ti	0.002	0.001	0.000	0.001	0.000	b.d.	b.d.	0.001	0.001	0.014	0.010	0.016	0.008	0.008	0.009	0.001
Cr	0.035	0.008	0.005	0.020	0.006	0.035	0.040	0.022	0.019	0.040	0.019	0.045	0.013	0.024	0.015	0.015
Al	0.150	0.029	0.039	0.079	0.038	0.090	0.095	0.085	0.068	0.176	0.118	0.192	0.092	0.114	0.104	0.069
Fe^{2+}	0.066	0.045	0.057	0.054	0.049	0.059	0.060	0.058	0.052	0.083	0.077	0.077	0.076	0.074	0.080	0.054
Mn	0.000	0.003	0.002	0.001	0.001	0.002	b.d.	b.d.	0.001	0.003	0.005	0.002	0.002	0.003	0.004	0.003
Ni	0.002	0.001	0.001	0.003	0.002	0.002	0.003	0.002	0.002	0.001	0.001	0.001	0.002	0.001	b.d.	0.001
Mg	0.903	0.961	0.973	0.944	0.972	0.940	0.939	0.946	0.960	0.871	0.926	0.858	0.944	0.931	0.920	0.914
Ca	0.917	0.960	0.957	0.930	0.947	0.893	0.891	0.960	0.961	0.907	0.902	0.916	0.917	0.912	0.901	0.952
Na	0.003	0.002	0.002	0.002	0.001	0.022	0.024	0.002	0.003	0.034	0.030	0.033	0.022	0.023	0.027	0.003
K	0.000	b.d.	0.001	0.000	b.d.	0.000	b.d.	b.d.	b.d.	0.000	b.d.	b.d.	b.d.	0.000	b.d.	b.d.
Total	**3.993**	**3.995**	**4.008**	**3.993**	**3.998**	**3.995**	**3.999**	**4.012**	**4.012**	**4.012**	**4.012**	**4.011**	**4.013**	**4.012**	**4.008**	**3.985**
Mg#	***0.932***	***0.955***	***0.944***	***0.946***	***0.952***	***0.941***	***0.940***	***0.942***	***0.949***	***0.913***	***0.923***	***0.918***	***0.925***	***0.926***	***0.920***	***0.944***
Cr#	***0.188***	***0.224***	***0.118***	***0.198***	***0.137***	***0.281***	***0.296***	***0.204***	***0.220***	***0.184***	***0.139***	***0.188***	***0.124***	***0.172***	***0.126***	***0.176***

Cr# calculated as Cr / (Cr + Al). b.d.: below detection limit.

Table 2.5: Major element composition of plagioclase (representative analyses)

	PLAGIOCLASE		
Rock	**pl harz**	**pl harz**	**pl harz**
	Pl	**Pl**	**Pl**
sample	PIA109	PIA120	PIA120
texture	matrix	vein core	vein rim
SiO_2	44.8	46.8	46.2
TiO_2			
Cr_2O_3			
Al_2O_3	34.8	34.8	35.0
Fe_2O_3	0.33	0.03	0.11
MnO			
NiO			
MgO			
CaO	18.4	16.8	17.2
Na_2O	0.98	2.08	1.74
K_2O	b.d.	0.02	0.01
H_2O			
Total	**99.3**	**100.4**	**100.3**
Stoich.	**8O**	**8O**	**8O**
	5 cat	**5 cat**	**5 cat**
Si	2.079	2.130	2.113
Ti			
Cr			
Al	1.904	1.866	1.887
Fe^{3+}	0.012	0.001	0.004
Mn			
Ni			
Mg			
Ca	0.917	0.818	0.842
Na	0.088	0.184	0.154
K	b.d.	0.001	0.000
H			
Total	**5.000**	**5.000**	**5.000**
An#	***0.912***	***0.817***	***0.845***

An# calculated as Ca / (Ca + Na).
Ba and Sr are below the detection limit.
b.d.: below detection limit.

Table 2.6: Major element composition of serpentine, talc and chlorite (representative analyses)

	SERPENTINE										TALC		CHLORITE		
Rock	**spl harz**	**spl harz**	**spl harz**	**spl harz**	**spl harz**	**spl harz**	**spl harz**	**pl harz**	**pl harz**	**pl harz**	**spl harz**	**pl harz**	**spl harz**	**pl harz**	**pl harz**
	Srp 1	**Srp 1**	**Srp 2**	**Srp 1**	**Srp 1**	**Srp 1**	**Srp 1**	**Srp 1**	**Srp 1**	**Srp 1**	**Tlc**	**Tlc**	**Chl 1**	**Chl 1**	**Chl 2**
sample	PI2	PIA27	PIA27	PIA44	PIA44	PIA44	PI6	PIA120	PIA109	PIA51	PIA27	PIA51	PI6	PIA120	PIA120
texture	vein	mesh-rim after ol	bastite after opx	mesh-rim after ol	bastite after opx	bastite after cpx	mesh-rim after ol	mesh-rim after ol	mesh-rim after ol	mesh-rim after ol					
SiO_2	41.9	38.8	40.9	39.8	39.4	42.5	42.6	42.4	40.9	41.7	60.5	61.5	33.3	31.0	24.4
TiO_2	0.01	b.d.	0.01	b.d.	0.02	0.01	0.01	0.03	0.01	b.d.	0.01	0.02	b.d.	0.03	0.03
Cr_2O_3	0.02	b.d.	0.34	0.03	0.48	0.58	0.01	0.03	0.03	0.01	0.54	0.15	2.56	0.01	0.05
Al_2O_3	0.34	0.01	0.48	0.32	1.66	0.63	0.20	0.54	0.53	0.47	2.06	1.08	13.3	20.1	20.2
FeO	5.42	4.89	2.78	6.51	7.98	7.72	6.19	3.56	4.95	5.39	1.50	2.07	3.64	5.53	32.9
MnO	0.14	0.20	0.09	0.11	0.16	0.04	0.17	0.08	0.12	0.12	0.02	0.02	0.03	0.02	0.66
NiO	0.11	0.08	0.07	0.05	0.05	b.d.	0.21	0.09	0.08	0.10	0.09	0.09	0.14	0.11	0.14
MgO	36.3	37.1	38.3	35.8	34.3	35.8	38.7	38.7	38.0	37.2	30.9	30.3	35.0	30.6	9.37
CaO	0.04	0.02	0.06	0.45	0.42	0.14	0.55	0.19	0.19	0.31	0.01	0.04	b.d.	0.04	0.27
Na_2O	0.04	0.02	0.03	0.07	0.08	0.02	0.56	0.05	0.05	0.01	0.09	0.35	0.04	0.06	0.18
K_2O	0.02	0.01	b.d.	0.01	0.04	b.d.	0.01	b.d.	0.04	0.02	0.01	0.01	b.d.	0.02	0.01
H_2O											4.71	4.70	12.7	12.7	10.9
Total	**84.3**	**81.1**	**83.1**	**83.2**	**84.6**	**87.4**	**89.2**	**85.6**	**84.8**	**85.4**	**100.4**	**100.3**	**100.9**	**100.3**	**99.0**
Stoich.	**9O**	**9O**	**9O**	**9O**	**9O**	**9O**	**9O**	**9O**	**9O**	**9O**	**12O**	**12O**	**18O**	**18O**	**18O**
											2OH	**2OH**	**8OH**	**8OH**	**8OH**
Si	2.045	1.978	2.005	1.993	1.958	2.025	1.988	2.021	1.989	2.017	3.850	3.922	3.137	2.936	2.685
Ti	0.000	b.d.	0.000	b.d.	0.001	0.001	0.000	0.001	0.000	b.d.	0.001	0.001	b.d.	0.002	0.003
Cr	0.001	b.d.	0.013	0.001	0.019	0.022	0.000	0.001	0.001	0.000	0.027	0.008	0.191	0.001	0.005
Al	0.020	0.000	0.028	0.019	0.097	0.036	0.011	0.030	0.030	0.027	0.155	0.081	1.480	2.238	2.615
Fe^{2+}	0.221	0.208	0.114	0.273	0.332	0.308	0.242	0.142	0.202	0.218	0.080	0.110	0.287	0.437	3.030
Mn	0.006	0.009	0.004	0.005	0.007	0.002	0.007	0.003	0.005	0.005	0.001	0.001	0.002	0.002	0.062
Ni	0.004	0.003	0.003	0.002	0.002	b.d.	0.008	0.004	0.003	0.004	0.005	0.005	0.011	0.009	0.013
Mg	2.642	2.820	2.801	2.677	2.541	2.545	2.694	2.748	2.751	2.681	2.934	2.880	4.917	4.309	1.539
Ca	0.002	0.001	0.003	0.024	0.022	0.007	0.028	0.010	0.010	0.016	0.001	0.003	b.d.	0.004	0.031
Na	0.004	0.002	0.003	0.007	0.008	0.002	0.050	0.005	0.005	0.001	0.012	0.043	0.008	0.011	0.039
K	0.001	0.000	b.d.	0.000	0.003	b.d.	0.000	b.d.	0.003	0.001	0.001	0.000	b.d.	0.003	0.002
H											2.000	2.000	8.000	8.000	8.000
Total	**4.947**	**5.023**	**4.975**	**5.000**	**4.989**	**4.946**	**5.030**	**4.965**	**4.999**	**4.971**	**7.065**	**7.055**	**10.032**	**9.950**	**10.022**
Mg#	***0.923***	***0.931***	***0.961***	***0.907***	***0.885***	***0.892***	***0.918***	***0.951***	***0.932***	***0.925***	***0.974***	***0.963***	***0.945***	***0.908***	***0.337***

b.d.: below detection limit.

Table 2.7: Major element composition of amphiboles (representative analyses)

	AMPHIBOLES						
Rock	**spl harz**	**spl harz**	**spl harz**	**spl harz**	**pl harz**	**pl harz**	**pl harz**
	Tr	**Ed hbl**	**Tr**	**Ath**	**Prg**	**Tr**	**Prg**
sample	PIA91	PIA27	PIA27	PIA27	PIA120	PIA120	PIA109
type	core	core	core	core	core	core	core
SiO_2	56.3	47.2	56.9	56.5	44.2	57.1	44.2
TiO_2	0.06	0.11	0.03	b.d.	2.21	0.10	1.74
Cr_2O_3	0.34	1.94	0.54	0.25	1.75	0.29	1.52
Al_2O_3	3.74	11.4	2.91	1.34	13.0	1.26	12.5
Fe_2O_3	n.c.	n.c.	n.c.	n.c.	n.c.	n.c.	n.c.
FeO	1.58	2.83	1.92	4.70	3.73	2.72	4.20
MnO	0.01	b.d.	0.04	0.08	0.12	0.15	0.08
NiO	0.09	0.13	0.05	0.10	0.14	0.06	0.09
MgO	22.2	19.3	22.8	33.8	17.6	22.8	18.4
CaO	13.2	12.2	12.3	0.45	12.3	13.1	12.1
Na_2O	0.49	2.02	0.78	0.02	2.73	0.36	3.18
K_2O	0.03	0.41	0.01	0.01	b.d.	0.02	0.01
H_2O	2.19	2.13	2.19	2.23	2.11	2.19	2.11
Total	**100.2**	**99.7**	**100.4**	**99.5**	**100.0**	**100.1**	**100.1**
Si	7.700	6.639	7.791	7.617	6.290	7.828	6.283
Ti	0.007	0.011	0.003	b.d.	0.237	0.010	0.187
Cr	0.037	0.216	0.059	0.026	0.196	0.032	0.171
Al	0.602	1.899	0.469	0.212	2.186	0.204	2.095
Fe^{3+}	n.c.	n.c.	n.c.	n.c.	n.c.	n.c.	n.c.
Fe^{2+}	0.181	0.333	0.219	0.530	0.443	0.312	0.499
Mn	0.002	b.d.	0.004	0.009	0.015	0.018	0.009
Ni	0.010	0.015	0.006	0.011	0.016	0.007	0.010
Mg	4.533	4.040	4.649	6.788	3.737	4.669	3.898
Ca	1.929	1.846	1.800	0.064	1.880	1.921	1.849
Na	0.129	0.552	0.207	0.006	0.753	0.097	0.876
K	0.004	0.074	0.002	0.001	0.001	0.004	0.003
H	2.000	2.000	2.000	2.000	2.000	2.000	2.000
Total	**15.134**	**15.626**	**15.209**	**15.267**	**15.753**	**15.100**	**15.879**
Mg#	***0.962***	***0.924***	***0.955***	***0.928***	***0.894***	***0.937***	***0.886***
(Na + K)A	***0.134***	***0.626***	***0.209***	***0.008***	***0.753***	***0.100***	***0.879***

(Na + K)A: Na + K on site A. n.c. = not calculated, b.d.: below detection limit. Data obtained by normalization with 23 oxygens and 15 cations + Na + K, except for anthophyllite: normalization with 23 oxygens and considering Fe3+=0.

Mg# of edenitic hornblende is between 0.92 and 0.99, and (Na + K) on site A ranges from 0.58 to 0.67 c.p.f.u (Table 2.7). Lower-temperature anthophyllite crystallized at edenitic hornblende rims during cooling (Fig. 2.4b) shows Mg# of 0.92-0.93. Mg# in tremolite ranges from 0.93 to 0.97.

Li, B AND Be CONTENTS OF ROCK-FORMING MINERALS

The results of light element analyses are listed in Table 2.8 and presented in Figure 2.8. In primary minerals, clinopyroxene shows variable Li values from 0.1 to 3.7 μg/g, the highest contents of all minerals (Fig. 2.8a). Li abundances are 0.5-1.1 μg/g in olivine, and 0.1-1.5 μg/g in orthopyroxene. Li zoning is frequent in olivine and pyroxenes, and usually Li decreases from core to rim. Rarely, Li can increase rimwards. In orthopyroxene, zoning is in some cases related to the presence of clinopyroxene exsolution lamellae and shows a very complex "wavy" pattern. Li concentration is lower than the detection limit in plagioclase (Fig. 2.8a).

Variable Li contents were measured in serpentine with values from < 0.005 to 1.4 μg/g (Fig. 2.8b, Table 2.8). Serpentine minerals are too small to be analyzed as single grains (see section

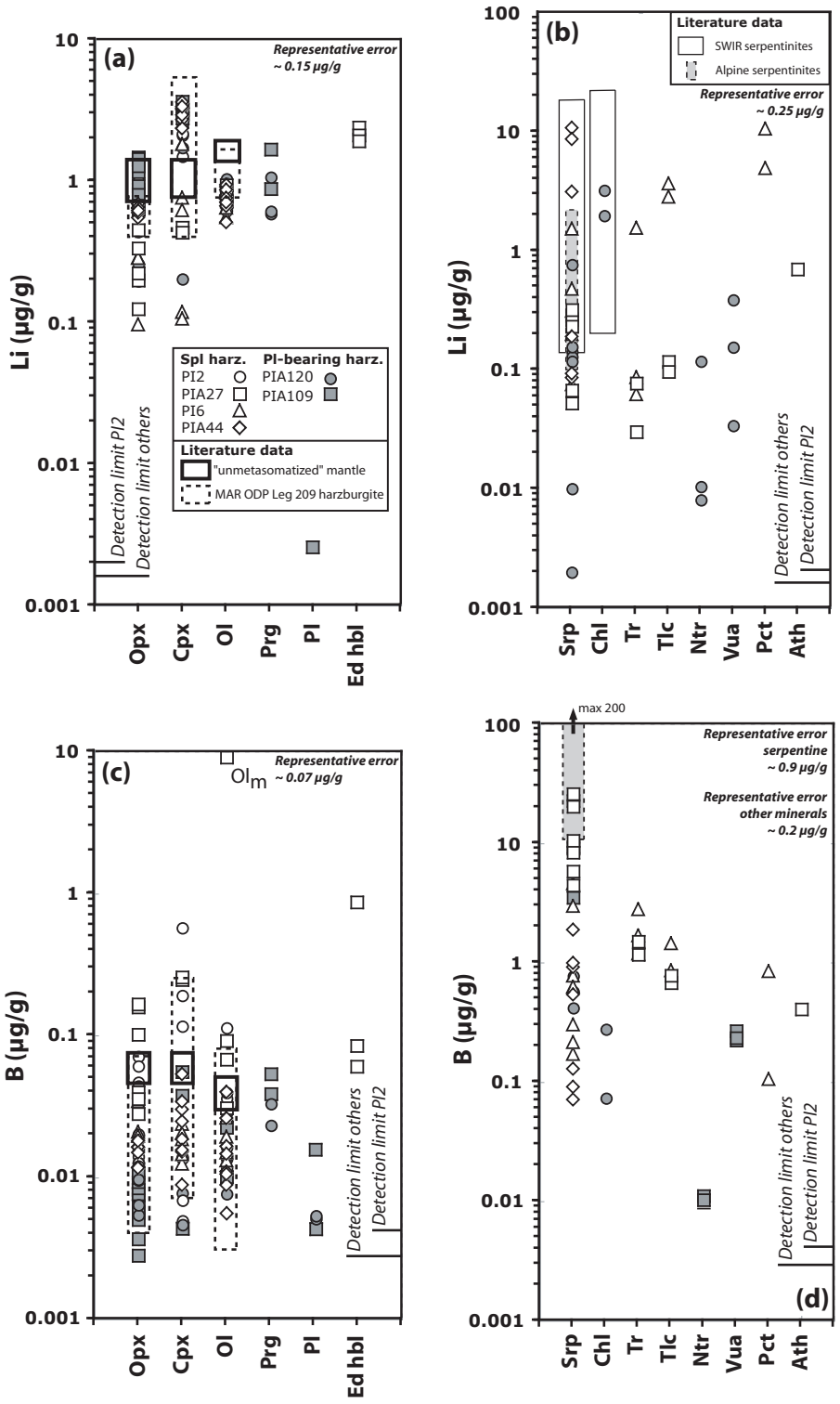


Fig. 2.8: (a) Li contents of primary mantle minerals and of high-temperature amphiboles. (b) Li contents of minerals related to serpentinization and retrograde. Li contents higher than 1.0 μg/g in serpentine are most likely due to mixture of different phases (see sections 'Nature of serpentine minerals' and 'Li, B, and Be contents of rock-forming minerals'). (c) B contents of primary mantle minerals and of high-temperature amphiboles. Ol_m: metamorphic olivine (d) B contents of minerals related to serpentinization and cooling (excepted for Ol_m). «Unmetasomatized» mantle data after Ottolini et al. (2004), Mid-Atlantic ridge ODP Leg 209 serpentinites after Vils et al. (in prep.), SWIR serpentinites after Decitre et al. (2002), and Alpine serpentinites after Scambelluri et al. (2004). Some values are below the detection limit for Li in plagioclase and serpentine, and for B in orthopyroxene, clinopyroxene, olivine, pargasite, plagioclase and natrolite.

on analytical techniques). Consequently, the results represent multi-grain values for serpentine. Only in case of sample PIA44, talc was identified within serpentine (see section 'The nature of serpentine minerals'). Consequently, serpentine (multigrain) analyses in this sample give higher values for Li (up to 11.2 μg/g; Fig. 2.8b; Table 2.8).

Li contents in amphiboles are variable (Fig. 2.8a-b), but edenitic hornblende has higher values (1.9-2.4 μg/g) than other amphiboles (pargasite, anthophyllite and tremolite). The alteration phases chlorite, talc and pectolite, have high Li concentrations, with 2.0-3.3, 0.1-3.8 and 5.1-11.0 μg/g, respectively (Fig. 2.8b). Natrolite and

vuagnatite have low Li concentrations < 0.4 μg/g (Table 2.8).

B concentrations in all primary minerals are low and range from < 0.008 up to 0.1, 0.4 and 0.6 μg/g, for olivine, orthopyroxene and clinopyroxene, respectively. Metamorphic olivine crystallized in sample PIA27 has the highest B content with 9.1 μg/g (only one grain was large enough to be analyzed). B concentrations are highly variable in serpentine (0.1 to 27.6 μg/g) (Fig. 2.8d). Contents can vary one order of magnitude in the same serpentine polymorph in one sample, at the millimeter scale. These contents were measured in pure serpentine and not in a mixture of different phases (see section 'The nature of the serpentine minerals'). B contents of alteration phases natrolite, vuagnatite and pectolite are low < 0.26 μg/g (Tabe 8).

Be contents of all minerals are generally below the detection limit (~ 1.4 ng/g). Only high temperature amphiboles (edenitic hornblende and pargasite) show a maximum value of 0.012 μg/g (Table 2.8).

Li, B AND Be CONTENTS OF WHOLE ROCK SAMPLES

Whole rock data are listed in Table 2.9. Li in harzburgites ranges from 0.5 to 1.1 μg/g, and no correlation exists between the degree of serpentinization and Li whole rock contents. The most serpentinized peridotites show a greater variation in Li contents. B contents range from 0.2 to 2.7 μg/g. Be contents are below detection limit (<1.6 ng/g) in all the samples.

DISCUSSION

The spinel and plagioclase-bearing harzburgites record different steps of evolution (see section 'Sample characteristics'). Primary mantle minerals were deformed during high-temperature plastic deformation. Textural and chemical characteristics strongly suggest that the Dramala peridotites were infiltrated by mafic melts and subjected to cooling and hydration, including formation of amphiboles, talc and serpentine. Finally, late alteration phases were formed very locally. Deformation, melt infiltration, hydration and cooling can potentially have modified the Li, B and Be content of the primary Dramala mantle. While the role of deformation cannot be assessed, we will discuss the impact of the other processes on the light element systematics.

Compositional effects of melt impregnation

Major element composition of minerals

Low modal clinopyroxene (Table 2.9), and olivine and spinel composition (Fig. 2.5 and 2.6) show that Pindos harzburgites were highly refractory before melt impregnation. They experienced extraction of at least 15% partial melt (Saccani & Photiades, 2004; Fig. 2.5b). Plagioclase-bearing harzburgites are less depleted than spinel harzburgites, which is consistent with the fact that they were refertilized by mafic melts to a greater extent (see section 'Interpretation of specific textures').

Spinel composition is highly sensitive to melt impregnation. Spinel in plagioclase-bearing harzburgites has lower Mg# and higher TiO_2 content than spinel in spinel harzburgites (Fig. 2.6a-b). Comparable Ti enrichment in spinel of impregnated depleted abyssal peridotites was mentionned by Dick & Bullen (1984) and Allan & Dick (1996). Also, plagioclase-bearing harzburgites from Othris are aligned exactly on the same trend (Dijkstra et al., 2001; Barth et al., 2003). In figure 2.6a, some spinels do not follow the partial melting trend defined by Dick & Bullen (1984) and Dick et al. (1984). Their shift in Mg# compared to the other spinels could be due to metasomatism during serpentinization, which can play an important role if grains are small.

Ti-rich clinopyroxene is associated with Ti-rich spinel in the plagioclase-bearing harzburgites (Fig. 2.7c). It is enriched in Al_2O_3, shows Na_2O values between 0.26 and 0.50 wt.%, and has lower Mg# compared to clinopyroxene from spinel harzburgite (Fig. 2.7c-d). These features were described in abyssal plagioclase-bearing peridotites (Allan & Dick, 1996) and in plagioclase-bearing harzburgites from Othris (Dijkstra et al., 2001; Barth et al. , 2003). Orthopyroxene from the plagioclase-bearing harzburgites has lower Mg# compared to the spinel harzburgites (Fig. 2.7a).

The composition of Cpx_{2i} from the plagioclase-bearing harzburgites corresponds to the most

Table 2.8: Li, Be and B contents of rock forming minerals (representative analyses)

Sample	N	Mineral	Li (µg/g)	2σ	Be (µg/g)	2σ	B (µg/g)	2σ
		OLIVINE						
PI2	13	Ol 1	0.73	0.03	0.002	0.002	0.11	0.02
		Ol 1	0.98	0.07	<0.0014		<0.0037	
		Ol 1	0.82	0.03	<0.0014		0.04	0.02
		Ol 1	0.62	0.05	<0.0014		0.016	0.009
PIA27	3	Ol 1	0.79	0.04	<0.0010		0.07	0.02
		Ol 1	0.95	0.05	<0.0010		0.03	0.01
		Ol 1	0.72	0.04	<0.0010		0.09	0.02
PIA27	1	Ol m	0.76	0.05	<0.0010		9	3
PI6	4	Ol 1	0.56	0.03	<0.0010		0.02	0.02
		Ol 1	0.65	0.04	<0.0010		0.03	0.01
		Ol 1	0.83	0.02	<0.0010		0.01	0.01
		Ol 1	0.86	0.04	<0.0010		0.01	0.01
PIA44	8	Ol 1	0.87	0.03	<0.0010		0.014	0.007
		Ol 1	0.51	0.02	<0.0010		0.026	0.006
		Ol 1	0.94	0.03	<0.0010		0.011	0.006
		Ol 1	0.67	0.04	<0.0010		0.009	0.005
PIA120	2	Ol 1	1.05	0.02	0.001	0.001	0.014	0.006
		Ol 1	0.97	0.02	<0.0010		0.007	0.003
PIA109	2	Ol 1	0.94	0.03	<0.0010		0.010	0.005
		Ol 1	0.72	0.02	<0.0010		0.022	0.008
		AMPHIBOLE						
PIA27	3	Ed hbl	2.4	0.1	0.002	0.001	0.08	0.01
		Ed hbl	2.1	0.2	<0.0010		0.06	0.02
	1	Ath	0.7	0.1	0.002	0.001	0.40	0.06
	2	Tr	0.03	0.01	<0.0010		1.17	0.06
		Tr	0.08	0.02	<0.0010		1.5	0.2
PI6	3	Tr	1.6	0.3	<0.0010		2.8	0.1
		Tr	0.09	0.02	0.001	0.001	1.7	0.1
		Tr	0.06	0.03	0.001	0.001	1.19	0.07
PIA120	3	Prg	0.6	0.1	0.003	0.001	<0.0026	
		Prg	1.1	0.1	0.004	0.001	0.02	0.01
		Prg	0.62	0.05	0.004	0.001	0.03	0.01
PIA109	2	Prg	1.7	0.1	0.012	0.003	0.04	0.01
		Prg	0.9	0.1	<0.0010		0.05	0.02

Sample	N	Mineral	Li (µg/g)	2σ	Be (µg/g)	2σ	B (µg/g)	2σ
		ORTHOPYROXENE						
PI2	25	Opx 1	1.14	0.07	<0.0014		0.07	0.01
		Opx 1	0.9	0.1	<0.0014		0.05	0.01
		Opx 1	0.70	0.09	<0.0014		0.02	0.01
		Opx 1	0.85	0.08	<0.0014		<0.0037	
	2	Opx 2	0.88	0.09	<0.0014		0.06	0.03
		Opx 2	0.7	0.1	<0.0014		0.39	0.05
PIA27	6	Opx 1	0.10	0.02	<0.0010		0.04	0.01
		Opx 1	0.20	0.03	<0.0010		0.03	0.01
		Opx 1	0.34	0.02	<0.0010		0.04	0.01
		Opx 1	0.45	0.07	<0.0010		0.17	0.03
PI6	4	Opx 1	0.10	0.03	0.001	0.001	0.02	0.01
		Opx 1	0.29	0.04	<0.0010		0.03	0.01
		Opx 1	0.29	0.07	<0.0010		0.02	0.01
PIA44	7	Opx 1	0.62	0.05	<0.0010		0.01	0.01
		Opx 1	0.69	0.06	<0.0010		0.01	0.01
		Opx 1	0.64	0.08	<0.0010		0.018	0.005
		Opx 1	0.55	0.03	<0.0010		0.02	0.01
PIA120	4	Opx 1	0.44	0.03	<0.0010		0.009	0.003
		Opx 1	0.66	0.05	<0.0010		0.010	0.004
		Opx 1	0.61	0.04	0.001	0.001	<0.0026	
		Opx 1	0.20	0.03	<0.0010		0.02	0.01
	2	Opx 2i	0.26	0.04	<0.0010		<0.0026	
		Opx 2i	0.26	0.02	<0.0010		0.03	0.01
PIA109	9	Opx 1	0.88	0.07	0.002	0.001	0.007	0.004
		Opx 1	0.64	0.05	0.002	0.001	0.009	0.005
		Opx 1	1.49	0.04	0.002	0.001	<0.0026	
		Opx 1	1.30	0.06	0.001	0.001	<0.0026	
	4	Opx 2i	0.64	0.04	0.002	0.001	0.008	0.003
		Opx 2i	0.94	0.04	0.001	0.001	0.011	0.004
		Opx 2i	0.81	0.05	<0.0010		0.007	0.004
		Opx 2i	0.68	0.04	0.001	0.001	<0.0026	
		PLAGIOCLASE						
PIA109	2	Pl	<0.0014		0.007	0.002	<0.0026	
		Pl	<0.0014		0.005	0.002	0.015	0.006

N: total number of analyses.

Table 2.8: continued

Sample	N	Mineral	Li (µg/g)	2σ	Be (µg/g)	2σ	B (µg/g)	2σ
		CLINOPYROXENE						
PI2	7	Cpx 1	3.3	0.2	<0.0014		<0.0037	
		Cpx 1	3.0	0.2	<0.0014		<0.0037	
		Cpx 1	2.5	0.1	<0.0014		0.58	0.07
		Cpx 1	1.5	0.1	<0.0014		0.12	0.03
	2	Cpx 2	3.2	0.2	<0.0014		<0.0037	
		Cpx 2	2.2	0.2	0.002	0.001	0.19	0.03
PIA27	2	Cpx exsol	0.47	0.04	<0.0010		0.25	0.03
		Cpx exsol	0.4	0.1	<0.0010		0.26	0.03
PI6	5	Cpx 1	0.6	0.1	0.003	0.002	0.020	0.009
		Cpx 1	0.8	0.1	<0.0010		0.02	0.01
		Cpx 1	0.11	0.03	<0.0010		0.01	0.01
		Cpx 1	1.8	0.1	<0.0010		0.023	0.009
PIA44	8	Cpx 1	2.4	0.1	<0.0010		0.015	0.008
		Cpx 1	3.0	0.2	0.001	0.001	0.02	0.01
		Cpx 1	2.7	0.1	<0.0010		0.03	0.01
		Cpx 1	3.7	0.2	<0.0010		0.05	0.01
PIA120	2	Cpx 1	1.7	0.1	0.004	0.005	<0.0026	
	2	Cpx 1	0.20	0.02	<0.0010		0.008	0.006
	2	Cpx 2i	1.5	0.1	0.003	0.002	0.03	0.01
	2	Cpx 2i	0.77	0.05	0.005	0.003	0.008	0.003
PIA109	2	Cpx 1	3.3	0.1	<0.0010		<0.0026	
	2	Cpx 1	3.7	0.1	0.004	0.002	<0.0026	
	2	Cpx 2i	2.8	0.1	0.004	0.001	0.06	0.01
	2	Cpx 2i	3.0	0.1	0.003	0.001	0.037	0.008
		ALTERATION PHASES AFTER PLAGIOCLASE						
PIA120	2	Chl 2	2.0	0.1	<0.0010		0.07	0.01
		Chl 2	3.3	0.2	<0.0010		0.27	0.05
	3	Ntr	0.01	0.01	<0.0010		0.007	0.003
		Ntr	0.1	0.1	<0.0010		0.010	0.004
		Ntr	0.01	0.01	<0.0010		0.009	0.005
	3	Vua	0.03	0.01	0.002	0.001	0.26	0.04
		Vua	0.4	0.1	0.001	0.001	0.22	0.03
		Vua	0.2	0.1	0.002	0.001	0.23	0.03
PI6	2	Pct	5.1	0.3	<0.0010		0.10	0.03
		Pct	11.0	0.5	<0.0010		0.8	0.3

Sample	N	Mineral	Li (µg/g)	2σ	Be (µg/g)	2σ	B (µg/g)	2σ
		SERPENTINE						
PIA27	3	Srp 1 (ol)	0.05	0.03	0.001	0.001	22	1
		Srp 1 (ol)	0.07	0.03	<0.0010		28	1
		Srp 1 (ol)	0.27	0.03	<0.0010		11.0	0.1
	3	Srp 2 (opx)	0.27	0.02	<0.0010		6	1
		Srp 2 (opx)	0.32	0.06	0.001	0.001	4.6	0.4
		Srp 2 (opx)	0.23	0.03	0.001	0.001	9	1
PI6	1	Srp (ol)	0.32	0.06	<0.0010		5	1
	3	Srp (opx)	0.08	0.02	<0.0010		3	1
		Srp (opx)	0.48	0.05	<0.0010		0.8	0.3
		Srp (opx)	0.20	0.04	<0.0010		0.6	0.2
PIA44	3	Srp (ol)	0.09	0.02	<0.0010		0.12	0.04
		Srp (ol)	0.19	0.03	<0.0010		0.07	0.02
		Srp (ol)	0.09	0.01	<0.0010		0.09	0.04
	2	Srp (opx)	(9.0)	0.5	0.001	0.001	(0.53)	0.03
		Srp (opx)	(3.2)	0.3	<0.0010		(1.0)	0.1
PIA120	3	Srp (ol)	0.78	0.05	<0.0010		0.41	0.03
		Srp (ol)	<0.0014		<0.0010		0.57	0.03
		Srp (ol)	<0.0014		<0.0010		0.8	0.1
PIA109	4	Srp (ol)	0.14	0.02	<0.0010		9	2
		Srp (ol)	0.13	0.02	<0.0010		10	1
		Srp (ol)	0.12	0.02	<0.0010		4	1
		Srp (ol)	0.16	0.02	<0.0010		24	5
		TALC						
PIA27	3	Tlc	0.15	0.03	<0.0010		4.0	0.6
		Tlc	0.12	0.03	<0.0010		0.7	0.1
		Tlc	0.10	0.02	<0.0010		0.8	0.1
PI6	2	Tlc	3.8	0.4	<0.0010		1.5	0.5
		Tlc	2.9	0.2	<0.0010		0.9	0.2

N: total number of analyses. Data in brackets represent mixtures of serpentine with talc (see comment in text).

Table 2.9: Whole rock data

PRESENT STUDY

Sample	Ol (%)	Cpx (%)	Opx (%)	Spl (%)	Pl (%)	Srp (%)	Other (%)		Li (µg/g)	Be (µg/g)	B (µg/g)
SPL HARZBURGITES									ICP-MS	ICP-MS	PGNAA
PI2	79.6	3.7	13.8	1.2		1.7			0.9	< 0.003	< 0.3
PIA91	78.0	3.9	16.0	1.9		0.0	0.2	Tr	1.0	< 0.003	
PIA27	64.5	0.2	6.6	1.0		19.1	8.6	Ed hbl, Tr, Ath, Tlc, Chl	0.6	< 0.003	1.1
PI6	46.3	0.8	3.0	0.7		46.9	2.3	Tr, Tlc, Pct	0.5	< 0.003	0.1
PIA44	36.8	1.0	5.0	1.6		55.4	0.2	Tr	0.8	< 0.003	< 0.3
PL-BEARING HARZBURGITES											
PIA120	35.7	1.9	5.0	0.3	2.0	41.1	14.0	Prg, Tr, Chl, Ntr, Vua, Pct	1.0	< 0.003	0.7
PIA51	66.1	4.7	18.2	1.9	0.2	8.5	0.4	Tr, Tlc, Chl, Vua	0.9	< 0.003	
PIA109	63.5	4.2	19.5	0.6	3.0	8.9	0.3	Prg, Tr	1.1	< 0.003	0.1

LITERATURE DATA

Paper	Data	Rock types	Li (µg/g)	Li (µg/g)	Li (µg/g)	Be (µg/g)	Be (µg/g)	Be (µg/g)	B (µg/g)	B (µg/g)	B (µg/g)
UNMETASOMATIZED MANTLE			av	max	min	av	max	min	av	max	min
Lyubetskaya & Korenaga (2007)	CAL	Primitive mantle composition	1.6			0.054			0.17		
McDonough & Sun (1995)	CAL	Primitive mantle composition	1.6			0.068			0.30		
Chaussidon & Jambon (1994)	CAL	Primitive mantle composition							0.25	0.35	0.15
Ottolini et al. (2004)	ANAL	Spl peridotites of Massif Central and Dreiser Weiher		1.80	1.60					0.10	0.07
Chaussidon & Libourel (1993)	EXP	Depleted mantle values estimated from experiments								0.30	0.05
Chaussidon & Marty (1995)	CAL	Depleted mantle values calculated								0.02	0.01
Salters & Stracke (2004)	CAL	Depleted mantle estimated composition	0.7			0.025			0.06		
ABYSSAL PERIDOTITES											
Thompson & Melson (1970)	ANAL	Dredged serpentinized peridotites, Vema fracture zone + Mid-Atlantic ridge								100	70
Bonatti et al. (1984)	ANAL	Dredged serpentinized peridotites, Vema + Romanche fracture zones, Atlantic							61	85	20
Spivack & Edmond (1987)	ANAL	Dredged serpentinized peridotites, Vema fracture zone, Atlantic							64	81	50
Decitre et al. (2002)	ANAL	Dredged fresh and serpentinized peridotites, South West Indian Ridge	3.5	8.2	0.6						
Niu (2004)	ANAL	Dredged abyssal peridotites, see details in the paper	6.0	13.7	0.6	0.044	0.212	0.001			
Boschi et al. (2008)	ANAL	Drilled serpentinized spl harzburgites, Atlantis Massif (30°N) Mid-Atlantic Ridge							66.6	90.6	34.0
Vils et al. (in prep.)	ANAL	Drilled serpentinized spl harzburgites, ODP Leg 209 Mid-Atlantic Ridge	0.7	3.4	0.1	0.0015	0.0080	0.0002	45.1	65.0	10.4
FOREARC PERIDOTITES											
Parkinson & Pearce (1998)	ANAL	Drilled serpentinized harzburgites, ODP Leg 125 Izu-Bonin-Mariana forearc	4.1	12.8	1.1						
Benton et al. (2001 and 2004)	ANAL	Drilled serpentinized peridotite clasts, Mariana forearc, Conical Seamount	5.9	18.9	1.6				24.3	57.5	6.8
Zanetti et al. (2006)	ANAL	Drilled serpentinized peridotites, ODP Leg 125+195 Izu-Bonin-Mariana forearc	4.7	12	1.6	0.11	0.16	0.07			
Savov et al. (2005)	ANAL	Serpentinized peridotites, Mariana Forearc, Conical Seamount	4.6	18.9	0.5				15.4	58.0	0.4
Wei et al. (2005)	ANAL	Serpentine muds, South Chamorro Seamount, Mariana forearc							58.7	79.0	39.4
PERIDOTITES INTERPRETED AS MODIFIED BY SLAB FLUIDS											
Scambelluri et al. (2004)	CAL	Serpentinized peridotite, Northern Apennine and Erro Tobbio	1.3						47.0		
Paquin et al. (2004)	CAL	Alpe Arami ultra-high pressure garnet peridotites				0.011			0.1		
Brooker et al. (2004)	ANAL	Metasomatized (hydrous fluid) spl lherzolites, Zabargad	3.2	4.1	2.5	0.063	0.213	0.012			
Ottolini et al. (2004)	ANAL	Metasomatized spl peridotites, Balmuccia and Zabargad	1.5	1.9	1.1				0.16	0.32	0.04
Scambelluri et al. (2006)	ANAL	Ulten spl peridotites and grt-amph peridotites		4.2	1.9		0.13	0.01			
OPHIOLITIC PERIDOTITES											
Marchesi et al. (2006)	ANAL	Mayari-Baracoa MOR- and transitional MOR-IAT-peridotites (Cuba)	0.35	0.70	0.23						
Li & Lee (2006)	ANAL	Feather River Ophiolite (California, USA)	0.95	3.09	0.23	0.03	0.06	0.01			
Agranier et al. (2007)	ANAL	Feather River Ophiolite (California, USA)	0.99	3.09	0.08				10.2	15.6	6.4

Literature data source, ANAL: analyzed, EXP: determined experimentally and CAL: calculated. Present-study results, ICP-MS: measured by Inductively Coupled Plasma Mass Spectrometry, PGNAA: measured by Prompt Gamma Neutron Activation Analysis. b.d.: below detection limit, av: average, max: maximum, min: minimum. ICP-MS Be detection limit: 0.0016 µg/g. For details about PGNAA detection limits see section 'Analytical techniques'.

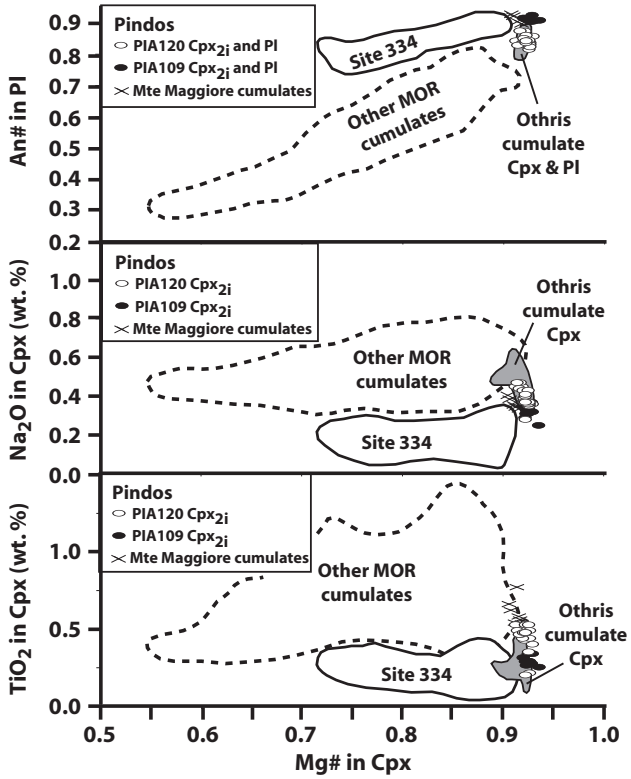


Fig. 2.9: Mineral compositions of melt-related (cumulate) minerals from the Pindos plagioclase-bearing harzburgites, compared to cumulate phases in oceanic rocks. Othris cumulates (grey field) from Dijkstra et al. (2001), Site 334 and other MOR cumulates fields from Ross & Elthon (1993), depleted cumulates of the Monte Maggiore (Corsica, France) ophiolitic peridotites from Rampone et al. (1997). Diagram modified from Fig. 1 of Ross & Elthon (1993).

depleted end of mid-ocean ridge cumulate compositions (Fig. 2.9). Anorthite contents in plagioclase ranges from 0.81 to 0.91 (Table 2.5, Fig. 2.9), which suggests that the melt was low in Na_2O. The crystallization of secondary orthopyroxene (Opx_{2i}), replacing olivine along the plagioclase-olivine boundary (Fig. 2.4d-e), indicates that the melt should have been relatively rich in silica. Clinopyroxene and plagioclase also have compositions similar to depleted cumulates crystallized in impregnated peridotites of the Monte Maggiore unit (Corsica, France, Rampone et al., 1997).

From all these chemical observations we conclude that the melt which impregnated the depleted harzburgites was depleted to ultra-depleted (i.e. melt produced by low-pressure partial melting of a refractory peridotite; Bloomer et al. 1989; Natland, 1989; Ross & Elthon, 1993; Sobolev & Shimizu, 1993; Dijkstra et al., 2001; Arai & Takemoto, 2007), or that the melt became depleted due to melt-rock reactions during percolation (Piccardo et al., 2004a).

Impact on Li, B and Be systematics

Bulk rock Li contents of all samples are similar to or higher than the depleted mantle value of Salters & Stracke (2004). Plagioclase-bearing harzburgites tend to have slightly higher Li contents than spinel harzburgites (Table 2.9), and there is a positive correlation between modal clinopyroxene and Li whole rock contents (Fig. 2.10). There is no difference between the Li contents of the primary mantle minerals in plagioclase-bearing harzburgites and in spinel harzburgites. In both rock types, clinopyroxene is enriched in Li compared to clinopyroxene from unmetazomatised mantle and shows a similar range of values (Fig. 2.11a). Li contents of olivine and orthopyroxene are comparable to or slightly lower than those of unmetasomatized mantle minerals (Fig. 2.11a-b). Values for Li in olivine are constant between 0.5 and 1.0 μg/g. This could be due to the extremely refractory character of the harzburgites prior to the infiltration event.

$^{opx/cpx}D_{Li}$ and $^{ol/cpx}D_{Li}$ of Pindos harzburgites are not those expected for equilibrated peridotites (Fig. 2.11a-b; Eggins et al., 1998; Seitz & Woodland, 2000; Kaliwoda, 2004; Ottolini et al., 2004; Kaeser et al., 2007). According to Seitz & Woodland (2000), Li enrichment in clinopyroxene can be related to metasomatism by mafic silicate melt or hydrous fluid. As textural evidence shows that melt infiltration occurred in the Dramala harzburgites, we consider that Li metasomatism is related to melt impregnation. Moreover, a similar Li metasomatism was observed in the Mid-Atlantic ridge ODP Leg 209 (Site 1274A) harzburgite by Vils et al. (in prep.), where melt metasomatism was described by Seyler et al. (2007). The preferential input of Li in clinopyroxene during impregnation of peridotites by mafic silicate melts was also observed by Eggins et al. (1998), Ottolini et al. (2004) and Woodland et al. (2004) (Fig. 2.11a).

Bulk rock B contents cannot be unequivocally related to melt infiltration, as they were potentially modified by serpentinization (see section 'Low-

temperature hydration - impact on Li, Be and B systematics'). Measured B abundances in primary minerals tend to be comparable to or even slightly lower than values for unmetasomatized mantle (Table 2.8, Fig. 2.8c). Measured bulk rock Be contents are two orders of magnitude lower than values for depleted or primitive mantle (Table 2.9), and Be contents of primary minerals are generally below detection limits (Table 2.8). The addition of little B (compared to Li) to the bulk rock during melt infiltration event, could be explained by the lower mineral/melt partition coefficients for B as compared to Li for olivine, clinopyroxene and orthopyroxene ($^{ol/melt}D_{Li}$ = 0.13-0.35, $^{cpx/melt}D_{Li}$ = 0.14-0.27, $^{opx/melt}D_{Li}$ = 0.20, $^{ol/melt}D_{B}$ = 0.003-0.008, $^{cpx/melt}D_{B}$ = 0.016-0.025, $^{opx/melt}D_{B}$ = 0.018; Brenan et al., 1998a). However, this cannot explain the overall depletion in Be, as Be and B show similar mineral/melt partition coefficients for olivine, clinopyroxene and orthopyroxene ($^{ol/melt}D_{Be}$ = 0.0015-0.0029, $^{cpx/melt}D_{Be}$ = 0.0025-0.021, $^{opx/melt}D_{Be}$ = 0.0016; Brenan et al., 1998a). The impregnating melt must have been poor in Li and B, and highly depleted in Be, in agreement with the postulated ultra-depleted character (see previous section).

In principle, the preferential enrichment of clinopyroxene in Li could alternatively be explained by fractionation upon cooling. This was observed in some slowly cooled orogenic peridotites (Alpe Arami, Central Swiss Alps) by Paquin et al. (2004). Coogan et al. (2005) performed experiments on Li diffusion between Li-doped olivine and clinopyroxene at high temperature (800 to 1000 °C). Li diffused into clinopyroxene within hours under these conditions. Jeffcoate et al. (2007) suggested a higher diffusivity of Li in clinopyroxene relative to olivine for some Hawaiian phenocrysts.

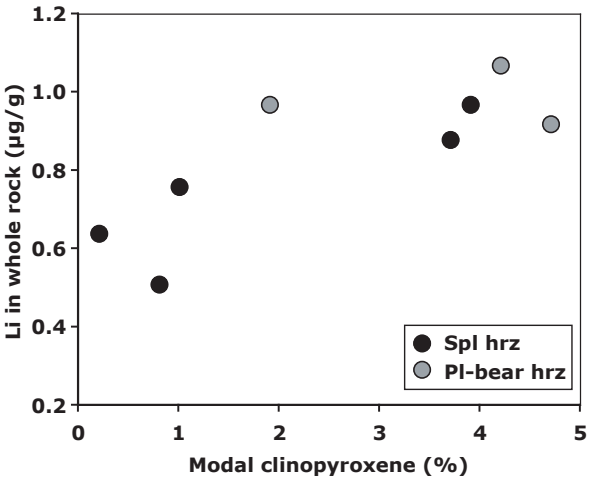


Fig. 2.10: Positive correlation between Li whole rock content (μg/g) and modal clinopyroxene (%) in the Dramala spinel (Spl hrz) and plagioclase-bearing (Pl-bear hrz) harzburgites.

In our samples, no systematic increase of Li at clinopyroxene rims was observed which could point to a diffusive enrichment of clinopyroxene during initial cooling. However, given the rapid diffusion of Li (Coogan et al. 2005), such an early enrichment pattern is unlikely to survive. In the Dramala samples, Li usually decreases rimward in olivine, orthopyroxene and clinopyroxene. This pattern most likely reflects late cooling during serpentinization, with some Li loss from primary minerals to serpentine, talc, tremolite and chlorite (Fig. 2.10a-b). In conclusion, diffusive repartitioning during initial high-temperature cooling may have contributed to Li enrichment in clinopyroxene. Nevertheless, the textural and chemical evidence for melt infiltration and the positive correlation between modal clinopyroxene and Li bulk rock contents suggest that there was Li input by a melt. Also, even if cooling accounts for a part of the Li enrichment in clinopyroxene, it cannot have created the Li enrichment observed in whole rock samples.

High-temperature hydration - impact on Li, B and Be systematics

Pargasite and edenitic hornblende are considered as high-temperature hydrous phases here. They pseudomorph clinopyroxene crystallized from a melt (sample PIA27; Fig. 2.4b) and replace clinopyroxene exsolutions in orthopyroxene clasts (samples PIA27, Fig. 2.4b; PIA109 and PIA120). These textures show that they were not crystallized from a melt but later from a high-temperature fluid.

As stated in the previous section, B contents of whole rock samples and minerals are similar to those of unmetasomatized mantle, and Be contents are considerably lower (Table 2.9). Li contents of primary minerals are also comparable to their respective values for unmetasomatized mantle (Fig. 2.8); only clinopyroxene and the bulk rock were enriched in Li by metasomatism of a mafic melt (see previous section). Therefore, high-temperature hydration cannot have added significant amounts of light elements to rocks and minerals. Its effect

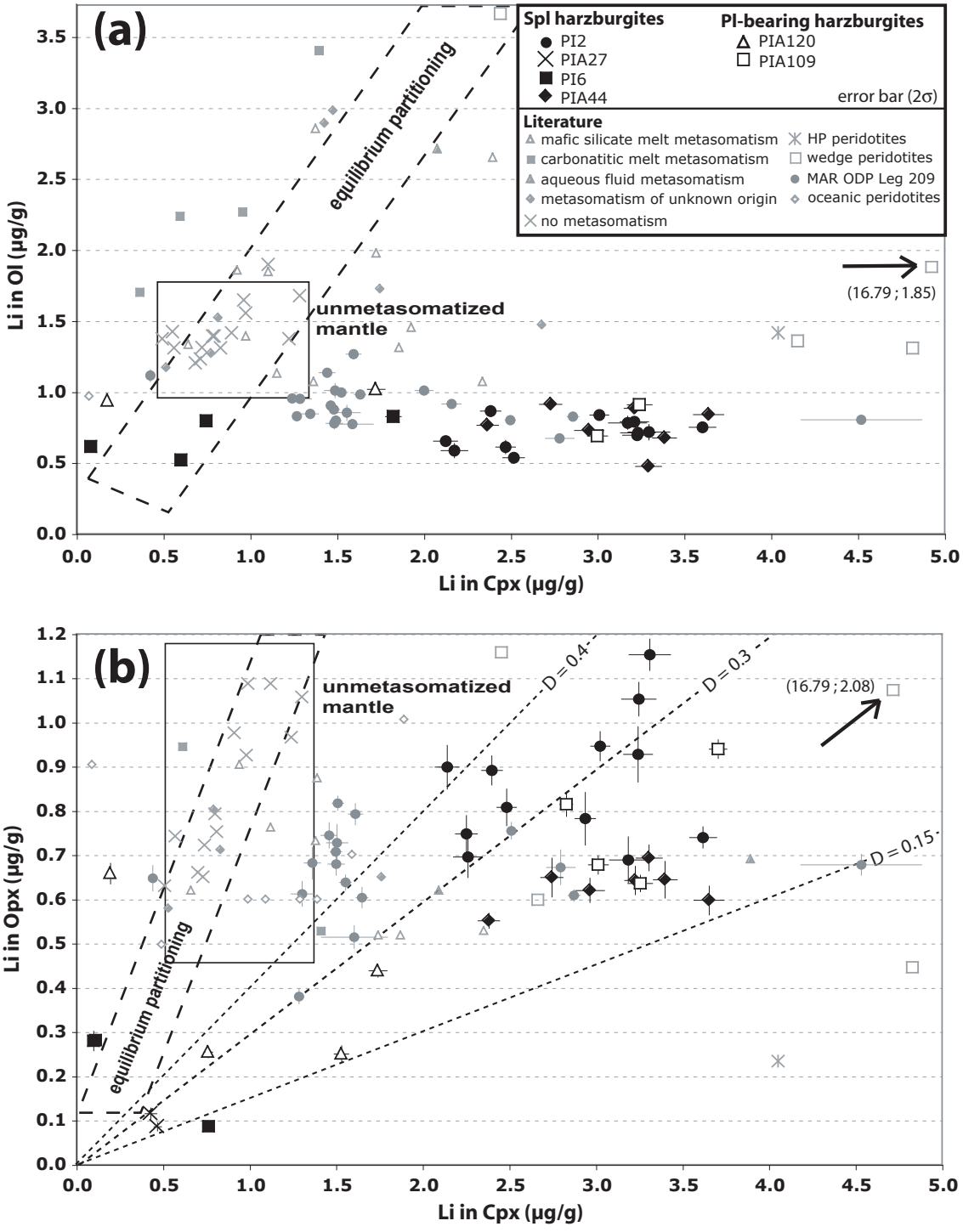


Fig. 2.11: Li-Li diagrams modified after Seitz & Woodland (2000) showing Li abundances in coexisting (a) clinopyroxene and olivine and (b) clinopyroxene and orthopyroxene from the Pindos spinel and plagioclase-bearing harzburgites. For sample PIA27, results represent clinopyroxene exsolutions in orthopyroxene. Equilibrium partitioning field after Seitz & Woodland (2000) and unmetasomatized mantle box after Ottolini et al. (2004). Mid-Atlantic ridge ODP Leg 209 serpentinites are represented for comparison (Vils et al., in prep.). Literature data: Eggins et al. (1998), Seitz & Woodland (2000), Decitre et al. (2002), Ottolini et al. (2004), Paquin et al. (2004), Scambelluri et al. (2004), Wagner & Deloule (2004), Woodland et al. (2004), Scambelluri et al. (2006), Kaliwoda (2004) and Kaeser et al. (2007).

seems to be limited to the formation of amphibole which has lower Li and B and higher Be contents than clinopyroxene. This is in line with amphibole-fluid partition coefficients for Be that are generally higher than those for B and Li (Brenan et al., 1998b).

The crystallization of hornblende and tremolite after clinopyroxene was described from the Zabargad peridotites by Agrinier et al. (1993), and interpreted as resulting from interaction of a seawater-derived fluid with peridotite. For peridotites from the Voltri massif (NW Italy), Hoogerduijn Strating et al. (1993) explained pargasite grown at the expense of clinopyroxene by a fluid related to a melt infiltration event. We used the partition coefficients for B and Be (no data for Li) between amphibole and fluid at high temperatures to calculate the composition of the fluid related to the formation of pargasite and edenitic hornblende in the Dramala harzburgites (Brenan et al. 1998b; $^{Amph/fluid}D_{Be} \sim 0.26$ and $^{Amph/fluid}D_{B} \sim 0.016$). However, there are several shortcomings to this approach. The experiments, in which the partition coefficients were determined, were performed in a basaltic system at 900°C and 2.0 GPa. The amphibole/fluid partition coefficients are probably dependent on temperature, pressure and pH, and no B partition coefficient were determined for hornblende at lower pressure. Only one fluid composition was calculated for pargasite and edenitic hornblende, as their Be and B contents are similar (Table 2.8). The calculated fluid composition ranges from < 0.01 to 0.02 μg/g and < 1.3 to 5.0 μg/g for Be and B respectively. This composition would be in agreement with seawater for B, but not for Be (seawater composition: Be ~ 0.0002 ng/g and B ~ 4.4 μg/g; Noakes & Hood, 1961, Measures & Edmond, 1982). However, edenitic hornblende and pargasite form at temperatures above 750°C (Lykins & Jenkins, 1992; Sharma & Jenkins, 1999). During high temperature alteration of oceanic basalts, B is preferentially partitioned into the liquid phase (Thompson & Melson, 1970). B loss from seawater during high temperature serpentinization is minimum (Bonatti et al., 1984). Measures & Edmond (1983) show that Be is strongly enriched in ridge crest hydrothermal solutions, with values 400 to 1600 times higher than seawater. It is therefore likely that seawater was heated and passed through mafic rocks or other peridotites before reacting with the Dramala mantle section.

Low-temperature hydration - impact on Li, B and Be systematics

Talc, tremolite, serpentine, magnetite, and the plagioclase alteration phases natrolite, vuagnatite, pectolite and chlorite are considered as low-temperature hydrous phases here. Textural observations (see section 'Sample characteristics') and comparison with literature data on orthopyroxene and olivine hydration (see section 'Interpretation of specific textures) show that the crystallization sequence with decreasing temperature is talc + tremolite ± serpentine ± olivine at T ≥ 350-400°C, followed by serpentine + magnetite at T < 250°C, followed by the plagioclase alteration phases down to T < 100°C.

Considering the high Li contents of talc and the high B contents of metamorphic olivine compared to the primary minerals (Table 2.8), the formation of these minerals by hydration of pyroxene at T ≥ 350-400°C should increase the bulk Li and B contents of the whole rock samples. However, the modes of talc and metamorphic olivine are very low, probably because cooling proceeded fast and fluid-rock ratios were low. Also, most of the talc was transformed to serpentine which likely removed most of the Li.

Serpentine is the major hydrous phase and can represent up to 55 vol. % of the whole rock. It is the major carrier of B with up to 28 μg/g (Fig. 2.8, Table 2.8). Its Be contents are < 3 ng/g. The Li contents are most likely less than 1 μg/g, and only considerably higher (up to 9 μg/g), if serpentine is intergrown with talc (Fig. 2.8, Table 2.8, see section 'Li, B and Be contents of rock-forming minerals'). Thus, serpentinization of the Dramala mantle by reaction with external fluid should have essentially increased the B whole rock contents and to a much lesser degree – if at all - also the Li whole rock contents. However, this is not what we observe. Measured B whole rock abundances (0.1 - 1.1 μg/g) are only slightly higher than values for unmetasomatized mantle (0.06 - 0.3 μg/g), and 1 to 2 orders of magnitude lower than values for drilled (10.4-65.0 μg/g see Table 2.9) or dredged (20-100 μg/g see Table 2.9) abyssal peridotites. Measured Li abundances (0.5 - 1.1 μg/g) in the whole rock samples from Dramala are close to the values for unmetasomatized mantle (0.7 - 1.6 μg/g), considerably lower than values for dredged abyssal peridotites (3.5 - 6.0 μg/g), but similar to values for drilled abyssal peridotites (0.7 μg/g). Also, there

is no positive correlation between the degree of serpentinization and the B contents, due to the fact that the B contents of serpentine are highly variable (0.1 - 28 μg/g). Some of the highest B contents in serpentine were found in low serpentinized peridotites (Fig. 2.8), where the percentage of serpentine is < 20 % (Table 2.9). We believe that several parameters may be responsible for the non-systematic behaviour of B (and to a lesser degree Li) during low-temperature hydration.

(1) Fluid-rock ratio and fluid composition: Fluid-rock ratio was probably low, as suggested by the fairly low degree of serpentinization in the Dramala mantle compared to drilled and dredged oceanic samples. Low fluid-rock ratios induce local differences in fluid composition and disequilibrium, as indicated by variable B contents of serpentine. Also, during serpentinization, the Dramala mantle may have been covered by igneous crust and was not exposed to seawater but to evolved fluids with highly variable compositions, which had interacted with the mafic crust before (Smith et al., 1995; Decitre et al., 2002).

(2) Temperature, pH and time: When depleted mantle rocks (Li ~ 0.7 μg/g, B ~ 0.06 μg/g; Salters & Stracke, 2004) react with seawater (Li ~ 0.2 μg/g, B ~ 4.44 μg/g; Li, 1982) at low temperatures and equilibrium conditions (Thompson & Melson, 1970; Seitz & Hart, 1973; Seyfried & Dibble, 1980; Bonatti et al., 1984; Spivack & Edmond, 1987; Decitre et al., 2002; Scambelluri et al., 2004; Paulick et al., 2006), they become enriched in B and Li. Seyfried & Dibble (1980) showed experimentally that B is preferentially incorporated in serpentine at low temperature (< 300°C). However, Boschi et al. (2008) demonstrated that B exchange between seawater and peridotites during serpentinization is mainly controlled by pH of the serpentinizing fluid. During the early-stage serpentinization when pH is low (4-6), the B-uptake in serpentine is low, while during the late-stage serpentinization when pH is higher (6-8), more B can be incorporated into serpentine.

Serpentinization in the Dramala harzburgite very likely began at temperatures above 350-400°C. In abyssal environments, known high-temperature fluids (> 350°C) such as those of the Logatchev and Rainbow hydrothermal fields (Mid-Atlantic ridge) show pH < 3 (Douville et al., 2002; Schmidt et al., 2006). It is possible that such fluids reacted with the Dramala mantle and produced low-B serpentine, which is in agreement with Boschi et al. (2008) observations. Then, serpentinization in the Dramala harzburgite continued down to low temperatures (and probably higher pH) and formed serpentine with a higher B-content. As cooling most likely proceeded quickly, serpentine could not re-equilibrate with seawater. This would explain the presence of high- and low-B serpentine. This hypothesis is in agreement with Boschi et al. (2008), who showed that processes related to low temperature marine weathering do not change the B content of serpentinites.

The very late formation of the plagioclase alteration phases should lead to an increase in Li contents due to the high abundances of this element in chlorite and pectolite. Again, the modes of these phases are extremely low so that the light element budget is not modified.

Summary

Before melt impregnation, hydration and cooling, the Dramala harzburgites represented depleted oceanic mantle characterized by extraction of more than 15% partial melt (Saccani & Photiades, 2004) and very low light element contents.

The infiltration of a mafic melt led to modal metasomatism in the plagioclase-bearing harzburgites and to mainly cryptic metasomatism in the spinel harzburgites. In both rock types, metasomatism added Li to clinopyroxene and to the bulk. Little or no B and no Be were added due to the depleted character of the melt.

Hydration and cooling at high temperatures formed amphibole but left the light element contents of bulk and primary minerals unchanged. The fluid calculated to be in equilibrium with the amphiboles could be reaction-modified seawater.

Serpentinization led to a very moderate increase in B (and eventually in Li) in most whole rock samples. Bulk Be contents and light element contents of all pre-existing minerals remained unchanged. The non-systematic behaviour of B in whole rock samples and serpentine may be explained by low fluid-rock ratios, decreasing temperature and lack of equilibrium due to fast exhumation.

The extremely low Be contents of minerals and whole rock samples remains enigmatic.

CONCLUSION

The Dramala harzburgites: MOR- rather than SSZ-type mantle

Bizimis et al. (2000) interpreted the Pindos harzburgites as supra-subduction zone (SSZ) mantle wedge peridotites, modified by subduction-related hydrous melting. This interpretation is based on the spoon-shaped rare earth element (REE) patterns of some Dramala harzburgites and clinopyroxenes (see 'Introduction'). Saccani & Photiades (2004) proposed a possible SSZ origin for the Pindos harzburgites, based on the composition of the associated lavas of the Aspropotamos complex (Fig. 2.2), which include IAT and boninites, in addition to N-MORB. The high Cr # of spinel in some samples of the Dramala Complex (> 0.6; Fig. 2.5a-b, and Economou-Eliopoulos & Vacondios, 1995) could be added to the previous arguments, but as set out in the introduction, none of these characteristics is distinctive of melting of the mantle in a SSZ setting. In addition, the lavas with IAT and boninite characteristics come from the Aspropotamos Complex which is only in tectonic contact with the Dramala Complex.

Dramala harzburgites have some textures typical of MOR-type mantle, for example, the presence of macroscopic plagioclase lenses and pods (Fig. 2.4d; Girardeau & Francheteau, 1993) and primary clinopyroxene grains with embayments filled by olivine, which are in optical continuity and associated with plagioclase (Fig. 2.4f; Seyler et al., 2001). High temperature amphibole is sparse in the Pindos peridotites. These amphiboles have very low Be contents (< 0.02 μg/g) compared to high-temperature amphiboles of SSZ-type peridotites

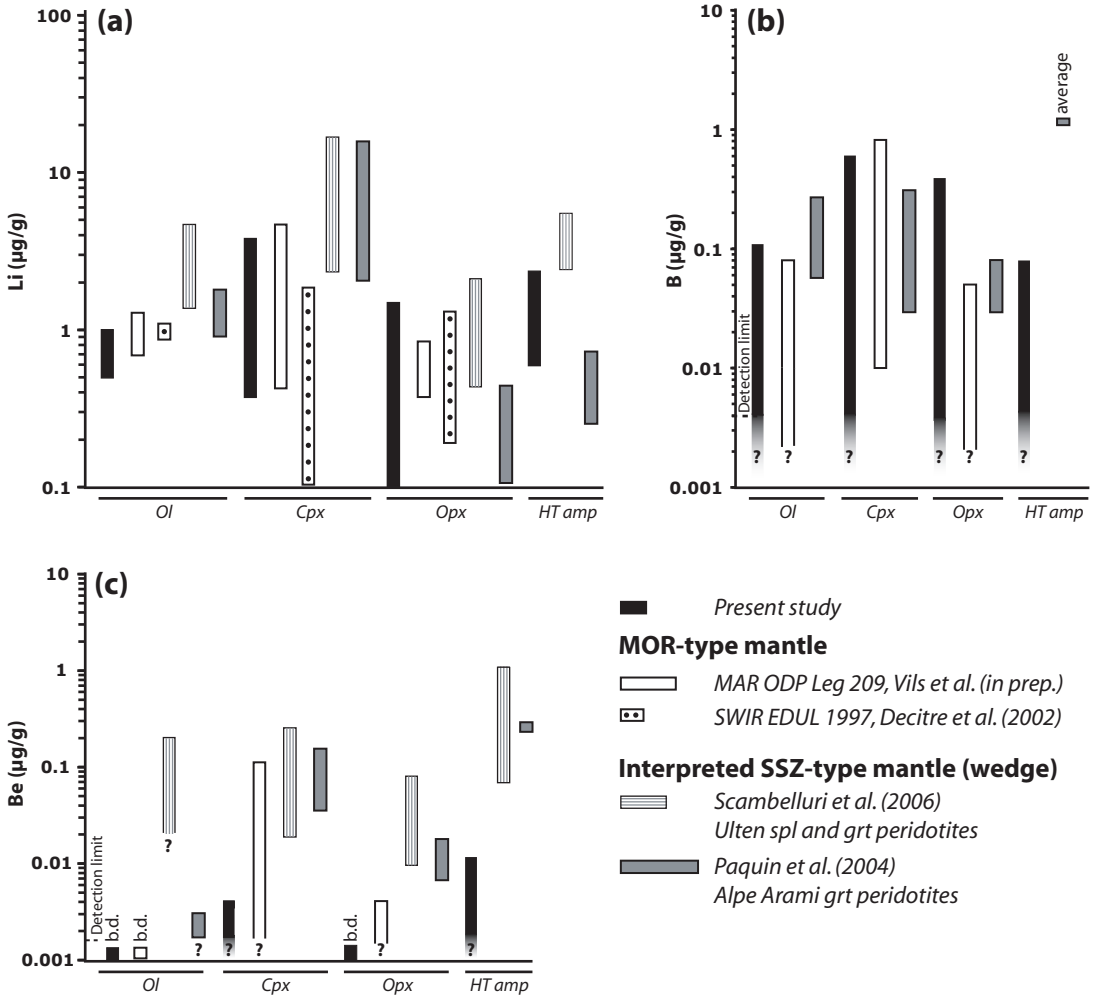


Fig. 2.12: (a) Li, (b) B and (c) Be contents of olivine, orthopyroxene, clinopyroxene and high temperature amphiboles from the Pindos mantle and from mid-ocean ridge (MOR)-type mantle and supra-subduction zone (SSZ)-type mantle. b.d.: below detection limit.

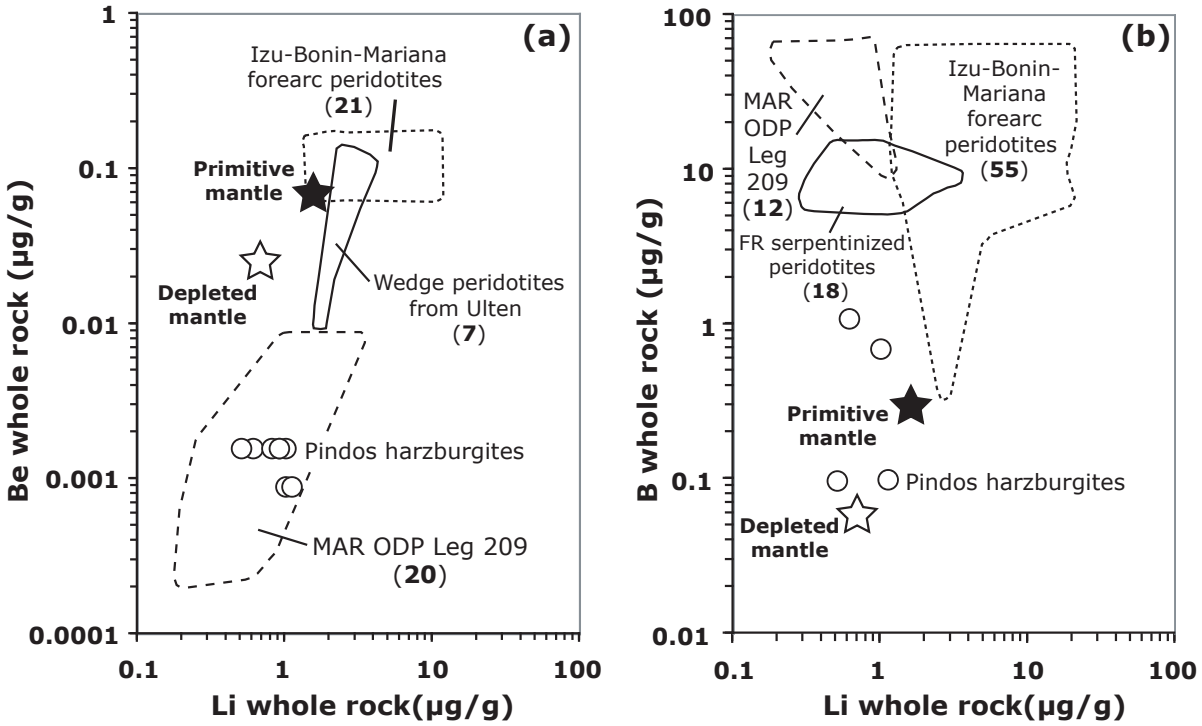


Fig. 2.13: (a) Li vs Be diagram of whole rock estimates from Pindos harzburgites. Detection limit values of the ICP-MS were plotted for Be as indicative in the Pindos harzburgites, as all results are below the detection limit. (b) Li vs B diagram of whole rock estimates from Pindos harzburgites. Mid-Atlantic ridge ODP Leg 209 peridotites of Vils et al. (in prep.), Ulten wedge peridotites from Scambelluri et al. (2006), Feather River (FR) serpentinized peridotites after Agranier et al. (2007) and Izu-Bonin-Mariana forearc peridotites of Benton et al. (2001 and 2004), Savov et al. (2005) and Zanetti et al. (2006) are represented for comparison. Depleted mantle after Salters & Stracke (2004) and primitive mantle after McDonough & Sun (1995). Note that bold numbers in brackets represent the number of samples analyzed. For Vils et al. (in prep.), Be data were calculated and Li data were measured.

(0.24 – 1.10 μg/g; Fig. 2.12c), and were probably formed during the interaction between Pindos harzburgite and seawater, but certainly not with a subduction-related fluid (see below).

In Figure 2.12, the Li, Be and B contents of the primary mantle minerals and high-temperature amphiboles of the Dramala harzburgites are compared to values for minerals from MOR-type peridotite and peridotite interpreted as related to SSZ-type settings. This comparison is problematic because there are no Li, B and Be mineral data for modern SSZ environments (Izu-Bonin-Mariana forearc), but only whole rock data (Table 2.9). Mineral data have to be taken from alpinotype peridotites that are interpreted as SSZ-related (Table 2.9). The light element contents of these minerals may have been modified during their emplacement into continental crust. Comparison between Dramala harzburgites and SSZ-attributed alpine peridotites (Paquin et al., 2004; Scambelluri et al., 2006) reveals many differences. Clinopyroxene and olivine from the SSZ-related samples is enriched in Li compared to Dramala clinopyroxene. An enrichment in B in olivine and high-temperature amphiboles of these peridotites is also characteristic. The most striking feature is the much higher Be content of clinopyroxene, orthopyroxene and high-temperature amphibole in minerals from SSZ-attributed alpine peridotites compared to Dramala. It is important to note that the measured Li, Be and B contents of all minerals from Dramala harzburgites are similar to the data from ODP Leg 209 sites 1272A and 1274A (Mid-Atlantic ridge; Vils et al., in prep.) and from the South West Indian ridge (Decitre et al., 2002), which represent MOR-type mantle.

Concerning whole rock data, Li, B and Be values are available for mantle from modern SSZ settings (Table 2.9). From Figure 2.13 and Table 2.9, it can be depicted that peridotites from the

Mariana and Izu-Bonin forearc have Li contents 4-10 times higher than those of Dramala mantle rocks, B contents are 2-3 orders of magnitude higher, and Be contents are at least 100 times higher. Be whole rock contents presented by Brooker et al. (2004) and Scambelluri et al. (2006) for Ulten and Zabargad wedge peridotites are also at least 1 order of magnitude higher than for Dramala samples. Li and Be whole rock contents for Dramala harzburgites are similar to those obtained by Vils et al. (in prep.) for ODP Leg 209 of the Mid-Atlantic ridge. B contents are much lower than published values for drilled serpentinized peridotites along the Mid-Atlantic ridge (11-91 μg/g; Boschi et al., 2008; Vils et al., in prep.), but this is probably due to higher temperatures during serpentinization (Fig. 2.12b).

In conclusion, the Dramala mantle shows many similarities with MOR-type mantle and many discrepancies to SSZ-type mantle. From the published data it seems that modern SSZ-related mantle is characterized by high contents of Li, Be and B. There is no difference in concentration level between drilled samples and those collected otherwise (Table 2.9). This means that alteration processes such as formation of clay minerals play no role, and that the elevated light element contents must be earlier features. Models predict that in SSZ settings, the mantle melts at relatively low temperatures due to influx of fluids released from a subducting slab (Davies & Stevenson, 1992 and references therein). These fluids are rich in B and Li, but also in Be (see 'Introduction'; Marschall et al., 2007, Li: 100 to 200 μg/g, B: 50-1200 μg/g, Be: 0.4-0.9 μg/g) and will enrich the mantle minerals in these elements. Moreover, as the geothermal gradient is lower than in MOR settings, serpentinization will probably take place at lower temperatures compared to MOR settings. Serpentine will thus be high in B and Li and add to the budget. It could be argued that with slow-spreading ridges, serpentinization continues down to low temperatures on the ocean floor and serpentine attains equilibrium with seawater. This is most likely true for modern MOR settings, but not necessarily for the Greek ophiolites. For Pindos and Vourinos ophiolites radiometric dating shows that crystallization of co-magmatic zircon in plagiogranite and gabbro (169-173 Ma; Liati et al., 2004) is virtually contemporaneous with formation of their metamorphic soles (169-176 Ma; Pe-Piper & Piper, 2002 and references therein). This means that the ophiolite mantle sections were hot and cooled quickly while being emplaced.

Tectonic setting of formation of the Pindos ophiolite

The Pindos ophiolite is a highly dismembered ophiolite, and there is no in situ contact between mantle harzburgite (Dramala complex) and the mafic rocks of the Aspropotamos complex (oceanic crust; Jones & Robertson, 1991). However, in some localities there are in situ contacts between the Dramala mantle and some MOR-type cumulates (Jones & Robertson, 1991). In the Aspropotamos complex, the crustal section shows successive phases of lava extrusion with a geochemical trend from high-Ti MORB to N-MORB/IAT (Island Arc Tholeiite) and finally to IAT-boninite-type for the youngest dykes (Capedri et al., 1980; Jones & Robertson, 1991; Jones et al., 1991; Kostopoulos, 1988; Pe-Piper et al., 2004; Beccaluva et al., 2005).

Li, Be and B contents of minerals and whole rock samples from Dramala harzburgite as well as textural and chemical evidence suggest that these rocks never interacted with subduction-related fluids or melts. Consequently, the Dramala mantle and the Aspropotamos crust apparently represent contrasting tectonic settings.

To resolve assemblage and evolution of the Pindos ophiolite is certainly beyond the scope of this paper, because an integrated structural, sedimentological, petrological and geochemical approach is required. Any proposed scenario must take into account (1) the juxtaposition of MOR-type mantle associated with (some) SSZ-type extrusives, (2) the occurrence of some ophicalcite in the Dramala mantle (Jones et al., 1991), showing that it was once exposed on the ocean floor, (3) the fact that the crustal section on top of the mantle is largely absent, which suggests that the Dramala mantle probably evolved in a slow-spreading environment, and (4) coincidence of the ages of plagiogranites, gabbros and metamorphic soles largely, indicating that oceanic spreading and thrusting were quasi-simultaneous. In addition, the Mesovouri mantle, cropping out in the southeastern part of the Pindos ophiolite (see Fig. 2), towards the Vourinos ophiolite, seems to be similar to the latter in terms of textures (A. Dijkstra, personal communication; no geochemical data available).

As the Vourinos ophiolite is commonly interpreted as SSZ-related, this could mean that the Dramala MOR-type mantle is juxtaposed with SSZ-type mantle, but at present this remains speculative.

(i) The Dramala mantle was formed in a back-arc setting, simultaneously with the Aspropotamos plutonics and extrusives, which formed in a forearc environment. These two units were later tectonically juxtaposed. Hawkins (2003) deduced from the observation of present-day SSZ-oceanic lithosphere, that crustal contraction would juxtapose arc, backarc and forearc crust. Therefore, rocks from different settings can be present in the same SSZ-ophiolite. The volcanic arc between the back-arc and forearc basins was probably a nascent arc. The presence of a MOR-type cumulate sequence at the top of the Dramala peridotite (Capedri et al., 1982; Rassios, 1991) is concordant with the fact that most extrusives present in back-arc environments have MORB character (Hawkins, 2003). Present-day equivalents would be the Lau Basin – Tonga Trench region of southwestern Pacific and the Mariana Trough – Mariana Trench region of the northwestern Pacific (Flower & Dilek, 2003).

(ii) The Dramala mantle was formed at a slow-spreading mid-ocean ridge, perhaps covered by a thin MOR-type crust, and was emplaced above an intra-oceanic subduction zone close to or directly at the ridge shortly after its formation (Boudier et al., 1988; Barth et. al., 2007). During this stage, island arc tholeiites and boninites erupted in a forearc setting, as proposed by Dilek & Flower (2003) and Flower & Dilek (2003). This can explain the presence of subduction-related lavas in association with MORB. However, it is difficult to imagine how the mantle preserved its MOR signature despite the passage of slab-derived fluids or melts. This would recquire that fluid flow from the slab is very localized.

ACKNOWLEDGEMENTS

We thank E. Gnos, A. Berger, T. Ludwig and H.-P. Meyer for analytical support and A. Dijkstra, O. Müntener and G. Suhr for comments and discussions. We thank H. Marschall for the whole rock analyses done at the University of Bristol. This work was financially supported by grants of the Swiss NSF (200020-112149) to A. Kalt. We also acknowledge financial support by the Swiss NSF grant 200021-103479/1 and by the Canton of Bern for the electron microprobe at the Institute of Geological Sciences, University of Bern.

N-MORB and ultra-depleted melt percolation in the Dramala harzburgites (Pindos ophiolite, Greece) and the famous spoon-shaped pattern

L. Pelletier[1], A.H. Dijkstra[1], A. Kalt[1] and T. Pettke[2]

[1]Institute of Geology and Hydrogeology, University of Neuchâtel, Emile Argand 11, CP158, 2009 Neuchâtel, Switzerland

[2]Institute of Geological Sciences, University of Bern, Baltzerstrasse 1-3, 3012 Bern, Switzerland

1st version manuscript - to be prepared for publication

Abstract

The Dramala harzburgites, which were tectonically assembled with subduction-related volcanics in the Pindos ophiolite (Greece), include spinel and plagioclase-bearing harzburgites, which followed a complex history of partial melting, melt percolation and melt impregnation. The Dramala mantle was subject to high degrees of partial melting (up to 22%), which mainly occurred in the spinel stability field, but probably began in the garnet peridotite field. This high degree of partial melting lead to very high Cr# in spinel (up to 0.67), to low modal clinopyroxene, to the depletion of the rock and its primary clinopyroxene in all the rare earth elements (REE) with a strong fractionation between light and heavy REEs ($[Ce/Yb]_N$ ratio of ~ 0.0001 in some clinopyroxene). The resulting spinel harzburgite was later percolated by an N-MORB type melt, which generated a spoon-shaped REE pattern in clinopyroxene and in the whole rock samples (mean $[Ce/Sm]_N$ of 1.42, mean $[Tb/Yb]_N$ of 0.08 in whole rock), by a selective enrichment in the light REEs compared to the heavy REEs. This melt metasomatism was accompanied by the crystallization of clinopyroxene, which was responsible for a Li enrichment in these rocks. This clinopyroxene crystallization explains the inconsistency observed between the high degree of partial melting and the modal content of clinopyroxene in some fresh Dramala spinel harzburgite (modal clinopyroxene 3-4%). Finally, the Dramala spinel harzburgite was percolated and impregnated by an ultra-depleted melt, with a REE composition similar to depleted and ultra-depleted melts reported in the literature. This ultra-depleted melt impregnation lead to the crystallization of plagioclase and clinopyroxene, turning the spinel harzburgite into a plagioclase-bearing harzburgite. Clinopyroxene from the Dramala plagioclase-bearing harzburgite is characterized by higher TiO_2, Na_2O, and lower Mg# compared to those in the Dramala spinel harzburgite, and plagioclase by $An_{0.81-0.91}$. Clinopyroxene and whole rock REE patterns resulting from this ultra-depleted melt impregnation are characterized by high light to heavy REE contents compared to those in the

Dramala spinel harzburgite, and by a strong fractionation between light and heavy REEs (mean $[Ce/Sm]_N$ of 0.05 in whole rock). A strong fractionation between light and middle REEs in plagioclase is also observed. All these results show that the Dramala mantle probably evolved in a mid-ocean ridge setting, and that the spoon-shaped REE pattern observed in clinopyroxene and whole rock samples from the Dramala spinel harzburgite could be related to N-MORB percolation in a depleted harzburgite. This scenario offers an alternative to the conventional hypothesis of subduction-related hydrous melting, postulated for some ophiolitic harzburgite (associated to subduction-related lavas), due to the observation of a spoon-shaped REE pattern in clinopyroxene or whole rock samples. This study shows that REE composition of clinopyroxene records a more detailed history of depletion and melt percolation than whole rock REE contents. In rare cases, clinopyroxene can conserve the REE pattern related high degrees partial melting, despite late melt percolation. The existence of ultra-depleted melt at mid-ocean ridges, which could be one component of MORB (generally considered as produced by polybaric melting of the mantle column beneath mid-ocean ridges), is a matter of debate. The present results confirm that this type of melt is certainly present at mid-ocean ridges, and could potentially be mixed with other melts to generate MORB.

Key words: supra-subduction zone ophiolite; harzburgite; trace elements; melt percolation; ultra-depleted melt; spoon-shaped pattern.

INTRODUCTION

The first detailed descriptions of ultra-depleted melts were reported from melt inclusions in olivine phenocrysts of MORB from the Mid-Atlantic ridge (Sobolev and Shimizu, 1993) and in primitive tholeiitic lavas from Iceland (Gurenko and Chaussidon, 1995). According to these authors, the ultra-depleted melts are characterized by TiO_2 between 0.2-1.0 wt. %, Mg# around 0.75, very low abundances of incompatible trace elements (except for Ti and Na) and extreme fractionation between light and heavy rare earth elements (REE). For comparison, the abundances of incompatible trace elements in primitive MORB are fifteen times higher (Sobolev and Shimizu, 1993). $[La/Sm]_N$ of such melts can be as low as 0.04, while primitive MORB shows a value of 0.35 (Sobolev and Shimizu, 1993).

In order to explain this very peculiar chemical composition, Sobolev and Shimizu (1993) postulated that these melts are very primitive trapped liquids, which represent the last fraction of melt produced in an ascending mantle column below a mid-ocean ridge. Moreover, their chemical composition cannot be produced by simple batch melting, but is produced during continuous (critical) melting (Sobolev and Shimizu, 1993; Gurenko and Chaussidon, 1995). This type of melting is characterized by low-degree partial melting, followed by melt extraction, but in contrast with fractional melting some melt is retained in the residue (Dick, 1976; Langmuir et al., 1977; Maaloe, 1982). This hypothesis is supported by experimental data, which shows that small fraction of partial melt can be efficiently extracted from the melting mantle (Riley and Kohlstedt, 1991). According to Sobolev and Shimizu (1993 and references therein), the ultra-depleted melts can be in equilibrium with a lherzolitic or an harzburgitic assemblage, and are produced at pressures ~ 5 kbar and temperatures of ~ 1250 °C. Gurenko and Chaussidon (1995) estimated that these melts can be produced at higher pressure (10-17 ± 5 kbar).

However, recent studies on melt inclusions revealed that the composition of ultra-depleted melt inclusions does not always reflect processes occurring in the mantle, but could be related to assimilation of gabbroic material into a hot primitive magma below a mid-ocean ridge (Danyushevsky et al., 2003). This process is supposed to occur in a high-porosity crystal mush, when the magma is passing through a zone of gabbroic cumulates. Moreover, Spandler et al. (2007) demonstrated that the REE content of melt inclusions can be drastically modified by rapid lattice diffusion in olivine, and that the REE pattern can be re-equilibrated with the host. It is therefore unclear whether the depleted character of melt inclusions is really representative of the depleted composition of the primary mantle melts from which they are derived.

In addition to ultra-depleted melt inclusions, ultra-depleted cumulates have been found along mid-ocean ridges. Some olivine gabbronorites collected at DSDP site 334 at the Mid-Atlantic ridge

have chemical characteristics similar to the melt inclusions described above (Ross and Elthon, 1993; Nonnotte et al., 2005). According to Nonnotte et al. (2005), these cumulates are mainly composed of Ca-rich plagioclase (An_{88}), Mg-rich clinopyroxene (Mg#: 0.87-0.89 with TiO_2: 0.09-0.14 wt. %) and orthopyroxene, associated with minor olivine. REE patterns of these clinopyroxenes mimic the ones from the ultra-depleted melt inclusions described above. They show very low concentrations in incompatible elements and a strong fractionation between light and heavy REEs with $[La/Sm]_N$ between 0.09 and 0.15 (Nonnotte et al., 2005). According to Ross and Elthon (1993) the calculated composition of the most depleted parental liquid related to these cumulates is strongly depleted (TiO_2 ~0.2 wt. %), shows very low concentrations in incompatible elements, and some fractionation between light and heavy REEs ($[La/Sm]_N$: 0.54).

(Ultra-)depleted melts are also observed in ophiolitic environments (Rampone et al., 1997; Dijkstra et al., 2003; Pelletier et al., submitted b). In this case, the depleted character of the melt is supposed to result from extensive reaction between an ascending melt and the surrounding peridotite during porous flow (Rampone et al., 1997; Piccardo et al., 2004), or to melting of already depleted peridotites at shallow levels (Dijkstra et al., 2003). In both cases, the melt is ascending and evolves from pyroxene-undersaturated to pyroxene-saturated, as deduced by Piccardo et al. (2004) in some Alpine-Apennine peridotites and by Dijkstra et al. (2003) in the Othris peridotites. According to Dijkstra et al. (2003), the increasing saturation of the melt in orthopyroxene is followed by a saturation in clinopyroxene and plagioclase during cooling. This process forms pyroxenes + plagioclase cumulates within the spinel peridotites (Rampone et al., 1997; Dijkstra et al., 2001 and 2003; Piccardo et al., 2004; Pelletier et al., submitted b), transforming the latter to plagioclase peridotites. Many plagioclase peridotites are commonly interpreted as resulting from impregnation of spinel peridotites by diffuse porous flow of melt, melt-rock reaction and fractional crystallization of plagioclase and pyroxenes (Dick, 1989; Rampone et al., 1997; Dijkstra et al., 2001 and 2003). The impregnated peridotites have a depleted character and contain Ca-rich plagioclase and Mg-rich clinopyroxene, as reported from the Monte Maggiore peridotites (Corsica, France) by Rampone et al. (1997), the Othris plagioclase peridotites (Greece) by Dijkstra et al. (2001 and 2003), and the Dramala plagioclase-bearing peridotites (Pindos, Greece) by Pelletier et al. (submitted b). In terms of trace elements, the calculated parental liquid of the cumulates found in some Othris plagioclase peridotites is strongly depleted in incompatible trace elements and shows a strong fractionation between light and heavy REEs (Dijkstra et al., 2003). The mineralogical composition and the trace element characteristics of these cumulates are similar to those observed in the DSDP site 334 cumulates of the Mid-Atlantic ridge (Ross and Elthon, 1993).

A recent study on the light element (Li, Be and B) content of Mg-rich clinopyroxene and Ca-rich plagioclase from the Dramala plagioclase-bearing peridotites (Pindos ophiolite, Greece) showed that these minerals could have crystallized as cumulates from an (ultra-)depleted melt (Pelletier et al., submitted b). This study also postulated that Dramala spinel peridotites could have been percolated by some melt. Bizimis et al. (2000) reported a spoon-shaped REE pattern in clinopyroxene and in the bulk of some Dramala spinel harzburgite, and postulated hydrous melting with subduction-related fluids in a supra-subduction zone setting. This interpretation is mainly based on the similar spoon-shaped REE pattern observed in some harzburgite from the Izu-Bonin-Mariana forearc mantle (Parkinson and Pearce, 1998; Ohara et al., 2002) and from the Lihir sub-arc mantle (Grégoire et al., 2001), but also on the fact that the spoon-shaped REE pattern in harzburgite is characteristic of some ophiolites where subduction-related lavas are reported (Bizimis et al., 2000; Godard et al., 2000; Barth et al., 2007). However, the spoon-shaped REE pattern was described in clinopyroxene from harzburgite from different mid-ocean ridges (Johnson et al., 1990; Wertz, 2003; Seyler et al., 2007), where hydrous-melting with subduction-related fluids can be definitely ruled out.

The objective of this paper is to test if the spoon-shaped REE pattern observed in the Dramala spinel harzburgite could be related to mafic melt metasomatism, which would represent an alternative to the common interpretation (subduction-related hydrous melting) made in some ophiolitic harzburgite. The first step will be the calculation with a model of the composition of the ultra-depleted melt postulated by Pelletier

et al. (submitted b), considering that the Dramala plagioclase-bearing harzburgite was generated by a mix of the Dramala spinel harzburgite (with its present-day composition) with a melt of unknown composition. The second step will be the estimation of the degree of melting recorded by the Dramala spinel harzburgite, in order to obtain the composition of the Dramala mantle before any melt percolation event. This depleted composition will then be used in a second modelling, where the depleted mantle column will be percolated by a melt of chosen composition. This model will be tested with the composition of the ultra-depleted melt calculated in the first step, but also with a N-MORB, in order to see if the spoon-shaped REE pattern observed in the Dramala spinel harzburgite could result from one of this type of melt percolation.

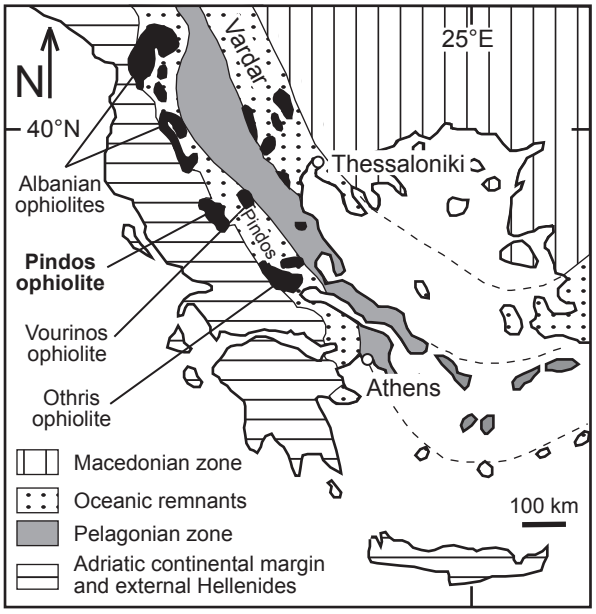


Fig. 3.1: The Pindos ophiolite within the Hellenides, modified after Channell and Kozur (1997).

GENERAL GEOLOGICAL FRAMEWORK

The Pindos, Vourinos and Othris ophiolites in Greece and the Albanian ophiolites belong to the Sub-Pelagonian ophiolites (Fig. 3.1). Their evolution is related to the history of the Neo-Tethys from the Triassic to the Tertiary. During the Triassic, sea-floor spreading began (Jones and Robertson, 1991; Pe-Piper and Piper, 2002; Robertson, 2002) and led to the formation of the oceanic lithosphere, which constitutes the "core" of these ophiolites.

During the Mid-Jurassic, oceanic lithosphere was still produced but convergence began and the ophiolites were displaced above a west- or east-dipping intra-oceanic subduction zone (Jones and Robertson, 1991). Later, this subduction zone collided with the Pelagonian margin and ophiolites were obducted onto the oceanic crust and eventually onto the accretionary prism. The metamorphic soles, mainly composed of metabasites and metasediments, were created at the base of these ophiolites during emplacement (Jones and Robertson, 1991; Ross and Zimmerman, 1996). Rocks of metamorphic soles were generally equilibrated under greenschist to amphibolite facies conditions (Pe-Piper and Piper, 2002 and references therein). Finally during Late Jurassic, ophiolites were emplaced by thrusting onto the Pelagonian continental crust.

The Sub-Pelagonian ophiolites are presently aligned in a NNW-SSE direction within the Hellenides mountain belt (Fig. 3.1). The Pindos and Vourinos ophiolites are connected beneath the Molasse-filled Mesohellenic Trough of the Sub-Pelagonian zone (Rassios and Moores, 2006). Pindos and Othris ophiolites are probably of the same origin and could be related along-strike to the South (Jones and Robertson, 1991).

The palaeogeographic position of the Neo-Tethyan ophiolites during the Jurassic is a matter of debate and two hypotheses have been put forward. i) All the ophiolites are allochtonous and were created in a single ocean basin, the Vardar ocean, situated to the east of the Pelagonian micro-continent. The actual position of the Sub-Pelagonian ophiolites would be due to post-collisional extensional movements (Aubouin, 1959; Dercourt et al., 1986, 1993; Jacobshagen, 1986). ii) The ophiolites are essentially autochtonous and were formed in different small ocean basins, with Pindos, Vourinos and Othris ophiolites formed in the Pindos basin, west of the Pelagonian continent (Robertson et al., 1991; Smith and Woodcock, 1976). The origin of these small oceans is still a matter of debate and could be placed in a fore-arc setting (Dilek and Flower, 2003), a back-arc environment (Stampfli et al., 1998) or a Red-sea type rift environment (Robertson et al., 1991).

According to Robertson and Shallo (2000), the Sub-Pelagonian ophiolites can be separated into two groups. i) The "Eastern-type", including the Eastern-Albanian and the Vourinos ophiolites,

which are classified as supra-subduction zone (SSZ)-type ophiolites. They are supposed to have formed above an intra-oceanic subduction zone during the Late Jurassic. ii) The "Western-type", with the Western-Albanian, the Pindos and the Othris ophiolites, which are supposed to represent mid-ocean ridge (MOR)-type ophiolites, formed at a slow-spreading mid-ocean ridge. During the Early Jurassic, they evolved to SSZ-type ophiolites at the onset of subduction.

Othris and Dramala (Pindos) mantle rocks show a similar tectono-magmatic evolution (Pelletier et al., submitted b), and were probably part of the same oceanic slab (Smith, 1979). They show mantle textures typically formed along slow-spreading mid-ocean ridges (Pearce et al., 1984; Rassios, 1991; Dijkstra et al., 2003). They are both characterized by the presence of highly tectonized peridotites and mylonites. Evidence of refertilization of depleted spinel peridotites by depleted melts was postulated in the two massifs to form their respective plagioclase-bearing peridotites (Dijkstra et al., 2001 and 2003; Pelletier et al., submitted b).

THE PINDOS OPHIOLITE

According to Jones and Robertson (1991) and to Rassios and Grivas (1998), the Pindos ophiolite can be subdivided into three units (Fig. 3.2): the Dramala complex (peridotite, mantle restite and cumulate), the Aspropotamos complex (crustal cumulate and extrusive) and the Loumnitsa unit (metamorphic sole of the ophiolite). The contact between the Dramala and the Aspropotamos complexes is tectonic.

The Dramala complex (Fig. 3.2) represents oceanic mantle, which mainly includes tectonized spinel harzburgite and minor plagioclase-bearing harzburgite or lherzolite. Some spinel harzburgites are highly depleted and can contain less than 4 modal % clinopyroxene (Pelletier et al., submitted b). A spoon-shaped trace-element pattern was described of clinopyroxenes from this unit and attributed to hydrous melting of the peridotite above a subduction zone (Bizimis et al., 2000). In contrast, Pelletier et al. (submitted b) showed that these harzburgites were impregnated or interacted with melts, which are responsible for the Li content of these harzburgites, and could be related to the spoon-shaped trace element pattern observed in these rocks. Other mantle rocks present in the massif are websterite, dunite and pyroxenite (Jones and Robertson, 1991; Pe-Piper and Piper, 2002; Ross and Zimmerman, 1996). Serpentinized equivalents of all rock types occur throughout the complex. The presence of ophicalcite in some harzburgites was mentioned by Jones et al. (1991), showing that these rocks were once exposed on the Neo-Tethyan ocean floor. In rare cases, the MOHO transition zone (petrological MOHO) is exposed (see crust-mantle boundary on Fig. 3.2). This transitional zone of approximately 0.5 to 1.0 km thickness is characterized by mantle restite intruded by many gabbro and dunite bodies, which progressively grades to a cumulate sequence (Rassios, 2004). Plagioclase-bearing peridotites mentioned above are mainly restricted to this transitional zone. The main cumulate sequence includes plagioclase-bearing dunite, troctolite and anorthosite gabbro (Capedri et al., 1982; Rassios, 1991), and is characterized by the crystallization sequence olivine-plagioclase-clinopyroxene. According to the Pearce et al. (1984) interpretation, this type of sequence is related to cumulates formed at mid-ocean ridges, rather than in supra-subduction zone settings.

The Aspropotamos complex (Fig. 3.2) is a piece of oceanic crust, which includes ultramafic and mafic cumulates, plagiogranite, sheeted dykes and pillow lavas. Magmatic zircons in one gabbro from this complex were dated by Liati et al. (2004) and gave ages of 171 ± 3 Ma. Lava affinities within the extrusive rocks evolved with time from high-Ti MORB (group 1) to transitional MORB / island arc tholeiites (group 2) to island arc tholeiites / boninite (group 3) type lavas (Capedri et al., 1980; Kostopoulos, 1988; Jones and Robertson, 1991; Jones et al., 1991; Pe-Piper et al., 2004; Saccani and Photiades, 2004; Beccaluva et al., 2005).

The Loumnitsa unit (Fig. 3.2) represents the metamorphic sole of the ophiolite, which mainly includes metasediments and metabasites with MORB and WPB (Within Plate Basalt) affinities (Jones and Robertson, 1991). These rocks are present between the Dramala mantle and the continental rocks, but also between the Dramala mantle and the Aspropotamos complex (Jones and Robertson, 1991). The rocks of the Loumnitsa unit were equilibrated under amphibolite facies conditions. K-Ar and Ar-Ar dating on hornblende from some

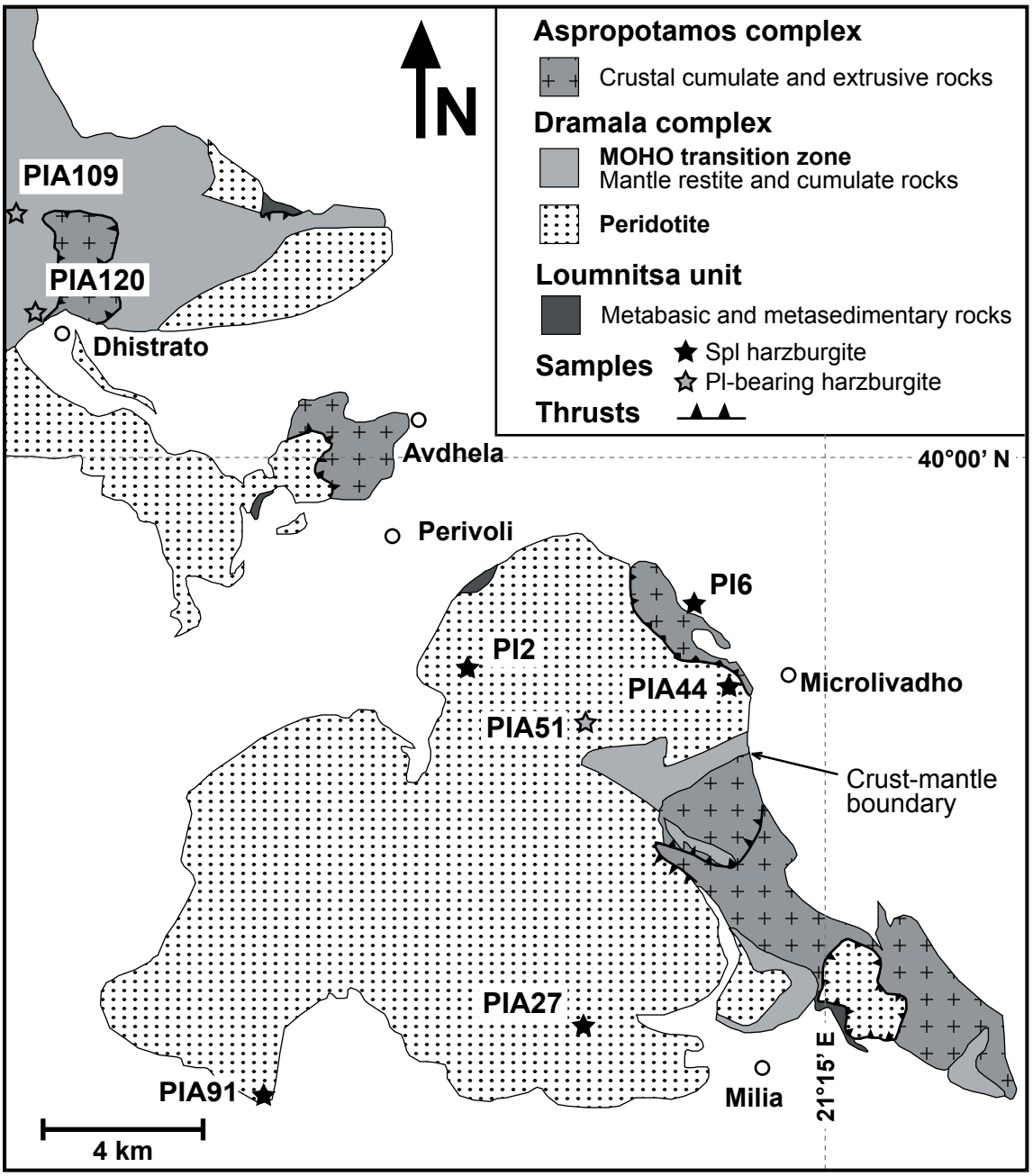


Fig. 3.2: Central part of the Pindos ophiolite showing the limits between the Dramala complex (mantle section and cumulate), the Aspropotamos complex (crustal cumulate and extrusive) and the Loumnitsa unit (metamorphic sole), and the position of the studied samples. The crust-mantle boundary (petrological MOHO) is exposed near to Microlivadho. Geology after Rassios (1991) and Rassios and Grivas (2001).

amphibolites gave ages of 165 ± 5 Ma and 176 ± 5 Ma (Pe-Piper and Piper, 2002 and references therein). These ages are contemporaneous with the one obtained on the gabbro from the Aspropotamos complex by Liati et al. (2004), showing that the intra-oceanic obduction began when the mantle section was still hot.

SELECTED SAMPLES AND MELT IMPREGNATION TEXTURES

Samples discussed below come from the Dramala complex (Fig. 3.2). Their textures, major and light (Li, Be, B) elements in minerals and light elements in the bulk rock have been described in

detail in a previous paper (Pelletier et al., submitted b). Samples are all clinopyroxene-bearing harzburgites and are subdivided into two groups. The first group includes the spinel harzburgite and the second group the plagioclase-bearing harzburgite collected in the MOHO transition zone (Fig. 3.2) mapped by Rassios and Grivas (1998), where melt impregnation textures were observed (Pelletier et al., submitted b). Microstructures range from coarse porphyroclastic to mylonitic (Mercier and Nicolas, 1975). Samples are serpentinized to various degrees, from completely fresh to highly serpentinized (up to 55 volume % serpentine). Samples described below were chosen in order to study their trace element content in clinopyroxene, plagioclase and in the bulk.

Spinel harzburgite

PI2 and PIA91 show a porphyroclastic texture, with a bimodal grain size distribution of orthopyroxene, clinopyroxene, olivine and spinel. Orthopyroxene and olivine porphyroclasts are frequent (maximum width ~ 2 mm), while clinopyroxene porphyroclasts are rare and can measure up to 1 mm in diameter. Neoblasts are smaller (< 0.5 mm). PIA27 shows no clinopyroxene porphyroclast, but is characterized by the presence of small cuspate clinopyroxene grains at olivine-orthopyroxene porphyroclasts joints. This clinopyroxene is replaced by edenitic hornblende formed during high-temperature hydration (Pelletier et al., submitted b). PI6 and PIA44 show a granoblastic texture, where cuspate clinopyroxene crystallized at triple junctions between orthopyroxene and olivine porphyroclasts (Fig. 3.3A). The shape and position of this interstitial clinopyroxene excludes a primary origin, it could alternatively have crystallized from incompletely extracted melts (Pelletier et al., submitted b) as deduced for similar textures in some depleted abyssal peridotites (Seyler et al., 2001) or orogenic peridotites (Piccardo et al., 2004b).

Plagioclase-bearing harzburgite

These rocks show different features, which can be directly related to melt percolation or to melt impregnation (Pelletier et al., submitted b). Sample PIA120 has a porphyroclastic texture, with clinopyroxene porphyroclast aggregates showing irregular outlines due to embayment of olivine. These clinopyroxenes are in optical continuity

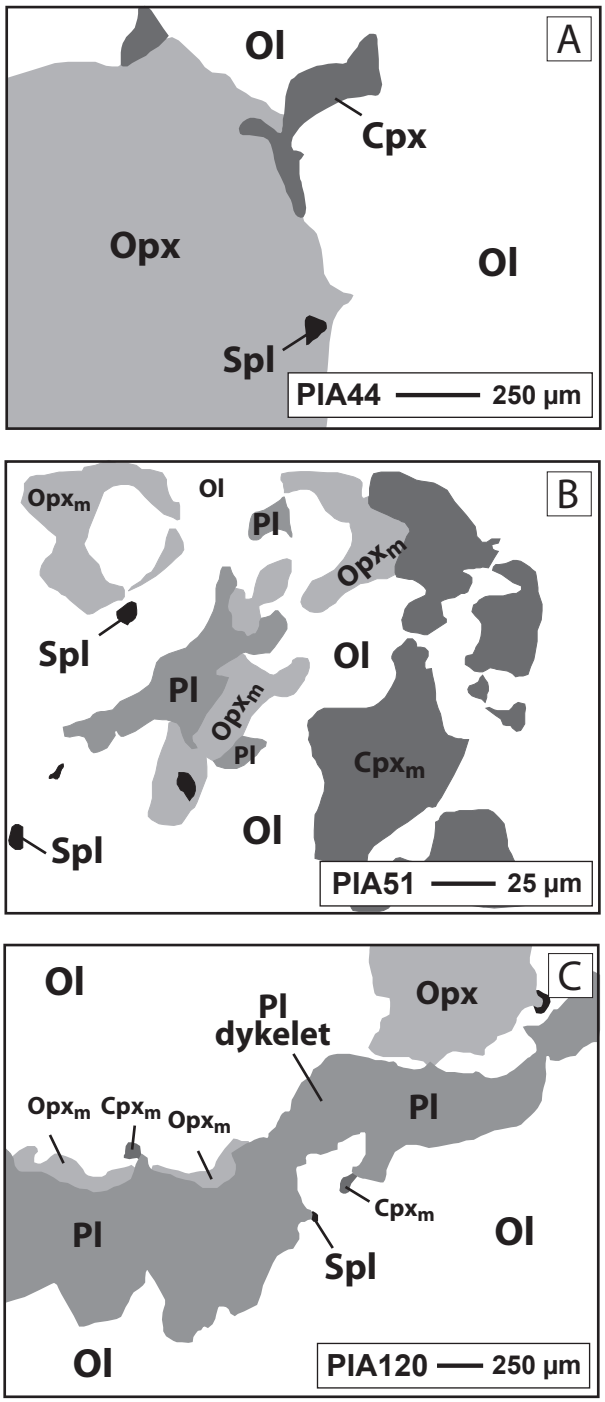


Fig. 3.3: (A) Lobed clinopyroxene grain in sample PIA44. Melt impregnation textures in sample (B) PIA51 and (C) PIA120. Cpx_m and Opx_m are related to the melt impregnation event. Mineral abbreviations after Kretz (1983).

and associated with plagioclase (Pelletier et al., submitted b). This texture is due to dissolution of primary clinopyroxene by pyroxene-undersaturated melt (Seyler et al., 2001; Dijkstra et al., 2003). In the same sample, millimeter-scale plagioclase dykelets

with igneous textures are present. Secondary clinopyroxene (Cpx_m) is usually associated with plagioclase in these dykelets (Fig. 3.3C). This mineralogical association is generally interpreted as due to porous flow of melt (Pearce et al., 2000; Dijkstra et al., 2001 and 2003 and references therein), and was interpreted as a cumulate assemblage in the Othris plagioclase-bearing peridotites (Dijkstra et al., 2001; Barth et al., 2007). This clinopyroxene-plagioclase association is also present in samples PIA51 and PIA109 (Fig. 3.3B). In the three plagioclase-bearing harzburgites, secondary undeformed orthopyroxene (Opx_m) crystallized at the contact between plagioclase and primary olivine (Fig. 3.3B-C). This texture is usually due to the replacement of olivine by orthopyroxene along the olivine-plagioclase contact during melt-rock reaction (Dijkstra et al., 2003; Piccardo et al., 2004b; Pelletier et al., submitted b).

All these textures could reflect the evolution of the melt composition either over time, or during cooling (Dijkstra et al., 2003; Piccardo et al., 2004b; Pelletier et al., submitted b). The corroded primary clinopyroxenes are most likely due to infiltration of pyroxene-undersaturated melt, while the crystallization of plagioclase + clinopyroxene association resulted from crystallization of a pyroxene-saturated melt (Pelletier et al., submitted b).

ANALYTICAL TECHNIQUES

Major element compositions of minerals were determined by electron microprobe (Cameca SX-50 and Jeol JXA-8200 at the Institute of Geological Sciences of the University of Bern, Cameca SX-51 at the Institute of Mineralogy of the Ruprecht-Karls University of Heidelberg, and Jeol JXA-8200 at the ETH Zürich) equipped with four to five wavelength-dispersive spectrometers. Operating conditions comprise an accelerating voltage of 15 kV and a 20 nA beam current. The spot size was about 3 μm except for hydrous minerals where a defocused beam was used (amphiboles, talc: 5 μm, serpentine: 1-10 μm, natrolite: 5-10 μm). Natural and synthetic oxides and silicates were used as standards. Backscattered electron (BSE) images were obtained at the Centre Suisse d'Electronique et de Microtechnique (CSEM, Neuchâtel), with a Philips XL-30 Scanning Electron Microscope, operated at 25 kV.

In situ trace element composition of minerals was determined by Laser Ablation-Inductively Coupled Plasma Mass Spectrometry (LA-ICPMS) at the Institute of Geological Sciences of the University of Bern. The system consists of a pulsed 193 nm ArF Excimer laser (Lambda Physik, Germany) with an energy-homogenized (Microlas, Germany) beam profile (Günther et al., 1997) coupled with an ELAN DRC-e ICP quadrupole mass spectrometer (QMS; Perkin Elmer, Canada). The depth-controlled ablation rate per shot was about 0.1 to 0.2 μm, depending on laser energy and matrix chemistry. The sample was loaded along with the SRM 610 glass standard from NIST in a ca. 16 cm^3 ablation cell and put on the stage of a modified petrographic microscope. Laser-ablation aerosol was carried to the ICP-QMS by a mixed He-Ar carrier gas. Analyses were performed in sequence, and each ablation was stored individually as transient (i.e. time resolved) signal in peak-hopping mode. Two analyses on the external standard at the beginning and the end of each set required for off-line data reduction bracketed up to 16 analyses of unknowns. The certified glass standard SRM 610 was used for the experiments as an external standard to calibrate analyte sensitivities, and bracketing standardization provided a linear drift correction. The analytical set-up was tuned for optimum performance across the entire mass range, by establishing robust plasma conditions as monitored by equal sensitivities for U and Th (e.g. Pettke, 2006). Oxide production rates monitored by ThO were always below 0.5%. Data reduction was done with Lamtrace program (S. Jackson, MacQuarie University, Sydney, Australia). EPMA data were used as internal standard, required to correct for differences in sensitivity between SRM 610 and the samples, by defining a relative sensitivity factor. Limits of detection (LOD) for each signal interval were calculated for individual analyses for each element as three times the standard deviation of the gas background signal divided by the element sensitivity (Longerich et al., 1996). It is worth noting that the smaller pit sizes result in higher LODs for a given element, since the background signal remains the same while the analyte signal per concentration unit of the sample and unit time decreases approximately by the square of the radius of the pit size (for ideal ablation).

Li, Be, Rb, Sr, Y, Ba, the heavy REEs (Dy to Lu) and U, Th and Pb were measured in whole rock by inductively coupled plasma mass spectrometry

(ICP-MS) at the Department of Earth Sciences, University of Bristol (United Kingdom). The samples and two ultramafic rock standards (PCC-1; UB-N) were dissolved using a HF-HNO3 multi-acid method on a hotplate. After evaporating the HF, samples were taken up in 2 % HNO3 at a dilution of ~500:1 of the original rock. ICP-MS analyses were performed on a Thermo Electron Element sector field ICP-MS in pulse-counting mode. Mass calibration was completed by using a multi-element solution (10 μg/L of each Li, B, Na, Sc, Fe, Co, Ga, Y, Rh, In, Ba, Lu, Tl, U in 5 % HNO3). Precision and reproducibility of solution ICP-MS analyses were < 12 %, except for Be, Ba, Lu, Pb, Th and U, where they were < 25 %. Detection limits were ~ 37 ng/g for Li and ~ 3 ng/g for Be. Measured intensities were normalised to solutions of USGS reference material PCC-1 (peridotite), except for Be, where ANRT reference material UB-N (serpentinite) was used. The published values for PCC-1 of 985 ng/g Li (Moriguti et al., 2004) was used to calculate the concentrations of Li. The accepted concentration of Be in UB-N is 200 ng/g (Govindaraju, 1994).

MAJOR ELEMENT COMPOSITION OF MINERALS

Despite the fact that plagioclase-bearing sample PIA51 shows evidence of melt impregnation, its major element composition of orthopyroxene, clinopyroxene and spinel is similar to the one of spinel harzburgites (Fig. 3.4A-B; Pelletier et al., submitted b). For this reason, this sample will be considered separately from the other plagioclase-bearing harzburgites in the following description of major element composition. Major element composition of clinopyroxene cores and plagioclase are presented in Tables 3.1 and 3.2.

Spinel in plagioclase-bearing harzburgite has lower Mg# and higher TiO_2 content than spinel in spinel harzburgite (Pelletier et al., submitted b), because spinel composition is highly sensitive to melt impregnation. Such Ti enrichment was observed by Dick and Bullen (1984) and Allan and Dick (1996) in spinel of impregnated depleted abyssal peridotites and in Othris plagioclase-bearing harzburgites (Dijkstra et al., 2001; Barth et al., 2003). TiO_2-rich clinopyroxene (0.18-0.50 wt. %) is associated with TiO_2-rich spinel (0.12-0.27 wt. %) in the plagioclase-bearing harzburgites. It is enriched in Al_2O_3 (1.7-4.7 wt. %), Na_2O (0.25-0.50 wt. %) and shows lower Mg# (Fig. 3.4A-B) compared to clinopyroxene from spinel harzburgite (Pelletier et al., submitted b). This is in agreement with observed compositions from abyssal plagioclase-bearing peridotite (Allan and Dick, 1996) and from Othris plagioclase-bearing harzburgite (Dijkstra et al., 2001; Barth et al., 2003). Orthopyroxene from the plagioclase-bearing harzburgite has lower Mg# compared to the spinel harzburgite (Pelletier et al., submitted b). The composition of Cpx_m from the plagioclase-bearing harzburgite corresponds to the most depleted end of mid-ocean ridge cumulate compositions and to cumulates found in the plagioclase-bearing peridotite from Othris (Fig. 3.4A; Dijkstra et al., 2001; Nonnotte et al., 2005). Anorthite contents in plagioclase ranges between 0.81 and 0.91.

TRACE ELEMENT COMPOSITION OF MINERALS

Clinopyroxene from all rocks is extremely depleted in Cs, Rb, Ba, Th, U, Nb and Ta, with values near to or below the detection limit (Table 3.3). Based on the trace element patterns of clinopyroxene, the Dramala harzburgites can be subdivided into three groups. The first group includes all spinel harzburgites (PI2, PIA91, PIA27, PI6, PIA44). Clinopyroxene from these rocks is depleted compared to the primitive mantle. It shows positive Ti, Sc and V anomalies (Fig. 3.5B) and low concentrations of Nd, Zr and Hf (Table 3.3). It is characterized by a spoon-shaped REE pattern (except for sample PI2), with an enrichment in the light REEs and a fractionation within the light and heavy REEs (Fig. 3.5A). $[La/Sm]_N$ and $[Gd/Yb]_N$ are approximately 0.13. In contrast, spinel harzburgite PI2 shows no spoon-shaped pattern but is characterized by an extreme fractionation between the light and heavy REEs, with $[Ce/Yb]_N$ of 0.0001, and very low Ce_N concentrations with a mean value < 0.001.

The second group includes plagioclase-bearing harzburgites PIA120 and PIA109. Clinopyroxene from these samples is enriched in nearly all trace elements compared to samples from the two previous groups (Fig. 3.5A-B; Table 3.3). It is characterized by a flat normalized pattern from Sm to Lu (Fig. 3.5A), and by negative Ti and Sr anomalies (Fig.

Table 3.1 Major element composition of clinopyroxene cores in spinel harzburgite and plagioclase-bearing harzburgite (representative analyses)

Rock	**Spl harz**	**Spl harz**	**Spl harz**	**Spl harz**	**Spl harz**	**Spl harz**	**Pl harz**	**Pl harz**	**Pl harz**	**Pl harz**	**Pl harz**
	Cpx	**Cpx**	**Cpx**	**Cpx**	**Cpx**	**Cpx**	**Cpx_m**	**Cpx_m**	**Cpx_m**	**Cpx_m**	**Cpx_m**
sample	**PI2**	**PI2**	**PIA91**	**PIA91**	**PIA44**	**PIA44**	**PIA120**	**PIA120**	**PIA109**	**PIA109**	**PIA51**
SiO2	53.8	53.9	53.8	53.9	53.1	53.1	52.8	52.9	53.7	52.9	54.2
TiO2	0.06	0.06	0.03	0.02	0.01	b.d.	0.42	0.45	0.17	0.26	0.01
Cr2O3	0.86	0.82	0.72	0.36	0.93	0.92	0.71	0.84	0.34	0.61	0.71
Al2O3	2.73	2.49	1.89	1.46	2.19	2.22	3.14	3.12	2.60	3.31	2.23
FeO	1.79	1.88	1.76	1.66	2.29	2.12	2.51	2.66	2.66	2.76	1.90
MnO	0.05	0.05	0.06	0.02	0.10	0.00	0.10	0.05	0.01	0.02	0.06
NiO	0.07	0.12	b.d.	0.05	0.05	0.05	0.05	0.04	b.d.	b.d.	0.02
MgO	17.3	17.4	17.5	17.7	17.9	17.9	16.7	16.5	17.2	17.0	16.8
CaO	24.2	24.3	23.7	24.1	23.3	23.5	23.2	23.4	23.9	23.1	24.3
Na2O	0.05	0.05	0.01	0.04	0.05	0.01	0.37	0.40	0.30	0.36	0.03
K2O	0.03	0.01	0.00	0.01	b.d.	b.d.	0.01	0.01	b.d.	0.02	b.d.
Total	101.0	101.0	99.5	99.3	99.9	99.8	100.0	100.3	100.8	100.4	100.2
Stoich.	6O	6O	6O	6O	6O	6O	6O	6O	6O	6O	6O
Si	1.934	1.937	1.957	1.966	1.931	1.933	1.921	1.919	1.936	1.918	1.960
Ti	0.002	0.002	0.001	0.001	0.000	b.d.	0.011	0.012	0.005	0.007	0.000
Cr	0.024	0.023	0.021	0.010	0.027	0.026	0.020	0.024	0.010	0.017	0.020
Al	0.116	0.106	0.081	0.063	0.094	0.095	0.135	0.134	0.111	0.141	0.095
Fe^{2+}	0.054	0.057	0.054	0.051	0.070	0.065	0.076	0.081	0.080	0.084	0.057
Mn	0.002	0.002	0.002	0.001	0.003	0.000	0.003	0.002	0.000	0.001	0.002
Ni	0.002	0.003	b.d.	0.002	0.001	0.001	0.001	0.001	b.d.	b.d.	0.001
Mg	0.926	0.930	0.949	0.960	0.972	0.969	0.906	0.891	0.924	0.919	0.906
Ca	0.933	0.936	0.925	0.942	0.909	0.916	0.903	0.911	0.924	0.896	0.940
Na	0.003	0.003	0.001	0.002	0.003	0.001	0.026	0.028	0.021	0.025	0.002
K	0.001	0.000	0.000	0.000	b.d.	b.d.	0.000	0.000	b.d.	0.001	b.d.
Total	3.997	3.999	3.991	3.998	4.010	4.007	4.003	4.004	4.010	4.009	3.983
Mg#	0.945	0.943	0.947	0.950	0.933	0.938	0.922	0.917	0.920	0.916	0.940
Cr#	0.174	0.181	0.204	0.141	0.222	0.218	0.132	0.153	0.081	0.110	0.176

Cr# calculated as Cr / (Cr + Al). Mg# calculated as Mg / (Mg + Fe^{2+}). b.d.: below detection limit.

Table 3.2 Major element composition of plagioclase in plagioclase-bearing harzburgite (representative analyses)

Sample	PIA109	PIA109	PIA109	PIA109	PIA109	PIA109	PIA109	PIA120	PIA120	PIA120	PIA120	PIA120	PIA120	PIA120	PIA120
SiO2	45.0	45.3	45.1	44.7	45.2	44.6	45.5	46.3	46.7	45.9	46.6	46.5	45.7	46.7	45.9
TiO2	0.02	< 0.01	0.01	< 0.01	0.01	0.01	0.01	0.01	< 0.01	n.a.	n.a.	n.a.	n.a.	n.a.	n.a.
Al2O3	35.1	35.7	35.4	35.1	35.2	34.8	34.6	34.2	33.8	35.3	34.9	35.1	35.5	34.8	35.5
Fe2O3	0.34	0.19	0.34	0.50	0.22	0.33	0.25	0.22	0.08	0.16	0.08	0.03	0.15	0.07	0.17
MnO	0.01	< 0.01	< 0.01	0.01	0.01	< 0.01	0.04	0.03	< 0.01	n.a.	n.a.	n.a.	n.a.	n.a.	n.a.
MgO	0.01	0.01	0.01	0.01	< 0.01	< 0.01	< 0.01	< 0.01	< 0.01	n.a.	n.a.	n.a.	n.a.	n.a.	n.a.
CaO	18.6	18.5	18.7	18.6	18.5	18.5	18.9	17.6	17.1	17.1	17.1	17.1	17.9	16.9	17.7
Na2O	1.03	1.06	0.96	0.98	1.08	0.94	1.05	1.56	1.77	1.78	1.82	1.86	1.38	2.13	1.66
K2O	< 0.01	< 0.01	0.01	0.01	0.02	< 0.01	0.01	< 0.01	0.01	0.02	< 0.01	0.02	< 0.01	0.03	< 0.01
Total	100.12	100.66	100.57	99.94	100.18	99.13	100.27	99.89	99.43	100.21	100.48	100.51	100.6	100.56	100.89
Stoich.	8 oxy 5 cat	8 oxy 5 cat	8 oxy 5 cat	8 oxy 5 cat	8 oxy 5 cat	8 oxy 5 cat	8 oxy 5 cat	8 oxy 5 cat	8 oxy 5 cat	8 oxy 5 cat	8 oxy 5 cat	8 oxy 5 cat	8 oxy 5 cat	8 oxy 5 cat	8 oxy 5 cat
Si	2.071	2.070	2.066	2.064	2.076	2.075	2.091	2.130	2.156	2.099	2.124	2.117	2.085	2.125	2.087
Ti	0.001	n.c.	0.000	n.c.	0.000	0.001	0.000	0.000	n.c.	n.a.	n.a.	n.a.	n.a.	n.a.	n.a.
Al	1.906	1.923	1.914	1.911	1.905	1.907	1.875	1.854	1.836	1.900	1.876	1.883	1.913	1.862	1.902
Fe^{3+}	0.012	0.007	0.012	0.018	0.008	0.011	0.009	0.008	0.003	0.006	0.003	0.001	0.005	0.003	0.006
Mn	0.001	n.c.	n.c.	0.001	0.000	n.c.	0.002	0.001	n.c.	n.a.	n.a.	n.a.	n.a.	n.a.	n.a.
Mg	0.001	0.001	0.001	0.001	n.c.	n.c.	n.c.	n.c.	n.c.	n.a.	n.a.	n.a.	n.a.	n.a.	n.a.
Ca	0.917	0.906	0.921	0.917	0.912	0.920	0.930	0.866	0.846	0.836	0.837	0.834	0.875	0.821	0.860
Na	0.092	0.094	0.085	0.088	0.096	0.085	0.094	0.139	0.159	0.158	0.161	0.164	0.122	0.188	0.146
K	n.c.	n.c.	0.001	0.000	0.001	n.c.	0.000	n.c.	0.001	0.001	0.000	0.001	0.000	0.002	0.000
An#	0.909	0.906	0.915	0.913	0.905	0.916	0.909	0.862	0.842	0.842	0.839	0.835	0.877	0.814	0.855

n.c.: not calculated. n.a.: not analyzed. An# calculated as Ca/(Ca+Na). Stoich.: stoichiometry, 8 oxy: 8 oxygens, 5 cat.: 5 cations.

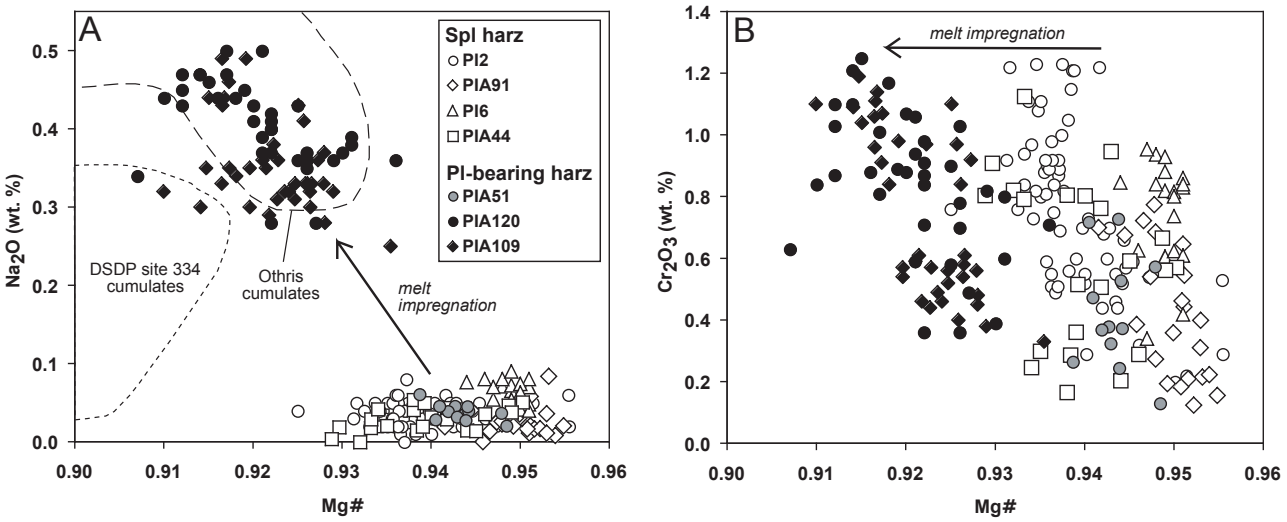


Fig. 3.4: (A-B) Effect of melt impregnation on major element composition of clinopyroxene in Dramala spinel and plagioclase-bearing harzburgites. Literature data plotted for comparison are depleted cumulates from DSDP site 334, after Nonnotte et al. (2005) and depleted cumulates from Othris plagioclase peridotite (Dijkstra et al., 2001).

3.5B). It shows a strong fractionation between the light and middle REEs, with $[La/Sm]_N$ of 0.001 for sample PIA120. Trace element concentrations were obtained on five plagioclase grains only (sample PIA120; Fig. 3.5C), because of small grain size and low concentrations. Plagioclase shows a strong fractionation within the light REEs, with an average $[La/Sm]_N$ of 0.1.

The third group includes plagioclase-bearing harzburgite PIA51, which mainly shows the same characteristics as spinel harzburgite with a spoon-shaped REE pattern (Fig. 3.5A). However, clinopyroxene from this sample is enriched in light REEs compared to clinopyroxene from spinel harzburgite, with $[La/Sm]_N$ about 2.59 (Fig. 3.5A). Moreover, this sample shows concentrations in Pr, Nd, Zr and Hf, intermediate between the spinel harzburgites and the other plagioclase-bearing harzburgites (Fig. 3.5B).

TRACE ELEMENT COMPOSITION OF WHOLE ROCK SAMPLES

Two different REE patterns can be observed in whole rock samples (Table 3.4; Fig. 3.6). The first pattern includes the spinel harzburgites and the plagioclase-bearing harzburgite PIA51. These rocks are characterized by a spoon-shaped REE pattern with fractionation within the light and the heavy REEs (Fig. 3.6). It shows a mean $[Ce/Sm]_N$ of 1.42 and a mean $[Tb/Yb]_N$ of 0.08. The second pattern represents plagioclase-bearing harzburgites PIA120 and PIA109, which are characterized by a flat heavy REEs pattern and a fractionation between the light and middle REEs with a mean $[Ce/Sm]_N$ of 0.05 (Fig. 3.6).

MELT IMPREGNATION MODEL

In order to calculate the composition of the melt which impregnated the plagioclase-bearing harzburgite, whole rock major element and REE contents of Dramala spinel and plagioclase-bearing harzburgites were used. It was postulated that the plagioclase-bearing harzburgite represents a mix of a certain quantity of trapped melt of unknown composition with a highly depleted Dramala spinel harzburgite. For each element, the following equation can be written:

$$C_{Pl\text{-}hrz} = F \cdot C_{melt} + (1 - F) \cdot C_{Spl\text{-}hrz}$$

where C is the concentration of the chosen element in the whole rock (measured in plagioclase-bearing harzburgite (Pl-hrz) and spinel harzburgite (Spl-hrz), and F (%) is the weight fraction of the impregnating

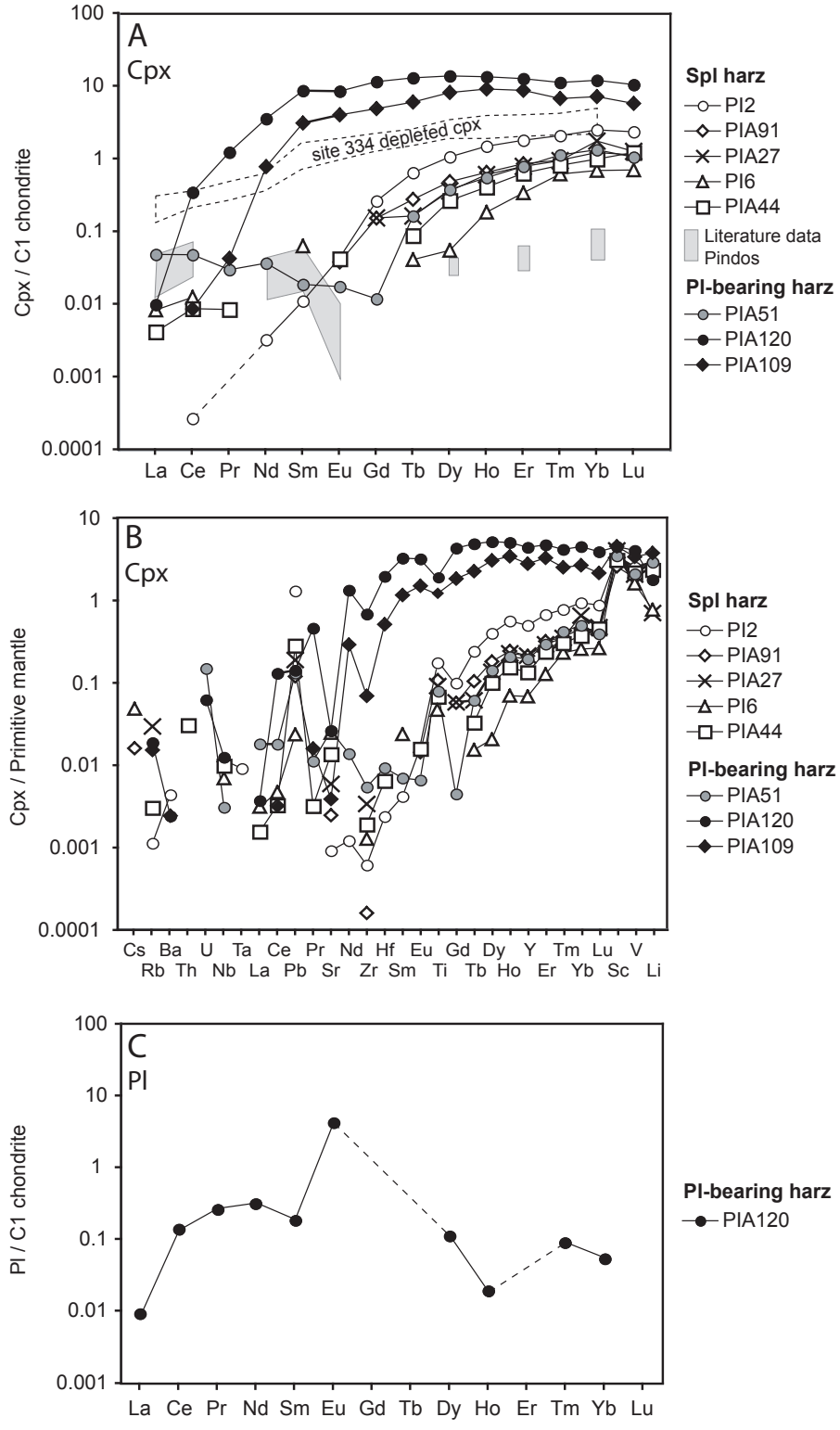


Fig. 3.5: (A) REE patterns of clinopyroxene from spinel and plagioclase-bearing harzburgites. Literature data plotted for comparison: clinopyroxene in depleted cumulates from DSDP site 334 after Nonnotte et al. (2005) and other clinopyroxene from Dramala spinel harzburgites (Pindos) after Bizimis et al. (2000). (B) Extended trace element patterns of clinopyroxene from spinel and plagioclase-bearing harzburgites. (C) REE patterns of plagioclase from the plagioclase-bearing harzburgite PIA120. Normalization to primitive mantle and to C1 chondrite after McDonough and Sun (1995).

Table 3.3 Composition of clinopyroxene in spinel harzburgite and plagioclase-bearing harzburgite (representative analyses)

	Rock	Spl harz	Spl harz	Spl harz	Spl harz	Spl harz	Spl harz	Spl harz	Spl harz	Spl harz	Spl harz	Spl harz	Spl harz	Spl harz	Spl harz
	Sample	PI2	PI2	PI2	PI2	PIA91	PIA91	PIA91	PIA91	PIA27	PIA27	PI6	PI6	PI6	PI6
Element	**Unit**														
Li	**µg/g**	5.0	4.4	4.8	4.9	3.5	3.6	4.0	5.9	1.0	1.3	1.6	1.3	1.1	0.9
B	**µg/g**	0.22	0.21	<0.16	<0.14	0.15	<0.10	<0.16	0.24	<0.76	<0.78	<0.56	<0.50	<0.50	<0.30
P	**µg/g**	5	4	4	4	3	3	3	4	9	9	4	5	6	3
Sc	**µg/g**	57.1	54.7	48.7	50.6	41.9	41.2	40.6	40.6	56.3	73.1	61.6	54.6	60.8	58.6
Ti	**µg/g**	202	214	195	199	140	133	135	109	109	113	55	58	52	57
V	**µg/g**	201	205	205	199	152	152	155	147	155	180	148	138	109	123
Co	**µg/g**	20.4	18.4	22.7	21.1	17.8	19.4	19.9	19.2	21.6	19.6	17.8	18.1	17.1	18.5
Ni	**µg/g**	338	313	369	344	312	335	352	336	383	361	301	312	307	327
Zn	**µg/g**	8.62	7.51	9.93	8.60	6.63	7.66	7.70	8.10	9.99	9.07	8.73	6.61	5.84	7.88
Ga	**µg/g**	1.73	1.63	1.80	1.64	1.13	1.10	1.10	1.06	1.22	1.18	0.957	1.02	0.578	0.631
Rb	**µg/g**	<0.003	<0.004	<0.004	<0.003	<0.004	<0.004	<0.004	<0.007	<0.022	0.035	<0.016	<0.016	<0.014	<0.006
Sr	**µg/g**	0.010	0.008	0.035	0.025	0.056	0.068	0.049	0.024	0.114	0.118	0.428	0.569	0.445	0.494
Y	**µg/g**	2.41	2.34	1.59	1.77	1.02	0.945	0.929	0.767	0.869	0.946	0.331	0.273	0.262	0.293
Zr	**µg/g**	0.009	0.007	0.007	0.007	0.005	<0.006	<0.004	<0.005	<0.034	0.07	0.023	<0.018	<0.024	0.03
Nb	**µg/g**	0.007	0.010	0.013	0.008	0.009	0.006	0.004	0.010	<0.016	<0.017	0.012	<0.012	<0.013	0.006
Sb	**µg/g**	0.031	0.024	0.041	0.042	0.027	0.026	0.021	0.030	<0.067	<0.063	<0.049	<0.046	<0.040	<0.018
Cs	**µg/g**	<0.002	<0.001	<0.001	<0.001	<0.002	0.002	<0.002	<0.002	<0.008	<0.011	<0.008	<0.003	<0.007	0.004
Ba	**µg/g**	<0.011	<0.016	0.041	0.130	0.025	0.047	0.023	<0.034	<0.119	<0.093	<0.054	<0.063	<0.081	<0.032
La	**µg/g**	<0.002	<0.002	<0.003	<0.002	<0.003	<0.002	<0.003	<0.004	<0.020	<0.014	0.008	<0.011	<0.010	<0.003
Ce	**µg/g**	<0.002	<0.002	<0.002	0.001	<0.002	<0.002	<0.003	<0.004	<0.013	<0.013	<0.011	0.021	<0.010	0.010
Pr	**µg/g**	<0.001	<0.002	<0.002	<0.001	<0.002	<0.001	<0.002	<0.003	<0.007	<0.013	<0.005	<0.008	<0.008	<0.003
Nd	**µg/g**	<0.007	<0.008	0.009	<0.010	<0.007	<0.007	<0.014	<0.013	<0.048	<0.045	<0.045	<0.037	<0.038	<0.022
Sm	**µg/g**	<0.013	<0.010	0.010	<0.012	<0.015	<0.012	<0.009	<0.015	<0.056	<0.065	<0.044	<0.042	0.038	<0.024
Eu	**µg/g**	0.005	<0.004	<0.004	0.005	0.004	<0.004	<0.005	0.009	<0.025	<0.018	<0.015	<0.016	<0.018	<0.007
Gd	**µg/g**	0.071	0.056	0.042	0.047	0.032	0.034	0.039	0.021	<0.085	0.062	<0.044	<0.042	<0.037	<0.019
Tb	**µg/g**	0.025	0.027	0.023	0.022	0.013	0.010	0.012	0.007	<0.009	0.012	<0.006	<0.006	0.006	<0.004
Dy	**µg/g**	0.312	0.256	0.206	0.253	0.126	0.123	0.116	0.102	0.103	0.078	<0.032	<0.029	0.026	0.029
Ho	**µg/g**	0.093	0.088	0.066	0.071	0.042	0.037	0.042	0.022	0.030	0.037	0.011	0.008	0.012	0.010
Er	**µg/g**	0.315	0.299	0.235	0.245	0.158	0.144	0.147	0.120	0.114	0.140	0.039	0.056	0.090	0.036
Tm	**µg/g**	0.059	0.057	0.040	0.045	0.030	0.019	0.024	0.024	0.024	0.023	0.020	0.012	0.017	0.013
Yb	**µg/g**	0.441	0.468	0.302	0.330	0.230	0.194	0.229	0.163	0.226	0.345	0.127	0.115	0.091	0.116
Lu	**µg/g**	0.069	0.069	0.039	0.048	0.033	0.027	0.032	0.022	0.037	0.026	0.013	0.028	0.020	0.009
Hf	**µg/g**	<0.006	<0.004	<0.004	<0.006	<0.006	<0.006	<0.005	<0.010	<0.024	<0.023	<0.027	<0.024	<0.027	<0.010
Ta	**µg/g**	0.002	<0.002	<0.001	<0.002	<0.001	<0.002	<0.001	<0.003	<0.011	<0.010	<0.007	<0.004	<0.007	<0.003
Pb	**µg/g**	0.277	0.208	0.207	0.155	0.032	0.030	0.019	<0.013	<0.050	0.056	<0.026	<0.019	<0.021	0.014
Th	**µg/g**	<0.002	<0.002	<0.002	<0.001	<0.002	<0.002	<0.002	<0.004	<0.011	<0.011	<0.007	<0.006	<0.007	<0.001
U	**µg/g**	<0.001	<0.002	<0.002	<0.002	<0.001	<0.002	<0.002	<0.003	<0.018	<0.010	<0.003	<0.008	<0.007	<0.003

Mg# calculated as (MgO/40.3)/[(MgO/40.3)+(FeO/71.85)]. Spl harz: spinel harzburgite.

Table 3.3 continued

	Rock	Spl harz	Spl harz	Spl harz	Pl harz	Pl harz	Pl harz	Pl harz	Pl harz	Pl harz	Pl harz	Pl harz	Pl harz	Pl harz	Pl harz	Pl harz
	Sample	PIA44	PIA44	PIA44	PIA44	PIA51	PIA51	PIA51	PIA51	PIA120	PIA120	PIA120	PIA120	PIA109	PIA109	PIA109
Element	**Unit**															
Li	**µg/g**	2.8	4.5	4.3	4.3	4.3	5.2	4.2	5.3	3.4	2.9	3.5	3.3	5.7	5.8	6.4
B	**µg/g**	0.38	0.12	<0.24	<0.16	0.11	<0.49	<0.45	<0.27	<0.16	<0.13	<0.27	<0.28	<0.94	<1.67	<1.68
P	**µg/g**	5	4	5	4	3	4	4	4	5	5	6	5	8	7	< 5
Sc	**µg/g**	53.8	49.2	51.3	47.4	51.4	55.8	63.9	54.7	69.3	69.1	70.3	65.1	68.1	74.0	75.1
Ti	**µg/g**	87	83	80	81	86	91	115	100	2380	2400	2447	2327	1660	1318	1454
V	**µg/g**	170	196	185	188	177	156	188	184	321	320	337	338	274	274	271
Co	**µg/g**	17.9	22.2	21.3	20.7	17.5	19.0	16.9	18.7	20.0	21.9	21.3	20.9	17.4	23.2	21.6
Ni	**µg/g**	333	359	343	345	308	335	302	306	317	344	341	347	264	363	353
Zn	**µg/g**	7.47	10.4	11.0	10.5	6.58	8.20	5.90	6.87	8.55	10.1	9.95	9.67	7.51	10.9	8.73
Ga	**µg/g**	1.09	1.38	1.33	1.21	1.28	0.946	1.20	1.45	4.10	4.17	4.62	4.35	2.91	2.60	1.96
Rb	**µg/g**	<0.011	<0.003	<0.006	0.009	<0.003	<0.017	<0.018	<0.009	0.016	0.015	<0.008	0.017	0.027	<0.042	<0.064
Sr	**µg/g**	0.326	0.297	0.263	0.258	0.564	0.525	0.465	0.551	0.547	0.519	0.428	0.493	0.094	0.135	<0.061
Y	**µg/g**	0.607	0.573	0.575	0.554	0.899	0.757	0.877	0.923	19.2	19.1	19.5	18.3	12.1	11.8	11.4
Zr	**µg/g**	0.031	0.019	0.012	0.020	0.053	0.069	0.066	0.050	7.27	6.98	7.43	7.00	0.800	0.694	0.664
Nb	**µg/g**	0.008	0.010	0.008	<0.008	0.010	<0.011	<0.011	<0.005	0.013	0.012	0.010	0.013	<0.017	<0.034	<0.034
Sb	**µg/g**	<0.041	0.020	0.021	0.022	0.026	<0.043	0.027	0.029	0.097	0.078	0.028	0.034	0.081	<0.072	<0.127
Cs	**µg/g**	<0.009	<0.002	<0.004	<0.005	<0.001	<0.009	<0.005	<0.004	<0.002	<0.002	<0.004	<0.003	<0.018	<0.029	<0.034
Ba	**µg/g**	<0.095	<0.018	<0.035	<0.024	<0.017	<0.058	<0.059	<0.030	0.077	<0.019	<0.028	0.049	<0.158	<0.211	<0.212
La	**µg/g**	<0.010	0.005	<0.004	<0.005	0.010	0.018	0.013	0.017	0.005	0.007	0.007	<0.004	<0.015	<0.029	<0.043
Ce	**µg/g**	<0.014	0.009	0.007	0.011	0.042	0.033	0.019	0.034	0.217	0.209	0.231	0.189	<0.009	0.016	<0.057
Pr	**µg/g**	<0.006	<0.002	<0.003	0.004	0.005	<0.008	<0.008	<0.006	0.133	0.129	0.137	0.132	0.012	<0.042	<0.028
Nd	**µg/g**	<0.039	<0.016	<0.009	<0.018	0.023	0.029	<0.047	0.033	1.616	1.770	1.721	1.594	0.277	0.358	0.445
Sm	**µg/g**	<0.044	<0.015	<0.026	<0.026	0.014	<0.028	<0.043	<0.031	1.312	1.434	1.445	1.283	0.444	0.578	0.369
Eu	**µg/g**	<0.009	0.012	<0.006	<0.006	0.005	<0.014	<0.011	<0.007	0.499	0.483	0.507	0.447	0.205	0.219	0.261
Gd	**µg/g**	<0.032	<0.012	<0.011	<0.016	0.012	<0.047	<0.037	<0.014	2.300	2.285	2.428	2.357	0.931	1.042	0.982
Tb	**µg/g**	<0.007	0.004	0.004	0.005	0.008	0.006	<0.005	0.009	0.525	0.515	0.487	0.494	0.234	0.258	0.172
Dy	**µg/g**	0.075	0.051	0.063	0.080	0.105	0.064	0.103	0.119	3.412	3.394	3.626	3.48	2.187	1.985	1.935
Ho	**µg/g**	0.025	0.021	0.021	0.028	0.031	0.036	0.025	0.035	0.769	0.767	0.779	0.758	0.554	0.498	0.465
Er	**µg/g**	0.119	0.124	0.080	0.083	0.153	0.111	0.116	0.152	2.146	2.094	2.176	1.904	1.474	1.512	1.274
Tm	**µg/g**	0.017	0.021	0.023	0.019	0.029	0.022	0.032	0.027	0.288	0.275	0.293	0.289	0.202	0.187	0.119
Yb	**µg/g**	0.116	0.167	0.182	0.139	0.191	0.239	0.278	0.193	2.007	1.855	1.999	1.834	1.458	1.071	0.963
Lu	**µg/g**	0.045	0.028	0.028	0.025	0.029	0.026	0.029	0.021	0.256	0.242	0.244	0.238	0.152	0.131	0.147
Hf	**µg/g**	<0.012	<0.006	0.009	<0.010	<0.005	0.013	<0.014	<0.011	0.591	0.515	0.539	0.527	0.127	0.145	0.159
Ta	**µg/g**	<0.009	<0.002	<0.004	<0.004	<0.001	<0.006	<0.005	<0.003	<0.002	<0.001	<0.004	<0.004	<0.012	<0.015	<0.034
Pb	**µg/g**	0.041	0.047	0.052	0.032	0.029	0.022	0.020	0.026	0.039	0.036	0.026	0.032	<0.031	<0.059	<0.089
Th	**µg/g**	0.012	<0.003	<0.003	<0.005	<0.002	<0.003	<0.004	<0.002	<0.002	<0.002	<0.003	<0.004	<0.007	<0.019	<0.023
U	**µg/g**	<0.006	<0.001	<0.003	<0.003	<0.002	0.006	0.009	<0.003	0.005	0.005	<0.003	<0.003	<0.009	<0.015	<0.021

Mg# calculated as (MgO/40.3)/[(MgO/40.3)+(FeO/71.85)]. Spl harz: spinel harzburgite, Pl harz: plagioclase-bearing harzburgite.

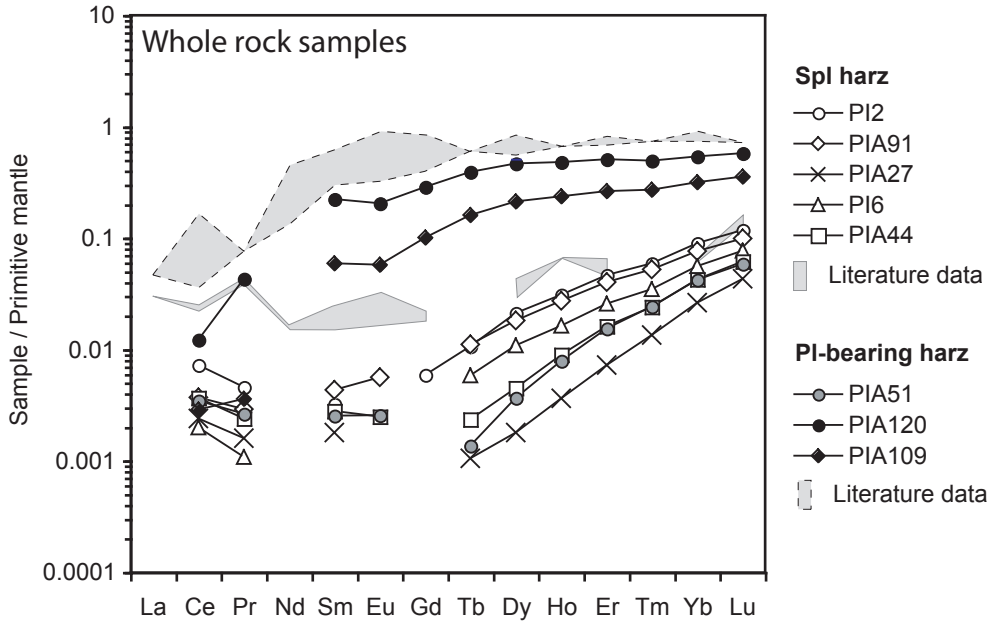


Fig. 3.6: REE patterns of bulk rock samples of spinel and plagioclase-bearing harzburgite. Literature data for some Pindos peridotites plotted for comparison: spinel and plagioclase-bearing harzburgite after Montigny et al. (1973) and Saccani and Photiades (2004). La concentration was to low to be measured on the ICP-MS.

melt. From this simple equation, the concentration of each element in the melt was deduced. In order to solve equation (1), one parameter should be chosen arbitrarily to characterize the melt composition. During the run of the model, the MgO/FeO ratio of the impregnating melt was assumed as known, which gives the following equation to define F:

$$F = \frac{(C^{MgO}_{Pl\text{-}hrz} - C^{MgO}_{Spl\text{-}hrz} - R_{melt}\cdot C^{FeO}_{Pl\text{-}hrz} + R_{melt}\cdot C^{FeO}_{Spl\text{-}hrz})}{(R_{melt}\cdot C^{FeO}_{Spl\text{-}hrz} - C^{MgO}_{Pl\text{-}hrz})}$$

where C^{MgO} and C^{FeO} represent the MgO and FeO concentrations in the rocks, respectively, and R_{melt} is the MgO/FeO ratio of the impregnating melt. From this assumption, C_{melt} can be determined from equation (1). Mg# presented in Figure 3.7 was calculated as:

$$Mg\# = \frac{[(MgO/40.30)/(FeO/71.85)]}{[(MgO/40.30)/(FeO/71.85)] + 1}$$

Strongly depleted spinel harzburgite should be used in order to calculate the composition of the melt for each element, otherwise some elements are more concentrated in the spinel harzburgite than in the plagioclase-bearing harzburgite (Ce, Pr, Sr) and the model is unusable. For this reason, sample PIA44 was chosen for modelling (PI2, PI6, PIA44, and a mean value of these three rocks were tested). Results of modelling for the three plagioclase-bearing harzburgites is given in Figure 3.7.

We investigated various calculated compositions for the impregnated material assuming values for its Mg# between 0.6 and 0.9. Mg# < 0.745 represent trapped evolved liquids, Mg# = 0.745 is our estimate for a trapped primitive melt in equilibrium with typical mantle olivine (see below), whereas values for Mg# > 0.745 represent a cumulate character for the impregnating material. The representative calculated composition of the impregnating material in samples PIA120, PIA109 and PIA51, is presented in Figure 3.7A to C.

DISCUSSION

Melt impregnation in plagioclase-bearing harzburgite

Using spinel harzbugite PIA44 as initial mantle composition and plagioclase harzburgites PIA120

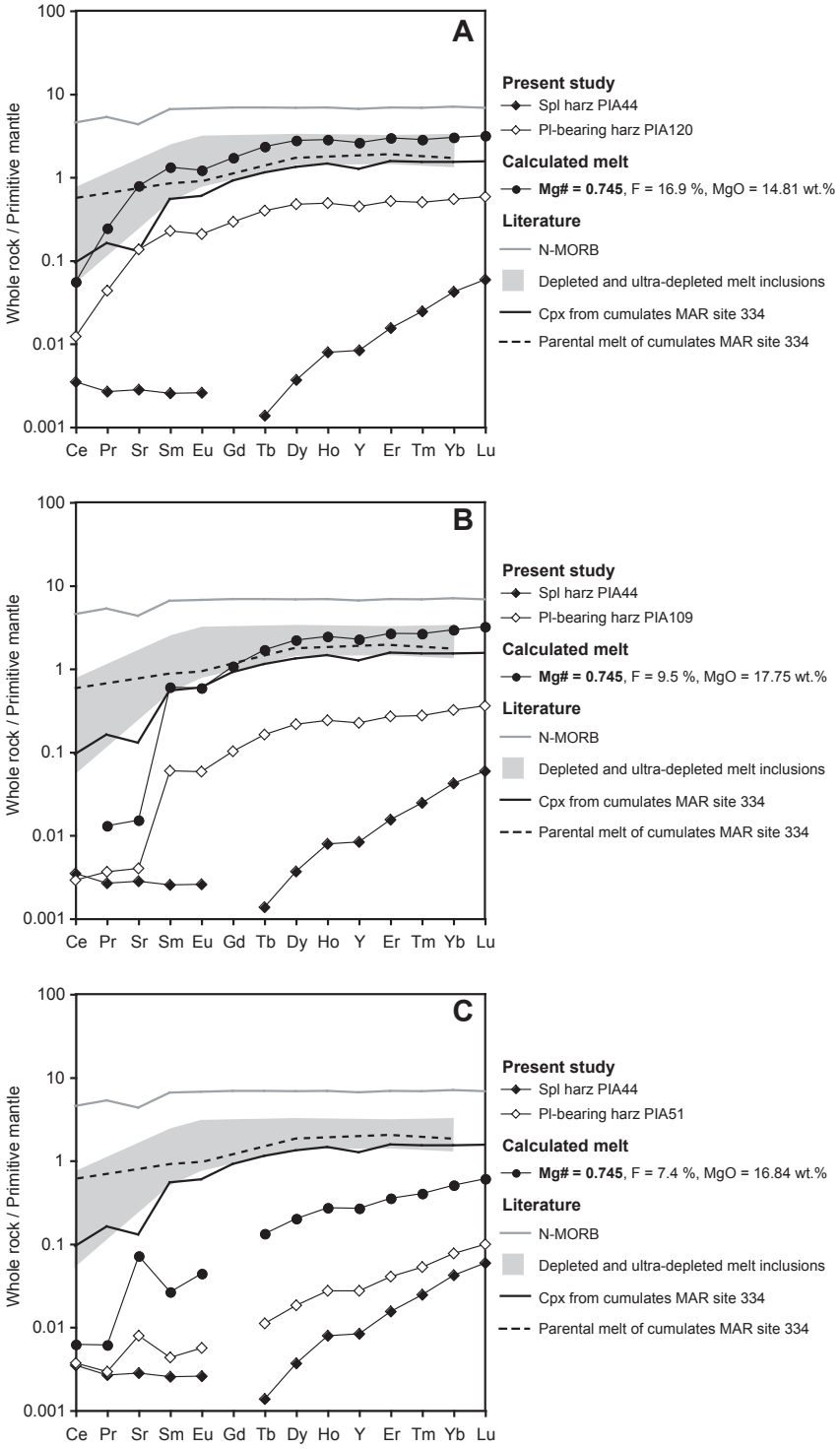


Fig. 3.7: Results of modelling of melt impregnation in plagioclase-bearing harzburgite from whole rock rare REE contents, giving the calculated composition of the impregnating melt: (A) Model for sample PIA120, (B) model for sample PIA109 and (C) model for sample PIA51. Black circles: model run assuming an Mg# of the impregnating melt of 0.745. Gd content of the spinel harzburgite PIA44 was considered as 0, because results were below the detection limit. Literature data: primitive mantle after McDonough and Sun (1995), N-MORB after Sun and McDonough (1989), depleted and ultra-depleted melt inclusions after Gurenko and Chaussidon (1995) and Sobolev and Shimizu (1993), clinopyroxene (Cpx) from depleted cumulates in DSDP site 334 after Nonnotte et al. (2005) and calculated composition of parental melt of DSDP site 334 cumulates after Ross and Elthon (1993).

Table 3.4 Whole rock composition of spinel harzburgite and plagioclase-bearing harzburgite

	Rock Sample	Spl harz PI2	Spl harz PIA91	Spl harz PIA27	Spl harz PI6	Spl harz PIA44	Pl harz PIA51	Pl harz PIA120	Pl harz PIA109
Element	Unit								
SiO2	wt. %	42.62	43.28	43.65	43.79	43.97	44.75	44.63	43.95
TiO2	wt. %	0.02	< 0.01	0.01	< 0.01	< 0.01	0.02	0.08	0.04
Al2O3	wt. %	0.84	0.66	0.52	0.42	0.70	0.89	2.76	1.93
Cr2O3	wt. %	0.40	0.45	0.43	0.51	0.45	0.39	0.38	0.35
Fe2O3	wt. %	9.16	8.95	8.82	9.00	9.02	9.23	9.14	9.26
MnO	wt. %	0.13	0.13	0.12	0.13	0.13	0.13	0.14	0.13
NiO	wt. %	0.31	0.31	0.31	0.32	0.31	0.29	0.26	0.29
MgO	wt. %	45.03	44.81	45.20	45.05	44.66	42.77	39.40	41.89
CaO	wt. %	1.01	1.00	0.61	0.59	0.84	1.23	2.78	1.75
Na2O	wt. %	0.12	0.15	0.08	0.04	0.34	0.98	0.23	0.24
K2O	wt. %	0.01	< 0.01	< 0.01	< 0.01	0.01	0.04	< 0.01	< 0.01
H2O	wt. %	0.3	n.a.	3.4	6.9	8.5	n.a.	7.4	1.7
Mg#		0.95	0.95	0.95	0.95	0.95	0.95	0.94	0.95
LOI	wt. %	< 0	< 0	2.7	6.2	7.8	1.0	6.6	1.1
Li	µg/g	0.88	0.97	0.64	0.51	0.76	0.92	0.97	1.07
Be	µg/g	< 0.0016	< 0.0016	< 0.0016	< 0.0016	< 0.0016	< 0.0016	< 0.0009	< 0.0009
Sc	µg/g	< 36	n.a.	8.6	< 55	12.4	n.a.	21.0	14.0
Co	µg/g	149	n.a.	122	103	105	n.a.	108	128
Ni	µg/g	2450	2460	2459	2496	2418	2304	2060	2241
Cu	µg/g	76	7	16	29	39	25	32	20
Zn	µg/g	48	48	44	46	47	48	49	51
Rb	µg/g	< 0.011	< 0.011	0.164	0.031	0.035	0.027	0.072	0.013
Sr	µg/g	0.05	0.10	0.41	0.32	0.06	0.17	2.85	0.08
Y	µg/g	0.133	0.073	0.042	0.017	0.036	0.118	1.902	0.954
Zr	µg/g	7	9	8	7	6	9	8	6
Ba	µg/g	0.26	< 0.16	0.26	< 0.16	< 0.16	< 0.16	< 0.17	< 0.17
Ce	µg/g	0.012	0.003	0.006	0.004	0.006	0.006	0.020	0.005
Pr	µg/g	0.0012	0.0003	0.0006	0.0004	0.0007	0.0007	0.0109	0.0009
Sm	µg/g	0.001	< 0.0005	0.001	0.001	0.001	0.002	0.091	0.024
Eu	µg/g	< 0.0003	< 0.0003	0.0004	< 0.0003	0.0004	0.0009	0.0317	0.0089
Gd	µg/g	0.0032	< 0.0031	< 0.0031	< 0.0031	< 0.0031	< 0.0031	0.1567	0.0550
Tb	µg/g	0.0011	0.0006	0.0002	0.0001	0.0001	0.0011	0.0389	0.0159
Dy	µg/g	0.0144	0.0074	0.0030	0.0012	0.0025	0.0123	0.3161	0.1439
Ho	µg/g	0.0046	0.0024	0.0013	0.0005	0.0012	0.0041	0.0720	0.0355
Er	µg/g	0.0205	0.0113	0.0071	0.0032	0.0068	0.0177	0.2237	0.1162
Tm	µg/g	0.0040	0.0024	0.0016	0.0009	0.0017	0.0036	0.0338	0.0186
Yb	µg/g	0.040	0.025	0.019	0.012	0.019	0.034	0.238	0.140
Lu	µg/g	0.0079	0.0052	0.0042	0.0029	0.0040	0.0067	0.0389	0.0241
Pb	µg/g	0.040	0.052	0.117	0.117	0.054	0.025	0.068	0.076
Th	µg/g	0.0018	0.0003	0.0009	0.0007	0.0006	0.0006	0.0001	0.0002
U	µg/g	0.0008	< 0.0003	0.0003	< 0.0003	< 0.0003	< 0.0003	0.0001	0.0002
B	µg/g	< 0.05	n.a.	1.05	0.10	< 0.04	n.a.	0.72	0.09
Cl	µg/g	< 77	n.a.	50	343	514	n.a.	292	129

LOI = Loss On Ignition. n.a. = not analyzed. Spl harz: spinel harzburgite, Pl harz: plagioclase-bearing harzburgite. Mg# calculated as (MgO/40.3)/[(MgO/40.3)+(Fe2O3/159.7)].

and PIA109 as products of melt impregnation, there is a good coincidence concerning the composition of the calculated melt between the two samples (Table 3.5; Fig. 3.7A-B). For any value of Mg# used, the patterns obtained by calculation were the same, but the REE concentrations vary for middle to heavy REEs. For samples PIA109 and PIA120, the modelled melt is characterized by a flat heavy REE pattern at one to three times the primitive mantle value (McDonough and Sun, 1995), and a strong fractionation between light and heavy REEs, with a $[Pr/Yb]_N$ ratio of 0.08 and 0.004, respectively (Fig. 3.7A-B). This melt has a similar REE pattern as those published for depleted and ultra-depleted melt inclusions (Sobolev and Shimizu, 1993; Gurenko and Chaussidon, 1995) or depleted and ultra-depleted cumulates from mid-ocean ridges (Ross and Elthon, 1993; Nonnotte et al., 2005). These melts show very low REE abundances (Table 3.5) compared to N-MORB (Fig. 3.7A-B). The strong depletion in light REEs rule out highly evolved liquids (where Mg# would be < 0.745), and the absence of strong inter-element fractionation (most importantly between Sr and Eu) makes cumulates unlikely (where Mg# would be >> 0.745). From this result, it can be deduced that in these two samples, melt-related plagioclase and clinopyroxene probably crystallized from a trapped ultra-depleted melt (primitive melt) with an Mg# of ~0.745.

Table 3.5
Modelization of melt composition in impregnated plagioclase-bearing harzburgite

Sample	PIA120	PIA109
Fixed parameter	Mg#	Mg#
Unit	0.745	0.745
(wt. %)		
SiO2	49.39	46.10
TiO2	0.48	0.42
Al2O3	13.01	13.74
Fe2O3	10.04	12.04
MnO	0.19	0.14
MgO	14.81	17.75
CaO	12.44	10.51
(µg/g)		
Ce	0.093	n.c.
Pr	0.062	0.003
Sr	16.673	0.322
Sm	0.536	0.244
Eu	0.187	0.090
Gd	0.935	0.582
Tb	0.231	0.167
Dy	1.873	1.497
Ho	0.424	0.364
Y	11.164	9.742
Er	1.301	1.164
Tm	0.193	0.180
Yb	1.326	1.305
Lu	0.213	0.217

n.c.: not calculated because value in plagioclase-bearing harzburgite higher than in spinel harzburgite.

Depleted to ultra-depleted melt composition was postulated by Pelletier et al. (submitted b) for the impregnating melt in the Dramala plagioclase-bearing harzburgite. In these rocks, clinopyroxene and plagioclase have major element compositions (Pelletier et al., submitted b; plagioclase: An_{81-91}; clinopyroxene: Mg# = 0.91-0.94 and TiO_2 = 0.18-0.50 wt. %) near to those observed in cumulates from DSDP site 334 (Nonnotte et al., 2005; plagioclase: An_{88-89}; clinopyroxene: Mg# = 0.87-0.89 and TiO_2 = 0.09-0.14 wt. %). Mg# of 0.745 is similar to Mg# measured in melt inclusions after Sobolev and Shimizu (1993; Mg# = 0.745) and Gurenko and Chaussidon (1995; Mg# = 0.682-0.747), and in depleted cumulates from the Garrett transform fault after Constantin (1999; Mg# = 0.772-0.849).

In contrast, the pattern obtained for the calculated melt in sample PIA51 during the model run is strongly depleted compared to published REE patterns of depleted and ultra-depleted melt inclusions or cumulates, and is characterized by a depletion in light REEs and a fractionation between middle and heavy REEs with a $[Tb/Yb]_N$ ratio of ~ 0.24. Due to this strong depletion and to the positive Sr anomaly observed in this sample, melt-related plagioclase and clinopyroxene probably does not represent a trapped melt, but cumulate phases crystallized from an ultra-depleted (primitive) percolating melt.

The fact that clinopyroxene and plagioclase represent cumulates, rather than a trapped melt in sample PIA51, explains the observed discrepancies between this sample and the other plagioclase-bearing harzburgites (Pelletier et al., submitted b). Samples PIA120 and PIA109 were collected in the MOHO transition zone mapped by Rassios (1991) and Rassios and Grivas (2001), while PIA51 was sampled in the peridotite zone where plagioclase-bearing harzburgites are rare (Fig. 3.2). Major

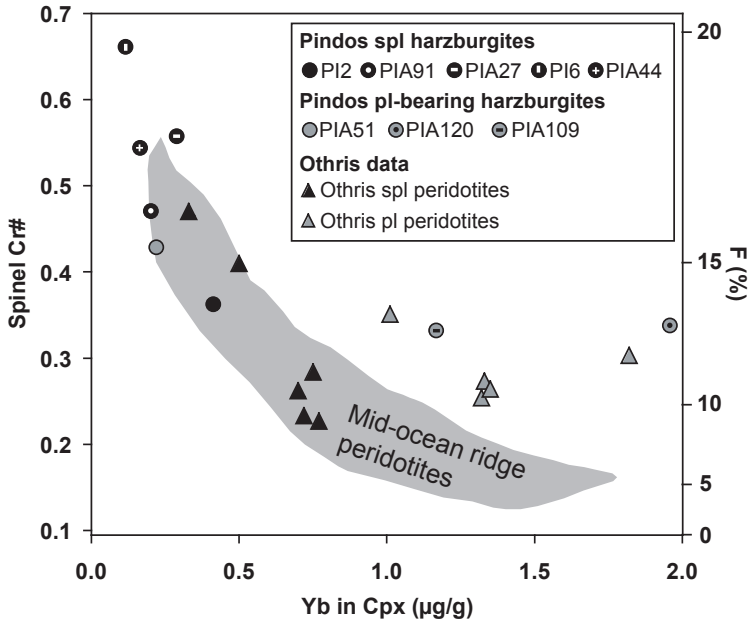


Fig. 3.8: Spinel Cr# vs. Yb (μg/g) in clinopyroxene (mean for each sample, clast core compositions) illustrating the depletion of the Dramala spinel harzburgite. Impregnated plagioclase-bearing harzburgite plotted for comparison. Diagram compiled from Hellebrand et al. (2001). Partial melting degree (F) given by Hellebrand et al. (2001) for pure fractional melting. Literature data: Othris plagioclase and spinel peridotites after Barth et al. (2003) and Dijkstra et al. (2003), mid-ocean ridge peridotites after Johnson and Dick (1992), Dick and Natland (1996), Ross and Elthon (1997), Hellebrand et al. (2001) and Seyler et al. (2007).

element composition of clinopyroxene from sample PIA51 is similar to the one of spinel harzburgites, with low Mg#, low TiO_2, Na_2O and Al_2O_3 compared to those of PIA120 and PIA109 (Fig. 3.4A-B; Pelletier et al., submitted b). Clinopyroxene from sample PIA51 is characterized by light REE contents systematically intermediate between those of clinopyroxene from plagioclase-bearing harzurgites PIA120 and PIA109 and clinopyroxene from spinel harzburgites (Fig. 3.5A). While PIA51 shows a spoon-shaped pattern in whole rock, samples PIA120 and PIA109 are characterized by a strong fractionation between light and heavy REEs (Fig. 3.6), because trapped melt induced an enrichment of the rock of all REEs, including the heavy REEs.

Melt infiltration in spinel harzburgite and the famous spoon-shaped pattern

In order to test if spinel harzburgite show evidence for interaction with a melt similar to the one observed in plagioclase-bearing harzburgite, and if this melt could be responsible for the spoon-shaped pattern, the first step consists in determining the degree of partial melting recorded in the spinel harzburgite. The composition of the depleted harzburgite obtained by the first step will then be used as the starting composition of the mantle column in the Percol-1D model of J.-L. Bodinier based on Navon and Stolper (1987), where the melt percolation of the ultra-depleted melt through a depleted harzburgite will be modelled.

The degree of partial melting prior to melt impregnation was estimated with two different methods: (i) From the Cr# of spinel (molar Cr/(Cr + Al) ratio), partial melting degree can be calculated for ideal pure fractional melting by a simple formula ($F = 0.1 \cdot \ln(Cr\#) + 0.24$), which was empirically defined by Hellebrand et al. (2001) for spinel Cr# between 0.10 and 0.60. This calculation can be applied to spinel clast cores from spinel harzburgite of the Dramala complex only. Cr# of rims and of smaller grains as well as spinel from plagioclase-bearing harzburgite could have been modified during different processes (diffusion, melt percolation or impregnation). Using this method, the degree of partial melting of the Dramala spinel harzburgite is estimated at 13-18% (Fig. 3.8), for

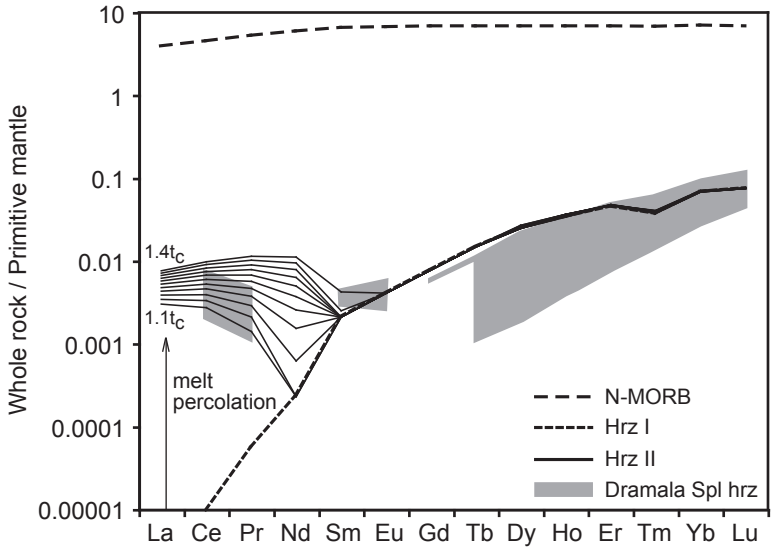


Fig. 3.9: Results of modelling of 22% non-modal near-fractional melting (Hrz I), and of N-MORB type melt percolation into Hrz I, in order to obtain spoon-shaped REE pattern (Hrz II) similar to those of the Dramala spinel harzburgite (Percol-1D model of J.-L. Bodinier based on Navon and Stolper, 1987). N-MORB after McDonough and Sun (1989). Modelling Hrz I parameters used: source modes, cpx = 0.18, opx = 0.23, ol = 0.57 and spl = 0.02; liquid modes, cpx = 0.74, opx = 0.44, ol = -0.2, spl = 0.02. Modelling Hrz II parameters used: grain size in cm, ol and opx = 0.1, cpx and spl = 0.03; diffusion coefficients in minerals = 10^{-14} $cm^2 \cdot s^{-1}$ and in melt = 10^{-8} $cm^2 \cdot s^{-1}$; melt fraction porosity = 1%; melt velocity = 1 $cm \cdot yr^{-1}$; realistic partition coefficients were used; t_c = time it takes for the fluid to pass through the modelled mantle column, e.g. if t_c is 100'000 years, it will take between 110'000 and 140'000 years to obtain the spoon-shaped pattern observed in the Dramala spinel harzburgite. Results of calculations with the ultra-depleted melt composition calculated from plagioclase-bearing harzburgite (see Table 3.5) give Hrz II similar to Hrz I.

Cr# between 0.32 and 0.57 (sample PI6 cannot be considered as its Cr# in spinel is 0.65-0.67, but it will give 20%); (ii) The degree of melting can also be estimated with a non-modal near-fractional melting model (details of the model in Dijkstra et al., submitted). The calculation is based on the REE composition of the depleted mantle as the source (Salters and Stracke, 2004), and on representative whole rock/melt partition coefficients for the REEs (Kennedy et al., 1993; Bédard, 1994; Hauri et al., 1994). Results in agreement with middle to heavy REE patterns of Dramala spinel harzburgite imply about 22% near-fractional melting with incremental batch melting steps of 0.1% (see Hrz I on Fig. 3.9).

Both calculations show that Dramala spinel harzburgite was highly depleted prior to melt impregnation, with up to 22% partial melting, leading to a strong depletion in the light REEs compared to the heavy REEs (see Hrz I on Fig. 3.9). This is in agreement with the REE pattern of clinopyroxene in sample PI2, which is strongly depleted in light REEs and shows a $[Ce/Yb]_N$ ratio of ~ 0.0001. There is a positive correlation between Cr# in clinopyroxene and Cr# in spinel in spinel harzburgite (except sample PIA44), which is aligned along the global abyssal peridotite dataset (Dick and Natland, 1996; Müntener and Manatschal, 2006). It shows that these rocks are probably residues of melting in the spinel peridotite field. However, the slope of the heavy REEs observed in the Dramala spinel harzburgite compared to the modelled trend, shows that melting in the garnet peridotite field (Hellebrand et al., 2002; Seyler et al., 2007) could have occurred in the Dramala spinel harzburgite. This garnet field melting could also explained the very high Cr# (Seyler et al., 2007) observed in sample PI6 (0.65-0.67). The different behaviour observed in sample PIA44 could be due to melt impregnation or re-equilibration in the plagioclase-stability field (Müntener and Manatschal, 2006).

In order to the test whether the observed spoon-shaped patterns could be the result of melt percolation, the Percol-1D model was run with a depleted mantle column after 22% non-modal

near-fractional melting (Hrz I in Fig. 3.9). In the first run, the depleted mantle column was infiltrated by the ultra-depleted melt calculated from Dramala plagioclase-bearing harzburgite. The results of modelling show that the spoon-shaped REE pattern observed in the Dramala spinel harzburgite cannot be obtained by percolation of an ultra-depleted melt, because this melt is in equilibrium with the depleted mantle column (Hrz I). Thus, the melt percolates without changing the composition of the depleted mantle column (Hrz I). In a second run, the depleted mantle column was infiltrated by a N-MORB type melt (Fig. 3.9). In contrast to the ultra-depleted melt, the N-MORB percolation generated a spoon-shaped REE pattern during modelling (Hrz II in Fig. 3.9), which is similar to the spoon-shaped pattern observed in Dramala spinel harzburgite (Fig. 3.9). This reflects strong disequilibrium between the depleted Dramala spinel harzburgite and the percolating N-MORB type melt, which lead to a selective enrichment in light REEs compared to heavy REEs.

As Pelletier et al. (submitted b) mentioned Li enrichment related to melt metasomatism (with contents ~ 1 μg/g) and very low Be and B contents (< 0.003 μg/g and < 0.1 μg/g) in fresh Dramala spinel harzburgite, the same modelling approach with an N-MORB melt was applied to Li, Be and B. The model was run with very low Li, Be and B concentrations in the depleted mantle column (0.0001 μg/g for the three elements), because these three elements are extremely incompatible during melting of peridotites (Brenan et al., 1998a). In the input, mineral/melt partition coefficients for olivine, clinopyroxene and orthopyroxene given by Brenan et al. (1998a) were used. Spinel/melt partition coefficents for these elements were estimated from spinel compositions in peridotites given by Ottolini et al. (2004). For Be and B, diffusion coefficients in minerals similar to those for the REEs were used, while for Li a higher diffusion coefficient was chosen according to Coogan et al. (2005). Average Li, Be and B contents of N-MORB were used (3.1 μg/g, 7 μg/g and 4 μg/g, respectively). The results show that Be and B whole rock contents observed in the Dramala spinel harzburgite can be obtained with the parameters used above for the REEs, and their whole rock contents do not drastically increase during percolation. On the contrary, for Li, it is impossible to attain during modelling the Li enrichment observed in the Dramala spinel harzburgite, unless the percolation time is hundred times the one required for the other elements (REEs, Be, B). This means that the Li metasomatism observed in the Dramala spinel harzburgite (Pelletier et al., submitted b) cannot be due to percolation only, but should be related to the crystallization of a cumulate phase within the depleted harzburgite, which could potentially retain a certain quantity of Li.

As mentioned before, the Dramala spinel harzburgite is a residue after up to 22% partial melting, which is close to the clinopyroxene-out boundary. For that reason, very low modal clinopyroxene should be observed in these rocks (about 1%). In contrary, the fresh spinel harzburgite contains about 3 to 4 modal % clinopyroxene (Pelletier et al., submitted b), which shows that clinopyroxene potentially crystallized during melt percolation in these rocks after their original depletion. This is in agreement with the lobed shape of some clinopyroxene observed in some Dramala spinel-harzburgite (Fig. 3.3A), which had already been related to melt percolation by Pelletier et al (submitted b). Crystallization of clinopyroxene could be responsible for the Li enrichment observed in these rocks. This would also explain the fact that clinopyroxene shows higher Li contents compared to olivine in some abyssal and ophiolitic harzburgites (Pelletier et al., submitted b; Vils et al., in prep.), despite the fact that the two minerals have similar $^{Li}D_{mineral/melt}$ (olivine: 0.13-0.35, cpx: 0.14-0.27; Brenan et al., 1998a). This process of clinopyroxene crystallization during melt percolation through depleted harzburgites coupled with spoon-shaped REE pattern in whole rock, was also observed in some harzburgites from the Oman ophiolite, and related to melt-rock reaction at decreasing melt mass (Godard et al., 2000).

In conclusion, this modelling shows that the spoon-shaped REE pattern observed in the Dramala spinel harzburgite can result from N-MORB percolation through a highly depleted spinel harzburgite, but not from ultra-depleted melt percolation. Li metasomatism observed by Pelletier et al. (submitted b) could be related to the crystallization of clinopyroxene as a cumulate phase during N-MORB percolation through depleted spinel harzburgite.

Evolution of the Dramala mantle over time

The Dramala mantle followed a complex

history of partial melting, melt percolation, and melt impregnation, which are resumed in Figure 3.10. The Dramala mantle was subject to up to 22% partial melting, which mainly occurred in the spinel stability field, but probably began in the garnet peridotite field, as shown by low heavy REE contents in the Dramala spinel harzburgite (Hrz I on Fig. 3.10). This high degree of partial melting generated high Cr# in spinel, up to 0.67, low modal percentage of clinopyroxene, and a depletion of the rock (Fig. 3.10) and its primary clinopyroxene (Fig. 3.5A sample PI2) in all the rare earth elements (REE) with a strong fractionation between light and heavy REEs ($[Ce/Yb]_N$ ratio of ~ 0.0001 in some clinopyroxene, Fig. 3.5A).

The resulting spinel harzburgite was later percolated by an N-MORB type melt, which generated the spoon-shaped REE pattern in clinopyroxene (Fig. 3.5A all Dramala spinel harzburgites except sample PI2, and Hrz II on Fig. 3.10) and whole rock samples (mean $[Ce/Sm]_N$ of 1.42, mean $[Tb/Yb]_N$ of 0.08 in whole rock, Fig. 3.6), by a selective enrichment in the light REEs compared to the heavy REEs. This melt metasomatism was accompanied by the crystallization of clinopyroxene, which was responsible for a Li enrichment in these rocks. The inconsistency observed between the degree of partial melting and the modal content of clinopyroxene in some fresh Dramala spinel harzburgite (modal clinopyroxene 3-4%; Pelletier et al., submitted b) is easily explained by this clinopyroxene crystallization during N-MORB percolation.

Finally, the Dramala spinel harzburgite was percolated and impregnated by an ultra-depleted melt, which shows a REE composition similar to published depleted and ultra-depleted melt compositions (Fig. 3.7A-B, Table 3.5; Ross and Elthon, 1993; Sobolev and Shimizu, 1993; Gurenko and Chaussidon, 1995; Nonnotte et al., 2005). This ultra-depleted melt impregnation lead to the crystallization of plagioclase and clinopyroxene, turning the spinel harzburgite into a plagioclase-bearing harzburgite. In sample PIA109 and PIA120, the ultra-depleted melt was certainly trapped, while in sample PIA51 clinopyroxene and plagioclase crystallized as cumulates. Clinopyroxene from the Dramala plagioclase-bearing harzburgite is characterized by higher TiO_2, Na_2O, and lower Mg# compared to those in the Dramala spinel harzburgite, and plagioclase by $An_{0.81-0.91}$. Clinopyroxene and whole rock REE patterns resulting from this ultra-depleted melt impregnation are characterized by high light to heavy REE contents compared to those in the Dramala spinel harzburgite, and by a strong fractionation between light and heavy REEs (mean $[Ce/Sm]_N$ of 0.05 in whole rock). Plagioclase also has a fractionation between the light and middle REEs (Fig. 3.5C).

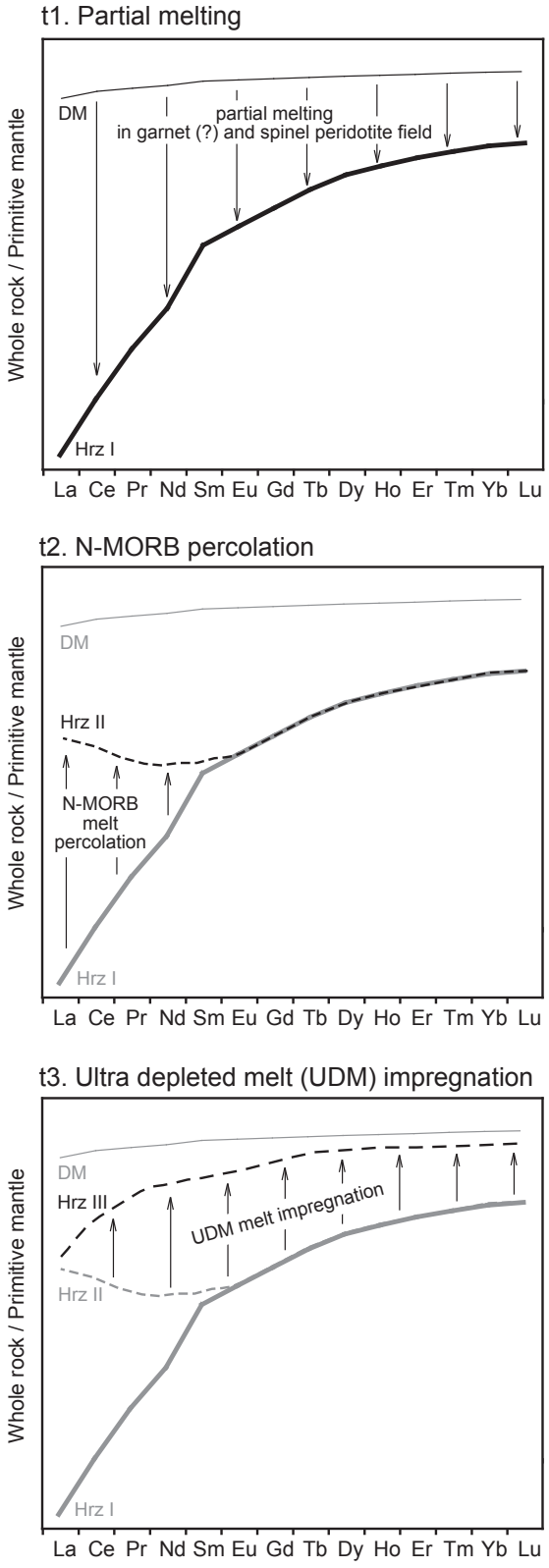
These results show that all steps of mantle evolution are potentially recorded by REEs and Li in clinopyroxene, while in whole rock the light REEs depletion due to high degree of partial melting cannot be identified anymore. This light REEs depletion in whole rock related to partial melting was overprinted during N-MORB percolation, while it was preserved in some primary clinopyroxenes.

CONCLUSION

All these results show that the Dramala mantle followed an evolution similar to present-day mid-ocean ridges, as postulated by Pelletier et al. (submitted b), and that the spoon-shaped REE pattern observed in clinopyroxene and whole rock samples from the Dramala spinel harzburgite could be related to a N-MORB percolation in a depleted harzburgite. This scenario offers an alternative to the first hypothesis of subduction-related hydrous melting, postulated by Bizimis et al. (2000) for the Dramala mantle from spoon-shaped REE patterns in clinopyroxene and whole rock. This study also shows that REE composition of clinopyroxene records a more detailed history of depletion and melt percolation than whole rock REE contents. In rare cases, clinopyroxene can conserve the REE pattern related to high degree partial melting, despite late melt percolation.

Present results demonstrate that ultra-depleted (primitive) melt could occur at mid-ocean ridges. These type of melts can be trapped within the cooling mantle or can percolate through it and lead to the crystallization of plagioclase + clinopyroxene cumulates. These ultra-depleted melts are probably one component of the MORB aggregate, which is normally considered as produced by polybaric melting of the mantle column beneath a mid-ocean ridge.

The Dramala mantle, which is part of the Pindos



Harzburgite I (Hrz I):

Very low modal Cpx

Cr# in spinel 0.32-0.67

WR and Cpx depletion in LREE to HREE

Harzburgite II (Hrz II):
Dramala spinel harzburgite

Crystallization of Cpx

Cr# in spinel 0.32-0.67

WR and Cpx enrichment in LREE

WR enrichment in Li, related to cpx crystallization

Harzburgite III (Hrz III):
Dramala plagioclase-bearing harzburgite

Crystallization of Plg and Cpx

TiO_2 enrichment in Cpx and Spl

High An# in Plg 0.81-0.91

WR and Cpx enrichment in LREE to HREE

Fig. 3.10: Evolution of the whole rock REE pattern of the Dramala mantle with time (t1, t2 and t3), and characteristic features related to each stage (mineralogy and/or major element chemistry). Hrz II and Hrz III correspond to the Dramala spinel and plagioclase-bearing harzburgites, respectively. Abbreviations: DM = depleted mantle, WR = whole rock, LREE, MREE and HREE are light, middle and heavy REEs, respectively.

ophiolite, was probably tectonically assembled with subduction-related volcanics (island arc tholeiites and boninites) of the Aspropotamos complex (Jones and Robertson, 1991), as postulated by Pelletier et al. (submitted b). These two units certainly represent contrasting tectonic settings. To resolve assemblage and evolution of the Pindos ophiolite is beyond the scope of this paper, but two scenarios can be postulated. (i) The Dramala mantle was formed in a back-arc setting, simultaneously with the Aspropotamos complex, which formed in a forearc environment. These units were later tectonically juxtaposed, as deduced from the observation of present-day supra-subduction zone oceanic lithosphere (Hawkins, 2003). Present-day equivalents would be the Lau Basin – Tonga Trench region of southwestern Pacific and the Mariana Trough – Mariana Trench region of the northwestern Pacific (Flower and Dilek, 2003). (ii) The Dramala mantle was formed at a mid-ocean ridge, and was emplaced above an intra-oceanic subduction zone close to or directly at the ridge shortly after its formation (Boudier et al., 1988; Barth et. al., 2007). During this stage, island arc tholeiites and boninites erupted in a forearc setting, as proposed by Dilek and Flower (2003) and Flower and Dilek (2003).

ACKNOWLEDGEMENTS

We thank E. Gnos, A. Berger and H.-P. Meyer for analytical support, and H. Marschall (University of Bristol) for the ICP-MS analyses. We are grateful to J.-L. Bodinier for the Percol-1D model. This work was financially supported by grants of the Swiss NSF (200020-112149) to A. Kalt. We acknowledge financial support by the Swiss NSF grant 200021-103479/1 and by the Canton of Bern for the electron microprobe facility at the Institute of Geological Sciences, University of Bern.

Li, Be and B mobility during emplacement of ultramafic rocks into the continental crust: the example of the Geisspfad body (Swiss-Italian Alps)

L. Pelletier[1], O. Müntener[2], A. Kalt[1], T.W. Vennemann[2], T. Belgya[3]

[1]Institute of Geology and Hydrogeology, University of Neuchâtel, Emile Argand 11, CP158, 2009 Neuchâtel, Switzerland
[2]Institute of Mineralogy and Geochemistry, University of Lausanne, Anthropole, 1015 Lausanne, Switzerland
[3]Institute of Isotopes, Hungarian Academy of Sciences, P.O. Box 77, 1525 Budapest, Hungary

Manuscript accepted by Chemical Geology with moderate revisions

Abstract

The Geisspfad ultramafic complex (Swiss-Italian Alps) represents a relict oceanic succession composed of serpentinites, ophicarbonates and metabasites, which was emplaced into the continental crust during Alpine collision. The Li, Be, and B contents of minerals and whole rock samples were determined, to evaluate the influence of continental crustal rocks on light element contents of serpentinized ultramafic rocks. Following peak metamorphic amphibolite facies conditions the Li, Be, and B contents of ultramafic rocks were modified during two successive stages of fluid flow. During the first stage at high temperature (425-525°C), the ultramafic rocks were enriched in Li, Be, and B. Fluids liberated from continental crustal rocks moved through the contact from the gneiss into the ultramafics on a distance ≤ 400 m, as suggested by the retrograde reaction olivine + tremolite + fluid -> antigorite + diopside in the serpentinites and the formation of antigorite + tremolite + calcite in ophicarbonates along the border of the ultramafic body. This retrograde recrystallization is monitored by the enrichment in Pb and U, the modification of Li, Be, and B and by the low δD values of –112 ‰ of some ophicarbonates at the border of the massif. Later, Li and Rb were leached from the ultramafic rocks along the sheared contact (maximum 150 m) at temperatures ≥ 300°C. In the centre of the massif, Li is preferentially concentrated in olivine, and Be and B in tremolite. On the contrary, at the outer rim of the massif, Li and Be are preferentially incorporated into diopside, and B into antigorite. This redistribution of light elements among olivine, tremolite, diopside and antigorite is readily explained by retrograde recrystallization

induced by externally derived fluids. Our results show that emplacement of altered ultramafic rocks into the continental crust changes mineral and whole rock light element budgets. Thus, light element budgets of (ultra) high pressure orogenic peridotites and subducted oceanic lithosphere are probably modified during emplacement, and only large ultramafic bodies (at least 1.0 km width) can potentially maintain the subduction-related light element systematics in their core.

Key words: Lithium; Beryllium; Boron; Serpentinite; Fluid metasomatism; Retrograde metamorphism

INTRODUCTION

Light elements, mainly Li and B, have been studied for some years in serpentinites from mid-ocean ridges (Bonatti et al., 1984; Früh-Green et al., 1996; Decitre et al., 2002; Niu, 2004; Paulick et al., 2006), forearc (Benton et al., 2001 and 2004; Savov et al., 2005; Wei et al., 2005), and ophiolitic (Scambelluri et al., 2004; Pelletier et al., submitted a) environments, as well as in rare high pressure serpentinites (Scambelluri et al. 2004; Marschall, 2005). These studies demonstrate that the interaction between peridotite and seawater can lead to a considerable enrichment of the serpentinites in B, and to a lesser extent in Li. In the Mariana forearc serpentinites, Li enrichment is more pronounced than at mid-ocean ridges, and is related to slab-derived fluids released by the subducting oceanic lithosphere (Benton et al., 2004). Be content of mid-ocean ridge and ophiolitic serpentinites is extremely low (e.g. ODP Leg 209: Vils et al. (in prep.), Pindos ophiolite: Pelletier et al. (submitted a)). Taken together, these data provide information about the potential input of light elements into subduction zones via serpentinites.

Recently, Scambelluri et al. (2004) studied the Li and B composition of the oceanic mantle under increasing pressure and temperature during Alpine subduction, using samples from the Alps, the Northern Apennine and the Sierra Nevada in Southern Spain. They showed that there is a progressive release of oceanic B with increasing pressure and temperature into the metamorphic fluid, but also that a significant quantity of B can be retained in high pressure phases (olivine and Ti-clinohumite), and potentially transported to the deep mantle. B capture by olivine at high pressure during antigorite breakdown was demonstrated experimentally by Tenthorey and Hermann (2004). Scambelluri et al. (2004) showed that Li contents of high pressure peridotites (4.9 μg/g; Betic Cordillera) derived from an oceanic serpentinite precursor are higher than those of oceanic serpentinites (1.3 μg/g; Erro Tobbio unit), suggesting a potential input due to an external source. Marschall (2005) studied Li, Be and B contents in high pressure serpentine and serpentinites of northern Syros (Greece) and Pfulwe Pass (Switzerland). The Syros serpentinites have Li (0.9-2.8 μg/g) and B (5.5-11.3 μg/g) concentrations slightly lower than those of the altered oceanic mantle (Li: ~ 3.5 μg/g, Decitre et al., 2002; B: 20-100 μg/g, Thompson and Melson, 1970, Bonatti et al., 1984, Spivack and Edmond, 1987), but are clearly enriched in Be (0.2-0.5 μg/g) compared to these rocks (~ 0.04 μg/g; Niu, 2004).

In order to study the slab-to-mantle wedge transfer of light elements, Li, Be, and B contents of high pressure garnet peridotites were investigated (Paquin et al., 2004; Scambelluri et al., 2006). Both data sets suggest a metasomatic overprint of these rocks by subduction-related fluid or melt, which modified the light element budget of the peridotites. In the Alpe Arami peridotites, an addition of Li, a limited addition of B and no change in the Be contents occurred (Paquin et al., 2004). In the Ulten peridotites, a clear enrichment in Li and to a lesser extent in Be were measured (Scambelluri et al., 2006).

All these studies focused on subducted serpentinites and high pressure wedge peridotites, but did not discuss the potential light element transfer during incorporation of these rocks into the crust. Li and Be contents of the continental crust (Rudnick and Gao, 2004 and references therein) are much higher than those of serpentinites or unmetasomatized peridotites (e.g. Decitre et al., 2002; e.g. review by Niu, 2004; Ottolini et al., 2004). B content of the continental crust (Rudnick and Gao, 2004 and references therein) is lower than or comparable to the one of serpentinites (Spivack and Edmond, 1987 and references therein), but clearly higher than values for unmetasomatized mantle. It is not known how the light element budget of ultramafic bodies is modified during emplacement into the continental crust, and if the light element

systematics observed in high pressure mantle rocks are only related to the subduction event. In order to exclude the influence of subduction-related fluids or melts, it is important to study an ultramafic body which was not subducted, but emplaced directly into the continental crust. The Geisspfad ultramafic massif meets these criteria.

The objective of the present study was to characterize the Li, Be and B contents (minerals and whole rock samples) of serpentinized peridotites during regional metamorphism in a continental environment. Samples of ultramafic rocks were collected along several profiles through the Geisspfad massif, to measure possible variations of the light element contents. Li, Be and B contents of minerals and whole rocks, $\delta^{18}O$ and δD values of the bulk rock and rare earth element contents of ultramafics were determined in order to constrain the nature and origin of the Geisspfad protolith, and to trace eventual metasomatism. The effects of the emplacement of ultramafic rocks into the continental crust on the light element budget will be discussed.

GEOLOGICAL SETTING

The Geisspfad ultramafic massif (Valais, Switzerland) is one of the largest ultramafic bodies in the Central Alps (Pastorelli et al., 1995) and is incorporated into the lower Penninic Monte Leone nappe (Fig. 4.1; Keusen, 1972; Pastorelli et al., 1995), which includes crystalline basement rocks and an overturned Mesozoic sedimentary cover. The nappe belonged to the distal European margin before the Alpine collision. In the Geisspfad region, the Monte Leone nappe includes gneisses of magmatic and sedimentary origin, Triassic dolomitic marbles and some calcschists (Pastorelli et al., 1995). The Geisspfad body and the gneiss were both metamorphosed under amphibolite facies conditions (Keusen, 1972) during Alpine metamorphism, meaning that the Geisspfad massif was certainly incorporated into the gneiss prior to this metamorphic event. Age and paleogeographic position of the Geisspfad ultramafic body are largely unknown.

During the Alpine orogeny, the ultramafic rocks

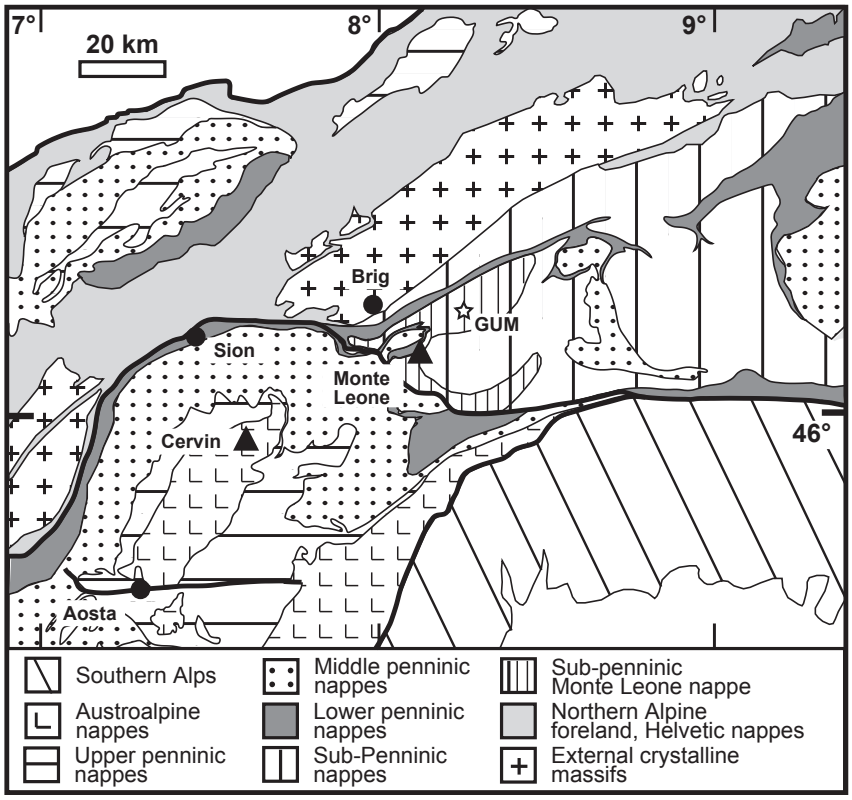


Fig. 4.1: General tectonic overview of the Central Alps (modified after Schmid et al., 2004). GUM: Location of the Geisspfad ultramafic massif.

of the Geisspfad body recrystallized under lower amphibolite facies conditions during prograde metamorphism (Keusen, 1972; Pastorelli et al., 1995). Pastorelli et al. (1995) estimated temperatures between 520 and 560 °C and pressures between 0.6 and 0.7 GPa for this metamorphism, selecting plagioclase-hornblende pairs in metabasites and using the geothermobarometer of Plyusnina (1982).

The Geisspfad ultramafic body is composed of various ultramafic and mafic rocks, mainly serpentinite, ophicarbonate and metabasic dykes (Fig. 4.2; Keusen, 1972; Pastorelli et al., 1995). Keusen (1972) and Pastorelli et al. (1995) defined a lherzolitic origin for the mantle protolith. In a fresh granular lherzolite from the Geisspfad ultramafic body, Pastorelli et al. (1995) described assemblages of orthopyroxene + clinopyroxene + spinel, which might represent breakdown products of precursor garnet. However, this fresh lherzolite was collected in loose blocks (east of Rothorn, Pastorelli S. personal communication), and was not found during sampling for the present study. The inferred garnet to spinel facies transition could be related to an uplift from deep lithospheric levels towards the sea floor. Metabasic dykes show a MORB tholeiitic affinity, and are usually rodingitized (Pastorelli, 1994). Pastorelli et al. (1995) concluded that the Geisspfad ultramafic body represents a piece of exhumed subcontinental mantle, which was probably emplaced in an ocean-continent transition environment during pre-Alpine rifting, by analogy to other ultramafic bodies in the Alps and Apennine (e.g. Müntener et al., 2000; Manatschal et al., 2003).

Different mafic lithologies were found at the contact between the Monte Leone gneiss and the serpentinite (Keusen 1972) and were interpreted as

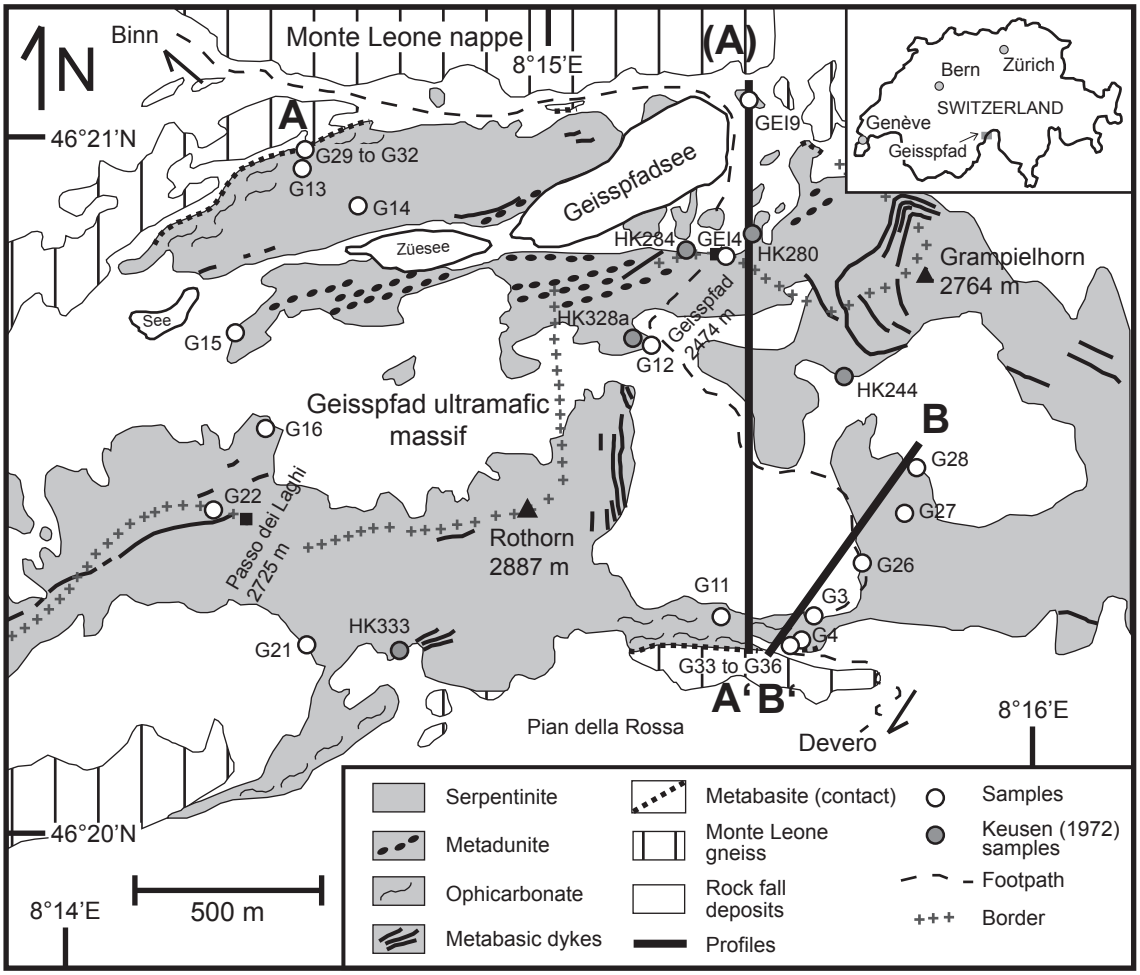


Fig. 4.2: Simplified geological map of the Geisspfad ultramafic massif (modified after Keusen, 1972), illustrating the contact between the ultramafic unit and the surrounding Monte Leone nappe. Profiles A-A' and B-B' refer to Figure 4.3.

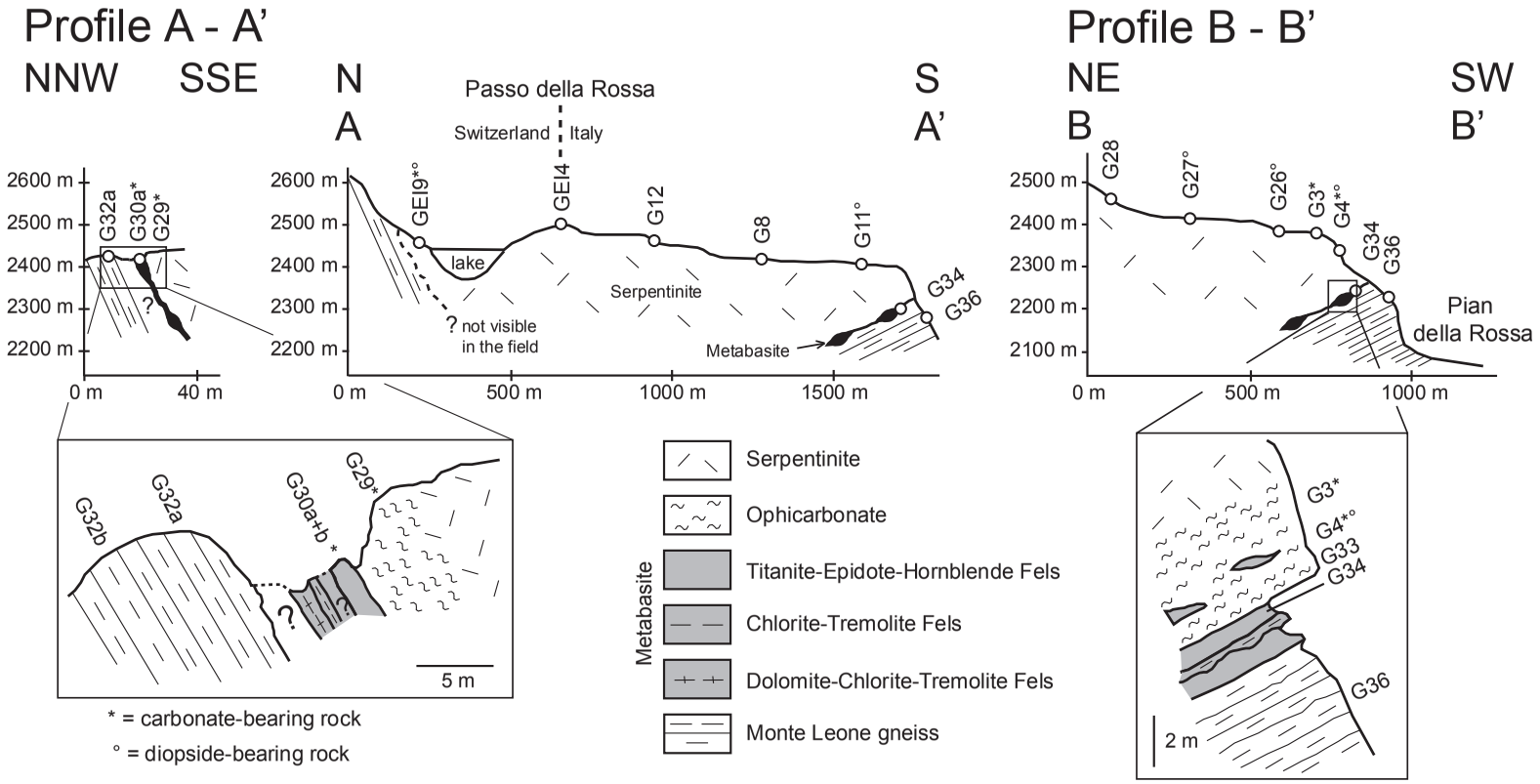


Fig. 4.3: Profiles of the contact between the ultramafic unit and the gneiss of the Monte Leone nappe, with position of the studied samples.

metabasalt and metagabbros (Pastorelli et al. 1995) (Fig. 4.2-4.3). They show a MORB affinity similar to metabasic dykes from the inner part of the massif, and they are generally rodingitized. Keusen (1972) mentioned the presence of ophidolomite in contact with the serpentinite.

ANALYTICAL TECHNIQUES

Major element contents of whole rock samples were measured by wavelength dispersive X-ray fluorescence (WD-XRF) at the Geosciences Department of the Fribourg University (Switzerland). Two grams of rock powder of each sample were dried for 6 to 12 hours in a furnace (110 °C), and the loss of weight was measured (humidity). Powders were later put in a furnace at 1000 °C for an hour under an oxidizing atmosphere. The final loss of weight was determined (Loss On Ignition, LOI), which represents the total loss of volatiles (H_2O and CO_2) and a gain of weight by oxidation of Fe^{2+}. 0.70 g of this dry powder was mixed with 6.65 g of dried lithium tetraborate ($Li_2B_4O_7$) and 0.35 g of dried lithium fluoride (LiF). This mix was put in a Pt-Au-ZrO crucible, in order to obtain a glass after 10 minutes heating at 1150 °C with a PHILIPS PERL'X-2. These glasses were measured with a PHILIPS PW1400 X-ray fluorescence spectrometer. Detection limit was ~ 0.01 wt. % and reproducibility between 0.01 and 0.25 % depending on the element. A correction factor was applied to the analytical results considering the calibration of the instrument with 40 international reference standards.

Li, Be and trace element whole rock contents were measured by inductively coupled plasma mass spectrometry (ICP-MS), using a VG PQ ExCell quadrupole ICP-MS at the Boston University. All the details concerning sample preparation, ICP parameters and standards used are described in Kelley et al. (2003). The same protocol was followed, except for the final sample dilution (1/1000 instead of 1/2000). Element concentrations were measured in analogue mode, for high-abundance elements (> 5 ppb in solution). For elements < 5 ppb in solution (e.g. REE, Rb, Y, Ba, and Zr), a pulse counting mode was applied. DNC-1 (USGS) standard reference material was run as an unknown and also compared with the values of Kelley et al. (2003). Precision was evaluated by the measurement of in-run replicates showing a relative standard deviation (RSD) < 2-3 % for all elements. Precision decreases with decreasing abundance, and RSD can reach 5 % for low-abundance elements.

B, S, Cl, and H_2O whole rock contents were measured by Prompt Gamma Neutron Activation Analysis (PGNAA) at the facility of the Budapest Research Reactor (BRR). B, S, Cl elemental and H_2O whole rock contents in geological samples were determined previously with high precision by this method (Gméling et al., 2005; Marschall et al., 2005; Pelletier et al., submitted a). All details concerning analytical procedure can be found in Molnár (2004), Révay et al. (2004), Marschall et al. (2005) and Pelletier et al. (submitted a). PGNAA is particularly useful for analyzing whole rock boron concentrations, because no sample preparation is needed, which avoids contamination problems (Anderson and Kasztovszky, 2004). The principle of the PGNAA method is the detection of prompt γ-rays that originate from the (n,γ)-reactions during neutron irradiation (Révay and Belgya, 2004). The detection limit for boron (0.01 to 0.03 μg/g) was different in each sample, depending on measurement time and the sample weight. Relative uncertainty is small (1 to 2 %), and can reach 5 % if the B content is lower than 1 μg/g. Relative uncertainties for S, Cl and H_2O were calculated at 6 to 8, 6 to 18 and 2 to 3 % respectively. Detection limits were approximately 500 μg/g for S, 28 μg/g for Cl and 10 μg/g for H_2O.

The oxygen isotope composition (^{16}O, ^{17}O, ^{18}O) of the samples was measured at the University of Lausanne (Switzerland), using a method similar to that described by Sharp (1990) and Rumble and Hoering (1994), and is described in more detail in Kasemann et al. (2001). Between 0.5 to 2.0 mg of sample rock powder was loaded into a small Pt-sample holder and pumped out to a vacuum of about 10^{-6} mbar. After prefluorination of the sample chamber overnight, the samples were heated with a CO_2 laser in pure F_2 at 50 mbars of pressure. Excess F_2 was separated from O_2 produced by conversion to Cl_2 using KCl held at 150°C. The extracted O_2 was collected on a molecular sieve (5A) and subsequently expanded into the inlet of a Finnigan MAT 253 mass spectrometer. Oxygen isotope compositions are given in the standard δ-notation, expressed relative to VSMOW in permil (‰). Replicate oxygen isotope analyses of an in-house standard, LS-1 quartz (n = 2), gave a precision of

better than 0.1 ‰ for $\delta^{18}O$. The accuracy of $\delta^{18}O$ values is commonly better than 0.2 ‰ compared to accepted $\delta^{18}O$ values for LS-1 of 18.10 ‰.
Hydrogen isotope compositions of whole rock powders were measured at the University of Lausanne (Switzerland), using high-temperature (1450°C) reduction methods with He carrier gas and a TC-EA linked to a Delta Plus XL mass spectrometer from Thermo-Finnigan on 2 to 4 mg sized samples according to a method adapted after Sharp et al. (2001). The results are given in the standard δ-notation, expressed relative to VSMOW in permil (‰). The precision of the in-house kaolinite standard and NBS-30 biotite for hydrogen isotope analyses was better than ± 2 ‰ for the method used; all values were normalized using a value of –125 ‰ for the kaolinite standard and – 65 ‰ for NBS-30 analyzed during the same period as the samples.

Light element compositions of minerals were measured in situ by secondary ion mass spectrometry (SIMS) with a modified Cameca ims 3f ion microprobe (equipped with a primary beam mass filter) at the Institute of Mineralogy of the Ruprecht-Karls University of Heidelberg (Germany). A protocol minimizing boron surface contamination during sample preparation and measurements was followed (Marschall and Ludwig, 2004). SIMS measurements were performed on points previously measured at the electron microprobe. The primary $^{16}O^-$ ion beam was set to 14.5 keV at a current of 20 nA. Positive secondary ions were accelerated to 4.5 keV and the energy window was set to 40 eV. The energy filtering technique was applied with an offset of ~ 75 eV at a mass resolution m/Δm (10%) of ~ 1020. Quantitative results were obtained using relative sensitivity factors with ^{30}Si as reference isotope for silicates (Ottolini et al., 1993), and ^{44}Ca for carbonates. Detection limits (the critical value; Currie, 1968) during silicate measurements for samples G3, G4 and G27 were calculated at 2.0, 2.0 and 3.7 ng/g (ppb) for Li, Be and B, respectively. For the other samples, values were lower at 1.4 for Li, 1.0 for Be and 2.6 ng/g for B. Detection limits for carbonate measurements were calculated at 1.4, 1.0 and 2.6 ng/g (ppb) for Li, Be and B, respectively. All rock-forming minerals were analysed, except for oxides and sulphides. For carbonates, SRM610 glass was used as a standard and contains about 2 wt. % CaO, which is much lower than CaO content in carbonates. Moreover, there is probably a matrix effect between silicates and carbonates, which is unknown. The results presented in this paper for carbonates are hence approximate values, and may be off by a factor of two (T. Ludwig, personal communication).

SAMPLE DESCRIPTION AND MINERALOGY

Two different types of ultramafic rocks are present in the Geisspfad body. They are distinguishable by their degree of deformation and by their modes. The transition between these two types is gradual from the core to the rim of the massif. The first type is weakly deformed serpentinite (Fig. 4.2, 4.3, 4.4a-b) and represents > 95 % of the ultramafic massif (Fig. 4.2). This rock is characterized by the absence of carbonate and by the rare presence of diopside. The second type is ophicarbonate (Fig. 4.2 and 4.3), which is intensely deformed and shows a well-developed foliation (Fig. 4.4e). This rock is characterized by the presence of carbonate and diopside and forms a belt of a few meters width around the serpentinite (Fig. 4.2-4.3). In all the studied samples, the serpentine mineral is antigorite (Pelletier et al., submitted b). Between the ophicarbonate and the Monte Leone gneiss, a 2 to 5 m thick metabasite can be observed. This metabasite is composed of various rock types with variable mineralogy. The contact between the metabasite and the gneiss is tectonic and sharp. In contrast, ophicarbonate boudins are often found in the metabasite, suggesting that this contact is rather primary than tectonic (Keusen, 1972). Chemical compositions of the main minerals (major elements) can be found in Tables a.1 to a.6 in the Appendix.

Serpentinite

The serpentinite is a forsterite-tremolite-antigorite fels, sometimes containing diopside (Fig. 4.4a, c, d), a typical assemblage in hydrated peridotites metamorphosed under amphibolite facies conditions (Evans and Trommsdorff, 1970). The assemblage forsterite + tremolite + antigorite was mentioned for the first time in the Geisspfad ultramafic body by Preiswerk (1901) and described as a metamorphic assemblage by Keusen (1970). This assemblage results from partial dehydration of the serpentinite during the reaction antigorite

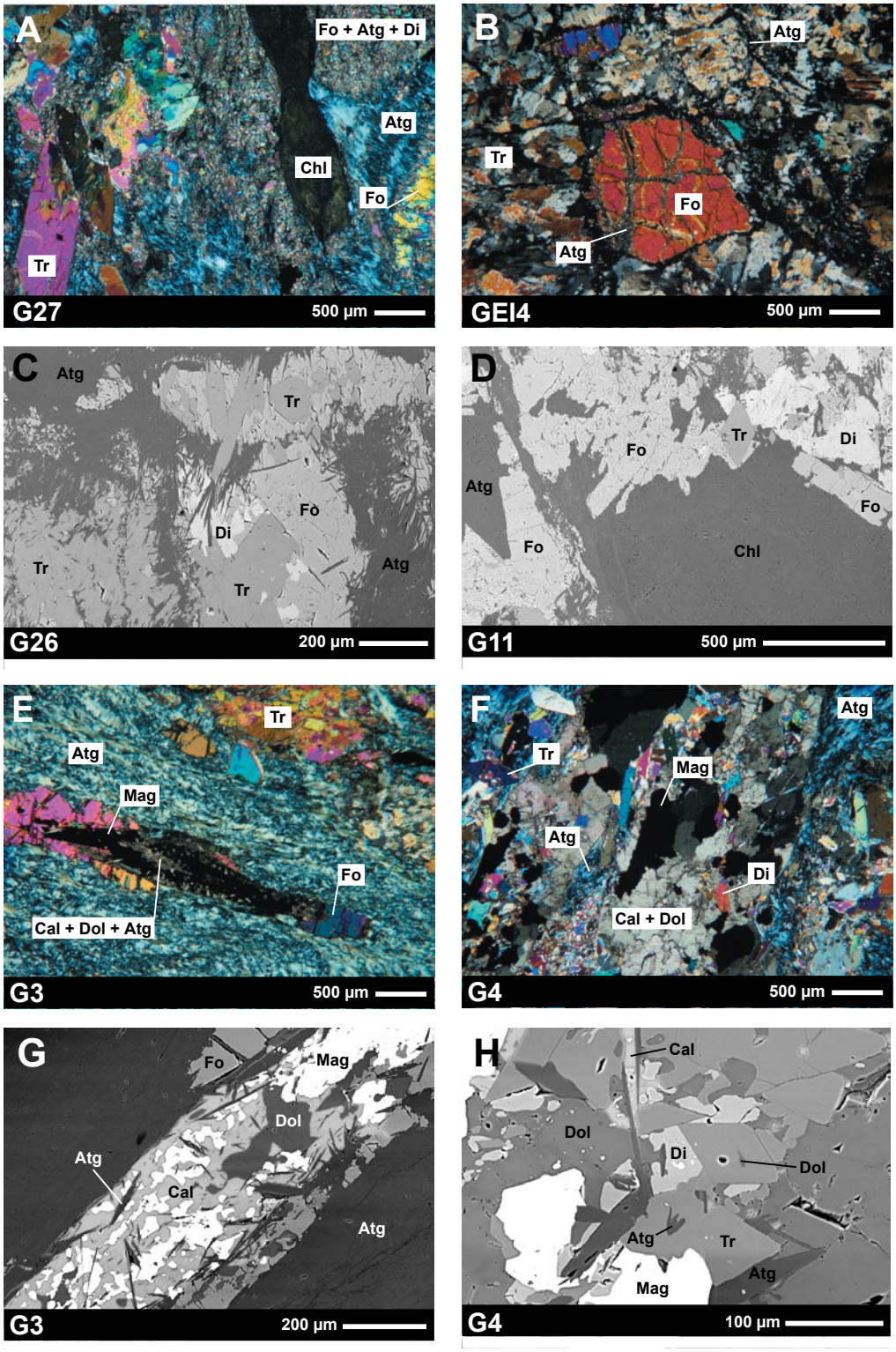


Fig. 4.4: Texture and mineralogy of the studied serpentinites (A to D) and ophicarbonates (E to H). C, D, G, H: backscattered electron images. Abbreviations: Atg: antigorite, Cal: calcite, Chl: chlorite, Di: diopside, Dol: dolomite, Fo: forsterite, Ilm: ilmenite, Mag: magnetite, Tr: tremolite.

+ diopside = forsterite + tremolite + fluid at approximately 0.6-0.7 GPa and 520-560°C (Pastorelli et al., 1995). In the centre of the massif, most samples are diopside-free and contain the prograde assemblage antigorite + forsterite + tremolite. However, in other samples two types of diopside can be distinguished. The first type is preserved as a relict (≤ 500 μm) in a single sample (G27), where chlorite crystallized after its former cleavages or exsolutions (?) creating a ghost crystal. The second diopside type is retrograde and is commonly found in serpentinite from the outer rim of the massif (Fig. 4.4c-d). This secondary diopside is smaller (≤ 200 μm) than the relic primary one. Modes and size of the different rock-forming minerals systematically change across the massif. Antigorite, diopside and magnetite increase in abundance, as forsterite decreases towards the rim of the massif. The length of the tremolite needles is smaller than 200 μm in the centre of the body, but can reach 2 cm at the rim. Forsterite shows a maximum size of 1 mm in the centre and often disappears at the rim of the massif.

No systematic major element variation was observed between minerals from the centre and from the rim of the massif. Antigorite has Mg# from 0.930 to 0.940, Al_2O_3 contents of ~ 3.00 wt.% and Cr_2O_3 between 0.10 and 1.00 wt.%. Forsterite has variable Mg# between 0.845 to 0.890. Its Ni content is comparable to those of olivines in the oceanic mantle (Allan and Dick, 1996), but its Mg# is lower (Arai, 1994). Amphibole is a nearly stoechiometric tremolite, and is zoned. It shows an increase of Ca and Si, and a decrease of Al, Na and K towards the rim. Diopside has a Cr_2O_3 content from below detection limit (< 0.01 wt.%) up to 0.26 wt.%. Diopside from serpentinite is richer in Cr compared to diopside from ophicarbonate. Chlorite shows Cr_2O_3 contents between 0.04 and 2.25 wt.%. Chlorite in the serpentinite is generally enriched in Cr compared to chlorite from the ophicarbonate.

Ophicarbonate

Antigorite-rich ophicarbonates are strongly deformed and are found at the border of the ultramafic massif (Fig. 4.4e, g). The rock is a tremolite-antigorite schist with calcite and/or dolomite, with minor diopside and forsterite (Fig. 4.4e-h). A retrograde assemblage antigorite + calcite + tremolite can be observed in these rocks, which was formed during the reaction diopside + dolomite + fluid = antigorite + calcite + tremolite (Connolly and Trommsdorff, 1991). This retrograde assemblage was formed simultaneously with retrograde diopside observed in serpentinite. Carbonate and diopside are not uniformly distributed in the samples, but are present in lenses (carbonate + antigorite + diopside + ilmenite + magnetite + Ni-rich sulphide), floating in an antigorite matrix (Fig. 4.4e-g). The retrograde assemblage is found in these lenses, where dolomite and diopside inclusions in tremolite are frequent (Fig. 4.4h). These lenses (up to 1 mm in diameter) are aligned along the foliation. Antigorite habitus changes between the matrix (anhedral) and the lenses (elongated needles).
Antigorite has Cr_2O_3 values between 0.09 and 0.31 wt.%. Its Cr content is generally lower than the Cr content of antigorite in serpentinite. Olivine (Fo_{89}) was found only in one sample (G3). Amphibole is a nearly stoechiometric tremolite, but lower in Na compared to the tremolite from serpentinite. Diopside has a Cr_2O_3 contents less than 0.09 wt.%. Calcite and dolomite both occur in the ophicarbonate, but in some cases calcite is the only carbonate present (sample GEI9). Calcite is nearly stoechiometric with up to 1.76 wt.% MgO while dolomite has a value around 17.0 wt.%, with substantial substitution of Mg by Fe.

Metabasite (contact)

The different metabasic rocks observed at the contact between the gneiss and the ultramafic rocks are titanite-epidote-hornblende fels with chlorite (+/- calcite and grossular), dolomite-chlorite-tremolite fels, and chlorite-tremolite fels. In some rocks, amphibole can form needles up to several centimetres length, and can even be asbestiform. Grossular usually crystallized in veins in association with titanite and calcite. Samples containing chlorite + tremolite ± dolomite were found in the centre of the metabasite (Fig. 4.3). They presumably formed a metasomatic "blackwall" between the ultramafic rocks and the gneiss, as was shown in some New England ultramafics by Sanford (1982).

The amphibole is a zoned tschermakitic hornblende with increasing Na_2O and Mg#, and decreasing K_2O towards the rim. Chlorite in metabasites is enriched in Al, Fe and Mn, and depleted in Ni, Cr and Mg compared to chlorite from serpentinite and ophicarbonate (Cr_2O_3 < 0.10 wt.%, Mg# from 0.750 to 0.820). Titanite has Al_2O_3 and Fe_2O_3 contents of ~ 1.50 and 0.80 wt.%,

respectively. Calcite and dolomite both occur in the metabasite, but were never found together. Calcite is nearly stoechiometric (MgO < 0.80 wt.%). Dolomite has MgO content of ~ 21.0 wt.%, and has higher FeO content (~ 1.95 wt.%) compared to calcite.

WHOLE ROCK COMPOSITION

Whole rock contents of major, light (Li, Be and B) and other trace elements were determined in the Geisspfad ultramafitites, as well as in the metabasite (contact) and in the Monte Leone gneiss.

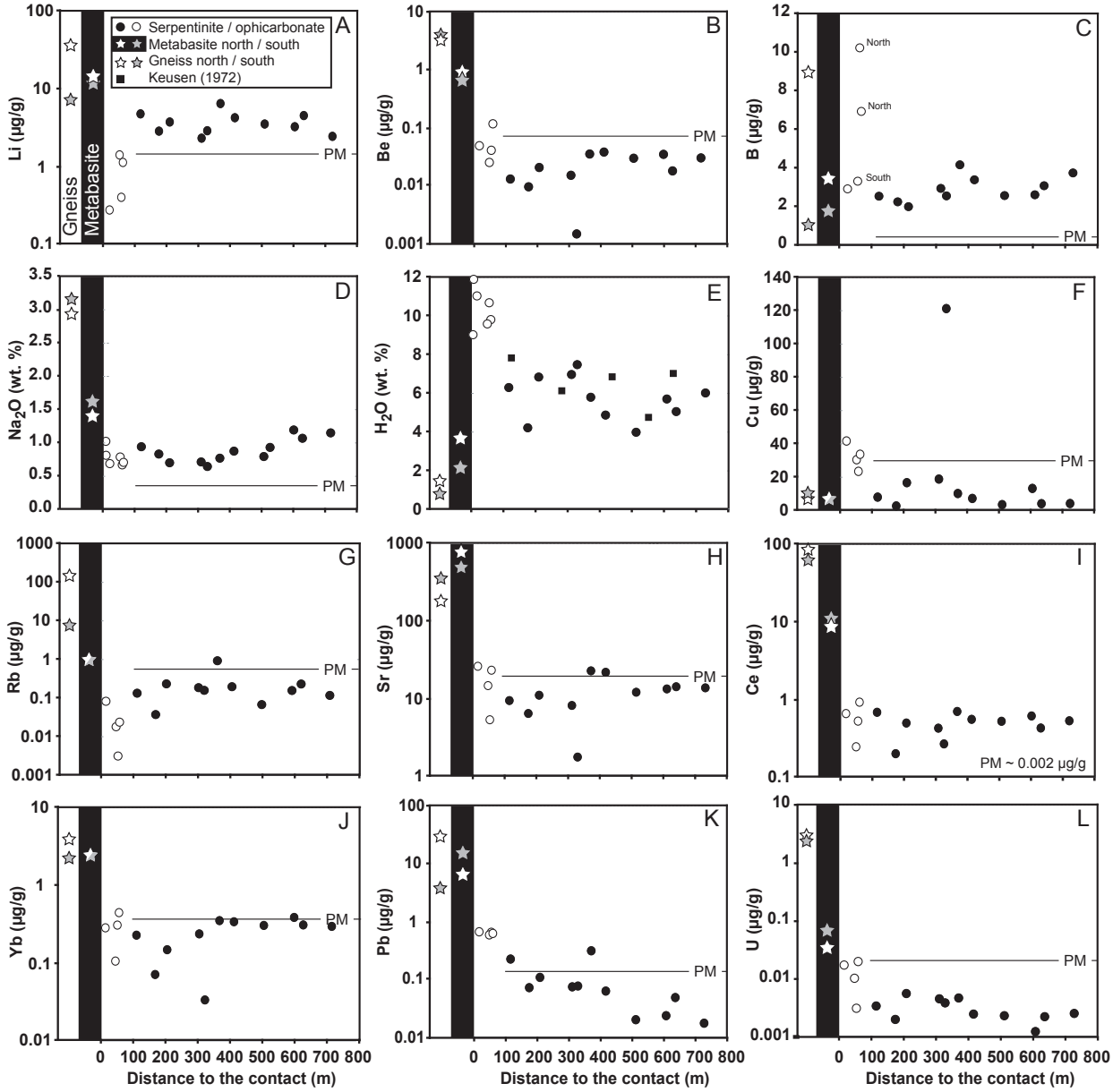


Fig. 4.5: Light (A to C), major (D and E) and trace elements (F to L) in whole rock samples of serpentinite, ophicarbonate, metabasite and Monte Leone gneiss. Values for serpentinite and ophicarbonate are plotted relative to their nearest orthogonal distance to the ophicarbonate - metabasite contact. For metabasite and gneiss, white stars represent samples from the northern contact (A on Figure 4.2 or 4.3), and grey stars from the southern contact (A' and B' on Figure 4.2 or 4.3). PM = primitive mantle (McDonough and Sun, 1995).

The results are listed in Tables 4.1 and 4.2, and are plotted in Figures 4.5 and 4.6.

Serpentinite and ophicarbonate

In terms of major element contents (SiO_2, Al_2O_3, Fe_2O_3, MgO, CaO, Na_2O), serpentinites and ophicarbonates are similar to orogenic, ophiolitic and abyssal peridotites (Bodinier and Godard, 2004) (Table 4.1, Fig. a.1 in the Appendix). Some major and trace elements display systematic variations across the massif (Fig. 4.5a-l), and can be subdivided into four types. All types show uniform concentrations in the centre of the massif (except for Pb).

Li and Rb represent the first type and show a decrease towards the contact. Li strongly decreases towards the margin from ~ 4 to < 1.5 μg/g (Fig. 4.5a), and has values in the centre of the massif comparable to South West Indian ridge serpentinites (mean value ~ 3.5 μg/g; Decitre et al., 2002), and to Mid-Atlantic ridge serpentinites (mean value ~ 0.7 μg/g; Vils et al., in prep.). Rb shows values in the centre of the massif similar to the primitive mantle value (McDonough and Sun, 1995). The second type includes Be, Cu, U and H_2O, which all increase towards the contact. Values for Be (< 0.06 μg/g; Fig. 4.5b) are slightly lower than the primitive mantle value ~ 0.068 μg/g (McDonough and Sun, 1995). Pb represents the third type, which is characterized by a continuous increase towards the rim, which can be observed over a distance of ~800 metres. The fourth type includes B, Sr, Ce, Yb, and Na_2O, which are ± constant over the entire massif (Fig. 4.5c). B content in serpentinite is about 3 μg/g, with the exception of the northern contact (~ 10 μg/g, samples GEI9 and G13; Fig. 4.2, 4.3 and 4.5c). The B content in the centre is about three times lower than the minimum mid-ocean ridge serpentinite value of about 10 μg/g (Fig. 4.6; Vils et al., in prep.). B contents are usually lower than values in Syros high pressure serpentinite (Marschall, 2005), except for some ophicarbonate (Fig. 4.6). Sr and Yb values in the centre of the massif are similar to the primitive mantle value (McDonough and Sun, 1995), while Ce content in serpentinite and ophicarbonate is 100 times higher than the primitive mantle value. The increase of many trace elements is within about 100 metres from the contact between the ophicarbonate and the metabasite.

Metabasite (contact) and Monte Leone gneiss

Three metabasites and two gneisses were analyzed (Table 4.2, Fig. 4.5). Metabasite shows rare earth element (REE) patterns (Fig. a.2 in the Appendix) comparable to normal mid-ocean ridge basalt (N-MORB). Li, Be, and B contents in the metabasite are ~ 13 μg/g, ~ 0.8 μg/g and ~ 2.5 μg/g, close to values of N-MORB.

The REE pattern of the gneiss shows a strong fractionation between the light and the heavy

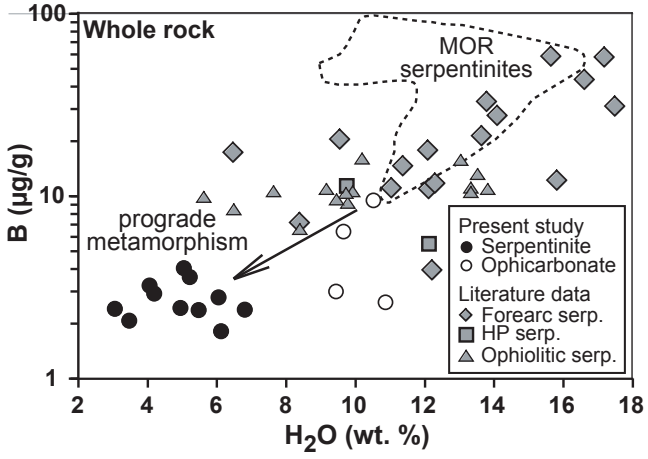


Fig. 4.6: H_2O (wt. %) versus B (μg/g) diagram of whole rock samples of serpentinite and ophicarbonate. Data from mid-ocean ridge (MOR), forearc, ophiolitic and high pressure serpentinites are plotted for comparison. MOR serpentinites: Atlantis Massif after Boschi et al. (2008), ODP Leg 209 after Vils et al. (in prep.), Romanche and Vema fracture zones after Bonatti et al. (1984). Forearc serpentinites: Mariana Forearc ODP Leg 125 after Savov et al. (2005). Ophiolitic serpentinites: Feather River Ophiolite, California (USA) after Agranier et al. (2007). High pressure serpentinites: Syros (Greece) after Marschall (2005).

Table 4.1. Whole rock composition of serpentinite and ophicarbonate

		Rock Sample D (m)	Serp GEI4 416	Serp G11 115	Serp G12 727	Serp G14 208	Serp G15 328	Serp G16 607	Serp G21 370	Serp G22 636	Serp G26 174	Serp G27 310	Serp G28 511	Serp G29 3
Method	**Element**	Unit												
XRF	**SiO2**	wt. %	44.21	44.70	45.00	44.84	43.97	44.32	44.86	43.69	43.94	43.67	43.80	46.93
	TiO2	wt. %	0.18	0.09	0.15	0.19	0.06	0.09	0.24	0.18	0.06	0.19	0.14	0.09
	Al2O3	wt. %	3.13	1.72	2.60	3.14	0.58	1.07	3.42	2.83	0.62	2.58	2.13	1.50
	Cr2O3	wt. %	0.36	0.42	0.38	0.38	0.55	0.39	0.36	0.35	0.37	0.34	0.34	0.37
	Fe2O3	wt. %	10.00	8.96	8.39	9.44	8.99	9.05	9.33	10.15	9.51	9.73	10.67	7.50
	MnO	wt. %	0.15	0.13	0.12	0.12	0.12	0.14	0.13	0.14	0.14	0.13	0.16	0.12
	NiO	wt. %	0.26	0.27	0.28	0.27	0.34	0.28	0.26	0.27	0.30	0.28	0.27	0.31
	MgO	wt. %	39.24	41.93	40.80	39.04	45.53	42.21	38.52	40.01	44.06	42.19	40.57	44.01
	CaO	wt. %	3.06	2.66	2.62	2.83	0.19	2.92	3.34	2.61	1.68	1.59	2.55	0.02
	Na2O	wt. %	0.86	0.93	1.13	0.68	0.63	1.18	0.75	1.05	0.81	0.70	0.78	0.79
	Mg#		0.89	0.91	0.91	0.90	0.91	0.91	0.89	0.89	0.91	0.90	0.89	0.92
	LOI	wt. %	4.1	5.5	5.2	6.1	6.8	4.9	5.0	4.2	3.5	6.0	3.0	11.6
ICP-MS	**Li**	µg/g	4.22	4.68	2.42	3.78	2.90	3.20	6.51	4.54	2.80	2.33	3.63	
	Be	µg/g	0.039	0.013	0.031	0.021	0.001	0.035	0.036	0.018	0.010	0.015	0.030	
	Sc	µg/g	14.0	14.1	14.3	13.2	9.5	16.0	16.0	12.9	10.8	14.2	10.6	
	V	µg/g	68	67	58	53	50	73	85	71	35	76	55	
	Co	µg/g	129	109	104	115	116	104	109	114	132	122	128	
	Ni	µg/g	2012	1963	2021	2050	2510	1858	1940	1962	2349	2140	2043	
	Cu	µg/g	8	9	5	17	122	14	11	4	2	19	3	
	Ga	µg/g	3.28	2.03	2.57	1.28	1.09	3.24	3.24	2.71	1.10	2.52	2.50	
	Zn	µg/g	57	50	51	48	52	50	49	49	52	50	62	
	Rb	µg/g	0.203	0.137	0.121	0.242	0.164	0.162	0.973	0.240	0.038	0.192	0.069	
	Sr	µg/g	21.95	9.33	13.67	10.95	1.67	13.27	22.93	14.20	6.29	8.03	12.00	
	Y	µg/g	3.618	2.101	3.002	1.380	0.202	4.397	3.821	3.094	0.469	2.240	2.933	
	Zr	µg/g	3.05	2.19	1.96	2.21	0.91	1.88	1.37	1.20	0.96	1.95	1.61	
	Cs	µg/g	0.028	0.033	0.030	0.029	0.015	0.017	0.094	0.020	0.010	0.016	0.012	
	Ba	µg/g	0.33	0.49	0.23	0.63	0.22	0.29	0.88	0.29	0.42	0.37	0.15	
	La	µg/g	0.130	0.217	0.135	0.166	0.128	0.138	0.196	0.111	0.068	0.143	0.138	
	Ce	µg/g	0.544	0.670	0.520	0.487	0.261	0.600	0.688	0.420	0.194	0.417	0.513	
	Pr	µg/g	0.104	0.102	0.094	0.078	0.029	0.118	0.129	0.082	0.026	0.071	0.094	
	Nd	µg/g	0.632	0.509	0.543	0.374	0.106	0.710	0.745	0.486	0.110	0.386	0.543	
	Sm	µg/g	0.260	0.163	0.216	0.102	0.018	0.298	0.282	0.211	0.024	0.144	0.214	
	Eu	µg/g	0.107	0.066	0.095	0.047	0.004	0.127	0.106	0.086	0.022	0.065	0.092	
	Gd	µg/g	0.410	0.236	0.341	0.146	0.022	0.493	0.442	0.350	0.034	0.238	0.333	
	Tb	µg/g	0.077	0.044	0.064	0.028	0.004	0.093	0.080	0.065	0.007	0.044	0.062	
	Dy	µg/g	0.530	0.307	0.440	0.192	0.025	0.645	0.560	0.452	0.054	0.311	0.419	
	Ho	µg/g	0.119	0.072	0.100	0.045	0.006	0.146	0.123	0.103	0.015	0.071	0.097	
	Er	µg/g	0.342	0.215	0.292	0.136	0.022	0.419	0.356	0.298	0.050	0.215	0.283	
	Yb	µg/g	0.347	0.232	0.302	0.150	0.033	0.395	0.359	0.315	0.071	0.241	0.311	
	Lu	µg/g	0.055	0.038	0.046	0.025	0.007	0.060	0.057	0.052	0.013	0.041	0.051	
	Hf	µg/g	0.130	0.059	0.096	0.067	0.024	0.107	0.084	0.079	0.020	0.083	0.074	
	Pb	µg/g	0.063	0.225	0.018	0.109	0.078	0.024	0.314	0.048	0.073	0.076	0.020	
	Th	µg/g	0.002	0.016	0.005	0.012	0.016	0.005	0.019	0.012	0.002	0.012	0.007	
	U	µg/g	0.002	0.003	0.003	0.006	0.004	0.001	0.005	0.002	0.002	0.004	0.002	
	TiO2	wt. %	0.129	0.049	0.102	0.051	0.021	0.138	0.192	0.133	0.015	0.148	0.095	
PGNAA	**B**	µg/g	3.24	2.37	3.60	1.82	2.39	2.44	4.03	2.92	2.08	2.78	2.41	
	Cl	µg/g	17	9	38	b.d.	28	44	13	28	19	b.d.	20	
	H2O	wt. %	4.9	6.3	6.0	6.8	7.5	5.7	5.8	5.1	4.2	7.0	4.0	
MS	**δD_{SMOW}**	‰	-89	-53	-39			-30	-49	-49		-56		
	$\delta 18O_{SMOW}$	‰	4.7	5.2	5.2			4.5		4.7				

Serp = serpentinite and Ophi = ophicarbonate. LOI = Loss On Ignition. Mg# calculated as (MgO/40.3)/[(MgO/40.3)+(0.8998*Fe2O3/74.85)]. D (m) = nearest orthogonal distance to the ophicarbonate - metabasite contact, b.d. = below detection limit.

Table 4.1. continued

		Rock Sample D (m)	Ophi G3 48	Ophi G4 16	Ophi GEI9 59	Ophi G13 54	Ophi G33 1
Method	**Element**	Unit					
XRF	**SiO2**	wt. %	45.69	44.68	45.18	44.87	48.76
	TiO2	wt. %	0.09	0.17	0.23	0.20	0.08
	Al2O3	wt. %	1.40	3.20	3.53	3.14	1.55
	Cr2O3	wt. %	0.41	0.35	0.38	0.38	0.34
	Fe2O3	wt. %	8.93	8.58	9.53	9.46	9.07
	MnO	wt. %	0.12	0.11	0.13	0.12	0.11
	NiO	wt. %	0.29	0.27	0.25	0.27	0.24
	MgO	wt. %	41.94	40.50	36.36	39.07	35.99
	CaO	wt. %	1.41	2.50	4.70	2.83	4.12
	Na2O	wt. %	0.77	0.67	0.68	0.65	1.01
	Mg#		0.91	0.91	0.89	0.90	0.89
	LOI	wt. %	9.2	11.9	9.5	10.2	8.5
ICP-MS	**Li**	µg/g	1.38	0.27	1.10	0.39	
	Be	µg/g	0.026	0.050	0.120	0.042	
	Sc	µg/g	12.0	13.6	15.8	14.4	
	V	µg/g	54	64	74	75	
	Co	µg/g	105	96	99	100	
	Ni	µg/g	2116	1833	1764	1910	
	Cu	µg/g	31	42	34	24	
	Ga	µg/g	2.29	3.10	3.30	3.15	
	Zn	µg/g	60	52	50	49	
	Rb	µg/g	0.018	0.084	0.024	0.003	
	Sr	µg/g	14.62	26.42	23.45	5.20	
	Y	µg/g	0.844	2.830	5.114	3.126	
	Zr	µg/g	0.46	0.90	2.53	1.87	
	Cs	µg/g	0.013	0.088	0.035	0.032	
	Ba	µg/g	1.10	0.71	12.12	0.15	
	La	µg/g	0.087	0.174	0.247	0.128	
	Ce	µg/g	0.240	0.644	0.907	0.514	
	Pr	µg/g	0.030	0.108	0.167	0.096	
	Nd	µg/g	0.122	0.592	0.965	0.560	
	Sm	µg/g	0.033	0.212	0.388	0.226	
	Eu	µg/g	0.013	0.071	0.165	0.085	
	Gd	µg/g	0.067	0.327	0.609	0.366	
	Tb	µg/g	0.014	0.060	0.114	0.068	
	Dy	µg/g	0.109	0.410	0.773	0.468	
	Ho	µg/g	0.028	0.093	0.172	0.107	
	Er	µg/g	0.086	0.270	0.484	0.305	
	Yb	µg/g	0.107	0.290	0.457	0.314	
	Lu	µg/g	0.019	0.048	0.069	0.052	
	Hf	µg/g	0.014	0.040	0.103	0.073	
	Pb	µg/g	0.582	0.656	0.608	0.629	
	Th	µg/g	0.005	0.014	0.006	0.004	
	U	µg/g	0.010	0.017	0.019	0.003	
	TiO2	wt. %	0.038	0.116	0.175	0.155	
PGNAA	**B**	µg/g	3.17	2.76	6.85	10.20	
	S	µg/g	846	748	522	525	
	Cl	µg/g	23	32	21	b.d.	
	H2O	wt. %	9.6	11.0	9.8	10.7	
MS	**δD_{SMOW}**	‰	-61	-112	-87		
	$\delta 18O_{SMOW}$	‰	4.9	4.9	4.1		

Serp = serpentinite and Ophi = ophicarbonate. LOI = Loss On Ignition
Mg# calculated as (MgO/40.3)/[(MgO/40.3)+(0.8998*Fe2O3/74.85)].
D (m) = nearest orthogonal distance to the ophicarbonate - metabasite contact. b.d. = below detection limit.

REE with La_N/Yb_N of 6.5 and 8.4 (Fig. a.2 from the Appendix). Li, Be, and B contents of the two gneisses are 7 and 36 μg/g, 0.9 and 8.8 μg/g, and 3.1 and 4.1 μg/g, respectively. These values are comparable to data of the continental crust (e.g. Rudnick and Gao, 2004).

Whole rock stable isotopic composition

Results are listed in Table 4.1 and plotted in Figure 4.7. $\delta^{18}O$ and δD values were measured in whole rocks (serpentinite and ophicarbonate). $\delta^{18}O$ is constant through the Geisspfad massif, in serpentinite and ophicarbonate, with a mean value of + 4.8 ‰. In contrast, δD values decrease from the centre to the rim of the massif, from – 30 ‰ to – 112 ‰ ,similar to other studies on serpentinites (Fig. 4.7; Wenner & Taylor, 1974; Früh-Green et al., 1996).

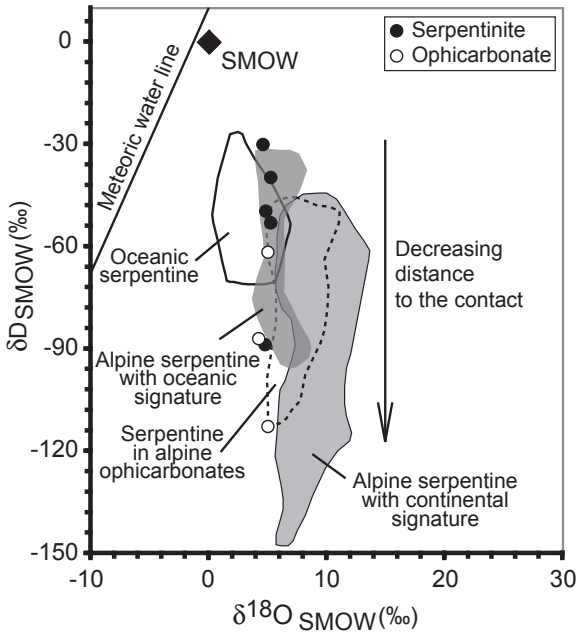


Fig. 4.7: Hydrogen and oxygen isotope ratios of whole rock samples of serpentinite and ophicarbonate. Meteoric water line and seawater (SMOW) are plotted for comparison, as well as data from serpentine mineral separates published in the literature. Oceanic serpentine: Wenner and Taylor (1974), Früh-Green et al. (1996). Alpine serpentine with oceanic signature: Burkhard and O'Neil (1988). Alpine serpentine with continental signature: Burkhard and O'Neil (1988), Früh-Green et al. (1990). Serpentine in alpine ophicarbonates: Pozzorini and Früh-Green (1996).

Table 4.2. Whole rock composition of metabasite and gneiss

		Rock	Metabas	Metabas	Metabas	Gneiss	Gneiss	Gneiss
		Sample	G30A	G30B	G34	G32A	G32B	G36
		D (m)	-1	-2	-1	-10	-15	-8
Method	**Element**	Unit						
XRF	**SiO2**	wt. %	39.79	41.81	43.78	70.86	70.57	72.12
	TiO2	wt. %	1.38	1.10	1.38	0.49	0.42	0.66
	Al2O3	wt. %	18.85	15.23	17.20	15.40	16.01	12.57
	Cr2O3	wt. %	0.06	0.06	0.05	b.d.	0.00	0.01
	Fe2O3	wt. %	11.33	10.97	10.88	3.23	2.53	5.38
	MnO	wt. %	0.17	0.18	0.19	0.04	0.04	0.12
	NiO	wt. %	0.03	0.05	0.03	0.00	0.00	0.00
	MgO	wt. %	11.61	13.32	9.75	1.18	0.79	1.93
	CaO	wt. %	16.03	15.85	15.79	1.62	2.18	4.56
	Na2O	wt. %	1.46	1.88	1.57	2.91	3.25	3.16
	K2O	wt. %	b.d.	b.d.	0.19	4.40	4.63	0.15
	Mg#		0.68	0.71	0.65	0.43	0.39	0.43
	LOI	wt. %	3.7	3.4	1.3	1.2	0.8	0.5
ICP-MS	**Li**	µg/g	14	12	12	36		7
	Be	µg/g	0.9	0.8	0.8	3.1		4.1
	Sc	µg/g	40.95	37.22	33.53	8.09		10.22
	V	µg/g	245.22	225.93	223.72	35.57		84.73
	Co	µg/g	82.8	77.3	68.5	81.2		83.1
	Ni	µg/g	257.5	236.8	245.4	13.5		31.3
	Cu	µg/g	5.5	5.1	5.1	9.8		10.6
	Ga	µg/g	20.2	18.6	18.5	30.2		18.3
	Zn	µg/g	49.2	45.0	70.1	55.9		58.3
	Rb	µg/g	1	1	1	163		8
	Sr	µg/g	978.5	933.3	536.1	187.1		379.3
	Y	µg/g	28.92	27.78	25.92	47.22		27.59
	Cs	µg/g	b.d.	b.d.	0.04	5.46		0.15
	Ba	µg/g	3	2	5	940		30
	La	µg/g	2.7	2.4	3.8	39.3		29.8
	Ce	µg/g	9.2	8.6	10.9	83.4		61.6
	Pr	µg/g	1.688	1.565	1.871	10.140		7.440
	Nd	µg/g	9.0	8.7	9.4	37.6		27.6
	Sm	µg/g	3.01	2.92	2.98	8.15		5.55
	Eu	µg/g	1.72	1.68	1.20	1.32		1.11
	Gd	µg/g	4.1	4.0	3.9	8.1		5.2
	Tb	µg/g	0.72	0.71	0.68	1.36		0.83
	Dy	µg/g	4.68	4.60	4.35	8.00		4.60
	Ho	µg/g	1.02	1.00	0.93	1.66		0.93
	Er	µg/g	2.86	2.81	2.59	4.68		2.61
	Yb	µg/g	2.70	2.65	2.44	4.13		2.41
	Lu	µg/g	0.41	0.40	0.37	0.58		0.35
	Pb	µg/g	6.4	6.3	15.0	29.1		3.8
	Th	µg/g	0.1	0.1	0.2	15.4		11.5
	U	µg/g	0.03	0.04	0.07	3.03		2.42
	TiO2	wt. %	1.459	1.318	1.153	0.460		0.590
PGNAA	**B**	µg/g	3.49		1.83	8.79		0.92
	Cl	µg/g	19		18	b.d.		20
	H2O	wt. %	3.9		2.1	1.5		0.9

Metabas = metabasite. LOI = Loss On Ignition. b.d. = below detection limit. Mg# calculated as (MgO/40.3)/[(MgO/40.3)+(0.8998*Fe2O3/74.85)]. D (m) = nearest orthogonal distance to the ophicarbonate - metabasite contact.

MINERAL COMPOSITION - LIGHT ELEMENTS (Li, Be AND B)

Light element contents of minerals were measured along two main profiles through the massif (A-A' and B-B', Fig. 4.2 and 4.3). Measurements from the serpentinite and ophicarbonate are presented together, because their mineralogical composition is similar. Results are shown in Table 4.3 and in Figures 4.8 to 4.10.

Serpentinite and ophicarbonate

Li contents are highly variable in all minerals (Fig. 4.8). Antigorite is poor in Li with values from < 0.1 up to 4.0 μg/g. Sample GEI4 (~ 420 m from the contact), which was collected where meta-dunite was mapped by Keusen (1972), shows the greatest variability in Li contents between 0.04 and 3.80 μg/g. Forsterite, tremolite and diopside have values of 1.7-10.1, 0.2-11.8 and 0.5-31.6 μg/g, respectively. Results for chlorite range from < 0.1 up to 1.8 μg/g. Calcite and dolomite are poor in Li with values < 0.2 μg/g.

The highest Be concentrations were measured in diopside (0.02-0.98 μg/g) and tremolite (0.04 and 0.29 μg/g). All the other minerals have Be contents < 0.05 μg/g.

The major B-bearing phases are antigorite and tremolite, with contents ranging from 0.8 to 35.3, and 1.7 to 19.7 μg/g, respectively. Forsterite (0.1 to 7.8 μg/g) and diopside (< 0.1 to 2.4 μg/g) have lower B contents. Chlorite may contain up to 3.1 μg/g of B, while calcite and dolomite have values < 0.2 μg/g.

In a cross section through the Geisspfad massif, Li contents of tremolite, antigorite and diopside increase towards the rim and then decrease towards the contact (Fig. 4.9a-c). A rimward increase in Be is observed in antigorite and diopside (Fig. 4.9e-f). B content also slightly increases in this direction in forsterite and diopside (Fig. 4.9g and i). In contrast, B and Be values in tremolite decreases towards the rim (Fig. 4.9d). This decrease is associated with an increase of the B and Be content in coexisting diopside.

Figure 4.10 illustrates the mean content of Li, Be, and B in minerals from serpentinite and ophicarbonate. The partitioning of each light element between the minerals of the assemblage antigorite + diopside + tremolite + forsterite is similar in the samples from the centre of the massif (Fig. 4.10a-c and 4.11, Table 4.4), except

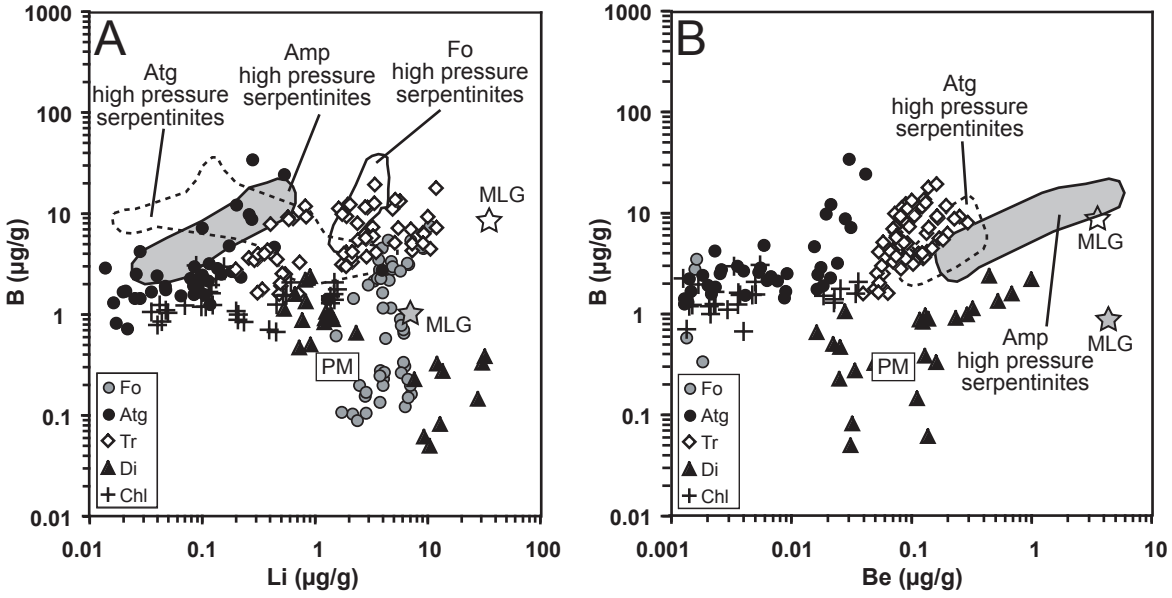


Fig. 4.8: (A) Li vs. B and (B) Be vs. B diagrams showing the concentrations of these elements in the rock-forming minerals of the Geisspfad serpentinites and ophicarbonates. High pressure serpentinites data after Scambelluri et al. (2004) and Marschall (2005). Mineral abbreviations: Amp = amphibole, Atg = antigorite, Chl = chlorite, Di = diopside, Fo = forsterite, Tr = tremolite. PM: primitive mantle (McDonough and Sun, 1995), MLG: Monte Leone Gneiss from present study, white star represents gneiss from the norhtern contact and grey star from the southern contact.

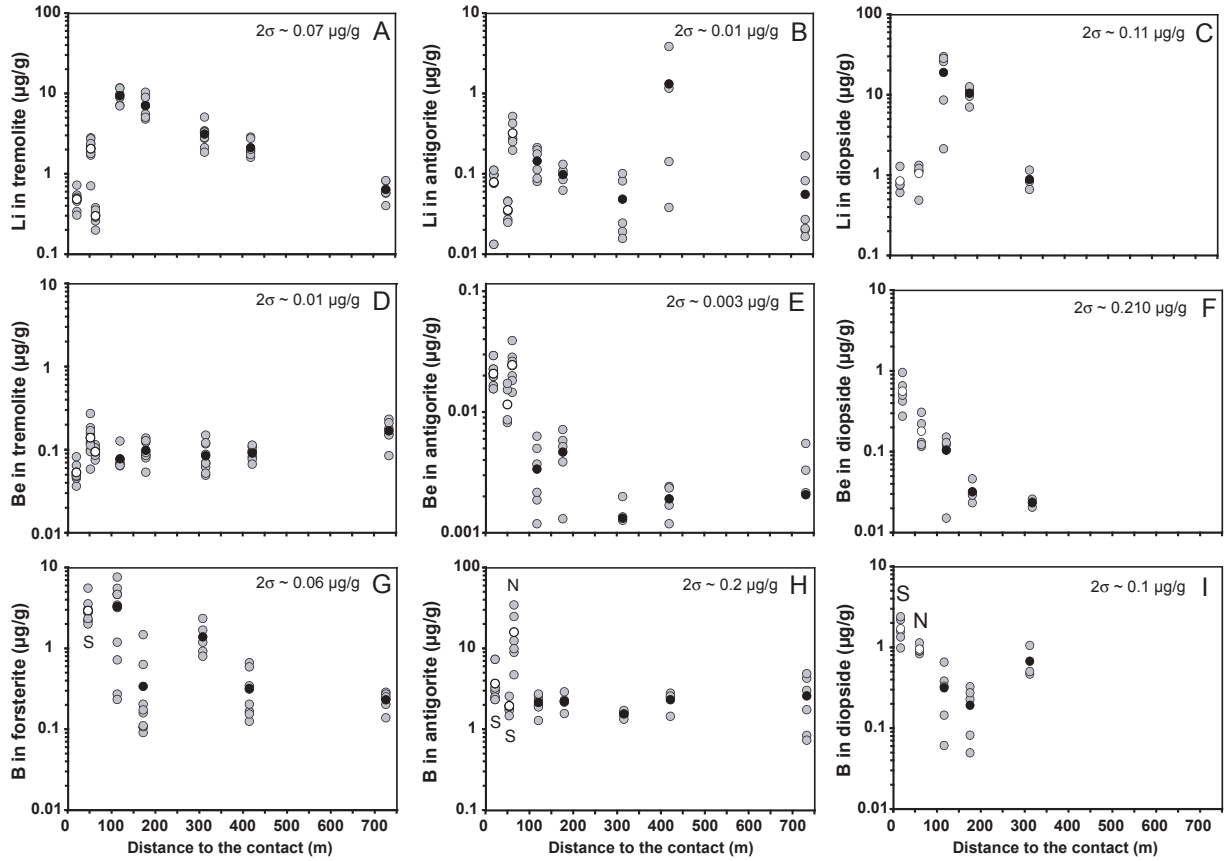


Fig. 4.9: Li, Be and B content of minerals in serpentinite and ophicarbonate as a function of their nearest orthogonal distance to the ophicarbonate – metabasite contact. Grey circles represent single measurements. Black circles are average values for serpentinite, and white circles are average values for ophicarbonate. N: northern contact, S: southern contact.

Table 4.4. Partition coefficients of equilibrated samples from the centre of the massif

Element	Min/min	GEI4 average	GEI4 1σ	G12 average	G12 1σ	G27 average	G27 1σ	All samples average	All samples 1σ
Li	Tr/Fo	0.4	0.1	0.17	0.04	0.6	0.2	0.3	0.2
	Tr/Di					3	1		
	Tr/Atg	18	23	23	14	107	83	54	68
	Atg/Di					0.06	0.05		
	Atg/Fo	0.2	0.3	0.01	0.01	0.01	0.01	0.1	0.2
	Fo/Di					6	1		
Be	Tr/Fo	175	134	500	196	114	44	261	215
	Tr/Di					4	1		
	Tr/Atg	26	19	235	248	76	46	125	168
	Atg/Di					0.06	0.02		
	Atg/Fo	3	2	6	4	1.6	0.8	4	3
	Fo/Di					0.032	0.003		
B	Tr/Fo	50	27	44	14	9	6	40	26
	Tr/Di					13	10		
	Tr/Atg	5	2	6	4	5	3	5	3
	Atg/Di					2.6	0.9		
	Atg/Fo	10	6	12	9	2.0	0.6	10	8
	Fo/Di					1.5	0.5		

Table 4.3. Light element composition of minerals (representative analyses)

Rock	Sample	N	Min	Li (µg/g)	2σ	Be (µg/g)	2σ	B (µg/g)	2σ
Serp	GEI4	4	Atg	3.80	0.05	0.003	0.002	2.9	0.1
	GEI4		Atg	1.24	0.04	<0.001		1.48	0.07
	GEI4		Atg	0.04	0.02	0.002	0.002	2.52	0.08
	G11	6	Atg	0.08	0.01	0.002	0.001	2.0	0.1
	G11		Atg	0.21	0.01	0.007	0.002	2.43	0.07
	G11		Atg	0.18	0.02	0.004	0.002	2.78	0.08
	G12	6	Atg	0.17	0.04	0.006	0.002	5.0	0.1
	G12		Atg	0.020	0.004	<0.001		1.78	0.05
	G12		Atg	0.02	0.01	<0.001		0.75	0.06
	G26	5	Atg	0.10	0.01	<0.001		2.3	0.1
	G26		Atg	0.06	0.01	0.004	0.003	1.60	0.07
	G26		Atg	0.13	0.02	0.005	0.004	3.0	0.2
	G27	5	Atg	0.10	0.01	<0.002		1.64	0.09
	G27		Atg	0.02	0.01	<0.002		1.75	0.08
	G27		Atg	0.02	0.01	<0.002		1.36	0.09
Ophi	G3	5	Atg	0.05	0.01	0.018	0.007	1.99	0.08
	G3		Atg	0.03	0.01	0.008	0.003	1.50	0.06
	G3		Atg	0.02	0.01	0.009	0.005	2.6	0.1
	G4	5	Atg	0.10	0.01	0.030	0.006	7.5	0.3
	G4		Atg	0.08	0.02	0.020	0.008	2.38	0.08
	G4		Atg	0.11	0.01	0.023	0.006	3.3	0.2
	GEI9	6	Atg	0.27	0.02	0.029	0.005	35.3	0.9
	GEI9		Atg	0.51	0.02	0.040	0.006	25	1
	GEI9		Atg	0.25	0.02	0.019	0.003	10.1	0.4
	GEI9		Atg	0.42	0.02	0.015	0.002	4.8	0.1
Serp	G11	5	Di	31.6	0.3	0.13	0.02	0.39	0.04
	G11		Di	27.4	0.3	0.11	0.01	0.15	0.03
	G11		Di	2.27	0.07	0.016	0.008	0.67	0.04
	G11		Di	9.1	0.2	0.13	0.01	0.06	0.02
	G26	5	Di	11.8	0.1	0.05	0.01	0.33	0.03
	G26		Di	7.5	0.1	0.025	0.008	0.23	0.03
	G26		Di	13.3	0.3	0.03	0.01	0.28	0.05
	G27	3	Di	1.23	0.04	0.027	0.008	1.1	0.1
	G27		Di	0.71	0.05	0.025	0.008	0.48	0.07
	G27		Di	0.89	0.05	0.022	0.007	0.52	0.05
Ophi	G4	5	Di	0.65	0.03	0.67	0.04	1.62	0.09
	G4		Di	0.80	0.05	0.98	0.05	2.2	0.1
	G4		Di	0.81	0.04	0.51	0.04	1.4	0.1
	GEI9	6	Di	1.19	0.03	0.121	0.006	0.85	0.06
	GEI9		Di	1.29	0.02	0.127	0.009	0.99	0.04
	GEI9		Di	0.52	0.02	0.32	0.01	1.16	0.04
Serp	GEI4	7	Tr	1.59	0.05	0.082	0.005	11.5	0.2
	GEI4		Tr	2.01	0.07	0.099	0.006	12.51	0.08
	GEI4		Tr	2.75	0.07	0.12	0.01	11.8	0.2
	G11	7	Tr	7.16	0.05	0.068	0.006	4.4	0.1
	G11		Tr	9.8	0.1	0.079	0.004	9.5	0.1
	G11		Tr	11.6	0.1	0.14	0.01	18.2	0.2
	G12	6	Tr	0.63	0.04	0.163	0.007	9.2	0.2
	G12		Tr	0.40	0.02	0.090	0.008	8.0	0.3
	G12		Tr	0.81	0.03	0.19	0.01	12.0	0.2
	G26	8	Tr	9.1	0.1	0.13	0.02	6.4	0.2
	G26		Tr	10.4	0.1	0.15	0.02	4.6	0.2
	G26		Tr	5.4	0.1	0.14	0.02	7.3	0.2
	G26		Tr	5.55	0.07	0.10	0.02	13.6	0.3
	G27	10	Tr	5.1	0.1	0.13	0.02	13.9	0.3
	G27		Tr	3.42	0.08	0.05	0.01	4.2	0.1
	G27		Tr	3.19	0.08	0.09	0.01	7.5	0.2
	G27		Tr	2.10	0.07	0.07	0.02	4.2	0.2
	G27		Tr	3.34	0.07	0.16	0.02	19.7	0.4
	G27		Tr	1.85	0.05	0.06	0.01	3.1	0.1
Ophi	G3	10	Tr	2.79	0.07	0.17	0.02	5.7	0.2
	G3		Tr	1.85	0.07	0.13	0.02	4.2	0.1
	G3		Tr	2.34	0.05	0.29	0.03	8.2	0.3
	G3		Tr	0.70	0.06	0.06	0.02	1.64	0.09
	G4	9	Tr	0.49	0.04	0.054	0.008	2.0	0.1
	G4		Tr	0.71	0.04	0.069	0.007	3.3	0.1
	G4		Tr	0.45	0.03	0.09	0.02	3.6	0.1
	G4		Tr	0.48	0.03	0.05	0.01	2.1	0.1
	GEI9	7	Tr	0.25	0.01	0.107	0.006	3.7	0.1
	GEI9		Tr	0.37	0.03	0.092	0.007	4.44	0.07
	GEI9		Tr	0.19	0.02	0.080	0.008	2.8	0.1
Metabas	G30a	5	Hbl	2.51	0.04	2.10	0.05	7.7	0.2
	G30a		Hbl	2.31	0.05	1.51	0.03	6.8	0.1
	G30a		Hbl	1.76	0.06	1.03	0.03	5.1	0.1
	G34	5	Hbl	9.3	0.1	0.59	0.02	1.99	0.09
	G34		Hbl	8.4	0.2	0.66	0.02	1.8	0.1
	G34		Hbl	11.5	0.2	0.75	0.02	2.30	0.09

N = total number of analysis. Abbreviations: Atg = antigorite, Di = diopside, Hbl = tschermakitic hornblende, Tr = tremolite. Serp = serpentinite, Ophi = ophicarbonate, Metabas = metaba

Table 4.3: continued

Rock	Sample	N	Min	Li (µg/g)	2σ	Be (µg/g)	2σ	B (µg/g)	2σ
Serp	GEI4	8	Fo	6.07	0.08	<0.001		0.13	0.02
	GEI4		Fo	5.88	0.09	0.002	0.002	0.35	0.02
	GEI4		Fo	6.49	0.09	<0.001		0.16	0.03
	GEI4		Fo	4.1	0.2	<0.001		0.60	0.04
	G11	12	Fo	8.8	0.1	<0.001		4.70	0.09
	G11		Fo	6.52	0.09	<0.001		3.24	0.07
	G11		Fo	4.57	0.07	<0.001		3.5	0.1
	G11		Fo	6.9	0.1	<0.001		5.6	0.1
	G11		Fo	6.45	0.05	<0.001		0.24	0.02
	G11		Fo	3.81	0.06	<0.001		4.7	0.1
	G11		Fo	4.56	0.05	<0.001		1.21	0.06
	G11		Fo	10.1	0.1	<0.001		7.8	0.1
	G12	6	Fo	3.90	0.07	<0.001		0.24	0.03
	G12		Fo	3.67	0.04	<0.001		0.29	0.02
	G12		Fo	3.86	0.06	<0.001		0.21	0.02
	G26	9	Fo	2.08	0.05	<0.001		0.11	0.02
	G26		Fo	1.66	0.06	<0.001		0.11	0.02
	G27	5	Fo	5.5	0.1	<0.002		0.9	0.1
	G27		Fo	5.6	0.1	<0.002		0.81	0.08
Ophi	G3	10	Fo	3.61	0.08	0.002	0.002	2.9	0.1
	G3		Fo	4.4	0.1	<0.002		2.29	0.09
	G3		Fo	3.5	0.1	0.002	0.002	3.6	0.2
Serp	GEI4	7	Chl	0.10	0.02	0.002	0.001	1.68	0.08
	GEI4		Chl	0.39	0.02	<0.001		0.7	0.2
	GEI4		Chl	0.12	0.02	0.002	0.001	1.3	0.2
	GEI4		Chl	0.13	0.03	<0.001		2	1
	G11	6	Chl	0.45	0.02	0.002	0.001	1.28	0.05
	G11		Chl	0.60	0.02	0.005	0.002	2.1	0.1
	G11		Chl	0.44	0.02	0.004	0.001	0.69	0.03
	G11		Chl	0.54	0.02	0.005	0.001	1.59	0.08
	G12	6	Chl	0.07	0.01	<0.001		1.3	0.1
	G12		Chl	0.12	0.01	0.002	0.001	2.0	0.2
	G12		Chl	0.09	0.01	0.005	0.002	3.1	0.1
	G12		Chl	0.03	0.01	<0.001		1.09	0.04
	G26	4	Chl	0.21	0.02	0.002	0.002	1.0	0.1
	G26		Chl	0.23	0.02	<0.001		0.86	0.05
	G26		Chl	0.20	0.02	<0.001		1.10	0.06
	G27	5	Chl	0.04	0.01	<0.002		0.87	0.08
	G27		Chl	0.04	0.01	0.004	0.003	1.27	0.08
	G27		Chl	0.05	0.01	0.003	0.002	1.12	0.07
Ophi	GEI9	6	Chl	1.35	0.04	0.022	0.003	1.3	0.1
	GEI9		Chl	1.46	0.04	0.022	0.003	1.4	0.1
	GEI9		Chl	1.46	0.04	0.035	0.004	2.13	0.09

Rock	Sample	N	Min	Li (µg/g)	2σ	Be (µg/g)	2σ	B (µg/g)	2σ
Metabas	G30a	4	Chl	27.6	0.1	0.013	0.002	0.7	0.1
	G30a		Chl	33.0	0.2	0.024	0.005	0.8	0.1
	G30a		Chl	33.4	0.4	0.019	0.005	2.0	0.3
	G34	5	Chl	75.2	0.9	0.021	0.003	2.0	0.3
	G34		Chl	65.5	0.4	0.021	0.003	0.8	0.2
	G34		Chl	62.9	0.5	0.021	0.005	0.31	0.06
	G34		Chl	63.7	0.7	0.223	0.009	1.5	0.1
Metabas	G30a	4	Ep	0.08	0.02	0.028	0.005	1.6	0.1
	G30a		Ep	0.82	0.02	0.025	0.004	1.22	0.06
	G30a		Ep	0.019	0.005	0.021	0.004	1.74	0.08
	G34	5	Ep	0.09	0.01	0.008	0.004	0.17	0.03
	G34		Ep	0.10	0.01	0.008	0.001	0.03	0.01
	G34		Ep	0.15	0.02	0.029	0.005	0.09	0.02
Metabas	G30a	3	Ttn	0.07	0.01	0.097	0.007	1.38	0.08
	G30a		Ttn	0.55	0.06	0.076	0.005	0.98	0.06
	G30a		Ttn	0.80	0.04	0.115	0.009	0.74	0.03
	G34	3	Ttn	3.78	0.06	0.41	0.01	0.88	0.06
	G34		Ttn	3.97	0.07	0.28	0.02	0.75	0.07
	G34		Ttn	0.02	0.01	0.04	0.01	0.20	0.03
Ophi	G3	5	Cal	0.020	0.004	<0.001		0.11	0.01
	G3		Cal	0.05	0.01	<0.001		0.05	0.02
	G3		Cal	0.008	0.002	<0.001		0.09	0.01
	G4	4	Cal	0.019	0.002	0.010	0.002	0.12	0.01
	G4		Cal	0.022	0.001	0.016	0.001	0.18	0.01
	G4		Cal	0.018	0.001	0.015	0.001	0.12	0.01
	GEI9	4	Cal	0.03	0.01	<0.001		0.12	0.02
	GEI9		Cal	0.006	0.001	<0.001		0.12	0.02
Ophi	G3	4	Dol	0.08	0.01	<0.001		0.15	0.01
	G3		Dol	0.026	0.004	<0.001		0.08	0.01
	G3		Dol	0.023	0.003	<0.001		0.08	0.01
	G4	5	Dol	0.171	0.004	<0.001		0.084	0.003
	G4		Dol	0.111	0.004	<0.001		0.068	0.002
	G4		Dol	0.026	0.001	<0.001		0.08	0.01

N = total number of analysis. Abbreviations: Cal = calcite, Chl = chlorite, Dol = dolomite, Ep = epidote, Fo = forsterite, Ttn = titanite. Serp = serpentinite, Ophi = ophicarbonate, Metab

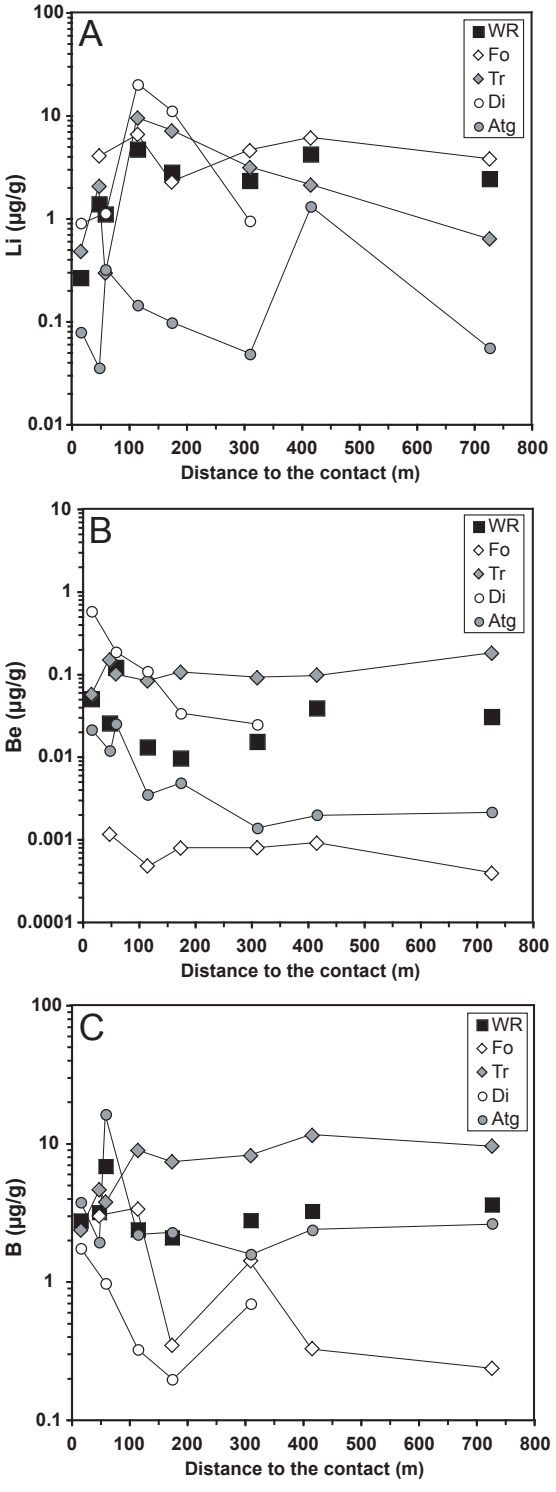


Fig. 4.10: Average (A) Li, (B) Be and (C) B contents in minerals and whole rock plotted relative to their nearest orthogonal distance to the ophicarbonate – metabasite contact. Abbreviations: Atg = antigorite, Di = diopside, Fo = forsterite, Tr = tremolite, WR = whole rock.

for some tremolite/antigorite pairs (Table 4.4). For example, $^{Be}D_{tremolite\text{-}forsterite}$ is >100 in samples GEI4, G12 and G27. In contrast, for all three light elements the partitioning varies near to the contact (Fig. 4.10a-c). In the centre of the massif, Li is preferentially incorporated into forsterite, and Be and B into tremolite (Fig. 4.10a). The Be concentration decreases in the order tremolite > diopside > antigorite > forsterite in the centre of the massif, while diopside has the highest Be contents at the rim of the massif (Fig. 4.10b). For B, the concentration decreases in the order tremolite > antigorite > forsterite > diopside in the centre of the massif, while antigorite sometimes contains more B than tremolite at the rim (Fig. 4.10c).

Metabasite (contact)

The major Li carrier in metabasic rocks is chlorite (27.6 to 75.2 μg/g), followed by tschermakitic hornblende (up to 11.5 μg/g). Epidote is poor in Li (< 0.8 μg/g), while titanite has values up to 4.0 μg/g. Tschermakitic hornblende and chlorite have Be contents up to 2.1 and 0.2 respectively. Tschermakitic hornblende has the highest B content, 7.7 μg/g, while chlorite has values between 0.3 and 2.0 μg/g. Epidote and titanite are both poor in Be (< 0.400 μg/g) and B (< 1.7 μg/g).

DISCUSSION

Nature of the protolith

REE patterns of serpentinite fall into two groups (Fig. 4.12). Rocks from group I (Fig. 4.12) show the classic 'N-MORB' REE pattern with a flat HREE segment at 1 to 2x the chondrite abundances, and a LREE fractionation (Ce_N/Sm_N = 0.48 to 0.99). This signature corresponds to fertile orogenic lherzolites (e.g. Bodinier and Godard 2004). According to Pastorelli et al. (1995), the protolith of the Geisspfad serpentinite is a subcontinental spinel lherzolite, which evolved in an ocean-continent transition environment during rifting. The REE pattern of group I serpentinites is in agreement with this hypothesis, but it could also correspond to slightly depleted subcontinental mantle.

Rocks from group II (G15 and G26) are characterized by a U-shaped REE pattern (Fig. 4.12), with fractionation of both light REE (Ce_N/Sm_N = 1.75 to 3.50), and heavy REE (Gd_N/Lu_N =

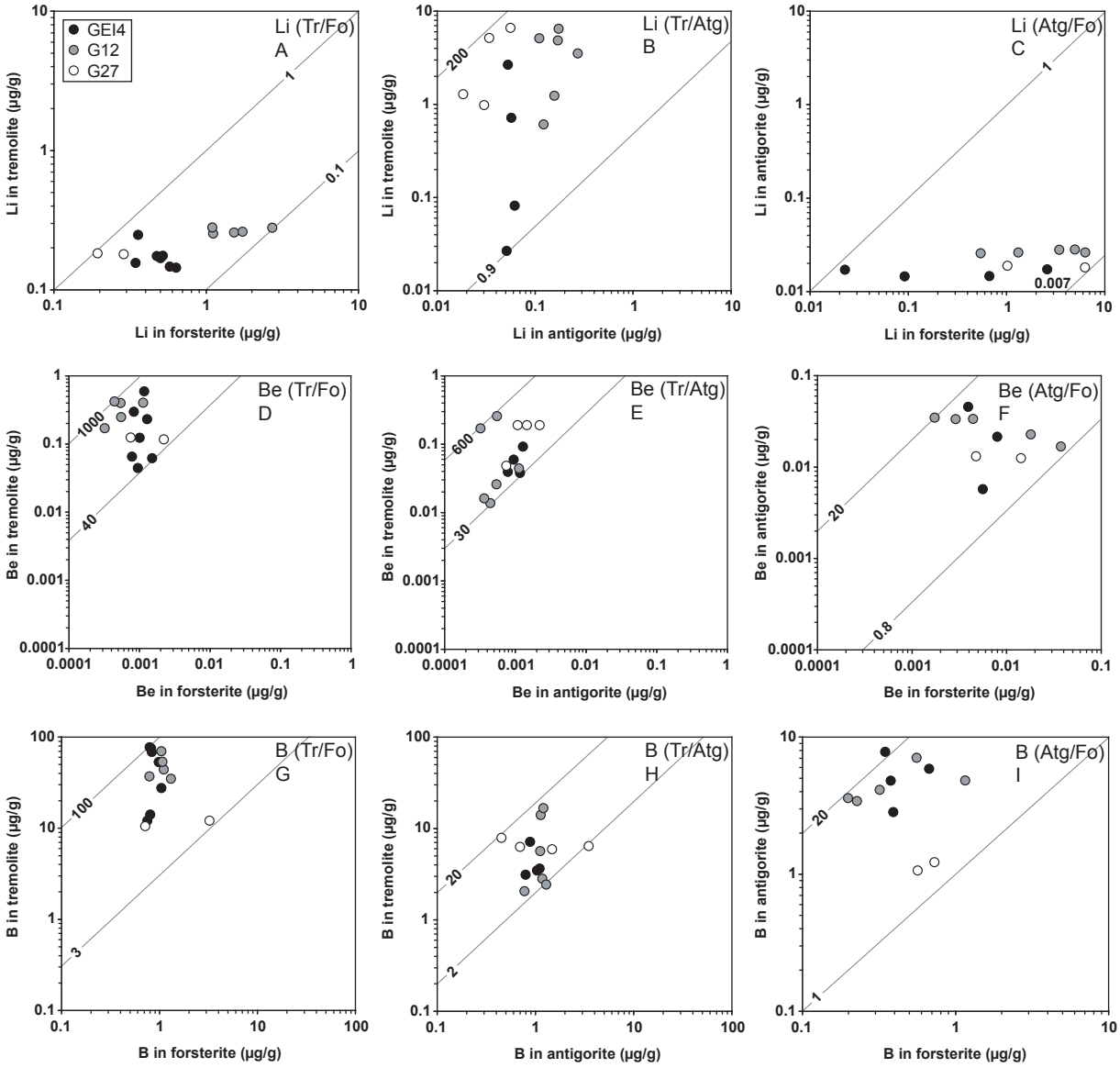


Fig. 4.11: Concentrations of (A-C) Li, (D-F) Be and (G-I) B in coexisting mineral pairs in samples GEI4, G12 and G27 from the centre of the massif. Diagonal lines mark constant partition coefficients (values given on lines).

0.33 to 0.42). The concentration of REE in whole rock samples of group II is approximately one order of magnitude lower than for group I. Group II samples show very low modal tremolite, and sample G15 is probably a meta-dunite (Keusen, 1972; Fig. 4.2). G15 and G26 have higher MgO and lower Al_2O_3 contents compared to serpentinites from group I (Fig. a.1 in the Appendix). Their patterns are similar to Huinan spinel harzburgite (Xu et al., 2003), which reacted with basaltic melts. Samples G15 and G26 might have dunitic and harzburgitic protoliths, respectively.

Serpentinization of the protolith

Ophicarbonates, metarodingites and serpentinites are present in the Geisspfad massif. This rock association was described in the present-day Iberia Abyssal Plain (Boillot et al., 1980), but also in Mesozoic ocean-continent transitions of the Alps (Platta-Val Malenco transect, Swiss-Italian Alps; Manatschal and Nievergelt, 1997; Müntener et al., 2000) and the northern Apennines (Marroni et al., 1998). In the centre of the massif, the Geisspfad serpentinite shows a hydrogen and oxygen whole rock isotopic composition (Fig. 4.7) similar to oceanic serpentine (mineral) drilled or

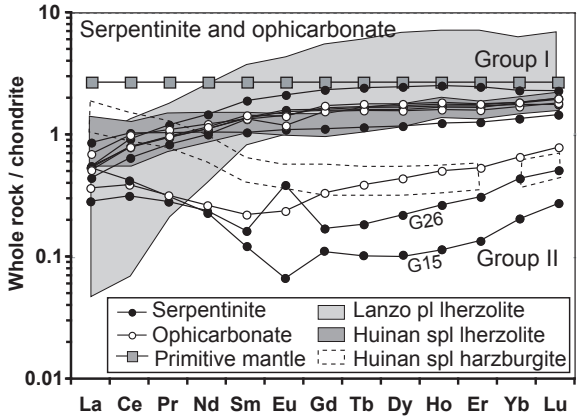


Fig. 4.12: Rare Earth Element (REE) signature of the Geisspfad serpentinites and ophicarbonates. Primitive mantle after McDonough and Sun (1995). Huinan spinel lherzolite and harzburgite after Xu et al. (2003), and Lanzo plagioclase lherzolite after Müntener et al. (2005) and Kaczmarek and Müntener (submitted) are plotted for comparison.

dredged on the ocean floor (Wenner and Taylor, 1974; Früh-Green et al., 1996). The $\delta^{18}O$ and δD values of the Geisspfad serpentinite thus support a reaction between peridotite and a seawater-derived fluid. Samples from the centre of the massif are hardly deformed and preserve a texture of static serpentinization (Fig. 4.4b). Figure 4.4b represents a mesh-rim texture after olivine, with serpentine being replaced by tremolite during amphibolite facies metamorphism. The mesh-rim texture after olivine is frequently observed in serpentinites from mid-ocean ridges (Wicks and Whittaker, 1977; O'Hanley, 1996). The increase in Cu whole rock content (up to 42 μg/g) at the rim of the ultramafic massif could be related to hydrothermal activity on the ocean floor related to volcanism (Zierenberg et al., 1998), or hosted by peridotite as in the present-day Logatchev hydrothermal field (Cu in the fluid: 2.8 μg/g; Schmidt et al., 2007). Serpentinization of the Geisspfad complex presumably occurred on the ocean floor. Oceanic serpentine usually found in oceanic environments (lizardite and chrysotile) was transformed to antigorite during prograde Alpine metamorphism and recrystallization (e.g. Trommsdorff and Evans, 1970).

Li, Be, and B budgets of the protolith before Alpine metamorphism

When constraining the Li, Be, and B contents of the protolith of the Geisspfad body, the ophicarbonate should not be considered. The increase in Pb and U whole rock contents (Fig. 4.5k-l), and the shift in δD values (Fig. 4.7) at the rim of the ultramafic massif clearly shows that (at least) the ophicarbonate reacted with crust-derived fluids. In contrast, the serpentinite (at least in the centre of the massif) seems to be unaffected by such fluids (Fig. 4.5). The serpentinites have average Pb and U abundances (0.095 and 0.003 μg/g) lower than the primitive mantle (0.150 and 0.020 μg/g; McDonough and Sun, 1995). For this reason, only the serpentinite will be used to estimate the protolith composition.

Partial dehydration of the Geisspfad serpentinite was driven by the reaction antigorite + diopside = forsterite + tremolite + fluid (0.6-0.7 GPa, 520-560°C; Pastorelli et al., 1995). Scambelluri et al. (2004) showed that Li is fairly immobile during serpentinite dehydration at high pressure (reaction: antigorite + brucite = forsterite + fluid). As diopside can contain up to ~ 5 μg/g of Li in oceanic serpentinites (Pelletier et al., submitted a; Vils et al., in prep.), its decomposition during prograde metamorphism could potentially liberate some Li into the fluid ($^{Li}D_{cpx\text{-}fluid} = 0.16$ after Brenan et al., 1998b). The antigorite consumed during the reaction could have played a role, as Li content in antigorite from high-pressure serpentinite ranges between 0.02 and 4.32 μg/g (Scambelluri et al., 2004; Marschall, 2005). However, some Li liberated during the reaction was probably stored in forsterite and tremolite, as shown by Scambelluri et al. (2004) for dehydration at high pressure. By analogy, the Li whole rock content of Geisspfad serpentinites probably decreased during prograde metamorphism, but this loss cannot be quantified. The whole rock Li content in Geisspfad serpentinite ranges from 2.3 to 6.5 μg/g. This value is similar to Li content in serpentinites from mid-ocean ridges (0.1-13.7 μg/g; Decitre et al., 2002; Niu, 2004; Vils et al., in prep.), but higher than the value of 1.6 μg/g attributed to the primitive mantle by McDonough and Sun (1995). This indicates that little Li is incorporated in ultramafic rocks during serpentinization (Pelletier et al., submitted a; Vils et al., in prep.). The Li content of the Geisspfad serpentinite is probably representative of the unmetamorphosed serpentinite precursor.

The Be content of the Geisspfad serpentinite varies between 0.013 and 0.039 μg/g, except for samples G15 and G26, which have lower values.

Our unpublished results indicate that no Be is added during serpentinization (Pelletier et al., submitted a; Vils et al., in prep.). Experiments and natural observations in basaltic systems suggest that Be is highly compatible during fluid production, with $^{Be}D_{cpx\text{-}fluid}$ = 1.8 (Brenan et al., 1998b) and $^{Be}D_{Ca\text{-}amphibole\text{-}fluid}$ = 4.14 (Marschall et al., 2007). By analogy, no Be should have been lost during prograde metamorphism, and Be content of the Geisspfad serpentinite should be representative of its protolith. The Geisspfad serpentinite has values lower than the primitive mantle (0.068 μg/g; McDonough and Sun, 1995), but similar to serpentinites from the Feather River ophiolite in California (Li and Lee, 2006) with values between 0.01 and 0.06 μg/g. Be is incompatible during melting of peridotite (Brenan et al., 1998a). For this reason, the lower Be content of the Geisspfad serpentinite compared to the primitive mantle can be explained by low degrees of partial melting of a fertile lherzolite protolith. Lanzo and Huinan lherzolites are residues after partial melting of < 6 to 12% (Bodinier, 1988) and of 0 to 15% (Xu et al., 2003), respectively. These lherzolites show a REE signature similar to the Geisspfad serpentinites (Fig. 4.12). The partial melting hypothesis is also confirmed by the extremely low whole rock Be contents of mid-Atlantic ridge ODP Leg 209 serpentinites (< 0.0080 μg/g; Vils et al., in prep.), and of the Pindos harzburgites (<0.0016 μg/g; Pelletier et al., submitted a), which represent residues after high degrees of partial melting (Saccani and Photiades, 2004; Seyler et al., 2007).

The B content of the Geisspfad serpentinite ranges from 1.8 to 4.0 μg/g. Ophicarbonate, rodingitization of some metabasites, and the $\delta^{18}O$ and δH isotopic compositions indicate that the Geisspfad serpentinite interacted with seawater. Rocks were probably highly serpentinized before prograde metamorphism, and B was primarily added to the rock during hydrothermal activity (Bonatti et al., 1984; Li and Lee, 2006; Pelletier et al., submitted a; Vils et al., in prep.). Serpentinization conditions in the Geisspfad body were probably comparable to those occurring in the present-day Iberia abyssal plain (Agrinier et al., 1996) at low temperature (< 200°C), by analogy with the postulated tectonic setting, but no B whole rock data exist. However, the B content of the Geisspfad serpentinite is lower than comparable low-temperature (T < 250°C, Bach et al., 2004) mid-ocean ridge serpentinites of ODP Leg 209 (10.4 - 65.0 μg/g; Vils et al., in prep.). B has a high fluid/rock partition coefficient (~ 60; Scambelluri et al., 2004) during partial dehydration at high pressure (reaction: antigorite + brucite = forsterite + fluid). Geisspfad serpentinites probably record a dehydration reaction, meaning that some B was lost during prograde metamorphism (Fig. 4.6). This B loss was coupled to a Cl loss, since Cl whole rock contents of the Geisspfad serpentinites are low (9-44 μg/g) compared to oceanic serpentinites (Barnes et al., 2006) and close to the primitive mantle value of 15 μg/g (Lyubetskaya and Korenaga, 2007). Coupled B and Cl loss during prograde metamorphism was also shown by Scambelluri et al. (2004).

Trace element behaviour related to retrograde metamorphism

In the centre of the massif, Li, Be, B, U, and Sr whole rock contents are homogeneous (Fig. 4.5). Li, Be, and B distribution between forsterite, antigorite, tremolite and diopside is also homogeneous (Fig. 4.9 and 4.10). Serpentinite from the centre seems to be related to the interaction with a seawater-related fluid (Fig. 4.7; Wenner and Taylor, 1974; Früh-Green et al., 1996). Considering these observations, metamorphism in the centre of the massif approached closed system behaviour, and Li, Be, and B contents of the minerals and the bulk record equilibrium.

On the contrary, at the rim of the massif, the mineralogical changes due to retrograde metamorphism are accompanied by different trace element systematics in minerals and whole rocks, which reflect disequilibrium: (i) A negative shift in the δD values of the bulk (Fig. 4.7); (ii) An increase of the fluid mobile elements Be, Rb, Pb, and U in whole rocks (Fig. 4.5); (iii) A change in the Li, Be, and B mineral-mineral partition coefficients compared to the centre of the massif (Fig. 4.10); (iv) A shift in the Li, Be, and B contents of the rock-forming minerals (Fig. 4.9). All these features can be explained by fluid-rock interaction in the contact zone between the Monte Leone gneiss and the ultramafic rocks during retrogression.

In tremolite, antigorite and diopside, Li increases from the centre of the massif to approximately 150 meters from the contact (Fig. 4.9a-c and 4.10a). Beyond this limit, Li content of all minerals decreases abruptly towards the

contact (Fig. 4.9a-c and 4.10a). The similar behaviour of Li in these minerals and in whole rocks shows that the low Li content observed in ophicarbonate is not due to the presence of Li-poor carbonates. The particular trend observed could reflect a two-stage evolution. Li in the ultramafic body increased during a first retrograde fluid flow, up to 400 meters inside the massif (Fig. 4.9a), which was responsible for the crystallization of retrograde diopside+antigorite at the expense of olivine+tremolite, and of the retrograde mineral assemblage observed in ophicarbonate. Temperature estimates in ophicarbonate (antigorite + dolomite + calcite) indicate that the retrograde assemblage formed at temperature between 425 and 525 °C (Connolly and Trommsdorff, 1991). Subsequently, Li was leached from the ultramafics along the contact during a second retrograde fluid flow (cryptic metasomatism), which was more localized (~ 150 m inside the massif; Fig. 4.13). Li leaching was accompanied by Rb leaching, which is observable in whole rocks (Fig. 4.5a and 4.g). By comparison, Li and Rb are leached from ultramafic rocks during high temperature hydrothermalism (T ≥ 300°C) on the seafloor (Schmidt et al., 2007). For this reason, the second retrograde fluid flow should have occurred at T ≥ 300°C.

Fluid induced recrystallization corresponding to the first retrograde fluid flow could also explain the increase in Be in the whole rocks (Fig. 4.5b and 4.10b), and in antigorite and diopside up to 100-150 meters from the contact (Fig. 4.9e-f). Tremolite shows no Be increase (Fig. 4.9d), but this is related to $^{Be}D_{Tr\text{-}Di}$ (Fig. 4.10b, Table 4.4), which is different in the centre of the massif (~ 4) and at its border (< 1). The Be increase is correlated with a Pb and U increase. Seitz and Hart (1973) showed that Pb and U can be enriched during hydrothermal alteration on the ocean floor in ultramafic systems. Li and Lee (2006) also mentioned high Pb contents (0.03-5.20 μg/g) in serpentinites from the Feather River ophiolite (California). However, the coupled increase of U, Pb and Be in the Geisspfad ultramafic rocks is better explained by interaction of these rocks with a (externally-derived) crustal fluid during emplacement into the crust.

Along the northern contact, there is an increase in the B content of the bulk (Fig. 4.5b) and of antigorite, and to a lesser extent of diopside (Fig. 4.9h-i). Along the southern contact, no B increase is observed (Fig. 4.5b), except in diopside (Fig. 4.9i). The difference in the B content between the north and the south is correlated to the B content in the surrounding gneiss (Fig. 4.5c; north: 8.79 μg/g; south: 0.92 μg/g). The gneiss showing the highest B concentration (G32a, North; Fig. 4.2) contains biotite, muscovite and chlorite, while the other gneiss (G36; South; Fig. 4.2) contains chlorite only. Muscovite and biotite are important carriers of B, compared to the other minerals, in medium- to low-grade metamorphic rocks (Grew, 1996). If the fluid is derived from the country rocks, as postulated for Li and Be, the difference in the B content of the ultramafics can be due to the B concentration in the fluid. It has long been known that B is leached during high temperature hydrothermal alteration of the oceanic crust (Thompson and Melson, 1970). Accordingly, the fluid composition could have evolved during its way through the Geisspfad metabasite during the first retrograde fluid flow, where B was leached at high temperature, and became enriched in the fluid. The second retrograde fluid flow should also be considered, because it probably modified the B budget along the contact. Interaction of serpentinites with moderate temperature fluid (T ≥ 300°C) on the ocean floor leads to B enrichment in whole rock, as shown by the B depletion of hydrothermal fluids compared to seawater in this environment (Schmidt et al., 2007).

In conclusion, the first retrograde fluid flow at temperature between 425 and 525°C induced modal metasomatism in serpentinite and ophicarbonate, and lead to the Li, Be, B, Pb, and U enrichment observed in whole rocks, but also to the Li, Be, and B enrichment of some rock-forming minerals. This first retrograde fluid flow was followed by a second retrograde fluid flow (Fig. 4.13), which mainly leached Li and Rb from ultramafics along the contact at temperature ≥ 300°C. This second retrograde fluid migration event was more localized than the first one, with a maximum penetration of ~ 150 m inside the ultramafic massif, and did not crystallize new minerals.

Origin of the fluid

As shown by the enrichment in U, Pb, Be, and the low δD values of the ultramafics at the contact, the first retrograde fluid flow is probably derived from the continental crust (Fig. 4.13). The positive correlation between the B content in the ultramafics at the rim of the massif and the B content in the

neighbouring gneiss, suggests a local origin of the fluid. The fluid propagated through the contact and probably reacted with the metabasite before infiltrating the ultramafics. Be is incompatible in most mineral phases from the metabasite, but compatible in Ca-amphibole ($^{Be}D_{Ca\text{-}amphibole/fluid}$: 4.14; Marschall et al., 2007). Be concentration in the fluid was probably high because Be whole rock content in serpentinite and ophicarbonate is 10 to 100 times higher than in oceanic serpentinites (Pelletier et al., submitted a), even if Be was probably compatible in tschermakitic hornblende from the metabasite (0.59-2.10 μg/g, Table 4.3).

Part of the original U and Pb present in the fluid was probably accommodated into the metabasite, because epidote group minerals (zoisite, allanite) usually contain major quantities of these elements (Zack et al., 2002). For the fluid mobile elements Sr, Ce, and Yb, no increase is observed in the ultramafics (Fig. 4.5). Rare earth elements (including Ce and Yb) are strongly compatible in allanite (Banks et al., 1994; Frei et al., 2004). Sr has a similar charge and ionic radius than Eu, Sr should therefore be compatible in this mineral. As allanite and epidote are monoclinic, they probably have similar behaviour during accommodation of rare earth elements in their structures. During the first retrograde fluid flow, Sr, Ce, and Yb were probably incorporated in epidote from the metabasite, and the fluid was depleted in these elements compared to the primitive (original) fluid when it reached the ultramafics.

In conclusion, the first retrograde fluid flow could be due to dehydration of the surrounding Monte Leone gneiss, and was produced during decompression and concomitant hydration of the ultramafics. This first retrograde fluid flow is responsible for most trace element systematics recorded by the border of the ultramafic rocks (Fig. 4.13). Similar fluid production during unloading of metamorphic crustal rocks at elevated temperature was observed in the Adula nappe (Central Alps) by Heinrich (1982) and postulated by Miller et al. (2002) in order to explain exhumation of high-pressure metamorphic belts. Fluid migration in the ultramafics was limited by the mechanical strength of the forsterite-tremolite-antigorite fels, which inhibited a fluid influx by brittle or plastic deformation. The origin and composition of the Li and Rb leaching fluid flow is uncertain, but probably limited to the strongly foliated rocks along the contact.

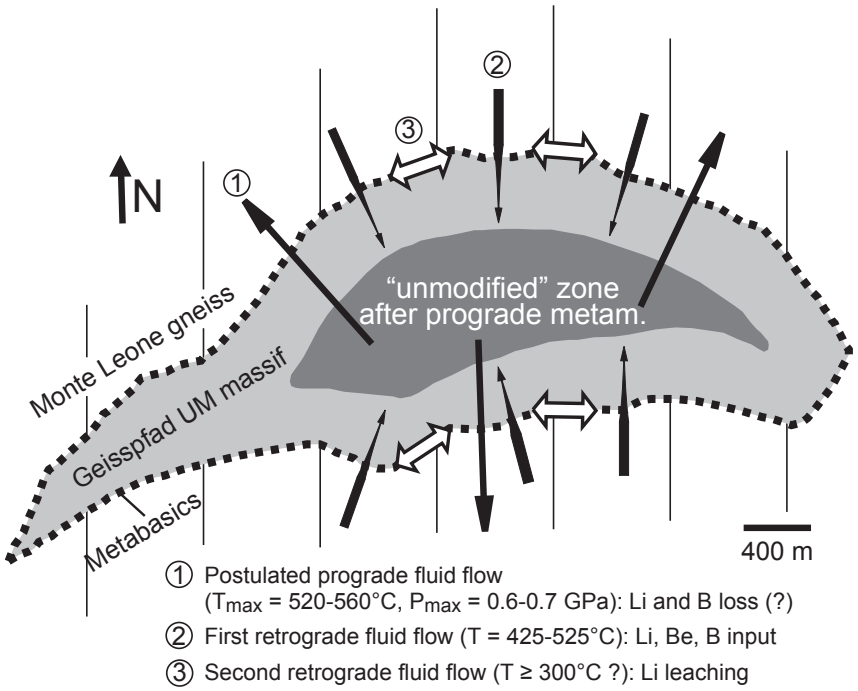


Fig. 4.13: Schematic representation of the different fluid migration events which occurred in the Geisspfad region between the ultramafic massif and the Monte Leone gneiss. The "unmodified" zone represents the rocks which conserved their prograde geochemical signature for all elements during exhumation and emplacement into the continental crust. Abbreviations: UM = ultramafic.

Implications for Li, Be and B studies in orogenic environments

According to the Pb content of the whole rocks, the first retrograde fluid flow affected the ultramafics on a distance of ~ 400 meters into the massif (Fig. 4.5k and 4.13). However, the effect on the Li, Be, and B contents of minerals and whole rocks seem to be modified on a distance of approximately 100-150 meters only (Fig. 4.5a-c and 4.9a, c, e, f, i), where the metasomatism was modal. Moreover, the second retrograde fluid flow also modified the Li signature in minerals and whole rocks. For these reasons, Li, Be, and B studies in ultramafic rocks from orogenic environments, such as ultrahigh pressure terranes, should always consider and quantify the modifications related to the emplacement into the continental crust.

Strong Li enrichment and negligible B and Be modifications were found in the Alpe Arami garnet peridotite by Paquin and Altherr (2002) and Paquin et al. (2004). The authors presented the Li content in olivine and clinopyroxene before and after an inferred metasomatic event. The Li increase in olivine is about 1 μg/g, while the Li increase in clinopyroxene ranges from 1 to 14 μg/g. They concluded that this enrichment is induced by subduction-related metasomatism. The lateral extent of the Alpe Arami garnet peridotite massif is approximately 1000 x 500 meters, with the freshest rocks (garnet peridotite) present in the centre of the massif, and retrograded rocks present at the rim (spinel-amphibole and chlorite peridotite). Alpe Arami is in direct contact with metagranites and metasediments. Considering the size of the massif, the studied samples were collected at a maximum distance of approximately 250 meters from the nearest contact. By comparison, results of the Geisspfad study for olivine and clinopyroxene, collected at a similar distance from the contact, are characterized by a Li enrichment of a few μg/g, and no Be or B enrichment compared to their protolith. The light element signature observed in the Alpe Arami garnet peridotite could thus potentially be related to its emplacement into the continental crust.

Scambelluri et al. (2006) presented Li and Be results from the Ulten zone peridotite (Eastern Italian Alps). This peridotite forms metric to decametric lenses in gneisses and migmatites. The authors described two different rock types metasomatized by subduction-related fluids or melts. Spinel peridotite was metasomatized by a hydrous melt, and garnet-amphibole peridotite reacted with some aqueous fluids. In the first case, they observed a strong Li (up to 24 μg/g), Pb and U enrichment in clinopyroxene, and $^{Cpx/ol}D_{Li}$ between 2.7 and 8.0. In the second case, they show bulk rock positive anomalies of Li, Pb, U, Cs, and Ba, and high Li contents in olivine, amphibole and clinopyroxene. Alternatively, all these features could have been produced during retrogression, and especially because the size of the ultramafic lenses are extremely small. In such small bodies, potential fluid migration is probably pervasive. Similar Li contents are observed in Geisspfad clinopyroxene (up to 31.65 μg/g) from the rim of the massif, where $^{Cpx/ol}D_{Li}$ is between 3 and 5 (Fig. 4.10a).

SUMMARY AND CONCLUSION

The Geisspfad massif shows mineralogical and geochemical evidence that altered ultramafic rocks might interact with the surrounding continental crust during their emplacement. In the Geisspfad ultramafics, two stages of retrograde fluid-rock interaction events are recorded along the rim of the massif, the first being induced by fluids released from the surrounding gneiss. Along a ~400m wide border zone of the ultramafic massif, the deformation increases, retrograde mineral assemblages are present, the δD is shifted to lower values, and the light and other trace element concentrations are modified in whole rocks. In terms of light elements, Li and Be in whole rocks are strongly enriched, while B might increase to a lesser extent, due to the interaction with the first high-temperature retrograde fluid (425-525°C). Effects of this first retrograde fluid migration is also observable by the increasing Li, Be, and B contents of minerals towards the rim of the massif. It modified the light element mineral-mineral distribution coefficients. Li content in whole rocks and minerals were leached during a second stage of retrograde fluid flow at temperature ≥ 300°C, which only affected ultramafic rocks near to the contact (maximum 150 m) and did not crystallize retrograde minerals. In order to avoid equivocal interpretations of Li, Be, and B distributions of orogenic ultramafic rocks, light element studies should focus on large bodies (at least 1.0 km width).

ACKNOWLEDGEMENTS

We thank E. Gnos, A. Berger, T. Ludwig and H.-P. Meyer for analytical support, T. Plank (Boston University) for the ICP-MS analyses, and B. Putlitz for her help during stable isotopic analyses. We are grateful to V. Serneels for whole rock analyses carried out at the University of Fribourg. This work was financially supported by grants of the Swiss NSF (200020-112149) to A. Kalt. We acknowledge financial support by the Swiss NSF grant 200021-103479/1 and by the Canton of Bern for the electron microprobe facility at the Institute of Geological Sciences, University of Bern. We also thank the Hungarian financial support to the Institute of Isotopes of the Hungarian Academy of Sciences in Budapest, GVOP-3.2.1-2004-04-0268/3.0 and NAP VENEUS05 Contract No. OMFB 00184/2006.

SUPPLEMENTARY DATA

Additional data associated with this article can be found in Appendix A of this manuscript, and will be available online on the website of *Chemical Geology*.

Li and B variability in serpentine: intracrystalline or intercrystalline ?

L. Pelletier[1], F. Vils[1], A. Kalt[1] and C. Groppo[2]

[1]Institute of Geology and Hydrogeology, University of Neuchâtel, Emile Argand 11, CP158, 2009 Neuchâtel, Switzerland
[2]Dept. of Mineralogical and Petrological Sciences, University of Turin, Via Valperga Caluso 35, 10125 Torino, Italy

Manuscript submitted to the European Journal of Mineralogy

Abstract

A combined secondary ion mass spectrometry (SIMS) and micro-Raman study was achieved in serpentine from oceanic, ophiolitic and alpine (metamorphic) serpentinites, in order to define the parameters controlling the observed variability of Li and B contents in different serpentine-related textures (bastite, mesh, matrix, vein). The micro-Raman study focused on points previously measured by SIMS, to define the nature of the serpentine matrix, mix of phases or single serpentine polymorph type. Results show that SIMS analyses were performed on single polymorph type, lizardite or chrysotile or antigorite. However, in some oceanic and ophiolitic serpentinites, lizardite can be intergrown with talc or tremolite or enstatite in bastite (serpentine formed after orthopyroxene). There is no dependence between the type of serpentine polymorph, lizardite, chrysotile or antigorite, and the measured Li and B contents. However, Li contents above 1.1 μg/g are characteristic for mix of lizardite with talc or tremolite or enstatite, in ophiolitic and oceanic bastite. In certain oceanic samples, the Li and B content seems to be directly related to the pre-serpentinization mineral. In these samples, the highest Li and B contents were measured in lizardite from bastite. This is not the case in ophiolitic serpentinites. Serpentine in alpine metamorphic serpentinites is antigorite. Unlike serpentine from oceanic or ophiolitic environments, antigorite from alpine serpentinites has a larger grain size than the SIMS spot size (15-30 μm). In this antigorite, Li and B variability is intracrystalline, because there is a negative correlation between Li and Mg^{2+} + Fe^{2+}, and between B^{3+} and Si^{4+}. The good correlation between calculated and measured bulk Li and B contents in alpine serpentinites confirm that grain boundary components are unlikely present in these rocks. In ophiolitic serpentine, there is a negative correlation between Li and Mg^{2+} + Fe^{2+}, showing that Li variability in these rocks is probably intracrystalline. The positive correlation between B^{3+} and Si^{4+} in oceanic and ophiolitic serpentinites, shows that some B is probably intercrystalline and related to grain boundary components.

Key words: lithium; boron; serpentine; micro-Raman spectroscopy; secondary ion mass spectrometry

INTRODUCTION

As the light elements Li and B are important tracers for mass transfer in subduction zones (Moran et al., 1992; Leeman, 1996; Brenan et al., 1998; Moriguti & Nakamura, 1998), numerous authors have analyzed Li and B contents of the altered oceanic lithosphere (Benton et al., 2001 and references therein; Bouman et al., 2004 and references therein). Li and B contents are low in fresh oceanic mantle or crust (Ryan & Langmuir, 1987, 1993; Decitre et al., 2002; Pelletier et al., submitted b), but can be clearly elevated in altered crust and serpentinized peridotites, due to the interaction of the rocks with seawater-related fluids (Thompson & Melson, 1970; Seyfried & Dibble, 1980; Bonatti et al., 1984; Seyfried et al., 1984 and 1998).

The first studies were focused on altered oceanic crust (Ryan & Langmuir, 1987 and 1993; Chaussidon & Jambon, 1994; Chan et al., 2002; Bouman et al., 2004), but more recently authors have taken an interest in the serpentinized oceanic mantle (Bonatti et al., 1984; Parkinson & Pearce, 1998; Benton et al., 2001 and 2004; Decitre et al., 2002; Früh-Green et al., 2004; Scambelluri et al., 2004; Savov et al., 2005; Wei et al., 2005; Paulick et al., 2006; Agranier et al., 2007), because it represents a huge reservoir compared to the oceanic crust. Studies demonstrated that there is a clear enrichment of B and to a lesser extent of Li in oceanic peridotites during serpentinization (Bonatti et al., 1984; Benton et al., 2001 and 2004; Agranier et al., 2007).

Li and B are enriched in serpentinite which reacted with seawater at low temperature and under equilibrium conditions (Thompson & Melson, 1970; Seitz & Hart, 1973; Seyfried & Dibble, 1980; Bonatti et al., 1984; Decitre et al., 2002; Paulick et al., 2006). This enrichment can be absent or even turn into depletion, if the serpentinizing fluid is not seawater, but fluid that evolved by interaction with the oceanic crust (Smith et al., 1995; Decitre et al., 2002). Also, B content of serpentinite is directly related to temperature of the fluid (Seyfried & Dibble, 1980; Bonatti et al., 1984), and probably to pH. Low pH favours the presence of trigonally coordinated B in the fluid (Spivack & Edmond, 1987; Schmidt et al., 2005), thus minimizing B incorporation into serpentine where it is tetrahedrally coordinated (Page, 1968). The highest B contents would be expected for serpentinites which reacted with low-temperature, high pH fluid (e.g. Lost City hydrothermal field at the Mid-Atlantic ridge; Allen & Seyfried, 2004) where more tetrahedrally coordinated B is present in the fluid.

Seitz & Hart (1973) provided the first in situ measurements of B in serpentine by thermal neutron irradiation in samples dredged from different mid-ocean ridges. Many years later, Li and B contents of serpentine were determined in situ by secondary ions mass spectrometry (Decitre et al., 2002; Scambelluri et al., 2004; Pelletier et al., submitted a and b; Vils et al., in prep.). Two studies focused on samples dredged from the South West Indian ridge (Decitre et al., 2002) and from the Mid-Atlantic ridge (Vils et al., in prep.). Other studies dealt with serpentine from the Pindos ophiolite in Greece (Pelletier et al., submitted b), from the metamorphic Geisspfad ultramafic massif in the Alps (Pelletier et al., submitted a) and from variably metamorphosed serpentinite bodies in the Alps, the Apennine and the Betic cordillera (Scambelluri et al., 2004). These studies showed that there is a large variability in the Li and B content of serpentine at the thin section scale, and sometimes at the micrometer scale (Decitre et al., 2002; Scambelluri et al., 2004; Pelletier et al., submitted a and b; Vils et al., in prep.). This variability sometimes exceeds one order of magnitude. It was observed in oceanic serpentine (Pelletier et al., submitted b; Vils et al., in prep.), but also in metamorphic serpentine (Pelletier et al., submitted a). For SIMS analyses a spot size between 15 and 30 μm is used, which is by far bigger than the grain size of most serpentine minerals (Decitre et al., 2002; Scambelluri et al., 2004; Pelletier et al., submitted b; Vils et al., in prep.), except for some metamorphosed serpentine (Pelletier et al., submitted a).

As most available data concern whole rock analysis or measurements obtained by SIMS, it cannot be determined if Li and B are present inside the serpentine structure or in the interstitials. Moreover in highly serpentinized peridotites, serpentine usually forms part of a matrix (Wicks & Whittaker, 1977; Savov et al., 2005). It is important

to check the mineralogical composition of this fine-grained serpentine matrix (grain size < 5 μm). Is this matrix constituted by a single serpentine polymorph, by a mix of different serpentine polymorphs or by a mix of different phases? This is important for Li and B contents, because other phases potentially present in serpentinites, like chlorite, brucite, talc or zeolites (Bach et al., 2004; D'Antonio & Kristensen, 2004; Paulick et al., 2006) can have high Li and/or B concentrations (Passaglia, 1978; Grew, 1996; Pelletier et al., submitted b).

Three serpentine polymorphs are present in nature, lizardite, chrysotile and antigorite (Whittaker & Zussman, 1956). Chrysotile can be divided into three subtypes, ortho-, clino- and parachrysotile (Whittaker & Zussman, 1956). Lizardite and chrysotile can be assembled in a complex form, called polygonal serpentine, where layers of lizardite are arranged as an outer shell around chrysotile fibers (Cressey & Zussman, 1976; Middleton & Whittaker, 1976). It is important to determine which polymorphs are present in the samples, and if they are mixed in the matrix, in order to test the relationship between the type of serpentine polymorph and the light element content. Such a relationship was described only once by Bonatti et al. (1984) in serpentinites from the Vema and Romanche fracture zones of the Mid-Atlantic ridge. The authors found an inverse temperature dependence of boron content in serpentine. Also, they described the following sequence of serpentine polymorph with increasing temperature: clinochrysotile + lizardite (30-80°C), lizardite + polygonal serpentine (80-120°C) and orthochrysotile (120-200°C).

A quick and reliable technique to determine the mineralogical composition of a serpentine matrix is micro-Raman spectroscopy (Rinaudo et al., 2003; Auzende et al., 2004; Groppo, 2005; Groppo et al., 2006). This technique allows the discrimination of chrysotile, lizardite and antigorite, and the identification of eventually associated phases, but not the determination of the three chrysotile subtypes or polygonal serpentine. These latter can be determined by X-ray diffraction on serpentine powder (Whittaker & Zussman, 1956), but the disadvantage is the loss of spatial information.

The objective of the present paper is to define the parameters controlling the Li and B variability in serpentine observed in peridotites serpentinized to various degrees. For that purpose, we use serpentinites from three different geological environments, oceanic, ophiolitic and alpine. Li and B contents of the samples are compiled from: Mid-Atlantic ridge ODP Leg 209 serpentinites given by Vils et al. (in prep), serpentinized peridotites from the Pindos ophiolite (Greece) given by Pelletier et al. (submitted b) and metamorphic serpentinites from the Geisspfad ultramafic body given by Pelletier et al. (submitted a). We present new micro-Raman data on serpentine from these serpentinites, in order to check whether the Li and B contents are controlled by the type of serpentine polymorph (one or more) or by phase mixtures. Moreover, we present calculated bulk Li and B contents of the samples, based on modes and mineral compositions, and we compare them to published Li and B whole rock data (Pelletier et al., submitted a and b; Vils et al., in prep.), in order to check if light elements could be localized on the interstitials.

SAMPLE CHARACTERISTICS

The samples described below were collected from different geological settings. They present variable degree of serpentinization, from 9 up to nearly 90 % of serpentine. To simplify nomenclature, all samples will be called serpentinites in the following. Samples will be classified into three groups, related to their geological setting: oceanic serpentinites, ophiolitic serpentinites and alpine serpentinites.

Oceanic serpentinites

Oceanic serpentinites were drilled during the Ocean Drilling Program (ODP) Leg 209 along the Mid-Atlantic ridge (15°20'N fracture Zone). Samples from the present study come from sites 1272A and 1274A. A precise description of serpentinite from these sites can be found in Kelemen et al. (2004) and Bach et al. (2004 and 2006). Details concerning serpentinization conditions were described by Bach et al. (2004 and 2006). Serpentinization is characterized by two different reactions (Bach et al., 2004 and 2006), the transformation of orthopyroxene to talc and tremolite (reaction I), and the reaction of olivine to serpentine, magnetite and brucite (reaction II). These reactions take place successively during cooling in the course of serpentinization, reaction

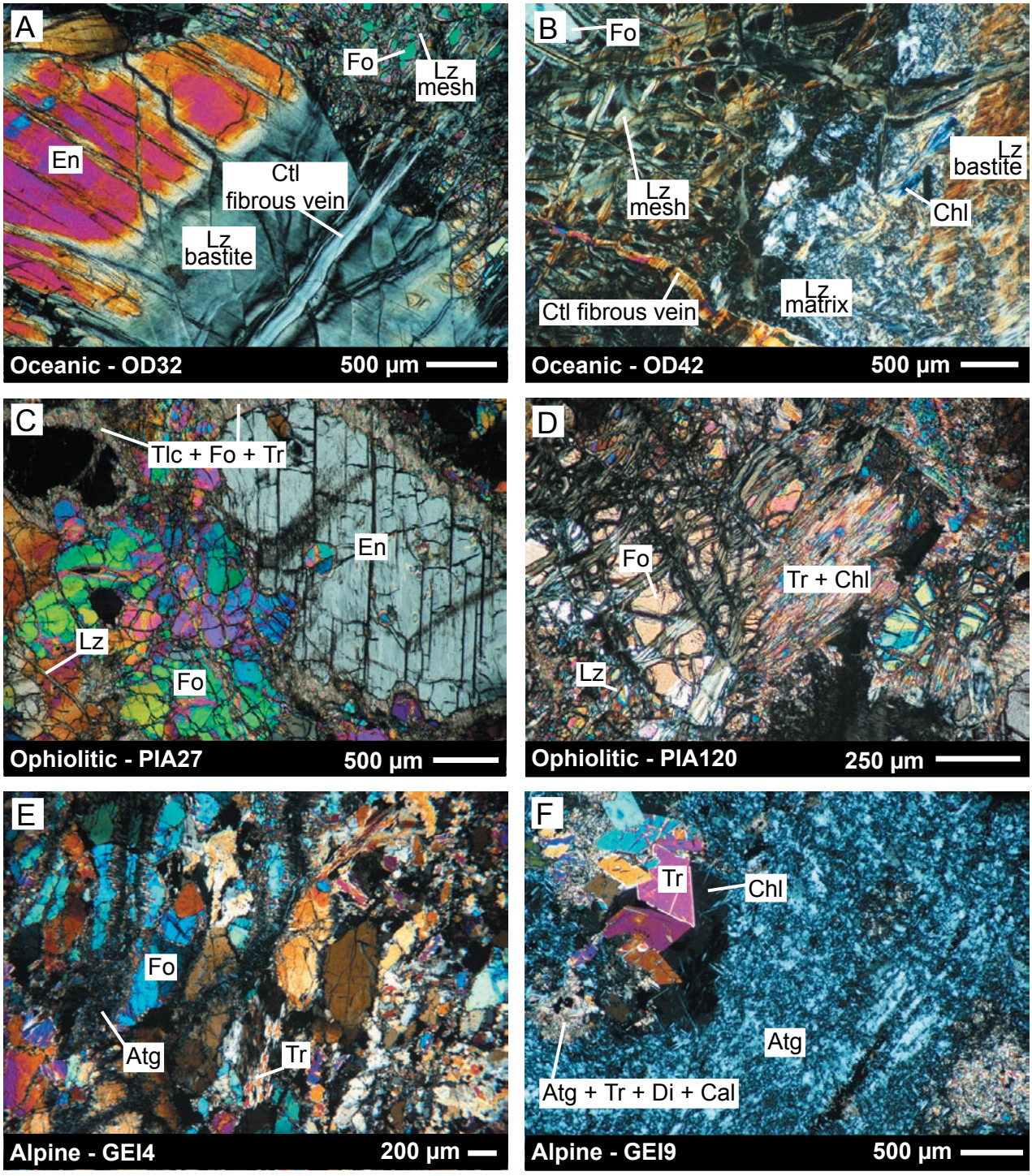


Fig. 5.1: Textures of the different serpentinite samples. A and B: oceanic serpentinites from the ODP Leg 209 sites 1272A and 1274A, C and D: ophiolitic serpentinites from the Pindos ophiolite and E and F: Alpine serpentinites from the Geisspfad ultramafic body. Abbreviations according to Kretz (1983).

I at T ≥ 350-400°C, and reaction II at T < 250°C (Bach et al., 2004). Samples from our study mainly contain serpentine associated with magnetite, and in the less serpentinized samples, some relics of diopside, enstatite, spinel and forsterite (Fig. 5.1a). Samples from site 1272A (OD2, OD18, OD28) contain up to 90% serpentine, while samples from site 1274A (OD32, OD34, OD42) show only 50 to 70%. Veins with serpentine flakes formed very early in the serpentinization history (Fig. 5.2a). It could have formed at high temperature (T ≥ 350-400 °C), simultaneously with the formation of talc after orthopyroxene in the bastite mentioned by Bach et al. (2004 and 2006). In these veins, serpentine flakes are pseudomorphosed by late serpentine (Fig. 5.2a). This late serpentine formation could be contemporaneous with the crystallization of serpentine after talc in bastite (Fig. 5.2b-f), and at the expense of olivine at lower temperature (Fig. 5.2d-f). The transformation of olivine to serpentine could have occurred at T < 250-300°C, according to Bach et al. (2004). Finally, fibrous veins formed during the late stage of serpentinization, crosscutting all the other textures (Fig. 5.2b-c). Brucite and iowaite were described by Bach et al. (2004) in some serpentinites from site 1274A, and are present in sample OD34.

Ophiolitic serpentinites

Ophiolitic serpentinites were collected in the Pindos ophiolite (northern Greece; PIA27, PIA44, PIA109, PIA120). A detailed description of these samples is presented in Pelletier et al. (submitted b). The samples show varying degrees of serpentinization, from nearly fresh (9 % serpentine) to moderately serpentinized (55 % serpentine). The less serpentinized samples are harzburgites with rare serpentine veins. They contain forsterite, rare diopside, enstatite, and spinel (Pelletier et al., submitted b). In addition to serpentine, some talc + tremolite coronas crystallized around orthopyroxene. The rocks show a crystallization sequence related to serpentinization under decreasing temperature (Pelletier et al., submitted b). The assemblage talc + tremolite ± serpentine ± olivine formed at T ≥ 350-400°C, followed by serpentine + magnetite formed at the expense of olivine at T < 250°C, and finally by the alteration of plagioclase to zeolite at T < 100°C (Pelletier et al., submitted b).

Alpine serpentinites

Three alpine serpentinites were collected from the Geisspfad ultramafic body in the Alps (GEI4, GEI9, G11). Detailed petrographic studies of this ultramafic body were performed by Keusen (1972), Pastorelli et al. (1995) and Pelletier et al. (submitted a). These serpentinites completely recrystallized under amphibolite-facies conditions (Keusen, 1972; Pastorelli et al., 1995; Pelletier et al., submitted a) during the alpine orogeny. Geisspfad serpentinites usually show an assemblage of serpentine, forsterite, tremolite, diopside and chlorite. However, in some samples, forsterite and/or diopside can be absent. In sample GEI9, calcite is present. The mineral assemblage antigorite + tremolite + forsterite ± diopside described by Keusen (1972) and Pastorelli et al. (1995) in the Geisspfad serpentinites, resulted from prograde metamorphism (Trommsdorff & Evans, 1974). Pastorelli et al. (1995) and Keusen (1972) defined peak metamorphic conditions of 520 to 560 °C and 0.6 to 0.7 GPa, and of 450 to 550 °C and ~ 0.5 GPa, respectively.

SERPENTINE TEXTURES

The following description of serpentine textures is based on the classification of Wicks & Whittaker (1977). In the following text, figures and tables, mineral abbreviations are used according to Kretz (1983).

Oceanic serpentinites

Serpentine in the oceanic samples shows four main textures. i) Pseudomorphic mesh texture after olivine (Fig. 5.1a and b, 5.2d to f), with replacement proceeding along fractures and grain boundaries. Very rare olivine is still present in the rocks. ii) Bastite texture after orthopyroxene, which is also pseudomorphic with serpentinization progressing along grain boundaries, cleavage planes and exsolution lamellae (Fig. 5.1a and b, 5.2b to f). In some cases, serpentinization is not complete and some orthopyroxene relics can be found in bastite (Fig. 5.2b). iii) Serpentine crystallized in veins. Three types of veins were observed: fibrous veins containing asbestiform serpentine minerals (Fig. 5.1a and b, 5.2a to c), other veins composed of serpentine flakes (Fig. 5.2a), and finally veins with extremely small serpentine minerals (< 5 μm,

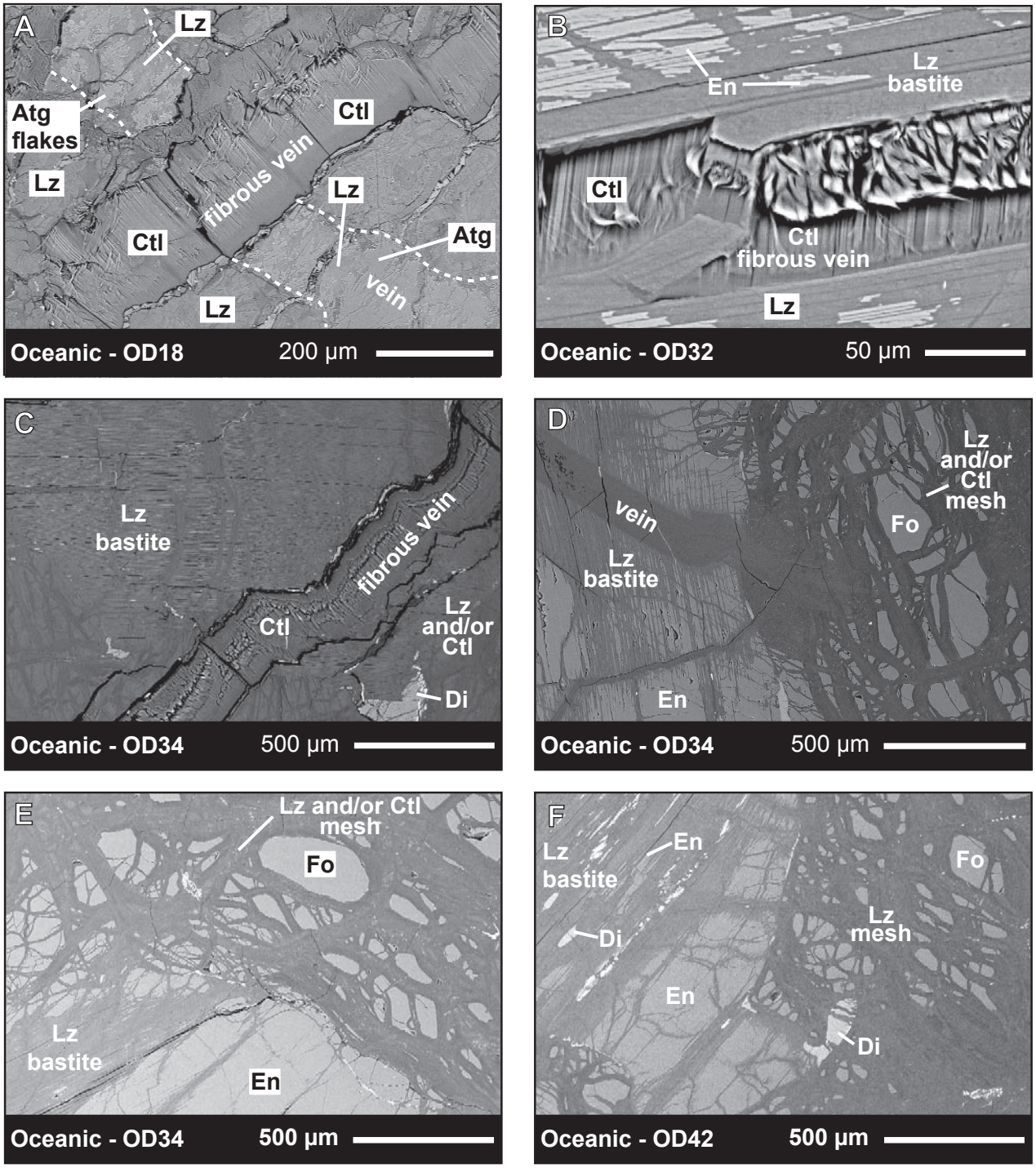


Fig. 5.2: Backscattered electron images of the different serpentine textures. A to F: oceanic serpentinites from the ODP Leg 209 sites 1272A and 1274A, G to J: ophiolitic serpentinites from the Pindos ophiolite and K and L: Alpine serpentinites from the Geisspfad ultramafic body. Abbreviations according to Kretz (1983).

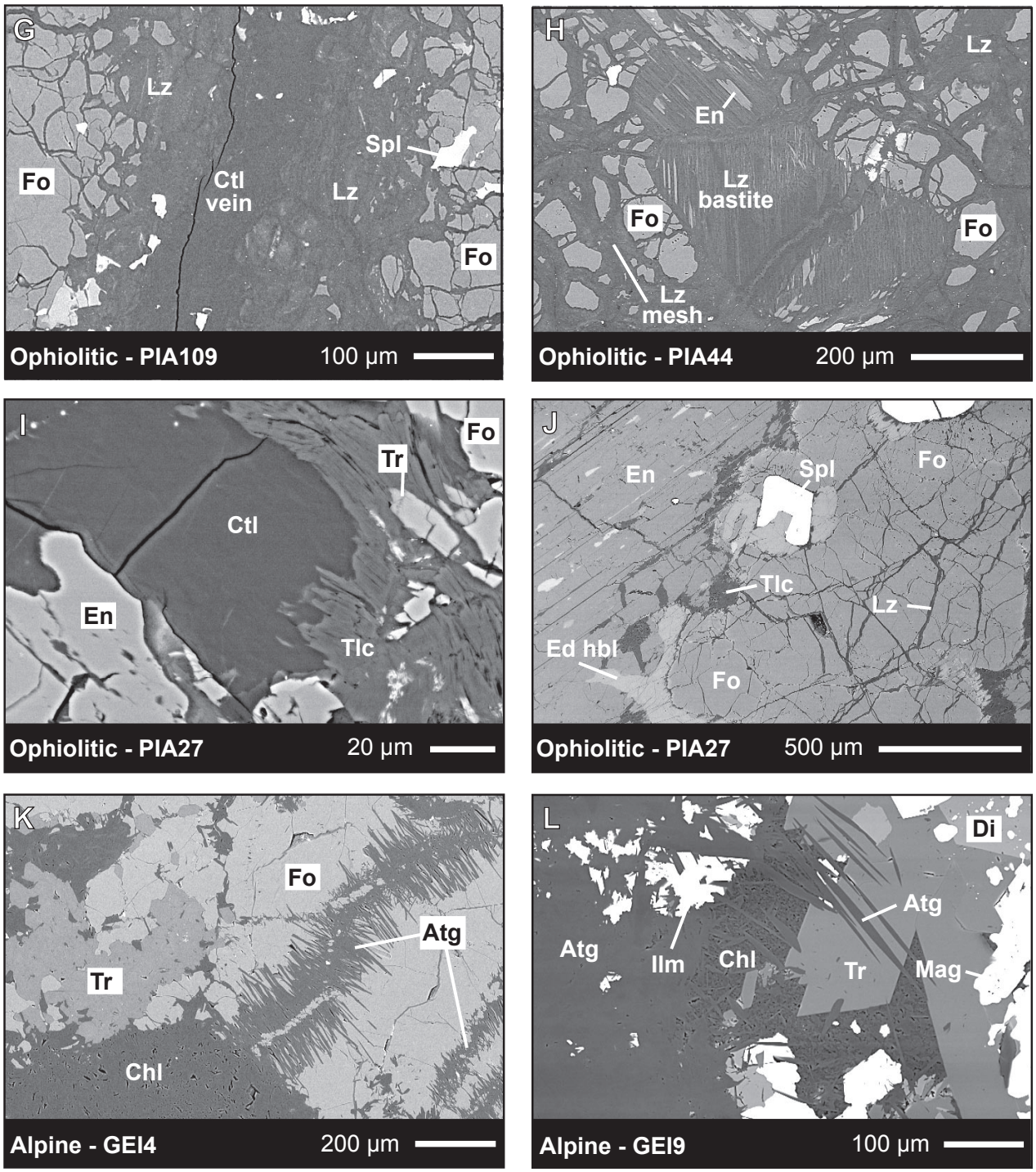


Fig. 5.2: continued.

Fig. 5.2d). In addition, serpentine often forms a fine-grained (< 5 μm) matrix, where the precursor minerals cannot be determined (Fig. 5.1b).

Ophiolitic serpentinites

Due to their low degree of serpentinization compared to the oceanic serpentinites, ophiolitic serpentinites present less complex textures. Mesh texture formed after olivine along grain boundaries (Fig. 5.1b and c, 5.2h and j), but the major parts of olivine grains are still preserved. Bastite pseudomorphic texture formed after orthopyroxene and rare clinopyroxene (Fig. 5.2h). Parts of orthopyroxene grains are usually preserved (Fig. 5.2h). Finally some veins were observed (Fig. 5.2g), where grain size is < 5 μm and where a difference in colour is observed from core to rim. Serpentine is dark in the centre of the vein and more light-coloured at the rim (Fig. 5.2g).

Alpine serpentinites

Serpentine in alpine serpentinites usually crystallized in veins, with serpentine needles growing outward from the centre of the vein (Fig. 5.1e and 5.2k). Needles can attain lengths up to 200 μm. These veins usually propagate in the rock through olivine crystals or along olivine grain boundaries. In the most serpentinized samples at the rim of the ultramafic body, two different types of serpentine can be observed. (i) Serpentine flakes in the matrix (< 50 μm) forming an interlocking texture (Fig. 5.1f and 5.2l). (ii) Serpentine in polycrystalline aggregates (serpentine + tremolite + diopside + magnetite + ilmenite + calcite) floating in the matrix, with crystals forming elongated needles (~ 200 μm length; Fig. 5.2l). An assemblage composed of serpentine and chlorite crystallized around these aggregates (Fig. 5.2l).

ANALYTICAL TECHNIQUES

All details concerning electron microprobe analysis (major elements in serpentine) and SIMS analysis (Li and B in serpentine) can be found in Pelletier et al. (submitted a and b) and Vils et al. (in prep.). Micro-Raman spectroscopy has been used as a technique complementary to optical microscopy and SEM-EDS, for rapid determination of serpentine polymorphs (Rinaudo et al., 2003; Groppo et al., 2006). Spectra were acquired on points previously measured by SIMS for Li and B contents. Micro-Raman spectra were acquired using an integrated micro/macro Raman system Jobin Yvon Mod at the Department of Mineralogical and Petrological Sciences, University of Torino (Italy). The system includes a microspectrometer Horiba Jobin Yvon HR800, an Olympus BX41 microscope and a CCD air-cooled detector. A polarized solid state Nd 80 mW laser operating at 532.11 nm was used as excitation source. Correct calibration of the instruments was verified by measuring the Stokes and anti-Stokes bands, and checking the position of the Si band at ~ 520.7 cm^{-1}. Each spectrum was acquired using a 50x objective, resulting in a 5 to 10 μm laser beam size on the sample. To optimize the signal to noise ratio, spectra were acquired using 10 scans of 5 to 10 seconds for each spectral region. The spectral regions from 1100 to 100 cm^{-1} and from 4000 to 3000 cm^{-1} were considered, because they are characteristic of serpentine minerals. The 4000 to 3000 cm-1 region was studied because the difference in asymmetry between chrysotile and lizardite peaks is observable in this range. Spectra were smoothed by an automatic basement line subtraction using the Origin 6.0 software. The serpentine polymorphs were determined by comparison with published data, where the positions of the different peaks related to each polymorphs are given (Rinaudo et al., 2003; Auzende et al., 2004; Groppo et al., 2006).

In order to test the potential presence of Li and B along grain boundaries, whole rock contents were studied. However, the information is only qualitative. Li and B in the bulk were first calculated, considering the Li and B contents of all the rock-forming minerals (serpentine, enstatite, diopside, forsterite, talc, chlorite, spinel, alteration phases, etc.). Modes of the mineralogy were calculated in weight percent based on a least-square fitting method (Herrmann & Berry, 2002) using whole rock X-Ray fluorescence (XRF) data, and mineral chemistry obtained on the electron microprobe (Pelletier et al., submitted a and b; Vils et al., in prep.). Li and B whole rock data were calculated using the modal mineral percentages and the light element abundances obtained by SIMS on the analyzed minerals. For spinel, values from Ottolini et al. (2004) were used. Secondly, Li and B content were measured by ICP-MS and PGNAA

respectively, in order to test the discrepancy between the calculated and the measured values.

IDENTIFICATION OF SERPENTINE POLYMORPHS

The spectra obtained for one type of serpentine polymorph in a single sample are similar, independent of the texture in which they crystallized. However, peaks can be slightly shifted depending on the type of sample analyzed, oceanic, ophiolitic or alpine. Representative position (wavenumbers) of the peaks related to the different polymorphs are presented in Table 5.1. Oceanic antigorite shows the typical 231, 689 and 1048 cm^{-1} bands (Fig. 5.3c), which can be related to O-H-O vibrations, and to the symmetric and asymmetric Si-O_b-Si stretching vibrations respectively (Kloprogge et al., 1999; Rinaudo et al., 2003; Groppo et al., 2006). In alpine antigorite, similar peaks were measured at 237, 689 and 1045 cm^{-1} (Fig. 5.3k). A 463 cm^{-1} band (Fig. 5.3c and k) was observed in oceanic and alpine antigorite, and could correspond to the Mg-OH translations and ν_6 SiO_4 vibrations described by Kloprogge et al. (1999) and Groppo et al. (2006). The 378 cm^{-1} band (Fig. 5.3c and k), also observed in oceanic and alpine antigorite, can be due to the symmetric bending ν_5 SiO_4 (Rinaudo et al., 2003, 2004; Kloprogge et al., 1999; Groppo et al., 2006). The broad peaks at 641 and 826 cm^{-1} are probably related to the epoxy resin (Fig. 5.3a and c). Oceanic antigorite is characterized by two distinct bands at 3668 and 3697 cm^{-1}, representing the O-H stretching bands (Fig. 5.3d; Auzende et al., 2004), while alpine antigorite shows only one band at 3664 cm^{-1} (Fig. 5.3l). The presence of only one band could be due to a higher pressure of crystallization, compared to the oceanic antigorite (Auzende et al., 2004). The shape of the band related to the O-H stretching band is directly related to the pressure of crystallization (Auzende et al., 2004).

The spectrum obtained for lizardite is similar to the one of antigorite (Fig. 5.3c), but the three typical bands 231, 387 and 693 cm^{-1} are shifted to higher wavenumbers (Fig. 5.3c, e and g; Rinaudo et al., 2003; Groppo et al., 2006). The chrysotile spectrum is also shifted to higher wavenumbers compared to lizardite (Fig. 5.3c; Rinaudo et al., 2003; Groppo et al., 2006), with values of 235, 391 and 695 cm^{-1}. The spectrum obtained for chrysotile is similar to the one of lizardite (Fig. 5.3g), but the two typical bands 229 and 688 cm^{-1} are shifted to 235 and 695 cm^{-1} (Fig. 5.3g; Rinaudo et al., 2003; Groppo et al., 2006). Lizardite and chrysotile are characterized by the absence of the 1048 cm^{-1} band compared to antigorite (Fig. 5.3c, e and g; Rinaudo

Table 5.1: Positions of the peaks related to the different serpentine polymorphs (representative analyses)

Texture	Pol.	Oceanic (cm^{-1})	Pol.	Ophiol. (cm^{-1})	Pol.	Alpine (cm^{-1})
Bastite (En)	Lz	691	Lz	688		
		387		384		
		233		229		
		3689		3681		
Mesh (Fo)	Lz	693	Lz	688		
		387		384		
		231		229		
		3688		3681		
	Ctl	695				
		391				
		235				
		3696				
Matrix (?)	Lz	693				
		387				
		231				
		3688				
Veins fibrous	Ctl	695				
		391				
		235				
		3696				
Veins flakes	Atg	1048				
		689				
		378				
		231				
		3697				
		3668				
Veins other			Ctl	695		
				389		
				235		
				3681		
Metam.					Atg	1045
						686
						378
						237
						3664

Metam.: metamorphic, Pol.: polymorph type, Ophiol.: ophiolitic. Underlined numbers obtained in the spectral region 4000 to 3000 cm^{-1}.

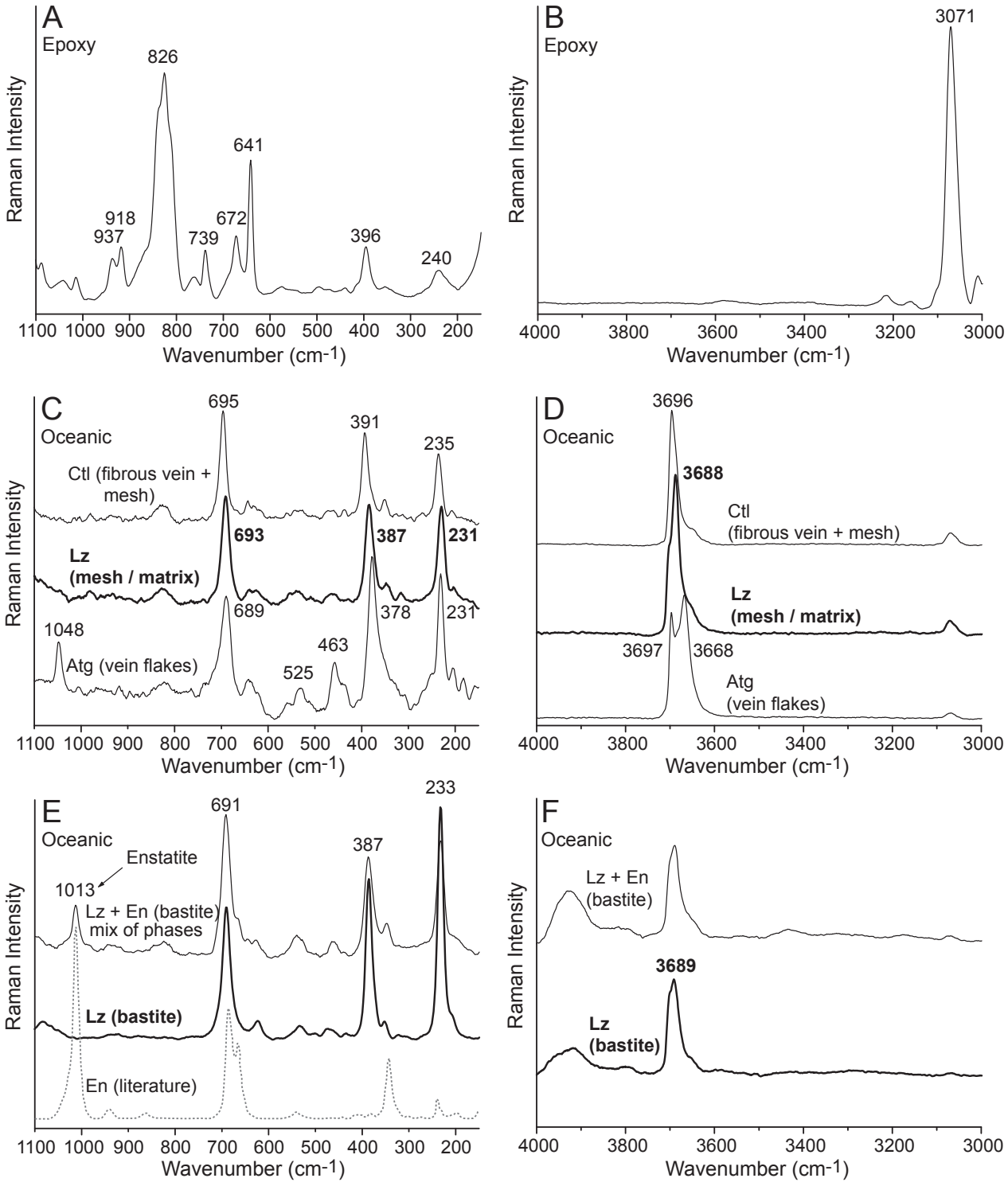


Fig. 5.3: Representative micro-Raman spectra of the frequency ranges 1100-100 cm^{-1} and their corresponding 4000-3000 cm^{-1}. Spectra of each line (a and b, c and d, etc.) were obtained on a single point. a and b: epoxy resin, c and d: mesh texture, matrix, fibrous vein and vein with flakes in oceanic serpentinites, e and f: bastite in oceanic serpentinites, g and h: mesh texture, bastite and vein in ophiolitic serpentinites, i and j: bastite in ophiolitic serpentinites, k and l: matrix and needle serpentine in Alpine serpentinites. Abbreviations according to Kretz (1983).

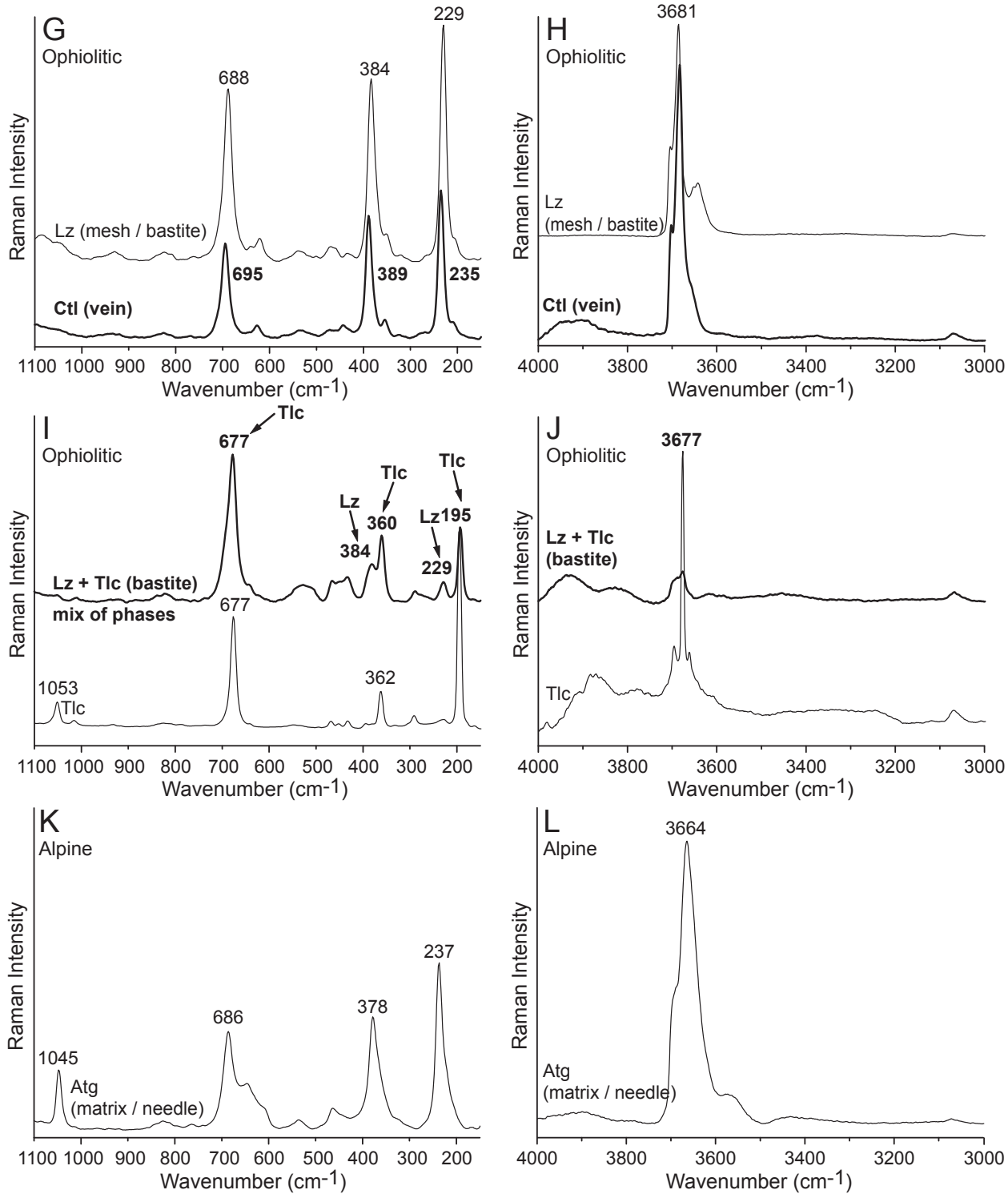


Fig. 5.3: continued

et al., 2003; Groppo et al., 2006). They usually show only one band in the 4000 to 3000 cm^{-1} spectral region around 3680 cm^{-1} (Fig. 5.3d; Auzende et al., 2004), but in some ophiolitic lizardite an additional peak at 3640 cm^{-1} can be observed (Fig. 5.3h). The asymmetry of the 3680 cm^{-1} band is reverse for lizardite and chrysotile (Fig. 5.3d, f and h; Auzende et al., 2004).

The mix of lizardite and enstatite in bastite is characterized by an additional 1013 cm^{-1} band, which is typical of enstatite and related to the Si-O_b stretching region (Fig. 5.3e). Lizardite and talc mix is characterized by a predominant talc signal (Fig. 5.3i), with 195, 360 and 677 cm^{-1} bands, which are specific to talc. This mix also shows a 3677 cm^{-1} band characteristic for talc in the O-H stretching vibration region (Fig. 5.3j).

DISCUSSION

Relation between texture and polymorphs

In oceanic serpentinites, mesh texture after olivine is composed of chrysotile and/or lizardite (Fig. 5.2d, 5.3c-d). Lizardite is the serpentine polymorph forming the bastite texture after orthopyroxene (Fig. 5.2c-f, 5.3e-f). In some bastite, a mixed signal for lizardite and enstatite was obtained (Fig. 5.3e and f). Mineralogical composition of the veins is variable, but is clearly related to the observed texture. Fibrous veins are composed of chrysotile (Fig. 5.2a, 5.3c-d), which shows an asbestiform habitus. Veins where flakes were observed are composed of antigorite (Fig. 5.2a, 5.3c-d), which is associated with late lizardite. Other veins where grain size is < 5 μm are usually composed of lizardite (Fig. 5.2d), but rare mixed signals of lizardite and chrysotile were obtained.

In ophiolitic serpentinites, lizardite is present in the mesh texture after olivine, and in the bastite (Fig. 5.2g-j). In some bastite (samples PIA27), a mix of lizardite and talc was measured (Fig. 5.3i-j). In the veins chrysotile crystallized in the centre and lizardite at the rim (Fig. 5.2g).

In alpine serpentinites, serpentine needles and serpentine in the matrix are both antigorite (Fig. 5.2k-l) and show similar absorption bands.

Major element composition of serpentine

The quality of the results was highly variable in terms of cation total (4.9 to 5.1) or oxide total (80 to 100 wt. %, including calculated H_2O). The best results are presented in Table 5.2 and are plotted in

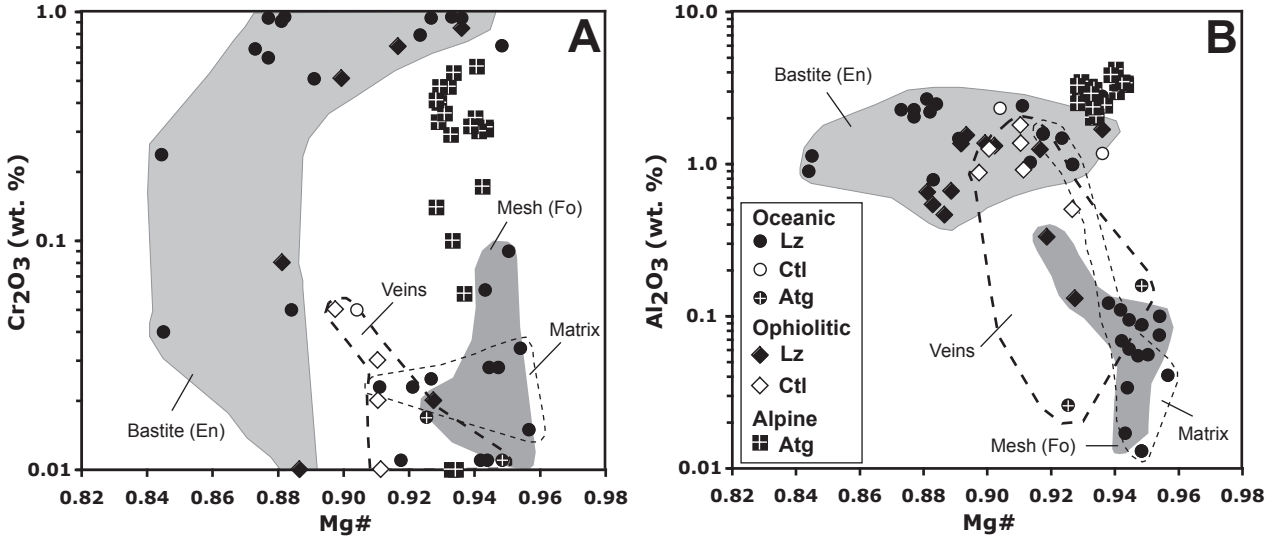


Fig. 5.4: (a) Mg# vs. Cr_2O_3 and (b) Mg# vs. Al_2O_3 (wt. %) content in serpentine as a function of the polymorph type. The textural sites are illustrated by the different fields. Oceanic serpentinites data from ODP Leg 209 sites 1272A and 1274A after Vils et al. (in prep.), ophiolitic serpentinites data from the Pindos ophiolite after Pelletier et al. (submitted b) and Alpine serpentinites data from the Geisspfad ultramafic body after Pelletier et al. (submitted a). Abbreviations: Bastite (En) = serpentine pseudomorph after orthopyroxene, Mesh (Fo) = serpentine in the mesh texture after olivine, Veins = include all type of veins, Matrix = serpentine from unknown precursor mineral.

Table 5.2: Major element composition of serpentine (representative analyses)

Setting	**Oceanic**	**Oceanic**	**Oceanic**	**Oceanic**	**Oceanic**	**Oceanic**	**Oceanic**	**Oceanic**	**Oceanic**	**Oceanic**	**Oceanic**	**Oceanic**
Sample	**OD18**	**OD18**	**OD28**	**OD32**	**OD32**	**OD42**	**OD42**	**OD28**	**OD28**	**OD32**	**OD42**	**OD28**
Pol.	**Atg**	**Atg**	**Lz**	**Lz**	**Lz**	**Lz**	**Lz**	**Lz**	**Ctl**	**Ctl**	**Ctl**	**Lz**
Texture	Vein	Vein	Bastite	Bastite	Bastite	Bastite	Bastite	Vein	Vein	Vein	Vein	Mesh
Repl.	-	-	En	En	En	En	En	-	-	-	-	Fo
SiO_2	43.2	45.0	40.7	40.0	40.0	42.1	40.9	40.3	41.1	39.6	42.8	41.3
TiO_2	b.d.	0.01	b.d.	0.02	0.01	b.d.	b.d.	b.d.	b.d.	b.d.	0.02	0.01
Cr_2O_3	0.01	0.02	0.71	0.51	0.94	0.04	0.24	0.02	b.d.	0.05	b.d.	b.d.
Al_2O_3	0.16	0.03	1.48	2.05	2.68	0.90	0.79	1.58	1.17	2.33	0.15	0.01
FeO	3.70	5.24	5.72	8.70	8.46	10.99	8.54	6.06	4.83	7.05	8.33	4.01
MnO	0.08	0.08	0.15	0.19	0.17	0.11	0.10	0.19	0.12	0.11	0.04	0.06
NiO	0.17	0.13	0.11					0.05	0.03			0.30
MgO	38.2	36.4	38.7	34.9	35.1	33.4	36.1	37.8	39.7	37.1	36.8	41.3
CaO	0.01	0.02	0.06	0.47	0.14	b.d.	0.03	0.04	0.03	0.03	0.03	0.02
Na_2O	0.01	0.01	0.01	0.01	0.03	0.01	0.01	0.04	b.d.	0.02	b.d.	0.01
K_2O	0.01	b.d.	b.d.	0.01	0.04	0.02	b.d.	0.01	b.d.	b.d.	b.d.	0.01
H_2O	12.5	12.8	12.5	12.3	12.5	12.4	12.4	12.2	12.5	12.4	12.7	12.5
Total	98.0	99.7	100.1	99.1	100.0	100.0	99.1	98.3	99.5	98.6	100.8	99.5
Stoich.	9 O	9 O	9 O	9 O	9 O	9 O	9 O	9 O	9 O	9 O	9 O	9 O
Si	2.058	2.113	1.929	1.941	1.924	2.034	1.980	1.943	1.948	1.917	2.028	1.954
Ti	b.d.	0.000	b.d.	0.001	0.000	b.d.	b.d.	b.d.	b.d.	b.d.	0.001	0.000
Cr	0.000	0.001	0.027	0.020	0.036	0.002	0.009	0.001	b.d.	0.002	b.d.	b.d.
Al	0.009	0.001	0.083	0.117	0.152	0.051	0.045	0.090	0.066	0.133	0.009	0.001
Fe^{2+}	0.147	0.206	0.227	0.353	0.340	0.444	0.346	0.244	0.192	0.285	0.330	0.159
Mn	0.003	0.003	0.006	0.008	0.007	0.005	0.004	0.008	0.005	0.005	0.002	0.002
Ni	0.007	0.005	0.004					0.002	0.001			0.011
Mg	2.711	2.554	2.736	2.525	2.513	2.404	2.606	2.717	2.806	2.673	2.598	2.913
Ca	0.000	0.001	0.003	0.025	0.007	b.d.	0.002	0.002	0.002	0.002	0.002	0.001
Na	0.001	0.001	0.001	0.001	0.003	0.001	0.001	0.004	b.d.	0.002	b.d.	0.000
K	0.001	b.d.	b.d.	0.000	0.002	0.001	b.d.	0.001	b.d.	b.d.	b.d.	0.000
H	3.985	3.999	3.956	3.995	3.997	3.996	3.998	3.923	3.954	3.993	3.997	3.938
Total	4.938	4.886	5.016	4.991	4.985	4.941	4.993	5.011	5.019	5.017	4.968	5.042
Mg#	0.948	0.925	0.923	0.877	0.881	0.844	0.883	0.917	0.936	0.904	0.887	0.948

Mg# calculated as Mg / (Mg + Fe^{2+}), all Fe considered as Fe^{2+}. b.d. = below detection limit. Pol.: polymorph type, Repl.: mineral replaced, Stoich.: stoichiometry.

Table 5.2: continued

Setting	**Ophiol.**	**Ophiol.**	**Ophiol.**	**Ophiol.**	**Ophiol.**	**Ophiol.**	**Alpine**	**Alpine**	**Alpine**	**Alpine**	**Alpine**	**Alpine**
Sample	**PIA44**	**PIA44**	**PIA109**	**PIA109**	**PIA120**	**PIA120**	**G11**	**G11**	**GEI9**	**GEI9**	**GEI4**	**GEI4**
Pol.	**Lz**	**Lz**	**Ctl**	**Ctl**	**Lz**	**Lz**	**Atg**	**Atg**	**Atg**	**Atg**	**Atg**	**Atg**
Texture	Bastite	Bastite	Vein	Vein	Mesh	Mesh	Metam	Metam	Metam	Metam	Metam	Metam
Repl.	En	En	-	-	Fo	Fo	-	-	-	-	-	-
SiO_2	42.7	41.6	41.6	40.8	40.1	40.3	42.3	42.8	42.9	42.8	42.0	42.6
TiO_2	0.01	b.d.	b.d.	0.03	b.d.	0.04	0.04	0.03	0.04	0.03	0.03	0.01
Cr_2O_3	0.85	0.51	0.05	0.03	0.02	b.d.	0.58	0.06	0.31	0.34	0.47	0.10
Al_2O_3	1.68	1.36	0.87	1.79	0.13	0.33	2.97	2.41	3.39	4.19	3.23	2.35
FeO	4.51	7.00	7.50	6.50	5.50	6.12	4.19	4.44	3.93	4.11	4.78	4.75
MnO	b.d.	0.30	0.05	0.13	0.11	0.07	0.05	0.03	0.06	0.08	0.05	0.03
NiO	0.08	0.10	0.00	0.00	0.31	0.27	0.20	0.19	0.13	0.18	0.12	0.15
MgO	37.1	35.1	36.9	37.1	39.5	38.8	37.3	37.0	36.8	36.3	36.8	37.3
CaO	0.17	0.75	0.06	0.20	0.19	0.03	0.02	b.d.	0.21	0.01	b.d.	0.01
Na_2O	0.07	0.03	0.01	b.d.	0.12	0.03	0.01	0.01	0.02	b.d.	0.01	0.01
K_2O	0.01	0.02	0.01	b.d.	b.d.	b.d.	b.d.	b.d.	b.d.	b.d.	0.01	0.02
H_2O	12.6	12.5	12.5	12.4	12.4	12.4	12.8	12.8	12.9	13.0	12.8	12.8
Total	99.7	99.2	99.4	99.0	98.4	98.4	100.5	99.7	100.7	101.0	100.4	100.1
Stoich.	9 O	9 O	9 O	9 O	9 O	9 O	9 O	9 O	9 O	9 O	9 O	9 O
Si	2.008	2.001	1.992	1.957	1.941	1.952	1.976	2.010	1.993	1.982	1.969	2.000
Ti	0.001	b.d.	b.d.	0.001	b.d.	0.001	0.001	0.001	0.001	0.001	0.001	0.000
Cr	0.031	0.019	0.002	0.001	0.001	b.d.	0.021	0.002	0.011	0.013	0.017	0.004
Al	0.093	0.077	0.049	0.101	0.007	0.019	0.163	0.133	0.185	0.229	0.178	0.130
Fe^{2+}	0.178	0.281	0.301	0.261	0.223	0.248	0.164	0.174	0.153	0.159	0.187	0.186
Mn	b.d.	0.012	0.002	0.005	0.005	0.003	0.002	0.001	0.002	0.003	0.002	0.001
Ni	0.003	0.004	0.000	0.000	0.012	0.011	0.008	0.007	0.005	0.007	0.005	0.006
Mg	2.603	2.516	2.634	2.654	2.851	2.800	2.594	2.591	2.544	2.503	2.572	2.605
Ca	0.009	0.039	0.003	0.010	0.010	0.002	0.001	b.d.	0.011	0.000	b.d.	0.000
Na	0.006	0.003	0.001	b.d.	0.011	0.003	0.001	0.001	0.002	b.d.	0.001	0.001
K	0.000	0.001	0.001	b.d.	b.d.	b.d.	b.d.	b.d.	b.d.	b.d.	0.001	0.001
H	3.949	3.995	3.983	3.970	4.000	4.000	4.000	3.999	4.000	3.997	4.000	4.000
Total	4.932	4.953	4.984	4.991	5.061	5.038	4.931	4.922	4.908	4.897	4.933	4.934
Mg#	0.936	0.899	0.898	0.911	0.928	0.919	0.941	0.937	0.943	0.940	0.932	0.933

Mg# calculated as Mg / (Mg + Fe^{2+}), all Fe considered as Fe^{2+}. b.d. = below detection limit. Pol.: polymorph type, Repl.: mineral replaced, Stoich.: stoichiometry.

Figure 5.4. In all type of samples, lizardite from bastite after orthopyroxene is enriched in Cr_2O_3 (up to 0.98 wt. %) and shows lower Mg# (Mg / Mg + Fe^{2+}) compared to chrysotile from all type of veins or lizardite from the mesh texture after olivine (Fig. 5.4a). Lizardite from bastite is enriched in Al_2O_3 (0.5-2.9 wt. %) compared to lizardite from the mesh texture, and shows high Mg# with values between 0.93 and 0.96 (Fig. 5.4a-b). Compared to lizardite or chrysotile from oceanic or ophiolitic serpentinites, antigorite from alpine serpentinites is usually enriched in Al_2O_3, with values up to 4.19 wt. % (Fig. 5.4b), and shows high Mg# between 0.92 and 0.95 (Fig. 5.4a-b). From these observations, we conclude that the chemical variability in serpentine from oceanic and ophiolitic serpentinites is controlled by the pre-serpentinization mineral (Fig. 5.4a-b), rather than by the type of serpentine polymorph (Fig. 5.4a-b).

Li and B content of serpentine

Li contents measured in oceanic and ophiolitic serpentine range between 0.003 and 10 μg/g, and between 0.002 and 0.8 μg/g, respectively (Fig. 5.5a, Table 5.3). In some samples, the variability represents up to three order of magnitude (Fig. 5.5a). In oceanic and ophiolitic samples, the Li contents between 3.2 and 31.8 μg/g were measured in bastite (Table 5.3), where mixtures of lizardite + talc, lizardite + tremolite or lizardite + enstatite were determined by micro-Raman. Li content in alpine antigorite varies between < 0.1 and 3.8 μg/g (Table 5.3). B contents of oceanic serpentine range between 0.1 and 16 μg/g (Fig. 5.5b, Table 5.3), while contents in ophiolitic serpentine range between 0.05 and 30 μg/g (Fig. 5.5b). Alpine serpentine shows values between 1 and 30 μg/g (Fig. 5.5b).

In conclusion, there is a large variability in the Li content of serpentine at the sample scale in all rock types (Fig. 5.5a). The variability is less pronounced in ophiolitic and alpine serpentinites, than in oceanic serpentinites, but can still represent two orders of magnitude (Fig. 5.5a). Moreover, Li contents in oceanic and ophiolitic serpentine below ~ 1.1 μg/g can be considered as "real" values, while higher concentrations can be attributed to mixture of phases. The variability of the B content in serpentine is smaller than the one observed for Li, and generally represents one to two orders of magnitude in a single sample (Fig. 5.5b).

As shown in Figure 5.6, no correlation exists between the type of serpentine polymorph (lizardite, chrysotile or antigorite) and the Li and B content of serpentine. The results obtained by SIMS represent multi-grain analysis of one single polymorph type, respectively, except for some bastite where lizardite can be mixed with talc, enstatite or tremolite (Table 5.3, Fig. 5.3e and i). In these cases, higher Li contents (> 1.1 μg/g) are observed (Table 5.3, Fig. 5.5a and 5.6b).

The variation in light element contents of pure serpentine is in cases related to the texture, and consequently to the precursor mineral, as for example at the ODP Leg 209 site 1272A (Fig. 5.6a). In these samples, lizardite in bastite and in the matrix is generally enriched in B compared to lizardite formed in mesh texture after olivine or to chrysotile crystallized in fibrous veins (Fig. 5.6a). The highest Li contents were usually measured in lizardite from bastite (Fig. 5.6a). The fact that Li content is highest in lizardite from bastite, is easily explainable by the fact that lizardite replaced talc, which was rich in Li (Pelletier et al., submitted b). Moreover, talc replaced orthopyroxene, which is rich in Li in serpentinized oceanic peridotites (Pelletier et al., submitted b; Vils et al., in prep.). In site 1272A there is a positive correlation between the Li and B content of lizardite from mesh texture after olivine (Fig. 5.6a). However, all these observations are not valid for the samples from site 1274A (Fig. 5.6b) or for ophiolitic serpentine (Fig. 5.6c). In site 1274A, the highest Li contents were measured in bastite. This is due to a mix of lizardite and enstatite, as was observed by micro-Raman spectroscopy (Fig. 5.4e and f). The major difference between the two ODP sites is the degree of serpentinization (Bach et al., 2004). The highest degree of serpentinization is found in samples from site 1272A, where the correlation between light element content and texture can be observed.

In the next paragraphs, cations exchange on cristallographic sites are tested. For this purpose, high quality major element analyses of serpentine were selected. As the ionic radius of Li^+ is 76 pm in 6-fold coordination (Shannon, 1976), Li^+ can substitute for octahedrally coordinated Mg^{2+} and Fe^{2+} (72 and 78 pm) in serpentine. There is a negative correlation between the Li^+ and the Mg^{2+} + Fe^{2+} contents in the ophiolitic and alpine serpentine (Fig. 5.7a). The latter result shows that in this case, the Li variability present in serpentine is

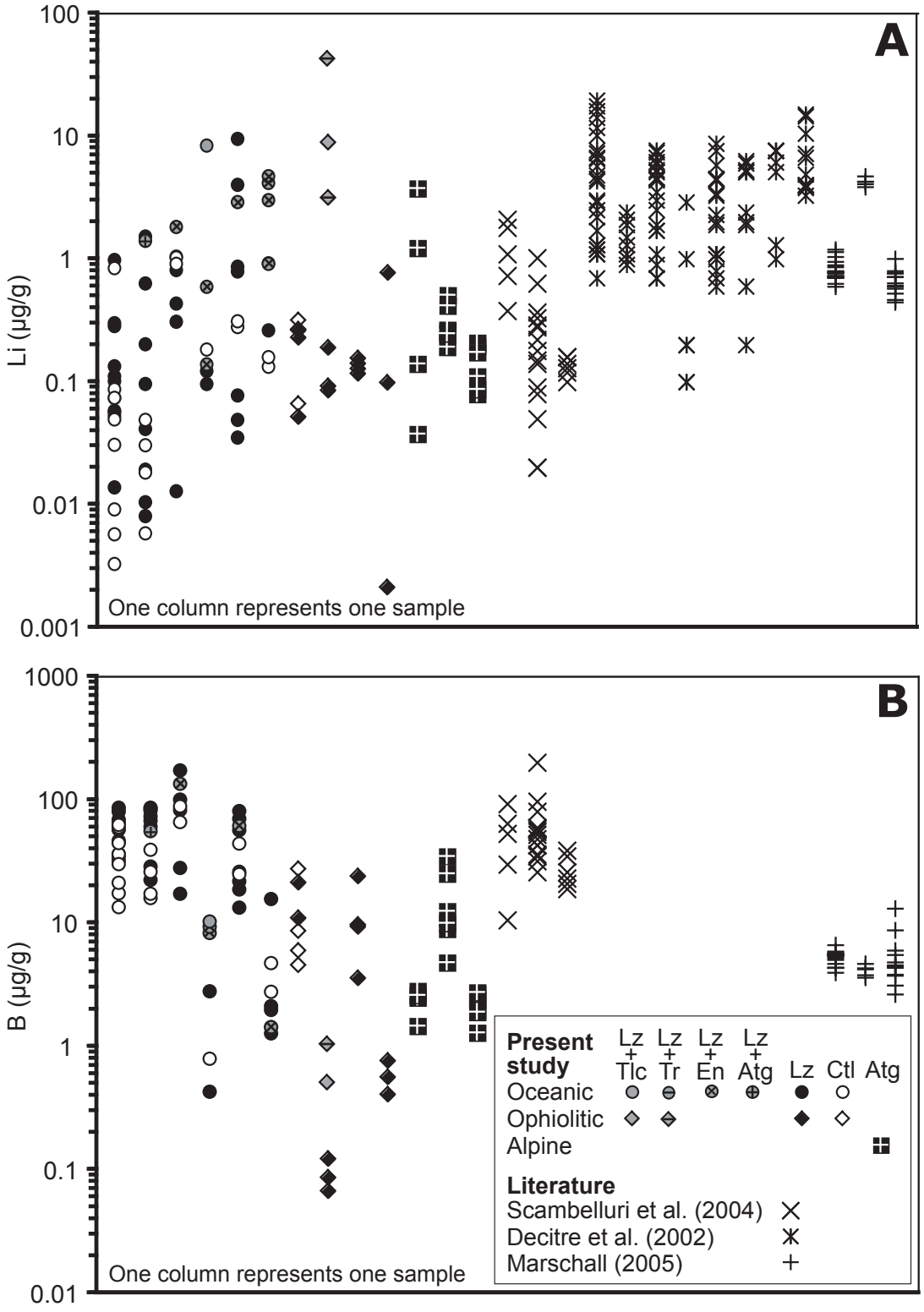


Fig. 5.5: Li (μg/g) and B (μg/g) contents of the different serpentine polymorphs and phase mixtures in the different thin sections. Oceanic serpentinites data from ODP Leg 209 sites 1272A and 1274A after Vils et al. (in prep.), ophiolitic serpentinites data from the Pindos ophiolite after Pelletier et al. (submitted b) and Alpine serpentinites data from the Geisspfad ultramafic body after Pelletier et al. (submitted a). Mineral abbreviations according to Kretz (1983).

Table 5.3: Li and B contents in serpentine (representative analyses)

Locality	Sample	Texture	Pol.	Repl.	Li (µg/g)	2σ	B (µg/g)	2σ
OCEANIC	OD2	Mesh	Lz	Fo	0.06	0.01	65.1	0.6
ODP Leg 209		Mesh	Lz	Fo	0.10	0.01	47.7	0.7
Site 1272A		Mesh	Lz	Fo	0.014	0.004	33.2	0.5
Vils et al.		Mesh	Ctl	Fo	0.009	0.003	64.1	0.7
(in prep.)		Mesh	Ctl	Fo	0.07	0.01	61.5	0.9
		Mesh	Lz + Ctl	Fo	0.03	0.01	37.1	0.5
		Bastite	Lz	En	0.28	0.02	83	2
		Bastite	Lz	En	0.05	0.01	36.0	0.5
		Bastite	Lz	En	1.0	0.1	89	1
		Vein	Lz		0.06	0.01	70.8	0.3
		Vein	Ctl		0.83	0.03	46	2
		Vein	Ctl		0.07	0.01	13.8	0.3
		Vein	Ctl		0.003	0.002	37.2	0.5
	OD18	Mesh	Lz	Fo	0.008	0.004	29.5	0.3
		Mesh	Lz	Fo	0.02	0.01	62.0	0.7
		Mesh	Lz	Fo	0.018	0.005	40.5	0.3
		Mesh	Ctl	Fo	0.006	0.002	26.6	0.2
		Bastite	Lz	Di	0.20	0.02	75.1	0.5
		Bastite	Lz	Di	0.09	0.01	82	3
		Bastite	Lz	Di	0.05	0.01	64.4	0.6
		Bastite	Lz	En	0.04	0.01	69.5	0.6
		Bastite	Lz	En	0.62	0.03	89	2
		Bastite	Lz	En	0.03	0.01	26.4	0.3
		Bastite	Lz	En	1.50	0.1	84	1
		Vein	Ctl		0.05	0.01	17.7	0.3
		Vein	Ctl		0.03	0.01	16.3	0.2
	OD28	Mesh	Lz	Fo	0.43	0.02	178	3
		Mesh	Lz	Fo	0.80	0.03	85	3
		Mesh	Lz	Fo	1.03	0.04	103.5	0.7
		Bastite	Lz	En	0.30	0.09	17.8	0.5
		Vein	Ctl		1.01	0.04	67	48
		Vein	Ctl		0.90	0.04	91	47
		Vein	Ctl		0.64	0.03	65	67
OCEANIC	OD32	Mesh	Lz	Fo	0.12	0.01	2.9	0.6
ODP Leg 209		Mesh	Lz	Fo	0.09	0.01	0.4	0.1
Site 1274A		Bastite	Lz (+ En)	En	0.14	0.01	8.5	0.4
Vils et al.		Bastite	Lz (+ En)	En	0.59	0.02	9.5	0.3
(in prep.)		Bastite	Lz (+ Tlc)	Di	54.4	0.4	3.5	0.6
		Bastite	Lz (+ Tlc)	Di	8.2	0.5	10.5	0.7
		Vein	Ctl		0.18	0.01	0.81	0.02
		Vein	Ctl		0.37	0.03	15.5	0.2

Pol.: polymorph type, Repl.: mineral replaced.

Table 5.3: continued

Locality	Sample	Texture	Pol.	Repl.	Li (µg/g)	2σ	B (µg/g)	2σ
OCEANIC	OD34	Mesh	Lz	Fo	0.78	0.03	83	1
ODP Leg 209		Mesh	Lz	Fo	0.08	0.01	13.6	0.3
Site 1274A		Mesh	Lz	Fo	0.05	0.01	22.4	0.4
Vils et al.		Mesh	Lz + Ctl	Fo	0.85	0.02	71.9	0.5
(in prep.)		Bastite	Lz (+ En)	En	4.0	0.1	26.6	0.3
		Bastite	Lz (+ En)	En	2.86	0.07	63.0	0.4
		Bastite	Lz (+ En)	En	9.4	0.2	58.1	0.8
		Vein	Ctl		0.27	0.02	25.6	0.3
		Vein	Ctl		0.29	0.02	20.1	0.4
		Vein	Ctl		0.31	0.02	45.2	0.6
	OD42	Mesh	Lz	Fo	0.26	0.01	1.5	0.2
		Mesh	Lz	Fo	0.91	0.03	1.3	0.3
		Bastite	Lz (+ En)	En	2.98	0.09	2.2	0.2
		Bastite	Lz (+ En)	En	4.1	0.6	16	1
		Bastite	Lz (+ En)	En	0.90	0.02	1.5	0.1
		Bastite	Lz (+ En)	En	4.6	0.1	2.0	0.2
		Vein	Ctl		0.11	0.01	4.0	0.1
		Vein	Ctl		0.13	0.02	2.82	0.06
		Vein	Lz		0.16	0.02	4.8	0.3
OPHIOLITIC	PIA27	Mesh	Lz	Fo	0.05	0.01	22	1
Pindos		Mesh	Lz	Fo	0.27	0.02	11.0	0.1
Pelletier et al.		Mesh	Ctl	Fo	0.07	0.01	27.6	0.8
(submitted b)		Bastite	Ctl	En	0.27	0.01	6.0	0.8
		Bastite	Ctl	En	0.32	0.03	4.6	0.4
		Bastite	Ctl	En	0.23	0.01	9	1
	PIA44	Mesh	Lz	Fo	0.09	0.01	0.12	0.04
		Mesh	Lz	Fo	0.19	0.02	0.07	0.02
		Mesh	Lz	Fo	0.09	0.01	0.09	0.04
		Bastite	Lz (+ Tlc)	En	11.2	0.3	1.9	0.3
		Bastite	Lz (+ Tlc)	En	9.0	0.2	0.53	0.03
		Bastite	Lz (+ Tr)	Di	31.8	0.3	0.9	0.4
		Bastite	Lz (+ Tr)	Di	3.2	0.1	0.99	0.09
	PIA120	Mesh	Lz	Fo	0.78	0.03	0.41	0.03
		Mesh	Lz	Fo	0.010	0.003	0.57	0.03
		Mesh	Lz	Fo	0.002	0.002	0.77	0.07
	PIA109	Vein	Lz		0.14	0.01	9	2
		Vein	Lz		0.12	0.01	4	1
		Vein	Lz		0.16	0.01	24	5
ALPINE	GEI4	Metam	Atg		3.80	0.05	2.9	0.1
Geisspfad		Metam	Atg		1.24	0.04	1.48	0.07
Pelletier et al.		Metam	Atg		0.04	0.02	2.52	0.08
(submitted a)	G11	Metam	Atg		0.08	0.01	2.0	0.1
		Metam	Atg		0.21	0.01	2.43	0.07
		Metam	Atg		0.18	0.02	2.78	0.08
	GEI9	Metam	Atg		0.27	0.02	35.3	0.9
		Metam	Atg		0.19	0.02	12.7	0.2
		Metam	Atg		0.51	0.02	25	1
		Metam	Atg		0.42	0.02	4.8	0.1

Pol.: polymorph type, Repl.: mineral replaced.

probably intracrystalline, and that Li^{+} preferentially replaces Mg^{2+} or Fe^{2+}. This observation can not be made in oceanic serpentine. During serpentine normalization, all Fe was assumed to be Fe^{2+}. However, Fe^{3+} could be present in these serpentine, which could potentially change the trends in Figure 5.7a. Moreover, the variation in Mg^{2+} and Fe^{2+} content of serpentine from the different textural sites (Fig. 5.4a-b, Table 5.2) in oceanic serpentine could also play a role in the plot.

In minerals, B^{3+} can be trigonally or tetrahedrally coordinated to oxygen (Hawthorne et al., 1996). In serpentine, B^{3+} should substitute for Si^{4+} or Al^{3+} on the tetrahedral site, as shown for the manandonite, an Al-, Li- and B-rich analogue of amesite (kaolinite-serpentine group) by Zheng & Bailey (1995). However, the presence of B^{3+} in the tetrahedral site generates a distortion of the TO_4 units (Zheng & Bailey, 1995), as B^{3+} has a very small ionic radius in this coordination state (11 pm). There is a negative correlation between the Si^{4+} and the B^{3+} content in alpine serpentine. In this case we can consider that the B variability in alpine serpentine is intracrystalline and that B^{3+} preferentially replace Si^{4+} on the tetrahedral site. This is in agreement with the fact that in alpine

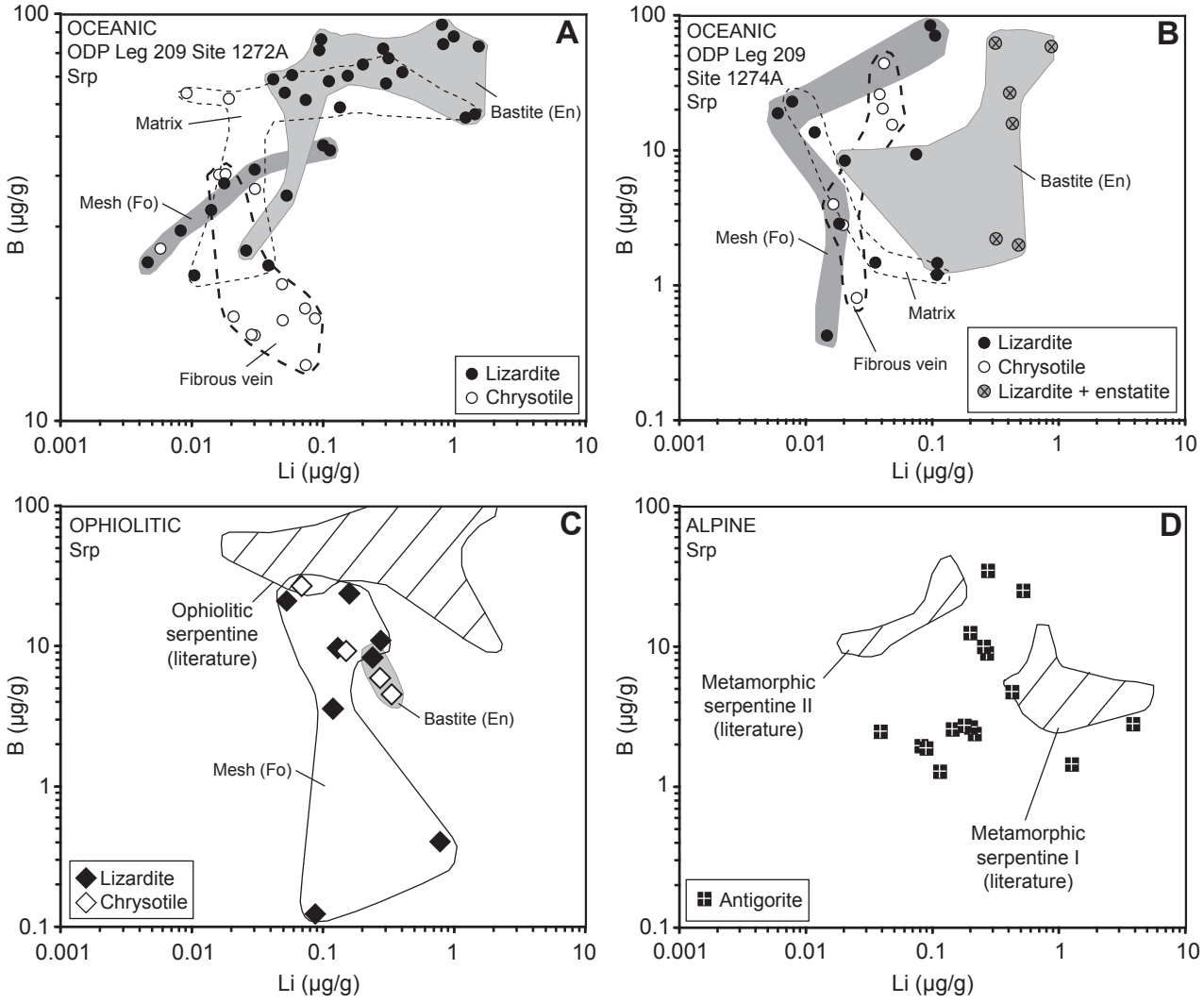


Fig. 5.6: Li (μg/g) and B (μg/g) content in oceanic serpentine (a-b), ophiolitic serpentine (c) and alpine serpentine (d) as a function of the polymorph type. Textural site information is illustrated by the different fields. Oceanic data after Vils et al. (in prep.), ophiolitic data after Pelletier et al. (submitted b) and alpine data after Pelletier et al. (submitted a). Literature data: ophiolitic serpentine after Scambelluri et al. (2004) and metamorphic serpentine (high pressure) after Scambelluri et al. (2004) and Marschall (2005).

serpentinites, serpentine minerals are larger than the spot size. A positive correlation between Si^{4+} and B^{3+} is visible in ophiolitic serpentine, and no correlation can be seen in oceanic serpentine. We can deduce that in ophiolitic or oceanic serpentine, part of the B is probably intercrystalline. However, as Si content in serpentine is variable, as shown by the heterogeneity of the microprobe analyses (small spot size), the Si content plotted in the diagram (Fig. 5.7b) is probably not representative of the bulk Si measured during SIMS analysis (large spot size).

In conclusion, we can consider that Li variability in alpine and ophiolitic serpentine is intracrystalline, while no information can be extracted for oceanic serpentine. The B variability in alpine serpentine is intracrystalline, while in oceanic and ophiolitic serpentine it should be intercrystalline.

Grain boundary effect

There is a good correlation between the analyzed and measured Li and B contents from the alpine serpentinites (Fig. 5.8a-b). In these samples, the grain size exceeds the SIMS spot size, including antigorite. This bulk rock correlation shows that no Li or B is present along grain boundaries in these samples. This is in agreement with the intracrystalline Li and B variability in alpine antigorite mentioned above (Fig. 5.5a-b). This variability can reach a maximum of two orders of magnitude for Li and one order of magnitude for B.

For ophiolitic serpentinites, there is a good correlation between the calculated and measured Li whole rock contents (Fig. 5.8a-b), in fresh rock (PIA109) and in moderately serpentinized samples (PIA44, PIA120). This is in agreement with the negative correlation between Li and Mg^{2+} + Fe^{2+} in ophiolitic serpentine, which shows that Li variability in this case is intracrystalline.

For B, there is a good correlation for ophiolitic and oceanic serpentinites, except for sample PIA109 (calculated: 1.0 μg/g, measured: 0.1 μg/g). This difference is probably due to calculation, because only three B contents were available in this low serpentinized sample, and range between 4 and 24 μg/g (Table 5.3). The B correlation of the other ophiolitic and oceanic serpentinites shows that the analyzed serpentine volume by SIMS was representative of the bulk serpentinites, because serpentine is the major B-bearing phase in ophiolitic and oceanic serpentinites (B concentration in primary phases is very low; Pelletier et al., submitted b and Vils et al., in prep.). However, this does not give any information on the presence of B at grain boundaries.

Sauerer et al. (1989) showed that in dioritic to granitic rocks, major quantity of B can be present at grain boundaries, and is related to alteration. This is in agreement with the postulated intercrystalline presence of B in ophiolitic and oceanic serpentinites mentioned above (see "Li and B content in serpentine"). The serpentine formed after plagioclase during alteration of the felsic rocks, is more concentrated in B than the grain boundary component (Sauerer et al., 1989). They also produced an image of the in-situ B distribution of a serpentine matrix in a siliceous dolomite marble, which shows that B content of the matrix is highly variable and heterogeneous at the micrometer scale, which is in agreement with our observations (Fig. 5.5b). However, these images do not say if the variability is intercrystalline or intracrystalline, because the resolution of the image is not high enough.

SUMMARY

In conclusion, SIMS analyses were obtained on single polymorph type, lizardite or chrysotile or antigorite, in all type of serpentinites. In bastites only (serpentine formed after orthopyroxene), lizardite can be intergrown with talc or tremolite or enstatite in some oceanic and ophiolitic serpentinites. No relation exists between the type of serpentine polymorph (lizardite, chrysotile or antigorite) and the measured Li and B contents. Li contents above ~ 1.1 μg/g are attributed to a mix of lizardite with talc or tremolite or enstatite, in ophiolitic and oceanic bastites. In some oceanic samples (ODP Leg 209 site 1272A), the Li and B content is related to the pre-serpentinization mineral. This is not the case in other serpentinites, ophiolitic or oceanic.

Study on antigorite from alpine serpentinites, shows that its Li and B variability is intracrystalline, and that Li preferentially replaces Mg and Fe^{2+} on the octahedral site, and B preferentially replaces Si on the tetrahedral site.

Li variability in ophiolitic serpentine is probably intracrystalline, while B variability is probably

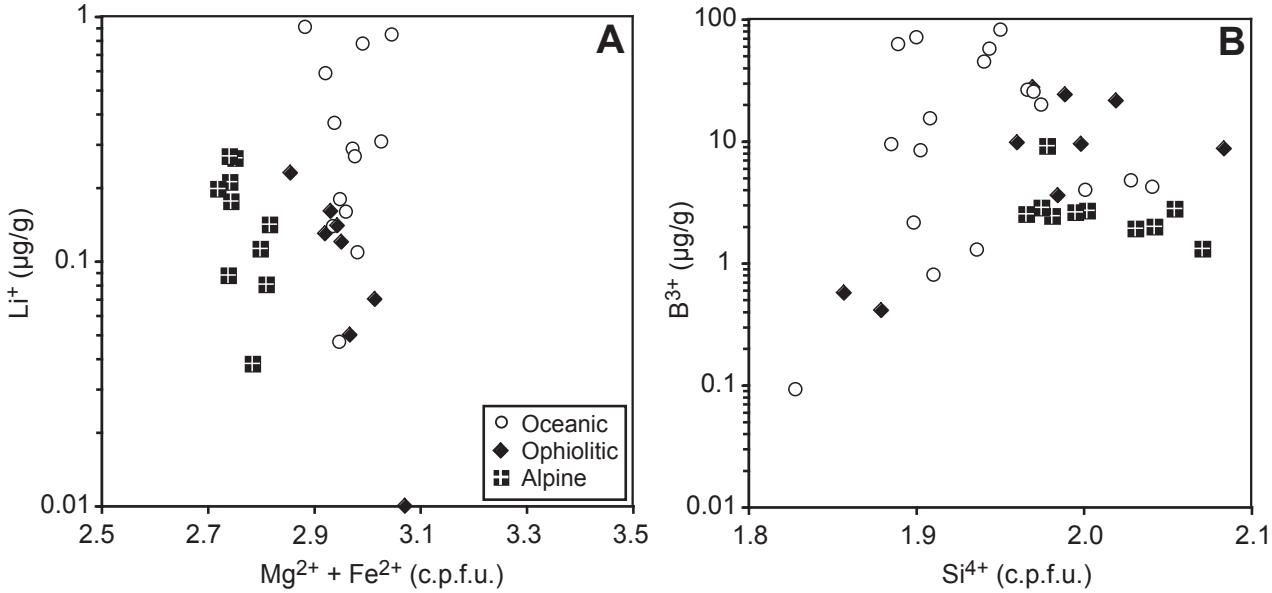


Fig. 5.7: Cation substitutions in the serpentine structure: (a) Mg^{2+} + Fe^{2+} vs. Li^{+} (μg/g) potentially represents substitution on the octahedral site, (b) Si^{4+} vs. B^{3+} (μg/g) potentially represents substitution on the tetrahedral site.

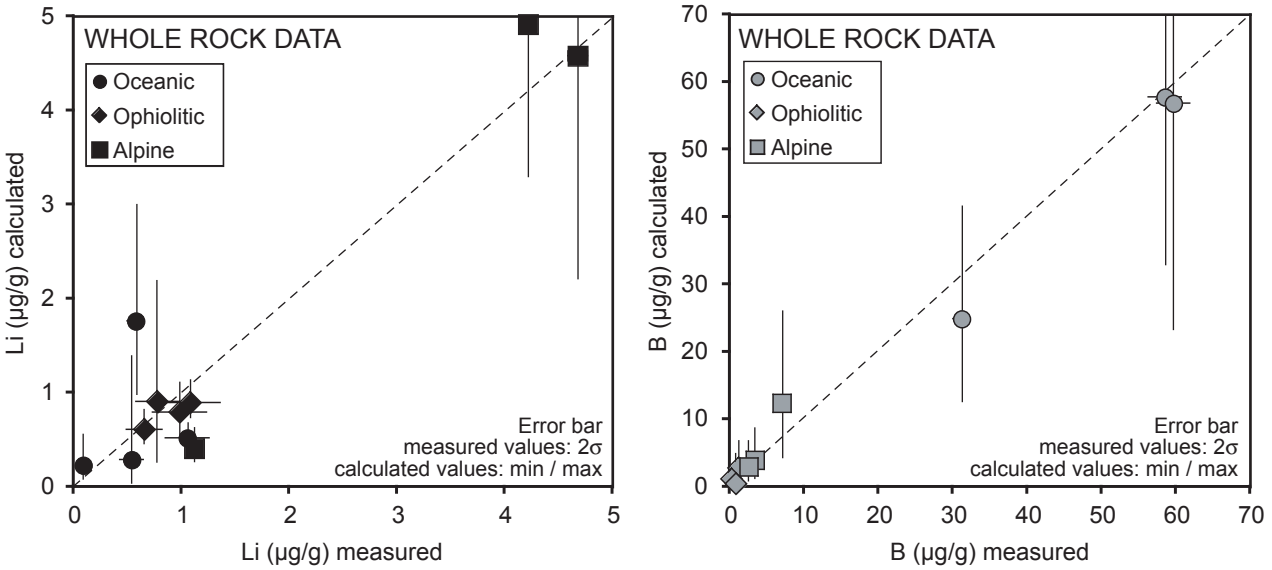


Fig. 5.8: Correlation between the Li (a) and B (b) (μg/g) whole rock contents measured and calculated. Li was measured by Inductively Coupled Plasma - Mass Spectrometry (ICP-MS) and B by Prompt Gamma Neutron Activation Analysis (PGNAA) (Pelletier et al., submitted a and b; Vils et al., in prep.).

intercrystalline and related to grain boundary components. Li and B variability in oceanic serpentine seems to be intercrystalline.

Chapter 6

Summary, conclusions and outlook

SUMMARY AND CONCLUSIONS

The results from the previous chapters lead to the identification of the main parameters and processes which potentially control the Li, Be and B contents in fresh and serpentinized oceanic peridotites, which are: (i) Li enrichment related to clinopyroxene crystallization during N-MORB type melt percolation. (ii) No Li, Be or B enrichment in harzburgite during ultra-depleted melt percolation and impregnation. (iii) Variable B enrichment during serpentinization, depending on the serpentinization parameters (temperature, pH, water/rock ratio). (iv) Modification of the Li, Be and B budget of the oceanic mantle related to retrograde fluid metasomatism during emplacement into the continental crust.

Additionally, the study of the Dramala harzburgites (Pindos ophiolite, Greece) contributes to the discussion on supra-subduction ophiolites. It clearly demonstrates that spoon-shaped rare earth element patterns observed in peridotites and their clinopyroxenes included in supra-subduction zone type ophiolites, does not necessarily imply an interaction of these peridotites with subduction-related fluids. All the trace element signatures observed in such peridotites, can be explained by mid-ocean ridge-type melt-related metasomatism.

Li, Be and B whole rock contents in oceanic peridotites from the different tectonic settings observed on Earth are presented in Figure 6.1.

Light elements in fresh oceanic peridotites and Li enrichment during melt-related metasomatism

The Li, Be and B content of minerals and whole rock samples from oceanic peridotites result from a complex history of depletion related to partial melting, followed by melt percolation and melt impregnation. Fresh harzburgites from the Dramala mantle of the Pindos ophiolite (Greece) show contents of approximately 0.9-1.1 μg/g for Li, < 0.003 μg/g for Be, and < 0.3 μg/g for B. During N-MORB percolation in these rocks, the crystallization of some clinopyroxene cumulate led to a Li enrichment in the rock. The use of a melt percolation model showed that N-MORB percolation through a depleted harzburgite cannot induce the Li content observed in these rocks. On the contrary, Be and B enrichment can occur during this percolation but their whole rock contents stay very low. Late ultra-depleted melt impregnation observed in some Dramala plagioclase-bearing harzburgite does not change Li, Be and B content of the latter, as the light element content in this type of melt is probably very low, and the melt seems to be in equilibrium with the depleted harzburgites.

B enrichment during serpentinization of oceanic peridotites

During serpentinization, there is a B enrichment in whole rock samples, while no Li or Be enrichment is observed. The primary mantle phases (olivine, clinopyroxene, orthopyroxene) conserve their original Li, Be and B contents during this process. The major B carrier phase is serpentine, and the B concentration in serpentine and serpentinites probably depends on temperature, pH and water/rock ratio during serpentinization. This is shown by the very different B contents in serpentine and serpentinites from the Dramala serpentinized harzburgites (Pindos ophiolite, Greece) compared to serpentinites from the Mid-Atlantic ridge ODP Leg 209. Pindos samples show low B whole rock content in highly serpentinized harzburgites (up to

1.1 μg/g) and highly heterogeneous B content in serpentine (0.1-28 μg/g), which probably reflect serpentinization occurring at high temperature and low water/rock ratio. In contrast, serpentinization in samples from the Mid-Atlantic ridge led to high B content in serpentine (up to 200 μg/g) and serpentinites (10-65 μg/g), which could be related to low temperature (Seyfried and Dibble, 1980; Bonatti et al., 1984) and high water/rock ratio.

Li and B contents in serpentine are heterogeneous at the micrometer scale in the Dramala and ODP Leg 209 samples, even if single polymorph types (antigorite, lizardite or chrysotile) were analyzed by SIMS (spot size ~ 15 μm). In serpentine, the highest Li contents (> 1.1 μg/g) are due to a mix of serpentine with other phases, like tremolite, talc or enstatite. It is not clear, if the observed Li and B variability is due to an intra- or intercrystalline factor.

Li, Be and B systematics during emplacement of oceanic peridotites into the continental crust

The study on the Geisspfad serpentinites showed that Li, Be and B contents in oceanic serpentinites are modified during emplacement into the continental crust, by some retrograde fluid flows. These fluids probably originate in the continental crust and have high Li, Be and B contents compared to the hydrothermally altered oceanic mantle metamorphosed under amphibolite facies conditions (which corresponds to the Geisspfad ultramafic body). The effect of fluid metasomatism is expressed by the Li, Be and B contents in minerals and whole rock samples, and by Li, Be and B partition coefficients between the different minerals. Two successive retrograde fluid flows were identified. The first fluid penetrated the ultramafics on about 400 meters, which induced the enrichment of the Geisspfad serpentinites in Li, Be and B. The second fluid travelled along the contact between the ultramafics and the crustal rocks, which led to a Li leaching in the Geisspfad serpentinites.

This result shows that studies on (ultra) high pressure orogenic peridotites conducted to constrain the Li, Be and B budget and systematics of subducted oceanic lithosphere should be treated with caution. As all of these rocks were emplaced into continental crust, their light element

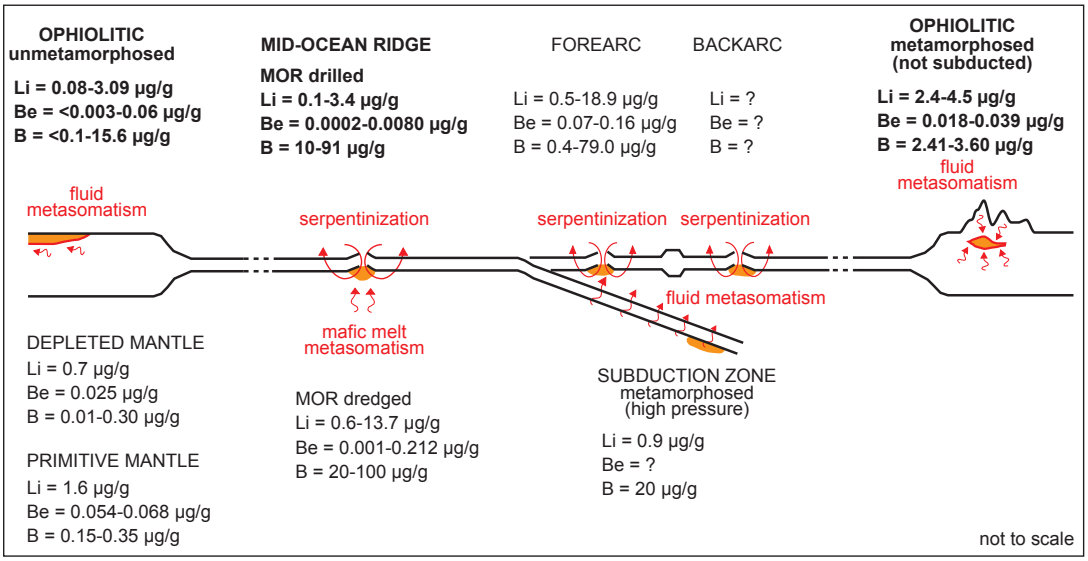


Fig. 6.1: Occurrences of serpentinized oceanic mantle and its Li, Be and B content. The contribution of the present thesis is presented in bold. Literature data: Thompson and Melson (1970), Bonatti et al. (1984), Spivack and Edmond (1987), Chaussidon and Libourel (1993), Chaussidon and Jambon (1994), Chaussidon and Marty (1995), McDonough and Sun (1995), Parkinson and Pearce (1998), Benton et al. (2001, 2004), Decitre et al. (2002), Brooker et al. (2004), Niu (2004), Ottolini et al. (2004), Paquin et al. (2004), Salters and Stracke (2004), Scambelluri et al. (2004, 2006), Savov et al. (2005), Wei et al. (2005), Li and Lee (2006), Marchesi et al. (2006), Zanetti et al. (2006), Agranier et al. (2007), Lyubetskaya and Korenaga (2007), Boschi et al. (2008), Pelletier et al. (submitted a, b, c), Vils et al. (in prep.).

systematics and budget were probably modified, and only large ultramafic bodies (about 1 km width) can potentially maintain the subduction-related light element systematics in the core.

Contribution to the discussion on supra-subduction zone ophiolites

The Dramala harzburgites (Pindos ophiolite, Greece) result from a complex history of depletion and melt percolation and/or impregnation. The modelization of N-MORB type melt percolation through a depleted harzburgite showed that the famous rare earth element (REE) spoon-shaped pattern (usually interpreted as due to subduction-related hydrous melting; Bizimis et al., 2000) can be due to a chromatographic effect during N-MORB percolation, which led to the fractionation of the different REEs. This chromatographic effect had already been modelized in some peridotites from the Oman ophiolite for all the REEs (Godard et al., 2000), but the study on the Dramala mantle brings new informations on the light elements behaviour during this process. During N-MORB percolation through the depleted Dramala harzburgites, there is no Li increase in these rocks, while Be and B whole rock contents can increase. However, Be and B contents of these harzburgites stay very low, due to the extreme depletion of the rock before melt percolation (up to 22% partial melting).

It shows that oceanic mantle with mid-ocean ridge type characteristics can be assembled with subduction-related volcanics in supra-subduction zone ophiolites. It also demonstrates that spoon-shaped REE patterns observed in peridotites from supra-subduction zone type ophiolites should not necessarily be related to hydrous-melting in a mantle wedge.

OUTLOOK

An important issue will be to calculate the Li, Be and B budget of the hydrothermally altered oceanic mantle, in order to define its light element input in subduction zones. Moreover, a study on Li and B isotopes could help in defining the contribution of the serpentinized mantle to the fluids present in arc magma sources, which are related to dehydration reactions in the subducting slab. These results should be compared to those obtained on the oceanic crust. These two topics are the subject of the companion thesis of Flurin Vils, which will be presented in 2008.

More experimental work should be done on serpentinization, in order to understand the parameters controlling the B content in serpentine and serpentinites, such as temperature, pH, water/rock ratio or silica activity. Experimental work should also be done to test Li and B isotopes fractionation during serpentinites dehydration in subduction zones under increasing pressure and temperature.

Li and B heterogeneity in serpentine should also be studied, in order to determine if Li and B variability measured in serpentine by secondary ion mass spectrometry (SIMS) is intra- or intercrystalline. However, no known analytical technique seems suitable to solve this question due to the extremely small grain size of the serpentine matrix.

In order to complete our knowledge on the Earth's Li, Be and B cycle, a study on some backarc oceanic peridotites (e.g. Mariana Trough) should be done. Moreover, as the Dramala harzburgites could have been formed in a similar setting, it could bring new informations on supra-subduction zone ophiolites. This study should include a quantification of Li, Be, B and other trace elements in minerals and whole rock samples. It would be important to define if the backarc mantle records any interaction with subduction-related fluids or melts, or only mid-ocean ridge type metasomatism.

Analytical techniques

DETERMINATION OF TEXTURE AND MINERALOGY

Secondary Electron Microscopy

Prior to the quantitative chemical analysis of minerals, texture and mineralogy were determined by secondary electron microscopy (SEM). The backscattered electron images (BSE) were acquired at the Centre Suisse d'Electronique et de Microtechnique (CSEM) in Neuchâtel (Switzerland), with a Philips XL-30 scanning electron microscope, operated at 25 kV.

Micro-Raman Spectroscopy

Micro-Raman spectroscopy was used as a technique complementary to optical microscopy and secondary electron microscopy, for a rapid determination of the different serpentine polymorphs (Rinaudo et al., 2003; Groppo et al., 2006). Micro-Raman spectra were acquired using an integrated micro/macro Raman system Jobin Yvon Mod at the Department of Mineralogical and Petrological Sciences, University of Torino (Italy). The system includes a microspectrometer Horiba Jobin Yvon HR800, an Olympus BX41 microscope and a CCD air-cooled detector. A polarized solid state Nd 80 mW laser operating at 532.11 nm was used as the excitation source. Correct calibration of the instruments was verified by measuring the Stokes and anti-Stokes bands, and checking the position of the Si band at ~ 520.7 cm^{-1}. Each spectrum was acquired using a 50x objective, resulting in a 5 to 10 μm laser beam size on the sample. To optimize the signal to noise ratio, spectra were acquired using 10 scans of 5 to 10 seconds for each spectral region. The spectral region from 1100 to 100 cm^{-1} and from 4000 to 3000 cm^{-1} were considered, because they are characteristic of serpentine minerals. The 4000 to 3000 cm-1 region was studied because the difference in asymmetry between chrysotile and lizardite peaks is pronounced. Spectra were smoothed by an automatic basement line substraction using the Origin 6.0 software. Complete spectra dataset are available in electronic format (enclosed CD-ROM).

IN SITU MINERAL ANALYSES

Electron Microprobe (EM)

Major element compositions of minerals were determined in situ by electron microprobe. Different machines were used: Cameca SX-50 and Jeol JXA-8200 at the Institute of Geological Sciences of the University of Bern (Switzerland), Cameca SX-51 at the Institute of Mineralogy of the Ruprecht-Karls University of Heidelberg (Germany), and Jeol JXA-8200 at the ETH Zürich (Switzerland). These microprobes are equipped with four to five wavelength-dispersive spectrometers. Operating conditions comprise an accelerating voltage of 15 kV and a 20 nA beam current. These conditions were set to 15 kV and 10 nA during carbonate measurement. The spot size was about 3 μm except for hydrous minerals and carbonates where a defocused beam was used (amphiboles, talc: 5 μm, serpentine: 3-15 μm, natrolite: 5-10 μm, calcite and dolomite: 15 μm). For serpentine, different spot sizes from ~ 3 to 15 μm were tested, in order to optimize totals obtained during measurement. However no systematic improvement was observed for a certain spot size. Natural and synthetic oxides and silicates were used as standards. Complete EM data are available in electronic format (enclosed CD-ROM).

Secondary Ion Mass Spectrometry (SIMS)

Li, Be and B compositions were measured in situ in minerals by secondary ion mass spectrometry

(SIMS) with a modified Cameca ims 3f ion microprobe (equipped with a primary beam mass filter) at the Institute of Mineralogy of the Ruprecht-Karls University of Heidelberg (Germany). These analyses were done in collaboration with T. Ludwig. The protocol established by Marschall and Ludwig (2004) was used for sample preparation and measurements to minimise boron surface contamination. Thin sections were prepared using pure glycol as lubricant and cooling liquid for sawing and polishing, because products containing boric acid cannot be used. Carbon coating used later for microprobe analysis was removed using γ-alumina powder (0.05 μm) and distilled water. After this polishing, thin sections were cleaned in an ultrasonic bath using ultra-pure water from a Milli-Q water purification system (Millipore). Three successive ultrasonic cleaning were applied of 5, 10 and10 minutes respectively. After cleaning, thin sections were coated with gold. During analysis, the pre-sputtering technique of Marschall & Ludwig (2004) was used to avoid eventual surface contamination. This method uses a field aperture (12 μm imaged field) in order to avoid the contamination produced at the rim of the crater during ablation of the sample.

SIMS measurements were performed on points previously measured at the electron microprobe. The primary $^{16}O^-$ ion beam was set to 14 – 14.5 keV/ 20 nA. Positive secondary ions were accelerated to 4.5 keV and the energy window was set to 40 eV. The energy filtering technique was applied with an offset of ~ 75 eV at a mass resolution m/Δm (10%) between 1018 to 1080. The surface imaged by the secondary ions was reduced from ~ 30 μm to ~ 12 μm by applying the field aperture (FA2; 750 μm). The instrumental design is illustrated in Fig. 7.1. Quantitative results were obtained using relative sensitivity factors with ^{30}Si as reference isotope (Ottolini et al., 1993) for silicates, and ^{44}Ca for carbonates. One analysis comprises 10 cycles for each element with an integration time of 8 s/cycle for Li, 16 s/cycle for Be and B, and 2 s/cycle for Si or Ca. Detection limits (the critical value; Currie, 1968) were calculated at 1.4, 1.0 and 2.6 ng/g (ppb) for Li, Be and B respectively. These detection limits are valid for all samples, except for PI2, G3, G4 and G27 where the integration time was changed to 4 s/cycle for Li, and 8 s/cycle for Be and B. In this case detection limits are higher with values of 2.0, 1.4 and 3.7 ng/g (ppb) for Li, Be and B respectively.

For carbonates, SRM610 glass was used as a standard and contains about 2 wt. % CaO, which is much lower than CaO content in carbonates. Moreover there is probably a matrix effect between silicates and carbonates, which is unknown. The results presented in this thesis for carbonates are rough values, and these results might be wrong by a factor of two (T. Ludwig personal communication). Complete SIMS data and standard details are available in electronic format (enclosed CD-ROM).

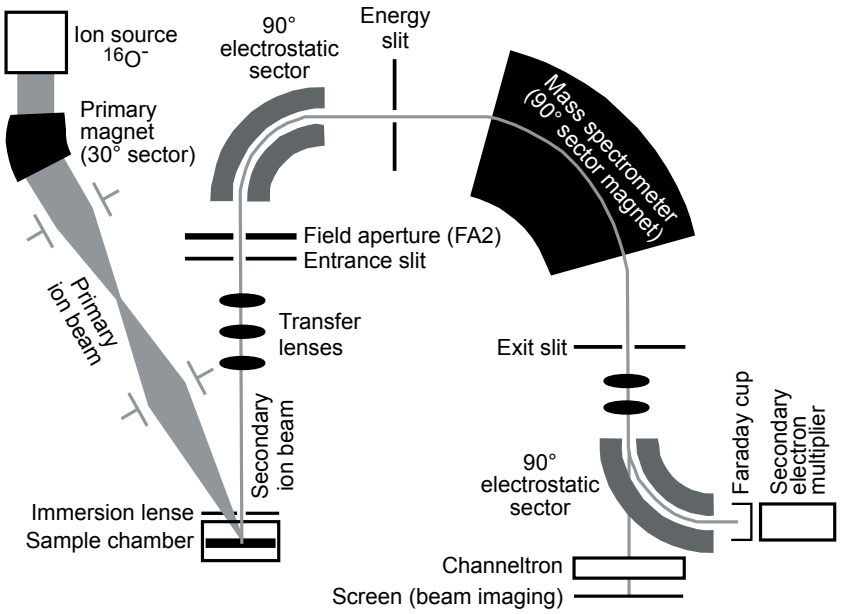


Fig. 7.1: Schematic representation of the SIMS used at the University of Heidelberg (Germany).

Laser Ablation – Inductively Coupled Plasma Mass Spectrometry (LA-ICPMS)

Forty isotopes (^{7}Li, ^{11}B, ^{25}Mg, ^{27}Al, ^{31}P, ^{42}Ca, ^{45}Sc, ^{49}Ti, ^{51}V, ^{59}Co, ^{62}Ni, ^{66}Zn, ^{71}Ga, ^{85}Rb, ^{88}Sr, ^{89}Y, ^{90}Zr, ^{93}Nb, ^{121}Sb, ^{133}Cs, ^{137}Ba, ^{139}La, ^{140}Ce, ^{141}Pr, ^{146}Nd, ^{147}Sm, ^{151}Eu, ^{157}Gd, ^{159}Tb, ^{163}Dy, ^{165}Ho, ^{167}Er, ^{169}Tm, ^{173}Tb, ^{175}Lu, ^{178}Hf, ^{181}Ta, ^{208}Pb, ^{232}Th, ^{238}U) were measured in situ in minerals from the Pindos ophiolite by Laser Ablation – Inductively Coupled Plasma Mass Spectrometry (LA-ICPMS) at the Institute of Geological Sciences of the University of Bern (Switzerland). These analyses were done in collaboration with Prof. T. Pettke. The machine combines a pulsed Geolas Pro 2006 193nm ArF excimer laser system (Lambda Physics, Germany) with an energy homogenized (Microlas, Germany) beam profile (Günther et al., 1997), with an Elan DRC-e quadrupole ICP mass spectrometer (QMS; Perkin Elmer, Canada). The following description is based on Günther et al. (1997), Heinrich et al. (2003) and Pettke et al. (2004). A schematic representation of the LA-ICPMS system of the Institute of Geological Sciences of the University of Bern is presented in Fig. 7.2.Details about the instrument and acquisition parameters can be found in Table 7.1.

The output energy was set to 100 mJ, resulting in an energy density of about 15 J/cm^2 on the sample surface. Different pit sizes were used (44-120 μm), depending on the size of the mineral and the eventual presence of exsolutions or mineral/fluid inclusions (Fig. 7.3). The ablation rate was about 0.1-0.2 μm/shot, and was depth-controlled. This control on the depth of the ablation crater is important, because drilling to deep would decrease the quality of the measurement by fractionation of the different elements (depth/diameter ratio should be < 1).

Polished thin sections were placed in the ablation chamber with the reference standard NIST SRM 610 glass. Prior to measurement the sample chamber was flushed with He gas, but the aerosol produced during the ablation process was transported to the ICPMS by Ar-He carrier gas. The Elan DRC-e quadrupole ICP mass spectrometer has a dwell time of 10 ms, which allows short ablation time. The measurement of major (in wt. %) and trace elements (up to the ng/g level) simultaneously was achieved by ions counting in dual detector mode.

The external standard was the NIST SRM 610 glass, which was measured twice before and twice after the analyses of 16 unknowns. This standard was used to calibrate the analyte sensivities and to apply a linear drift correction. Raw data were reduced with the LAMTRACE program (modified after S.E. Jackson) to quantify the results. During the reduction process, an internal standard was needed to calculate final concentrations and detection limits. This internal standard was a known

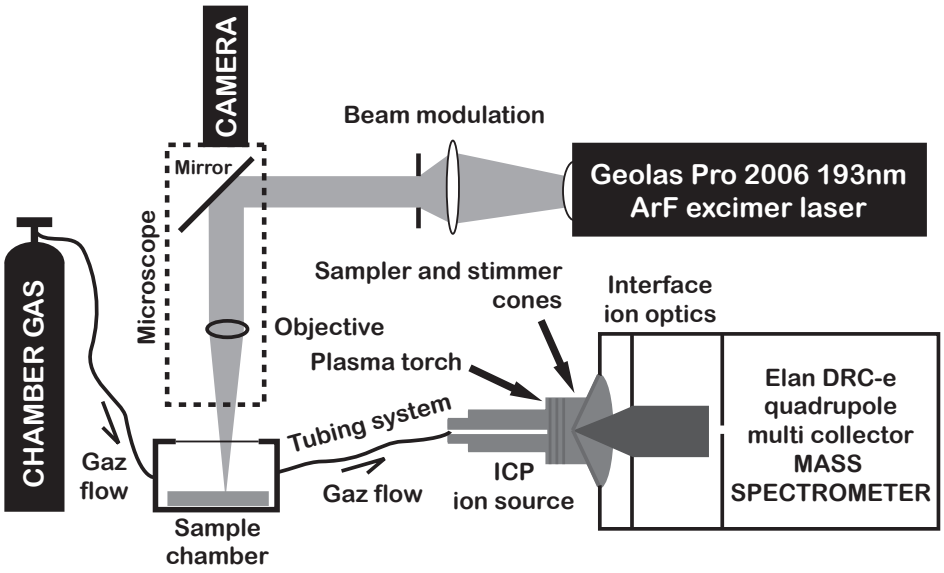


Fig. 7.2: Schematic representation of the LA-ICPMS system used at the University of Bern (Switzerland).

Table 7.1: LA-ICPMS instrument and data acuisition parameters

Geolas Pro 2006 Laser system (Excimer 193 nm ArF laser)	
Output energy	100 mJ
Energy density on sample	ca. 15 J/cm^2, homogeneous energy distribution
Pulse duration	15 ns
Repetition rate	10 Hz
Pit sizes	Between 24 and 120 µm
Ablation cell volume	ca. 16 cm^3
Cell gas flow	0.9-1.0 l min^{-1} He
ELAN DRC-e quadrupole ICPMS	
Nebulizer gas flow	0.75-0.85 l min-1 Ar
Auxiliary gas flow	0.70-0.80 l min-1 Ar
Cool gas flow	15.0-16.0 l min-1 Ar
rf power	1450 kV
Detector mode	Dual, 8 orders of magnitude linear dynamic range
Quadrupole settling time	3 ms
Detector housing vacuum	1.5-2.8*10^{-5} Torr during analysis
Data acquisition parameters	
Sweeps per reading	1
Readings per replicate	200-300
Replicates	1
Dwell time per isotope	10 ms
Points per peak	1 per measurement
Oxide production rate	Tuned to $S_U = S_{Th}$ and < 0.2% ThO

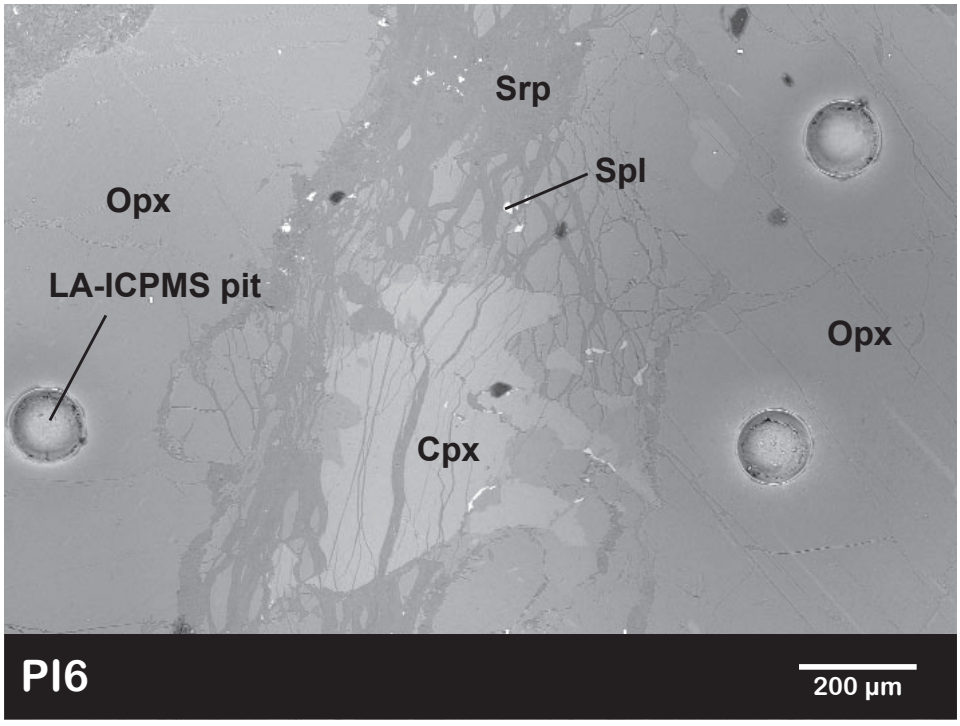


Fig. 7.3: LA-ICPMS pits on spinel harzburgite PI6 of the Pindos ophiolite (Greece). Abbreviations: Opx = orthopyroxene, Cpx = clinopyroxene, Spl = spinel, Srp = serpentine.

concentration (previously measured on the electron microprobe) of an element in the analyzed mineral in wt.% oxides (CaO for clinopyroxene, Al_2O_3 for orthopyroxene, spinel and plagioclase, MgO for olivine). Before calculation the transient signal (background and ablation signal) of each element was filtered in order to remove eventual spikes. Detection limits represent the minimum detectable signal intensity, and were calculated as 3 times the standard deviation of the background signal divided by the element sensitivity (Longerich et al., 1996). Complete LA-ICPMS data and standard details are available in electronic format (enclosed CD-ROM).

WHOLE ROCK ANALYSES

Wavelength Dispersive X-Ray Fluorescence (WD-XRF)

Major element whole rock contents were measured by wavelength dispersive X-ray fluorescence (WD-XRF) at the Geosciences Department of the Fribourg University (Switzerland). Two grams of rock powders of each sample were dried for 6 to 12 hours in a oven (110 °C), and the loss of weight was measured (humidity). Powders were later put in a oven at 1000 °C for an hour under an oxidizing atmosphere. The final loss of weight was measured and called Loss of Ignition (LOI), which represents the loss of volatiles, H_2O and CO_2, and a gain of weight by Fe^{2+} oxidation. 0.70 g of this burnt powder was mixed with 6.65 g of dried lithium tetraborate ($Li_2B_4O_7$) and 0.35 g of dried lithium fuoride (LiF). This mix was put in a Pt-Au-ZrO crucible, in order to obtain a glass after 10 minutes heating at 1150 °C with a PHILIPS PERL'X-2. These glasses were measured with a PHILIPS PW1400 spectrometer. Analysis program BAS2005 was used for major elements. Detection limit was 0.01 wt. % and reproducibility between 0.01 and 0.25 % depending on the element. A correction factor was applied to the analytical results considering the calibration of the instrument with 40 international reference standards.

Inductively Coupled Plasma Mass Spectrometry (ICPMS)

For Pindos and Vourinos samples, Li, Be, Rb, Sr, Y, Ba, the heavy rare earth elements (Dy to Lu) and U, Th and Pb were measured in whole rock by inductively coupled plasma mass spectrometry (ICP-MS) at the Department of Earth Sciences, University of Bristol (United Kingdom). The samples and two ultramafic rock standards (PCC-1; UB-N) were dissolved using a HF-HNO3 multi-acid method on a hotplate. After evaporating the HF, samples were taken up in 2 % HNO3 at a dilution of ~500:1 of the original rock. ICP-MS analyses were performed on a Thermo Electron Element sector field ICP-MS in pulse-counting mode. Mass calibration was completed by using a multi-element solution (10 μg/L of each Li, B, Na, Sc, Fe, Co, Ga, Y, Rh, In, Ba, Lu, Tl, U in 5 % HNO3). Precision and reproducibility of solution ICP-MS analyses were < 12 %, except for Be, Ba, Lu, Pb, Th and U, where they were < 25 %. Detection limits were ~ 37 ng/g for Li and ~ 3 ng/g for Be. Measured intensities were normalised to solutions of USGS reference material PCC-1 (peridotite), except for Be, where ANRT reference material UB-N (serpentinite) was used. The published values for PCC-1 of 985 ng/g Li (Moriguti et al., 2004) was used to calculate the concentrations of Li. The accepted concentration of Be in UB-N is 200 ng/g (Govindaraju, 1994).

For Geisspfad samples, Li, Be and trace element whole rock contents were measured by inductively coupled plasma mass spectrometry (ICP-MS), using a VG PQ ExCell quadrupole ICP-MS at the Boston University. All the details concerning sample preparation by acid digestion and measurement parameters are described in Kelley et al. (2003). The same protocol was followed, except for the final sample dilution (1/1000 instead of 1/2000), because of low concentrations. Measurements were performed using the analogue setting mode, usually used for high-abundance elements (> 5 ppb in solution). However for most samples, REE, Rb, Y, Ba and Zr were collected in pulse counting mode, usually used for low-abundance elements (< 5 ppb in solution). Calibration standards used in the analyses are BIR-1, W-2 (USGS) and MAR-1 (Mid-Atlantic Ridge basalt, Lamont in-house standard), using the values published in Kelley et al. (2003). DNC-1 (USGS) standard reference material was run as an unknown and also compared with the values of Kelley et al. (2003). Precision was evaluated by the measurement of in-run replicates showing a relative standard deviation (RSD) < 2-3 % for all elements. Precision decreases with decreasing abundance, and RSD can reach 5 % for low-concentrated elements. Details about standards are available in electronic format (enclosed CD-ROM).

Prompt Gamma Neutron Activation Analysis (PGNAA)

B, S, Cl and H_2O whole rock contents were measured by PGNAA (Prompt Gamma Neutron Activation Analysis) at the prompt gamma activation analysis facility of the Budapest Research Reactor (BRR). This method has already been used to analyze B whole rock contents in geological samples (Gméling et al., 2005; Marschall et al., 2005). PGNAA is especially useful for analyzing whole rock boron concentrations. In contrast to other geoanalytical methods, sample preparation procedures are not needed, and hence contamination problems are eliminated (Anderson & Kasztovszky, 2004). Analyses were performed on rock powders. The principle of the PGNAA method is the detection of prompt γ-rays that originate from the (n,γ)-reactions during neutron irradiation (Révay & Belgya, 2004). The detection limit was different in each sample, depending on measurement time and the sample weight, but ranges from 0.01 to 0.03 μg/g for B. The detection limit is inversely proportional to the measurement time and to the sensitivity of the given element. B has a small relative uncertainty (1 to 2 %), but is above 5 % only if the B content goes under 1 μg/g. S and Cl have relative uncertainties of 6 to 8 %, and 4 to 18 % respectively. H_2O has a small relative uncertainty (2 to 4 %). Samples were heat-sealed in fluorinated ethylene propylene (FEP) film, which produces negligible background. The analytical system is located at a cold neutron beam, which is extracted from the cold neutron source of the 10 MW research reactor. The neutrons are guided 35 m away from the reactor core by means of evacuated, curved, horizontal guides without significant loss.

The samples were irradiated in a cold neutron beam of $5 \cdot 10^7$ $cm^{-2}s^{-1}$ flux. The cross-section of the neutron beam was 4 cm^2. The neutron flux was stable during the whole reactor operation period and homogeneous in the area of the beam. Because the samples are practically transparent to neutrons, average bulk compositions of the investigated volume were obtained. All of the samples were thinner than 5 mm; thus the self-absorption of neutrons and γ-photons was negligible. The emitted gamma radiation was detected with a High Purity Germanium – Bismuth Germanate detector system, and the signals were processed with a multichannel analyzer. The measurement system has been described by Molnár (2004) and Révay et al. (2004). The measurement time for each individual sample varied between 2600 and 11200 seconds. The spectra were evaluated with Hypermet-PC software and the element identification was performed using a prompt-gamma library (Révay et al., 2001). Details about accuracy of this method can be found in electronic format (enclosed CD-ROM).

Oxygen and Hydrogen Isotope Analyses

The oxygen and hydrogen isotope analyses were done at the University of Lausanne (Switzerland), using whole rock powders. The oxygen isotope composition (^{16}O, ^{17}O, ^{18}O) of the Geisspfad samples were measured using a method similar to that described by Sharp (1990) and Rumble & Hoering (1994), and is described in more detail in Kasemann et al. (2001). Between 0.5 to 2.0 mg of sample rock powder was loaded into a small Pt-sample holder and pumped out to a vacuum of about 10^{-6} mbar. After prefluorination of the sample chamber overnight, the samples were heated with a CO_2-laser in 50 mbars of pure F_2. Excess F_2 was separated from the O_2 produced by conversion to Cl_2 using KCl held at 150°C. The extracted O_2 was collected on a molecular sieve (5A) and subsequently expanded into the inlet of a Finnigan MAT 253 isotope ratio mass spectrometer. Oxygen isotope compositions are given in the standard δ-notation, expressed relative to VSMOW in permil (‰). Replicate oxygen isotope analyses of an in-house standard, LS-1 quartz (n = 2), gave a precision of 0.002 ‰ for $\delta^{18}O$. The accuracy of $\delta^{18}O$ values is commonly better than 0.02 ‰ compared to accepted $\delta^{18}O$ values for LS-1 of 18.10 ‰.

Measurements of the hydrogen isotope compositions of whole rocks were made using high-temperature (1450°C) reduction methods with He-carrier gas and a TC-EA linked to a Delta Plus XL mass spectrometer from Thermo-Finnigan on 2 to 4 mg sized samples according to a method adapted after Sharp et al. (2001). The results are given in the standard δ-notation, expressed relative to VSMOW in permil (‰). The precision of the in-house kaolinite standard and NBS-30 biotite for hydrogen isotope analyses was better than ± 2 ‰ for the method used; all values were normalized using a value of –125 ‰ for the kaolinite standard and – 66 ‰ for NBS-30 analyzed during the same period as the samples. Details about standards can be found in electronic format (enclosed CD-ROM).

Appendix A

Supplement to chapter 4

The electronic version of this supplement will be available on the website of Chemical Geology

ANALYTICAL TECHNIQUES - MICROPROBE ANALYSES

Major element compositions of minerals were determined by electron microprobe, using a Jeol JXA-8200 at the Institute of Geological Sciences of the University of Bern and a Cameca SX-51 at the Institute of Mineralogy of the Ruprecht-Karls University of Heidelberg. These microprobes are equipped with five and four wavelength-dispersive spectrometers, respectively. Operating conditions used for silicates comprise an accelerating voltage of 15 kV and a 20 nA beam current. These conditions were set to 15 kV and 10 nA during carbonate measurement. The spot size was about 3 μm except for some minerals where a defocused beam was used (amphibole, chlorite, epidote, titanite: 10 μm; calcite, dolomite: 15 μm). Different spot sizes were tested for serpentine, but the best cation and oxide totals were obtained with a 3 μm spot size. Natural and synthetic oxides, silicates, sulfides, sulfates and carbonates were used as standards. Backscattered electron (BSE) images were obtained at the Centre Suisse d'Electronique et de Microtechnique (CSEM, Neuchâtel), with a Philips XL-30 Scanning Electron Microscope, operated at 25 kV.

MINERAL CHEMISTRY - MAJOR ELEMENTS

Microprobe analyses were normalized considering Fe as Fe^{2+} in all minerals, except for amphiboles where Fe^{2+} and Fe^{3+} were calculated, and epidote and titanite where all Fe was considered as Fe^{3+}. Mg# was calculated as Mg / [Mg + Fe^{2+}] for all minerals.

WHOLE ROCK CHEMISTRY - RARE EARTH ELEMENTS (REE)

Serpentinite and ophicarbonate show two different rare earth element (REE) signatures (see group I and II on Fig. 4.12). The REE group I is characterized by a rather homogeneous pattern, a variable light REE fractionation (Ce_N/Sm_N = 0.48 to 0.99), a nearly flat heavy REE pattern, and is LREE depleted compared to the primitive mantle trend of McDonough & Sun (1995). This group I is also similar to trends obtained on Lanzo plagioclase lherzolites and Huinan spinel lherzolites (Xu et al., 2003; Müntener et al., 2005; Kaczmarek & Müntener, submitted; Fig. 4.12), which represent ocean-continent transition mantle. The REE group II (Fig. 4.12) is characterized by a U-shaped REE pattern, with fractionation of both light REE (Ce_N/Sm_N = 1.75 to 3.50), and heavy REE (Gd_N/Lu_N = 0.33 to 0.42). The concentration of REE in the whole rock from group II is approximately one order of magnitude lower than for group I. This signature is similar to some Huinan harzburgites of Xu et al. (2003; Fig. 4.12).

Blackwall rocks show a single rare earth element (REE) pattern (Fig. a.2 in the Appendix). This REE pattern is characterized by a rather homogeneous curve, with a light REE fractionation (Ce_N/Sm_N ~ 0.78), a nearly flat heavy REE pattern, and is comparable to the normal mid-ocean ridge basalt (N-MORB) trend of Sun & McDonough (1989).

In the gneiss, REE trend shows a strong fractionation between the light and the heavy REE (Fig. a.2 in the Appendix), with a clear light REE enrichment (Ce_N/Yb_N ~ 6.01).

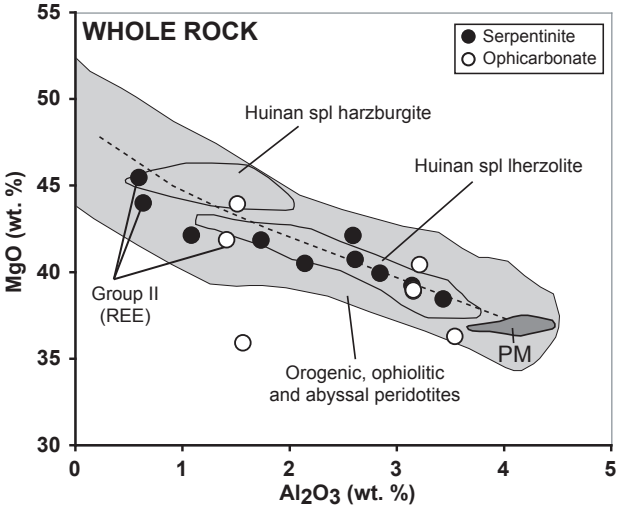


Fig. a.1: Al_2O_3 (wt. %) versus MgO (wt. %) diagram of whole rock serpentinites and ophicarbonates. Data of Huinan spinel lherzolite and harzburgite after Xu et al. (2003) are plotted for comparison. Orogenic, ophiolitic and abyssal peridotite field after Bodinier & Godard (2004). Primitive mantle estimates after Green et al. (1979), Jagoutz et al. (1979) and McDonough & Sun (1995). Dashed line represents a near fractional melting trend of a starting primitive spinel peridotite (Niu, 1997; Takazawa et al., 2000; Xu et al., 2003). Group II (REE) refers to Fig. 4.12.

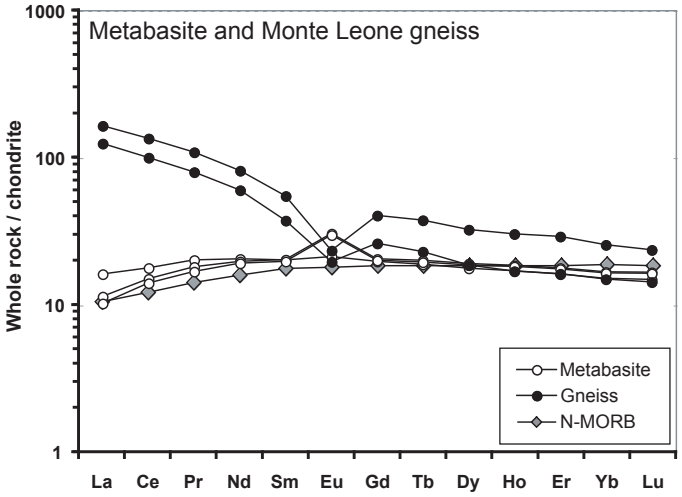


Fig. a.2: Rare earth element (REE) abundances in whole rock metabasite and gneiss. REE data were normalized by the chondrite (McDonough & Sun, 1995). N-MORB after Sun & McDonough (1989) is plotted for comparison.

Table a.1: Major element composition of antigorite (representative analyses)

Rock	Serp	Serp	Serp	Serp	Serp	Serp	Serp	Serp	Serp	Serp	Serp	Serp	Ophi	Ophi	Ophi	Ophi
Sample	GEI4	GEI4	GEI4	G11	G11	G12	G12	G26	G26	G27	G27	G27	G3	G4	G4	GEI9
SiO_2	42.6	42.1	42.6	42.3	42.8	42.8	42.7	42.2	41.9	42.6	42.5	42.5	42.9	42.2	42.4	42.9
TiO_2	0.01	0.04	0.04	0.04	0.03	0.03	0.01	0.02	0.02	0.02	0.03	0.04	0.02	0.03	0.02	0.04
Cr_2O_3	0.10	0.54	0.29	0.58	0.06	0.12	0.43	0.97	1.01	0.23	0.37	0.29	0.17	0.09	0.18	0.31
Al_2O_3	2.35	3.08	2.88	2.97	2.41	2.77	3.11	2.82	2.93	2.97	3.10	3.21	2.47	3.25	3.06	3.39
FeO	4.75	4.64	4.76	4.19	4.44	3.89	4.12	3.83	3.62	4.57	4.37	4.46	4.48	4.62	4.88	3.93
MnO	0.03	0.08	0.03	0.05	0.03	0.05	b.d.	0.03	b.d.	0.04	0.05	0.04	b.d.	0.09	0.09	0.06
NiO	0.15	0.18	0.20	0.20	0.19	0.17	0.19	0.16	0.19	0.12	0.12	0.15	0.20	0.09	0.03	0.13
MgO	37.3	36.7	37.1	37.3	37.0	38.0	36.5	37.4	37.2	37.1	37.4	37.2	37.5	36.6	36.7	36.8
CaO	0.01	0.01	b.d.	0.02	b.d.	b.d.	b.d.	b.d.	b.d.	b.d.	b.d.	b.d.	b.d.	b.d.	0.01	0.21
Na_2O	0.01	0.01	b.d.	b.d.	b.d.	b.d.	b.d.	b.d.	b.d.	b.d.	0.03	0.02	b.d.	b.d.	b.d.	0.02
K_2O	0.02	b.d.	b.d.	b.d.	b.d.	b.d.	b.d.	b.d.	b.d.	b.d.	0.02	b.d.	b.d.	b.d.	b.d.	b.d.
H_2O	12.8	12.8	12.9	12.8	12.8	12.9	12.8	12.8	12.7	12.9	12.9	12.9	12.9	12.7	12.8	12.9
Total	100.1	100.1	100.8	100.5	99.7	100.8	99.9	100.3	99.6	100.5	100.9	100.8	100.5	99.8	100.2	100.7
Stoich.	9 O	9 O	9 O	9 O	9 O	9 O	9 O	9 O	9 O	9 O	9 O	9 O	9 O	9 O	9 O	9 O
Si	2.000	1.977	1.987	1.976	2.010	1.987	2.000	1.974	1.970	1.987	1.975	1.978	2.000	1.983	1.988	1.993
Ti	0.000	0.001	0.001	0.001	0.001	0.001	0.000	0.001	0.001	0.001	0.001	0.001	0.001	0.001	0.001	0.001
Cr	0.004	0.020	0.011	0.021	0.002	0.004	0.016	0.036	0.038	0.008	0.014	0.011	0.006	0.003	0.007	0.011
Al	0.130	0.170	0.158	0.163	0.133	0.152	0.172	0.155	0.163	0.163	0.170	0.176	0.136	0.180	0.169	0.185
Fe^{2+}	0.186	0.182	0.186	0.164	0.174	0.151	0.161	0.150	0.142	0.178	0.170	0.173	0.175	0.182	0.191	0.153
Mn	0.001	0.003	0.001	0.002	0.001	0.002	0.000	0.001	b.d.	0.001	0.002	0.002	0.000	0.004	0.004	0.002
Ni	0.006	0.007	0.008	0.008	0.007	0.006	0.007	0.006	0.007	0.004	0.005	0.006	0.007	0.004	0.001	0.005
Mg	2.605	2.565	2.575	2.594	2.591	2.630	2.549	2.605	2.607	2.582	2.594	2.578	2.604	2.567	2.563	2.544
Ca	0.000	0.000	b.d.	0.001	b.d.	b.d.	b.d.	b.d.	b.d.	b.d.	b.d.	b.d.	b.d.	b.d.	0.001	0.011
Na	0.001	0.001	b.d.	b.d.	b.d.	b.d.	b.d.	b.d.	b.d.	b.d.	0.002	0.002	b.d.	b.d.	b.d.	0.002
K	0.001	b.d.	b.d.	b.d.	b.d.	b.d.	b.d.	b.d.	b.d.	b.d.	0.001	b.d.	b.d.	b.d.	b.d.	b.d.
H	4.000	4.000	4.000	4.000	3.999	4.000	3.997	4.000	4.000	4.000	4.000	4.000	3.998	3.997	3.998	4.000
Total	8.934	8.927	8.927	8.930	8.920	8.933	8.903	8.929	8.928	8.926	8.934	8.927	8.926	8.921	8.921	8.908
Mg#	0.933	0.934	0.933	0.941	0.937	0.946	0.940	0.946	0.948	0.935	0.939	0.937	0.937	0.934	0.931	0.943

b.d.: below detection limit, Serp: serpentinite, Ophi: ophicarbonate.

Table a.2: Major element composition of forsterite (representative analyses)

Rock	Serp	Serp	Serp	Serp	Serp	Serp	Serp	Serp	Serp	Serp	Serp	Serp	Serp	Ophi	Ophi	Ophi
Sample	GEI4	GEI4	GEI4	G8	G8	G11	G11	G12	G12	G26	G26	G27	G27	G3	G3	G3
SiO_2	39.9	39.6	39.5	40.7	40.3	40.0	40.2	40.3	40.5	40.2	40.5	39.7	40.5	40.2	39.9	40.1
TiO_2	b.d.	0.01	b.d.	b.d.	b.d.	b.d.	0.02	b.d.	b.d.	b.d.	0.01	b.d.	b.d.	0.02	b.d.	0.01
Cr_2O_3	0.02	0.02	b.d.	b.d.	b.d.	0.07	0.12	0.03	b.d.	b.d.	0.03	0.01	b.d.	b.d.	b.d.	0.03
Al_2O_3	0.01	b.d.	b.d.	0.02	0.27	0.02	b.d.	b.d.	0.02	b.d.	b.d.	b.d.	b.d.	0.01	b.d.	b.d.
FeO	14.3	14.8	14.4	13.7	13.2	13.3	13.2	11.7	13.1	11.6	11.8	13.0	13.1	11.3	11.7	11.5
MnO	0.22	0.19	0.18	0.17	0.14	0.24	0.17	0.21	0.19	0.23	0.24	0.24	0.29	0.35	0.42	0.36
NiO	0.30	0.38	0.34	0.22	0.27	0.45	0.36	0.34	0.39	0.33	0.36	0.34	0.33	0.34	0.28	0.27
MgO	45.8	45.2	45.3	46.1	46.6	46.4	46.6	46.9	46.5	47.2	47.9	45.8	46.6	48.0	47.1	47.8
CaO	b.d.	0.02	0.01	0.01	0.01	0.01	0.01	0.01	b.d.	b.d.	0.02	0.01	0.02	0.01	b.d.	b.d.
Na_2O	b.d.	b.d.	b.d.	0.01	b.d.	b.d.	0.01	b.d.	b.d.	b.d.	b.d.	0.01	b.d.	b.d.	0.01	b.d.
K_2O	b.d.	b.d.	b.d.	b.d.	b.d.	b.d.	b.d.	b.d.	b.d.	b.d.	b.d.	b.d.	0.01	b.d.	0.01	b.d.
Total	100.5	100.2	99.7	100.9	100.9	100.5	100.6	99.5	100.7	99.5	100.9	99.1	100.8	100.2	99.4	100.0
Stoich.	4 O	4 O	4 O	4 O	4 O	4 O	4 O	4 O	4 O	4 O	4 O	4 O	4 O	4 O	4 O	4 O
Si	0.993	0.991	0.992	1.005	0.996	0.994	0.995	1.003	1.002	1.000	0.995	0.998	1.000	0.993	0.995	0.993
Ti	b.d.	0.000	b.d.	b.d.	b.d.	b.d.	0.000	b.d.	b.d.	b.d.	0.000	b.d.	b.d.	0.000	b.d.	0.000
Cr	0.000	0.000	b.d.	b.d.	b.d.	0.001	0.002	0.001	b.d.	b.d.	0.001	0.000	b.d.	b.d.	b.d.	0.001
Al	0.000	b.d.	b.d.	0.001	0.008	0.001	b.d.	b.d.	0.001	b.d.	b.d.	b.d.	b.d.	0.000	b.d.	b.d.
Fe^{2+}	0.298	0.309	0.302	0.284	0.273	0.276	0.274	0.243	0.270	0.240	0.243	0.273	0.271	0.234	0.243	0.237
Mn	0.005	0.004	0.004	0.003	0.003	0.005	0.004	0.004	0.004	0.005	0.005	0.005	0.006	0.007	0.009	0.007
Ni	0.006	0.008	0.007	0.004	0.005	0.009	0.007	0.007	0.008	0.007	0.007	0.007	0.006	0.007	0.006	0.005
Mg	1.699	1.687	1.695	1.697	1.716	1.719	1.721	1.738	1.713	1.749	1.753	1.718	1.715	1.764	1.753	1.763
Ca	b.d.	0.001	0.000	0.000	0.000	0.000	0.000	0.000	b.d.	b.d.	0.000	0.000	0.000	0.000	b.d.	b.d.
Na	b.d.	b.d.	b.d.	0.000	b.d.	b.d.	0.000	b.d.	b.d.	b.d.	b.d.	0.000	b.d.	b.d.	0.000	b.d.
K	b.d.	b.d.	b.d.	b.d.	b.d.	b.d.	b.d.	b.d.	b.d.	b.d.	b.d.	b.d.	0.000	b.d.	0.000	b.d.
Total	3.000	3.000	3.000	2.995	3.000	3.005	3.003	2.996	2.998	3.000	3.004	3.002	3.000	3.007	3.006	3.007
Mg#	0.851	0.845	0.849	0.857	0.863	0.862	0.863	0.877	0.864	0.879	0.878	0.863	0.863	0.883	0.878	0.881

b.d.: below detection limit, Serp: serpentinite, Ophi: ophicarbonate.

Table a.3: Major element composition of amphibole (representative analyses)

Rock	Serp	Serp	Serp	Serp	Serp	Serp	Serp	Serp	Serp	Serp	Serp	Serp	Serp	Serp	Serp	Serp
Sample	GEI4	GEI4	GEI4	G8	G8	G8	G11	G11	G11	G12	G12	G12	G26	G26	G26	G27
Name	Tr	Tr	Tr	Tr	Tr	Tr	Tr	Tr	Tr	Tr	Tr	Tr	Tr	Tr	Tr	Tr
SiO_2	57.4	57.3	57.7	58.2	57.4	58.0	57.5	58.5	57.7	57.6	58.1	58.1	58.2	57.9	57.9	58.2
TiO_2	0.10	0.08	0.04	0.05	0.04	0.05	0.04	0.06	0.03	0.03	0.03	0.03	0.04	0.06	0.04	0.05
Cr_2O_3	0.07	0.05	0.02	b.d.	0.04	0.09	0.01	0.11	0.08	0.05	0.02	0.02	0.08	0.01	0.10	0.06
Al_2O_3	0.94	0.91	0.70	1.03	1.14	1.20	0.88	0.82	0.77	0.85	0.72	0.71	0.63	0.76	0.62	0.81
Fe_2O_3	n.c.	n.c.	n.c.	n.c.	n.c.	n.c.	n.c.	n.c.	n.c.	n.c.	n.c.	n.c.	n.c.	n.c.	n.c.	n.c.
FeO	2.13	2.00	2.02	1.97	2.15	2.29	2.03	2.22	1.86	2.05	2.27	2.05	1.70	1.69	1.66	1.90
MnO	0.10	0.02	0.05	0.04	0.01	0.10	0.07	0.10	0.03	b.d.	0.12	b.d.	0.02	0.03	0.04	0.03
NiO	0.09	0.05	0.10	0.08	0.16	0.22	0.01	b.d.	0.16	0.20	0.23	0.10	0.13	0.11	0.08	0.10
MgO	23.3	23.4	23.4	22.6	22.5	22.8	22.5	22.9	22.5	22.5	22.6	22.8	23.3	23.4	23.1	23.0
CaO	13.4	13.3	13.2	12.8	12.9	12.7	13.2	13.2	13.5	13.1	13.1	13.1	13.6	13.3	13.7	13.5
Na_2O	0.88	0.92	0.84	0.85	0.91	1.05	0.80	0.69	0.68	0.88	0.79	0.81	0.69	0.81	0.62	0.65
K_2O	0.07	0.06	0.05	0.03	0.02	0.03	0.09	0.07	0.06	0.04	0.04	0.04	0.05	0.06	0.04	0.05
H_2O	2.19	2.18	2.18	2.17	2.16	2.18	2.16	2.19	2.17	2.16	2.17	2.18	2.19	2.19	2.19	2.19
Total	100.6	100.3	100.2	99.8	99.4	100.7	99.2	100.8	99.5	99.4	100.1	100.0	100.5	100.4	100.1	100.6
Stoich.	23 O 15 cat + Na + K	23 O 15 cat + Na + K	23 O 15 cat + Na + K	23 O 15 cat + Na + K	23 O 15 cat + Na + K	23 O 15 cat + Na + K	23 O 15 cat + Na + K	23 O 15 cat + Na + K	23 O 15 cat + Na + K	23 O 15 cat + Na + K	23 O 15 cat + Na + K	23 O 15 cat + Na + K	23 O 15 cat + Na + K	23 O 15 cat + Na + K	23 O 15 cat + Na + K	23 O 15 cat + Na + K
Si	7.854	7.865	7.918	8.034	7.972	7.965	7.989	7.990	7.990	7.991	8.008	8.012	7.946	7.935	7.942	7.960
Ti	0.010	0.008	0.004	0.005	0.004	0.005	0.004	0.006	0.004	0.003	0.003	0.003	0.004	0.006	0.004	0.006
Cr	0.007	0.005	0.002	0.000	0.005	0.010	0.001	0.012	0.009	0.005	0.002	0.002	0.008	0.001	0.011	0.006
Al	0.152	0.147	0.113	0.168	0.187	0.194	0.144	0.132	0.125	0.139	0.117	0.115	0.101	0.123	0.100	0.131
Fe^{3+}	n.c.	n.c.	n.c.	n.c.	n.c.	n.c.	n.c.	n.c.	n.c.	n.c.	n.c.	n.c.	n.c.	n.c.	n.c.	n.c.
Fe^{2+}	0.243	0.230	0.232	0.227	0.250	0.263	0.236	0.254	0.215	0.238	0.262	0.236	0.194	0.194	0.190	0.217
Mn	0.012	0.003	0.006	0.005	0.002	0.011	0.008	0.012	0.004	b.d.	0.013	b.d.	0.003	0.003	0.005	0.004
Ni	0.010	0.005	0.011	0.009	0.018	0.024	0.001	0.000	0.018	0.022	0.025	0.011	0.014	0.012	0.009	0.011
Mg	4.756	4.778	4.778	4.659	4.651	4.662	4.654	4.659	4.640	4.651	4.641	4.687	4.745	4.773	4.720	4.683
Ca	1.957	1.958	1.938	1.892	1.912	1.867	1.964	1.936	1.995	1.950	1.929	1.934	1.985	1.953	2.019	1.983
Na	0.234	0.244	0.225	0.227	0.244	0.279	0.215	0.182	0.183	0.237	0.210	0.217	0.182	0.216	0.164	0.171
K	0.012	0.011	0.008	0.005	0.004	0.006	0.017	0.012	0.011	0.007	0.006	0.007	0.009	0.011	0.007	0.009
H	2.000	2.000	2.000	2.000	2.000	2.000	1.999	2.000	2.000	1.999	1.999	1.999	2.000	2.000	2.000	2.000
Total	15.247	15.254	15.233	15.232	15.248	15.285	15.232	15.194	15.194	15.243	15.216	15.224	15.191	15.226	15.171	15.180
Mg#	0.951	0.954	0.954	0.953	0.949	0.947	0.952	0.948	0.956	0.951	0.947	0.952	0.961	0.961	0.961	0.956
NaK (A)	0.146	0.135	0.081	0.232	0.248	0.285	0.232	0.194	0.194	0.243	0.216	0.224	0.191	0.226	0.171	0.180

n.c.: not calculated, b.d.: below detection limit, Serp: serpentinite, Tr: tremolite.

Table a.3: continued

Rock	Serp	Serp	Ophi	Ophi	Ophi	Ophi	Ophi	Ophi	Ophi	Ophi	Ophi	Metabas	Metabas	Metabas	Metabas	Metabas
Sample	G27	G27	G3	G3	G3	G4	G4	G4	GEI9	GEI9	GEI9	G30a	G30a	G30a	G34	G34
Name	Tr	Tr	Tr	Tr	Tr	Tr	Tr	Tr	Tr	Tr	Tr	Hbl	Hbl	Hbl	Hbl	Hbl
SiO_2	58.3	58.0	59.0	58.9	58.7	59.1	58.7	58.7	58.5	58.4	58.0	43.2	43.8	44.2	43.4	41.6
TiO_2	0.05	0.07	0.03	0.02	0.02	0.03	0.04	0.05	0.03	0.04	0.04	0.31	0.30	0.32	0.33	0.25
Cr_2O_3	0.05	b.d.	b.d.	0.10	0.03	b.d.	0.10	b.d.	b.d.	b.d.	0.07	0.01	0.07	0.05	0.03	b.d.
Al_2O_3	0.86	0.76	0.23	0.18	0.31	0.08	0.19	0.11	0.28	0.36	0.39	12.94	12.67	12.53	13.28	17.14
Fe_2O_3	n.c.	n.c.	n.c.	n.c.	n.c.	n.c.	n.c.	n.c.	n.c.	n.c.	n.c.	7.00	6.55	6.07	6.32	4.97
FeO	1.89	1.90	1.78	1.66	1.86	1.63	1.75	1.52	1.49	1.56	1.57	5.69	5.37	4.70	5.62	6.69
MnO	0.04	0.06	0.13	0.05	0.12	0.17	0.18	0.09	0.10	0.07	0.07	0.27	0.24	0.22	0.22	0.19
NiO	0.10	0.10	b.d.	0.12	0.02	0.19	0.08	0.05	0.10	0.02	0.10	0.00	0.08	b.d.	0.08	b.d.
MgO	23.1	23.0	23.5	23.7	23.6	23.7	23.3	23.2	23.2	23.3	22.9	13.2	13.8	14.3	13.8	9.2
CaO	13.5	13.2	13.4	13.6	13.4	13.6	13.6	13.6	13.7	13.6	13.5	13.9	13.7	14.0	13.1	16.4
Na_2O	0.74	0.71	0.21	0.15	0.31	0.05	0.09	0.05	0.12	0.18	0.19	1.18	1.16	1.19	1.18	0.85
K_2O	0.05	0.04	0.04	0.04	0.06	0.01	0.01	0.01	0.04	0.04	0.03	0.54	0.53	0.46	0.45	0.40
H_2O	2.20	2.18	2.20	2.21	2.20	2.21	2.20	2.19	2.19	2.19	2.17	2.07	2.08	2.08	2.07	2.05
Total	100.9	100.0	100.5	100.8	100.5	100.8	100.1	99.6	99.7	99.8	99.1	100.3	100.3	100.1	99.9	99.8
Stoich.	23 O 15 cat + Na + K	23 O 15 cat + Na + K	23 O 15 cat + Na + K	23 O 15 cat + Na + K	23 O 15 cat + Na + K	23 O 15 cat + Na + K	23 O 15 cat + Na + K	23 O 15 cat + Na + K	23 O 15 cat + Na + K	23 O 15 cat + Na + K	23 O 15 cat + Na + K	23 O 15 cat + Na + K	23 O 15 cat + Na + K	23 O 15 cat + Na + K	23 O 15 cat + Na + K	23 O 15 cat + Na + K
Si	7.947	7.969	8.024	7.987	7.984	8.004	8.006	8.048	8.009	8.002	8.014	6.262	6.317	6.362	6.276	6.068
Ti	0.005	0.007	0.003	0.002	0.002	0.003	0.004	0.005	0.003	0.005	0.005	0.034	0.033	0.035	0.036	0.027
Cr	0.005	b.d.	b.d.	0.011	0.003	b.d.	0.011	b.d.	b.d.	b.d.	0.007	0.002	0.008	0.006	0.003	b.d.
Al	0.138	0.123	0.036	0.029	0.049	0.013	0.030	0.018	0.046	0.058	0.063	2.212	2.157	2.126	2.266	2.949
Fe^{3+}	n.c.	n.c.	n.c.	n.c.	n.c.	n.c.	n.c.	n.c.	n.c.	n.c.	n.c.	0.764	0.712	0.657	0.689	0.545
Fe^{2+}	0.216	0.218	0.203	0.188	0.212	0.185	0.200	0.174	0.171	0.179	0.181	0.690	0.648	0.565	0.681	0.816
Mn	0.005	0.007	0.015	0.006	0.014	0.020	0.021	0.011	0.012	0.008	0.009	0.033	0.030	0.027	0.027	0.024
Ni	0.011	0.011	b.d.	0.013	0.002	0.020	0.009	0.006	0.011	0.002	0.012	0.000	0.009	b.d.	0.009	b.d.
Mg	4.696	4.718	4.765	4.788	4.786	4.781	4.737	4.736	4.736	4.758	4.719	2.844	2.966	3.069	2.976	1.999
Ca	1.978	1.946	1.955	1.976	1.947	1.974	1.983	2.003	2.012	1.989	1.990	2.159	2.121	2.152	2.037	2.570
Na	0.195	0.190	0.055	0.041	0.081	0.012	0.023	0.012	0.031	0.049	0.052	0.330	0.326	0.332	0.332	0.240
K	0.008	0.006	0.008	0.006	0.010	0.002	0.002	0.002	0.006	0.007	0.005	0.100	0.098	0.085	0.084	0.074
H	2.000	2.000	2.000	2.000	2.000	2.000	2.000	2.000	1.999	1.999	2.000	2.000	2.000	2.000	2.000	2.000
Total	15.203	15.196	15.063	15.047	15.091	15.014	15.024	15.015	15.037	15.056	15.057	15.430	15.423	15.417	15.416	15.314
Mg#	0.956	0.956	0.959	0.962	0.958	0.963	0.959	0.965	0.965	0.964	0.963	0.805	0.821	0.844	0.814	0.710
NaK (A)	0.203	0.196	0.063	0.047	0.091	0.014	0.024	0.015	0.037	0.056	0.057	0.430	0.423	0.417	0.416	0.314

n.c.: not calculated, b.d.: below detection limit, Serp: serpentinite, Ophi: ophicarbonate, Metabas: metabasite, Tr: tremolite, Hbl: tschermakitic hornblende.

Table a.4: Major element composition of diopside (representative analyses)

Rock	Serp	Serp	Serp	Serp	Serp	Serp	Serp	Ophi	Ophi	Ophi	Ophi	Ophi	Ophi	Ophi	Ophi	Ophi
Sample	G11	G11	G11	G11	G26	G26	G27	G4	G4	G4	GEI9	GEI9	GEI9	GEI9	GEI9	GEI9
SiO_2	55.4	55.6	55.4	54.9	55.6	55.9	55.6	55.7	55.3	55.7	54.6	55.1	55.3	54.9	54.9	54.9
TiO_2	b.d.	0.03	0.02	b.d.	0.03	0.03	0.02	0.01	0.03	0.02	0.01	0.01	0.03	0.03	0.03	0.02
Cr_2O_3	0.20	b.d.	0.11	0.25	0.07	0.15	0.26	0.05	b.d.	b.d.	0.07	b.d.	0.06	b.d.	0.09	0.03
Al_2O_3	0.05	0.03	0.04	0.10	0.01	0.05	0.21	0.18	0.04	0.03	0.02	0.02	b.d.	0.03	0.13	0.23
FeO	1.35	1.65	1.68	1.98	1.14	1.66	1.18	1.68	1.99	1.59	0.94	1.12	1.26	1.17	1.26	1.24
MnO	0.06	b.d.	0.02	0.12	b.d.	0.03	0.04	0.13	0.12	0.13	0.16	0.06	0.14	0.20	0.05	0.11
NiO	0.03	0.10	b.d.	b.d.	b.d.	b.d.	0.04	0.03	b.d.	b.d.	0.06	0.04	0.02	b.d.	b.d.	b.d.
MgO	17.4	17.5	17.1	16.8	17.5	17.0	17.8	17.9	16.9	17.3	17.0	17.1	17.1	17.3	17.8	18.5
CaO	25.8	25.9	25.9	25.4	26.3	25.6	25.5	24.6	25.8	26.0	26.2	26.0	26.0	25.7	25.1	24.2
Na_2O	0.13	0.06	0.09	0.23	0.08	0.25	0.22	0.18	0.18	0.08	0.08	0.06	0.08	0.11	0.08	0.08
K_2O	b.d.	b.d.	0.01	b.d.	b.d.	b.d.	b.d.	0.01	b.d.	b.d.	b.d.	b.d.	0.01	b.d.	b.d.	0.01
Total	100.4	100.9	100.4	99.8	100.7	100.7	100.9	100.5	100.3	100.9	99.2	99.5	100.0	99.5	99.4	99.3
Stoich.	6 O	6 O	6 O	6 O	6 O	6 O	6 O	6 O	6 O	6 O	6 O	6 O	6 O	6 O	6 O	6 O
Si	2.002	2.002	2.005	2.003	2.001	2.013	1.996	2.007	2.005	2.007	2.001	2.007	2.007	2.002	2.000	1.997
Ti	b.d.	0.001	0.000	b.d.	0.001	0.001	0.000	0.000	0.001	0.001	0.000	0.000	0.001	0.001	0.001	0.000
Cr	0.006	b.d.	0.003	0.007	0.002	0.004	0.007	0.001	b.d.	b.d.	0.002	b.d.	0.002	b.d.	0.003	0.001
Al	0.002	0.001	0.002	0.004	0.000	0.002	0.009	0.007	0.002	0.001	0.001	0.001	b.d.	0.001	0.006	0.010
Fe^{2+}	0.041	0.050	0.051	0.060	0.034	0.050	0.036	0.051	0.060	0.048	0.029	0.034	0.038	0.036	0.038	0.038
Mn	0.002	b.d.	0.000	0.004	b.d.	0.001	0.001	0.004	0.004	0.004	0.005	0.002	0.004	0.006	0.001	0.003
Ni	0.001	0.003	b.d.	b.d.	b.d.	b.d.	0.001	0.001	b.d.	b.d.	0.002	0.001	0.000	b.d.	b.d.	b.d.
Mg	0.940	0.937	0.924	0.913	0.942	0.915	0.954	0.960	0.913	0.927	0.926	0.928	0.927	0.942	0.966	1.002
Ca	0.998	1.000	1.002	0.993	1.014	0.988	0.982	0.951	1.003	1.002	1.029	1.016	1.009	1.005	0.979	0.944
Na	0.009	0.004	0.007	0.016	0.005	0.017	0.016	0.013	0.012	0.006	0.005	0.004	0.005	0.008	0.005	0.006
K	b.d.	b.d.	0.000	b.d.	b.d.	b.d.	b.d.	0.001	b.d.	b.d.	b.d.	b.d.	0.000	b.d.	b.d.	0.000
Total	3.999	3.998	3.995	4.000	4.000	3.992	4.003	3.995	4.000	3.995	4.000	3.994	3.995	4.000	3.998	4.000
Mg#	0.958	0.950	0.948	0.938	0.965	0.948	0.964	0.950	0.938	0.951	0.970	0.964	0.960	0.964	0.962	0.964

b.d.: below detection limit, Serp: serpentinite, Ophi: ophicarbonate.

Table a.5: Major element composition of chlorite (representative analyses)

Rock	Serp	Serp	Serp	Serp	Serp	Serp	Serp	Serp	Serp	Serp	Ophi	Ophi	Metabas	Metabas	Metabas	Metabas
Sample	GEI4	GEI4	GEI4	G8	G12	G12	G27	G27	G27	G27	GEI9	GEI9	G30a	G30a	G34	G34
SiO_2	34.0	34.4	34.5	35.1	33.5	33.0	34.0	33.6	33.9	33.9	36.7	34.5	29.2	28.4	27.9	27.7
TiO_2	0.01	0.05	b.d.	0.01	0.03	0.06	0.02	0.03	0.03	0.01	0.03	0.01	0.03	0.03	0.09	0.07
Cr_2O_3	0.93	1.00	1.07	0.04	2.05	1.19	1.73	2.25	1.80	1.80	0.38	0.16	0.09	b.d.	0.01	b.d.
Al_2O_3	12.8	13.0	12.8	13.2	13.8	15.3	13.3	13.3	13.4	13.4	10.7	13.3	20.7	21.5	22.3	22.1
FeO	4.36	4.42	4.10	3.68	3.13	3.47	3.81	4.14	3.88	3.86	4.35	4.43	10.4	11.3	13.0	13.4
MnO	0.04	0.01	0.03	0.08	b.d.	0.01	b.d.	b.d.	b.d.	b.d.	0.00	0.03	0.19	0.20	0.18	0.20
NiO	0.25	0.19	0.18	0.20	0.25	0.18	0.19	0.17	0.18	0.19	0.34	0.25	0.07	0.06	b.d.	0.01
MgO	34.4	34.6	34.7	34.4	33.9	33.5	34.2	33.7	34.1	34.2	34.7	34.2	26.7	25.8	23.9	23.6
CaO	0.01	0.03	0.04	0.03	0.02	0.01	b.d.	b.d.	b.d.	b.d.	0.02	0.03	0.04	0.02	0.05	0.04
Na_2O	b.d.	0.01	0.02	0.01	0.02	0.02	0.02	0.02	0.02	0.01	b.d.	b.d.	b.d.	b.d.	b.d.	b.d.
K_2O	b.d.	b.d.	b.d.	0.01	b.d.	b.d.	b.d.	0.01	b.d.	b.d.	b.d.	0.01	b.d.	b.d.	b.d.	b.d.
H_2O	12.6	12.7	12.7	12.7	12.6	12.6	12.7	12.6	12.7	12.7	12.7	12.6	12.3	12.3	12.2	12.1
Total	99.4	100.5	100.2	99.5	99.3	99.4	99.8	99.9	99.9	100.0	99.9	99.5	99.7	99.7	99.5	99.3
Stoich.	9 O 4 OH	9 O 4 OH	9 O 4 OH	9 O 4 OH	9 O 4 OH	9 O 4 OH	9 O 4 OH	9 O 4 OH	9 O 4 OH	9 O 4 OH	9 O 4 OH	9 O 4 OH	9 O 4 OH	9 O 4 OH	9 O 4 OH	9 O 4 OH
Si	1.621	1.622	1.629	1.657	1.591	1.567	1.608	1.597	1.605	1.603	1.729	1.636	1.421	1.390	1.374	1.373
Ti	0.000	0.002	b.d.	0.000	0.001	0.002	0.001	0.001	0.001	0.000	0.001	0.000	0.001	0.001	0.003	0.003
Cr	0.035	0.037	0.040	0.002	0.077	0.044	0.065	0.085	0.067	0.067	0.014	0.006	0.003	b.d.	0.000	b.d.
Al	0.719	0.721	0.714	0.735	0.773	0.855	0.740	0.745	0.746	0.746	0.594	0.744	1.186	1.242	1.298	1.290
Fe^{2+}	0.174	0.174	0.162	0.145	0.124	0.138	0.151	0.164	0.154	0.153	0.172	0.176	0.421	0.463	0.536	0.557
Mn	0.002	0.000	0.001	0.003	b.d.	0.000	b.d.	b.d.	b.d.	b.d.	0.000	0.001	0.008	0.008	0.007	0.008
Ni	0.009	0.007	0.007	0.008	0.010	0.007	0.007	0.006	0.007	0.007	0.013	0.009	0.003	0.002	b.d.	0.001
Mg	2.440	2.432	2.438	2.421	2.405	2.368	2.415	2.388	2.406	2.413	2.441	2.416	1.938	1.881	1.753	1.745
Ca	0.001	0.002	0.002	0.002	0.001	0.001	b.d.	b.d.	b.d.	b.d.	0.001	0.001	0.002	0.001	0.003	0.002
Na	b.d.	0.001	0.002	0.001	0.002	0.002	0.002	0.002	0.002	0.001	b.d.	b.d.	b.d.	b.d.	b.d.	b.d.
K	b.d.	b.d.	b.d.	0.001	b.d.	b.d.	b.d.	0.000	b.d.	b.d.	b.d.	0.000	b.d.	b.d.	b.d.	b.d.
H	4.000	4.000	4.000	3.998	3.996	4.000	4.000	4.000	4.000	4.000	3.995	3.994	4.000	4.000	4.000	4.000
Total	5.002	4.998	4.995	4.975	4.984	4.983	4.989	4.988	4.988	4.990	4.965	4.989	4.983	4.989	4.974	4.979
Mg#	0.934	0.933	0.938	0.943	0.951	0.945	0.941	0.936	0.940	0.940	0.934	0.932	0.822	0.803	0.766	0.758

b.d.: below detection limit, Serp: serpentinite, Ophi: ophicarbonate, Metabas: metabasite.

Table a.6: Major element composition of epidote and titanite (representative analyses)

Rock	Metabas	Metabas	Metabas	Metabas	Metabas	Metabas	Metabas	Metabas	Metabas	Metabas	Metabas	Metabas	Metabas	Metabas	Metabas
Sample	G30a	G30a	G30a	G30a	G34	G34	G34	G34	G30a	G30a	G30a	G34	G34	G34	G34
Name	Ep	Ep	Ep	Ep	Ep	Ep	Ep	Ep	Ttn	Ttn	Ttn	Ttn	Ttn	Ttn	Ttn
SiO_2	38.10	37.79	38.28	37.49	38.21	37.78	38.62	38.35	30.73	30.54	31.11	30.70	31.09	31.16	30.95
TiO_2	0.08	0.22	0.08	0.19	0.12	0.08	0.12	0.08	34.55	34.95	37.08	37.86	37.73	37.20	37.61
Al_2O_3	27.01	26.04	27.49	25.88	28.25	27.34	28.78	27.09	2.26	2.16	1.49	0.97	1.28	1.37	1.32
Fe_2O_3	9.37	10.60	7.98	10.57	7.27	8.75	6.62	8.55	1.29	0.82	0.56	0.41	0.29	0.58	0.54
MnO	0.02	0.44	0.05	0.25	0.12	0.15	0.12	0.12	0.05	0.03	b.d.	b.d.	b.d.	b.d.	b.d.
MgO	0.01	0.08	0.03	0.12	0.05	0.02	0.03	0.02	1.98	0.88	b.d.	b.d.	b.d.	b.d.	b.d.
CaO	24.07	23.61	24.74	24.28	24.74	24.40	24.37	24.66	29.47	31.31	28.93	29.07	28.99	28.98	28.96
Na_2O	0.01	b.d.	b.d.	0.01	0.02	0.02	b.d.	b.d.	b.d.	0.03	b.d.	0.01	0.02	b.d.	0.01
H_2O	2.09	2.08	2.10	2.08	2.10	2.09	2.11	2.10							
Total	100.76	100.86	100.75	100.86	100.88	100.63	100.77	100.97	100.33	100.71	99.17	99.03	99.41	99.29	99.39
Stoich.	12 O 1 OH	12 O 1 OH	12 O 1 OH	12 O 1 OH	12 O 1 OH	12 O 1 OH	12 O 1 OH	12 O 1 OH	5 O	5 O	5 O	5 O	5 O	5 O	5 O
Si	2.730	2.721	2.736	2.705	2.722	2.712	2.741	2.741	1.001	0.996	1.022	1.012	1.019	1.022	1.015
Ti	0.005	0.012	0.004	0.010	0.006	0.004	0.006	0.004	0.847	0.857	0.916	0.938	0.930	0.918	0.928
Al	2.281	2.210	2.316	2.201	2.372	2.313	2.408	2.282	0.087	0.083	0.058	0.038	0.049	0.053	0.051
Fe^{3+}	0.505	0.574	0.429	0.574	0.390	0.473	0.354	0.460	0.032	0.020	0.014	0.010	0.007	0.014	0.013
Mn	0.001	0.027	0.003	0.015	0.008	0.009	0.007	0.008	0.001	0.001	b.d.	b.d.	b.d.	b.d.	b.d.
Mg	0.001	0.009	0.003	0.013	0.005	0.003	0.003	0.002	0.096	0.043	b.d.	b.d.	b.d.	b.d.	b.d.
Ca	1.848	1.821	1.895	1.877	1.888	1.876	1.853	1.888	1.029	1.094	1.018	1.027	1.018	1.019	1.018
Na	0.001	b.d.	b.d.	0.001	0.002	0.003	b.d.	b.d.	b.d.	0.003	b.d.	0.001	0.002	b.d.	0.001
Total	7.372	7.375	7.387	7.397	7.392	7.393	7.372	7.384	3.093	3.096	3.027	3.026	3.024	3.026	3.025

b.d.: below detection limit, Metabas: metabasite, Ep: epidote, Ttn: titanite.

Appendix B

Thermobarometric study on Dramala harzburgites (Pindos ophiolite, Greece)

Part of Dramala spinel and plagioclase-bearing harzburgites, display porphyroclastic textures. Orthopyroxene and clinopyroxene clasts show exsolution lamellae. The bimodal grain size distribution is associated with a difference in the major element composition of clasts and blasts of clinopyroxene and orthopyroxene (see example for sample PI2 in Fig. b.1a-b). Clinopyroxene clasts show higher Al(Ts) components compared to blasts (Fig. b.1a), while orthopyroxene clasts are enriched in Cr compared to blasts (Fig. b.1b). Moreover, clinopyroxene, orthopyroxene and spinel clasts show pronounced zoning (Fig. b.2a-c). Clinopyroxene and orthopyroxene are characterized by a rimward decrease in Al and Cr (Fig. b.2a-b). Spinel clasts show increasing Al and decreasing Cr contents rimwards (Fig. b.2c). For orthopyroxene, clinopyroxene and spinel clasts, composition at the rim is similar to the one of the corresponding blasts.

As exsolution lamellae in pyroxene clasts and the difference in composition between clasts and blasts reflect cooling, geothermometric calculations were performed on spinel and plagioclase-bearing harzburgites in order to constrain the temperature evolution of the Dramala mantle over time. Thermometry was applied to clast cores, clast rims and blasts. Temperature related to melt impregnation in plagioclase-bearing harzburgites cannot be evaluated because all minerals partially or completely reequilibrated at lower temperature. Geobarometers can be used neither in spinel harzburgites nor in plagioclase-bearing harzburgites, because there is a lack of equilibrium between clinopyroxene and orthopyroxene in these rocks. However, rough pressure estimates can be gained from the plagioclase-spinel and the spinel-garnet facies transitions, and from the position of the depleted peridotite solidus.

In order to apply geothermometry on pyroxene clast cores, their primary composition before exsolution was recalculated. High-quality contrasted backscattered electron images of exsolution lamellae were obtained by secondary electron microscopy. The percentage of exsolution lamellae was determined using the Image SXM program (v. 1.74, July 2004, Steve Barrett). Primary composition was recalculated considering the percentage of exsolution lamellae and of the host, and their respective major element compositions obtained by electron microprobe analysis.

APPLICATION OF THERMOBAROMETERS

Different geothermometers were applied: (i) The two pyroxenes thermometer ($T_{2Px\text{-}BK90}$) and the Ca-in-orthopyroxene thermometer ($T_{Ca\text{-}opx\text{-}BK90}$) after Brey & Köhler (1990), which are experimentally calibrated between 10 and 60 kbar for four-phase lherzolites. (ii) The Seitz et al. (1999) thermometer based on Cr partitioning between orthopyroxene and clinopyroxene ($T_{Cr\text{-}cpx\text{-}opx\text{-}S99}$). (iii) The Witt-Eickschen & Seck (1991) thermometer based on Al and Cr contents in orthopyroxene ($T_{Al,\ Cr\text{-}opx\text{-}WS91}$). Representative thermometric results are presented in Table b.1 and in Figure b.3.

For clast rims and blasts, all geothermometers cited above give concordant results, while for clast cores major differences are observed. The Ca-in-orthopyroxene thermometer of Brey & Köhler (1990) and the Cr-partitioning between clinopyroxene and orthopyroxene thermometer of

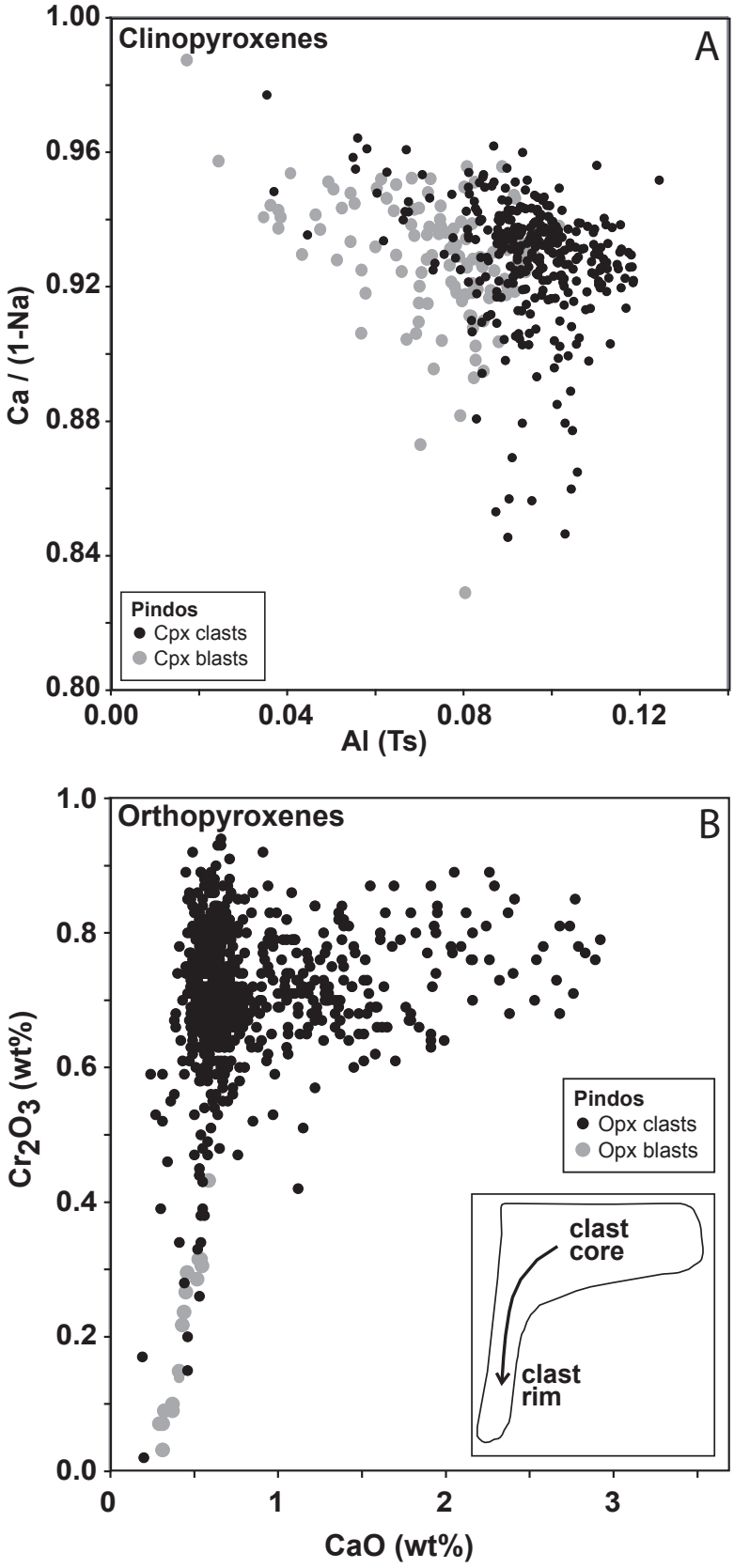


Fig. b.1: (A) Compositional variations of the clinopyroxene clasts and blasts of sample PI2. (B) Compositional variations of the orthopyroxene clasts and blasts of sample PI2.

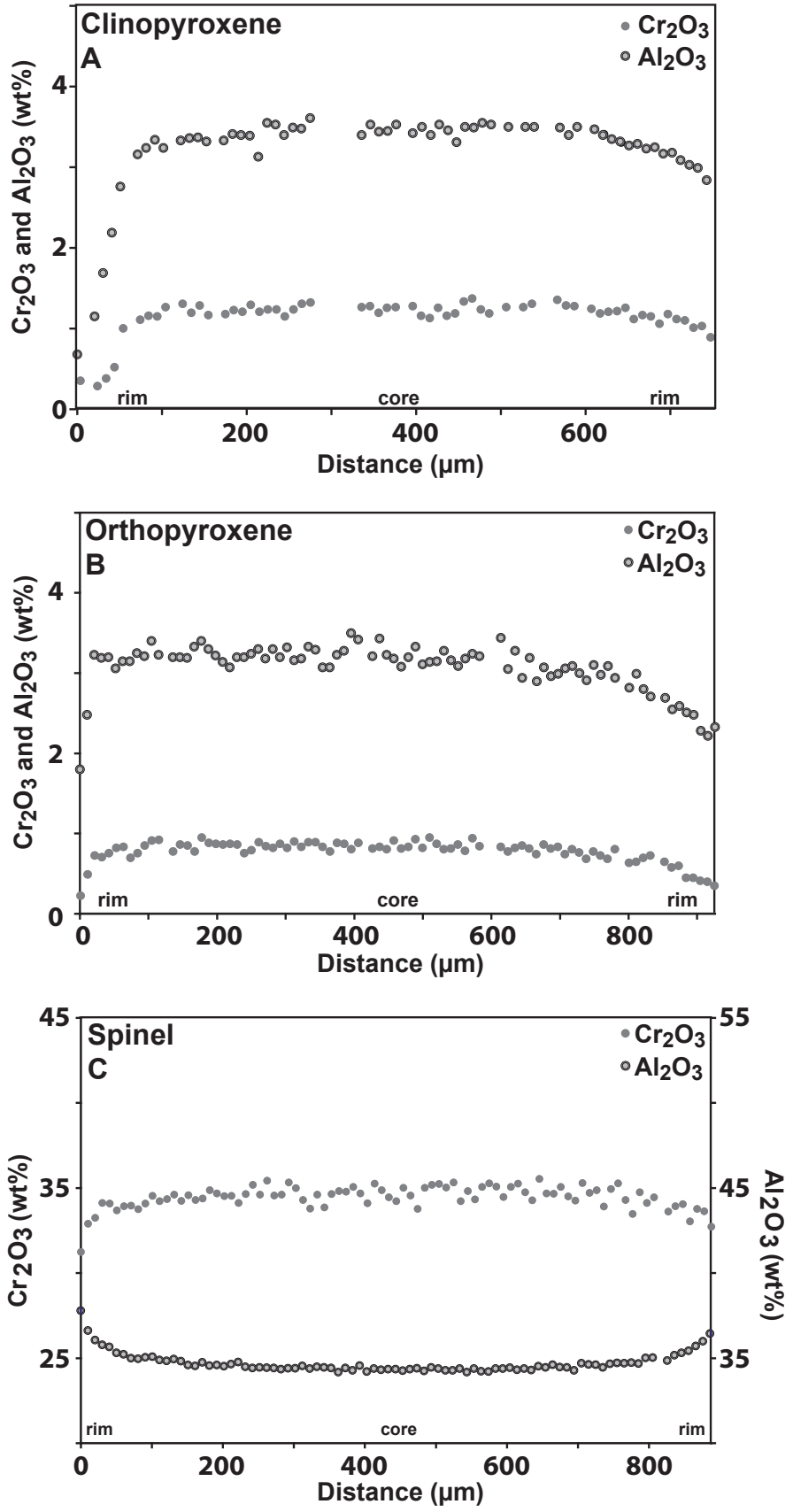


Fig. b.2: Cr_2O_3 and Al_2O_3 (wt. %) zoning in clasts from sample PI2: (A) clinopyroxene, (B) orthopyroxene and (C) spinel.

Seitz et al. (1999) give the highest temperatures. The two pyroxenes thermometer of Brey & Köhler (1990) and the Al and Cr contents in orthopyroxene thermometer of Witt-Eickschen & Seck (1991) systematically give lower temperatures (Table b.1). This difference is probably due to the lack of equilibrium between orthopyroxene and clinopyroxene clast cores, which can be tested in a Ca-in-orthopyroxene versus Ca-in-clinopyroxene plot (Brey & Köhler, 1990). Results given in the following text refer to the Ca-in-orthopyroxene thermometer of Brey & Köhler (1990) and are presented in Figure b.3.

P-T EVOLUTION OF THE DRAMALA HARZBURGITES

Thermometric calculations and rough pressure constraints yield ~1160-1280°C and ~0.4-1.9 GPa for the initial high temperature stage (Fig. b.3) preserved in orthopyroxene clast cores. This stage certainly corresponds to high temperature equilibration of the rock after the end of partial melting, which generated the spinel harzburgites. This high temperature stage was followed by dynamic recrystallization, which led to the observed porphyroclastic texture. This deformation was followed by the N-MORB melt impregnation (refer to chapter 3), which led to the crystallization of clinopyroxene in spinel harzburgites, which appears undeformed under the optical microscope. In the plagioclase-bearing harzburgites, the plagioclase and clinopyroxene from the dykelets are aligned along the foliation planes, but are undeformed, which suggests that deformation was not active during ultra-depleted melt impregnation (refer to chapter 3) in these rocks. Finally, the rocks were subject to cooling down to ~790-990°C and ~0.2-1.4 GPa, which is preserved in orthopyroxene clast rims and blasts, and could correspond to the moving of the harzburgites off the axis of the mid-ocean ridge.

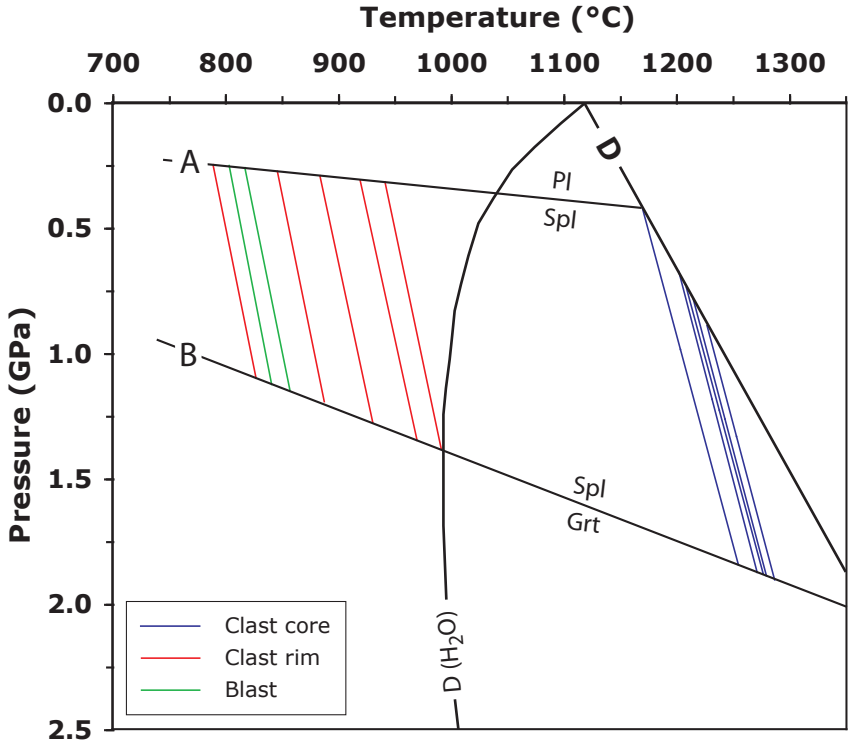


Fig. b.3: Selected temperature estimates for the Dramala harzburgites for the Ca-in-orthopyroxene thermometer after Brey & Köhler (1990). Maximum pressure is constrained by the transition of the spinel to garnet peridotite facies, and minimum pressure by the transition of the plagioclase to spinel peridotite facies or by the depleted peridotite solidus (D). Transition line between plagioclase and spinel peridotite facies (A) calculated for the Othris peridotites by Dijkstra et al. (2001). Transition from spinel to garnet peridotite facies (B), depleted peridotite solidus (D) and depleted peridotite solidus with H_2O ($D(H_2O)$) after Juteau & Maury (1999).

Table b.1: Results of thermometric calculations for Pindos harzburgites

Rock	Sample	Type	$T_{2Px\text{-}BK90}$	$T_{Ca\text{-}opx\text{-}BK90}$	$T_{Cr\text{-}cpx\text{-}opx\text{-}S99}$	$T_{Al,Cr\text{-}opx\text{-}WS91}$
Spl hrz	PI2	clast core	965 ± 6	1206 ± 58	1274 ± 202	1007 ± 47
	PI2	clast rim	784 ± 102	877 ± 17	704 ± 1	863 ± 67
	PI2	blast	776 ± 33	836 ± 43	816 ± 204	779 ± 70
Spl hrz	PIA27	clast core	-	1220 ± 2	-	-
	PIA27	clast rim	-	918 ± 17	-	-
Spl hrz	PIA44	clast core	1003 ± 7	1222 ± 66	-	913 ± 78
	PIA44	clast rim	714 ± 8	972 ± 16	-	836 ± 25
Pl-bear hrz	PIA120	clast core	820 ± 3	1235 ± 54	1159 ± 115	1079 ± 54
	PIA120	clast rim	750 ± 19	953 ± 50	-	787 ± 57
Pl-bear hrz	PIA109	clast core	-	1228 ± 44	-	-
	PIA109	clast rim	819 ± 17	825 ± 46	-	746 ± 120
	PIA109	blast	772 ± 37	836 ± 34	-	-

Temperatures calculated at $P_{assumed}$ = 1.0 GPa. Errors = 1σ. BK90: Brey & Köhler (1990), S99: Seitz et al. (1999), WS91: Witt-Eickschen & Seck (1991). Spl hrz: spinel harzburgite, Pl-bear hrz: plagioclase-bearing harzburgite.

Li zoning in orthopyroxene

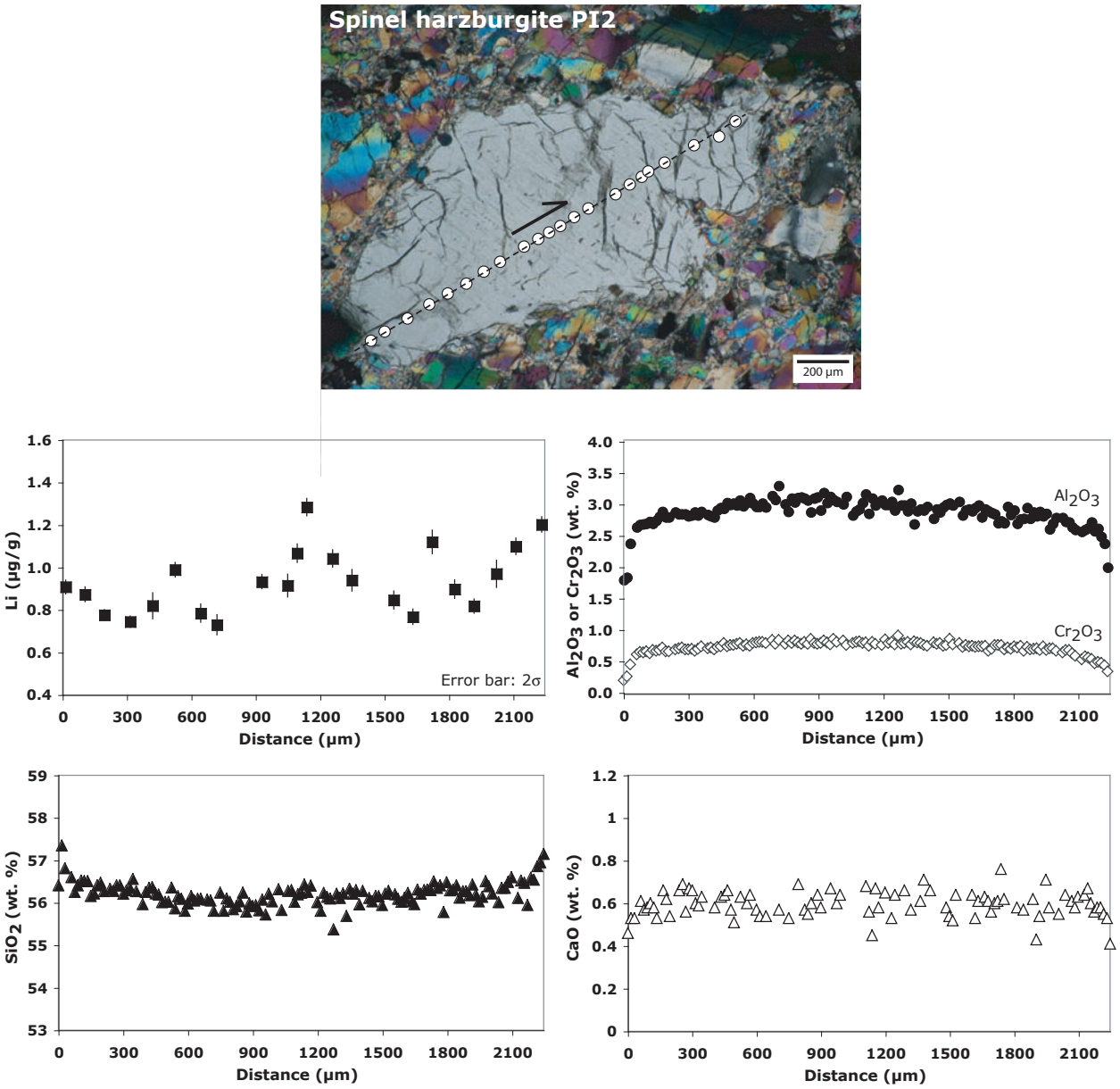


Fig. c.1: Peculiar Li zoning found in an orthopyroxene clast from spinel harzburgite PI2 (Pindos ophiolite, Greece), where clinopyroxene exsolution lamellae are frequent. Clinopyroxene exsolution lamellae were deleted in the CaO (wt. %) profile.

Four profiles were performed by secondary ion mass spectrometry (SIMS) on four different orthopyroxene clasts from two fresh spinel harzburgites (sample PI2, Pindos ophiolite, and sample VOU2, Vourinos ophiolite). One SIMS analysis takes 15 minutes. For this reason, a limited number of profiles were done, because about 30 samples were analyzed in detail for this thesis (electron microprobe, SIMS, LA-ICPMS, micro-Raman).

In samples PI2 and VOU2, the two profiles obtained on the SIMS for each sample were different. One profile shows no variation in its Li content, except for a Li increase or decrease rimward (50-100 μm). The second profile was more complex and present two or three Li peaks through the grain (Fig. c.1). This variation in the Li content of orthopyroxene could be related to the presence of exsolution lamellae of clinopyroxene. This zoning could result from a Li diffusion after the formation of the exsolution lamellae, because Li preferentially diffuses into clinopyroxene at high temperature (Coogan et al., 2005; Jeffcoate et al., 2007). Alternatively, this variation could be due to the ^{Li}Cpx/Opx partition coefficient during the formation of the exsolution lamellae.

The Li contents presented in the previous chapters of this thesis for orthopyroxene were shot in the centre of the grains.

Appendix D

Bulk rock fusion using an iridium-strip heater: Preliminary results

INTRODUCTION

Bulk rock fusion using an iridium strip heater was first proposed by Nicholls in 1974. This technique allows the preparation of homogeneous glass beads by direct fusion of rock powders. These glasses can later be quantitatively analyzed with current analytical methods. No sample preparation is needed for this technique. For this reason, we decided to use this method to produce glasses, where bulk Li and B contents of peridotites could be analyzed by secondary ion mass spectrometry (SIMS) or laser ablation inductively coupled plasma mass spectrometry (LA-ICP-MS). The lack of sample preparation will avoid any light element contamination, which can be caused during sample preparation for conventional analytical techniques (inductively coupled plasma mass spectrometry, thermal ionization mass spectrometry), where column chemistry is used. This technique is also quicker than the existing ones. Nicholls (1974) obtained homogeneous glasses from many mafic rocks, but mentioned the presence of quenched crystals in rare heterogeneous glasses from ultramafic samples. The challenge was to produce homogeneous glasses from peridotite powders, and to avoid any loss of light element during heating and fusion, because Li and B are moderately volatile (McDonough & Sun, 1995).

SAMPLE PREPARATION AND FUSION TECHNIQUE

Rock powders were obtained in a tungsten mill, from harzburgites from the Pindos and Vourinos ophiolites. Rock powder (< 400 mg) was placed on an iridium-strip as shown in Figure c.1. Iridium is used because it has a high melting point around 2410 °C, and because it normally does not absorb iron from the sample (Nicholls, 1974). The iridium-strip heater was placed in a chamber, where pre-vacuum was achieved, before flushing the chamber with an argon gas (Fig. d.1). The use of the argon atmosphere is supposed to avoid oxidation of iron during fusion. This would potentially allow the determination of the Fe^{2+}/Fe^{3+} ratio in the glass.

During the first attempts, the temperature was not calibrated. However, we later estimated that the melting temperature was probably > 1400 °C. The strip was heated until all the powder was transformed to glass during approximately 10-15 seconds. However in some cases, it was not possible to melt chromite which had not been completely powdered during crushing. After fusion, the melt was quenched by turning off the power and simultaneously by applying a jet of argon.

Glasses were mounted in an epoxy resin (Fig. d.2), and prepared following the procedure of Marschall & Ludwig (2004) for thin sections, in order to avoid any boron contamination during sample preparation for analysis.

RESULTS

Heterogeneous glass

All ultramafic glasses obtained are heterogeneous and present quenched crystals. These crystals can be observed with a binocular microscope, and are easily mapped by SEM (secondary electron microscopy; Fig. d.3). Glasses

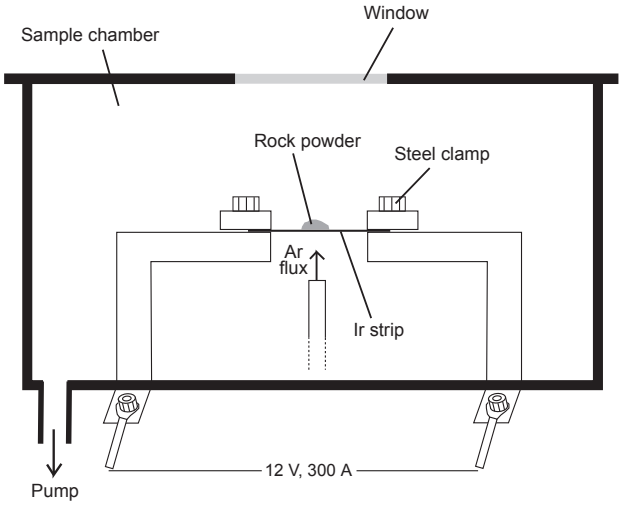


Fig. d.1: Schematic representation of the iridium-strip heater used to prepare glasses by direct fusion of rock powder. The size of the iridium-strip is approximately 20x8 mm with a thickness of 0.15 mm.

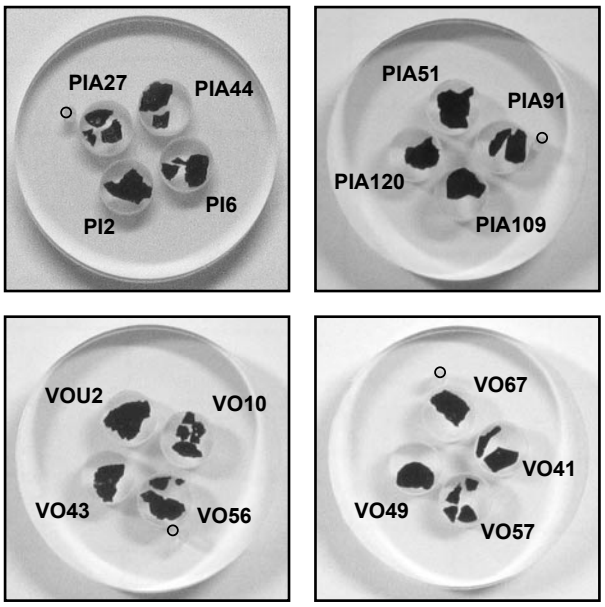


Fig. d.2: Glasses mounted in the epoxy resin.

present a spinifex texture, which resembles the one of komatiites. The glass matrix appears dark on backscattered electron images, while the crystals are brighter (Fig. d.3). These images also show that gas was produced during melting of the most serpentinized samples (PI6, PIA27, PIA44; Fig. d.3).

Major element composition

Elemental maps obtained on the electron microprobe show that Si, Al, Fe and Ca are concentrated in the bright crystals, while Mg stayed in the matrix (Fig. d.4). The composition of the dark matrix is stoechiometrically similar to forsterite (Table d.1), while the composition of the bright crystals is more variable but seems to correspond to an orthopyroxene solid solution (Table d.2). Microprobe analyses also show this chemical heterogeneity in the major elements. The composition of the whole rocks obtained by XRF always plot in between the composition of the host and the crystals (Fig. d.5).

Li and B composition

The heterogeneous glasses were measured by LA-ICP-MS with the largest spot size of 120 μm, in order to potentially measure a similar quantity of crystals and host. The results obtained are similar to the one obtained by solution ICP-MS for Li, and by prompt gamma neutron activation analysis for B (Fig. d.6). The formation of the quenched crystals probably fractionated Li and B between the dark matrix and the bright crystals, because Brenan et al. (1998a) showed that olivine and orthopyroxene have different mineral/melt partition coefficients during melting in the ultramafic system. They give $^{ol/melt}D_{Li}$ = 0.13-0.35, $^{opx/melt}D_{Li}$ = 0.20, $^{ol/melt}D_{B}$ = 0.003-0.008 and $^{ol/melt}D_{B}$ = 0.018. However, as the crystals are very small, we can consider that the use of a large spot size of 120 μm during measurement by LA-ICP-MS gives a representative value of the Li and B content of the whole rock.

This iridium-strip heater method is still in development in Neuchâtel. Improvements and detailed results will be published in 2008 by Flurin Vils.

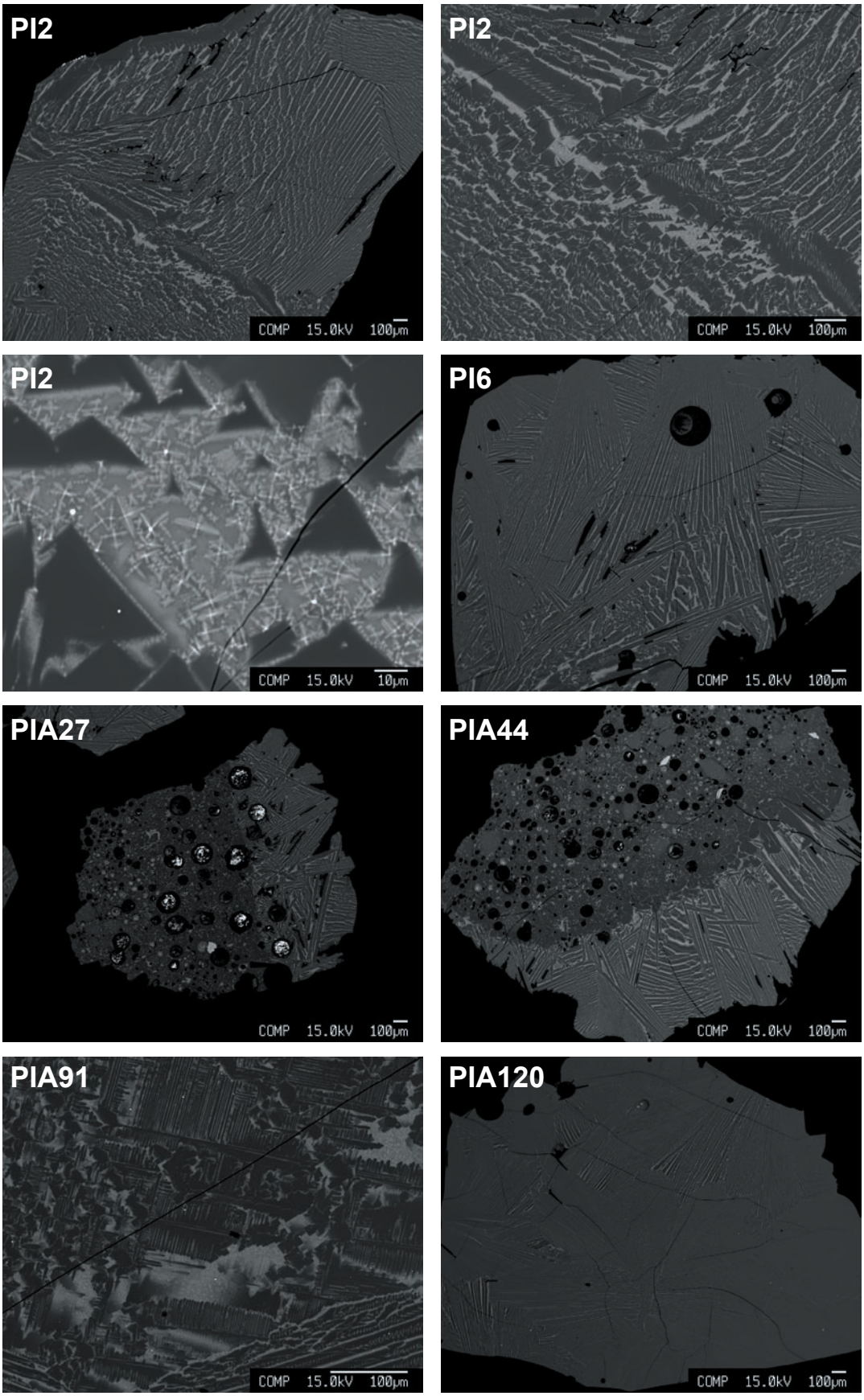


Fig. d.3: Backscattered electron images of the Pindos glasses. The spinifex texture is easily recognizable.

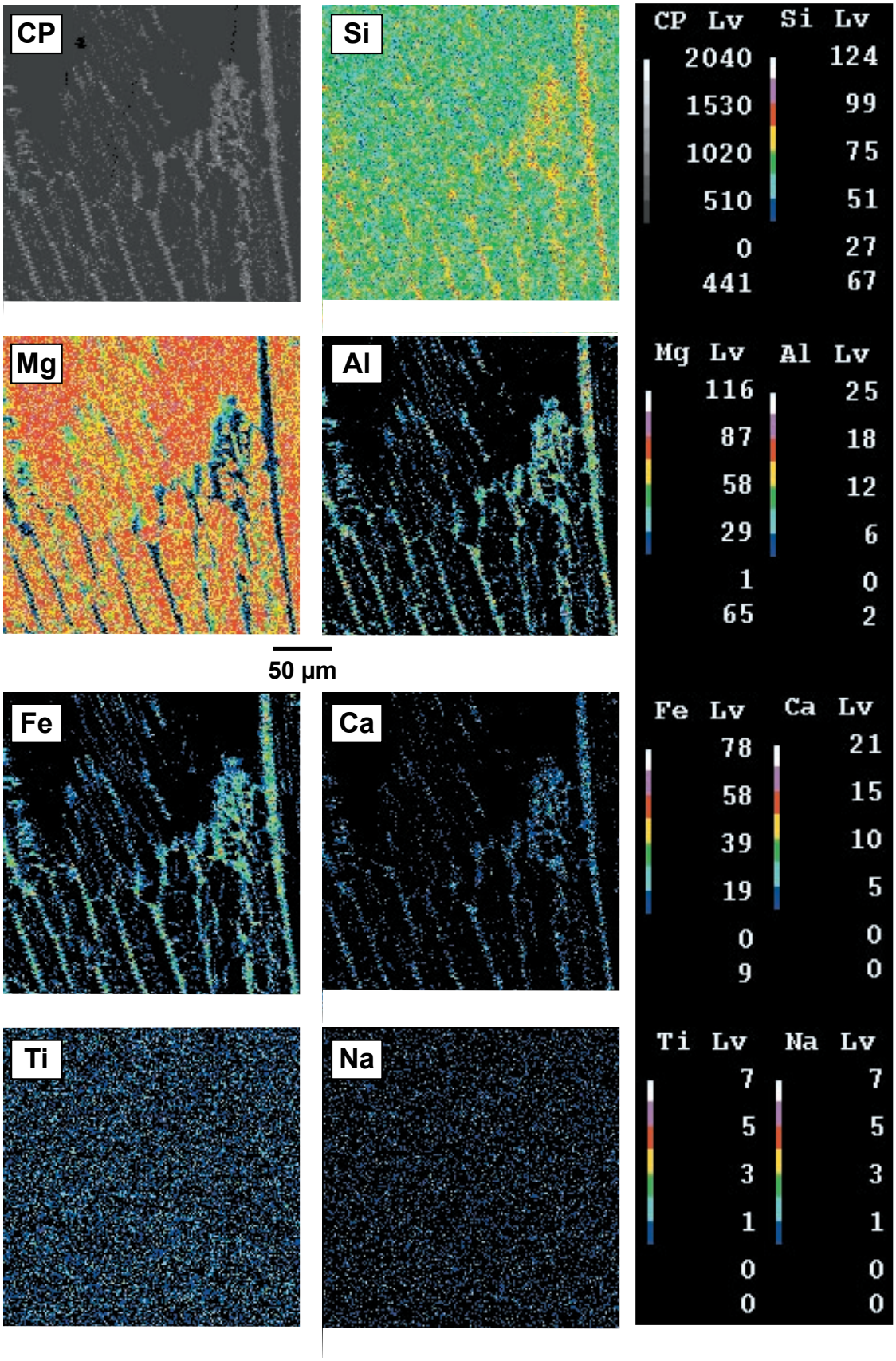


Fig. d.4: Elemental maps of the glasses obtained by electron microprobe illustrating the chemical heterogeneity of the glasses.

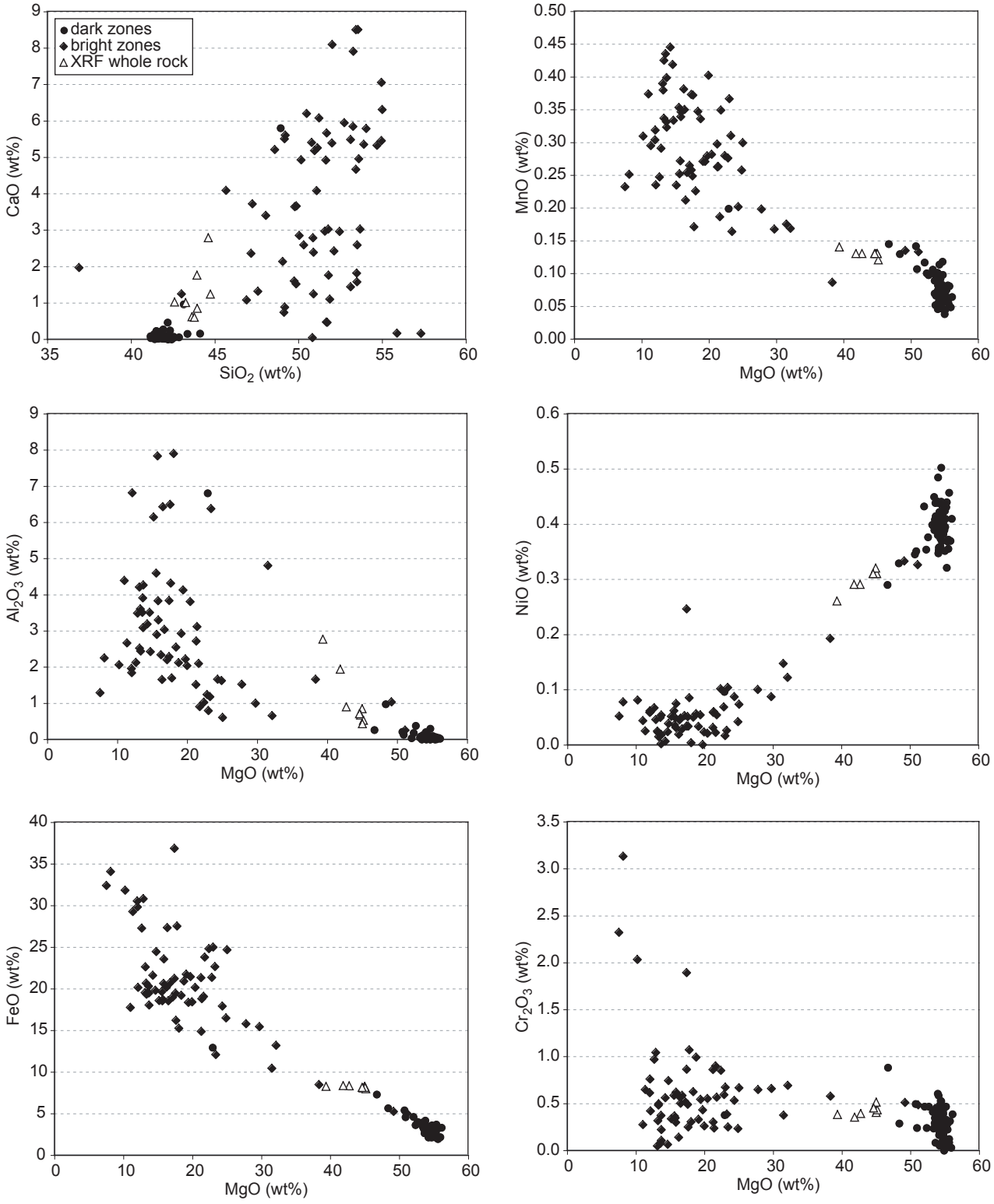


Fig. d.5: Comparison between the major element compositions of the dark (~forsterite) and bright zones (~orthopyroxene solid solution), and the composition of the whole rocks obtained by X-ray fluorescence.

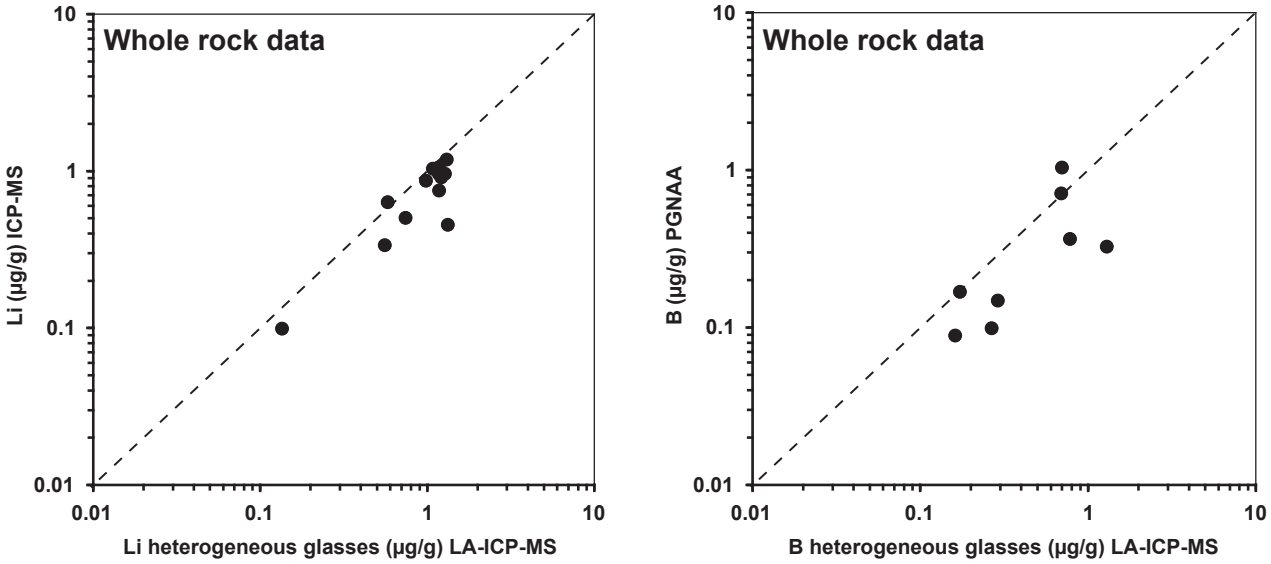


Fig. d.6: Comparison between the Li and B contents obtained on the different heterogeneous glasses and the Li and B contents obtained by conventional methods (ICP-MS for Li and prompt gamma neutron activation analysis for B).

Table D.1: Representative microprobe analyses of the dark zones

Sample	PI2	PI6	PIA27	PIA44	PIA120	PIA109	PIA51	VO41	VO57	VO67
SiO2	41.71	41.59	43.36	41.81	41.50	41.81	41.90	41.23	42.32	41.98
TiO2	0.00	0.01	0.00	0.00	0.00	0.00	0.00	0.00	0.00	0.00
Cr2O3	0.25	0.44	0.50	0.28	0.59	0.26	0.28	0.39	0.06	0.07
Al2O3	0.09	0.06	0.21	0.06	0.21	0.06	0.04	0.04	0.00	0.02
FeO	2.51	2.60	5.42	3.16	3.47	2.85	3.12	3.15	2.10	2.29
MnO	0.04	0.06	0.14	0.08	0.09	0.06	0.07	0.07	0.06	0.04
NiO	0.35	0.39	0.35	0.36	0.41	0.36	0.42	0.44	0.32	0.39
MgO	55.07	54.76	50.71	54.19	54.06	54.46	55.07	54.17	55.36	54.99
CaO	0.06	0.05	0.15	0.06	0.23	0.07	0.09	0.07	0.07	0.02
Na2O	0.00	0.01	0.02	0.00	0.00	0.00	0.00	0.00	0.04	0.01
K2O	0.00	0.00	0.00	0.00	0.00	0.00	0.00	0.00	0.00	0.00
Total	100.10	99.97	100.87	99.99	100.55	99.93	100.99	99.56	100.33	99.82

Table D.2: Representative microprobe analyses of the bright zones

Sample	PIA91	PI6	PIA27	PIA44	PIA120	PIA109	PIA51	VO41	VO57	VO67
SiO2	52.02	53.52	52.46	53.49	48.06	50.97	51.80	53.12	49.19	51.67
TiO2	0.03	0.01	0.02	0.01	0.09	0.12	0.02	0.01	0.02	0.01
Cr2O3	0.56	0.43	0.33	0.90	0.37	0.49	0.64	0.53	0.85	0.69
Al2O3	3.18	2.21	2.92	2.09	4.80	6.49	1.51	1.65	1.02	0.65
FeO	21.59	21.43	21.70	19.05	10.41	19.43	15.75	17.88	24.78	13.18
MnO	0.44	0.28	0.27	0.19	0.17	0.25	0.20	0.20	0.28	0.17
NiO	0.01	0.00	0.03	0.02	0.15	0.05	0.10	0.09	0.10	0.12
MgO	14.30	19.76	19.15	21.64	31.54	17.56	27.82	24.37	22.40	32.14
CaO	8.09	2.58	2.95	1.81	3.39	5.17	1.75	1.43	0.88	0.46
Na2O	0.00	0.11	0.20	0.03	0.39	0.12	0.05	0.11	0.07	0.02
K2O	0.00	0.01	0.00	0.01	0.00	0.00	0.01	0.07	0.00	0.00
Total	100.22	100.35	100.03	99.24	99.37	100.64	99.65	99.45	99.59	99.12

Appendix E

Mineralogical composition of the studied samples

Table E.1 Mineralogy of the studied samples - Pindos ophiolite

	PI2	PIA91	PIA27	PI6	PIA44	PIA120	PIA109	PIA51
Orthopyroxene	x	x	x	x	x	x	x	x
Clinopyroxene	x	x		x	x	x	x	x
Olivine	x	x	x	x	x	x	x	x
Spinel	x	x	x	x	x	x	x	x
Plagioclase						x	x	x
Edenitic hornblende			x					
Pargasite						x	x	
Serpentine			x	x	x	x		
Tremolite			x	x	x			
Anthophyllite			x	x				
Talc			x					
Chlorite			x			x		
Vuagnatite						x		
Natrolite						x		
Pectolite						x		

Table E.2 Mineralogy of the studied samples - Geisspfad ultramafic body

Ultramafics	G3	G4	G8	G11	G12	G26	G27	GEI4	GEI9
Olivine	x		x	x	x	x	x	x	
Diopside		x		x		x	x		x
Serpentine	x	x		x	x	x	x	x	x
Tremolite	x	x	x	x	x	x	x	x	x
Chlorite			x	x	x	x	x	x	x
Talc			x						
Calcite	x	x							x
Dolomite	x	x							
Ilmenite								x	

Metabasites	G30a	G30b	G31	G34
Tschermakitic hornblende	x	x		x
Epidote	x	x		x
Titanite	x	x		x
Chlorite	x	x	x	x
Calcite	x	x		
Dolomite			x	
Tremolite			x	

Gneiss	G32a	G32b	G36
Quartz	x	x	x
Albite	x		x
Alkali feldspar	x	x	
Biotite	x	x	
Muscovite	x	x	
Chlorite	x		x
Garnet			x
Apatite			x
Epidote		x	x
Titanite	x		
Ilmenite			x

References

Agranier, A., Lee, C.-T.A., Li, Z.-X.A., Leeman, W.P. (2007). Fluid mobile element budgets in serpentinized oceanic lithospheric mantle: Insights from B, As, Li, Pb, PGEs and Os isotopes in the Feather River Ophiolite, California. Chemical Geology, doi: 10.1016/j.chemgeo.2007.08.008.

Agrinier, P., Mével, C., Bosch, D., Javoy, M. (1993). Metasomatic hydrous fluids in amphibole peridotites from Zabargad Island (Red Sea). Earth and Planetary Science Letters 120, 187-205.

Allan, J.F., Dick, H.J.B. (1996). Cr-rich spinel as a tracer for melt migration and melt-wall rock interaction in the mantle: Hess Deep, leg 147. Proceedings of the Ocean Drilling Program, Scientific Results 147, 157-172.

Allen, D.E., Seyfried, W.E.J. (2003). Compositional controls on vent fluids from ultramafic-hosted hydrothermal systems at mid-ocean ridges: An experimental study at 400°C, 500 bars. Geochimica et Cosmochimica Acta 67, 1531-1542.

Allen, D.E., Seyfried, W.E.J. (2004). Serpentinization and heat generation: Constraints from Lost City and Rainbow hydrothermal systems. Geochimica et Cosmochimica Acta 68, 1347-1354.

Anderson, D.L., Kasztovszky, Zs. (2004). Application of PGAA with neutron beam. In: Molnár, G.L. (Ed.), Handbook of prompt gamma activation analysis with neutron beams. Springer: Kluwer Academic Publisher, 148-152.

Arai, S. (1994). Characterization of spinel peridotites by olivine spinel compositional relationships – Review and interpretation. Chemical Geology 113, 191-204.

Arai, S., Matsukage, K. (1996). Petrology of the gabbro-troctolite-peridotite complex from Hess Deep, Equatorial Pacific: Implications for mantle-melt interaction within the oceanic lithosphere. Proceedings of the Ocean Drilling Program, Scientific Results 147, 135-155.

Arai, S., Takemoto, Y. (2007). Mantle wehrlite from Hess Deep as a crystal cumulate from an ultra-depleted primary melt in East Pacific Rise. Geophysical Research Letters 34, L08302, doi.: 10.1029/2006GL029198.

Aubouin, J. (1959). Contribution à l'étude géologique de la Grèce Septentrionale. Athènes: Annales géologiques des Pays Helléniques.

Auzende, A.-L., Daniel, I., Reynard, B., Lemaire, C., Guyot, F. (2004): High-pressure behaviour of serpentine minerals: a Raman spectroscopic study. Physics and Chemistry of Minerals 31, 269-277.

Ayers, J. (1998). Trace element modeling of aqueous fluid - peridotite interaction in the mantle wedge of subduction zones. Contributions to Mineralogy and Petrology 132, 390-404.

Bach, W., Alt, J.C., Niu, Y., Humphris, S.E., Erzinger, J., Dick, H.J.B. (2001). The geochemical consequences of late-stage low-grade alteration of lower oceanic crust at the SW Indian Ridge: Results from ODP Hole 735B (Leg 176). Geochimica et Cosmochimica Acta 65, 3267-3287.

Bach, W., Garrido, C.J., Paulick, H., Harvey, J., Rosner, M. (2004). Seawater-peridotite interactions: First insights from ODP Leg 209, MAR 15°N. Geochemistry Geophysics Geosystems 5, doi: 10.1029/2004GC000744.

Bach, W., Paulick, H., Garrido, C.J., Ildefonse, B., Meurer, W.P., Humphris, S.E. (2006). Unraveling the sequence of serpentinization reactions: petrography, mineral chemistry, and petrophysics of serpentinites from MAR 15°N (ODP Leg 209, Site 1274). Geophysical Research Letters 33, doi: 10.1029/2006GL025681.

Banks, D.A., Yardley, B.W.D., Campell, A.R., Jarvis, K.E. (1994). REE composition of an aqueous magmatic fluid: A fluid inclusion study from the Capitan Pluton, New Mexico, USA. Chemical Geology 110, 299-314.

Barnes, J.D., Selverstone, J., Sharp, Z.D. (2006). Chlorine isotope chemistry of serpentinites from Elba, Italy, as an indicator of fluid source and subsequent tectonic history. Geochemistry, Geophysics and Geosystems 7(8), doi: 10.1029/2006GC001296.

Barth, M.G., Mason, P.R.D., Davies, G.R., Dijkstra, A.H., Drury, M.R. (2003). Geochemistry of the Othris Ophiolite, Greece: Evidence for Refertilization? Journal of Petrology 44, 1759-1785.

Barth, M.G., Mason, P.R.D., Davies, G.R., Drury, M.R. (2007). The Othris ophiolite, Greece: A snapshot of subduction initiation at a mid-ocean ridge. Lithos, in press, doi: 10.1016/j.lithos.200706.018.

Bebout, G.E., Ryan, J.G., Leeman, W.P. (1993). B-Be systematics in subduction-related metamorphic rocks: Characterization of the subducted component. Geochimica et Cosmochimica Acta 57, 2227-2237.

Bebout, G.E., Ryan, J.G., Leeman, W.P., Bebout, A.E. (1999). Fractionation of trace elements by subduction-zone metamorphism - effect of convergent-margin thermal evolution. Earth and Planetary Science Letters 171, 63-81.

Beccaluva, L., Coltorti, M., Giunta, G., Siena, F. (2004). Tethyan vs. Cordilleran ophiolites: a reappraisal of distinctive tectono-magmatic features of supra-subduction complexes in relation to the subduction mode. Tectonophysics 393, 163-174.

Beccaluva, L., Coltorti, M., Saccani, E., Siena, F. (2005). Magma generation and crustal accretion as evidenced by supra-subduction ophiolites of the Albanide-Hellenide Subpelagonian zone. The Island Arc 14, 551-563.

Beccaluva, L., Ohnenstetter, D., Ohnenstetter, M., Paupy, A. (1984). Two magmatic series with island arc affinities within the Vourinos ophiolite. Contributions to Mineralogy and Petrology 85, 253-271.

Bédard, J.H. (1994). A procedure for calculating the equilibrium distribution of trace-elements among the minerals of cumulate rocks, and the concentration of trace-elements in the coexisting liquids. Chemical Geology 118 (1-4), 143-153.

Benoît, M., Ceuleneer, G., Polve, M. (1999). The remelting of hydrothermally altered peridotite at mid-ocean ridges by intruding mantle diapirs. Nature 402, 514-518.

Benton, L.D., Ryan, J.G., Savov, I.P. (2004). Lithium abundance and isotope systematics of forearc serpentinites, Conical Seamount, Mariana forearc: Insights into the mechanics of slab-mantle exchange during subduction. Geochemistry, Geophysics and Geosystems 5, doi: 10.1029/2004GC000708.

Benton, L.D., Ryan, J.G., Tera, F. (2001). Boron isotope systematics of slab fluids as inferred from a serpentine seamount, Mariana forearc. Earth and Planetary Science Letters 187, 273-282.

Bizimis, M., Salters, V.J.M., Bonatti, E. (2000). Trace and REE content of clinopyroxenes from supra-subduction zone peridotites. Implications for melting and enrichment processes in island arcs. Chemical Geology 165, 67-85.

Bloomer, S.H., Natland, J.H., Fischer, R.L. (1989). Mineral relationships in gabbroic rocks from fracture zones of Indian Ocean ridges: evidence for extensive fractionation, parental diversity, and boundary-layer recrystallization. In: Saunders, A. D., Norry, M.J. (ed.) Magmatism in the Ocean Basins. London: Geological Society of London Special Publication 42, 107-124.

Blundy, J., Dalton, J. (2000). Experimental comparison of trace element partitioning between clinopyroxene and melt in carbonate and silicate systems, and implications for mantle metasomatism. Contributions to Mineralogy and Petrology 139, 356-371.

Bodinier, J.L. (1988). Geochemistry and petrogenesis of the Lanzo peridotite body, western Alps. Tectonophysics 149, 67-88.

Bodinier, J.-L., Godard, M. (2004). Orogenic, ophiolitic, and abyssal peridotites. In: R.W. Carlson, H.D. Holland and K.K. Turekian (Editors), Treatise on Geochemistry Volume 2: The mantle and core. Elsevier, Oxford, 103-170.

Boillot, G., Grimaud, S., Mauffret, A., Mougenot, D., Kornprobst, J., Mergoildaniel, J., Torrent, G. (1980). Ocean-continent boundary off the Iberian margin – a serpentinite diapir west of the Galicia Bank. Earth and Planetary Science Letters 48, 23-34.

Bonatti, E., Lawrence, J.R., Morandi, N. (1984). Serpentinization of oceanic peridotites: temperature dependence of mineralogy and boron content. Earth and Planetary Science Letters 70, 88-94.

Boschi, C., Dini, A., Früh-Green, G.L., Kelley, D.S. (2008). Isotopic and element exchange during serpentinization and metasomatism at the Atlantis Massif (MAR 30°N): Insights from B and Sr isotope data. Geochimica et Cosmochimica Acta, doi: 10.1016/j.gca.2008.01.013.

Boudier, F., Ceuleneer, G., Nicolas, A. (1988). Shear zones, thrusts and related magmatism in the Oman ophiolite – initiation of thrusting on an oceanic ridge. Tectonophysics 151, 275-296.

Bouman, C. (2004). Lithium isotope systematics at subduction zones. Amsterdam: Vrije Universiteit - Faculteit der Aard- en Levenswetenschappen.

Bouman, C., Elliott, T., Vroon, P.Z. (2004). Lithium inputs to subduction zones. Chemical Geology 212, 59-79.

Brenan, J.M., Neroda, E., Lundstrom, C.C., Shaw, H.F., Ryerson, F.J., Phinney, D.L. (1998a). Behaviour of boron, beryllium, and lithium during melting and crystallization: Constraints from mineral-melt partitioning experiments. Geochimica et Cosmochimica Acta 62, 2129-2141.

Brenan, J.M., Ryerson, F.J., Shaw, H.F. (1998b). The role of aqueous fluids in the slab-to-mantle transfer of boron, beryllium, and lithium during subduction: Experiments and models. Geochimica et Cosmochimica Acta 62, 3337-3347.

Brey, G.P., Köhler, T. (1990). Geothermobarometry in Four-phase Lherzolites II. New Thermobarometers, and Practical Assessment of Existing Thermobarometers. Journal of Petrology 31, 1353-1378.

Broeker, W.S., Peng, T.-H. (1982). Tracers in the sea. New York (USA): Lamont-Doherty Geological Observatory.

Bromiley, G.D., Pawley, A.R. (2003). The stability of antigorite in the systems MgO-SiO2-H2O (MSH) and MgO-Al2O3-SiO2-H2O (MASH): The effects of Al^{3+} substitution on high-pressure stability. American Mineralogist 88, 99-108.

Brooker, R.A., James, R.H., Blundy, J.D. (2004). Trace elements and Li isotope systematics in Zabargad peridotites: evidence of ancient subduction processes in the Red Sea mantle. Chemical Geology 212, 179-204.

Burkhard, D.J.M., O'Neil, J.R. (1988). Contrasting serpentinization processes in the eastern Central Alps. Contributions to Mineralogy and Petrology 99, 498-506.

Capedri, S., Venturelli, G., Bébien, J., Toscani, L. (1981). Low and high-Ti ophiolites in northern Pindos: petrological and geological constraints. Bulletin Volcanologique 44, 439-444.

Capedri, S., Venturelli, G., Bocchi, G., Dostal, J., Garuti, G., Rossi, A. (1980). The geochemistry and petrogenesis of an ophiolitic sequence from Pindos, Greece. Contributions to Mineralogy and Petrology 74, 189-200.

Capedri, S., Venturelli, G., Toscani, L. (1982). Petrology of an ophiolitic cumulate sequence from Pindos, Greece. Geological Journal 17, 223-242.

Chan, L.-H., Alt, J.C., Teagle, D.A.H. (2002): Lithium and lithium isotope profiles through the upper oceanic crust: a study of seawater-basalt exchange at ODP Sites 504B and 896A. Earth and Planetary Science Letters 201, 187-201.

Chan, L.-H., Edmond, J.M., Thompson, G., Gillis, K. (1992). Lithium isotopic composition of submarine basalts: implications for the lithium cycle in the oceans. Earth and Planetary Science Letters 108, 151-160.

Chan, L.-H., Kastner, M. (2000). Lithium isotopic compositions of pore fluids and sediments in the Costa Rica subduction zone: implications for fluid processes and sediment contribution to the arc volcanoes. Earth and Planetary Science Letters 183, 275-290.

Chan, L.H., Leeman, W.P., You, C.F. (1999). Lithium isotopic composition of Central American Volcanic Arc lavas: implications for modification of subarc mantle by slab-derived fluids. Chemical Geology 160, 255-280.

Chan, L.-H., Leeman, W.P., You, C.-F. (2002). Lithium isotopic composition of Central American volcanic arc lavas: implications for modification of subarc mantle by slab-derived fluids: correction. Chemical Geology 182, 293-300.

Channell, J.E.T., Kozur, H.W. (1997). How many oceans? Meliata, Vardar, and Pindos oceans in Mesozoic Alpine paleogeography. Geology 25, 183-186.

Chaussidon, M., Jambon, A. (1994). Boron content and isotopic composition of oceanic basalts: Geochemical and cosmochemical implications. Earth and Planetary Science Letters 121, 277-291.

Chaussidon, M., Libourel, G. (1993). Boron partitioning in the upper mantle: An experimental and ion probe study. Geochimica et Cosmochimica Acta 57, 5053-5062.

Chaussidon, M., Marty, B. (1995). Primitive Boron Isotope Composition of the Mantle. Science 269, 383-386.

Connolly, J.A.D., Trommsdorff, V. (1991). Petrogenetic grids for metacarbonate rocks: pressure-temperature phase-diagram projection for mixed-volatile systems. Contributions to Mineralogy and Petrology 108, 93-105.

Constantin, M. (1999). Gabbroic intrusions and magmatic metasomatism in harzburgites from the Garrett transform fault: implications for the nature of the mantle-crust transition at fast-spreading ridges. Contributions to Mineralogy and Petrology 136, 111-130.

Coogan, L.A., Kasemann, S., Chakraborty, S. (2005). Rates of hydrothermal cooling of new oceanic upper crust derived from lithium-geospeedometry. Earth and Planetary Science Letters 240, 415-424.

Crawford, A.J., Falloon, T.J., Green, D.H. (1989). Classification, petrogenesis and tectonic setting of boninites. In: Crawford, A. J. (ed.) Boninites and related rocks. London: Unwin Hyman, 1-49.

Cressey, B.A., Zussman, J. (1976): Electron microscope studies of serpentinites. The Canadian Mineralogist 14, 307-313.

Currie, L.A. (1968). Limits for qualitative detection and quantitative determination. Analytical Chemistry 40, 586-593.

D'Antonio, M., Kristensen, M.B. (2005). Hydrothermal alteration of oceanic crust in the West Philippine Sea Basin (Ocean Drilling Program Leg 195, Site 1201): inferences from a mineral chemistry investigation. Mineralogy and Petrology 83, 87-112.

Danyushevsky, L.V., Eggins, S.M., Falloon, T.J., Christie, D.M. (2000). H2O abundance in depleted to moderately enriched mid-ocean ridge magmas; part I: incompatible behaviour, implications for mantle storage, and origin of regional variations. Journal of Petrology 41, 1329-1364.

Danyushevsky, L.V., Perfit, M.R., Eggins, S.M., Falloon, T.J. (2003). Crustal origin for coupled "ultra-depleted" and "plagioclase" signatures in MORB olivine-hosted melt inclusions: evidence from the Siqueiros Transform Fault, East Pacific Rise. Contributions to Mineralogy and Petrology 144, 619-637.

Davies, J.H., Stevenson, D.J. (1992). Physical model of source region of subduction zone volcanics. Journal of Geophysical Research - Solid Earth 97, 2037-2070.

Decitre, S., Deloule, E., Reisberg, L., James, R., Agrinier, P., Mével, C. (2002). Behavior of Li and its isotopes during serpentinization of oceanic peridotites. Geochemistry, Geophysics and Geosystems 3, doi: 10.1029/2001GC000178.

Dercourt, J., Ricou, L.F., Vrielynck, B. (1993). Atlas of Tethys Palaeoenvironmental Maps. Paris: Gauthier-Villars.

Dercourt, J., Zonenshain, L.P., Ricou, L.E., Kazmin, V.G., Lepichon, X., Knipper, A.L., Grandjacquet, C., Sbortshikov, I.M., Geyssant, J., Lepvrier, C., Pechersky, D.H., Boulin, J., Sibuet, J.C., Savostin, L.A., Sorokhtin, O., Westphal, M., Bazhenov, M.L., Lauer, J.P., Bijuduval, B. (1986). Geological evolution of the Tethys belt from the Atlantic to the Pamirs since the Lias. Tectonophysics 123, 241-315.

Dick, H.J.B. (1976). The origin and emplacement of the Josephine peridotite of Southwestern Oregon. Unpublished PhD Thesis. New Haven: Yale University.

Dick, H.J.B. (1989). Abyssal peridotites, very slow spreading ridges and ocean ridge magmatism. In: Saunders, A. D., Norry, M.J. (ed.) Magmatism in the Ocean Basins. London: Geological Society of London Special Publication 42, 107-124.

Dick, H.J.B., Bullen, T. (1984). Chromian spinel as a petrogenetic indicator in abyssal and alpine-type peridotites and spatially associated lavas. Contributions to Mineralogy and Petrology 86, 54-76.

Dick, H.J.B., Fisher, R.L., Bryan, W.B. (1984). Mineralogical variability of the uppermost mantle along mid-ocean ridges. Earth and Planetary Science Letters 69, 88-106.

Dick, H.J.B., Natland, J.H. (1996). Late stage melt evolution and transport in the shallow mantle beneath the East Pacific Rise. Proceedings of the Ocean Drilling Program, Scientific Results 147, 103-134.

Dick, H.J.B., Ozawa, K., Meyer, P.S., Niu, Y., Robinson, P.T., Constantin, M., Hebert, R., Natland, J.H., Hirth, G. & Mackie, S.M. (2002). Primary silicate mineral chemistry of a 1.5-km section of a very slow spreading lower ocean crust: ODP Hole 735B, Southwest Indian Ridge. In: Natland, J. H., Dick, H. J. B., Miller, D. J. and Von Herzen, R. P. (ed.) Proceedings of the Ocean Drilling Program, Scientific Results 176, 1-60 (CD-ROM).

Dijkstra, A.H., Barth, M.G., Drury, M.R., Mason, P.R.D., Vissers, R.L.M. (2003). Diffuse porous melt flow and melt-rock reaction in the mantle lithosphere at a slow-spreading ridge: A structural petrology and LA-ICP-MS study of the Othris Peridotite Massif (Greece). Geochemistry Geophysics Geosystems 4, doi: 10.1029/2001GC000278.

Dijkstra, A.H., Cawood, P.A. (2004). Base-up growth of ocean crust by multiple phases of magmatism: field evidence from Macquarie Island. Journal of the Geological Society of London 161, 739-742.

Dijkstra, A.H., Drury, M.R., Vissers, R.L.M. (2001). Structural Petrology of Plagioclase Peridotites in the West Othris Mountains (Greece): Melt Impregnation in Mantle Lithosphere. Journal of Petrology 42, 5-24.

Dijkstra, A.H., Mason, P.R.D., Spandler, C., Cawood, P.A. (2008). Extreme depletion, melt-rock reaction and melt percolation in oceanic peridotites on Macquarie Island: implications for processes in the cold mantle lid in the modern oceans. Journal of Petrology, accepted with revisions.

Dilek, Y. (2003). Ophiolite pulses, mantle plumes and orogeny. In: Dilek, Y. and Robinson, P. T. (ed.) Ophiolites in Earth History. London: The Geological Society of London Special Publications 218, 9-19.

Dilek, Y., Flower, M.F.J. (2003). Arc-trench rollback and forearc accretion: 2. A model template for ophiolites in Albania, Cyprus, and Oman. In: Dilek, Y., Robinson, P.T. (ed.) Ophiolites in Earth History. London: Geological Society of London Special Publication 218, 43-68.

Domanik, K.J., Hervig, R.L., Peacock, S.M. (1993). Beryllium and boron in subduction zone minerals: an ion microprobe study. Geochimica et Cosmochimica Acta 57, 4997-5010.

Douville, E., Charlou, J.L., Oelkers, E.H., Bianvenu, P., Jove Colon, C.F., Donval, J.P., Fouquet, Y., Prieur, D., Appriou, P. (2002). The Rainbow vent fluids (36°14'N, MAR): The influence of ultramafic rocks and phase separation on trace metal contents on Mid-Atlantic ridge hydrothermal fluids. Chemical Geology 184, 37-48.

Economou-Eliopoulos, M., Tarkian, M., Sambanis, G. (1999). On the geochemistry of chromitites from the Pindos ophiolite complex, Greece. Chemie der Erde 59, 19-31.

Economou-Eliopoulos, M., Vacondios, I. (1995). Geochemistry of chromitites and host rocks from the Pindos ophiolite complex, northwestern Greece. Chemical Geology 122, 99-108.

Edwards, S.J., Pearce, J.A., Freeman, J. (2000). New insights concerning the influence of water during the formation of podiform chromitite. In: Dilek, Y., Moores, E.M., Elthon, D., Nicolas, A. (ed.) Ophiolites and Oceanic crust: New Insights from Field Studies and Ocean Drilling Program. Boulder, Colorado: Geological Society of America Special Paper 349, 139-147.

Eggins, S.M., Rudnick, R.L., McDonough, W.F. (1998). The composition of peridotites and their minerals: a laser-ablation ICP-MS study. Earth and Planetary Science Letters 154, 53-71.

Escartin, J., Mével, C., MacLeod, C.J., McCraig, A. (2003). Constraints on deformation conditions and the origin of oceanic detachments, the Mid-Atlantic Ridge core complex at 15°45'N. Geochemistry Geophysics Geosystems 4, doi: 10.1029/2002GC000472.

Evans, B.W., Trommsdorff, V. (1970). Regional metamorphism of ultramafic rocks in the Central Alps: Parageneses in the system CaO-MgO-SiO2-H2O. Schweiz. Mineral. Petrogr. Mitt. 50, 481-492.

Filippidis, A. (1982). Experimental study of the serpentinization of Mg-Fe-Ni olivine in the presence of sulfur. The Canadian Mineralogist 20, 567-574.

Filippidis, A. (1996). Chemical variation of olivine in the serpentinite of the central section in the Xerolivado chrome mine of Vourinos, Greece. Neues Jahrbuch für Mineralogie - Abhandlungen 170, 189-205.

Flower, M.F.J., Dilek, Y. (2003). Arc-trench rollback and forearc accretion: 1. A collision-induced mantle flow model for Tethyan ophiolites. In: Dilek, Y., Robinson P.T. (ed.) Ophiolites in Earth History. London: Geological Society of London Special Publication 218, 21-41.

Frei, D., Liebscher, A., Franz, G., Dulski, P. (2004). Trace element geochemistry of epidote minerals. Reviews in Mineralogy & Geochemistry 56, 553-605.

Froitzheim, N., Schmid, S.M., Frey, M. (1996). Mesozoic paleogeography and the timing of eclogite-facies metamorphism on the Alps: A working hypothesis. Eclogae geol. Helv. 89, 81-110.

Frost, B.R., Beard, J.S. (2007). On Silica Activity and Serpentinization. Journal of Petrology 48, 1351-1368.

Früh-Green, G.L., Connolly, J.A.D., Plas, A., Kelley, D.S., Grobéty, B. (2004): Serpentinization of oceanic peridotites: implications for geochemical cycles and biological activity. In: The subseafloor biosphere at mid-ocean ridges. Geophysical Monograph Series 144, 119-136.

Früh-Green, G.L., Plas, A., Lécuyer, C. (1996). Petrologic and stable isotope constraints on hydrothermal alteration and serpentinization of the EPR shallow mantle at Hess Deep (site 895). Proceedings of the Ocean Drilling Program Scientific Results 147, 255-288.

Früh-Green, G.L., Weissert, H., Bernoulli, D. (1990). A Multiple Fluid History Recorded in Alpine Ophiolites. Journal of the Geological Society 147, 959-970.

Fujiwara, T., Lin, J., Matsumoto, T., Kelemen, P.B., Tucholke, B.E. & Casey, J.F. (2003). Crustal evolution of the Mid-Atlantic Ridge near the Fifteen-Twenty Fracture Zone in the last 5 Ma. Geochemistry Geophysics Geosystems 4, doi: 10.1029/2002GC000364.

Gaetani, G.A., Grove, G.L., Bryan, W.B. (1994). Experimental phase relations of basaltic andesite from Hole 839B under hydrous and anhydrous conditions. Proceedings of the Ocean Drilling Program, Scientific Results 135, 557-563.

Gao, S., Luo, T., Zhang, B., Zhang, H., Han, Y., Zhao, Z., Hu, Y. (1998). Chemical composition of the continental crust as revealed by studies in East China. Geochimica et Cosmochimica Acta 62, 1959-1975.

Girardeau, J., Francheteau, J. (1993). Plagioclase-wehrlites and peridotites on the East pacific Rise (Hess Deep) and the Mid-Atlantic Ridge (DSDP Site 334): evidence for magma percolation in the oceanic upper mantle. Earth and Planetary Science Letters 115, 137-149.

Gméling, K., Harangi, Sz., Kasztovszky, Zs. (2005). Boron and chlorine concentration of volcanic rocks: an application of prompt gamma activation analysis. Journal of Radioanalytical and Nuclear Chemistry 265, 201-212.

Godard, M., Jousselin, D., Bodinier, J.-L. (2000). Relationships between geochemistry and structure beneath a palaeo-spreading centre: a study of the mantle section in the Oman ophiolite. Earth and Planetary Science Letters 180, 133-148.

Govindaraju, K. (1994). 1994 compilation of working values and sample description for 383 geostandards. Geostandards Newsletter 18, 1-158.

Green, D.H., Hibberson, W.O., Jacques, A.L. (1979). Petrogenesis of mid-ocean basalts. In: Elhinny, H. W. (ed.) The Earth, its origin, structure and evolution. London: Academic Press, 265-299.

Grégoire, M., McInnes, B.I.A., O'Reilly, S.Y. (2001). Hydrous metasomatism of oceanic sub-arc mantle, Lihir, Papua New Guinea, Part 2. Trace element characteristics of slab-derived fluids. Lithos 59, 91-108.

Grew, E.S. (1996): Borosilicates (exclusive of tourmaline) and Boron in rock-forming minerals in metamorphic environments. In: Grew, E. S. (ed.) Boron: mineralogy, petrology and geochemistry. Washington DC: Mineralogical Society of America, Reviews in Mineralogy 33, 387-502.

Groppo, C. (2005): Asbestos hazard in Western Alps: Petrology, characterization and quantitative determination of fibrous minerals in the asbestos-bearing serpentinites of the Piemonte zone (Susa and Lanzo Valleys). Unpublished PhD Thesis, Torino: Universita degli Studi di Torino, 179 p.

Groppo, C., Rinaudo, C., Cairo, S., Gastaldi, D., Compagnoni, R. (2006). Micro-Raman spectroscopy for a quick and reliable identification of serpentine minerals from ultramafics. European Journal of Mineralogy 18, 319-329.

Günther, D., Frischknecht, R., Heinrich, C.A., Kahlert, H.J. (1997). Capabilities of an Argon Fluoride 193 nm excimer laser for laser ablation inductively coupled plasma mass spectrometry microanalysis of geological materials. Journal of Analytical Atomic Spectrometry 12, 939-944.

Gurenko, A.A., Chaussidon, M. (1995). Enriched and depleted primitive melts included in olivine from Icelandic tholeiites: Origin by continous melting of a single mantle column. Geochimica et Cosmochimica Acta 59 (14), 2905-2917.

Haase, K.M., Stroncik, N.A., Hekinian, R., Stoffers, P. (2005). Nb-depleted andesites from the Pacific-Antarctic Rise as analogs for early continental crust. Geology 33, 921-924.

Hauri, E.H., Wagner, T.P., Grove, T.L. (1994). Experimental and natural partitioning of Th, U, Pb and other trace-elements between garnet, clinopyroxene and basaltic melts. Chemical Geology 117 (1-4), 149-166.

Hawkins, J.W. (2003). Geology of supra-subduction zones – Implications for the origin of ophiolites. Geological Society of America Special Paper 373, 227-268.

Hawthorne, F.C., Burns, P.C., Grice, J.D. (1996): The crystal chemistry of boron. In: Grew, E. S. (ed.) Boron: mineralogy, petrology and geochemistry. Washington DC: Mineralogical Society of America, Reviews in Mineralogy 33, 41-116.

Hawthorne, F.C., Huminicki, D.M.C. (2002). The crystal chemistry of beryllium. In: Grew, E. S. (ed.) Beryllium: mineralogy, petrology and geochemistry. Washington DC: Mineralogical Society of America, Reviews in Mineralogy 50, 333-403.

Heinrich, C.A. (1982). Kyanite-eclogite to amphibolite facies evolution of hydrous mafic and pelitic rocks, Adula nappe, Central Alps. Contributions to Mineralogy and Petrology 81, 30-38.

Heinrich, C.A., Pettke, T., Halter, W.E., Aigner-Torres, M., Audetat, A., Günther, D., Hattendorf, B., Bleiner, D., Guillong, M., Horn, I. (2003). Quantitative multi-element analysis of minerals, fluid and melt inclusions by laser-ablation inductively-coupled-plasma mass-spectrometry. Geochimica et Cosmochimica Acta 67, 3473-3497.

Hellebrand, E., Snow, J.E., Dick, H.J.B., Hofmann, A.W. (2001). Coupled major and trace elements as indicators of the extent of melting in mid-ocean-ridge peridotites. Nature 410, 677-681.

Hellebrand, E., Snow, J.E., Hoppe, P., Hofmann, A.W. (2002). Garnet-field melting and late-stage refertilization in “residual” abyssal peridotites from the Central Indian Ridge. Journal of Petrology 43, 2305-2338.

Hellebrand, E., Snow, J.E., Mühe, R. (2002). Mantle melting beneath Gakkel Ridge (Arctic Ocean): abyssal peridotite spinel compositions. Chemical Geology 182, 227-235.

Herrmann, W. & Berry, R.F. (2002): MINSQ - a least squares spreadsheet method for calculating mineral proportions from whole rock major element analyses. Geochemistry: Exploration, Environment, Analysis 2, 361-368.

Hoefs, J., Sywall, M. (1997). Lithium isotope composition of Quaternary and Tertiary biogene carbonates and global lithium isotope balance. Geochimica et Cosmochimica Acta 61, 2679-2690.

Hoogerduijn Strating, E.H., Rampone, E., Piccardo, G.B., Drury, M.R., Vissers, R.L.M. (1993). Subsolidus emplacement of mantle peridotites during incipient oceanic rifting and opening of the Mesozoic Tethys (Voltri Massif, NW Italy). Journal of Petrology 34, 901-927.

Ishikawa, T., Nakamura, E. (1993). Boron isotope systematics of marine sediments. Earth and Planetary Science Letters 117, 567-580.

Ishikawa, T., Nakamura, E. (1994). Origin of the slab component in arc lavas from across-arc variation of B and Pb isotopes. Nature 370, 205-208.

Jacobshagen, V. (1986). Geologie von Griechenland. Berlin-Stuttgart: Borntraeger.

Jagoutz, E., Palme, H., Baddenhausen, H., Blum, K., Cendales, M., Dreibus, G., Spettel, B., Lorenz, V., Vanke, H. (1979). The abundance of major, minor and trace elements in the earth's mantle as derived from primitive ultramafic nodules. Geochimica et Cosmochimica Acta 11, 2031-2050.

Jeffcoate, A.B., Elliott, T., Kasemann, S.A., Ionov, D., Cooper, K., Brooker, R. (2007). Li isotope fractionation in peridotites and mafic melts. Geochimica et Cosmochimica Acta 71, 202-218.

Johnson, K.T.M., Dick, H.J.B. (1992). Open system melting and temporal and spatial variation of peridotite and basalt at the Atlantis-II fracture-zone. Journal of Geophysical Research-Solid Earth 97(B6), 9219-9241.

Johnson, M.C., Planck, T. (1999). Dehydration and melting experiments constrain the fate of subducted sediments. Geochemistry, Geophysics and Geosystems 1, doi: 10.1029/1999GC000014.

Jones, G., Robertson, A.H.F. (1991). Tectono-stratigraphy and evolution of the Mesozoic Pindos ophiolite and related units, northwestern Greece. Journal of the Geological Society of London 148, 267-288.

Jones, G., Robertson, A.H.F., Cann, J.R. (1991). Genesis and Emplacement of the Supra-Subduction Zone Pindos Ophiolite, Northwestern Greece. In: Peters, T., et al. (ed.) Ophiolite Genesis and Evolution of the Oceanic Lithosphere. Sultanate of Oman: Ministry of Petroleum and Minerals, 771-799.

Juteau, T., Maury, R. (1999). Géologie de la croûte océanique - Pétrologie et dynamique endogènes. Paris: Dunod, 367 p.

Kaczmarek, M.-A., Müntener, O. (2008) Juxtaposition of melt impregnation and high temperature shear zones in the upper mantle (Lanzo peridotite, N-Italy) II: whole rock geochemistry. Journal of Petrology, submitted.

Kaeser, B., Kalt, A., Ludwig, T. (2007). Li, Be and B Abundances in Minerals of Peridotite Xenoliths from Marsabit (Kenya): Disequilibrium Processes and Implications for Subduction Zone Signatures. Geochemistry, Geophysics, Geosystems 8, doi: 10.1029/2006GC001555.

Kaliwoda, M. (2004). Mantel-Xenolithe des Harrat Uwayrid (Saudi-Arabien): Archive der stofflichen une thermischen Entwicklung des lithosphärischen Erdmantels im Bereich eines passiven Kontinentalrandes. Unpublished PhD Thesis. Heidelberg (Germany): Mathematisch-Naturwissenschaftlichen Gesamtfakultät, Ruprecht-Karls-Universität, 365 p.

Kamenetsky, V.S., Everard, J.L., Crawford, A.J., Varne, R., Eggins, S.M., Lanyon, R. (2000). Enriched end-member or primitive MORB melts: petrology and geochemistry of glasses from Macquarie Island (SW Pacific). Journal of Petrology 41, 411-430.

Kasemann, S., Meixner, A., Rocholl, A., Vennemann, T., Schmitt, A., Wiedenbeck, M. (2001). Boron and oxygen isotope composition of certified reference materials NIST SRM 610/612, and reference materials JB-2G and JR-2G. Geostandards Newsletter 25, 405-416.

Kelemen, P.B., Kikawa, E., Miller, D.J., Abe, N., Bach, W., Carlson, R.L., Casey, J.F., Chambers, L.M., Cheadle, M., Cirpiani, A., Dick, H.J.B., Faul, U., Garces, M., Garrido, C., Gee, J.S., Godard, M.M., Graham, D.W., Griffin, D.W., Harvey, J., Ildefonse, B., Iturrino, G.J., Josef, J., Meurer, W.P., Paulick, H., Rosner, M., Schroeder, T., Seyler, M. & Takazawa, E. (2004). Proceedings of the Ocean Drilling Program - Drilling Mantle Peridotite along the Mid-Atlantic Ridge from 14° to 16°. Initial Reports 209, 1-139.

Kelemen, P.B., Kikawa, E., Miller, D.J., Abe, N., Bach, W., Carlson, R.L., Casey, J.F., Chambers, L.M., Cheadle, M., Cipriani, A., Dick, H.J.B., Faul, U., Garces, M., Garrido, C., Gee, J.S., Godard, M.M., Graham, D.W., Griffin, D.W., Harvey, J., Ildefonse, B., Iturrino, G.J., Josef, J., Meurer, W.P., Paulick, H., Rosner, M., Schroeder, T., Seyler, M., Takazawa, E., Mrozewski, S. (2003). Leg 209 Preliminary Report. Drilling Mantle Peridotite along the Mid-Atlantic Ridge from 14° to 16°N. Proceedings of the Ocean Drilling Program, Part A: Initial Reports 209, 1-160.

Kelley, K.A., Plank, T., Ludden, J., Staudigel, H. (2003). Composition of altered oceanic crust at ODP Sites 801 and 1149. Geochemistry Geophysics Geosystems 4, doi: 10.1029/2002GC000435.

Kennedy, A.K., Lofgren, G.E., Wasserburg, G.J. (1993). An experimental-study of trace-element partitioning between olivine, orthopyorxene and melt in chondrules - equilibrium values and kinetic effects. Earth and Planetary Science Letters 115 (1-4), 177-195.

Keusen, H.-R. (1970). Genese der basischen und ultrabasischen Gesteine vom Geisspfad (Wallis, Schweiz). Vortragsreferat DMG. Fortschritte der Mineralogie 48(1), 14-16.

Keusen, H.-R. (1972): Mineralogie une Petrographie des metamorphen Ultramafitit-Complexes vom Geisspfad (Penninische Alpen). Schweizerische Mineralogische und Petrographische Mitteilungen 52, 385-478.

Keusen, H.R., Peters, T. (1980). Preiswerkite, and Al-rich trioctahedral sodium mica from the Geisspfad ultramafic complex (Penninic Alps). American Mineralogist 65, 1134-1137.

Klein, E.M., Karsten, J.L. (1995). Ocean-ridge basalts with convergent-margin geochemical affinities from the Chile Ridge. Nature 374, 52-57.

Kloprogge, J.T., Frost, R.L., Rintoul, L. (1999): Single crystal Raman microscopic study of the asbestos mineral chrysotile. Physical Chemistry Chemical Physics 1(10), 2559-2564.

Kostopoulos, D. (1988). Geochemistry and tectonic setting of the Pindos ophiolite, northwestern Greece. Unpublished PhD Thesis. Newcastle-upon-Tyne (England): Newcastle University, 498 p.

Kretz, R. (1983). Symbols for rock-forming minerals. American Mineralogist 68, 277-279.

Langmuir, C.H., Bender, J.F., Bence, A.E., Hanson, G.N., Taylor, S.R. (1977). Petrogenesis of basalts from the FAMOUS area: Mid-Atlantic Ridge. Earth and Planetary Science Letters 36, 133-156.

Leeman, W.P. (1996). Boron and other fluid-mobile elements in volcanic arc lavas: implications for subduction processes. In: Bebout, G. E., Scholl, D., Kirby, S., Platt, J.P. (ed.) Subduction top to bottom. AGU Geophysical Monograph Series 96, 269-276.

Leeman, W.P., Tonarini, S., Chan, L.-H., Borg, L.E. (2004). Boron and lithium isotopic variations in a hot subduction zone - the southern Washington Cascades. Chemical Geology 212, 101-124.

Li, Y.-H. (1982). A brief discussion on the mean oceanic residence time of elements. Geochimica et Cosmochimica Acta 46, 2671-2675.

Li, Z.-X.A., Lee, C.-T.A. (2006). Geochemical investigation of serpentinized oceanic lithospheric mantle in the Feather River Ophiolite, California: Implications for the recycling rate of water by subduction. Chemical Geology 235, 161-185.

Liati, A., Gebauer, D., Fanning, C.M. (2004). The age of ophiolitic rocks of the Hellenides (Vourinos, Pindos, Crete): first U-Pb ion microprobe (SHRIMP) zircon ages. Chemical Geology 207, 171-188.

Longerich, H.P., Jackson, S.E., Günther, D. (1996). Laser Ablation Inductively Coupled Plasma Mass Spectrometric Transient Signal Data Acquisition and Analyte Concentration Calculation*. Journal of Analytical Spectrometry 11, 899-904.

Lykins, R.W., Jenkins, D.M. (1992). Experimental determination of pargasite stability relations in the presence of orthopyroxene. Contributions to Mineralogy and Petrology 112, 405-413.

Lyubetskaya, T., Korenaga, J. (2007). Chemical composition of Earth's primitive mantle and its variance: 1. Method and results. Journal of Geophysical Research 112, 1-21.

Makris, J. (1977). Geophysical investigations of the Hellenides. Hamburger Geophysikalische Einzelschriften 33.

Maaloe, S. (1982). Geochemical aspects of permeability controlled partial melting and fractional crystallization. Geochimica et Cosmochimica Acta 46, 43-57.

Manatschal, G., Müntener, O., Desmurs, L., Bernoulli, D. (2003). An ancient ocean-continent transition in the Alps: the Totalp, Err-Platta, and Malenco units in the eastern Central Alps (Graubünden and northern Italy). Eclogae geol. Helv. 96, 131-146.

Manatschal, G., Nievergelt, P. (1997). A continent-ocean transition recorded in the Err and Platta nappes (Eastern Switzerland). Eclogae Geol. Helv. 90, 3-27.

Marchesi, C., Garrido, C.J., Godard, M., Proenza, J.A., Gervilla, F., Blanco-Moreno, J. (2006). Petrogenesis of highly depleted peridotites and gabbroic rocks from the Mayari-Baracoa Ophiolitic Belt (eastern Cuba). Contributions to Mineralogy and Petrology 151, 717-736.

Marroni, M., Molli, G., Montanini, A., Tribuzio, R., 1998. The association of continental crust rocks with ophiolites in the Northern Apennines (Italy): implications for the continent-ocean transition in the Western Tethys. Tectonophysics 292: 43-66.

Marschall, H.R. (2005): Lithium, Beryllium and Boron in high pressure metamorphic rocks from Syros (Greece). Ruprecht-Karls Universität Heidelberg (Germany). Unpublished PhD Thesis, 411 p.

Marschall, H.R., Altherr, R., Ludwig, T., Kalt, A., Gméling, K., Kasztovszky, Z. (2006). Partitioning and budget of Li, Be and B in high-pressure metamorphic rocks. Geochimica et Cosmochimica Acta 70, 4750-4769.

Marschall, H.R., Altherr, R., Rüpke, L. (2007). Squeezing out the slab – modelling the release of Li, Be and B during progressive high-pressure metamorphism. Chemical Geology 239, 323-335.

Marschall, H.R., Kasztovszky, Z., Gméling, K., Altherr, R. (2005). Chemical analysis of high-pressure metamorphic rocks by PGNAA: Comparison with results from XRF and solution ICP-MS. Journal of Radioanalytical and Nuclear Chemistry 265, 339-348.

Marschall, H.R., Ludwig, T. (2004). The low-boron contest: minimising surface contamination and analysing boron concentrations at the ng/g-level by secondary ion mass spectrometry. Mineralogy and Petrology 81, 265-278.

McDonough, W.F., Sun, S.-S. (1995). The composition of the Earth. Chemical Geology 120, 223-253.

McInnes, B.I.A., Grégoire, M., Binns, R.A., Herzig, P.M., Hannington, M.D. (2001). Hydrous metasomatism of oceanic sub-arc mantle, Lihir, Papua New Guinea: petrology and geochemistry of fluid-metasomatised mantle wedge xenoliths. Earth and Planetary Science Letters 188, 169-183.

Measures, C.I., Edmond, J.M. (1982). Beryllium in the Water Column of the Central North Pacific. Nature 297 (5861), 51-53.

Measures, C.I., Edmond, J.M. (1983). The geochemical cycle of ^{9}Be: a reconnaissance. Earth and Planetary Science Letters 66, 101-110.

Mercier, J.C.C., Nicolas, A. (1975). Textures and Fabrics of Upper-Mantle Peridotites as Illustrated by Xenoliths from Basalts. Journal of the Geological Society of London 148, 267-288.

Metcalf, R.V., Wallin, E.T., Willse, K.R., Muller, E.R. (2000). Geology and geochemistry of the ophiolitic Trinity terrane, California: Evidence of middle Paleozoic depleted supra-subduction zone mag,atism in a proto-arc setting. In: Dilek, Y., Moores, E.M., Elthon, D., Nicolas, A. (ed.) Ophiolites and Oceanic crust: New Insights from Field Studies and the Ocean Drilling Program. Boulder, Colorado: Geological Society of America Special Paper 349, 403-418.

Mével, C. (2003). Serpentinization of abyssal peridotites at mid-ocean ridges. C.R. Geoscience 335, 825-852.

Middleton, A.P., Whittaker, E.J.W. (1976): Structure of povlentype chrysotile. The Canadian Mineralogist 14, 301-306.

Miller, J.A., Buick, I.S., Cartwright, I., Barnicoat, A. (2002). Fluid processes during the exhumation of high-P metamorphic belts. Mineralogical Magazine 66(1), 93-119.

Molnár, G.L. (2004). Handbook of prompt gamma activation analysis with neutron beams. Springer: Kluwer Academic Publisher.

Montigny, R., Bougault, H., Bottinga, Y., Allègre, C.J. (1973). Trace element geochemistry and genesis of the Pindos ophiolite suite. Geochimica et Cosmochimica Acta 37, 2135-2147.

Moores, E.M., Kellogg, L.H., Dilek, Y. (2000). Tethyan ophiolites, mantle convection, and tectonic "historical contingency": A resolution of the "ophiolite conundrum". In: Dilek, Y., Moores, E.M., Elthon, D., Nicolas, A. (ed.) Ophiolies and Oceanic crust: New Insights from Field Studies and Ocean Drilling Program. Boulder, Colorado: Geological Society of America Special Paper 349, 3-12.

Moran, A.E., Sisson, V.B., Leeman, W.P. (1992). Boron depletion during progressive metamorphism: implications for subduction processes. Earth and Planetary Science Letters 111, 331-349.

Moriguti, T., Makishima, A., Nakamura, E. (2004). Determination of Lithium Contents in Silicates by Isotope Dilution ICP-MS and its Evaluation by Isotope Dilution Thermal Ionisation Mass Spectrometry. Geostandards and Geoanalytical Research 28, 371-382.

Moriguti, T., Nakamura, E. (1998). Across-arc variation of Li isotopes in lavas and implications for crust / mantle recycling at subduction zones. Earth and Planetary Science Letters 163, 167-174.

Morozov, N.P. (1968). Geochemistry of rare earth alkali elements in the oceans and seas. Oceanology 8, 169-178.

Müntener, O., Hermann, J., Trommsdorff, V. (2000). Cooling history and exhumation of lower-crustal granulite and upper mantle (Malenco, Eastern Central Alps). Journal of Petrology 41, 175-200.

Müntener, O., Manatschal, G. (2006). High degrees of melt extraction recorded by spinel harzburgite of the Newfoundland margin: The role of inheritance and consequences for the evolution of the southern North Atlantic. Earth and Planetary Science Letters 252, 437-452.

Müntener, O., Piccardo, G.B., Polino, R., Zanetti, A. (2005). Revisiting the Lanzo peridotite (NW-Italy): ‚Asthenospherization' of ancient mantle lithosphere. Ofioliti 30(2), 111-124.

Murton, B.J. (1989). Tectonic controls on boninite genesis. In: Saunders, A. D., Norry, M.J. (ed.) Magmatism in the Ocean Basins. London: Geological Society of London Special Publication 42, 347-377.

Natland, J.H. (1989). Partial melting of a lithologically heterogeneous mantle: inferences from crystallization histories of magnesian abyssal tholeiites from the Siqueiros Fracture Zone. In: Saunders, A. D., Norry, M.J. (ed.) Magmatism in the Ocean Basins. London: Geological Society of London Special Publication 42, 41-70.

Natland, J.H., Tarney, J. (1982). Petrologic evolution of the Mariana arc and back-arc basin system – A synthesis of drilling results in the South Philippine Sea. Initial reports of Deep-Sea Drilling Projects 60, 877-908.

Navon, O., Stolper, E. (1987). Geochemical consequences of melt percolation: The upper mantle as a chromatographic column. Journal of Geology 95, 285-307.

Nicholls, I.A. (1974). A direct fusion method of preparing silicate rock glasses for energy-dispersive electron microprobe analysis. Chemical Geology 14, 151-157.

Niu, Y. (1997). Mantle melting and melt extraction processes beneath ocean ridges: evidence from abyssal peridotites. Journal of Petrology 38, 1047-1074.

Niu, Y. (2004). Bulk-rock major and trace element compositions of abyssal peridotites: Implications for mantle melting, melt extraction and post-melting processes beneath mid-ocean ridges. Journal of Petrology 45, 2423-2458.

Niu, Y., Batiza, R. (1997). Trace element evidence from seamounts for recycled oceanic crust in the Eastern Pacific mantle. Earth and Planetary Science Letters 148, 471-483.

Noakes, J.E., Hood, D.W. (1961). Boron-boric acid complexes in sea-water. Deep Sea Research 8, 121-129.

Nonnotte, P., Ceuleneer, G., Benoît, M. (2005). Genesis of andesitic-boninitic magmas at mid-ocean ridges by melting of hydrated peridotites: Geochemical evidence from DSDP Site 334 gabbronorites. Earth and Planetary Science Letters 236, 632-653.

O'Hanley, D.S. (1996). Serpentinites: Record of Tectonic and Petrological History. Oxford: Oxford University Press.

Ohara, Y., Stern, R.J., Ishii, T., Yurimoto, H., Yamazaki, T. (2002). Peridotites from the mariana Trough: first look at the mantle beneath an active back-arc basin. Contributions to Mineralogy and Petrology 143, 1-18.

Olsher, U., Izatt, R.M., Bradshaw, J.S., Dalley, N.K. (1991). Coordination chemistry of lithium ion: a crystal and molecular structure review. Chemical Reviews 91, 137-164.

Ottolini, L., Bottazzi, P., Vannucci, R. (1993). Quantification of Lithium, Beryllium, and Boron in Silicates by Secondary Ion Mass Spectrometry Using Conventional Energy Filtering. Analytical Chemistry 65, 1960-1968.

Ottolini, L., Le Fèvre, B., Vannucci, R. (2004). Direct assessment of mantle boron and lithium contents and distribution by SIMS analyses of peridotite minerals. Earth and Planetary Science Letters 228, 19-36.

Page, N.J. (1968). Chemical differences among the serpentine «polymorphs». American Mineralogist 53, 201-215.

Paquin, J., Altherr, R. (2002). Subduction-related lithium metasomatism during exhumation of the Alpe Arami ultrahigh-pressure garnet peridotite (Central Alps, Switzerland). Contributions to Mineralogy and Petrology 143, 623-640.

Paquin, J., Altherr, R., Ludwig, T. (2004). Li-Be-B systematics in the ultrahigh-pressure garnet peridotite from Alpe Arami (Central Swiss Alps): implications for slab-to-mantle wedge transfer. Earth and Planetary Science Letters 218, 507-519.

Parkinson, I.J., Pearce, J.A. (1998). Peridotites from the Izu-Bonin-Mariana forearc (ODP Leg 125): Evidence for mantle melting and melt-mantle interaction in a supra-subduction zone setting. Journal of Petrology 39, 1577-1618.

Passaglia, E. (1978): Lattice-constant variations in cation-exchanged chabazites. In: Sand, L. B. and Mumpton, F. A. (ed.) Natural Zeolites: Occurrence, Properties, Use. London: Pergamon Press, 45-52.

Pastorelli, S. (1994). Il complesso ultrafemico di Geisspfad e i suori rapporti con le rocce incassanti. unpublished diploma thesis Thesis, Facolta' di scienze M.F.N. Universita' degli studi di Torino, Torino, 119 p.

Pastorelli, S., Martinotti, G., Piccardo, G.B., Rampone, E., Scambelluri, M. (1995): The Geisspfad Complex and its relationships with the Monte Leone Nappe (Lower Pennine, Western Alps). In: Polino, R., Sacchi, R. (ed.) Atti del Convegno Rapporti Alpi-Appennino 1994. Roma: Accad. Naz. Scienze, Scritti e Documenti 14, 349-358.

Paulick, H., Bach, W., Godard, M., De Hoog, J.C.M., Suhr, G., Harvey, J. (2006). Geochemistry of abyssal peridotites (Mid-Atlantic Ridge, 15°20'N, ODP Leg 209): Implications for fluid/rock interactions in slow spreading environments. Chemical Geology 234, 179-210.

Peacock, S.M., Hervig, R.L. (1999). Boron isotopic composition of subduction-zone metamorphic rocks. Chemical Geology 160, 281-290.

Pearce, J.A. (2003). Supra-subduction zone ophiolites: The search for modern analogues. Geological Society of America Special Paper 373, 269-293.

Pearce, J.A., Barker, P.F., Edwards, S.J., Parkinson, I.J., Leat, P.T. (2000). Geochemistry and tectonic significance of peridotites from the South Sandwich arc-basin system, South Atlantic. Contributions to Mineralogy and Petrology 139, 36-53.

Pearce, J.A., Lippard, S.J., Roberts, S. (1984). Characteristics and tectonic significance of supra-subduction zone ophiolites. In: Kokelaar, B. P., Howells, M.F. (ed.) Marginal Basin Geology. London: Geological Society of London Special Publication 16, 77-89.

Pelletier, L., Müntener, O., Kalt, A., Venneman, T., Belgya, T. (2008a). Li, Be and B mobility during emplacement of ultramafic rocks into the continental crust: the example of the Geisspfad ultramafic body (Swiss Alps). Chemical Geology, submitted.

Pelletier, L., Vils, F., Kalt, A., Gméling, K. (2008b). Li, B and Be contents of harzburgites from the Dramala Complex (Pindos ophiolite, Greece): a MOR-type mantle in a supra-subduction zone environment. Journal of Petrology, submitted.

Pelletier, L., Vils, V., Kalt, A. and Groppo, C. (2008c). Li and B variability in serpentine: intracrystalline or intercrystalline ? European Journal of Mineralogy, submitted.

Pe-Piper, G., Piper, D.J.W. (2002). The igneous rocks of Greece. The anatomy of an orogen. Berlin: Gebrüder Borntraeger.

Pe-Piper, G., Tsikouras, B., Hatzipanagiotou, K. (2004). Evolution of boninites and island-arc tholeiites in the Pindos Ophiolite, Greece. Geological Magazine 141, 455-469.

Perfit, M.R., Ridley, W.I., Jonasson, I. (1999). Geologic, petrologic, and geochemical relationships between magmatism and massive sulfide mineralization along the eastern Galapagos spreading center. In: Barrie, C. T. and Hannington, M. D. (ed.) Volcanic-associated massive sulfide deposits; processes and examples in modern and ancient settings. Reviews in Economic Geology vol. 8. Socorro, NM, USA: Society of Economic Geologists, 75-100.

Pettke, T. (2006). In situ laser-ablation ICPMS analysis of melt inclusions and prospects for constraining subduction zone magmatism. Mineralogical Association of Canada, Montréal, Québec Short course 36, 51-80.

Pettke, T., Halter, W.E., Webster, J.D., Aigner-Torres, M., Heinrich, C.A. (2004). Accurate quantification of melt inclusion chemistry by LA-ICPMS: a comparison with EMP and SIMS and advantages and possible limitations of these methods. Lithos 78, 333-361.

Piccardo, G.B., Müntener, O., Zanetti, A. (2004a). Alpine-Apennine ophiolitic peridotites: new concepts on their composition and evolution. Ofioliti 29, 63-74.

Piccardo, G.B., Müntener, O., Zanetti, A., Romairone, A., Bruzzone, S., Poggi, E., Spagnolo, G. (2004b). The Lanzo South peridotite: melt/peridotite interaction in the mantle lithosphere of the Jurassic Ligurian Tethys. Ofioliti 29, 37-62.

Plank, T., Langmuir, C.H. (1993). Tracing trace elements from sediment input to volcanic output at subduction zones. Nature 362, 739-743.

Plyusnina, L.P. (1982). Geothermometry and geobarometry of plagioclase-hornblende bearing assemblages. Contributions to Mineralogy and Petrology 80(2), 140-146.

Pozzorini, D., Früh-Green, G.L. (1996). Stable isotope systematics of the Ventina Ophicarbonate Zone, Bergell contact aureole. Schweiz. Mineral. Petrogr. Mitt. 76, 549-564.

Preiswerk, H. (1901). Über Dunitserpentin am Geisspfadpass im Oberwallis. Dissertation University of Basel (Switzerland), Birkhäuser.

Rampone, E., Piccardo, G.B., Vannucci, R., Bottazzi, P. (1997). Chemistry and origin of trapped melts in ophiolitic peridotites. Geochimica et Cosmochimica Acta 61, 4557-4569.

Rassios, A. (1991). Internal structure and pseudostratigraphy of the Dramala peridotite massif Pindos Mountains, Greece. Bulletin of the Geological Society of Greece 25, 293-305.

Rassios, A. (2004). A Geologist's Guide to West Macedonia, Greece. Grevena (Greece): The Grevena Development Agency.

Rassios, A., Grivas, E. (1998). Geologic and metallogenic map of the Pindos imbricated ophiolite and associated units.

Rassios, A., Grivas, E. (2001). Ore potential in the Pindos and Vourinos ophiolites. Institute of Geology and Mineral Exploration Rept. Regional Branch West Macedonia, 12 maps.

Rassios, A., Grivas, E., Konstantopoulou, G., Vakondios, I. (1994). The geometry and structures forming around the ductile - brittle transition in the Vourinos-Pindos-Othrys oceanic slab. Bull. Geol. Soc. Greece 30, 109-121.

Rassios, A.H.E., Moores, E.M. (2006). Heterogeneous mantle complex, crustal processes, and obduction kinematics in a unified Pindos-Vourinos ophiolitic slab (northern Greece). Geological Society of London Special Publications 260, 237-266.

Regelous, M., Niu, Y., Wendt, J.I., Batiza, R., Greig, A., Collerson, K.D. (1999). Variations in the geochemistry of magmatism on the East Pacific Rise at 10°30' N since 800 ka. Earth and Planetary Science Letters 168, 45-63.

Révay, Zs., Belgya, T. (2004). Principles of PGAA method. In: Molnár, G.L. (Ed.), Handbook of prompt gamma activation analysis with neutron beams. Springer: Kluwer Academic Publisher, 1-30.

Révay, Zs., Belgya, T., Kasztovszky, Zs., Weil, J.L., Molnár, G.L. (2004). Cold neutron PGAA facility at Budapest. Nuclear Instruments and Methods in Physics Research Section B: Beam Interactions with Materials and Atoms 213, 385-388.

Révay, Z., Molnár, G.L., Belgya, T., Kasztovszky, Z., Firestone, R.B. (2001). A new gamma-ray spectrum catalog and library for PGAA. Journal of Radioanalytical and Nuclear Chemistry 248 (2), 395-399.

Riley, G.N.J., Kohlstedt, D.L. (1991). Kinetics of melt migration in upper mantle-type rocks. Earth and Planetary Science Letters 105, 500-521.

Rinaudo, C., Belluso, E., Gastaldi, D. (2004): Assessment of the use of Raman spectroscopy for the determination of amphibole asbestos. Mineralogical Magazine 68, 455-465.

Rinaudo, C., Gastaldi, D., Belluso, E. (2003): Characterization of chrysotile, antigorite and lizardite by FT-Raman spectroscopy. The Canadian Mineralogist 41, 883-890.

Robertson, A.H.F. (2002). Overview of the genesis and emplacement of Mesozoic ophiolites in the Eastern Mediterranean Tethyan region. Lithos 65, 1-67.

Robertson, A.H.F., Clift, P.D., Degnan, P., Jones, G. (1991). Paleoceanography of the Eastern Mediterranean Neotethys. Paleogeography, Paleoclimatology, Paleoecology 87, 289-343.

Robertson, A., Shallo, M. (2000). Mesozoic-Tertiary tectonic evolution of Albania in its regional Eastern Mediterranean context. Tectonophysics 316, 197-254.

Robertson, A.H.F., Ustaömer, T., Pickett, E.A., Collins, A., Andrew, T. & Dixon, J.E. (2004). Testing models of Late Palaeozoic-early Mesozoic orogeny: support for an evolving one-Tethys model. Journal of the Geological Society of London 161, 501-511.

Roddick, J.C., Cameron, W.E., Smith, A.G. (1979). Permo-Triassic and Jurassic 40Ar-39Ar ages from Greek ophiolites and associated rocks. Nature 279, 788-790.

Rose, E.F., Shimizu, N., Layne, G.D., Grove, T.L. (2001). Melt production beneath Mt. Shasta from boron data in primitive melt inclusions. Science 293, 281-283.

Rosner, M., Erzinger, J., Franz, G., Trumbull, R.B. (2003). Slab-derived boron isotope signatures in arc volcanic rocks from the Central Andes and evidence for boron isotope fractionation during progressive slab dehydration. Geochemistry, Geophysics and Geosystems 4, doi: 10.1029/2002GC000438.

Ross, K., Elthon, D. (1993). Cumulates from strongly depleted mid-ocean ridge basalt. Nature 365, 826-829.

Ross, K., Elthon, D. (1997). Extreme incompatible trace-element depletion of diopside in residual mantle from south of the Kane Fracture Zone. In: Karson, J. A., Cannat, M., Miller, D. J. and Elthon, D. (ed.) Proceedings of the Ocean Drilling Program: Scientific Results. College Station, TX: Ocean Drilling Program, 277-284.

Ross, J.V., Zimmerman, J. (1996). Comparison of evolution and tectonic significance of the Pindos and Vourinos ophiolite suites, northern Greece. Tectonophysics 256, 1-15.

Rudnick, R.L., Gao, S. (2004). Composition of the Continental Crust. In: Holland, H.D., Turekian, K.K. (Ed.), Treatise on Geochemistry 3, 1-64.

Rumble, D., Hoering, T.C. (1994). Analysis of oxygen and sulfur isotope ratios in oxide and sulfide minerals by spot heating with a carbon dioxide laser in a fluorine atmosphere. Accounts of Chemical Research 27, 237-241.

Rüpke, L.H., Morgan, J.P., Hort, M., Connolly, J.A.D. (2002). Are the regional variations in Central American arc lavas due to differing basalt versus peridotitic slab sources of fluids? Geology 30, 1035-1038.

Ryan, J.G. (2002). Trace-element systematics of beryllium in terrestrial materials. In: Grew, E. S. (ed.) Beryllium - Mineralogy, Petrology and Geochemistry. Reviews in Mineralogy and Geochemistry 50, 121-145.

Ryan, J.G., Langmuir, C.H. (1987): The systematics of lithium abundances in young volcanic rocks*. Geochimica et Cosmochimica Acta 51, 1727-1741.

Ryan, J.G., Langmuir, C.H. (1988). Beryllium systematics in young volcanic rocks: Implications for 10Be*. Geochimica et Cosmochimica Acta 52, 237-244.

Ryan, J.G., Langmuir, C.H. (1993): The systematics of boron abundances in young volcanic rocks. Geochimica et Cosmochimica Acta 57, 1489-1498.

Saccani, E., Photiades, A. (2004). Mid-ocean ridge and supra-subduction affinities in the Pindos ophiolites (Greece): implications for magma genesis in forearc setting. Lithos 73, 229-253.

Salters, V.J.M., Stracke, A. (2004). Composition of the depleted mantle. Geochemistry, Geophysics and Geosystems 5, doi: 10.1029/2003GC000597.

Sanford, R.F. (1982). Growth of ultramafic reaction zones in greenschist to amphibolite facies metamorphism. American Journal of Science 282, 543-616.

Sano, T., Hasenka, T., Shimaoka, A., Yonezawa, C., Fukuoka, T. (2001). Boron contents of Japan Trench sediments and Iwate basaltic lavas, Northeastern Japan: estimation of sediment-derived fluid contribution in mantle wedge. Earth and Planetary Science Letters 186, 187-198.

Sauerer, A., Troll, G., Matthies, D. (1989): Microdistribution of boron: particle-track images from samples of a Caledonian igneous complex. Terra Nova, 1, 359-364.

Savov, I.P., Ryan, J.G., D'Antonio, M., Kelly, K., Mattie, P. (2005). Geochemistry of serpentinized peridotites from the Mariana Forearc Conical Seamount, ODP Leg 125: Implications for the elemental recycling at subduction zones. Geochemistry Geophysics Geosystems 6, doi: 10.1029/2004GC000777.

Scambelluri, M., Hermann, J., Morten, L., Rampone, E. (2006). Melt-versus fluid-induced metasomatism in spinel to garnet wedge peridotites (Ulten Zone, Eastern Italian Alps): clues from trace element and Li abundances. Contributions to Mineralogy and Petrology 151, 372-394.

Scambelluri, M., Müntener, O., Ottolini, L., Pettke, T.T., Vannucci, R. (2004). The fate of B, Cl and Li in the subducted oceanic mantle and in the antigorite breakdown fluids. Earth and Planetary Science Letters 222, 217-234.

Scambelluri, M., Philippot, P. (2004). Volatile and mobile element recycling during subduction of the oceanic lithosphere. Insights from metasediments and serpentinites of the Alps. Periodico di Mineralogia 73, 221-233.

Schmid, S.M., Fugenschuh, B., Kissling, E., Schuster, R. (2004). Tectonic map and overall architecture of the Alpine orogen. Eclogae Geol. Helv. 97 (1), 93-117.

Schmidt, K., Koschinsky-Fritsche, A., Garbe-Schönberg, D. (2006). Detailed geochemical investigation of hydrothermal fluids from Logatchev field, 15°N, MAR. Supplement to Geochimica et Cosmochimica Acta 70, A563.

Schmidt, K., Koschinsky, A., Garbe-Schönberg, D., De Carvalho, L.M., Seifert, R. (2007). Geochemistry of hydrothermal fluids from the ultramafic-hosted Logatchev hydrothermal field, 15°N on the Mid-Atlantic Ridge: Temporal and spatial investigation. Chemical Geology 242, 1-21.

Schmidt, C., Thomas, R., Heinrich, W. (2005). Boron speciation in aqueous fluids at 22 to 600°C and 0.1 MPa to 2 GPa. Geochimica et Cosmochimica Acta 69, 275-281.

Seitz, H.-M., Altherr, R., Ludwig, T. (1999). Partitioning of transition elements between orthopyroxene and clinopyroxene in peridotitic and websteritic xenoliths: New empirical geothermometers. Geochimica et Cosmochimica Acta 63, 3967-3982.

Seitz, M.G., Hart, S.R. (1973). Uranium and boron distributions in some oceanic ultramafic rocks. Earth and Planetary Science Letters 21, 97-107.

Seitz, H.-M., Woodland, A.B. (2000). The distribution of lithium in peridotitic and pyroxenitic mantle lithologies - an indicator of magmatic and metasomatic processes. Chemical Geology 166, 47-64.

Seyfried, W.E., Chen, X., Chan, L.-H. (1998): Trace element mobility and lithium isotope exchange during hydrothermal alteration of seafloor weathered basalt: An experimental study at 350°C, 500 bars. Geochimica et Cosmochimica Acta 62, 949-960.

Seyfried Jr., W.E., Dibble Jr., W.E. (1980). Seawater-peridotite interaction at 300°C and 500 bars: implications for the origin of oceanic serpentinites. Geochimica et Cosmochimica Acta 44, 309-321.

Seyfried Jr., W.E., Janecky, D.R., Mottl, M.J. (1984). Alteration of the oceanic crust: Implications for geochemical cycles of lithium and boron. Geochimica et Cosmochimica Acta 48, 557-569.

Seyler, M., Lorand, J.P., Dick, H.J.B., Drouin, M. (2007). Pervasive melt percolation reactions in ultra-depleted refractory harzburgites at the Mid-Atlantic Ridge, 15° 20'N: ODP Hole 1274A. Contributions to Mineralogy and Petrology 153, 303-319.

Seyler, M., Toplis, M.J., Lorand, J.P., Luguet, A., Cannat, M. (2001). Clinopyroxene microtextures reveal incompletely extracted melts in abyssal peridotites. Geology 29, 155-158.

Shannon, R.D. (1976): Revised effective ionic radii in halides and chalcogenides. Acta Crystallographica A32, 751-767.

Sharma, A., Jenkins, D.M. (1999). Hydrothermal synthesis of amphiboles along the tremolite-pargasite join and in the ternary system tremolite-pargasite-cummingtonite. American Mineralogist 84, 1304-1318.

Sharp, Z.D. (1990). A laser-based microanalytical method for the in-situ determination of oxygen isotope ratios of silicates and oxides. Geochimica et Cosmochimica Acta 54, 1353-1357.

Sharp, Z.D., Atudorei, V. and Durakiewicz, T. (2001). A rapid method for determination of hydrogen and oxygen isotope ratios from water and hydrous minerals. Chemical Geology 178 (1-4), 197-210.

Smith, A.G. (1979). Othris, Pindos and Vourinos Ophiolites and the pelagonian zone. Proc. Colloq. Geol. Aegean Region 6, 1369-1374.

Smith, H.J., Leeman, W.P., Davidson, J., Spivack, A.J. (1997). The Boron isotopic composition of arc lavas from Martinique, Lesser Antilles. Earth and Planetary Science Letters 146, 303-314.

Smith, A.G., Spivack, A.J., Staudigel, H., Hart, S.R. (1995). The boron isotopic composition of altered oceanic crust. Chemical Geology 126, 119-135.

Smith, A.G., Woodcock, N.H. (1976). Emplacement model for some Tethyan ophiolites. Geology 4, 635-656.

Sobolev, A.V., Shimizu, N. (1993). Ultra-depleted primary melt included in an olivine from the Mid-Atlantic Ridge. Nature 363, 151-154.

Sovatzoglou-Skounakis, E., Economou-Eliopoulos, M. (1997). Fe-Cu-Ni-Co sulfide mineralizations from the Pindos and Veria ophiolite complexes, Greece. Ofioliti 22, 227-230.

Spandler, C., O'Neill, H.S.C., Kamenetsky, V.S. (2007). Survival times of anomalous melt inclusions from element diffusion in olivine and chromite. Nature 447 (7142), 303-306.

Spivack, A.J., Edmond, J.M. (1987). Boron isotope exchange between seawater and the oceanic crust. Geochimica et Cosmochimica Acta 51, 1033-1043.

Spivack, A.J., You, C.F. (1997). Boron isotopic geochemistry of carbonates and pore waters, Ocean Drilling Program Site 851. Earth and Planetary Science Letters 152, 113-122.

Spray, J.G., Bebien, J., Rex, D.C, Roddick, J.C. (1984). Age constraints on the igneous and metamorphic evolution of the Hellenic-Dinaric ophiolites. In: Dixon, J. E., Robertson A.H.F. (ed.) The Geological Evolution of the Eastern Mediterranean. London: Geological Society of London Special Publication 17, 619-627.

Spray, J.G., Roddick, J.C. (1980). Petrology and 40Ar-39Ar geochronology of some hellenic sub-ophiolitic metamorphic rocks. Contributions to Mineralogy and Petrology 72, 43-55.

Stampfli, G., Mosar, J., Bono, A. de, Vavasis, I. (1998). Late Paleozoic, early Mesozoic plate tectonics of the western Tethys. Bull. Soc. Geol. Greece 32, 113-120.

Steck, A., Bigioggero, B., Dal Piaz, G.V., Escher, A., Martinotti, G., Masson, H. (1999). Carte tectonique des Alpes de Suisse occidentale et des régions avoisinantes 1:100 000. Service hydrologique et géologique national carte géologique spéciale N°123, feuille 42 Oberwallis.

Sturm, M.E., Klein, E.M., Karsten, J.L., Karson, J.A. (2000). Evidence for subduction-related contamination of the mantle beneath the Southern Chile Ridge: Implications for ambiguous ophiolite compositions. In: Dilek, Y., Moores, E.M., Elthon, D., Nicolas, A. (ed.) Ophiolites and Oceanic crust: New Insights from Field Studies and Ocean Drilling Program. Boulder, Colorado: Geological Society of America Special Paper 349, 13-20.

Sun, S.-S., McDonough, W.F. (1989). Chemical and isotopic systematics of oceanic basalts: implications for mantle composition and processes. In: Saunders, A. D., Norry, M.J. (ed.) Magmatism in the Ocean Basins. London: Geological Society of London Special Publication 42, 313-345.

Takahashi, E., Uto, K., Schilling, J.-G. (1987). Primary magma compositions and Mg/Fe ratios of their mantle residues along Mid Atlantic Ridge 29° N to 73° N. Technical report of ISEI Okayama University Series 9, 1-4.

Tatsumi, Y. (1989). Migration of fluid phases and genesis of basalt magma at subduction zones. Journal of Geophysical Research 94, 4697-4707.

Tenthorey, E., Hermann, J. (2004). Composition of fluids during serpentinite breakdown in subduction zones: Evidence for limited boron mobility. Geology 32, 865-868.

Thompson, G., Melson, W.G. (1970). Boron contents of serpentinites and metabasalts in the oceanic crust: implications for the boron cycle in the oceans. Earth and Planetary Science Letters 8, 61-65.

Thuizat, R., Whitechurch, H., Montigny, R., Juteau, T. (1981). K-Ar dating of some intra-ophiolite metamorphic soles from the East Mediterranean: New evidence for oceanic thrusting before obduction. Earth and Planetary Science Letters 52, 302-310.

Tomascak, P.B., Ryan, G.R., Defant, M.J. (2000). Lithium isotope evidence for light element decoupling in the Panama subarc mantle. Geology 28, 507-510.

Tomascak, P.B., Widom, E., Benton, L.D., Goldstein, S.L., Ryan, J.G. (2002). The control of lithium budgets in island arcs. Earth and Planetary Science Letters 196, 227-238.

Trommsdorff, V., Evans, B.W. (1974): Alpine metamorphism of peridotite rocks. Schweizerische Mineralogische und Petrographische Mitteilungen 54(2-3), 333-352.

Tucholke, B.E., Lin, J., Kleinrock, M.C. (1998). Megamullions and mullion structure defining oceanic metamorphic core complexes on the Mid-Atlantic ridge. Journal of Geophysical Research - Solid Earth 103 (B5), 9857-9866.

Ulmer, P., Trommsdorff, V. (1995). Serpentine stability to mantle depths and subduction-related magmatism. Science 268, 858-861.

Wagner, C., Deloule, E. (2004). Li and ∂7Li behaviour in mantle metasomatic processes. Supplement to Geochemica et Cosmochemica Acta 68, A49.

Wallin, E.T., Metcalf, R.V. (1998). Supra-subduction zone ophiolite formed in an extensional forearc: Trinity terrane, Klamath Mountains, California. Journal of Geology 106, 591-608.

Wei, W., Kastner, M., Deyhle, A., Spivack, A.J. (2005). Geochemical cycling of fluorine, chlorine, bromine, and boron and implications for fluid-rock reactions in Mariana forearc, South Chamorro Seamount, ODP Leg 195. Proceedings of the Ocean Drilling Program, Scientific Results 195, 1-23.

Wenner, D.B., Taylor Jr., H.P., 1974. D/H and 18O/16O studies of serpentinization of ultramafic rocks. Geochimica et Cosmochimica Acta 38, 1255-1286.

Wertz, K.L. (2003). From seafloor spreading to uplift: the structural and geochemical evolution of Macquarie Island on the Australian-Pacific plate boundary. Unpublished PhD Thesis. Austin (USA): University of Texas, 169 p.

Whittaker, E.J.W., Zussman, J. (1956): The characterization of serpentine minerals by X-ray diffraction. Mineralogical Magazine 233, 107-126.

Witt-Eickschen, G., Seck, H.A. (1991). Solubility of Ca and Al in orthopyroxene from spinel peridotite: an improved version of an empirical geothermometer. Contributions to Mineralogy and Petrology 106, 431-439.

Wicks, F.J., Whittaker, E.J.W. (1977). Serpentine textures and serpentinization. The Canadian Mineralogist 15, 459-488.

Woodland, A.B., Seitz, H.-M., Yaxley, G.M. (2004). Varying behaviour of Li in metasomatised spinel peridotite xenoliths from western Victoria, Australia. Lithos 75, 55-66.

Xu, Y.-G., Menzies, M.A., Thirlwall, M.F., Huang, X.-L., Liu, Y., Chen, X.-M. (2003). «Reactive» harzburgites from Huinan, NE China: Products of the lithosphere-asthenosphere interaction during lithospheric thinning? Geochimica et Cosmochimica Acta 67(3), 487-505.

You, C.F., Butterfield, D.A., Spivack, A.J., Gieskes, J.M., Gamo, T., Campbell, A.J. (1994). Boron and halide systematics in submarine hydrothermal systems: effects of phase separation and sedimentary contributions. Earth and Planetary Science Letters 123, 227-238.

You, C.F., Chan, L.H., Spivack, A.J., Gieskes, J.M. (1995a). Lithium, boron, and their isotopes in sediments and pora waters of Ocean Drilling program Site 808, nankai Trough: implications for fluid expulsion in accretionary prisms. Geology 23, 37-40.

You, C.-F., Spivack, A.J., Gieskes, J.M., Rosenbauer, R., Bischoff, J.L. (1995b). Experimental study of boron geochemistry: Implications for fluid processes in subduction zones. Geochimica et Cosmochimica Acta 59, 2435-2442.

Zack, T., Foley, S.F., Rivers, T. (2002). Equilibrium and disequilibrium trace element partitioning in hydrous eclogites (Trescolmen, Central Alps). Journal of Petrology 43(10), 1947-1974.

Zanetti, A., D'Antonio, M., Spadea, P., Raffone, N., Vannucci, R., Brugeir, O. (2006). Petrogenesis of mantle peridotites from the Izu-Bonin-Mariana (IBM) forearc. Ofioliti 31(2), 189-206.

Zheng, H., Bailey, S.W. (1995): The crystal structure of manandonite-2H2. American Mineralogist 80, 387-393.

Zierenberg, R.A., Fouquet, R.A., Miller, D.J., Bahr, J.M., Naker, P.A., Bjerkgard, T., Brunner, C.A., Duckworth, R.C., Gable, R., Gieskes, J.M., Goodfellow, W.D., Groschel-Becker, H.M., Guerin, G., Ishibashi, J., Iturrino, G., James, R.H., Lackschewitz, K.S., Marquez, L.L., Nehlig, P., Peter, J.M., Rigsby, C.A., Schultheiss, P., Shanks, W.C., Simoneit, B.R.T., Summit, M., Teagle, D.A.H., Urabt, M., Zuffa, G.G., 1998. The deep structure of a sea-floor hydrothermal deposit. Nature 392 (6675): 485-488.

Publications, manuscript and abstracts

PUBLISHED PAPER

2006 **Pelletier L.** and Müntener O.: High-pressure metamorphism of the Lanzo peridotite and its oceanic cover, and some consequences for the Sesia-Lanzo zone (northwestern Italian Alps), Lithos, 90, 111-130.

SUBMITTED PAPERS

2008 **Pelletier L.**, Vils F. and Kalt A.: Li, B and Be contents of the Pindos harzburgites (Greece): a MOR-type mantle in a supra-subduction zone environment, accepted by the Journal of Petrology (with minor revisions).

2008 **Pelletier L.**, Müntener O., Kalt A., Vennemann T.W. and Belgya T.: Li, Be and B mobility during emplacement of ultramafic rocks in the continental crust: the example of the Geisspfad body (Swiss-Italian Alps), accepted by Chemical Geology (with moderate revisions).

2008 **Pelletier L.**, Vils F., Kalt A. and Groppo C.: Li and B variability in serpentine: intracrystalline or intercrystalline ?, submitted to the European Journal of Mineralogy.

2008 Vils F., **Pelletier L**., kalt A., Müntener O., Ludwig T.: The lithium, boron and beryllium content of serpentinized peridotites from ODP leg 209 (sites 1272A and 1724A): implications for lithium and boron budgets of oceanic lithosphere, submitted to Geochimica et Cosmochimica Acta.

PAPERS IN PREPARATION

2008 Vils F., Tonarini S., Seitz H.-M., Kalt A., **Pelletier L**.: Boron, lithium and strontium isotopes as tracers of seawater-serpentinite interaction at Mid-Atlantic ridge, ODP Leg 209.

2008 **Pelletier L.**, Kalt A., Dijkstra A., Pettke T.: Interaction of the Dramala harzburgites (Pindos ophiolite, Greece) with ultra-depleted melt.

UNPUBLISHED MANUSCRIPT

2003 **Pelletier L.**: Relations entre une croûte océanique et sa couverture sédimenatire: l'exemple du massif de Lanzo (Alpes piémontaises, Italie). Diploma thesis, University of Neuchâtel (CH), 83 p.

CONFERENCE ABSTRACTS

2006 **Pelletier L.**, Vils F. and Kalt A.: Li, Be and B in Pindos mantle rocks (Greece) evidence against a supra-subduction origin, 4th Swiss Geoscience Meeting (Bern), abstract book, 155.

2006 **Pelletier L.**, Vils F. and Kalt A.: Li, Be and B in Pindos and Vourinos mantle rocks (Greece): Evidence against a supra-subduction origin, Suppl. to Geochimica et Cosmochimica Acta, 70(18), A481.

2006 Vils F., **Pelletier L.**, Kalt A. and Müntener O.: Potential input of light elements into subduction zones – Insights from ODP Leg 209, Suppl. to Geochimica et Cosmochimica Acta, 70(18), A674.

2006 Vils F., **Pelletier L**., Kalt A., Müntener O. and Ludwig T.: Light element (Li, Be and B) concentrations in peridotites from the Mid-Atlantic-Ridge; ODP Leg 209, Geophysical Research Abstracts, 8, 06000.

2005 **Pelletier L.** and Kalt A.: Relation between melt percolation and light element contents (Li, Be and B) in peridotites from the Pindos ophiolite (Greece), Ofioliti, 30(2), 204.

2005 **Pelletier L.**, Vils F., Kalt A. and Ludwig T.: The oceanic mantle as an important repository for light elements (Li, Be and B), Geophysical Research Abstracts, 7, 01988.

2005 **Pelletier L**. and Kalt A.: Relation between melt percolation and light element contents (Li, Be and B) in peridotites from the Pindos ophiolite (Greece), Ofioliti, 30(2), 231.

2005 Vils F., **Pelletier L**., Kalt A. and Müntener O.: The Pindos and Vourinos ophiolites (Northern Greece): mineral compositions and thermobarometry, Geophysical Research Abstracts, 7, 01986.

2004 **Pelletier L.** & Müntener O.: High pressure metamorphic evolution of oceanic crust: the example of the Lanzo massif and its sedimentary cover (western Alps), Geophysical Research Abstracts, 6, 01550.

THE OCEANIC MANTLE AS AN IMPORTANT REPOSITORY FOR THE LIGHT ELEMENTS Li, Be AND B

Thèse présentée à la Faculté des Sciences
Institut de Géologie et d'Hydrogéologie
Université de Neuchâtel

pour l'obtention du grade de docteur ès sciences par **Laure Pelletier**

soutenue le 22 janvier 2008

Complementary appendix

1 Sample localization and mineralogy
2 Geisspfad ultramafic body
4 Mid-Atlantic ridge ODP leg 209 sites 1272A and 1274A
6 Pindos ophiolite

9 Micro-Raman
11 Geisspfad ultramafic body
14 Mid-Atlantic ridge ODP leg 209 sites 1272A and 1274A
20 Pindos ophiolite
24 Vourinos ophiolite

27 Electron microprobe (EMPA) - major elements
28 Geisspfad ultramafic body
62 Pindos ophiolite

175 Mineral profiles - major and light elements (Li, B)
176 Geisspfad ultramafic body
180 Pindos ophiolite

207 Secondary ion mass spectrometry (SIMS) - light elements (Li, Be, B)
208 Geisspfad ultramafic body
212 Pindos ophiolite

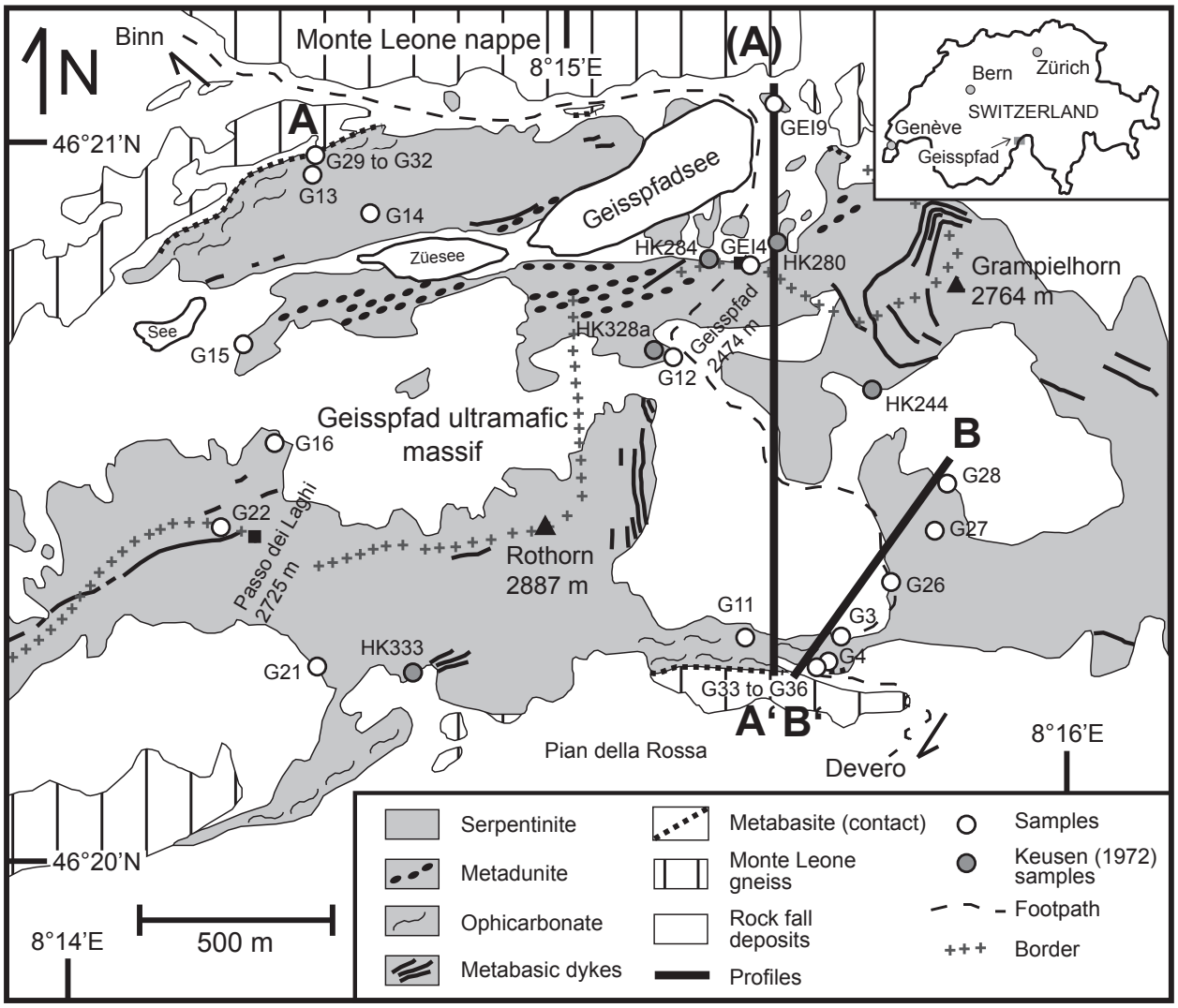
217 Laser ablation - inductively coupled plasma mass spectrometry (LA-ICPMS) - Li, B and other trace elements
218 Pindos ophiolite

225 Standard data
226 ICP-MS Boston (USA) and Bristol (UK)
230 PGNAA
231 LA-ICPMS
234 Stable isotopes

Université de Neuchâtel unine

Sample localization and mineralogy

Geisspfad ultramafic body



Geisspfad ultramafic body: mineralogy of the studied samples

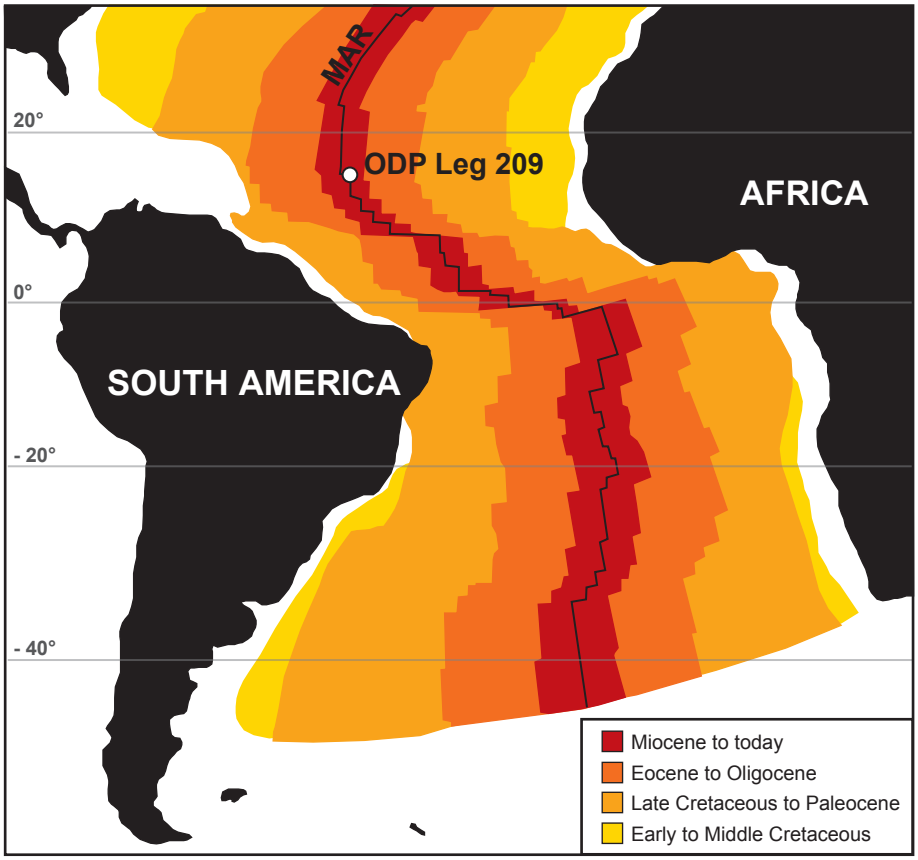
Sample	Rock type	Fo	Di	Atg	Tr	Chl	Cal	Dol	Ilm
G11	Serpentinite	x	x	x	x	x			
G12	Serpentinite	x		x	x	x			
G26	Serpentinite	x	x	x	x	x			
G27	Serpentinite	x	x	x	x	x			
GEI4	Serpentinite	x		x	x	x			x
G3	Ophicarbonate	x		x	x		x	x	
G4	Ophicarbonate		x	x	x		x	x	
GEI9	Ophicarbonate		x	x	x	x	x		

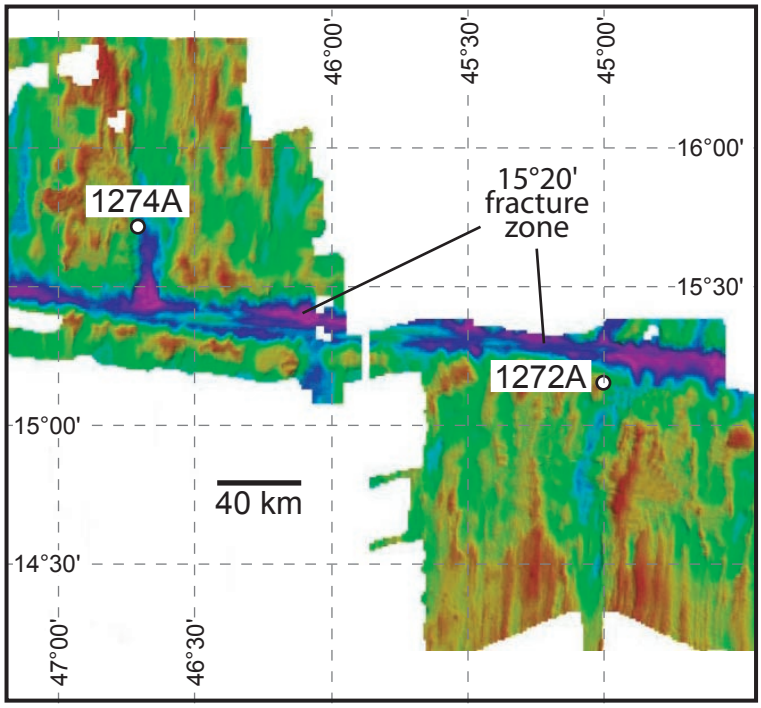
Sample	Rock type	Tsch hbl	Ep	Tit	Chl	Cal	Dol	Tr
G30a	Metabasite	x	x	x	x	x		
G30b	Metabasite	x	x	x	x	x		
G31	Metabasite				x		x	x
G34	Metabasite	x	x	x	x			

Sample	Rock type	Qtz	Ab	Kfsp	Bt	Ms	Chl	Grt	Ap	Ep	Tit	Ilm
G32a	Gneiss	x	x	x	x	x	x				x	
G32b	Gneiss	x		x	x	x				x		
G36	Gneiss	x	x				x	x	x	x		x

Abbreviations: Fo = forsterite, Di = diopside, Atg = antigorite, Tr = tremolite, Chl = chlorite, Cal = calcite, Dol = dolomite, Ilm = ilmenite, Tsch hbl = tschermakitic hornblende, Ep = epidote, Tit = titanite, Qtz = Quartz, Ab = albite, Kfsp = alkali feldspar, Bt = biotite, Ms = muscovite, Grt = garnet, Ap = apatite.

Mid-Atlantic ridge ODP Leg 209 sites 1272A and 1274A

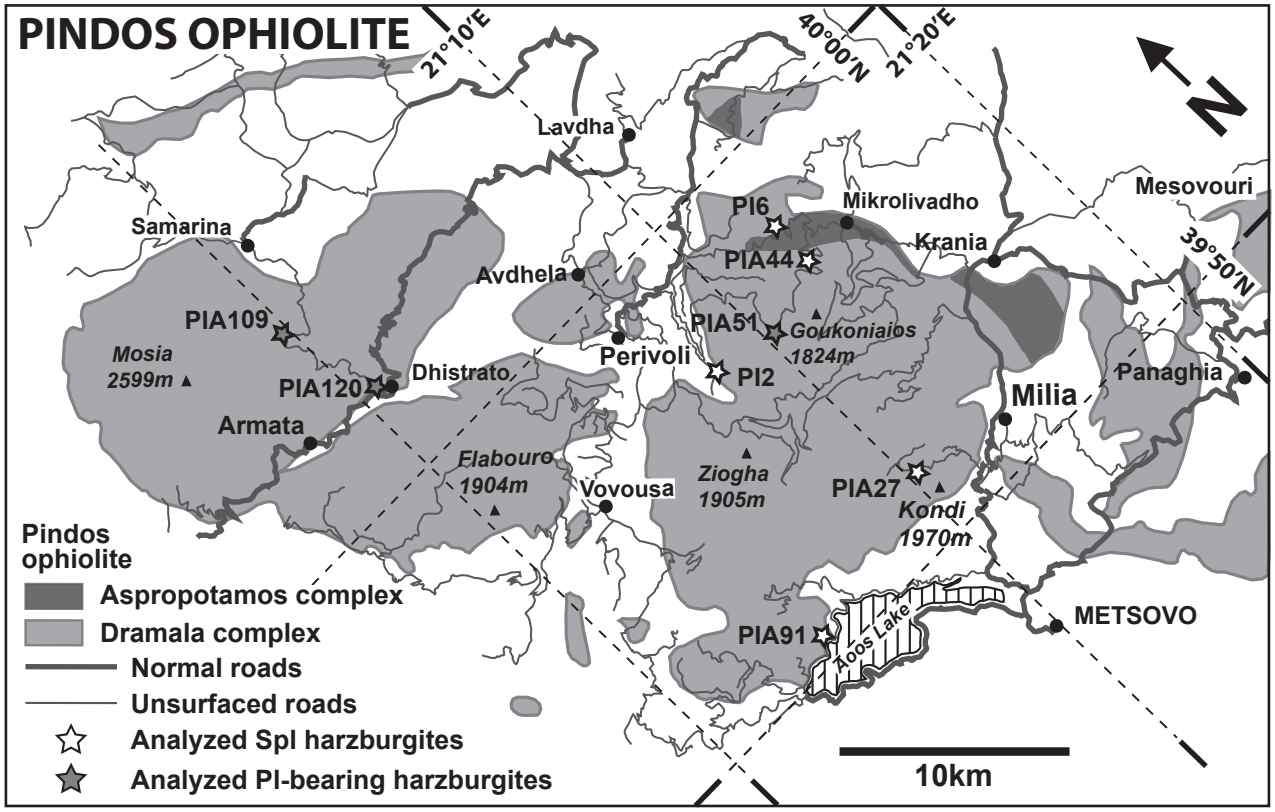




Mid-Atlantic ridge ODP Leg 209 sites 1272A and 1274A: mineralogy of the studied samples

Sample	Site	ODP number	Rock type	Cpx	Opx	Ol	Spl	Srp	Mag	Bru	Phl	Chl
OD2	**1272A**	209-1272A-13R-1, W, 103.5-106.5	Serp spinel harz			x	x	x	x			
OD18	**1272A**	209-1272A-23R-2, W, 22-25	Serp spinel harz				x	x	x			
OD28	**1272A**	209-1272A-27R-1, W, 28-31.5	Serp spinel harz	x	x	x	x	x	x			
OD32	**1274A**	209-1274A-1R-1, W, 88-92	Serp spinel harz	x	x	x	x	x	x			
OD34	**1274A**	209-1274A-3R-1, W, 35-38	Serp spinel harz	x	x	x	x	x	x	x		
OD42	**1274A**	209-1274A-6R-2, W, 68-70	Serp spinel harz	x	x	x	x	x	x		x	x

Abbreviations: Cpx = clinopyroxene, Opx = orthopyroxene, Ol = olivine, Spl = spinel, Srp = serpentine, Mag = magnetite, Bru = brucite, Phl = phlogopite, Chl = chlorite, Serp spinel harz = serpentinized spinel harzburgite.


PINDOS OPHIOLITE
21°10'E
40°00'N
21°20'E
N
39°50'N
Lavdha
Mesovouri
Mikrolivadho
PI6
Samarina
Krania
PIA44
Avdhela
PIA109
PIA51
Goukoniaios
1824m
Mosia
2599m
Perivoli
PI2
Dhistrato
PIA120
Panaghia
Milia
Armata
Elabouro
1904m
Ziogha
1905m
Vovousa
PIA27
Kondi
1970m
METSOVO
PIA91
Aoos Lake
10km
Pindos
ophiolite
Aspropotamos complex
Dramala complex
Normal roads
Unsurfaced roads
Analyzed Spl harzburgites
Analyzed Pl-bearing harzburgites

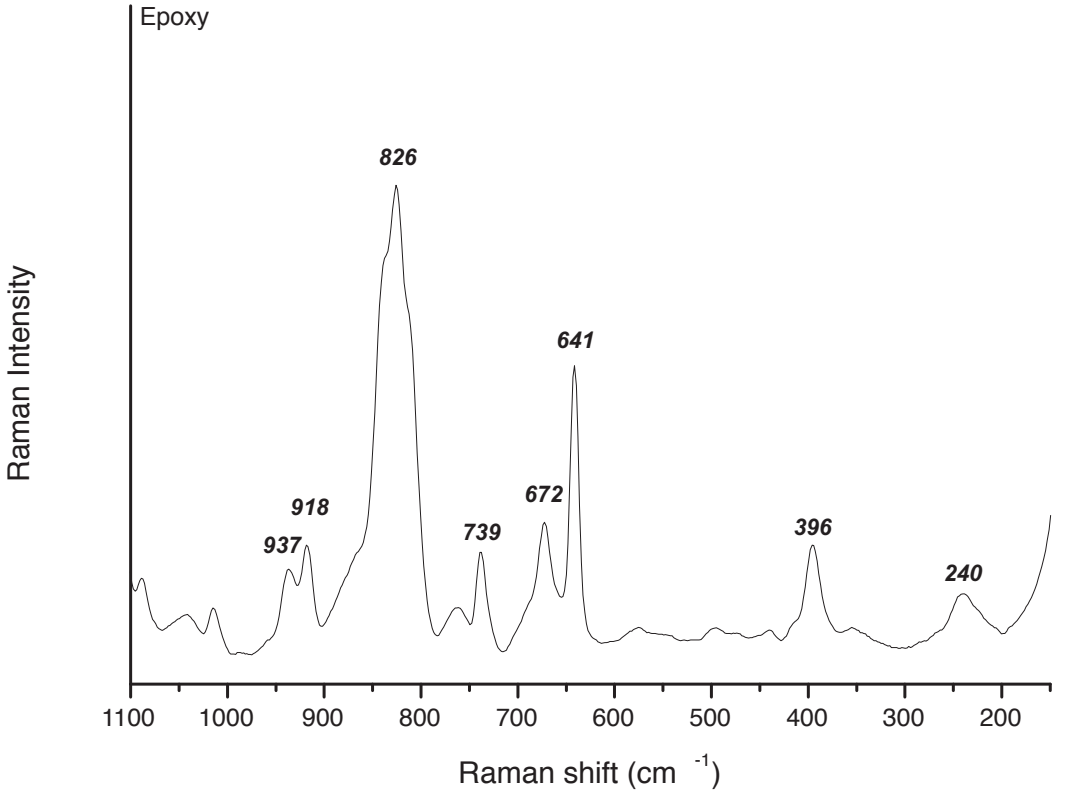
Pindos ophiolite - Dramala complex: mineralogy of the studied samples

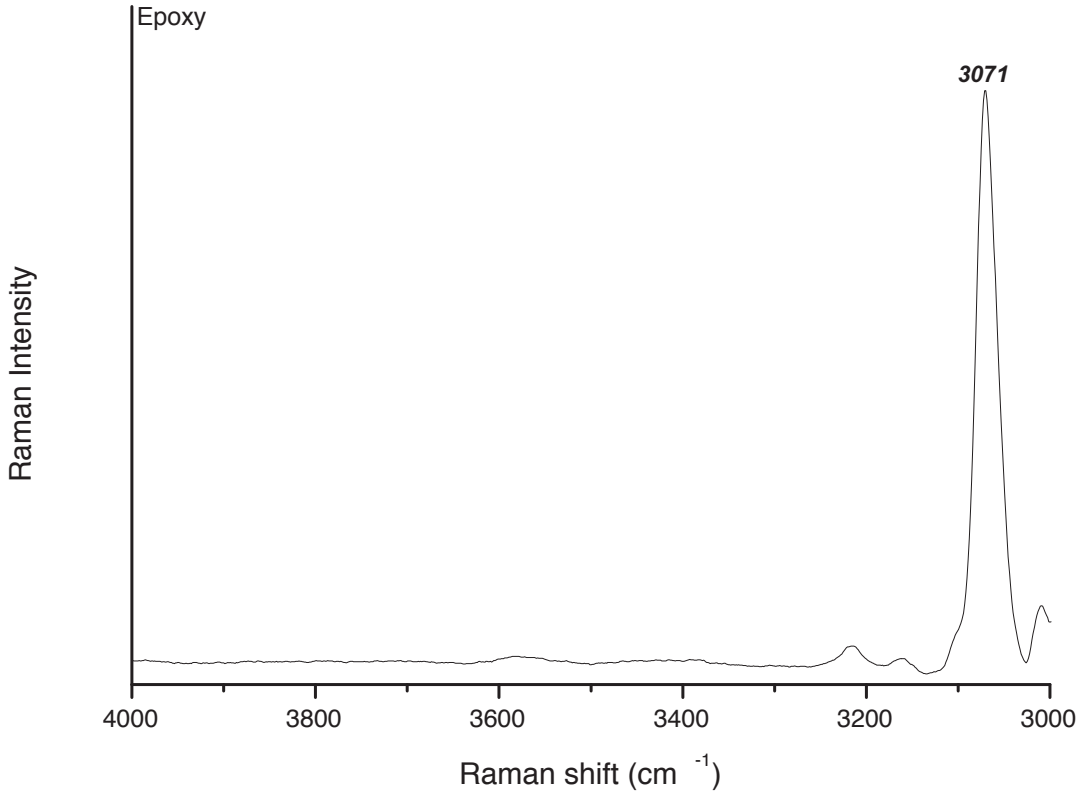
Sample	Rock type	Opx	Cpx	Ol	Spl	Pl	Ed hbl	Prg	Srp	Tr	Ath	Tlc	Chl	Vua	Ntr	Pct
PI2	Spl harzburgite	x	x	x	x											
PIA91	Spl harzburgite	x	x	x	x											
PIA27	Spl harzburgite	x		x	x		x		x	x	x	x	x			
PI6	Spl harzburgite	x	x	x	x				x	x	x					
PIA44	Spl harzburgite	x	x	x	x				x	x						
PIA120	Pl-bear harzburgite	x	x	x	x	x		x	x				x	x	x	x
PIA109	Pl-bear harzburgite	x	x	x	x	x		x								
PIA51	Pl-bear harzburgite	x	x	x	x	x										

Abbreviations: Spl harzburgite = spinel harzburgite, Pl-bear harzburgite = plagioclase-bearing harzburgite, Opx = orthopyroxene, Cpx = clinopyroxene, Ol = olivine, Spl = spinel, Pl = plagioclase, Ed hbl = edenitic hornblende, Prg = pargasite, Srp = serpentine, Tr = tremolite, Ath = anthophyllite, Tlc = talc, Chl = chlorite, Vua = vuagnatite, Ntr = natrolite, Pct = pectolite.

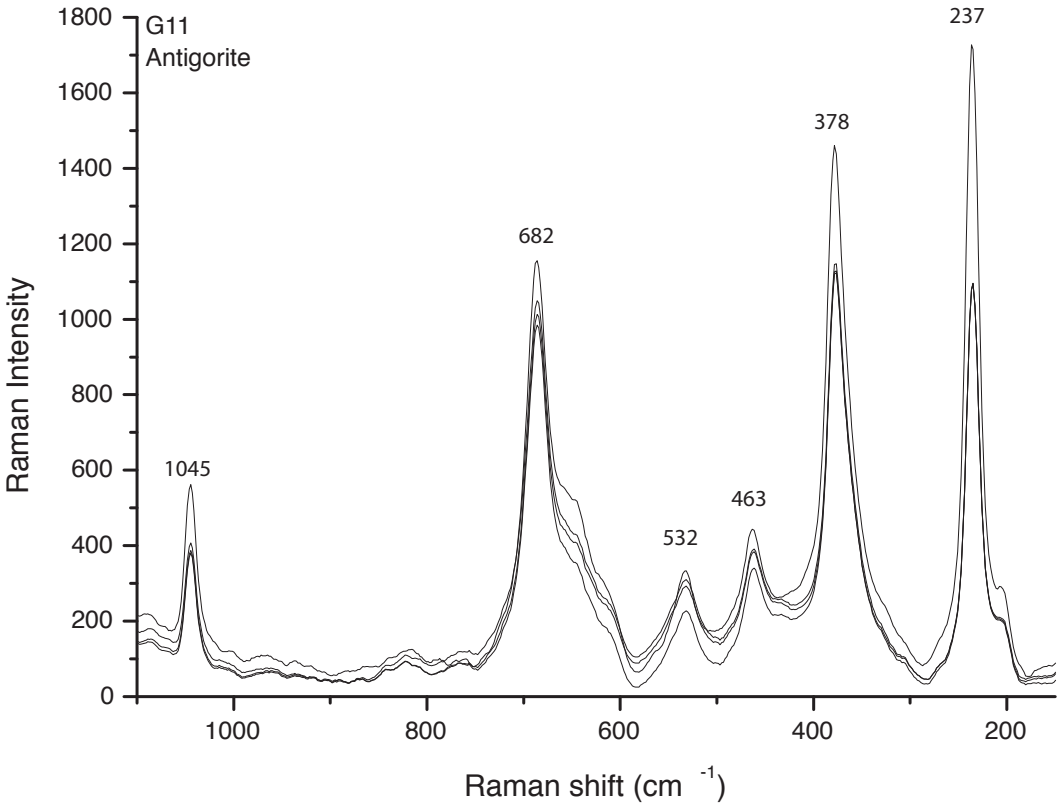
Micro-Raman

Epoxy

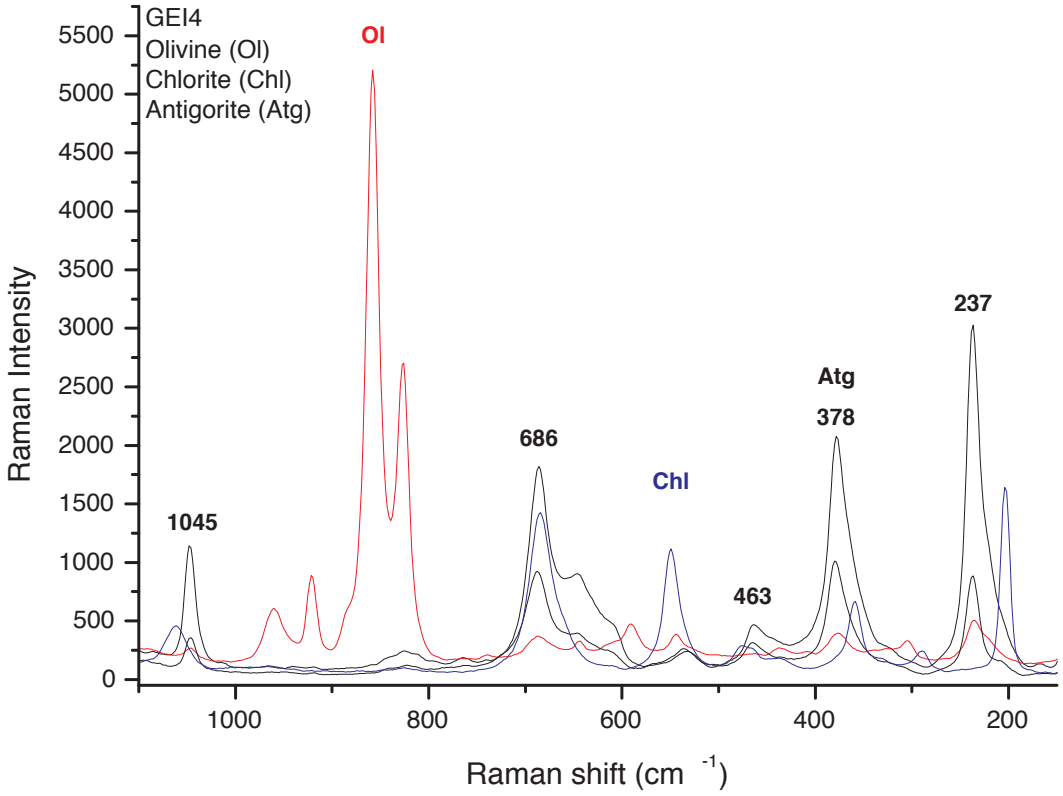

Epoxy
826
641
672
918
937
739
396
240
Raman Intensity
1100
1000
900
800
700
600
500
400
300
200
Raman shift (cm -1)


Epoxy
3071
Raman Intensity
4000
3800
3600
3400
3200
3000
Raman shift (cm -1)

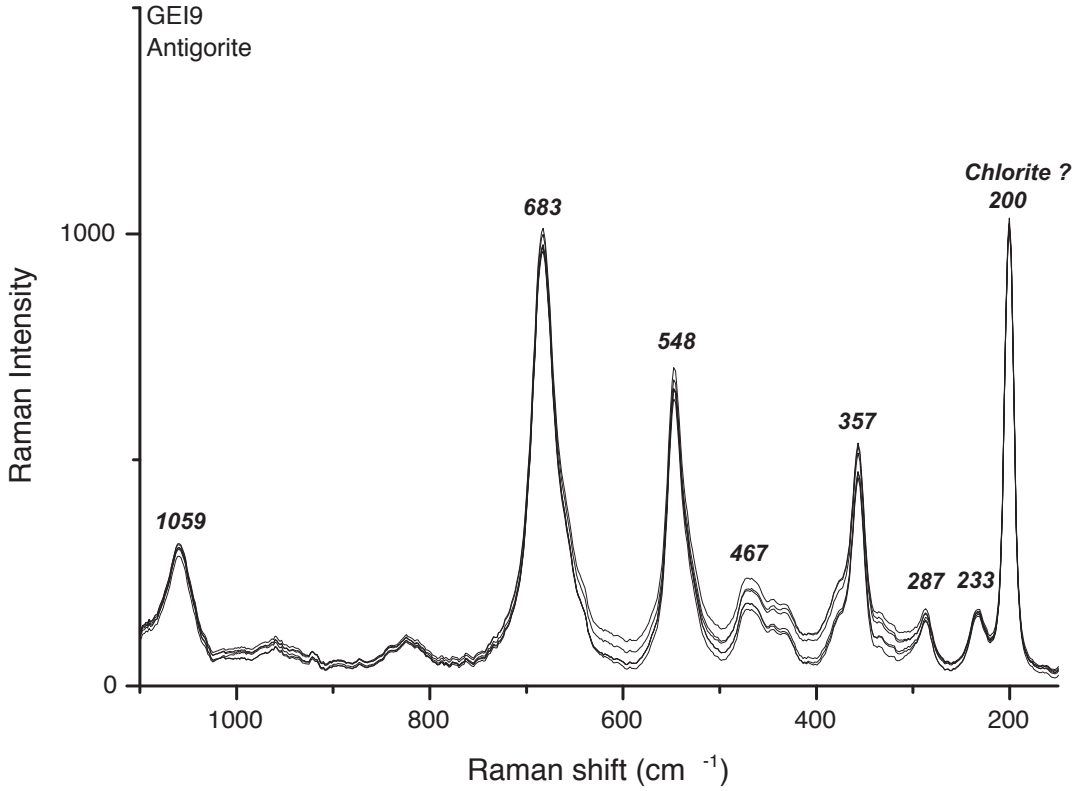
Geisspfad ultramafic body
Serpentinite G11
Antigorite

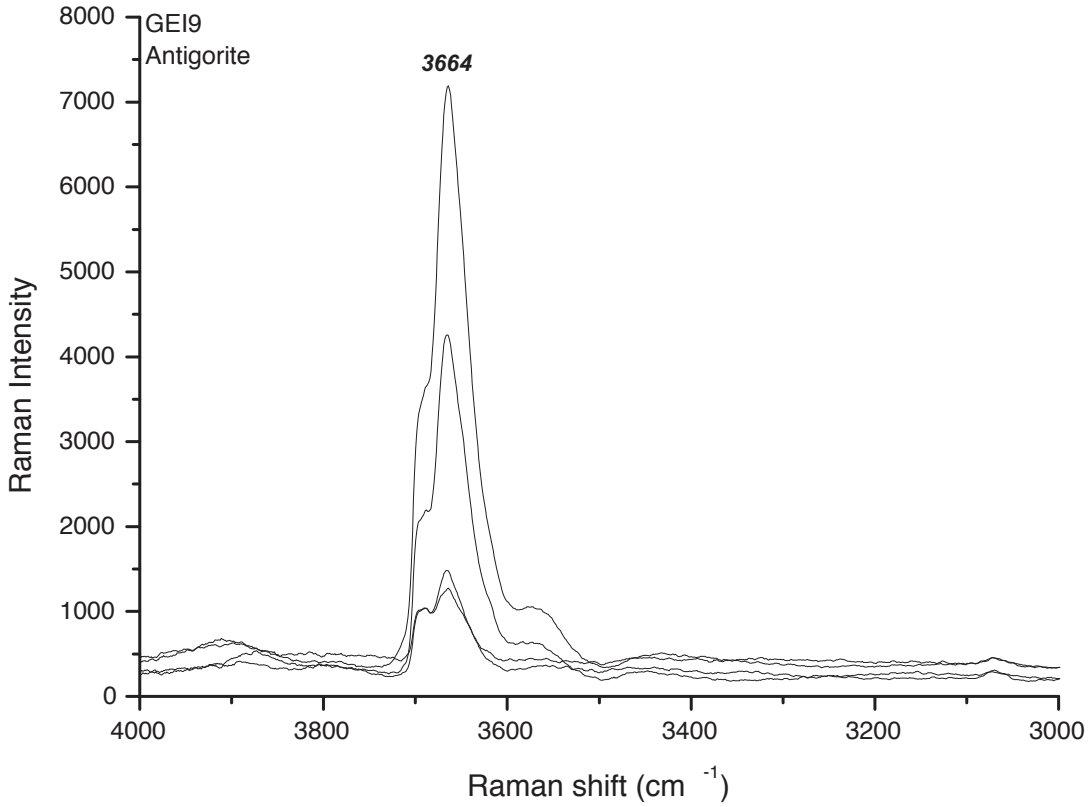


Geisspfad ultramafic body
Serpentinite GEI4
Olivine, chlorite and antigorite

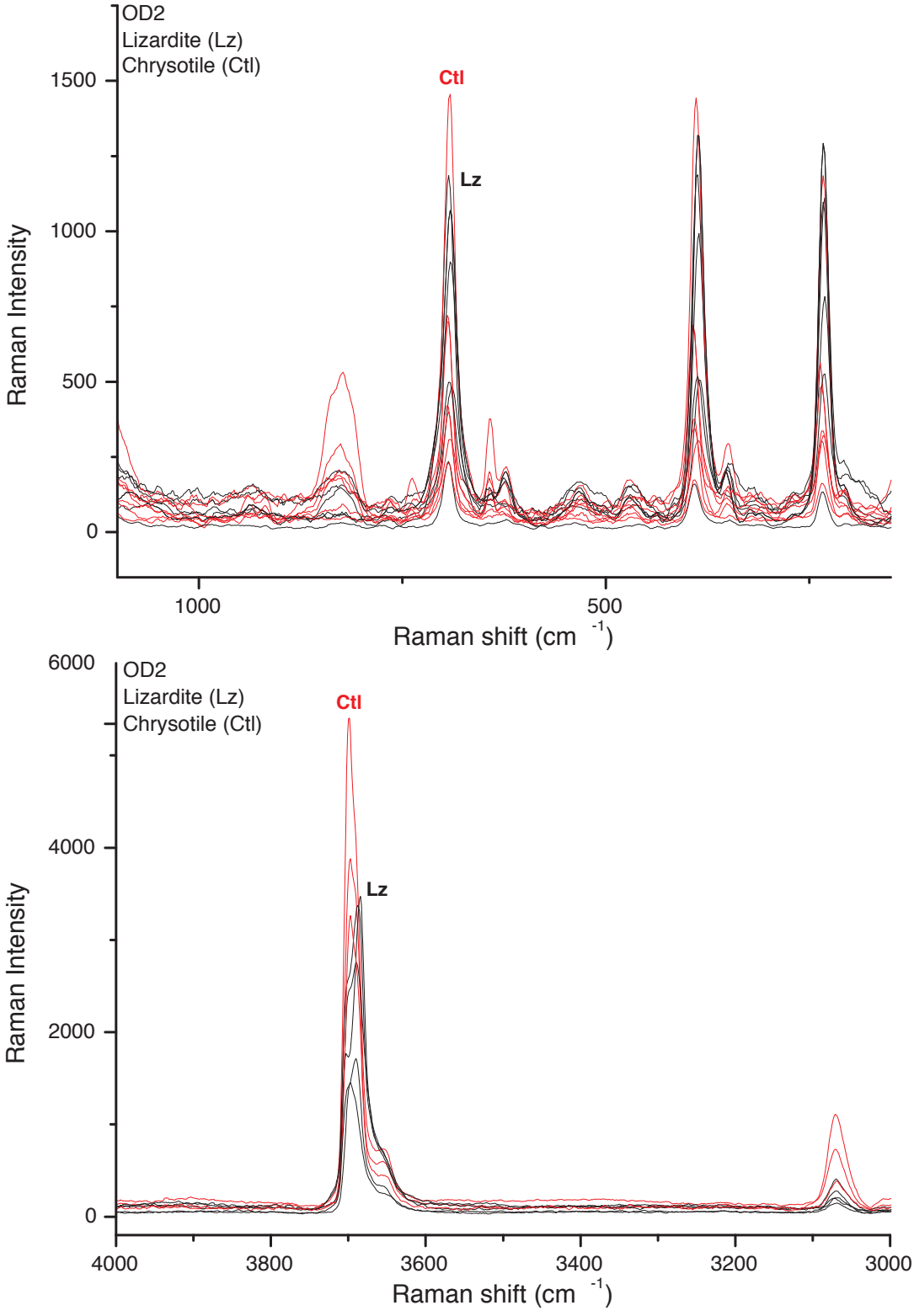


Geisspfad ultramafic body
Ophicarbonate GEI9
Antigorite

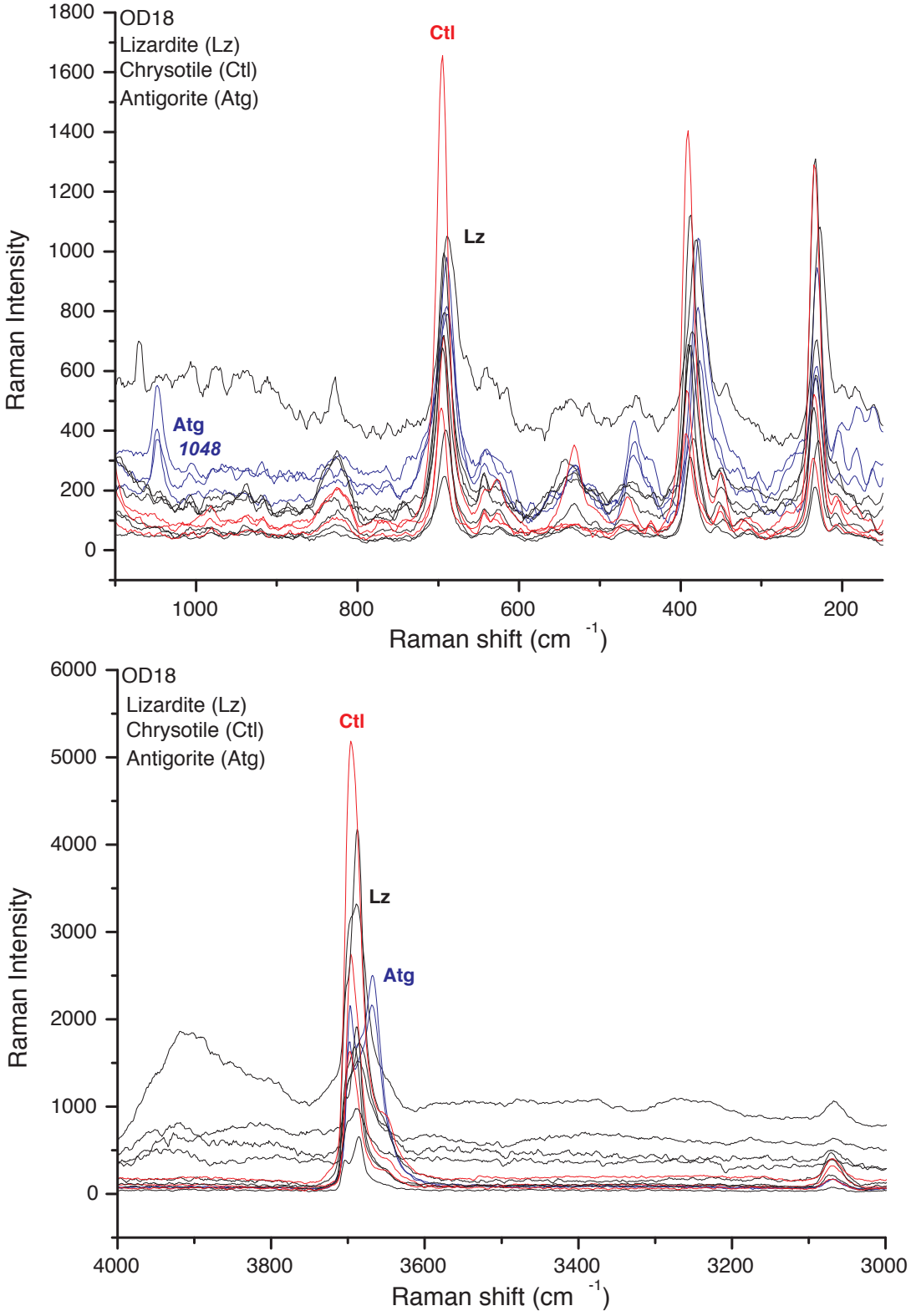




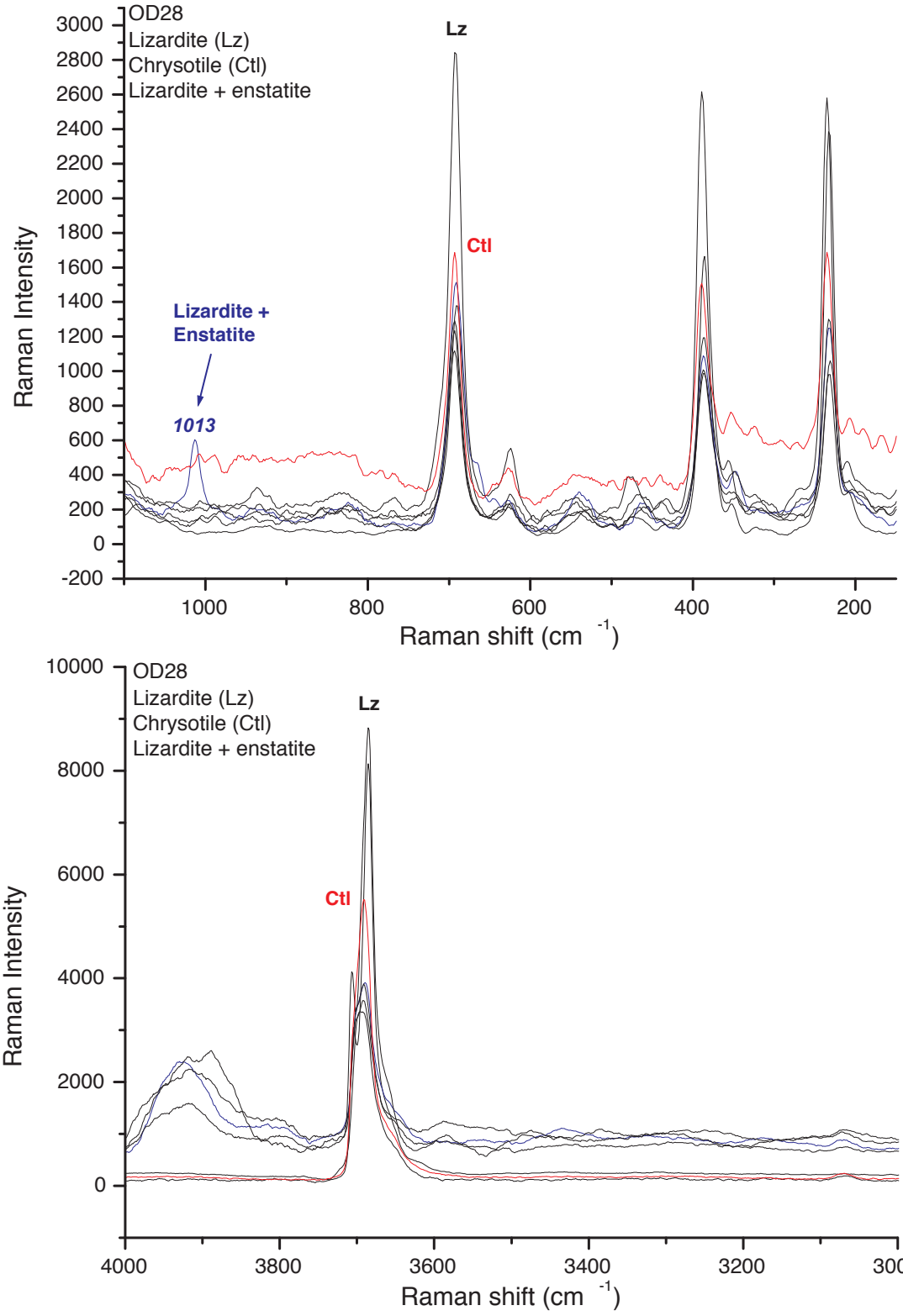
Ocean Drilling Program leg 209 site 1272A
Serpentinite OD2
Lizardite and chrysotile



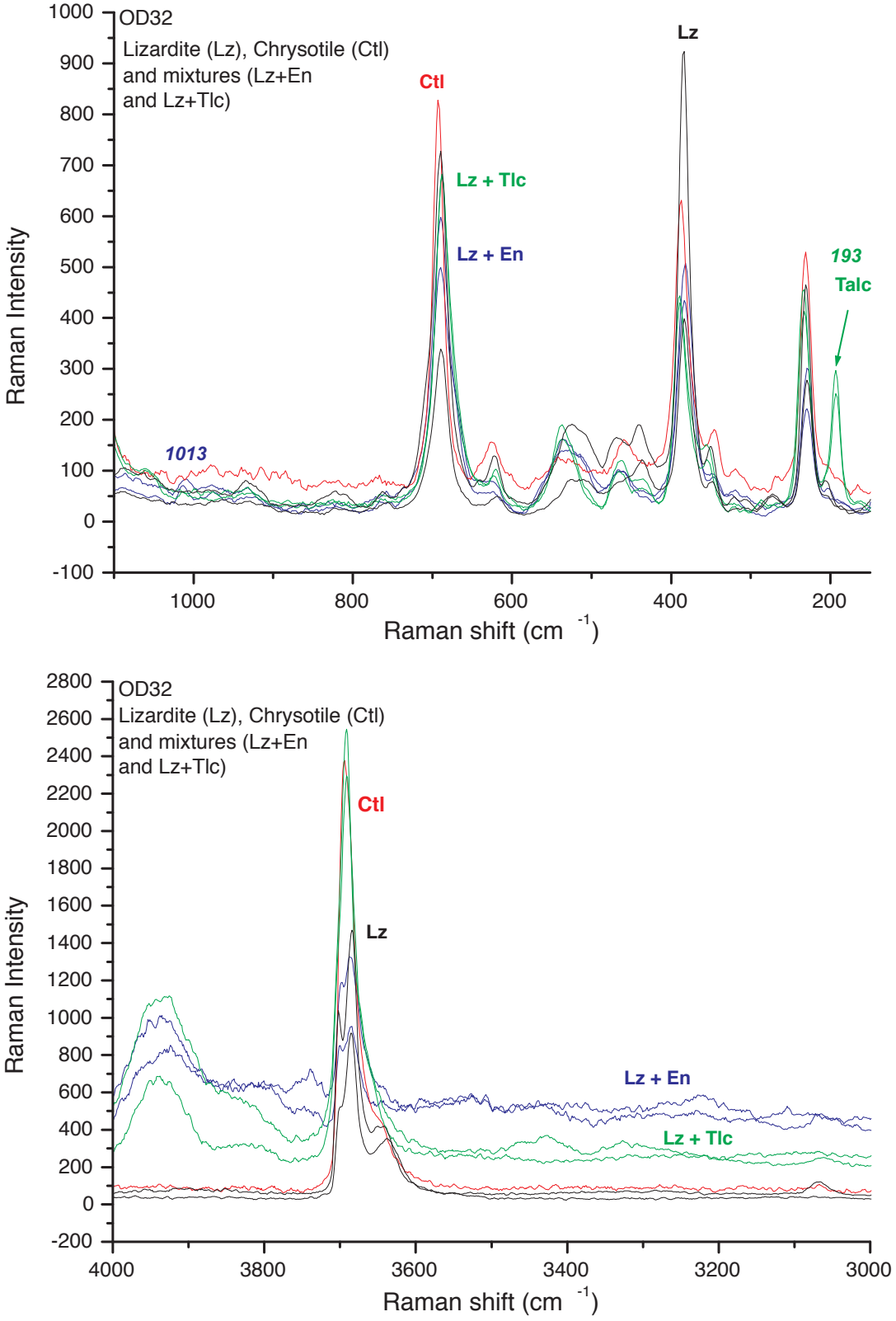
Ocean Drilling Program leg 209 site 1272A
Serpentinite OD18
Lizardite, chrysotile and antigorite



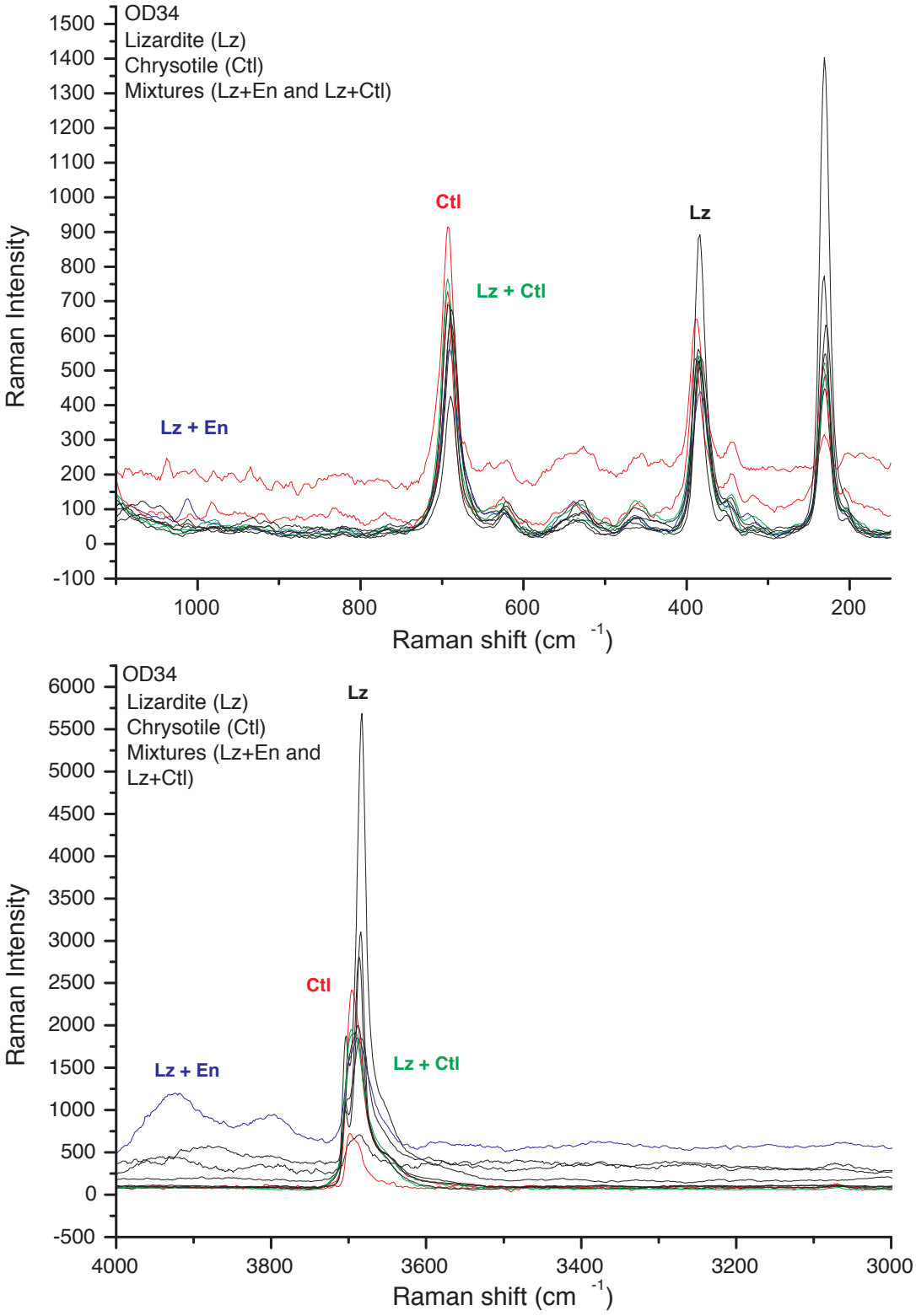
Ocean Drilling Program leg 209 site 1272A
Serpentinite OD28
Lizardite and chrysotile



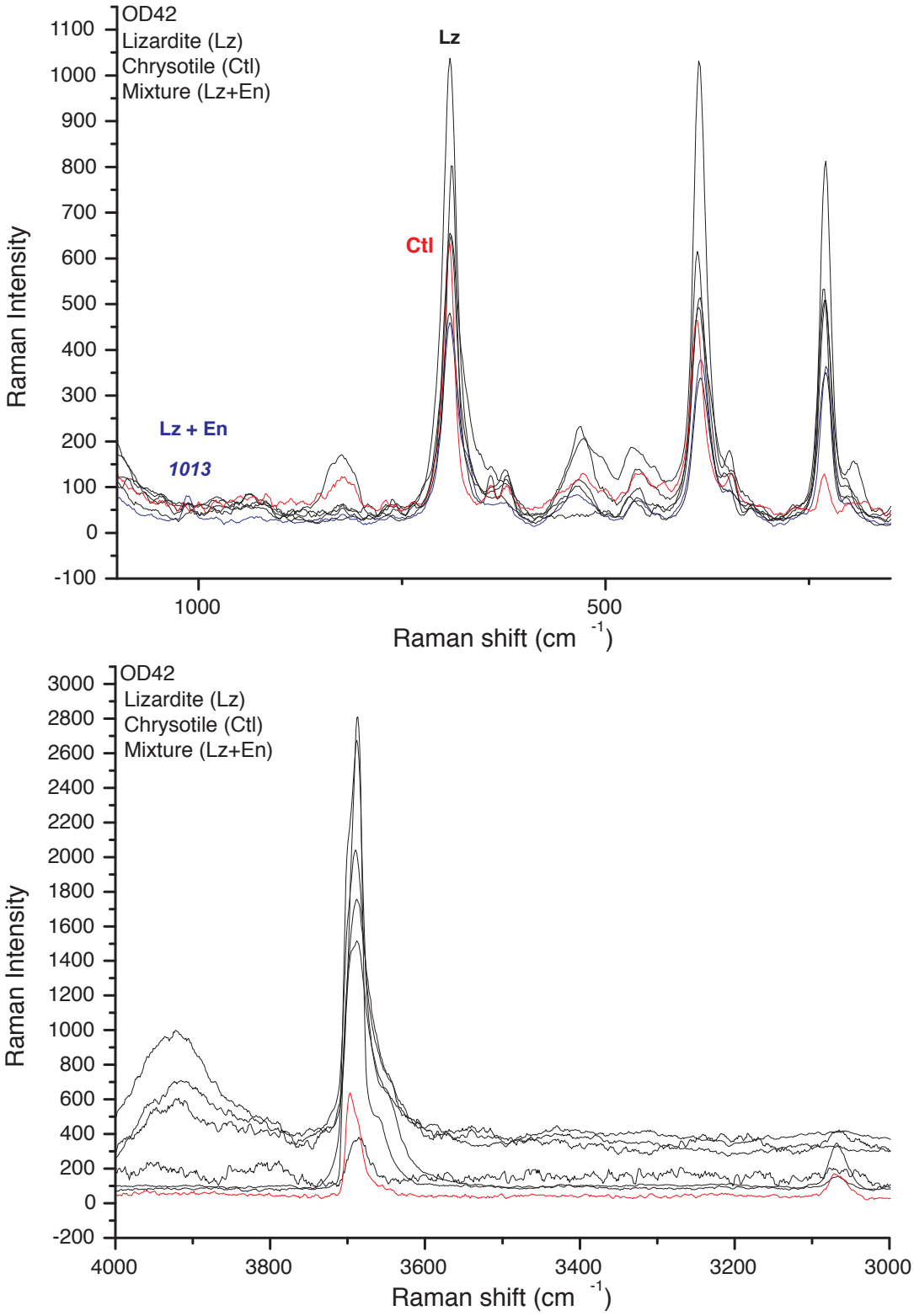
Ocean Drilling Program leg 209 site 1274A
Serpentinite OD32
Lizardite, chrysotile and mixtures



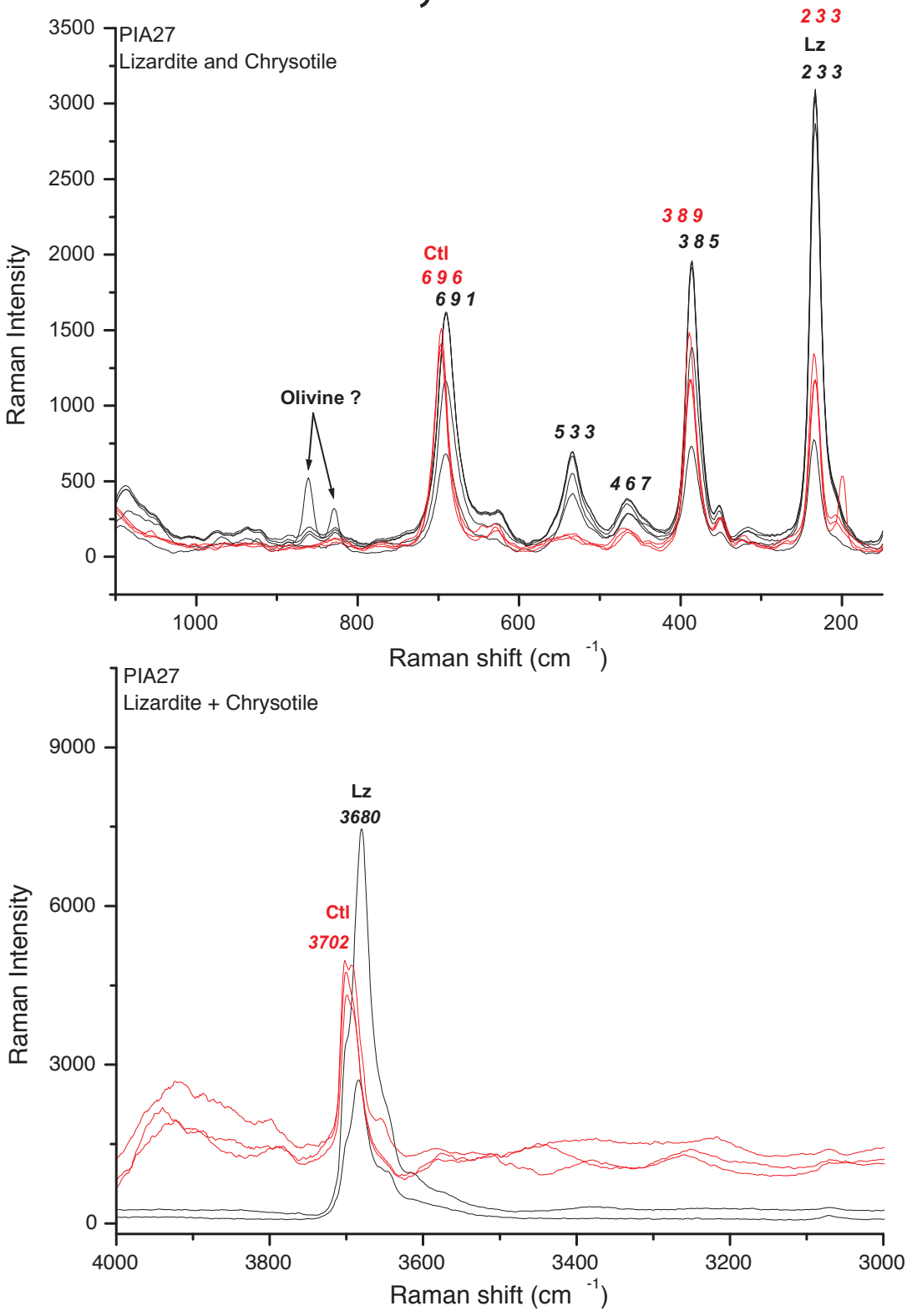
Ocean Drilling Program leg 209 site 1274A
Serpentinite OD34
Lizardite, chrysotile and mixtures



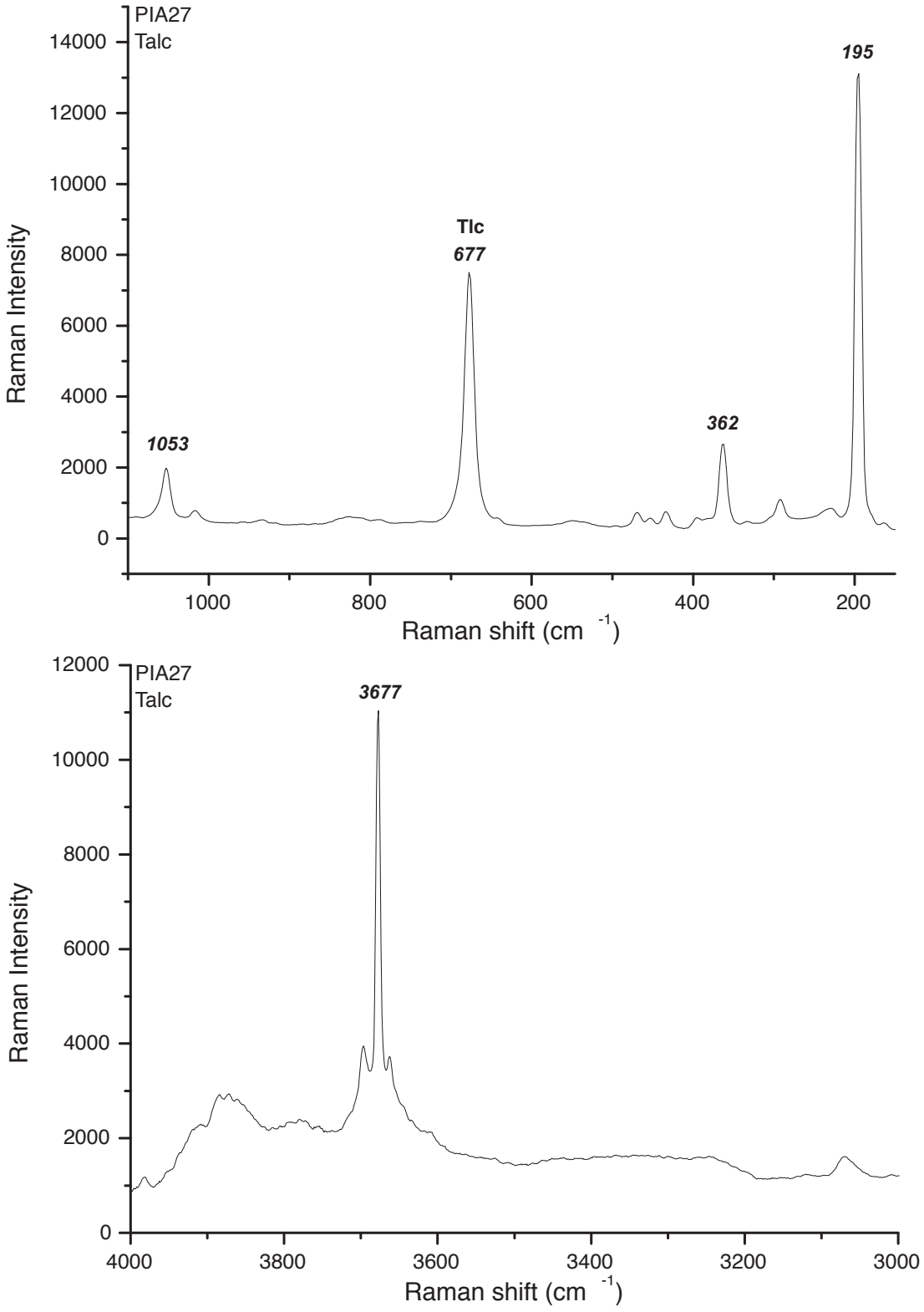
Ocean Drilling Program leg 209 site 1274A
Serpentinite OD42
Lizardite, chrysotile and mixture



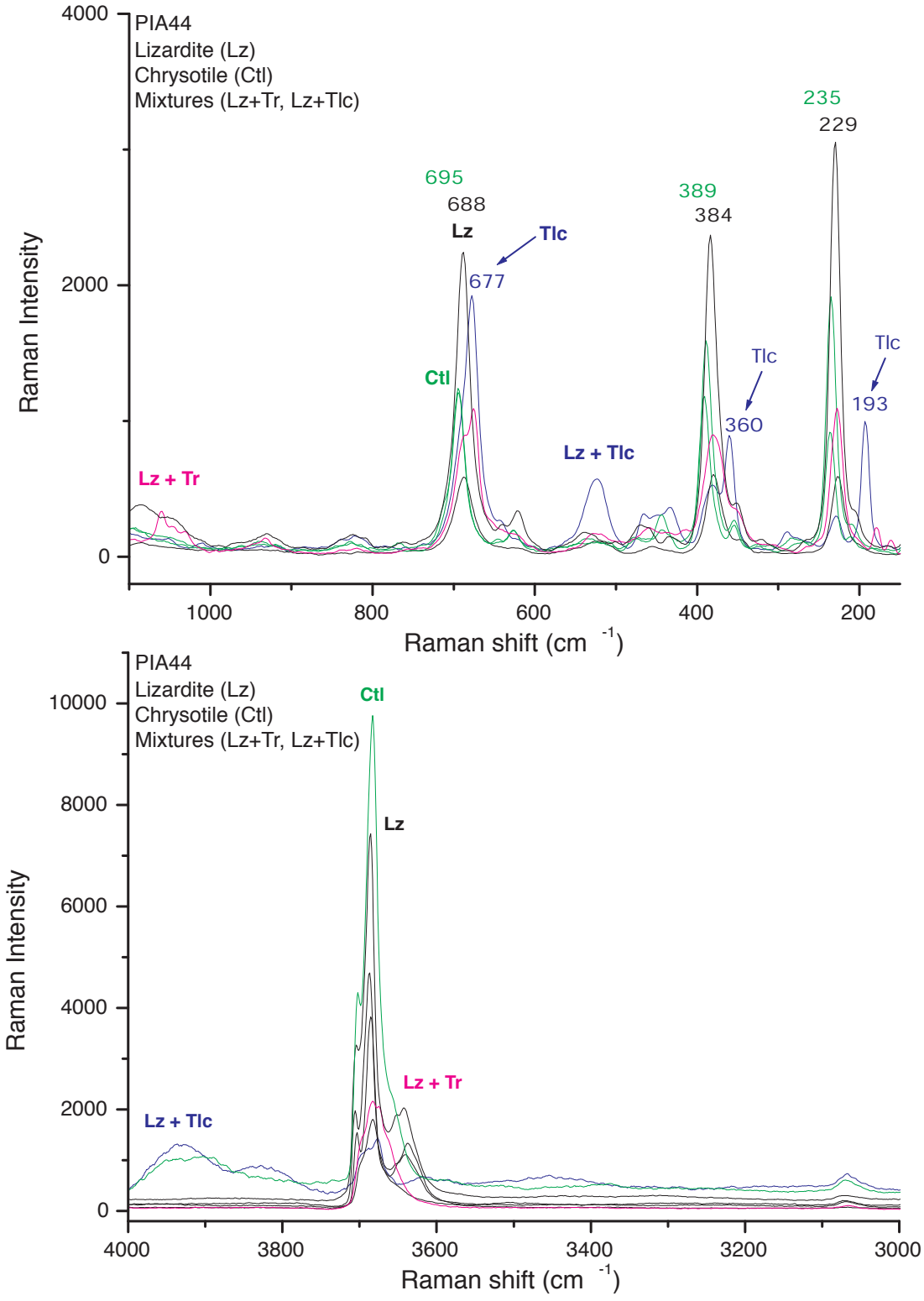
Pindos ophiolite - Dramala complex
Spinel harzburgite PIA27
Lizardite and chrysotile



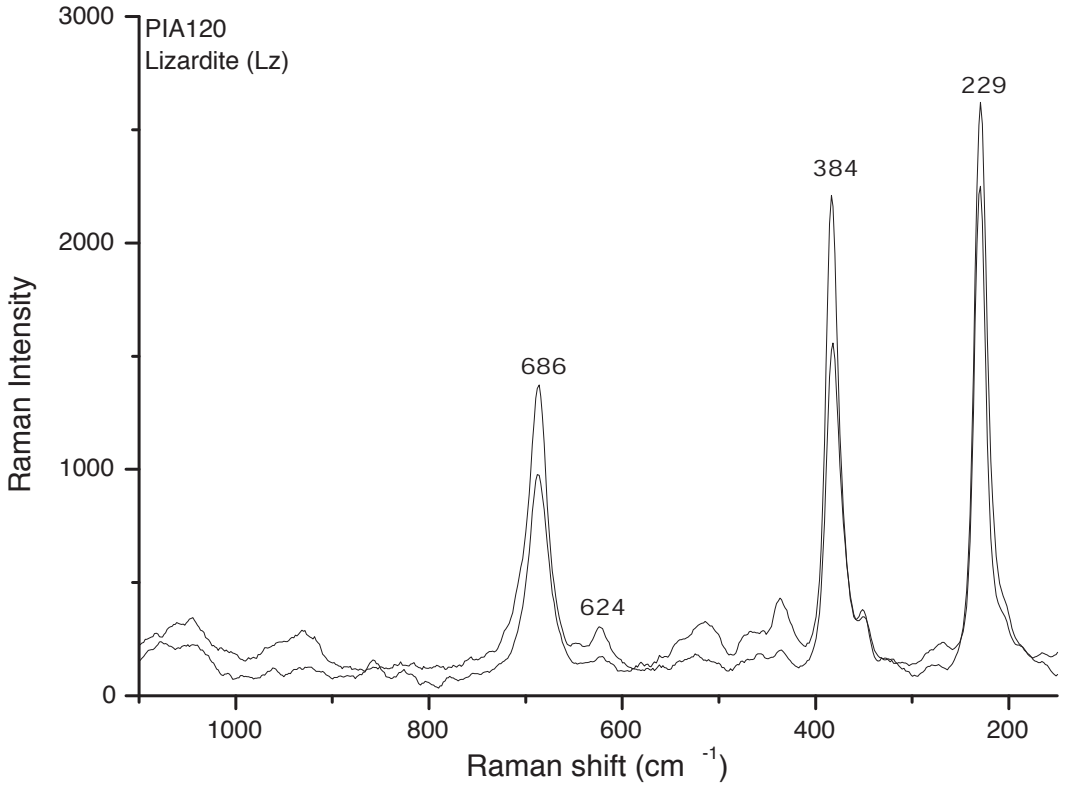
Pindos ophiolite - Dramala complex
Spinel harzburgite PIA27
Talc

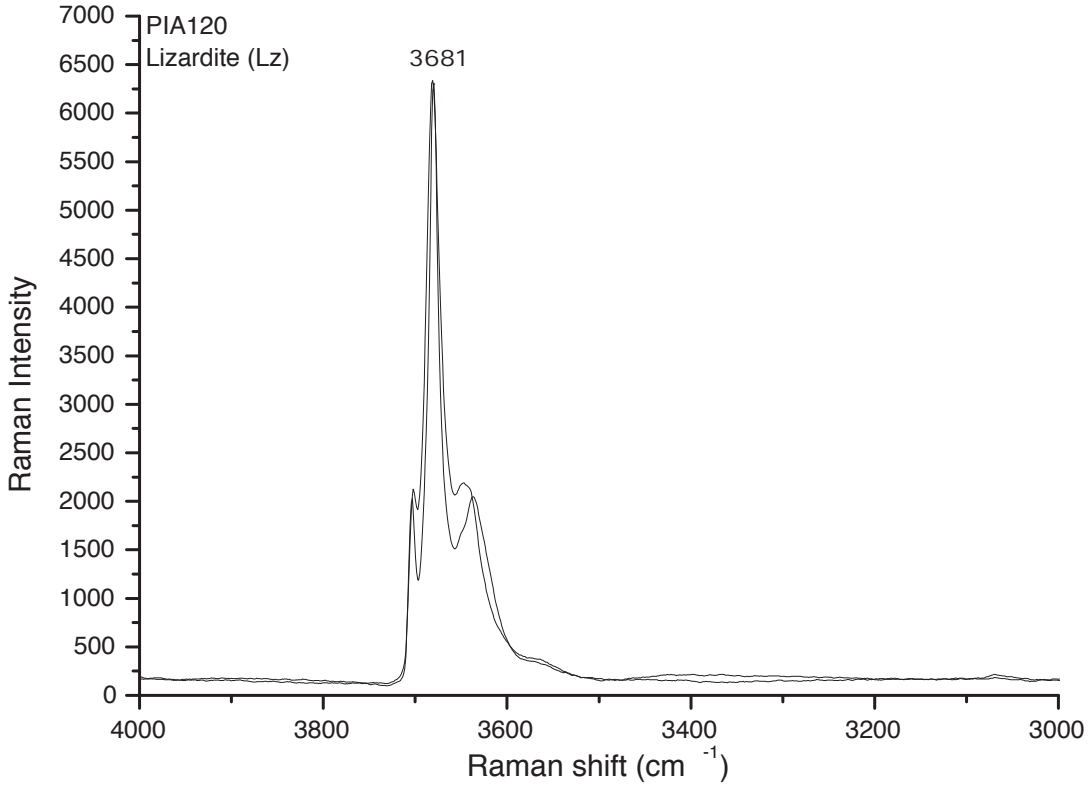


Pindos ophiolite - Dramala complex
Spinel harzburgite PIA44
Lizardite, chrysotile and mixtures

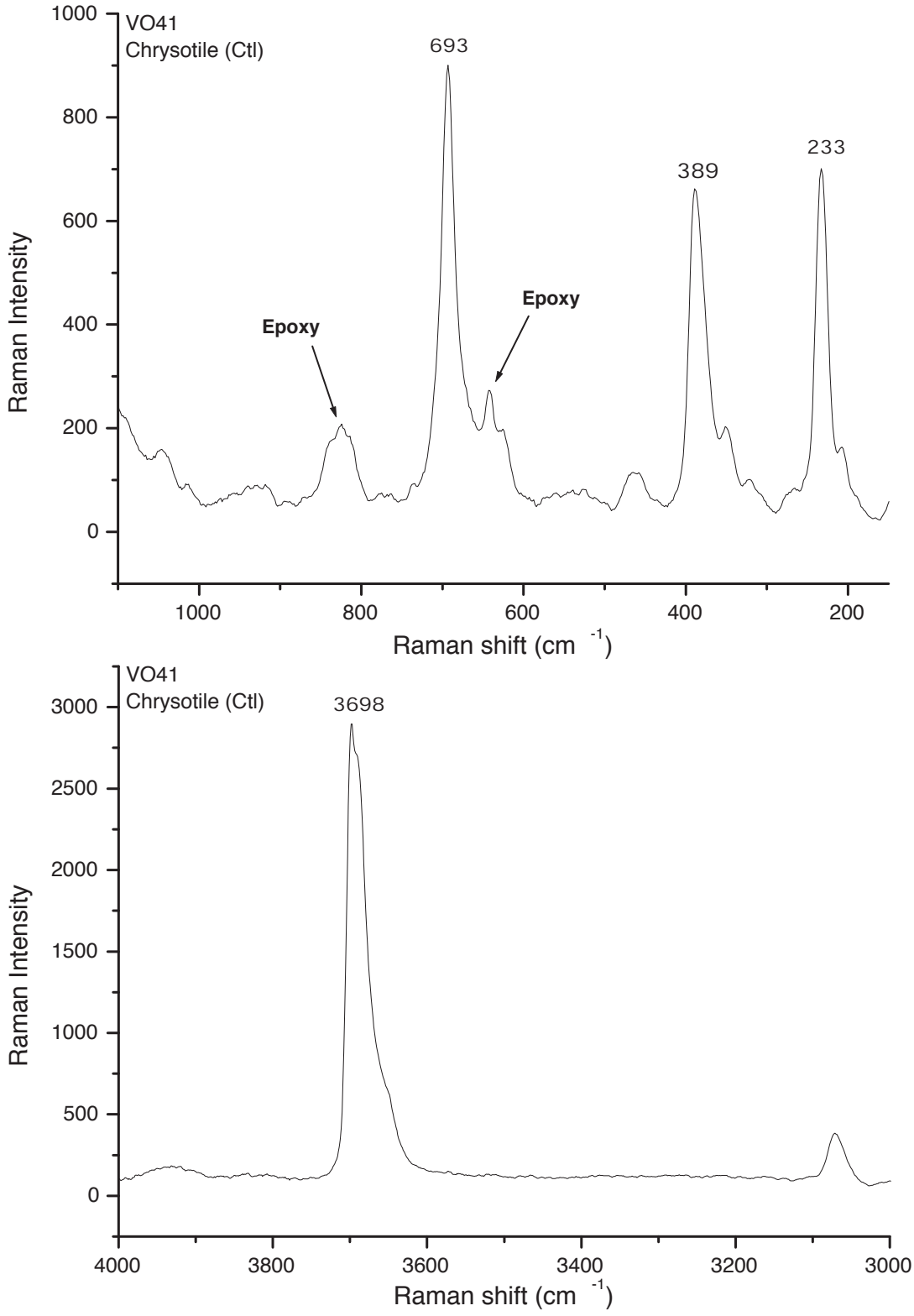


Pindos ophiolite - Dramala complex
Plagioclase-bearing harzburgite PIA120
Lizardite

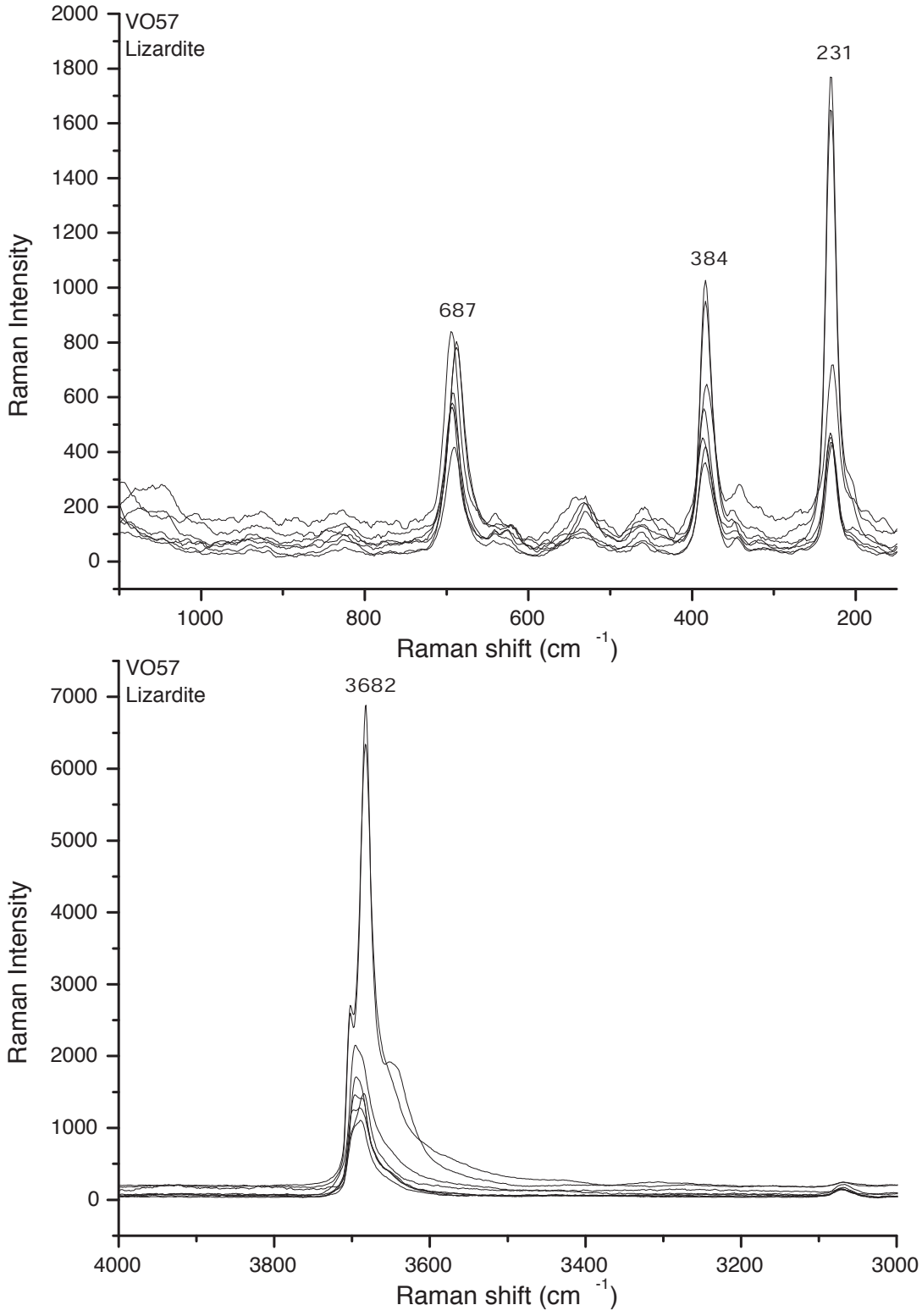




Vourinos ophiolite
Spinel harzburgite VO41
Chrysotile



Vourinos ophiolite
Spinel harzburgite VO57
Lizardite



Electron microprobe (EMPA) major elements

Major element composition of amphibole from the Geisspfad ultramafic body

Sample		G8	G8	G8	G8	G8	G8	G8	G8	G8	G8	G8	G8	G8	G8	G8	G8	G8
Rock		Serp	Serp	Serp	Serp	Serp	Serp	Serp	Serp	Serp	Serp	Serp	Serp	Serp	Serp	Serp	Serp	Serp
Mineral		Tr	Tr	Tr	Tr	Tr	Tr	Tr	Tr	Tr	Tr	Tr	Tr	Tr	Tr	Tr	Tr	Tr
Wt.%	SiO2	58.48	57.56	57.15	58.64	57.27	56.89	57.50	58.07	58.01	56.91	57.08	58.18	57.41	56.26	56.64	57.71	58.01
	TiO2	0.03	0.05	0.08	0.05	0.10	0.12	0.04	0.04	0.04	0.11	0.09	0.05	0.04	0.08	0.08	0.05	0.05
	Cr2O3	0.13	0.23	0.30	0.14	0.54	0.69	0.21	0.02	0.07	0.51	0.53	b.d.	0.04	0.03	0.12	0.02	0.09
	Al2O3	0.51	1.21	1.90	0.69	1.37	1.84	1.68	0.89	0.58	1.59	1.51	1.03	1.14	2.18	1.81	0.97	1.20
	Fe2O3	n.c.	n.c.	n.c.	n.c.	n.c.	n.c.	n.c.	n.c.	n.c.	n.c.	n.c.	n.c.	n.c.	n.c.	n.c.	n.c.	n.c.
	FeO	2.23	2.32	2.53	2.28	2.33	2.42	2.65	2.55	2.35	2.68	2.97	1.97	2.15	2.48	2.35	2.12	2.29
	MnO	0.17	0.03	0.15	0.09	b.d.	0.01	0.07	0.03	0.14	0.15	0.06	0.04	0.01	0.07	0.18	0.03	0.10
	NiO	0.20	b.d.	0.04	b.d.	b.d.	0.16	0.16	0.10	0.07	0.09	0.15	0.08	0.16	0.08	0.01	0.02	0.22
	MgO	23.01	22.42	22.27	22.66	22.47	22.34	22.67	22.44	22.66	22.42	22.26	22.64	22.47	22.05	21.89	22.44	22.78
	CaO	12.14	12.04	12.35	12.36	11.63	11.88	11.89	11.92	12.41	11.58	11.60	12.79	12.85	12.75	12.87	12.65	12.69
	Na2O	0.80	1.37	1.49	1.08	1.72	1.81	1.47	1.46	0.83	1.71	1.71	0.85	0.91	1.22	1.06	0.95	1.05
	K2O	0.03	0.02	0.04	0.02	0.04	0.04	0.07	0.04	0.03	0.05	0.04	0.03	0.02	0.05	0.04	0.03	0.03
	H2O	2.17	2.15	2.17	2.17	2.14	2.16	2.17	2.15	2.16	2.15	2.15	2.17	2.16	2.15	2.15	2.15	2.18
	Total	99.89	99.40	100.47	100.19	99.61	100.36	100.59	99.71	99.35	99.96	100.16	99.84	99.37	99.40	99.19	99.15	100.69
Cations	Si	8.072	8.033	7.909	8.100	8.007	7.911	7.941	8.094	8.057	7.938	7.957	8.034	7.972	7.840	7.906	8.036	7.965
	Ti	0.004	0.005	0.009	0.005	0.011	0.013	0.004	0.004	0.004	0.011	0.010	0.005	0.004	0.008	0.008	0.006	0.005
	Cr	0.014	0.025	0.032	0.016	0.059	0.076	0.023	0.002	0.007	0.056	0.058	b.d.	0.005	0.004	0.013	0.002	0.010
	Al	0.083	0.198	0.310	0.112	0.226	0.301	0.274	0.146	0.096	0.262	0.247	0.168	0.187	0.358	0.298	0.160	0.194
	Fe3+	n.c.	n.c.	n.c.	n.c.	n.c.	n.c.	n.c.	n.c.	n.c.	n.c.	n.c.	n.c.	n.c.	n.c.	n.c.	n.c.	n.c.
	Fe2+	0.257	0.271	0.293	0.263	0.272	0.281	0.306	0.297	0.273	0.313	0.346	0.227	0.250	0.289	0.274	0.247	0.263
	Mn	0.020	0.004	0.018	0.011	b.d.	0.001	0.008	0.004	0.017	0.018	0.007	0.005	0.002	0.008	0.021	0.003	0.011
	Ni	0.022	b.d.	0.005	b.d.	b.d.	0.018	0.018	0.011	0.008	0.010	0.017	0.009	0.018	0.009	0.001	0.002	0.024
	Mg	4.734	4.663	4.593	4.665	4.682	4.630	4.666	4.662	4.691	4.661	4.625	4.659	4.651	4.580	4.554	4.657	4.662
	Ca	1.795	1.800	1.831	1.829	1.742	1.770	1.759	1.780	1.847	1.730	1.732	1.892	1.912	1.904	1.925	1.887	1.867
	Na	0.214	0.371	0.400	0.290	0.466	0.488	0.394	0.395	0.225	0.462	0.462	0.227	0.244	0.330	0.287	0.256	0.279
	K	0.005	0.004	0.007	0.004	0.007	0.008	0.013	0.007	0.005	0.009	0.008	0.005	0.004	0.008	0.007	0.005	0.006
	H	2.000	2.000	2.000	2.000	2.000	2.000	2.000	2.000	2.000	2.000	2.000	2.000	2.000	2.000	2.000	2.000	2.000
	Sum	15.219	15.375	15.407	15.294	15.473	15.496	15.406	15.402	15.229	15.471	15.470	15.232	15.248	15.338	15.294	15.261	15.285
	Al4	0.000	0.000	0.091	0.000	0.000	0.089	0.059	0.000	0.000	0.062	0.043	0.000	0.028	0.160	0.094	0.000	0.035
	Al6	0.083	0.198	0.219	0.112	0.226	0.211	0.215	0.146	0.096	0.200	0.204	0.168	0.159	0.198	0.204	0.160	0.159
	Mg #	0.948	0.945	0.940	0.947	0.945	0.943	0.938	0.940	0.945	0.937	0.930	0.953	0.949	0.941	0.943	0.950	0.947
	NaK (A)	0.219	0.375	0.407	0.294	0.473	0.496	0.406	0.402	0.229	0.471	0.470	0.232	0.248	0.338	0.294	0.261	0.285

Abbreviations: Tr = tremolite, Serp = serpentinite, b.d. = below detection, n.c. = not calculated. Mg# calculated as (MgO/40.3) / (MgO/40.3 + FeO/71.85).

Major element composition of amphibole from the Geisspfad ultramafic body continued

Sample		G8	G8	G8	G8	G11	G11	G11	G11	G11	G11	G11	G11	G11	G11	G11	G11	G11	G11	G11
Rock		Serp	Serp	Serp	Serp	Serp	Serp	Serp	Serp	Serp	Serp	Serp	Serp	Serp	Serp	Serp	Serp	Serp	Serp	Serp
Mineral		Tr	Tr	Tr	Tr	Tr	Tr	Tr	Tr	Tr	Tr	Tr	Tr	Tr	Tr	Tr	Tr	Tr	Tr	Tr
Wt.%	SiO2	56.36	57.20	56.07	56.14	57.40	57.61	57.00	57.36	57.33	57.47	57.54	57.63	57.55	57.78	57.50	57.69	57.57	57.20	57.16	56.95
	TiO2	0.08	0.06	0.12	0.06	0.05	0.06	0.06	0.06	0.05	0.04	0.07	0.06	0.07	0.05	0.07	0.07	0.05	0.07	0.06	0.06
	Cr2O3	0.09	0.07	0.13	0.24	0.05	0.02	b.d.	0.04	0.04	0.01	0.05	0.10	0.03	0.03	0.13	0.10	0.05	0.11	0.17	0.19
	Al2O3	2.05	1.55	2.32	2.04	0.88	1.03	1.01	0.96	0.94	0.88	0.90	0.85	0.87	0.88	0.99	1.05	1.13	1.13	1.18	1.49
	Fe2O3	n.c.	n.c.	n.c.	n.c.	n.c.	n.c.	n.c.	n.c.	n.c.	n.c.	n.c.	n.c.	n.c.	n.c.	n.c.	n.c.	n.c.	n.c.	n.c.	n.c.
	FeO	2.35	2.51	2.58	2.70	1.96	1.88	2.04	1.77	1.91	2.03	2.06	2.10	1.86	1.91	2.01	2.33	2.07	1.94	2.27	2.45
	MnO	0.15	0.13	0.08	0.11	0.07	0.12	0.04	0.08	0.02	0.07	0.04	b.d.	0.05	0.10	0.05	0.05	0.11	0.01	0.07	0.11
	NiO	0.03	0.05	0.11	b.d.	0.10	0.01	0.12	0.08	b.d.	0.01	0.09	0.21	0.10	0.04	0.01	0.04	0.02	0.16	0.08	0.15
	MgO	22.04	22.03	21.87	22.04	22.48	22.62	22.68	23.06	22.54	22.46	22.31	22.50	22.39	22.16	22.15	22.19	21.96	22.22	22.50	22.26
	CaO	12.73	12.24	12.44	11.97	13.21	13.09	13.12	13.05	13.11	13.19	13.26	13.11	13.23	13.16	12.99	13.02	12.90	12.91	12.95	12.58
	Na2O	1.27	1.24	1.48	1.64	0.78	0.93	0.91	0.87	0.82	0.80	0.78	0.69	0.79	0.79	0.94	0.99	1.03	1.14	1.07	1.33
	K2O	0.04	0.05	0.05	0.05	0.09	0.10	0.10	0.10	0.10	0.09	0.09	0.08	0.09	0.10	0.10	0.12	0.12	0.11	0.12	0.14
	H2O	2.15	2.15	2.14	2.14	2.16	2.16	2.16	2.17	2.15	2.16	2.16	2.16	2.16	2.15	2.15	2.16	2.15	2.15	2.16	2.15
	Total	99.33	99.27	99.39	99.13	99.22	99.62	99.24	99.60	99.02	99.20	99.36	99.51	99.20	99.16	99.07	99.82	99.17	99.15	99.80	99.87
Cations	Si	7.864	7.995	7.843	7.884	7.976	7.979	7.922	7.928	7.980	7.989	7.993	7.984	8.002	8.046	8.026	8.004	8.042	7.990	7.927	7.923
	Ti	0.008	0.006	0.013	0.007	0.005	0.006	0.006	0.006	0.006	0.004	0.007	0.006	0.007	0.005	0.007	0.007	0.006	0.007	0.006	0.006
	Cr	0.010	0.007	0.015	0.027	0.005	0.002	b.d.	0.004	0.004	0.001	0.006	0.011	0.004	0.003	0.014	0.011	0.006	0.012	0.019	0.021
	Al	0.337	0.256	0.383	0.338	0.144	0.168	0.166	0.157	0.155	0.144	0.147	0.139	0.143	0.145	0.162	0.172	0.186	0.187	0.193	0.244
	Fe3+	n.c.	n.c.	n.c.	n.c.	n.c.	n.c.	n.c.	n.c.	n.c.	n.c.	n.c.	n.c.	n.c.	n.c.	n.c.	n.c.	n.c.	n.c.	n.c.	n.c.
	Fe2+	0.274	0.293	0.302	0.317	0.228	0.218	0.237	0.205	0.222	0.236	0.239	0.243	0.216	0.222	0.235	0.270	0.242	0.227	0.263	0.285
	Mn	0.017	0.015	0.009	0.013	0.008	0.014	0.005	0.010	0.002	0.008	0.005	b.d.	0.005	0.012	0.006	0.006	0.013	0.001	0.008	0.013
	Ni	0.004	0.006	0.013	b.d.	0.012	0.001	0.013	0.008	b.d.	0.001	0.010	0.023	0.012	0.005	0.001	0.004	0.002	0.018	0.009	0.017
	Mg	4.583	4.589	4.559	4.613	4.656	4.670	4.698	4.750	4.676	4.654	4.619	4.646	4.640	4.599	4.608	4.589	4.572	4.626	4.651	4.616
	Ca	1.903	1.833	1.864	1.801	1.967	1.942	1.953	1.932	1.955	1.964	1.973	1.946	1.971	1.963	1.942	1.935	1.931	1.932	1.924	1.875
	Na	0.344	0.337	0.401	0.447	0.209	0.249	0.245	0.232	0.221	0.215	0.211	0.186	0.214	0.214	0.253	0.266	0.280	0.309	0.288	0.360
	K	0.007	0.009	0.008	0.010	0.015	0.017	0.018	0.018	0.018	0.017	0.016	0.015	0.017	0.018	0.018	0.022	0.021	0.019	0.022	0.025
	H	2.000	2.000	2.000	2.000	2.000	2.000	2.000	1.999	2.000	1.999	1.999	2.000	2.000	1.999	2.000	2.000	2.000	1.999	1.999	1.999
	Sum	15.351	15.346	15.409	15.456	15.225	15.266	15.263	15.250	15.239	15.232	15.227	15.201	15.231	15.232	15.272	15.288	15.301	15.328	15.310	15.385
	Al4	0.136	0.005	0.157	0.116	0.024	0.021	0.078	0.072	0.020	0.011	0.007	0.016	0.000	0.000	0.000	0.000	0.000	0.010	0.073	0.077
	Al6	0.201	0.251	0.225	0.222	0.120	0.147	0.087	0.084	0.135	0.133	0.140	0.124	0.143	0.145	0.162	0.172	0.186	0.177	0.120	0.167
	Mg #	0.944	0.940	0.938	0.936	0.953	0.955	0.952	0.959	0.955	0.952	0.951	0.950	0.955	0.954	0.952	0.944	0.950	0.953	0.946	0.942
	NaK (A)	0.351	0.346	0.409	0.456	0.225	0.266	0.263	0.250	0.239	0.232	0.227	0.201	0.231	0.232	0.272	0.288	0.301	0.328	0.310	0.385

Abbreviations: Tr = tremolite, Serp = serpentinite, b.d. = below detection, n.c. = not calculated. Mg# calculated as (MgO/40.3) / (MgO/40.3 + FeO/71.85).

Major element composition of amphibole from the Geisspfad ultramafic body continued

Sample		G11	G11	G11	G11	G11	G11	G11	G11	G11	G11	G11	G11	G11	G11	G11	G11	G11	G11	G12
Rock		Serp	Serp	Serp	Serp	Serp	Serp	Serp	Serp	Serp	Serp	Serp	Serp	Serp	Serp	Serp	Serp	Serp	Serp	Serp
Mineral		Tr	Tr	Tr	Tr	Tr	Tr	Tr	Tr	Tr	Tr	Tr	Tr	Tr	Tr	Tr	Tr	Tr	Tr	Tr
Wt.%	SiO2	56.97	57.20	57.32	58.45	57.49	57.42	57.72	57.80	57.53	57.22	57.10	57.28	56.94	56.77	57.25	57.59	57.59	57.19	57.54	57.65
	TiO2	0.07	0.06	0.05	0.06	0.06	0.02	0.03	0.04	0.01	0.07	0.06	0.06	0.05	0.08	0.05	0.05	0.07	0.05	0.06	0.03
	Cr2O3	0.05	0.12	0.10	0.11	0.18	0.10	0.08	0.08	b.d.	0.09	0.19	0.09	b.d.	0.09	0.11	0.02	0.06	0.14	0.09	0.07
	Al2O3	1.34	1.08	0.94	0.82	0.80	0.77	0.77	0.81	0.24	1.13	1.07	1.03	1.22	1.22	0.83	0.79	0.87	0.93	0.81	0.85
	Fe2O3	n.c.	n.c.	n.c.	n.c.	n.c.	n.c.	n.c.	n.c.	n.c.	n.c.	n.c.	n.c.	n.c.	n.c.	n.c.	n.c.	n.c.	n.c.	n.c.	n.c.
	FeO	2.27	2.19	2.04	2.22	2.05	2.04	1.86	2.15	1.96	2.03	2.01	1.98	2.06	2.13	1.98	2.09	1.77	1.86	1.80	1.93
	MnO	0.07	0.04	b.d.	0.10	0.02	0.10	0.03	0.05	0.04	0.09	0.05	b.d.	0.07	0.06	b.d.	0.03	0.03	0.05	0.07	0.08
	NiO	0.08	0.16	0.12	b.d.	0.04	0.06	0.16	0.08	0.12	0.17	0.07	0.08	0.02	0.14	0.20	0.07	0.11	0.09	0.07	0.03
	MgO	22.38	22.17	22.28	22.87	22.56	22.49	22.49	22.58	23.89	22.83	22.25	22.34	22.41	22.21	22.50	22.40	22.88	22.68	23.03	22.61
	CaO	12.51	12.91	13.14	13.22	13.32	13.44	13.45	13.39	12.88	12.88	13.10	13.12	13.01	12.93	13.29	13.24	13.66	13.68	13.61	13.05
	Na2O	1.37	1.06	0.79	0.69	0.61	0.60	0.68	0.68	0.51	0.84	0.87	0.85	0.99	1.19	0.76	0.66	0.76	0.75	0.70	0.83
	K2O	0.13	0.12	0.09	0.07	0.06	0.07	0.06	0.05	0.03	0.10	0.09	0.09	0.11	0.12	0.09	0.07	0.09	0.09	0.06	0.05
	H2O	2.15	2.15	2.15	2.19	2.16	2.16	2.17	2.17	2.18	2.17	2.15	2.15	2.15	2.14	2.16	2.16	2.18	2.17	2.18	2.16
	Total	99.38	99.26	99.03	100.80	99.36	99.26	99.51	99.87	99.39	99.61	99.01	99.06	99.03	99.08	99.22	99.18	100.07	99.67	100.05	99.35
Cations	Si	7.956	7.982	7.989	7.990	7.964	7.963	7.990	7.973	7.917	7.917	7.965	7.980	7.941	7.941	7.955	8.000	7.921	7.902	7.907	7.998
	Ti	0.007	0.007	0.005	0.006	0.006	0.002	0.004	0.004	0.001	0.008	0.007	0.006	0.006	0.008	0.005	0.005	0.007	0.006	0.007	0.003
	Cr	0.005	0.013	0.011	0.012	0.019	0.011	0.009	0.008	b.d.	0.010	0.021	0.010	b.d.	0.010	0.013	0.002	0.007	0.015	0.010	0.008
	Al	0.220	0.178	0.155	0.132	0.131	0.125	0.125	0.132	0.039	0.183	0.176	0.168	0.201	0.201	0.137	0.130	0.141	0.152	0.132	0.139
	Fe3+	n.c.	n.c.	n.c.	n.c.	n.c.	n.c.	n.c.	n.c.	n.c.	n.c.	n.c.	n.c.	n.c.	n.c.	n.c.	n.c.	n.c.	n.c.	n.c.	n.c.
	Fe2+	0.265	0.256	0.238	0.254	0.237	0.237	0.215	0.248	0.226	0.235	0.234	0.231	0.240	0.249	0.230	0.243	0.204	0.215	0.207	0.224
	Mn	0.008	0.004	b.d.	0.012	0.002	0.011	0.004	0.005	0.005	0.010	0.006	b.d.	0.008	0.007	b.d.	0.004	0.004	0.006	0.009	0.009
	Ni	0.009	0.018	0.013	b.d.	0.005	0.007	0.018	0.009	0.013	0.019	0.008	0.009	0.002	0.015	0.022	0.007	0.012	0.010	0.008	0.004
	Mg	4.658	4.611	4.628	4.659	4.658	4.648	4.640	4.642	4.900	4.708	4.626	4.639	4.658	4.630	4.660	4.638	4.691	4.670	4.717	4.675
	Ca	1.872	1.930	1.962	1.936	1.977	1.997	1.995	1.979	1.899	1.909	1.958	1.958	1.944	1.938	1.978	1.970	2.013	2.025	2.004	1.940
	Na	0.371	0.286	0.214	0.182	0.163	0.160	0.183	0.182	0.137	0.226	0.235	0.229	0.267	0.323	0.206	0.178	0.202	0.200	0.187	0.223
	K	0.023	0.020	0.017	0.012	0.010	0.012	0.011	0.009	0.004	0.018	0.016	0.017	0.020	0.021	0.016	0.013	0.015	0.015	0.011	0.008
	H	2.000	2.000	1.999	2.000	2.000	2.000	2.000	2.000	2.000	2.000	2.000	2.000	2.000	1.999	1.999	1.999	2.000	2.000	2.000	1.999
	Sum	15.394	15.306	15.231	15.194	15.174	15.172	15.194	15.191	15.142	15.243	15.251	15.246	15.287	15.344	15.221	15.191	15.217	15.215	15.198	15.231
	Al4	0.044	0.018	0.011	0.010	0.036	0.037	0.010	0.027	0.039	0.083	0.035	0.020	0.059	0.059	0.045	0.000	0.079	0.098	0.093	0.002
	Al6	0.176	0.161	0.143	0.121	0.095	0.088	0.116	0.105	0.000	0.101	0.141	0.148	0.142	0.142	0.092	0.130	0.063	0.053	0.039	0.137
	Mg #	0.946	0.947	0.951	0.948	0.951	0.952	0.956	0.949	0.956	0.952	0.952	0.953	0.951	0.949	0.953	0.950	0.958	0.956	0.958	0.954
	NaK (A)	0.394	0.306	0.231	0.194	0.174	0.172	0.194	0.191	0.142	0.243	0.251	0.246	0.287	0.344	0.221	0.191	0.217	0.215	0.198	0.231

Abbreviations: Tr = tremolite, Serp = serpentinite, b.d. = below detection, n.c. = not calculated. Mg# calculated as (MgO/40.3) / (MgO/40.3 + FeO/71.85).

Major element composition of amphibole from the Geisspfad ultramafic body continued

Sample		G12	G12	G12	G12	G12	G12	G26	G26	G26	G26	G26	G26	G26	G26	G26	G26	G26	G27	G27
Rock		Serp	Serp	Serp	Serp	Serp	Serp	Serp	Serp	Serp	Serp	Serp	Serp	Serp	Serp	Serp	Serp	Serp	Serp	Serp
Mineral		Tr	Tr	Tr	Tr	Tr	Tr	Tr	Tr	Tr	Tr	Tr	Tr	Tr	Tr	Tr	Tr	Tr	Tr	Tr
Wt.%	SiO2	57.68	57.56	58.07	58.31	58.14	57.50	57.44	58.01	57.64	57.90	57.23	57.31	57.76	56.25	58.12	58.15	57.94	57.91	57.74	57.75
	TiO2	0.05	0.03	0.03	0.06	0.03	0.04	0.04	0.02	0.04	0.03	0.03	0.04	0.03	0.06	0.04	0.04	0.06	0.04	0.06	0.06
	Cr2O3	b.d.	0.05	0.02	0.10	0.02	0.03	0.30	0.06	0.08	0.12	0.19	0.15	0.07	0.27	0.10	0.08	0.01	0.10	0.05	0.08
	Al2O3	0.96	0.85	0.72	0.64	0.71	0.83	1.22	0.59	0.81	0.66	1.16	0.95	0.56	1.51	0.61	0.63	0.76	0.62	0.96	0.99
	Fe2O3	n.c.	n.c.	n.c.	n.c.	n.c.	n.c.	n.c.	n.c.	n.c.	n.c.	n.c.	n.c.	n.c.	n.c.	n.c.	n.c.	n.c.	n.c.	n.c.	n.c.
	FeO	1.82	2.05	2.27	2.12	2.05	1.74	1.92	1.95	1.85	1.78	1.75	2.07	1.82	1.62	1.67	1.70	1.69	1.66	1.95	1.98
	MnO	0.10	b.d.	0.12	0.07	b.d.	0.06	b.d.	0.04	0.04	0.06	b.d.	0.01	0.04	0.05	0.07	0.02	0.03	0.04	0.04	0.07
	NiO	0.13	0.20	0.23	0.15	0.10	0.09	0.10	0.08	0.06	0.04	0.13	0.14	0.17	0.13	0.07	0.13	0.11	0.08	0.14	0.09
	MgO	22.90	22.48	22.58	22.64	22.82	23.25	22.71	22.70	22.96	22.24	22.82	22.86	22.51	22.89	23.21	23.30	23.38	23.09	23.17	23.00
	CaO	13.05	13.11	13.06	12.80	13.10	13.32	12.64	11.83	12.92	13.10	12.97	12.94	13.27	13.34	13.42	13.56	13.31	13.74	13.42	13.33
	Na2O	0.89	0.88	0.79	0.97	0.81	0.83	1.31	1.66	0.92	0.89	1.27	1.07	0.73	1.14	0.70	0.69	0.81	0.62	0.83	0.84
	K2O	0.04	0.04	0.04	0.03	0.04	0.04	0.12	0.12	0.07	0.04	0.13	0.09	0.04	0.13	0.05	0.05	0.06	0.04	0.06	0.06
	H2O	2.17	2.16	2.17	2.17	2.18	2.18	2.16	2.14	2.17	2.15	2.16	2.17	2.16	2.16	2.19	2.19	2.19	2.19	2.19	2.19
	Total	99.78	99.41	100.08	100.08	99.99	99.92	99.98	99.22	99.57	99.02	99.84	99.79	99.18	99.56	100.24	100.54	100.35	100.12	100.59	100.42
Cations	Si	7.962	7.991	8.008	8.053	8.012	7.910	7.961	8.131	7.977	8.075	7.931	7.934	8.024	7.797	7.967	7.946	7.935	7.942	7.900	7.921
	Ti	0.005	0.003	0.003	0.007	0.003	0.005	0.004	0.002	0.004	0.003	0.003	0.004	0.003	0.007	0.004	0.004	0.006	0.004	0.006	0.006
	Cr	b.d.	0.005	0.002	0.011	0.002	0.003	0.033	0.007	0.009	0.013	0.021	0.017	0.008	0.030	0.011	0.008	0.001	0.011	0.005	0.008
	Al	0.156	0.139	0.117	0.105	0.115	0.134	0.199	0.098	0.132	0.108	0.189	0.155	0.092	0.247	0.099	0.101	0.123	0.100	0.154	0.159
	Fe3+	n.c.	n.c.	n.c.	n.c.	n.c.	n.c.	n.c.	n.c.	n.c.	n.c.	n.c.	n.c.	n.c.	n.c.	n.c.	n.c.	n.c.	n.c.	n.c.	n.c.
	Fe2+	0.210	0.238	0.262	0.245	0.236	0.200	0.223	0.228	0.215	0.208	0.203	0.239	0.212	0.188	0.191	0.194	0.194	0.190	0.223	0.227
	Mn	0.011	b.d.	0.013	0.009	b.d.	0.008	b.d.	0.005	0.005	0.007	b.d.	0.001	0.005	0.006	0.008	0.003	0.003	0.005	0.004	0.008
	Ni	0.014	0.022	0.025	0.017	0.011	0.010	0.012	0.009	0.007	0.005	0.015	0.016	0.019	0.015	0.007	0.014	0.012	0.009	0.015	0.010
	Mg	4.712	4.651	4.641	4.661	4.687	4.767	4.692	4.743	4.736	4.623	4.712	4.716	4.661	4.729	4.742	4.745	4.773	4.720	4.725	4.702
	Ca	1.930	1.950	1.929	1.894	1.934	1.963	1.877	1.777	1.915	1.957	1.925	1.919	1.975	1.981	1.971	1.985	1.953	2.019	1.967	1.959
	Na	0.237	0.237	0.210	0.260	0.217	0.222	0.351	0.451	0.247	0.240	0.340	0.286	0.197	0.305	0.187	0.182	0.216	0.164	0.220	0.222
	K	0.007	0.007	0.006	0.006	0.007	0.007	0.022	0.022	0.013	0.008	0.023	0.016	0.008	0.022	0.009	0.009	0.011	0.007	0.010	0.010
	H	2.000	1.999	1.999	1.998	1.999	2.000	2.000	2.000	2.000	2.000	2.000	2.000	2.000	2.000	2.000	2.000	2.000	2.000	2.000	2.000
	Sum	15.244	15.243	15.216	15.266	15.224	15.229	15.372	15.474	15.260	15.248	15.363	15.302	15.205	15.328	15.195	15.191	15.226	15.171	15.230	15.233
	Al4	0.038	0.009	0.000	0.000	0.000	0.090	0.039	0.000	0.023	0.000	0.069	0.066	0.000	0.203	0.033	0.054	0.065	0.058	0.100	0.079
	Al6	0.118	0.130	0.117	0.105	0.115	0.044	0.160	0.098	0.109	0.108	0.120	0.089	0.092	0.045	0.066	0.047	0.058	0.042	0.054	0.080
	Mg #	0.957	0.951	0.947	0.950	0.952	0.960	0.955	0.954	0.957	0.957	0.959	0.952	0.957	0.962	0.961	0.961	0.961	0.961	0.955	0.954
	NaK (A)	0.244	0.243	0.216	0.266	0.224	0.229	0.372	0.474	0.260	0.248	0.363	0.302	0.205	0.328	0.195	0.191	0.226	0.171	0.230	0.233

Abbreviations: Tr = tremolite, Serp = serpentinite, b.d. = below detection, n.c. = not calculated. Mg# calculated as (MgO/40.3) / (MgO/40.3 + FeO/71.85).

Major element composition of amphibole from the Geisspfad ultramafic body continued

Sample		G27	G27	G27	G27	G27	G27	G27	G27	G27	G27	G27	G27	G27	G27	G27	G27	G27	G27	G27
Rock		Serp	Serp	Serp	Serp	Serp	Serp	Serp	Serp	Serp	Serp	Serp	Serp	Serp	Serp	Serp	Serp	Serp	Serp	Serp
Mineral		Tr	Tr	Tr	Tr	Tr	Tr	Tr	Tr	Tr	Tr	Tr	Tr	Tr	Tr	Tr	Tr	Tr	Tr	Tr
Wt.%	SiO2	57.27	57.78	57.56	57.56	57.45	57.81	57.64	57.79	57.62	57.71	57.64	57.55	57.93	57.73	57.80	57.66	57.44	57.31	57.64	57.68
	TiO2	0.06	0.06	0.06	0.06	0.05	0.05	0.08	0.07	0.05	0.06	0.06	0.05	0.07	0.07	0.05	0.05	0.06	0.08	0.06	0.04
	Cr2O3	0.06	0.01	0.03	b.d.	0.02	b.d.	0.06	0.04	0.08	0.10	0.06	0.02	b.d.	0.04	0.04	b.d.	0.15	b.d.	b.d.	0.09
	Al2O3	1.02	1.04	0.95	1.03	1.00	1.02	0.95	0.96	1.02	1.01	0.99	1.05	0.87	0.85	0.86	0.73	1.15	0.81	1.09	0.88
	Fe2O3	n.c.	n.c.	n.c.	n.c.	n.c.	n.c.	n.c.	n.c.	n.c.	n.c.	n.c.	n.c.	n.c.	n.c.	n.c.	n.c.	n.c.	n.c.	n.c.	n.c.
	FeO	1.96	1.96	1.93	1.93	1.98	2.00	1.94	1.96	1.95	1.99	1.98	1.93	1.89	1.87	1.95	1.89	2.10	1.98	2.07	1.92
	MnO	0.04	0.01	0.04	0.06	0.06	0.04	0.06	0.04	0.04	0.05	0.04	0.05	0.02	0.01	0.03	0.04	0.05	0.06	0.05	0.02
	NiO	0.08	0.10	0.08	0.09	0.09	0.06	0.06	0.06	0.10	0.07	0.13	0.09	0.12	0.11	0.07	0.08	0.11	0.08	0.08	0.09
	MgO	23.03	23.13	22.96	23.12	22.83	22.96	22.88	23.12	22.83	23.08	23.20	23.03	23.07	23.08	23.14	22.94	22.96	22.68	22.97	22.80
	CaO	13.14	13.32	13.33	13.18	12.84	13.10	13.30	13.11	13.32	13.30	13.07	13.35	13.50	13.62	13.64	13.77	12.80	13.67	13.13	13.48
	Na2O	0.91	0.88	0.87	0.95	0.95	0.94	0.87	0.90	0.94	0.93	0.88	0.87	0.77	0.76	0.79	0.68	1.05	0.76	0.97	0.74
	K2O	0.06	0.07	0.07	0.07	0.06	0.07	0.06	0.07	0.07	0.06	0.07	0.06	0.05	0.04	0.04	0.04	0.07	0.04	0.07	0.06
	H2O	2.17	2.19	2.18	2.18	2.16	2.18	2.18	2.18	2.18	2.19	2.18	2.18	2.19	2.19	2.19	2.18	2.17	2.17	2.18	2.18
	Total	99.81	100.55	100.06	100.22	99.51	100.23	100.08	100.30	100.21	100.54	100.30	100.24	100.49	100.37	100.61	100.06	100.11	99.63	100.32	99.97
Cations	Si	7.902	7.913	7.924	7.912	7.960	7.951	7.937	7.936	7.931	7.910	7.912	7.905	7.932	7.911	7.903	7.922	7.921	7.920	7.924	7.943
	Ti	0.006	0.006	0.006	0.006	0.006	0.005	0.008	0.007	0.005	0.006	0.006	0.005	0.007	0.007	0.005	0.005	0.007	0.008	0.007	0.004
	Cr	0.007	0.001	0.003	b.d.	0.002	b.d.	0.006	0.004	0.009	0.011	0.007	0.002	b.d.	0.004	0.004	b.d.	0.016	b.d.	b.d.	0.010
	Al	0.166	0.168	0.155	0.167	0.164	0.165	0.154	0.156	0.166	0.164	0.160	0.170	0.140	0.137	0.139	0.118	0.186	0.131	0.177	0.142
	Fe3+	n.c.	n.c.	n.c.	n.c.	n.c.	n.c.	n.c.	n.c.	n.c.	n.c.	n.c.	n.c.	n.c.	n.c.	n.c.	n.c.	n.c.	n.c.	n.c.	n.c.
	Fe2+	0.226	0.224	0.222	0.222	0.229	0.230	0.223	0.225	0.224	0.228	0.227	0.222	0.216	0.214	0.223	0.217	0.242	0.229	0.238	0.221
	Mn	0.005	0.001	0.005	0.006	0.007	0.004	0.007	0.005	0.005	0.005	0.005	0.006	0.003	0.001	0.003	0.004	0.006	0.007	0.005	0.002
	Ni	0.009	0.011	0.009	0.010	0.011	0.007	0.007	0.007	0.011	0.007	0.014	0.010	0.013	0.013	0.008	0.008	0.012	0.009	0.009	0.010
	Mg	4.736	4.721	4.711	4.736	4.715	4.707	4.696	4.732	4.684	4.715	4.746	4.715	4.708	4.714	4.716	4.698	4.719	4.672	4.706	4.680
	Ca	1.942	1.954	1.966	1.941	1.906	1.930	1.962	1.929	1.964	1.953	1.922	1.965	1.980	1.999	1.998	2.027	1.891	2.024	1.934	1.989
	Na	0.245	0.234	0.233	0.252	0.255	0.251	0.233	0.238	0.251	0.246	0.234	0.232	0.205	0.201	0.211	0.181	0.280	0.203	0.258	0.198
	K	0.010	0.012	0.011	0.012	0.011	0.012	0.010	0.011	0.013	0.010	0.011	0.011	0.009	0.008	0.007	0.007	0.013	0.007	0.013	0.010
	H	2.000	2.000	2.000	2.000	2.000	2.000	2.000	2.000	2.000	2.000	2.000	2.000	2.000	2.000	2.000	2.000	2.000	2.000	2.000	2.000
	Sum	15.255	15.246	15.244	15.264	15.266	15.263	15.244	15.250	15.264	15.256	15.245	15.244	15.215	15.209	15.217	15.188	15.293	15.210	15.271	15.209
	Al4	0.098	0.087	0.076	0.088	0.040	0.049	0.063	0.064	0.069	0.090	0.088	0.095	0.068	0.089	0.097	0.078	0.079	0.080	0.076	0.057
	Al6	0.069	0.081	0.078	0.079	0.124	0.117	0.091	0.091	0.097	0.074	0.072	0.075	0.073	0.047	0.042	0.040	0.107	0.052	0.101	0.085
	Mg #	0.954	0.955	0.955	0.955	0.954	0.953	0.955	0.955	0.954	0.954	0.954	0.955	0.956	0.957	0.955	0.956	0.951	0.953	0.952	0.955
	NaK (A)	0.255	0.246	0.244	0.264	0.266	0.263	0.244	0.250	0.264	0.256	0.245	0.244	0.215	0.209	0.217	0.188	0.293	0.210	0.271	0.209

Abbreviations: Tr = tremolite, Serp = serpentinite, b.d. = below detection, n.c. = not calculated. Mg# calculated as (MgO/40.3) / (MgO/40.3 + FeO/71.85).

Major element composition of amphibole from the Geisspfad ultramafic body continued

Sample		G27	G27	G27	G27	G27	G27	G27	G27	G27	G27	G27	G27	G27	G27	G27	G27	G27	G27	G27
Rock		Serp	Serp	Serp	Serp	Serp	Serp	Serp	Serp	Serp	Serp	Serp	Serp	Serp	Serp	Serp	Serp	Serp	Serp	Serp
Mineral		Tr	Tr	Tr	Tr	Tr	Tr	Tr	Tr	Tr	Tr	Tr	Tr	Tr	Tr	Tr	Tr	Tr	Tr	Tr
Wt.%	SiO2	58.00	58.24	57.94	57.99	57.57	57.83	57.87	57.94	57.66	58.05	57.70	57.58	57.66	57.30	57.03	57.07	57.30	57.82	57.55	57.58
	TiO2	0.04	0.05	0.07	0.07	0.04	0.08	0.04	0.04	0.05	0.05	0.06	0.06	0.05	0.06	0.07	0.05	0.08	0.04	0.07	0.05
	Cr2O3	0.02	0.06	0.06	0.07	0.07	0.03	b.d.	b.d.	b.d.	0.08	0.08	0.06	0.04	b.d.	0.09	0.08	0.02	0.08	0.02	0.06
	Al2O3	0.78	0.81	0.89	0.93	0.95	0.92	0.91	0.97	0.95	0.99	1.02	1.13	1.02	1.28	1.29	1.38	1.36	0.96	0.95	0.94
	Fe2O3	n.c.	n.c.	n.c.	n.c.	n.c.	n.c.	n.c.	n.c.	n.c.	n.c.	n.c.	n.c.	n.c.	n.c.	n.c.	n.c.	n.c.	n.c.	n.c.	n.c.
	FeO	1.89	1.90	1.89	1.89	1.94	1.98	1.89	1.88	1.94	1.94	1.96	1.96	1.91	2.22	2.19	2.26	2.21	1.89	1.98	1.94
	MnO	0.03	0.03	0.04	0.04	0.05	0.03	0.06	0.04	0.02	0.05	0.03	0.07	0.03	0.06	0.05	0.07	0.06	0.06	0.02	0.05
	NiO	0.10	0.10	0.07	0.05	0.07	0.05	0.08	0.08	0.06	0.10	0.10	0.10	0.14	0.11	0.10	0.05	0.06	0.08	0.09	0.09
	MgO	23.22	22.99	23.16	23.10	23.03	22.98	22.99	22.83	22.91	23.01	23.06	22.78	22.95	22.89	22.65	22.68	22.76	22.87	22.91	22.91
	CaO	13.57	13.54	13.51	13.57	13.06	13.43	13.28	13.10	13.36	13.24	13.23	13.05	13.14	12.78	12.68	12.81	12.69	13.14	13.33	13.40
	Na2O	0.66	0.65	0.73	0.74	0.84	0.81	0.80	0.87	0.88	0.89	0.95	0.96	0.94	1.19	1.22	1.19	1.18	0.86	0.81	0.78
	K2O	0.04	0.05	0.05	0.05	0.06	0.06	0.06	0.06	0.06	0.06	0.07	0.07	0.07	0.09	0.08	0.10	0.08	0.06	0.05	0.06
	H2O	2.19	2.19	2.19	2.20	2.18	2.19	2.18	2.18	2.18	2.19	2.18	2.17	2.18	2.17	2.16	2.17	2.17	2.18	2.18	2.18
	Total	100.54	100.62	100.59	100.70	99.85	100.39	100.16	99.99	100.07	100.64	100.44	99.99	100.12	100.17	99.61	99.91	99.97	100.05	99.96	100.03
Cations	Si	7.924	7.960	7.919	7.921	7.936	7.932	7.952	7.984	7.937	7.949	7.919	7.945	7.939	7.910	7.923	7.903	7.926	7.963	7.926	7.923
	Ti	0.004	0.006	0.007	0.007	0.004	0.008	0.005	0.005	0.005	0.005	0.006	0.006	0.005	0.006	0.007	0.006	0.008	0.004	0.007	0.005
	Cr	0.002	0.006	0.006	0.007	0.008	0.003	b.d.	b.d.	b.d.	0.009	0.008	0.007	0.004	b.d.	0.010	0.008	0.002	0.009	0.002	0.006
	Al	0.125	0.131	0.143	0.150	0.155	0.149	0.147	0.158	0.154	0.160	0.165	0.184	0.165	0.208	0.211	0.226	0.221	0.156	0.154	0.152
	Fe3+	n.c.	n.c.	n.c.	n.c.	n.c.	n.c.	n.c.	n.c.	n.c.	n.c.	n.c.	n.c.	n.c.	n.c.	n.c.	n.c.	n.c.	n.c.	n.c.	n.c.
	Fe2+	0.216	0.217	0.216	0.216	0.224	0.227	0.217	0.217	0.223	0.222	0.225	0.226	0.220	0.256	0.254	0.262	0.256	0.218	0.228	0.223
	Mn	0.003	0.004	0.005	0.005	0.005	0.004	0.007	0.005	0.003	0.006	0.004	0.008	0.003	0.008	0.006	0.008	0.007	0.007	0.003	0.006
	Ni	0.011	0.011	0.008	0.006	0.008	0.006	0.009	0.008	0.007	0.011	0.011	0.011	0.016	0.013	0.011	0.006	0.007	0.009	0.010	0.010
	Mg	4.728	4.683	4.718	4.703	4.732	4.698	4.708	4.689	4.700	4.696	4.717	4.685	4.710	4.709	4.690	4.681	4.693	4.695	4.703	4.698
	Ca	1.986	1.983	1.978	1.986	1.929	1.973	1.955	1.934	1.970	1.942	1.945	1.929	1.938	1.890	1.887	1.901	1.881	1.939	1.967	1.975
	Na	0.175	0.171	0.192	0.196	0.225	0.217	0.214	0.232	0.234	0.236	0.254	0.257	0.250	0.319	0.328	0.319	0.318	0.231	0.216	0.207
	K	0.007	0.009	0.008	0.009	0.010	0.010	0.010	0.011	0.011	0.010	0.012	0.012	0.012	0.016	0.015	0.018	0.014	0.011	0.009	0.010
	H	2.000	2.000	2.000	2.000	2.000	2.000	2.000	2.000	2.000	2.000	2.000	2.000	2.000	2.000	2.000	2.000	2.000	2.000	2.000	2.000
	Sum	15.183	15.180	15.200	15.205	15.235	15.227	15.224	15.243	15.245	15.245	15.265	15.270	15.262	15.335	15.343	15.337	15.332	15.242	15.226	15.217
	Al4	0.076	0.040	0.081	0.079	0.064	0.068	0.048	0.016	0.063	0.051	0.081	0.055	0.061	0.090	0.077	0.097	0.074	0.037	0.074	0.077
	Al6	0.050	0.091	0.062	0.071	0.091	0.081	0.099	0.142	0.091	0.109	0.084	0.128	0.104	0.118	0.134	0.129	0.148	0.119	0.081	0.075
	Mg #	0.956	0.956	0.956	0.956	0.955	0.954	0.956	0.956	0.955	0.955	0.954	0.954	0.955	0.948	0.949	0.947	0.948	0.956	0.954	0.955
	NaK (A)	0.183	0.180	0.200	0.205	0.235	0.227	0.224	0.243	0.245	0.245	0.265	0.270	0.262	0.335	0.343	0.337	0.332	0.242	0.226	0.217

Abbreviations: Tr = tremolite, Serp = serpentinite, b.d. = below detection, n.c. = not calculated. Mg# calculated as (MgO/40.3) / (MgO/40.3 + FeO/71.85).

Major element composition of amphibole from the Geisspfad ultramafic body continued

Sample		G27	G27	G27	G27	G27	G27	G27	G27	G27	G27	G27	G27	G27	G27	G27	G27	G27	G27	G27
Rock		Serp	Serp	Serp	Serp	Serp	Serp	Serp	Serp	Serp	Serp	Serp	Serp	Serp	Serp	Serp	Serp	Serp	Serp	Serp
Mineral		Tr	Tr	Tr	Tr	Tr	Tr	Tr	Tr	Tr	Tr	Tr	Tr	Tr	Tr	Tr	Tr	Tr	Tr	Tr
Wt.%	SiO2	57.62	57.72	58.24	57.87	58.27	57.97	57.68	57.86	57.68	57.73	57.48	57.84	57.58	57.60	57.09	57.79	57.72	57.93	57.52	57.56
	TiO2	0.05	0.05	0.05	0.05	0.05	0.05	0.05	0.05	0.04	0.06	0.06	0.05	0.06	0.06	0.06	0.05	0.07	0.05	0.05	0.06
	Cr2O3	0.01	b.d.	0.03	b.d.	0.05	0.01	b.d.	0.07	0.02	0.04	0.01	0.04	0.08	0.06	0.11	0.08	0.03	0.08	b.d.	b.d.
	Al2O3	0.93	0.89	0.79	0.86	0.86	0.86	0.98	0.88	0.92	1.01	1.12	0.95	1.09	1.04	1.08	1.19	1.07	1.06	1.00	1.04
	Fe2O3	n.c.	n.c.	n.c.	n.c.	n.c.	n.c.	n.c.	n.c.	n.c.	n.c.	n.c.	n.c.	n.c.	n.c.	n.c.	n.c.	n.c.	n.c.	n.c.	n.c.
	FeO	1.94	1.97	1.77	1.93	1.89	1.93	1.88	1.84	1.88	1.95	1.94	1.91	2.04	2.05	1.98	2.03	2.01	2.00	1.98	1.99
	MnO	0.04	0.04	0.04	0.06	0.04	0.04	0.04	0.05	0.04	0.05	0.05	0.05	0.07	0.03	0.03	0.03	0.04	0.05	0.03	0.06
	NiO	0.10	0.10	0.12	0.08	0.10	0.11	0.11	0.08	0.04	0.06	0.09	0.08	0.08	0.11	0.11	0.09	0.09	0.03	0.09	0.08
	MgO	22.99	22.98	23.43	23.17	23.10	23.12	22.93	23.25	23.08	23.11	23.02	23.08	22.98	22.94	22.68	23.06	23.26	23.03	22.86	23.05
	CaO	13.15	13.15	13.55	13.14	13.54	13.31	13.19	13.37	13.28	13.31	13.08	13.17	13.05	12.92	12.89	13.07	13.01	13.06	13.15	13.10
	Na2O	0.79	0.73	0.72	0.75	0.74	0.78	0.84	0.80	0.83	0.90	0.95	0.90	1.04	1.00	0.99	1.02	1.00	0.96	0.88	0.89
	K2O	0.05	0.05	0.05	0.05	0.05	0.04	0.06	0.05	0.05	0.06	0.06	0.06	0.07	0.07	0.07	0.08	0.07	0.07	0.07	0.07
	H2O	2.18	2.18	2.20	2.18	2.20	2.19	2.18	2.19	2.18	2.19	2.18	2.18	2.18	2.17	2.16	2.19	2.19	2.19	2.17	2.18
	Total	99.84	99.86	100.98	100.14	100.88	100.41	99.94	100.48	100.05	100.46	100.03	100.30	100.32	100.05	99.25	100.66	100.55	100.51	99.82	100.08
Cations	Si	7.940	7.950	7.922	7.944	7.947	7.943	7.947	7.918	7.932	7.914	7.917	7.943	7.921	7.943	7.938	7.920	7.911	7.948	7.941	7.921
	Ti	0.005	0.005	0.005	0.005	0.005	0.006	0.005	0.006	0.004	0.006	0.007	0.005	0.006	0.007	0.007	0.005	0.007	0.005	0.006	0.006
	Cr	0.001	b.d.	0.003	b.d.	0.005	0.001	b.d.	0.007	0.002	0.004	0.001	0.004	0.009	0.007	0.012	0.008	0.003	0.009	b.d.	b.d.
	Al	0.151	0.145	0.127	0.139	0.138	0.138	0.159	0.142	0.148	0.163	0.181	0.153	0.178	0.169	0.177	0.192	0.173	0.172	0.163	0.169
	Fe3+	n.c.	n.c.	n.c.	n.c.	n.c.	n.c.	n.c.	n.c.	n.c.	n.c.	n.c.	n.c.	n.c.	n.c.	n.c.	n.c.	n.c.	n.c.	n.c.	n.c.
	Fe2+	0.224	0.227	0.201	0.222	0.216	0.221	0.217	0.211	0.216	0.224	0.223	0.219	0.235	0.236	0.230	0.233	0.230	0.229	0.229	0.229
	Mn	0.005	0.005	0.004	0.007	0.005	0.005	0.005	0.005	0.005	0.005	0.005	0.005	0.008	0.003	0.004	0.003	0.005	0.006	0.004	0.007
	Ni	0.011	0.011	0.013	0.009	0.011	0.012	0.012	0.008	0.005	0.007	0.010	0.009	0.008	0.012	0.012	0.010	0.010	0.003	0.010	0.008
	Mg	4.722	4.717	4.750	4.741	4.696	4.721	4.708	4.742	4.730	4.722	4.726	4.724	4.712	4.715	4.700	4.710	4.751	4.709	4.704	4.728
	Ca	1.941	1.940	1.975	1.933	1.978	1.954	1.947	1.960	1.956	1.955	1.930	1.937	1.923	1.909	1.920	1.919	1.910	1.920	1.945	1.931
	Na	0.211	0.196	0.190	0.200	0.195	0.208	0.224	0.211	0.222	0.239	0.252	0.240	0.277	0.266	0.266	0.271	0.266	0.256	0.237	0.238
	K	0.008	0.009	0.008	0.008	0.008	0.007	0.011	0.009	0.008	0.011	0.010	0.010	0.012	0.012	0.013	0.014	0.012	0.013	0.013	0.013
	H	2.000	2.000	2.000	2.000	2.000	2.000	2.000	2.000	2.000	2.000	2.000	2.000	2.000	2.000	2.000	2.000	2.000	2.000	2.000	2.000
	Sum	15.219	15.204	15.198	15.208	15.203	15.215	15.235	15.221	15.230	15.250	15.263	15.250	15.289	15.279	15.279	15.285	15.277	15.269	15.250	15.251
	Al4	0.060	0.050	0.078	0.056	0.053	0.057	0.053	0.082	0.068	0.086	0.083	0.057	0.079	0.057	0.062	0.080	0.089	0.052	0.059	0.079
	Al6	0.091	0.095	0.049	0.084	0.085	0.081	0.106	0.060	0.080	0.077	0.098	0.096	0.099	0.112	0.115	0.112	0.083	0.119	0.103	0.090
	Mg #	0.955	0.954	0.959	0.955	0.956	0.955	0.956	0.957	0.956	0.955	0.955	0.956	0.953	0.952	0.953	0.953	0.954	0.954	0.954	0.954
	NaK (A)	0.219	0.204	0.198	0.208	0.203	0.215	0.235	0.221	0.230	0.250	0.263	0.250	0.289	0.279	0.279	0.285	0.277	0.269	0.250	0.251

Abbreviations: Tr = tremolite, Serp = serpentinite, b.d. = below detection, n.c. = not calculated. Mg# calculated as (MgO/40.3) / (MgO/40.3 + FeO/71.85).

Major element composition of amphibole from the Geisspfad ultramafic body continued

Sample		G27	G27	G27	GEI4	GEI4	GEI4	GEI4	GEI4	GEI4	GEI4	GEI4	GEI4	GEI4	GEI4	GEI4	GEI4	GEI4	GEI4	GEI4
Rock		Serp	Serp	Serp	Serp	Serp	Serp	Serp	Serp	Serp	Serp	Serp	Serp	Serp	Serp	Serp	Serp	Serp	Serp	Serp
Mineral		Tr	Tr	Tr	Tr	Tr	Tr	Tr	Tr	Tr	Tr	Tr	Tr	Tr	Tr	Tr	Tr	Tr	Tr	Tr
Wt.%	SiO2	57.63	57.96	57.89	57.26	57.22	55.26	54.04	56.09	56.93	56.57	56.64	57.09	56.27	56.49	56.98	56.11	57.22	57.58	56.65	57.20
	TiO2	0.06	0.07	0.06	0.04	0.06	0.08	0.13	0.08	0.05	0.07	0.05	0.04	0.06	0.04	0.04	0.07	0.07	0.04	0.07	0.07
	Cr2O3	0.03	b.d.	0.04	0.13	0.18	0.54	0.61	0.58	0.03	0.08	0.05	0.04	0.20	0.19	0.22	0.60	0.04	0.25	0.52	0.26
	Al2O3	0.89	0.76	0.74	1.06	0.92	1.96	2.80	1.72	1.10	1.22	0.98	1.00	1.51	1.49	1.26	1.73	1.11	0.90	1.53	1.07
	Fe2O3	n.c.	n.c.	n.c.	n.c.	n.c.	n.c.	n.c.	n.c.	n.c.	n.c.	n.c.	n.c.	n.c.	n.c.	n.c.	n.c.	n.c.	n.c.	n.c.	n.c.
	FeO	1.96	1.90	1.93	2.22	2.34	2.18	2.40	2.02	2.39	2.26	2.46	2.32	2.57	2.36	2.18	2.11	2.13	2.33	2.49	2.06
	MnO	0.04	0.06	0.06	0.05	0.12	b.d.	0.04	0.03	0.05	0.03	0.03	0.04	0.03	0.04	0.07	0.04	0.06	0.04	0.13	0.03
	NiO	0.07	0.10	0.07	0.06	0.11	0.07	0.07	0.06	0.04	0.09	0.08	0.09	0.11	0.11	0.09	0.11	0.08	0.11	0.10	0.07
	MgO	23.23	23.02	23.13	23.26	23.33	22.71	22.29	22.79	23.22	23.11	23.62	23.32	23.13	23.22	23.14	22.72	23.25	23.23	22.94	23.22
	CaO	13.34	13.21	13.50	13.04	12.27	12.78	12.73	12.85	12.82	12.89	12.52	12.95	12.37	12.61	12.88	12.55	12.76	12.31	12.43	13.12
	Na2O	0.78	0.71	0.67	1.03	1.46	1.52	1.85	1.24	1.18	1.24	0.94	1.03	1.64	1.46	1.08	1.45	1.16	1.36	1.47	1.02
	K2O	0.04	0.04	0.04	0.07	0.10	0.14	0.17	0.10	0.08	0.10	0.06	0.06	0.12	0.09	0.08	0.13	0.07	0.10	0.11	0.10
	H2O	2.19	2.18	2.19	2.18	2.17	2.15	2.14	2.16	2.17	2.17	2.17	2.18	2.16	2.17	2.18	2.16	2.18	2.17	2.17	2.18
	Total	100.25	100.01	100.33	100.42	100.27	99.38	99.26	99.72	100.08	99.82	99.59	100.16	100.17	100.27	100.20	99.78	100.13	100.41	100.63	100.42
Cations	Si	7.902	7.969	7.930	7.863	7.907	7.713	7.584	7.782	7.854	7.831	7.821	7.856	7.797	7.800	7.848	7.802	7.887	7.942	7.817	7.857
	Ti	0.006	0.007	0.007	0.004	0.006	0.008	0.014	0.009	0.005	0.007	0.005	0.004	0.006	0.004	0.004	0.007	0.007	0.004	0.007	0.007
	Cr	0.003	b.d.	0.004	0.014	0.020	0.059	0.068	0.063	0.004	0.008	0.006	0.005	0.022	0.020	0.024	0.066	0.005	0.027	0.056	0.028
	Al	0.143	0.123	0.120	0.172	0.150	0.323	0.463	0.281	0.179	0.199	0.160	0.162	0.247	0.243	0.204	0.283	0.181	0.147	0.249	0.174
	Fe3+	n.c.	n.c.	n.c.	n.c.	n.c.	n.c.	n.c.	n.c.	n.c.	n.c.	n.c.	n.c.	n.c.	n.c.	n.c.	n.c.	n.c.	n.c.	n.c.	n.c.
	Fe2+	0.225	0.218	0.221	0.255	0.270	0.254	0.282	0.234	0.276	0.262	0.284	0.267	0.298	0.273	0.251	0.245	0.245	0.269	0.288	0.237
	Mn	0.005	0.007	0.007	0.005	0.014	b.d.	0.005	0.003	0.006	0.003	0.003	0.005	0.003	0.005	0.009	0.005	0.007	0.005	0.016	0.004
	Ni	0.008	0.011	0.008	0.007	0.013	0.008	0.008	0.007	0.005	0.010	0.009	0.010	0.013	0.013	0.009	0.013	0.009	0.012	0.012	0.008
	Mg	4.748	4.718	4.722	4.761	4.805	4.724	4.663	4.712	4.776	4.767	4.861	4.783	4.777	4.778	4.751	4.709	4.776	4.776	4.718	4.754
	Ca	1.960	1.946	1.981	1.919	1.816	1.911	1.914	1.910	1.896	1.912	1.852	1.909	1.837	1.865	1.901	1.871	1.884	1.820	1.838	1.931
	Na	0.208	0.190	0.179	0.275	0.390	0.412	0.504	0.334	0.316	0.332	0.252	0.275	0.440	0.392	0.288	0.391	0.310	0.363	0.394	0.272
	K	0.006	0.006	0.007	0.013	0.019	0.025	0.030	0.019	0.014	0.018	0.010	0.011	0.021	0.016	0.015	0.023	0.013	0.018	0.020	0.018
	H	2.000	2.000	2.000	2.000	2.000	2.000	2.000	2.000	2.000	2.000	2.000	2.000	2.000	2.000	2.000	2.000	2.000	2.000	2.000	2.000
	Sum	15.214	15.196	15.187	15.288	15.409	15.437	15.534	15.353	15.330	15.350	15.262	15.286	15.461	15.407	15.303	15.415	15.323	15.381	15.414	15.289
	Al4	0.098	0.031	0.070	0.137	0.093	0.287	0.416	0.218	0.146	0.169	0.160	0.144	0.203	0.200	0.152	0.198	0.113	0.058	0.183	0.143
	Al6	0.046	0.093	0.050	0.035	0.057	0.036	0.047	0.063	0.033	0.029	0.000	0.019	0.044	0.043	0.052	0.085	0.067	0.089	0.066	0.031
	Mg #	0.955	0.956	0.955	0.949	0.947	0.949	0.943	0.953	0.945	0.948	0.945	0.947	0.941	0.946	0.950	0.951	0.951	0.947	0.943	0.953
	NaK (A)	0.214	0.196	0.187																	

Abbreviations: Tr = tremolite, Serp = serpentinite, b.d. = below detection, n.c. = not calculated. Mg# calculated as (MgO/40.3) / (MgO/40.3 + FeO/71.85).

Major element composition of amphibole from the Geisspfad ultramafic body continued

Sample		GEI4	GEI4	GEI4	GEI4	GEI4	GEI4	GEI4	GEI4	GEI4	GEI4	GEI4	GEI4	GEI4	GEI4	G3	G3	G3	G3	G3	G3
Rock		Serp	Serp	Serp	Serp	Serp	Serp	Serp	Serp	Serp	Serp	Serp	Serp	Serp	Serp	Ophi	Ophi	Ophi	Ophi	Ophi	Ophi
Mineral		Tr	Tr	Tr	Tr	Tr	Tr	Tr	Tr	Tr	Tr	Tr	Tr	Tr	Tr	Tr	Tr	Tr	Tr	Tr	Tr
Wt.%	SiO2	56.85	56.15	57.39	56.82	57.36	57.30	57.34	57.70	57.52	57.45	56.38	55.21	55.56	56.09	59.00	59.17	58.91	58.65	58.52	58.96
	TiO2	0.05	0.06	0.10	0.05	0.05	0.08	0.05	0.04	0.03	0.05	0.09	0.09	0.08	0.05	0.03	0.01	0.02	0.02	0.01	0.01
	Cr2O3	0.07	0.42	0.07	0.04	0.11	0.05	0.17	0.02	0.07	0.08	0.28	0.51	0.19	0.33	0.00	0.05	0.10	0.03	0.08	0.01
	Al2O3	1.20	1.65	0.94	1.35	0.98	0.91	1.02	0.70	0.75	0.98	1.65	2.30	2.07	1.63	0.23	0.14	0.18	0.31	0.24	0.16
	Fe2O3	n.c.	n.c.	n.c.	n.c.	n.c.	n.c.	n.c.	n.c.	n.c.	n.c.	n.c.	n.c.	n.c.	n.c.	n.c.	n.c.	n.c.	n.c.	n.c.	n.c.
	FeO	2.39	2.16	2.13	2.39	1.99	2.00	2.14	2.02	2.25	2.10	2.08	2.59	2.31	2.60	1.78	1.65	1.66	1.86	1.76	1.71
	MnO	0.06	0.06	0.10	0.09	b.d.	0.02	0.03	0.05	0.08	0.03	0.08	0.05	0.06	0.13	0.13	0.08	0.05	0.12	0.16	0.08
	NiO	0.09	0.09	0.09	0.08	0.12	0.05	0.10	0.10	0.08	0.08	0.14	0.07	0.08	0.10	b.d.	0.10	0.12	0.02	0.09	0.08
	MgO	23.23	22.96	23.32	23.05	23.33	23.36	23.23	23.36	23.21	23.19	22.88	22.64	23.19	23.11	23.50	23.26	23.70	23.59	22.95	23.01
	CaO	12.75	12.86	13.35	12.89	13.11	13.32	13.10	13.18	12.68	13.00	12.90	12.54	12.58	12.04	13.41	13.48	13.61	13.35	13.40	13.46
	Na2O	1.17	1.47	0.88	1.26	0.97	0.92	1.04	0.84	1.04	1.09	1.31	1.83	1.34	1.85	0.21	0.15	0.15	0.31	0.23	0.14
	K2O	0.10	0.11	0.07	0.09	0.07	0.06	0.08	0.05	0.10	0.11	0.09	0.12	0.15	0.15	0.04	0.04	0.04	0.06	0.05	0.03
	H2O	2.17	2.17	2.19	2.17	2.18	2.18	2.18	2.18	2.17	2.18	2.17	2.16	2.16	2.16	2.20	2.20	2.21	2.20	2.18	2.19
	Total	100.12	100.15	100.62	100.28	100.27	100.25	100.48	100.22	99.97	100.35	100.06	100.11	99.79	100.23	100.54	100.33	100.76	100.51	99.67	99.84
Cations	Si	7.841	7.769	7.854	7.835	7.877	7.865	7.871	7.918	7.940	7.902	7.797	7.681	7.694	7.790	8.024	8.066	7.987	7.984	8.045	8.082
	Ti	0.005	0.006	0.010	0.005	0.005	0.008	0.005	0.004	0.003	0.005	0.009	0.009	0.009	0.005	0.003	0.001	0.002	0.002	0.001	0.001
	Cr	0.007	0.046	0.007	0.004	0.012	0.005	0.018	0.002	0.007	0.008	0.031	0.056	0.021	0.037	0.000	0.006	0.011	0.003	0.009	0.001
	Al	0.194	0.270	0.152	0.219	0.158	0.147	0.165	0.113	0.121	0.159	0.268	0.377	0.339	0.266	0.036	0.022	0.029	0.049	0.038	0.025
	Fe3+	n.c.	n.c.	n.c.	n.c.	n.c.	n.c.	n.c.	n.c.	n.c.	n.c.	n.c.	n.c.	n.c.	n.c.	n.c.	n.c.	n.c.	n.c.	n.c.	n.c.
	Fe2+	0.275	0.250	0.243	0.276	0.229	0.230	0.246	0.232	0.260	0.242	0.240	0.301	0.268	0.302	0.203	0.188	0.188	0.212	0.203	0.196
	Mn	0.008	0.007	0.012	0.011	b.d.	0.003	0.004	0.006	0.009	0.003	0.010	0.006	0.007	0.015	0.015	0.010	0.006	0.014	0.019	0.009
	Ni	0.010	0.010	0.010	0.009	0.014	0.005	0.012	0.011	0.009	0.009	0.016	0.008	0.009	0.011	b.d.	0.011	0.013	0.002	0.010	0.008
	Mg	4.776	4.735	4.756	4.737	4.776	4.778	4.752	4.778	4.776	4.756	4.716	4.693	4.787	4.783	4.765	4.727	4.788	4.786	4.702	4.700
	Ca	1.884	1.907	1.957	1.905	1.929	1.958	1.927	1.938	1.875	1.915	1.912	1.869	1.866	1.792	1.955	1.970	1.976	1.947	1.974	1.977
	Na	0.312	0.394	0.234	0.336	0.257	0.244	0.276	0.225	0.279	0.292	0.352	0.494	0.361	0.498	0.055	0.039	0.041	0.081	0.062	0.037
	K	0.018	0.019	0.012	0.016	0.013	0.011	0.013	0.008	0.017	0.019	0.016	0.022	0.027	0.027	0.008	0.007	0.006	0.010	0.009	0.005
	H	2.000	2.000	2.000	2.000	2.000	2.000	2.000	2.000	2.000	2.000	2.000	2.000	2.000	2.000	2.000	2.000	2.000	2.000	2.000	2.000
	Sum	15.331	15.413	15.247	15.352	15.270	15.254	15.289	15.233	15.296	15.311	15.369	15.516	15.388	15.524	15.063	15.046	15.047	15.091	15.071	15.042
	Al4	0.159	0.231	0.146	0.165	0.123	0.135	0.129	0.082	0.060	0.098	0.203	0.319	0.306	0.210	0.000	0.000	0.013	0.016	0.000	0.000
	Al6	0.035	0.039	0.005	0.054	0.036	0.012	0.036	0.031	0.062	0.061	0.066	0.058	0.033	0.056	0.036	0.022	0.016	0.034	0.038	0.025
	Mg #	0.945	0.950	0.951	0.945	0.954	0.954	0.951	0.954	0.948	0.952	0.952	0.940	0.947	0.941	0.959	0.962	0.962	0.958	0.959	0.960
	NaK (A)															0.063	0.046	0.047	0.091	0.071	0.042

Abbreviations: Tr = tremolite, Serp = serpentinite, Ophi = ophicarbonate, b.d. = below detection, n.c. = not calculated. Mg# calculated as (MgO/40.3) / (MgO/40.3 + FeO/71.85).

Major element composition of amphibole from the Geisspfad ultramafic body continued

Sample		G3	G4	G4	G4	G4	G4	GEI9	GEI9	GEI9	GEI9	GEI9	GEI9	GEI9	GEI9	GEI9	GEI9	GEI9	GEI9	GEI9
Rock		Ophi	Ophi	Ophi	Ophi	Ophi	Ophi	Ophi	Ophi	Ophi	Ophi	Ophi	Ophi	Ophi	Ophi	Ophi	Ophi	Ophi	Ophi	Ophi
Mineral		Tr	Tr	Tr	Tr	Tr	Tr	Tr	Tr	Tr	Tr	Tr	Tr	Tr	Tr	Tr	Tr	Tr	Tr	Tr
Wt.%	SiO2	58.26	59.11	58.65	58.88	58.81	58.71	58.51	58.23	57.96	58.37	58.47	58.43	59.33	58.95	57.76	58.69	58.38	58.37	58.69	58.77
	TiO2	0.02	0.03	0.04	0.04	0.03	0.05	0.05	0.04	0.06	0.04	0.03	0.04	0.04	0.04	0.06	0.05	0.06	0.04	0.05	0.04
	Cr2O3	0.08	b.d.	0.10	b.d.	0.03	b.d.	b.d.	0.09	0.02	b.d.	b.d.	b.d.	0.05	0.04	b.d.	0.02	0.02	b.d.	b.d.	b.d.
	Al2O3	0.15	0.08	0.19	0.11	0.18	0.11	0.35	0.40	0.38	0.32	0.28	0.36	0.33	0.46	0.40	0.38	0.40	0.37	0.34	0.37
	Fe2O3	n.c.	n.c.	n.c.	n.c.	n.c.	n.c.	n.c.	n.c.	n.c.	n.c.	n.c.	n.c.	n.c.	n.c.	n.c.	n.c.	n.c.	n.c.	n.c.	n.c.
	FeO	1.72	1.63	1.75	1.57	1.63	1.52	1.41	1.51	1.56	1.45	1.49	1.56	1.51	1.66	1.64	1.36	1.44	1.38	1.43	1.30
	MnO	0.09	0.17	0.18	0.07	0.20	0.09	0.07	0.10	0.09	0.02	0.10	0.07	0.09	0.07	0.16	0.10	0.14	0.01	0.13	0.09
	NiO	b.d.	0.19	0.08	0.05	0.04	0.05	0.09	0.03	0.14	0.12	0.10	0.02	b.d.	0.07	0.20	0.05	0.03	0.15	0.08	0.11
	MgO	22.92	23.69	23.28	23.04	22.80	23.18	23.12	22.66	23.07	22.73	23.20	23.31	23.28	23.76	23.30	23.29	22.96	22.89	22.81	22.85
	CaO	13.49	13.61	13.56	13.66	13.51	13.64	13.63	13.56	13.65	13.63	13.71	13.56	13.60	13.36	13.41	13.50	13.51	13.49	13.53	13.56
	Na2O	0.17	0.05	0.09	0.06	0.08	0.05	0.15	0.24	0.21	0.19	0.12	0.18	0.19	0.23	0.25	0.26	0.25	0.24	0.20	0.19
	K2O	0.03	0.01	0.01	0.02	0.02	0.01	0.03	0.04	0.03	0.02	0.04	0.04	0.04	0.03	0.03	0.03	0.04	0.05	0.03	0.03
	H2O	2.17	2.21	2.20	2.19	2.18	2.19	2.19	2.17	2.18	2.17	2.19	2.19	2.21	2.21	2.18	2.19	2.18	2.17	2.18	2.18
	Total	99.11	100.77	100.11	99.68	99.51	99.60	99.61	99.06	99.34	99.05	99.73	99.77	100.66	100.89	99.39	99.92	99.39	99.16	99.47	99.49
Cations	Si	8.043	8.004	8.006	8.072	8.087	8.048	8.027	8.052	7.979	8.064	8.009	8.002	8.062	7.982	7.946	8.030	8.038	8.056	8.077	8.083
	Ti	0.002	0.003	0.004	0.004	0.003	0.005	0.005	0.004	0.006	0.004	0.003	0.005	0.004	0.004	0.006	0.005	0.006	0.004	0.005	0.004
	Cr	0.009	b.d.	0.011	b.d.	0.003	b.d.	b.d.	0.010	0.002	b.d.	b.d.	b.d.	0.005	0.005	b.d.	0.002	0.002	b.d.	b.d.	b.d.
	Al	0.024	0.013	0.030	0.018	0.030	0.018	0.056	0.065	0.062	0.052	0.046	0.058	0.053	0.073	0.064	0.062	0.064	0.060	0.056	0.060
	Fe3+	n.c.	n.c.	n.c.	n.c.	n.c.	n.c.	n.c.	n.c.	n.c.	n.c.	n.c.	n.c.	n.c.	n.c.	n.c.	n.c.	n.c.	n.c.	n.c.	n.c.
	Fe2+	0.199	0.185	0.200	0.180	0.188	0.174	0.162	0.175	0.180	0.168	0.171	0.179	0.172	0.188	0.189	0.156	0.166	0.159	0.165	0.150
	Mn	0.011	0.020	0.021	0.008	0.024	0.011	0.009	0.012	0.010	0.003	0.012	0.008	0.010	0.008	0.018	0.012	0.016	0.001	0.015	0.010
	Ni	b.d.	0.020	0.009	0.005	0.004	0.006	0.010	0.003	0.015	0.013	0.011	0.002	b.d.	0.008	0.022	0.005	0.003	0.017	0.009	0.012
	Mg	4.716	4.781	4.737	4.707	4.672	4.736	4.728	4.670	4.734	4.680	4.736	4.758	4.715	4.795	4.778	4.749	4.712	4.708	4.679	4.684
	Ca	1.996	1.974	1.983	2.006	1.990	2.003	2.003	2.009	2.013	2.017	2.012	1.989	1.980	1.938	1.976	1.979	1.993	1.995	1.995	1.998
	Na	0.046	0.012	0.023	0.015	0.020	0.012	0.041	0.064	0.057	0.051	0.031	0.049	0.050	0.059	0.068	0.068	0.067	0.065	0.054	0.050
	K	0.005	0.002	0.002	0.003	0.004	0.002	0.005	0.007	0.005	0.003	0.006	0.007	0.007	0.005	0.005	0.004	0.006	0.008	0.005	0.006
	H	2.000	2.000	2.000	2.000	2.000	2.000	2.000	1.999	1.999	2.000	1.999	1.999	2.000	2.000	2.000	1.999	1.999	2.000	2.000	2.000
	Sum	15.051	15.014	15.024	15.018	15.024	15.015	15.046	15.071	15.062	15.054	15.037	15.056	15.057	15.065	15.073	15.073	15.073	15.073	15.059	15.056
	Al4	0.000	0.000	0.000	0.000	0.000	0.000	0.000	0.000	0.021	0.000	0.000	0.000	0.000	0.018	0.054	0.000	0.000	0.000	0.000	0.000
	Al6	0.024	0.013	0.030	0.018	0.030	0.018	0.056	0.065	0.041	0.052	0.046	0.058	0.053	0.055	0.011	0.062	0.064	0.060	0.056	0.060
	Mg #	0.960	0.963	0.959	0.963	0.961	0.965	0.967	0.964	0.963	0.965	0.965	0.964	0.965	0.962	0.962	0.968	0.966	0.967	0.966	0.969
	NaK (A)	0.051	0.014	0.024	0.018	0.024	0.015	0.046	0.071	0.062	0.054	0.037	0.056	0.057	0.065	0.073	0.073	0.073	0.073	0.059	0.056

Abbreviations: Tr = tremolite, Ophi = ophicarbonate, b.d. = below detection, n.c. = not calculated. Mg# calculated as (MgO/40.3) / (MgO/40.3 + FeO/71.85).

Major element composition of amphibole from the Geisspfad ultramafic body continued

Sample		GEI9	GEI9	GEI9	GEI9	GEI9	GEI9	GEI9	GEI9	GEI9	GEI9	GEI9	GEI9	GEI9	GEI9	GEI9	GEI9	GEI9
Rock		Ophi	Ophi	Ophi	Ophi	Ophi	Ophi	Ophi	Ophi	Ophi	Ophi	Ophi	Ophi	Ophi	Ophi	Ophi	Ophi	Ophi
Mineral		Tr	Tr	Tr	Tr	Tr	Tr	Tr	Tr	Tr	Tr	Tr	Tr	Tr	Tr	Tr	Tr	Tr
Wt.%	SiO2	58.72	58.78	58.67	58.04	58.30	58.36	58.51	58.24	58.06	58.91	58.96	59.17	59.48	58.74	59.12	58.54	58.65
	TiO2	0.04	0.04	0.04	0.04	0.05	0.05	0.06	0.05	0.04	0.05	0.04	0.01	0.03	0.03	0.04	0.06	0.04
	Cr2O3	0.04	0.03	0.07	0.07	0.01	0.03	b.d.	0.03	b.d.	b.d.	b.d.	0.06	b.d.	0.04	0.02	0.04	0.03
	Al2O3	0.21	0.34	0.34	0.39	0.34	0.32	0.31	0.32	0.33	0.30	0.31	0.13	0.16	0.27	0.27	0.39	0.34
	Fe2O3	n.c.	n.c.	n.c.	n.c.	n.c.	n.c.	n.c.	n.c.	n.c.	n.c.	n.c.	n.c.	n.c.	n.c.	n.c.	n.c.	n.c.
	FeO	1.34	1.45	1.54	1.57	1.45	1.44	1.53	1.55	1.64	1.45	1.24	1.24	1.38	1.42	1.55	1.86	1.63
	MnO	0.13	0.13	0.11	0.07	0.12	0.01	0.01	0.12	0.20	0.11	0.05	0.13	0.08	0.07	0.01	0.09	0.19
	NiO	0.04	0.06	b.d.	0.10	0.04	b.d.	0.15	b.d.	0.09	0.11	0.05	b.d.	b.d.	b.d.	0.02	0.03	0.01
	MgO	22.89	22.96	22.74	22.93	22.81	22.92	23.03	22.96	22.62	23.08	23.00	23.07	23.35	23.03	23.34	22.81	22.75
	CaO	13.77	13.54	13.51	13.45	13.54	13.60	13.53	13.52	13.64	13.62	13.69	13.83	13.75	13.80	13.59	13.56	13.59
	Na2O	0.11	0.17	0.21	0.19	0.21	0.22	0.20	0.21	0.19	0.16	0.16	0.08	0.07	0.12	0.10	0.23	0.22
	K2O	0.02	0.03	0.03	0.03	0.03	0.02	0.04	0.04	0.04	0.02	0.02	0.02	0.02	0.03	0.02	0.03	0.03
	H2O	2.18	2.19	2.18	2.17	2.17	2.17	2.18	2.17	2.17	2.19	2.19	2.19	2.21	2.19	2.20	2.18	2.18
	Total	99.51	99.71	99.44	99.06	99.07	99.15	99.55	99.21	99.02	100.01	99.70	99.93	100.53	99.74	100.27	99.83	99.66
Cations	Si	8.068	8.065	8.081	8.014	8.053	8.050	8.041	8.031	8.032	8.057	8.082	8.089	8.078	8.048	8.051	8.036	8.064
	Ti	0.005	0.004	0.004	0.005	0.005	0.005	0.006	0.005	0.005	0.006	0.004	0.001	0.003	0.003	0.004	0.006	0.004
	Cr	0.005	0.003	0.008	0.007	0.001	0.003	b.d.	0.003	b.d.	b.d.	b.d.	0.006	b.d.	0.005	0.002	0.005	0.003
	Al	0.035	0.055	0.056	0.063	0.055	0.053	0.050	0.052	0.054	0.048	0.050	0.021	0.026	0.044	0.043	0.064	0.055
	Fe3+	n.c.	n.c.	n.c.	n.c.	n.c.	n.c.	n.c.	n.c.	n.c.	n.c.	n.c.	n.c.	n.c.	n.c.	n.c.	n.c.	n.c.
	Fe2+	0.154	0.166	0.177	0.181	0.167	0.166	0.176	0.179	0.190	0.166	0.142	0.142	0.157	0.163	0.177	0.214	0.187
	Mn	0.016	0.015	0.013	0.009	0.013	0.001	0.001	0.014	0.023	0.013	0.006	0.015	0.009	0.008	0.001	0.011	0.022
	Ni	0.004	0.007	b.d.	0.012	0.005	b.d.	0.017	b.d.	0.010	0.012	0.006	b.d.	b.d.	b.d.	0.002	0.004	0.001
	Mg	4.687	4.695	4.668	4.719	4.696	4.712	4.717	4.719	4.664	4.704	4.699	4.701	4.726	4.703	4.738	4.667	4.662
	Ca	2.027	1.990	1.994	1.990	2.004	2.010	1.992	1.997	2.022	1.996	2.010	2.025	2.001	2.026	1.983	1.994	2.002
	Na	0.030	0.046	0.056	0.052	0.055	0.058	0.052	0.056	0.050	0.043	0.042	0.020	0.018	0.031	0.026	0.061	0.060
	K	0.004	0.005	0.005	0.005	0.006	0.004	0.007	0.006	0.006	0.004	0.003	0.004	0.003	0.005	0.003	0.005	0.006
	H	2.000	2.000	2.000	2.000	2.000	2.000	1.999	2.000	1.999	2.000	2.000	2.000	2.000	2.000	1.999	1.999	2.000
	Sum	15.034	15.051	15.061	15.057	15.061	15.062	15.059	15.062	15.056	15.047	15.045	15.024	15.020	15.036	15.029	15.066	15.066
	Al4	0.000	0.000	0.000	0.000	0.000	0.000	0.000	0.000	0.000	0.000	0.000	0.000	0.000	0.000	0.000	0.000	0.000
	Al6	0.035	0.055	0.056	0.063	0.055	0.053	0.050	0.052	0.054	0.048	0.050	0.021	0.026	0.044	0.043	0.064	0.055
	Mg #	0.968	0.966	0.963	0.963	0.966	0.966	0.964	0.964	0.961	0.966	0.971	0.971	0.968	0.967	0.964	0.956	0.961
	NaK (A)	0.034	0.051	0.061	0.057	0.061	0.062	0.059	0.062	0.056	0.047	0.045	0.024	0.020	0.036	0.029	0.066	0.066

Abbreviations: Tr = tremolite, Ophi = ophicarbonate, b.d. = below detection, n.c. = not calculated. Mg# calculated as (MgO/40.3) / (MgO/40.3 + FeO/71.85).

Major element composition of amphibole from the Geisspfad ultramafic body

Sample		G34	G34	G34	G34	G34	G34	G34	G34	G34	G34	G34	G34	G34	G34	G34	G34
Rock		Metab	Metab	Metab	Metab	Metab	Metab	Metab	Metab	Metab	Metab	Metab	Metab	Metab	Metab	Metab	Metab
Mineral		Ts hbl	Ts hbl	Ts hbl	Ts hbl	Ts hbl	Ts hbl	Ts hbl	Ts hbl	Ts hbl	Ts hbl	Ts hbl	Ts hbl	Ts hbl	Ts hbl	Ts hbl	Ts hbl
Wt.%	SiO2	42.97	41.73	42.87	43.09	43.03	42.84	43.46	43.04	43.07	42.81	42.91	43.11	42.80	42.88	43.17	42.78
	TiO2	0.33	4.09	0.33	0.33	0.33	0.32	0.32	0.32	0.33	0.31	0.37	0.41	0.36	0.35	0.33	0.35
	Cr2O3	0.03	0.06	0.04	0.02	0.10	0.07	0.07	0.04	0.10	b.d.	0.01	b.d.	0.05	0.11	0.01	b.d.
	Al2O3	13.15	11.99	13.43	13.14	13.06	13.33	12.96	13.08	13.09	13.21	13.24	13.13	12.97	13.08	13.07	13.27
	Fe2O3	6.51	2.55	5.68	5.71	6.09	5.98	5.47	5.69	5.45	6.00	5.94	5.85	6.49	6.67	5.49	6.38
	FeO	5.90	7.97	6.20	6.23	6.41	6.26	6.71	6.70	7.00	6.70	6.22	6.62	5.85	6.13	6.68	6.27
	MnO	0.22	0.18	0.22	0.23	0.23	0.24	0.25	0.23	0.24	0.24	0.23	0.21	0.23	0.26	0.22	0.22
	NiO	b.d.	b.d.	b.d.	0.06	0.04	0.07	0.12	0.08	b.d.	b.d.	b.d.	b.d.	0.08	0.02	0.06	0.08
	MgO	13.53	12.09	13.48	13.45	13.37	13.36	13.38	13.19	13.13	12.99	13.40	13.28	13.44	13.43	13.28	13.26
	CaO	13.10	14.87	12.95	13.07	12.91	12.99	12.97	12.93	12.98	13.09	13.01	13.22	13.18	12.97	12.96	13.05
	Na2O	1.19	1.10	1.23	1.20	1.17	1.23	1.18	1.16	1.23	1.16	1.18	1.25	1.22	1.21	1.17	1.24
	K2O	0.52	0.48	0.53	0.52	0.51	0.55	0.50	0.52	0.52	0.55	0.53	0.55	0.55	0.52	0.50	0.51
	H2O	2.06	2.03	2.05	2.05	2.05	2.05	2.06	2.05	2.05	2.05	2.05	2.06	2.05	2.06	2.05	2.05
	Total	99.52	99.15	99.01	99.10	99.28	99.29	99.45	99.05	99.18	99.11	99.10	99.68	99.26	99.68	99.00	99.47
Cations	Si	6.260	6.156	6.268	6.298	6.287	6.259	6.335	6.305	6.306	6.276	6.274	6.280	6.259	6.248	6.319	6.246
	Ti	0.037	0.454	0.036	0.037	0.036	0.035	0.035	0.035	0.036	0.034	0.041	0.045	0.039	0.038	0.036	0.039
	Cr	0.004	0.007	0.005	0.003	0.011	0.008	0.008	0.005	0.012	b.d.	0.002	b.d.	0.006	0.012	0.002	b.d.
	Al	2.258	2.085	2.315	2.264	2.249	2.296	2.227	2.259	2.259	2.283	2.282	2.255	2.236	2.247	2.255	2.284
	Fe3+	0.714	0.283	0.624	0.628	0.669	0.658	0.600	0.627	0.600	0.662	0.654	0.641	0.714	0.732	0.605	0.701
	Fe2+	0.719	0.983	0.758	0.761	0.784	0.764	0.817	0.821	0.856	0.821	0.761	0.806	0.715	0.747	0.817	0.766
	Mn	0.028	0.023	0.027	0.028	0.028	0.029	0.031	0.029	0.030	0.029	0.029	0.026	0.028	0.032	0.028	0.028
	Ni	b.d.	b.d.	b.d.	0.007	0.004	0.008	0.015	0.010	b.d.	b.d.	b.d.	0.000	0.009	0.002	0.007	0.009
	Mg	2.938	2.658	2.938	2.930	2.911	2.909	2.907	2.880	2.865	2.838	2.920	2.883	2.929	2.917	2.897	2.886
	Ca	2.044	2.350	2.029	2.046	2.021	2.033	2.025	2.029	2.036	2.056	2.038	2.063	2.065	2.025	2.032	2.041
	Na	0.335	0.315	0.349	0.341	0.331	0.348	0.333	0.331	0.348	0.331	0.335	0.352	0.345	0.341	0.332	0.350
	K	0.097	0.090	0.099	0.097	0.094	0.103	0.093	0.098	0.097	0.103	0.099	0.102	0.103	0.096	0.094	0.094
	H	2.000	2.000	2.000	2.000	2.000	2.000	2.000	2.000	2.000	2.000	2.000	2.000	2.000	2.000	2.000	2.000
	Sum	15.432	15.405	15.448	15.438	15.425	15.451	15.426	15.428	15.445	15.434	15.434	15.454	15.448	15.436	15.426	15.444
	Al4	1.740	1.844	1.732	1.702	1.713	1.741	1.665	1.695	1.694	1.724	1.726	1.720	1.741	1.752	1.681	1.754
	Al6	0.518	0.241	0.583	0.561	0.536	0.555	0.562	0.564	0.565	0.559	0.556	0.535	0.494	0.495	0.575	0.530
	Mg #	0.803	0.730	0.795	0.794	0.788	0.792	0.781	0.778	0.770	0.776	0.793	0.782	0.804	0.796	0.780	0.790
	NaK (A)	0.432	0.405	0.448	0.438	0.425	0.451	0.426	0.428	0.445	0.434	0.434	0.454	0.448	0.436	0.426	0.444

Abbreviations: Ts hbl = tschermakitic hornblende, Metab = metabasite, b.d. = below detection. Mg# calculated as (MgO/40.3) / (MgO/40.3 + FeO/71.85).

Major element composition of amphibole from the Geisspfad ultramafic body continued

Sample		G30	G30	G30	G30	G30	G30	G30	G30	G30	G30	G30	G31	G34	G34	G34	G34	G34	G34	G34	G34
Rock		Metab	Metab	Metab	Metab	Metab	Metab	Metab	Metab	Metab	Metab	Metab	Metab	Metab	Metab	Metab	Metab	Metab	Metab	Metab	Metab
Mineral		Ts hbl	Ts hbl	Ts hbl	Ts hbl	Ts hbl	Ts hbl	Ts hbl	Ts hbl	Ts hbl	Ts hbl	Ts hbl	Ts hbl	Ts hbl	Ts hbl	Ts hbl	Ts hbl	Ts hbl	Ts hbl	Ts hbl	Ts hbl
Wt.%	SiO2	42.94	43.46	43.19	42.92	43.20	43.75	44.21	43.28	44.00	43.33	42.84	58.47	49.05	43.84	47.61	43.99	46.74	43.81	43.58	43.35
	TiO2	0.33	0.30	0.31	0.31	0.28	0.30	0.32	0.34	0.32	0.33	0.31	0.01	0.26	0.52	0.34	0.53	0.39	0.53	0.34	0.33
	Cr2O3	0.06	0.14	0.01	0.01	0.13	0.07	0.05	0.09	b.d.	0.03	0.13	0.09	0.04	0.19	0.07	0.12	0.01	0.12	b.d.	0.03
	Al2O3	12.99	13.17	12.94	13.63	12.64	12.67	12.53	13.07	13.05	13.26	13.06	0.14	9.69	15.58	11.50	15.31	12.44	15.13	13.16	13.28
	Fe2O3	6.62	6.68	7.00	6.27	8.00	6.55	6.07	7.52	6.75	5.10	6.37	n.c.	0.83	0.59	0.24	0.67	0.30	1.52	5.76	6.32
	FeO	5.92	5.32	5.69	5.73	3.29	5.37	4.70	5.00	4.24	6.46	6.74	2.88	8.21	10.46	9.63	10.51	9.65	9.80	5.63	5.62
	MnO	0.27	0.25	0.27	0.24	0.21	0.24	0.22	0.25	0.20	0.24	0.27	0.12	0.23	0.25	0.24	0.25	0.24	0.26	0.21	0.22
	NiO	0.03	b.d.	b.d.	0.22	0.15	0.08	b.d.	0.05	0.10	b.d.	0.04	0.10	0.14	0.02	0.18	b.d.	b.d.	b.d.	0.11	0.08
	MgO	13.31	13.76	13.16	13.55	15.07	13.78	14.31	13.71	14.43	13.55	12.98	22.43	15.32	11.97	14.18	12.10	13.74	12.21	13.99	13.79
	CaO	13.22	13.59	13.90	13.01	12.69	13.71	13.96	13.79	13.93	13.07	13.04	13.67	12.81	12.23	12.33	12.22	12.43	12.33	13.05	13.13
	Na2O	1.13	1.19	1.18	1.20	1.06	1.16	1.19	1.20	1.27	1.21	1.17	0.02	0.66	1.05	0.78	1.08	0.86	0.98	1.20	1.18
	K2O	0.52	0.52	0.54	0.55	0.43	0.53	0.46	0.57	0.41	0.58	0.55	0.02	0.17	0.42	0.26	0.41	0.24	0.46	0.43	0.45
	H2O	2.05	2.08	2.07	2.06	2.07	2.08	2.08	2.09	2.10	2.06	2.05	2.19	2.10	2.06	2.09	2.06	2.08	2.06	2.07	2.07
	Total	99.40	100.48	100.26	99.71	99.21	100.29	100.11	100.96	100.79	99.21	99.56	100.15	99.52	99.18	99.46	99.26	99.12	99.21	99.54	99.86
Cations	Si	6.270	6.263	6.262	6.235	6.259	6.317	6.362	6.223	6.290	6.318	6.264	8.018	7.003	6.378	6.840	6.396	6.741	6.374	6.316	6.276
	Ti	0.036	0.033	0.034	0.034	0.030	0.033	0.035	0.037	0.035	0.036	0.034	0.001	0.028	0.057	0.037	0.058	0.042	0.058	0.037	0.036
	Cr	0.007	0.016	0.002	0.001	0.015	0.008	0.006	0.010	b.d.	0.003	0.015	0.010	0.005	0.022	0.008	0.014	0.002	0.013	b.d.	0.003
	Al	2.236	2.237	2.212	2.334	2.159	2.157	2.126	2.215	2.199	2.279	2.251	0.023	1.631	2.672	1.947	2.624	2.115	2.595	2.248	2.266
	Fe3+	0.728	0.725	0.764	0.685	0.872	0.712	0.657	0.814	0.726	0.560	0.701	n.c.	0.089	0.065	0.026	0.074	0.032	0.167	0.628	0.689
	Fe2+	0.723	0.642	0.690	0.696	0.399	0.648	0.565	0.602	0.507	0.787	0.824	0.330	0.981	1.272	1.157	1.278	1.164	1.192	0.683	0.681
	Mn	0.033	0.030	0.033	0.030	0.026	0.030	0.027	0.030	0.024	0.030	0.034	0.014	0.028	0.031	0.030	0.030	0.029	0.032	0.026	0.027
	Ni	0.004	b.d.	b.d.	0.026	0.017	0.009	b.d.	0.006	0.011	b.d.	0.005	0.011	0.016	0.003	0.021	b.d.	b.d.	b.d.	0.013	0.009
	Mg	2.897	2.956	2.844	2.934	3.254	2.966	3.069	2.938	3.075	2.945	2.829	4.584	3.260	2.595	3.036	2.622	2.954	2.648	3.022	2.976
	Ca	2.068	2.098	2.159	2.025	1.970	2.121	2.152	2.124	2.133	2.042	2.043	2.008	1.959	1.906	1.898	1.903	1.921	1.922	2.026	2.037
	Na	0.321	0.334	0.330	0.339	0.296	0.326	0.332	0.336	0.351	0.341	0.332	0.006	0.182	0.295	0.216	0.304	0.239	0.276	0.337	0.332
	K	0.097	0.096	0.100	0.102	0.080	0.098	0.085	0.104	0.075	0.109	0.103	0.004	0.031	0.077	0.048	0.076	0.044	0.086	0.080	0.084
	H	2.000	2.000	2.000	2.000	2.000	2.000	2.000	2.000	2.000	2.000	2.000	2.000	2.000	2.000	2.000	2.000	2.000	2.000	2.000	2.000
	Sum	15.418	15.430	15.430	15.441	15.376	15.423	15.417	15.440	15.425	15.449	15.435	15.009	15.214	15.372	15.265	15.380	15.283	15.362	15.417	15.416
	Al4	1.730	1.737	1.738	1.765	1.741	1.683	1.638	1.777	1.710	1.682	1.736	0.000	0.997	1.622	1.160	1.604	1.259	1.626	1.684	1.724
	Al6	0.506	0.500	0.474	0.569	0.417	0.474	0.488	0.439	0.489	0.597	0.515	0.023	0.634	1.049	0.787	1.020	0.856	0.969	0.565	0.543
	Mg #	0.800	0.822	0.805	0.808	0.891	0.821	0.844	0.830	0.859	0.789	0.774	0.933	0.769	0.671	0.724	0.672	0.717	0.690	0.816	0.814
	NaK (A)	0.418	0.430	0.430	0.441	0.376	0.423	0.417	0.440	0.425	0.449	0.435	0.009	0.214	0.372	0.265	0.380	0.283	0.362	0.417	0.416

Abbreviations: Ts hbl = tschermakitic hornblende, Metab = metabasite, b.d. = below detection, n.c. = not calculated. Mg# calculated as (MgO/40.3) / (MgO/40.3 + FeO/71.85).

Major element composition of antigorite from the Geisspfad ultramafic body

Sample		G11	G11	G12	G12	G12	G12	G26	G26	G26	G27	G27	G27	G27	G27	G27	GEI4	GEI4
Rock		Serp	Serp	Serp	Serp	Serp	Serp	Serp	Serp	Serp	Serp	Serp	Serp	Serp	Serp	Serp	Serp	Serp
Mineral		Atg	Atg	Atg	Atg	Atg	Atg	Atg	Atg	Atg	Atg	Atg	Atg	Atg	Atg	Atg	Atg	Atg
Wt.%	SiO2	42.31	42.78	43.25	42.81	41.68	42.71	42.22	41.87	41.71	42.60	42.47	41.95	42.82	42.53	42.39	42.44	42.27
	TiO2	0.04	0.03	0.03	0.03	0.04	0.01	0.02	0.02	0.01	0.02	0.03	0.04	0.03	0.04	0.04	0.03	0.03
	Cr2O3	0.58	0.06	0.28	0.12	0.47	0.43	0.97	1.01	1.26	0.23	0.37	0.64	0.32	0.29	0.41	0.40	0.33
	Al2O3	2.97	2.41	2.49	2.77	3.74	3.11	2.82	2.93	3.36	2.97	3.10	3.55	2.97	3.21	3.46	3.11	3.04
	FeO	4.19	4.44	3.74	3.89	3.88	4.12	3.83	3.62	3.82	4.57	4.37	4.52	4.54	4.46	4.65	5.02	5.07
	MnO	0.05	0.03	0.04	0.05	0.01	b.d.	0.03	0.01	0.01	0.04	0.05	0.02	0.01	0.04	0.03	0.11	b.d.
	NiO	0.20	0.19	0.15	0.17	0.19	0.19	0.16	0.19	0.19	0.12	0.12	0.09	0.17	0.15	0.14	0.14	0.14
	MgO	37.27	37.00	37.62	38.01	36.40	36.53	37.38	37.17	36.22	37.13	37.43	36.65	37.20	37.18	36.81	36.96	37.19
	CaO	0.02	b.d.	0.01	b.d.	0.01	b.d.	0.01	b.d.	b.d.	0.01	b.d.	b.d.	0.01	0.01	b.d.	0.01	0.01
	H2O	12.84	12.76	12.91	12.92	12.69	12.80	12.83	12.74	12.69	12.85	12.90	12.81	12.91	12.89	12.88	12.88	12.86
	Total	100.48	99.70	100.51	100.78	99.12	99.90	100.27	99.57	99.27	100.53	100.85	100.26	100.99	100.80	100.81	101.10	100.94
Cations	Si	1.976	2.010	2.010	1.987	1.968	2.000	1.974	1.970	1.970	1.987	1.975	1.964	1.989	1.978	1.974	1.975	1.971
	Ti	0.001	0.001	0.001	0.001	0.001	0.000	0.001	0.001	0.000	0.001	0.001	0.001	0.001	0.001	0.001	0.001	0.001
	Cr	0.021	0.002	0.010	0.004	0.018	0.016	0.036	0.038	0.047	0.008	0.014	0.024	0.012	0.011	0.015	0.015	0.012
	Al	0.163	0.133	0.136	0.152	0.208	0.172	0.155	0.163	0.187	0.163	0.170	0.196	0.163	0.176	0.190	0.170	0.167
	Fe2+	0.164	0.174	0.145	0.151	0.153	0.161	0.150	0.142	0.151	0.178	0.170	0.177	0.176	0.173	0.181	0.195	0.198
	Mn	0.002	0.001	0.001	0.002	0.000	b.d.	0.001	0.000	0.000	0.001	0.002	0.001	0.000	0.002	0.001	0.004	b.d.
	Ni	0.008	0.007	0.006	0.006	0.007	0.007	0.006	0.007	0.007	0.004	0.005	0.003	0.006	0.006	0.005	0.005	0.005
	Mg	2.594	2.591	2.605	2.630	2.561	2.549	2.605	2.607	2.549	2.582	2.594	2.558	2.575	2.578	2.555	2.564	2.584
	Ca	0.001	b.d.	0.000	b.d.	0.001	b.d.	0.000	b.d.	b.d.	0.000	b.d.	b.d.	0.000	0.000	b.d.	0.000	0.001
	H	4.000	3.999	4.000	4.000	3.997	3.997	4.000	4.000	3.999	4.000	4.000	4.000	4.000	4.000	4.000	4.000	4.000
	Sum	4.930	4.921	4.915	4.933	4.917	4.906	4.929	4.928	4.912	4.926	4.930	4.924	4.923	4.926	4.922	4.931	4.938
	Mg #	0.941	0.937	0.947	0.946	0.944	0.940	0.946	0.948	0.944	0.935	0.939	0.935	0.936	0.937	0.934	0.929	0.929

Abbreviations: Fo = forsterite, Serp = serpentinite, b.d. = below detection. Mg# calculated as (MgO/40.3) / (MgO/40.3 + FeO/71.85).

Major element composition of antigorite from the Geisspfad ultramafic body continued

Sample		GEI4	GEI4	GEI4	GEI4	GEI4	GEI4	GEI4	GEI4	GEI4	GEI4	G3	G4	G4	G4	G4	G4	GEI9
Rock		Serp	Serp	Serp	Serp	Serp	Serp	Serp	Serp	Serp	Serp	Ophi	Ophi	Ophi	Ophi	Ophi	Ophi	Ophi
Mineral		Atg	Atg	Atg	Atg	Atg	Atg	Atg	Atg	Atg	Atg	Atg	Atg	Atg	Atg	Atg	Atg	Atg
Wt.%	SiO2	43.62	42.02	43.15	42.98	42.01	42.63	41.91	42.12	41.61	42.64	42.89	42.20	41.82	42.42	41.76	42.10	42.94
	TiO2	0.04	0.03	0.03	0.04	0.04	0.01	0.02	0.04	0.05	0.04	0.02	0.03	0.02	0.02	0.04	0.04	0.04
	Cr2O3	0.01	0.47	0.01	0.14	0.36	0.10	0.47	0.54	0.41	0.29	0.17	0.09	0.29	0.18	0.22	0.52	0.31
	Al2O3	2.01	3.23	2.06	2.51	3.22	2.35	3.46	3.08	3.26	2.88	2.47	3.25	3.80	3.06	3.43	3.28	3.39
	FeO	4.78	4.78	4.67	5.11	4.90	4.75	4.97	4.64	5.05	4.76	4.48	4.62	4.16	4.88	4.27	4.09	3.93
	MnO	0.03	0.05	0.03	0.04	0.08	0.03	0.02	0.08	0.02	0.03	b.d.	0.09	0.09	0.09	0.08	0.11	0.06
	NiO	0.18	0.12	0.19	0.12	0.15	0.15	0.15	0.18	0.18	0.20	0.20	0.09	0.12	0.03	0.09	0.23	0.13
	MgO	37.35	36.83	37.26	37.15	37.02	37.26	36.74	36.66	36.70	37.06	37.47	36.65	37.01	36.70	36.33	36.81	36.77
	CaO	b.d.	b.d.	0.01	0.01	b.d.	0.01	0.02	0.01	0.02	b.d.	0.01	b.d.	0.02	0.01	0.18	0.11	0.21
	H2O	12.91	12.80	12.82	12.89	12.82	12.78	12.82	12.77	12.74	12.87	12.86	12.75	12.80	12.79	12.68	12.79	12.92
	Total	100.93	100.33	100.23	100.99	100.60	100.07	100.58	100.12	100.04	100.77	100.55	99.77	100.13	100.17	99.08	100.09	100.71
Cations	Si	2.026	1.969	2.019	2.000	1.965	2.000	1.961	1.977	1.960	1.987	2.000	1.983	1.957	1.988	1.976	1.973	1.993
	Ti	0.001	0.001	0.001	0.001	0.002	0.000	0.001	0.001	0.002	0.001	0.001	0.001	0.001	0.001	0.001	0.001	0.001
	Cr	0.000	0.017	0.000	0.005	0.013	0.004	0.017	0.020	0.015	0.011	0.006	0.003	0.011	0.007	0.008	0.019	0.011
	Al	0.110	0.178	0.114	0.138	0.178	0.130	0.191	0.170	0.181	0.158	0.136	0.180	0.210	0.169	0.192	0.181	0.185
	Fe2+	0.186	0.187	0.183	0.199	0.192	0.186	0.195	0.182	0.199	0.186	0.175	0.182	0.163	0.191	0.169	0.160	0.153
	Mn	0.001	0.002	0.001	0.002	0.003	0.001	0.001	0.003	0.001	0.001	b.d.	0.004	0.004	0.004	0.003	0.005	0.002
	Ni	0.007	0.005	0.007	0.005	0.006	0.006	0.006	0.007	0.007	0.008	0.007	0.004	0.004	0.001	0.003	0.009	0.005
	Mg	2.586	2.572	2.598	2.577	2.581	2.605	2.563	2.565	2.576	2.575	2.604	2.567	2.582	2.563	2.562	2.571	2.544
	Ca	b.d.	b.d.	0.000	0.000	b.d.	0.000	0.001	0.000	0.001	b.d.	0.000	b.d.	0.001	0.001	0.009	0.006	0.011
	H	4.000	4.000	4.000	4.000	4.000	4.000	4.000	4.000	4.000	4.000	3.998	3.997	3.997	3.998	4.000	3.998	4.000
	Sum	4.917	4.932	4.923	4.926	4.938	4.932	4.934	4.926	4.940	4.927	4.928	4.924	4.932	4.924	4.923	4.925	4.906
	Mg #	0.933	0.932	0.934	0.928	0.931	0.933	0.929	0.934	0.928	0.933	0.937	0.934	0.941	0.931	0.938	0.941	0.943

Abbreviations: Fo = forsterite, Serp = serpentinite, Ophi = ophicarbonate, b.d. = below detection. Mg# calculated as (MgO/40.3) / (MgO/40.3 + FeO/71.85).

Major element composition of forsterite from the Geisspfad ultramafic body

Sample		G8	G8	G8	G11	G11	G11	G11	G11	G11	G11	G11	G11	G11	G11	G11	G11
Rock		Serp	Serp	Serp	Serp	Serp	Serp	Serp	Serp	Serp	Serp	Serp	Serp	Serp	Serp	Serp	Serp
Mineral		Fo	Fo	Fo	Fo	Fo	Fo	Fo	Fo	Fo	Fo	Fo	Fo	Fo	Fo	Fo	Fo
Wt.%	SiO2	40.50	40.67	40.34	40.93	40.09	40.68	40.51	40.29	40.02	40.57	40.60	40.20	40.01	40.18	40.16	40.68	40.60
	TiO2	b.d.	b.d.	b.d.	0.01	0.02	0.01	0.01	0.01	b.d.	0.01	0.01	0.01	0.01	b.d.	0.02	0.01	b.d.
	Cr2O3	0.05	b.d.	b.d.	0.08	0.03	b.d.	0.03	b.d.	0.07	b.d.	0.04	0.04	0.01	b.d.	0.02	b.d.	0.03
	Al2O3	b.d.	0.02	0.27	0.01	0.01	0.01	0.01	b.d.	0.02	b.d.	b.d.	0.02	0.01	b.d.	0.01	0.02	0.03
	FeO	13.64	13.73	13.21	12.63	13.16	13.11	12.60	13.04	13.29	13.21	12.91	13.15	12.97	12.87	12.96	13.11	13.51
	MnO	0.22	0.17	0.14	0.34	0.31	0.22	0.13	0.30	0.24	0.34	0.21	0.27	0.26	0.21	0.29	0.21	0.25
	NiO	0.36	0.22	0.27	0.42	0.21	0.39	0.47	0.31	0.45	0.35	0.24	0.31	0.40	0.41	0.33	0.39	0.34
	MgO	45.71	46.07	46.64	46.41	45.86	46.44	46.00	46.30	46.42	45.99	45.87	45.49	45.36	45.58	45.83	46.09	45.83
	CaO	0.01	0.01	0.01	b.d.	0.02	0.01	b.d.	0.01	0.01	0.02	0.02	0.03	0.03	0.04	0.03	b.d.	0.01
	Na2O	0.01	0.01	b.d.	b.d.	0.01	b.d.	0.01	b.d.	b.d.	b.d.	b.d.	b.d.	b.d.	b.d.	b.d.	b.d.	b.d.
	Total	100.49	100.90	100.88	100.83	99.70	100.86	99.77	100.26	100.52	100.48	99.90	99.52	99.05	99.29	99.65	100.50	100.60
Cations	Si	1.006	1.005	0.996	1.008	1.002	1.004	1.008	1.001	0.994	1.006	1.010	1.006	1.006	1.007	1.004	1.007	1.006
	Ti	b.d.	b.d.	b.d.	0.000	0.000	0.000	0.000	0.000	b.d.	0.000	0.000	0.000	0.000	b.d.	0.000	0.000	b.d.
	Cr	0.001	b.d.	b.d.	0.002	0.001	b.d.	0.001	b.d.	0.001	b.d.	0.001	0.001	0.000	b.d.	0.000	b.d.	0.001
	Al	b.d.	0.001	0.008	0.000	0.000	0.000	0.000	b.d.	0.001	b.d.	b.d.	0.001	0.000	b.d.	0.000	0.000	0.001
	Fe2+	0.283	0.284	0.273	0.260	0.275	0.271	0.262	0.271	0.276	0.274	0.269	0.275	0.273	0.270	0.271	0.271	0.280
	Mn	0.005	0.003	0.003	0.007	0.006	0.005	0.003	0.006	0.005	0.007	0.004	0.006	0.006	0.004	0.006	0.004	0.005
	Ni	0.007	0.004	0.005	0.008	0.004	0.008	0.009	0.006	0.009	0.007	0.005	0.006	0.008	0.008	0.007	0.008	0.007
	Mg	1.692	1.697	1.716	1.704	1.708	1.708	1.707	1.714	1.719	1.699	1.701	1.697	1.700	1.702	1.707	1.701	1.693
	Ca	0.000	0.000	0.000	b.d.	0.000	0.000	b.d.	0.000	0.000	0.000	0.000	0.001	0.001	0.001	0.001	b.d.	0.000
	Na	0.001	0.000	b.d.	b.d.	0.000	b.d.	0.001	b.d.	b.d.	b.d.	b.d.	b.d.	b.d.	b.d.	b.d.	b.d.	b.d.
	Sum	2.994	2.995	3.000	2.990	2.997	2.996	2.991	2.999	3.005	2.994	2.990	2.993	2.994	2.993	2.996	2.992	2.993
	Mg #	0.857	0.857	0.863	0.868	0.861	0.863	0.867	0.864	0.862	0.861	0.864	0.860	0.862	0.863	0.863	0.862	0.858

Abbreviations: Fo = forsterite, Serp = serpentinite, b.d. = below detection. Mg# calculated as (MgO/40.3) / (MgO/40.3 + FeO/71.85).

Major element composition of forsterite from the Geisspfad ultramafic body continued

Sample		G11	G11	G11	G11	G11	G11	G11	G11	G11	G11	G11	G11	G11	G11	G11	G11	G11
Rock		Serp	Serp	Serp	Serp	Serp	Serp	Serp	Serp	Serp	Serp	Serp	Serp	Serp	Serp	Serp	Serp	Serp
Mineral		Fo	Fo	Fo	Fo	Fo	Fo	Fo	Fo	Fo	Fo	Fo	Fo	Fo	Fo	Fo	Fo	Fo
Wt.%	SiO2	40.11	40.21	39.91	40.44	40.48	40.71	40.16	40.33	40.03	40.68	40.37	40.04	40.11	40.71	40.33	40.44	40.37
	TiO2	b.d.	0.01	b.d.	0.01	b.d.	b.d.	0.02	b.d.	b.d.	0.01	0.01	b.d.	0.02	b.d.	0.01	b.d.	b.d.
	Cr2O3	0.02	0.06	0.07	0.03	0.01	0.10	0.12	0.05	b.d.	0.02	0.03	0.07	b.d.	0.10	b.d.	b.d.	0.03
	Al2O3	0.02	0.01	0.04	0.02	0.02	b.d.	b.d.	0.01	0.02	0.02	0.01	b.d.	0.43	0.01	b.d.	b.d.	0.01
	FeO	13.57	13.60	13.77	13.41	13.24	13.16	13.21	13.17	13.04	13.18	13.39	13.08	13.01	13.79	13.45	12.76	13.17
	MnO	0.35	0.25	0.27	0.19	0.23	0.25	0.17	0.20	0.31	0.24	0.21	0.19	0.27	0.31	0.21	0.23	0.21
	NiO	0.34	0.39	0.49	0.31	0.34	0.31	0.36	0.39	0.44	0.34	0.33	0.44	0.23	0.36	0.42	0.48	0.46
	MgO	44.89	45.29	45.28	45.90	45.84	46.05	46.59	46.56	45.32	45.99	45.78	46.16	45.52	45.47	45.56	46.09	46.24
	CaO	0.01	0.02	b.d.	b.d.	0.01	b.d.	0.01	b.d.	b.d.	0.01	0.01	0.01	0.04	0.01	b.d.	b.d.	0.01
	Na2O	0.01	b.d.	b.d.	0.01	0.02	b.d.	0.01	b.d.	0.01	0.01	0.01	b.d.	0.08	b.d.	b.d.	0.02	b.d.
	Total	99.31	99.84	99.83	100.32	100.18	100.58	100.63	100.70	99.16	100.50	100.13	99.99	99.72	100.75	99.98	100.02	100.50
Cations	Si	1.008	1.006	1.000	1.005	1.006	1.007	0.995	0.998	1.006	1.008	1.005	0.998	1.001	1.009	1.006	1.006	1.001
	Ti	b.d.	0.000	b.d.	0.000	b.d.	b.d.	0.000	b.d.	b.d.	0.000	0.000	b.d.	0.000	b.d.	0.000	b.d.	b.d.
	Cr	0.000	0.001	0.001	0.001	0.000	0.002	0.002	0.001	b.d.	0.000	0.001	0.001	b.d.	0.002	b.d.	b.d.	0.001
	Al	0.000	0.000	0.001	0.001	0.000	b.d.	b.d.	0.000	0.000	0.001	0.000	b.d.	0.013	0.000	b.d.	b.d.	0.000
	Fe2+	0.285	0.284	0.289	0.279	0.275	0.272	0.274	0.273	0.274	0.273	0.279	0.273	0.272	0.286	0.281	0.265	0.273
	Mn	0.007	0.005	0.006	0.004	0.005	0.005	0.004	0.004	0.007	0.005	0.004	0.004	0.006	0.006	0.004	0.005	0.004
	Ni	0.007	0.008	0.010	0.006	0.007	0.006	0.007	0.008	0.009	0.007	0.007	0.009	0.005	0.007	0.008	0.010	0.009
	Mg	1.682	1.688	1.691	1.700	1.699	1.698	1.721	1.717	1.698	1.698	1.699	1.715	1.693	1.679	1.694	1.708	1.709
	Ca	0.000	0.001	b.d.	b.d.	0.000	b.d.	0.000	b.d.	b.d.	0.000	0.000	0.000	0.001	0.000	b.d.	b.d.	0.000
	Na	0.000	b.d.	b.d.	0.001	0.001	b.d.	0.000	b.d.	0.000	0.001	0.000	b.d.	0.004	b.d.	b.d.	0.001	b.d.
	Sum	2.991	2.993	2.998	2.995	2.994	2.991	3.003	3.001	2.994	2.992	2.995	3.001	2.994	2.990	2.994	2.995	2.998
	Mg #	0.855	0.856	0.854	0.859	0.861	0.862	0.863	0.863	0.861	0.861	0.859	0.863	0.862	0.855	0.858	0.866	0.862

Abbreviations: Fo = forsterite, Serp = serpentinite, b.d. = below detection. Mg# calculated as (MgO/40.3) / (MgO/40.3 + FeO/71.85).

Major element composition of forsterite from the Geisspfad ultramafic body continued

Sample		G11	G11	G11	G11	G12	G12	G12	G26	G26	G26	G26	G26	G26	G26	G26	G27	G27
Rock		Serp	Serp	Serp	Serp	Serp	Serp	Serp	Serp	Serp	Serp	Serp	Serp	Serp	Serp	Serp	Serp	Serp
Mineral		Fo	Fo	Fo	Fo	Fo	Fo	Fo	Fo	Fo	Fo	Fo	Fo	Fo	Fo	Fo	Fo	Fo
Wt.%	SiO2	40.33	40.83	40.59	40.51	40.34	40.73	40.54	40.78	40.82	40.56	40.63	40.52	40.40	40.18	40.54	39.68	40.67
	TiO2	b.d.	b.d.	b.d.	0.02	b.d.	b.d.	b.d.	b.d.	0.01	b.d.	b.d.	0.01	0.01	b.d.	0.01	b.d.	0.01
	Cr2O3	0.02	0.01	0.01	b.d.	0.03	0.01	b.d.	0.05	0.15	0.01	b.d.	0.03	b.d.	b.d.	0.03	0.01	0.05
	Al2O3	b.d.	b.d.	b.d.	b.d.	b.d.	b.d.	0.02	0.01	0.16	b.d.	b.d.	0.02	b.d.	b.d.	b.d.	b.d.	b.d.
	FeO	12.88	12.99	12.95	12.53	11.67	12.20	13.07	11.14	11.03	11.69	11.24	11.30	11.62	11.56	11.84	12.97	12.98
	MnO	0.27	0.26	0.20	0.26	0.21	0.14	0.19	0.23	0.14	0.17	0.14	0.22	0.21	0.23	0.24	0.24	0.24
	NiO	0.48	0.29	0.42	0.28	0.34	0.31	0.39	0.44	0.30	0.31	0.35	0.33	0.42	0.33	0.36	0.34	0.38
	MgO	46.47	46.37	46.61	46.24	46.88	46.84	46.49	48.07	47.75	47.27	47.09	47.68	46.81	47.17	47.90	45.81	46.54
	CaO	0.01	0.01	0.01	0.01	0.01	b.d.	b.d.	0.01	0.01	0.01	0.01	b.d.	b.d.	b.d.	0.02	0.01	0.02
	Na2O	b.d.	0.02	0.02	0.01	b.d.	b.d.	b.d.	0.01	0.01	b.d.	b.d.	b.d.	0.02	b.d.	b.d.	0.01	0.01
	Total	100.45	100.78	100.80	99.86	99.47	100.24	100.69	100.75	100.37	100.01	99.45	100.10	99.48	99.46	100.93	99.08	100.90
Cations	Si	1.000	1.007	1.002	1.007	1.003	1.007	1.002	1.000	1.002	1.003	1.008	1.000	1.005	1.000	0.995	0.998	1.003
	Ti	b.d.	b.d.	b.d.	0.000	b.d.	b.d.	b.d.	b.d.	0.000	b.d.	b.d.	0.000	0.000	b.d.	0.000	b.d.	0.000
	Cr	0.000	0.000	0.000	b.d.	0.001	0.000	b.d.	0.001	0.003	0.000	b.d.	0.001	b.d.	b.d.	0.001	0.000	0.001
	Al	b.d.	b.d.	b.d.	b.d.	b.d.	b.d.	0.001	0.000	0.005	b.d.	b.d.	0.001	b.d.	b.d.	b.d.	b.d.	b.d.
	Fe2+	0.267	0.268	0.267	0.260	0.243	0.252	0.270	0.228	0.227	0.242	0.233	0.233	0.242	0.240	0.243	0.273	0.268
	Mn	0.006	0.005	0.004	0.006	0.004	0.003	0.004	0.005	0.003	0.004	0.003	0.005	0.004	0.005	0.005	0.005	0.005
	Ni	0.010	0.006	0.008	0.006	0.007	0.006	0.008	0.009	0.006	0.006	0.007	0.006	0.008	0.007	0.007	0.007	0.008
	Mg	1.717	1.705	1.715	1.713	1.738	1.725	1.713	1.756	1.748	1.742	1.741	1.754	1.735	1.749	1.753	1.718	1.711
	Ca	0.000	0.000	0.000	0.000	0.000	b.d.	b.d.	0.000	0.000	0.000	0.000	b.d.	b.d.	b.d.	0.000	0.000	0.001
	Na	b.d.	0.001	0.001	0.000	b.d.	b.d.	b.d.	0.001	0.000	b.d.	b.d.	b.d.	0.001	b.d.	b.d.	0.000	0.000
	Sum	3.000	2.993	2.998	2.993	2.996	2.993	2.998	3.000	2.994	2.997	2.992	2.999	2.995	3.000	3.004	3.002	2.996
	Mg #	0.865	0.864	0.865	0.868	0.877	0.873	0.864	0.885	0.885	0.878	0.882	0.883	0.878	0.879	0.878	0.863	0.865

Abbreviations: Fo = forsterite, Serp = serpentinite, b.d. = below detection. Mg# calculated as (MgO/40.3) / (MgO/40.3 + FeO/71.85).

Major element composition of forsterite from the Geisspfad ultramafic body continued

Sample		G27	G27	G27	G27	G27	GEI4	GEI4	GEI4	GEI4	GEI4	GEI4	GEI4	GEI4	GEI4	GEI4	GEI4
Rock		Serp	Serp	Serp	Serp	Serp	Serp	Serp	Serp	Serp	Serp	Serp	Serp	Serp	Serp	Serp	Serp
Mineral		Fo	Fo	Fo	Fo	Fo	Fo	Fo	Fo	Fo	Fo	Fo	Fo	Fo	Fo	Fo	Fo
Wt.%	SiO2	40.47	40.49	40.53	40.46	40.55	39.88	39.68	39.85	39.73	39.99	39.94	40.09	39.85	39.88	39.87	39.81	39.88
	TiO2	b.d.	b.d.	b.d.	b.d.	b.d.	b.d.	b.d.	b.d.	0.03	0.01	0.01	b.d.	0.02	0.01	b.d.	b.d.	b.d.
	Cr2O3	b.d.	0.03	b.d.	b.d.	0.03	b.d.	0.03	b.d.	0.01	0.02	b.d.	0.02	0.02	0.03	b.d.	0.03	0.02
	Al2O3	0.02	0.02	b.d.	b.d.	b.d.	0.02	b.d.	b.d.	0.01	0.01	b.d.	0.01	0.01	0.02	0.01	b.d.	0.01
	FeO	12.96	12.83	12.82	13.13	13.06	14.51	14.70	14.48	14.20	14.67	14.66	14.61	14.60	14.59	14.27	14.85	14.30
	MnO	0.24	0.25	0.26	0.29	0.23	0.30	0.28	0.24	0.18	0.37	0.23	0.27	0.24	0.31	0.27	0.29	0.22
	NiO	0.31	0.34	0.31	0.33	0.36	0.34	0.36	0.37	0.33	0.41	0.40	0.31	0.31	0.33	0.40	0.36	0.30
	MgO	46.32	46.67	46.70	46.56	46.63	45.45	45.39	45.45	45.42	45.46	45.36	45.09	45.62	45.71	45.73	45.24	45.79
	CaO	b.d.	0.02	b.d.	0.02	0.01	b.d.	0.02	0.01	0.07	0.01	0.01	0.01	0.02	0.02	0.01	b.d.	b.d.
	Na2O	b.d.	b.d.	b.d.	b.d.	0.01	b.d.	b.d.	b.d.	b.d.	0.01	0.02	b.d.	0.01	0.02	0.01	0.01	b.d.
	Total	100.33	100.66	100.62	100.78	100.87	100.50	100.46	100.40	99.98	100.96	100.63	100.41	100.70	100.92	100.57	100.59	100.52
Cations	Si	1.004	1.001	1.002	1.000	1.001	0.995	0.990	0.994	0.995	0.994	0.995	1.002	0.991	0.990	0.992	0.993	0.993
	Ti	b.d.	b.d.	b.d.	b.d.	b.d.	b.d.	b.d.	b.d.	0.001	0.000	0.000	b.d.	0.000	0.000	b.d.	b.d.	b.d.
	Cr	b.d.	0.001	b.d.	b.d.	0.001	b.d.	0.001	b.d.	0.000	0.000	b.d.	0.000	0.000	0.001	b.d.	0.001	0.000
	Al	0.001	0.001	b.d.	b.d.	b.d.	0.000	b.d.	b.d.	0.000	0.000	b.d.	0.000	0.000	0.001	0.000	b.d.	0.000
	Fe2+	0.269	0.265	0.265	0.271	0.270	0.303	0.307	0.302	0.297	0.305	0.306	0.306	0.304	0.303	0.297	0.310	0.298
	Mn	0.005	0.005	0.006	0.006	0.005	0.006	0.006	0.005	0.004	0.008	0.005	0.006	0.005	0.007	0.006	0.006	0.005
	Ni	0.006	0.007	0.006	0.006	0.007	0.007	0.007	0.007	0.007	0.008	0.008	0.006	0.006	0.007	0.008	0.007	0.006
	Mg	1.712	1.719	1.720	1.715	1.715	1.689	1.688	1.690	1.695	1.684	1.685	1.680	1.692	1.691	1.696	1.682	1.699
	Ca	b.d.	0.000	b.d.	0.000	0.000	b.d.	0.001	0.000	0.002	0.000	0.000	0.000	0.001	0.000	0.000	b.d.	b.d.
	Na	b.d.	b.d.	b.d.	b.d.	0.000	b.d.	b.d.	b.d.	b.d.	0.001	0.001	b.d.	0.001	0.001	0.000	0.001	b.d.
	Sum	2.996	2.999	2.998	3.000	2.999	3.000	3.000	3.000	3.000	3.000	3.000	3.000	3.000	3.000	3.000	3.000	3.000
	Mg #	0.864	0.866	0.867	0.863	0.864	0.848	0.846	0.848	0.851	0.847	0.846	0.846	0.848	0.848	0.851	0.844	0.851

Abbreviations: Fo = forsterite, Serp = serpentinite, b.d. = below detection. Mg# calculated as (MgO/40.3) / (MgO/40.3 + FeO/71.85).

Major element composition of forsterite from the Geisspfad ultramafic body continued

Sample		GEI4	GEI4	GEI4	GEI4	GEI4	GEI4	GEI4	GEI4	GEI4	GEI4	GEI4	GEI4	GEI4	GEI4	GEI4	GEI4	GEI4
Rock		Serp	Serp	Serp	Serp	Serp	Serp	Serp	Serp	Serp	Serp	Serp	Serp	Serp	Serp	Serp	Serp	Serp
Mineral		Fo	Fo	Fo	Fo	Fo	Fo	Fo	Fo	Fo	Fo	Fo	Fo	Fo	Fo	Fo	Fo	Fo
Wt.%	SiO2	39.61	39.76	39.65	39.74	40.13	39.75	39.76	39.86	39.51	39.78	39.92	39.87	40.02	39.83	39.93	39.78	39.64
	TiO2	0.01	0.01	b.d.	0.02	b.d.	0.03	b.d.	0.01	b.d.	b.d.	0.01	0.06	b.d.	0.01	0.02	b.d.	0.03
	Cr2O3	0.02	b.d.	b.d.	0.03	0.05	0.02	0.03	0.03	b.d.	0.02	0.01	b.d.	0.02	b.d.	0.02	0.03	0.02
	Al2O3	b.d.	0.01	b.d.	b.d.	b.d.	b.d.	b.d.	0.01	b.d.	0.01	b.d.	0.01	0.01	0.01	0.01	0.01	b.d.
	FeO	14.75	14.43	14.48	14.35	14.44	14.29	13.91	14.34	14.39	14.66	14.46	14.43	14.72	14.28	14.67	14.46	14.51
	MnO	0.19	0.28	0.33	0.27	0.30	0.27	0.32	0.29	0.18	0.27	0.28	0.24	0.23	0.25	0.29	0.31	0.29
	NiO	0.38	0.36	0.37	0.33	0.38	0.41	0.38	0.37	0.34	0.41	0.37	0.35	0.32	0.36	0.36	0.36	0.31
	MgO	45.23	45.66	45.48	45.54	45.32	45.44	45.58	45.50	45.27	45.54	45.50	45.33	45.67	45.43	45.42	45.50	45.31
	CaO	0.02	0.01	0.01	0.01	b.d.	0.01	b.d.	0.02	0.01	b.d.	0.03	0.06	0.01	0.02	0.03	0.05	0.07
	Na2O	b.d.	b.d.	b.d.	b.d.	b.d.	b.d.	b.d.	b.d.	b.d.	b.d.	b.d.	b.d.	b.d.	0.01	b.d.	b.d.	b.d.
	Total	100.21	100.52	100.32	100.29	100.62	100.22	99.98	100.43	99.70	100.69	100.58	100.35	101.00	100.20	100.75	100.50	100.18
Cations	Si	0.991	0.990	0.990	0.992	1.000	0.993	0.994	0.994	0.992	0.990	0.995	0.996	0.993	0.995	0.994	0.992	0.992
	Ti	0.000	0.000	b.d.	0.000	b.d.	0.001	b.d.	0.000	b.d.	b.d.	0.000	0.001	b.d.	0.000	0.000	b.d.	0.001
	Cr	0.000	b.d.	b.d.	0.001	0.001	0.000	0.001	0.001	b.d.	0.000	0.000	b.d.	0.000	b.d.	0.000	0.001	0.000
	Al	b.d.	0.000	b.d.	b.d.	b.d.	b.d.	b.d.	0.000	b.d.	0.000	b.d.	0.000	0.000	0.000	0.000	0.000	b.d.
	Fe2+	0.309	0.301	0.303	0.300	0.301	0.299	0.291	0.299	0.302	0.305	0.301	0.301	0.305	0.299	0.306	0.302	0.304
	Mn	0.004	0.006	0.007	0.006	0.006	0.006	0.007	0.006	0.004	0.006	0.006	0.005	0.005	0.005	0.006	0.007	0.006
	Ni	0.008	0.007	0.007	0.007	0.008	0.008	0.008	0.008	0.007	0.008	0.007	0.007	0.006	0.007	0.007	0.007	0.006
	Mg	1.687	1.695	1.693	1.694	1.684	1.692	1.699	1.692	1.695	1.690	1.690	1.688	1.689	1.692	1.685	1.691	1.690
	Ca	0.001	0.000	0.000	0.000	b.d.	0.000	b.d.	0.000	0.000	b.d.	0.001	0.002	0.000	0.001	0.001	0.001	0.002
	Na	b.d.	b.d.	b.d.	b.d.	b.d.	b.d.	b.d.	b.d.	b.d.	b.d.	b.d.	b.d.	b.d.	0.001	b.d.	b.d.	b.d.
	Sum	3.000	2.999	3.000	3.000	3.000	2.999	3.000	3.000	3.000	3.000	3.000	3.000	3.000	3.000	3.000	3.000	3.000
	Mg #	0.845	0.849	0.848	0.850	0.848	0.850	0.854	0.850	0.849	0.847	0.849	0.848	0.847	0.850	0.847	0.849	0.848

Abbreviations: Fo = forsterite, Serp = serpentinite, b.d. = below detection. Mg# calculated as (MgO/40.3) / (MgO/40.3 + FeO/71.85).

Major element composition of forsterite from the Geisspfad ultramafic body continued

Sample		GEI4	GEI4	G3	G3	G3	G3	G3	G3	G3
Rock		Serp	Serp	Ophi	Ophi	Ophi	Ophi	Ophi	Ophi	Ophi
Mineral		Fo	Fo	Fo	Fo	Fo	Fo	Fo	Fo	Fo
Wt.%	SiO2	39.91	39.87	40.22	40.38	39.86	40.11	40.25	40.26	40.24
	TiO2	0.01	b.d.	0.02	b.d.	b.d.	0.01	b.d.	b.d.	b.d.
	Cr2O3	0.01	0.01	b.d.	b.d.	b.d.	0.03	0.03	b.d.	0.05
	Al2O3	0.01	0.01	0.01	b.d.	b.d.	b.d.	b.d.	0.03	0.02
	FeO	14.45	14.78	11.35	11.84	11.66	11.47	11.43	11.76	11.94
	MnO	0.21	0.33	0.35	0.31	0.42	0.36	0.30	0.33	0.33
	NiO	0.39	0.39	0.34	0.37	0.28	0.27	0.28	0.18	0.28
	MgO	45.29	45.31	47.95	47.19	47.13	47.79	47.62	46.56	46.60
	CaO	0.12	0.09	0.01	b.d.	b.d.	b.d.	0.01	0.01	0.01
	Na2O	b.d.	0.02	b.d.	b.d.	0.01	b.d.	b.d.	b.d.	b.d.
	Total	100.40	100.81	100.25	100.10	99.35	100.04	99.92	99.13	99.48
Cations	Si	0.996	0.993	0.993	1.000	0.995	0.993	0.997	1.005	1.003
	Ti	0.000	b.d.	0.000	b.d.	b.d.	0.000	b.d.	b.d.	b.d.
	Cr	0.000	0.000	b.d.	b.d.	b.d.	0.001	0.001	b.d.	0.001
	Al	0.000	0.000	0.000	b.d.	b.d.	b.d.	b.d.	0.001	0.001
	Fe2+	0.302	0.308	0.234	0.245	0.243	0.237	0.237	0.246	0.249
	Mn	0.005	0.007	0.007	0.006	0.009	0.007	0.006	0.007	0.007
	Ni	0.008	0.008	0.007	0.007	0.006	0.005	0.006	0.004	0.006
	Mg	1.685	1.681	1.764	1.741	1.753	1.763	1.757	1.732	1.731
	Ca	0.003	0.002	0.000	b.d.	b.d.	b.d.	0.000	0.000	0.000
	Na	b.d.	0.001	b.d.	b.d.	0.000	b.d.	b.d.	b.d.	b.d.
	Sum	2.999	3.000	3.007	3.000	3.006	3.007	3.003	2.995	2.997
	Mg #	0.848	0.845	0.883	0.877	0.878	0.881	0.881	0.876	0.874

Abbreviations: Fo = forsterite, Serp = serpentinite, b.d. = below detection.
Mg# calculated as (MgO/40.3) / (MgO/40.3 + FeO/71.85).

Major element composition of diopside from the Geisspfad ultramafic body

Sample		G11	G11	G11	G11	G11	G11	G11	G11	G11	G11	G11	G11	G11	G11	G11	G11	G11
Rock		Serp	Serp	Serp	Serp	Serp	Serp	Serp	Serp	Serp	Serp	Serp	Serp	Serp	Serp	Serp	Serp	Serp
Mineral		Di	Di	Di	Di	Di	Di	Di	Di	Di	Di	Di	Di	Di	Di	Di	Di	Di
Wt.%	SiO2	52.09	52.92	52.85	52.70	52.64	53.01	52.71	52.88	52.97	53.07	52.77	55.22	55.38	55.66	55.83	55.62	53.39
	TiO2	0.34	0.35	0.32	0.35	0.30	0.33	0.30	0.31	0.30	0.33	0.32	0.04	b.d.	0.01	b.d.	0.03	0.32
	Cr2O3	0.67	0.80	0.81	0.72	0.75	0.79	0.69	0.87	0.81	0.82	0.91	0.15	0.20	0.11	0.04	b.d.	0.99
	Al2O3	4.86	4.59	4.60	4.53	4.55	4.60	4.56	4.50	4.56	4.56	4.23	0.43	0.05	0.03	0.04	0.03	4.65
	FeO	2.54	2.56	2.56	2.57	2.54	2.44	2.44	2.54	2.46	2.46	2.13	1.46	1.35	1.54	1.57	1.65	2.60
	MnO	0.09	0.05	0.09	0.07	0.07	0.08	0.13	0.07	0.07	0.07	0.08	0.04	0.06	0.06	0.09	b.d.	0.06
	NiO	0.07	0.02	0.04	0.05	0.02	0.07	0.03	0.03	0.04	0.03	0.06	0.03	0.03	b.d.	0.10	0.10	0.01
	MgO	15.20	15.63	15.83	15.84	15.67	15.52	15.47	15.76	15.59	15.53	15.60	17.76	17.44	17.64	17.30	17.46	15.23
	CaO	22.20	22.49	22.55	22.59	22.64	22.72	22.66	22.61	22.77	22.08	22.63	25.66	25.77	25.96	25.82	25.93	22.56
	Na2O	1.10	1.07	1.02	1.08	1.12	1.21	1.17	1.05	1.01	1.08	1.32	0.28	0.13	0.13	0.10	0.06	1.11
	K2O	0.01	b.d.	b.d.	b.d.	b.d.	b.d.	b.d.	b.d.	0.01	0.01	b.d.	0.01	b.d.	b.d.	b.d.	b.d.	b.d.
	Total	99.16	100.48	100.68	100.49	100.31	100.76	100.17	100.63	100.59	100.04	100.05	101.08	100.39	101.15	100.91	100.89	100.92
Cations	Si	1.908	1.912	1.907	1.906	1.908	1.912	1.912	1.909	1.912	1.922	1.916	1.984	2.002	1.999	2.008	2.002	1.920
	Ti	0.009	0.009	0.009	0.009	0.008	0.009	0.008	0.008	0.008	0.009	0.009	0.001	b.d.	0.000	b.d.	0.001	0.009
	Cr	0.019	0.023	0.023	0.021	0.022	0.023	0.020	0.025	0.023	0.024	0.026	0.004	0.006	0.003	0.001	b.d.	0.028
	Al	0.210	0.195	0.196	0.193	0.194	0.196	0.195	0.192	0.194	0.195	0.181	0.018	0.002	0.001	0.002	0.001	0.197
	Fe2+	0.078	0.077	0.077	0.078	0.077	0.074	0.074	0.077	0.074	0.074	0.065	0.044	0.041	0.046	0.047	0.050	0.078
	Mn	0.003	0.001	0.003	0.002	0.002	0.002	0.004	0.002	0.002	0.002	0.002	0.001	0.002	0.002	0.003	b.d.	0.002
	Ni	0.002	0.001	0.001	0.001	0.001	0.002	0.001	0.001	0.001	0.001	0.002	0.001	0.001	b.d.	0.003	0.003	0.000
	Mg	0.830	0.842	0.851	0.854	0.846	0.834	0.836	0.848	0.839	0.838	0.844	0.951	0.940	0.944	0.928	0.937	0.816
	Ca	0.871	0.871	0.872	0.875	0.879	0.878	0.881	0.875	0.881	0.857	0.880	0.988	0.998	0.999	0.995	1.000	0.869
	Na	0.078	0.075	0.072	0.075	0.079	0.084	0.082	0.074	0.071	0.076	0.093	0.020	0.009	0.009	0.007	0.004	0.077
	K	0.000	b.d.	b.d.	b.d.	b.d.	b.d.	b.d.	b.d.	0.000	0.000	b.d.	0.000	b.d.	b.d.	b.d.	b.d.	b.d.
	Sum	4.008	4.007	4.011	4.015	4.016	4.013	4.013	4.011	4.006	3.998	4.018	4.013	3.999	4.003	3.994	3.998	3.997
	Mg #	0.914	0.916	0.917	0.917	0.917	0.919	0.919	0.917	0.919	0.918	0.929	0.956	0.958	0.953	0.952	0.950	0.913

Abbreviations: Di = diopside, Serp = serpentinite, b.d. = below detection. Mg# calculated as (MgO/40.3) / (MgO/40.3 + FeO/71.85).

Major element composition of diopside from the Geisspfad ultramafic body continued

Sample		G11	G11	G11	G26	G26	G26	G26	G26	G26	G27	G27	G27	G27	G27	G27	G27	G4
Rock		Serp	Serp	Serp	Serp	Serp	Serp	Serp	Serp	Serp	Serp	Serp	Serp	Serp	Serp	Serp	Serp	Ophi
Mineral		Di	Di	Di	Di	Di	Di	Di	Di	Di	Di	Di	Di	Di	Di	Di	Di	Di
Wt.%	SiO2	53.39	55.42	54.94	55.55	53.65	53.93	55.86	54.22	54.19	55.56	56.15	55.79	54.76	55.89	55.85	55.55	55.18
	TiO2	0.34	0.02	b.d.	0.03	0.05	0.09	0.03	0.10	0.11	0.01	0.02	0.02	0.13	b.d.	0.02	0.02	0.02
	Cr2O3	0.64	0.11	0.25	0.07	0.48	0.65	0.15	0.49	0.70	0.01	0.02	0.10	0.40	b.d.	0.08	0.26	0.04
	Al2O3	4.53	0.04	0.10	0.01	2.85	2.71	0.05	2.52	2.34	0.03	0.01	0.77	0.46	0.07	0.01	0.21	0.06
	FeO	2.59	1.68	1.98	1.14	2.17	1.97	1.66	2.17	2.04	1.28	1.29	1.28	2.46	1.27	1.26	1.18	1.82
	MnO	0.06	0.02	0.12	b.d.	b.d.	0.08	0.03	0.04	0.06	0.04	0.01	0.05	0.06	0.04	0.05	0.04	0.15
	NiO	b.d.	b.d.	b.d.	b.d.	0.05	0.11	b.d.	0.05	0.01	0.02	0.05	0.03	0.04	0.02	0.03	0.04	0.07
	MgO	15.60	17.14	16.80	17.55	16.38	16.53	17.04	16.70	16.70	17.54	17.47	17.52	16.57	17.53	17.41	17.82	16.87
	CaO	22.90	25.85	25.42	26.29	23.54	23.94	25.59	24.42	24.37	26.72	26.26	25.82	25.18	26.14	26.43	25.52	25.39
	Na2O	0.98	0.09	0.23	0.08	0.51	0.47	0.25	0.44	0.43	0.03	0.04	0.06	0.50	0.04	0.03	0.22	0.13
	K2O	b.d.	0.01	b.d.	b.d.	0.01	b.d.	b.d.	b.d.	b.d.	0.01	b.d.	b.d.	b.d.	b.d.	b.d.	b.d.	0.01
	Total	101.04	100.37	99.85	100.71	99.67	100.48	100.68	101.15	100.96	101.24	101.32	101.45	100.56	101.02	101.17	100.86	99.74
Cations	Si	1.918	2.005	2.003	2.001	1.951	1.948	2.013	1.948	1.950	1.995	2.009	1.992	1.988	2.006	2.004	1.996	2.010
	Ti	0.009	0.000	b.d.	0.001	0.001	0.002	0.001	0.003	0.003	0.000	0.001	0.001	0.003	b.d.	0.001	0.000	0.000
	Cr	0.018	0.003	0.007	0.002	0.014	0.019	0.004	0.014	0.020	0.000	0.001	0.003	0.012	b.d.	0.002	0.007	0.001
	Al	0.192	0.002	0.004	0.000	0.122	0.115	0.002	0.107	0.099	0.001	0.000	0.033	0.020	0.003	0.000	0.009	0.003
	Fe2+	0.078	0.051	0.060	0.034	0.066	0.059	0.050	0.065	0.061	0.038	0.039	0.038	0.075	0.038	0.038	0.036	0.056
	Mn	0.002	0.000	0.004	b.d.	b.d.	0.003	0.001	0.001	0.002	0.001	0.000	0.002	0.002	0.001	0.002	0.001	0.005
	Ni	b.d.	b.d.	b.d.	b.d.	0.001	0.003	b.d.	0.002	0.000	0.000	0.001	0.001	0.001	0.001	0.001	0.001	0.002
	Mg	0.835	0.924	0.913	0.942	0.888	0.890	0.915	0.894	0.896	0.939	0.932	0.932	0.896	0.938	0.931	0.954	0.916
	Ca	0.881	1.002	0.993	1.014	0.917	0.926	0.988	0.940	0.940	1.028	1.006	0.987	0.979	1.005	1.016	0.982	0.991
	Na	0.068	0.007	0.016	0.005	0.036	0.033	0.017	0.030	0.030	0.002	0.003	0.004	0.035	0.003	0.002	0.016	0.009
	K	b.d.	0.000	b.d.	b.d.	0.001	b.d.	b.d.	b.d.	b.d.	0.000	b.d.	b.d.	b.d.	b.d.	b.d.	b.d.	0.000
	Sum	4.002	3.995	4.000	4.000	3.998	3.999	3.992	4.004	4.002	4.005	3.991	3.992	4.011	3.994	3.996	4.003	3.992
	Mg #	0.915	0.948	0.938	0.965	0.931	0.937	0.948	0.932	0.936	0.961	0.960	0.961	0.923	0.961	0.961	0.964	0.943

Abbreviations: Di = diopside, Serp = serpentinite, Ophi = ophicarbonate, b.d. = below detection. Mg# calculated as (MgO/40.3) / (MgO/40.3 + FeO/71.85).

Major element composition of diopside from the Geisspfad ultramafic body continued

Sample		G4	G4	G4	G4	GEI9	GEI9	GEI9	GEI9	GEI9	GEI9	GEI9	GEI9	GEI9	GEI9	GEI9	GEI9
Rock		Ophi	Ophi	Ophi	Ophi	Ophi	Ophi	Ophi	Ophi	Ophi	Ophi	Ophi	Ophi	Ophi	Ophi	Ophi	Ophi
Mineral		Di	Di	Di	Di	Di	Di	Di	Di	Di	Di	Di	Di	Di	Di	Di	Di
Wt.%	SiO2	55.73	55.28	55.81	55.74	55.22	55.31	54.63	54.62	55.08	55.29	55.17	55.55	55.82	55.82	55.45	54.92	54.88
	TiO2	0.01	0.03	0.01	0.02	0.02	0.01	0.02	0.01	0.01	0.03	0.03	0.01	0.01	b.d.	0.01	0.03	0.03
	Cr2O3	0.05	b.d.	b.d.	b.d.	0.08	b.d.	b.d.	0.07	b.d.	0.06	b.d.	b.d.	0.04	0.02	b.d.	b.d.	0.09
	Al2O3	0.18	0.04	0.04	0.03	0.02	0.04	b.d.	0.02	0.02	b.d.	0.03	0.01	0.01	0.05	0.04	0.03	0.13
	FeO	1.68	1.99	1.65	1.59	0.95	1.20	1.06	0.94	1.12	1.26	1.27	0.99	1.22	0.21	1.13	1.17	1.26
	MnO	0.13	0.12	0.16	0.13	0.19	0.16	0.21	0.16	0.06	0.14	0.11	0.21	0.09	0.02	0.15	0.20	0.05
	NiO	0.03	b.d.	0.02	b.d.	b.d.	b.d.	0.01	0.06	0.04	0.02	0.15	0.01	0.01	b.d.	0.08	b.d.	b.d.
	MgO	17.89	16.90	17.23	17.28	17.06	16.94	16.98	16.97	17.09	17.14	16.84	17.14	17.80	17.67	17.33	17.34	17.78
	CaO	24.65	25.80	25.72	25.98	25.99	26.12	26.10	26.23	26.01	25.96	25.83	26.09	25.85	26.40	25.64	25.74	25.07
	Na2O	0.18	0.18	0.14	0.08	0.07	0.04	0.06	0.08	0.06	0.08	0.09	0.07	0.06	0.08	0.08	0.11	0.08
	K2O	0.01	b.d.	b.d.	b.d.	b.d.	b.d.	b.d.	b.d.	b.d.	0.01	b.d.	b.d.	b.d.	b.d.	b.d.	b.d.	b.d.
	Total	100.55	100.34	100.80	100.86	99.61	99.82	99.07	99.16	99.50	99.99	99.51	100.07	100.92	100.28	99.92	99.53	99.36
Cations	Si	2.007	2.005	2.010	2.007	2.009	2.010	2.002	2.001	2.007	2.007	2.012	2.011	2.004	2.010	2.010	2.002	2.000
	Ti	0.000	0.001	0.000	0.001	0.001	0.000	0.001	0.000	0.000	0.001	0.001	0.000	0.000	b.d.	0.000	0.001	0.001
	Cr	0.001	b.d.	b.d.	b.d.	0.002	b.d.	b.d.	0.002	b.d.	0.002	b.d.	b.d.	0.001	0.001	b.d.	b.d.	0.003
	Al	0.007	0.002	0.002	0.001	0.001	0.002	b.d.	0.001	0.001	b.d.	0.001	0.000	0.000	0.002	0.002	0.001	0.006
	Fe2+	0.051	0.060	0.050	0.048	0.029	0.036	0.032	0.029	0.034	0.038	0.039	0.030	0.037	0.006	0.034	0.036	0.038
	Mn	0.004	0.004	0.005	0.004	0.006	0.005	0.006	0.005	0.002	0.004	0.003	0.006	0.003	0.001	0.005	0.006	0.001
	Ni	0.001	b.d.	0.001	b.d.	b.d.	b.d.	0.000	0.002	0.001	0.000	0.004	0.000	0.000	b.d.	0.002	b.d.	b.d.
	Mg	0.960	0.913	0.925	0.927	0.925	0.918	0.928	0.926	0.928	0.927	0.915	0.925	0.953	0.948	0.936	0.942	0.966
	Ca	0.951	1.003	0.992	1.002	1.013	1.017	1.025	1.029	1.016	1.009	1.009	1.012	0.994	1.018	0.996	1.005	0.979
	Na	0.013	0.012	0.010	0.006	0.005	0.003	0.004	0.005	0.004	0.005	0.007	0.005	0.004	0.006	0.006	0.008	0.005
	K	0.001	b.d.	b.d.	b.d.	b.d.	b.d.	b.d.	b.d.	b.d.	0.000	b.d.	b.d.	b.d.	b.d.	b.d.	b.d.	b.d.
	Sum	3.995	4.000	3.994	3.995	3.991	3.990	3.999	4.000	3.994	3.995	3.990	3.991	3.997	3.992	3.992	4.000	3.998
	Mg #	0.950	0.938	0.949	0.951	0.970	0.962	0.966	0.970	0.964	0.960	0.960	0.969	0.963	0.993	0.965	0.964	0.962

Abbreviations: Di = diopside, Ophi = ophicarbonate, b.d. = below detection. Mg# calculated as (MgO/40.3) / (MgO/40.3 + FeO/71.85).

Major element composition of chlorite from the Geisspfad ultramafic body

Sample		G8	G8	G8	G11	G11	G11	G12	G12	G12	G12	G26	G26	G27	G27	G27	G27	G27
Rock		Serp	Serp	Serp	Serp	Serp	Serp	Serp	Serp	Serp	Serp	Serp	Serp	Serp	Serp	Serp	Serp	Serp
Mineral		Chl	Chl	Chl	Chl	Chl	Chl	Chl	Chl	Chl	Chl	Chl	Chl	Chl	Chl	Chl	Chl	Chl
Wt.%	SiO2	35.35	35.11	33.75	32.36	33.83	33.04	33.46	34.48	34.26	33.02	32.98	34.62	33.95	33.61	33.89	34.10	33.80
	TiO2	b.d.	0.01	0.02	0.09	0.01	0.04	0.03	0.03	0.03	0.06	0.02	0.02	0.02	0.03	0.03	0.02	0.03
	Cr2O3	0.01	0.04	2.12	1.87	2.57	2.16	2.05	1.87	1.79	1.19	3.45	1.36	1.73	2.25	1.80	2.03	1.43
	Al2O3	13.35	13.22	13.62	15.15	12.85	13.57	13.79	13.10	13.08	15.28	12.16	12.35	13.26	13.30	13.36	13.22	13.57
	FeO	3.69	3.68	3.74	4.75	4.03	3.95	3.13	2.68	2.81	3.47	3.75	3.37	3.81	4.14	3.88	3.94	3.75
	MnO	0.12	0.08	b.d.	b.d.	b.d.	b.d.	b.d.	b.d.	b.d.	0.01	b.d.	0.02	b.d.	b.d.	b.d.	0.01	b.d.
	NiO	0.08	0.20	0.20	0.23	0.26	0.25	0.25	0.32	0.19	0.18	0.31	0.30	0.19	0.17	0.18	0.19	0.20
	MgO	33.84	34.42	32.97	31.46	32.85	32.35	33.93	33.98	34.04	33.48	33.28	34.21	34.20	33.72	34.08	34.04	33.74
	CaO	0.11	0.03	0.02	0.01	0.01	0.01	0.02	0.02	0.02	0.01	0.01	0.01	b.d.	b.d.	b.d.	0.02	b.d.
	Na2O	0.01	0.01	b.d.	b.d.	0.01	b.d.	0.02	0.01	0.02	0.02	b.d.	0.02	0.02	0.02	0.02	0.01	b.d.
	K2O	0.01	0.01	b.d.	b.d.	b.d.	b.d.	b.d.	0.02	0.01	b.d.	0.01	0.01	b.d.	0.01	b.d.	b.d.	b.d.
	H2O	12.65	12.70	12.56	12.41	12.51	12.37	12.60	12.64	12.59	12.64	12.38	12.57	12.66	12.62	12.66	12.70	12.59
	Total	99.34	99.54	99.01	98.35	98.94	97.76	99.33	99.15	98.87	99.36	98.36	98.91	99.85	99.87	99.90	100.29	99.12
Cations	Si	1.670	1.657	1.612	1.563	1.622	1.601	1.591	1.636	1.630	1.567	1.597	1.650	1.608	1.597	1.605	1.610	1.610
	Ti	b.d.	0.000	0.001	0.003	0.001	0.002	0.001	0.001	0.001	0.002	0.001	0.001	0.001	0.001	0.001	0.001	0.001
	Cr	0.000	0.002	0.080	0.071	0.097	0.083	0.077	0.070	0.067	0.044	0.132	0.051	0.065	0.085	0.067	0.076	0.054
	Al	0.744	0.735	0.767	0.863	0.726	0.775	0.773	0.732	0.734	0.855	0.694	0.694	0.740	0.745	0.746	0.736	0.762
	Fe2+	0.146	0.145	0.149	0.192	0.162	0.160	0.124	0.106	0.112	0.138	0.152	0.134	0.151	0.164	0.154	0.156	0.149
	Mn	0.005	0.003	b.d.	b.d.	b.d.	b.d.	b.d.	b.d.	b.d.	0.000	b.d.	0.001	b.d.	b.d.	b.d.	0.000	b.d.
	Ni	0.003	0.008	0.008	0.009	0.010	0.010	0.010	0.012	0.007	0.007	0.012	0.012	0.007	0.006	0.007	0.007	0.007
	Mg	2.383	2.421	2.347	2.265	2.347	2.337	2.405	2.402	2.414	2.368	2.402	2.431	2.415	2.388	2.406	2.396	2.396
	Ca	0.006	0.002	0.001	0.000	0.000	0.001	0.001	0.001	0.001	0.001	0.000	0.001	b.d.	b.d.	b.d.	0.001	b.d.
	Na	0.001	0.001	b.d.	b.d.	0.001	b.d.	0.002	0.001	0.002	0.002	b.d.	0.002	0.002	0.002	0.002	0.001	b.d.
	K	0.001	0.001	b.d.	b.d.	b.d.	b.d.	b.d.	0.001	0.001	b.d.	0.001	0.001	b.d.	0.000	b.d.	b.d.	b.d.
	H	3.987	3.998	3.999	3.997	3.999	3.997	3.996	4.000	3.998	4.000	3.998	3.997	4.000	4.000	4.000	4.000	4.000
	Sum	4.958	4.975	4.964	4.967	4.966	4.968	4.984	4.963	4.969	4.983	4.990	4.978	4.989	4.988	4.988	4.984	4.981
	Mg #	0.942	0.943	0.940	0.922	0.936	0.936	0.951	0.958	0.956	0.945	0.941	0.948	0.941	0.936	0.940	0.939	0.941

Abbreviations: Chl = chlorite, Serp = serpentinite, b.d. = below detection. Mg# calculated as (MgO/40.3) / (MgO/40.3 + FeO/71.85).

Major element composition of chlorite from the Geisspfad ultramafic body continued

Sample		G27	G27	G27	GEI4	GEI4	GEI4	GEI4	GEI4	GEI4	GEI4	GEI4	GEI4	GEI4	GEI4	GEI9	GEI9	GEI9
Rock		Serp	Serp	Serp	Serp	Serp	Serp	Serp	Serp	Serp	Serp	Serp	Serp	Serp	Serp	Ophi	Ophi	Ophi
Mineral		Chl	Chl	Chl	Chl	Chl	Chl	Chl	Chl	Chl	Chl	Chl	Chl	Chl	Chl	Chl	Chl	Chl
Wt.%	SiO2	33.31	33.89	33.53	34.03	34.02	33.78	34.24	33.94	34.43	34.36	34.06	34.53	33.95	33.93	36.66	34.87	34.48
	TiO2	0.03	0.01	0.05	0.01	0.03	0.03	0.03	0.03	0.05	0.05	0.09	b.d.	0.03	0.04	0.03	0.02	0.01
	Cr2O3	2.36	1.80	1.96	0.93	0.92	1.04	1.02	1.00	1.00	0.19	1.19	1.07	1.33	0.90	0.38	0.62	0.16
	Al2O3	13.30	13.37	14.43	12.80	13.00	13.05	12.46	12.90	12.98	12.94	12.93	12.83	12.77	13.04	10.68	13.37	13.30
	FeO	3.97	3.86	4.32	4.36	4.30	4.23	4.12	4.24	4.42	4.67	4.24	4.10	4.12	4.15	4.35	4.35	4.43
	MnO	b.d.	b.d.	0.01	0.04	0.03	b.d.	b.d.	0.02	0.01	0.05	0.01	0.03	b.d.	0.02	b.d.	0.06	0.03
	NiO	0.16	0.19	0.21	0.25	0.19	0.16	0.18	0.20	0.19	0.21	0.20	0.18	0.21	0.22	0.34	0.28	0.25
	MgO	33.41	34.22	33.64	34.37	34.00	34.24	34.39	34.09	34.64	34.89	33.83	34.67	33.99	34.14	34.72	33.38	34.17
	CaO	b.d.	b.d.	b.d.	0.01	0.02	b.d.	0.02	0.01	0.03	0.02	0.24	0.04	0.11	0.06	0.02	0.03	0.03
	Na2O	0.02	0.01	b.d.	b.d.	0.02	b.d.	b.d.	0.03	0.01	b.d.	0.05	0.02	0.02	b.d.	b.d.	b.d.	b.d.
	K2O	b.d.	b.d.	0.01	b.d.	0.01	b.d.	0.01	b.d.	b.d.	0.01	0.01	b.d.	0.03	0.01	b.d.	b.d.	0.01
	H2O	12.53	12.68	12.76	12.59	12.56	12.56	12.56	12.55	12.73	12.68	12.59	12.71	12.55	12.56	12.70	12.65	12.62
	Total	99.09	100.03	100.91	99.40	99.11	99.09	99.02	99.00	100.50	100.07	99.45	100.19	99.12	99.07	99.93	99.69	99.54
Cations	Si	1.594	1.603	1.576	1.621	1.624	1.613	1.635	1.622	1.622	1.625	1.622	1.629	1.622	1.619	1.729	1.651	1.636
	Ti	0.001	0.000	0.002	0.000	0.001	0.001	0.001	0.001	0.002	0.002	0.003	b.d.	0.001	0.001	0.001	0.001	0.000
	Cr	0.089	0.067	0.073	0.035	0.035	0.039	0.038	0.038	0.037	0.007	0.045	0.040	0.050	0.034	0.014	0.023	0.006
	Al	0.750	0.746	0.800	0.719	0.731	0.734	0.701	0.727	0.721	0.721	0.726	0.714	0.719	0.734	0.594	0.746	0.744
	Fe2+	0.159	0.153	0.170	0.174	0.172	0.169	0.165	0.170	0.174	0.185	0.169	0.162	0.164	0.166	0.172	0.172	0.176
	Mn	b.d.	b.d.	0.001	0.002	0.001	b.d.	b.d.	0.001	0.000	0.002	0.001	0.001	b.d.	0.001	b.d.	0.002	0.001
	Ni	0.006	0.007	0.008	0.009	0.007	0.006	0.007	0.008	0.007	0.008	0.008	0.007	0.008	0.009	0.013	0.011	0.009
	Mg	2.383	2.413	2.357	2.440	2.419	2.437	2.447	2.428	2.432	2.459	2.402	2.438	2.420	2.429	2.441	2.356	2.416
	Ca	b.d.	b.d.	b.d.	0.001	0.001	b.d.	0.001	0.001	0.002	0.001	0.012	0.002	0.006	0.003	0.001	0.001	0.001
	Na	0.002	0.001	b.d.	b.d.	0.002	b.d.	b.d.	0.002	0.001	b.d.	0.004	0.002	0.002	b.d.	b.d.	b.d.	b.d.
	K	b.d.	b.d.	0.000	b.d.	0.001	b.d.	0.001	b.d.	b.d.	0.000	0.001	b.d.	0.002	0.000	b.d.	b.d.	0.000
	H	4.000	4.000	4.000	4.000	4.000	4.000	4.000	4.000	4.000	4.000	4.000	4.000	4.000	4.000	3.995	3.994	3.994
	Sum	4.986	4.990	4.986	5.002	4.994	5.000	4.995	4.996	4.998	5.010	4.992	4.995	4.995	4.996	4.965	4.963	4.989
	Mg #	0.938	0.940	0.933	0.934	0.934	0.935	0.937	0.935	0.933	0.930	0.934	0.938	0.936	0.936	0.934	0.932	0.932

Abbreviations: Chl = chlorite, Serp = serpentinite, Ophi = ophicarbonate, b.d. = below detection. Mg# calculated as (MgO/40.3) / (MgO/40.3 + FeO/71.85).

Major element composition of chlorite from the Geisspfad ultramafic body continued

Sample		G30	G30	G30	G34	G34	G34	G34
Rock		Metabas	Metabas	Metabas	Metabas	Metabas	Metabas	Metabas
Mineral		Chl	Chl	Chl	Chl	Chl	Chl	Chl
Wt.%	SiO2	29.21	29.40	28.41	27.25	27.30	27.85	27.71
	TiO2	0.03	0.03	0.03	0.08	0.05	0.09	0.07
	Cr2O3	0.09	0.01	b.d.	0.17	0.08	0.01	b.d.
	Al2O3	20.69	20.80	21.54	22.62	22.92	22.32	22.09
	FeO	10.35	10.08	11.32	12.79	12.56	13.00	13.43
	MnO	0.19	0.20	0.20	0.18	0.18	0.18	0.20
	NiO	0.07	0.18	0.06	0.13	0.05	b.d.	0.01
	MgO	26.73	26.64	25.81	23.50	23.50	23.85	23.63
	CaO	0.04	0.05	0.02	0.06	0.07	0.05	0.04
	Na2O	b.d.	b.d.	b.d.	b.d.	b.d.	b.d.	b.d.
	K2O	b.d.	b.d.	b.d.	b.d.	b.d.	b.d.	b.d.
	H2O	12.33	12.35	12.26	12.07	12.09	12.16	12.10
	Total	99.73	99.75	99.65	98.85	98.80	99.50	99.28
Cations	Si	1.421	1.428	1.390	1.354	1.354	1.374	1.373
	Ti	0.001	0.001	0.001	0.003	0.002	0.003	0.003
	Cr	0.003	0.001	b.d.	0.007	0.003	0.000	b.d.
	Al	1.186	1.191	1.242	1.325	1.340	1.298	1.290
	Fe2+	0.421	0.409	0.463	0.531	0.521	0.536	0.557
	Mn	0.008	0.008	0.008	0.008	0.008	0.007	0.008
	Ni	0.003	0.007	0.002	0.005	0.002	b.d.	0.001
	Mg	1.938	1.928	1.881	1.741	1.738	1.753	1.745
	Ca	0.002	0.002	0.001	0.003	0.004	0.003	0.002
	Na	b.d.	b.d.	b.d.	b.d.	b.d.	b.d.	b.d.
	K	b.d.	b.d.	b.d.	b.d.	b.d.	b.d.	b.d.
	H	4.000	4.000	4.000	4.000	4.000	4.000	4.000
	Sum	4.983	4.976	4.989	4.977	4.972	4.974	4.979
	Mg #	0.822	0.825	0.803	0.766	0.769	0.766	0.758

Abbreviations: Chl = chlorite, Metabas = metabasite, b.d. = below detection.
Mg# calculated as (MgO/40.3) / (MgO/40.3 + FeO/71.85).

Major element composition of epidote from the Geisspfad ultramafic body

Sample		G30	G30	G30	G30	G30	G30	G30	G30	G30	G30	G34	G34	G34	G34	G34
Rock		Metabas	Metabas	Metabas	Metabas	Metabas	Metabas	Metabas	Metabas	Metabas	Metabas	Metabas	Metabas	Metabas	Metabas	Metabas
Mineral		Ep	Ep	Ep	Ep	Ep	Ep	Ep	Ep	Ep	Ep	Ep	Ep	Ep	Ep	Ep
Wt.%	SiO2	38.28	38.10	37.79	38.28	37.49	37.98	38.33	37.81	38.01	37.85	38.25	38.65	38.49	38.21	38.64
	TiO2	0.33	0.08	0.22	0.08	0.19	0.12	0.24	0.12	0.09	0.10	0.08	0.12	0.10	0.12	0.18
	Al2O3	25.83	27.01	26.04	27.49	25.88	26.85	26.92	26.88	26.86	25.50	27.63	28.74	27.54	28.25	30.22
	Fe2O3	10.45	9.37	10.60	7.98	10.57	9.42	8.88	9.40	9.17	11.34	8.50	7.14	8.41	7.27	5.23
	MnO	0.06	0.02	0.44	0.05	0.25	0.04	0.11	0.08	0.07	0.09	0.17	0.15	0.11	0.12	0.02
	MgO	0.07	0.01	0.08	0.03	0.12	0.01	0.06	0.05	0.04	0.03	0.03	0.03	0.03	0.05	0.06
	CaO	23.44	24.07	23.61	24.74	24.28	25.11	24.65	24.63	24.97	24.81	24.61	24.43	24.48	24.74	24.96
	Na2O	0.03	0.01	b.d.	b.d.	0.01	b.d.	b.d.	b.d.	b.d.	b.d.	b.d.	b.d.	b.d.	0.02	0.01
	H2O	2.08	2.09	2.08	2.10	2.08	2.10	2.10	2.09	2.10	2.09	2.11	2.12	2.11	2.10	2.13
	Total	100.58	100.76	100.86	100.75	100.86	101.63	101.29	101.06	101.31	101.81	101.38	101.39	101.26	100.88	101.46
Cations	Si	2.754	2.730	2.721	2.736	2.705	2.710	2.734	2.710	2.717	2.713	2.722	2.732	2.738	2.722	2.714
	Ti	0.018	0.005	0.012	0.004	0.010	0.006	0.013	0.006	0.005	0.005	0.005	0.007	0.005	0.006	0.010
	Al	2.191	2.281	2.210	2.316	2.201	2.258	2.263	2.271	2.263	2.155	2.317	2.394	2.309	2.372	2.502
	Fe3+	0.566	0.505	0.574	0.429	0.574	0.506	0.477	0.507	0.493	0.612	0.455	0.380	0.450	0.390	0.276
	Mn	0.004	0.001	0.027	0.003	0.015	0.003	0.007	0.005	0.004	0.006	0.010	0.009	0.006	0.008	0.001
	Mg	0.008	0.001	0.009	0.003	0.013	0.001	0.006	0.005	0.004	0.003	0.003	0.003	0.003	0.005	0.006
	Ca	1.807	1.848	1.821	1.895	1.877	1.919	1.884	1.891	1.912	1.905	1.876	1.850	1.866	1.888	1.878
	Na	0.004	0.001	b.d.	b.d.	0.001	b.d.	b.d.	b.d.	b.d.	b.d.	b.d.	b.d.	b.d.	0.002	0.002
	Sum	7.351	7.372	7.375	7.387	7.397	7.402	7.383	7.395	7.400	7.399	7.388	7.375	7.377	7.392	7.388

Abbreviations: Ep = epidote, Metabas = Metabasite, b.d. = below detection.

Major element composition of epidote from the Geisspfad ultramafic body continued

Sample		G34	G34	G34	G34	G34	G34	G34	G34	G34	G34	G34	G34	G34	G34	G34
Rock		Metabas	Metabas	Metabas	Metabas	Metabas	Metabas	Metabas	Metabas	Metabas	Metabas	Metabas	Metabas	Metabas	Metabas	Metabas
Mineral		Ep	Ep	Ep	Ep	Ep	Ep	Ep	Ep	Ep	Ep	Ep	Ep	Ep	Ep	Ep
Wt.%	SiO2	38.23	38.09	38.29	37.78	38.44	38.54	38.49	38.21	38.73	38.25	38.57	38.88	38.69	38.62	38.68
	TiO2	0.16	0.13	0.16	0.08	0.15	0.09	0.10	0.11	0.11	0.09	0.11	0.11	0.14	0.12	0.11
	Al2O3	27.35	26.90	28.08	27.34	28.91	27.89	28.59	27.20	28.35	27.01	28.27	28.55	28.76	28.78	28.77
	Fe2O3	8.83	9.37	7.42	8.75	7.28	7.86	7.46	9.13	7.60	9.14	7.87	7.31	6.92	6.62	6.93
	MnO	0.22	0.16	0.12	0.15	0.13	0.16	0.11	0.18	0.11	0.14	0.12	0.11	0.16	0.12	0.11
	MgO	0.03	0.01	0.05	0.02	0.03	b.d.	0.05	0.03	0.05	0.03	0.04	0.04	0.05	0.03	0.01
	CaO	24.47	24.64	25.00	24.40	24.34	24.77	24.78	24.69	24.92	24.77	24.55	24.89	24.52	24.37	24.68
	Na2O	b.d.	0.01	b.d.	0.02	0.02	b.d.	b.d.	b.d.	b.d.	b.d.	b.d.	b.d.	b.d.	b.d.	b.d.
	H2O	2.11	2.10	2.11	2.09	2.12	2.11	2.12	2.11	2.13	2.10	2.12	2.13	2.12	2.11	2.12
	Total	101.39	101.41	101.23	100.63	101.42	101.42	101.70	101.66	102.00	101.54	101.65	102.02	101.37	100.77	101.41
Cations	Si	2.723	2.720	2.721	2.712	2.717	2.735	2.719	2.719	2.729	2.725	2.727	2.735	2.734	2.741	2.733
	Ti	0.009	0.007	0.009	0.004	0.008	0.005	0.005	0.006	0.006	0.005	0.006	0.006	0.007	0.006	0.006
	Al	2.296	2.264	2.352	2.313	2.409	2.333	2.380	2.281	2.355	2.268	2.356	2.367	2.396	2.408	2.396
	Fe3+	0.473	0.503	0.397	0.473	0.387	0.420	0.396	0.489	0.403	0.490	0.419	0.387	0.368	0.354	0.368
	Mn	0.013	0.010	0.007	0.009	0.008	0.010	0.006	0.011	0.007	0.008	0.007	0.006	0.010	0.007	0.007
	Mg	0.003	0.001	0.006	0.003	0.003	b.d.	0.005	0.003	0.005	0.003	0.004	0.004	0.006	0.003	0.001
	Ca	1.867	1.885	1.904	1.876	1.843	1.883	1.875	1.882	1.881	1.891	1.860	1.876	1.856	1.853	1.868
	Na	b.d.	0.001	b.d.	0.003	0.003	b.d.	b.d.	b.d.	b.d.	b.d.	b.d.	b.d.	b.d.	b.d.	b.d.
	Sum	7.384	7.391	7.395	7.393	7.378	7.384	7.387	7.391	7.386	7.391	7.380	7.382	7.377	7.372	7.379

Abbreviations: Ep = epidote, Metabas = Metabasite, b.d. = below detection.

Major element composition of epidote from the Geisspfad ultramafic body continued

Sample		G34	G34	G34	G34	G34	G34	G34	G34	G34	G34	G34	G34	G34	G34	G34
Rock		Metabas	Metabas	Metabas	Metabas	Metabas	Metabas	Metabas	Metabas	Metabas	Metabas	Metabas	Metabas	Metabas	Metabas	Metabas
Mineral		Ep	Ep	Ep	Ep	Ep	Ep	Ep	Ep	Ep	Ep	Ep	Ep	Ep	Ep	Ep
Wt.%	SiO2	38.74	38.76	38.35	38.30	38.12	38.71	38.55	38.44	38.75	38.52	38.47	38.62	38.77	38.51	38.50
	TiO2	0.10	0.08	0.08	0.08	0.09	0.09	0.11	0.11	0.08	0.10	0.12	0.16	0.12	0.14	0.14
	Al2O3	28.80	27.83	27.09	27.02	27.38	27.55	28.22	28.47	28.38	28.42	28.49	28.39	28.82	28.56	28.51
	Fe2O3	6.86	7.68	8.55	9.21	8.43	7.81	7.24	7.48	7.37	7.03	7.32	7.81	7.44	7.36	7.05
	MnO	0.10	0.11	0.12	0.14	0.12	0.12	0.12	0.12	0.12	0.14	0.13	0.18	0.13	0.15	0.16
	MgO	0.01	0.01	0.02	0.02	0.02	0.02	0.01	0.02	0.02	0.03	0.03	0.04	0.03	0.02	0.05
	CaO	24.84	24.84	24.66	24.77	24.82	24.68	24.71	25.09	24.69	24.94	24.61	24.40	24.63	24.59	24.37
	Na2O	b.d.	0.02	b.d.	0.01	0.01	b.d.	b.d.	b.d.	b.d.	0.01	0.01	b.d.	b.d.	b.d.	0.02
	H2O	2.13	2.12	2.10	2.11	2.10	2.11	2.11	2.12	2.12	2.12	2.12	2.12	2.13	2.12	2.11
	Total	101.58	101.45	100.97	101.65	101.08	101.09	101.07	101.85	101.53	101.30	101.29	101.72	102.08	101.45	100.91
Cations	Si	2.733	2.747	2.741	2.726	2.722	2.754	2.738	2.715	2.739	2.730	2.726	2.727	2.725	2.725	2.734
	Ti	0.005	0.004	0.004	0.004	0.005	0.005	0.006	0.006	0.004	0.005	0.006	0.008	0.006	0.008	0.008
	Al	2.395	2.325	2.282	2.267	2.305	2.310	2.362	2.370	2.364	2.374	2.380	2.363	2.388	2.382	2.387
	Fe3+	0.364	0.410	0.460	0.493	0.453	0.418	0.387	0.397	0.392	0.375	0.390	0.415	0.393	0.392	0.377
	Mn	0.006	0.006	0.008	0.008	0.007	0.008	0.007	0.007	0.007	0.008	0.008	0.011	0.008	0.009	0.010
	Mg	0.001	0.002	0.002	0.002	0.002	0.002	0.001	0.002	0.002	0.004	0.004	0.005	0.003	0.002	0.005
	Ca	1.877	1.886	1.888	1.889	1.899	1.881	1.880	1.898	1.870	1.894	1.868	1.846	1.855	1.864	1.854
	Na	b.d.	0.002	b.d.	0.001	0.001	b.d.	b.d.	b.d.	b.d.	0.001	0.001	b.d.	b.d.	b.d.	0.002
	Sum	7.382	7.382	7.384	7.390	7.394	7.377	7.381	7.396	7.378	7.391	7.383	7.375	7.378	7.381	7.377

Abbreviations: Ep = epidote, Metabas = Metabasite, b.d. = below detection.

Major element composition of epidote from the Geisspfad ultramafic body continued

Sample		G34	G34	G34	G34	G34	G34	G34	G34	G34	G34
Rock		Metabas	Metabas	Metabas	Metabas	Metabas	Metabas	Metabas	Metabas	Metabas	Metabas
Mineral		Ep	Ep	Ep	Ep	Ep	Ep	Ep	Ep	Ep	Ep
Wt.%	SiO2	38.46	38.32	37.91	38.01	38.46	38.45	38.45	38.35	38.44	38.65
	TiO2	0.11	0.09	0.12	0.13	0.14	0.12	0.12	0.10	0.10	0.10
	Al2O3	26.92	27.04	26.88	26.98	27.44	27.18	27.38	27.11	27.65	27.95
	Fe2O3	9.92	9.55	9.68	9.15	9.18	8.95	9.15	8.97	8.67	7.86
	MnO	0.14	0.11	0.13	0.17	0.15	0.16	0.16	0.15	0.15	0.14
	MgO	0.02	0.02	0.05	0.02	0.04	0.02	0.01	0.02	0.02	0.01
	CaO	24.76	24.55	24.67	24.65	24.77	24.24	24.59	24.50	24.65	24.78
	Na2O	b.d.	b.d.	b.d.	b.d.	b.d.	b.d.	0.01	b.d.	0.02	b.d.
	H2O	2.12	2.11	2.10	2.10	2.12	2.10	2.12	2.10	2.12	2.12
	Total	102.45	101.79	101.54	101.22	102.29	101.23	101.99	101.31	101.82	101.60
Cations	Si	2.721	2.724	2.707	2.718	2.718	2.740	2.724	2.734	2.724	2.737
	Ti	0.006	0.005	0.007	0.007	0.007	0.006	0.006	0.006	0.005	0.005
	Al	2.245	2.266	2.262	2.274	2.286	2.283	2.286	2.278	2.309	2.333
	Fe3+	0.528	0.511	0.520	0.492	0.488	0.480	0.488	0.481	0.462	0.419
	Mn	0.008	0.006	0.008	0.010	0.009	0.010	0.010	0.009	0.009	0.008
	Mg	0.002	0.002	0.005	0.003	0.004	0.002	0.002	0.002	0.002	0.001
	Ca	1.877	1.870	1.887	1.888	1.875	1.851	1.866	1.871	1.871	1.880
	Na	b.d.	b.d.	b.d.	b.d.	b.d.	b.d.	0.001	b.d.	0.003	b.d.
	Sum	7.387	7.383	7.395	7.392	7.388	7.372	7.383	7.381	7.386	7.382

Abbreviations: Ep = epidote, Metabas = Metabasite, b.d. = below detection.

Major element composition of titanite from the Geisspfad ultramafic body

Sample		G30a	G30a	G30a	G30a	G30a	G30a	G30a	G30a	G30a	G30a	G34	G34	G34	G34
Rock		Metabas	Metabas	Metabas	Metabas	Metabas	Metabas	Metabas	Metabas	Metabas	Metabas	Metabas	Metabas	Metabas	Metabas
Mineral		Tit	Tit	Tit	Tit	Tit	Tit	Tit	Tit	Tit	Tit	Tit	Tit	Tit	Tit
Wt.%	SiO2	30.73	31.08	30.87	30.54	31.36	31.00	31.11	31.03	31.03	30.97	30.70	31.21	31.09	31.16
	TiO2	34.55	34.90	37.34	34.95	34.25	36.75	37.08	35.55	35.79	34.67	37.86	37.67	37.73	37.20
	Al2O3	2.26	2.54	0.86	2.16	3.50	1.51	1.49	2.47	2.26	2.97	0.97	0.98	1.28	1.37
	Fe2O3	1.29	1.31	0.91	0.82	1.10	0.62	0.56	0.60	0.41	0.98	0.41	0.60	0.29	0.58
	MnO	0.05	0.03	0.04	0.03	0.03	b.d.	b.d.	b.d.	b.d.	b.d.	b.d.	b.d.	b.d.	b.d.
	MgO	1.98	1.82	b.d.	0.88	0.08	b.d.	b.d.	0.01	0.01	b.d.	b.d.	b.d.	b.d.	b.d.
	CaO	29.47	30.30	32.33	31.31	31.59	29.03	28.93	29.21	28.74	28.80	29.07	28.81	28.99	28.98
	Na2O	b.d.	b.d.	0.01	0.03	b.d.	b.d.	b.d.	0.01	0.02	b.d.	0.01	b.d.	0.02	b.d.
	Total	100.33	101.98	102.37	100.71	101.90	98.91	99.17	98.88	98.27	98.39	99.03	99.27	99.41	99.29
Cations	Si	1.001	0.997	0.995	0.996	1.007	1.021	1.022	1.022	1.026	1.024	1.012	1.024	1.019	1.022
	Ti	0.847	0.842	0.905	0.857	0.827	0.911	0.916	0.880	0.890	0.862	0.938	0.930	0.930	0.918
	Al	0.087	0.096	0.033	0.083	0.133	0.059	0.058	0.096	0.088	0.116	0.038	0.038	0.049	0.053
	Fe3+	0.032	0.032	0.022	0.020	0.027	0.015	0.014	0.015	0.010	0.024	0.010	0.015	0.007	0.014
	Mn	0.001	0.001	0.001	0.001	0.001	b.d.	b.d.	b.d.	b.d.	b.d.	b.d.	b.d.	b.d.	b.d.
	Mg	0.096	0.087	0.000	0.043	0.004	b.d.	b.d.	0.000	0.001	b.d.	b.d.	b.d.	b.d.	b.d.
	Ca	1.029	1.042	1.116	1.094	1.087	1.025	1.018	1.030	1.018	1.020	1.027	1.013	1.018	1.019
	Na	b.d.	b.d.	0.001	0.002	b.d.	b.d.	b.d.	0.001	0.001	b.d.	0.001	b.d.	0.002	b.d.
	Sum	3.093	3.097	3.073	3.096	3.086	3.031	3.027	3.043	3.035	3.045	3.026	3.020	3.024	3.026

Abbreviations:Tit = titanite, Metabas = Metabasite, b.d. = below detection.

Major element composition of titanite from the Geisspfad ultramafic body

Sample		G34	G34	G34	G34
Rock		Metabas	Metabas	Metabas	Metabas
Mineral		Tit	Tit	Tit	Tit
Wt.%	SiO2	30.93	30.90	30.95	31.36
	TiO2	37.12	37.67	37.61	35.81
	Al2O3	1.37	1.06	1.32	2.29
	Fe2O3	0.60	0.49	0.54	0.67
	MnO	b.d.	b.d.	b.d.	b.d.
	MgO	b.d.	b.d.	b.d.	0.10
	CaO	28.78	28.77	28.96	28.71
	Na2O	0.01	b.d.	0.01	0.04
	Total	98.81	98.89	99.39	98.98
Cations	Si	1.020	1.018	1.015	1.029
	Ti	0.920	0.934	0.928	0.884
	Al	0.053	0.041	0.051	0.089
	Fe3+	0.015	0.012	0.013	0.017
	Mn	b.d.	b.d.	b.d.	b.d.
	Mg	b.d.	b.d.	b.d.	0.005
	Ca	1.017	1.016	1.018	1.010
	Na	0.001	b.d.	0.001	0.002
	Sum	3.026	3.021	3.025	3.035

Abbreviations:Tit = titanite, Metabas = Metabasite, b.d. = below detection.

Major element composition of talc from the Geisspfad ultramafic body

Sample		G8	G8	G8	G8	G8	G8
Rock		Serp	Serp	Serp	Serp	Serp	Serp
Mineral		Tlc	Tlc	Tlc	Tlc	Tlc	Tlc
Wt.%	SiO2	63.09	62.28	62.50	62.40	62.99	62.64
	TiO2	0.03	0.04	0.04	0.01	0.04	0.03
	Cr2O3	b.d.	0.07	0.05	0.01	b.d.	b.d.
	Al2O3	0.39	0.70	0.47	0.33	0.40	0.36
	FeO	1.38	1.40	1.37	1.36	1.31	1.60
	MnO	b.d.	b.d.	0.02	b.d.	0.05	0.02
	NiO	0.34	0.26	0.13	0.16	0.32	0.35
	MgO	29.59	29.01	29.01	29.27	29.08	28.71
	CaO	b.d.	0.01	0.02	0.01	0.01	0.01
	Na2O	0.20	0.34	0.23	0.11	0.17	0.17
	K2O	0.01	0.01	0.02	0.01	0.02	0.01
	H2O	4.70	4.65	4.65	4.64	4.67	4.63
	Total	99.75	98.80	98.53	98.31	99.07	98.57
Cations	Si	4.020	4.008	4.027	4.028	4.036	4.040
	Ti	0.001	0.002	0.002	0.001	0.002	0.001
	Cr	b.d.	0.003	0.002	0.000	b.d.	b.d.
	Al	0.030	0.053	0.036	0.025	0.030	0.027
	Fe2+	0.074	0.075	0.074	0.073	0.070	0.086
	Mn	b.d.	b.d.	0.001	b.d.	0.003	0.001
	Ni	0.017	0.014	0.007	0.008	0.016	0.018
	Mg	2.810	2.783	2.786	2.816	2.777	2.760
	Ca	b.d.	0.001	0.001	0.000	0.001	0.001
	Na	0.025	0.043	0.029	0.013	0.022	0.022
	K	0.000	0.001	0.001	0.001	0.001	0.001
	H	1.998	1.997	1.998	1.999	1.997	1.993
	Sum	6.977	6.983	6.967	6.966	6.958	6.956
	Mg #	0.975	0.974	0.974	0.975	0.975	0.970

Abbreviations: Tlc = talc, Serp = serpentinite, b.d. = below detection.
Mg# calculated as (MgO/40.3) / (MgO/40.3 + FeO/71.85).

Major element composition of calcite from the Geisspfad ultramafic body

Sample		G3	G3	G3	G3	G3	G3	G3	G3	G3	GEI9	GEI9	GEI9	GEI9	GEI9	GEI9	GEI9
Rock		Ophi	Ophi	Ophi	Ophi	Ophi	Ophi	Ophi	Ophi	Ophi	Ophi	Ophi	Ophi	Ophi	Ophi	Ophi	Ophi
Mineral		Cal	Cal	Cal	Cal	Cal	Cal	Cal	Cal	Cal	Cal	Cal	Cal	Cal	Cal	Cal	Cal
Wt. %	SiO2	0.03	b.d.	0.03	b.d.	0.02	0.01	b.d.	0.02	0.24	0.05	0.02	0.02	0.00	0.07	b.d.	0.01
	Al2O3	n.a.	n.a.	n.a.	n.a.	n.a.	n.a.	n.a.	n.a.	n.a.	n.a.	n.a.	n.a.	n.a.	n.a.	n.a.	n.a.
	FeO	0.77	0.61	0.40	1.34	1.33	1.47	1.30	0.24	0.32	0.18	0.18	0.14	0.22	0.20	0.23	0.22
	MnO	0.12	0.08	0.15	0.22	0.23	0.41	0.42	0.19	0.27	0.21	0.19	0.21	0.25	0.19	0.21	0.24
	MgO	1.72	1.76	1.53	17.03	16.86	16.66	16.66	1.52	1.60	1.04	1.11	1.26	1.36	1.29	1.24	1.46
	CaO	50.14	52.26	52.33	29.40	29.13	29.55	29.56	52.95	52.45	53.56	53.18	56.89	53.69	53.73	54.23	54.59
	Na2O	0.02	b.d.	0.02	0.02	b.d.	0.01	b.d.	b.d.	0.01	b.d.	0.02	b.d.	0.01	0.01	0.02	b.d.
	K2O	b.d.	b.d.	0.02	0.01	b.d.	0.01	b.d.	b.d.	b.d.	0.01	0.01	0.01	b.d.	b.d.	0.01	b.d.
	SrO	0.10	0.19	0.17	0.15	0.14	0.13	0.04	0.06	0.10	0.08	0.08	0.02	0.14	0.08	0.07	0.05
	BaO	n.a.	n.a.	n.a.	n.a.	n.a.	n.a.	n.a.	n.a.	n.a.	n.a.	n.a.	n.a.	n.a.	n.a.	n.a.	n.a.
	SO3	b.d.	b.d.	b.d.	0.02	b.d.	b.d.	0.02	0.03	b.d.	0.05	b.d.	0.07	0.03	0.01	0.02	b.d.
	CO2	47.10	45.10	45.34	51.78	52.29	51.76	52.01	44.99	45.00	44.80	45.19	41.37	44.30	44.42	43.98	43.41
	Total	100.00	100.00	99.98	99.97	100.00	100.00	100.00	100.00	99.99	99.98	99.99	99.99	99.99	100.00	100.01	99.98

Abbreviations: Cal = calcite, Ophi = ophicarbonate, b.d. = below detection, n.a. = not analyzed.

Major element composition of calcite from the Geisspfad ultramafic body

Sample		G30	G30	G30	G30	G30	G30	G30	G30
Rock		Metabas	Metabas	Metabas	Metabas	Metabas	Metabas	Metabas	Metabas
Mineral		Cal	Cal	Cal	Cal	Cal	Cal	Cal	Cal
Wt. %	SiO2	0.02	0.01	b.d.	0.01	0.06	b.d.	0.03	0.02
	Al2O3	0.09	0.01	0.02	0.12	0.13	0.02	0.16	0.12
	FeO	0.44	0.31	0.43	0.34	0.21	0.32	0.23	0.45
	MnO	0.37	0.41	0.14	0.28	0.31	0.07	0.33	0.16
	MgO	0.80	0.80	0.73	0.61	0.49	0.62	0.55	0.54
	CaO	53.24	53.34	53.10	52.94	53.28	53.79	52.95	53.07
	Na2O	b.d.	0.01	0.02	0.02	b.d.	0.02	b.d.	b.d.
	K2O	b.d.	b.d.	b.d.	0.01	b.d.	b.d.	b.d.	b.d.
	SrO	0.11	0.07	0.14	0.09	0.10	0.05	0.06	0.10
	BaO	0.06	b.d.	b.d.	0.05	b.d.	b.d.	b.d.	b.d.
	SO3	n.a.	n.a.	n.a.	n.a.	n.a.	n.a.	n.a.	n.a.
	CO2	43.29	43.23	42.93	42.77	42.87	43.20	42.68	42.77
	Total	98.42	98.18	97.51	97.24	97.46	98.09	96.98	97.23

Abbreviations: Cal = calcite, Metabas = Metabasite, b.d. = below detection, n.a. = not analyzed.

Major element composition of olivine from the Dramala spinel harzburgite and plagioclase-bearing harzburgite

Sample		PI2	PI2	PI2	PI2	PI2	PI2	PI2	PI2	PI2	PI2	PI2	PI2	PI2	PI2	PI2	PI2
Rock		Spl hrz	Spl hrz	Spl hrz	Spl hrz	Spl hrz	Spl hrz	Spl hrz	Spl hrz	Spl hrz	Spl hrz	Spl hrz	Spl hrz	Spl hrz	Spl hrz	Spl hrz	Spl hrz
Mineral		Ol	Ol	Ol	Ol	Ol	Ol	Ol	Ol	Ol	Ol	Ol	Ol	Ol	Ol	Ol	Ol
Type		Clast	Clast	Clast	Clast	Clast	Clast	Clast	Clast	Clast	Clast	Clast	Clast	Clast	Clast	Clast	Clast
Wt.%	SiO2	42.04	41.68	41.98	42.02	41.90	41.89	42.00	41.81	42.00	41.76	41.74	41.83	41.95	41.79	42.03	41.18
	TiO2	b.d.	b.d.	0.01	0.01	b.d.	0.01	0.01	b.d.	b.d.	0.01	0.01	0.03	0.01	b.d.	b.d.	b.d.
	Cr2O3	0.02	b.d.	0.01	b.d.	b.d.	b.d.	b.d.	b.d.	0.01	0.04	b.d.	b.d.	0.01	0.03	b.d.	0.02
	Al2O3	b.d.	0.02	b.d.	b.d.	0.02	b.d.	b.d.	b.d.	b.d.	0.01	b.d.	b.d.	b.d.	b.d.	b.d.	0.01
	FeO	8.29	8.62	8.75	8.52	8.76	8.95	9.35	8.97	9.08	9.15	8.95	9.03	8.74	8.59	8.80	9.03
	MnO	0.16	0.11	0.14	0.13	0.16	0.19	0.12	0.13	0.13	0.14	0.20	0.12	0.11	0.10	0.12	0.12
	NiO	0.48	0.46	0.43	0.51	0.41	0.50	0.44	0.39	0.47	0.41	0.39	0.41	0.42	0.50	0.36	0.40
	MgO	50.20	49.85	49.95	50.28	50.08	49.71	49.85	49.86	50.10	49.65	50.02	50.02	50.00	49.92	50.27	49.93
	CaO	0.08	0.06	0.02	0.01	0.02	0.03	0.02	0.02	0.02	0.02	0.02	0.03	0.02	0.01	0.02	0.02
	Na2O	b.d.	0.02	0.01	0.01	0.01	b.d.	0.01	0.01	b.d.	b.d.	0.01	b.d.	b.d.	b.d.	0.01	b.d.
	K2O	b.d.	b.d.	b.d.	b.d.	b.d.	0.02	b.d.	0.01	b.d.	0.01	b.d.	b.d.	b.d.	b.d.	b.d.	0.01
	Total	101.27	100.82	101.30	101.49	101.36	101.30	101.80	101.20	101.81	101.20	101.34	101.47	101.26	100.94	101.61	100.72
Cations	Si	1.010	1.008	1.010	1.009	1.008	1.010	1.008	1.008	1.007	1.008	1.006	1.006	1.010	1.009	1.008	0.999
	Ti	b.d.	b.d.	0.000	0.000	b.d.	0.000	0.000	b.d.	b.d.	0.000	0.000	0.001	0.000	b.d.	b.d.	b.d.
	Cr	0.000	b.d.	0.000	b.d.	b.d.	b.d.	b.d.	b.d.	0.000	0.001	b.d.	b.d.	0.000	0.001	b.d.	0.000
	Al	b.d.	0.001	b.d.	b.d.	0.001	b.d.	b.d.	b.d.	b.d.	0.000	b.d.	b.d.	b.d.	b.d.	b.d.	0.000
	Fe2+	0.167	0.174	0.176	0.171	0.176	0.180	0.188	0.181	0.182	0.185	0.180	0.182	0.176	0.173	0.176	0.183
	Mn	0.003	0.002	0.003	0.003	0.003	0.004	0.002	0.003	0.003	0.003	0.004	0.002	0.002	0.002	0.002	0.002
	Ni	0.009	0.009	0.008	0.010	0.008	0.010	0.008	0.008	0.009	0.008	0.008	0.008	0.008	0.010	0.007	0.008
	Mg	1.798	1.796	1.791	1.799	1.795	1.786	1.784	1.792	1.791	1.786	1.796	1.794	1.793	1.796	1.797	1.806
	Ca	0.002	0.002	0.001	0.000	0.001	0.001	0.001	0.001	0.001	0.001	0.001	0.001	0.001	0.000	0.001	0.001
	Na	b.d.	0.001	0.000	0.000	0.000	b.d.	0.000	0.000	b.d.	b.d.	0.000	b.d.	b.d.	b.d.	0.000	b.d.
	K	b.d.	b.d.	b.d.	b.d.	b.d.	0.001	b.d.	0.000	b.d.	0.000	b.d.	b.d.	b.d.	b.d.	b.d.	0.000
	SumCAT	2.990	2.993	2.990	2.992	2.992	2.991	2.992	2.992	2.993	2.992	2.995	2.993	2.990	2.991	2.992	3.000
	Mg #	0.915	0.912	0.911	0.913	0.911	0.908	0.905	0.908	0.908	0.906	0.909	0.908	0.911	0.912	0.911	0.908

Abbreviations: Ol = olivine, Metam = metamorphic, Spl hrz = spinel harzburgite, b.d. = below detection limit.
Mg# calculated as (MgO/40.3) / (MgO/40.3 + FeO/71.85).

Major element composition of olivine from the Dramala spinel harzburgite and plagioclase-bearing harzburgite continued

Sample		PI2	PI2	PI2	PI2	PI2	PI2	PI2	PI2	PI2	PI2	PI2	PI2	PI2	PI2	PI2	PI2
Rock		Spl hrz	Spl hrz	Spl hrz	Spl hrz	Spl hrz	Spl hrz	Spl hrz	Spl hrz	Spl hrz	Spl hrz	Spl hrz	Spl hrz	Spl hrz	Spl hrz	Spl hrz	Spl hrz
Mineral		Ol	Ol	Ol	Ol	Ol	Ol	Ol	Ol	Ol	Ol	Ol	Ol	Ol	Ol	Ol	Ol
Type		Clast	Clast	Clast	Clast	Clast	Clast	Clast	Clast	Clast	Clast	Clast	Clast	Clast	Clast	Clast	Clast
Wt.%	SiO2	41.60	41.32	41.48	41.24	41.65	41.92	41.69	41.19	40.76	40.82	40.47	40.76	41.66	41.52	41.50	41.40
	TiO2	b.d.	0.02	0.01	0.03	b.d.	0.02	0.01	0.01	b.d.	b.d.	b.d.	0.01	0.00	0.02	b.d.	0.01
	Cr2O3	0.03	b.d.	0.01	b.d.	0.30	0.06	b.d.	0.01	0.01	0.02	0.01	b.d.	0.01	b.d.	0.01	0.01
	Al2O3	0.01	0.01	0.02	0.01	0.03	b.d.	b.d.	b.d.	b.d.	b.d.	b.d.	b.d.	b.d.	0.01	b.d.	b.d.
	FeO	8.65	8.61	8.36	9.05	8.34	8.60	8.94	9.12	9.47	9.34	9.22	8.58	8.81	9.21	8.98	8.76
	MnO	0.09	0.13	0.14	0.17	0.17	0.19	0.12	0.21	0.14	0.13	0.13	0.12	0.15	0.14	0.15	0.13
	NiO	0.38	0.53	0.44	0.45	0.38	0.39	0.34	0.37	0.35	0.36	0.40	0.38	0.35	0.34	0.36	0.38
	MgO	50.35	50.25	50.44	50.36	50.56	50.28	50.17	50.14	50.06	49.83	49.87	50.35	50.27	49.88	49.97	50.11
	CaO	b.d.	0.02	0.01	b.d.	0.02	b.d.	0.02	0.01	0.01	0.01	0.01	0.01	0.01	0.04	0.02	0.02
	Na2O	0.02	0.02	b.d.	0.01	b.d.	b.d.	b.d.	b.d.	b.d.	b.d.	b.d.	b.d.	b.d.	b.d.	b.d.	0.01
	K2O	b.d.	b.d.	0.01	b.d.	b.d.	b.d.	b.d.	0.01	0.01	0.01	b.d.	b.d.	b.d.	0.01	0.01	b.d.
	Total	101.13	100.91	100.92	101.32	101.45	101.46	101.29	101.07	100.81	100.52	100.11	100.21	101.26	101.17	101.00	100.83
Cations	Si	1.003	1.000	1.001	0.996	1.001	1.007	1.004	0.997	0.991	0.995	0.990	0.993	1.004	1.003	1.003	1.002
	Ti	b.d.	0.000	0.000	0.001	b.d.	0.000	0.000	0.000	b.d.	b.d.	b.d.	0.000	0.000	0.000	b.d.	0.000
	Cr	0.001	b.d.	0.000	b.d.	0.006	0.001	b.d.	0.000	0.000	0.000	0.000	b.d.	0.000	b.d.	0.000	0.000
	Al	0.000	0.000	0.001	0.000	0.001	b.d.	b.d.	b.d.	b.d.	b.d.	b.d.	b.d.	b.d.	0.000	b.d.	b.d.
	Fe2+	0.174	0.174	0.169	0.183	0.168	0.173	0.180	0.185	0.193	0.190	0.189	0.175	0.177	0.186	0.182	0.177
	Mn	0.002	0.003	0.003	0.003	0.003	0.004	0.002	0.004	0.003	0.003	0.003	0.002	0.003	0.003	0.003	0.003
	Ni	0.007	0.010	0.009	0.009	0.007	0.008	0.007	0.007	0.007	0.007	0.008	0.007	0.007	0.007	0.007	0.007
	Mg	1.809	1.812	1.815	1.812	1.810	1.800	1.801	1.809	1.814	1.810	1.819	1.828	1.805	1.796	1.801	1.807
	Ca	b.d.	0.001	0.000	b.d.	0.001	b.d.	0.001	0.000	0.000	0.000	0.000	0.000	0.000	0.001	0.001	0.001
	Na	0.001	0.001	b.d.	0.000	b.d.	b.d.	b.d.	b.d.	b.d.	b.d.	b.d.	b.d.	b.d.	b.d.	b.d.	0.000
	K	b.d.	b.d.	0.000	b.d.	b.d.	b.d.	b.d.	0.000	0.000	0.000	b.d.	b.d.	b.d.	0.000	0.000	b.d.
	SumCAT	2.997	3.000	2.998	3.004	2.996	2.992	2.995	3.003	3.009	3.005	3.009	3.007	2.996	2.997	2.997	2.998
	Mg #	0.912	0.912	0.915	0.908	0.915	0.912	0.909	0.907	0.904	0.905	0.906	0.913	0.910	0.906	0.908	0.911

Abbreviations: Ol = olivine, Metam = metamorphic, Spl hrz = spinel harzburgite, b.d. = below detection limit.
Mg# calculated as (MgO/40.3) / (MgO/40.3 + FeO/71.85).

Major element composition of olivine from the Dramala spinel harzburgite and plagioclase-bearing harzburgite continued

Sample		PI2	PI2	PI2	PI2	PI2	PI2	PI2	PI2	PI2	PI2	PI2	PI2	PI2	PI2	PI2	PI2
Rock		Spl hrz	Spl hrz	Spl hrz	Spl hrz	Spl hrz	Spl hrz	Spl hrz	Spl hrz	Spl hrz	Spl hrz	Spl hrz	Spl hrz	Spl hrz	Spl hrz	Spl hrz	Spl hrz
Mineral		Ol	Ol	Ol	Ol	Ol	Ol	Ol	Ol	Ol	Ol	Ol	Ol	Ol	Ol	Ol	Ol
Type		Clast	Clast	Clast	Clast	Clast	Clast	Clast	Clast	Clast	Clast	Clast	Clast	Clast	Clast	Clast	Clast
Wt.%	SiO2	41.58	41.22	41.25	40.99	41.06	41.17	41.22	41.02	40.96	41.11	41.13	41.00	41.01	41.28	41.09	41.00
	TiO2	0.02	b.d.	b.d.	b.d.	0.02	b.d.	b.d.	b.d.	b.d.	0.02	0.02	b.d.	b.d.	b.d.	b.d.	0.01
	Cr2O3	b.d.	0.01	0.04	b.d.	0.02	0.02	b.d.	b.d.	b.d.	b.d.	b.d.	0.03	0.01	0.02	0.01	0.03
	Al2O3	b.d.	b.d.	b.d.	0.01	b.d.	0.01	b.d.	b.d.	0.02	b.d.	b.d.	0.01	b.d.	0.01	0.01	0.01
	FeO	8.86	8.83	8.84	9.35	8.53	9.29	8.82	8.47	9.19	9.38	9.36	8.96	9.25	9.23	9.42	9.41
	MnO	0.13	0.07	0.15	0.10	0.11	0.12	0.09	0.13	0.11	0.13	0.18	0.15	0.11	0.13	0.19	0.15
	NiO	0.40	0.36	0.43	0.36	0.43	0.40	0.37	0.39	0.38	0.42	0.35	0.36	0.42	0.35	0.35	0.40
	MgO	50.16	50.13	50.21	49.98	50.54	49.90	49.97	50.35	50.08	49.76	50.07	50.02	50.35	50.24	49.94	49.98
	CaO	0.01	0.01	b.d.	0.11	0.06	0.01	0.05	0.03	0.02	0.02	0.03	0.02	0.01	0.04	0.02	0.02
	Na2O	b.d.	0.01	b.d.	b.d.	0.01	b.d.	0.01	0.01	0.01	b.d.	0.01	0.01	b.d.	0.01	b.d.	b.d.
	K2O	b.d.	b.d.	b.d.	b.d.	0.01	b.d.	b.d.	b.d.	0.01	b.d.	0.01	b.d.	b.d.	b.d.	b.d.	b.d.
	Total	101.16	100.64	100.92	100.90	100.79	100.92	100.53	100.40	100.78	100.84	101.16	100.56	101.16	101.31	101.03	101.01
Cations	Si	1.003	1.000	0.999	0.995	0.994	0.998	1.001	0.997	0.995	0.998	0.996	0.997	0.993	0.997	0.996	0.995
	Ti	0.000	b.d.	b.d.	b.d.	0.000	b.d.	b.d.	b.d.	b.d.	0.000	0.000	b.d.	b.d.	b.d.	b.d.	0.000
	Cr	b.d.	0.000	0.001	b.d.	0.000	0.000	b.d.	b.d.	b.d.	b.d.	b.d.	0.001	0.000	0.000	0.000	0.001
	Al	b.d.	b.d.	b.d.	0.000	b.d.	0.000	b.d.	b.d.	0.001	b.d.	b.d.	0.000	b.d.	0.000	0.000	0.000
	Fe2+	0.179	0.179	0.179	0.190	0.173	0.188	0.179	0.172	0.187	0.190	0.189	0.182	0.187	0.186	0.191	0.191
	Mn	0.003	0.001	0.003	0.002	0.002	0.002	0.002	0.003	0.002	0.003	0.004	0.003	0.002	0.003	0.004	0.003
	Ni	0.008	0.007	0.008	0.007	0.008	0.008	0.007	0.008	0.007	0.008	0.007	0.007	0.008	0.007	0.007	0.008
	Mg	1.804	1.812	1.811	1.808	1.824	1.803	1.808	1.823	1.813	1.801	1.807	1.812	1.816	1.808	1.805	1.807
	Ca	0.000	0.000	b.d.	0.003	0.002	0.000	0.001	0.001	0.001	0.001	0.001	0.001	0.000	0.001	0.001	0.001
	Na	b.d.	0.000	b.d.	b.d.	0.000	b.d.	0.000	0.000	0.000	b.d.	0.000	0.000	b.d.	0.000	b.d.	b.d.
	K	b.d.	b.d.	b.d.	b.d.	0.000	b.d.	b.d.	b.d.	0.000	b.d.	0.000	b.d.	b.d.	b.d.	b.d.	b.d.
	SumCAT	2.997	3.000	3.001	3.005	3.005	3.001	2.999	3.004	3.005	3.001	3.004	3.003	3.007	3.003	3.004	3.005
	Mg #	0.910	0.910	0.910	0.905	0.914	0.905	0.910	0.914	0.907	0.904	0.905	0.909	0.907	0.907	0.904	0.904

Abbreviations: Ol = olivine, Metam = metamorphic, Spl hrz = spinel harzburgite, b.d. = below detection limit.
Mg# calculated as (MgO/40.3) / (MgO/40.3 + FeO/71.85).

Major element composition of olivine from the Dramala spinel harzburgite and plagioclase-bearing harzburgite continued

Sample		PI2	PI2	PI2	PI2	PI2	PI2	PI2	PI2	PI2	PI2	PI2	PI2	PI2	PI2	PI2	PI2
Rock		Spl hrz	Spl hrz	Spl hrz	Spl hrz	Spl hrz	Spl hrz	Spl hrz	Spl hrz	Spl hrz	Spl hrz	Spl hrz	Spl hrz	Spl hrz	Spl hrz	Spl hrz	Spl hrz
Mineral		Ol	Ol	Ol	Ol	Ol	Ol	Ol	Ol	Ol	Ol	Ol	Ol	Ol	Ol	Ol	Ol
Type		Clast	Clast	Clast	Clast	Clast	Clast	Clast	Clast	Clast	Clast	Clast	Clast	Clast	Clast	Clast	Clast
Wt.%	SiO2	41.13	41.20	40.98	41.35	41.23	41.24	41.06	40.99	41.20	40.98	41.35	41.06	41.07	41.23	41.29	41.16
	TiO2	b.d.	b.d.	b.d.	b.d.	0.01	b.d.	0.02	b.d.	b.d.	b.d.	b.d.	b.d.	b.d.	b.d.	0.01	0.01
	Cr2O3	0.01	b.d.	0.01	0.01	b.d.	b.d.	0.02	b.d.	b.d.	0.01	0.01	b.d.	b.d.	b.d.	b.d.	0.01
	Al2O3	b.d.	b.d.	b.d.	b.d.	b.d.	0.01	b.d.	0.01	b.d.	b.d.	b.d.	0.01	0.01	0.01	0.01	0.01
	FeO	9.51	8.77	9.31	9.15	9.12	9.44	8.53	9.35	8.77	9.31	9.15	8.89	8.95	8.71	9.32	8.97
	MnO	0.17	0.10	0.17	0.14	0.20	0.12	0.11	0.10	0.10	0.17	0.14	0.16	0.17	0.11	0.07	0.17
	NiO	0.39	0.37	0.38	0.34	0.39	0.40	0.43	0.36	0.37	0.38	0.34	0.40	0.44	0.29	0.42	0.36
	MgO	49.96	49.90	49.80	49.95	49.88	49.95	50.54	49.98	49.90	49.80	49.95	50.17	50.15	50.25	50.36	50.22
	CaO	0.02	0.03	0.03	0.04	0.03	0.02	0.06	0.11	0.03	0.03	0.04	b.d.	b.d.	b.d.	0.01	0.06
	Na2O	b.d.	b.d.	0.02	b.d.	0.01	b.d.	0.01	b.d.	b.d.	0.02	b.d.	0.01	0.01	b.d.	b.d.	b.d.
	K2O	b.d.	b.d.	b.d.	b.d.	b.d.	b.d.	0.01	b.d.	b.d.	b.d.	b.d.	b.d.	0.01	b.d.	0.01	b.d.
	Total	101.19	100.37	100.70	100.98	100.87	101.18	100.79	100.90	100.37	100.70	100.98	100.70	100.81	100.60	101.50	100.97
Cations	Si	0.996	1.002	0.997	1.001	1.000	0.998	0.994	0.995	1.002	0.997	1.001	0.997	0.996	1.000	0.996	0.997
	Ti	b.d.	b.d.	b.d.	b.d.	0.000	b.d.	0.000	b.d.	b.d.	b.d.	b.d.	b.d.	b.d.	b.d.	0.000	0.000
	Cr	0.000	b.d.	0.000	0.000	b.d.	b.d.	0.000	b.d.	b.d.	0.000	0.000	b.d.	b.d.	b.d.	b.d.	0.000
	Al	b.d.	b.d.	b.d.	b.d.	b.d.	0.000	b.d.	0.000	b.d.	b.d.	b.d.	0.000	0.000	0.000	0.000	0.000
	Fe2+	0.193	0.178	0.189	0.185	0.185	0.191	0.173	0.190	0.178	0.189	0.185	0.180	0.182	0.177	0.188	0.182
	Mn	0.003	0.002	0.004	0.003	0.004	0.002	0.002	0.002	0.002	0.004	0.003	0.003	0.003	0.002	0.001	0.003
	Ni	0.008	0.007	0.007	0.007	0.008	0.008	0.008	0.007	0.007	0.007	0.007	0.008	0.009	0.006	0.008	0.007
	Mg	1.803	1.808	1.805	1.802	1.803	1.802	1.824	1.808	1.808	1.805	1.802	1.815	1.813	1.816	1.810	1.812
	Ca	0.001	0.001	0.001	0.001	0.001	0.001	0.002	0.003	0.001	0.001	0.001	b.d.	b.d.	b.d.	0.000	0.002
	Na	b.d.	b.d.	0.001	b.d.	0.000	b.d.	0.000	b.d.	b.d.	0.001	b.d.	0.000	0.000	b.d.	b.d.	b.d.
	K	b.d.	b.d.	b.d.	b.d.	b.d.	b.d.	0.000	b.d.	b.d.	b.d.	b.d.	b.d.	0.000	b.d.	0.000	b.d.
	SumCAT	3.004	2.998	3.004	2.999	3.000	3.002	3.005	3.005	2.998	3.004	2.999	3.004	3.004	3.000	3.004	3.003
	Mg #	0.904	0.910	0.905	0.907	0.907	0.904	0.914	0.905	0.910	0.905	0.907	0.910	0.909	0.911	0.906	0.909

Abbreviations: Ol = olivine, Metam = metamorphic, Spl hrz = spinel harzburgite, b.d. = below detection limit.
Mg# calculated as (MgO/40.3) / (MgO/40.3 + FeO/71.85).

Major element composition of olivine from the Dramala spinel harzburgite and plagioclase-bearing harzburgite continued

Sample		PI2	PIA91	PIA91	PIA27	PIA27	PIA27	PIA27	PIA27	PIA27	PIA27	PIA27	PIA27	PIA27	PI6	PI6	PI6
Rock		Spl hrz	Spl hrz	Spl hrz	Spl hrz	Spl hrz	Spl hrz	Spl hrz	Spl hrz	Spl hrz	Spl hrz	Spl hrz	Spl hrz	Spl hrz	Spl hrz	Spl hrz	Spl hrz
Mineral		Ol	Ol	Ol	Ol	Ol	Ol	Ol	Ol	Ol	Ol	Ol	Ol	Ol	Ol	Ol	Ol
Type		Clast	Clast	Clast	Clast	Clast	Clast	Clast	Clast	Metam	Metam	Metam	Metam	Metam	Clast	Clast	Clast
Wt.%	SiO2	41.16	40.73	40.74	40.87	41.02	40.91	41.12	41.23	40.22	40.19	40.11	39.92	40.34	42.04	41.71	41.99
	TiO2	0.02	b.d.	b.d.	b.d.	0.03	b.d.	0.01	b.d.	0.03	b.d.	0.05	b.d.	b.d.	b.d.	b.d.	b.d.
	Cr2O3	0.01	b.d.	b.d.	b.d.	0.01	0.03	b.d.	b.d.	b.d.	0.03	0.06	0.07	0.05	0.01	b.d.	0.05
	Al2O3	b.d.	0.01	b.d.	b.d.	b.d.	0.03	b.d.	b.d.	b.d.	b.d.	0.02	0.01	b.d.	0.01	b.d.	b.d.
	FeO	8.61	7.91	7.94	8.11	8.44	8.42	8.52	8.45	13.09	12.54	13.00	13.10	12.52	8.77	8.55	8.39
	MnO	0.14	0.11	0.09	0.12	0.09	0.16	0.06	0.13	0.25	0.28	0.28	0.27	0.27	0.11	0.15	0.10
	NiO	0.39	0.35	0.37	0.28	0.26	0.37	0.46	0.45	0.16	0.20	0.13	0.27	0.13	0.40	0.38	0.41
	MgO	50.24	49.23	49.40	50.36	50.63	50.38	50.57	50.55	46.71	46.60	46.37	46.65	46.51	51.83	51.98	52.00
	CaO	0.01	0.05	0.01	0.02	0.02	0.01	0.01	0.01	0.01	0.01	0.02	0.01	0.01	0.02	0.02	0.02
	Na2O	0.01	0.01	0.01	0.01	b.d.	b.d.	b.d.	b.d.	b.d.	b.d.	b.d.	b.d.	b.d.	0.03	b.d.	b.d.
	K2O	b.d.	0.01	0.01	b.d.	b.d.	b.d.	0.01	b.d.	b.d.	b.d.	0.01	b.d.	0.01	b.d.	b.d.	0.02
	Total	100.59	98.40	98.57	99.78	100.50	100.32	100.76	100.83	100.47	99.84	100.03	100.30	99.83	103.24	102.81	102.97
Cations	Si	0.998	1.006	1.005	0.997	0.995	0.995	0.996	0.997	0.997	1.000	0.998	0.993	1.003	0.994	0.990	0.994
	Ti	0.000	b.d.	b.d.	b.d.	0.000	b.d.	0.000	b.d.	0.000	b.d.	0.001	b.d.	b.d.	b.d.	b.d.	b.d.
	Cr	0.000	b.d.	b.d.	b.d.	0.000	0.001	b.d.	b.d.	b.d.	0.001	0.001	0.001	0.001	0.000	b.d.	0.001
	Al	b.d.	0.000	b.d.	b.d.	b.d.	0.001	b.d.	b.d.	b.d.	b.d.	0.000	0.000	b.d.	0.000	b.d.	b.d.
	Fe2+	0.175	0.163	0.164	0.165	0.171	0.171	0.172	0.171	0.271	0.261	0.270	0.272	0.260	0.173	0.170	0.166
	Mn	0.003	0.002	0.002	0.003	0.002	0.003	0.001	0.003	0.005	0.006	0.006	0.006	0.006	0.002	0.003	0.002
	Ni	0.008	0.007	0.007	0.006	0.005	0.007	0.009	0.009	0.003	0.004	0.003	0.005	0.003	0.008	0.007	0.008
	Mg	1.816	1.813	1.816	1.831	1.830	1.826	1.825	1.823	1.725	1.728	1.720	1.729	1.724	1.826	1.839	1.834
	Ca	0.000	0.001	0.000	0.001	0.001	0.000	0.000	0.000	0.000	0.000	0.001	0.000	0.000	0.001	0.000	0.000
	Na	0.000	0.000	0.000	0.000	b.d.	b.d.	b.d.	b.d.	b.d.	b.d.	b.d.	b.d.	b.d.	0.001	b.d.	b.d.
	K	b.d.	0.000	0.000	b.d.	b.d.	b.d.	0.000	b.d.	b.d.	b.d.	0.000	b.d.	0.000	b.d.	b.d.	0.000
	SumCAT	3.001	2.994	2.995	3.003	3.005	3.004	3.004	3.003	3.003	3.000	3.000	3.007	2.997	3.006	3.010	3.006
	Mg #	0.912	0.917	0.917	0.917	0.914	0.914	0.914	0.914	0.864	0.869	0.864	0.864	0.869	0.913	0.916	0.917

Abbreviations: Ol = olivine, Metam = metamorphic, Spl hrz = spinel harzburgite, b.d. = below detection limit.
Mg# calculated as (MgO/40.3) / (MgO/40.3 + FeO/71.85).

Major element composition of olivine from the Dramala spinel harzburgite and plagioclase-bearing harzburgite continued

Sample		PI6	PI6	PI6	PI6	PI6	PI6	PI6	PI6	PI6	PI6	PI6	PI6	PI6	PI6	PI6	PIA44
Rock		Spl hrz	Spl hrz	Spl hrz	Spl hrz	Spl hrz	Spl hrz	Spl hrz	Spl hrz	Spl hrz	Spl hrz	Spl hrz	Spl hrz	Spl hrz	Spl hrz	Spl hrz	Spl hrz
Mineral		Ol	Ol	Ol	Ol	Ol	Ol	Ol	Ol	Ol	Ol	Ol	Ol	Ol	Ol	Ol	Ol
Type		Clast	Clast	Clast	Clast	Clast	Clast	Clast	Clast	Clast	Clast	Clast	Clast	Clast	Clast	Clast	Clast
Wt.%	SiO2	42.20	42.19	41.90	42.13	42.02	42.10	41.82	41.77	41.96	42.02	41.92	41.91	41.81	41.89	41.53	40.57
	TiO2	b.d.	b.d.	b.d.	0.02	b.d.	b.d.	0.03	b.d.	b.d.	0.01	0.01	b.d.	0.01	b.d.	0.04	b.d.
	Cr2O3	b.d.	0.06	b.d.	0.01	0.01	b.d.	b.d.	b.d.	b.d.	0.02	b.d.	b.d.	b.d.	0.02	b.d.	b.d.
	Al2O3	b.d.	0.01	b.d.	b.d.	b.d.	b.d.	b.d.	b.d.	0.01	b.d.	b.d.	b.d.	0.02	b.d.	b.d.	b.d.
	FeO	8.72	8.67	8.64	8.78	8.50	8.49	8.62	8.45	8.63	8.59	8.60	8.71	8.59	8.73	8.71	8.43
	MnO	0.14	0.09	0.13	0.12	0.14	0.15	0.13	0.14	0.10	0.12	0.15	0.11	0.13	0.15	0.11	0.05
	NiO	0.40	0.43	0.39	0.38	0.41	0.40	0.46	0.46	0.43	0.41	0.43	0.41	0.43	0.42	0.46	0.06
	MgO	51.59	51.94	51.90	52.17	51.90	52.15	52.08	51.56	52.13	52.12	52.16	52.10	51.93	52.15	52.20	50.09
	CaO	b.d.	0.02	0.01	0.01	0.02	0.03	0.01	0.03	0.01	0.02	0.02	0.01	0.02	0.03	0.02	0.01
	Na2O	0.01	b.d.	b.d.	b.d.	b.d.	b.d.	b.d.	b.d.	b.d.	b.d.	b.d.	b.d.	b.d.	0.01	b.d.	b.d.
	K2O	b.d.	b.d.	b.d.	b.d.	b.d.	0.01	0.01	b.d.	0.01	0.00	0.02	b.d.	b.d.	b.d.	b.d.	b.d.
	Total	103.09	103.42	102.98	103.62	103.05	103.36	103.15	102.46	103.27	103.34	103.31	103.26	102.98	103.43	103.07	99.21
Cations	Si	0.998	0.995	0.993	0.992	0.994	0.993	0.990	0.994	0.991	0.992	0.990	0.991	0.991	0.989	0.985	0.996
	Ti	b.d.	b.d.	b.d.	0.000	b.d.	b.d.	0.000	b.d.	b.d.	0.000	0.000	b.d.	0.000	b.d.	0.001	b.d.
	Cr	b.d.	0.001	b.d.	0.000	0.000	b.d.	b.d.	b.d.	b.d.	0.000	b.d.	b.d.	b.d.	0.000	b.d.	b.d.
	Al	b.d.	0.000	b.d.	b.d.	b.d.	b.d.	b.d.	b.d.	0.000	b.d.	b.d.	b.d.	0.001	b.d.	b.d.	b.d.
	Fe2+	0.173	0.171	0.171	0.173	0.168	0.167	0.171	0.168	0.171	0.170	0.170	0.172	0.170	0.172	0.173	0.173
	Mn	0.003	0.002	0.003	0.002	0.003	0.003	0.003	0.003	0.002	0.002	0.003	0.002	0.003	0.003	0.002	0.001
	Ni	0.008	0.008	0.007	0.007	0.008	0.008	0.009	0.009	0.008	0.008	0.008	0.008	0.008	0.008	0.009	0.001
	Mg	1.819	1.826	1.833	1.831	1.831	1.834	1.837	1.829	1.836	1.834	1.837	1.836	1.834	1.836	1.845	1.833
	Ca	b.d.	0.000	0.000	0.000	0.001	0.001	0.000	0.001	0.000	0.000	0.001	0.000	0.001	0.001	0.000	0.000
	Na	0.000	b.d.	b.d.	b.d.	b.d.	b.d.	b.d.	b.d.	b.d.	b.d.	b.d.	b.d.	b.d.	0.000	b.d.	b.d.
	K	b.d.	b.d.	b.d.	b.d.	b.d.	0.000	0.000	b.d.	0.000	0.000	0.000	b.d.	b.d.	b.d.	b.d.	b.d.
	SumCAT	3.001	3.004	3.007	3.007	3.005	3.007	3.010	3.005	3.009	3.007	3.010	3.009	3.008	3.010	3.015	3.004
	Mg #	0.913	0.914	0.915	0.914	0.916	0.916	0.915	0.916	0.915	0.915	0.915	0.914	0.915	0.914	0.914	0.914

Abbreviations: Ol = olivine, Metam = metamorphic, Spl hrz = spinel harzburgite, b.d. = below detection limit.
Mg# calculated as (MgO/40.3) / (MgO/40.3 + FeO/71.85).

Major element composition of olivine from the Dramala spinel harzburgite and plagioclase-bearing harzburgite continued

Sample		PIA44	PIA44	PIA44	PIA44	PIA120	PIA120	PIA120	PIA120	PIA120	PIA120	PIA120	PIA120
Rock		Spl hrz	Spl hrz	Spl hrz	Spl hrz	Pl-bear hrz	Pl-bear hrz	Pl-bear hrz	Pl-bear hrz	Pl-bear hrz	Pl-bear hrz	Pl-bear hrz	Pl-bear hrz
Mineral		Ol	Ol	Ol	Ol	Ol	Ol	Ol	Ol	Ol	Ol	Ol	Ol
Type		Clast	Clast	Clast	Clast	Clast	Clast	Clast	Clast	Clast	Clast	Clast	Clast
Wt.%	SiO2	40.52	40.56	40.60	40.64	40.87	40.73	40.54	40.78	41.36	40.76	40.88	40.69
	TiO2	b.d.	b.d.	b.d.	0.01	0.02	b.d.	0.01	0.01	0.03	b.d.	b.d.	b.d.
	Cr2O3	b.d.	b.d.	0.05	0.02	0.02	0.05	0.10	b.d.	0.01	0.01	0.02	0.03
	Al2O3	b.d.	0.01	b.d.	b.d.	0.01	b.d.	0.02	0.01	0.02	0.01	0.02	b.d.
	FeO	8.30	8.36	8.57	8.55	9.97	10.40	9.80	10.23	9.97	10.52	10.17	10.12
	MnO	0.14	0.14	0.14	0.04	0.15	0.09	0.15	0.11	0.16	0.18	0.17	0.17
	NiO	0.11	0.11	0.18	0.45	0.31	0.37	0.41	0.47	0.41	0.32	0.23	0.29
	MgO	50.42	49.87	50.27	50.57	49.59	49.65	49.33	49.78	49.28	48.84	49.48	49.79
	CaO	b.d.	0.02	0.01	b.d.	0.01	b.d.	0.02	0.02	b.d.	0.02	b.d.	0.03
	Na2O	b.d.	b.d.	0.02	b.d.	b.d.	b.d.	b.d.	0.02	b.d.	0.01	b.d.	b.d.
	K2O	b.d.	b.d.	b.d.	b.d.	b.d.	b.d.	0.01	b.d.	0.01	0.01	0.01	b.d.
	Total	99.49	99.08	99.84	100.28	100.95	101.29	100.39	101.43	101.25	100.68	100.98	101.12
Cations	Si	0.992	0.997	0.992	0.990	0.994	0.990	0.992	0.989	1.002	0.997	0.995	0.989
	Ti	b.d.	b.d.	b.d.	0.000	0.000	b.d.	0.000	0.000	0.001	b.d.	b.d.	b.d.
	Cr	b.d.	b.d.	0.001	0.000	0.000	0.001	0.002	b.d.	0.000	0.000	0.000	0.001
	Al	b.d.	0.000	b.d.	b.d.	0.000	b.d.	0.001	0.000	0.001	0.000	0.001	b.d.
	Fe2+	0.170	0.172	0.175	0.174	0.203	0.211	0.201	0.208	0.202	0.215	0.207	0.206
	Mn	0.003	0.003	0.003	0.001	0.003	0.002	0.003	0.002	0.003	0.004	0.004	0.004
	Ni	0.002	0.002	0.003	0.009	0.006	0.007	0.008	0.009	0.008	0.006	0.005	0.006
	Mg	1.840	1.827	1.831	1.836	1.798	1.798	1.799	1.800	1.780	1.780	1.794	1.805
	Ca	b.d.	0.001	0.000	b.d.	0.000	b.d.	0.001	0.001	b.d.	0.001	b.d.	0.001
	Na	b.d.	b.d.	0.001	b.d.	b.d.	b.d.	b.d.	0.001	b.d.	0.000	b.d.	b.d.
	K	b.d.	b.d.	b.d.	b.d.	b.d.	b.d.	0.000	b.d.	0.000	0.000	0.000	b.d.
	SumCAT	3.008	3.003	3.008	3.010	3.005	3.010	3.007	3.011	2.997	3.003	3.005	3.010
	Mg #	0.915	0.914	0.913	0.913	0.899	0.895	0.900	0.897	0.898	0.892	0.897	0.898

Abbreviations: Ol = olivine, Metam = metamorphic, Spl hrz = spinel harzburgite, Pl-bear hrz = plagioclase-bearing harzburgite, b.d. = below detection limit.
Mg# calculated as (MgO/40.3) / (MgO/40.3 + FeO/71.85).

Major element composition of olivine from the Dramala spinel harzburgite and plagioclase-bearing harzburgite continued

Sample		PIA120	PIA120	PIA109	PIA109	PIA109	PIA109	PIA109	PIA109	PIA109	PIA109	PIA109
Rock		Pl-bear hrz	Pl-bear hrz	Pl-bear hrz	Pl-bear hrz	Pl-bear hrz	Pl-bear hrz	Pl-bear hrz	Pl-bear hrz	Pl-bear hrz	Pl-bear hrz	Pl-bear hrz
Mineral		Ol	Ol	Ol	Ol	Ol	Ol	Ol	Ol	Ol	Ol	Ol
Type		Clast	Clast	Clast	Clast	Clast	Clast	Clast	Clast	Clast	Clast	Clast
Wt.%	SiO2	41.79	40.87	41.67	41.61	41.57	41.31	41.52	41.52	41.53	41.27	41.44
	TiO2	0.01	b.d.	b.d.	0.02	0.05	0.01	0.03	b.d.	0.01	0.02	b.d.
	Cr2O3	0.02	b.d.	b.d.	b.d.	b.d.	0.02	0.03	0.06	0.03	b.d.	b.d.
	Al2O3	0.03	0.02	b.d.	0.01	b.d.	b.d.	b.d.	b.d.	b.d.	b.d.	b.d.
	FeO	9.90	10.02	9.88	9.50	9.88	9.95	9.55	9.63	9.29	9.68	9.53
	MnO	0.14	0.11	0.12	0.09	0.19	0.17	0.18	0.13	0.17	0.15	0.10
	NiO	0.44	0.43	0.35	0.39	0.43	0.33	0.35	0.38	0.39	0.37	0.37
	MgO	49.34	49.23	50.26	50.79	50.48	49.81	50.14	49.90	50.39	50.16	50.09
	CaO	b.d.	0.02	b.d.	b.d.	0.03	0.01	0.02	0.01	0.03	0.02	0.03
	Na2O	0.03	0.01	b.d.	b.d.	0.02	b.d.	b.d.	b.d.	b.d.	b.d.	b.d.
	K2O	b.d.	0.01	0.01	b.d.	b.d.	b.d.	b.d.	b.d.	0.01	0.01	0.02
	Total	101.70	100.72	102.29	102.41	102.65	101.61	101.82	101.63	101.85	101.68	101.58
Cations	Si	1.007	0.997	0.999	0.995	0.994	0.998	0.999	1.001	0.998	0.995	0.999
	Ti	0.000	b.d.	b.d.	0.000	0.001	0.000	0.001	b.d.	0.000	0.000	b.d.
	Cr	0.000	b.d.	b.d.	b.d.	b.d.	0.000	0.001	0.001	0.001	b.d.	b.d.
	Al	0.001	0.001	b.d.	0.000	b.d.	b.d.	b.d.	b.d.	b.d.	b.d.	b.d.
	Fe2+	0.199	0.204	0.198	0.190	0.198	0.201	0.192	0.194	0.187	0.195	0.192
	Mn	0.003	0.002	0.002	0.002	0.004	0.003	0.004	0.003	0.003	0.003	0.002
	Ni	0.009	0.008	0.007	0.007	0.008	0.006	0.007	0.007	0.008	0.007	0.007
	Mg	1.772	1.790	1.795	1.810	1.799	1.793	1.798	1.793	1.805	1.803	1.800
	Ca	b.d.	0.001	b.d.	b.d.	0.001	0.000	0.001	0.000	0.001	0.001	0.001
	Na	0.001	0.000	b.d.	b.d.	0.001	b.d.	b.d.	b.d.	b.d.	b.d.	b.d.
	K	b.d.	0.000	0.000	b.d.	b.d.	b.d.	b.d.	b.d.	0.000	0.000	0.001
	SumCAT	2.993	3.003	3.001	3.005	3.005	3.002	3.000	2.999	3.002	3.005	3.001
	Mg #	0.899	0.898	0.901	0.905	0.901	0.899	0.903	0.902	0.906	0.902	0.904

Abbreviations: Ol = olivine, Metam = metamorphic, Pl-bear hrz = plagioclase-bearing harzburgite, b.d. = below detection limit.
Mg# calculated as (MgO/40.3) / (MgO/40.3 + FeO/71.85).

Major element composition of olivine from the Dramala spinel harzburgite and plagioclase-bearing harzburgite continued

Sample		PIA109	PIA109	PIA109	PIA109	PIA109	PIA109	PIA109	PIA109	PIA109	PIA109	PIA109
Rock		Pl-bear hrz	Pl-bear hrz	Pl-bear hrz	Pl-bear hrz	Pl-bear hrz	Pl-bear hrz	Pl-bear hrz	Pl-bear hrz	Pl-bear hrz	Pl-bear hrz	Pl-bear hrz
Mineral		Ol	Ol	Ol	Ol	Ol	Ol	Ol	Ol	Ol	Ol	Ol
Type		Clast	Clast	Clast	Clast	Clast	Clast	Clast	Clast	Clast	Clast	Clast
Wt.%	SiO2	41.39	41.56	41.41	41.68	41.46	41.22	41.16	41.16	40.99	41.01	40.72
	TiO2	0.02	0.01	0.01	0.04	0.02	0.04	0.02	0.02	0.03	0.01	b.d.
	Cr2O3	b.d.	0.01	b.d.	b.d.	b.d.	0.03	b.d.	0.05	0.03	0.02	b.d.
	Al2O3	b.d.	b.d.	0.01	b.d.	0.02	b.d.	b.d.	0.01	0.29	0.05	0.19
	FeO	9.87	9.39	9.63	9.85	9.67	9.72	10.02	10.12	10.79	10.62	10.60
	MnO	0.12	0.13	0.16	0.15	0.10	0.21	0.17	0.15	0.15	0.12	0.11
	NiO	0.40	0.41	0.39	0.40	0.38	0.42	0.40	0.40	0.00	0.00	0.00
	MgO	50.18	50.74	50.48	50.42	50.05	50.37	50.46	50.11	49.97	50.03	49.86
	CaO	0.03	0.02	0.03	0.01	0.02	0.02	0.01	0.02	0.00	0.01	0.01
	Na2O	b.d.	0.02	0.02	0.01	0.02	b.d.	b.d.	b.d.	b.d.	b.d.	b.d.
	K2O	b.d.	b.d.	b.d.	b.d.	b.d.	0.01	b.d.	b.d.	b.d.	b.d.	b.d.
	Total	102.01	102.29	102.14	102.56	101.74	102.04	102.24	102.04	102.25	101.87	101.49
Cations	Si	0.995	0.995	0.994	0.997	0.998	0.992	0.989	0.992	0.987	0.990	0.987
	Ti	0.000	0.000	0.000	0.001	0.000	0.001	0.000	0.000	0.001	0.000	b.d.
	Cr	b.d.	0.000	b.d.	b.d.	b.d.	0.001	b.d.	0.001	0.001	0.000	b.d.
	Al	b.d.	b.d.	0.000	b.d.	0.001	b.d.	b.d.	0.000	0.008	0.001	0.005
	Fe2+	0.199	0.188	0.193	0.197	0.195	0.196	0.201	0.204	0.217	0.214	0.215
	Mn	0.002	0.003	0.003	0.003	0.002	0.004	0.003	0.003	0.003	0.002	0.002
	Ni	0.008	0.008	0.008	0.008	0.007	0.008	0.008	0.008	0.000	0.000	0.000
	Mg	1.799	1.810	1.806	1.797	1.796	1.806	1.808	1.799	1.792	1.800	1.801
	Ca	0.001	0.001	0.001	0.000	0.001	0.001	0.000	0.001	0.000	0.000	0.000
	Na	b.d.	0.001	0.001	0.000	0.001	b.d.	b.d.	b.d.	b.d.	b.d.	b.d.
	K	b.d.	b.d.	b.d.	b.d.	b.d.	0.000	b.d.	b.d.	b.d.	b.d.	b.d.
	SumCAT	3.004	3.005	3.006	3.003	3.001	3.008	3.010	3.007	3.009	3.009	3.010
	Mg #	0.901	0.906	0.903	0.901	0.902	0.902	0.900	0.898	0.892	0.894	0.893

Abbreviations: Ol = olivine, Metam = metamorphic, Pl-bear hrz = plagioclase-bearing harzburgite, b.d. = below detection limit.
Mg# calculated as (MgO/40.3) / (MgO/40.3 + FeO/71.85).

Major element composition of orthopyroxene from the Dramala spinel harzburgite and plagioclase-bearing harzburgite

Sample		PI2	PI2	PI2	PI2	PI2	PI2	PI2	PI2	PI2	PI2	PI2	PI2	PI2	PI2	PI2	PI2
Rock		Spl hrz	Spl hrz	Spl hrz	Spl hrz	Spl hrz	Spl hrz	Spl hrz	Spl hrz	Spl hrz	Spl hrz	Spl hrz	Spl hrz	Spl hrz	Spl hrz	Spl hrz	Spl hrz
Mineral		Opx	Opx	Opx	Opx	Opx	Opx	Opx	Opx	Opx	Opx	Opx	Opx	Opx	Opx	Opx	Opx
Type		Exs Cpx	Exs Cpx	Exs Cpx	Cl core	Cl core	Cl core	Cl core	Cl core	Cl core	Cl core	Cl core	Cl core	Cl core	Cl core	Cl core	Cl core
Wt.%	**SiO2**	53.25	53.03	52.69	55.55	56.24	56.11	56.46	56.53	56.37	56.31	56.25	56.36	56.52	56.03	56.11	56.57
	TiO2	0.08	0.05	0.08	0.01	b.d.	0.03	b.d.	0.03	0.03	b.d.	0.01	0.05	b.d.	0.02	0.01	0.03
	Cr2O3	0.89	0.96	0.94	0.78	0.55	0.60	0.65	0.66	0.64	0.71	0.65	0.64	0.61	0.63	0.64	0.63
	Al2O3	2.63	2.85	2.86	3.04	2.71	2.98	3.04	3.05	2.96	3.06	3.07	3.10	3.16	3.08	3.10	3.16
	FeO	1.73	1.85	1.97	5.46	5.72	5.80	5.91	5.75	5.92	5.74	5.75	5.76	5.84	5.97	5.69	5.74
	MnO	0.03	0.03	0.09	0.10	0.21	0.15	0.17	0.15	0.15	0.17	0.18	0.17	0.11	0.09	0.08	0.13
	NiO	0.08	0.04	0.03	0.16	0.10	0.12	0.05	0.07	0.01	0.09	0.08	0.06	0.07	0.01	0.06	0.11
	MgO	17.11	16.98	17.02	33.54	34.25	33.72	33.99	33.82	34.01	33.78	33.45	34.02	33.89	33.92	33.10	33.87
	CaO	25.02	24.74	24.59	1.56	0.61	0.77	0.69	0.76	0.83	0.72	0.96	0.73	0.72	0.88	1.99	0.65
	Na2O	0.04	0.02	0.01	b.d.	0.01	0.01	0.01	b.d.	b.d.	0.01	0.02	b.d.	0.02	0.01	0.01	b.d.
	K2O	0.01	b.d.	0.01	0.01	b.d.	b.d.	b.d.	b.d.	b.d.	0.02	0.01	b.d.	b.d.	b.d.	0.01	0.01
	Total	100.87	100.55	100.29	100.21	100.40	100.29	100.97	100.82	100.92	100.61	100.43	100.89	100.94	100.64	100.80	100.90
Cations	**Si**	1.922	1.920	1.914	1.917	1.932	1.930	1.929	1.933	1.928	1.930	1.932	1.926	1.930	1.922	1.926	1.932
	Ti	0.002	0.001	0.002	0.000	b.d.	0.001	b.d.	0.001	0.001	b.d.	0.000	0.001	b.d.	0.001	0.000	0.001
	Cr	0.025	0.027	0.027	0.021	0.015	0.016	0.018	0.018	0.017	0.019	0.018	0.017	0.016	0.017	0.017	0.017
	Al	0.112	0.122	0.122	0.124	0.110	0.121	0.122	0.123	0.119	0.124	0.124	0.125	0.127	0.125	0.125	0.127
	Fe2+	0.052	0.056	0.060	0.158	0.164	0.167	0.169	0.164	0.169	0.165	0.165	0.165	0.167	0.171	0.163	0.164
	Mn	0.001	0.001	0.003	0.003	0.006	0.004	0.005	0.004	0.004	0.005	0.005	0.005	0.003	0.003	0.002	0.004
	Ni	0.002	0.001	0.001	0.004	0.003	0.003	0.001	0.002	0.000	0.002	0.002	0.002	0.002	0.000	0.002	0.003
	Mg	0.921	0.916	0.922	1.725	1.753	1.729	1.731	1.723	1.734	1.726	1.713	1.733	1.725	1.735	1.693	1.724
	Ca	0.968	0.959	0.957	0.058	0.022	0.028	0.025	0.028	0.030	0.026	0.035	0.027	0.026	0.032	0.073	0.024
	Na	0.003	0.001	0.001	b.d.	0.001	0.001	0.001	b.d.	b.d.	0.001	0.001	b.d.	0.001	0.001	0.001	b.d.
	K	0.000	b.d.	0.000	0.000	b.d.	b.d.	b.d.	b.d.	b.d.	0.001	0.000	b.d.	b.d.	b.d.	0.000	0.000
	Sum	4.009	4.005	4.009	4.010	4.006	4.001	4.001	3.996	4.003	3.999	3.997	4.001	3.999	4.007	4.003	3.996
	Mg #	0.946	0.942	0.939	0.916	0.914	0.912	0.911	0.913	0.911	0.913	0.912	0.913	0.912	0.910	0.912	0.913

Abbreviations: Opx = orthopyroxene, Spl hrz = spinel harzburgite, Exs Cpx = exsolution lamellae in Cpx, Cl core = clast core, b.d. = below detection limit.
Mg# calculated as (MgO/40.3) / (MgO/40.3 + FeO/71.85).

Major element composition of orthopyroxene from the Dramala spinel harzburgite and plagioclase-bearing harzburgite continued

Sample		PI2	PI2	PI2	PI2	PI2	PI2	PI2	PI2	PI2	PI2	PI2	PI2	PI2	PI2	PI2	PI2
Rock		Spl hrz	Spl hrz	Spl hrz	Spl hrz	Spl hrz	Spl hrz	Spl hrz	Spl hrz	Spl hrz	Spl hrz	Spl hrz	Spl hrz	Spl hrz	Spl hrz	Spl hrz	Spl hrz
Mineral		Opx	Opx	Opx	Opx	Opx	Opx	Opx	Opx	Opx	Opx	Opx	Opx	Opx	Opx	Opx	Opx
Type		Cl core	Cl core	Cl core	Cl core	Cl core	Cl core	Cl core	Cl core	Cl core	Cl core	Cl core	Cl core	Cl core	Cl core	Cl core	Cl core
Wt.%	**SiO2**	56.29	56.28	55.95	56.20	56.13	56.28	56.14	56.16	56.40	56.48	56.24	56.26	56.29	56.17	56.32	55.97
	TiO2	b.d.	0.02	0.03	0.02	b.d.	0.02	0.03	0.01	0.03	b.d.	0.03	0.01	0.03	b.d.	0.01	0.01
	Cr2O3	0.73	0.71	0.73	0.65	0.69	0.74	0.71	0.69	0.68	0.64	0.73	0.78	0.66	0.73	0.69	0.70
	Al2O3	3.14	3.04	3.02	3.03	3.09	3.05	2.98	3.10	2.93	3.00	3.09	3.07	3.06	3.09	2.94	3.13
	FeO	5.65	5.85	5.58	5.76	5.75	5.86	5.90	5.78	5.55	5.69	5.70	5.75	5.50	5.49	5.66	5.65
	MnO	0.17	0.12	0.17	0.14	0.21	0.17	0.21	0.13	0.12	0.05	0.13	0.12	0.12	0.19	0.16	0.17
	NiO	0.06	0.11	0.06	0.07	0.06	0.06	0.09	0.04	0.04	0.09	0.06	0.07	0.08	0.07	0.07	0.04
	MgO	33.44	34.04	33.38	33.87	33.92	33.88	33.74	33.80	33.02	33.72	34.14	33.42	33.24	33.25	33.12	33.78
	CaO	1.39	0.65	1.53	0.66	0.70	0.70	1.08	0.66	1.53	0.90	0.66	0.97	1.62	1.51	1.55	0.77
	Na2O	b.d.	0.01	b.d.	b.d.	0.02	0.02	0.01	0.03	b.d.	0.01	b.d.	0.04	0.02	b.d.	0.01	0.01
	K2O	0.01	0.02	b.d.	0.01	b.d.	b.d.	0.02	0.01	b.d.	b.d.	0.01	b.d.	b.d.	0.02	0.01	b.d.
	Total	100.88	100.85	100.45	100.41	100.57	100.78	100.91	100.41	100.30	100.58	100.79	100.49	100.62	100.52	100.54	100.23
Cations	**Si**	1.927	1.926	1.925	1.930	1.926	1.927	1.924	1.928	1.940	1.935	1.924	1.932	1.931	1.930	1.935	1.926
	Ti	b.d.	0.001	0.001	0.001	b.d.	0.001	0.001	0.000	0.001	b.d.	0.001	0.000	0.001	b.d.	0.000	0.000
	Cr	0.020	0.019	0.020	0.018	0.019	0.020	0.019	0.019	0.018	0.017	0.020	0.021	0.018	0.020	0.019	0.019
	Al	0.127	0.123	0.122	0.123	0.125	0.123	0.120	0.125	0.119	0.121	0.125	0.124	0.124	0.125	0.119	0.127
	Fe2+	0.162	0.167	0.161	0.165	0.165	0.168	0.169	0.166	0.160	0.163	0.163	0.165	0.158	0.158	0.163	0.163
	Mn	0.005	0.003	0.005	0.004	0.006	0.005	0.006	0.004	0.003	0.001	0.004	0.003	0.003	0.006	0.005	0.005
	Ni	0.002	0.003	0.002	0.002	0.002	0.002	0.002	0.001	0.001	0.002	0.002	0.002	0.002	0.002	0.002	0.001
	Mg	1.706	1.736	1.712	1.733	1.734	1.729	1.723	1.730	1.693	1.722	1.741	1.710	1.700	1.702	1.696	1.732
	Ca	0.051	0.024	0.056	0.024	0.026	0.026	0.040	0.024	0.056	0.033	0.024	0.036	0.060	0.056	0.057	0.028
	Na	b.d.	0.001	b.d.	b.d.	0.001	0.001	0.001	0.002	b.d.	0.001	b.d.	0.003	0.001	b.d.	0.001	0.001
	K	0.000	0.001	b.d.	0.000	b.d.	b.d.	0.001	0.000	b.d.	b.d.	0.000	b.d.	b.d.	0.001	0.000	b.d.
	Sum	4.000	4.004	4.003	4.000	4.003	4.001	4.006	4.000	3.991	3.996	4.003	3.997	3.998	3.998	3.996	4.002
	Mg #	0.913	0.912	0.914	0.913	0.913	0.912	0.911	0.912	0.914	0.914	0.914	0.912	0.915	0.915	0.913	0.914

Abbreviations: Opx = orthopyroxene, Spl hrz = spinel harzburgite, Cl core = clast core, b.d. = below detection limit.
Mg# calculated as (MgO/40.3) / (MgO/40.3 + FeO/71.85).

Major element composition of orthopyroxene from the Dramala spinel harzburgite and plagioclase-bearing harzburgite continued

Sample		PI2	PI2	PI2	PI2	PI2	PI2	PI2	PI2	PI2	PI2	PI2	PI2	PI2	PI2	PI2	PI2
Rock		Spl hrz	Spl hrz	Spl hrz	Spl hrz	Spl hrz	Spl hrz	Spl hrz	Spl hrz	Spl hrz	Spl hrz	Spl hrz	Spl hrz	Spl hrz	Spl hrz	Spl hrz	Spl hrz
Mineral		Opx	Opx	Opx	Opx	Opx	Opx	Opx	Opx	Opx	Opx	Opx	Opx	Opx	Opx	Opx	Opx
Type		Cl core	Cl core	Cl core	Cl core	Cl core	Cl core	Cl core	Cl core	Cl core	Cl core	Cl core	Cl core	Cl core	Cl core	Cl core	Cl core
Wt.%	SiO2	55.98	56.00	56.14	56.15	55.68	56.23	56.09	55.84	55.91	56.10	55.99	56.19	56.33	56.22	56.11	56.20
	TiO2	0.02	0.01	0.03	0.03	b.d.	0.01	0.05	0.02	0.01	0.01	b.d.	0.02	b.d.	b.d.	0.02	0.02
	Cr2O3	0.76	0.67	0.68	0.75	0.73	0.72	0.69	0.78	0.64	0.75	0.74	0.64	0.70	0.69	0.74	0.67
	Al2O3	2.97	3.10	3.10	3.11	3.07	3.05	3.10	3.16	3.16	3.12	3.00	3.14	3.09	3.12	3.10	3.15
	FeO	5.55	5.80	5.76	6.00	5.19	5.89	5.81	5.67	5.94	5.77	5.78	5.66	5.64	5.52	5.73	5.93
	MnO	0.11	0.14	0.12	0.10	0.11	0.19	0.08	0.10	0.14	0.12	0.15	0.14	0.17	0.16	0.11	0.07
	NiO	0.07	0.04	0.10	0.08	0.07	0.06	0.09	0.13	0.08	0.12	0.10	0.08	0.11	0.13	0.10	0.08
	MgO	32.87	33.70	33.65	34.12	31.81	33.63	33.72	33.41	33.75	33.32	33.71	33.83	33.70	33.25	33.59	33.69
	CaO	2.16	0.72	0.70	0.61	3.40	1.19	0.78	0.73	0.73	1.32	0.90	0.70	0.90	1.58	0.77	0.66
	Na2O	b.d.	b.d.	b.d.	b.d.	0.01	0.02	0.01	0.02	b.d.	0.01	b.d.	0.01	b.d.	b.d.	b.d.	b.d.
	K2O	b.d.	0.01	b.d.	b.d.	b.d.	b.d.	b.d.	b.d.	b.d.	b.d.	0.01	0.01	b.d.	0.01	b.d.	b.d.
	Total	100.49	100.19	100.28	100.95	100.07	100.99	100.42	99.86	100.36	100.64	100.38	100.42	100.64	100.68	100.27	100.47
Cations	Si	1.928	1.928	1.930	1.921	1.929	1.925	1.927	1.928	1.923	1.926	1.926	1.928	1.930	1.929	1.930	1.929
	Ti	0.001	0.000	0.001	0.001	b.d.	0.000	0.001	0.001	0.000	0.000	b.d.	0.001	b.d.	b.d.	0.001	0.001
	Cr	0.021	0.018	0.018	0.020	0.020	0.019	0.019	0.021	0.017	0.020	0.020	0.017	0.019	0.019	0.020	0.018
	Al	0.121	0.126	0.126	0.125	0.125	0.123	0.126	0.129	0.128	0.126	0.122	0.127	0.125	0.126	0.126	0.127
	Fe2+	0.160	0.167	0.166	0.172	0.150	0.169	0.167	0.164	0.171	0.166	0.166	0.162	0.162	0.158	0.165	0.170
	Mn	0.003	0.004	0.003	0.003	0.003	0.006	0.002	0.003	0.004	0.003	0.004	0.004	0.005	0.005	0.003	0.002
	Ni	0.002	0.001	0.003	0.002	0.002	0.002	0.002	0.004	0.002	0.003	0.003	0.002	0.003	0.004	0.003	0.002
	Mg	1.687	1.729	1.724	1.740	1.642	1.716	1.727	1.720	1.730	1.705	1.728	1.730	1.721	1.700	1.722	1.724
	Ca	0.080	0.027	0.026	0.022	0.126	0.044	0.029	0.027	0.027	0.049	0.033	0.026	0.033	0.058	0.028	0.024
	Na	b.d.	b.d.	b.d.	b.d.	0.001	0.001	0.001	0.001	b.d.	0.001	b.d.	0.001	b.d.	b.d.	b.d.	b.d.
	K	b.d.	0.000	b.d.	b.d.	b.d.	b.d.	b.d.	b.d.	b.d.	b.d.	0.000	0.000	b.d.	0.000	b.d.	b.d.
	Sum	4.001	4.000	3.997	4.006	3.999	4.004	4.000	3.997	4.004	4.000	4.003	3.999	3.998	3.999	3.997	3.998
	Mg #	0.913	0.912	0.912	0.910	0.916	0.911	0.912	0.913	0.910	0.911	0.912	0.914	0.914	0.915	0.913	0.910

Abbreviations: Opx = orthopyroxene, Spl hrz = spinel harzburgite, Cl core = clast core, b.d. = below detection limit.
Mg# calculated as (MgO/40.3) / (MgO/40.3 + FeO/71.85).

Major element composition of orthopyroxene from the Dramala spinel harzburgite and plagioclase-bearing harzburgite continued

Sample		PI2	PI2	PI2	PI2	PI2	PI2	PI2	PI2	PI2	PI2	PI2	PI2	PI2	PI2	PI2	PI2
Rock		Spl hrz	Spl hrz	Spl hrz	Spl hrz	Spl hrz	Spl hrz	Spl hrz	Spl hrz	Spl hrz	Spl hrz	Spl hrz	Spl hrz	Spl hrz	Spl hrz	Spl hrz	Spl hrz
Mineral		Opx	Opx	Opx	Opx	Opx	Opx	Opx	Opx	Opx	Opx	Opx	Opx	Opx	Opx	Opx	Opx
Type		Cl core	Cl core	Cl core	Cl core	Cl core	Cl core	Cl core	Cl core	Cl core	Cl core	Cl core	Cl core	Cl core	Cl core	Cl core	Cl core
Wt.%	SiO2	55.96	56.29	56.09	55.98	56.30	56.09	56.20	56.25	56.15	56.14	56.27	56.02	56.07	56.23	56.04	56.04
	TiO2	0.04	b.d.	0.05	0.04	b.d.	0.03	b.d.	0.04	0.02	0.02	0.03	0.02	0.01	0.04	0.01	0.03
	Cr2O3	0.73	0.66	0.67	0.66	0.72	0.67	0.74	0.72	0.67	0.68	0.66	0.66	0.70	0.68	0.66	0.69
	Al2O3	3.12	3.08	3.08	3.07	3.06	3.12	2.97	3.08	3.11	3.03	3.05	3.11	3.06	3.03	3.10	2.97
	FeO	5.68	5.81	5.62	5.83	5.97	5.74	5.72	5.46	5.87	5.51	5.67	5.68	5.83	5.72	5.57	5.80
	MnO	0.15	0.15	0.13	0.13	0.11	0.14	0.20	0.09	0.17	0.14	0.06	0.13	0.09	0.17	0.12	0.12
	NiO	0.08	0.07	0.08	0.16	0.09	0.08	0.08	0.10	0.12	0.08	0.16	0.08	0.07	0.11	0.09	0.11
	MgO	33.43	33.50	33.84	34.06	33.74	33.93	33.91	33.38	33.94	32.89	33.81	33.06	33.54	33.86	33.74	33.25
	CaO	0.97	0.79	0.68	0.71	0.72	0.76	0.71	1.30	0.59	1.79	0.73	1.34	1.29	0.76	0.72	1.76
	Na2O	b.d.	0.02	b.d.	0.01	0.02	0.01	0.02	b.d.	b.d.	b.d.	b.d.	b.d.	b.d.	0.03	b.d.	b.d.
	K2O	b.d.	0.01	b.d.	0.01	0.01	0.01	0.01	0.01	b.d.	b.d.	b.d.	b.d.	b.d.	0.03	0.01	0.01
	Total	100.16	100.38	100.24	100.66	100.74	100.58	100.56	100.43	100.64	100.28	100.44	100.10	100.66	100.66	100.06	100.78
Cations	Si	1.928	1.934	1.928	1.921	1.929	1.924	1.928	1.932	1.925	1.934	1.931	1.932	1.925	1.928	1.930	1.925
	Ti	0.001	b.d.	0.001	0.001	b.d.	0.001	b.d.	0.001	0.001	0.001	0.001	0.001	0.000	0.001	0.000	0.001
	Cr	0.020	0.018	0.018	0.018	0.020	0.018	0.020	0.020	0.018	0.019	0.018	0.018	0.019	0.018	0.018	0.019
	Al	0.127	0.125	0.125	0.124	0.124	0.126	0.120	0.125	0.126	0.123	0.123	0.126	0.124	0.122	0.126	0.120
	Fe2+	0.164	0.167	0.162	0.167	0.171	0.165	0.164	0.157	0.168	0.159	0.163	0.164	0.167	0.164	0.160	0.167
	Mn	0.004	0.004	0.004	0.004	0.003	0.004	0.006	0.003	0.005	0.004	0.002	0.004	0.003	0.005	0.003	0.003
	Ni	0.002	0.002	0.002	0.004	0.002	0.002	0.002	0.003	0.003	0.002	0.004	0.002	0.002	0.003	0.002	0.003
	Mg	1.716	1.715	1.734	1.742	1.723	1.735	1.734	1.708	1.734	1.688	1.729	1.699	1.716	1.730	1.732	1.702
	Ca	0.036	0.029	0.025	0.026	0.026	0.028	0.026	0.048	0.022	0.066	0.027	0.050	0.047	0.028	0.027	0.065
	Na	b.d.	0.001	b.d.	0.001	0.001	0.001	0.001	b.d.	b.d.	b.d.	b.d.	b.d.	b.d.	0.002	b.d.	b.d.
	K	b.d.	0.000	b.d.	0.000	0.000	0.000	0.000	0.000	b.d.	b.d.	b.d.	b.d.	b.d.	0.001	0.000	0.000
	Sum	3.998	3.996	3.999	4.008	4.000	4.004	4.003	3.996	4.002	3.995	3.998	3.995	4.003	4.003	3.998	4.005
	Mg #	0.913	0.911	0.915	0.912	0.910	0.913	0.914	0.916	0.912	0.914	0.914	0.912	0.911	0.913	0.915	0.911

Abbreviations: Opx = orthopyroxene, Spl hrz = spinel harzburgite, Cl core = clast core, b.d. = below detection limit.
Mg# calculated as (MgO/40.3) / (MgO/40.3 + FeO/71.85).

Major element composition of orthopyroxene from the Dramala spinel harzburgite and plagioclase-bearing harzburgite continued

Sample		PI2	PI2	PI2	PI2	PI2	PI2	PI2	PI2	PI2	PI2	PI2	PI2	PI2	PI2	PI2	PI2
Rock		Spl hrz	Spl hrz	Spl hrz	Spl hrz	Spl hrz	Spl hrz	Spl hrz	Spl hrz	Spl hrz	Spl hrz	Spl hrz	Spl hrz	Spl hrz	Spl hrz	Spl hrz	Spl hrz
Mineral		Opx	Opx	Opx	Opx	Opx	Opx	Opx	Opx	Opx	Opx	Opx	Opx	Opx	Opx	Opx	Opx
Type		Cl core	Cl core	Cl core	Cl core	Cl core	Cl core	Cl core	Cl core	Cl core	Cl core	Cl core	Cl core	Cl core	Cl core	Cl core	Cl core
Wt.%	SiO2	56.03	56.11	56.21	56.42	56.14	56.14	56.29	56.23	55.95	56.22	56.24	56.25	54.73	56.06	55.75	56.27
	TiO2	0.01	0.04	0.01	0.01	0.01	0.03	0.02	0.03	0.04	0.03	0.02	0.01	0.01	0.01	0.02	0.02
	Cr2O3	0.67	0.71	0.75	0.69	0.68	0.74	0.69	0.65	0.67	0.67	0.73	0.56	0.79	0.72	0.76	0.72
	Al2O3	3.08	3.04	3.02	2.98	3.04	2.99	3.06	3.09	3.06	3.01	3.06	3.03	3.02	2.91	3.05	2.99
	FeO	5.61	5.84	5.74	5.73	5.82	5.84	5.76	5.81	5.90	5.68	5.89	5.82	5.70	5.72	5.65	5.90
	MnO	0.18	0.12	0.09	0.14	0.12	0.15	0.12	0.14	0.14	0.20	0.13	0.16	0.15	0.11	0.19	0.15
	NiO	0.13	0.13	0.07	0.06	0.09	0.11	0.12	0.08	0.10	0.03	0.09	0.13	0.04	0.11	0.13	0.07
	MgO	33.29	34.02	33.80	33.79	33.67	33.99	33.85	33.72	33.84	33.82	33.93	33.82	32.95	34.03	33.16	33.86
	CaO	1.37	0.80	0.94	0.93	0.72	0.70	0.74	0.77	0.78	0.77	0.67	0.73	1.38	0.85	1.38	0.64
	Na2O	0.01	b.d.	b.d.	0.01	0.01	0.03	b.d.	b.d.	b.d.	b.d.	0.01	0.02	0.02	0.02	b.d.	b.d.
	K2O	0.02	0.02	b.d.	b.d.	b.d.	0.02	0.01	0.01	b.d.	b.d.	b.d.	b.d.	b.d.	0.01	0.01	b.d.
	Total	100.40	100.83	100.63	100.76	100.30	100.74	100.66	100.53	100.48	100.43	100.77	100.53	98.79	100.55	100.10	100.62
Cations	Si	1.928	1.922	1.927	1.931	1.931	1.924	1.929	1.929	1.923	1.930	1.926	1.930	1.917	1.925	1.925	1.929
	Ti	0.000	0.001	0.000	0.000	0.000	0.001	0.001	0.001	0.001	0.001	0.001	0.000	0.000	0.000	0.001	0.001
	Cr	0.018	0.019	0.020	0.019	0.018	0.020	0.019	0.018	0.018	0.018	0.020	0.015	0.022	0.020	0.021	0.020
	Al	0.125	0.123	0.122	0.120	0.123	0.121	0.124	0.125	0.124	0.122	0.124	0.123	0.125	0.118	0.124	0.121
	Fe2+	0.161	0.167	0.165	0.164	0.167	0.167	0.165	0.167	0.170	0.163	0.169	0.167	0.167	0.164	0.163	0.169
	Mn	0.005	0.003	0.003	0.004	0.003	0.004	0.003	0.004	0.004	0.006	0.004	0.005	0.004	0.003	0.006	0.004
	Ni	0.004	0.004	0.002	0.002	0.002	0.003	0.003	0.002	0.003	0.001	0.002	0.004	0.001	0.003	0.004	0.002
	Mg	1.707	1.737	1.727	1.724	1.726	1.737	1.729	1.724	1.734	1.730	1.732	1.730	1.720	1.741	1.707	1.730
	Ca	0.051	0.029	0.035	0.034	0.027	0.026	0.027	0.028	0.029	0.028	0.025	0.027	0.052	0.031	0.051	0.024
	Na	0.001	b.d.	b.d.	0.001	0.001	0.002	b.d.	b.d.	b.d.	b.d.	0.001	0.001	0.001	0.001	b.d.	b.d.
	K	0.001	0.001	b.d.	b.d.	b.d.	0.001	0.000	0.000	b.d.	b.d.	b.d.	b.d.	b.d.	0.000	0.000	b.d.
	Sum	4.001	4.006	4.001	3.999	3.999	4.006	4.000	3.999	4.005	3.999	4.002	4.001	4.010	4.007	4.002	4.000
	Mg #	0.914	0.912	0.913	0.913	0.912	0.912	0.913	0.912	0.911	0.914	0.911	0.912	0.912	0.914	0.913	0.911

Abbreviations: Opx = orthopyroxene, Spl hrz = spinel harzburgite, Cl core = clast core, b.d. = below detection limit.
Mg# calculated as (MgO/40.3) / (MgO/40.3 + FeO/71.85).

Major element composition of orthopyroxene from the Dramala spinel harzburgite and plagioclase-bearing harzburgite continued

Sample		PI2	PI2	PI2	PI2	PI2	PI2	PI2	PI2	PI2	PI2	PI2	PI2	PI2	PI2	PI2	PI2
Rock		Spl hrz	Spl hrz	Spl hrz	Spl hrz	Spl hrz	Spl hrz	Spl hrz	Spl hrz	Spl hrz	Spl hrz	Spl hrz	Spl hrz	Spl hrz	Spl hrz	Spl hrz	Spl hrz
Mineral		Opx	Opx	Opx	Opx	Opx	Opx	Opx	Opx	Opx	Opx	Opx	Opx	Opx	Opx	Opx	Opx
Type		Cl core	Cl core	Cl core	Cl core	Cl core	Cl core	Cl core	Cl core	Cl core	Cl core	Cl core	Cl core	Cl core	Cl core	Cl core	Cl core
Wt.%	SiO2	56.32	55.96	56.03	56.23	56.04	56.04	56.33	55.83	56.24	56.24	56.14	56.06	55.66	55.75	56.44	56.38
	TiO2	b.d.	0.01	0.05	0.02	0.03	0.02	b.d.	0.01	b.d.	0.02	0.01	b.d.	0.03	0.01	b.d.	0.01
	Cr2O3	0.69	0.66	0.67	0.68	0.63	0.63	0.68	0.70	0.72	0.68	0.72	0.75	0.67	0.68	0.57	0.72
	Al2O3	3.11	3.01	3.01	3.04	3.02	2.82	3.02	2.95	3.02	3.06	3.04	3.09	3.05	3.03	3.04	2.96
	FeO	5.62	5.83	5.89	5.75	5.74	5.48	5.72	5.80	5.81	5.69	5.83	5.79	5.69	5.85	5.74	5.90
	MnO	0.14	0.11	0.17	0.17	0.17	0.12	0.11	0.11	0.15	0.17	0.17	0.14	0.15	0.15	0.14	0.15
	NiO	0.15	0.11	0.06	0.08	0.07	0.07	0.04	0.11	0.05	0.11	0.18	0.11	0.08	0.10	0.05	0.06
	MgO	33.95	33.60	33.88	33.45	33.68	33.03	33.97	34.04	33.83	33.76	33.80	33.86	33.84	33.80	33.98	33.87
	CaO	0.64	1.06	0.68	0.82	1.05	1.91	0.74	0.65	0.71	0.74	0.67	0.70	0.65	0.83	0.67	0.79
	Na2O	b.d.	b.d.	b.d.	b.d.	0.03	b.d.	0.01	b.d.	0.02	0.03	b.d.	0.03	0.01	b.d.	b.d.	0.03
	K2O	0.02	b.d.	0.01	b.d.	b.d.	0.01	0.01	b.d.	b.d.	b.d.	b.d.	0.02	b.d.	b.d.	b.d.	b.d.
	Total	100.64	100.35	100.45	100.24	100.46	100.13	100.63	100.20	100.55	100.50	100.56	100.55	99.83	100.20	100.63	100.87
Cations	Si	1.929	1.926	1.925	1.934	1.926	1.934	1.930	1.923	1.929	1.930	1.927	1.924	1.923	1.922	1.932	1.929
	Ti	b.d.	0.000	0.001	0.001	0.001	0.001	b.d.	0.000	b.d.	0.001	0.000	b.d.	0.001	0.000	b.d.	0.000
	Cr	0.019	0.018	0.018	0.018	0.017	0.017	0.018	0.019	0.020	0.018	0.020	0.020	0.018	0.019	0.015	0.019
	Al	0.126	0.122	0.122	0.123	0.122	0.115	0.122	0.120	0.122	0.124	0.123	0.125	0.124	0.123	0.123	0.119
	Fe2+	0.161	0.168	0.169	0.165	0.165	0.158	0.164	0.167	0.167	0.163	0.167	0.166	0.164	0.169	0.164	0.169
	Mn	0.004	0.003	0.005	0.005	0.005	0.004	0.003	0.003	0.004	0.005	0.005	0.004	0.004	0.004	0.004	0.004
	Ni	0.004	0.003	0.002	0.002	0.002	0.002	0.001	0.003	0.001	0.003	0.005	0.003	0.002	0.003	0.001	0.002
	Mg	1.733	1.724	1.735	1.715	1.725	1.699	1.734	1.748	1.730	1.727	1.729	1.732	1.743	1.737	1.734	1.728
	Ca	0.023	0.039	0.025	0.030	0.039	0.071	0.027	0.024	0.026	0.027	0.025	0.026	0.024	0.031	0.025	0.029
	Na	b.d.	b.d.	b.d.	b.d.	0.002	b.d.	0.001	b.d.	0.001	0.002	b.d.	0.002	0.001	b.d.	b.d.	0.002
	K	0.001	b.d.	0.000	b.d.	b.d.	0.000	0.000	b.d.	b.d.	b.d.	b.d.	0.001	b.d.	b.d.	b.d.	b.d.
	Sum	3.999	4.003	4.003	3.994	4.004	4.000	4.001	4.007	4.001	4.000	4.001	4.004	4.005	4.007	3.999	4.002
	Mg #	0.915	0.911	0.911	0.912	0.913	0.915	0.914	0.913	0.912	0.914	0.912	0.912	0.914	0.911	0.913	0.911

Abbreviations: Opx = orthopyroxene, Spl hrz = spinel harzburgite, Cl core = clast core, b.d. = below detection limit.
Mg# calculated as (MgO/40.3) / (MgO/40.3 + FeO/71.85).

Major element composition of orthopyroxene from the Dramala spinel harzburgite and plagioclase-bearing harzburgite continued

Sample		PI2	PI2	PI2	PI2	PI2	PI2	PI2	PI2	PI2	PI2	PI2	PI2	PI2	PI2	PI2	PI2
Rock		Spl hrz	Spl hrz	Spl hrz	Spl hrz	Spl hrz	Spl hrz	Spl hrz	Spl hrz	Spl hrz	Spl hrz	Spl hrz	Spl hrz	Spl hrz	Spl hrz	Spl hrz	Spl hrz
Mineral		Opx	Opx	Opx	Opx	Opx	Opx	Opx	Opx	Opx	Opx	Opx	Opx	Opx	Opx	Opx	Opx
Type		Cl core	Cl core	Cl core	Cl core	Cl core	Cl core	Cl core	Cl core	Cl core	Cl core	Cl core	Cl core	Cl core	Cl core	Cl core	Cl core
Wt.%	SiO2	56.14	56.23	56.29	56.32	56.33	56.33	56.33	56.54	55.93	55.85	56.02	56.36	56.02	55.94	55.84	56.01
	TiO2	b.d.	b.d.	0.02	b.d.	b.d.	b.d.	0.02	0.02	b.d.	0.01	0.01	0.02	0.03	b.d.	0.02	0.02
	Cr2O3	0.85	0.70	0.72	0.65	0.72	0.65	0.70	0.72	0.67	0.69	0.72	0.68	0.63	0.72	0.68	0.73
	Al2O3	2.95	3.07	3.07	3.06	3.08	3.10	3.09	3.06	3.10	3.13	3.08	3.03	3.20	3.12	3.14	3.08
	FeO	5.81	5.62	5.59	5.82	5.60	5.78	5.63	5.77	5.68	5.83	5.68	5.76	5.83	5.75	5.65	5.83
	MnO	0.16	0.16	0.15	0.13	0.16	0.20	0.13	0.08	0.15	0.12	0.17	0.16	0.17	0.13	0.09	0.18
	NiO	0.07	0.05	0.07	b.d.	0.14	0.12	0.14	0.03	0.12	0.11	0.09	0.08	0.07	0.04	0.05	0.06
	MgO	33.90	33.53	33.63	33.49	33.55	33.62	33.49	33.60	33.81	33.92	33.51	33.27	33.87	33.87	33.43	34.02
	CaO	0.76	1.37	1.04	1.13	1.14	1.17	1.36	1.14	0.82	0.69	1.44	1.48	0.71	0.90	1.20	0.71
	Na2O	b.d.	0.02	0.01	b.d.	b.d.	b.d.	0.02	b.d.	0.02	0.01	0.01	0.01	0.01	b.d.	b.d.	b.d.
	K2O	b.d.	0.01	0.01	b.d.	b.d.	b.d.	b.d.	b.d.	0.02	b.d.	b.d.	0.02	b.d.	b.d.	b.d.	b.d.
	Total	100.64	100.76	100.60	100.60	100.72	100.97	100.91	100.96	100.32	100.36	100.73	100.87	100.54	100.47	100.10	100.64
Cations	Si	1.926	1.927	1.930	1.932	1.930	1.927	1.928	1.932	1.924	1.921	1.923	1.931	1.923	1.922	1.925	1.921
	Ti	b.d.	b.d.	0.001	b.d.	b.d.	b.d.	0.001	0.001	b.d.	0.000	0.000	0.001	0.001	b.d.	0.001	0.001
	Cr	0.023	0.019	0.020	0.018	0.020	0.018	0.019	0.019	0.018	0.019	0.020	0.018	0.017	0.020	0.019	0.020
	Al	0.119	0.124	0.124	0.124	0.124	0.125	0.125	0.123	0.126	0.127	0.125	0.122	0.129	0.126	0.128	0.125
	Fe2+	0.167	0.161	0.160	0.167	0.160	0.165	0.161	0.165	0.163	0.168	0.163	0.165	0.167	0.165	0.163	0.167
	Mn	0.005	0.005	0.004	0.004	0.005	0.006	0.004	0.002	0.004	0.003	0.005	0.005	0.005	0.004	0.003	0.005
	Ni	0.002	0.001	0.002	b.d.	0.004	0.003	0.004	0.001	0.003	0.003	0.002	0.002	0.002	0.001	0.001	0.002
	Mg	1.733	1.713	1.718	1.712	1.713	1.714	1.708	1.711	1.734	1.739	1.714	1.699	1.733	1.734	1.718	1.739
	Ca	0.028	0.050	0.038	0.042	0.042	0.043	0.050	0.042	0.030	0.025	0.053	0.054	0.026	0.033	0.044	0.026
	Na	b.d.	0.001	0.001	b.d.	b.d.	b.d.	0.001	b.d.	0.001	0.001	0.001	0.001	0.001	b.d.	b.d.	b.d.
	K	b.d.	0.000	0.000	b.d.	b.d.	b.d.	b.d.	b.d.	0.001	b.d.	b.d.	0.001	b.d.	b.d.	b.d.	b.d.
	Sum	4.003	4.002	3.998	3.998	3.998	4.001	4.000	3.996	4.005	4.006	4.005	3.999	4.004	4.005	4.001	4.006
	Mg #	0.912	0.914	0.915	0.911	0.914	0.912	0.914	0.912	0.914	0.912	0.913	0.911	0.912	0.913	0.913	0.912

Abbreviations: Opx = orthopyroxene, Spl hrz = spinel harzburgite, Cl core = clast core, b.d. = below detection limit.
Mg# calculated as (MgO/40.3) / (MgO/40.3 + FeO/71.85).

Major element composition of orthopyroxene from the Dramala spinel harzburgite and plagioclase-bearing harzburgite continued

Sample		PI2	PI2	PI2	PI2	PI2	PI2	PI2	PI2	PI2	PI2	PI2	PI2	PI2	PI2	PI2	PI2
Rock		Spl hrz	Spl hrz	Spl hrz	Spl hrz	Spl hrz	Spl hrz	Spl hrz	Spl hrz	Spl hrz	Spl hrz	Spl hrz	Spl hrz	Spl hrz	Spl hrz	Spl hrz	Spl hrz
Mineral		Opx	Opx	Opx	Opx	Opx	Opx	Opx	Opx	Opx	Opx	Opx	Opx	Opx	Opx	Opx	Opx
Type		Cl core	Cl core	Cl core	Cl core	Cl core	Cl core	Cl core	Cl core	Cl core	Cl core	Cl core	Cl core	Cl core	Cl core	Cl core	Cl core
Wt.%	**SiO2**	56.16	55.99	56.19	55.96	56.35	55.92	55.89	55.98	55.96	56.14	56.15	56.15	56.42	55.93	56.32	56.38
	TiO2	0.03	0.03	0.03	0.05	b.d.	0.02	0.02	0.02	0.02	0.03	0.03	0.02	0.03	0.01	b.d.	0.01
	Cr2O3	0.65	0.64	0.68	0.67	0.82	0.74	0.68	0.70	0.69	0.66	0.77	0.75	0.72	0.65	0.68	0.71
	Al2O3	3.09	3.08	3.01	3.19	3.15	3.09	3.17	3.16	3.06	3.14	3.00	3.22	3.05	3.12	3.14	3.03
	FeO	5.64	5.49	5.60	5.42	5.67	5.87	5.82	5.79	5.58	5.84	5.66	5.58	5.67	5.86	5.70	5.91
	MnO	0.18	0.16	0.15	0.10	0.15	0.14	0.15	0.21	0.13	0.15	0.13	0.16	0.11	0.19	0.13	0.17
	NiO	0.04	0.07	0.10	0.04	0.11	0.08	0.00	0.08	0.09	0.14	0.09	0.10	0.04	0.06	0.14	0.04
	MgO	33.35	33.24	33.43	33.44	33.85	33.86	33.46	33.82	33.49	33.77	34.10	33.26	33.98	34.05	33.89	34.07
	CaO	1.37	1.91	1.42	1.22	0.60	0.63	1.12	0.80	1.23	0.87	0.61	1.39	0.61	0.62	0.51	0.66
	Na2O	b.d.	b.d.	b.d.	b.d.	b.d.	b.d.	0.04	0.02	0.02	0.01	b.d.	0.03	0.01	b.d.	b.d.	b.d.
	K2O	b.d.	b.d.	b.d.	b.d.	b.d.	0.03	0.02	b.d.	0.01	0.02	0.01	0.01	b.d.	b.d.	0.02	b.d.
	Total	100.51	100.61	100.61	100.09	100.70	100.38	100.37	100.58	100.28	100.77	100.55	100.67	100.64	100.49	100.53	100.98
Cations	**Si**	1.929	1.924	1.929	1.927	1.929	1.923	1.924	1.922	1.926	1.924	1.926	1.926	1.931	1.921	1.930	1.927
	Ti	0.001	0.001	0.001	0.001	b.d.	0.001	0.001	0.001	0.001	0.001	0.001	0.001	0.001	0.000	b.d.	0.000
	Cr	0.018	0.017	0.018	0.018	0.022	0.020	0.019	0.019	0.019	0.018	0.021	0.020	0.019	0.018	0.018	0.019
	Al	0.125	0.125	0.122	0.129	0.127	0.125	0.129	0.128	0.124	0.127	0.121	0.130	0.123	0.126	0.127	0.122
	Fe2+	0.162	0.158	0.161	0.156	0.162	0.169	0.167	0.166	0.161	0.167	0.162	0.160	0.162	0.168	0.163	0.169
	Mn	0.005	0.005	0.004	0.003	0.004	0.004	0.004	0.006	0.004	0.004	0.004	0.005	0.003	0.006	0.004	0.005
	Ni	0.001	0.002	0.003	0.001	0.003	0.002	0.000	0.002	0.002	0.004	0.002	0.003	0.001	0.002	0.004	0.001
	Mg	1.707	1.702	1.710	1.716	1.727	1.736	1.716	1.730	1.718	1.725	1.743	1.701	1.733	1.743	1.731	1.735
	Ca	0.050	0.070	0.052	0.045	0.022	0.023	0.041	0.029	0.045	0.032	0.022	0.051	0.022	0.023	0.019	0.024
	Na	b.d.	b.d.	b.d.	b.d.	b.d.	b.d.	0.003	0.001	0.001	0.001	b.d.	0.002	0.001	b.d.	b.d.	b.d.
	K	b.d.	b.d.	b.d.	b.d.	b.d.	0.001	0.001	b.d.	0.000	0.001	0.000	0.000	b.d.	b.d.	0.001	b.d.
	Sum	3.999	4.004	4.000	3.998	3.997	4.004	4.004	4.005	4.002	4.004	4.003	3.999	3.997	4.007	3.997	4.002
	Mg #	0.913	0.915	0.914	0.917	0.914	0.911	0.911	0.912	0.915	0.912	0.915	0.914	0.914	0.912	0.914	0.911

Abbreviations: Opx = orthopyroxene, Spl hrz = spinel harzburgite, Cl core = clast core, b.d. = below detection limit.
Mg# calculated as (MgO/40.3) / (MgO/40.3 + FeO/71.85).

Major element composition of orthopyroxene from the Dramala spinel harzburgite and plagioclase-bearing harzburgite continued

Sample		PI2	PI2	PI2	PI2	PI2	PI2	PI2	PI2	PI2	PI2	PI2	PI2	PI2	PI2	PI2	PI2
Rock		Spl hrz	Spl hrz	Spl hrz	Spl hrz	Spl hrz	Spl hrz	Spl hrz	Spl hrz	Spl hrz	Spl hrz	Spl hrz	Spl hrz	Spl hrz	Spl hrz	Spl hrz	Spl hrz
Mineral		Opx	Opx	Opx	Opx	Opx	Opx	Opx	Opx	Opx	Opx	Opx	Opx	Opx	Opx	Opx	Opx
Type		Cl core	Cl core	Cl core	Cl core	Cl core	Cl core	Cl core	Cl core	Cl core	Cl core	Cl core	Cl core	Cl core	Cl core	Cl core	Cl core
Wt.%	SiO2	56.42	56.30	56.27	56.42	56.59	56.20	55.94	56.08	55.58	55.77	56.38	56.54	56.14	56.48	56.29	56.50
	TiO2	b.d.	0.01	b.d.	0.05	0.01	b.d.	0.04	0.04	0.03	0.04	0.01	0.02	0.01	0.02	b.d.	0.02
	Cr2O3	0.71	0.70	0.72	0.66	0.77	0.67	0.74	0.63	0.67	0.81	0.70	0.71	0.73	0.76	0.64	0.68
	Al2O3	3.16	3.16	3.24	3.09	3.06	3.24	3.25	2.90	2.89	3.11	2.87	3.12	3.10	3.06	3.21	3.02
	FeO	5.60	5.32	5.53	5.67	5.59	5.80	5.80	5.67	5.07	5.77	5.82	5.85	5.61	5.64	5.90	5.79
	MnO	0.15	0.13	0.16	0.08	0.15	0.15	0.10	0.15	0.09	0.13	0.15	0.15	0.17	0.12	0.11	0.16
	NiO	0.11	0.05	0.01	0.06	0.05	0.08	0.08	0.07	0.05	0.04	0.04	0.06	0.07	0.06	0.03	0.04
	MgO	33.86	32.61	33.87	33.66	33.77	33.83	33.73	33.70	31.18	34.02	33.47	33.81	33.47	34.05	33.81	33.78
	CaO	0.60	2.53	0.61	1.18	0.91	0.65	0.72	0.84	5.00	0.59	1.34	0.64	1.27	0.62	0.74	0.89
	Na2O	0.01	0.01	b.d.	b.d.	0.04	0.01	0.03	b.d.	0.03	b.d.	b.d.	b.d.	b.d.	0.01	b.d.	0.01
	K2O	b.d.	0.01	b.d.	b.d.	b.d.	b.d.	0.01	b.d.	b.d.	0.01	b.d.	b.d.	b.d.	0.01	b.d.	0.01
	Total	100.62	100.83	100.41	100.87	100.94	100.63	100.44	100.08	100.59	100.29	100.78	100.90	100.57	100.83	100.73	100.90
Cations	Si	1.931	1.931	1.929	1.929	1.932	1.926	1.922	1.932	1.924	1.919	1.933	1.932	1.927	1.930	1.927	1.932
	Ti	b.d.	0.000	b.d.	0.001	0.000	b.d.	0.001	0.001	0.001	0.001	0.000	0.001	0.000	0.001	b.d.	0.001
	Cr	0.019	0.019	0.020	0.018	0.021	0.018	0.020	0.017	0.018	0.022	0.019	0.019	0.020	0.021	0.017	0.018
	Al	0.127	0.128	0.131	0.125	0.123	0.131	0.132	0.118	0.118	0.126	0.116	0.126	0.125	0.123	0.130	0.122
	Fe2+	0.160	0.153	0.159	0.162	0.160	0.166	0.167	0.163	0.147	0.166	0.167	0.167	0.161	0.161	0.169	0.166
	Mn	0.004	0.004	0.005	0.002	0.004	0.004	0.003	0.004	0.003	0.004	0.004	0.004	0.005	0.003	0.003	0.005
	Ni	0.003	0.001	0.000	0.002	0.001	0.002	0.002	0.002	0.001	0.001	0.001	0.002	0.002	0.002	0.001	0.001
	Mg	1.727	1.667	1.731	1.716	1.719	1.728	1.727	1.731	1.609	1.745	1.710	1.722	1.713	1.734	1.725	1.721
	Ca	0.022	0.093	0.022	0.043	0.033	0.024	0.027	0.031	0.185	0.022	0.049	0.023	0.047	0.023	0.027	0.033
	Na	0.001	0.001	b.d.	b.d.	0.003	0.001	0.002	b.d.	0.002	b.d.	b.d.	b.d.	b.d.	0.001	b.d.	0.001
	K	b.d.	0.000	b.d.	b.d.	b.d.	b.d.	0.000	b.d.	b.d.	0.000	b.d.	b.d.	b.d.	0.000	b.d.	0.000
	Sum	3.996	3.996	3.996	3.998	3.997	4.000	4.002	3.999	4.008	4.006	4.000	3.995	4.000	3.998	3.999	3.998
	Mg #	0.915	0.916	0.916	0.914	0.915	0.912	0.912	0.914	0.916	0.913	0.911	0.912	0.914	0.915	0.911	0.912

Abbreviations: Opx = orthopyroxene, Spl hrz = spinel harzburgite, Cl core = clast core, b.d. = below detection limit.
Mg# calculated as (MgO/40.3) / (MgO/40.3 + FeO/71.85).

Major element composition of orthopyroxene from the Dramala spinel harzburgite and plagioclase-bearing harzburgite continued

Sample		PI2	PI2	PI2	PI2	PI2	PI2	PI2	PI2	PI2	PI2	PI2	PI2	PI2	PI2	PI2	PI2
Rock		Spl hrz	Spl hrz	Spl hrz	Spl hrz	Spl hrz	Spl hrz	Spl hrz	Spl hrz	Spl hrz	Spl hrz	Spl hrz	Spl hrz	Spl hrz	Spl hrz	Spl hrz	Spl hrz
Mineral		Opx	Opx	Opx	Opx	Opx	Opx	Opx	Opx	Opx	Opx	Opx	Opx	Opx	Opx	Opx	Opx
Type		Cl core	Cl core	Cl core	Cl core	Cl core	Cl core	Cl core	Cl core	Cl core	Cl core	Cl core	Cl core	Cl core	Cl core	Cl core	Cl core
Wt.%	SiO2	56.09	56.12	56.15	56.46	55.19	56.20	56.37	56.27	56.52	56.59	56.39	56.34	56.37	56.42	56.71	56.54
	TiO2	0.01	0.01	0.03	0.01	0.02	b.d.	0.02	0.02	0.01	0.01	0.02	b.d.	0.02	0.03	0.04	0.01
	Cr2O3	0.67	0.64	0.73	0.68	0.61	0.67	0.66	0.63	0.71	0.70	0.65	0.69	0.64	0.73	0.64	0.74
	Al2O3	3.20	3.20	3.11	3.18	2.97	3.14	3.15	3.11	3.07	2.77	2.99	3.16	3.14	2.99	3.13	3.12
	FeO	5.88	5.98	5.79	5.76	5.67	5.77	5.76	5.94	5.63	5.56	5.60	5.74	5.66	5.36	5.68	5.64
	MnO	0.13	0.16	0.16	0.11	0.12	0.15	0.10	0.14	0.15	0.13	0.13	0.12	0.18	0.09	0.09	0.17
	NiO	0.07	0.04	0.10	0.11	0.05	0.11	0.07	0.08	0.05	0.05	0.13	0.15	0.10	0.12	b.d.	0.07
	MgO	33.62	33.97	33.99	34.00	33.18	34.04	34.06	33.94	33.68	33.53	33.55	33.92	33.60	32.57	33.97	33.59
	CaO	1.26	0.63	0.63	0.54	1.51	0.50	0.53	0.60	0.82	1.28	1.48	0.74	1.27	2.66	0.60	1.07
	Na2O	b.d.	b.d.	b.d.	b.d.	b.d.	0.02	0.01	0.02	0.01	b.d.	b.d.	b.d.	b.d.	b.d.	0.02	b.d.
	K2O	b.d.	b.d.	b.d.	0.01	0.02	0.01	0.02	0.01	0.01	b.d.	b.d.	0.01	b.d.	b.d.	b.d.	b.d.
	Total	100.93	100.75	100.69	100.86	99.34	100.61	100.75	100.76	100.66	100.62	100.94	100.87	100.98	100.97	100.88	100.95
Cations	Si	1.921	1.923	1.924	1.929	1.921	1.926	1.928	1.927	1.935	1.939	1.929	1.927	1.927	1.933	1.934	1.932
	Ti	0.000	0.000	0.001	0.000	0.001	b.d.	0.001	0.001	0.000	0.000	0.001	b.d.	0.001	0.001	0.001	0.000
	Cr	0.018	0.017	0.020	0.018	0.017	0.018	0.018	0.017	0.019	0.019	0.018	0.019	0.017	0.020	0.017	0.020
	Al	0.129	0.129	0.126	0.128	0.122	0.127	0.127	0.126	0.124	0.112	0.121	0.127	0.127	0.121	0.126	0.126
	Fe2+	0.168	0.171	0.166	0.165	0.165	0.165	0.165	0.170	0.161	0.159	0.160	0.164	0.162	0.154	0.162	0.161
	Mn	0.004	0.005	0.005	0.003	0.004	0.004	0.003	0.004	0.004	0.004	0.004	0.003	0.005	0.003	0.003	0.005
	Ni	0.002	0.001	0.003	0.003	0.001	0.003	0.002	0.002	0.001	0.001	0.004	0.004	0.003	0.003	b.d.	0.002
	Mg	1.716	1.734	1.736	1.731	1.722	1.739	1.736	1.732	1.718	1.713	1.711	1.729	1.712	1.664	1.727	1.710
	Ca	0.046	0.023	0.023	0.020	0.056	0.018	0.019	0.022	0.030	0.047	0.054	0.027	0.047	0.098	0.022	0.039
	Na	b.d.	b.d.	b.d.	b.d.	b.d.	0.001	0.001	0.001	0.001	b.d.	b.d.	b.d.	b.d.	b.d.	0.001	b.d.
	K	b.d.	b.d.	b.d.	0.000	0.001	0.000	0.001	0.000	0.000	b.d.	b.d.	0.000	b.d.	b.d.	b.d.	b.d.
	Sum	4.005	4.004	4.003	3.998	4.009	4.002	4.000	4.002	3.994	3.995	4.001	4.001	4.000	3.995	3.994	3.995
	Mg #	0.911	0.910	0.913	0.913	0.913	0.913	0.913	0.911	0.914	0.915	0.914	0.913	0.914	0.915	0.914	0.914

Abbreviations: Opx = orthopyroxene, Spl hrz = spinel harzburgite, Cl core = clast core, b.d. = below detection limit.
Mg# calculated as (MgO/40.3) / (MgO/40.3 + FeO/71.85).

Major element composition of orthopyroxene from the Dramala spinel harzburgite and plagioclase-bearing harzburgite continued

Sample		PI2	PI2	PI2	PI2	PI2	PI2	PI2	PI2	PI2	PI2	PI2	PI2	PI2	PI2	PI2	PI2
Rock		Spl hrz	Spl hrz	Spl hrz	Spl hrz	Spl hrz	Spl hrz	Spl hrz	Spl hrz	Spl hrz	Spl hrz	Spl hrz	Spl hrz	Spl hrz	Spl hrz	Spl hrz	Spl hrz
Mineral		Opx	Opx	Opx	Opx	Opx	Opx	Opx	Opx	Opx	Opx	Opx	Opx	Opx	Opx	Opx	Opx
Type		Cl core	Cl core	Cl core	Cl core	Cl core	Cl core	Cl core	Cl core	Cl core	Cl core	Cl core	Cl core	Cl core	Cl core	Cl core	Cl core
Wt.%	SiO2	56.50	56.54	56.26	56.92	56.66	56.20	56.42	56.24	56.20	56.52	55.99	56.26	55.86	56.12	55.95	56.23
	TiO2	0.01	0.04	0.03	0.01	0.02	0.03	0.03	b.d.	0.01	0.03	0.02	b.d.	0.05	0.04	0.01	0.03
	Cr2O3	0.66	0.66	0.67	0.52	0.59	0.65	0.67	0.71	0.72	0.75	0.77	0.84	0.79	0.83	0.87	0.75
	Al2O3	3.06	3.07	3.04	2.77	3.19	3.29	3.16	3.27	3.32	3.26	3.30	3.30	3.22	3.19	3.23	3.22
	FeO	5.66	5.74	5.83	5.74	5.79	5.94	5.72	5.57	5.88	5.63	5.55	5.68	5.38	5.80	5.66	5.81
	MnO	0.16	0.18	0.16	0.13	0.11	0.15	0.17	0.14	0.15	0.18	0.14	0.12	0.13	0.14	0.13	0.16
	NiO	0.06	0.09	0.12	0.16	0.08	0.11	0.07	0.06	0.10	0.05	0.10	0.10	0.07	0.03	0.10	0.11
	MgO	34.11	34.02	34.13	33.81	33.91	33.87	33.94	33.73	33.95	33.87	32.88	33.44	32.00	33.92	33.20	33.93
	CaO	0.64	0.57	0.68	0.85	0.56	0.61	0.51	1.10	0.55	0.54	2.04	1.22	3.35	0.67	1.69	0.67
	Na2O	b.d.	0.01	0.01	b.d.	0.01	0.01	b.d.	b.d.	0.04	b.d.	b.d.	0.01	0.01	0.01	0.02	b.d.
	K2O	b.d.	b.d.	b.d.	b.d.	b.d.	b.d.	0.01	b.d.	0.02	b.d.	b.d.	0.01	b.d.	b.d.	0.02	b.d.
	Total	100.86	100.92	100.93	100.91	100.92	100.86	100.70	100.82	100.94	100.83	100.79	100.98	100.86	100.75	100.88	100.91
Cations	Si	1.930	1.931	1.924	1.944	1.933	1.923	1.930	1.924	1.921	1.930	1.922	1.924	1.922	1.922	1.919	1.923
	Ti	0.000	0.001	0.001	0.000	0.001	0.001	0.001	b.d.	0.000	0.001	0.001	b.d.	0.001	0.001	0.000	0.001
	Cr	0.018	0.018	0.018	0.014	0.016	0.018	0.018	0.019	0.019	0.020	0.021	0.023	0.021	0.022	0.024	0.020
	Al	0.123	0.124	0.123	0.111	0.128	0.133	0.127	0.132	0.134	0.131	0.134	0.133	0.131	0.129	0.131	0.130
	Fe2+	0.162	0.164	0.167	0.164	0.165	0.170	0.164	0.159	0.168	0.161	0.159	0.162	0.155	0.166	0.162	0.166
	Mn	0.005	0.005	0.005	0.004	0.003	0.004	0.005	0.004	0.004	0.005	0.004	0.003	0.004	0.004	0.004	0.005
	Ni	0.002	0.002	0.003	0.004	0.002	0.003	0.002	0.002	0.003	0.001	0.003	0.003	0.002	0.001	0.003	0.003
	Mg	1.737	1.732	1.740	1.721	1.725	1.727	1.731	1.720	1.730	1.724	1.682	1.704	1.641	1.731	1.697	1.729
	Ca	0.023	0.021	0.025	0.031	0.020	0.022	0.019	0.040	0.020	0.020	0.075	0.045	0.123	0.025	0.062	0.025
	Na	b.d.	0.001	0.001	b.d.	0.001	0.001	b.d.	b.d.	0.003	b.d.	b.d.	0.001	0.001	0.001	0.001	b.d.
	K	b.d.	b.d.	b.d.	b.d.	b.d.	b.d.	0.000	b.d.	0.001	b.d.	b.d.	0.000	b.d.	b.d.	0.001	b.d.
	Sum	3.999	3.998	4.005	3.993	3.994	4.002	3.997	4.000	4.004	3.993	4.000	3.999	4.001	4.002	4.004	4.001
	Mg #	0.915	0.914	0.913	0.913	0.913	0.910	0.914	0.915	0.911	0.915	0.913	0.913	0.914	0.912	0.913	0.912

Abbreviations: Opx = orthopyroxene, Spl hrz = spinel harzburgite, Cl core = clast core, b.d. = below detection limit.
Mg# calculated as (MgO/40.3) / (MgO/40.3 + FeO/71.85).

Major element composition of orthopyroxene from the Dramala spinel harzburgite and plagioclase-bearing harzburgite continued

Sample		PI2	PI2	PI2	PI2	PI2	PI2	PI2	PI2	PI2	PI2	PI2	PI2	PI2	PI2	PI2	PI2
Rock		Spl hrz	Spl hrz	Spl hrz	Spl hrz	Spl hrz	Spl hrz	Spl hrz	Spl hrz	Spl hrz	Spl hrz	Spl hrz	Spl hrz	Spl hrz	Spl hrz	Spl hrz	Spl hrz
Mineral		Opx	Opx	Opx	Opx	Opx	Opx	Opx	Opx	Opx	Opx	Opx	Opx	Opx	Opx	Opx	Opx
Type		Cl core	Cl core	Cl core	Cl core	Cl core	Cl core	Cl core	Cl core	Cl core	Cl core	Cl core	Cl core	Cl core	Cl core	Cl core	Cl core
Wt.%	SiO2	56.23	56.02	56.20	56.08	56.18	56.52	56.18	56.20	56.39	56.19	56.18	55.58	56.27	56.42	56.23	56.05
	TiO2	0.03	0.04	0.04	b.d.	0.06	0.05	0.01	0.02	0.03	0.04	b.d.	0.02	0.02	0.01	0.02	0.02
	Cr2O3	0.84	0.83	0.81	0.73	0.77	0.00	0.83	0.87	0.78	0.79	0.79	0.82	0.69	0.82	0.81	0.80
	Al2O3	3.22	3.20	3.20	3.35	3.30	3.11	3.34	3.44	3.45	3.45	3.35	3.21	3.30	3.27	3.38	3.40
	FeO	5.82	5.27	5.79	5.68	5.55	5.76	5.63	5.73	5.69	5.70	5.76	5.68	5.55	5.67	5.77	5.53
	MnO	0.14	0.09	0.15	0.18	0.12	0.13	0.15	0.10	0.12	0.10	0.15	0.16	0.15	0.14	0.16	0.10
	NiO	0.07	0.08	0.08	0.10	0.08	0.09	0.09	0.06	0.08	0.02	0.10	0.12	0.05	0.05	0.13	0.08
	MgO	33.94	32.06	33.79	33.73	33.01	33.69	33.11	33.91	33.68	33.70	33.95	33.86	33.88	33.85	33.81	33.23
	CaO	0.64	3.00	0.67	1.12	1.89	0.87	1.64	0.61	0.57	0.55	0.63	0.79	0.59	0.71	0.59	1.27
	Na2O	0.01	b.d.	0.02	b.d.	b.d.	b.d.	b.d.	0.01	0.01	b.d.	b.d.	0.02	b.d.	b.d.	b.d.	b.d.
	K2O	0.02	b.d.	b.d.	0.02	b.d.	b.d.	b.d.	b.d.	b.d.	b.d.	b.d.	b.d.	b.d.	b.d.	0.01	0.01
	Total	100.96	100.59	100.75	100.99	100.96	100.22	100.98	100.95	100.80	100.54	100.91	100.26	100.50	100.94	100.91	100.49
Cations	Si	1.922	1.929	1.925	1.918	1.924	1.941	1.923	1.919	1.927	1.925	1.920	1.915	1.927	1.926	1.922	1.924
	Ti	0.001	0.001	0.001	b.d.	0.002	0.001	0.000	0.001	0.001	0.001	b.d.	0.001	0.001	0.000	0.001	0.001
	Cr	0.023	0.023	0.022	0.020	0.021	0.000	0.022	0.023	0.021	0.021	0.021	0.022	0.019	0.022	0.022	0.022
	Al	0.130	0.130	0.129	0.135	0.133	0.126	0.135	0.138	0.139	0.139	0.135	0.130	0.133	0.132	0.136	0.138
	Fe2+	0.166	0.152	0.166	0.162	0.159	0.165	0.161	0.164	0.163	0.163	0.165	0.164	0.159	0.162	0.165	0.159
	Mn	0.004	0.003	0.004	0.005	0.003	0.004	0.004	0.003	0.003	0.003	0.004	0.005	0.004	0.004	0.005	0.003
	Ni	0.002	0.002	0.002	0.003	0.002	0.002	0.002	0.002	0.002	0.001	0.003	0.003	0.001	0.001	0.004	0.002
	Mg	1.729	1.645	1.725	1.720	1.685	1.724	1.689	1.726	1.715	1.721	1.730	1.739	1.730	1.723	1.723	1.700
	Ca	0.023	0.111	0.025	0.041	0.069	0.032	0.060	0.022	0.021	0.020	0.023	0.029	0.022	0.026	0.022	0.047
	Na	0.001	b.d.	0.001	b.d.	b.d.	b.d.	b.d.	0.001	0.001	b.d.	b.d.	0.001	b.d.	b.d.	b.d.	b.d.
	K	0.001	b.d.	b.d.	0.001	b.d.	b.d.	b.d.	b.d.	b.d.	b.d.	b.d.	b.d.	b.d.	b.d.	0.000	0.000
	Sum	4.002	3.994	4.000	4.005	3.998	3.995	3.998	3.999	3.993	3.994	4.001	4.009	3.996	3.996	3.999	3.996
	Mg #	0.912	0.916	0.912	0.914	0.914	0.912	0.913	0.913	0.913	0.913	0.913	0.914	0.916	0.914	0.913	0.915

Abbreviations: Opx = orthopyroxene, Spl hrz = spinel harzburgite, Cl core = clast core, b.d. = below detection limit.
Mg# calculated as (MgO/40.3) / (MgO/40.3 + FeO/71.85).

Major element composition of orthopyroxene from the Dramala spinel harzburgite and plagioclase-bearing harzburgite continued

Sample		PI2	PI2	PI2	PI2	PI2	PI2	PI2	PI2	PI2	PI2	PI2	PI2	PI2	PI2	PI2	PI2
Rock		Spl hrz	Spl hrz	Spl hrz	Spl hrz	Spl hrz	Spl hrz	Spl hrz	Spl hrz	Spl hrz	Spl hrz	Spl hrz	Spl hrz	Spl hrz	Spl hrz	Spl hrz	Spl hrz
Mineral		Opx	Opx	Opx	Opx	Opx	Opx	Opx	Opx	Opx	Opx	Opx	Opx	Opx	Opx	Opx	Opx
Type		Cl core	Cl core	Cl core	Cl core	Cl core	Cl core	Cl core	Cl core	Cl core	Cl core	Cl core	Cl core	Cl core	Cl core	Cl core	Cl core
Wt.%	SiO2	56.49	56.24	56.19	56.31	56.33	56.24	56.25	56.32	56.24	56.21	56.55	56.43	56.18	56.68	55.43	56.75
	TiO2	0.02	b.d.	0.02	0.03	0.02	b.d.	0.02	b.d.	0.01	0.05	0.01	0.01	0.03	b.d.	0.04	0.03
	Cr2O3	0.83	0.80	0.78	0.81	0.66	0.82	0.80	0.74	0.82	0.76	0.78	0.75	0.76	0.59	0.58	0.60
	Al2O3	3.26	3.27	3.18	3.31	3.18	3.27	3.09	3.23	3.34	3.26	3.19	3.21	3.07	3.00	2.71	2.90
	FeO	5.79	5.70	5.43	5.83	5.95	5.77	5.55	5.92	5.84	5.54	5.84	5.84	5.45	6.00	5.63	5.63
	MnO	0.08	0.14	0.16	0.16	0.21	0.16	0.16	0.16	0.13	0.15	0.14	0.10	0.14	0.19	0.17	0.12
	NiO	0.05	0.16	0.10	0.07	0.04	0.04	0.08	0.06	0.13	0.06	0.02	0.13	0.12	0.10	0.06	0.06
	MgO	33.86	33.92	32.92	33.75	34.03	33.94	32.78	33.86	33.87	33.86	33.67	33.73	32.95	33.77	34.08	34.15
	CaO	0.60	0.59	2.09	0.60	0.53	0.58	2.16	0.59	0.56	0.92	0.65	0.70	2.15	0.59	0.55	0.70
	Na2O	b.d.	b.d.	0.01	0.01	0.01	0.03	0.03	b.d.	0.02	b.d.	0.01	0.03	0.01	0.01	0.01	0.01
	K2O	b.d.	0.02	0.01	b.d.	b.d.	0.01	b.d.	0.01	b.d.	b.d.	0.01	b.d.	0.01	b.d.	b.d.	b.d.
	Total	100.98	100.84	100.89	100.88	100.96	100.86	100.92	100.89	100.96	100.81	100.87	100.93	100.87	100.93	99.26	100.95
Cations	Si	1.928	1.924	1.926	1.925	1.925	1.923	1.929	1.926	1.922	1.923	1.932	1.929	1.927	1.937	1.926	1.936
	Ti	0.001	b.d.	0.001	0.001	0.001	b.d.	0.001	b.d.	0.000	0.001	0.000	0.000	0.001	b.d.	0.001	0.001
	Cr	0.022	0.022	0.021	0.022	0.018	0.022	0.022	0.020	0.022	0.021	0.021	0.020	0.021	0.016	0.016	0.016
	Al	0.131	0.132	0.128	0.133	0.128	0.132	0.125	0.130	0.135	0.131	0.128	0.129	0.124	0.121	0.111	0.117
	Fe2+	0.165	0.163	0.156	0.167	0.170	0.165	0.159	0.169	0.167	0.158	0.167	0.167	0.156	0.171	0.164	0.161
	Mn	0.002	0.004	0.005	0.005	0.006	0.005	0.005	0.005	0.004	0.004	0.004	0.003	0.004	0.005	0.005	0.003
	Ni	0.001	0.004	0.003	0.002	0.001	0.001	0.002	0.002	0.004	0.002	0.001	0.004	0.003	0.003	0.002	0.002
	Mg	1.722	1.729	1.682	1.720	1.733	1.730	1.675	1.726	1.725	1.726	1.715	1.718	1.684	1.720	1.765	1.736
	Ca	0.022	0.022	0.077	0.022	0.019	0.021	0.079	0.022	0.021	0.034	0.024	0.026	0.079	0.022	0.020	0.026
	Na	b.d.	b.d.	0.001	0.001	0.001	0.002	0.002	b.d.	0.001	b.d.	0.001	0.002	0.001	0.001	0.001	0.001
	K	b.d.	0.001	0.000	b.d.	b.d.	0.000	b.d.	0.000	b.d.	b.d.	0.000	b.d.	0.000	b.d.	b.d.	b.d.
	Sum	3.995	4.000	3.999	3.997	4.002	4.001	3.998	3.999	4.000	4.000	3.993	3.997	4.001	3.995	4.010	3.997
	Mg #	0.912	0.914	0.915	0.912	0.911	0.913	0.913	0.911	0.912	0.916	0.911	0.911	0.915	0.909	0.915	0.915

Abbreviations: Opx = orthopyroxene, Spl hrz = spinel harzburgite, Cl core = clast core, b.d. = below detection limit.
Mg# calculated as (MgO/40.3) / (MgO/40.3 + FeO/71.85).

Major element composition of orthopyroxene from the Dramala spinel harzburgite and plagioclase-bearing harzburgite continued

Sample		PI2	PI2	PI2	PI2	PI2	PI2	PI2	PI2	PI2	PI2	PI2	PI2	PI2	PI2	PI2	PI2
Rock		Spl hrz	Spl hrz	Spl hrz	Spl hrz	Spl hrz	Spl hrz	Spl hrz	Spl hrz	Spl hrz	Spl hrz	Spl hrz	Spl hrz	Spl hrz	Spl hrz	Spl hrz	Spl hrz
Mineral		Opx	Opx	Opx	Opx	Opx	Opx	Opx	Opx	Opx	Opx	Opx	Opx	Opx	Opx	Opx	Opx
Type		Cl core	Cl core	Cl core	Cl core	Cl core	Cl core	Cl core	Cl core	Cl core	Cl core	Cl core	Cl core	Cl core	Cl core	Cl core	Cl core
Wt.%	SiO2	56.06	55.95	55.78	55.80	56.36	56.33	55.21	56.58	56.50	56.08	56.14	56.33	56.13	56.54	56.32	56.30
	TiO2	0.04	0.03	0.05	0.01	0.02	0.03	0.03	b.d.	0.01	0.01	0.01	b.d.	b.d.	b.d.	0.01	0.02
	Cr2O3	0.64	0.63	0.79	0.81	0.69	0.72	0.64	0.77	0.71	0.71	0.89	0.82	0.81	0.84	0.83	0.83
	Al2O3	2.71	2.61	3.15	3.08	3.03	2.99	3.19	3.15	3.20	3.33	3.40	3.30	3.22	3.16	3.33	3.29
	FeO	5.68	5.67	5.68	5.80	5.63	5.74	5.85	5.82	5.85	5.95	5.93	5.86	5.95	5.65	5.82	5.60
	MnO	0.19	0.16	0.14	0.15	0.13	0.12	0.12	0.13	0.13	0.13	0.12	0.15	0.13	0.14	0.15	0.18
	NiO	0.10	0.09	0.06	0.03	0.07	0.05	0.11	0.04	0.07	0.05	0.08	0.07	0.07	0.04	0.07	0.12
	MgO	33.60	34.22	34.11	34.09	33.87	34.19	33.65	33.84	33.79	33.47	33.72	33.82	33.65	34.05	34.15	33.26
	CaO	1.62	0.70	0.61	0.72	0.56	0.55	0.71	0.66	0.62	1.00	0.60	0.53	0.65	0.49	0.60	1.36
	Na2O	0.01	b.d.	b.d.	0.03	b.d.	0.02	b.d.	b.d.	0.01	b.d.	b.d.	0.02	0.04	b.d.	b.d.	b.d.
	K2O	b.d.	b.d.	b.d.	0.01	0.02	b.d.	0.01	b.d.	0.02	b.d.	b.d.	b.d.	b.d.	b.d.	b.d.	b.d.
	Total	100.65	100.06	100.37	100.53	100.38	100.74	99.52	100.99	100.91	100.73	100.89	100.90	100.65	100.91	101.28	100.96
Cations	Si	1.927	1.929	1.917	1.917	1.934	1.927	1.916	1.931	1.930	1.923	1.921	1.925	1.925	1.930	1.919	1.926
	Ti	0.001	0.001	0.001	0.000	0.001	0.001	0.001	b.d.	0.000	0.000	0.000	b.d.	b.d.	0.000	0.000	0.001
	Cr	0.017	0.017	0.021	0.022	0.019	0.019	0.018	0.021	0.019	0.019	0.024	0.022	0.022	0.023	0.022	0.022
	Al	0.110	0.106	0.128	0.125	0.123	0.121	0.131	0.127	0.129	0.135	0.137	0.133	0.130	0.127	0.134	0.133
	Fe2+	0.163	0.163	0.163	0.167	0.162	0.164	0.170	0.166	0.167	0.171	0.170	0.167	0.171	0.161	0.166	0.160
	Mn	0.006	0.005	0.004	0.004	0.004	0.003	0.004	0.004	0.004	0.004	0.003	0.004	0.004	0.004	0.004	0.005
	Ni	0.003	0.002	0.002	0.001	0.002	0.001	0.003	0.001	0.002	0.001	0.002	0.002	0.002	0.001	0.002	0.003
	Mg	1.721	1.759	1.748	1.746	1.732	1.744	1.741	1.721	1.721	1.710	1.719	1.723	1.720	1.732	1.734	1.696
	Ca	0.060	0.026	0.022	0.027	0.021	0.020	0.026	0.024	0.023	0.037	0.022	0.019	0.024	0.018	0.022	0.050
	Na	0.001	b.d.	b.d.	0.002	b.d.	0.001	b.d.	b.d.	0.001	b.d.	b.d.	0.001	0.003	b.d.	b.d.	b.d.
	K	b.d.	b.d.	b.d.	0.000	0.001	b.d.	0.000	b.d.	0.001	b.d.	b.d.	b.d.	b.d.	b.d.	b.d.	b.d.
	Sum	4.009	4.008	4.007	4.010	3.996	4.002	4.009	3.995	3.996	4.000	3.999	3.998	4.000	3.996	4.003	3.996
	Mg #	0.913	0.915	0.915	0.913	0.915	0.914	0.911	0.912	0.911	0.909	0.910	0.911	0.910	0.915	0.913	0.914

Abbreviations: Opx = orthopyroxene, Spl hrz = spinel harzburgite, Cl core = clast core, b.d. = below detection limit.
Mg# calculated as (MgO/40.3) / (MgO/40.3 + FeO/71.85).

Major element composition of orthopyroxene from the Dramala spinel harzburgite and plagioclase-bearing harzburgite continued

Sample		PI2	PI2	PI2	PI2	PI2	PI2	PI2	PI2	PI2	PI2	PI2	PI2	PI2	PI2	PI2	PI2
Rock		Spl hrz	Spl hrz	Spl hrz	Spl hrz	Spl hrz	Spl hrz	Spl hrz	Spl hrz	Spl hrz	Spl hrz	Spl hrz	Spl hrz	Spl hrz	Spl hrz	Spl hrz	Spl hrz
Mineral		Opx	Opx	Opx	Opx	Opx	Opx	Opx	Opx	Opx	Opx	Opx	Opx	Opx	Opx	Opx	Opx
Type		Cl core	Cl core	Cl core	Cl core	Cl core	Cl core	Cl core	Cl core	Cl core	Cl core	Cl core	Cl core	Cl core	Cl core	Cl core	Cl core
Wt.%	SiO2	56.35	56.40	56.27	56.33	56.28	56.40	56.32	56.60	56.28	56.76	56.58	56.51	56.66	56.23	56.81	56.25
	TiO2	0.04	0.02	0.03	0.01	0.05	0.01	b.d.	b.d.	b.d.	0.01	0.03	b.d.	0.05	0.02	b.d.	b.d.
	Cr2O3	0.81	0.82	0.87	0.76	0.72	0.71	0.79	0.68	0.74	0.62	0.66	0.62	0.74	0.65	0.58	0.65
	Al2O3	3.28	3.42	3.33	3.11	3.18	3.05	2.94	2.90	3.09	2.91	2.98	3.09	2.94	2.58	2.99	2.68
	FeO	5.73	5.73	5.72	5.72	5.92	5.67	5.82	5.41	5.84	5.60	5.84	5.80	5.81	5.23	5.69	6.01
	MnO	0.12	0.09	0.13	0.17	0.17	0.14	0.17	0.13	0.12	0.14	0.18	0.16	0.16	0.09	0.09	0.11
	NiO	0.04	0.12	0.04	0.04	0.08	0.14	0.08	0.06	0.13	0.05	0.11	0.09	0.10	0.04	0.06	0.10
	MgO	33.75	33.76	33.55	33.58	33.89	33.82	33.68	32.79	34.09	34.20	34.24	34.01	34.08	31.49	34.15	34.21
	CaO	0.72	0.57	0.67	1.02	0.58	0.76	1.08	2.38	0.55	0.58	0.63	0.49	0.51	4.53	0.54	0.57
	Na2O	b.d.	0.01	b.d.	b.d.	b.d.	b.d.	0.01	b.d.	b.d.	0.02	b.d.	0.02	b.d.	0.05	0.03	b.d.
	K2O	b.d.	b.d.	0.01	b.d.	0.02	b.d.	0.01	b.d.	b.d.	b.d.	0.02	0.01	0.01	b.d.	0.01	0.01
	Total	100.84	100.94	100.62	100.74	100.89	100.70	100.90	100.95	100.84	100.89	101.27	100.80	101.06	100.91	100.95	100.59
Cations	Si	1.926	1.925	1.928	1.929	1.925	1.931	1.929	1.938	1.925	1.936	1.928	1.932	1.933	1.937	1.937	1.931
	Ti	0.001	0.001	0.001	0.000	0.001	0.000	b.d.	0.000	0.000	0.000	0.001	b.d.	0.001	0.001	b.d.	0.000
	Cr	0.022	0.022	0.024	0.021	0.019	0.019	0.021	0.018	0.020	0.017	0.018	0.017	0.020	0.018	0.016	0.018
	Al	0.132	0.138	0.134	0.126	0.128	0.123	0.119	0.117	0.125	0.117	0.120	0.125	0.118	0.105	0.120	0.108
	Fe2+	0.164	0.164	0.164	0.164	0.169	0.162	0.167	0.155	0.167	0.160	0.166	0.166	0.166	0.151	0.162	0.172
	Mn	0.003	0.003	0.004	0.005	0.005	0.004	0.005	0.004	0.003	0.004	0.005	0.005	0.005	0.003	0.003	0.003
	Ni	0.001	0.003	0.001	0.001	0.002	0.004	0.002	0.002	0.004	0.001	0.003	0.002	0.003	0.001	0.002	0.003
	Mg	1.720	1.718	1.713	1.714	1.728	1.726	1.719	1.673	1.738	1.739	1.739	1.733	1.733	1.617	1.735	1.750
	Ca	0.026	0.021	0.025	0.037	0.021	0.028	0.040	0.087	0.020	0.021	0.023	0.018	0.019	0.167	0.020	0.021
	Na	b.d.	0.001	b.d.	b.d.	b.d.	b.d.	0.001	b.d.	b.d.	0.001	b.d.	0.001	b.d.	0.003	0.002	b.d.
	K	b.d.	b.d.	0.000	b.d.	0.001	b.d.	0.000	b.d.	b.d.	b.d.	0.001	0.000	0.000	b.d.	0.000	0.000
	Sum	3.996	3.994	3.993	3.997	4.000	3.998	4.002	3.994	4.002	3.997	4.003	3.998	3.997	4.003	3.996	4.007
	Mg #	0.913	0.913	0.913	0.913	0.911	0.914	0.912	0.915	0.912	0.916	0.913	0.913	0.913	0.915	0.915	0.910

Abbreviations: Opx = orthopyroxene, Spl hrz = spinel harzburgite, Cl core = clast core, b.d. = below detection limit.
Mg# calculated as (MgO/40.3) / (MgO/40.3 + FeO/71.85).

Major element composition of orthopyroxene from the Dramala spinel harzburgite and plagioclase-bearing harzburgite continued

Sample		PI2	PI2	PI2	PI2	PI2	PI2	PI2	PI2	PI2	PI2	PI2	PI2	PI2	PI2	PI2	PI2
Rock		Spl hrz	Spl hrz	Spl hrz	Spl hrz	Spl hrz	Spl hrz	Spl hrz	Spl hrz	Spl hrz	Spl hrz	Spl hrz	Spl hrz	Spl hrz	Spl hrz	Spl hrz	Spl hrz
Mineral		Opx	Opx	Opx	Opx	Opx	Opx	Opx	Opx	Opx	Opx	Opx	Opx	Opx	Opx	Opx	Opx
Type		Cl core	Cl core	Cl core	Cl core	Cl core	Cl core	Cl core	Cl core	Cl core	Cl core	Cl core	Cl core	Cl core	Cl core	Cl core	Cl core
Wt.%	SiO2	56.41	56.52	56.51	56.41	56.27	56.56	56.33	56.28	56.41	56.21	56.29	56.36	56.56	56.35	56.22	56.01
	TiO2	0.01	0.02	b.d.	0.03	0.02	0.01	0.01	0.02	0.01	0.02	0.04	b.d.	0.02	0.01	b.d.	0.03
	Cr2O3	0.64	0.66	0.68	0.72	0.66	0.68	0.69	0.71	0.69	0.69	0.70	0.67	0.70	0.69	0.74	0.74
	Al2O3	2.69	2.70	2.70	2.89	2.80	2.79	2.88	2.85	2.85	2.82	2.83	2.88	2.83	2.80	2.95	3.03
	FeO	5.92	5.83	5.84	6.00	5.78	5.79	5.83	6.03	5.69	5.97	5.85	5.90	5.79	5.66	5.85	5.76
	MnO	0.12	0.20	0.17	0.14	0.14	0.16	0.10	0.12	0.14	0.09	0.13	0.09	0.17	0.13	0.13	0.10
	NiO	0.06	0.09	0.11	0.10	0.07	0.04	0.08	0.06	0.11	0.06	0.12	0.08	0.08	0.09	0.09	0.11
	MgO	34.19	34.32	34.38	34.02	33.64	34.17	34.00	33.99	34.22	34.27	34.26	34.14	34.10	33.63	34.04	34.24
	CaO	0.58	0.60	0.53	0.62	1.59	0.61	0.66	0.69	0.67	0.66	0.60	0.59	0.63	1.59	0.64	0.57
	Na2O	b.d.	0.01	0.03	0.01	0.01	0.01	b.d.	b.d.	b.d.	0.01	b.d.	b.d.	0.01	b.d.	0.01	0.01
	K2O	b.d.	b.d.	b.d.	b.d.	b.d.	b.d.	b.d.	b.d.	0.01	0.01	0.01	b.d.	b.d.	b.d.	b.d.	b.d.
	Total	100.62	100.95	100.95	100.94	100.98	100.82	100.58	100.75	100.80	100.81	100.83	100.71	100.89	100.95	100.67	100.60
Cations	Si	1.934	1.932	1.931	1.929	1.927	1.934	1.931	1.929	1.930	1.925	1.927	1.930	1.933	1.930	1.927	1.921
	Ti	0.000	0.001	b.d.	0.001	0.001	0.000	0.000	0.001	0.000	0.001	0.001	b.d.	0.001	0.000	b.d.	0.001
	Cr	0.017	0.018	0.018	0.019	0.018	0.018	0.019	0.019	0.019	0.019	0.019	0.018	0.019	0.019	0.020	0.020
	Al	0.109	0.109	0.109	0.117	0.113	0.112	0.116	0.115	0.115	0.114	0.114	0.116	0.114	0.113	0.119	0.122
	Fe2+	0.170	0.167	0.167	0.172	0.166	0.166	0.167	0.173	0.163	0.171	0.167	0.169	0.165	0.162	0.168	0.165
	Mn	0.003	0.006	0.005	0.004	0.004	0.005	0.003	0.003	0.004	0.003	0.004	0.003	0.005	0.004	0.004	0.003
	Ni	0.002	0.002	0.003	0.003	0.002	0.001	0.002	0.002	0.003	0.002	0.003	0.002	0.002	0.002	0.002	0.003
	Mg	1.747	1.748	1.751	1.734	1.717	1.741	1.738	1.736	1.745	1.750	1.748	1.743	1.737	1.716	1.739	1.750
	Ca	0.021	0.022	0.019	0.023	0.058	0.022	0.024	0.025	0.025	0.024	0.022	0.022	0.023	0.058	0.024	0.021
	Na	b.d.	0.001	0.002	0.001	0.001	0.001	b.d.	b.d.	b.d.	0.001	b.d.	b.d.	0.001	b.d.	0.001	0.001
	K	b.d.	b.d.	b.d.	b.d.	b.d.	b.d.	b.d.	b.d.	0.000	0.000	0.000	b.d.	b.d.	b.d.	b.d.	b.d.
	Sum	4.003	4.005	4.006	4.002	4.007	4.001	4.001	4.003	4.003	4.008	4.006	4.003	4.000	4.004	4.004	4.007
	Mg #	0.911	0.913	0.913	0.910	0.912	0.913	0.912	0.909	0.915	0.911	0.913	0.912	0.913	0.914	0.912	0.914

Abbreviations: Opx = orthopyroxene, Spl hrz = spinel harzburgite, Cl core = clast core, b.d. = below detection limit.
Mg# calculated as (MgO/40.3) / (MgO/40.3 + FeO/71.85).

Major element composition of orthopyroxene from the Dramala spinel harzburgite and plagioclase-bearing harzburgite continued

Sample		PI2	PI2	PI2	PI2	PI2	PI2	PI2	PI2	PI2	PI2	PI2	PI2	PI2	PI2	PI2	PI2
Rock		Spl hrz	Spl hrz	Spl hrz	Spl hrz	Spl hrz	Spl hrz	Spl hrz	Spl hrz	Spl hrz	Spl hrz	Spl hrz	Spl hrz	Spl hrz	Spl hrz	Spl hrz	Spl hrz
Mineral		Opx	Opx	Opx	Opx	Opx	Opx	Opx	Opx	Opx	Opx	Opx	Opx	Opx	Opx	Opx	Opx
Type		Cl core	Cl core	Cl core	Cl core	Cl core	Cl core	Cl core	Cl core	Cl core	Cl core	Cl core	Cl core	Cl core	Cl core	Cl core	Cl core
Wt.%	SiO2	56.02	56.36	55.87	56.09	55.98	56.16	56.09	56.09	56.05	55.81	56.24	56.10	56.02	55.85	55.92	56.03
	TiO2	0.01	0.01	0.03	0.03	0.04	0.02	0.02	b.d.	0.02	0.01	0.02	b.d.	0.03	0.01	0.01	b.d.
	Cr2O3	0.76	0.78	0.79	0.77	0.79	0.80	0.81	0.79	0.78	0.84	0.78	0.79	0.83	0.80	0.78	0.81
	Al2O3	3.00	2.99	3.07	3.03	3.02	2.97	3.02	2.96	3.08	3.30	3.01	3.10	3.04	3.11	3.12	3.10
	FeO	5.92	5.87	5.58	5.71	5.81	6.07	5.75	5.87	6.08	5.75	5.89	5.86	6.04	5.29	6.10	6.07
	MnO	0.22	0.15	0.12	0.14	0.12	0.12	0.23	0.13	0.20	0.11	0.16	0.16	0.13	0.18	0.20	0.09
	NiO	0.08	0.11	0.09	0.09	0.12	0.11	0.11	0.11	0.11	0.09	0.13	0.08	0.12	0.07	0.10	0.07
	MgO	34.32	33.98	33.05	34.07	34.11	34.12	34.20	33.69	34.07	33.48	34.18	33.85	34.00	32.89	33.98	33.98
	CaO	0.51	0.63	1.73	0.64	0.57	0.54	0.54	1.05	0.57	1.22	0.53	0.98	0.69	1.61	0.57	0.55
	Na2O	b.d.	b.d.	b.d.	0.01	b.d.	0.04	0.03	b.d.	0.02	0.02	b.d.	0.04	b.d.	0.02	b.d.	0.01
	K2O	b.d.	0.01	b.d.	0.01	0.01	b.d.	0.01	b.d.	b.d.	b.d.	0.01	b.d.	0.02	b.d.	b.d.	b.d.
	Total	100.84	100.89	100.33	100.59	100.57	100.95	100.81	100.69	100.98	100.63	100.95	100.96	100.92	99.83	100.78	100.71
Cations	Si	1.919	1.928	1.925	1.924	1.921	1.922	1.921	1.925	1.919	1.917	1.923	1.921	1.919	1.931	1.918	1.922
	Ti	0.000	0.000	0.001	0.001	0.001	0.001	0.001	b.d.	0.001	0.000	0.001	b.d.	0.001	0.000	0.000	b.d.
	Cr	0.021	0.021	0.022	0.021	0.021	0.022	0.022	0.021	0.021	0.023	0.021	0.021	0.022	0.022	0.021	0.022
	Al	0.121	0.121	0.125	0.122	0.122	0.120	0.122	0.120	0.124	0.134	0.121	0.125	0.123	0.127	0.126	0.125
	Fe2+	0.170	0.168	0.161	0.164	0.167	0.174	0.165	0.168	0.174	0.165	0.168	0.168	0.173	0.153	0.175	0.174
	Mn	0.006	0.004	0.004	0.004	0.003	0.003	0.007	0.004	0.006	0.003	0.005	0.005	0.004	0.005	0.006	0.003
	Ni	0.002	0.003	0.002	0.002	0.003	0.003	0.003	0.003	0.003	0.002	0.004	0.002	0.003	0.002	0.003	0.002
	Mg	1.752	1.732	1.698	1.742	1.745	1.741	1.746	1.724	1.739	1.714	1.742	1.727	1.736	1.695	1.737	1.737
	Ca	0.019	0.023	0.064	0.024	0.021	0.020	0.020	0.039	0.021	0.045	0.019	0.036	0.025	0.060	0.021	0.020
	Na	b.d.	b.d.	b.d.	0.001	b.d.	0.003	0.002	b.d.	0.001	0.001	b.d.	0.003	b.d.	0.001	b.d.	0.001
	K	b.d.	0.000	b.d.	0.000	0.000	b.d.	0.000	b.d.	b.d.	b.d.	0.000	b.d.	0.001	b.d.	b.d.	b.d.
	Sum	4.010	4.001	4.001	4.004	4.006	4.008	4.008	4.004	4.008	4.005	4.005	4.007	4.008	3.995	4.008	4.005
	Mg #	0.912	0.912	0.913	0.914	0.913	0.909	0.914	0.911	0.909	0.912	0.912	0.911	0.909	0.917	0.909	0.909

Abbreviations: Opx = orthopyroxene, Spl hrz = spinel harzburgite, Cl core = clast core, b.d. = below detection limit.
Mg# calculated as (MgO/40.3) / (MgO/40.3 + FeO/71.85).

Major element composition of orthopyroxene from the Dramala spinel harzburgite and plagioclase-bearing harzburgite continued

Sample		PI2	PI2	PI2	PI2	PI2	PI2	PI2	PI2	PI2	PI2	PI2	PI2	PI2	PI2	PI2	PI2
Rock		Spl hrz	Spl hrz	Spl hrz	Spl hrz	Spl hrz	Spl hrz	Spl hrz	Spl hrz	Spl hrz	Spl hrz	Spl hrz	Spl hrz	Spl hrz	Spl hrz	Spl hrz	Spl hrz
Mineral		Opx	Opx	Opx	Opx	Opx	Opx	Opx	Opx	Opx	Opx	Opx	Opx	Opx	Opx	Opx	Opx
Type		Cl core	Cl core	Cl core	Cl core	Cl core	Cl core	Cl core	Cl core	Cl core	Cl core	Cl core	Cl core	Cl core	Cl core	Cl core	Cl core
Wt.%	SiO2	55.79	55.99	55.92	55.82	56.07	55.72	56.03	55.52	56.28	56.02	56.20	56.43	56.25	54.94	56.01	55.81
	TiO2	0.01	0.01	0.03	0.02	0.03	0.03	b.d.	0.04	0.03	0.02	0.04	0.02	0.01	0.02	b.d.	0.04
	Cr2O3	0.86	0.79	0.78	0.83	0.80	0.77	0.81	0.81	0.79	0.82	0.79	0.75	0.81	0.83	0.76	0.85
	Al2O3	2.88	3.10	3.12	3.19	3.03	3.13	3.05	2.91	2.83	2.93	3.03	2.86	3.10	3.03	3.07	3.00
	FeO	5.23	5.81	5.88	5.62	6.23	5.71	5.74	5.21	5.63	5.79	5.76	5.81	5.83	4.48	5.94	5.59
	MnO	0.08	0.13	0.12	0.18	0.14	0.13	0.15	0.20	0.18	0.13	0.16	0.16	0.22	0.10	0.18	0.06
	NiO	0.05	0.08	0.09	0.10	0.11	0.08	0.14	0.08	0.11	0.09	0.06	0.10	0.10	0.09	0.14	0.09
	MgO	31.98	34.26	34.04	33.28	33.86	32.94	33.85	30.61	33.72	33.50	34.12	34.19	33.82	28.46	34.11	33.04
	CaO	3.61	0.64	0.58	0.84	0.67	1.28	0.64	4.98	1.09	1.39	0.68	0.45	0.67	8.80	0.65	2.41
	Na2O	b.d.	b.d.	b.d.	0.02	b.d.	b.d.	0.02	0.02	b.d.	b.d.	0.02	b.d.	b.d.	b.d.	b.d.	0.01
	K2O	b.d.	0.01	b.d.	0.01	b.d.	b.d.	b.d.	b.d.	0.01	b.d.	0.02	b.d.	0.01	0.01	0.02	0.01
	Total	100.49	100.82	100.56	99.91	100.94	99.79	100.43	100.38	100.67	100.69	100.88	100.77	100.82	100.76	100.88	100.91
Cations	Si	1.927	1.917	1.920	1.928	1.921	1.929	1.925	1.928	1.930	1.924	1.923	1.931	1.926	1.916	1.919	1.918
	Ti	0.000	0.000	0.001	0.001	0.001	0.001	b.d.	0.001	0.001	0.001	0.001	0.001	0.000	0.001	b.d.	0.001
	Cr	0.023	0.021	0.021	0.023	0.022	0.021	0.022	0.022	0.021	0.022	0.021	0.020	0.022	0.023	0.021	0.023
	Al	0.117	0.125	0.126	0.130	0.122	0.128	0.124	0.119	0.114	0.119	0.122	0.115	0.125	0.125	0.124	0.121
	Fe2+	0.151	0.166	0.169	0.162	0.179	0.165	0.165	0.151	0.161	0.166	0.165	0.166	0.167	0.131	0.170	0.161
	Mn	0.002	0.004	0.003	0.005	0.004	0.004	0.004	0.006	0.005	0.004	0.005	0.005	0.006	0.003	0.005	0.002
	Ni	0.001	0.002	0.002	0.003	0.003	0.002	0.004	0.002	0.003	0.002	0.002	0.003	0.003	0.003	0.004	0.002
	Mg	1.646	1.749	1.742	1.713	1.729	1.699	1.734	1.584	1.724	1.715	1.740	1.744	1.726	1.480	1.742	1.692
	Ca	0.134	0.023	0.021	0.031	0.025	0.047	0.024	0.185	0.040	0.051	0.025	0.016	0.025	0.329	0.024	0.089
	Na	b.d.	b.d.	b.d.	0.001	b.d.	b.d.	0.001	0.001	b.d.	b.d.	0.001	b.d.	b.d.	b.d.	b.d.	0.001
	K	b.d.	0.000	b.d.	0.000	b.d.	b.d.	b.d.	b.d.	0.000	b.d.	0.001	b.d.	0.000	0.000	0.001	0.000
	Sum	4.002	4.009	4.006	3.997	4.006	3.996	4.003	4.001	4.001	4.005	4.005	4.001	4.000	4.010	4.009	4.010
	Mg #	0.916	0.913	0.912	0.913	0.906	0.911	0.913	0.913	0.914	0.912	0.913	0.913	0.912	0.919	0.911	0.913

Abbreviations: Opx = orthopyroxene, Spl hrz = spinel harzburgite, Cl core = clast core, b.d. = below detection limit.
Mg# calculated as (MgO/40.3) / (MgO/40.3 + FeO/71.85).

Major element composition of orthopyroxene from the Dramala spinel harzburgite and plagioclase-bearing harzburgite continued

Sample		PI2	PI2	PI2	PI2	PI2	PI2	PI2	PI2	PI2	PI2	PI2	PI2	PI2	PI2	PI2	PI2
Rock		Spl hrz	Spl hrz	Spl hrz	Spl hrz	Spl hrz	Spl hrz	Spl hrz	Spl hrz	Spl hrz	Spl hrz	Spl hrz	Spl hrz	Spl hrz	Spl hrz	Spl hrz	Spl hrz
Mineral		Opx	Opx	Opx	Opx	Opx	Opx	Opx	Opx	Opx	Opx	Opx	Opx	Opx	Opx	Opx	Opx
Type		Cl core	Cl core	Cl core	Cl core	Cl core	Cl core	Cl core	Cl core	Cl core	Cl core	Cl core	Cl core	Cl core	Cl core	Cl core	Cl core
Wt.%	SiO2	56.23	56.14	56.10	56.11	55.69	56.21	56.30	55.96	56.28	56.11	56.15	55.95	56.21	56.28	56.20	56.09
	TiO2	0.01	0.02	0.02	b.d.	b.d.	0.01	b.d.	0.01	b.d.	0.05	0.02	b.d.	0.01	0.01	0.03	b.d.
	Cr2O3	0.79	0.81	0.77	0.79	0.77	0.80	0.79	0.76	0.75	0.80	0.75	0.76	0.86	0.77	0.79	0.73
	Al2O3	3.00	3.05	2.91	2.99	3.02	2.90	2.93	2.91	2.97	2.78	2.96	3.00	3.02	2.99	3.05	2.83
	FeO	6.03	5.99	5.71	5.98	5.46	6.06	5.75	5.38	5.75	5.71	5.78	5.67	5.85	6.07	5.60	5.62
	MnO	0.14	0.17	0.21	0.12	0.12	0.17	0.11	0.15	0.16	0.17	0.14	0.18	0.14	0.11	0.18	0.18
	NiO	0.07	0.07	0.08	0.12	0.06	0.11	0.10	0.05	0.11	0.08	0.07	0.12	0.10	0.09	0.09	0.06
	MgO	34.09	33.90	33.68	33.75	32.54	34.07	33.89	32.74	33.94	33.24	34.12	33.64	34.21	33.95	33.53	32.93
	CaO	0.53	0.64	1.17	0.94	2.83	0.61	0.71	2.26	0.66	1.82	0.58	0.54	0.52	0.64	1.10	2.32
	Na2O	b.d.	b.d.	b.d.	b.d.	b.d.	b.d.	b.d.	0.01	0.02	b.d.	0.01	0.02	b.d.	0.01	b.d.	0.01
	K2O	b.d.	b.d.	b.d.	b.d.	b.d.	b.d.	0.01	b.d.	0.01	b.d.	0.01	b.d.	b.d.	b.d.	b.d.	b.d.
	Total	100.89	100.79	100.65	100.80	100.49	100.94	100.59	100.23	100.65	100.76	100.59	99.88	100.92	100.92	100.57	100.77
Cations	Si	1.924	1.924	1.926	1.924	1.922	1.925	1.931	1.931	1.929	1.928	1.926	1.931	1.922	1.926	1.929	1.928
	Ti	0.000	0.001	0.001	b.d.	b.d.	0.000	b.d.	0.000	b.d.	0.001	0.001	b.d.	0.000	0.000	0.001	b.d.
	Cr	0.021	0.022	0.021	0.021	0.021	0.022	0.021	0.021	0.020	0.022	0.020	0.021	0.023	0.021	0.021	0.020
	Al	0.121	0.123	0.118	0.121	0.123	0.117	0.118	0.118	0.120	0.113	0.120	0.122	0.122	0.121	0.123	0.115
	Fe2+	0.173	0.172	0.164	0.171	0.158	0.173	0.165	0.155	0.165	0.164	0.166	0.164	0.167	0.174	0.161	0.162
	Mn	0.004	0.005	0.006	0.003	0.004	0.005	0.003	0.004	0.005	0.005	0.004	0.005	0.004	0.003	0.005	0.005
	Ni	0.002	0.002	0.002	0.003	0.002	0.003	0.003	0.001	0.003	0.002	0.002	0.003	0.003	0.002	0.002	0.002
	Mg	1.739	1.731	1.723	1.725	1.674	1.739	1.732	1.684	1.734	1.702	1.744	1.731	1.744	1.732	1.715	1.687
	Ca	0.019	0.023	0.043	0.035	0.105	0.022	0.026	0.084	0.024	0.067	0.021	0.020	0.019	0.023	0.040	0.085
	Na	b.d.	b.d.	b.d.	b.d.	b.d.	b.d.	b.d.	0.001	0.001	b.d.	0.001	0.001	b.d.	0.001	b.d.	0.001
	K	b.d.	b.d.	b.d.	b.d.	b.d.	b.d.	0.000	b.d.	0.000	b.d.	0.000	b.d.	b.d.	b.d.	b.d.	b.d.
	Sum	4.004	4.003	4.004	4.005	4.006	4.006	4.000	3.999	4.002	4.004	4.004	3.998	4.005	4.003	3.998	4.005
	Mg #	0.910	0.910	0.913	0.910	0.914	0.909	0.913	0.916	0.913	0.912	0.913	0.914	0.912	0.909	0.914	0.913

Abbreviations: Opx = orthopyroxene, Spl hrz = spinel harzburgite, Cl core = clast core, b.d. = below detection limit.
Mg# calculated as (MgO/40.3) / (MgO/40.3 + FeO/71.85).

Major element composition of orthopyroxene from the Dramala spinel harzburgite and plagioclase-bearing harzburgite continued

Sample		PI2	PI2	PI2	PI2	PI2	PI2	PI2	PI2	PI2	PI2	PI2	PI2	PI2	PI2	PI2	PI2
Rock		Spl hrz	Spl hrz	Spl hrz	Spl hrz	Spl hrz	Spl hrz	Spl hrz	Spl hrz	Spl hrz	Spl hrz	Spl hrz	Spl hrz	Spl hrz	Spl hrz	Spl hrz	Spl hrz
Mineral		Opx	Opx	Opx	Opx	Opx	Opx	Opx	Opx	Opx	Opx	Opx	Opx	Opx	Opx	Opx	Opx
Type		Cl core	Cl core	Cl core	Cl core	Cl core	Cl core	Cl core	Cl core	Cl core	Cl core	Cl core	Cl core	Cl core	Cl core	Cl core	Cl core
Wt.%	SiO2	56.11	56.23	56.31	56.21	56.30	56.31	56.30	56.35	55.78	56.29	56.41	56.12	56.27	56.18	56.03	56.14
	TiO2	0.02	0.02	0.02	0.02	0.01	0.03	0.01	0.02	0.02	0.03	0.02	0.03	0.01	0.02	0.02	0.02
	Cr2O3	0.74	0.75	0.74	0.75	0.67	0.70	0.76	0.76	0.72	0.74	0.75	0.67	0.69	0.70	0.74	0.68
	Al2O3	2.93	2.90	2.80	2.93	2.90	2.87	2.85	2.74	2.97	2.91	2.77	2.78	2.78	2.88	2.82	2.86
	FeO	5.93	5.89	5.93	6.09	6.15	5.96	5.98	5.67	5.38	6.06	5.95	5.84	6.03	6.21	6.16	6.07
	MnO	0.14	0.20	0.15	0.12	0.16	0.10	0.13	0.18	0.14	0.15	0.12	0.07	0.14	0.10	0.14	0.13
	NiO	0.09	0.09	0.11	0.08	0.09	0.12	0.09	0.08	0.09	0.11	0.06	0.12	0.10	0.06	0.11	0.09
	MgO	34.11	34.17	34.25	34.01	33.83	34.05	33.97	34.18	32.79	34.06	34.22	33.35	33.99	34.08	34.06	34.12
	CaO	0.64	0.53	0.63	0.61	0.56	0.60	0.61	0.62	1.63	0.58	0.57	1.79	0.62	0.43	0.71	0.58
	Na2O	0.01	b.d.	b.d.	b.d.	0.04	0.01	b.d.	b.d.	0.01	0.01	0.02	0.01	0.02	0.01	b.d.	b.d.
	K2O	b.d.	b.d.	b.d.	0.01	b.d.	0.02	b.d.	0.02	0.01	b.d.	0.01	b.d.	b.d.	b.d.	b.d.	b.d.
	Total	100.72	100.78	100.94	100.83	100.71	100.77	100.70	100.62	99.54	100.94	100.90	100.78	100.65	100.67	100.79	100.69
Cations	Si	1.924	1.926	1.926	1.926	1.931	1.929	1.930	1.931	1.934	1.926	1.930	1.928	1.931	1.927	1.923	1.926
	Ti	0.001	0.001	0.001	0.001	0.000	0.001	0.000	0.001	0.001	0.001	0.001	0.001	0.000	0.001	0.001	0.001
	Cr	0.020	0.020	0.020	0.020	0.018	0.019	0.021	0.021	0.020	0.020	0.020	0.018	0.019	0.019	0.020	0.018
	Al	0.118	0.117	0.113	0.118	0.117	0.116	0.115	0.111	0.121	0.117	0.112	0.113	0.112	0.116	0.114	0.116
	Fe2+	0.170	0.169	0.170	0.174	0.176	0.171	0.171	0.163	0.156	0.173	0.170	0.168	0.173	0.178	0.177	0.174
	Mn	0.004	0.006	0.004	0.003	0.005	0.003	0.004	0.005	0.004	0.004	0.003	0.002	0.004	0.003	0.004	0.004
	Ni	0.002	0.002	0.003	0.002	0.002	0.003	0.002	0.002	0.003	0.003	0.002	0.003	0.003	0.002	0.003	0.002
	Mg	1.743	1.744	1.746	1.737	1.729	1.739	1.736	1.746	1.695	1.737	1.745	1.707	1.738	1.742	1.742	1.744
	Ca	0.024	0.019	0.023	0.022	0.021	0.022	0.022	0.023	0.061	0.021	0.021	0.066	0.023	0.016	0.026	0.021
	Na	0.001	b.d.	b.d.	b.d.	0.003	0.001	b.d.	b.d.	0.001	0.001	0.001	0.001	0.001	0.001	b.d.	b.d.
	K	b.d.	b.d.	b.d.	0.000	b.d.	0.001	b.d.	0.001	0.000	b.d.	0.000	b.d.	b.d.	b.d.	b.d.	b.d.
	Sum	4.007	4.005	4.007	4.005	4.003	4.004	4.002	4.003	3.995	4.005	4.005	4.006	4.004	4.005	4.010	4.007
	Mg #	0.911	0.912	0.911	0.909	0.907	0.911	0.910	0.915	0.916	0.909	0.911	0.911	0.909	0.907	0.908	0.909

Abbreviations: Opx = orthopyroxene, Spl hrz = spinel harzburgite, Cl core = clast core, b.d. = below detection limit.
Mg# calculated as (MgO/40.3) / (MgO/40.3 + FeO/71.85).

Major element composition of orthopyroxene from the Dramala spinel harzburgite and plagioclase-bearing harzburgite continued

Sample		PI2	PI2	PI2	PI2	PI2	PI2	PI2	PI2	PI2	PI2	PI2	PI2	PI2	PI2	PI2	PI2
Rock		Spl hrz	Spl hrz	Spl hrz	Spl hrz	Spl hrz	Spl hrz	Spl hrz	Spl hrz	Spl hrz	Spl hrz	Spl hrz	Spl hrz	Spl hrz	Spl hrz	Spl hrz	Spl hrz
Mineral		Opx	Opx	Opx	Opx	Opx	Opx	Opx	Opx	Opx	Opx	Opx	Opx	Opx	Opx	Opx	Opx
Type		Cl core	Cl core	Cl core	Cl core	Cl core	Cl core	Cl core	Cl core	Cl core	Cl core	Cl core	Cl core	Cl core	Cl core	Cl core	Cl core
Wt.%	SiO2	56.39	56.22	56.35	56.49	56.60	56.48	56.11	56.52	56.47	55.95	56.59	56.54	56.61	56.45	56.54	56.41
	TiO2	b.d.	0.04	0.01	0.01	0.02	0.02	0.06	0.02	0.01	0.02	0.05	0.01	b.d.	0.03	0.02	0.02
	Cr2O3	0.71	0.67	0.68	0.63	0.59	0.60	0.53	0.58	0.56	0.54	0.47	0.49	0.66	0.66	0.66	0.65
	Al2O3	2.70	2.79	2.72	2.64	2.60	2.56	2.57	2.60	2.63	2.72	2.58	2.62	2.60	2.63	2.65	2.67
	FeO	5.76	6.03	6.08	5.89	5.93	5.99	6.13	6.26	6.14	6.23	6.13	6.06	5.80	6.00	5.78	5.93
	MnO	0.19	0.14	0.18	0.18	0.16	0.14	0.10	0.14	0.14	0.14	0.12	0.17	0.08	0.15	0.16	0.18
	NiO	0.10	0.09	0.10	0.11	0.10	0.08	0.12	0.08	0.09	0.10	0.07	0.03	0.10	0.10	0.06	0.09
	MgO	33.89	34.25	34.07	34.22	34.15	33.86	33.93	34.11	34.13	34.08	34.32	34.08	34.19	34.15	34.12	34.12
	CaO	1.03	0.55	0.61	0.58	0.63	0.66	0.64	0.67	0.60	0.56	0.58	0.58	0.55	0.58	0.52	0.57
	Na2O	b.d.	0.03	0.02	0.01	0.01	0.02	0.01	b.d.	b.d.	b.d.	b.d.	b.d.	b.d.	b.d.	0.02	b.d.
	K2O	b.d.	0.02	b.d.	0.03	b.d.	b.d.	b.d.	b.d.	b.d.	b.d.	b.d.	b.d.	0.01	b.d.	b.d.	0.02
	Total	100.77	100.83	100.82	100.79	100.79	100.41	100.20	100.98	100.77	100.34	100.91	100.58	100.60	100.75	100.53	100.66
Cations	Si	1.933	1.926	1.931	1.934	1.937	1.941	1.934	1.934	1.935	1.927	1.935	1.939	1.939	1.934	1.938	1.934
	Ti	b.d.	0.001	0.000	0.000	0.001	0.001	0.002	0.001	0.000	0.001	0.001	0.000	b.d.	0.001	0.001	0.001
	Cr	0.019	0.018	0.018	0.017	0.016	0.016	0.014	0.016	0.015	0.015	0.013	0.013	0.018	0.018	0.018	0.018
	Al	0.109	0.113	0.110	0.107	0.105	0.104	0.104	0.105	0.106	0.110	0.104	0.106	0.105	0.106	0.107	0.108
	Fe2+	0.165	0.173	0.174	0.169	0.170	0.172	0.177	0.179	0.176	0.179	0.175	0.174	0.166	0.172	0.166	0.170
	Mn	0.006	0.004	0.005	0.005	0.005	0.004	0.003	0.004	0.004	0.004	0.003	0.005	0.002	0.004	0.005	0.005
	Ni	0.003	0.002	0.003	0.003	0.003	0.002	0.003	0.002	0.002	0.003	0.002	0.001	0.003	0.003	0.002	0.002
	Mg	1.731	1.749	1.740	1.746	1.742	1.734	1.743	1.740	1.743	1.750	1.749	1.742	1.746	1.744	1.743	1.744
	Ca	0.038	0.020	0.022	0.021	0.023	0.024	0.024	0.025	0.022	0.021	0.021	0.021	0.020	0.021	0.019	0.021
	Na	b.d.	0.002	0.001	0.001	0.001	0.001	0.001	b.d.	b.d.	b.d.	b.d.	b.d.	b.d.	b.d.	0.001	b.d.
	K	b.d.	0.001	b.d.	0.001	b.d.	b.d.	b.d.	b.d.	b.d.	b.d.	b.d.	b.d.	0.000	b.d.	b.d.	0.001
	Sum	4.003	4.009	4.005	4.005	4.002	3.999	4.005	4.005	4.004	4.010	4.005	4.001	4.000	4.003	3.999	4.003
	Mg #	0.913	0.910	0.909	0.912	0.911	0.910	0.908	0.907	0.908	0.907	0.909	0.909	0.913	0.910	0.913	0.911

Abbreviations: Opx = orthopyroxene, Spl hrz = spinel harzburgite, Cl core = clast core, b.d. = below detection limit.
Mg# calculated as (MgO/40.3) / (MgO/40.3 + FeO/71.85).

Major element composition of orthopyroxene from the Dramala spinel harzburgite and plagioclase-bearing harzburgite continued

Sample		PI2	PI2	PI2	PI2	PI2	PI2	PI2	PI2	PI2	PI2	PI2	PI2	PI2	PI2	PI2	PI2
Rock		Spl hrz	Spl hrz	Spl hrz	Spl hrz	Spl hrz	Spl hrz	Spl hrz	Spl hrz	Spl hrz	Spl hrz	Spl hrz	Spl hrz	Spl hrz	Spl hrz	Spl hrz	Spl hrz
Mineral		Opx	Opx	Opx	Opx	Opx	Opx	Opx	Opx	Opx	Opx	Opx	Opx	Opx	Opx	Opx	Opx
Type		Cl core	Cl core	Cl core	Cl core	Cl core	Cl core	Cl core	Cl core	Cl core	Cl core	Cl core	Cl core	Cl core	Cl core	Cl core	Cl core
Wt.%	SiO2	56.53	56.43	56.28	56.19	56.18	56.17	56.28	56.29	56.38	56.36	56.17	56.20	56.12	56.15	56.09	56.26
	TiO2	b.d.	0.01	0.01	0.02	0.03	b.d.	0.01	b.d.	0.01	0.02	0.03	b.d.	0.02	0.02	0.02	0.05
	Cr2O3	0.67	0.73	0.68	0.71	0.67	0.72	0.67	0.74	0.75	0.72	0.71	0.73	0.69	0.73	0.71	0.70
	Al2O3	2.71	2.79	2.81	2.88	2.92	2.90	2.88	2.88	2.92	2.99	2.99	2.97	2.94	2.92	2.95	2.93
	FeO	5.90	5.91	5.66	5.91	5.87	5.91	6.12	6.00	5.96	6.05	5.71	5.99	5.94	5.75	5.82	5.75
	MnO	0.15	0.14	0.14	0.13	0.17	0.08	0.10	0.07	0.09	0.15	0.13	0.14	0.14	0.17	0.12	0.16
	NiO	0.12	0.11	0.08	0.05	0.09	0.10	0.11	0.07	0.08	0.05	0.06	0.13	0.09	0.10	0.06	0.09
	MgO	34.18	33.90	34.04	34.08	34.06	33.84	34.08	33.98	33.98	33.93	33.14	33.76	33.99	33.91	33.44	33.93
	CaO	0.56	0.71	0.59	0.68	0.61	0.71	0.69	0.64	0.70	0.67	1.14	0.71	0.79	0.65	1.30	0.66
	Na2O	0.03	0.01	b.d.	0.01	0.01	b.d.	b.d.	b.d.	b.d.	0.02	b.d.	b.d.	0.02	0.01	0.01	0.01
	K2O	b.d.	0.01	b.d.	b.d.	b.d.	b.d.	b.d.	0.01	b.d.	b.d.	0.01	b.d.	b.d.	b.d.	b.d.	0.02
	Total	100.85	100.75	100.29	100.66	100.61	100.43	100.94	100.68	100.87	100.96	100.09	100.63	100.74	100.41	100.52	100.56
Cations	Si	1.934	1.933	1.934	1.927	1.927	1.930	1.926	1.930	1.929	1.928	1.936	1.929	1.924	1.929	1.928	1.930
	Ti	b.d.	0.000	0.000	0.001	0.001	b.d.	0.000	b.d.	0.000	0.001	0.001	b.d.	0.001	0.001	0.001	0.001
	Cr	0.018	0.020	0.018	0.019	0.018	0.020	0.018	0.020	0.020	0.019	0.019	0.020	0.019	0.020	0.019	0.019
	Al	0.109	0.113	0.114	0.116	0.118	0.117	0.116	0.116	0.118	0.121	0.121	0.120	0.119	0.118	0.120	0.118
	Fe2+	0.169	0.169	0.163	0.169	0.168	0.170	0.175	0.172	0.171	0.173	0.165	0.172	0.170	0.165	0.167	0.165
	Mn	0.004	0.004	0.004	0.004	0.005	0.002	0.003	0.002	0.003	0.004	0.004	0.004	0.004	0.005	0.003	0.005
	Ni	0.003	0.003	0.002	0.001	0.002	0.003	0.003	0.002	0.002	0.001	0.002	0.004	0.002	0.003	0.002	0.002
	Mg	1.743	1.731	1.743	1.742	1.741	1.733	1.739	1.736	1.733	1.730	1.703	1.727	1.737	1.736	1.713	1.735
	Ca	0.021	0.026	0.022	0.025	0.022	0.026	0.025	0.024	0.026	0.025	0.042	0.026	0.029	0.024	0.048	0.024
	Na	0.002	0.001	b.d.	0.001	0.001	b.d.	b.d.	b.d.	b.d.	0.001	b.d.	b.d.	0.001	0.001	0.001	0.001
	K	b.d.	0.000	b.d.	b.d.	b.d.	b.d.	b.d.	0.000	b.d.	b.d.	0.000	b.d.	b.d.	b.d.	b.d.	0.001
	Sum	4.003	4.001	4.000	4.005	4.004	4.001	4.006	4.002	4.002	4.002	3.993	4.001	4.007	4.002	4.002	4.001
	Mg #	0.912	0.911	0.915	0.911	0.912	0.911	0.908	0.910	0.910	0.909	0.912	0.909	0.911	0.913	0.911	0.913

Abbreviations: Opx = orthopyroxene, Spl hrz = spinel harzburgite, Cl core = clast core, b.d. = below detection limit.
Mg# calculated as (MgO/40.3) / (MgO/40.3 + FeO/71.85).

Major element composition of orthopyroxene from the Dramala spinel harzburgite and plagioclase-bearing harzburgite continued

Sample		PI2	PI2	PI2	PI2	PI2	PI2	PI2	PI2	PI2	PI2	PI2	PI2	PI2	PI2	PI2	PI2
Rock		Spl hrz	Spl hrz	Spl hrz	Spl hrz	Spl hrz	Spl hrz	Spl hrz	Spl hrz	Spl hrz	Spl hrz	Spl hrz	Spl hrz	Spl hrz	Spl hrz	Spl hrz	Spl hrz
Mineral		Opx	Opx	Opx	Opx	Opx	Opx	Opx	Opx	Opx	Opx	Opx	Opx	Opx	Opx	Opx	Opx
Type		Cl core	Cl core	Cl core	Cl core	Cl core	Cl core	Cl core	Cl core	Cl core	Cl core	Cl core	Cl core	Cl core	Cl core	Cl core	Cl core
Wt.%	SiO2	55.09	56.41	56.18	56.33	56.36	56.02	56.25	56.16	56.22	55.99	56.15	56.14	56.36	56.28	56.30	56.16
	TiO2	0.02	0.01	0.02	0.02	0.02	0.02	b.d.	0.04	b.d.	0.03	0.03	b.d.	b.d.	b.d.	0.05	0.01
	Cr2O3	0.74	0.69	0.76	0.73	0.68	0.74	0.70	0.78	0.72	0.73	0.72	0.75	0.69	0.67	0.68	0.66
	Al2O3	2.93	2.95	2.92	2.92	2.85	2.89	2.93	3.05	2.91	3.00	2.96	2.98	2.83	2.88	2.96	2.97
	FeO	5.95	6.20	6.12	5.88	5.77	5.92	5.90	5.80	6.05	6.12	5.91	5.88	6.16	5.89	6.10	6.24
	MnO	0.16	0.17	0.14	0.13	0.20	0.22	0.13	0.13	0.16	0.07	0.21	0.19	0.07	0.16	0.21	0.17
	NiO	0.06	0.07	0.09	0.09	0.09	0.11	0.06	0.07	0.09	0.10	0.10	0.07	0.05	0.09	0.08	0.08
	MgO	33.30	33.90	33.90	33.88	34.30	34.01	33.79	34.20	33.97	34.05	34.22	34.25	34.11	34.09	34.01	34.08
	CaO	0.79	0.55	0.49	0.66	0.49	0.40	0.89	0.41	0.48	0.48	0.53	0.46	0.48	0.38	0.48	0.48
	Na2O	0.01	b.d.	b.d.	b.d.	b.d.	b.d.	b.d.	b.d.	b.d.	b.d.	0.01	0.02	b.d.	b.d.	b.d.	b.d.
	K2O	b.d.	b.d.	b.d.	b.d.	b.d.	b.d.	b.d.	b.d.	b.d.	b.d.	b.d.	b.d.	0.01	0.01	b.d.	b.d.
	Total	99.05	100.95	100.62	100.64	100.76	100.33	100.65	100.64	100.60	100.57	100.84	100.74	100.76	100.45	100.87	100.85
Cations	Si	1.923	1.930	1.928	1.931	1.929	1.927	1.929	1.924	1.929	1.923	1.923	1.923	1.931	1.932	1.927	1.924
	Ti	0.001	0.000	0.001	0.001	0.001	0.001	b.d.	0.001	b.d.	0.001	0.001	b.d.	b.d.	b.d.	0.001	0.000
	Cr	0.020	0.019	0.021	0.020	0.018	0.020	0.019	0.021	0.020	0.020	0.019	0.020	0.019	0.018	0.018	0.018
	Al	0.121	0.119	0.118	0.118	0.115	0.117	0.118	0.123	0.118	0.121	0.119	0.120	0.114	0.117	0.119	0.120
	Fe2+	0.174	0.177	0.176	0.169	0.165	0.170	0.169	0.166	0.174	0.176	0.169	0.168	0.176	0.169	0.175	0.179
	Mn	0.005	0.005	0.004	0.004	0.006	0.006	0.004	0.004	0.005	0.002	0.006	0.006	0.002	0.005	0.006	0.005
	Ni	0.002	0.002	0.002	0.002	0.002	0.003	0.002	0.002	0.002	0.003	0.003	0.002	0.001	0.002	0.002	0.002
	Mg	1.732	1.729	1.734	1.731	1.750	1.744	1.728	1.746	1.737	1.743	1.747	1.749	1.742	1.744	1.735	1.740
	Ca	0.030	0.020	0.018	0.024	0.018	0.015	0.033	0.015	0.018	0.018	0.019	0.017	0.018	0.014	0.018	0.018
	Na	0.001	b.d.	b.d.	b.d.	b.d.	b.d.	b.d.	b.d.	b.d.	b.d.	0.001	0.001	b.d.	b.d.	b.d.	b.d.
	K	b.d.	b.d.	b.d.	b.d.	b.d.	b.d.	b.d.	b.d.	b.d.	b.d.	b.d.	b.d.	0.000	0.000	b.d.	b.d.
	Sum	4.007	4.001	4.002	4.000	4.004	4.004	4.002	4.003	4.002	4.006	4.007	4.007	4.003	4.001	4.002	4.006
	Mg #	0.909	0.907	0.908	0.911	0.914	0.911	0.911	0.913	0.909	0.908	0.912	0.912	0.908	0.912	0.909	0.907

Abbreviations: Opx = orthopyroxene, Spl hrz = spinel harzburgite, Cl core = clast core, b.d. = below detection limit.
Mg# calculated as (MgO/40.3) / (MgO/40.3 + FeO/71.85).

Major element composition of orthopyroxene from the Dramala spinel harzburgite and plagioclase-bearing harzburgite continued

Sample		PI2	PI2	PI2	PI2	PI2	PI2	PI2	PI2	PI2	PI2	PI2	PI2	PI2	PI2	PI2	PI2
Rock		Spl hrz	Spl hrz	Spl hrz	Spl hrz	Spl hrz	Spl hrz	Spl hrz	Spl hrz	Spl hrz	Spl hrz	Spl hrz	Spl hrz	Spl hrz	Spl hrz	Spl hrz	Spl hrz
Mineral		Opx	Opx	Opx	Opx	Opx	Opx	Opx	Opx	Opx	Opx	Opx	Opx	Opx	Opx	Opx	Opx
Type		Cl core	Cl core	Cl core	Cl core	Cl core	Cl core	Cl core	Cl core	Cl core	Cl rim	Cl rim	Cl rim	Cl rim	Cl rim	Cl rim	Cl rim
Wt.%	SiO2	56.22	56.33	55.38	56.46	56.30	56.42	56.66	56.66	56.74	57.10	57.26	56.41	56.81	56.99	55.95	56.66
	TiO2	0.03	0.03	0.02	0.02	0.01	b.d.	0.03	0.03	b.d.	0.02	0.03	b.d.	0.02	b.d.	0.03	b.d.
	Cr2O3	0.71	0.67	0.68	0.64	0.65	0.63	0.64	0.61	0.56	0.38	0.28	0.20	0.45	0.42	0.70	0.60
	Al2O3	2.92	2.90	3.10	2.93	2.76	2.70	2.68	2.66	2.44	2.48	2.33	1.80	2.38	2.48	2.46	3.11
	FeO	5.94	6.20	6.27	5.92	6.06	5.96	5.95	5.93	5.83	5.72	5.77	5.68	5.90	5.68	5.72	5.78
	MnO	0.18	0.21	0.14	0.11	0.11	0.12	0.15	0.12	0.13	0.10	0.14	0.10	0.13	0.18	0.12	0.14
	NiO	0.09	0.06	0.13	0.13	0.09	0.11	0.06	0.11	0.09	0.10	0.11	0.11	0.08	0.04	0.04	0.05
	MgO	33.90	33.93	33.72	33.97	34.03	34.32	34.25	34.32	34.40	34.52	34.42	34.37	34.56	34.03	34.03	33.85
	CaO	0.46	0.47	0.39	0.49	0.49	0.48	0.42	0.47	0.38	0.54	0.44	0.46	0.53	1.12	0.66	0.56
	Na2O	b.d.	b.d.	b.d.	b.d.	b.d.	b.d.	0.02	0.01	0.01	0.01	0.01	b.d.	0.01	b.d.	0.02	0.03
	K2O	0.01	b.d.	b.d.	b.d.	b.d.	b.d.	b.d.	0.04	b.d.	b.d.	b.d.	0.01	b.d.	b.d.	0.01	b.d.
	Total	100.46	100.80	99.83	100.67	100.50	100.74	100.86	100.96	100.58	100.97	100.79	99.14	100.87	100.94	99.74	100.78
Cations	Si	1.931	1.930	1.918	1.934	1.933	1.932	1.937	1.936	1.943	1.946	1.954	1.958	1.941	1.946	1.935	1.936
	Ti	0.001	0.001	0.001	0.001	0.000	b.d.	0.001	0.001	b.d.	0.001	0.001	b.d.	0.001	b.d.	0.001	b.d.
	Cr	0.019	0.018	0.019	0.017	0.018	0.017	0.017	0.016	0.015	0.010	0.008	0.005	0.012	0.011	0.019	0.016
	Al	0.118	0.117	0.127	0.118	0.112	0.109	0.108	0.107	0.098	0.100	0.094	0.074	0.096	0.100	0.100	0.125
	Fe2+	0.171	0.178	0.182	0.170	0.174	0.171	0.170	0.169	0.167	0.163	0.165	0.165	0.169	0.162	0.165	0.165
	Mn	0.005	0.006	0.004	0.003	0.003	0.003	0.004	0.003	0.004	0.003	0.004	0.003	0.004	0.005	0.004	0.004
	Ni	0.002	0.002	0.004	0.004	0.002	0.003	0.002	0.003	0.002	0.003	0.003	0.003	0.002	0.001	0.001	0.001
	Mg	1.735	1.733	1.741	1.734	1.742	1.752	1.745	1.747	1.756	1.753	1.751	1.778	1.760	1.732	1.754	1.724
	Ca	0.017	0.017	0.014	0.018	0.018	0.018	0.015	0.017	0.014	0.020	0.016	0.017	0.019	0.041	0.024	0.020
	Na	b.d.	b.d.	b.d.	b.d.	b.d.	b.d.	0.001	0.001	0.001	0.001	0.001	b.d.	0.001	b.d.	0.001	0.002
	K	0.000	b.d.	b.d.	b.d.	b.d.	b.d.	b.d.	0.002	b.d.	b.d.	b.d.	0.000	b.d.	b.d.	0.000	b.d.
	Sum	4.000	4.002	4.009	3.998	4.002	4.005	4.000	4.003	4.000	3.999	3.995	4.003	4.005	3.998	4.005	3.994
	Mg #	0.910	0.907	0.906	0.911	0.909	0.911	0.911	0.912	0.913	0.915	0.914	0.915	0.913	0.914	0.914	0.913

Abbreviations: Opx = orthopyroxene, Spl hrz = spinel harzburgite, Cl core = clast core, Cl rim = clast rim, b.d. = below detection limit.
Mg# calculated as (MgO/40.3) / (MgO/40.3 + FeO/71.85).

Major element composition of orthopyroxene from the Dramala spinel harzburgite and plagioclase-bearing harzburgite continued

Sample		**PI2**	**PI2**	**PI2**	**PI2**	**PI2**	**PI2**	**PI2**	**PI2**
Rock		**Spl hrz**	**Spl hrz**	**Spl hrz**	**Spl hrz**	**Spl hrz**	**Spl hrz**	**Spl hrz**	**Spl hrz**
Mineral		**Opx**	**Opx**	**Opx**	**Opx**	**Opx**	**Opx**	**Opx**	**Opx**
Type		**Cl rim**	**Blast**	**Blast**	**Blast**	**Blast**	**Blast**	**Blast**	**Blast**
Wt.%	**SiO2**	56.34	56.89	56.98	56.67	58.18	57.96	57.55	56.60
	TiO2	0.02	0.02	0.01	0.04	0.02	0.01	b.d.	0.02
	Cr2O3	0.62	0.31	0.23	0.28	0.02	0.06	0.14	0.43
	Al2O3	2.96	2.09	1.86	1.92	0.54	0.57	1.19	2.30
	FeO	5.75	6.12	5.72	5.90	5.85	5.67	6.02	5.71
	MnO	0.10	0.20	0.22	0.17	0.22	0.20	0.16	0.18
	NiO	0.04	0.07	0.07	0.05	0.10	0.10	0.08	0.09
	MgO	33.26	34.60	34.77	34.71	35.65	35.80	34.99	34.29
	CaO	1.58	0.49	0.40	0.48	0.27	0.27	0.37	0.55
	Na2O	0.02	b.d.	0.03	0.02	b.d.	0.01	b.d.	b.d.
	K2O	0.02	b.d.	0.02	0.01	b.d.	b.d.	b.d.	b.d.
	Total	100.71	100.79	100.31	100.25	100.85	100.65	100.50	100.17
Cations	**Si**	1.933	1.947	1.955	1.948	1.984	1.980	1.971	1.946
	Ti	0.001	0.001	0.000	0.001	0.001	0.000	b.d.	0.001
	Cr	0.017	0.008	0.006	0.008	0.001	0.002	0.004	0.012
	Al	0.120	0.084	0.075	0.078	0.022	0.023	0.048	0.093
	Fe2+	0.165	0.175	0.164	0.170	0.167	0.162	0.172	0.164
	Mn	0.003	0.006	0.006	0.005	0.006	0.006	0.005	0.005
	Ni	0.001	0.002	0.002	0.001	0.003	0.003	0.002	0.002
	Mg	1.701	1.765	1.778	1.779	1.812	1.823	1.786	1.757
	Ca	0.058	0.018	0.015	0.018	0.010	0.010	0.014	0.020
	Na	0.001	b.d.	0.002	0.001	b.d.	0.001	b.d.	b.d.
	K	0.001	b.d.	0.001	0.000	b.d.	b.d.	b.d.	b.d.
	Sum	4.000	4.006	4.005	4.009	4.004	4.008	4.003	4.001
	Mg #	0.912	0.910	0.916	0.913	0.916	0.918	0.912	0.915

Abbreviations: Opx = orthopyroxene, Spl hrz = spinel harzburgite, Cl rim = clast rim, b.d. = below detection limit. Mg# calculated as (MgO/40.3) / (MgO/40.3 + FeO/71.85).

Major element composition of orthopyroxene from the Dramala spinel harzburgite and plagioclase-bearing harzburgite continued

Sample		PI2	PI2	PI2	PIA91	PIA91	PIA91	PIA91	PIA91	PIA91	PIA91	PIA91	PIA91	PIA91	PIA91	PIA91	PIA91
Rock		Spl hrz	Spl hrz	Spl hrz	Spl hrz	Spl hrz	Spl hrz	Spl hrz	Spl hrz	Spl hrz	Spl hrz	Spl hrz	Spl hrz	Spl hrz	Spl hrz	Spl hrz	Spl hrz
Mineral		Opx	Opx	Opx	Opx	Opx	Opx	Opx	Opx	Opx	Opx	Opx	Opx	Opx	Opx	Opx	Opx
Type		Blast	Blast	Blast	Cl core	Cl core	Cl core	Cl core	Cl core	Cl core	Cl core	Cl core	Cl core	Cl core	Cl core	Cl core	Cl core
Wt.%	SiO2	57.86	57.10	57.54	57.15	57.47	57.44	56.91	56.77	57.00	56.85	56.87	57.15	57.30	57.04	56.87	56.70
	TiO2	0.04	0.01	b.d.	0.01	0.01	0.01	0.02	0.02	0.02	0.02	0.01	0.01	0.02	0.02	0.01	0.02
	Cr2O3	0.09	0.31	0.21	0.18	0.22	0.26	0.28	0.37	0.40	0.38	0.38	0.40	0.36	0.39	0.35	0.37
	Al2O3	1.10	1.97	1.55	1.18	1.37	1.45	1.64	1.71	1.75	1.77	1.75	1.67	1.66	1.69	1.63	1.59
	FeO	5.75	6.10	5.87	5.45	5.51	5.32	5.29	5.25	5.22	5.24	5.07	5.32	5.30	5.45	5.27	5.45
	MnO	0.10	0.11	0.19	0.25	0.18	0.06	0.06	0.12	0.11	0.14	0.22	0.09	0.16	0.19	0.13	0.08
	NiO	0.07	0.09	0.09	0.19	0.16	0.11	0.14	0.13	0.09	0.22	0.03	0.13	0.04	0.13	0.00	0.09
	MgO	35.28	34.62	35.00	34.56	34.63	34.68	34.60	34.45	34.29	34.11	34.37	34.39	34.22	34.45	34.38	34.25
	CaO	0.33	0.50	0.39	0.41	0.43	0.50	0.56	0.62	0.63	0.71	0.70	0.71	0.72	0.72	0.71	0.71
	Na2O	b.d.	b.d.	0.01	0.02	0.02	0.04	0.01	0.02	0.03	b.d.	b.d.	b.d.	0.03	0.02	0.06	0.05
	K2O	0.01	0.01	b.d.	b.d.	b.d.	0.01	b.d.	b.d.	b.d.	0.01	0.01	b.d.	b.d.	b.d.	0.01	b.d.
	Total	100.63	100.82	100.85	99.40	99.99	99.89	99.51	99.46	99.54	99.45	99.40	99.86	99.81	100.10	99.42	99.31
Cations	Si	1.976	1.952	1.964	1.976	1.975	1.973	1.964	1.961	1.966	1.965	1.964	1.966	1.971	1.961	1.965	1.964
	Ti	0.001	0.000	b.d.	0.000	0.000	0.000	0.001	0.000	0.000	0.001	0.000	0.000	0.001	0.001	0.000	0.000
	Cr	0.002	0.008	0.006	0.005	0.006	0.007	0.008	0.010	0.011	0.011	0.010	0.011	0.010	0.011	0.010	0.010
	Al	0.044	0.079	0.062	0.048	0.056	0.059	0.067	0.070	0.071	0.072	0.071	0.068	0.067	0.068	0.066	0.065
	Fe2+	0.164	0.174	0.168	0.158	0.158	0.153	0.153	0.152	0.151	0.151	0.146	0.153	0.152	0.157	0.152	0.158
	Mn	0.003	0.003	0.005	0.007	0.005	0.002	0.002	0.003	0.003	0.004	0.006	0.003	0.005	0.005	0.004	0.002
	Ni	0.002	0.002	0.002	0.005	0.005	0.003	0.004	0.003	0.003	0.006	0.001	0.004	0.001	0.003	0.000	0.002
	Mg	1.795	1.764	1.780	1.781	1.774	1.776	1.780	1.774	1.763	1.757	1.769	1.764	1.755	1.765	1.771	1.768
	Ca	0.012	0.018	0.014	0.015	0.016	0.018	0.021	0.023	0.023	0.026	0.026	0.026	0.026	0.027	0.026	0.026
	Na	b.d.	b.d.	0.001	0.001	0.001	0.003	0.000	0.001	0.002	b.d.	b.d.	b.d.	0.002	0.001	0.004	0.004
	K	0.000	0.000	b.d.	b.d.	b.d.	0.001	b.d.	b.d.	b.d.	0.000	0.000	b.d.	b.d.	b.d.	0.000	b.d.
	Sum	4.000	4.004	4.003	3.998	3.995	3.995	3.998	3.999	3.993	3.993	3.995	3.994	3.991	3.999	3.999	4.000
	Mg #	0.916	0.910	0.914	0.919	0.918	0.921	0.921	0.921	0.921	0.921	0.924	0.920	0.920	0.918	0.921	0.918

Abbreviations: Opx = orthopyroxene, Spl hrz = spinel harzburgite, Cl core = clast core, b.d. = below detection limit.
Mg# calculated as (MgO/40.3) / (MgO/40.3 + FeO/71.85).

Major element composition of orthopyroxene from the Dramala spinel harzburgite and plagioclase-bearing harzburgite continued

Sample		PIA91	PIA91	PIA91	PIA91	PIA91	PIA91	PIA91	PIA91	PIA91	PIA91	PIA91	PIA91	PIA91	PIA91	PIA91	PIA91
Rock		Spl hrz	Spl hrz	Spl hrz	Spl hrz	Spl hrz	Spl hrz	Spl hrz	Spl hrz	Spl hrz	Spl hrz	Spl hrz	Spl hrz	Spl hrz	Spl hrz	Spl hrz	Spl hrz
Mineral		Opx	Opx	Opx	Opx	Opx	Opx	Opx	Opx	Opx	Opx	Opx	Opx	Opx	Opx	Opx	Opx
Type		Cl core	Cl core	Cl core	Cl core	Cl core	Cl core	Cl core	Cl core	Cl core	Cl core	Cl core	Cl core	Cl core	Cl core	Cl core	Cl core
Wt.%	SiO2	57.54	57.12	57.23	57.30	56.58	56.87	56.90	56.55	56.97	56.75	56.65	57.14	56.71	56.72	57.10	56.50
	TiO2	0.01	b.d.	0.01	b.d.	b.d.	0.02	0.01	0.03	0.01	0.01	0.02	0.02	0.01	b.d.	0.01	0.01
	Cr2O3	0.36	0.36	0.33	0.34	0.44	0.50	0.54	0.54	0.60	0.58	0.60	0.55	0.61	0.58	0.57	0.58
	Al2O3	1.51	1.68	1.65	1.46	1.97	1.96	1.93	1.94	1.86	1.98	1.93	1.99	1.95	1.95	1.95	1.84
	FeO	5.18	5.63	5.23	5.82	5.36	5.23	5.08	4.92	4.96	5.18	5.22	5.19	5.28	5.13	5.22	5.19
	MnO	0.15	0.16	0.14	0.22	0.07	0.11	0.06	0.18	0.07	0.13	0.14	0.03	0.12	0.05	0.06	0.12
	NiO	0.17	0.13	0.12	0.14	0.09	b.d.	0.10	b.d.	0.10	0.17	0.02	0.10	0.02	b.d.	0.10	0.10
	MgO	34.40	34.35	34.31	34.73	34.32	34.39	34.11	34.31	33.92	34.16	33.85	34.22	34.08	33.98	34.22	34.09
	CaO	0.73	0.71	0.68	0.61	0.60	0.63	0.68	0.64	1.16	0.80	0.87	0.67	0.59	1.02	0.77	0.66
	Na2O	0.01	0.04	b.d.	b.d.	0.02	0.03	0.02	b.d.	0.03	0.01	b.d.	0.05	b.d.	b.d.	b.d.	b.d.
	K2O	b.d.	b.d.	0.01	b.d.	b.d.	0.01	b.d.	0.01	b.d.	b.d.	0.01	b.d.	b.d.	b.d.	b.d.	0.01
	Total	100.05	100.19	99.71	100.62	99.46	99.74	99.43	99.11	99.68	99.78	99.31	99.96	99.38	99.43	100.02	99.11
Cations	Si	1.975	1.963	1.971	1.963	1.955	1.958	1.964	1.958	1.964	1.956	1.961	1.962	1.960	1.960	1.961	1.959
	Ti	0.000	b.d.	0.000	b.d.	b.d.	0.001	0.000	0.001	0.000	0.000	0.001	0.000	0.000	b.d.	0.000	0.000
	Cr	0.010	0.010	0.009	0.009	0.012	0.014	0.015	0.015	0.016	0.016	0.017	0.015	0.017	0.016	0.016	0.016
	Al	0.061	0.068	0.067	0.059	0.080	0.080	0.079	0.079	0.075	0.080	0.079	0.081	0.079	0.079	0.079	0.075
	Fe2+	0.149	0.162	0.151	0.167	0.155	0.151	0.147	0.142	0.143	0.149	0.151	0.149	0.153	0.148	0.150	0.151
	Mn	0.004	0.005	0.004	0.006	0.002	0.003	0.002	0.005	0.002	0.004	0.004	0.001	0.004	0.001	0.002	0.004
	Ni	0.005	0.003	0.003	0.004	0.003	b.d.	0.003	b.d.	0.003	0.005	0.001	0.003	0.001	b.d.	0.003	0.003
	Mg	1.759	1.759	1.761	1.773	1.768	1.765	1.755	1.770	1.743	1.755	1.746	1.752	1.756	1.750	1.752	1.762
	Ca	0.027	0.026	0.025	0.022	0.022	0.023	0.025	0.024	0.043	0.030	0.032	0.025	0.022	0.038	0.029	0.024
	Na	0.000	0.003	b.d.	b.d.	0.001	0.002	0.001	b.d.	0.002	0.001	b.d.	0.003	b.d.	b.d.	b.d.	b.d.
	K	b.d.	b.d.	0.000	b.d.	b.d.	0.000	b.d.	0.000	b.d.	b.d.	0.000	b.d.	b.d.	b.d.	b.d.	0.000
	Sum	3.990	4.000	3.991	4.003	3.999	3.996	3.990	3.995	3.991	3.996	3.991	3.991	3.992	3.993	3.991	3.995
	Mg #	0.922	0.916	0.921	0.914	0.919	0.921	0.923	0.926	0.924	0.922	0.920	0.922	0.920	0.922	0.921	0.921

Abbreviations: Opx = orthopyroxene, Spl hrz = spinel harzburgite, Cl core = clast core, b.d. = below detection limit.
Mg# calculated as (MgO/40.3) / (MgO/40.3 + FeO/71.85).

Major element composition of orthopyroxene from the Dramala spinel harzburgite and plagioclase-bearing harzburgite continued

Sample		PIA91	PIA91	PIA91	PIA91	PI6	PI6	PI6	PI6	PI6	PI6	PI6	PI6	PI6	PI6	PI6	PI6
Rock		Spl hrz	Spl hrz	Spl hrz	Spl hrz	Spl hrz	Spl hrz	Spl hrz	Spl hrz	Spl hrz	Spl hrz	Spl hrz	Spl hrz	Spl hrz	Spl hrz	Spl hrz	Spl hrz
Mineral		Opx	Opx	Opx	Opx	Opx	Opx	Opx	Opx	Opx	Opx	Opx	Opx	Opx	Opx	Opx	Opx
Type		Cl rim	Cl rim	Cl rim	Cl rim	Cl core	Cl core	Cl core	Cl core	Cl core	Cl core	Cl core	Cl core	Cl core	Cl core	Cl core	Cl core
Wt.%	SiO2	57.89	57.51	57.91	57.21	56.62	56.76	56.86	56.33	57.50	57.10	57.13	57.36	57.22	57.40	57.36	57.45
	TiO2	b.d.	0.02	b.d.	0.01	b.d.	0.04	b.d.	0.01	0.02	0.01	0.04	b.d.	0.03	0.01	b.d.	0.01
	Cr2O3	0.03	0.22	0.06	0.22	0.31	0.26	0.64	0.70	0.28	0.42	0.44	0.44	0.50	0.48	0.46	0.52
	Al2O3	0.37	1.43	0.55	1.48	1.89	1.86	1.96	1.92	1.28	1.25	1.28	1.22	1.24	1.24	1.22	1.31
	FeO	5.56	5.72	5.36	5.16	5.38	5.37	5.58	5.40	5.67	5.95	5.98	5.38	6.17	5.92	5.79	6.06
	MnO	0.17	0.06	0.17	0.16	0.10	0.01	0.08	0.07	0.09	0.11	0.10	0.15	0.13	0.12	0.14	0.15
	NiO	0.16	0.20	0.11	b.d.	b.d.	0.16	0.12	b.d.	0.14	0.09	0.11	0.06	0.10	0.06	0.10	0.08
	MgO	35.34	34.73	35.23	34.52	34.27	34.30	34.40	34.35	34.95	34.87	34.79	34.38	34.69	34.98	34.60	34.76
	CaO	0.25	0.36	0.23	0.47	0.77	0.79	0.76	0.86	0.66	0.56	0.90	0.82	0.54	0.59	0.58	0.59
	Na2O	0.02	b.d.	0.05	b.d.	b.d.	0.01	0.01	0.01	b.d.	0.01	b.d.	b.d.	0.01	b.d.	0.02	b.d.
	K2O	b.d.	b.d.	b.d.	b.d.	0.01	b.d.	0.01	0.01	b.d.	0.02	b.d.	b.d.	b.d.	b.d.	b.d.	b.d.
	Total	99.78	100.25	99.67	99.23	99.34	99.57	100.41	99.65	100.60	100.39	100.77	99.81	100.63	100.80	100.27	100.93
Cations	Si	1.992	1.972	1.993	1.976	1.959	1.960	1.951	1.947	1.967	1.962	1.958	1.976	1.963	1.963	1.970	1.964
	Ti	b.d.	0.000	b.d.	0.000	b.d.	0.001	b.d.	0.000	0.001	0.000	0.001	b.d.	0.001	0.000	b.d.	0.000
	Cr	0.001	0.006	0.002	0.006	0.008	0.007	0.017	0.019	0.008	0.011	0.012	0.012	0.014	0.013	0.012	0.014
	Al	0.015	0.058	0.022	0.060	0.077	0.076	0.079	0.078	0.052	0.051	0.052	0.050	0.050	0.050	0.049	0.053
	Fe2+	0.160	0.164	0.154	0.149	0.156	0.155	0.160	0.156	0.162	0.171	0.171	0.155	0.177	0.169	0.166	0.173
	Mn	0.005	0.002	0.005	0.005	0.003	0.000	0.002	0.002	0.002	0.003	0.003	0.004	0.004	0.003	0.004	0.004
	Ni	0.004	0.005	0.003	b.d.	b.d.	0.005	0.003	b.d.	0.004	0.002	0.003	0.002	0.003	0.002	0.003	0.002
	Mg	1.813	1.775	1.807	1.777	1.767	1.765	1.759	1.769	1.782	1.785	1.777	1.765	1.774	1.783	1.771	1.771
	Ca	0.009	0.013	0.008	0.017	0.028	0.029	0.028	0.032	0.024	0.021	0.033	0.030	0.020	0.022	0.021	0.022
	Na	0.001	b.d.	0.003	b.d.	b.d.	0.001	0.001	0.000	b.d.	0.001	b.d.	b.d.	0.001	b.d.	0.001	b.d.
	K	b.d.	b.d.	b.d.	b.d.	0.001	b.d.	0.000	0.000	b.d.	0.001	b.d.	b.d.	b.d.	b.d.	b.d.	b.d.
	Sum	4.000	3.996	3.997	3.991	3.999	3.998	4.001	4.005	4.002	4.008	4.009	3.994	4.005	4.005	3.999	4.003
	Mg #	0.919	0.915	0.921	0.923	0.919	0.919	0.917	0.919	0.917	0.913	0.912	0.919	0.909	0.913	0.914	0.911

Abbreviations: Opx = orthopyroxene, Spl hrz = spinel harzburgite, Cl core = clast core, b.d. = below detection limit.
Mg# calculated as (MgO/40.3) / (MgO/40.3 + FeO/71.85).

Major element composition of orthopyroxene from the Dramala spinel harzburgite and plagioclase-bearing harzburgite continued

Sample		PI6	PI6	PI6	PI6	PI6	PI6	PI6	PI6	PI6	PI6	PI6	PI6	PI6	PI6	PI6	PI6
Rock		Spl hrz	Spl hrz	Spl hrz	Spl hrz	Spl hrz	Spl hrz	Spl hrz	Spl hrz	Spl hrz	Spl hrz	Spl hrz	Spl hrz	Spl hrz	Spl hrz	Spl hrz	Spl hrz
Mineral		Opx	Opx	Opx	Opx	Opx	Opx	Opx	Opx	Opx	Opx	Opx	Opx	Opx	Opx	Opx	Opx
Type		Cl core	Cl core	Cl core	Cl core	Cl core	Cl core	Cl core	Cl core	Cl core	Cl core	Cl core	Cl core	Cl core	Cl core	Cl core	Cl core
Wt.%	**SiO2**	57.12	57.07	56.97	56.92	57.11	56.97	57.15	57.04	57.10	57.06	56.93	57.14	57.17	56.96	57.04	56.28
	TiO2	b.d.	0.02	b.d.	b.d.	0.03	b.d.	0.01	0.04	b.d.	b.d.	b.d.	0.03	0.01	0.02	b.d.	0.04
	Cr2O3	0.52	0.49	0.50	0.52	0.49	0.53	0.53	0.52	0.55	0.54	0.60	0.52	0.54	0.54	0.56	0.56
	Al2O3	1.41	1.26	1.32	1.28	1.25	1.28	1.36	1.24	1.34	1.23	1.35	1.24	1.24	1.29	1.28	1.49
	FeO	5.86	5.85	5.79	5.60	5.76	5.74	5.64	5.69	5.85	5.46	5.72	5.56	5.65	5.71	5.79	5.09
	MnO	0.20	0.16	0.15	0.20	0.15	0.15	0.12	0.19	0.10	0.13	0.17	0.17	0.15	0.12	0.15	0.12
	NiO	0.10	0.05	0.10	0.09	0.10	0.10	0.09	0.09	0.14	0.09	0.06	0.08	0.09	0.11	0.10	0.10
	MgO	34.66	34.85	34.51	34.48	34.45	34.55	34.23	33.92	34.70	34.04	34.29	34.65	34.58	33.89	34.54	32.63
	CaO	0.64	0.56	0.61	0.74	0.76	0.96	0.76	1.36	0.71	1.35	0.67	0.73	0.87	1.30	1.10	2.54
	Na2O	b.d.	0.01	b.d.	b.d.	0.01	b.d.	0.02	b.d.	b.d.	b.d.	b.d.	b.d.	0.01	0.01	0.02	0.06
	K2O	b.d.	0.01	b.d.	b.d.	b.d.	b.d.	0.01	b.d.	b.d.	b.d.	b.d.	b.d.	b.d.	b.d.	b.d.	0.02
	Total	100.51	100.33	99.95	99.83	100.11	100.28	99.92	100.09	100.49	99.90	99.79	100.12	100.31	99.95	100.58	98.93
Cations	**Si**	1.960	1.961	1.964	1.965	1.966	1.960	1.970	1.967	1.960	1.969	1.966	1.966	1.965	1.967	1.959	1.966
	Ti	b.d.	0.001	b.d.	b.d.	0.001	b.d.	0.000	0.001	b.d.	b.d.	b.d.	0.001	0.000	0.001	b.d.	0.001
	Cr	0.014	0.013	0.014	0.014	0.013	0.014	0.014	0.014	0.015	0.015	0.016	0.014	0.015	0.015	0.015	0.015
	Al	0.057	0.051	0.054	0.052	0.051	0.052	0.055	0.050	0.054	0.050	0.055	0.050	0.050	0.053	0.052	0.061
	Fe2+	0.168	0.168	0.167	0.162	0.166	0.165	0.163	0.164	0.168	0.158	0.165	0.160	0.162	0.165	0.166	0.149
	Mn	0.006	0.005	0.004	0.006	0.004	0.004	0.004	0.006	0.003	0.004	0.005	0.005	0.004	0.004	0.004	0.004
	Ni	0.003	0.001	0.003	0.002	0.003	0.003	0.002	0.002	0.004	0.002	0.002	0.002	0.002	0.003	0.003	0.003
	Mg	1.773	1.785	1.774	1.774	1.768	1.772	1.758	1.744	1.775	1.751	1.765	1.777	1.771	1.744	1.768	1.699
	Ca	0.024	0.021	0.023	0.027	0.028	0.035	0.028	0.050	0.026	0.050	0.025	0.027	0.032	0.048	0.040	0.095
	Na	b.d.	0.001	b.d.	b.d.	0.001	b.d.	0.001	b.d.	b.d.	b.d.	b.d.	b.d.	0.001	0.001	0.001	0.004
	K	b.d.	0.000	b.d.	b.d.	b.d.	b.d.	0.000	b.d.	b.d.	b.d.	b.d.	b.d.	b.d.	b.d.	b.d.	0.001
	Sum	4.004	4.007	4.002	4.002	4.001	4.006	3.996	3.999	4.005	3.998	3.999	4.001	4.003	3.999	4.009	3.997
	Mg #	0.913	0.914	0.914	0.916	0.914	0.915	0.915	0.914	0.914	0.917	0.914	0.917	0.916	0.914	0.914	0.920

Abbreviations: Opx = orthopyroxene, Spl hrz = spinel harzburgite, Cl core = clast core, b.d. = below detection limit.
Mg# calculated as (MgO/40.3) / (MgO/40.3 + FeO/71.85).

Major element composition of orthopyroxene from the Dramala spinel harzburgite and plagioclase-bearing harzburgite continued

Sample		PI6	PI6	PI6	PI6	PI6	PI6	PI6	PI6	PI6	PI6	PI6	PI6	PI6	PI6	PI6	PI6
Rock		Spl hrz	Spl hrz	Spl hrz	Spl hrz	Spl hrz	Spl hrz	Spl hrz	Spl hrz	Spl hrz	Spl hrz	Spl hrz	Spl hrz	Spl hrz	Spl hrz	Spl hrz	Spl hrz
Mineral		Opx	Opx	Opx	Opx	Opx	Opx	Opx	Opx	Opx	Opx	Opx	Opx	Opx	Opx	Opx	Opx
Type		Cl core	Cl core	Cl core	Cl core	Cl core	Cl core	Cl core	Cl core	Cl core	Cl core	Cl core	Cl core	Cl core	Cl core	Cl core	Cl core
Wt.%	SiO2	56.81	56.36	56.68	56.77	57.14	57.10	56.93	57.23	56.75	57.21	57.05	56.75	56.80	56.95	57.02	57.40
	TiO2	0.03	b.d.	0.03	b.d.	0.01	0.01	b.d.	b.d.	0.03	b.d.	b.d.	0.01	0.02	b.d.	b.d.	b.d.
	Cr2O3	0.55	0.52	0.57	0.59	0.52	0.54	0.55	0.55	0.53	0.50	0.57	0.52	0.56	0.58	0.52	0.50
	Al2O3	1.27	1.45	1.33	1.28	1.27	1.30	1.26	1.33	1.28	1.27	1.26	1.33	1.24	1.23	1.29	1.13
	FeO	5.70	5.46	5.72	5.70	6.00	5.63	5.88	5.90	5.93	5.50	5.56	5.76	5.52	5.61	5.97	5.80
	MnO	0.16	0.07	0.10	0.16	0.18	0.13	0.12	0.08	0.19	0.09	0.16	0.06	0.17	0.17	0.14	0.10
	NiO	0.13	0.07	0.09	0.12	0.12	0.12	0.11	0.12	0.09	0.08	0.11	0.12	0.13	0.04	0.09	0.07
	MgO	34.18	32.95	34.24	34.36	34.89	34.22	34.26	34.65	34.49	34.43	34.60	33.98	33.82	34.33	34.23	34.41
	CaO	0.98	2.53	1.00	1.06	0.55	1.36	1.32	0.84	0.86	0.98	0.81	1.50	1.73	1.08	0.78	0.97
	Na2O	b.d.	b.d.	0.01	0.03	b.d.	b.d.	b.d.	b.d.	0.03	0.01	b.d.	b.d.	b.d.	0.01	b.d.	0.03
	K2O	b.d.	b.d.	0.02	b.d.	b.d.	b.d.	b.d.	b.d.	b.d.	b.d.	b.d.	0.01	0.02	0.04	b.d.	b.d.
	Total	99.81	99.41	99.79	100.07	100.68	100.41	100.43	100.70	100.18	100.07	100.12	100.04	100.01	100.04	100.04	100.41
Cations	Si	1.964	1.961	1.960	1.959	1.959	1.963	1.959	1.961	1.957	1.969	1.964	1.960	1.963	1.964	1.966	1.971
	Ti	0.001	b.d.	0.001	b.d.	0.000	0.000	b.d.	b.d.	0.001	b.d.	b.d.	0.000	0.001	b.d.	b.d.	b.d.
	Cr	0.015	0.014	0.016	0.016	0.014	0.015	0.015	0.015	0.014	0.014	0.016	0.014	0.015	0.016	0.014	0.014
	Al	0.052	0.059	0.054	0.052	0.051	0.053	0.051	0.054	0.052	0.052	0.051	0.054	0.051	0.050	0.052	0.046
	Fe2+	0.165	0.159	0.165	0.164	0.172	0.162	0.169	0.169	0.171	0.158	0.160	0.166	0.160	0.162	0.172	0.167
	Mn	0.005	0.002	0.003	0.005	0.005	0.004	0.003	0.002	0.006	0.003	0.005	0.002	0.005	0.005	0.004	0.003
	Ni	0.004	0.002	0.003	0.003	0.003	0.003	0.003	0.003	0.002	0.002	0.003	0.003	0.004	0.001	0.002	0.002
	Mg	1.761	1.709	1.765	1.767	1.783	1.753	1.758	1.770	1.773	1.766	1.775	1.749	1.742	1.764	1.760	1.761
	Ca	0.036	0.094	0.037	0.039	0.020	0.050	0.049	0.031	0.032	0.036	0.030	0.056	0.064	0.040	0.029	0.036
	Na	b.d.	b.d.	0.001	0.002	b.d.	b.d.	b.d.	b.d.	0.002	0.001	b.d.	b.d.	b.d.	0.001	b.d.	0.002
	K	b.d.	b.d.	0.001	b.d.	b.d.	b.d.	b.d.	b.d.	b.d.	b.d.	b.d.	0.000	0.001	0.002	b.d.	b.d.
	Sum	4.002	4.002	4.005	4.008	4.008	4.003	4.008	4.005	4.010	3.999	4.003	4.006	4.004	4.004	4.000	4.000
	Mg #	0.914	0.915	0.914	0.915	0.912	0.915	0.912	0.913	0.912	0.918	0.917	0.913	0.916	0.916	0.911	0.914

Abbreviations: Opx = orthopyroxene, Spl hrz = spinel harzburgite, Cl core = clast core, b.d. = below detection limit.
Mg# calculated as (MgO/40.3) / (MgO/40.3 + FeO/71.85).

Major element composition of orthopyroxene from the Dramala spinel harzburgite and plagioclase-bearing harzburgite continued

Sample		PI6	PI6	PI6	PI6	PI6	PI6	PI6	PI6	PI6	PI6	PI6	PI6	PI6	PI6	PI6	PI6
Rock		Spl hrz	Spl hrz	Spl hrz	Spl hrz	Spl hrz	Spl hrz	Spl hrz	Spl hrz	Spl hrz	Spl hrz	Spl hrz	Spl hrz	Spl hrz	Spl hrz	Spl hrz	Spl hrz
Mineral		Opx	Opx	Opx	Opx	Opx	Opx	Opx	Opx	Opx	Opx	Opx	Opx	Opx	Opx	Opx	Opx
Type		Cl core	Cl core	Cl core	Cl core	Cl core	Cl core	Cl core	Cl core	Cl core	Cl core	Cl core	Cl core	Cl core	Cl core	Cl core	Cl core
Wt.%	SiO2	57.00	57.22	57.06	56.89	57.09	56.93	57.11	57.06	57.14	57.09	56.99	56.85	56.98	57.16	57.12	57.35
	TiO2	b.d.	b.d.	0.02	0.01	0.02	b.d.	0.03	0.02	0.02	b.d.	0.03	0.01	b.d.	b.d.	0.01	0.02
	Cr2O3	0.57	0.52	0.54	0.56	0.54	0.52	0.50	0.52	0.48	0.52	0.51	0.47	0.50	0.50	0.46	0.50
	Al2O3	1.25	1.28	1.25	1.24	1.26	1.26	1.27	1.23	1.24	1.32	1.18	1.18	1.30	1.26	1.22	1.23
	FeO	5.87	5.96	5.67	5.70	5.72	5.81	5.45	5.55	5.82	5.95	5.55	5.70	5.75	5.72	5.69	5.81
	MnO	0.17	0.18	0.07	0.10	0.15	0.13	0.16	0.13	0.14	0.09	0.13	0.17	0.16	0.13	0.12	0.12
	NiO	0.09	0.11	0.12	0.12	0.09	0.07	0.08	0.10	0.09	0.08	0.09	0.12	0.06	0.08	0.08	0.09
	MgO	34.47	34.51	34.66	34.57	34.88	34.65	34.61	34.09	34.67	34.46	33.84	34.59	34.32	34.67	34.05	34.55
	CaO	0.76	1.06	0.82	1.02	0.80	0.86	0.98	1.57	0.94	0.82	2.36	0.84	1.28	0.60	1.66	0.65
	Na2O	b.d.	b.d.	b.d.	b.d.	b.d.	0.01	0.02	b.d.	0.01	0.02	0.01	0.01	b.d.	b.d.	0.02	b.d.
	K2O	b.d.	0.01	b.d.	b.d.	b.d.	0.01	0.02	b.d.	0.01	0.03	0.02	0.01	b.d.	0.02	b.d.	b.d.
	Total	100.18	100.85	100.21	100.21	100.55	100.25	100.23	100.27	100.56	100.38	100.71	99.95	100.35	100.14	100.43	100.32
Cations	Si	1.963	1.960	1.963	1.959	1.958	1.960	1.963	1.965	1.961	1.963	1.959	1.962	1.961	1.966	1.965	1.969
	Ti	b.d.	b.d.	0.001	0.000	0.001	b.d.	0.001	0.001	0.001	b.d.	0.001	0.000	b.d.	b.d.	0.000	0.001
	Cr	0.016	0.014	0.015	0.015	0.015	0.014	0.014	0.014	0.013	0.014	0.014	0.013	0.014	0.014	0.013	0.014
	Al	0.051	0.052	0.051	0.050	0.051	0.051	0.051	0.050	0.050	0.053	0.048	0.048	0.053	0.051	0.049	0.050
	Fe2+	0.169	0.171	0.163	0.164	0.164	0.167	0.157	0.160	0.167	0.171	0.160	0.165	0.165	0.165	0.164	0.167
	Mn	0.005	0.005	0.002	0.003	0.004	0.004	0.005	0.004	0.004	0.003	0.004	0.005	0.005	0.004	0.003	0.003
	Ni	0.002	0.003	0.003	0.003	0.002	0.002	0.002	0.003	0.002	0.002	0.002	0.003	0.002	0.002	0.002	0.002
	Mg	1.770	1.762	1.777	1.775	1.783	1.778	1.773	1.749	1.773	1.766	1.734	1.779	1.760	1.777	1.746	1.768
	Ca	0.028	0.039	0.030	0.038	0.029	0.032	0.036	0.058	0.035	0.030	0.087	0.031	0.047	0.022	0.061	0.024
	Na	b.d.	b.d.	b.d.	b.d.	b.d.	0.001	0.001	b.d.	0.001	0.001	0.001	0.001	b.d.	b.d.	0.001	b.d.
	K	b.d.	0.000	b.d.	b.d.	b.d.	0.000	0.001	b.d.	0.000	0.001	0.001	0.000	b.d.	0.001	b.d.	b.d.
	Sum	4.004	4.007	4.004	4.008	4.008	4.008	4.004	4.003	4.007	4.005	4.010	4.008	4.006	4.002	4.005	3.998
	Mg #	0.913	0.912	0.916	0.915	0.916	0.914	0.919	0.916	0.914	0.912	0.916	0.915	0.914	0.915	0.914	0.914

Abbreviations: Opx = orthopyroxene, Spl hrz = spinel harzburgite, Cl core = clast core, b.d. = below detection limit.
Mg# calculated as (MgO/40.3) / (MgO/40.3 + FeO/71.85).

Major element composition of orthopyroxene from the Dramala spinel harzburgite and plagioclase-bearing harzburgite continued

Sample		PI6	PI6	PI6	PI6	PI6	PI6	PI6	PI6	PI6	PI6	PI6	PI6	PI6	PI6	PI6	PI6
Rock		Spl hrz	Spl hrz	Spl hrz	Spl hrz	Spl hrz	Spl hrz	Spl hrz	Spl hrz	Spl hrz	Spl hrz	Spl hrz	Spl hrz	Spl hrz	Spl hrz	Spl hrz	Spl hrz
Mineral		Opx	Opx	Opx	Opx	Opx	Opx	Opx	Opx	Opx	Opx	Opx	Opx	Opx	Opx	Opx	Opx
Type		Cl core	Cl core	Cl core	Cl core	Cl core	Cl core	Cl core	Cl core	Cl core	Cl core	Cl core	Cl core	Cl core	Cl core	Cl core	Cl core
Wt.%	SiO2	57.25	57.22	56.94	57.30	57.26	57.00	56.94	57.33	57.16	57.05	56.93	56.78	57.15	56.60	57.01	56.49
	TiO2	0.01	0.02	0.03	b.d.	b.d.	b.d.	b.d.	0.03	0.01	b.d.	b.d.	0.03	0.02	0.02	0.01	0.03
	Cr2O3	0.43	0.40	0.43	0.39	0.33	0.26	0.27	0.24	0.23	0.37	0.38	0.43	0.54	0.54	0.55	0.51
	Al2O3	1.17	1.18	1.16	1.07	1.04	1.13	1.24	0.97	1.41	1.20	1.16	1.20	1.26	1.27	1.28	1.28
	FeO	5.74	5.67	5.58	5.79	5.77	5.70	5.78	5.74	6.09	6.10	6.06	5.80	5.74	5.53	5.79	5.75
	MnO	0.12	0.15	0.16	0.18	0.17	0.10	0.10	0.15	0.16	0.15	0.14	0.14	0.14	0.12	0.11	0.22
	NiO	0.12	0.10	0.09	0.11	0.07	0.06	0.09	0.09	0.07	0.07	0.06	0.11	0.09	0.09	0.08	0.11
	MgO	35.04	34.83	34.86	35.13	35.06	34.99	35.05	35.22	35.04	34.73	34.76	34.58	35.00	34.26	34.53	34.35
	CaO	0.48	0.58	0.47	0.46	0.37	0.39	0.44	0.48	0.37	0.63	0.67	0.70	0.62	0.70	0.81	0.94
	Na2O	b.d.	b.d.	b.d.	b.d.	b.d.	b.d.	0.02	b.d.	0.01	0.01	0.01	0.02	0.01	b.d.	0.01	0.02
	K2O	b.d.	b.d.	0.02	b.d.	0.01	b.d.	b.d.	b.d.	b.d.	b.d.	b.d.	b.d.	0.01	b.d.	b.d.	b.d.
	Total	100.36	100.15	99.74	100.43	100.08	99.63	99.93	100.25	100.55	100.31	100.17	99.79	100.58	99.13	100.18	99.70
Cations	Si	1.965	1.967	1.965	1.966	1.970	1.968	1.962	1.969	1.960	1.963	1.962	1.962	1.959	1.966	1.963	1.957
	Ti	0.000	0.001	0.001	b.d.	b.d.	b.d.	b.d.	0.001	0.000	b.d.	b.d.	0.001	0.001	0.001	0.000	0.001
	Cr	0.012	0.011	0.012	0.011	0.009	0.007	0.007	0.007	0.006	0.010	0.010	0.012	0.015	0.015	0.015	0.014
	Al	0.047	0.048	0.047	0.043	0.042	0.046	0.050	0.039	0.057	0.049	0.047	0.049	0.051	0.052	0.052	0.052
	Fe2+	0.165	0.163	0.161	0.166	0.166	0.165	0.167	0.165	0.175	0.175	0.175	0.168	0.165	0.161	0.167	0.167
	Mn	0.003	0.004	0.005	0.005	0.005	0.003	0.003	0.004	0.005	0.004	0.004	0.004	0.004	0.004	0.003	0.006
	Ni	0.003	0.003	0.002	0.003	0.002	0.002	0.002	0.002	0.002	0.002	0.002	0.003	0.002	0.003	0.002	0.003
	Mg	1.792	1.785	1.793	1.796	1.797	1.801	1.800	1.803	1.790	1.781	1.785	1.781	1.788	1.774	1.772	1.774
	Ca	0.018	0.021	0.017	0.017	0.014	0.014	0.016	0.018	0.014	0.023	0.025	0.026	0.023	0.026	0.030	0.035
	Na	b.d.	b.d.	b.d.	b.d.	b.d.	b.d.	0.001	b.d.	0.001	0.001	0.001	0.001	0.001	b.d.	0.001	0.001
	K	b.d.	b.d.	0.001	b.d.	0.000	b.d.	b.d.	b.d.	b.d.	b.d.	b.d.	b.d.	0.000	b.d.	b.d.	b.d.
	Sum	4.005	4.003	4.005	4.007	4.005	4.005	4.010	4.007	4.009	4.008	4.010	4.007	4.008	4.000	4.004	4.010
	Mg #	0.916	0.916	0.918	0.915	0.915	0.916	0.915	0.916	0.911	0.910	0.911	0.914	0.916	0.917	0.914	0.914

Abbreviations: Opx = orthopyroxene, Spl hrz = spinel harzburgite, Cl core = clast core, b.d. = below detection limit.
Mg# calculated as (MgO/40.3) / (MgO/40.3 + FeO/71.85).

Major element composition of orthopyroxene from the Dramala spinel harzburgite and plagioclase-bearing harzburgite continued

Sample		PI6	PI6	PI6	PI6	PI6	PI6	PI6	PI6	PI6	PI6	PI6	PI6	PI6	PI6	PI6	PI6
Rock		Spl hrz	Spl hrz	Spl hrz	Spl hrz	Spl hrz	Spl hrz	Spl hrz	Spl hrz	Spl hrz	Spl hrz	Spl hrz	Spl hrz	Spl hrz	Spl hrz	Spl hrz	Spl hrz
Mineral		Opx	Opx	Opx	Opx	Opx	Opx	Opx	Opx	Opx	Opx	Opx	Opx	Opx	Opx	Opx	Opx
Type		Cl core	Cl core	Cl core	Cl core	Cl core	Cl core	Cl core	Cl core	Cl core	Cl core	Cl core	Cl core	Cl core	Cl core	Cl core	Cl core
Wt.%	SiO2	56.88	56.81	56.52	56.85	56.74	56.92	56.93	56.93	57.27	57.06	57.25	57.09	56.85	57.07	57.05	57.02
	TiO2	0.02	0.01	b.d.	b.d.	0.02	b.d.	b.d.	b.d.	b.d.	0.01	b.d.	0.01	b.d.	b.d.	b.d.	0.01
	Cr2O3	0.53	0.52	0.53	0.56	0.62	0.58	0.58	0.55	0.56	0.58	0.56	0.58	0.60	0.57	0.63	0.61
	Al2O3	1.30	1.33	1.30	1.39	1.42	1.34	1.37	1.36	1.31	1.40	1.39	1.37	1.41	1.35	1.41	1.39
	FeO	5.83	5.75	5.68	5.64	5.48	5.95	5.94	5.76	5.96	5.77	5.69	5.97	5.80	5.85	5.79	5.78
	MnO	0.10	0.15	0.06	0.19	0.17	0.14	0.15	0.18	0.13	0.16	0.13	0.12	0.05	0.10	0.13	0.16
	NiO	0.07	0.11	0.13	0.08	0.07	0.07	0.11	0.07	0.09	0.09	0.11	0.10	0.10	0.04	0.09	0.10
	MgO	34.74	34.61	34.11	34.25	33.86	34.78	34.89	34.51	34.70	34.21	34.36	34.65	34.46	33.93	34.48	34.42
	CaO	0.60	0.57	1.18	0.83	2.06	0.62	0.52	0.73	0.57	1.31	0.83	0.72	0.58	0.98	0.72	0.81
	Na2O	b.d.	b.d.	0.01	b.d.	b.d.	b.d.	0.01	0.03	0.02	b.d.	0.01	b.d.	b.d.	b.d.	0.01	0.02
	K2O	b.d.	0.02	b.d.	b.d.	b.d.	0.01	b.d.	b.d.	0.02	0.01	0.01	b.d.	0.01	b.d.	b.d.	0.01
	Total	100.07	99.88	99.52	99.79	100.44	100.41	100.50	100.12	100.63	100.60	100.34	100.61	99.86	99.89	100.31	100.33
Cations	Si	1.960	1.961	1.960	1.964	1.954	1.957	1.955	1.961	1.963	1.959	1.966	1.959	1.962	1.970	1.961	1.961
	Ti	0.001	0.000	b.d.	b.d.	0.001	b.d.	b.d.	b.d.	b.d.	0.000	b.d.	0.000	b.d.	b.d.	b.d.	0.000
	Cr	0.014	0.014	0.015	0.015	0.017	0.016	0.016	0.015	0.015	0.016	0.015	0.016	0.016	0.016	0.017	0.017
	Al	0.053	0.054	0.053	0.057	0.058	0.054	0.055	0.055	0.053	0.057	0.056	0.055	0.057	0.055	0.057	0.056
	Fe2+	0.168	0.166	0.165	0.163	0.158	0.171	0.171	0.166	0.171	0.166	0.163	0.171	0.167	0.169	0.166	0.166
	Mn	0.003	0.004	0.002	0.006	0.005	0.004	0.004	0.005	0.004	0.005	0.004	0.003	0.001	0.003	0.004	0.005
	Ni	0.002	0.003	0.004	0.002	0.002	0.002	0.003	0.002	0.002	0.002	0.003	0.003	0.003	0.001	0.002	0.003
	Mg	1.784	1.780	1.763	1.763	1.738	1.782	1.786	1.772	1.773	1.751	1.759	1.772	1.772	1.746	1.767	1.764
	Ca	0.022	0.021	0.044	0.031	0.076	0.023	0.019	0.027	0.021	0.048	0.031	0.026	0.021	0.036	0.027	0.030
	Na	b.d.	b.d.	0.001	b.d.	b.d.	b.d.	0.001	0.002	0.001	b.d.	0.001	b.d.	b.d.	b.d.	0.001	0.001
	K	b.d.	0.001	b.d.	b.d.	b.d.	0.000	b.d.	b.d.	0.001	0.000	0.000	b.d.	0.000	b.d.	b.d.	0.000
	Sum	4.006	4.005	4.006	4.000	4.008	4.009	4.010	4.005	4.004	4.004	3.999	4.006	4.002	3.995	4.002	4.003
	Mg #	0.914	0.915	0.915	0.915	0.917	0.912	0.913	0.914	0.912	0.914	0.915	0.912	0.914	0.912	0.914	0.914

Abbreviations: Opx = orthopyroxene, Spl hrz = spinel harzburgite, Cl core = clast core, b.d. = below detection limit.
Mg# calculated as (MgO/40.3) / (MgO/40.3 + FeO/71.85).

Major element composition of orthopyroxene from the Dramala spinel harzburgite and plagioclase-bearing harzburgite continued

Sample		PI6	PI6	PI6	PI6	PI6	PI6	PI6	PI6	PI6	PI6	PI6	PI6	PI6	PI6	PI6	PI6
Rock		Spl hrz	Spl hrz	Spl hrz	Spl hrz	Spl hrz	Spl hrz	Spl hrz	Spl hrz	Spl hrz	Spl hrz	Spl hrz	Spl hrz	Spl hrz	Spl hrz	Spl hrz	Spl hrz
Mineral		Opx	Opx	Opx	Opx	Opx	Opx	Opx	Opx	Opx	Opx	Opx	Opx	Opx	Opx	Opx	Opx
Type		Cl core	Cl core	Cl core	Cl core	Cl core	Cl core	Cl core	Cl core	Cl core	Cl core	Cl core	Cl core	Cl core	Cl core	Cl core	Cl core
Wt.%	SiO2	57.11	56.94	56.98	57.19	57.28	56.95	57.09	56.85	56.91	57.23	57.13	57.32	57.02	56.99	57.09	57.05
	TiO2	0.04	b.d.	b.d.	0.02	b.d.	b.d.	0.01	0.03	b.d.	b.d.	0.03	0.01	b.d.	0.01	0.02	0.04
	Cr2O3	0.56	0.58	0.56	0.59	0.58	0.63	0.58	0.62	0.57	0.58	0.58	0.60	0.53	0.56	0.62	0.58
	Al2O3	1.33	1.24	1.36	1.36	1.37	1.36	1.37	1.37	1.24	1.38	1.36	1.36	1.32	1.32	1.31	1.33
	FeO	5.77	5.45	5.94	5.81	5.74	5.62	5.87	5.80	5.54	5.88	5.90	5.78	5.70	5.79	5.54	5.98
	MnO	0.08	0.13	0.19	0.14	0.09	0.16	0.16	0.11	0.11	0.14	0.12	0.16	0.13	0.15	0.10	0.12
	NiO	0.12	0.09	0.11	0.09	0.08	0.09	0.11	0.10	0.13	0.09	0.13	0.10	0.09	0.13	0.09	0.11
	MgO	34.75	33.54	34.67	34.60	34.59	34.63	34.47	33.87	32.78	34.46	33.98	34.58	34.21	34.11	33.76	34.78
	CaO	0.65	1.44	0.51	0.56	0.60	0.99	0.82	0.97	2.70	0.64	1.06	0.62	0.82	0.70	1.61	0.78
	Na2O	b.d.	0.02	b.d.	0.01	b.d.	b.d.	b.d.	0.01	0.02	b.d.	b.d.	0.01	0.01	0.01	b.d.	0.01
	K2O	0.02	b.d.	0.01	0.03	0.01	b.d.	b.d.	0.02	b.d.	b.d.	0.02	b.d.	0.01	0.02	0.01	0.01
	Total	100.43	99.43	100.33	100.40	100.34	100.43	100.48	99.75	100.00	100.40	100.31	100.54	99.84	99.79	100.15	100.79
Cations	Si	1.960	1.974	1.960	1.963	1.966	1.957	1.961	1.966	1.970	1.965	1.966	1.965	1.968	1.969	1.967	1.955
	Ti	0.001	b.d.	b.d.	0.001	b.d.	b.d.	0.000	0.001	b.d.	b.d.	0.001	0.000	b.d.	0.000	0.001	0.001
	Cr	0.015	0.016	0.015	0.016	0.016	0.017	0.016	0.017	0.016	0.016	0.016	0.016	0.014	0.015	0.017	0.016
	Al	0.054	0.051	0.055	0.055	0.055	0.055	0.055	0.056	0.051	0.056	0.055	0.055	0.054	0.054	0.053	0.054
	Fe2+	0.166	0.158	0.171	0.167	0.165	0.161	0.169	0.168	0.160	0.169	0.170	0.166	0.165	0.167	0.160	0.171
	Mn	0.002	0.004	0.006	0.004	0.003	0.005	0.005	0.003	0.003	0.004	0.003	0.005	0.004	0.004	0.003	0.003
	Ni	0.003	0.003	0.003	0.002	0.002	0.002	0.003	0.003	0.004	0.002	0.004	0.003	0.002	0.004	0.002	0.003
	Mg	1.778	1.733	1.777	1.771	1.769	1.773	1.765	1.746	1.692	1.764	1.743	1.767	1.760	1.756	1.734	1.776
	Ca	0.024	0.053	0.019	0.021	0.022	0.036	0.030	0.036	0.100	0.024	0.039	0.023	0.030	0.026	0.059	0.029
	Na	b.d.	0.001	b.d.	0.001	b.d.	b.d.	b.d.	0.001	0.001	b.d.	b.d.	0.001	0.001	0.001	b.d.	0.001
	K	0.001	b.d.	0.000	0.001	0.000	b.d.	b.d.	0.001	b.d.	b.d.	0.001	b.d.	0.000	0.001	0.000	0.000
	Sum	4.004	3.993	4.006	4.001	3.999	4.007	4.003	3.997	3.997	3.999	3.998	4.000	3.998	3.997	3.997	4.010
	Mg #	0.915	0.916	0.912	0.914	0.915	0.917	0.913	0.912	0.913	0.913	0.911	0.914	0.915	0.913	0.916	0.912

Abbreviations: Opx = orthopyroxene, Spl hrz = spinel harzburgite, Cl core = clast core, b.d. = below detection limit.
Mg# calculated as (MgO/40.3) / (MgO/40.3 + FeO/71.85).

Major element composition of orthopyroxene from the Dramala spinel harzburgite and plagioclase-bearing harzburgite continued

Sample		PI6	PI6	PI6	PI6	PI6	PI6	PI6	PI6	PI6	PI6	PI6	PI6	PI6	PI6	PI6	PI6
Rock		Spl hrz	Spl hrz	Spl hrz	Spl hrz	Spl hrz	Spl hrz	Spl hrz	Spl hrz	Spl hrz	Spl hrz	Spl hrz	Spl hrz	Spl hrz	Spl hrz	Spl hrz	Spl hrz
Mineral		Opx	Opx	Opx	Opx	Opx	Opx	Opx	Opx	Opx	Opx	Opx	Opx	Opx	Opx	Opx	Opx
Type		Cl core	Cl core	Cl core	Cl core	Cl core	Cl core	Cl core	Cl core	Cl core	Cl core	Cl core	Cl core	Cl core	Cl core	Cl core	Cl core
Wt.%	SiO2	56.34	56.95	56.98	56.82	57.22	56.93	57.20	57.39	57.36	57.28	57.10	57.18	57.27	56.90	53.84	56.95
	TiO2	0.02	0.02	0.04	b.d.	0.01	0.01	b.d.	0.03	0.03	0.02	0.02	0.03	0.02	0.02	0.04	b.d.
	Cr2O3	0.61	0.60	0.61	0.59	0.58	0.48	0.52	0.41	0.58	0.61	0.60	0.61	0.61	0.65	0.82	0.68
	Al2O3	1.48	1.33	1.23	1.34	1.32	1.19	1.29	1.28	1.28	1.33	1.31	1.38	1.36	1.41	1.35	1.47
	FeO	5.63	5.83	5.49	5.75	5.93	5.88	6.02	6.01	4.73	4.88	4.99	4.48	4.60	4.84	1.54	4.51
	MnO	0.15	0.20	0.13	0.20	0.11	0.13	0.14	0.15	0.09	0.16	0.11	0.07	0.02	0.12	0.10	0.13
	NiO	0.11	0.08	0.07	0.09	0.04	0.05	0.10	0.12	0.06	0.08	0.08	0.11	0.08	0.11	0.08	0.09
	MgO	33.68	34.56	34.36	33.89	34.34	34.92	34.68	34.79	34.21	34.50	34.44	33.94	34.56	33.86	18.52	34.16
	CaO	1.46	0.60	1.56	1.12	0.67	0.49	0.59	0.60	0.91	0.61	0.54	1.29	0.54	1.31	23.26	0.99
	Na2O	0.01	b.d.	0.01	0.03	b.d.	0.01	0.01	b.d.	0.01	0.01	b.d.	0.03	0.02	b.d.	0.08	0.01
	K2O	b.d.	b.d.	b.d.	0.02	0.01	b.d.	b.d.	0.01	b.d.	b.d.	0.01	b.d.	b.d.	b.d.	0.00	0.02
	Total	99.49	100.17	100.48	99.85	100.23	100.09	100.55	100.79	99.26	99.48	99.20	99.12	99.08	99.22	99.63	99.01
Cations	Si	1.957	1.961	1.958	1.965	1.968	1.961	1.963	1.964	1.981	1.975	1.975	1.978	1.978	1.971	1.956	1.972
	Ti	0.001	0.001	0.001	b.d.	0.000	0.000	b.d.	0.001	0.001	0.001	0.001	0.001	0.001	0.001	0.001	b.d.
	Cr	0.017	0.016	0.017	0.016	0.016	0.013	0.014	0.011	0.016	0.017	0.016	0.017	0.017	0.018	0.024	0.019
	Al	0.061	0.054	0.050	0.055	0.054	0.048	0.052	0.052	0.052	0.054	0.053	0.056	0.055	0.058	0.058	0.060
	Fe2+	0.164	0.168	0.158	0.166	0.171	0.169	0.173	0.172	0.137	0.141	0.144	0.130	0.133	0.140	0.047	0.131
	Mn	0.004	0.006	0.004	0.006	0.003	0.004	0.004	0.004	0.003	0.005	0.003	0.002	0.001	0.004	0.003	0.004
	Ni	0.003	0.002	0.002	0.003	0.001	0.001	0.003	0.003	0.002	0.002	0.002	0.003	0.002	0.003	0.002	0.003
	Mg	1.744	1.774	1.760	1.747	1.760	1.793	1.774	1.775	1.761	1.773	1.775	1.750	1.779	1.748	1.003	1.763
	Ca	0.054	0.022	0.057	0.041	0.025	0.018	0.022	0.022	0.034	0.023	0.020	0.048	0.020	0.049	0.905	0.037
	Na	0.001	b.d.	0.001	0.002	b.d.	0.001	0.001	b.d.	0.001	0.001	b.d.	0.002	0.001	b.d.	0.006	0.001
	K	b.d.	b.d.	b.d.	0.001	0.000	b.d.	b.d.	0.000	b.d.	b.d.	0.000	b.d.	b.d.	b.d.	0.000	0.001
	Sum	4.004	4.003	4.008	4.001	3.997	4.008	4.004	4.004	3.985	3.990	3.990	3.986	3.986	3.991	4.005	3.989
	Mg #	0.914	0.914	0.918	0.913	0.912	0.914	0.911	0.912	0.928	0.926	0.925	0.931	0.931	0.926	0.955	0.931

Abbreviations: Opx = orthopyroxene, Spl hrz = spinel harzburgite, Cl core = clast core, b.d. = below detection limit.
Mg# calculated as (MgO/40.3) / (MgO/40.3 + FeO/71.85).

Major element composition of orthopyroxene from the Dramala spinel harzburgite and plagioclase-bearing harzburgite continued

Sample		PI6	PI6	PI6	PI6	PI6	PI6	PI6	PI6	PI6	PI6	PI6	PI6	PI6	PI6	PI6	PI6
Rock		Spl hrz	Spl hrz	Spl hrz	Spl hrz	Spl hrz	Spl hrz	Spl hrz	Spl hrz	Spl hrz	Spl hrz	Spl hrz	Spl hrz	Spl hrz	Spl hrz	Spl hrz	Spl hrz
Mineral		Opx	Opx	Opx	Opx	Opx	Opx	Opx	Opx	Opx	Opx	Opx	Opx	Opx	Opx	Opx	Opx
Type		Cl core	Cl core	Cl core	Cl core	Cl core	Cl core	Cl core	Cl core	Cl core	Cl core	Cl core	Cl core	Cl core	Cl core	Cl core	Cl core
Wt.%	SiO2	56.89	57.07	53.69	57.24	57.14	56.88	57.16	57.23	57.25	54.20	57.17	57.06	57.22	56.97	56.77	57.17
	TiO2	0.04	0.03	0.02	0.01	b.d.	b.d.	0.03	b.d.	0.01	0.04	0.01	b.d.	0.02	0.03	0.02	b.d.
	Cr2O3	0.63	0.68	0.86	0.68	0.60	0.65	0.62	0.62	0.61	0.83	0.69	0.62	0.63	0.57	0.63	0.56
	Al2O3	1.43	1.45	1.33	1.44	1.37	1.49	1.43	1.46	1.45	1.35	1.48	1.44	1.40	1.36	1.35	1.30
	FeO	4.38	4.76	1.43	4.77	4.78	4.80	4.78	4.84	4.82	1.65	4.81	4.86	4.86	4.62	4.63	4.70
	MnO	0.13	0.09	0.07	0.11	0.14	0.14	0.14	0.07	0.10	0.09	0.06	0.15	0.14	0.10	0.12	0.15
	NiO	0.08	0.11	0.09	0.06	0.09	0.12	0.09	0.09	0.11	0.07	0.06	0.17	0.12	0.08	0.08	0.09
	MgO	34.33	34.36	17.62	34.30	33.68	34.30	34.68	34.33	34.15	18.20	34.61	34.57	34.44	34.02	34.09	34.66
	CaO	1.26	0.56	24.48	0.83	1.94	1.04	0.46	0.99	0.93	23.89	0.52	0.56	0.72	1.31	1.33	0.55
	Na2O	0.01	b.d.	0.06	0.01	0.01	b.d.	0.01	0.01	b.d.	0.06	0.01	0.02	b.d.	b.d.	b.d.	b.d.
	K2O	b.d.	b.d.	b.d.	b.d.	b.d.	b.d.	b.d.	0.01	b.d.	0.00	0.01	b.d.	b.d.	0.02	b.d.	b.d.
	Total	99.18	99.11	99.65	99.45	99.75	99.42	99.40	99.65	99.43	100.38	99.43	99.45	99.55	99.08	99.02	99.18
Cations	Si	1.968	1.973	1.956	1.974	1.972	1.966	1.971	1.971	1.975	1.958	1.971	1.969	1.972	1.974	1.969	1.975
	Ti	0.001	0.001	0.001	0.000	b.d.	b.d.	0.001	b.d.	0.000	0.001	0.000	b.d.	0.001	0.001	0.001	b.d.
	Cr	0.017	0.019	0.025	0.019	0.016	0.018	0.017	0.017	0.017	0.024	0.019	0.017	0.017	0.016	0.017	0.015
	Al	0.058	0.059	0.057	0.059	0.056	0.061	0.058	0.059	0.059	0.057	0.060	0.059	0.057	0.056	0.055	0.053
	Fe2+	0.127	0.138	0.044	0.138	0.138	0.139	0.138	0.139	0.139	0.050	0.139	0.140	0.140	0.134	0.134	0.136
	Mn	0.004	0.003	0.002	0.003	0.004	0.004	0.004	0.002	0.003	0.003	0.002	0.004	0.004	0.003	0.004	0.004
	Ni	0.002	0.003	0.003	0.002	0.002	0.003	0.002	0.002	0.003	0.002	0.002	0.005	0.003	0.002	0.002	0.003
	Mg	1.770	1.771	0.957	1.763	1.732	1.767	1.782	1.762	1.756	0.980	1.778	1.778	1.769	1.757	1.762	1.785
	Ca	0.047	0.021	0.956	0.031	0.072	0.039	0.017	0.037	0.034	0.924	0.019	0.021	0.027	0.049	0.049	0.020
	Na	0.001	b.d.	0.004	0.001	0.001	b.d.	0.001	0.001	b.d.	0.004	0.001	0.001	b.d.	b.d.	b.d.	b.d.
	K	b.d.	b.d.	b.d.	b.d.	b.d.	b.d.	b.d.	0.000	b.d.	0.000	0.000	b.d.	b.d.	0.001	b.d.	b.d.
	Sum	3.994	3.987	4.004	3.988	3.993	3.995	3.991	3.991	3.987	4.003	3.990	3.994	3.990	3.991	3.994	3.991
	Mg #	0.933	0.928	0.956	0.928	0.926	0.927	0.928	0.927	0.927	0.952	0.928	0.927	0.927	0.929	0.929	0.929

Abbreviations: Opx = orthopyroxene, Spl hrz = spinel harzburgite, Cl core = clast core, b.d. = below detection limit.
Mg# calculated as (MgO/40.3) / (MgO/40.3 + FeO/71.85).

Major element composition of orthopyroxene from the Dramala spinel harzburgite and plagioclase-bearing harzburgite continued

Sample		PI6	PI6	PI6	PI6	PI6	PI6	PI6	PI6	PI6	PI6	PI6	PI6	PI6	PI6	PI6	PIA44
Rock		Spl hrz	Spl hrz	Spl hrz	Spl hrz	Spl hrz	Spl hrz	Spl hrz	Spl hrz	Spl hrz	Spl hrz	Spl hrz	Spl hrz	Spl hrz	Spl hrz	Spl hrz	Spl hrz
Mineral		Opx	Opx	Opx	Opx	Opx	Opx	Opx	Opx	Opx	Opx	Opx	Opx	Opx	Opx	Opx	Opx
Type		Cl core	Cl core	Cl core	Cl core	Cl core	Cl rim	Cl rim	Cl rim	Cl rim	Cl rim	Cl rim	Cl rim	Cl rim	Cl rim	Cl rim	Cl core
Wt.%	SiO2	57.22	56.96	57.20	57.24	57.37	57.66	57.84	57.67	57.95	57.76	57.33	57.06	57.19	58.36	57.55	56.54
	TiO2	0.02	0.01	b.d.	b.d.	0.02	b.d.	0.01	0.04	b.d.	0.03	0.02	0.02	0.02	0.03	0.03	0.01
	Cr2O3	0.59	0.55	0.51	0.47	0.42	0.19	0.17	0.15	0.12	0.15	0.23	0.27	0.34	0.46	0.23	0.45
	Al2O3	1.34	1.38	1.09	1.32	1.18	0.98	0.83	0.85	0.81	0.76	0.96	0.88	1.01	1.25	0.99	2.23
	FeO	4.90	4.54	4.30	4.68	4.88	5.63	5.95	5.72	5.92	5.82	5.97	5.92	5.97	5.71	4.96	5.34
	MnO	0.15	0.12	0.11	0.19	0.13	0.21	0.16	0.18	0.18	0.17	0.09	0.18	0.17	0.17	0.13	0.13
	NiO	0.10	0.13	0.07	0.07	0.09	0.10	0.10	0.07	0.09	0.09	0.07	0.12	0.08	0.08	0.11	0.08
	MgO	33.97	34.58	33.53	34.73	34.74	35.05	35.29	35.07	35.32	35.40	35.03	34.66	35.11	36.02	34.80	32.57
	CaO	1.39	0.83	3.00	0.56	0.51	0.45	0.42	0.42	0.40	0.40	0.42	0.42	0.42	0.41	0.47	2.12
	Na2O	b.d.	b.d.	b.d.	b.d.	b.d.	0.01	b.d.	b.d.	b.d.	b.d.	b.d.	b.d.	0.01	0.03	b.d.	0.04
	K2O	0.01	b.d.	b.d.	0.01	b.d.	0.01	b.d.	b.d.	b.d.	b.d.	b.d.	b.d.	b.d.	b.d.	b.d.	0.03
	Total	99.69	99.10	99.81	99.27	99.34	100.29	100.77	100.17	100.79	100.58	100.12	99.53	100.32	102.51	99.27	99.54
Cations	Si	1.973	1.970	1.974	1.975	1.979	1.977	1.976	1.980	1.979	1.976	1.972	1.975	1.965	1.960	1.986	1.960
	Ti	0.001	0.000	b.d.	b.d.	0.001	b.d.	0.000	0.001	b.d.	0.001	0.001	0.001	0.001	0.001	0.001	0.000
	Cr	0.016	0.015	0.014	0.013	0.011	0.005	0.005	0.004	0.003	0.004	0.006	0.007	0.009	0.012	0.006	0.012
	Al	0.054	0.056	0.044	0.054	0.048	0.040	0.033	0.034	0.033	0.031	0.039	0.036	0.041	0.049	0.040	0.091
	Fe2+	0.141	0.131	0.124	0.135	0.141	0.161	0.170	0.164	0.169	0.167	0.172	0.171	0.172	0.160	0.143	0.155
	Mn	0.004	0.004	0.003	0.006	0.004	0.006	0.005	0.005	0.005	0.005	0.003	0.005	0.005	0.005	0.004	0.004
	Ni	0.003	0.004	0.002	0.002	0.002	0.003	0.003	0.002	0.002	0.002	0.002	0.003	0.002	0.002	0.003	0.002
	Mg	1.746	1.783	1.725	1.786	1.786	1.791	1.797	1.794	1.797	1.805	1.796	1.788	1.798	1.803	1.790	1.683
	Ca	0.051	0.031	0.111	0.021	0.019	0.017	0.015	0.015	0.015	0.015	0.015	0.016	0.015	0.015	0.017	0.079
	Na	b.d.	b.d.	b.d.	b.d.	b.d.	0.001	b.d.	b.d.	b.d.	b.d.	b.d.	b.d.	0.001	0.002	b.d.	0.003
	K	0.000	b.d.	b.d.	0.000	b.d.	0.000	b.d.	b.d.	b.d.	b.d.	b.d.	b.d.	b.d.	b.d.	b.d.	0.001
	Sum	3.991	3.994	3.997	3.992	3.991	4.001	4.004	4.000	4.003	4.006	4.005	4.003	4.009	4.009	3.990	3.990
	Mg #	0.925	0.931	0.933	0.930	0.927	0.917	0.914	0.916	0.914	0.916	0.913	0.913	0.913	0.918	0.926	0.916

Abbreviations: Opx = orthopyroxene, Spl hrz = spinel harzburgite, Cl core = clast core, Cl rim = clast rim, b.d. = below detection limit.
Mg# calculated as (MgO/40.3) / (MgO/40.3 + FeO/71.85).

Major element composition of orthopyroxene from the Dramala spinel harzburgite and plagioclase-bearing harzburgite continued

Sample		PIA44	PIA44	PIA44	PIA44	PIA44	PIA44	PIA44	PIA44
Rock		Spl hrz	Spl hrz	Spl hrz	Spl hrz	Spl hrz	Spl hrz	Spl hrz	Spl hrz
Mineral		Opx	Opx	Opx	Opx	Opx	Opx	Opx	Opx
Type		Cl core	Cl core	Cl core	Cl core	Cl core	Cl core	Cl core	Cl core
Wt.%	SiO2	57.22	55.88	55.83	56.00	56.37	56.27	56.53	56.62
	TiO2	0.01	0.03	0.01	b.d.	b.d.	0.01	b.d.	0.02
	Cr2O3	0.46	0.03	0.15	0.12	0.63	0.66	0.18	0.42
	Al2O3	1.73	1.85	1.85	1.76	1.84	1.86	1.62	1.72
	FeO	5.84	5.49	5.40	5.61	5.84	5.61	5.45	5.69
	MnO	0.18	0.09	0.04	0.12	0.03	0.10	0.13	0.12
	NiO	0.14	0.00	0.06	0.01	0.14	0.08	b.d.	b.d.
	MgO	34.03	33.57	33.73	34.07	34.38	34.36	34.21	34.30
	CaO	1.14	1.31	1.29	0.92	0.75	0.88	0.68	0.80
	Na2O	b.d.	b.d.	b.d.	0.01	b.d.	0.01	b.d.	b.d.
	K2O	b.d.	0.01	b.d.	b.d.	b.d.	b.d.	b.d.	b.d.
	Total	100.75	98.25	98.36	98.61	99.97	99.83	98.79	99.70
Cations	Si	1.960	1.958	1.955	1.955	1.946	1.945	1.966	1.956
	Ti	0.000	0.001	0.000	b.d.	b.d.	0.000	b.d.	0.001
	Cr	0.012	0.001	0.004	0.003	0.017	0.018	0.005	0.012
	Al	0.070	0.076	0.076	0.072	0.075	0.076	0.066	0.070
	Fe2+	0.167	0.161	0.158	0.164	0.169	0.162	0.158	0.164
	Mn	0.005	0.003	0.001	0.004	0.001	0.003	0.004	0.004
	Ni	0.004	0.000	0.002	0.000	0.004	0.002	b.d.	b.d.
	Mg	1.738	1.754	1.760	1.773	1.769	1.770	1.773	1.766
	Ca	0.042	0.049	0.049	0.035	0.028	0.032	0.025	0.030
	Na	b.d.	b.d.	b.d.	0.000	b.d.	0.001	b.d.	b.d.
	K	b.d.	0.001	b.d.	b.d.	b.d.	b.d.	b.d.	b.d.
	Sum	3.999	4.003	4.005	4.007	4.008	4.009	3.998	4.002
	Mg #	0.912	0.916	0.918	0.915	0.913	0.916	0.918	0.915

Abbreviations: Opx = orthopyroxene, Spl hrz = spinel harzburgite, Cl core = clast core, b.d. = below detection limit.
Mg# calculated as (MgO/40.3) / (MgO/40.3 + FeO/71.85).

Major element composition of orthopyroxene from the Dramala spinel harzburgite and plagioclase-bearing harzburgite continued

Sample		PIA44	PIA44	PIA44	PIA44	PIA44	PIA44	PIA44	PIA44	PIA44	PIA44	PIA44	PIA44	PIA44	PIA44	PIA44	PIA44
Rock		Spl hrz	Spl hrz	Spl hrz	Spl hrz	Spl hrz	Spl hrz	Spl hrz	Spl hrz	Spl hrz	Spl hrz	Spl hrz	Spl hrz	Spl hrz	Spl hrz	Spl hrz	Spl hrz
Mineral		Opx	Opx	Opx	Opx	Opx	Opx	Opx	Opx	Opx	Opx	Opx	Opx	Opx	Opx	Opx	Opx
Type		Cl core	Cl core	Cl core	Cl core	Cl core	Cl core	Cl core	Cl core	Cl core	Cl core	Cl core	Cl core	Cl core	Cl core	Cl core	Cl core
Wt.%	SiO2	56.53	56.73	56.66	56.38	56.89	56.66	56.67	56.93	56.84	56.78	56.84	56.72	56.47	56.64	56.53	56.62
	TiO2	0.01	0.02	0.01	0.02	b.d.	b.d.	0.02	b.d.	b.d.	0.17	b.d.	0.02	0.01	b.d.	0.01	0.01
	Cr2O3	0.55	0.15	0.52	0.58	0.49	0.62	0.62	0.52	0.43	0.57	0.66	0.66	0.54	0.63	0.15	0.56
	Al2O3	1.78	1.77	1.79	1.76	1.80	1.79	1.74	1.83	1.77	1.79	1.75	1.82	1.83	1.81	1.87	1.87
	FeO	5.61	5.29	5.61	5.48	5.81	5.36	5.39	5.60	5.94	5.73	5.58	5.64	5.71	5.62	5.42	5.23
	MnO	0.08	0.10	0.02	0.11	0.13	0.14	0.06	0.05	0.11	0.05	0.12	0.12	0.16	0.10	0.11	0.09
	NiO	b.d.	0.06	0.03	0.18	b.d.	0.01	0.05	0.09	0.02	b.d.	0.15	0.11	b.d.	0.09	0.06	0.11
	MgO	34.22	34.12	34.11	33.66	34.39	34.22	34.36	34.53	34.23	34.23	34.18	34.32	34.23	34.18	34.15	34.08
	CaO	0.85	0.83	0.86	1.67	0.64	0.86	0.80	0.60	0.87	0.74	1.05	1.02	0.96	0.87	0.92	0.71
	Na2O	b.d.	b.d.	b.d.	b.d.	b.d.	0.01	b.d.	b.d.	b.d.	b.d.	b.d.	b.d.	b.d.	b.d.	b.d.	b.d.
	K2O	b.d.	b.d.	b.d.	b.d.	b.d.	b.d.	0.01	0.01	0.01	b.d.	b.d.	b.d.	b.d.	b.d.	0.01	b.d.
	Total	99.62	99.06	99.61	99.83	100.15	99.68	99.71	100.15	100.22	100.05	100.32	100.42	99.90	99.95	99.21	99.26
Cations	Si	1.954	1.966	1.958	1.951	1.957	1.956	1.956	1.956	1.956	1.955	1.954	1.949	1.950	1.953	1.959	1.960
	Ti	0.000	0.001	0.000	0.000	b.d.	b.d.	0.000	b.d.	b.d.	0.004	b.d.	0.000	0.000	b.d.	0.000	0.000
	Cr	0.015	0.004	0.014	0.016	0.013	0.017	0.017	0.014	0.012	0.015	0.018	0.018	0.015	0.017	0.004	0.015
	Al	0.072	0.072	0.073	0.072	0.073	0.073	0.071	0.074	0.072	0.073	0.071	0.074	0.074	0.074	0.076	0.076
	Fe2+	0.162	0.153	0.162	0.159	0.167	0.155	0.155	0.161	0.171	0.165	0.160	0.162	0.165	0.162	0.157	0.151
	Mn	0.002	0.003	0.001	0.003	0.004	0.004	0.002	0.001	0.003	0.001	0.003	0.003	0.005	0.003	0.003	0.003
	Ni	b.d.	0.002	0.001	0.005	b.d.	0.000	0.001	0.002	0.001	b.d.	0.004	0.003	b.d.	0.002	0.002	0.003
	Mg	1.764	1.763	1.757	1.736	1.763	1.761	1.768	1.768	1.756	1.757	1.752	1.757	1.762	1.757	1.764	1.758
	Ca	0.032	0.031	0.032	0.062	0.024	0.032	0.030	0.022	0.032	0.027	0.039	0.038	0.035	0.032	0.034	0.026
	Na	b.d.	b.d.	b.d.	b.d.	b.d.	0.001	b.d.	b.d.	b.d.	b.d.	b.d.	b.d.	b.d.	b.d.	b.d.	b.d.
	K	b.d.	b.d.	b.d.	b.d.	b.d.	b.d.	0.000	0.000	0.000	b.d.	b.d.	b.d.	b.d.	b.d.	0.000	b.d.
	Sum	4.002	3.995	3.998	4.004	4.000	3.999	4.000	4.000	4.002	3.997	4.001	4.005	4.006	4.001	4.000	3.994
	Mg #	0.916	0.920	0.915	0.916	0.913	0.919	0.919	0.917	0.911	0.914	0.916	0.916	0.914	0.916	0.918	0.921

Abbreviations: Opx = orthopyroxene, Spl hrz = spinel harzburgite, Cl core = clast core, b.d. = below detection limit.
Mg# calculated as (MgO/40.3) / (MgO/40.3 + FeO/71.85).

Major element composition of orthopyroxene from the Dramala spinel harzburgite and plagioclase-bearing harzburgite continued

Sample		PIA44	PIA44	PIA44	PIA44	PIA44	PIA44	PIA44	PIA44	PIA44	PIA44	PIA44	PIA44	PIA44	PIA44	PIA44	PIA44
Rock		Spl hrz	Spl hrz	Spl hrz	Spl hrz	Spl hrz	Spl hrz	Spl hrz	Spl hrz	Spl hrz	Spl hrz	Spl hrz	Spl hrz	Spl hrz	Spl hrz	Spl hrz	Spl hrz
Mineral		Opx	Opx	Opx	Opx	Opx	Opx	Opx	Opx	Opx	Opx	Opx	Opx	Opx	Opx	Opx	Opx
Type		Cl core	Cl core	Cl core	Cl core	Cl core	Cl core	Cl core	Cl core	Cl core	Cl core	Cl core	Cl core	Cl core	Cl core	Cl core	Cl core
Wt.%	SiO2	56.66	56.62	56.84	56.79	56.57	56.14	56.67	56.60	56.67	56.36	56.24	56.75	56.32	56.41	56.31	53.61
	TiO2	b.d.	0.01	0.01	b.d.	b.d.	0.01	b.d.	0.02	0.01	0.01	0.01	0.01	b.d.	b.d.	0.01	0.03
	Cr2O3	0.58	0.59	0.61	0.64	0.65	0.64	0.51	0.65	0.63	0.57	0.81	0.66	0.52	0.63	0.54	0.87
	Al2O3	1.86	1.81	1.77	1.88	1.85	1.83	1.83	1.69	1.84	1.88	1.87	1.91	1.84	1.86	1.88	1.83
	FeO	5.73	5.36	5.52	5.56	5.51	5.03	5.61	5.37	5.21	5.41	5.66	5.60	5.50	5.67	5.17	1.73
	MnO	0.11	0.14	0.00	0.08	0.03	0.08	0.00	0.12	0.08	0.12	0.11	0.11	0.13	0.08	0.07	0.03
	NiO	0.11	0.05	0.07	0.10	0.07	0.08	0.19	0.04	0.12	0.05	0.11	0.05	0.11	0.15	0.09	0.01
	MgO	34.37	34.34	34.45	34.17	34.18	32.81	33.99	33.53	34.02	34.20	34.16	34.35	34.10	34.04	33.43	18.01
	CaO	0.84	0.85	0.86	0.99	0.89	2.97	0.91	1.74	1.00	1.14	0.93	0.90	0.93	1.48	1.89	24.44
	Na2O	0.01	b.d.	b.d.	b.d.	0.01	b.d.	0.01	b.d.	0.01	0.02	0.03	0.01	0.01	0.01	b.d.	0.02
	K2O	b.d.	b.d.	b.d.	0.02	0.01	0.02	b.d.	b.d.	b.d.	0.01	0.01	0.01	b.d.	b.d.	0.01	b.d.
	Total	100.26	99.77	100.13	100.23	99.77	99.60	99.72	99.75	99.59	99.75	99.95	100.36	99.46	100.33	99.39	100.59
Cations	Si	1.950	1.954	1.954	1.953	1.953	1.950	1.958	1.958	1.958	1.948	1.943	1.950	1.952	1.944	1.954	1.937
	Ti	b.d.	0.000	0.000	b.d.	b.d.	0.000	b.d.	0.000	0.000	0.000	0.000	0.000	b.d.	b.d.	0.000	0.001
	Cr	0.016	0.016	0.016	0.018	0.018	0.017	0.014	0.018	0.017	0.015	0.022	0.018	0.014	0.017	0.015	0.025
	Al	0.075	0.074	0.072	0.076	0.075	0.075	0.075	0.069	0.075	0.077	0.076	0.077	0.075	0.076	0.077	0.078
	Fe2+	0.165	0.155	0.159	0.160	0.159	0.146	0.162	0.155	0.150	0.156	0.164	0.161	0.159	0.163	0.150	0.052
	Mn	0.003	0.004	0.000	0.002	0.001	0.002	0.000	0.003	0.002	0.003	0.003	0.003	0.004	0.002	0.002	0.001
	Ni	0.003	0.001	0.002	0.003	0.002	0.002	0.005	0.001	0.003	0.001	0.003	0.001	0.003	0.004	0.002	0.000
	Mg	1.762	1.766	1.765	1.751	1.759	1.699	1.750	1.729	1.752	1.762	1.759	1.758	1.761	1.748	1.729	0.970
	Ca	0.031	0.032	0.032	0.036	0.033	0.110	0.034	0.065	0.037	0.042	0.034	0.033	0.034	0.055	0.070	0.946
	Na	0.000	b.d.	b.d.	b.d.	0.001	b.d.	0.000	b.d.	0.001	0.001	0.002	0.001	0.001	0.000	b.d.	0.001
	K	b.d.	b.d.	b.d.	0.001	0.000	0.001	b.d.	b.d.	b.d.	0.001	0.001	0.000	b.d.	b.d.	0.000	b.d.
	Sum	4.005	4.001	4.001	4.000	4.001	4.004	3.998	3.998	3.996	4.007	4.008	4.003	4.004	4.010	4.000	4.011
	Mg #	0.915	0.920	0.917	0.916	0.917	0.921	0.915	0.918	0.921	0.918	0.915	0.916	0.917	0.915	0.920	0.949

Abbreviations: Opx = orthopyroxene, Spl hrz = spinel harzburgite, Cl core = clast core, b.d. = below detection limit.
Mg# calculated as (MgO/40.3) / (MgO/40.3 + FeO/71.85).

Major element composition of orthopyroxene from the Dramala spinel harzburgite and plagioclase-bearing harzburgite continued

Sample		PIA44	PIA44	PIA44	PIA44	PIA44	PIA44	PIA44	PIA44	PIA44	PIA44	PIA44	PIA44	PIA44	PIA44	PIA44	PIA44
Rock		Spl hrz	Spl hrz	Spl hrz	Spl hrz	Spl hrz	Spl hrz	Spl hrz	Spl hrz	Spl hrz	Spl hrz	Spl hrz	Spl hrz	Spl hrz	Spl hrz	Spl hrz	Spl hrz
Mineral		Opx	Opx	Opx	Opx	Opx	Opx	Opx	Opx	Opx	Opx	Opx	Opx	Opx	Opx	Opx	Opx
Type		Cl core	Cl core	Cl core	Cl core	Cl core	Cl core	Cl core	Cl core	Cl core	Cl core	Cl core	Cl core	Cl core	Cl core	Cl core	Cl core
Wt.%	SiO2	56.63	56.42	56.54	56.16	56.54	56.53	56.29	56.46	56.47	56.36	56.71	56.36	56.49	56.45	56.36	56.30
	TiO2	b.d.	0.02	b.d.	0.03	0.01	b.d.	b.d.	0.04	b.d.	b.d.	b.d.	0.02	b.d.	0.03	b.d.	b.d.
	Cr2O3	0.70	0.67	0.72	0.57	0.69	0.47	0.71	0.55	0.55	0.66	0.67	0.65	0.66	0.61	0.67	0.49
	Al2O3	1.91	1.84	1.85	1.85	1.91	1.89	1.85	1.89	1.86	1.73	1.83	1.91	1.91	1.91	1.90	1.82
	FeO	5.08	5.20	5.63	5.68	5.42	5.61	5.40	5.90	5.23	5.43	5.40	5.40	5.46	5.28	5.47	5.17
	MnO	0.05	0.20	0.06	0.06	0.13	0.13	0.06	0.12	0.03	0.14	0.14	0.08	0.00	0.09	0.05	0.10
	NiO	0.10	0.09	0.05	0.10	0.11	0.10	0.06	0.07	0.02	0.07	0.12	0.06	0.16	0.15	0.07	0.01
	MgO	34.18	33.18	34.17	34.06	34.21	34.19	33.95	34.24	32.64	33.84	34.06	33.97	34.48	34.15	34.12	32.98
	CaO	0.81	2.61	0.95	0.88	0.90	0.91	1.33	0.88	3.25	1.51	0.96	1.12	0.84	0.92	0.89	2.69
	Na2O	b.d.	b.d.	0.01	b.d.	b.d.	b.d.	b.d.	b.d.	b.d.	b.d.	b.d.	b.d.	b.d.	b.d.	b.d.	b.d.
	K2O	0.01	b.d.	b.d.	b.d.	b.d.	b.d.	b.d.	b.d.	0.01	b.d.	b.d.	0.01	b.d.	b.d.	b.d.	0.01
	Total	99.46	100.22	99.97	99.39	99.93	99.84	99.65	100.15	100.08	99.73	99.88	99.58	99.99	99.57	99.53	99.56
Cations	Si	1.957	1.948	1.950	1.949	1.950	1.952	1.949	1.947	1.953	1.951	1.956	1.951	1.947	1.952	1.951	1.954
	Ti	b.d.	0.001	b.d.	0.001	0.000	b.d.	b.d.	0.001	b.d.	b.d.	b.d.	0.000	b.d.	0.001	b.d.	b.d.
	Cr	0.019	0.018	0.020	0.016	0.019	0.013	0.020	0.015	0.015	0.018	0.018	0.018	0.018	0.017	0.018	0.014
	Al	0.078	0.075	0.075	0.076	0.078	0.077	0.075	0.077	0.076	0.070	0.074	0.078	0.077	0.078	0.078	0.075
	Fe2+	0.147	0.150	0.162	0.165	0.156	0.162	0.156	0.170	0.151	0.157	0.156	0.156	0.157	0.153	0.158	0.150
	Mn	0.001	0.006	0.002	0.002	0.004	0.004	0.002	0.003	0.001	0.004	0.004	0.002	0.000	0.003	0.002	0.003
	Ni	0.003	0.002	0.001	0.003	0.003	0.003	0.002	0.002	0.001	0.002	0.003	0.002	0.004	0.004	0.002	0.000
	Mg	1.760	1.708	1.756	1.762	1.758	1.759	1.752	1.759	1.683	1.746	1.751	1.752	1.771	1.760	1.760	1.706
	Ca	0.030	0.097	0.035	0.033	0.033	0.034	0.049	0.032	0.121	0.056	0.036	0.042	0.031	0.034	0.033	0.100
	Na	b.d.	b.d.	0.000	b.d.	b.d.	b.d.	b.d.	b.d.	b.d.	b.d.	b.d.	b.d.	b.d.	b.d.	b.d.	b.d.
	K	0.000	b.d.	b.d.	b.d.	b.d.	b.d.	b.d.	b.d.	0.001	b.d.	b.d.	0.000	b.d.	b.d.	b.d.	0.000
	Sum	3.995	4.005	4.003	4.005	4.002	4.003	4.004	4.007	4.001	4.005	3.998	4.001	4.006	4.000	4.001	4.002
	Mg #	0.923	0.919	0.915	0.914	0.918	0.916	0.918	0.912	0.917	0.917	0.918	0.918	0.918	0.920	0.917	0.919

Abbreviations: Opx = orthopyroxene, Spl hrz = spinel harzburgite, Cl core = clast core, b.d. = below detection limit.
Mg# calculated as (MgO/40.3) / (MgO/40.3 + FeO/71.85).

Major element composition of orthopyroxene from the Dramala spinel harzburgite and plagioclase-bearing harzburgite continued

Sample		PIA44	PIA44	PIA44	PIA44	PIA44	PIA44	PIA44	PIA44	PIA44	PIA44	PIA44	PIA44	PIA44	PIA44	PIA44	PIA44
Rock		Spl hrz	Spl hrz	Spl hrz	Spl hrz	Spl hrz	Spl hrz	Spl hrz	Spl hrz	Spl hrz	Spl hrz	Spl hrz	Spl hrz	Spl hrz	Spl hrz	Spl hrz	Spl hrz
Mineral		Opx	Opx	Opx	Opx	Opx	Opx	Opx	Opx	Opx	Opx	Opx	Opx	Opx	Opx	Opx	Opx
Type		Cl core	Cl core	Cl core	Cl core	Cl core	Cl core	Cl core	Cl core	Cl core	Cl core	Cl core	Cl core	Cl core	Cl core	Cl core	Cl core
Wt.%	SiO2	56.67	56.70	56.52	56.40	55.99	56.30	56.57	56.12	56.45	56.45	56.38	56.47	56.56	56.43	56.06	56.05
	TiO2	b.d.	0.02	0.01	0.03	0.05	0.02	0.01	b.d.	0.01	b.d.	b.d.	0.01	b.d.	0.01	0.02	0.01
	Cr2O3	0.62	0.17	0.55	0.73	0.74	0.71	0.51	0.66	0.58	0.61	0.61	0.61	0.58	0.57	0.57	0.77
	Al2O3	1.92	1.94	1.84	1.88	2.00	1.87	1.89	1.91	1.87	1.93	1.85	1.89	1.95	1.92	1.86	1.87
	FeO	5.58	5.73	5.42	5.22	4.85	5.16	5.73	5.43	5.65	5.44	5.67	5.17	5.17	5.50	5.80	5.38
	MnO	0.07	0.11	0.14	0.10	0.04	0.04	0.06	0.10	0.05	0.06	0.14	0.11	0.06	0.09	0.07	0.18
	NiO	0.16	0.08	0.10	0.06	0.09	b.d.	0.16	0.07	0.15	0.04	0.16	0.03	0.12	0.21	0.14	0.17
	MgO	34.31	34.21	33.91	33.89	32.10	33.95	34.24	34.24	33.99	34.44	34.19	34.24	33.92	34.27	33.99	34.25
	CaO	0.86	0.80	1.09	1.27	3.77	0.92	0.73	0.81	1.46	0.68	0.98	0.87	1.10	0.93	0.92	0.75
	Na2O	b.d.	b.d.	0.01	0.01	0.03	0.03	0.02	0.03	b.d.	b.d.	0.01	0.01	0.01	0.01	b.d.	b.d.
	K2O	0.01	b.d.	b.d.	b.d.	0.02	0.02	0.01	0.01	0.01	b.d.	0.01	0.01	b.d.	b.d.	b.d.	b.d.
	Total	100.19	99.77	99.59	99.59	99.66	99.03	99.92	99.37	100.21	99.64	99.98	99.42	99.47	99.94	99.43	99.42
Cations	Si	1.950	1.957	1.956	1.951	1.947	1.955	1.952	1.946	1.946	1.950	1.947	1.954	1.956	1.947	1.947	1.944
	Ti	b.d.	0.001	0.000	0.001	0.001	0.000	0.000	b.d.	0.000	b.d.	b.d.	0.000	b.d.	0.000	0.001	0.000
	Cr	0.017	0.005	0.015	0.020	0.020	0.020	0.014	0.018	0.016	0.017	0.017	0.017	0.016	0.016	0.016	0.021
	Al	0.078	0.079	0.075	0.077	0.082	0.077	0.077	0.078	0.076	0.078	0.075	0.077	0.079	0.078	0.076	0.076
	Fe2+	0.161	0.165	0.157	0.151	0.141	0.150	0.165	0.157	0.163	0.157	0.164	0.149	0.150	0.159	0.168	0.156
	Mn	0.002	0.003	0.004	0.003	0.001	0.001	0.002	0.003	0.002	0.002	0.004	0.003	0.002	0.003	0.002	0.005
	Ni	0.004	0.002	0.003	0.002	0.002	b.d.	0.004	0.002	0.004	0.001	0.004	0.001	0.003	0.006	0.004	0.005
	Mg	1.759	1.760	1.749	1.748	1.664	1.757	1.761	1.770	1.747	1.773	1.760	1.765	1.749	1.762	1.759	1.771
	Ca	0.032	0.030	0.040	0.047	0.140	0.034	0.027	0.030	0.054	0.025	0.036	0.032	0.041	0.034	0.034	0.028
	Na	b.d.	b.d.	0.000	0.000	0.002	0.002	0.002	0.002	b.d.	b.d.	0.000	0.001	0.001	0.000	b.d.	b.d.
	K	0.001	b.d.	b.d.	b.d.	0.001	0.001	0.000	0.001	0.000	b.d.	0.000	0.000	b.d.	b.d.	b.d.	b.d.
	Sum	4.003	4.001	3.999	4.000	4.002	3.997	4.004	4.007	4.008	4.003	4.007	4.000	3.996	4.006	4.007	4.007
	Mg #	0.916	0.914	0.918	0.920	0.922	0.921	0.914	0.918	0.915	0.919	0.915	0.922	0.921	0.917	0.913	0.919

Abbreviations: Opx = orthopyroxene, Spl hrz = spinel harzburgite, Cl core = clast core, b.d. = below detection limit.
Mg# calculated as (MgO/40.3) / (MgO/40.3 + FeO/71.85).

Major element composition of orthopyroxene from the Dramala spinel harzburgite and plagioclase-bearing harzburgite continued

Sample		PIA44	PIA44	PIA44	PIA44	PIA44	PIA44	PIA44	PIA44	PIA44	PIA44	PIA44	PIA44	PIA44	PIA44	PIA44	PIA44
Rock		Spl hrz	Spl hrz	Spl hrz	Spl hrz	Spl hrz	Spl hrz	Spl hrz	Spl hrz	Spl hrz	Spl hrz	Spl hrz	Spl hrz	Spl hrz	Spl hrz	Spl hrz	Spl hrz
Mineral		Opx	Opx	Opx	Opx	Opx	Opx	Opx	Opx	Opx	Opx	Opx	Opx	Opx	Opx	Opx	Opx
Type		Cl core	Cl core	Cl core	Cl core	Cl core	Cl core	Cl core	Cl core	Cl core	Cl core	Cl core	Cl core	Cl core	Cl core	Cl core	Cl core
Wt.%	SiO2	56.64	56.45	56.42	56.38	56.31	56.42	56.63	56.22	56.51	56.36	56.64	56.47	56.31	56.56	56.39	56.26
	TiO2	0.04	b.d.	0.03	b.d.	0.02	b.d.	b.d.	0.03	0.01	0.03	0.01	0.03	0.02	b.d.	b.d.	b.d.
	Cr2O3	0.64	0.58	0.70	0.68	0.59	0.66	0.56	0.62	0.59	0.65	0.67	0.68	0.47	0.56	0.62	0.69
	Al2O3	1.89	1.83	1.85	1.87	1.88	1.91	1.84	1.83	1.89	1.88	1.86	1.89	1.87	1.88	1.86	1.86
	FeO	5.68	5.68	5.44	5.44	5.55	5.21	5.39	5.51	5.06	5.52	5.49	5.59	5.69	5.44	5.10	5.25
	MnO	0.13	0.06	0.06	0.04	0.02	0.11	0.12	0.00	0.17	0.08	0.15	0.11	0.09	0.05	0.16	0.16
	NiO	0.04	0.09	0.07	0.05	0.12	0.09	0.18	0.11	0.10	0.12	0.09	0.10	0.01	0.05	0.14	0.15
	MgO	34.30	34.36	34.45	34.37	34.43	34.35	34.16	34.30	34.28	34.13	34.05	34.33	34.18	34.28	34.15	34.17
	CaO	0.85	0.80	0.87	0.68	0.65	0.70	1.12	0.71	0.83	0.99	1.13	0.86	0.86	0.77	0.85	0.83
	Na2O	b.d.	b.d.	b.d.	0.01	b.d.	b.d.	b.d.	0.01	b.d.	0.03	0.02	b.d.	b.d.	b.d.	b.d.	b.d.
	K2O	b.d.	b.d.	b.d.	0.01	b.d.	0.01	0.01	0.01	0.01	0.02	0.01	b.d.	b.d.	b.d.	0.02	b.d.
	Total	100.21	99.83	99.88	99.52	99.56	99.47	100.00	99.35	99.44	99.81	100.11	100.07	99.48	99.57	99.29	99.37
Cations	Si	1.949	1.949	1.946	1.950	1.948	1.951	1.952	1.949	1.954	1.948	1.951	1.946	1.951	1.954	1.954	1.950
	Ti	0.001	b.d.	0.001	b.d.	0.000	b.d.	b.d.	0.001	0.000	0.001	0.000	0.001	0.001	b.d.	b.d.	b.d.
	Cr	0.017	0.016	0.019	0.019	0.016	0.018	0.015	0.017	0.016	0.018	0.018	0.019	0.013	0.015	0.017	0.019
	Al	0.077	0.074	0.075	0.076	0.077	0.078	0.075	0.075	0.077	0.077	0.076	0.077	0.076	0.076	0.076	0.076
	Fe2+	0.164	0.164	0.157	0.157	0.161	0.151	0.155	0.160	0.146	0.159	0.158	0.161	0.165	0.157	0.148	0.152
	Mn	0.004	0.002	0.002	0.001	0.001	0.003	0.004	0.000	0.005	0.002	0.004	0.003	0.003	0.002	0.005	0.005
	Ni	0.001	0.002	0.002	0.001	0.003	0.002	0.005	0.003	0.003	0.003	0.002	0.003	0.000	0.001	0.004	0.004
	Mg	1.759	1.768	1.772	1.772	1.775	1.771	1.755	1.772	1.767	1.758	1.748	1.764	1.765	1.765	1.764	1.765
	Ca	0.031	0.029	0.032	0.025	0.024	0.026	0.041	0.026	0.031	0.036	0.042	0.032	0.032	0.028	0.032	0.031
	Na	b.d.	b.d.	b.d.	0.001	b.d.	b.d.	b.d.	0.000	b.d.	0.002	0.001	b.d.	b.d.	b.d.	b.d.	b.d.
	K	b.d.	b.d.	b.d.	0.000	b.d.	0.001	0.000	0.000	0.000	0.001	0.000	b.d.	b.d.	b.d.	0.001	b.d.
	Sum	4.003	4.006	4.006	4.003	4.005	4.001	4.003	4.004	3.999	4.006	4.002	4.005	4.004	4.000	4.000	4.002
	Mg #	0.915	0.915	0.919	0.918	0.917	0.922	0.919	0.917	0.923	0.917	0.917	0.916	0.915	0.918	0.923	0.921

Abbreviations: Opx = orthopyroxene, Spl hrz = spinel harzburgite, Cl core = clast core, b.d. = below detection limit.
Mg# calculated as (MgO/40.3) / (MgO/40.3 + FeO/71.85).

Major element composition of orthopyroxene from the Dramala spinel harzburgite and plagioclase-bearing harzburgite continued

Sample		PIA44	PIA44	PIA44	PIA44	PIA44	PIA44	PIA44	PIA44	PIA44	PIA44	PIA44	PIA44	PIA44	PIA44	PIA44	PIA44
Rock		Spl hrz	Spl hrz	Spl hrz	Spl hrz	Spl hrz	Spl hrz	Spl hrz	Spl hrz	Spl hrz	Spl hrz	Spl hrz	Spl hrz	Spl hrz	Spl hrz	Spl hrz	Spl hrz
Mineral		Opx	Opx	Opx	Opx	Opx	Opx	Opx	Opx	Opx	Opx	Opx	Opx	Opx	Opx	Opx	Opx
Type		Cl core	Cl core	Cl core	Cl core	Cl core	Cl core	Cl core	Cl core	Cl core	Cl core	Cl core	Cl core	Cl core	Cl core	Cl core	Cl core
Wt.%	SiO2	56.47	56.44	56.55	56.31	56.83	56.31	56.46	56.36	56.05	56.37	56.20	56.53	56.34	56.33	56.52	56.92
	TiO2	b.d.	b.d.	b.d.	0.01	0.01	0.02	0.02	0.02	0.02	b.d.	b.d.	b.d.	b.d.	0.01	0.01	b.d.
	Cr2O3	0.62	0.59	0.50	0.50	0.23	0.59	0.69	0.67	0.59	0.66	0.64	0.61	0.60	0.66	0.58	0.60
	Al2O3	1.87	1.85	1.87	1.90	1.85	1.89	1.89	1.82	1.93	1.83	1.85	1.87	1.84	1.85	1.84	1.80
	FeO	5.50	5.24	5.34	5.12	5.62	5.30	5.90	5.39	5.49	5.58	5.57	5.41	5.30	5.57	5.75	5.49
	MnO	0.13	0.05	0.11	0.01	0.09	0.11	0.14	0.09	0.00	0.08	0.03	0.04	0.08	0.03	0.11	0.18
	NiO	0.16	0.11	0.11	0.06	0.10	0.05	0.10	0.04	0.10	0.15	0.01	0.07	0.04	0.14	0.20	0.13
	MgO	34.44	34.11	34.20	34.09	34.21	33.66	34.26	34.10	33.17	34.20	34.28	34.16	34.12	33.76	34.43	34.28
	CaO	0.84	0.86	0.91	0.96	0.88	1.70	0.92	1.00	2.57	0.96	0.95	0.90	1.03	1.59	0.89	0.91
	Na2O	b.d.	b.d.	0.01	b.d.	0.01	0.01	0.01	b.d.	0.01	0.02	b.d.	b.d.	b.d.	b.d.	b.d.	0.01
	K2O	b.d.	b.d.	0.02	0.02	b.d.	b.d.	0.01	0.01	b.d.	b.d.	0.01	0.01	b.d.	b.d.	0.01	b.d.
	Total	100.02	99.24	99.60	98.98	99.84	99.62	100.38	99.51	99.92	99.84	99.53	99.61	99.36	99.93	100.32	100.32
Cations	Si	1.947	1.956	1.955	1.956	1.959	1.950	1.944	1.951	1.943	1.948	1.947	1.954	1.952	1.948	1.945	1.955
	Ti	b.d.	b.d.	b.d.	0.000	0.000	0.000	0.001	0.000	0.000	b.d.	b.d.	b.d.	b.d.	0.000	0.000	b.d.
	Cr	0.017	0.016	0.014	0.014	0.006	0.016	0.019	0.018	0.016	0.018	0.018	0.017	0.016	0.018	0.016	0.016
	Al	0.076	0.075	0.076	0.078	0.075	0.077	0.077	0.074	0.079	0.074	0.075	0.076	0.075	0.075	0.075	0.073
	Fe2+	0.159	0.152	0.154	0.149	0.162	0.153	0.170	0.156	0.159	0.161	0.161	0.156	0.154	0.161	0.165	0.158
	Mn	0.004	0.001	0.003	0.000	0.003	0.003	0.004	0.003	0.000	0.002	0.001	0.001	0.002	0.001	0.003	0.005
	Ni	0.004	0.003	0.003	0.002	0.003	0.001	0.003	0.001	0.003	0.004	0.000	0.002	0.001	0.004	0.005	0.004
	Mg	1.770	1.762	1.762	1.764	1.758	1.738	1.758	1.760	1.714	1.761	1.770	1.760	1.762	1.740	1.766	1.755
	Ca	0.031	0.032	0.034	0.036	0.033	0.063	0.034	0.037	0.095	0.035	0.035	0.033	0.038	0.059	0.033	0.034
	Na	b.d.	b.d.	0.001	b.d.	0.001	0.000	0.001	b.d.	0.001	0.001	b.d.	b.d.	b.d.	b.d.	b.d.	0.001
	K	b.d.	b.d.	0.001	0.001	b.d.	b.d.	0.000	0.000	b.d.	b.d.	0.000	0.000	b.d.	b.d.	0.000	b.d.
	Sum	4.007	3.998	4.001	3.999	4.000	4.003	4.009	4.002	4.010	4.006	4.007	4.000	4.002	4.006	4.009	4.000
	Mg #	0.918	0.921	0.919	0.922	0.916	0.919	0.912	0.919	0.915	0.916	0.916	0.918	0.920	0.915	0.914	0.918

Abbreviations: Opx = orthopyroxene, Spl hrz = spinel harzburgite, Cl core = clast core, b.d. = below detection limit.
Mg# calculated as (MgO/40.3) / (MgO/40.3 + FeO/71.85).

Major element composition of orthopyroxene from the Dramala spinel harzburgite and plagioclase-bearing harzburgite continued

Sample		PIA44	PIA44	PIA44	PIA44	PIA44	PIA44	PIA44	PIA44	PIA44	PIA44	PIA44	PIA44	PIA44	PIA44	PIA44	PIA44
Rock		Spl hrz	Spl hrz	Spl hrz	Spl hrz	Spl hrz	Spl hrz	Spl hrz	Spl hrz	Spl hrz	Spl hrz	Spl hrz	Spl hrz	Spl hrz	Spl hrz	Spl hrz	Spl hrz
Mineral		Opx	Opx	Opx	Opx	Opx	Opx	Opx	Opx	Opx	Opx	Opx	Opx	Opx	Opx	Opx	Opx
Type		Cl core	Cl core	Cl core	Cl core	Cl core	Cl core	Cl core	Cl core	Cl core	Cl core	Cl core	Cl core	Cl core	Cl core	Cl core	Cl core
Wt.%	SiO2	56.68	56.76	56.64	56.31	56.48	56.43	56.48	56.30	56.30	56.45	56.28	56.36	56.57	56.58	56.62	56.39
	TiO2	0.02	0.01	0.02	b.d.	0.01	0.02	b.d.	b.d.	0.02	b.d.	0.01	0.02	0.01	b.d.	b.d.	b.d.
	Cr2O3	0.57	0.47	0.41	0.50	0.46	0.52	0.66	0.48	0.25	0.55	0.47	0.56	0.41	0.51	0.48	0.55
	Al2O3	1.83	1.66	1.70	1.76	1.82	1.79	1.86	1.85	1.85	1.86	1.82	1.83	1.85	1.88	1.85	1.86
	FeO	5.58	5.59	5.74	5.50	5.53	5.14	5.52	5.62	5.59	5.48	5.37	5.53	5.33	5.49	5.48	5.41
	MnO	0.19	0.04	0.13	0.07	0.07	0.09	0.20	0.05	0.02	0.19	0.12	0.06	0.07	b.d.	0.08	0.11
	NiO	0.07	0.13	0.12	0.03	0.08	0.08	0.03	0.08	0.01	0.03	0.18	0.10	0.09	0.05	0.05	0.03
	MgO	34.18	34.62	34.48	34.33	34.32	34.28	34.16	34.13	33.97	34.12	34.25	34.37	34.13	34.11	34.03	34.15
	CaO	0.93	0.84	0.91	0.93	1.01	1.00	1.05	1.08	1.11	1.10	1.14	1.14	1.17	1.10	1.13	1.14
	Na2O	0.02	0.01	0.02	0.02	0.04	0.01	b.d.	b.d.	b.d.	b.d.	0.01	0.02	0.02	0.01	b.d.	0.01
	K2O	0.01	b.d.	0.02	b.d.	0.01	b.d.	b.d.	b.d.	0.01	b.d.	0.01	0.01	b.d.	b.d.	0.01	0.01
	Total	100.09	100.15	100.18	99.44	99.81	99.36	99.95	99.58	99.13	99.78	99.64	100.00	99.64	99.72	99.72	99.65
Cations	Si	1.953	1.953	1.951	1.951	1.950	1.954	1.949	1.950	1.956	1.951	1.948	1.945	1.955	1.954	1.956	1.950
	Ti	0.000	0.000	0.000	b.d.	0.000	0.001	b.d.	b.d.	0.001	b.d.	0.000	0.000	0.000	b.d.	b.d.	b.d.
	Cr	0.016	0.013	0.011	0.014	0.012	0.014	0.018	0.013	0.007	0.015	0.013	0.015	0.011	0.014	0.013	0.015
	Al	0.074	0.067	0.069	0.072	0.074	0.073	0.075	0.076	0.076	0.076	0.074	0.075	0.075	0.076	0.075	0.076
	Fe2+	0.161	0.161	0.165	0.159	0.160	0.149	0.159	0.163	0.162	0.158	0.155	0.159	0.154	0.159	0.158	0.156
	Mn	0.006	0.001	0.004	0.002	0.002	0.003	0.006	0.001	0.001	0.006	0.003	0.002	0.002	b.d.	0.002	0.003
	Ni	0.002	0.004	0.003	0.001	0.002	0.002	0.001	0.002	0.000	0.001	0.005	0.003	0.003	0.001	0.001	0.001
	Mg	1.755	1.776	1.770	1.773	1.767	1.769	1.757	1.762	1.759	1.757	1.767	1.768	1.758	1.756	1.752	1.760
	Ca	0.034	0.031	0.033	0.034	0.037	0.037	0.039	0.040	0.041	0.041	0.042	0.042	0.043	0.041	0.042	0.042
	Na	0.002	0.001	0.002	0.001	0.002	0.001	b.d.	b.d.	b.d.	b.d.	0.001	0.001	0.001	0.000	b.d.	0.001
	K	0.001	b.d.	0.001	b.d.	0.000	b.d.	b.d.	b.d.	0.000	b.d.	0.000	0.000	b.d.	b.d.	0.000	0.000
	Sum	4.003	4.007	4.010	4.007	4.008	4.002	4.004	4.006	4.003	4.004	4.009	4.011	4.002	4.001	4.000	4.005
	Mg #	0.916	0.917	0.915	0.918	0.917	0.922	0.917	0.915	0.916	0.917	0.919	0.917	0.919	0.917	0.917	0.918

Abbreviations: Opx = orthopyroxene, Spl hrz = spinel harzburgite, Cl core = clast core, b.d. = below detection limit.
Mg# calculated as (MgO/40.3) / (MgO/40.3 + FeO/71.85).

Major element composition of orthopyroxene from the Dramala spinel harzburgite and plagioclase-bearing harzburgite continued

Sample		PIA44	PIA44	PIA44	PIA44	PIA44	PIA44	PIA44	PIA44	PIA44	PIA44	PIA44	PIA44	PIA44	PIA44	PIA44	PIA44
Rock		Spl hrz	Spl hrz	Spl hrz	Spl hrz	Spl hrz	Spl hrz	Spl hrz	Spl hrz	Spl hrz	Spl hrz	Spl hrz	Spl hrz	Spl hrz	Spl hrz	Spl hrz	Spl hrz
Mineral		Opx	Opx	Opx	Opx	Opx	Opx	Opx	Opx	Opx	Opx	Opx	Opx	Opx	Opx	Opx	Opx
Type		Cl core	Cl core	Cl core	Cl core	Cl core	Cl core	Cl core	Cl core	Cl core	Cl core	Cl core	Cl core	Cl core	Cl core	Cl core	Cl core
Wt.%	SiO2	56.31	56.22	56.29	56.46	56.63	56.25	56.53	56.48	56.41	56.18	56.19	56.39	56.26	56.23	56.31	56.66
	TiO2	b.d.	0.01	0.02	0.04	0.02	0.02	b.d.	0.02	b.d.	b.d.	0.01	0.01	0.01	0.01	b.d.	b.d.
	Cr2O3	0.56	0.48	0.59	0.41	0.18	0.56	0.40	0.27	0.21	0.46	0.51	0.48	0.53	0.62	0.61	0.46
	Al2O3	1.83	1.83	1.92	1.84	1.85	1.82	1.90	1.83	1.83	1.83	1.86	1.80	1.84	1.83	1.80	1.81
	FeO	5.72	5.61	5.55	5.48	5.34	5.70	5.55	5.40	5.43	5.38	5.41	5.51	5.51	5.37	5.61	5.61
	MnO	0.13	0.14	0.10	0.06	0.08	0.13	0.12	0.10	0.08	0.12	0.11	0.11	0.12	0.04	0.05	0.18
	NiO	0.05	0.04	0.00	0.10	0.00	0.19	0.10	b.d.	0.06	0.05	0.01	0.10	0.07	0.10	0.07	0.08
	MgO	34.08	34.13	34.25	34.10	34.17	34.17	34.16	34.19	34.03	34.14	34.06	34.06	34.10	34.08	34.07	34.20
	CaO	1.14	1.12	1.12	1.14	1.09	0.99	1.08	1.09	1.12	1.11	1.12	1.08	1.13	1.15	1.13	1.14
	Na2O	b.d.	b.d.	0.01	b.d.	b.d.	b.d.	0.01	b.d.	0.01	0.03	0.02	0.04	0.02	b.d.	0.01	b.d.
	K2O	b.d.	b.d.	b.d.	b.d.	b.d.	b.d.	0.01	0.01	b.d.	0.01	0.01	b.d.	0.01	b.d.	0.01	b.d.
	Total	99.83	99.57	99.86	99.63	99.37	99.83	99.84	99.39	99.18	99.30	99.30	99.59	99.60	99.43	99.67	100.12
Cations	Si	1.948	1.948	1.944	1.953	1.960	1.946	1.952	1.956	1.958	1.950	1.950	1.952	1.948	1.949	1.949	1.952
	Ti	b.d.	0.000	0.001	0.001	0.000	0.001	b.d.	0.000	b.d.	b.d.	0.000	0.000	0.000	0.000	b.d.	b.d.
	Cr	0.015	0.013	0.016	0.011	0.005	0.015	0.011	0.008	0.006	0.013	0.014	0.013	0.014	0.017	0.017	0.012
	Al	0.075	0.075	0.078	0.075	0.075	0.074	0.077	0.075	0.075	0.075	0.076	0.074	0.075	0.075	0.073	0.073
	Fe2+	0.165	0.163	0.160	0.158	0.155	0.165	0.160	0.156	0.158	0.156	0.157	0.160	0.160	0.156	0.162	0.162
	Mn	0.004	0.004	0.003	0.002	0.002	0.004	0.003	0.003	0.002	0.003	0.003	0.003	0.003	0.001	0.002	0.005
	Ni	0.001	0.001	0.000	0.003	0.000	0.005	0.003	b.d.	0.002	0.001	0.000	0.003	0.002	0.003	0.002	0.002
	Mg	1.757	1.763	1.763	1.758	1.762	1.762	1.758	1.765	1.760	1.766	1.762	1.758	1.760	1.761	1.758	1.756
	Ca	0.042	0.041	0.041	0.042	0.041	0.037	0.040	0.040	0.041	0.041	0.042	0.040	0.042	0.043	0.042	0.042
	Na	b.d.	b.d.	0.001	b.d.	b.d.	b.d.	0.000	b.d.	0.001	0.002	0.001	0.002	0.001	b.d.	0.001	b.d.
	K	b.d.	b.d.	b.d.	b.d.	b.d.	b.d.	0.000	0.000	b.d.	0.000	0.000	b.d.	0.000	b.d.	0.000	b.d.
	Sum	4.007	4.008	4.008	4.003	4.000	4.009	4.005	4.003	4.003	4.008	4.005	4.005	4.007	4.005	4.006	4.005
	Mg #	0.914	0.916	0.917	0.917	0.919	0.914	0.916	0.919	0.918	0.919	0.918	0.917	0.917	0.919	0.915	0.916

Abbreviations: Opx = orthopyroxene, Spl hrz = spinel harzburgite, Cl core = clast core, b.d. = below detection limit.
Mg# calculated as (MgO/40.3) / (MgO/40.3 + FeO/71.85).

Major element composition of orthopyroxene from the Dramala spinel harzburgite and plagioclase-bearing harzburgite continued

Sample		PIA44	PIA44	PIA44	PIA44	PIA44	PIA44	PIA44	PIA44	PIA44	PIA44	PIA44	PIA44	PIA44	PIA44	PIA44	PIA44
Rock		Spl hrz	Spl hrz	Spl hrz	Spl hrz	Spl hrz	Spl hrz	Spl hrz	Spl hrz	Spl hrz	Spl hrz	Spl hrz	Spl hrz	Spl hrz	Spl hrz	Spl hrz	Spl hrz
Mineral		Opx	Opx	Opx	Opx	Opx	Opx	Opx	Opx	Opx	Opx	Opx	Opx	Opx	Opx	Opx	Opx
Type		Cl core	Cl core	Cl core	Cl core	Cl core	Cl core	Cl core	Cl rim	Cl rim	Cl rim	Cl rim	Cl rim	Cl rim	Cl rim	Cl rim	Cl rim
Wt.%	SiO2	56.35	56.36	56.40	56.50	56.58	56.43	56.37	56.72	56.59	56.89	56.46	56.33	56.62	56.61	56.49	56.51
	TiO2	0.02	b.d.	0.02	b.d.	0.01	b.d.	b.d.	0.02	0.03	b.d.	b.d.	0.02	0.04	b.d.	b.d.	b.d.
	Cr2O3	0.47	0.46	0.52	0.59	0.54	0.51	0.47	0.15	0.52	0.44	0.50	0.49	0.54	0.34	0.47	0.47
	Al2O3	1.83	1.82	1.80	1.85	1.77	1.72	1.67	1.67	1.71	1.72	1.77	1.72	1.69	1.53	1.64	1.59
	FeO	5.30	5.46	5.49	5.69	5.91	5.54	5.27	5.93	5.95	5.69	5.74	5.90	5.60	5.33	5.68	5.39
	MnO	0.13	0.07	0.11	0.15	0.10	0.11	0.16	0.11	0.01	0.11	0.14	0.18	0.18	0.05	0.05	0.06
	NiO	0.07	0.06	0.11	0.12	0.19	0.13	0.13	0.04	0.01	0.11	0.11	0.07	0.01	0.10	0.07	0.11
	MgO	34.13	34.13	34.14	34.26	34.36	34.37	34.26	34.58	34.44	34.63	34.33	34.14	34.42	34.63	34.36	34.21
	CaO	1.12	1.13	1.10	1.15	0.98	0.99	0.95	0.64	0.76	0.53	0.70	0.78	0.89	0.75	0.88	0.86
	Na2O	b.d.	b.d.	b.d.	b.d.	b.d.	0.01	0.01	0.03	0.04	0.01	0.02	b.d.	0.02	0.02	0.02	0.03
	K2O	0.01	0.01	b.d.	b.d.	b.d.	0.01	0.01	b.d.	0.01	0.01	b.d.	0.01	0.01	0.01	0.01	0.01
	Total	99.43	99.49	99.69	100.31	100.42	99.81	99.30	99.89	100.07	100.13	99.76	99.62	100.01	99.38	99.67	99.23
Cations	Si	1.952	1.952	1.951	1.946	1.947	1.950	1.955	1.957	1.951	1.956	1.952	1.952	1.952	1.959	1.954	1.960
	Ti	0.001	b.d.	0.001	b.d.	0.000	b.d.	b.d.	0.001	0.001	b.d.	b.d.	0.000	0.001	b.d.	b.d.	b.d.
	Cr	0.013	0.012	0.014	0.016	0.015	0.014	0.013	0.004	0.014	0.012	0.014	0.013	0.015	0.009	0.013	0.013
	Al	0.075	0.074	0.073	0.075	0.072	0.070	0.068	0.068	0.070	0.070	0.072	0.070	0.069	0.062	0.067	0.065
	Fe2+	0.153	0.158	0.159	0.164	0.170	0.160	0.153	0.171	0.172	0.164	0.166	0.171	0.161	0.154	0.164	0.156
	Mn	0.004	0.002	0.003	0.004	0.003	0.003	0.005	0.003	0.000	0.003	0.004	0.005	0.005	0.002	0.001	0.002
	Ni	0.002	0.002	0.003	0.003	0.005	0.004	0.004	0.001	0.000	0.003	0.003	0.002	0.000	0.003	0.002	0.003
	Mg	1.762	1.762	1.760	1.758	1.762	1.770	1.771	1.778	1.770	1.775	1.769	1.763	1.769	1.787	1.771	1.768
	Ca	0.042	0.042	0.041	0.042	0.036	0.037	0.035	0.024	0.028	0.020	0.026	0.029	0.033	0.028	0.032	0.032
	Na	b.d.	b.d.	b.d.	b.d.	b.d.	0.001	0.001	0.002	0.002	0.001	0.001	b.d.	0.001	0.001	0.001	0.002
	K	0.000	0.000	b.d.	b.d.	b.d.	0.000	0.000	b.d.	0.001	0.000	b.d.	0.000	0.000	0.000	0.000	0.000
	Sum	4.004	4.005	4.005	4.009	4.010	4.008	4.005	4.008	4.008	4.003	4.006	4.006	4.006	4.006	4.007	4.002
	Mg #	0.920	0.918	0.917	0.915	0.912	0.917	0.921	0.912	0.912	0.916	0.914	0.912	0.916	0.921	0.915	0.919

Abbreviations: Opx = orthopyroxene, Spl hrz = spinel harzburgite, Cl core = clast core, Cl rim = clast rim, b.d. = below detection limit.
Mg# calculated as (MgO/40.3) / (MgO/40.3 + FeO/71.85).

Major element composition of orthopyroxene from the Dramala spinel harzburgite and plagioclase-bearing harzburgite continued

Sample		PIA120	PIA120	PIA120	PIA120	PIA120	PIA120	PIA120	PIA51
Rock		Pl-b hrz	Pl-b hrz	Pl-b hrz	Pl-b hrz	Pl-b hrz	Pl-b hrz	Pl-b hrz	Pl-b hrz
Mineral		Opx	Opx	Opx	Opx	Opx	Opx	Opx	Opx
Type		Melt r	Cl core	Cl core	Cl core	Cl core	Cl core	Cl rim	Cl core
Wt.%	SiO2	55.63	55.62	55.61	55.02	55.46	55.50	55.97	55.62
	TiO2	0.14	0.19	0.16	0.25	0.20	0.13	0.17	0.09
	Cr2O3	2.54	2.85	2.87	3.30	3.13	2.78	2.20	0.71
	Al2O3	0.48	0.56	0.62	0.63	0.89	0.63	0.43	4.02
	FeO	6.80	6.34	6.64	6.22	6.82	6.71	6.26	6.49
	MnO	0.11	0.24	0.15	0.17	0.18	0.14	0.21	0.15
	NiO	0.07	0.04	0.08	0.08	0.02	0.11	0.08	0.07
	MgO	33.21	32.70	32.99	31.91	33.03	33.48	33.85	33.67
	CaO	0.81	2.08	1.56	2.53	1.22	0.64	0.93	0.05
	Na2O	0.01	0.04	b.d.	0.05	0.03	b.d.	b.d.	0.04
	K2O	0.02	b.d.	0.02	b.d.	0.03	0.02	b.d.	b.d.
	Total	99.82	100.66	100.70	100.16	101.01	100.14	100.10	100.91
Cations	Si	1.946	1.935	1.934	1.929	1.924	1.936	1.947	1.905
	Ti	0.004	0.005	0.004	0.007	0.005	0.003	0.004	0.002
	Cr	0.070	0.078	0.079	0.091	0.086	0.077	0.060	0.019
	Al	0.020	0.023	0.025	0.026	0.036	0.026	0.018	0.162
	Fe2+	0.199	0.184	0.193	0.182	0.198	0.196	0.182	0.186
	Mn	0.003	0.007	0.004	0.005	0.005	0.004	0.006	0.004
	Ni	0.002	0.001	0.002	0.002	0.001	0.003	0.002	0.002
	Mg	1.731	1.696	1.710	1.667	1.708	1.740	1.755	1.719
	Ca	0.030	0.078	0.058	0.095	0.045	0.024	0.035	0.002
	Na	0.001	0.003	b.d.	0.003	0.002	b.d.	b.d.	0.003
	K	0.001	b.d.	0.001	b.d.	0.001	0.001	b.d.	b.d.
	Sum	4.006	4.010	4.010	4.008	4.011	4.010	4.010	4.004
	Mg #	0.897	0.902	0.899	0.901	0.896	0.899	0.906	0.902

Abbreviations: Opx = orthopyroxene, Pl-b hrz = plagioclase-bearing harzburgite, Melt r = melt related,
Cl core = clast core, Cl rim = clast rim, b.d. = below detection limit. Mg# calculated as (MgO/40.3) / (MgO/40.3 + FeO/71.85).

Major element composition of clinopyroxene from the Dramala spinel harzburgite and plagioclase-bearing harzburgite

Sample		PI2	PI2	PI2	PI2	PI2	PI2	PI2	PI2	PI2	PI2	PI2	PI2	PI2	PI2	PI2
Rock		Spl hrz	Spl hrz	Spl hrz	Spl hrz	Spl hrz	Spl hrz	Spl hrz	Spl hrz	Spl hrz	Spl hrz	Spl hrz	Spl hrz	Spl hrz	Spl hrz	Spl hrz
Mineral		Cpx	Cpx	Cpx	Cpx	Cpx	Cpx	Cpx	Cpx	Cpx	Cpx	Cpx	Cpx	Cpx	Cpx	Cpx
Type		Exs Opx	Exs Opx	Cl core	Cl core	Cl core	Cl core	Cl core	Cl core	Cl core	Cl core	Cl core	Cl core	Cl core	Cl core	Cl core
Wt.%	SiO2	52.85	52.43	53.81	54.33	54.44	54.19	53.62	54.23	54.14	54.38	52.86	53.74	53.68	53.18	53.55
	TiO2	0.04	0.04	0.04	0.05	0.03	0.03	0.06	0.05	0.04	0.04	0.05	0.07	0.06	0.05	0.05
	Cr2O3	0.80	1.22	0.60	0.52	0.60	0.61	0.69	0.75	0.71	0.55	0.88	0.90	0.93	0.96	0.91
	Al2O3	2.73	3.61	1.99	1.98	2.18	2.26	2.19	2.34	2.15	1.86	2.68	2.89	2.83	2.70	2.88
	FeO	1.75	2.06	2.11	1.80	1.81	1.79	2.15	1.73	1.66	1.59	2.11	1.89	1.86	1.70	1.84
	MnO	0.07	0.11	0.04	0.06	0.05	0.06	0.11	0.07	0.05	0.01	0.09	0.06	0.04	0.07	0.02
	NiO	0.04	0.08	b.d.	0.11	0.02	b.d.	0.06	0.02	b.d.	0.07	0.13	0.02	0.04	0.07	0.04
	MgO	16.91	16.75	17.93	17.62	17.53	17.54	18.08	17.41	17.48	17.60	17.87	17.29	17.38	17.16	17.15
	CaO	24.80	24.09	23.22	24.42	24.30	24.33	23.21	24.14	24.53	24.51	23.14	24.02	23.88	23.78	24.11
	Na2O	0.02	0.04	0.01	0.05	0.03	0.04	0.06	0.02	0.04	0.01	0.02	0.01	0.05	0.18	0.08
	K2O	b.d.	0.01	b.d.	b.d.	b.d.	b.d.	0.01	b.d.	b.d.	b.d.	b.d.	b.d.	0.01	0.08	0.01
	Total	100.01	100.44	99.75	100.94	100.99	100.85	100.24	100.76	100.80	100.62	99.83	100.89	100.76	99.93	100.64
Cations	Si	1.923	1.901	1.953	1.952	1.953	1.948	1.940	1.949	1.948	1.958	1.923	1.932	1.932	1.932	1.931
	Ti	0.001	0.001	0.001	0.001	0.001	0.001	0.002	0.001	0.001	0.001	0.001	0.002	0.002	0.001	0.001
	Cr	0.023	0.035	0.017	0.015	0.017	0.017	0.020	0.021	0.020	0.016	0.025	0.026	0.026	0.028	0.026
	Al	0.117	0.154	0.085	0.084	0.092	0.096	0.093	0.099	0.091	0.079	0.115	0.122	0.120	0.116	0.122
	Fe2+	0.053	0.062	0.064	0.054	0.054	0.054	0.065	0.052	0.050	0.048	0.064	0.057	0.056	0.052	0.055
	Mn	0.002	0.003	0.001	0.002	0.002	0.002	0.003	0.002	0.002	0.000	0.003	0.002	0.001	0.002	0.001
	Ni	0.001	0.002	b.d.	0.003	0.001	b.d.	0.002	0.001	b.d.	0.002	0.004	0.001	0.001	0.002	0.001
	Mg	0.917	0.905	0.970	0.944	0.937	0.940	0.975	0.933	0.937	0.944	0.969	0.926	0.932	0.929	0.922
	Ca	0.967	0.936	0.903	0.940	0.934	0.937	0.900	0.930	0.945	0.945	0.902	0.925	0.921	0.925	0.931
	Na	0.001	0.003	0.001	0.003	0.002	0.003	0.004	0.001	0.003	0.001	0.001	0.001	0.003	0.013	0.006
	K	b.d.	0.000	b.d.	b.d.	b.d.	b.d.	0.000	b.d.	b.d.	b.d.	b.d.	b.d.	0.000	0.004	0.000
	Sum	4.006	4.005	3.995	3.999	3.993	3.996	4.004	3.990	3.997	3.994	4.007	3.993	3.995	4.003	3.997
	Mg #	0.945	0.935	0.938	0.946	0.945	0.946	0.937	0.947	0.949	0.952	0.938	0.942	0.943	0.947	0.943

Abbreviations: Cpx = clinopyroxene, Spl hrz = spinel harzburgite, Exs Opx = exsolution lamellae in Opx, Cl core = clast core, b.d. = below detection limit.
Mg# calculated as (MgO/40.3) / (MgO/40.3 + FeO/71.85).

Major element composition of clinopyroxene from the Dramala spinel harzburgite and plagioclase-bearing harzburgite continued

Sample		PI2	PI2	PI2	PI2	PI2	PI2	PI2	PI2	PI2	PI2	PI2	PI2	PI2	PI2	PI2
Rock		Spl hrz	Spl hrz	Spl hrz	Spl hrz	Spl hrz	Spl hrz	Spl hrz	Spl hrz	Spl hrz	Spl hrz	Spl hrz	Spl hrz	Spl hrz	Spl hrz	Spl hrz
Mineral		Cpx	Cpx	Cpx	Cpx	Cpx	Cpx	Cpx	Cpx	Cpx	Cpx	Cpx	Cpx	Cpx	Cpx	Cpx
Type		Cl core	Cl core	Cl core	Cl core	Cl core	Cl core	Cl core	Cl core	Cl core	Cl core	Cl core	Cl core	Cl core	Cl core	Cl core
Wt.%	SiO2	53.73	53.43	53.56	53.70	53.78	53.55	53.31	53.63	53.78	52.95	54.04	54.58	54.07	53.97	54.24
	TiO2	0.03	0.06	0.07	0.05	0.05	0.04	0.03	0.05	0.03	0.09	0.03	0.05	0.04	0.03	0.03
	Cr2O3	0.98	1.01	0.95	1.00	0.87	0.90	0.74	0.91	0.92	0.82	0.83	0.39	0.52	0.55	0.51
	Al2O3	2.77	2.81	2.86	2.82	2.84	2.83	2.36	2.71	2.74	2.58	2.47	1.70	2.03	2.07	2.10
	FeO	1.89	1.78	1.83	1.80	1.88	1.91	1.91	2.09	2.05	2.40	1.86	2.01	2.03	2.06	2.17
	MnO	0.09	0.10	0.05	0.07	0.08	0.09	0.06	0.06	0.03	0.09	0.06	0.09	0.08	0.07	0.08
	NiO	b.d.	0.04	0.08	0.06	0.06	0.11	0.15	0.02	0.06	0.53	0.06	b.d.	0.01	0.06	0.04
	MgO	17.26	17.27	17.16	17.15	17.18	17.29	17.84	17.39	17.46	17.72	17.46	17.94	17.79	18.09	17.88
	CaO	24.10	24.04	24.07	24.20	24.11	24.01	23.77	23.81	23.74	22.90	24.04	24.19	23.88	23.03	23.83
	Na2O	0.03	0.06	0.04	0.04	0.02	0.05	0.04	0.04	0.05	0.04	0.04	0.02	0.01	0.03	0.06
	K2O	0.01	b.d.	b.d.	0.02	b.d.	b.d.	0.01	b.d.	b.d.	b.d.	0.02	b.d.	0.02	0.01	0.01
	Total	100.89	100.60	100.67	100.91	100.87	100.78	100.22	100.71	100.86	100.12	100.91	100.97	100.48	99.97	100.95
Cations	Si	1.933	1.928	1.931	1.932	1.934	1.929	1.932	1.933	1.934	1.925	1.942	1.959	1.951	1.953	1.949
	Ti	0.001	0.002	0.002	0.001	0.001	0.001	0.001	0.001	0.001	0.002	0.001	0.001	0.001	0.001	0.001
	Cr	0.028	0.029	0.027	0.028	0.025	0.026	0.021	0.026	0.026	0.024	0.024	0.011	0.015	0.016	0.014
	Al	0.117	0.120	0.122	0.120	0.120	0.120	0.101	0.115	0.116	0.111	0.105	0.072	0.086	0.088	0.089
	Fe2+	0.057	0.054	0.055	0.054	0.057	0.058	0.058	0.063	0.062	0.073	0.056	0.060	0.061	0.062	0.065
	Mn	0.003	0.003	0.002	0.002	0.002	0.003	0.002	0.002	0.001	0.003	0.002	0.003	0.002	0.002	0.002
	Ni	b.d.	0.001	0.002	0.002	0.002	0.003	0.004	0.001	0.002	0.015	0.002	b.d.	0.000	0.002	0.001
	Mg	0.925	0.929	0.922	0.919	0.921	0.928	0.963	0.934	0.936	0.960	0.935	0.960	0.957	0.976	0.957
	Ca	0.929	0.929	0.930	0.933	0.929	0.927	0.923	0.919	0.915	0.892	0.926	0.930	0.923	0.893	0.917
	Na	0.002	0.004	0.003	0.003	0.001	0.003	0.003	0.003	0.003	0.003	0.003	0.001	0.001	0.002	0.004
	K	0.000	b.d.	b.d.	0.001	b.d.	b.d.	0.000	b.d.	b.d.	b.d.	0.001	b.d.	0.001	0.000	0.000
	Sum	3.995	3.998	3.995	3.995	3.993	3.998	4.008	3.997	3.996	4.007	3.995	3.998	3.998	3.995	4.001
	Mg #	0.942	0.945	0.944	0.944	0.942	0.942	0.943	0.937	0.938	0.929	0.944	0.941	0.940	0.940	0.936

Abbreviations: Cpx = clinopyroxene, Spl hrz = spinel harzburgite, Cl core = clast core, b.d. = below detection limit.
Mg# calculated as (MgO/40.3) / (MgO/40.3 + FeO/71.85).

Major element composition of clinopyroxene from the Dramala spinel harzburgite and plagioclase-bearing harzburgite continued

Sample		PI2	PI2	PI2	PI2	PI2	PI2	PI2	PI2	PI2	PI2	PI2	PI2	PI2	PI2	PI2
Rock		Spl hrz	Spl hrz	Spl hrz	Spl hrz	Spl hrz	Spl hrz	Spl hrz	Spl hrz	Spl hrz	Spl hrz	Spl hrz	Spl hrz	Spl hrz	Spl hrz	Spl hrz
Mineral		Cpx	Cpx	Cpx	Cpx	Cpx	Cpx	Cpx	Cpx	Cpx	Cpx	Cpx	Cpx	Cpx	Cpx	Cpx
Type		Cl core	Cl core	Cl core	Cl core	Cl core	Cl core	Cl core	Cl core	Cl core	Cl core	Cl core	Cl core	Cl core	Cl core	Cl core
Wt.%	SiO2	54.28	54.54	54.63	54.47	55.10	53.46	53.71	53.56	54.06	53.05	52.44	52.83	53.08	54.03	53.70
	TiO2	0.02	0.07	0.03	b.d.	0.02	0.03	0.06	0.02	0.03	0.07	0.05	0.05	0.06	0.05	0.04
	Cr2O3	0.49	0.42	0.33	0.25	0.23	0.50	0.66	0.52	0.53	0.64	0.84	0.67	0.64	0.38	0.51
	Al2O3	2.00	1.69	1.54	1.43	1.15	1.90	1.70	1.52	1.12	2.01	2.74	2.54	2.56	1.42	1.99
	FeO	2.15	2.06	2.00	2.07	1.86	1.86	1.69	1.75	1.66	1.66	1.70	1.74	1.79	1.58	1.87
	MnO	0.06	0.08	0.11	0.06	0.04	0.07	0.06	0.04	0.07	0.07	0.05	0.03	0.08	0.02	0.07
	NiO	0.12	0.04	0.08	0.03	0.08	0.03	b.d.	0.05	0.11	b.d.	0.05	0.03	0.04	0.05	0.11
	MgO	17.83	17.86	18.12	18.66	18.23	17.56	17.57	17.70	18.00	17.30	17.08	16.93	17.17	17.87	18.14
	CaO	23.66	23.76	23.98	23.39	24.14	23.83	23.82	24.04	24.09	24.17	24.09	24.32	24.14	24.33	23.68
	Na2O	0.02	0.02	0.03	0.04	0.03	0.04	0.04	0.03	0.03	0.05	0.01	0.03	0.06	0.04	0.02
	K2O	0.01	b.d.	0.02	b.d.	b.d.	0.01	b.d.	0.01	0.01	b.d.	b.d.	0.01	b.d.	0.01	b.d.
	Total	100.64	100.54	100.87	100.40	100.88	99.29	99.31	99.24	99.71	99.02	99.05	99.18	99.62	99.78	100.13
Cations	Si	1.955	1.964	1.963	1.963	1.977	1.952	1.959	1.958	1.966	1.944	1.924	1.935	1.934	1.962	1.944
	Ti	0.001	0.002	0.001	b.d.	0.001	0.001	0.002	0.001	0.001	0.002	0.001	0.001	0.002	0.001	0.001
	Cr	0.014	0.012	0.009	0.007	0.007	0.014	0.019	0.015	0.015	0.019	0.024	0.019	0.018	0.011	0.015
	Al	0.085	0.072	0.065	0.061	0.049	0.082	0.073	0.065	0.048	0.087	0.118	0.110	0.110	0.061	0.085
	Fe2+	0.065	0.062	0.060	0.062	0.056	0.057	0.052	0.053	0.050	0.051	0.052	0.053	0.055	0.048	0.057
	Mn	0.002	0.002	0.003	0.002	0.001	0.002	0.002	0.001	0.002	0.002	0.002	0.001	0.002	0.001	0.002
	Ni	0.003	0.001	0.002	0.001	0.002	0.001	b.d.	0.001	0.003	b.d.	0.001	0.001	0.001	0.001	0.003
	Mg	0.957	0.959	0.970	1.002	0.975	0.956	0.955	0.964	0.976	0.945	0.934	0.924	0.933	0.967	0.979
	Ca	0.913	0.917	0.923	0.903	0.928	0.932	0.931	0.941	0.939	0.949	0.947	0.954	0.942	0.947	0.919
	Na	0.001	0.001	0.002	0.003	0.002	0.003	0.003	0.002	0.002	0.004	0.001	0.002	0.004	0.003	0.001
	K	0.000	b.d.	0.001	b.d.	b.d.	0.000	b.d.	0.000	0.000	b.d.	b.d.	0.000	b.d.	0.000	b.d.
	Sum	3.996	3.993	4.001	4.004	3.996	4.000	3.995	4.003	4.003	4.003	4.004	4.001	4.002	4.002	4.006
	Mg #	0.937	0.939	0.942	0.941	0.946	0.944	0.949	0.947	0.951	0.949	0.947	0.945	0.945	0.953	0.945

Abbreviations: Cpx = clinopyroxene, Spl hrz = spinel harzburgite, Cl core = clast core, b.d. = below detection limit.
Mg# calculated as (MgO/40.3) / (MgO/40.3 + FeO/71.85).

Major element composition of clinopyroxene from the Dramala spinel harzburgite and plagioclase-bearing harzburgite continued

Sample		PI2	PI2	PI2	PI2	PI2	PI2	PI2	PI2	PI2	PI2	PI2	PI2	PI2	PI2	PI2
Rock		Spl hrz	Spl hrz	Spl hrz	Spl hrz	Spl hrz	Spl hrz	Spl hrz	Spl hrz	Spl hrz	Spl hrz	Spl hrz	Spl hrz	Spl hrz	Spl hrz	Spl hrz
Mineral		Cpx	Cpx	Cpx	Cpx	Cpx	Cpx	Cpx	Cpx	Cpx	Cpx	Cpx	Cpx	Cpx	Cpx	Cpx
Type		Cl core	Cl core	Cl core	Cl core	Cl core	Cl core	Cl core	Cl core	Cl core	Cl core	Cl core	Cl core	Cl core	Cl core	Cl core
Wt.%	SiO2	53.60	53.66	53.62	53.56	53.36	53.44	53.28	53.35	53.52	53.58	53.94	53.54	53.35	53.42	53.48
	TiO2	0.03	0.08	0.04	0.07	0.05	0.03	0.03	0.05	0.05	0.02	0.03	0.05	0.04	0.02	b.d.
	Cr2O3	0.52	0.55	0.59	0.68	0.60	0.70	0.73	0.70	0.66	0.57	0.56	0.57	1.03	1.02	0.89
	Al2O3	2.17	2.21	2.25	2.29	2.42	2.41	2.40	2.48	2.26	2.18	2.08	1.89	2.44	2.73	2.77
	FeO	1.86	1.90	2.17	1.95	2.04	2.02	1.98	1.90	1.87	1.74	2.00	1.97	2.16	2.20	2.18
	MnO	0.07	0.07	0.05	0.05	0.08	0.08	0.01	0.09	0.09	0.07	0.09	0.09	0.07	0.12	0.05
	NiO	0.07	0.04	0.05	0.02	0.05	0.02	0.07	b.d.	b.d.	0.03	0.03	0.04	0.01	0.06	0.01
	MgO	17.69	17.81	17.75	17.81	17.63	17.63	17.51	17.53	17.77	17.59	17.74	18.14	17.63	17.66	17.73
	CaO	23.82	23.83	23.52	23.62	23.54	23.80	23.76	23.84	23.98	24.05	23.97	23.69	23.87	23.51	23.38
	Na2O	0.04	0.03	0.03	0.05	0.03	0.04	0.05	0.05	0.04	0.03	0.03	0.06	0.01	0.02	0.06
	K2O	b.d.	0.01	0.01	b.d.	b.d.	b.d.	0.01	b.d.	b.d.	0.01	b.d.	b.d.	b.d.	0.01	b.d.
	Total	99.87	100.19	100.08	100.10	99.80	100.17	99.83	99.99	100.24	99.87	100.47	100.04	100.61	100.77	100.55
Cations	Si	1.946	1.942	1.943	1.940	1.939	1.936	1.937	1.936	1.937	1.945	1.947	1.942	1.928	1.926	1.929
	Ti	0.001	0.002	0.001	0.002	0.001	0.001	0.001	0.001	0.001	0.001	0.001	0.001	0.001	0.001	b.d.
	Cr	0.015	0.016	0.017	0.019	0.017	0.020	0.021	0.020	0.019	0.016	0.016	0.016	0.029	0.029	0.025
	Al	0.093	0.094	0.096	0.098	0.104	0.103	0.103	0.106	0.096	0.093	0.089	0.081	0.104	0.116	0.118
	Fe2+	0.056	0.057	0.066	0.059	0.062	0.061	0.060	0.058	0.057	0.053	0.060	0.060	0.065	0.066	0.066
	Mn	0.002	0.002	0.002	0.002	0.002	0.002	0.000	0.003	0.003	0.002	0.003	0.003	0.002	0.004	0.002
	Ni	0.002	0.001	0.001	0.001	0.001	0.001	0.002	b.d.	b.d.	0.001	0.001	0.001	0.000	0.002	0.000
	Mg	0.957	0.961	0.959	0.961	0.955	0.952	0.949	0.948	0.959	0.952	0.955	0.981	0.950	0.949	0.953
	Ca	0.926	0.924	0.913	0.916	0.916	0.924	0.925	0.927	0.930	0.935	0.927	0.921	0.924	0.908	0.904
	Na	0.003	0.002	0.002	0.004	0.002	0.003	0.004	0.004	0.003	0.002	0.002	0.004	0.001	0.001	0.004
	K	b.d.	0.000	0.000	b.d.	b.d.	b.d.	0.000	b.d.	b.d.	0.000	b.d.	b.d.	b.d.	0.000	b.d.
	Sum	4.001	4.002	4.001	4.001	4.000	4.003	4.002	4.002	4.005	4.001	4.001	4.010	4.005	4.002	4.001
	Mg #	0.944	0.944	0.936	0.942	0.939	0.940	0.940	0.943	0.944	0.947	0.941	0.943	0.936	0.935	0.935

Abbreviations: Cpx = clinopyroxene, Spl hrz = spinel harzburgite, Cl core = clast core, b.d. = below detection limit.
Mg# calculated as (MgO/40.3) / (MgO/40.3 + FeO/71.85).

Major element composition of clinopyroxene from the Dramala spinel harzburgite and plagioclase-bearing harzburgite continued

Sample		PI2	PI2	PI2	PI2	PI2	PI2	PI2	PI2	PI2	PI2	PI2	PI2	PI2	PI2	PI2
Rock		Spl hrz	Spl hrz	Spl hrz	Spl hrz	Spl hrz	Spl hrz	Spl hrz	Spl hrz	Spl hrz	Spl hrz	Spl hrz	Spl hrz	Spl hrz	Spl hrz	Spl hrz
Mineral		Cpx	Cpx	Cpx	Cpx	Cpx	Cpx	Cpx	Cpx	Cpx	Cpx	Cpx	Cpx	Cpx	Cpx	Cpx
Type		Cl core	Cl core	Cl core	Cl core	Cl core	Cl core	Cl core	Cl core	Cl core	Cl core	Cl core	Cl core	Cl core	Cl core	Cl core
Wt.%	SiO2	53.50	53.56	53.33	52.72	53.44	53.46	53.10	53.72	53.25	53.49	53.31	53.46	53.47	53.33	53.29
	TiO2	0.04	b.d.	0.02	0.03	0.03	0.04	0.06	0.08	0.07	0.04	0.06	0.05	0.07	0.05	0.06
	Cr2O3	1.04	0.97	0.90	0.96	0.93	1.04	0.80	0.90	0.82	0.91	0.95	0.93	0.95	0.93	0.84
	Al2O3	2.77	2.81	2.79	2.74	2.70	2.62	2.71	2.71	2.71	2.80	2.82	2.75	2.79	2.83	2.91
	FeO	2.14	2.13	2.18	2.35	2.06	2.08	1.78	2.02	1.89	1.89	1.86	1.86	1.93	1.99	1.95
	MnO	0.05	0.07	0.08	0.05	0.11	0.03	0.07	0.10	0.08	0.09	0.07	0.09	0.06	0.07	0.06
	NiO	0.08	0.04	0.10	0.01	0.02	0.07	0.02	0.04	0.10	0.03	0.05	0.03	0.04	0.11	0.06
	MgO	17.69	17.68	17.62	18.25	17.60	17.64	17.39	17.40	17.43	17.21	17.56	17.35	17.38	17.50	17.39
	CaO	23.16	23.41	23.27	22.18	23.28	23.46	23.90	23.67	23.65	23.84	23.83	23.72	23.79	23.57	23.56
	Na2O	0.05	0.01	0.01	0.04	0.03	0.03	0.02	0.05	0.03	0.02	0.03	0.03	0.05	0.07	0.04
	K2O	b.d.	b.d.	0.02	0.01	b.d.	0.01	b.d.	b.d.	0.01	b.d.	b.d.	b.d.	0.01	0.02	0.01
	Total	100.52	100.68	100.32	99.34	100.20	100.48	99.85	100.69	100.04	100.32	100.54	100.27	100.54	100.47	100.17
Cations	Si	1.930	1.929	1.929	1.923	1.933	1.931	1.929	1.935	1.931	1.934	1.924	1.933	1.930	1.927	1.929
	Ti	0.001	b.d.	0.001	0.001	0.001	0.001	0.002	0.002	0.002	0.001	0.002	0.001	0.002	0.001	0.002
	Cr	0.030	0.028	0.026	0.028	0.027	0.030	0.023	0.026	0.024	0.026	0.027	0.027	0.027	0.027	0.024
	Al	0.118	0.119	0.119	0.118	0.115	0.112	0.116	0.115	0.116	0.119	0.120	0.117	0.119	0.121	0.124
	Fe2+	0.065	0.064	0.066	0.072	0.062	0.063	0.054	0.061	0.057	0.057	0.056	0.056	0.058	0.060	0.059
	Mn	0.002	0.002	0.002	0.002	0.003	0.001	0.002	0.003	0.002	0.003	0.002	0.003	0.002	0.002	0.002
	Ni	0.002	0.001	0.003	0.000	0.001	0.002	0.001	0.001	0.003	0.001	0.001	0.001	0.001	0.003	0.002
	Mg	0.951	0.949	0.950	0.992	0.949	0.950	0.942	0.934	0.942	0.927	0.945	0.935	0.935	0.942	0.938
	Ca	0.895	0.903	0.902	0.867	0.902	0.908	0.930	0.913	0.919	0.923	0.922	0.919	0.920	0.912	0.914
	Na	0.003	0.001	0.001	0.003	0.002	0.002	0.001	0.003	0.002	0.001	0.002	0.002	0.003	0.005	0.003
	K	b.d.	b.d.	0.001	0.000	b.d.	0.000	b.d.	b.d.	0.000	b.d.	b.d.	b.d.	0.000	0.001	0.000
	Sum	3.997	3.997	3.999	4.005	3.996	3.999	4.000	3.994	3.999	3.993	4.001	3.995	3.997	4.001	3.997
	Mg #	0.936	0.937	0.935	0.933	0.938	0.938	0.946	0.939	0.943	0.942	0.944	0.943	0.941	0.940	0.941

Abbreviations: Cpx = clinopyroxene, Spl hrz = spinel harzburgite, Cl core = clast core, b.d. = below detection limit.
Mg# calculated as (MgO/40.3) / (MgO/40.3 + FeO/71.85).

Major element composition of clinopyroxene from the Dramala spinel harzburgite and plagioclase-bearing harzburgite continued

Sample		PI2	PI2	PI2	PI2	PI2	PI2	PI2	PI2	PI2	PI2	PI2	PI2	PI2	PI2	PI2
Rock		Spl hrz	Spl hrz	Spl hrz	Spl hrz	Spl hrz	Spl hrz	Spl hrz	Spl hrz	Spl hrz	Spl hrz	Spl hrz	Spl hrz	Spl hrz	Spl hrz	Spl hrz
Mineral		Cpx	Cpx	Cpx	Cpx	Cpx	Cpx	Cpx	Cpx	Cpx	Cpx	Cpx	Cpx	Cpx	Cpx	Cpx
Type		Cl core	Cl core	Cl core	Cl core	Cl core	Cl core	Cl core	Cl core	Cl core	Cl core	Cl core	Cl core	Cl core	Cl core	Cl core
Wt.%	SiO2	52.93	52.98	53.18	53.28	53.42	53.03	53.09	53.35	53.34	53.43	53.20	53.37	53.29	53.36	53.29
	TiO2	0.05	0.07	0.03	0.04	0.07	b.d.	0.04	0.03	0.01	0.02	0.01	0.05	0.06	0.03	0.02
	Cr2O3	0.90	0.96	0.91	1.11	1.00	0.99	1.05	0.92	1.00	0.98	0.90	0.88	0.82	0.90	0.87
	Al2O3	3.03	3.03	3.11	3.09	3.04	3.13	3.04	3.09	3.01	3.06	3.00	2.96	3.05	3.09	2.98
	FeO	2.13	2.02	1.96	2.03	2.09	2.04	2.03	2.39	2.06	2.22	2.18	2.19	2.05	2.03	2.05
	MnO	0.04	0.12	0.08	0.05	0.10	0.08	0.09	0.07	0.10	0.06	0.14	0.06	0.08	0.05	0.09
	NiO	0.05	0.06	b.d.	b.d.	0.05	0.04	0.05	0.07	0.03	0.07	b.d.	0.05	0.03	0.02	b.d.
	MgO	17.51	17.26	17.53	17.44	17.34	17.54	17.23	18.20	17.32	18.27	17.83	17.84	17.28	17.35	17.49
	CaO	23.02	23.62	23.52	23.12	23.29	23.03	23.56	22.35	23.55	22.19	22.87	22.79	23.59	23.27	23.74
	Na2O	0.04	0.06	0.04	0.05	0.05	0.05	0.03	0.03	0.05	0.05	0.04	0.04	0.02	0.02	0.03
	K2O	0.01	b.d.	0.01	0.01	b.d.	b.d.	0.01	b.d.	b.d.	b.d.	b.d.	b.d.	0.01	b.d.	b.d.
	Total	99.71	100.18	100.37	100.22	100.45	99.93	100.22	100.50	100.47	100.35	100.17	100.23	100.28	100.12	100.56
Cations	Si	1.924	1.921	1.921	1.926	1.928	1.923	1.923	1.922	1.926	1.926	1.925	1.928	1.927	1.930	1.923
	Ti	0.001	0.002	0.001	0.001	0.002	b.d.	0.001	0.001	0.000	0.001	0.000	0.001	0.002	0.001	0.001
	Cr	0.026	0.028	0.026	0.032	0.029	0.028	0.030	0.026	0.029	0.028	0.026	0.025	0.023	0.026	0.025
	Al	0.130	0.129	0.132	0.132	0.129	0.134	0.130	0.131	0.128	0.130	0.128	0.126	0.130	0.132	0.127
	Fe2+	0.065	0.061	0.059	0.061	0.063	0.062	0.061	0.072	0.062	0.067	0.066	0.066	0.062	0.061	0.062
	Mn	0.001	0.004	0.002	0.002	0.003	0.002	0.003	0.002	0.003	0.002	0.004	0.002	0.002	0.002	0.003
	Ni	0.001	0.002	b.d.	b.d.	0.001	0.001	0.001	0.002	0.001	0.002	b.d.	0.001	0.001	0.001	b.d.
	Mg	0.949	0.933	0.944	0.940	0.933	0.948	0.930	0.977	0.932	0.981	0.961	0.961	0.931	0.935	0.941
	Ca	0.897	0.917	0.910	0.895	0.901	0.895	0.914	0.863	0.911	0.857	0.886	0.882	0.914	0.902	0.918
	Na	0.003	0.004	0.003	0.004	0.003	0.004	0.002	0.002	0.004	0.003	0.003	0.003	0.001	0.001	0.002
	K	0.000	b.d.	0.000	0.000	b.d.	b.d.	0.000	b.d.	b.d.	b.d.	b.d.	b.d.	0.000	b.d.	b.d.
	Sum	3.998	4.001	4.000	3.993	3.993	3.997	3.997	3.999	3.997	3.997	4.000	3.996	3.995	3.991	4.001
	Mg #	0.936	0.938	0.941	0.939	0.937	0.939	0.938	0.931	0.937	0.936	0.936	0.936	0.938	0.938	0.938

Abbreviations: Cpx = clinopyroxene, Spl hrz = spinel harzburgite, Cl core = clast core, b.d. = below detection limit.
Mg# calculated as (MgO/40.3) / (MgO/40.3 + FeO/71.85).

Major element composition of clinopyroxene from the Dramala spinel harzburgite and plagioclase-bearing harzburgite continued

Sample		PI2	PI2	PI2	PI2	PI2	PI2	PI2	PI2	PI2	PI2	PI2	PI2	PI2	PI2	PI2
Rock		Spl hrz	Spl hrz	Spl hrz	Spl hrz	Spl hrz	Spl hrz	Spl hrz	Spl hrz	Spl hrz	Spl hrz	Spl hrz	Spl hrz	Spl hrz	Spl hrz	Spl hrz
Mineral		Cpx	Cpx	Cpx	Cpx	Cpx	Cpx	Cpx	Cpx	Cpx	Cpx	Cpx	Cpx	Cpx	Cpx	Cpx
Type		Cl core	Cl core	Cl core	Cl core	Cl core	Cl core	Cl core	Cl core	Cl core	Cl core	Cl core	Cl core	Cl core	Cl core	Cl core
Wt.%	SiO2	53.31	53.30	53.47	53.57	53.41	53.55	53.64	53.21	53.52	53.38	53.29	53.44	53.72	53.63	53.80
	TiO2	0.02	0.02	0.03	0.05	0.03	0.07	0.07	0.04	0.02	0.02	0.05	b.d.	0.05	0.01	0.04
	Cr2O3	0.89	0.71	0.86	0.74	0.77	0.76	0.74	0.63	0.80	0.73	0.83	0.74	0.81	0.63	0.74
	Al2O3	2.89	2.83	2.76	2.83	2.74	2.75	2.79	2.58	2.74	2.77	2.91	2.87	2.73	2.52	2.43
	FeO	2.05	2.01	2.06	2.16	2.10	2.11	2.14	2.13	2.04	2.00	1.94	1.96	2.09	1.98	2.02
	MnO	0.08	0.07	0.09	0.06	0.07	0.10	0.08	0.08	0.08	0.09	0.06	0.06	0.07	0.04	0.11
	NiO	b.d.	0.06	0.05	0.08	0.06	0.09	0.02	0.07	0.03	0.01	0.07	0.07	0.04	0.02	0.05
	MgO	17.34	17.65	17.63	17.83	17.43	17.35	18.07	18.01	17.55	17.57	17.28	17.65	17.59	17.76	17.77
	CaO	23.65	23.17	23.32	23.10	23.45	23.71	23.12	22.46	23.60	23.66	23.71	23.37	23.61	23.26	23.72
	Na2O	0.01	0.03	0.05	0.05	0.03	0.03	0.04	0.04	0.03	0.03	0.06	0.05	0.03	0.05	0.04
	K2O	0.01	b.d.	b.d.	0.01	b.d.	b.d.	0.01	b.d.	0.01	b.d.	0.01	0.01	0.02	0.01	0.01
	Total	100.25	99.85	100.32	100.48	100.09	100.52	100.72	99.25	100.42	100.26	100.21	100.22	100.76	99.91	100.73
Cations	Si	1.929	1.933	1.932	1.932	1.935	1.933	1.929	1.939	1.933	1.931	1.929	1.932	1.934	1.943	1.938
	Ti	0.001	0.001	0.001	0.001	0.001	0.002	0.002	0.001	0.001	0.001	0.001	b.d.	0.001	0.000	0.001
	Cr	0.025	0.020	0.025	0.021	0.022	0.022	0.021	0.018	0.023	0.021	0.024	0.021	0.023	0.018	0.021
	Al	0.123	0.121	0.118	0.120	0.117	0.117	0.118	0.111	0.117	0.118	0.124	0.122	0.116	0.108	0.103
	Fe2+	0.062	0.061	0.062	0.065	0.064	0.064	0.064	0.065	0.062	0.060	0.059	0.059	0.063	0.060	0.061
	Mn	0.002	0.002	0.003	0.002	0.002	0.003	0.002	0.002	0.002	0.003	0.002	0.002	0.002	0.001	0.003
	Ni	b.d.	0.002	0.001	0.002	0.002	0.003	0.001	0.002	0.001	0.000	0.002	0.002	0.001	0.001	0.001
	Mg	0.935	0.954	0.950	0.958	0.941	0.934	0.969	0.978	0.945	0.947	0.932	0.951	0.944	0.959	0.954
	Ca	0.917	0.900	0.903	0.892	0.910	0.917	0.891	0.877	0.913	0.917	0.920	0.905	0.910	0.903	0.915
	Na	0.001	0.002	0.004	0.003	0.002	0.002	0.003	0.003	0.002	0.002	0.004	0.004	0.002	0.004	0.003
	K	0.000	b.d.	b.d.	0.000	b.d.	b.d.	0.000	b.d.	0.000	b.d.	0.000	0.000	0.001	0.000	0.000
	Sum	3.996	3.997	3.998	3.998	3.996	3.996	4.001	3.997	3.998	4.000	3.998	3.998	3.997	3.996	4.001
	Mg #	0.938	0.940	0.938	0.936	0.937	0.936	0.938	0.938	0.939	0.940	0.941	0.941	0.938	0.941	0.940

Abbreviations: Cpx = clinopyroxene, Spl hrz = spinel harzburgite, Cl core = clast core, b.d. = below detection limit.
Mg# calculated as (MgO/40.3) / (MgO/40.3 + FeO/71.85).

Major element composition of clinopyroxene from the Dramala spinel harzburgite and plagioclase-bearing harzburgite continued

Sample		PI2	PI2	PI2	PI2	PI2	PI2	PI2	PI2	PI2	PI2	PI2	PI2	PI2	PI2	PI2
Rock		Spl hrz	Spl hrz	Spl hrz	Spl hrz	Spl hrz	Spl hrz	Spl hrz	Spl hrz	Spl hrz	Spl hrz	Spl hrz	Spl hrz	Spl hrz	Spl hrz	Spl hrz
Mineral		Cpx	Cpx	Cpx	Cpx	Cpx	Cpx	Cpx	Cpx	Cpx	Cpx	Cpx	Cpx	Cpx	Cpx	Cpx
Type		Cl core	Cl core	Cl core	Cl core	Cl core	Cl core	Cl core	Cl core	Cl core	Cl core	Cl core	Cl core	Cl core	Cl core	Cl core
Wt.%	SiO2	53.91	53.56	53.60	53.45	53.27	53.49	53.40	53.43	53.32	53.27	53.37	53.39	53.34	53.28	53.22
	TiO2	0.08	0.04	0.05	0.04	0.01	0.07	0.01	0.08	0.05	0.06	0.05	0.01	0.03	0.05	0.02
	Cr2O3	0.62	0.81	0.82	0.79	0.78	0.81	0.81	0.78	0.85	0.81	0.79	0.82	0.83	0.84	0.85
	Al2O3	2.45	2.82	2.81	2.87	2.85	2.87	2.97	2.83	2.75	2.82	2.76	2.78	2.73	2.88	2.84
	FeO	1.93	1.96	1.93	1.93	1.92	2.02	1.99	1.94	1.99	1.86	1.83	1.85	1.83	1.80	1.79
	MnO	0.04	0.07	0.14	0.14	0.09	0.11	0.08	0.07	0.06	0.03	0.13	0.06	0.04	0.07	0.02
	NiO	0.02	0.06	0.13	0.07	b.d.	0.04	0.07	0.02	0.09	0.02	0.01	0.06	b.d.	0.04	0.04
	MgO	17.54	17.39	17.69	17.30	17.21	17.38	17.33	17.28	17.23	17.33	17.35	17.32	17.25	17.14	17.06
	CaO	23.47	23.88	23.35	24.00	24.03	23.91	24.05	23.86	23.99	23.93	24.03	24.10	23.91	24.19	24.07
	Na2O	0.05	0.02	0.02	0.04	0.01	0.03	0.04	0.05	0.06	0.06	0.03	0.04	0.07	0.04	0.06
	K2O	0.01	b.d.	b.d.	0.01	b.d.	b.d.	b.d.	b.d.	b.d.	b.d.	0.01	0.01	b.d.	b.d.	0.01
	Total	100.12	100.61	100.54	100.64	100.17	100.73	100.75	100.34	100.39	100.19	100.36	100.44	100.03	100.33	99.98
Cations	Si	1.948	1.931	1.932	1.928	1.930	1.928	1.925	1.932	1.929	1.929	1.930	1.930	1.934	1.928	1.931
	Ti	0.002	0.001	0.001	0.001	0.000	0.002	0.000	0.002	0.001	0.002	0.001	0.000	0.001	0.001	0.001
	Cr	0.018	0.023	0.023	0.023	0.022	0.023	0.023	0.022	0.024	0.023	0.023	0.023	0.024	0.024	0.024
	Al	0.104	0.120	0.119	0.122	0.122	0.122	0.126	0.121	0.117	0.120	0.118	0.118	0.117	0.123	0.121
	Fe2+	0.058	0.059	0.058	0.058	0.058	0.061	0.060	0.059	0.060	0.056	0.055	0.056	0.055	0.054	0.054
	Mn	0.001	0.002	0.004	0.004	0.003	0.003	0.002	0.002	0.002	0.001	0.004	0.002	0.001	0.002	0.001
	Ni	0.001	0.002	0.004	0.002	b.d.	0.001	0.002	0.001	0.003	0.001	0.000	0.002	b.d.	0.001	0.001
	Mg	0.945	0.935	0.950	0.930	0.929	0.934	0.931	0.931	0.929	0.935	0.935	0.933	0.932	0.924	0.923
	Ca	0.909	0.923	0.902	0.928	0.933	0.923	0.929	0.924	0.930	0.928	0.931	0.933	0.929	0.938	0.936
	Na	0.004	0.001	0.001	0.003	0.001	0.002	0.003	0.004	0.004	0.004	0.002	0.003	0.005	0.003	0.004
	K	0.000	b.d.	b.d.	0.000	b.d.	b.d.	b.d.	b.d.	b.d.	b.d.	0.000	0.000	b.d.	b.d.	0.000
	Sum	3.990	3.997	3.996	4.000	3.998	3.999	4.002	3.997	4.001	4.000	4.000	4.001	3.998	3.999	3.997
	Mg #	0.942	0.941	0.942	0.941	0.941	0.939	0.939	0.941	0.939	0.943	0.944	0.943	0.944	0.944	0.944

Abbreviations: Cpx = clinopyroxene, Spl hrz = spinel harzburgite, Cl core = clast core, b.d. = below detection limit.
Mg# calculated as (MgO/40.3) / (MgO/40.3 + FeO/71.85).

Major element composition of clinopyroxene from the Dramala spinel harzburgite and plagioclase-bearing harzburgite continued

Sample		PI2	PI2	PI2	PI2	PI2	PI2	PI2	PI2	PI2	PI2	PI2	PI2	PI2	PI2	PI2
Rock		Spl hrz	Spl hrz	Spl hrz	Spl hrz	Spl hrz	Spl hrz	Spl hrz	Spl hrz	Spl hrz	Spl hrz	Spl hrz	Spl hrz	Spl hrz	Spl hrz	Spl hrz
Mineral		Cpx	Cpx	Cpx	Cpx	Cpx	Cpx	Cpx	Cpx	Cpx	Cpx	Cpx	Cpx	Cpx	Cpx	Cpx
Type		Cl core	Cl core	Cl core	Cl core	Cl core	Cl core	Cl core	Cl core	Cl core	Cl core	Cl core	Cl core	Cl core	Cl core	Cl core
Wt.%	SiO2	53.10	53.39	52.99	53.29	53.48	53.32	53.34	53.35	53.20	53.25	53.28	53.07	52.97	53.04	52.94
	TiO2	0.07	0.08	0.07	0.02	0.05	0.05	0.05	0.05	0.04	0.05	0.04	0.03	0.05	0.02	0.06
	Cr2O3	0.94	0.90	0.78	0.99	0.90	0.85	0.97	0.90	0.95	0.95	0.97	1.01	0.95	0.94	1.02
	Al2O3	2.88	2.90	2.73	2.93	2.91	2.96	2.94	3.08	3.08	3.06	2.79	3.20	3.10	3.21	3.09
	FeO	1.81	1.84	1.92	1.72	1.79	1.90	1.92	1.84	1.91	1.84	1.76	1.94	1.87	1.80	1.88
	MnO	0.10	0.08	0.04	0.04	0.04	0.07	0.11	0.10	0.12	0.10	0.10	0.11	0.05	0.03	0.12
	NiO	0.07	0.09	0.02	0.05	b.d.	0.02	0.01	0.05	0.04	0.04	0.02	0.03	0.04	b.d.	b.d.
	MgO	17.18	17.29	17.91	17.25	17.28	17.38	17.05	17.03	17.05	17.26	17.19	16.87	17.03	17.06	17.21
	CaO	23.72	24.25	23.22	23.99	23.98	23.92	23.75	24.08	23.91	23.87	23.84	24.08	24.07	24.18	24.13
	Na2O	0.02	0.03	0.02	0.05	0.06	0.03	0.09	0.02	0.07	0.07	0.04	0.05	0.06	0.04	b.d.
	K2O	b.d.	b.d.	b.d.	b.d.	b.d.	b.d.	b.d.	0.01	b.d.	0.01	0.01	b.d.	b.d.	b.d.	b.d.
	Total	99.89	100.85	99.70	100.33	100.49	100.50	100.23	100.51	100.37	100.50	100.04	100.39	100.19	100.32	100.45
Cations	Si	1.929	1.923	1.926	1.927	1.930	1.925	1.931	1.926	1.925	1.923	1.932	1.921	1.920	1.919	1.916
	Ti	0.002	0.002	0.002	0.001	0.001	0.001	0.001	0.001	0.001	0.001	0.001	0.001	0.001	0.001	0.002
	Cr	0.027	0.026	0.022	0.028	0.026	0.024	0.028	0.026	0.027	0.027	0.028	0.029	0.027	0.027	0.029
	Al	0.123	0.123	0.117	0.125	0.124	0.126	0.125	0.131	0.131	0.130	0.119	0.137	0.132	0.137	0.132
	Fe2+	0.055	0.055	0.058	0.052	0.054	0.057	0.058	0.056	0.058	0.056	0.053	0.059	0.057	0.054	0.057
	Mn	0.003	0.002	0.001	0.001	0.001	0.002	0.003	0.003	0.004	0.003	0.003	0.003	0.002	0.001	0.004
	Ni	0.002	0.003	0.001	0.001	b.d.	0.001	0.000	0.001	0.001	0.001	0.001	0.001	0.001	b.d.	b.d.
	Mg	0.930	0.928	0.970	0.930	0.929	0.935	0.920	0.917	0.919	0.929	0.929	0.910	0.920	0.920	0.928
	Ca	0.923	0.936	0.904	0.929	0.927	0.925	0.921	0.932	0.927	0.924	0.926	0.934	0.935	0.937	0.935
	Na	0.001	0.002	0.001	0.004	0.004	0.002	0.006	0.001	0.005	0.005	0.003	0.004	0.004	0.003	b.d.
	K	b.d.	b.d.	b.d.	b.d.	b.d.	b.d.	b.d.	0.000	b.d.	0.000	0.000	b.d.	b.d.	b.d.	b.d.
	Sum	3.995	4.001	4.003	3.998	3.996	3.999	3.994	3.995	3.998	4.000	3.995	3.997	4.000	4.000	4.002
	Mg #	0.944	0.944	0.943	0.947	0.945	0.942	0.941	0.943	0.941	0.944	0.946	0.939	0.942	0.944	0.942

Abbreviations: Cpx = clinopyroxene, Spl hrz = spinel harzburgite, Cl core = clast core, b.d. = below detection limit.
Mg# calculated as (MgO/40.3) / (MgO/40.3 + FeO/71.85).

Major element composition of clinopyroxene from the Dramala spinel harzburgite and plagioclase-bearing harzburgite continued

Sample		PI2	PI2	PI2	PI2	PI2	PI2	PI2	PI2	PI2	PI2	PI2	PI2	PI2	PI2	PI2
Rock		Spl hrz	Spl hrz	Spl hrz	Spl hrz	Spl hrz	Spl hrz	Spl hrz	Spl hrz	Spl hrz	Spl hrz	Spl hrz	Spl hrz	Spl hrz	Spl hrz	Spl hrz
Mineral		Cpx	Cpx	Cpx	Cpx	Cpx	Cpx	Cpx	Cpx	Cpx	Cpx	Cpx	Cpx	Cpx	Cpx	Cpx
Type		Cl core	Cl core	Cl core	Cl core	Cl core	Cl core	Cl core	Cl core	Cl core	Cl core	Cl core	Cl core	Cl core	Cl core	Cl core
Wt.%	SiO2	53.10	53.37	53.05	53.00	52.77	53.21	53.06	52.81	53.28	53.03	52.93	53.05	53.09	54.35	53.73
	TiO2	0.06	0.05	0.02	b.d.	0.02	0.03	0.06	0.03	0.05	0.07	0.04	0.05	0.05	0.04	0.04
	Cr2O3	0.90	0.96	0.99	1.04	0.95	0.95	0.95	1.05	0.94	0.89	1.03	0.86	0.81	0.46	0.95
	Al2O3	3.03	3.07	3.16	3.26	3.05	3.23	3.18	3.07	3.06	2.99	2.90	2.91	2.70	2.19	2.76
	FeO	1.87	1.91	1.89	1.87	1.80	1.87	1.78	2.02	1.82	1.91	1.84	1.75	1.92	1.88	1.86
	MnO	0.08	0.08	0.13	0.09	0.10	0.06	0.11	0.06	0.10	0.10	0.07	0.07	0.03	0.13	0.03
	NiO	0.06	0.04	0.09	0.05	b.d.	0.09	0.08	0.04	0.06	0.04	0.05	0.04	0.08	0.04	0.03
	MgO	17.16	17.24	17.11	16.96	17.15	17.05	17.30	17.21	17.22	17.26	17.09	17.17	17.12	17.60	17.17
	CaO	23.79	24.01	23.83	23.86	24.01	23.81	24.01	24.03	23.80	23.86	23.93	24.08	24.64	23.97	24.17
	Na2O	0.04	0.02	0.05	0.03	0.05	0.02	0.04	0.06	0.06	0.08	0.05	0.04	0.06	0.02	0.04
	K2O	b.d.	b.d.	b.d.	0.01	0.01	b.d.	0.01	0.01	b.d.	b.d.	b.d.	b.d.	b.d.	b.d.	b.d.
	Total	100.09	100.75	100.32	100.17	99.91	100.32	100.58	100.39	100.39	100.23	99.93	100.02	100.50	100.68	100.78
Cations	Si	1.925	1.923	1.921	1.921	1.919	1.924	1.916	1.914	1.925	1.922	1.924	1.925	1.923	1.955	1.934
	Ti	0.002	0.001	0.001	b.d.	0.001	0.001	0.002	0.001	0.001	0.002	0.001	0.001	0.001	0.001	0.001
	Cr	0.026	0.027	0.028	0.030	0.027	0.027	0.027	0.030	0.027	0.025	0.030	0.025	0.023	0.013	0.027
	Al	0.129	0.130	0.135	0.139	0.131	0.138	0.135	0.131	0.130	0.128	0.124	0.124	0.115	0.093	0.117
	Fe2+	0.057	0.058	0.057	0.057	0.055	0.057	0.054	0.061	0.055	0.058	0.056	0.053	0.058	0.057	0.056
	Mn	0.002	0.002	0.004	0.003	0.003	0.002	0.003	0.002	0.003	0.003	0.002	0.002	0.001	0.004	0.001
	Ni	0.002	0.001	0.003	0.001	b.d.	0.003	0.002	0.001	0.002	0.001	0.001	0.001	0.002	0.001	0.001
	Mg	0.927	0.926	0.923	0.916	0.929	0.919	0.931	0.930	0.927	0.932	0.926	0.929	0.924	0.943	0.921
	Ca	0.924	0.927	0.924	0.926	0.935	0.922	0.929	0.933	0.921	0.926	0.932	0.936	0.956	0.924	0.932
	Na	0.003	0.001	0.004	0.002	0.004	0.001	0.003	0.004	0.004	0.006	0.004	0.003	0.004	0.001	0.003
	K	b.d.	b.d.	b.d.	0.000	0.000	b.d.	0.000	0.000	b.d.	b.d.	b.d.	b.d.	b.d.	b.d.	b.d.
	Sum	3.997	3.997	3.999	3.996	4.004	3.993	4.003	4.007	3.997	4.003	4.000	4.000	4.009	3.992	3.994
	Mg #	0.942	0.941	0.942	0.942	0.944	0.942	0.945	0.938	0.944	0.942	0.943	0.946	0.941	0.943	0.943

Abbreviations: Cpx = clinopyroxene, Spl hrz = spinel harzburgite, Cl core = clast core, b.d. = below detection limit.
Mg# calculated as (MgO/40.3) / (MgO/40.3 + FeO/71.85).

Major element composition of clinopyroxene from the Dramala spinel harzburgite and plagioclase-bearing harzburgite continued

Sample		PI2	PI2	PI2	PI2	PI2	PI2	PI2	PI2	PI2	PI2	PI2	PI2	PI2	PI2	PI2
Rock		Spl hrz	Spl hrz	Spl hrz	Spl hrz	Spl hrz	Spl hrz	Spl hrz	Spl hrz	Spl hrz	Spl hrz	Spl hrz	Spl hrz	Spl hrz	Spl hrz	Spl hrz
Mineral		Cpx	Cpx	Cpx	Cpx	Cpx	Cpx	Cpx	Cpx	Cpx	Cpx	Cpx	Cpx	Cpx	Cpx	Cpx
Type		Cl core	Cl core	Cl core	Cl core	Cl core	Cl core	Cl core	Cl core	Cl core	Cl core	Cl core	Cl core	Cl core	Cl core	Cl core
Wt.%	SiO2	53.25	53.13	53.25	53.25	53.12	53.07	53.22	52.96	53.00	53.01	53.18	52.93	52.95	53.19	52.86
	TiO2	0.04	0.06	0.06	0.05	0.06	0.07	0.02	0.05	0.06	0.04	0.05	0.02	0.02	0.07	0.06
	Cr2O3	1.06	1.11	1.10	1.22	1.26	1.24	1.12	1.13	1.18	1.16	1.16	1.19	1.19	1.10	1.19
	Al2O3	3.16	3.24	3.34	3.24	3.33	3.37	3.32	3.33	3.41	3.40	3.13	3.55	3.53	3.40	3.49
	FeO	1.88	2.02	2.02	2.03	2.06	2.01	1.97	1.96	2.03	2.03	1.93	2.10	2.08	1.95	2.10
	MnO	0.07	0.07	0.07	0.10	0.08	0.10	0.10	0.06	0.09	0.12	0.14	0.12	0.12	0.06	0.08
	NiO	0.03	b.d.	b.d.	0.03	0.02	0.06	0.07	0.03	0.07	b.d.	0.06	b.d.	0.08	0.07	0.01
	MgO	17.18	17.14	17.04	17.14	16.95	17.04	16.84	16.87	16.89	16.99	16.85	16.95	16.76	16.80	16.77
	CaO	23.94	23.95	23.74	23.85	23.77	23.51	23.99	24.10	23.86	23.65	24.00	23.76	23.73	24.08	23.66
	Na2O	0.06	0.02	0.06	0.04	0.04	0.06	0.04	0.04	0.04	0.04	0.05	0.04	0.04	0.02	0.06
	K2O	b.d.	b.d.	b.d.	0.01	b.d.	b.d.	0.02	b.d.	0.03	b.d.	b.d.	b.d.	0.02	b.d.	0.01
	Total	100.67	100.74	100.68	100.96	100.69	100.53	100.71	100.53	100.66	100.44	100.55	100.66	100.52	100.74	100.29
Cations	Si	1.920	1.916	1.920	1.917	1.917	1.917	1.920	1.915	1.914	1.916	1.922	1.911	1.915	1.918	1.915
	Ti	0.001	0.002	0.002	0.001	0.002	0.002	0.001	0.001	0.002	0.001	0.001	0.001	0.001	0.002	0.002
	Cr	0.030	0.032	0.031	0.035	0.036	0.035	0.032	0.032	0.034	0.033	0.033	0.034	0.034	0.031	0.034
	Al	0.134	0.138	0.142	0.137	0.142	0.143	0.141	0.142	0.145	0.145	0.133	0.151	0.150	0.145	0.149
	Fe2+	0.057	0.061	0.061	0.061	0.062	0.061	0.059	0.059	0.061	0.061	0.058	0.063	0.063	0.059	0.064
	Mn	0.002	0.002	0.002	0.003	0.002	0.003	0.003	0.002	0.003	0.004	0.004	0.004	0.004	0.002	0.002
	Ni	0.001	b.d.	b.d.	0.001	0.001	0.002	0.002	0.001	0.002	b.d.	0.002	b.d.	0.002	0.002	0.000
	Mg	0.923	0.921	0.916	0.919	0.912	0.917	0.906	0.909	0.909	0.915	0.908	0.912	0.903	0.903	0.905
	Ca	0.925	0.925	0.917	0.920	0.919	0.910	0.927	0.934	0.923	0.916	0.929	0.919	0.919	0.930	0.918
	Na	0.004	0.001	0.004	0.003	0.003	0.004	0.003	0.003	0.003	0.003	0.004	0.003	0.003	0.001	0.004
	K	b.d.	b.d.	b.d.	0.000	b.d.	b.d.	0.001	b.d.	0.001	b.d.	b.d.	b.d.	0.001	b.d.	0.000
	Sum	3.998	3.998	3.994	3.998	3.994	3.994	3.995	3.998	3.997	3.995	3.995	3.997	3.995	3.993	3.994
	Mg #	0.942	0.938	0.938	0.938	0.936	0.938	0.938	0.939	0.937	0.937	0.940	0.935	0.935	0.939	0.934

Abbreviations: Cpx = clinopyroxene, Spl hrz = spinel harzburgite, Cl core = clast core, b.d. = below detection limit.
Mg# calculated as (MgO/40.3) / (MgO/40.3 + FeO/71.85).

Major element composition of clinopyroxene from the Dramala spinel harzburgite and plagioclase-bearing harzburgite continued

Sample		PI2	PI2	PI2	PI2	PI2	PI2	PI2	PI2	PI2	PI2	PI2	PI2	PI2	PI2	PI2
Rock		Spl hrz	Spl hrz	Spl hrz	Spl hrz	Spl hrz	Spl hrz	Spl hrz	Spl hrz	Spl hrz	Spl hrz	Spl hrz	Spl hrz	Spl hrz	Spl hrz	Spl hrz
Mineral		Cpx	Cpx	Cpx	Cpx	Cpx	Cpx	Cpx	Cpx	Cpx	Cpx	Cpx	Cpx	Cpx	Cpx	Cpx
Type		Cl core	Cl core	Cl core	Cl core	Cl core	Cl core	Cl core	Cl core	Cl core	Cl core	Cl core	Cl core	Cl core	Cl core	Cl core
Wt.%	SiO2	52.93	53.07	53.10	53.00	53.19	53.20	53.08	53.25	52.84	53.20	53.07	52.94	52.86	53.02	53.04
	TiO2	0.03	0.05	0.02	0.02	0.06	0.03	0.04	0.04	0.05	0.02	0.05	0.04	0.05	0.03	0.05
	Cr2O3	1.22	1.23	1.15	1.21	1.22	1.23	1.11	1.08	1.21	1.11	1.14	1.29	1.33	1.19	1.14
	Al2O3	3.40	3.53	3.44	3.45	3.53	3.41	3.50	3.40	3.53	3.46	3.31	3.50	3.49	3.55	3.53
	FeO	1.85	2.00	1.99	1.98	2.20	2.10	2.14	2.15	1.96	2.07	1.90	2.03	1.98	2.06	2.08
	MnO	0.08	0.12	0.06	0.08	0.01	0.06	0.05	0.07	0.09	0.09	0.06	0.08	0.07	0.03	0.07
	NiO	0.03	b.d.	0.07	0.09	0.06	0.06	0.03	0.05	0.05	0.05	0.04	0.04	0.01	0.03	0.09
	MgO	16.71	16.81	17.02	16.96	16.82	16.87	16.89	17.26	16.89	16.75	16.85	16.84	16.67	17.00	16.79
	CaO	24.11	24.16	23.90	23.88	23.76	23.74	23.89	23.35	24.00	24.01	24.19	23.89	23.92	23.58	23.98
	Na2O	0.06	0.01	0.04	0.05	0.05	0.04	0.05	0.03	0.04	0.05	0.03	0.01	0.03	0.02	0.05
	K2O	0.02	b.d.	b.d.	b.d.	0.01	b.d.	b.d.	0.01	0.01	b.d.	0.02	b.d.	b.d.	0.01	b.d.
	Total	100.44	100.98	100.79	100.72	100.91	100.74	100.78	100.69	100.67	100.81	100.66	100.66	100.41	100.52	100.82
Cations	Si	1.915	1.911	1.914	1.913	1.915	1.918	1.914	1.919	1.909	1.918	1.916	1.912	1.913	1.914	1.913
	Ti	0.001	0.001	0.001	0.001	0.002	0.001	0.001	0.001	0.001	0.001	0.001	0.001	0.001	0.001	0.001
	Cr	0.035	0.035	0.033	0.035	0.035	0.035	0.032	0.031	0.035	0.032	0.033	0.037	0.038	0.034	0.033
	Al	0.145	0.150	0.146	0.147	0.150	0.145	0.149	0.144	0.150	0.147	0.141	0.149	0.149	0.151	0.150
	Fe2+	0.056	0.060	0.060	0.060	0.066	0.063	0.065	0.065	0.059	0.062	0.057	0.061	0.060	0.062	0.063
	Mn	0.002	0.004	0.002	0.002	0.000	0.002	0.002	0.002	0.003	0.003	0.002	0.002	0.002	0.001	0.002
	Ni	0.001	b.d.	0.002	0.003	0.002	0.002	0.001	0.001	0.001	0.001	0.001	0.001	0.000	0.001	0.003
	Mg	0.901	0.902	0.914	0.912	0.903	0.907	0.908	0.927	0.909	0.900	0.907	0.906	0.899	0.915	0.902
	Ca	0.935	0.932	0.923	0.923	0.917	0.917	0.923	0.901	0.929	0.927	0.936	0.924	0.928	0.912	0.926
	Na	0.004	0.001	0.003	0.003	0.003	0.003	0.003	0.002	0.003	0.003	0.002	0.001	0.002	0.001	0.003
	K	0.001	b.d.	b.d.	b.d.	0.000	b.d.	b.d.	0.000	0.000	b.d.	0.001	b.d.	b.d.	0.000	b.d.
	Sum	3.996	3.996	3.997	3.998	3.993	3.992	3.996	3.994	3.999	3.994	3.997	3.995	3.993	3.993	3.996
	Mg #	0.942	0.937	0.938	0.939	0.932	0.935	0.934	0.935	0.939	0.935	0.941	0.937	0.938	0.936	0.935

Abbreviations: Cpx = clinopyroxene, Spl hrz = spinel harzburgite, Cl core = clast core, b.d. = below detection limit.
Mg# calculated as (MgO/40.3) / (MgO/40.3 + FeO/71.85).

Major element composition of clinopyroxene from the Dramala spinel harzburgite and plagioclase-bearing harzburgite continued

Sample		PI2	PI2	PI2	PI2	PI2	PI2	PI2	PI2	PI2	PI2	PI2	PI2	PI2	PI2	PI2
Rock		Spl hrz	Spl hrz	Spl hrz	Spl hrz	Spl hrz	Spl hrz	Spl hrz	Spl hrz	Spl hrz	Spl hrz	Spl hrz	Spl hrz	Spl hrz	Spl hrz	Spl hrz
Mineral		Cpx	Cpx	Cpx	Cpx	Cpx	Cpx	Cpx	Cpx	Cpx	Cpx	Cpx	Cpx	Cpx	Cpx	Cpx
Type		Cl core	Cl core	Cl core	Cl core	Cl core	Cl core	Cl core	Cl core	Cl core	Cl core	Cl core	Cl core	Cl core	Cl core	Cl core
Wt.%	SiO2	53.11	53.10	52.99	53.17	53.04	53.11	52.69	53.21	53.19	53.14	53.32	53.10	53.33	53.47	53.17
	TiO2	0.04	0.01	0.04	0.05	0.03	0.06	0.05	0.01	0.06	0.01	0.04	0.04	0.05	0.05	0.05
	Cr2O3	1.22	1.22	1.26	1.31	1.24	1.23	1.14	1.16	1.17	1.21	1.07	1.12	1.10	1.01	1.07
	Al2O3	3.50	3.50	3.50	3.49	3.40	3.50	3.40	3.35	3.32	3.27	3.29	3.23	3.25	3.17	3.09
	FeO	1.89	2.12	2.00	2.05	2.17	2.04	2.12	2.01	2.19	2.15	2.06	2.03	2.20	2.48	2.02
	MnO	0.06	0.07	0.08	0.04	0.06	0.05	0.12	0.07	0.09	0.08	0.07	0.07	0.06	0.09	0.11
	NiO	0.01	0.05	0.04	0.09	0.06	0.05	0.07	0.04	0.01	0.04	0.03	0.04	0.06	0.05	0.03
	MgO	16.71	16.74	16.81	16.90	16.80	16.86	16.75	16.90	17.03	17.07	17.03	16.87	17.44	18.27	17.11
	CaO	24.20	24.05	23.93	23.84	24.09	23.92	23.62	23.91	23.85	23.66	23.76	24.16	23.42	21.96	23.75
	Na2O	0.06	0.03	0.03	0.04	0.03	0.03	0.04	0.05	0.06	0.06	0.05	0.02	0.04	b.d.	0.05
	K2O	b.d.	0.01	0.01	b.d.	b.d.	b.d.	b.d.	0.01	b.d.	b.d.	0.02	0.01	b.d.	b.d.	0.02
	Total	100.80	100.90	100.69	100.98	100.92	100.85	100.00	100.72	100.97	100.69	100.74	100.69	100.95	100.55	100.47
Cations	Si	1.915	1.914	1.913	1.913	1.913	1.914	1.915	1.919	1.915	1.918	1.922	1.918	1.918	1.924	1.922
	Ti	0.001	0.000	0.001	0.001	0.001	0.002	0.001	0.000	0.002	0.000	0.001	0.001	0.001	0.001	0.001
	Cr	0.035	0.035	0.036	0.037	0.035	0.035	0.033	0.033	0.033	0.035	0.030	0.032	0.031	0.029	0.031
	Al	0.149	0.149	0.149	0.148	0.145	0.149	0.146	0.142	0.141	0.139	0.140	0.137	0.138	0.134	0.132
	Fe2+	0.057	0.064	0.060	0.062	0.065	0.061	0.064	0.061	0.066	0.065	0.062	0.061	0.066	0.075	0.061
	Mn	0.002	0.002	0.002	0.001	0.002	0.002	0.004	0.002	0.003	0.002	0.002	0.002	0.002	0.003	0.003
	Ni	0.000	0.001	0.001	0.003	0.002	0.001	0.002	0.001	0.000	0.001	0.001	0.001	0.002	0.001	0.001
	Mg	0.898	0.899	0.904	0.906	0.903	0.905	0.908	0.908	0.914	0.918	0.915	0.908	0.935	0.980	0.922
	Ca	0.935	0.929	0.925	0.919	0.931	0.923	0.920	0.924	0.920	0.915	0.917	0.935	0.902	0.846	0.920
	Na	0.004	0.002	0.002	0.003	0.002	0.002	0.003	0.003	0.004	0.004	0.003	0.001	0.003	b.d.	0.004
	K	b.d.	0.000	0.000	b.d.	b.d.	b.d.	b.d.	0.000	b.d.	b.d.	0.001	0.000	b.d.	b.d.	0.001
	Sum	3.995	3.995	3.995	3.994	3.998	3.994	3.995	3.995	3.998	3.997	3.994	3.997	3.998	3.993	3.997
	Mg #	0.940	0.934	0.937	0.936	0.932	0.936	0.934	0.937	0.933	0.934	0.936	0.937	0.934	0.929	0.938

Abbreviations: Cpx = clinopyroxene, Spl hrz = spinel harzburgite, Cl core = clast core, b.d. = below detection limit.
Mg# calculated as (MgO/40.3) / (MgO/40.3 + FeO/71.85).

Major element composition of clinopyroxene from the Dramala spinel harzburgite and plagioclase-bearing harzburgite continued

Sample		PI2	PI2	PI2	PI2	PI2	PI2	PI2	PI2	PI2	PI2	PI2	PI2	PI2	PI2	PI2
Rock		Spl hrz	Spl hrz	Spl hrz	Spl hrz	Spl hrz	Spl hrz	Spl hrz	Spl hrz	Spl hrz	Spl hrz	Spl hrz	Spl hrz	Spl hrz	Spl hrz	Spl hrz
Mineral		Cpx	Cpx	Cpx	Cpx	Cpx	Cpx	Cpx	Cpx	Cpx	Cpx	Cpx	Cpx	Cpx	Cpx	Cpx
Type		Cl core	Cl core	Cl core	Cl core	Cl core	Cl core	Cl core	Cl core	Cl core	Cl core	Cl core	Cl core	Cl core	Cl core	Cl core
Wt.%	SiO2	53.57	53.67	53.91	54.07	54.35	54.23	54.43	54.08	53.90	53.78	53.82	53.89	54.08	54.00	54.03
	TiO2	0.05	0.03	0.03	0.04	0.04	0.04	0.04	0.02	0.04	0.04	0.03	0.04	0.05	0.05	0.02
	Cr2O3	1.05	0.98	0.67	0.71	0.68	0.80	0.72	0.75	0.74	0.79	0.75	0.64	0.76	0.73	0.67
	Al2O3	3.03	2.84	2.17	2.14	2.14	2.08	2.10	2.05	2.47	2.54	2.55	2.52	2.50	2.38	2.37
	FeO	2.02	2.02	1.70	2.04	1.86	1.74	2.08	2.03	1.88	2.02	2.01	2.00	2.07	2.19	2.04
	MnO	0.03	0.11	0.12	0.04	0.11	0.07	0.08	0.07	0.10	0.08	0.08	0.05	0.04	0.08	0.10
	NiO	b.d.	0.08	0.05	0.03	0.02	0.08	0.03	0.06	0.04	0.05	0.03	0.13	0.13	0.07	0.01
	MgO	17.16	17.38	17.48	17.62	17.67	17.72	17.85	17.88	17.55	17.39	17.67	17.56	17.65	17.69	17.69
	CaO	23.86	23.61	24.33	24.20	24.08	24.12	23.56	23.33	23.76	23.83	23.78	23.68	23.56	23.53	23.44
	Na2O	0.03	0.03	0.05	0.04	0.03	0.01	0.06	0.05	0.02	0.06	0.02	0.04	0.04	0.06	0.03
	K2O	b.d.	0.01	0.03	b.d.	b.d.	b.d.	0.01	b.d.	b.d.	b.d.	b.d.	b.d.	b.d.	b.d.	0.01
	Total	100.80	100.76	100.54	100.93	100.98	100.89	100.96	100.32	100.50	100.58	100.74	100.55	100.88	100.78	100.41
Cations	Si	1.928	1.932	1.946	1.945	1.951	1.949	1.953	1.952	1.943	1.940	1.937	1.943	1.943	1.943	1.948
	Ti	0.001	0.001	0.001	0.001	0.001	0.001	0.001	0.001	0.001	0.001	0.001	0.001	0.001	0.001	0.001
	Cr	0.030	0.028	0.019	0.020	0.019	0.023	0.020	0.021	0.021	0.023	0.021	0.018	0.022	0.021	0.019
	Al	0.129	0.121	0.092	0.091	0.091	0.088	0.089	0.087	0.105	0.108	0.108	0.107	0.106	0.101	0.101
	Fe2+	0.061	0.061	0.051	0.061	0.056	0.052	0.062	0.061	0.057	0.061	0.060	0.060	0.062	0.066	0.062
	Mn	0.001	0.003	0.004	0.001	0.003	0.002	0.002	0.002	0.003	0.002	0.002	0.002	0.001	0.002	0.003
	Ni	b.d.	0.002	0.001	0.001	0.001	0.002	0.001	0.002	0.001	0.001	0.001	0.004	0.004	0.002	0.000
	Mg	0.921	0.933	0.940	0.945	0.945	0.949	0.955	0.962	0.943	0.935	0.948	0.943	0.945	0.949	0.951
	Ca	0.920	0.911	0.941	0.933	0.926	0.928	0.906	0.902	0.918	0.921	0.917	0.914	0.907	0.907	0.906
	Na	0.002	0.002	0.003	0.003	0.002	0.001	0.004	0.003	0.001	0.004	0.001	0.003	0.003	0.004	0.002
	K	b.d.	0.000	0.001	b.d.	b.d.	b.d.	0.000	b.d.	b.d.	b.d.	b.d.	b.d.	b.d.	b.d.	0.000
	Sum	3.992	3.994	4.000	4.000	3.994	3.995	3.994	3.995	3.993	3.996	3.998	3.995	3.993	3.997	3.992
	Mg #	0.938	0.939	0.948	0.939	0.944	0.948	0.939	0.940	0.943	0.939	0.940	0.940	0.938	0.935	0.939

Abbreviations: Cpx = clinopyroxene, Spl hrz = spinel harzburgite, Cl core = clast core, b.d. = below detection limit.
Mg# calculated as (MgO/40.3) / (MgO/40.3 + FeO/71.85).

Major element composition of clinopyroxene from the Dramala spinel harzburgite and plagioclase-bearing harzburgite continued

Sample		PI2	PI2	PI2	PI2	PI2	PI2	PI2	PI2	PI2	PI2	PI2	PI2	PI2	PI2	PI2
Rock		Spl hrz	Spl hrz	Spl hrz	Spl hrz	Spl hrz	Spl hrz	Spl hrz	Spl hrz	Spl hrz	Spl hrz	Spl hrz	Spl hrz	Spl hrz	Spl hrz	Spl hrz
Mineral		Cpx	Cpx	Cpx	Cpx	Cpx	Cpx	Cpx	Cpx	Cpx	Cpx	Cpx	Cpx	Cpx	Cpx	Cpx
Type		Cl core	Cl core	Cl core	Cl core	Cl core	Cl core	Cl core	Cl core	Cl core	Cl core	Cl core	Cl core	Cl core	Cl core	Cl core
Wt.%	SiO2	53.98	54.00	53.86	53.67	54.12	54.36	54.16	54.12	53.84	54.14	54.12	53.54	53.38	53.25	53.41
	TiO2	0.03	0.03	0.04	0.06	0.04	0.04	0.06	0.02	0.06	0.02	0.02	0.04	0.04	0.05	0.05
	Cr2O3	0.73	0.67	0.76	0.59	0.72	0.80	0.69	0.70	0.64	0.66	0.67	0.74	0.73	0.81	0.79
	Al2O3	2.40	2.41	2.42	2.34	2.39	2.44	2.43	2.41	2.44	2.35	2.29	2.55	2.60	2.65	2.72
	FeO	2.11	2.20	1.99	2.08	2.61	2.07	2.12	2.14	2.13	1.98	2.03	2.13	2.11	2.04	2.06
	MnO	0.04	0.13	0.08	0.04	0.12	0.08	0.03	0.11	0.05	0.03	0.04	0.02	0.08	0.03	0.06
	NiO	0.01	0.01	0.04	0.08	0.02	b.d.	0.06	0.02	0.06	0.02	0.09	0.04	0.07	0.01	0.04
	MgO	17.99	17.88	17.57	17.79	19.37	18.23	17.74	17.69	18.09	17.63	17.67	17.30	17.03	17.09	16.91
	CaO	23.04	23.35	23.68	23.67	21.53	22.94	23.65	23.70	23.24	24.05	23.78	23.92	24.03	24.11	24.47
	Na2O	0.04	0.02	0.04	0.01	0.03	0.02	0.02	0.07	0.01	0.01	0.02	0.03	0.01	0.04	0.05
	K2O	b.d.	b.d.	b.d.	0.01	b.d.	0.01	0.01	b.d.	b.d.	b.d.	0.01	b.d.	0.02	b.d.	b.d.
	Total	100.37	100.70	100.48	100.34	100.95	100.99	100.97	100.98	100.56	100.89	100.74	100.31	100.10	100.08	100.56
Cations	Si	1.946	1.943	1.943	1.940	1.937	1.946	1.944	1.943	1.939	1.945	1.947	1.938	1.937	1.933	1.931
	Ti	0.001	0.001	0.001	0.002	0.001	0.001	0.002	0.001	0.002	0.001	0.001	0.001	0.001	0.001	0.001
	Cr	0.021	0.019	0.022	0.017	0.020	0.023	0.020	0.020	0.018	0.019	0.019	0.021	0.021	0.023	0.023
	Al	0.102	0.102	0.103	0.100	0.101	0.103	0.103	0.102	0.104	0.100	0.097	0.109	0.111	0.113	0.116
	Fe2+	0.064	0.066	0.060	0.063	0.078	0.062	0.064	0.064	0.064	0.059	0.061	0.064	0.064	0.062	0.062
	Mn	0.001	0.004	0.002	0.001	0.004	0.002	0.001	0.003	0.002	0.001	0.001	0.001	0.002	0.001	0.002
	Ni	0.000	0.000	0.001	0.002	0.001	b.d.	0.002	0.001	0.002	0.001	0.003	0.001	0.002	0.000	0.001
	Mg	0.966	0.959	0.945	0.958	1.033	0.973	0.949	0.947	0.971	0.944	0.948	0.933	0.921	0.925	0.911
	Ca	0.890	0.900	0.915	0.917	0.826	0.880	0.909	0.912	0.897	0.926	0.917	0.927	0.934	0.938	0.948
	Na	0.003	0.001	0.003	0.001	0.002	0.001	0.001	0.005	0.001	0.001	0.001	0.002	0.001	0.003	0.004
	K	b.d.	b.d.	b.d.	0.000	b.d.	0.000	0.000	b.d.	b.d.	b.d.	0.000	b.d.	0.001	b.d.	b.d.
	Sum	3.993	3.996	3.995	4.001	4.002	3.991	3.994	3.998	3.999	3.995	3.995	3.997	3.996	3.999	4.000
	Mg #	0.938	0.935	0.940	0.938	0.930	0.940	0.937	0.936	0.938	0.941	0.939	0.935	0.935	0.937	0.936

Abbreviations: Cpx = clinopyroxene, Spl hrz = spinel harzburgite, Cl core = clast core, b.d. = below detection limit.
Mg# calculated as (MgO/40.3) / (MgO/40.3 + FeO/71.85).

Major element composition of clinopyroxene from the Dramala spinel harzburgite and plagioclase-bearing harzburgite continued

Sample		PI2	PI2	PI2	PI2	PI2	PI2	PI2	PI2	PI2	PI2	PI2	PI2	PI2	PI2	PI2
Rock		Spl hrz	Spl hrz	Spl hrz	Spl hrz	Spl hrz	Spl hrz	Spl hrz	Spl hrz	Spl hrz	Spl hrz	Spl hrz	Spl hrz	Spl hrz	Spl hrz	Spl hrz
Mineral		Cpx	Cpx	Cpx	Cpx	Cpx	Cpx	Cpx	Cpx	Cpx	Cpx	Cpx	Cpx	Cpx	Cpx	Cpx
Type		Cl core	Cl core	Cl core	Cl core	Cl core	Cl core	Cl core	Cl core	Cl core	Cl core	Cl core	Cl core	Cl core	Cl core	Cl core
Wt.%	SiO2	53.17	52.98	53.22	53.29	53.04	53.16	53.61	53.10	53.20	53.36	52.64	53.54	53.64	53.58	53.62
	TiO2	0.03	0.07	0.06	0.02	0.06	0.05	0.03	0.07	0.07	0.04	0.05	0.06	0.01	0.06	0.03
	Cr2O3	0.79	0.84	0.79	0.80	0.87	0.81	0.76	0.76	0.73	0.75	0.68	0.70	0.61	0.64	0.66
	Al2O3	2.70	2.75	2.70	2.71	2.68	2.73	2.73	2.67	2.68	2.62	2.40	2.41	2.44	2.25	2.46
	FeO	2.15	2.22	2.21	2.15	2.02	2.10	2.61	2.20	2.14	2.07	2.42	2.08	2.50	1.77	1.79
	MnO	0.13	0.11	0.08	0.08	0.11	0.04	0.11	0.09	0.03	0.10	0.06	0.03	0.11	0.05	0.05
	NiO	b.d.	0.07	0.06	0.05	0.03	0.07	0.06	0.03	0.07	0.02	0.04	0.06	0.05	0.03	b.d.
	MgO	17.21	17.38	17.26	17.35	16.89	17.08	18.04	17.06	17.04	17.16	17.97	17.25	18.89	17.25	17.42
	CaO	24.08	23.74	24.22	24.13	24.29	24.18	22.04	24.15	24.21	23.99	22.71	24.12	22.04	24.30	24.52
	Na2O	0.03	0.02	0.02	0.02	0.04	0.05	0.04	0.04	0.04	0.01	0.03	0.02	0.02	0.04	0.04
	K2O	0.01	b.d.	b.d.	0.03	b.d.	0.01	b.d.	0.02	b.d.	b.d.	0.01	b.d.	0.01	b.d.	0.01
	Total	100.30	100.18	100.62	100.63	100.03	100.28	100.03	100.19	100.21	100.12	99.01	100.27	100.32	99.97	100.60
Cations	Si	1.928	1.923	1.925	1.926	1.929	1.928	1.939	1.928	1.930	1.935	1.930	1.939	1.935	1.945	1.935
	Ti	0.001	0.002	0.002	0.001	0.002	0.001	0.001	0.002	0.002	0.001	0.001	0.002	0.000	0.002	0.001
	Cr	0.023	0.024	0.023	0.023	0.025	0.023	0.022	0.022	0.021	0.022	0.020	0.020	0.017	0.018	0.019
	Al	0.115	0.118	0.115	0.115	0.115	0.117	0.116	0.114	0.115	0.112	0.104	0.103	0.104	0.096	0.105
	Fe2+	0.065	0.067	0.067	0.065	0.061	0.064	0.079	0.067	0.065	0.063	0.074	0.063	0.075	0.054	0.054
	Mn	0.004	0.003	0.002	0.002	0.003	0.001	0.003	0.003	0.001	0.003	0.002	0.001	0.003	0.002	0.002
	Ni	b.d.	0.002	0.002	0.001	0.001	0.002	0.002	0.001	0.002	0.001	0.001	0.002	0.001	0.001	b.d.
	Mg	0.930	0.940	0.930	0.935	0.916	0.923	0.973	0.923	0.922	0.928	0.982	0.931	1.016	0.933	0.937
	Ca	0.935	0.923	0.938	0.934	0.946	0.939	0.854	0.940	0.941	0.932	0.892	0.936	0.852	0.945	0.948
	Na	0.002	0.001	0.001	0.001	0.003	0.004	0.003	0.003	0.003	0.001	0.002	0.001	0.001	0.003	0.003
	K	0.000	b.d.	b.d.	0.001	b.d.	0.000	b.d.	0.001	b.d.	b.d.	0.000	b.d.	0.000	b.d.	0.000
	Sum	4.004	4.005	4.005	4.006	4.001	4.003	3.992	4.004	4.001	3.997	4.008	3.998	4.005	3.998	4.004
	Mg #	0.935	0.933	0.933	0.935	0.937	0.935	0.925	0.933	0.934	0.937	0.930	0.937	0.931	0.946	0.945

Abbreviations: Cpx = clinopyroxene, Spl hrz = spinel harzburgite, Cl core = clast core, b.d. = below detection limit.
Mg# calculated as (MgO/40.3) / (MgO/40.3 + FeO/71.85).

Major element composition of clinopyroxene from the Dramala spinel harzburgite and plagioclase-bearing harzburgite continued

Sample		PI2	PI2	PI2	PI2	PI2	PI2	PI2	PI2	PI2	PI2	PI2	PI2	PI2	PI2	PI2
Rock		Spl hrz	Spl hrz	Spl hrz	Spl hrz	Spl hrz	Spl hrz	Spl hrz	Spl hrz	Spl hrz	Spl hrz	Spl hrz	Spl hrz	Spl hrz	Spl hrz	Spl hrz
Mineral		Cpx	Cpx	Cpx	Cpx	Cpx	Cpx	Cpx	Cpx	Cpx	Cpx	Cpx	Cpx	Cpx	Cpx	Cpx
Type		Cl core	Cl core	Cl core	Cl core	Cl core	Cl core	Cl core	Cl core	Cl core	Cl core	Cl core	Cl core	Cl core	Cl core	Cl core
Wt.%	SiO2	53.56	53.59	53.42	53.27	53.54	53.28	53.47	53.59	53.65	53.61	53.62	53.64	53.42	53.69	53.68
	TiO2	0.04	0.03	0.04	0.06	0.05	0.06	0.05	0.06	0.04	0.04	0.04	0.07	0.05	0.03	0.05
	Cr2O3	0.69	0.74	0.72	0.76	0.72	0.65	0.73	0.67	0.72	0.69	0.67	0.69	0.71	0.68	0.70
	Al2O3	2.36	2.58	2.67	2.69	2.65	2.48	2.56	2.60	2.43	2.44	2.39	2.43	2.64	2.40	2.40
	FeO	1.68	1.83	1.88	1.89	1.91	1.98	1.82	1.82	1.78	1.95	1.82	1.75	1.81	1.97	1.85
	MnO	0.05	0.07	0.08	0.05	0.09	0.02	0.07	0.10	0.03	0.05	0.09	0.05	0.13	0.07	0.08
	NiO	0.06	0.06	0.06	0.08	0.06	0.05	0.02	0.05	0.02	0.04	0.03	0.02	0.03	0.09	0.05
	MgO	17.22	17.38	17.13	17.34	17.35	17.46	17.17	17.64	17.39	17.47	17.34	17.46	17.25	17.43	17.26
	CaO	24.32	24.05	24.28	24.11	23.95	23.42	24.30	23.78	24.03	24.12	24.14	24.26	24.07	24.23	24.08
	Na2O	0.04	0.08	0.03	0.04	0.05	0.04	0.04	0.06	0.03	0.05	0.04	0.05	0.03	0.04	0.01
	K2O	0.01	b.d.	b.d.	0.02	b.d.	0.01	0.01	b.d.	b.d.	0.02	b.d.	b.d.	0.01	b.d.	b.d.
	Total	100.03	100.41	100.31	100.31	100.37	99.45	100.24	100.37	100.12	100.48	100.18	100.42	100.15	100.63	100.16
Cations	Si	1.943	1.936	1.934	1.929	1.935	1.941	1.936	1.935	1.942	1.937	1.942	1.938	1.935	1.938	1.944
	Ti	0.001	0.001	0.001	0.002	0.001	0.002	0.001	0.002	0.001	0.001	0.001	0.002	0.001	0.001	0.001
	Cr	0.020	0.021	0.021	0.022	0.021	0.019	0.021	0.019	0.021	0.020	0.019	0.020	0.020	0.019	0.020
	Al	0.101	0.110	0.114	0.115	0.113	0.107	0.109	0.111	0.104	0.104	0.102	0.103	0.113	0.102	0.102
	Fe2+	0.051	0.055	0.057	0.057	0.058	0.060	0.055	0.055	0.054	0.059	0.055	0.053	0.055	0.059	0.056
	Mn	0.002	0.002	0.002	0.002	0.003	0.001	0.002	0.003	0.001	0.002	0.003	0.002	0.004	0.002	0.002
	Ni	0.002	0.002	0.002	0.002	0.002	0.001	0.001	0.001	0.001	0.001	0.001	0.001	0.001	0.003	0.001
	Mg	0.931	0.936	0.924	0.936	0.935	0.948	0.927	0.950	0.938	0.941	0.936	0.940	0.932	0.938	0.932
	Ca	0.945	0.931	0.942	0.935	0.928	0.914	0.943	0.920	0.932	0.934	0.937	0.939	0.934	0.937	0.934
	Na	0.003	0.006	0.002	0.003	0.004	0.003	0.003	0.004	0.002	0.004	0.003	0.004	0.002	0.003	0.001
	K	0.000	b.d.	b.d.	0.001	b.d.	0.000	0.000	b.d.	b.d.	0.001	b.d.	b.d.	0.000	b.d.	b.d.
	Sum	3.998	4.000	3.999	4.003	3.998	3.996	3.999	4.000	3.996	4.002	3.998	4.000	3.998	4.002	3.994
	Mg #	0.948	0.944	0.942	0.942	0.942	0.940	0.944	0.945	0.946	0.941	0.944	0.947	0.944	0.940	0.943

Abbreviations: Cpx = clinopyroxene, Spl hrz = spinel harzburgite, Cl core = clast core, b.d. = below detection limit.
Mg# calculated as (MgO/40.3) / (MgO/40.3 + FeO/71.85).

Major element composition of clinopyroxene from the Dramala spinel harzburgite and plagioclase-bearing harzburgite continued

Sample		PI2	PI2	PI2	PI2	PI2	PI2	PI2	PI2	PI2	PI2	PI2	PI2	PI2	PI2	PI2
Rock		Spl hrz	Spl hrz	Spl hrz	Spl hrz	Spl hrz	Spl hrz	Spl hrz	Spl hrz	Spl hrz	Spl hrz	Spl hrz	Spl hrz	Spl hrz	Spl hrz	Spl hrz
Mineral		Cpx	Cpx	Cpx	Cpx	Cpx	Cpx	Cpx	Cpx	Cpx	Cpx	Cpx	Cpx	Cpx	Cpx	Cpx
Type		Cl core	Cl core	Cl core	Cl core	Cl core	Cl core	Cl core	Cl core	Cl core	Cl core	Cl core	Cl core	Cl core	Cl core	Cl core
Wt.%	SiO2	53.99	53.11	53.19	53.21	53.44	53.29	53.20	52.64	53.13	53.33	53.28	53.32	53.03	53.17	52.92
	TiO2	0.04	0.04	0.05	0.04	0.02	0.06	0.03	0.08	0.06	0.02	0.05	0.07	0.06	0.06	0.04
	Cr2O3	0.71	0.71	0.88	0.86	0.87	0.88	0.87	0.95	0.89	0.90	0.92	0.89	0.97	0.92	0.94
	Al2O3	2.40	2.54	2.73	2.81	2.78	2.87	2.84	3.06	2.93	2.87	2.92	2.99	3.00	2.98	2.96
	FeO	1.73	1.74	1.94	1.88	2.13	2.28	1.84	2.20	2.06	2.12	2.06	2.15	2.14	2.08	2.18
	MnO	0.08	0.07	0.07	0.13	0.08	0.06	0.09	0.06	0.09	0.12	0.17	0.09	0.07	0.10	0.07
	NiO	0.05	0.06	0.06	0.03	0.04	0.05	0.03	0.01	0.02	0.07	0.07	0.04	0.05	0.03	0.05
	MgO	17.61	17.21	17.35	17.34	17.32	17.29	17.31	17.32	17.24	17.33	17.22	17.68	16.99	17.12	17.06
	CaO	23.83	24.14	24.03	24.04	23.88	23.68	24.22	23.25	24.00	23.83	23.85	22.55	24.11	24.08	23.95
	Na2O	0.02	0.05	0.04	0.02	0.03	0.08	0.04	0.03	0.04	0.02	0.04	0.06	0.02	0.04	0.03
	K2O	b.d.	b.d.	b.d.	b.d.	0.01	b.d.	b.d.	b.d.	b.d.	b.d.	b.d.	0.02	b.d.	b.d.	b.d.
	Total	100.46	99.67	100.34	100.36	100.60	100.54	100.47	99.60	100.46	100.61	100.58	99.86	100.44	100.58	100.20
Cations	Si	1.946	1.934	1.926	1.926	1.930	1.926	1.924	1.919	1.922	1.926	1.925	1.932	1.921	1.922	1.921
	Ti	0.001	0.001	0.001	0.001	0.001	0.002	0.001	0.002	0.002	0.001	0.001	0.002	0.002	0.002	0.001
	Cr	0.020	0.020	0.025	0.025	0.025	0.025	0.025	0.027	0.025	0.026	0.026	0.025	0.028	0.026	0.027
	Al	0.102	0.109	0.117	0.120	0.118	0.122	0.121	0.131	0.125	0.122	0.124	0.128	0.128	0.127	0.127
	Fe2+	0.052	0.053	0.059	0.057	0.064	0.069	0.056	0.067	0.062	0.064	0.062	0.065	0.065	0.063	0.066
	Mn	0.002	0.002	0.002	0.004	0.002	0.002	0.003	0.002	0.003	0.004	0.005	0.003	0.002	0.003	0.002
	Ni	0.001	0.002	0.002	0.001	0.001	0.001	0.001	0.000	0.001	0.002	0.002	0.001	0.001	0.001	0.001
	Mg	0.946	0.934	0.936	0.935	0.932	0.931	0.933	0.941	0.930	0.933	0.927	0.955	0.917	0.922	0.923
	Ca	0.920	0.942	0.932	0.932	0.924	0.917	0.938	0.908	0.930	0.922	0.923	0.875	0.935	0.932	0.931
	Na	0.001	0.004	0.003	0.001	0.002	0.006	0.003	0.002	0.003	0.001	0.003	0.004	0.001	0.003	0.002
	K	b.d.	b.d.	b.d.	b.d.	0.000	b.d.	b.d.	b.d.	b.d.	b.d.	b.d.	0.001	b.d.	b.d.	b.d.
	Sum	3.993	4.002	4.003	4.002	4.000	4.001	4.004	4.000	4.002	4.000	4.000	3.992	4.001	4.001	4.002
	Mg #	0.948	0.946	0.941	0.943	0.935	0.931	0.944	0.933	0.937	0.936	0.937	0.936	0.934	0.936	0.933

Abbreviations: Cpx = clinopyroxene, Spl hrz = spinel harzburgite, Cl core = clast core, b.d. = below detection limit.
Mg# calculated as (MgO/40.3) / (MgO/40.3 + FeO/71.85).

Major element composition of clinopyroxene from the Dramala spinel harzburgite and plagioclase-bearing harzburgite continued

Sample		PI2	PI2	PI2	PI2	PI2	PI2	PI2	PI2	PI2	PI2	PI2	PI2	PI2	PI2	PI2
Rock		Spl hrz	Spl hrz	Spl hrz	Spl hrz	Spl hrz	Spl hrz	Spl hrz	Spl hrz	Spl hrz	Spl hrz	Spl hrz	Spl hrz	Spl hrz	Spl hrz	Spl hrz
Mineral		Cpx	Cpx	Cpx	Cpx	Cpx	Cpx	Cpx	Cpx	Cpx	Cpx	Cpx	Cpx	Cpx	Cpx	Cpx
Type		Cl core	Cl core	Cl core	Cl core	Cl core	Cl core	Cl core	Cl core	Cl core	Cl core	Cl core	Cl core	Cl core	Cl core	Cl core
Wt.%	SiO2	53.21	52.91	52.88	53.18	53.16	53.01	53.29	53.05	53.22	53.08	53.16	52.98	53.00	53.13	53.13
	TiO2	0.04	0.03	0.06	0.02	0.05	0.06	0.04	0.04	0.07	0.02	0.03	0.04	0.05	0.03	0.02
	Cr2O3	0.92	0.88	0.91	0.94	0.90	0.93	0.95	0.94	0.89	0.87	0.95	0.91	0.87	0.84	0.89
	Al2O3	2.96	2.96	2.96	3.01	2.88	2.92	2.92	3.08	2.92	2.93	2.99	2.95	2.88	2.93	2.89
	FeO	2.12	2.02	2.05	1.93	2.00	1.85	1.98	2.05	1.96	2.09	2.17	2.03	1.95	2.14	2.00
	MnO	0.08	0.11	0.07	0.09	0.08	0.09	0.09	0.07	0.10	0.06	b.d.	0.03	0.10	0.07	0.10
	NiO	0.03	0.03	0.07	0.01	0.09	0.05	0.04	0.06	0.04	0.05	0.07	0.06	0.08	0.09	0.02
	MgO	17.29	17.10	16.96	17.09	17.09	17.13	17.03	17.10	17.16	17.07	17.08	17.21	17.08	17.18	17.09
	CaO	23.98	24.03	24.23	24.06	24.18	24.06	24.02	23.59	23.92	24.01	23.90	23.98	24.22	23.90	23.98
	Na2O	0.03	0.02	0.02	0.03	0.03	b.d.	0.03	0.01	0.06	0.04	0.06	0.02	0.05	0.04	0.03
	K2O	b.d.	b.d.	0.02	b.d.	b.d.	b.d.	b.d.	0.01	b.d.	b.d.	b.d.	b.d.	b.d.	b.d.	b.d.
	Total	100.66	100.09	100.23	100.36	100.46	100.10	100.39	100.00	100.34	100.22	100.41	100.21	100.28	100.35	100.15
Cations	Si	1.921	1.922	1.920	1.924	1.924	1.924	1.928	1.925	1.926	1.925	1.924	1.921	1.922	1.924	1.927
	Ti	0.001	0.001	0.002	0.001	0.001	0.002	0.001	0.001	0.002	0.001	0.001	0.001	0.001	0.001	0.001
	Cr	0.026	0.025	0.026	0.027	0.026	0.027	0.027	0.027	0.025	0.025	0.027	0.026	0.025	0.024	0.026
	Al	0.126	0.127	0.127	0.128	0.123	0.125	0.125	0.132	0.125	0.125	0.128	0.126	0.123	0.125	0.124
	Fe2+	0.064	0.061	0.062	0.058	0.061	0.056	0.060	0.062	0.059	0.063	0.066	0.062	0.059	0.065	0.061
	Mn	0.002	0.003	0.002	0.003	0.002	0.003	0.003	0.002	0.003	0.002	b.d.	0.001	0.003	0.002	0.003
	Ni	0.001	0.001	0.002	0.000	0.003	0.001	0.001	0.002	0.001	0.001	0.002	0.002	0.002	0.003	0.001
	Mg	0.931	0.926	0.918	0.922	0.922	0.926	0.918	0.925	0.926	0.923	0.921	0.930	0.923	0.927	0.924
	Ca	0.928	0.935	0.942	0.933	0.938	0.935	0.931	0.917	0.927	0.933	0.927	0.932	0.941	0.927	0.932
	Na	0.002	0.001	0.001	0.002	0.002	b.d.	0.002	0.001	0.004	0.003	0.004	0.001	0.004	0.003	0.002
	K	b.d.	b.d.	0.001	b.d.	b.d.	b.d.	b.d.	0.000	0.000	b.d.	b.d.	b.d.	b.d.	b.d.	b.d.
	Sum	4.002	4.002	4.003	3.998	4.001	3.999	3.996	3.995	3.999	4.001	4.000	4.002	4.004	4.002	3.999
	Mg #	0.936	0.938	0.936	0.940	0.938	0.943	0.939	0.937	0.940	0.936	0.933	0.938	0.940	0.935	0.938

Abbreviations: Cpx = clinopyroxene, Spl hrz = spinel harzburgite, Cl core = clast core, b.d. = below detection limit.
Mg# calculated as (MgO/40.3) / (MgO/40.3 + FeO/71.85).

Major element composition of clinopyroxene from the Dramala spinel harzburgite and plagioclase-bearing harzburgite continued

Sample		PI2	PI2	PI2	PI2	PI2	PI2	PI2	PI2	PI2	PI2	PI2	PI2	PI2	PI2	PI2
Rock		Spl hrz	Spl hrz	Spl hrz	Spl hrz	Spl hrz	Spl hrz	Spl hrz	Spl hrz	Spl hrz	Spl hrz	Spl hrz	Spl hrz	Spl hrz	Spl hrz	Spl hrz
Mineral		Cpx	Cpx	Cpx	Cpx	Cpx	Cpx	Cpx	Cpx	Cpx	Cpx	Cpx	Cpx	Cpx	Cpx	Cpx
Type		Cl core	Cl core	Cl core	Cl core	Cl core	Cl core	Cl core	Cl core	Cl core	Cl core	Cl core	Cl core	Cl core	Cl core	Cl core
Wt.%	SiO2	53.16	53.02	52.89	53.20	52.80	52.96	53.12	53.32	53.33	53.21	53.25	53.23	53.23	53.34	53.29
	TiO2	0.05	0.02	0.06	0.05	0.02	0.03	0.04	0.04	0.06	0.08	0.04	0.06	0.02	0.03	0.03
	Cr2O3	0.87	0.89	0.84	0.90	0.89	0.88	0.80	0.91	0.88	0.83	0.78	0.82	0.85	0.82	0.82
	Al2O3	2.90	2.84	2.87	2.89	2.80	2.84	2.84	2.85	2.84	2.81	2.72	2.68	2.67	2.63	2.58
	FeO	2.09	2.11	1.98	2.09	1.99	2.09	2.10	2.13	2.01	2.01	2.00	2.01	2.10	1.92	1.86
	MnO	0.08	0.05	0.10	0.10	0.10	0.09	0.03	0.10	0.10	0.07	0.12	0.14	0.09	0.12	0.12
	NiO	0.05	0.07	0.04	0.09	0.04	0.04	b.d.	0.04	0.06	0.10	b.d.	0.02	0.10	0.04	0.04
	MgO	17.16	17.06	17.08	17.02	16.97	17.25	17.24	17.20	17.12	17.26	17.28	17.18	17.39	17.33	17.31
	CaO	24.04	24.01	24.09	24.28	24.11	23.98	24.06	23.88	24.06	23.81	23.85	23.92	24.12	23.96	24.02
	Na2O	0.02	0.03	b.d.	0.03	0.06	0.03	0.03	0.06	b.d.	0.06	0.05	0.05	0.05	0.02	0.03
	K2O	b.d.	b.d.	b.d.	0.01	b.d.	b.d.	b.d.	b.d.	b.d.	0.02	b.d.	0.01	b.d.	0.01	0.01
	Total	100.42	100.10	99.95	100.66	99.78	100.19	100.26	100.53	100.46	100.26	100.09	100.12	100.62	100.22	100.11
Cations	Si	1.924	1.926	1.924	1.923	1.925	1.922	1.925	1.927	1.929	1.928	1.931	1.931	1.925	1.932	1.933
	Ti	0.001	0.001	0.002	0.001	0.001	0.001	0.001	0.001	0.002	0.002	0.001	0.002	0.001	0.001	0.001
	Cr	0.025	0.026	0.024	0.026	0.026	0.025	0.023	0.026	0.025	0.024	0.022	0.024	0.024	0.023	0.024
	Al	0.124	0.122	0.123	0.123	0.120	0.121	0.121	0.121	0.121	0.120	0.116	0.115	0.114	0.112	0.110
	Fe2+	0.063	0.064	0.060	0.063	0.061	0.063	0.064	0.064	0.061	0.061	0.061	0.061	0.063	0.058	0.056
	Mn	0.002	0.002	0.003	0.003	0.003	0.003	0.001	0.003	0.003	0.002	0.004	0.004	0.003	0.004	0.004
	Ni	0.001	0.002	0.001	0.003	0.001	0.001	b.d.	0.001	0.002	0.003	b.d.	0.001	0.003	0.001	0.001
	Mg	0.926	0.924	0.926	0.917	0.922	0.933	0.931	0.927	0.923	0.932	0.934	0.929	0.937	0.936	0.936
	Ca	0.932	0.934	0.939	0.940	0.942	0.932	0.934	0.925	0.932	0.924	0.927	0.930	0.934	0.930	0.933
	Na	0.001	0.002	b.d.	0.002	0.004	0.002	0.002	0.004	b.d.	0.004	0.004	0.004	0.004	0.001	0.002
	K	b.d.	b.d.	b.d.	0.000	b.d.	b.d.	b.d.	b.d.	b.d.	0.001	b.d.	0.000	b.d.	0.000	0.000
	Sum	4.001	4.001	4.001	4.002	4.004	4.005	4.003	4.000	3.997	4.001	4.000	4.000	4.007	4.000	4.001
	Mg #	0.936	0.935	0.939	0.936	0.938	0.936	0.936	0.935	0.938	0.939	0.939	0.938	0.937	0.941	0.943

Abbreviations: Cpx = clinopyroxene, Spl hrz = spinel harzburgite, Cl core = clast core, b.d. = below detection limit.
Mg# calculated as (MgO/40.3) / (MgO/40.3 + FeO/71.85).

Major element composition of clinopyroxene from the Dramala spinel harzburgite and plagioclase-bearing harzburgite continued

Sample		PI2	PI2	PI2	PI2	PI2	PI2	PI2	PI2	PI2	PI2	PI2	PI2	PI2	PI2	PI2
Rock		Spl hrz	Spl hrz	Spl hrz	Spl hrz	Spl hrz	Spl hrz	Spl hrz	Spl hrz	Spl hrz	Spl hrz	Spl hrz	Spl hrz	Spl hrz	Spl hrz	Spl hrz
Mineral		Cpx	Cpx	Cpx	Cpx	Cpx	Cpx	Cpx	Cpx	Cpx	Cpx	Cpx	Cpx	Cpx	Cpx	Cpx
Type		Cl core	Cl core	Cl rim	Cl rim	Cl rim	Cl rim	Cl rim	Cl rim	Cl rim	Cl rim	Cl rim	Cl rim	Cl rim	Cl rim	Cl rim
Wt.%	SiO2	53.40	52.94	54.85	54.53	53.61	53.69	53.73	53.55	55.30	52.94	53.48	54.27	53.94	54.63	53.70
	TiO2	0.02	0.05	0.05	0.05	0.05	0.06	0.07	0.07	0.02	0.02	0.10	0.06	0.06	0.04	0.08
	Cr2O3	0.79	0.95	0.24	0.45	0.59	0.56	0.61	0.76	0.22	0.95	0.79	0.73	0.58	0.20	0.77
	Al2O3	2.56	2.99	1.25	1.57	2.44	2.43	2.36	2.64	1.15	2.75	2.60	1.96	2.10	0.98	2.37
	FeO	1.95	2.23	1.91	1.68	1.92	2.06	1.68	1.70	1.65	1.87	1.97	1.60	1.71	1.87	1.94
	MnO	0.08	0.05	0.07	0.04	0.07	0.05	0.09	0.10	0.06	0.09	0.05	0.12	0.12	0.03	0.05
	NiO	0.04	0.03	0.03	0.09	0.04	0.03	0.05	0.07	0.02	0.09	b.d.	0.02	0.06	0.07	0.04
	MgO	17.27	16.99	18.18	17.86	17.60	17.56	17.27	17.35	18.13	17.33	17.42	17.53	17.32	18.02	17.51
	CaO	23.94	24.06	24.28	24.42	23.67	23.44	24.61	24.20	24.29	24.21	24.30	24.63	24.61	24.41	24.10
	Na2O	0.06	0.03	0.05	0.05	0.05	0.01	0.02	0.01	0.05	0.02	0.01	0.02	0.02	0.05	0.04
	K2O	b.d.	b.d.	b.d.	b.d.	0.01	b.d.	b.d.	0.01	b.d.	b.d.	0.02	b.d.	b.d.	b.d.	b.d.
	Total	100.11	100.32	100.91	100.74	100.05	99.89	100.49	100.46	100.89	100.27	100.74	100.94	100.52	100.30	100.60
Cations	Si	1.936	1.920	1.969	1.962	1.942	1.946	1.941	1.934	1.981	1.920	1.929	1.950	1.948	1.975	1.938
	Ti	0.001	0.001	0.001	0.001	0.001	0.002	0.002	0.002	0.001	0.001	0.003	0.002	0.002	0.001	0.002
	Cr	0.023	0.027	0.007	0.013	0.017	0.016	0.017	0.022	0.006	0.027	0.023	0.021	0.017	0.006	0.022
	Al	0.109	0.128	0.053	0.067	0.104	0.104	0.100	0.112	0.049	0.118	0.111	0.083	0.089	0.042	0.101
	Fe2+	0.059	0.068	0.057	0.051	0.058	0.062	0.051	0.051	0.049	0.057	0.059	0.048	0.052	0.057	0.059
	Mn	0.002	0.002	0.002	0.001	0.002	0.002	0.003	0.003	0.002	0.003	0.002	0.004	0.004	0.001	0.002
	Ni	0.001	0.001	0.001	0.003	0.001	0.001	0.001	0.002	0.001	0.003	b.d.	0.001	0.002	0.002	0.001
	Mg	0.933	0.918	0.973	0.958	0.950	0.949	0.930	0.934	0.968	0.937	0.936	0.939	0.932	0.971	0.942
	Ca	0.930	0.935	0.934	0.941	0.918	0.910	0.952	0.936	0.932	0.941	0.939	0.948	0.952	0.945	0.932
	Na	0.004	0.002	0.003	0.003	0.004	0.001	0.001	0.001	0.003	0.001	0.001	0.001	0.001	0.004	0.003
	K	b.d.	b.d.	b.d.	b.d.	0.000	b.d.	b.d.	0.000	b.d.	b.d.	0.001	b.d.	b.d.	b.d.	b.d.
	Sum	3.999	4.002	4.001	3.999	3.998	3.992	3.999	3.998	3.992	4.007	4.003	3.997	3.998	4.002	4.000
	Mg #	0.940	0.931	0.944	0.950	0.942	0.938	0.948	0.948	0.951	0.943	0.940	0.951	0.948	0.945	0.941

Abbreviations: Cpx = clinopyroxene, Spl hrz = spinel harzburgite, Cl core = clast core, Cl rim = clast rim, b.d. = below detection limit.
Mg# calculated as (MgO/40.3) / (MgO/40.3 + FeO/71.85).

Major element composition of clinopyroxene from the Dramala spinel harzburgite and plagioclase-bearing harzburgite continued

Sample		PI2	PI2	PI2	PI2	PI2	PI2	PI2	PI2	PI2	PI2	PI2	PI2	PI2	PI2	PI2
Rock		Spl hrz	Spl hrz	Spl hrz	Spl hrz	Spl hrz	Spl hrz	Spl hrz	Spl hrz	Spl hrz	Spl hrz	Spl hrz	Spl hrz	Spl hrz	Spl hrz	Spl hrz
Mineral		Cpx	Cpx	Cpx	Cpx	Cpx	Cpx	Cpx	Cpx	Cpx	Cpx	Cpx	Cpx	Cpx	Cpx	Cpx
Type		Cl rim	Cl rim	Cl rim	Cl rim	Cl rim	Cl rim	Cl rim	Cl rim	Cl rim	Cl rim	Cl rim	Cl rim	Cl rim	Cl rim	Cl rim
Wt.%	**SiO2**	53.24	53.52	53.36	53.07	53.24	53.28	53.53	53.55	53.82	54.01	54.07	53.68	53.61	53.86	53.10
	TiO2	0.04	0.03	0.02	0.05	0.06	0.04	0.04	0.05	0.05	0.06	0.06	0.02	0.03	0.10	0.05
	Cr2O3	0.72	0.83	0.87	0.93	0.94	0.89	0.84	0.71	0.55	0.49	0.40	0.60	0.64	0.44	0.74
	Al2O3	2.22	2.63	2.75	2.75	2.68	2.55	2.45	2.06	1.96	1.93	1.74	2.25	2.37	1.93	2.72
	FeO	1.96	1.83	2.03	2.23	1.95	1.91	1.85	1.93	1.87	1.92	2.03	1.89	1.81	1.85	1.86
	MnO	0.04	0.09	0.08	0.12	0.14	0.05	0.08	0.06	0.07	0.05	0.05	0.13	0.02	0.06	0.06
	NiO	0.05	0.02	0.00	0.06	0.03	0.04	0.08	0.04	0.03	0.06	0.09	b.d.	0.03	0.04	0.05
	MgO	17.81	17.28	17.33	17.16	17.17	17.20	17.43	17.61	17.64	17.76	17.62	17.33	17.36	17.35	17.22
	CaO	23.78	24.10	23.88	23.98	24.15	24.39	24.34	24.22	24.34	24.29	24.47	24.41	24.27	24.72	24.38
	Na2O	0.01	0.05	0.06	0.01	0.05	0.05	0.06	0.03	0.03	0.02	0.01	0.05	0.02	0.03	0.02
	K2O	b.d.	0.01	b.d.	b.d.	b.d.	b.d.	0.01	0.02	0.01	0.01	0.01	b.d.	0.01	0.03	0.01
	Total	99.87	100.39	100.38	100.36	100.41	100.40	100.71	100.28	100.37	100.60	100.55	100.36	100.17	100.41	100.21
Cations	**Si**	1.935	1.935	1.930	1.924	1.928	1.930	1.932	1.940	1.947	1.948	1.953	1.943	1.942	1.949	1.926
	Ti	0.001	0.001	0.001	0.001	0.002	0.001	0.001	0.001	0.001	0.002	0.002	0.001	0.001	0.003	0.001
	Cr	0.021	0.024	0.025	0.027	0.027	0.025	0.024	0.020	0.016	0.014	0.011	0.017	0.018	0.013	0.021
	Al	0.095	0.112	0.117	0.118	0.114	0.109	0.104	0.088	0.084	0.082	0.074	0.096	0.101	0.082	0.116
	Fe2+	0.060	0.055	0.061	0.068	0.059	0.058	0.056	0.058	0.057	0.058	0.061	0.057	0.055	0.056	0.056
	Mn	0.001	0.003	0.002	0.004	0.004	0.002	0.002	0.002	0.002	0.002	0.002	0.004	0.001	0.002	0.002
	Ni	0.001	0.001	0.000	0.002	0.001	0.001	0.002	0.001	0.001	0.002	0.003	b.d.	0.001	0.001	0.001
	Mg	0.965	0.931	0.934	0.927	0.927	0.928	0.938	0.951	0.951	0.955	0.949	0.935	0.937	0.936	0.931
	Ca	0.926	0.933	0.925	0.932	0.937	0.946	0.941	0.940	0.943	0.939	0.947	0.946	0.942	0.958	0.947
	Na	0.001	0.004	0.004	0.001	0.004	0.004	0.004	0.002	0.002	0.001	0.001	0.004	0.001	0.002	0.001
	K	b.d.	0.000	b.d.	b.d.	b.d.	b.d.	0.000	0.001	0.000	0.000	0.000	b.d.	0.000	0.001	0.000
	Sum	4.006	3.998	4.000	4.003	4.002	4.004	4.005	4.006	4.004	4.003	4.003	4.002	3.999	4.003	4.005
	Mg #	0.942	0.944	0.938	0.932	0.940	0.941	0.944	0.942	0.944	0.943	0.939	0.942	0.945	0.944	0.943

Abbreviations: Cpx = clinopyroxene, Spl hrz = spinel harzburgite, Cl rim = clast rim, b.d. = below detection limit.
Mg# calculated as (MgO/40.3) / (MgO/40.3 + FeO/71.85).

Major element composition of clinopyroxene from the Dramala spinel harzburgite and plagioclase-bearing harzburgite continued

Sample		PI2	PI2	PI2	PI2	PI2	PI2	PI2	PI2	PI2	PI2	PI2	PI2	PI2	PI2	PI2
Rock		Spl hrz	Spl hrz	Spl hrz	Spl hrz	Spl hrz	Spl hrz	Spl hrz	Spl hrz	Spl hrz	Spl hrz	Spl hrz	Spl hrz	Spl hrz	Spl hrz	Spl hrz
Mineral		Cpx	Cpx	Cpx	Cpx	Cpx	Cpx	Cpx	Cpx	Cpx	Cpx	Cpx	Cpx	Cpx	Cpx	Cpx
Type		Cl rim	Cl rim	Cl rim	Cl rim	Cl rim	Cl rim	Cl rim	Blast	Blast	Blast	Blast	Blast	Blast	Blast	Blast
Wt.%	SiO2	53.29	53.34	53.09	54.16	54.01	53.97	54.75	53.59	54.74	54.16	54.35	53.52	53.58	53.71	54.89
	TiO2	0.07	0.08	0.08	0.11	0.06	0.08	0.03	0.07	0.01	0.05	0.03	0.04	0.06	0.04	0.04
	Cr2O3	0.85	0.76	0.75	0.53	0.73	0.54	0.20	0.55	0.18	0.44	0.29	0.59	0.57	0.51	0.07
	Al2O3	2.85	2.79	3.10	1.77	1.98	1.74	0.94	2.12	0.92	1.73	1.32	2.34	2.08	2.23	0.42
	FeO	1.90	1.79	1.88	1.45	1.73	1.75	1.67	2.15	1.90	1.94	2.03	1.80	1.83	2.14	1.51
	MnO	0.02	0.06	0.15	0.05	0.04	0.07	0.08	0.10	0.07	0.05	0.05	0.06	0.11	0.10	0.02
	NiO	0.05	0.01	0.01	0.05	0.02	0.03	0.04	0.06	0.03	0.03	0.06	0.04	0.03	0.03	0.03
	MgO	17.23	17.07	16.89	17.45	17.51	17.61	17.79	17.67	18.13	17.63	17.90	17.49	17.50	17.79	18.11
	CaO	23.97	24.34	24.60	24.74	24.66	24.90	25.23	24.16	24.81	24.57	24.54	23.69	24.46	24.11	25.50
	Na2O	0.04	0.05	0.05	0.06	0.03	0.02	0.04	0.02	0.02	0.04	0.03	0.05	0.04	b.d.	0.03
	K2O	0.01	b.d.	b.d.	b.d.	b.d.	0.01	0.01	b.d.	0.02	b.d.	b.d.	b.d.	b.d.	b.d.	b.d.
	Total	100.28	100.29	100.60	100.37	100.77	100.72	100.78	100.49	100.83	100.64	100.60	99.62	100.26	100.66	100.62
Cations	Si	1.929	1.931	1.919	1.956	1.946	1.948	1.973	1.939	1.971	1.954	1.962	1.946	1.942	1.938	1.980
	Ti	0.002	0.002	0.002	0.003	0.002	0.002	0.001	0.002	0.000	0.001	0.001	0.001	0.002	0.001	0.001
	Cr	0.024	0.022	0.021	0.015	0.021	0.015	0.006	0.016	0.005	0.013	0.008	0.017	0.016	0.015	0.002
	Al	0.122	0.119	0.132	0.075	0.084	0.074	0.040	0.090	0.039	0.074	0.056	0.100	0.089	0.095	0.018
	Fe2+	0.057	0.054	0.057	0.044	0.052	0.053	0.050	0.065	0.057	0.059	0.061	0.055	0.055	0.065	0.046
	Mn	0.001	0.002	0.005	0.002	0.001	0.002	0.002	0.003	0.002	0.002	0.002	0.002	0.003	0.003	0.001
	Ni	0.001	0.000	0.000	0.001	0.001	0.001	0.001	0.002	0.001	0.001	0.002	0.001	0.001	0.001	0.001
	Mg	0.929	0.921	0.910	0.939	0.940	0.947	0.955	0.953	0.973	0.948	0.963	0.948	0.945	0.957	0.974
	Ca	0.929	0.944	0.953	0.957	0.952	0.963	0.974	0.936	0.957	0.950	0.949	0.923	0.950	0.932	0.986
	Na	0.003	0.004	0.004	0.004	0.002	0.001	0.003	0.001	0.001	0.003	0.002	0.004	0.003	b.d.	0.002
	K	0.000	b.d.	b.d.	b.d.	b.d.	0.000	0.000	b.d.	0.001	b.d.	b.d.	b.d.	b.d.	b.d.	b.d.
	Sum	3.998	3.998	4.003	3.998	4.001	4.007	4.005	4.007	4.008	4.003	4.006	3.996	4.006	4.006	4.010
	Mg #	0.942	0.944	0.941	0.955	0.947	0.947	0.950	0.936	0.944	0.942	0.940	0.945	0.945	0.937	0.955

Abbreviations: Cpx = clinopyroxene, Spl hrz = spinel harzburgite, Cl rim = clast rim, b.d. = below detection limit.
Mg# calculated as (MgO/40.3) / (MgO/40.3 + FeO/71.85).

Major element composition of clinopyroxene from the Dramala spinel harzburgite and plagioclase-bearing harzburgite continued

Sample		PI2	PI2	PI2	PI2	PI2	PI2	PI2	PI2	PI2	PIA91	PIA91	PIA91	PIA91	PIA91	PIA91
Rock		Spl hrz	Spl hrz	Spl hrz	Spl hrz	Spl hrz	Spl hrz	Spl hrz	Spl hrz	Spl hrz	Spl hrz	Spl hrz	Spl hrz	Spl hrz	Spl hrz	Spl hrz
Mineral		Cpx	Cpx	Cpx	Cpx	Cpx	Cpx	Cpx	Cpx	Cpx	Cpx	Cpx	Cpx	Cpx	Cpx	Cpx
Type		Blast	Blast	Blast	Blast	Blast	Blast	Blast	Blast	Blast	Cl core	Cl core	Cl core	Cl core	Cl core	Cl core
Wt.%	SiO2	53.53	53.28	53.71	53.68	53.31	53.42	53.19	52.98	53.31	53.50	54.02	53.99	53.92	53.66	54.14
	TiO2	0.05	0.02	0.04	0.05	0.06	0.06	0.02	0.07	0.04	0.03	0.03	0.03	0.04	0.04	0.03
	Cr2O3	0.82	0.69	0.72	0.58	0.88	0.87	0.88	0.82	0.89	0.59	0.64	0.64	0.70	0.68	0.67
	Al2O3	2.68	2.59	2.63	2.31	2.35	2.42	2.89	2.58	2.56	1.55	1.74	1.81	1.88	1.90	1.95
	FeO	1.74	1.81	1.93	1.86	1.95	2.07	1.90	1.65	2.00	1.70	1.62	2.04	1.92	1.72	1.84
	MnO	0.05	0.06	0.03	0.09	0.09	0.08	0.10	0.11	0.04	b.d.	0.04	0.06	b.d.	b.d.	0.05
	NiO	0.01	0.04	b.d.	b.d.	0.08	0.02	b.d.	0.01	0.02	0.04	0.03	0.11	0.03	0.05	0.11
	MgO	17.15	17.46	17.31	17.34	17.61	17.69	17.15	17.13	17.61	17.51	17.51	17.38	17.35	17.58	17.57
	CaO	24.29	23.85	24.04	24.00	23.86	23.92	23.99	24.60	23.69	24.18	24.12	23.86	24.00	23.51	23.75
	Na2O	0.03	0.03	0.02	0.03	0.05	0.04	0.04	0.05	0.04	0.01	0.05	b.d.	0.02	0.02	0.04
	K2O	0.01	b.d.	b.d.	b.d.	b.d.	b.d.	0.02	0.02	b.d.	b.d.	0.01	0.01	0.01	0.01	b.d.
	Total	100.36	99.83	100.43	99.94	100.24	100.59	100.18	100.02	100.20	99.11	99.80	99.93	99.87	99.18	100.16
Cations	Si	1.935	1.935	1.939	1.947	1.932	1.930	1.928	1.926	1.931	1.958	1.961	1.960	1.957	1.958	1.958
	Ti	0.001	0.001	0.001	0.001	0.002	0.002	0.001	0.002	0.001	0.001	0.001	0.001	0.001	0.001	0.001
	Cr	0.023	0.020	0.021	0.017	0.025	0.025	0.025	0.024	0.025	0.017	0.018	0.018	0.020	0.020	0.019
	Al	0.114	0.111	0.112	0.099	0.100	0.103	0.123	0.111	0.109	0.067	0.074	0.078	0.081	0.082	0.083
	Fe2+	0.053	0.055	0.058	0.056	0.059	0.063	0.058	0.050	0.061	0.052	0.049	0.062	0.058	0.052	0.056
	Mn	0.002	0.002	0.001	0.003	0.003	0.002	0.003	0.003	0.001	b.d.	0.001	0.002	b.d.	b.d.	0.001
	Ni	0.000	0.001	b.d.	b.d.	0.002	0.001	b.d.	0.000	0.001	0.001	0.001	0.003	0.001	0.001	0.003
	Mg	0.924	0.945	0.931	0.937	0.951	0.952	0.926	0.928	0.951	0.955	0.947	0.940	0.939	0.956	0.947
	Ca	0.941	0.928	0.930	0.933	0.927	0.926	0.931	0.958	0.919	0.948	0.938	0.928	0.933	0.919	0.920
	Na	0.002	0.002	0.001	0.002	0.004	0.003	0.003	0.004	0.003	0.001	0.003	b.d.	0.001	0.002	0.003
	K	0.000	b.d.	b.d.	b.d.	b.d.	b.d.	0.001	0.001	b.d.	b.d.	0.000	0.000	0.001	0.001	b.d.
	Sum	3.996	4.000	3.994	3.995	4.005	4.006	3.999	4.007	4.002	4.000	3.994	3.992	3.992	3.992	3.992
	Mg #	0.946	0.945	0.941	0.943	0.942	0.938	0.941	0.949	0.940	0.948	0.951	0.938	0.942	0.948	0.945

Abbreviations: Cpx = clinopyroxene, Spl hrz = spinel harzburgite, Cl core = clast core, b.d. = below detection limit.
Mg# calculated as (MgO/40.3) / (MgO/40.3 + FeO/71.85).

Major element composition of clinopyroxene from the Dramala spinel harzburgite and plagioclase-bearing harzburgite continued

Sample		PIA91	PIA91	PIA91	PIA91	PIA91	PIA91	PIA91	PIA91	PIA91	PIA91	PIA91	PIA91	PIA91	PIA91	PIA91
Rock		Spl hrz	Spl hrz	Spl hrz	Spl hrz	Spl hrz	Spl hrz	Spl hrz	Spl hrz	Spl hrz	Spl hrz	Spl hrz	Spl hrz	Spl hrz	Spl hrz	Spl hrz
Mineral		Cpx	Cpx	Cpx	Cpx	Cpx	Cpx	Cpx	Cpx	Cpx	Cpx	Cpx	Cpx	Cpx	Cpx	Cpx
Type		Cl core	Cl core	Cl core	Cl core	Cl core	Cl core	Cl core	Cl core	Cl core	Cl core	Cl core	Cl core	Cl core	Cl core	Cl core
Wt.%	SiO2	53.99	54.08	53.91	54.06	54.13	53.71	54.30	53.93	54.41	54.32	54.16	54.42	54.23	54.57	54.35
	TiO2	0.02	0.03	0.02	0.01	0.06	0.03	0.03	0.04	0.02	0.04	0.02	0.01	0.04	0.03	0.04
	Cr2O3	0.68	0.73	0.72	0.70	0.67	0.71	0.69	0.55	0.31	0.44	0.34	0.38	0.39	0.44	0.32
	Al2O3	1.85	1.86	1.91	1.81	1.87	1.88	1.83	1.58	1.28	1.42	1.23	1.25	1.26	1.38	1.23
	FeO	1.79	1.93	1.73	1.62	1.69	1.75	1.86	1.69	1.46	1.75	1.80	1.68	1.82	1.63	1.75
	MnO	0.04	0.02	0.02	0.06	0.07	b.d.	b.d.	b.d.	0.03	0.03	0.05	0.05	0.03	0.07	0.04
	NiO	0.10	b.d.	0.09	0.07	0.10	0.13	0.11	0.13	0.04	0.03	0.02	0.05	0.10	0.13	0.20
	MgO	17.47	17.90	17.47	17.44	17.41	17.42	17.52	17.60	17.62	17.70	17.89	17.80	17.82	17.80	17.71
	CaO	23.92	23.44	23.77	23.83	23.99	23.80	24.00	23.73	24.25	24.00	23.89	23.93	23.80	24.06	24.11
	Na2O	0.03	0.02	0.07	0.01	0.05	0.06	0.03	0.04	0.06	b.d.	0.01	0.01	b.d.	0.06	0.03
	K2O	0.01	0.01	0.01	0.01	0.01	b.d.	0.01	b.d.	b.d.	b.d.	b.d.	b.d.	b.d.	b.d.	b.d.
	Total	99.91	100.01	99.71	99.64	100.07	99.48	100.39	99.29	99.48	99.73	99.41	99.59	99.48	100.18	99.77
Cations	Si	1.958	1.957	1.958	1.964	1.960	1.957	1.960	1.966	1.978	1.971	1.972	1.977	1.973	1.972	1.974
	Ti	0.001	0.001	0.001	0.000	0.002	0.001	0.001	0.001	0.001	0.001	0.000	0.000	0.001	0.001	0.001
	Cr	0.020	0.021	0.021	0.020	0.019	0.020	0.020	0.016	0.009	0.013	0.010	0.011	0.011	0.013	0.009
	Al	0.079	0.079	0.082	0.078	0.080	0.081	0.078	0.068	0.055	0.061	0.053	0.053	0.054	0.059	0.053
	Fe2+	0.054	0.058	0.053	0.049	0.051	0.053	0.056	0.052	0.044	0.053	0.055	0.051	0.055	0.049	0.053
	Mn	0.001	0.001	0.001	0.002	0.002	b.d.	b.d.	b.d.	0.001	0.001	0.002	0.002	0.001	0.002	0.001
	Ni	0.003	b.d.	0.003	0.002	0.003	0.004	0.003	0.004	0.001	0.001	0.001	0.002	0.003	0.004	0.006
	Mg	0.944	0.966	0.946	0.944	0.939	0.946	0.943	0.956	0.955	0.957	0.971	0.964	0.966	0.959	0.959
	Ca	0.930	0.909	0.925	0.927	0.930	0.929	0.928	0.927	0.944	0.933	0.932	0.931	0.928	0.931	0.938
	Na	0.002	0.002	0.005	0.001	0.004	0.004	0.002	0.003	0.004	b.d.	0.001	0.001	b.d.	0.004	0.002
	K	0.000	0.000	0.000	0.000	0.001	b.d.	0.000	b.d.	b.d.	b.d.	b.d.	b.d.	b.d.	b.d.	b.d.
	Sum	3.993	3.993	3.993	3.988	3.991	3.994	3.991	3.992	3.992	3.991	3.996	3.991	3.993	3.994	3.995
	Mg #	0.946	0.943	0.947	0.950	0.948	0.947	0.944	0.949	0.956	0.947	0.947	0.950	0.946	0.951	0.947

Abbreviations: Cpx = clinopyroxene, Spl hrz = spinel harzburgite, Cl core = clast core, b.d. = below detection limit.
Mg# calculated as (MgO/40.3) / (MgO/40.3 + FeO/71.85).

Major element composition of clinopyroxene from the Dramala spinel harzburgite and plagioclase-bearing harzburgite continued

Sample		PIA91	PIA91	PIA91	PIA91	PIA91	PIA91	PIA27	PIA27	PIA27	PIA27	PIA27	PI6	PI6	PI6	PI6
Rock		Spl hrz	Spl hrz	Spl hrz	Spl hrz	Spl hrz	Spl hrz	Spl hrz	Spl hrz	Spl hrz	Spl hrz	Spl hrz	Spl hrz	Spl hrz	Spl hrz	Spl hrz
Mineral		Cpx	Cpx	Cpx	Cpx	Cpx	Cpx	Cpx	Cpx	Cpx	Cpx	Cpx	Cpx	Cpx	Cpx	Cpx
Type		Cl core	Cl core	Cl rim	Cl rim	Cl rim	Cl rim	Cl core	Cl core	Cl core	Cl core	Cl core	Cl core	Cl core	Cl core	Cl core
Wt.%	SiO2	54.34	54.76	54.34	54.57	54.30	55.00	53.97	53.61	53.76	53.98	53.79	54.29	53.98	54.12	53.86
	TiO2	0.03	0.01	0.02	0.03	0.01	0.03	0.02	0.06	0.04	b.d.	b.d.	0.04	0.03	0.02	0.04
	Cr2O3	0.24	0.17	0.38	0.22	0.21	0.12	1.27	1.16	1.18	1.23	1.40	0.80	0.84	0.85	0.88
	Al2O3	1.13	0.85	1.34	1.00	0.88	0.66	2.00	2.13	1.99	2.11	2.24	1.34	1.40	1.41	1.44
	FeO	1.67	1.57	1.45	1.54	1.62	1.62	1.99	1.89	1.71	1.96	1.99	1.63	1.76	1.86	1.79
	MnO	0.05	0.07	0.13	0.02	0.05	0.10	b.d.	b.d.	0.04	0.08	b.d.	0.04	0.10	0.07	0.03
	NiO	b.d.	0.05	0.12	0.05	0.08	0.09	b.d.	0.01	b.d.	0.07	0.11	0.02	0.02	0.05	0.05
	MgO	17.81	18.05	17.63	17.90	17.87	18.11	17.51	17.45	17.28	17.40	17.41	17.70	17.62	17.58	17.47
	CaO	24.13	24.37	24.24	24.06	24.22	24.16	23.16	23.02	23.65	22.99	22.99	24.80	24.91	24.84	24.68
	Na2O	0.02	0.05	0.03	0.01	0.02	0.02	0.30	0.31	0.27	0.31	0.34	0.09	0.05	0.09	0.08
	K2O	0.01	b.d.	0.01	0.01	b.d.	b.d.	b.d.	b.d.	b.d.	0.01	b.d.	b.d.	0.01	0.01	b.d.
	Total	99.42	99.96	99.69	99.41	99.26	99.91	100.23	99.63	99.93	100.13	100.27	100.75	100.72	100.90	100.32
Cations	Si	1.978	1.983	1.973	1.984	1.981	1.991	1.952	1.949	1.951	1.954	1.946	1.957	1.950	1.952	1.953
	Ti	0.001	0.000	0.001	0.001	0.000	0.001	0.001	0.002	0.001	b.d.	b.d.	0.001	0.001	0.001	0.001
	Cr	0.007	0.005	0.011	0.006	0.006	0.004	0.036	0.033	0.034	0.035	0.040	0.023	0.024	0.024	0.025
	Al	0.048	0.036	0.057	0.043	0.038	0.028	0.085	0.091	0.085	0.090	0.095	0.057	0.060	0.060	0.062
	Fe2+	0.051	0.048	0.044	0.047	0.049	0.049	0.060	0.057	0.052	0.059	0.060	0.049	0.053	0.056	0.054
	Mn	0.001	0.002	0.004	0.001	0.001	0.003	b.d.	b.d.	0.001	0.002	b.d.	0.001	0.003	0.002	0.001
	Ni	b.d.	0.001	0.004	0.001	0.002	0.003	b.d.	0.000	b.d.	0.002	0.003	0.001	0.001	0.001	0.001
	Mg	0.966	0.974	0.954	0.970	0.972	0.977	0.944	0.946	0.935	0.939	0.939	0.951	0.949	0.945	0.944
	Ca	0.941	0.945	0.943	0.937	0.947	0.937	0.898	0.897	0.920	0.892	0.891	0.958	0.964	0.960	0.959
	Na	0.001	0.004	0.002	0.001	0.001	0.001	0.021	0.022	0.019	0.021	0.024	0.006	0.004	0.006	0.006
	K	0.000	b.d.	0.000	0.000	b.d.	b.d.	b.d.	b.d.	b.d.	0.000	b.d.	b.d.	0.000	0.000	b.d.
	Sum	3.994	3.998	3.993	3.991	3.998	3.993	3.997	3.998	3.998	3.995	3.999	4.005	4.009	4.009	4.006
	Mg #	0.950	0.953	0.956	0.954	0.952	0.952	0.940	0.943	0.947	0.941	0.940	0.951	0.947	0.944	0.946

Abbreviations: Cpx = clinopyroxene, Spl hrz = spinel harzburgite, Cl core = clast core, Cl rim = clast rim, b.d. = below detection limit.
Mg# calculated as (MgO/40.3) / (MgO/40.3 + FeO/71.85).

Major element composition of clinopyroxene from the Dramala spinel harzburgite and plagioclase-bearing harzburgite continued

Sample		PI6	PI6	PI6	PI6	PI6	PI6	PI6	PI6	PI6	PI6	PI6	PI6	PI6	PI6	PI6
Rock		Spl hrz	Spl hrz	Spl hrz	Spl hrz	Spl hrz	Spl hrz	Spl hrz	Spl hrz	Spl hrz	Spl hrz	Spl hrz	Spl hrz	Spl hrz	Spl hrz	Spl hrz
Mineral		Cpx	Cpx	Cpx	Cpx	Cpx	Cpx	Cpx	Cpx	Cpx	Cpx	Cpx	Cpx	Cpx	Cpx	Cpx
Type		Cl core	Cl core	Cl core	Cl core	Cl core	Cl core	Cl core	Cl core	Cl core	Cl core	Cl core	Cl core	Cl core	Cl core	Cl core
Wt.%	SiO2	53.98	53.97	54.05	53.87	53.74	54.00	53.63	53.86	54.06	54.14	53.57	53.86	54.09	54.07	54.10
	TiO2	0.03	0.01	0.01	0.02	0.01	b.d.	b.d.	b.d.	0.03	b.d.	0.02	0.02	b.d.	0.03	b.d.
	Cr2O3	0.85	0.81	0.83	0.86	0.94	0.84	0.86	0.88	0.84	0.78	0.85	0.82	0.84	0.74	0.68
	Al2O3	1.42	1.40	1.40	1.43	1.47	1.42	1.56	1.41	1.41	1.30	1.44	1.35	1.36	1.31	1.21
	FeO	1.66	1.75	1.69	1.89	1.88	1.70	1.61	1.68	1.62	1.80	1.83	1.74	1.72	1.73	1.54
	MnO	0.09	0.04	0.08	b.d.	0.03	0.05	0.15	0.09	0.06	0.11	0.05	0.09	0.09	b.d.	b.d.
	NiO	0.03	0.03	0.05	0.01	0.01	0.05	0.02	b.d.	b.d.	0.06	0.08	0.02	0.04	0.05	0.02
	MgO	17.58	17.52	17.52	17.53	17.46	17.56	17.42	17.52	17.51	18.02	17.47	17.53	17.58	17.50	17.63
	CaO	24.76	24.69	24.53	24.75	24.60	24.66	24.47	24.53	24.73	24.32	24.62	24.64	24.73	24.82	24.67
	Na2O	0.06	0.08	0.05	0.08	0.08	0.08	0.07	0.09	0.08	0.04	0.09	0.08	0.07	0.05	0.05
	K2O	b.d.	0.01	b.d.	b.d.	0.03	b.d.	b.d.	b.d.	0.01	0.01	b.d.	b.d.	b.d.	b.d.	b.d.
	Total	100.46	100.31	100.21	100.44	100.25	100.36	99.79	100.06	100.35	100.58	100.02	100.15	100.52	100.30	99.90
Cations	Si	1.953	1.956	1.959	1.951	1.951	1.956	1.953	1.956	1.957	1.956	1.950	1.955	1.956	1.959	1.965
	Ti	0.001	0.000	0.000	0.001	0.000	b.d.	b.d.	b.d.	0.001	b.d.	0.001	0.001	b.d.	0.001	b.d.
	Cr	0.024	0.023	0.024	0.025	0.027	0.024	0.025	0.025	0.024	0.022	0.024	0.024	0.024	0.021	0.020
	Al	0.061	0.060	0.060	0.061	0.063	0.061	0.067	0.060	0.060	0.055	0.062	0.058	0.058	0.056	0.052
	Fe2+	0.050	0.053	0.051	0.057	0.057	0.051	0.049	0.051	0.049	0.054	0.056	0.053	0.052	0.052	0.047
	Mn	0.003	0.001	0.002	b.d.	0.001	0.002	0.005	0.003	0.002	0.003	0.002	0.003	0.003	b.d.	b.d.
	Ni	0.001	0.001	0.001	0.000	0.000	0.001	0.001	b.d.	b.d.	0.002	0.002	0.001	0.001	0.001	0.001
	Mg	0.948	0.946	0.946	0.946	0.945	0.948	0.945	0.948	0.945	0.970	0.948	0.949	0.948	0.945	0.954
	Ca	0.960	0.959	0.953	0.961	0.957	0.957	0.955	0.954	0.959	0.941	0.960	0.958	0.958	0.963	0.960
	Na	0.004	0.006	0.004	0.006	0.006	0.006	0.005	0.006	0.006	0.003	0.006	0.006	0.005	0.004	0.004
	K	b.d.	0.000	b.d.	b.d.	0.001	b.d.	b.d.	b.d.	0.000	0.000	b.d.	b.d.	b.d.	b.d.	b.d.
	Sum	4.005	4.005	4.001	4.008	4.008	4.005	4.004	4.004	4.003	4.007	4.010	4.006	4.005	4.003	4.001
	Mg #	0.950	0.947	0.949	0.943	0.943	0.948	0.951	0.949	0.951	0.947	0.944	0.947	0.948	0.947	0.953

Abbreviations: Cpx = clinopyroxene, Spl hrz = spinel harzburgite, Cl core = clast core, b.d. = below detection limit.
Mg# calculated as (MgO/40.3) / (MgO/40.3 + FeO/71.85).

Major element composition of clinopyroxene from the Dramala spinel harzburgite and plagioclase-bearing harzburgite continued

Sample		PI6	PI6	PI6	PI6	PI6	PI6	PI6	PIA44	PIA44	PIA44	PIA44	PIA44	PIA44	PIA44	PIA44
Rock		Spl hrz	Spl hrz	Spl hrz	Spl hrz	Spl hrz	Spl hrz	Spl hrz	Spl hrz	Spl hrz	Spl hrz	Spl hrz	Spl hrz	Spl hrz	Spl hrz	Spl hrz
Mineral		Cpx	Cpx	Cpx	Cpx	Cpx	Cpx	Cpx	Cpx	Cpx	Cpx	Cpx	Cpx	Cpx	Cpx	Cpx
Type		Cl core	Cl core	Cl core	Cl rim	Cl rim	Cl rim	Cl rim	Cl core	Cl core	Cl core	Cl core	Cl core	Cl core	Cl core	Cl core
Wt.%	SiO2	54.35	54.26	54.26	54.26	54.07	54.30	54.29	53.26	53.32	53.15	53.01	53.06	52.99	53.17	53.37
	TiO2	0.03	0.01	0.03	b.d.	0.02	b.d.	0.05	0.03	b.d.	0.01	b.d.	b.d.	0.05	0.03	0.01
	Cr2O3	0.69	0.62	0.55	0.72	0.77	0.51	0.42	0.97	0.34	0.91	0.79	1.13	0.94	0.20	0.36
	Al2O3	1.19	1.13	1.09	1.28	1.34	0.97	1.02	2.26	2.28	2.33	2.30	2.31	2.35	2.20	1.94
	FeO	1.65	1.55	1.46	1.71	1.78	1.44	1.59	2.22	2.39	2.43	2.30	2.30	2.17	2.14	2.07
	MnO	0.11	0.07	0.04	0.11	0.03	0.05	0.09	0.05	b.d.	b.d.	0.04	b.d.	0.04	0.02	0.04
	NiO	0.02	0.04	0.03	0.10	0.05	b.d.	0.03	0.03	b.d.	b.d.	0.03	0.08	b.d.	b.d.	0.05
	MgO	17.54	17.60	17.68	17.66	17.64	17.80	17.80	17.98	17.91	18.01	18.00	18.00	18.05	17.87	17.88
	CaO	24.67	24.92	24.94	24.74	24.74	24.90	24.86	23.38	23.25	23.28	23.08	23.17	23.22	23.37	23.81
	Na2O	0.04	0.07	0.07	0.07	0.07	0.06	0.03	0.02	0.01	0.02	0.02	0.03	0.02	b.d.	0.02
	K2O	0.01	b.d.	0.01	b.d.	b.d.	0.01	0.02	b.d.	b.d.	b.d.	0.01	b.d.	b.d.	0.01	0.01
	Total	100.30	100.27	100.16	100.65	100.51	100.04	100.20	100.18	99.50	100.13	99.57	100.07	99.83	99.02	99.57
Cations	Si	1.967	1.965	1.966	1.960	1.956	1.969	1.967	1.931	1.943	1.929	1.933	1.927	1.927	1.945	1.945
	Ti	0.001	0.000	0.001	b.d.	0.001	b.d.	0.001	0.001	b.d.	0.000	b.d.	b.d.	0.001	0.001	0.000
	Cr	0.020	0.018	0.016	0.021	0.022	0.015	0.012	0.028	0.010	0.026	0.023	0.032	0.027	0.006	0.010
	Al	0.051	0.048	0.047	0.054	0.057	0.041	0.044	0.097	0.098	0.099	0.099	0.099	0.101	0.095	0.083
	Fe2+	0.050	0.047	0.044	0.052	0.054	0.044	0.048	0.067	0.073	0.074	0.070	0.070	0.066	0.066	0.063
	Mn	0.003	0.002	0.001	0.003	0.001	0.002	0.003	0.001	b.d.	b.d.	0.001	b.d.	0.001	0.001	0.001
	Ni	0.001	0.001	0.001	0.003	0.001	b.d.	0.001	0.001	b.d.	b.d.	0.001	0.002	b.d.	b.d.	0.002
	Mg	0.946	0.950	0.955	0.951	0.951	0.962	0.961	0.971	0.973	0.974	0.978	0.975	0.979	0.975	0.972
	Ca	0.957	0.967	0.968	0.957	0.959	0.967	0.965	0.908	0.907	0.905	0.902	0.901	0.905	0.916	0.930
	Na	0.003	0.005	0.005	0.005	0.005	0.004	0.002	0.001	0.001	0.001	0.001	0.002	0.002	b.d.	0.001
	K	0.000	b.d.	0.000	b.d.	b.d.	0.000	0.001	b.d.	b.d.	b.d.	0.000	b.d.	b.d.	0.000	0.001
	Sum	3.998	4.004	4.004	4.005	4.006	4.005	4.005	4.007	4.004	4.009	4.007	4.008	4.009	4.004	4.009
	Mg #	0.950	0.953	0.956	0.948	0.946	0.957	0.952	0.935	0.930	0.930	0.933	0.933	0.937	0.937	0.939

Abbreviations: Cpx = clinopyroxene, Spl hrz = spinel harzburgite, Cl core = clast core, b.d. = below detection limit.
Mg# calculated as (MgO/40.3) / (MgO/40.3 + FeO/71.85).

Major element composition of clinopyroxene from the Dramala spinel harzburgite and plagioclase-bearing harzburgite continued

Sample		PIA44	PIA44	PIA44	PIA44	PIA44	PIA120	PIA120	PIA120	PIA120	PIA120	PIA120	PIA120	PIA120	PIA120	PIA120
Rock		Spl hrz	Spl hrz	Spl hrz	Spl hrz	Spl hrz	Pl-b hrz	Pl-b hrz	Pl-b hrz	Pl-b hrz	Pl-b hrz	Pl-b hrz	Pl-b hrz	Pl-b hrz	Pl-b hrz	Pl-b hrz
Mineral		Cpx	Cpx	Cpx	Cpx	Cpx	Cpx	Cpx	Cpx	Cpx	Cpx	Cpx	Cpx	Cpx	Cpx	Cpx
Type		Cl core	Cl core	Cl core	Cl core	Cl core	Ex Opx	Ex Opx	Ex Opx	Ex Opx	Ex Opx	Ex Opx	Ex Opx	Melt r	Melt r	Melt r
Wt.%	SiO2	53.47	53.51	53.27	53.79	53.37	52.31	52.68	52.30	52.48	51.88	52.04	52.03	52.83	52.86	52.52
	TiO2	0.02	0.02	0.02	0.03	0.03	0.59	0.62	0.61	0.62	0.65	0.61	0.71	0.42	0.45	0.46
	Cr2O3	0.84	0.70	0.35	0.56	0.81	1.20	1.21	1.18	1.16	1.24	1.20	1.21	0.71	0.84	0.87
	Al2O3	1.67	1.73	1.97	1.71	2.04	3.73	3.78	3.80	3.77	4.06	3.94	4.08	3.14	3.12	3.50
	FeO	2.01	1.95	1.82	1.86	2.14	2.34	2.45	2.45	2.48	2.28	2.40	2.18	2.51	2.66	2.48
	MnO	0.02	0.06	0.04	b.d.	0.09	0.05	0.07	0.08	0.09	0.07	0.03	0.08	0.10	0.05	0.10
	NiO	b.d.	0.12	0.05	0.07	0.03	0.03	b.d.	0.01	0.01	0.05	0.04	0.04	0.05	0.04	0.07
	MgO	18.54	17.57	17.24	17.50	18.09	16.08	16.08	15.89	16.16	15.87	16.02	16.00	16.71	16.46	16.48
	CaO	23.15	24.89	24.75	24.77	23.31	23.71	23.59	23.44	23.64	23.82	23.71	23.64	23.19	23.43	23.56
	Na2O	0.07	0.05	0.03	0.05	0.05	0.44	0.44	0.45	0.46	0.47	0.47	0.47	0.37	0.40	0.40
	K2O	0.02	0.01	b.d.	0.01	b.d.	0.02	0.01	b.d.	b.d.	b.d.	b.d.	0.02	0.01	0.01	0.01
	Total	99.80	100.61	99.54	100.35	99.96	100.50	100.93	100.21	100.87	100.39	100.46	100.46	100.04	100.32	100.45
Cations	Si	1.943	1.938	1.945	1.949	1.938	1.898	1.902	1.902	1.897	1.886	1.890	1.888	1.921	1.919	1.906
	Ti	0.001	0.000	0.001	0.001	0.001	0.016	0.017	0.017	0.017	0.018	0.017	0.019	0.011	0.012	0.013
	Cr	0.024	0.020	0.010	0.016	0.023	0.034	0.035	0.034	0.033	0.036	0.034	0.035	0.020	0.024	0.025
	Al	0.071	0.074	0.085	0.073	0.087	0.160	0.161	0.163	0.161	0.174	0.169	0.175	0.135	0.134	0.150
	Fe2+	0.061	0.059	0.056	0.056	0.065	0.071	0.074	0.075	0.075	0.069	0.073	0.066	0.076	0.081	0.075
	Mn	0.001	0.002	0.001	b.d.	0.003	0.002	0.002	0.002	0.003	0.002	0.001	0.002	0.003	0.002	0.003
	Ni	b.d.	0.003	0.001	0.002	0.001	0.001	b.d.	0.000	0.000	0.001	0.001	0.001	0.001	0.001	0.002
	Mg	1.004	0.949	0.939	0.945	0.979	0.870	0.865	0.861	0.871	0.860	0.867	0.865	0.906	0.891	0.891
	Ca	0.901	0.966	0.968	0.961	0.907	0.922	0.912	0.913	0.916	0.928	0.923	0.919	0.903	0.911	0.916
	Na	0.005	0.004	0.002	0.004	0.004	0.031	0.031	0.032	0.032	0.033	0.033	0.033	0.026	0.028	0.028
	K	0.001	0.000	b.d.	0.000	b.d.	0.001	0.000	b.d.	b.d.	b.d.	b.d.	0.001	0.000	0.000	0.000
	Sum	4.012	4.016	4.008	4.008	4.008	4.005	3.999	3.999	4.005	4.008	4.008	4.005	4.003	4.004	4.009
	Mg #	0.943	0.941	0.944	0.944	0.938	0.925	0.921	0.920	0.921	0.925	0.922	0.929	0.922	0.917	0.922

Abbreviations: Cpx = clinopyroxene, Spl hrz = spinel harzburgite, Pl-b hrz = plagioclase-bearing harzburgite, Cl core = clast core, Ex Opx = exsolution lamellae in Opx, Melt r = melt related, b.d. = below detection limit. Mg# calculated as (MgO/40.3) / (MgO/40.3 + FeO/71.85).

Major element composition of clinopyroxene from the Dramala spinel harzburgite and plagioclase-bearing harzburgite continued

Sample		PIA120	PIA120	PIA120	PIA120	PIA120	PIA120	PIA120	PIA120	PIA120	PIA120	PIA120	PIA120	PIA120	PIA120	PIA120
Rock		Pl-b hrz	Pl-b hrz	Pl-b hrz	Pl-b hrz	Pl-b hrz	Pl-b hrz	Pl-b hrz	Pl-b hrz	Pl-b hrz	Pl-b hrz	Pl-b hrz	Pl-b hrz	Pl-b hrz	Pl-b hrz	Pl-b hrz
Mineral		Cpx	Cpx	Cpx	Cpx	Cpx	Cpx	Cpx	Cpx	Cpx	Cpx	Cpx	Cpx	Cpx	Cpx	Cpx
Type		Melt r	Melt r	Melt r	Cl core	Cl core	Cl core	Cl core	Cl core	Cl core	Cl core	Cl core	Cl core	Cl core	Cl core	Cl rim
Wt.%	SiO2	52.76	53.44	52.89	52.57	53.26	52.90	52.60	52.97	51.26	51.38	51.95	51.70	51.70	52.20	53.83
	TiO2	0.29	0.38	0.39	0.46	0.48	0.33	0.48	0.41	0.51	0.46	0.41	0.44	0.46	0.41	0.22
	Cr2O3	0.61	0.59	0.78	0.90	0.98	0.63	1.17	0.88	1.36	1.26	1.14	1.12	1.10	0.84	0.43
	Al2O3	2.65	2.67	2.83	3.50	3.33	2.72	3.79	3.46	4.07	3.94	3.54	3.58	3.47	3.21	2.10
	FeO	2.25	2.58	2.36	2.37	2.50	3.21	2.57	2.73	2.68	2.54	2.76	2.74	2.55	2.73	2.46
	MnO	0.06	0.04	0.05	0.07	0.10	0.07	0.08	0.10	0.09	0.07	0.13	0.11	0.12	0.08	0.10
	NiO	0.01	0.05	0.04	0.03	0.07	0.05	0.06	0.08	0.02	0.02	0.06	0.03	0.06	0.04	0.03
	MgO	16.95	16.86	16.66	16.34	16.45	17.48	16.13	16.64	15.91	15.93	16.37	17.18	16.25	16.88	17.28
	CaO	23.59	23.63	23.52	23.63	23.38	22.14	23.05	22.64	23.05	23.00	22.96	22.57	23.24	22.34	23.98
	Na2O	0.31	0.37	0.37	0.43	0.40	0.34	0.44	0.44	0.48	0.56	0.44	0.43	0.46	0.41	0.30
	K2O	b.d.	0.02	b.d.	0.01	0.01	0.01	b.d.	0.01	0.01	0.03	0.01	b.d.	b.d.	0.01	b.d.
	Total	99.48	100.63	99.89	100.31	100.96	99.88	100.37	100.36	99.44	99.19	99.77	99.90	99.41	99.15	100.73
Cations	Si	1.929	1.932	1.926	1.909	1.919	1.927	1.908	1.919	1.883	1.891	1.900	1.888	1.899	1.915	1.944
	Ti	0.008	0.010	0.011	0.013	0.013	0.009	0.013	0.011	0.014	0.013	0.011	0.012	0.013	0.011	0.006
	Cr	0.018	0.017	0.022	0.026	0.028	0.018	0.034	0.025	0.040	0.037	0.033	0.032	0.032	0.024	0.012
	Al	0.114	0.114	0.122	0.150	0.141	0.117	0.162	0.148	0.176	0.171	0.153	0.154	0.150	0.139	0.089
	Fe2+	0.069	0.078	0.072	0.072	0.075	0.098	0.078	0.083	0.082	0.078	0.084	0.084	0.078	0.084	0.074
	Mn	0.002	0.001	0.002	0.002	0.003	0.002	0.002	0.003	0.003	0.002	0.004	0.003	0.004	0.002	0.003
	Ni	0.000	0.001	0.001	0.001	0.002	0.001	0.002	0.002	0.001	0.001	0.002	0.001	0.002	0.001	0.001
	Mg	0.923	0.909	0.904	0.884	0.884	0.949	0.872	0.898	0.871	0.874	0.893	0.935	0.889	0.923	0.930
	Ca	0.924	0.915	0.918	0.919	0.903	0.864	0.896	0.879	0.907	0.907	0.900	0.883	0.914	0.878	0.928
	Na	0.022	0.026	0.026	0.030	0.028	0.024	0.031	0.031	0.034	0.040	0.031	0.030	0.033	0.029	0.021
	K	b.d.	0.001	b.d.	0.000	0.000	0.000	b.d.	0.000	0.000	0.001	0.000	b.d.	b.d.	0.000	b.d.
	Sum	4.009	4.005	4.004	4.006	3.997	4.009	3.997	3.999	4.012	4.014	4.011	4.022	4.014	4.007	4.009
	Mg #	0.931	0.921	0.926	0.925	0.921	0.907	0.918	0.916	0.914	0.918	0.914	0.918	0.919	0.917	0.926

Abbreviations: Cpx = clinopyroxene, Pl-b hrz = plagioclase-bearing harzburgite, Cl core = clast core, Cl rim = clast rim,
Melt r = melt related, b.d. = below detection limit. Mg# calculated as (MgO/40.3) / (MgO/40.3 + FeO/71.85).

Major element composition of clinopyroxene from the Dramala spinel spinel harzburgite and plagioclase-bearing harzburgite continued

Sample		PIA120	PIA109	PIA109	PIA109
Rock		Pl-b hrz	Pl-b hrz	Pl-b hrz	Pl-b hrz
Mineral		Cpx	Cpx	Cpx	Cpx
Type		Cl rim	Melt r	Melt r	Cl rim
Wt.%	SiO2	53.68	53.67	52.93	53.16
	TiO2	0.37	0.17	0.26	0.32
	Cr2O3	0.79	0.34	0.61	0.92
	Al2O3	2.82	2.60	3.31	2.72
	FeO	2.27	2.66	2.76	2.40
	MnO	0.06	0.01	0.02	0.07
	NiO	0.08	b.d.	b.d.	0.09
	MgO	16.83	17.18	17.01	17.17
	CaO	23.59	23.92	23.09	23.78
	Na2O	0.38	0.30	0.36	0.36
	K2O	b.d.	b.d.	0.02	b.d.
	Total	100.87	100.85	100.37	100.99
Cations	Si	1.934	1.936	1.918	1.918
	Ti	0.010	0.005	0.007	0.009
	Cr	0.022	0.010	0.017	0.026
	Al	0.120	0.111	0.141	0.116
	Fe2+	0.068	0.080	0.084	0.072
	Mn	0.002	0.000	0.001	0.002
	Ni	0.002	b.d.	b.d.	0.003
	Mg	0.904	0.924	0.919	0.924
	Ca	0.910	0.924	0.896	0.919
	Na	0.027	0.021	0.025	0.025
	K	b.d.	b.d.	0.001	b.d.
	Sum	3.999	4.010	4.009	4.014
	Mg #	0.930	0.920	0.916	0.927

Abbreviations: Cpx = clinopyroxene, Pl-bear hrz = plagioclase-bearing harzburgite, Cl rim = clast rim, Melt r = melt related, b.d. = below detection limit.
Mg# calculated as (MgO/40.3) / (MgO/40.3 + FeO/71.85).

Major element composition of spinel from the Dramala spinel harzburgite and plagioclase-bearing harzburgite

Sample		PI2	PI2	PI2	PI2	PI2	PI2	PI2	PI2	PI2	PI2	PI2	PI2	PI2	PI2	PI2	PI2
Rock		Spl hrz	Spl hrz	Spl hrz	Spl hrz	Spl hrz	Spl hrz	Spl hrz	Spl hrz	Spl hrz	Spl hrz	Spl hrz	Spl hrz	Spl hrz	Spl hrz	Spl hrz	Spl hrz
Mineral		Spl	Spl	Spl	Spl	Spl	Spl	Spl	Spl	Spl	Spl	Spl	Spl	Spl	Spl	Spl	Spl
Type		Cl core	Cl core	Cl core	Cl core	Cl core	Cl core	Cl core	Cl core	Cl core	Cl core	Cl core	Cl core	Cl core	Cl core	Cl core	Cl core
Wt.%	SiO2	0.03	0.02	b.d.	0.01	0.01	0.04	0.02	0.04	0.01	b.d.	0.02	b.d.	0.02	b.d.	0.01	0.02
	TiO2	0.05	0.02	0.00	0.06	b.d.	0.06	0.03	0.05	0.03	0.06	0.04	0.03	0.05	0.06	0.07	0.05
	Cr2O3	34.25	33.63	34.13	34.08	33.69	33.93	33.97	33.76	34.09	34.54	34.23	34.35	34.61	34.24	34.58	34.30
	Al2O3	34.41	35.15	35.77	35.65	35.30	35.21	34.99	34.96	35.05	35.07	34.88	34.83	34.93	34.82	34.58	34.53
	Fe2O3	1.47	1.46	0.93	1.12	1.24	0.79	1.16	1.34	1.32	0.85	0.98	1.28	0.93	1.52	0.58	1.32
	FeO	12.82	13.11	13.55	13.50	13.25	13.59	13.72	13.35	13.31	13.44	13.42	13.35	13.78	13.39	13.46	13.37
	MnO	0.15	0.13	0.08	0.10	b.d.	0.06	0.09	0.05	0.14	0.09	0.10	0.05	0.06	0.16	0.15	0.08
	NiO	0.16	0.11	0.15	0.18	0.19	0.16	0.15	0.15	0.10	0.14	0.17	0.13	0.14	0.14	0.13	0.19
	ZnO	0.12	0.21	0.19	0.14	0.14	0.08	0.14	0.21	0.21	0.13	0.12	0.20	0.20	0.19	0.22	0.17
	MgO	15.73	15.64	15.57	15.61	15.54	15.42	15.24	15.33	15.50	15.45	15.45	15.55	15.36	15.45	15.26	15.36
	CaO	b.d.	b.d.	0.01	b.d.	0.03	b.d.	b.d.	b.d.	0.01	b.d.	b.d.	b.d.	b.d.	0.02	b.d.	b.d.
	Na2O	b.d.	b.d.	0.01	0.02	0.01	0.01	0.01	0.05	0.02	0.03	b.d.	b.d.	b.d.	0.01	b.d.	0.02
	K2O	b.d.	b.d.	0.00	0.01	0.01	b.d.	0.01	0.01	b.d.	0.01	b.d.	b.d.	b.d.	0.01	b.d.	b.d.
	Total	99.18	99.48	100.39	100.48	99.40	99.35	99.53	99.30	99.79	99.81	99.41	99.77	100.08	100.01	99.04	99.41
Cations	Si	0.001	0.001	b.d.	0.000	0.000	0.001	0.001	0.001	0.000	b.d.	0.001	b.d.	0.001	b.d.	0.000	0.001
	Ti	0.001	0.000	0.000	0.001	b.d.	0.001	0.001	0.001	0.001	0.001	0.001	0.001	0.001	0.001	0.002	0.001
	Cr	0.786	0.769	0.773	0.771	0.770	0.777	0.778	0.774	0.778	0.788	0.784	0.785	0.789	0.781	0.796	0.787
	Al	1.178	1.198	1.208	1.203	1.203	1.202	1.195	1.195	1.193	1.193	1.191	1.186	1.187	1.184	1.187	1.182
	Fe3+	0.032	0.032	0.020	0.024	0.027	0.017	0.025	0.029	0.029	0.018	0.021	0.028	0.020	0.033	0.013	0.029
	Fe2+	0.311	0.317	0.324	0.323	0.320	0.329	0.332	0.324	0.321	0.324	0.325	0.322	0.332	0.323	0.328	0.325
	Mn	0.004	0.003	0.002	0.002	b.d.	0.001	0.002	0.001	0.003	0.002	0.002	0.001	0.001	0.004	0.004	0.002
	Ni	0.004	0.003	0.003	0.004	0.004	0.004	0.003	0.003	0.002	0.003	0.004	0.003	0.003	0.003	0.003	0.004
	Zn	0.003	0.004	0.004	0.003	0.003	0.002	0.003	0.004	0.004	0.003	0.003	0.004	0.004	0.004	0.005	0.004
	Mg	0.681	0.674	0.665	0.666	0.670	0.665	0.658	0.663	0.667	0.665	0.667	0.670	0.660	0.664	0.663	0.665
	Ca	b.d.	b.d.	0.000	b.d.	0.001	b.d.	b.d.	b.d.	0.000	b.d.	b.d.	b.d.	b.d.	0.001	b.d.	b.d.
	Na	b.d.	b.d.	0.001	0.001	0.001	0.001	0.001	0.003	0.001	0.002	b.d.	b.d.	b.d.	0.001	b.d.	0.001
	K	b.d.	b.d.	0.000	0.000	0.000	b.d.	0.000	0.000	b.d.	0.000	b.d.	b.d.	b.d.	0.000	b.d.	b.d.
	Mg #	0.686	0.680	0.672	0.673	0.677	0.669	0.664	0.672	0.675	0.672	0.672	0.675	0.665	0.673	0.669	0.672
FeCr2O4 (Chromit)		0.122	0.122	0.125	0.124	0.123	0.128	0.129	0.125	0.125	0.128	0.127	0.126	0.131	0.126	0.130	0.128

Abbreviations: Spl = spinel, Spl hrz = spinel harzburgite, Cl core = clast core, b.d. = below detection limit. Mg# calculated as (MgO/40.3) / (MgO/40.3 + FeO/71.85).

Major element composition of spinel from the Dramala spinel harzburgite and plagioclase-bearing harzburgite continued

Sample		PI2	PI2	PI2	PI2	PI2	PI2	PI2	PI2	PI2	PI2	PI2	PI2	PI2	PI2	PI2	PI2
Rock		Spl hrz	Spl hrz	Spl hrz	Spl hrz	Spl hrz	Spl hrz	Spl hrz	Spl hrz	Spl hrz	Spl hrz	Spl hrz	Spl hrz	Spl hrz	Spl hrz	Spl hrz	Spl hrz
Mineral		Spl	Spl	Spl	Spl	Spl	Spl	Spl	Spl	Spl	Spl	Spl	Spl	Spl	Spl	Spl	Spl
Type		Cl core	Cl core	Cl core	Cl core	Cl core	Cl core	Cl core	Cl core	Cl core	Cl core	Cl core	Cl core	Cl core	Cl core	Cl core	Cl core
Wt.%	SiO2	b.d.	0.02	0.02	0.02	0.02	0.01	0.01	0.01	0.05	0.04	b.d.	b.d.	0.01	0.02	0.01	b.d.
	TiO2	0.02	0.02	0.08	0.07	0.06	0.04	0.03	0.05	0.04	0.06	0.03	0.02	0.04	0.03	0.02	0.03
	Cr2O3	34.39	34.88	34.68	34.53	34.55	34.12	34.64	35.19	34.62	35.43	34.56	34.61	35.33	35.00	34.30	34.61
	Al2O3	34.75	34.56	34.59	34.51	34.64	34.76	34.48	34.41	34.45	34.43	34.41	34.35	34.40	34.39	34.54	34.49
	Fe2O3	1.16	1.18	1.09	1.49	0.89	1.12	0.92	0.55	0.87	0.70	1.85	1.14	0.94	1.10	1.49	1.47
	FeO	13.25	13.37	13.66	13.17	13.47	13.37	13.44	13.51	13.29	13.51	13.07	13.37	13.23	13.23	13.27	13.16
	MnO	0.14	0.08	0.22	0.13	0.11	0.07	0.09	0.01	0.17	0.13	0.03	0.18	0.08	0.18	0.08	0.13
	NiO	0.14	0.15	0.18	0.16	0.13	0.10	0.13	0.16	0.11	0.14	0.10	0.15	0.11	0.11	0.13	0.12
	ZnO	0.20	0.12	0.10	0.29	0.16	0.13	0.18	0.13	0.11	0.11	0.12	0.17	0.12	0.14	0.07	0.22
	MgO	15.42	15.46	15.29	15.50	15.38	15.42	15.29	15.34	15.40	15.42	15.70	15.30	15.67	15.42	15.46	15.45
	CaO	0.05	0.02	b.d.	b.d.	b.d.	0.01	b.d.	b.d.	b.d.	b.d.	0.03	b.d.	0.01	b.d.	b.d.	0.01
	Na2O	0.01	0.03	0.01	0.02	b.d.	b.d.	0.01	0.02	0.02	0.03	0.02	b.d.	b.d.	0.03	0.02	0.04
	K2O	b.d.	b.d.	b.d.	0.01	0.01	0.02	0.01	b.d.	b.d.	b.d.	0.01	b.d.	b.d.	0.02	0.02	b.d.
	Total	99.53	99.89	99.92	99.90	99.42	99.18	99.23	99.38	99.13	100.00	99.93	99.29	99.95	99.67	99.42	99.74
Cations	Si	b.d.	0.001	0.001	0.001	0.001	0.000	0.000	0.000	0.001	0.001	b.d.	b.d.	0.000	0.001	0.000	b.d.
	Ti	0.000	0.000	0.002	0.002	0.001	0.001	0.001	0.001	0.001	0.001	0.001	0.000	0.001	0.001	0.000	0.001
	Cr	0.788	0.797	0.793	0.789	0.793	0.784	0.797	0.808	0.796	0.809	0.789	0.796	0.806	0.802	0.787	0.792
	Al	1.187	1.177	1.179	1.176	1.185	1.190	1.182	1.178	1.181	1.172	1.171	1.178	1.171	1.174	1.181	1.177
	Fe3+	0.025	0.026	0.024	0.032	0.019	0.025	0.020	0.012	0.019	0.015	0.040	0.025	0.021	0.024	0.033	0.032
	Fe2+	0.321	0.323	0.330	0.318	0.327	0.325	0.327	0.328	0.323	0.326	0.316	0.325	0.319	0.321	0.322	0.319
	Mn	0.003	0.002	0.005	0.003	0.003	0.002	0.002	0.000	0.004	0.003	0.001	0.004	0.002	0.004	0.002	0.003
	Ni	0.003	0.003	0.004	0.004	0.003	0.002	0.003	0.004	0.003	0.003	0.002	0.004	0.003	0.003	0.003	0.003
	Zn	0.004	0.003	0.002	0.006	0.003	0.003	0.004	0.003	0.002	0.002	0.003	0.004	0.003	0.003	0.001	0.005
	Mg	0.666	0.666	0.659	0.668	0.665	0.668	0.663	0.664	0.668	0.664	0.676	0.664	0.674	0.666	0.668	0.667
	Ca	0.002	0.001	b.d.	b.d.	b.d.	0.000	b.d.	b.d.	b.d.	b.d.	0.001	b.d.	0.000	b.d.	b.d.	0.000
	Na	0.001	0.002	0.001	0.001	b.d.	b.d.	0.001	0.001	0.001	0.002	0.001	b.d.	b.d.	0.002	0.001	0.002
	K	b.d.	b.d.	b.d.	0.000	0.000	0.001	0.000	b.d.	b.d.	b.d.	0.000	b.d.	b.d.	0.001	0.001	b.d.
	Mg #	0.675	0.673	0.666	0.677	0.671	0.673	0.670	0.669	0.674	0.670	0.682	0.671	0.679	0.675	0.675	0.677
FeCr2O4	(Chromit)	0.126	0.129	0.131	0.125	0.129	0.127	0.130	0.132	0.129	0.132	0.124	0.129	0.129	0.128	0.127	0.126

Abbreviations: Spl = spinel, Spl hrz = spinel harzburgite, Cl core = clast core, b.d. = below detection limit. Mg# calculated as (MgO/40.3) / (MgO/40.3 + FeO/71.85).

Major element composition of spinel from the Dramala spinel harzburgite and plagioclase-bearing harzburgite continued

Sample		PI2	PI2	PI2	PI2	PI2	PI2	PI2	PI2	PI2	PI2	PI2	PI2	PI2	PI2	PI2	PI2
Rock		Spl hrz	Spl hrz	Spl hrz	Spl hrz	Spl hrz	Spl hrz	Spl hrz	Spl hrz	Spl hrz	Spl hrz	Spl hrz	Spl hrz	Spl hrz	Spl hrz	Spl hrz	Spl hrz
Mineral		Spl	Spl	Spl	Spl	Spl	Spl	Spl	Spl	Spl	Spl	Spl	Spl	Spl	Spl	Spl	Spl
Type		Cl core	Cl core	Cl core	Cl core	Cl core	Cl core	Cl core	Cl core	Cl core	Cl core	Cl core	Cl core	Cl core	Cl core	Cl core	Cl core
Wt.%	SiO2	b.d.	0.04	0.04	0.04	0.05	0.02	0.02	0.04	b.d.	0.01	0.01	0.02	0.05	0.05	0.02	b.d.
	TiO2	0.05	0.04	0.04	0.06	0.01	b.d.	0.06	0.02	0.06	b.d.	0.04	0.03	0.05	0.04	0.04	0.04
	Cr2O3	34.65	34.82	34.79	35.06	34.69	35.25	34.87	34.46	34.22	35.01	34.56	35.01	35.18	35.24	35.04	35.33
	Al2O3	34.42	34.17	34.41	34.28	34.56	34.37	34.30	34.34	34.35	34.26	34.35	34.24	34.45	34.38	34.28	34.28
	Fe2O3	1.59	0.94	0.66	0.97	0.84	0.93	0.64	1.34	1.63	1.01	1.41	1.11	0.66	1.18	1.46	0.75
	FeO	13.36	13.47	13.47	13.31	13.47	13.34	13.41	13.45	13.21	13.44	13.23	13.24	13.58	13.66	13.27	13.36
	MnO	0.04	0.04	0.07	0.08	0.06	0.08	0.06	0.10	0.10	0.01	0.09	0.07	0.14	0.07	0.15	0.08
	NiO	0.13	0.12	0.17	0.12	0.14	0.16	0.10	0.19	0.19	0.11	0.13	0.13	0.10	0.11	0.15	0.11
	ZnO	0.20	0.17	0.09	0.17	0.17	0.18	0.21	0.18	0.15	0.15	0.20	0.23	0.23	0.19	0.15	0.23
	MgO	15.48	15.31	15.29	15.52	15.35	15.39	15.30	15.33	15.45	15.42	15.48	15.42	15.31	15.35	15.57	15.40
	CaO	b.d.	0.01	0.01	b.d.	0.02	0.01	b.d.	0.01	b.d.	b.d.	b.d.	b.d.	0.01	b.d.	0.01	0.01
	Na2O	0.02	0.01	0.02	0.01	b.d.	0.03	b.d.	b.d.	0.01	b.d.	0.01	0.02	0.01	0.03	b.d.	0.01
	K2O	0.01	b.d.	b.d.	b.d.	0.02	b.d.	0.02	b.d.	b.d.	b.d.	b.d.	0.01	0.01	0.02	0.01	b.d.
	Total	99.94	99.14	99.06	99.61	99.38	99.76	99.00	99.46	99.37	99.42	99.51	99.53	99.77	100.32	100.15	99.60
Cations	Si	b.d.	0.001	0.001	0.001	0.001	0.001	0.001	0.001	b.d.	0.000	0.000	0.001	0.001	0.001	0.001	b.d.
	Ti	0.001	0.001	0.001	0.001	0.000	b.d.	0.001	0.000	0.001	b.d.	0.001	0.001	0.001	0.001	0.001	0.001
	Cr	0.792	0.802	0.801	0.803	0.796	0.807	0.804	0.791	0.786	0.804	0.793	0.803	0.806	0.803	0.800	0.810
	Al	1.173	1.174	1.181	1.171	1.183	1.173	1.179	1.176	1.176	1.173	1.175	1.171	1.176	1.169	1.166	1.172
	Fe3+	0.035	0.021	0.015	0.021	0.018	0.020	0.014	0.029	0.036	0.022	0.031	0.024	0.014	0.026	0.032	0.016
	Fe2+	0.323	0.328	0.328	0.322	0.327	0.323	0.327	0.327	0.321	0.327	0.321	0.321	0.329	0.329	0.320	0.324
	Mn	0.001	0.001	0.002	0.002	0.001	0.002	0.001	0.002	0.002	0.000	0.002	0.002	0.003	0.002	0.004	0.002
	Ni	0.003	0.003	0.004	0.003	0.003	0.004	0.002	0.004	0.004	0.003	0.003	0.003	0.002	0.003	0.003	0.003
	Zn	0.004	0.004	0.002	0.004	0.004	0.004	0.005	0.004	0.003	0.003	0.004	0.005	0.005	0.004	0.003	0.005
	Mg	0.667	0.665	0.664	0.670	0.664	0.664	0.665	0.664	0.669	0.668	0.669	0.667	0.661	0.660	0.670	0.666
	Ca	b.d.	0.000	0.000	b.d.	0.001	0.000	b.d.	0.000	b.d.	b.d.	b.d.	b.d.	0.000	b.d.	0.000	0.000
	Na	0.001	0.001	0.001	0.001	b.d.	0.002	b.d.	b.d.	0.001	b.d.	0.001	0.001	0.001	0.002	b.d.	0.001
	K	0.000	b.d.	b.d.	b.d.	0.001	b.d.	0.001	b.d.	b.d.	b.d.	b.d.	0.000	0.000	0.001	0.000	b.d.
	Mg #	0.674	0.670	0.669	0.675	0.670	0.673	0.670	0.670	0.676	0.672	0.676	0.675	0.668	0.667	0.677	0.673
FeCr2O4	(Chromit)	0.128	0.132	0.131	0.129	0.130	0.130	0.131	0.129	0.126	0.131	0.127	0.129	0.132	0.132	0.128	0.131

Abbreviations: Spl = spinel, Spl hrz = spinel harzburgite, Cl core = clast core, b.d. = below detection limit. Mg# calculated as (MgO/40.3) / (MgO/40.3 + FeO/71.85).

Major element composition of spinel from the Dramala spinel harzburgite and plagioclase-bearing harzburgite continued

Sample		PI2	PI2	PI2	PI2	PI2	PI2	PI2	PI2	PI2	PI2	PI2	PI2	PI2	PI2	PI2	PI2
Rock		Spl hrz	Spl hrz	Spl hrz	Spl hrz	Spl hrz	Spl hrz	Spl hrz	Spl hrz	Spl hrz	Spl hrz	Spl hrz	Spl hrz	Spl hrz	Spl hrz	Spl hrz	Spl hrz
Mineral		Spl	Spl	Spl	Spl	Spl	Spl	Spl	Spl	Spl	Spl	Spl	Spl	Spl	Spl	Spl	Spl
Type		Cl core	Cl core	Cl core	Cl core	Cl core	Cl core	Cl core	Cl core	Cl core	Cl core	Cl core	Cl core	Cl core	Cl core	Cl core	Cl core
Wt.%	SiO2	0.01	0.03	0.02	0.03	0.02	b.d.	0.03	b.d.	0.04	0.04	b.d.	0.03	0.05	0.06	0.04	0.01
	TiO2	0.01	0.06	0.04	0.06	0.05	0.04	0.04	0.05	b.d.	0.02	0.05	0.05	b.d.	0.01	0.07	0.05
	Cr2O3	34.82	34.33	35.06	35.27	35.09	34.47	35.07	35.25	34.75	34.28	35.54	34.69	34.66	35.06	34.26	35.30
	Al2O3	34.17	34.38	34.22	34.21	34.37	34.38	34.43	34.31	34.38	34.29	34.52	34.44	34.61	34.47	34.27	34.70
	Fe2O3	1.97	1.11	0.88	0.64	1.07	1.19	0.72	0.95	1.38	1.58	0.59	1.26	1.21	0.80	1.35	0.76
	FeO	13.00	13.19	13.39	13.45	13.32	13.24	13.51	13.65	13.21	13.34	13.87	13.51	13.48	13.54	13.24	13.87
	MnO	0.15	0.10	0.09	0.10	0.04	0.01	0.09	0.13	0.11	0.12	0.05	0.06	0.10	0.12	0.09	0.10
	NiO	0.14	0.16	0.15	0.18	0.12	0.09	0.11	0.12	0.13	0.16	0.11	0.17	0.12	0.12	0.16	0.08
	ZnO	0.14	0.20	0.27	0.09	0.16	0.23	0.11	0.20	0.14	0.25	0.16	0.14	0.21	0.14	0.26	0.17
	MgO	15.63	15.44	15.30	15.37	15.54	15.37	15.43	15.31	15.48	15.27	15.33	15.42	15.43	15.42	15.40	15.33
	CaO	0.02	b.d.	b.d.	b.d.	b.d.	b.d.	b.d.	b.d.	b.d.	0.02	b.d.	b.d.	b.d.	b.d.	0.01	b.d.
	Na2O	0.03	b.d.	b.d.	0.01	0.02	0.02	b.d.	b.d.	0.03	0.01	b.d.	0.01	0.01	b.d.	b.d.	b.d.
	K2O	b.d.	b.d.	0.02	b.d.	b.d.	0.02	b.d.	b.d.	0.01	0.02	b.d.	b.d.	b.d.	b.d.	b.d.	0.02
	Total	100.09	99.00	99.44	99.41	99.80	99.06	99.54	99.97	99.66	99.40	100.22	99.78	99.88	99.74	99.15	100.39
Cations	Si	0.000	0.001	0.001	0.001	0.001	b.d.	0.001	b.d.	0.001	0.001	b.d.	0.001	0.001	0.002	0.001	0.000
	Ti	0.000	0.001	0.001	0.001	0.001	0.001	0.001	0.001	b.d.	0.000	0.001	0.001	b.d.	0.000	0.002	0.001
	Cr	0.795	0.791	0.806	0.810	0.803	0.794	0.804	0.807	0.796	0.788	0.811	0.794	0.792	0.802	0.789	0.804
	Al	1.163	1.181	1.173	1.172	1.172	1.180	1.177	1.171	1.174	1.175	1.174	1.175	1.179	1.176	1.176	1.178
	Fe3+	0.043	0.024	0.019	0.014	0.023	0.026	0.016	0.021	0.030	0.035	0.013	0.027	0.026	0.017	0.030	0.016
	Fe2+	0.314	0.321	0.325	0.327	0.322	0.323	0.328	0.330	0.320	0.324	0.335	0.327	0.326	0.328	0.322	0.334
	Mn	0.004	0.002	0.002	0.002	0.001	0.000	0.002	0.003	0.003	0.003	0.001	0.001	0.002	0.003	0.002	0.002
	Ni	0.003	0.004	0.004	0.004	0.003	0.002	0.003	0.003	0.003	0.004	0.003	0.004	0.003	0.003	0.004	0.002
	Zn	0.003	0.004	0.006	0.002	0.003	0.005	0.002	0.004	0.003	0.005	0.003	0.003	0.004	0.003	0.006	0.004
	Mg	0.673	0.670	0.663	0.666	0.670	0.667	0.667	0.660	0.668	0.662	0.659	0.665	0.665	0.665	0.668	0.658
	Ca	0.001	b.d.	b.d.	b.d.	b.d.	b.d.	b.d.	b.d.	b.d.	0.001	b.d.	b.d.	b.d.	b.d.	0.000	b.d.
	Na	0.002	b.d.	b.d.	0.001	0.001	0.001	b.d.	b.d.	0.002	0.001	b.d.	0.001	0.001	b.d.	b.d.	b.d.
	K	b.d.	b.d.	0.001	b.d.	b.d.	0.001	b.d.	b.d.	0.000	0.001	b.d.	b.d.	b.d.	b.d.	b.d.	0.001
	Mg #	0.682	0.676	0.671	0.671	0.675	0.674	0.671	0.667	0.676	0.671	0.663	0.670	0.671	0.670	0.675	0.663
FeCr2O4 (Chromit)		0.125	0.127	0.131	0.132	0.129	0.128	0.132	0.133	0.127	0.128	0.135	0.130	0.129	0.131	0.127	0.134

Abbreviations: Spl = spinel, Spl hrz = spinel harzburgite, Cl core = clast core, b.d. = below detection limit. Mg# calculated as (MgO/40.3) / (MgO/40.3 + FeO/71.85).

Major element composition of spinel from the Dramala spinel harzburgite and plagioclase-bearing harzburgite continued

Sample		PI2	PI2	PI2	PI2	PI2	PI2	PI2	PI2	PI2	PI2	PI2	PI2	PI2	PI2	PI2	PI2
Rock		Spl hrz	Spl hrz	Spl hrz	Spl hrz	Spl hrz	Spl hrz	Spl hrz	Spl hrz	Spl hrz	Spl hrz	Spl hrz	Spl hrz	Spl hrz	Spl hrz	Spl hrz	Spl hrz
Mineral		Spl	Spl	Spl	Spl	Spl	Spl	Spl	Spl	Spl	Spl	Spl	Spl	Spl	Spl	Spl	Spl
Type		Cl core	Cl core	Cl core	Cl core	Cl core	Cl core	Cl core	Cl core	Cl core	Cl core	Cl core	Cl core	Cl core	Cl core	Cl core	Cl core
Wt.%	SiO2	0.01	0.02	b.d.	0.05	b.d.	0.03	b.d.	0.03	0.01	b.d.	0.02	0.04	0.03	0.02	0.02	0.06
	TiO2	0.04	0.05	0.06	0.05	0.03	0.07	0.05	0.07	0.01	0.03	0.05	0.04	0.05	0.01	0.05	0.01
	Cr2O3	34.71	34.87	33.92	34.95	35.28	34.29	33.48	34.76	34.12	34.45	33.94	34.05	34.32	28.47	34.43	33.19
	Al2O3	34.62	34.61	34.44	34.66	34.71	34.69	34.73	34.67	35.01	35.02	35.16	35.30	34.41	40.06	34.90	35.62
	Fe2O3	1.26	1.14	1.58	1.31	0.88	1.46	1.80	0.64	1.23	0.87	0.84	1.01	1.38	1.32	1.35	0.80
	FeO	13.36	13.82	13.14	13.67	13.79	13.39	13.02	13.80	13.33	13.36	13.59	13.66	12.72	13.10	13.20	13.79
	MnO	0.07	0.07	0.08	0.09	0.15	0.17	0.10	0.04	0.03	0.12	0.15	0.10	0.19	0.06	0.14	0.04
	NiO	0.13	0.12	0.18	0.17	0.17	0.18	0.11	0.09	0.14	0.18	0.11	0.15	0.12	0.09	0.16	0.12
	ZnO	0.17	0.11	0.14	0.16	0.20	0.17	0.20	0.20	0.19	0.26	0.11	0.17	0.18	0.12	0.08	0.17
	MgO	15.51	15.39	15.44	15.52	15.28	15.49	15.53	15.25	15.50	15.34	15.34	15.32	15.75	16.15	15.74	15.24
	CaO	b.d.	b.d.	b.d.	0.02	0.01	0.02	b.d.	0.02	0.01	0.01	b.d.	b.d.	b.d.	0.03	b.d.	b.d.
	Na2O	0.02	b.d.	0.01	b.d.	0.01	b.d.	0.02	b.d.	0.01	0.03	0.01	0.04	b.d.	0.03	b.d.	0.01
	K2O	b.d.	b.d.	0.01	b.d.	b.d.	b.d.	b.d.	0.01	0.01	b.d.	b.d.	b.d.	b.d.	b.d.	b.d.	b.d.
	Total	99.90	100.20	99.00	100.65	100.51	99.96	99.04	99.58	99.60	99.67	99.32	99.88	99.15	99.46	100.07	99.05
Cations	Si	0.000	0.001	b.d.	0.001	b.d.	0.001	b.d.	0.001	0.000	b.d.	0.001	0.001	0.001	0.001	0.001	0.002
	Ti	0.001	0.001	0.001	0.001	0.001	0.002	0.001	0.002	0.000	0.001	0.001	0.001	0.001	0.000	0.001	0.000
	Cr	0.793	0.795	0.781	0.793	0.803	0.783	0.770	0.797	0.780	0.788	0.778	0.776	0.788	0.637	0.783	0.761
	Al	1.179	1.177	1.182	1.173	1.178	1.181	1.190	1.185	1.193	1.194	1.201	1.200	1.178	1.335	1.184	1.218
	Fe3+	0.027	0.025	0.035	0.028	0.019	0.032	0.039	0.014	0.027	0.019	0.018	0.022	0.030	0.028	0.029	0.017
	Fe2+	0.323	0.333	0.320	0.328	0.332	0.323	0.317	0.335	0.322	0.323	0.329	0.329	0.309	0.310	0.318	0.334
	Mn	0.002	0.002	0.002	0.002	0.004	0.004	0.002	0.001	0.001	0.003	0.004	0.002	0.005	0.001	0.003	0.001
	Ni	0.003	0.003	0.004	0.004	0.004	0.004	0.003	0.002	0.003	0.004	0.003	0.003	0.003	0.002	0.004	0.003
	Zn	0.004	0.002	0.003	0.003	0.004	0.004	0.004	0.004	0.004	0.006	0.002	0.004	0.004	0.003	0.002	0.004
	Mg	0.668	0.662	0.670	0.664	0.655	0.667	0.673	0.659	0.668	0.661	0.663	0.659	0.682	0.681	0.675	0.659
	Ca	b.d.	b.d.	b.d.	0.001	0.000	0.001	b.d.	0.001	0.000	0.000	b.d.	b.d.	b.d.	0.001	b.d.	b.d.
	Na	0.001	b.d.	0.001	b.d.	0.001	b.d.	0.001	b.d.	0.001	0.002	0.001	0.002	b.d.	0.002	b.d.	0.001
	K	b.d.	b.d.	0.000	b.d.	b.d.	b.d.	b.d.	0.000	0.000	b.d.	b.d.	b.d.	b.d.	b.d.	b.d.	b.d.
	Mg #	0.674	0.665	0.677	0.669	0.664	0.674	0.680	0.663	0.675	0.672	0.668	0.667	0.688	0.687	0.680	0.663
FeCr2O4 (Chromit)		0.128	0.132	0.125	0.130	0.133	0.126	0.122	0.133	0.126	0.127	0.128	0.128	0.121	0.099	0.124	0.127

Abbreviations: Spl = spinel, Spl hrz = spinel harzburgite, Cl core = clast core, b.d. = below detection limit. Mg# calculated as (MgO/40.3) / (MgO/40.3 + FeO/71.85).

Major element composition of spinel from the Dramala spinel harzburgite and plagioclase-bearing harzburgite continued

Sample		PI2	PI2	PI2	PI2	PI2	PI2	PI2	PI2	PI2	PI2	PI2	PI2	PI2	PI2	PI2	PI2
Rock		Spl hrz	Spl hrz	Spl hrz	Spl hrz	Spl hrz	Spl hrz	Spl hrz	Spl hrz	Spl hrz	Spl hrz	Spl hrz	Spl hrz	Spl hrz	Spl hrz	Spl hrz	Spl hrz
Mineral		Spl	Spl	Spl	Spl	Spl	Spl	Spl	Spl	Spl	Spl	Spl	Spl	Spl	Spl	Spl	Spl
Type		Cl core	Cl core	Cl core	Cl core	Cl core	Cl core	Cl core	Cl core	Cl core	Cl core	Cl core	Cl core	Cl core	Cl core	Cl core	Cl core
Wt.%	SiO2	0.02	0.03	0.01	0.03	b.d.	0.02	0.02	0.03	0.03	0.03	0.05	0.05	0.04	b.d.	0.04	0.03
	TiO2	b.d.	0.04	0.06	0.05	0.06	0.02	0.03	0.06	0.03	0.03	0.04	0.03	0.03	0.03	0.06	0.04
	Cr2O3	33.72	34.60	34.35	34.31	34.40	34.68	34.18	35.03	34.57	34.80	34.79	34.83	34.29	34.61	34.67	33.78
	Al2O3	35.42	35.31	34.91	35.15	34.82	34.95	34.58	34.71	34.78	35.01	34.93	35.07	34.75	35.05	34.96	34.88
	Fe2O3	0.78	0.66	0.48	0.43	0.52	0.75	1.10	0.46	0.78	0.59	0.67	0.59	0.92	1.24	0.27	1.15
	FeO	13.75	13.70	13.58	13.92	13.70	13.42	13.45	13.45	13.68	13.74	13.93	13.77	13.64	13.36	13.87	13.64
	MnO	0.05	0.11	0.12	0.11	b.d.	0.02	0.04	0.18	0.13	0.11	0.16	0.12	0.13	0.08	0.10	0.18
	NiO	0.13	0.18	0.15	0.18	0.18	0.18	0.12	0.14	0.14	0.17	0.18	0.15	0.14	0.12	0.16	0.17
	ZnO	0.15	0.19	0.17	0.16	0.23	0.19	0.22	0.17	0.15	0.18	0.16	0.14	0.24	0.20	0.12	0.17
	MgO	15.25	15.33	15.26	15.12	15.08	15.46	15.33	15.39	15.23	15.30	15.21	15.34	15.21	15.61	15.22	15.16
	CaO	0.01	b.d.	b.d.	0.01	0.01	b.d.	b.d.	0.02	0.01	0.01	b.d.	b.d.	b.d.	b.d.	b.d.	b.d.
	Na2O	0.01	0.03	b.d.	b.d.	0.03	0.02	b.d.	b.d.	0.01	0.01	b.d.	0.02	b.d.	0.02	b.d.	0.01
	K2O	b.d.	0.01	b.d.	0.01	b.d.	b.d.	b.d.	0.01	0.01	b.d.	0.01	b.d.	0.01	b.d.	b.d.	b.d.
	Total	99.29	100.19	99.09	99.48	99.03	99.71	99.08	99.65	99.55	99.99	100.14	100.11	99.40	100.32	99.47	99.21
Cations	Si	0.001	0.001	0.000	0.001	b.d.	0.001	0.001	0.001	0.001	0.001	0.001	0.001	0.001	b.d.	0.001	0.001
	Ti	b.d.	0.001	0.001	0.001	0.001	0.000	0.001	0.001	0.001	0.001	0.001	0.001	0.001	0.001	0.001	0.001
	Cr	0.772	0.787	0.790	0.786	0.792	0.792	0.787	0.802	0.792	0.794	0.793	0.793	0.787	0.786	0.795	0.776
	Al	1.210	1.197	1.197	1.201	1.196	1.190	1.187	1.184	1.189	1.191	1.188	1.191	1.189	1.187	1.195	1.195
	Fe3+	0.017	0.014	0.011	0.009	0.011	0.016	0.024	0.010	0.017	0.013	0.015	0.013	0.020	0.027	0.006	0.025
	Fe2+	0.333	0.329	0.330	0.337	0.334	0.324	0.328	0.326	0.332	0.332	0.336	0.332	0.331	0.321	0.336	0.332
	Mn	0.001	0.003	0.003	0.003	b.d.	0.000	0.001	0.004	0.003	0.003	0.004	0.003	0.003	0.002	0.002	0.004
	Ni	0.003	0.004	0.004	0.004	0.004	0.004	0.003	0.003	0.003	0.004	0.004	0.003	0.003	0.003	0.004	0.004
	Zn	0.003	0.004	0.004	0.003	0.005	0.004	0.005	0.004	0.003	0.004	0.003	0.003	0.005	0.004	0.003	0.004
	Mg	0.659	0.657	0.661	0.653	0.655	0.666	0.665	0.664	0.658	0.658	0.654	0.659	0.658	0.668	0.658	0.657
	Ca	0.000	b.d.	b.d.	0.000	0.000	b.d.	b.d.	0.001	0.000	0.000	b.d.	b.d.	b.d.	b.d.	b.d.	b.d.
	Na	0.001	0.002	b.d.	b.d.	0.002	0.001	b.d.	b.d.	0.001	0.001	b.d.	0.001	b.d.	0.001	b.d.	0.001
	K	b.d.	0.000	b.d.	0.000	b.d.	b.d.	b.d.	0.000	0.000	b.d.	0.000	b.d.	0.000	b.d.	b.d.	b.d.
	Mg #	0.664	0.666	0.667	0.659	0.662	0.673	0.670	0.671	0.665	0.665	0.661	0.665	0.665	0.676	0.662	0.665
FeCr2O4 (Chromit)		0.000	0.000	0.000	0.000	0.000	0.000	0.000	0.000	0.000	0.000	0.000	0.000	0.000	0.000	0.000	0.000

Abbreviations: Spl = spinel, Spl hrz = spinel harzburgite, Cl core = clast core, b.d. = below detection limit. Mg# calculated as (MgO/40.3) / (MgO/40.3 + FeO/71.85).

Major element composition of spinel from the Dramala spinel harzburgite and plagioclase-bearing harzburgite continued

Sample		PI2	PI2	PI2	PI2	PI2	PI2	PI2	PI2	PI2	PI2	PI2	PI2	PI2	PI2	PI2
Rock		Spl hrz	Spl hrz	Spl hrz	Spl hrz	Spl hrz	Spl hrz	Spl hrz	Spl hrz	Spl hrz	Spl hrz	Spl hrz	Spl hrz	Spl hrz	Spl hrz	Spl hrz
Mineral		Spl	Spl	Spl	Spl	Spl	Spl	Spl	Spl	Spl	Spl	Spl	Spl	Spl	Spl	Spl
Type		Cl core	Cl core	Cl core	Cl core	Cl core	Cl core	Cl core	Cl core	Cl core	Cl core	Cl core	Cl rim	Cl rim	Cl rim	Cl rim	Cl rim
Wt.%	SiO2	0.01	0.02	0.01	0.04	0.01	0.03	0.01	0.01	b.d.	0.01	0.01	0.05	b.d.	0.02	0.03	0.02
	TiO2	0.05	0.01	0.03	0.03	0.05	0.03	0.03	0.04	0.03	0.05	b.d.	0.05	b.d.	b.d.	0.03	0.03
	Cr2O3	34.62	34.24	34.56	33.47	33.99	33.54	32.78	31.89	31.48	31.65	32.02	32.90	33.25	31.70	33.48	33.78
	Al2O3	34.99	35.08	35.44	35.51	35.66	35.87	36.36	38.49	38.20	38.13	37.87	36.61	36.06	37.15	35.26	35.06
	Fe2O3	0.51	1.01	0.35	1.13	0.45	0.88	0.93	0.13	0.12	0.76	0.64	0.84	1.00	1.44	1.60	1.27
	FeO	14.08	13.65	13.87	13.38	13.91	13.72	13.39	13.07	13.12	12.95	12.84	13.55	13.20	11.87	12.98	12.90
	MnO	0.09	0.08	0.12	0.08	0.05	0.14	0.02	0.03	0.06	0.12	0.04	0.14	0.05	0.17	0.17	0.14
	NiO	0.16	0.13	0.16	0.11	0.10	0.10	0.12	0.10	0.13	0.15	0.10	0.12	0.11	0.21	0.16	0.06
	ZnO	0.12	0.18	0.15	0.19	0.15	0.13	0.19	0.22	0.20	0.22	0.13	0.17	0.15	0.14	0.17	0.15
	MgO	15.08	15.25	15.19	15.54	15.28	15.47	15.62	16.24	15.84	16.17	16.16	15.61	15.69	16.47	15.75	15.77
	CaO	b.d.	b.d.	0.02	b.d.	b.d.	0.01	0.02	0.02	0.02	b.d.	0.03	0.04	0.01	0.11	b.d.	0.01
	Na2O	0.01	0.02	0.03	b.d.	0.01	b.d.	0.01	b.d.	0.03	0.01	0.03	0.02	0.02	b.d.	b.d.	b.d.
	K2O	b.d.	0.03	b.d.	0.02	0.01	b.d.	b.d.	b.d.	b.d.	b.d.	0.01	b.d.	b.d.	b.d.	b.d.	b.d.
	Total	99.72	99.70	99.93	99.50	99.67	99.92	99.48	100.24	99.23	100.22	99.88	100.10	99.54	99.28	99.63	99.19
Cations	Si	0.000	0.001	0.000	0.001	0.000	0.001	0.000	0.000	b.d.	0.000	0.000	0.001	b.d.	0.001	0.001	0.001
	Ti	0.001	0.000	0.001	0.001	0.001	0.001	0.001	0.001	0.001	0.001	b.d.	0.001	b.d.	b.d.	0.001	0.001
	Cr	0.793	0.783	0.788	0.764	0.775	0.762	0.746	0.713	0.711	0.709	0.719	0.744	0.756	0.716	0.763	0.773
	Al	1.194	1.196	1.204	1.209	1.213	1.216	1.233	1.282	1.287	1.273	1.268	1.234	1.223	1.252	1.199	1.197
	Fe3+	0.011	0.022	0.008	0.025	0.010	0.019	0.020	0.003	0.003	0.016	0.014	0.018	0.022	0.031	0.035	0.028
	Fe2+	0.341	0.330	0.334	0.323	0.336	0.330	0.322	0.309	0.313	0.307	0.305	0.324	0.318	0.284	0.313	0.312
	Mn	0.002	0.002	0.003	0.002	0.001	0.003	0.000	0.001	0.001	0.003	0.001	0.003	0.001	0.004	0.004	0.003
	Ni	0.004	0.003	0.004	0.003	0.002	0.002	0.003	0.002	0.003	0.003	0.002	0.003	0.003	0.005	0.004	0.001
	Zn	0.003	0.004	0.003	0.004	0.003	0.003	0.004	0.005	0.004	0.005	0.003	0.004	0.003	0.003	0.004	0.003
	Mg	0.651	0.657	0.653	0.669	0.657	0.663	0.670	0.684	0.675	0.683	0.684	0.665	0.673	0.702	0.677	0.681
	Ca	b.d.	b.d.	0.001	b.d.	b.d.	0.000	0.001	0.001	0.001	b.d.	0.001	0.001	0.000	0.003	b.d.	0.000
	Na	0.001	0.001	0.002	b.d.	0.001	b.d.	0.001	b.d.	0.002	0.001	0.002	0.001	0.001	b.d.	b.d.	b.d.
	K	b.d.	0.001	b.d.	0.001	0.000	b.d.	b.d.	b.d.	b.d.	b.d.	0.000	b.d.	b.d.	b.d.	b.d.	b.d.
	Mg #	0.656	0.666	0.661	0.674	0.662	0.668	0.675	0.689	0.683	0.690	0.692	0.673	0.679	0.712	0.684	0.685
FeCr2O4 (Chromit)		0.000	0.000	0.000	0.000	0.000	0.000	0.000	0.000	0.000	0.000	0.000	0.120	0.120	0.102	0.119	0.121

Abbreviations: Spl = spinel, Spl hrz = spinel harzburgite, Cl core = clast core, Cl rim = clast rim, b.d. = below detection limit.
Mg# calculated as (MgO/40.3) / (MgO/40.3 + FeO/71.85).

Major element composition of spinel from the Dramala spinel harzburgite and plagioclase-bearing harzburgite continued

Sample		PI2	PI2	PI2	PI2	PI2	PI2	PI2	PI2	PI2	PI2	PI2	PI2	PI2	PI2	PI2	PIA91
Rock		Spl hrz	Spl hrz	Spl hrz	Spl hrz	Spl hrz	Spl hrz	Spl hrz	Spl hrz	Spl hrz	Spl hrz	Spl hrz	Spl hrz	Spl hrz	Spl hrz	Spl hrz	Spl hrz
Mineral		Spl	Spl	Spl	Spl	Spl	Spl	Spl	Spl	Spl	Spl	Spl	Spl	Spl	Spl	Spl	Spl
Type		Cl rim	Cl rim	Cl rim	Cl rim	Cl rim	Cl rim	Cl rim	Cl rim	Cl rim	Cl rim	Blast	Blast	Blast	Blast	Blast	Cl core
Wt.%	SiO2	0.03	0.04	0.03	0.01	0.02	0.02	0.03	0.02	0.03	0.03	0.08	0.03	0.02	0.03	0.03	0.03
	TiO2	0.03	b.d.	0.03	0.02	0.03	0.05	b.d.	0.05	0.01	0.04	0.03	0.02	0.04	0.03	0.01	0.02
	Cr2O3	31.06	33.78	33.64	32.73	32.24	34.41	32.13	32.23	31.34	38.69	24.02	26.38	25.51	24.01	26.30	43.77
	Al2O3	37.27	35.71	35.98	36.45	36.11	35.00	36.45	36.90	37.99	31.71	44.65	42.79	43.01	43.08	41.60	25.55
	Fe2O3	1.60	0.70	1.02	1.04	1.56	1.20	1.06	0.87	0.64	0.87	1.10	1.38	1.69	2.42	2.52	1.94
	FeO	13.00	13.43	13.59	13.36	13.26	13.03	13.44	13.34	13.29	13.19	12.25	12.38	12.66	12.54	12.74	13.99
	MnO	0.16	0.08	0.08	0.13	0.20	0.17	0.07	0.13	0.02	b.d.	0.49	0.53	0.52	0.49	0.55	0.84
	NiO	0.11	0.13	0.10	0.18	0.08	0.13	0.15	0.12	0.18	0.13	0.16	0.17	0.12	0.26	0.19	0.22
	ZnO	0.25	0.23	0.08	0.14	0.11	0.22	0.20	0.17	0.19	0.19	0.04	0.32	0.25	0.28	0.28	b.d.
	MgO	15.88	15.51	15.65	15.63	15.63	15.76	15.48	15.71	15.76	15.48	17.18	16.83	16.67	16.49	16.42	13.81
	CaO	b.d.	b.d.	0.04	b.d.	b.d.	b.d.	b.d.	b.d.	b.d.	b.d.	b.d.	b.d.	b.d.	b.d.	b.d.	0.01
	Na2O	b.d.	0.01	0.01	b.d.	b.d.	b.d.	b.d.	b.d.	0.04	0.01	b.d.	b.d.	b.d.	b.d.	b.d.	n.a.
	K2O	b.d.	b.d.	b.d.	0.01	b.d.	b.d.	b.d.	0.01	b.d.	0.01	b.d.	b.d.	b.d.	b.d.	b.d.	n.a.
	Total	99.39	99.62	100.25	99.70	99.24	99.99	99.01	99.55	99.49	100.36	100.01	100.83	100.48	99.62	100.64	100.19
Cations	Si	0.001	0.001	0.001	0.000	0.001	0.001	0.001	0.001	0.001	0.001	0.002	0.001	0.000	0.001	0.001	0.001
	Ti	0.001	b.d.	0.001	0.000	0.001	0.001	b.d.	0.001	0.000	0.001	0.001	0.000	0.001	0.001	0.000	0.001
	Cr	0.704	0.770	0.761	0.743	0.735	0.783	0.734	0.731	0.708	0.890	0.523	0.576	0.558	0.530	0.579	1.044
	Al	1.259	1.213	1.214	1.234	1.228	1.188	1.241	1.247	1.279	1.088	1.449	1.393	1.404	1.417	1.366	0.909
	Fe3+	0.034	0.015	0.022	0.022	0.034	0.026	0.023	0.019	0.014	0.019	0.023	0.029	0.035	0.051	0.053	0.044
	Fe2+	0.312	0.324	0.325	0.321	0.320	0.314	0.325	0.320	0.317	0.321	0.282	0.286	0.293	0.293	0.297	0.353
	Mn	0.004	0.002	0.002	0.003	0.005	0.004	0.002	0.003	0.000	b.d.	0.011	0.012	0.012	0.012	0.013	0.021
	Ni	0.003	0.003	0.002	0.004	0.002	0.003	0.003	0.003	0.004	0.003	0.004	0.004	0.003	0.006	0.004	0.005
	Zn	0.005	0.005	0.002	0.003	0.002	0.005	0.004	0.004	0.004	0.004	0.001	0.007	0.005	0.006	0.006	b.d.
	Mg	0.678	0.666	0.668	0.669	0.672	0.676	0.667	0.672	0.671	0.672	0.705	0.693	0.688	0.686	0.682	0.621
	Ca	b.d.	b.d.	0.001	b.d.	b.d.	b.d.	b.d.	b.d.	b.d.	b.d.	b.d.	b.d.	b.d.	b.d.	b.d.	0.000
	Na	b.d.	0.001	0.001	b.d.	b.d.	b.d.	b.d.	b.d.	0.002	0.001	b.d.	b.d.	b.d.	b.d.	b.d.	n.a.
	K	b.d.	b.d.	b.d.	0.000	b.d.	b.d.	b.d.	0.000	b.d.	0.000	b.d.	b.d.	b.d.	b.d.	b.d.	n.a.
	Mg #	0.685	0.673	0.672	0.676	0.678	0.683	0.672	0.677	0.679	0.677	0.714	0.708	0.701	0.701	0.697	0.638
FeCr2O4 (Chromit)		0.109	0.125	0.124	0.119	0.118	0.123	0.119	0.000	0.000	0.000	0.074	0.082	0.082	0.077	0.086	0.184

Abbreviations: Spl = spinel, Spl hrz = spinel harzburgite, Cl rim = clast rim, b.d. = below detection limit. Mg# calculated as (MgO/40.3) / (MgO/40.3 + FeO/71.85).

Major element composition of spinel from the Dramala spinel harzburgite and plagioclase-bearing harzburgite continued

Sample		PIA91	PIA91	PIA91	PIA91	PIA91	PIA91	PIA91	PIA91	PIA91	PIA27	PIA27	PIA27	PIA44	PIA44	PIA44	PIA44
Rock		Spl hrz	Spl hrz	Spl hrz	Spl hrz	Spl hrz	Spl hrz	Spl hrz	Spl hrz	Spl hrz	Spl hrz	Spl hrz	Spl hrz	Spl hrz	Spl hrz	Spl hrz	Spl hrz
Mineral		Spl	Spl	Spl	Spl	Spl	Spl	Spl	Spl	Spl	Spl	Spl	Spl	Spl	Spl	Spl	Spl
Type		Cl core	Cl core	Cl core	Cl rim	Cl rim	Cl rim	Blast	Blast	Blast	Cl core	Cl core	Cl rim	Cl core	Cl core	Cl core	Cl core
Wt.%	SiO2	0.04	0.03	0.03	0.04	0.13	0.01	0.04	0.05	0.06	0.08	0.06	0.06	0.01	0.05	0.03	0.03
	TiO2	0.02	0.07	0.04	0.03	0.03	0.02	0.03	b.d.	0.02	0.02	0.03	0.03	0.03	0.01	0.04	b.d.
	Cr2O3	43.70	43.64	43.20	37.57	29.70	38.24	32.37	28.69	35.70	43.47	44.99	41.42	43.86	44.28	44.46	44.83
	Al2O3	25.30	26.04	26.67	31.84	38.73	30.34	35.69	38.76	32.61	24.18	23.20	25.45	24.43	24.58	24.48	24.30
	Fe2O3	2.59	1.65	1.61	1.55	0.41	1.97	1.28	1.45	1.48	2.58	2.67	2.21	2.96	2.61	2.55	2.80
	FeO	13.30	13.66	13.93	13.22	14.56	14.04	14.20	14.50	14.21	14.73	13.98	17.81	14.76	14.81	14.50	14.37
	MnO	0.83	0.85	0.80	0.76	0.62	0.75	0.65	0.60	0.72	0.80	0.81	0.86	0.86	0.80	0.84	0.86
	NiO	0.13	0.12	0.07	0.08	0.06	0.07	0.16	0.19	0.03	0.09	0.09	0.15	0.07	0.04	0.12	0.13
	ZnO	0.10	0.13	0.17	0.30	0.28	0.29	0.11	0.20	0.19	0.18	0.29	0.45	0.10	0.02	0.02	0.09
	MgO	14.26	14.12	14.09	14.99	14.79	14.17	14.58	14.54	14.34	13.01	13.40	10.93	13.22	13.40	13.51	13.57
	CaO	0.01	b.d.	0.01	b.d.	0.04	0.02	0.07	0.22	0.01	b.d.	b.d.	b.d.	0.01	b.d.	b.d.	b.d.
	Na2O	n.a.	n.a.	n.a.	n.a.	n.a.	n.a.	n.a.	n.a.	n.a.	n.a.	n.a.	n.a.	n.a.	n.a.	n.a.	n.a.
	K2O	n.a.	n.a.	n.a.	n.a.	n.a.	n.a.	n.a.	n.a.	n.a.	n.a.	n.a.	n.a.	n.a.	n.a.	n.a.	n.a.
	Total	100.27	100.32	100.60	100.37	99.34	99.92	99.18	99.20	99.37	99.14	99.53	99.37	100.30	100.60	100.54	100.98
Cations	Si	0.001	0.001	0.001	0.001	0.004	0.000	0.001	0.002	0.002	0.002	0.002	0.002	0.000	0.002	0.001	0.001
	Ti	0.000	0.002	0.001	0.001	0.001	0.001	0.001	b.d.	0.000	0.000	0.001	0.001	0.001	0.000	0.001	b.d.
	Cr	1.040	1.036	1.021	0.867	0.673	0.895	0.744	0.652	0.831	1.058	1.093	1.014	1.055	1.060	1.064	1.070
	Al	0.898	0.922	0.940	1.095	1.309	1.059	1.224	1.313	1.132	0.877	0.840	0.929	0.876	0.877	0.874	0.865
	Fe3+	0.059	0.037	0.036	0.034	0.009	0.044	0.028	0.031	0.033	0.060	0.062	0.051	0.068	0.059	0.058	0.064
	Fe2+	0.335	0.343	0.348	0.323	0.349	0.348	0.345	0.348	0.350	0.379	0.359	0.461	0.375	0.375	0.367	0.363
	Mn	0.021	0.022	0.020	0.019	0.015	0.019	0.016	0.015	0.018	0.021	0.021	0.023	0.022	0.021	0.022	0.022
	Ni	0.003	0.003	0.002	0.002	0.001	0.002	0.004	0.004	0.001	0.002	0.002	0.004	0.002	0.001	0.003	0.003
	Zn	0.002	0.003	0.004	0.007	0.006	0.006	0.002	0.004	0.004	0.004	0.007	0.010	0.002	0.000	0.000	0.002
	Mg	0.640	0.632	0.628	0.652	0.632	0.626	0.632	0.623	0.629	0.597	0.614	0.505	0.599	0.605	0.610	0.611
	Ca	0.000	b.d.	0.000	b.d.	0.001	0.001	0.002	0.007	0.000	b.d.	b.d.	b.d.	0.000	b.d.	b.d.	b.d.
	Na	n.a.	n.a.	n.a.	n.a.	n.a.	n.a.	n.a.	n.a.	n.a.	n.a.	n.a.	n.a.	n.a.	n.a.	n.a.	n.a.
	K	n.a.	n.a.	n.a.	n.a.	n.a.	n.a.	n.a.	n.a.	n.a.	n.a.	n.a.	n.a.	n.a.	n.a.	n.a.	n.a.
	Mg #	0.657	0.648	0.643	0.669	0.644	0.643	0.647	0.641	0.643	0.612	0.631	0.523	0.615	0.617	0.624	0.627
FeCr2O4 (Chromit)		0.174	0.177	0.177	0.140	0.117	0.156	0.128	0.113	0.145	0.200	0.196	0.233	0.198	0.198	0.195	0.194

Abbreviations: Spl = spinel, Spl hrz = spinel harzburgite, Cl core = clast core, Cl rim = clast rim, b.d. = below detection limit, n.a. = not analyzed.
Mg# calculated as (MgO/40.3) / (MgO/40.3 + FeO/71.85).

Major element composition of spinel from the Dramala spinel harzburgite and plagioclase-bearing harzburgite continued

Sample		PIA44	PIA44	PIA44	PIA44	PIA44	PIA44	PIA44	PIA44	PIA44	PIA44	PIA44	PIA44	PIA44	PIA44	PIA44	PIA44
Rock		Spl hrz	Spl hrz	Spl hrz	Spl hrz	Spl hrz	Spl hrz	Spl hrz	Spl hrz	Spl hrz	Spl hrz	Spl hrz	Spl hrz	Spl hrz	Spl hrz	Spl hrz	Spl hrz
Mineral		Spl	Spl	Spl	Spl	Spl	Spl	Spl	Spl	Spl	Spl	Spl	Spl	Spl	Spl	Spl	Spl
Type		Cl core	Cl core	Cl core	Cl core	Cl core	Cl core	Cl core	Cl core	Cl core	Cl core	Cl core	Cl core	Cl core	Cl core	Cl core	Cl rim
Wt.%	SiO2	0.01	0.02	0.01	b.d.	0.02	b.d.	0.02	b.d.	0.04	0.04	0.02	0.01	0.03	0.01	0.04	0.09
	TiO2	0.04	0.01	0.04	0.03	0.04	0.05	0.05	0.05	0.03	0.02	0.04	0.03	0.01	0.04	0.01	0.02
	Cr2O3	44.66	44.83	44.79	44.44	44.22	43.62	43.47	44.49	44.73	44.88	44.72	44.93	44.91	45.18	43.84	46.23
	Al2O3	24.07	24.08	24.19	24.21	24.29	24.18	24.64	24.74	24.15	23.90	23.86	23.85	23.65	23.51	24.51	22.02
	Fe2O3	2.81	2.69	2.82	2.97	2.97	3.58	3.01	2.30	2.68	2.57	2.93	2.82	2.92	2.89	3.39	2.99
	FeO	14.29	14.50	14.63	14.59	15.09	14.58	14.89	15.06	15.05	15.08	15.09	15.11	15.38	15.01	14.73	15.33
	MnO	0.83	0.86	0.85	0.86	0.84	0.82	0.82	0.82	0.87	0.85	0.85	0.84	0.83	0.86	0.79	0.87
	NiO	0.18	0.02	0.07	0.02	0.10	0.06	0.11	0.11	0.26	b.d.	b.d.	b.d.	0.02	0.14	0.06	0.02
	ZnO	b.d.	0.13	0.00	0.23	b.d.	0.26	b.d.	0.09	0.09	0.19	0.17	0.24	0.00	0.08	0.17	0.21
	MgO	13.54	13.42	13.49	13.34	13.15	13.27	13.22	13.19	13.05	13.05	13.07	13.02	12.94	13.03	13.40	12.64
	CaO	0.01	0.02	b.d.	b.d.	b.d.	0.01	b.d.	b.d.	b.d.	b.d.	b.d.	b.d.	0.01	0.01	0.01	0.01
	Na2O	n.a.	n.a.	n.a.	n.a.	n.a.	n.a.	n.a.	n.a.	n.a.	n.a.	n.a.	n.a.	n.a.	n.a.	n.a.	n.a.
	K2O	n.a.	n.a.	n.a.	n.a.	n.a.	n.a.	n.a.	n.a.	n.a.	n.a.	n.a.	n.a.	n.a.	n.a.	n.a.	n.a.
	Total	100.44	100.58	100.88	100.68	100.72	100.43	100.24	100.84	100.95	100.58	100.73	100.85	100.69	100.74	100.95	100.44
Cations	Si	0.000	0.001	0.000	b.d.	0.001	b.d.	0.000	b.d.	0.001	0.001	0.000	0.000	0.001	0.000	0.001	0.003
	Ti	0.001	0.000	0.001	0.001	0.001	0.001	0.001	0.001	0.001	0.001	0.001	0.001	0.000	0.001	0.000	0.001
	Cr	1.072	1.075	1.071	1.066	1.061	1.049	1.045	1.064	1.072	1.080	1.075	1.079	1.082	1.088	1.047	1.125
	Al	0.861	0.861	0.862	0.865	0.869	0.867	0.883	0.882	0.863	0.857	0.855	0.854	0.849	0.844	0.873	0.799
	Fe3+	0.064	0.062	0.064	0.068	0.068	0.082	0.069	0.052	0.061	0.059	0.067	0.064	0.067	0.066	0.077	0.069
	Fe2+	0.363	0.368	0.370	0.370	0.383	0.371	0.378	0.381	0.381	0.384	0.384	0.384	0.392	0.382	0.372	0.395
	Mn	0.021	0.022	0.022	0.022	0.022	0.021	0.021	0.021	0.022	0.022	0.022	0.021	0.021	0.022	0.020	0.023
	Ni	0.004	0.000	0.002	0.000	0.002	0.001	0.003	0.003	0.006	b.d.	b.d.	b.d.	0.000	0.003	0.001	0.001
	Zn	b.d.	0.003	0.000	0.005	b.d.	0.006	b.d.	0.002	0.002	0.004	0.004	0.005	0.000	0.002	0.004	0.005
	Mg	0.613	0.607	0.608	0.603	0.595	0.602	0.599	0.595	0.590	0.592	0.592	0.590	0.587	0.591	0.603	0.580
	Ca	0.000	0.001	b.d.	b.d.	b.d.	0.000	b.d.	b.d.	b.d.	b.d.	b.d.	b.d.	0.000	0.000	0.000	0.000
	Na	n.a.	n.a.	n.a.	n.a.	n.a.	n.a.	n.a.	n.a.	n.a.	n.a.	n.a.	n.a.	n.a.	n.a.	n.a.	n.a.
	K	n.a.	n.a.	n.a.	n.a.	n.a.	n.a.	n.a.	n.a.	n.a.	n.a.	n.a.	n.a.	n.a.	n.a.	n.a.	n.a.
	Mg #	0.628	0.623	0.622	0.620	0.608	0.619	0.613	0.610	0.607	0.607	0.607	0.606	0.600	0.607	0.619	0.595
FeCr2O4 (Chromit)		0.194	0.198	0.198	0.197	0.203	0.194	0.197	0.202	0.204	0.207	0.206	0.207	0.212	0.208	0.195	0.221

Abbreviations: Spl = spinel, Spl hrz = spinel harzburgite, Cl core = clast core, Cl rim = clast rim, b.d. = below detection limit, n.a. = not analyzed.
Mg# calculated as (MgO/40.3) / (MgO/40.3 + FeO/71.85).

Major element composition of spinel from the Dramala spinel harzburgite and plagioclase-bearing harzburgite continued

Sample		PIA44	PIA44	PIA44	PIA44	PIA120	PIA120	PIA120	PIA120	PIA120	PIA120	PIA120	PIA120	PIA120	PIA120	PIA120	PIA120
Rock		Spl hrz	Spl hrz	Spl hrz	Spl hrz	Pl-b hrz	Pl-b hrz	Pl-b hrz	Pl-b hrz	Pl-b hrz	Pl-b hrz	Pl-b hrz	Pl-b hrz	Pl-b hrz	Pl-b hrz	Pl-b hrz	Pl-b hrz
Mineral		Spl	Spl	Spl	Spl	Spl	Spl	Spl	Spl	Spl	Spl	Spl	Spl	Spl	Spl	Spl	Spl
Type		Cl rim	Cl rim	Cl rim	Cl rim	Melt r	Melt r	Cl core	Cl core	Cl core	Cl core	Cl core	Cl core	Cl core	Cl core	Cl core	Cl core
Wt.%	SiO2	0.05	0.04	0.05	0.01	0.04	0.04	0.03	0.04	0.03	0.04	0.01	0.02	0.04	0.02	0.05	0.05
	TiO2	0.04	0.05	b.d.	0.02	0.13	0.16	0.25	0.26	0.26	0.25	0.23	0.24	0.26	0.21	0.21	0.21
	Cr2O3	41.80	44.32	42.50	43.08	25.23	27.94	30.71	29.95	30.08	29.45	30.03	30.66	28.64	28.90	28.65	28.41
	Al2O3	25.35	24.76	25.08	25.02	39.53	38.32	34.77	35.71	35.91	36.06	35.55	34.75	38.13	38.04	38.24	38.32
	Fe2O3	4.00	2.27	3.05	3.18	4.10	3.20	3.26	3.39	3.22	3.40	3.23	3.50	2.28	2.64	2.77	2.75
	FeO	14.63	14.99	14.69	15.06	15.05	14.73	16.67	16.27	16.35	16.05	15.81	16.08	15.32	14.77	15.07	14.89
	MnO	0.82	0.83	0.83	0.85	0.15	0.11	0.08	0.09	0.05	0.01	0.04	0.15	0.05	0.09	0.08	0.11
	NiO	0.05	0.10	0.06	0.09	0.16	0.22	0.15	0.16	0.17	0.18	0.16	0.14	0.20	0.19	0.23	0.17
	ZnO	0.07	0.09	0.02	0.10	0.21	0.13	n.a.	n.a.	n.a.	n.a.	n.a.	n.a.	n.a.	n.a.	n.a.	n.a.
	MgO	13.48	13.24	13.26	13.13	14.68	14.90	13.51	13.85	13.98	14.03	13.94	13.72	14.72	15.04	15.03	15.08
	CaO	0.02	b.d.	0.01	0.01	0.15	0.15	b.d.	b.d.	0.03	0.01	b.d.	0.03	0.07	0.05	0.03	0.01
	Na2O	n.a.	n.a.	n.a.	n.a.	0.01	0.02	b.d.	0.03	b.d.	0.02	0.05	0.03	0.02	0.03	b.d.	0.02
	K2O	n.a.	n.a.	n.a.	n.a.	b.d.	b.d.	0.01	0.01	b.d.	0.01	b.d.	b.d.	b.d.	b.d.	0.01	b.d.
	Total	100.30	100.70	99.55	100.55	99.44	99.92	99.44	99.76	100.07	99.51	99.05	99.32	99.73	99.97	100.38	100.01
Cations	Si	0.001	0.001	0.002	0.000	0.001	0.001	0.001	0.001	0.001	0.001	0.000	0.001	0.001	0.001	0.001	0.001
	Ti	0.001	0.001	b.d.	0.001	0.003	0.003	0.006	0.006	0.006	0.005	0.005	0.005	0.006	0.005	0.004	0.005
	Cr	1.000	1.060	1.025	1.032	0.571	0.632	0.713	0.689	0.689	0.677	0.695	0.711	0.649	0.653	0.645	0.641
	Al	0.904	0.883	0.902	0.894	1.334	1.292	1.203	1.225	1.227	1.237	1.226	1.202	1.289	1.282	1.284	1.289
	Fe3+	0.091	0.052	0.070	0.073	0.088	0.069	0.072	0.074	0.070	0.074	0.071	0.077	0.049	0.057	0.059	0.059
	Fe2+	0.370	0.379	0.375	0.381	0.360	0.352	0.409	0.396	0.396	0.391	0.387	0.395	0.367	0.353	0.359	0.355
	Mn	0.021	0.021	0.022	0.022	0.004	0.003	0.002	0.002	0.001	0.000	0.001	0.004	0.001	0.002	0.002	0.003
	Ni	0.001	0.002	0.001	0.002	0.004	0.005	0.004	0.004	0.004	0.004	0.004	0.003	0.005	0.004	0.005	0.004
	Zn	0.002	0.002	0.000	0.002	0.004	0.003	n.a.	n.a.	n.a.	n.a.	n.a.	n.a.	n.a.	n.a.	n.a.	n.a.
	Mg	0.608	0.597	0.603	0.593	0.626	0.635	0.591	0.601	0.604	0.608	0.608	0.600	0.629	0.641	0.638	0.642
	Ca	0.001	b.d.	0.000	0.000	0.005	0.005	b.d.	b.d.	0.001	0.000	b.d.	0.001	0.002	0.002	0.001	0.000
	Na	n.a.	n.a.	n.a.	n.a.	0.001	0.001	b.d.	0.002	b.d.	0.001	0.003	0.002	0.001	0.002	b.d.	0.001
	K	n.a.	n.a.	n.a.	n.a.	b.d.	b.d.	0.000	0.000	b.d.	0.000	b.d.	b.d.	b.d.	b.d.	0.000	b.d.
	Mg #	0.622	0.612	0.617	0.609	0.635	0.643	0.591	0.603	0.604	0.609	0.611	0.603	0.631	0.645	0.640	0.644
FeCr2O4 (Chromit)		0.185	0.201	0.192	0.197	0.103	0.111	0.145	0.136	0.136	0.132	0.134	0.140	0.119	0.115	0.115	0.113

Abbreviations: Spl = spinel, Spl hrz = spinel harzburgite, Pl-b hrz = plagioclase-bearing harzburgite, Cl core = clast core, Cl rim = clast rim, b.d. = below detection limit, n.a. = not analyzed. Mg# calculated as (MgO/40.3) / (MgO/40.3 + FeO/71.85).

Major element composition of spinel from the Dramala spinel harzburgite and plagioclase-bearing harzburgite continued

Sample		PIA120	PIA120	PIA120	PIA120	PIA120	PIA120	PIA109	PIA51	PIA51	PIA51	PIA51	PIA51	PIA51	PIA51
Rock		Pl-b hrz	Pl-b hrz	Pl-b hrz	Pl-b hrz	Pl-b hrz	Pl-b hrz	Pl-b hrz	Pl-b hrz	Pl-b hrz	Pl-b hrz	Pl-b hrz	Pl-b hrz	Pl-b hrz	Pl-b hrz
Mineral		Spl	Spl	Spl	Spl	Spl	Spl	Spl	Spl	Spl	Spl	Spl	Spl	Spl	Spl
Type		Cl core	Cl core	Cl core	Cl core	Cl rim	Cl rim	Melt r	Melt r	Melt r	Melt r	Cl core	Cl core	Cl core	Cl rim
Wt.%	SiO2	0.02	0.05	0.02	0.04	0.04	0.07	0.02	0.03	0.04	0.07	0.03	0.03	0.03	0.06
	TiO2	0.20	0.22	0.25	0.23	0.25	0.27	0.14	0.02	0.02	b.d.	b.d.	0.01	0.04	0.03
	Cr2O3	27.79	27.23	27.44	27.21	33.38	31.06	29.47	31.87	30.57	31.45	40.39	35.38	41.81	39.11
	Al2O3	38.73	39.27	39.26	39.24	31.82	34.24	35.28	34.84	35.24	35.51	26.64	31.77	25.28	27.54
	Fe2O3	2.83	2.99	2.99	3.42	3.64	3.03	4.39	2.77	3.43	2.59	4.40	3.21	3.72	3.66
	FeO	14.57	14.65	14.54	14.40	17.14	17.47	14.92	14.15	14.30	14.51	13.85	14.53	14.92	14.97
	MnO	0.18	0.04	0.11	0.08	0.13	0.10	0.63	0.62	0.65	0.62	0.82	0.70	0.86	0.73
	NiO	0.22	0.14	0.23	0.22	0.07	0.21	0.23	0.13	0.14	0.06	b.d.	0.04	0.12	0.01
	ZnO	n.a.	n.a.	n.a.	n.a.	n.a.	n.a.	0.25	0.19	0.42	0.24	0.27	0.12	0.27	0.03
	MgO	15.18	15.44	15.45	15.54	12.90	12.87	14.05	14.52	14.29	14.49	14.02	14.17	13.06	13.46
	CaO	0.03	0.02	b.d.	0.02	b.d.	b.d.	0.01	0.01	0.01	b.d.	0.01	0.01	b.d.	0.01
	Na2O	0.01	b.d.	b.d.	0.02	0.01	0.02	b.d.	b.d.	b.d.	b.d.	b.d.	b.d.	b.d.	b.d.
	K2O	b.d.	0.01	0.02	0.01	b.d.	b.d.	b.d.	b.d.	b.d.	b.d.	b.d.	b.d.	b.d.	b.d.
	Total	99.75	100.06	100.31	100.42	99.38	99.34	99.39	99.15	99.11	99.54	100.43	99.97	100.11	99.61
Cations	Si	0.001	0.001	0.001	0.001	0.001	0.002	0.001	0.001	0.001	0.002	0.001	0.001	0.001	0.002
	Ti	0.004	0.005	0.005	0.005	0.006	0.006	0.003	0.000	0.000	b.d.	b.d.	0.000	0.001	0.001
	Cr	0.627	0.611	0.614	0.608	0.787	0.725	0.681	0.736	0.707	0.723	0.957	0.824	1.005	0.933
	Al	1.303	1.313	1.311	1.308	1.118	1.192	1.215	1.200	1.215	1.216	0.942	1.103	0.906	0.979
	Fe3+	0.061	0.064	0.064	0.073	0.082	0.067	0.096	0.061	0.075	0.057	0.099	0.071	0.085	0.083
	Fe2+	0.348	0.348	0.344	0.340	0.427	0.432	0.365	0.346	0.350	0.353	0.347	0.358	0.379	0.378
	Mn	0.004	0.001	0.003	0.002	0.003	0.003	0.016	0.015	0.016	0.015	0.021	0.017	0.022	0.019
	Ni	0.005	0.003	0.005	0.005	0.002	0.005	0.005	0.003	0.003	0.001	b.d.	0.001	0.003	0.000
	Zn	n.a.	n.a.	n.a.	n.a.	n.a.	n.a.	0.005	0.004	0.009	0.005	0.006	0.003	0.006	0.001
	Mg	0.646	0.653	0.652	0.655	0.573	0.567	0.612	0.633	0.623	0.628	0.627	0.622	0.592	0.605
	Ca	0.001	0.001	b.d.	0.001	b.d.	b.d.	0.000	0.000	0.000	b.d.	0.000	0.000	b.d.	0.000
	Na	0.001	b.d.	b.d.	0.001	0.001	0.001	b.d.	b.d.	b.d.	b.d.	b.d.	b.d.	b.d.	b.d.
	K	b.d.	0.000	0.001	0.000	b.d.	b.d.	b.d.	b.d.	b.d.	b.d.	b.d.	b.d.	b.d.	b.d.
	Mg #	0.650	0.653	0.655	0.658	0.573	0.568	0.627	0.647	0.640	0.640	0.643	0.635	0.609	0.616
FeCr2O4	(Chromit)	0.109	0.106	0.105	0.103	0.167	0.156	0.124	0.127	0.123	0.127	0.166	0.147	0.190	0.176

Abbreviations: Spl = spinel, Pl-b hrz = plagioclase-bearing harzburgite, Cl core = clast core, Cl rim = clast rim, Melt r = melt related, b.d. = below detection lim
n.a. = not analyzed. Mg# calculated as (MgO/40.3) / (MgO/40.3 + FeO/71.85).

Major element composition of plagioclase from the Dramala plagioclase-bearing harzburgite

Sample		PIA109	PIA109	PIA109	PIA109	PIA109	PIA109	PIA109	PIA109	PIA109	PIA109	PIA109	PIA109	PIA109
Rock		Pl-b hrz	Pl-b hrz	Pl-b hrz	Pl-b hrz	Pl-b hrz	Pl-b hrz	Pl-b hrz	Pl-b hrz	Pl-b hrz	Pl-b hrz	Pl-b hrz	Pl-b hrz	Pl-b hrz
Mineral		Pl	Pl	Pl	Pl	Pl	Pl	Pl	Pl	Pl	Pl	Pl	Pl	Pl
Wt.%	SiO2	44.98	44.19	45.25	45.70	45.08	44.74	45.16	45.40	47.44	44.77	44.60	45.09	45.46
	TiO2	0.02	0.01	b.d.	0.02	0.01	b.d.	0.01	0.05	0.05	0.05	0.01	b.d.	0.01
	Al2O3	35.13	34.58	35.67	31.87	35.42	35.14	35.16	32.06	23.72	34.79	34.79	35.33	34.58
	Fe2O3	0.34	1.06	0.19	1.49	0.34	0.50	0.22	0.86	1.63	0.33	0.33	0.11	0.25
	FeO	b.d.	b.d.	b.d.	b.d.	b.d.	b.d.	b.d.	b.d.	b.d.	b.d.	b.d.	0.16	b.d.
	MnO	0.01	0.01	b.d.	0.07	b.d.	0.01	0.01	b.d.	0.03	0.01	b.d.	0.01	0.04
	MgO	0.01	1.63	0.01	1.95	0.01	0.01	b.d.	1.67	6.24	b.d.	b.d.	b.d.	b.d.
	CaO	18.60	18.00	18.48	18.87	18.74	18.55	18.52	19.19	20.14	18.44	18.46	18.64	18.87
	SrO	0.01	b.d.	b.d.	b.d.	0.01	b.d.	b.d.	b.d.	0.03	b.d.	b.d.	b.d.	n.a.
	BaO	b.d.	0.04	0.00	0.10	b.d.	0.08	0.07	b.d.	b.d.	b.d.	0.04	0.06	n.a.
	Na2O	1.03	0.77	1.06	0.94	0.96	0.98	1.08	1.05	0.98	0.98	0.94	0.83	1.05
	K2O	b.d.	0.02	b.d.	0.02	0.01	0.01	0.02	0.01	0.03	b.d.	b.d.	b.d.	0.01
	Total	100.14	100.31	100.66	101.01	100.58	100.02	100.25	100.29	100.28	99.37	99.17	100.24	100.28
Cations	Si	2.071	2.027	2.070	2.088	2.066	2.064	2.076	2.083	2.166	2.078	2.075	2.077	2.091
	Ti	0.001	0.000	b.d.	0.001	0.000	b.d.	0.000	0.002	0.002	0.002	0.001	b.d.	0.000
	Al	1.906	1.869	1.923	1.716	1.914	1.911	1.905	1.734	1.276	1.903	1.907	1.918	1.875
	Fe3	0.012	0.037	0.007	0.051	0.012	0.018	0.008	0.030	0.056	0.011	0.011	0.004	0.009
	Fe2	b.d.	b.d.	b.d.	b.d.	b.d.	b.d.	b.d.	b.d.	b.d.	b.d.	b.d.	0.006	b.d.
	Mn	0.001	0.000	b.d.	0.003	b.d.	0.001	0.000	b.d.	0.001	0.000	b.d.	0.001	0.002
	Mg	0.001	0.112	0.001	0.133	0.001	0.001	b.d.	0.114	0.425	b.d.	b.d.	b.d.	b.d.
	Ca	0.917	0.884	0.906	0.923	0.921	0.917	0.912	0.943	0.985	0.917	0.920	0.920	0.930
	Sr	0.000	b.d.	b.d.	b.d.	0.000	b.d.	b.d.	b.d.	0.001	b.d.	b.d.	b.d.	n.a.
	Ba	b.d.	0.001	0.000	0.002	b.d.	0.002	0.001	b.d.	b.d.	b.d.	0.001	0.001	n.a.
	Na	0.092	0.069	0.094	0.083	0.085	0.088	0.096	0.094	0.087	0.089	0.085	0.075	0.094
	K	b.d.	0.001	b.d.	0.001	0.001	0.000	0.001	0.001	0.002	b.d.	b.d.	b.d.	0.000
	An #	0.909	0.928	0.906	0.918	0.915	0.913	0.905	0.910	0.919	0.912	0.916	0.925	0.909

Abbreviations: Pl = plagioclase, Pl-b hrz = plagioclase-bearing harzburgite, b.d. = below detection limit.
An# calculated as Ca / (Ca + Na).

Major element composition of plagioclase from the Dramala plagioclase-bearing harzburgite continued

Sample		PIA120	PIA120	PIA120	PIA120	PIA120	PIA120	PIA120	PIA120	PIA120	PIA120	PIA120	PIA120
Rock		Pl-b hrz	Pl-b hrz	Pl-b hrz	Pl-b hrz	Pl-b hrz	Pl-b hrz	Pl-b hrz	Pl-b hrz	Pl-b hrz	Pl-b hrz	Pl-b hrz	Pl-b hrz
Mineral		Pl	Pl	Pl	Pl	Pl	Pl	Pl	Pl	Pl	Pl	Pl	Pl
Wt.%	SiO2	47.28	46.30	46.71	45.92	46.56	45.87	46.46	45.66	46.73	45.91	46.78	46.83
	TiO2	b.d.	0.01	b.d.	n.a.	n.a.	n.a.	n.a.	n.a.	n.a.	n.a.	n.a.	n.a.
	Al2O3	34.07	34.20	33.75	35.26	34.89	35.76	35.06	35.54	34.75	35.50	35.11	35.16
	Fe2O3	0.00	0.22	0.08	0.16	0.08	0.26	0.03	0.15	0.07	0.17	0.11	0.12
	FeO	0.06	b.d.	b.d.	b.d.	b.d.	b.d.	b.d.	b.d.	b.d.	b.d.	b.d.	b.d.
	MnO	0.01	0.03	b.d.	n.a.	n.a.	n.a.	n.a.	n.a.	n.a.	n.a.	n.a.	n.a.
	MgO	b.d.	b.d.	b.d.	n.a.	n.a.	n.a.	n.a.	n.a.	n.a.	n.a.	n.a.	n.a.
	CaO	17.19	17.57	17.11	17.07	17.13	18.03	17.08	17.87	16.85	17.65	17.18	17.03
	SrO	b.d.	0.11	b.d.	n.a.	n.a.	n.a.	n.a.	n.a.	n.a.	n.a.	b.d.	b.d.
	BaO	0.04	b.d.	0.04	n.a.	n.a.	n.a.	n.a.	n.a.	n.a.	n.a.	b.d.	b.d.
	Na2O	1.77	1.56	1.77	1.78	1.82	1.50	1.86	1.38	2.13	1.66	1.82	1.94
	K2O	b.d.	b.d.	0.01	0.02	b.d.	0.01	0.02	b.d.	0.03	b.d.	0.01	b.d.
	Total	100.42	99.99	99.47	100.21	100.49	101.43	100.50	100.61	100.56	100.88	101.01	101.07
Cations	Si	2.162	2.130	2.156	2.099	2.124	2.077	2.117	2.085	2.125	2.087	2.123	2.122
	Ti	b.d.	0.000	b.d.	n.a.	n.a.	n.a.	n.a.	n.a.	n.a.	n.a.	n.a.	n.a.
	Al	1.836	1.854	1.836	1.900	1.876	1.908	1.883	1.913	1.862	1.902	1.878	1.877
	Fe3	0.000	0.008	0.003	0.006	0.003	0.009	0.001	0.005	0.003	0.006	0.004	0.004
	Fe2	0.002	b.d.	b.d.	b.d.	b.d.	b.d.	b.d.	b.d.	b.d.	b.d.	b.d.	b.d.
	Mn	0.000	0.001	b.d.	n.a.	n.a.	n.a.	n.a.	n.a.	n.a.	n.a.	n.a.	n.a.
	Mg	b.d.	b.d.	b.d.	n.a.	n.a.	n.a.	n.a.	n.a.	n.a.	n.a.	n.a.	n.a.
	Ca	0.842	0.866	0.846	0.836	0.837	0.874	0.834	0.875	0.821	0.860	0.835	0.827
	Sr	b.d.	0.003	b.d.	n.a.	n.a.	n.a.	n.a.	n.a.	n.a.	n.a.	b.d.	b.d.
	Ba	0.001	b.d.	0.001	n.a.	n.a.	n.a.	n.a.	n.a.	n.a.	n.a.	b.d.	b.d.
	Na	0.157	0.139	0.159	0.158	0.161	0.131	0.164	0.122	0.188	0.146	0.160	0.171
	K	b.d.	b.d.	0.001	0.001	b.d.	0.001	0.001	b.d.	0.002	b.d.	0.001	b.d.
	An #	0.843	0.862	0.842	0.842	0.839	0.869	0.835	0.877	0.814	0.855	0.043	0.052

Abbreviations: Pl = plagioclase, Pl-b hrz = plagioclase-bearing harzburgite, b.d. = below detection limit, n.a. = not analyzed.
An# calculated as Ca / (Ca + Na).

Major element composition of amphibole from the Dramala spinel harzburgite and plagioclase-bearing harzburgite

Sample		PIA27	PIA27	PIA27	PIA27	PIA27	PIA27	PIA27	PIA27	PIA27	PIA27	PIA27	PIA27	PIA27	PIA27	PIA27	PIA27
Rock		Spl hrz	Spl hrz	Spl hrz	Spl hrz	Spl hrz	Spl hrz	Spl hrz	Spl hrz	Spl hrz	Spl hrz	Spl hrz	Spl hrz	Spl hrz	Spl hrz	Spl hrz	Spl hrz
Mineral		Ed hbl	Ed hbl	Ed hbl	Ed hbl	Ed hbl	Ed hbl	Ed hbl	Ed hbl	Ed hbl	Ed hbl	Ed hbl	Ed hbl	Ed hbl	Ed hbl	Ed hbl	Ed hbl
Wt.%	SiO2	46.77	46.83	46.61	46.80	46.95	47.16	46.98	46.95	47.00	47.00	47.32	46.93	47.06	46.97	46.99	47.01
	TiO2	0.14	0.11	0.13	0.12	0.07	0.11	0.12	0.13	0.14	0.11	0.16	0.10	0.13	0.10	0.12	0.11
	Cr2O3	2.23	2.34	2.05	2.05	1.94	1.94	2.07	2.01	1.94	2.03	1.83	1.94	2.03	2.04	2.13	1.98
	Al2O3	11.57	11.77	11.77	11.71	11.58	11.45	11.53	11.46	11.66	11.57	11.50	11.58	11.59	11.55	11.48	11.71
	Fe2O3	n.c.	n.c.	n.c.	n.c.	n.c.	n.c.	n.c.	n.c.	n.c.	n.c.	n.c.	n.c.	n.c.	n.c.	n.c.	n.c.
	FeO	2.52	2.71	2.55	2.91	2.65	2.83	2.61	2.54	2.77	2.57	2.52	2.69	2.54	2.55	2.66	2.51
	MnO	b.d.	b.d.	b.d.	b.d.	b.d.	b.d.	b.d.	b.d.	b.d.	b.d.	b.d.	b.d.	b.d.	b.d.	b.d.	b.d.
	NiO	0.14	0.14	0.11	0.15	0.16	0.13	0.15	0.19	0.10	0.17	0.00	0.18	0.10	0.09	0.06	0.18
	MgO	19.14	19.19	19.16	19.28	19.19	19.25	19.15	19.25	19.21	19.18	19.23	19.29	19.21	19.17	19.03	19.17
	CaO	12.16	12.17	12.17	12.09	12.15	12.24	12.10	12.14	12.03	12.21	12.06	12.15	12.12	12.19	12.14	12.19
	Na2O	2.02	2.13	2.10	2.10	2.01	2.02	2.01	1.99	2.10	2.12	2.09	2.14	2.13	2.09	2.11	2.13
	K2O	0.43	0.44	0.43	0.47	0.40	0.41	0.43	0.46	0.41	0.42	0.40	0.42	0.43	0.43	0.41	0.42
	H2O	2.12	2.13	2.12	2.13	2.12	2.13	2.12	2.12	2.13	2.12	2.12	2.13	2.12	2.12	2.12	2.13
	Total	99.22	99.96	99.19	99.80	99.23	99.68	99.25	99.24	99.49	99.51	99.24	99.54	99.45	99.29	99.23	99.54
Cations	Si	6.616	6.587	6.594	6.589	6.634	6.639	6.643	6.636	6.632	6.634	6.687	6.619	6.645	6.641	6.654	6.631
	Ti	0.014	0.012	0.014	0.012	0.008	0.011	0.013	0.014	0.014	0.012	0.017	0.011	0.014	0.010	0.012	0.012
	Cr	0.249	0.260	0.229	0.228	0.217	0.216	0.231	0.224	0.217	0.227	0.205	0.216	0.227	0.228	0.238	0.221
	Al	1.929	1.951	1.964	1.943	1.929	1.899	1.921	1.909	1.939	1.925	1.916	1.926	1.929	1.925	1.916	1.948
	Fe3+	n.c.	n.c.	n.c.	n.c.	n.c.	n.c.	n.c.	n.c.	n.c.	n.c.	n.c.	n.c.	n.c.	n.c.	n.c.	n.c.
	Fe2+	0.298	0.319	0.301	0.342	0.313	0.333	0.308	0.300	0.327	0.304	0.297	0.318	0.300	0.302	0.315	0.297
	Mn	b.d.	b.d.	b.d.	b.d.	b.d.	b.d.	b.d.	b.d.	b.d.	b.d.	b.d.	b.d.	b.d.	b.d.	b.d.	b.d.
	Ni	0.016	0.016	0.012	0.016	0.018	0.015	0.016	0.021	0.012	0.019	0.000	0.020	0.011	0.010	0.006	0.020
	Mg	4.035	4.023	4.040	4.045	4.040	4.040	4.035	4.056	4.041	4.034	4.051	4.055	4.043	4.039	4.017	4.030
	Ca	1.843	1.834	1.845	1.824	1.839	1.846	1.832	1.839	1.819	1.846	1.826	1.835	1.833	1.846	1.841	1.841
	Na	0.554	0.580	0.575	0.573	0.551	0.552	0.550	0.544	0.574	0.581	0.573	0.585	0.584	0.574	0.579	0.582
	K	0.078	0.079	0.077	0.085	0.071	0.074	0.078	0.083	0.073	0.075	0.073	0.076	0.078	0.078	0.074	0.076
	H	2.000	2.000	2.000	2.000	2.000	2.000	2.000	2.000	2.000	2.000	2.000	2.000	2.000	2.000	2.000	2.000
	Sum	15.633	15.659	15.652	15.659	15.623	15.626	15.628	15.627	15.647	15.656	15.645	15.661	15.661	15.652	15.653	15.659
	Al IV	1.3841	1.4133	1.4056	1.4110	1.3658	1.3605	1.3573	1.3640	1.3678	1.3663	1.3127	1.3811	1.3551	1.3589	1.3462	1.3686
	Al VI	0.5444	0.5373	0.5580	0.5321	0.5637	0.5386	0.5638	0.5453	0.5711	0.5588	0.6031	0.5447	0.5735	0.5657	0.5696	0.5790
	Mg #	0.9313	0.9266	0.9306	0.9220	0.9280	0.9239	0.9290	0.9311	0.9252	0.9300	0.9316	0.9274	0.9310	0.9305	0.9272	0.9315
	NaK (A)	0.6326	0.6592	0.6518	0.6585	0.6228	0.6256	0.6282	0.6270	0.6469	0.6559	0.6453	0.6610	0.6613	0.6517	0.6529	0.6586

Abbreviations: Ed hbl = edenitic hornblende, Spl hrz = spinel harzburgite, b.d. = below detection limit, n.c. = not calculated. Mg# calculated as (MgO/40.3) / (MgO/40.3 + FeO/71.85)

Major element composition of amphibole from the Dramala spinel harzburgite and plagioclase-bearing harzburgite continued

Sample		PIA27	PIA27	PIA27	PIA27	PIA27	PIA27	PIA27	PIA27	PIA27	PIA27	PIA27	PIA120	PIA120	PIA120	PIA120	PIA120
Rock		Spl hrz	Spl hrz	Spl hrz	Spl hrz	Spl hrz	Spl hrz	Spl hrz	Spl hrz	Spl hrz	Spl hrz	Spl hrz	Pl-b hrz	Pl-b hrz	Pl-b hrz	Pl-b hrz	Pl-b hrz
Mineral		Ed hbl	Ed hbl	Ed hbl	Ed hbl	Ed hbl	Ed hbl	Ed hbl	Ed hbl	Ed	Ed	Tr	Prg hbl	Prg hbl	Prg hbl	Prg hbl	Prg hbl
Wt.%	SiO2	47.21	46.91	47.61	47.54	47.98	47.69	47.57	47.33	48.11	47.98	58.34	44.03	43.92	45.73	44.26	44.23
	TiO2	0.10	0.09	0.02	0.03	0.05	0.04	0.05	0.08	0.03	0.05	b.d.	2.00	1.88	1.94	1.90	1.91
	Cr2O3	1.97	2.08	1.38	1.37	1.38	1.39	1.57	1.59	1.43	1.44	0.09	2.55	2.44	1.83	2.01	1.97
	Al2O3	11.57	11.64	11.32	11.24	11.01	11.28	11.38	11.59	10.93	10.87	0.25	13.12	12.87	12.29	12.78	12.74
	Fe2O3	n.c.	n.c.	n.c.	n.c.	n.c.	n.c.	n.c.	n.c.	n.c.	n.c.	n.c.	n.c.	n.c.	n.c.	n.c.	n.c.
	FeO	2.39	2.46	2.44	2.56	2.67	2.49	2.44	2.60	2.51	2.40	1.86	3.69	3.67	3.55	3.46	3.63
	MnO	b.d.	b.d.	b.d.	b.d.	b.d.	b.d.	b.d.	b.d.	b.d.	b.d.	0.06	0.06	0.13	0.04	0.09	0.05
	NiO	0.16	0.10	0.09	0.13	0.21	0.05	0.11	0.13	0.20	0.13	0.05	0.09	0.10	0.09	0.12	0.11
	MgO	19.14	19.16	19.61	19.51	19.76	19.51	19.57	19.47	19.65	19.55	23.63	17.35	17.48	17.77	17.52	17.70
	CaO	12.13	12.23	12.32	12.14	12.09	12.14	12.29	12.10	12.26	12.15	12.77	12.23	12.32	12.47	12.37	12.39
	Na2O	2.11	2.03	1.96	1.99	1.94	1.99	2.04	2.07	1.82	1.80	0.05	2.92	3.01	2.87	2.97	2.90
	K2O	0.41	0.42	0.58	0.59	0.56	0.55	0.53	0.57	0.55	0.60	0.01	b.d.	0.01	0.01	b.d.	0.01
	H2O	2.12	2.12	2.13	2.12	2.14	2.13	2.13	2.13	2.14	2.12	2.18	2.10	2.10	2.12	2.09	2.10
	Total	99.29	99.24	99.45	99.21	99.78	99.26	99.68	99.65	99.61	99.10	99.28	100.14	99.93	100.71	99.57	99.74
Cations	Si	6.673	6.630	6.700	6.714	6.733	6.727	6.686	6.662	6.756	6.774	8.010	6.279	6.278	6.469	6.337	6.315
	Ti	0.011	0.010	0.002	0.003	0.005	0.005	0.005	0.008	0.003	0.005	b.d.	0.214	0.202	0.206	0.205	0.205
	Cr	0.220	0.233	0.153	0.153	0.153	0.155	0.175	0.176	0.159	0.161	0.010	0.287	0.276	0.205	0.227	0.222
	Al	1.928	1.939	1.878	1.871	1.821	1.875	1.886	1.923	1.809	1.809	0.040	2.205	2.168	2.049	2.157	2.144
	Fe3+	n.c.	n.c.	n.c.	n.c.	n.c.	n.c.	n.c.	n.c.	n.c.	n.c.	n.c.	n.c.	n.c.	n.c.	n.c.	n.c.
	Fe2+	0.282	0.291	0.287	0.302	0.313	0.294	0.286	0.306	0.294	0.284	0.214	0.440	0.439	0.420	0.414	0.433
	Mn	b.d.	b.d.	b.d.	b.d.	b.d.	b.d.	b.d.	b.d.	b.d.	b.d.	0.007	0.007	0.016	0.005	0.011	0.006
	Ni	0.018	0.011	0.010	0.015	0.023	0.006	0.012	0.015	0.022	0.014	0.005	0.010	0.011	0.010	0.014	0.013
	Mg	4.032	4.036	4.112	4.106	4.134	4.103	4.100	4.085	4.112	4.115	4.836	3.688	3.724	3.746	3.738	3.766
	Ca	1.836	1.851	1.857	1.836	1.817	1.835	1.851	1.824	1.844	1.837	1.878	1.868	1.887	1.890	1.897	1.895
	Na	0.578	0.556	0.534	0.544	0.529	0.544	0.555	0.565	0.494	0.494	0.014	0.807	0.834	0.787	0.824	0.803
	K	0.073	0.076	0.103	0.106	0.100	0.099	0.095	0.103	0.099	0.108	0.001	b.d.	0.002	0.002	b.d.	0.002
	H	2.000	2.000	2.000	2.000	2.000	2.000	2.000	2.000	2.000	2.000	2.000	2.000	2.000	2.000	2.000	2.000
	Sum	15.651	15.632	15.638	15.650	15.629	15.644	15.650	15.668	15.593	15.602	15.015	15.807	15.836	15.789	15.824	15.804
	Al IV	1.3271	1.3698	1.2998	1.2857	1.2670	1.2725	1.3145	1.3381	1.2437	1.2259	0.0000	1.7211	1.7224	1.5313	1.6634	1.6851
	Al VI	0.6007	0.5689	0.5778	0.5849	0.5541	0.6023	0.5712	0.5852	0.5653	0.5836	0.0405	0.4843	0.4460	0.5179	0.4933	0.4589
	Mg #	0.9347	0.9328	0.9347	0.9314	0.9295	0.9331	0.9348	0.9304	0.9332	0.9355	0.9577	0.8934	0.8946	0.8992	0.9003	0.8968
	NaK (A)	0.6510	0.6319	0.6376	0.6500	0.6290	0.6436	0.6498	0.6678	0.5926	0.6019	0.0152	0.8073	0.8359	0.7888	0.8243	0.8045

Abbreviations: Ed hbl = edenitic hornblende, Ed = edenite, Tr = tremolite, Prg hbl = pargasitic hornblende, Spl hrz = spinel harzburgite, Pl-b hrz = plagioclase-bearing harzburgite, b.d. = below detection limit, n.c. = not calculated. Mg# calculated as (MgO/40.3) / (MgO/40.3 + FeO/71.85).

Major element composition of amphibole from the Dramala spinel harzburgite and plagioclase-bearing harzburgite continued

Sample		PIA120	PIA120	PIA120	PIA120	PIA120	PIA120	PIA120	PIA120	PIA120	PIA120	PIA120	PIA120	PIA109	PIA109	PIA109	PIA109
Rock		Pl-b hrz	Pl-b hrz	Pl-b hrz	Pl-b hrz	Pl-b hrz	Pl-b hrz	Pl-b hrz	Pl-b hrz	Pl-b hrz	Pl-b hrz	Pl-b hrz	Pl-b hrz	Pl-b hrz	Pl-b hrz	Pl-b hrz	Pl-b hrz
Mineral		Prg hbl	Prg hbl	Prg hbl	Prg hbl	Prg hbl	Prg	Prg	Prg	Prg	Tr	Tr	Tr	Prg hbl	Prg hbl	Prg hbl	Prg hbl
Wt.%	SiO2	44.47	44.66	44.23	44.07	43.76	43.73	43.01	43.71	42.46	58.33	56.95	57.06	44.33	43.97	44.18	44.20
	TiO2	2.25	2.19	2.21	2.47	2.20	2.09	2.18	2.21	2.21	0.06	0.09	0.10	1.94	1.81	1.74	1.87
	Cr2O3	1.76	1.61	1.75	1.81	2.28	2.57	2.18	1.74	2.72	0.12	0.39	0.29	1.70	2.23	1.52	1.51
	Al2O3	12.88	12.63	13.04	13.34	12.98	12.77	12.89	13.18	13.39	0.54	1.27	1.26	12.71	12.41	12.50	12.57
	Fe2O3	n.c.	n.c.	n.c.	n.c.	n.c.	n.c.	n.c.	n.c.	n.c.	n.c.	n.c.	n.c.	n.c.	n.c.	n.c.	n.c.
	FeO	3.82	3.68	3.73	3.99	3.60	3.73	3.79	3.95	3.72	2.32	2.52	2.72	3.94	3.82	4.20	4.12
	MnO	0.12	0.05	0.12	0.06	0.02	0.02	0.06	0.08	0.07	0.08	0.03	0.15	0.03	0.06	0.08	b.d.
	NiO	0.09	0.13	0.14	0.13	0.08	0.03	0.01	0.10	b.d.	0.04	0.02	0.06	0.09	0.06	0.09	0.15
	MgO	17.55	17.71	17.63	17.34	17.21	17.59	17.50	17.49	17.11	23.24	22.68	22.83	18.10	18.14	18.39	18.02
	CaO	12.36	12.32	12.34	12.40	12.26	12.51	12.41	12.44	12.19	13.03	13.14	13.07	12.20	12.29	12.14	12.47
	Na2O	2.95	3.00	2.73	3.02	3.01	3.00	3.16	2.85	3.18	0.21	0.39	0.36	3.33	3.32	3.18	3.29
	K2O	0.02	b.d.	b.d.	0.01	0.02	b.d.	b.d.	b.d.	0.03	b.d.	0.01	0.02	b.d.	b.d.	0.01	b.d.
	H2O	2.11	2.10	2.11	2.11	2.09	2.10	2.08	2.10	2.07	2.19	2.18	2.19	2.11	2.10	2.11	2.11
	Total	100.38	100.08	100.03	100.75	99.51	100.14	99.27	99.85	99.15	100.16	99.67	100.11	100.48	100.21	100.14	100.31
Cations	Si	6.323	6.363	6.290	6.254	6.288	6.237	6.193	6.237	6.137	7.973	7.848	7.829	6.300	6.268	6.282	6.290
	Ti	0.241	0.235	0.236	0.264	0.238	0.224	0.236	0.237	0.240	0.006	0.009	0.010	0.207	0.194	0.186	0.200
	Cr	0.198	0.181	0.197	0.203	0.259	0.290	0.248	0.196	0.311	0.013	0.042	0.031	0.191	0.251	0.171	0.170
	Al	2.159	2.121	2.186	2.231	2.198	2.147	2.188	2.217	2.281	0.087	0.206	0.204	2.129	2.085	2.095	2.109
	Fe3+	n.c.	n.c.	n.c.	n.c.	n.c.	n.c.	n.c.	n.c.	n.c.	n.c.	n.c.	n.c.	n.c.	n.c.	n.c.	n.c.
	Fe2+	0.454	0.438	0.444	0.473	0.433	0.445	0.456	0.471	0.450	0.265	0.290	0.312	0.468	0.455	0.499	0.490
	Mn	0.014	0.006	0.014	0.007	0.002	0.002	0.007	0.010	0.009	0.009	0.004	0.017	0.004	0.007	0.010	b.d.
	Ni	0.010	0.015	0.016	0.015	0.009	0.003	0.001	0.011	b.d.	0.004	0.002	0.007	0.010	0.007	0.010	0.017
	Mg	3.719	3.761	3.737	3.667	3.686	3.739	3.756	3.719	3.686	4.734	4.658	4.669	3.834	3.854	3.897	3.822
	Ca	1.883	1.880	1.880	1.885	1.887	1.912	1.914	1.902	1.887	1.908	1.940	1.921	1.857	1.877	1.849	1.901
	Na	0.813	0.829	0.753	0.831	0.838	0.830	0.882	0.788	0.891	0.056	0.104	0.096	0.917	0.918	0.877	0.908
	K	0.004	b.d.	b.d.	0.002	0.004	b.d.	b.d.	b.d.	0.006	b.d.	0.002	0.004	b.d.	b.d.	0.002	b.d.
	H	2.000	2.000	2.000	2.000	2.000	2.000	2.000	2.000	2.000	2.000	2.000	2.000	2.000	2.000	2.000	2.000
	Sum	15.817	15.829	15.753	15.833	15.842	15.830	15.882	15.788	15.897	15.056	15.106	15.099	15.917	15.918	15.878	15.908
	Al IV	1.6774	1.6373	1.7099	1.7462	1.7122	1.7627	1.8069	1.7634	1.8634	0.0273	0.1522	0.1713	1.7004	1.7316	1.7180	1.7097
	Al VI	0.4811	0.4837	0.4760	0.4852	0.4862	0.3843	0.3809	0.4532	0.4178	0.0597	0.0541	0.0325	0.4286	0.3538	0.3771	0.3990
	Mg #	0.8912	0.8956	0.8939	0.8857	0.8950	0.8937	0.8917	0.8875	0.8913	0.9470	0.9413	0.9373	0.8912	0.8943	0.8864	0.8863
	NaK (A)	0.8167	0.8286	0.7527	0.8326	0.8421	0.8295	0.8821	0.7883	0.8965	0.0556	0.1059	0.0993	0.9174	0.9176	0.8784	0.9077

Abbreviations: Tr = tremolite, Prg hbl = pargasitic hornblende, Prg = pargasite, Pl-b hrz = plagioclase-bearing harzburgite,
b.d. = below detection limit, n.c. = not calculated. Mg# calculated as (MgO/40.3) / (MgO/40.3 + FeO/71.85).

Major element composition of amphibole from the Dramala spinel harzburgite and plagioclase-bearing

Sample		PIA109	PIA109	PIA109	PIA109	PIA109	PIA109	PIA109	PIA109	PIA109
Rock		Pl-b hrz	Pl-b hrz	Pl-b hrz	Pl-b hrz	Pl-b hrz	Pl-b hrz	Pl-b hrz	Pl-b hrz	Pl-b hrz
Mineral		Prg hbl	Prg hbl	Prg hbl	Prg hbl	Prg	Prg	Prg	Prg	Prg
Wt.%	SiO2	44.43	44.18	44.47	44.15	43.43	43.94	43.89	43.97	43.83
	TiO2	1.74	1.82	1.09	1.21	1.63	1.85	1.78	1.88	1.91
	Cr2O3	1.81	1.43	1.27	1.05	1.76	1.45	2.21	2.10	1.54
	Al2O3	12.71	13.16	13.53	13.85	13.42	13.51	12.47	12.60	12.76
	Fe2O3	n.c.	n.c.	n.c.	n.c.	n.c.	n.c.	n.c.	n.c.	n.c.
	FeO	4.00	4.29	4.44	4.47	4.43	4.55	4.07	3.93	4.24
	MnO	0.06	0.07	0.07	0.05	b.d.	0.02	0.04	0.05	0.06
	NiO	0.11	b.d.	b.d.	b.d.	b.d.	b.d.	0.05	0.18	0.12
	MgO	18.41	17.63	18.04	17.83	17.42	17.67	18.13	17.93	17.89
	CaO	12.39	12.21	12.21	12.42	12.17	12.31	12.55	12.70	12.69
	Na2O	3.37	3.17	3.09	3.18	3.39	3.23	3.30	3.32	3.42
	K2O	0.02	b.d.	b.d.	0.01	b.d.	0.04	0.04	0.01	b.d.
	H2O	2.13	2.10	2.12	2.12	2.09	2.11	2.11	2.11	2.11
	Total	101.18	100.06	100.33	100.34	99.74	100.68	100.64	100.78	100.57
Cations	Si	6.267	6.300	6.294	6.255	6.230	6.233	6.233	6.240	6.233
	Ti	0.185	0.195	0.116	0.129	0.176	0.197	0.190	0.201	0.204
	Cr	0.202	0.161	0.142	0.118	0.200	0.163	0.248	0.236	0.173
	Al	2.113	2.212	2.257	2.313	2.269	2.259	2.088	2.108	2.139
	Fe3+	n.c.	n.c.	n.c.	n.c.	n.c.	n.c.	n.c.	n.c.	n.c.
	Fe2+	0.472	0.512	0.525	0.530	0.531	0.540	0.483	0.466	0.504
	Mn	0.007	0.008	0.008	0.006	b.d.	0.002	0.005	0.006	0.007
	Ni	0.012	b.d.	b.d.	b.d.	b.d.	b.d.	0.006	0.021	0.014
	Mg	3.870	3.747	3.805	3.765	3.724	3.736	3.838	3.792	3.792
	Ca	1.872	1.865	1.851	1.885	1.870	1.871	1.909	1.931	1.933
	Na	0.921	0.876	0.848	0.873	0.943	0.888	0.909	0.913	0.943
	K	0.004	b.d.	b.d.	0.002	b.d.	0.007	0.007	0.002	b.d.
	H	2.000	2.000	2.000	2.000	2.000	2.000	2.000	2.000	2.000
	Sum	15.925	15.876	15.848	15.875	15.943	15.895	15.916	15.915	15.943
	Al IV	1.7333	1.7003	1.7060	1.7450	1.7703	1.7673	1.7667	1.7601	1.7668
	Al VI	0.3798	0.5116	0.5512	0.5679	0.4988	0.4916	0.3208	0.3476	0.3721
	Mg #	0.8913	0.8799	0.8787	0.8767	0.8751	0.8738	0.8881	0.8905	0.8826
	NaK (A)	0.9251	0.8763	0.8478	0.8752	0.9427	0.8954	0.9158	0.9152	0.9429

Abbreviations: Prg hbl = pargasitic hornblende, Prg = pargasite, Pl-b hrz = plagioclase-bearing harzburgite, b.d. = below detection limit, n.c. = not calculated. Mg# calculated as (MgO/40.3) / (MgO/40.3 + FeO/71.85).

Major element composition of serpentine from the Dramala spinel harzburgite and plagioclase-bearing harzburgite

Sample		PI6	PI6	PI6	PIA44	PIA44	PIA44	PIA44	PIA120	PIA120	PIA120	PIA120	PIA120	PIA120	PIA120	PIA120
Rock		Spl hrz	Spl hrz	Spl hrz	Spl hrz	Spl hrz	Spl hrz	Spl hrz	Pl-b hrz	Pl-b hrz	Pl-b hrz	Pl-b hrz	Pl-b hrz	Pl-b hrz	Pl-b hrz	Pl-b hrz
Mineral		Srp	Srp	Srp	Srp	Srp	Srp	Srp	Srp	Srp	Srp	Srp	Srp	Srp	Srp	Srp
Texture		Mesh	Bastite	Bastite	Bastite	Bastite	Bastite	Bastite	Mesh	Mesh	Mesh	Mesh	Mesh	Mesh	Mesh	Mesh
Wt.%	SiO2	41.65	40.83	42.22	42.66	42.47	40.67	41.60	40.10	42.37	40.34	42.16	41.64	41.03	41.89	38.41
	TiO2	0.02	b.d.	b.d.	0.01	0.01	b.d.	b.d.	b.d.	0.03	0.04	0.05	b.d.	0.04	0.01	0.06
	Cr2O3	0.02	b.d.	0.20	0.85	0.58	0.71	0.51	0.02	0.03	b.d.	b.d.	0.01	b.d.	b.d.	0.02
	Al2O3	0.22	0.07	0.05	1.68	0.63	1.24	1.36	0.13	0.54	0.33	0.66	0.46	1.54	0.54	0.80
	FeO	8.13	7.39	7.53	4.51	7.72	5.83	7.00	5.50	3.56	6.12	7.88	7.97	7.44	8.28	6.98
	MnO	0.28	0.35	0.22	b.d.	0.04	0.14	0.30	0.11	0.08	0.07	0.25	0.21	0.15	0.11	0.14
	NiO	0.11	0.12	0.16	0.08	b.d.	0.05	0.10	0.31	0.09	0.27	0.05	0.22	0.52	0.21	0.44
	MgO	36.28	37.16	37.17	37.10	35.80	36.00	35.11	39.52	38.65	38.82	35.34	34.97	35.07	35.04	38.75
	CaO	0.47	0.45	0.40	0.17	0.14	1.30	0.75	0.19	0.19	0.03	0.31	0.34	0.26	0.29	0.30
	Na2O	0.07	0.05	0.14	0.07	0.02	0.03	0.03	0.12	0.05	0.03	0.13	0.16	0.35	0.14	0.03
	K2O	0.02	0.02	0.02	0.01	b.d.	0.02	0.02	b.d.	b.d.	b.d.	0.06	0.08	0.09	0.09	b.d.
	ZnO	0.02	0.05	n.a.	n.a.	n.a.	n.a.	n.a.	n.a.	n.a.	n.a.	n.a.	n.a.	n.a.	n.a.	n.a.
	H2O	12.47	12.37	12.63	12.58	12.32	12.37	12.45	12.39	12.57	12.39	12.47	12.32	12.38	12.39	12.23
	Total	99.75	98.85	100.74	99.71	99.74	98.35	99.22	98.39	98.16	98.44	99.36	98.38	98.87	98.99	98.16
Cations	Si	2.003	1.980	2.006	2.008	2.025	1.970	2.001	1.941	2.021	1.952	2.027	2.027	1.987	2.027	1.883
	Ti	0.001	b.d.	b.d.	0.001	0.001	b.d.	b.d.	b.d.	0.001	0.001	0.002	b.d.	0.001	0.000	0.002
	Cr	0.001	b.d.	0.007	0.031	0.022	0.027	0.019	0.001	0.001	b.d.	b.d.	0.000	b.d.	b.d.	0.001
	Al	0.012	0.004	0.003	0.093	0.036	0.071	0.077	0.007	0.030	0.019	0.037	0.026	0.088	0.031	0.046
	Fe2+	0.327	0.300	0.299	0.178	0.308	0.236	0.281	0.223	0.142	0.248	0.317	0.324	0.301	0.335	0.286
	Mn	0.011	0.014	0.009	b.d.	0.002	0.006	0.012	0.005	0.003	0.003	0.010	0.009	0.006	0.005	0.006
	Ni	0.004	0.005	0.006	0.003	b.d.	0.002	0.004	0.012	0.003	0.011	0.002	0.009	0.020	0.008	0.017
	Mg	2.601	2.686	2.632	2.603	2.545	2.599	2.516	2.851	2.748	2.800	2.533	2.537	2.531	2.527	2.832
	Ca	0.024	0.023	0.021	0.009	0.007	0.067	0.039	0.010	0.010	0.002	0.016	0.018	0.013	0.015	0.016
	Na	0.007	0.005	0.013	0.006	0.002	0.003	0.003	0.011	0.005	0.003	0.012	0.015	0.033	0.013	0.003
	K	0.001	0.001	0.001	0.000	b.d.	0.001	0.001	b.d.	b.d.	b.d.	0.004	0.005	0.006	0.006	b.d.
	Zn	0.001	0.002	n.a.	n.a.	n.a.	n.a.	n.a.	n.a.	n.a.	n.a.	n.a.	n.a.	n.a.	n.a.	n.a.
	H	4.000	4.000	4.000	3.949	3.918	3.995	3.995	4.000	4.000	4.000	4.000	4.000	4.000	4.000	4.000
	Sum	4.993	5.020	4.997	4.932	4.946	4.983	4.953	5.061	4.964	5.038	4.960	4.970	4.987	4.967	5.092
	Mg #	0.888	0.900	0.898	0.936	0.892	0.917	0.899	0.928	0.951	0.919	0.889	0.887	0.894	0.883	0.908

Abbreviations: Srp = serpentine, Mesh = serpentine after olivine, Bastite = serpentine after orthopyroxene, Spl hrz = spinel harzburgite, Pl-b hrz = plagioclase-bearing harzburgite, b.d. = below detection, n.a. = not analyzed. Mg# calculated as (MgO/40.3) / (MgO/40.3 + FeO/71.85).

Major element composition of serpentine from the Dramala spinel harzburgite and plagioclase-bearing harzburgite continued

Sample		**PIA109**	**PIA109**	**PIA109**	**PIA109**	**PIA109**	**PIA109**	**PIA51**
Rock		**Pl-b hrz**	**Pl-b hrz**	**Pl-b hrz**	**Pl-b hrz**	**Pl-b hrz**	**Pl-b hrz**	**Pl-b hrz**
Mineral		**Srp**	**Srp**	**Srp**	**Srp**	**Srp**	**Srp**	**Srp**
Texture		**Bastite**	**Bastite**	**Bastite**	**Bastite**	**Vein**	**Vein**	**Vein**
Wt.%	**SiO2**	38.08	42.08	41.18	41.88	40.90	40.89	42.21
	TiO2	b.d.	b.d.	0.03	b.d.	b.d.	b.d.	b.d.
	Cr2O3	b.d.	0.08	b.d.	b.d.	0.05	0.02	0.03
	Al2O3	0.50	0.65	1.35	1.31	1.35	1.36	0.27
	FeO	5.84	8.31	7.66	7.01	6.71	6.50	5.27
	MnO	0.05	0.17	0.14	0.15	0.04	0.16	0.08
	NiO	0.24	0.15	0.04	0.05	b.d.	b.d.	0.10
	MgO	41.51	34.64	35.45	36.37	37.03	37.18	37.65
	CaO	0.15	0.35	0.14	0.21	0.14	0.16	0.22
	Na2O	0.02	0.06	0.10	0.08	0.03	b.d.	0.01
	K2O	0.03	0.05	0.05	0.01	b.d.	0.02	0.01
	ZnO	n.a.	n.a.	n.a.	n.a.	n.a.	n.a.	n.a.
	H2O	12.36	12.40	12.38	12.56	12.33	12.35	12.50
	Total	98.78	98.94	98.52	99.63	98.58	98.64	98.36
Cations	**Si**	1.848	2.035	1.995	1.999	1.971	1.969	2.026
	Ti	b.d.	b.d.	0.001	b.d.	b.d.	b.d.	b.d.
	Cr	b.d.	0.003	b.d.	b.d.	0.002	0.001	0.001
	Al	0.029	0.037	0.077	0.074	0.077	0.077	0.015
	Fe2+	0.237	0.336	0.310	0.280	0.270	0.262	0.211
	Mn	0.002	0.007	0.006	0.006	0.002	0.007	0.003
	Ni	0.009	0.006	0.002	0.002	b.d.	b.d.	0.004
	Mg	3.003	2.497	2.560	2.588	2.660	2.668	2.693
	Ca	0.008	0.018	0.007	0.011	0.007	0.008	0.011
	Na	0.002	0.006	0.009	0.007	0.003	b.d.	0.001
	K	0.002	0.003	0.003	0.001	b.d.	0.001	0.001
	Zn	n.a.	n.a.	n.a.	n.a.	n.a.	n.a.	n.a.
	H	4.000	4.000	4.000	4.000	3.962	3.966	4.000
	Sum	5.139	4.949	4.971	4.968	4.991	4.993	4.967
	Mg #	0.927	0.881	0.892	0.902	0.908	0.911	0.927

Abbreviations: Srp = serpentine, Mesh = serpentine after olivine, Bastite = serpentine after orthopyroxene, Pl-b hrz = plagioclase-bearing harzburgite, b.d. = below detection, n.a. = not analyzed. Mg# calculated as (MgO/40.3) / (MgO/40.3 + FeO/71.85).

Major element composition of talc from the Dramala spinel harzburgite and plagioclase-bearing harzburgite

Sample		**PIA27**	**PIA27**	**PI6**	**PI6**	**PIA51**	**PIA51**	**PIA51**
Rock		**Spl hrz**	**Spl hrz**	**Spl hrz**	**Spl hrz**	**Pl-b hrz**	**Pl-b hrz**	**Pl-b hrz**
Mineral		**Tlc**	**Tlc**	**Tlc**	**Tlc**	**Tlc**	**Tlc**	**Tlc**
Wt.%	**SiO2**	61.03	60.47	59.09	55.92	59.36	60.76	61.49
	TiO2	0.01	0.01	0.01	0.01	b.d.	0.01	0.02
	Cr2O3	0.35	0.54	0.44	0.39	0.64	0.59	0.15
	Al2O3	1.12	2.06	1.05	0.48	1.95	1.89	1.08
	FeO	0.99	1.50	2.66	4.34	1.85	1.77	2.07
	MnO	0.04	0.02	0.05	0.04	b.d.	b.d.	0.02
	NiO	0.14	0.09	0.06	0.07	0.09	0.12	0.09
	MgO	30.45	30.92	32.19	33.62	30.29	29.79	30.30
	CaO	0.01	0.01	0.04	0.07	0.02	0.05	0.04
	Na2O	0.15	0.09	0.03	0.21	0.08	0.03	0.35
	K2O	b.d.	0.01	0.01	0.02	0.03	0.01	0.01
	ZnO	b.d.	b.d.	0.05	b.d.	b.d.	b.d.	b.d.
	H2O	4.66	4.71	4.66	4.56	4.63	4.68	4.70
	Total	98.94	100.43	100.32	99.73	98.94	99.70	100.33
Cations	**Si**	3.926	3.850	3.802	3.677	3.845	3.894	3.922
	Ti	0.001	0.001	0.000	0.000	b.d.	0.001	0.001
	Cr	0.018	0.027	0.023	0.020	0.033	0.030	0.008
	Al	0.085	0.155	0.079	0.038	0.149	0.143	0.081
	Fe2+	0.053	0.080	0.143	0.239	0.100	0.095	0.110
	Mn	0.002	0.001	0.003	0.002	b.d.	b.d.	0.001
	Ni	0.007	0.005	0.003	0.004	0.005	0.006	0.005
	Mg	2.920	2.934	3.087	3.295	2.924	2.846	2.880
	Ca	0.001	0.001	0.003	0.005	0.002	0.003	0.003
	Na	0.018	0.012	0.003	0.026	0.010	0.004	0.043
	K	b.d.	0.001	0.000	0.002	0.003	0.001	0.000
	Zn	b.d.	b.d.	0.002	b.d.	b.d.	b.d.	b.d.
	H	2.000	2.000	2.000	2.000	2.000	2.000	2.000
	Sum	7.031	7.065	7.148	7.308	7.070	7.022	7.055
	Mg #	0.982	0.974	0.956	0.932	0.967	0.968	0.963

Abbreviations: Tlc = talc, Spl hrz = spinel harzburgite, Pl-b hrz = plagioclase-bearing harzburgite, b.d. = below detection.
Mg# calculated as (MgO/40.3) / (MgO/40.3 + FeO/71.85).

Major element composition of chlorite from the Dramala spinel harzburgite and plagioclase-bearing harzburgite

Sample		PIA27	PI6	PI6	PIA120	PIA120	PIA120
Rock		Spl hrz	Spl hrz	Spl hrz	Pl-b hrz	Pl-b hrz	Pl-b hrz
Mineral		Chl	Chl	Chl	Chl	Chl	Chl
Wt.%	SiO2	41.24	33.32	33.66	24.38	21.70	26.14
	TiO2	0.01	b.d.	b.d.	0.03	b.d.	b.d.
	Cr2O3	1.24	2.56	2.22	0.05	0.11	b.d.
	Al2O3	9.58	13.34	12.97	20.15	22.73	18.80
	FeO	2.09	3.64	3.16	32.90	40.24	28.99
	MnO	b.d.	0.03	0.06	0.66	1.87	1.31
	NiO	0.12	0.14	0.09	0.14	b.d.	b.d.
	MgO	32.86	35.04	35.55	9.37	1.89	4.08
	CaO	0.01	b.d.	0.08	0.27	0.21	9.36
	Na2O	0.08	0.04	0.03	0.18	0.34	0.37
	K2O	b.d.	b.d.	b.d.	0.01	0.03	0.04
	ZnO	b.d.	b.d.	0.01	b.d.	b.d.	b.d.
	H2O	13.01	12.74	12.75	10.89	10.48	10.73
	Total	100.24	100.86	100.58	99.03	99.60	99.82
Cations	Si	3.803	3.137	3.168	2.685	2.483	2.873
	Ti	0.001	b.d.	b.d.	0.002	b.d.	b.d.
	Cr	0.090	0.191	0.165	0.004	0.010	b.d.
	Al	1.041	1.480	1.439	2.616	3.066	2.436
	Fe2+	0.161	0.287	0.249	3.030	3.850	2.665
	Mn	b.d.	0.002	0.005	0.062	0.181	0.122
	Ni	0.009	0.011	0.007	0.012	b.d.	b.d.
	Mg	4.517	4.917	4.986	1.538	0.322	0.668
	Ca	0.001	b.d.	0.008	0.032	0.026	1.102
	Na	0.015	0.008	0.005	0.038	0.075	0.079
	K	b.d.	b.d.	b.d.	0.001	0.004	0.006
	Zn	b.d.	b.d.	0.001	b.d.	b.d.	b.d.
	H	8.000	8.000	8.000	8.000	8.000	7.866
	Sum	9.638	10.032	10.033	10.022	10.019	9.951
	Mg #	0.966	0.945	0.952	0.337	0.077	0.201

Abbreviations: Chl = chlorite, Spl hrz = spinel harzburgite, Pl-b hrz = plagioclase-bearing harzburgite, b.d. = below detection limit.
Mg# calculated as (MgO/40.3) / (MgO/40.3 + FeO/71.85).

Major element composition of vuagnatite from the Dramala plagioclase-bearing harzburgite

Sample		PIA120	PIA120	PIA120	PIA120	PIA120	PIA120	PIA120
Rock		Pl-b hrz	Pl-b hrz	Pl-b hrz	Pl-b hrz	Pl-b hrz	Pl-b hrz	Pl-b hrz
Mineral		Vua	Vua	Vua	Vua	Vua	Vua	Vua
Wt.%	SiO2	33.59	33.65	33.69	33.06	33.52	33.51	33.53
	TiO2	0.03	0.03	b.d.	n.a.	n.a.	n.a.	n.a.
	Al2O3	27.77	27.96	28.05	29.52	29.55	29.57	29.66
	FeO	0.23	0.60	0.22	0.16	0.29	0.15	0.19
	Cr2O3	0.06	b.d.	0.01	n.a.	n.a.	n.a.	n.a.
	MnO	0.04	0.05	0.10	n.a.	n.a.	n.a.	n.a.
	NiO	b.d.	b.d.	b.d.	n.a.	n.a.	n.a.	n.a.
	MgO	0.01	b.d.	b.d.	n.a.	n.a.	n.a.	n.a.
	CaO	31.82	31.47	31.23	31.19	31.35	31.82	31.68
	Na2O	b.d.	0.02	b.d.	0.04	b.d.	0.01	0.07
	K2O	b.d.	0.01	b.d.	b.d.	0.02	0.01	0.01
	H2O	5.02	5.03	5.02	5.06	5.10	5.12	5.12
	Total	98.56	98.82	98.31	99.03	99.83	100.19	100.25
Cations	Si	1.003	1.002	1.006	0.979	0.985	0.982	0.982
	Al	0.977	0.982	0.987	1.031	1.023	1.021	1.024
	Fe2+	0.006	0.015	0.005	0.004	0.007	0.004	0.005
	Ti	0.001	0.001	b.d.	n.a.	n.a.	n.a.	n.a.
	Cr	0.001	b.d.	0.000	n.a.	n.a.	n.a.	n.a.
	Mn	0.001	0.001	0.003	n.a.	n.a.	n.a.	n.a.
	Ni	b.d.	b.d.	b.d.	n.a.	n.a.	n.a.	n.a.
	Mg	0.000	b.d.	b.d.	n.a.	n.a.	n.a.	n.a.
	Ca	1.018	1.004	0.999	0.990	0.987	0.999	0.994
	Na	b.d.	0.001	b.d.	0.002	b.d.	0.001	0.004
	K	b.d.	0.001	b.d.	b.d.	0.001	0.000	0.001
	H	1.000	1.000	1.000	1.000	1.000	1.000	1.000
	Sum	3.007	3.007	3.000	3.007	3.004	3.007	3.008

Abbreviations: Vua = vuagnatite, Pl-b hrz = plagioclase-bearing harzburgite, b.d. = below detection limit, n.a. = not analyzed.

Major element composition of pectolite from the Dramala plagioclase-bearing harzburgite

Sample		PIA120	PIA120	PIA120	PIA120	PIA120	PIA120	PIA120
Rock		Pl-b hrz	Pl-b hrz	Pl-b hrz	Pl-b hrz	Pl-b hrz	Pl-b hrz	Pl-b hrz
Mineral		Pct	Pct	Pct	Pct	Pct	Pct	Pct
Wt.%	SiO2	53.35	54.09	54.41	53.32	53.52	53.49	53.19
	TiO2	b.d.	0.03	b.d.	0.01	n.a.	n.a.	n.a.
	Al2O3	0.46	0.56	0.18	0.86	0.19	0.19	0.42
	Cr2O3	b.d.	b.d.	b.d.	0.03	n.a.	n.a.	n.a.
	FeO	0.25	0.61	0.11	0.26	0.17	0.18	0.21
	MnO	0.86	0.24	0.63	0.09	n.a.	n.a.	n.a.
	NiO	b.d.	b.d.	b.d.	b.d.	n.a.	n.a.	n.a.
	MgO	b.d.	0.26	b.d.	b.d.	n.a.	n.a.	n.a.
	CaO	33.43	33.80	33.29	34.20	33.12	33.05	33.11
	Na2O	9.31	8.78	9.14	8.76	9.29	9.23	9.10
	K2O	0.01	b.d.	b.d.	0.02	0.02	0.01	0.01
	H2O	2.70	2.73	2.72	2.71	2.68	2.68	2.67
	Total	100.37	101.10	100.49	100.27	98.99	98.83	98.71
Cations	Si	2.958	2.965	2.998	2.950	2.992	2.995	2.983
	Ti	b.d.	0.001	b.d.	0.000	n.a.	n.a.	n.a.
	Al	0.030	0.037	0.012	0.056	0.013	0.012	0.028
	Cr	b.d.	b.d.	b.d.	0.001	n.a.	n.a.	n.a.
	Fe2+	0.012	0.028	0.005	0.012	0.008	0.009	0.010
	Mn	0.040	0.011	0.030	0.004	n.a.	n.a.	n.a.
	Ni	b.d.	b.d.	b.d.	b.d.	n.a.	n.a.	n.a.
	Mg	b.d.	0.021	b.d.	b.d.	n.a.	n.a.	n.a.
	Ca	1.986	1.985	1.965	2.027	1.984	1.982	1.989
	Na	1.000	0.933	0.976	0.940	1.007	1.002	0.989
	K	0.001	b.d.	b.d.	0.001	0.001	0.001	0.000
	H	1.000	1.000	1.000	1.000	1.000	1.000	1.000
	Sum	6.027	5.982	5.985	5.992	6.006	6.001	5.998

Abbreviations: Pct = pectolite, Pl-b hrz = plagioclase-bearing harzburgite, b.d. = below detection limit, n.a. = not analyzed.

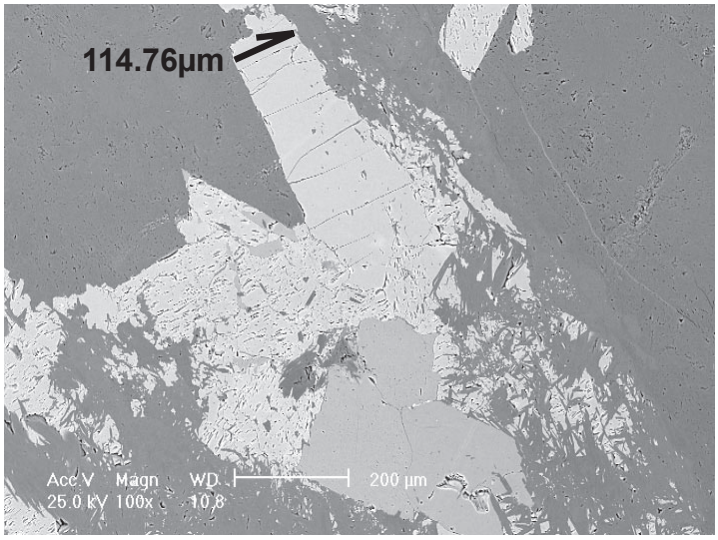
Major element composition of natrolite from the Dramala plagioclase-bearing harzburgite

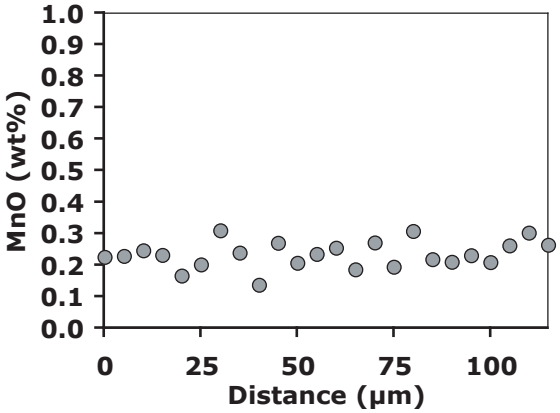
Sample		**PIA120**
Rock		**Pl-b hrz**
Mineral		**Ntr**
Wt.%	**SiO2**	47.12
	Al2O3	27.49
	FeO	0.02
	CaO	0.26
	Na2O	15.53
	K2O	0.03
	H2O	9.56
	Total	100.00
Cations	**Si**	2.975
	Al	2.045
	Fe2+	0.001
	Ca	0.017
	Na	1.901
	K	0.003
	H	0.531
	Sum	7.473

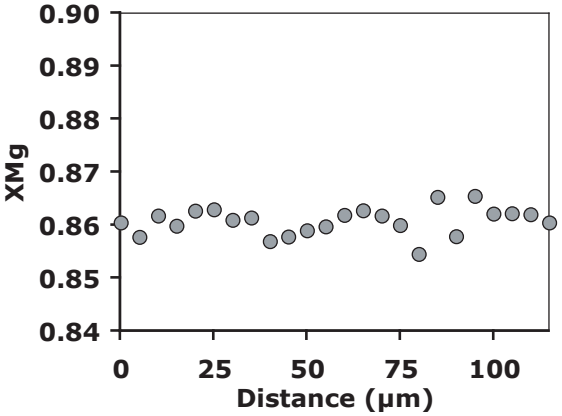
Abbreviations: Ntr = natrolite,
Pl-b hrz = plagioclase-bearing harzburgite.

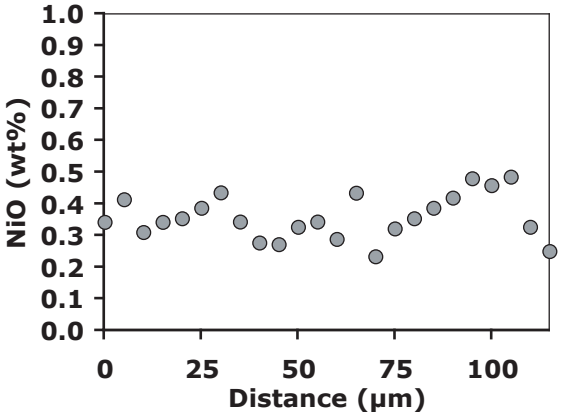
Mineral profiles
major and light elements (Li, B)

Geisspfad ultramafic body
Serpentinite G11 - Olivine
g11olc3

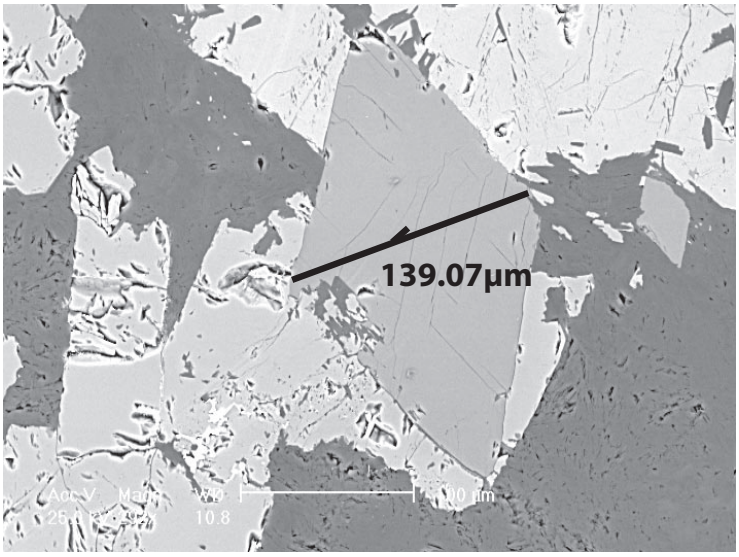


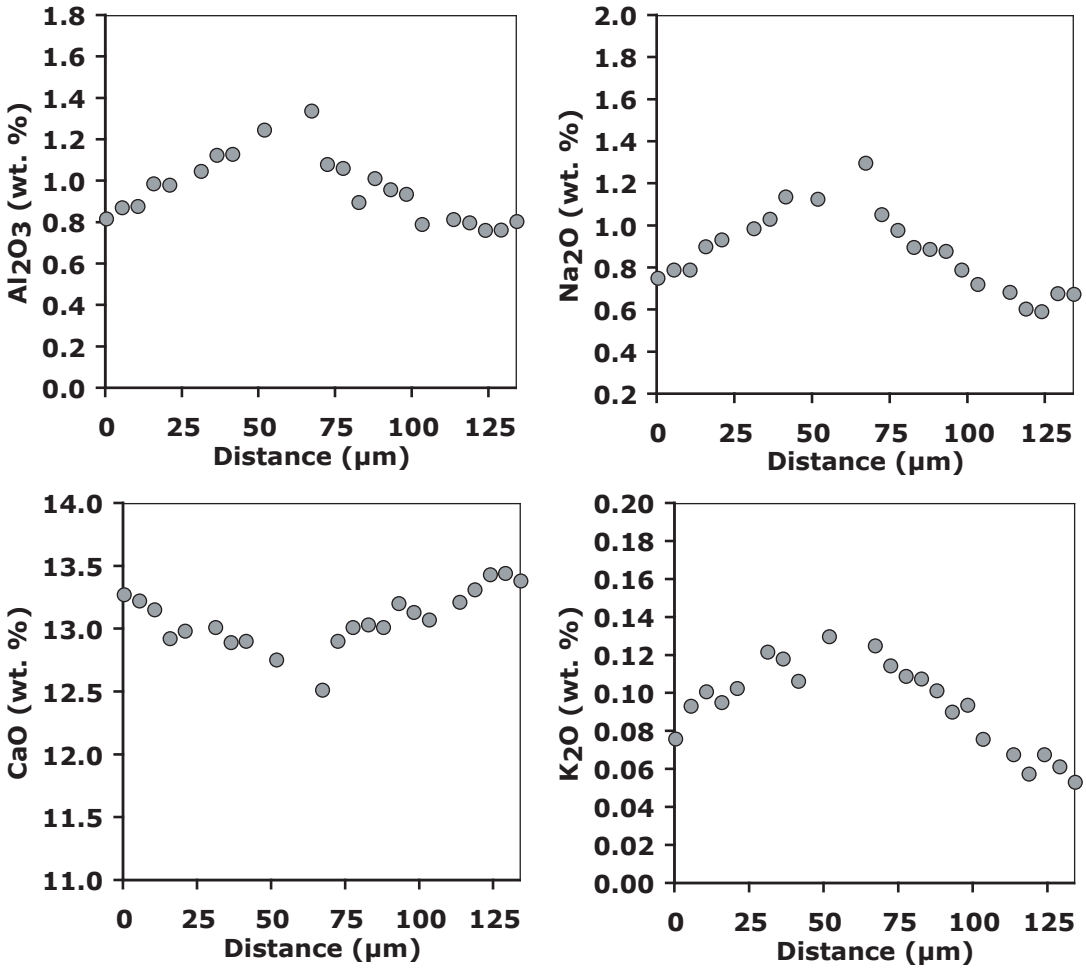




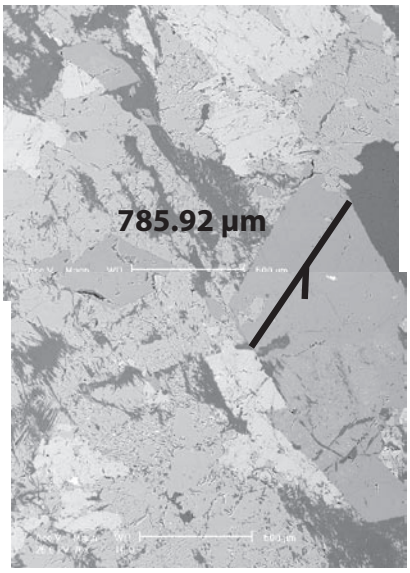


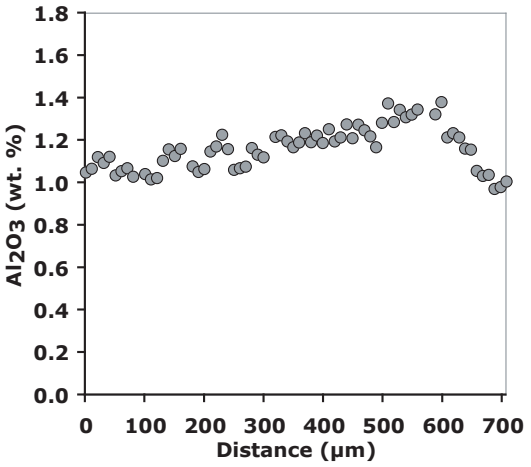
Geisspfad ultramafic body
Serpentinite G11 - Tremolite
g11trec1

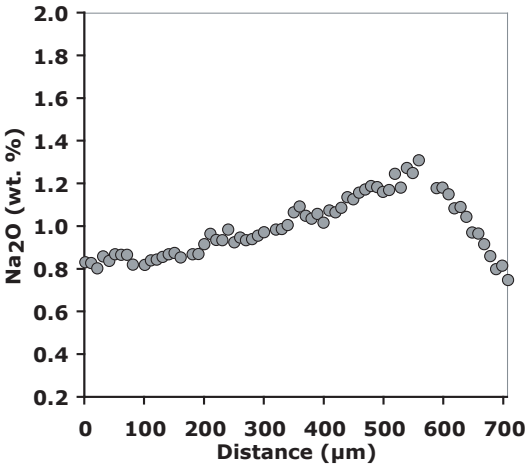


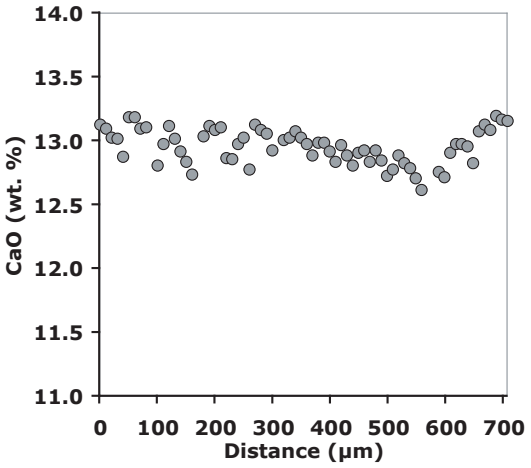


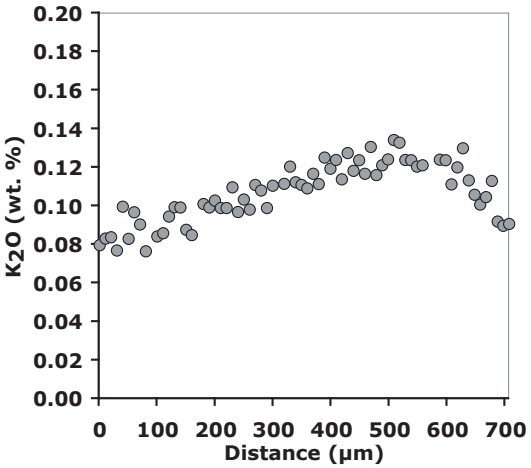
Geisspfad ultramafic body
Serpentinite G11 - Tremolite
g11trec2



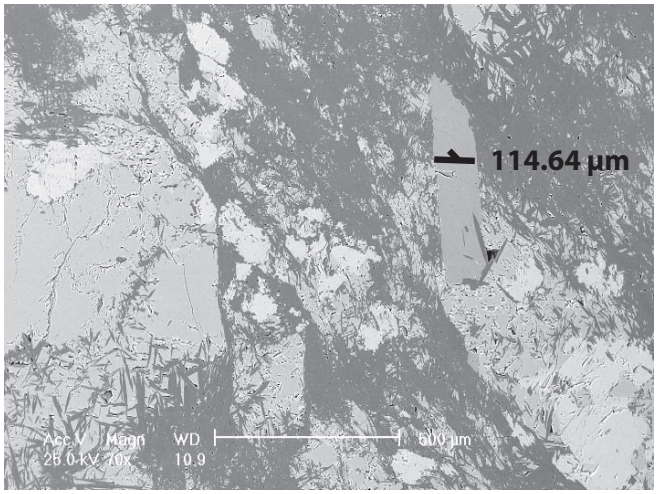


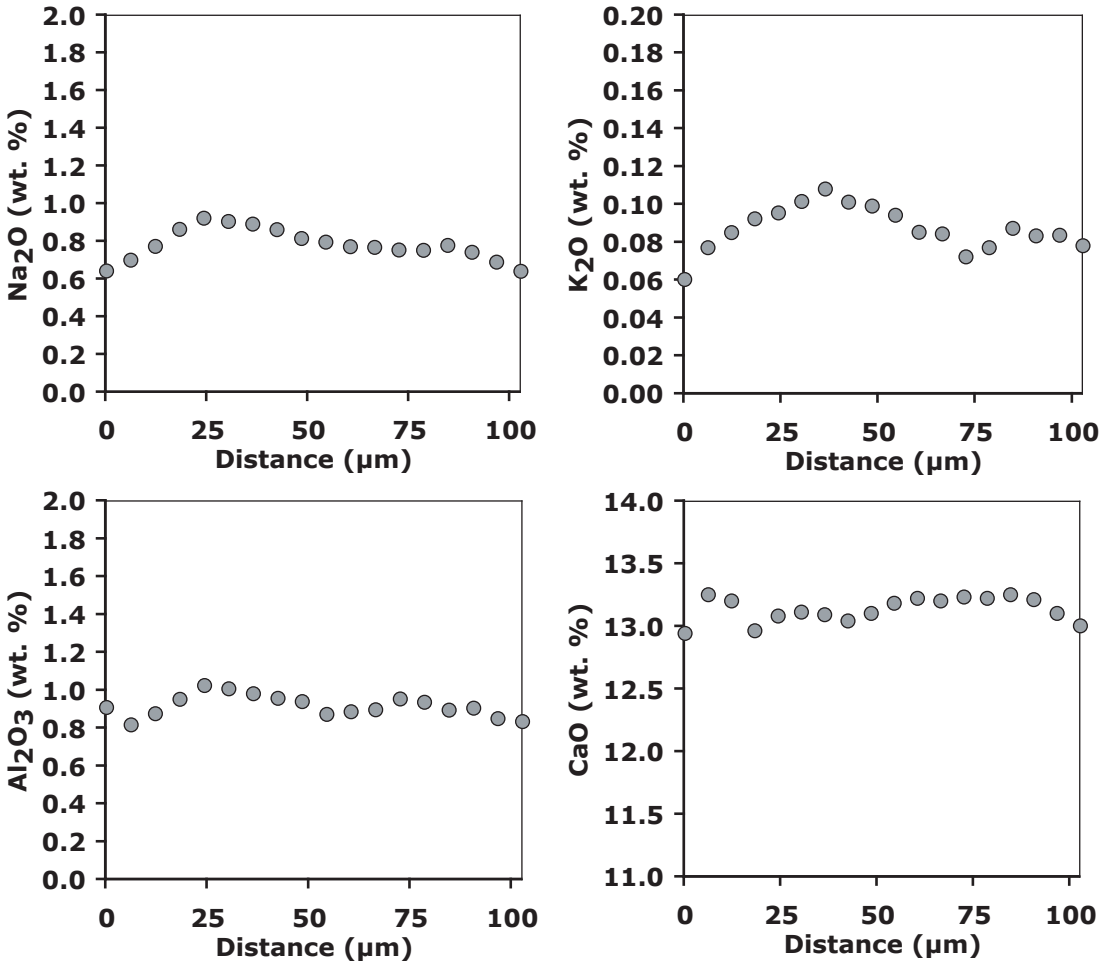




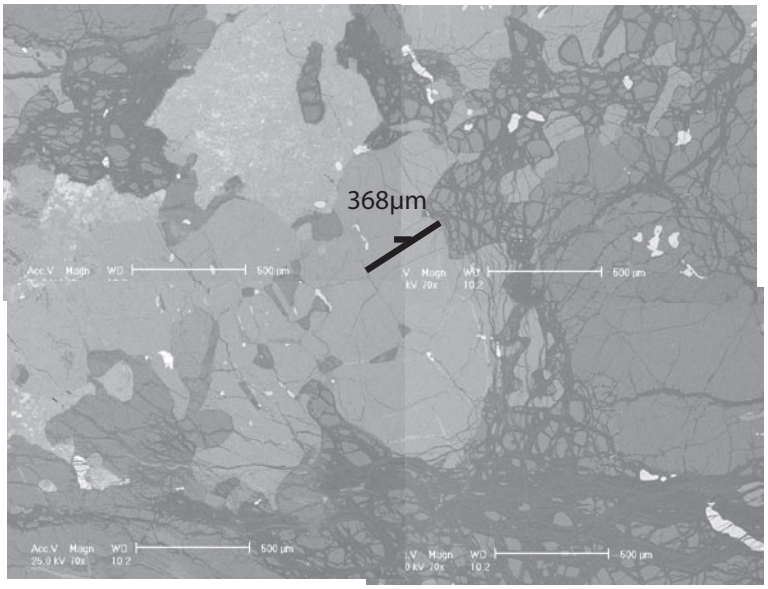


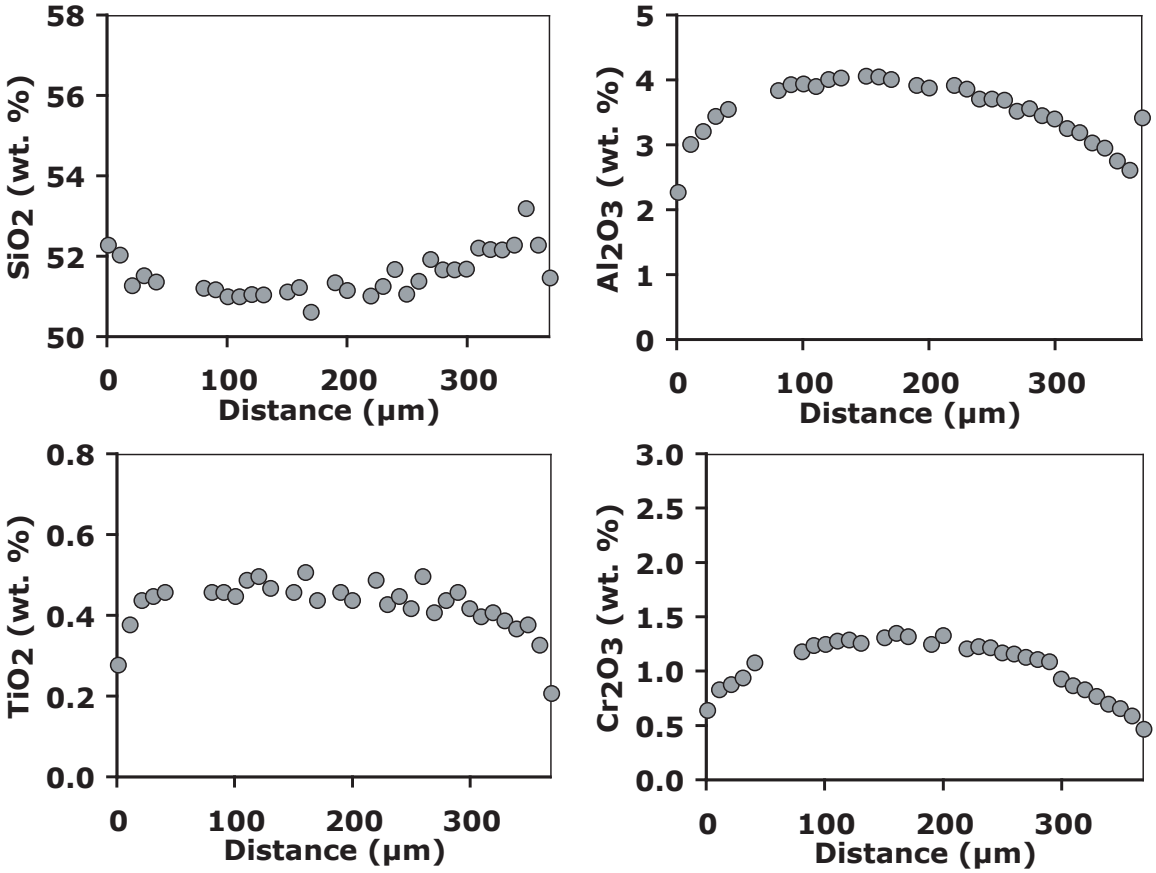
Geisspfad ultramafic body
Serpentinite G11 - Tremolite
g11trec4



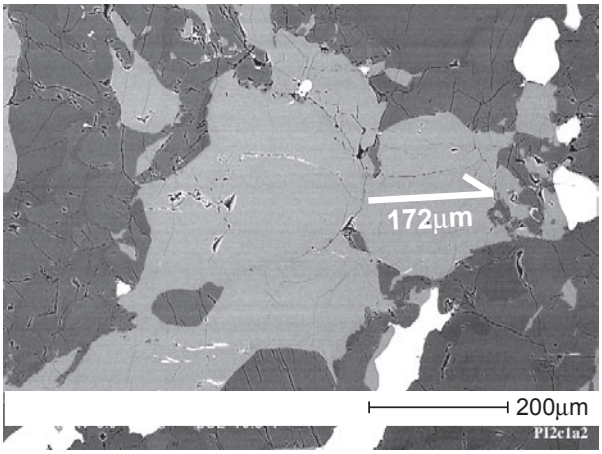


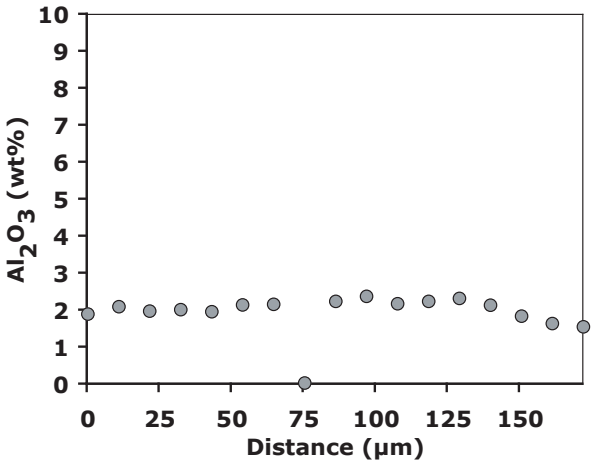
Pindos ophiolite - Dramala complex
Plagioclase-bearing harzburgite PlA120 - Clinopyroxene 12cpc2

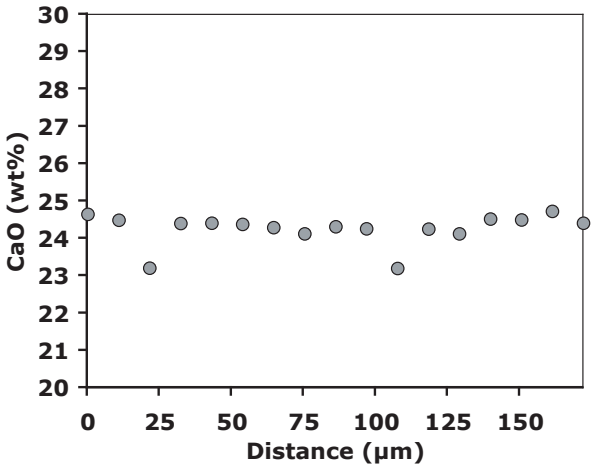


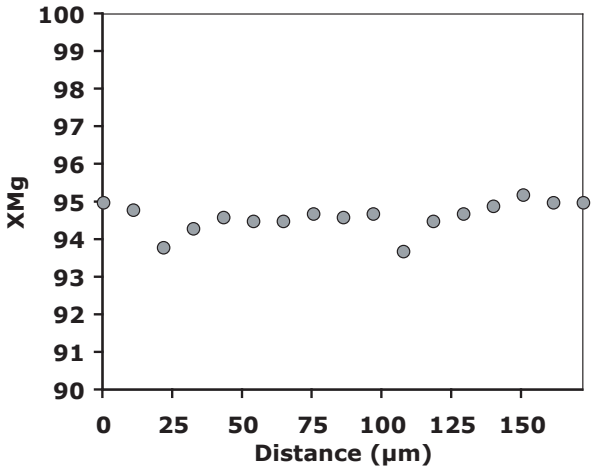


Pindos ophiolite - Dramala complex
Spinel harzburgite Pl2 - Clinopyroxene blast
pi2c1cpxc1

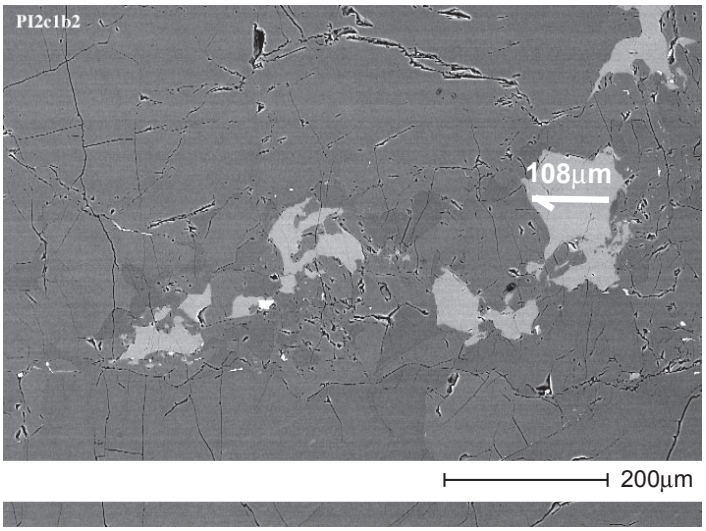


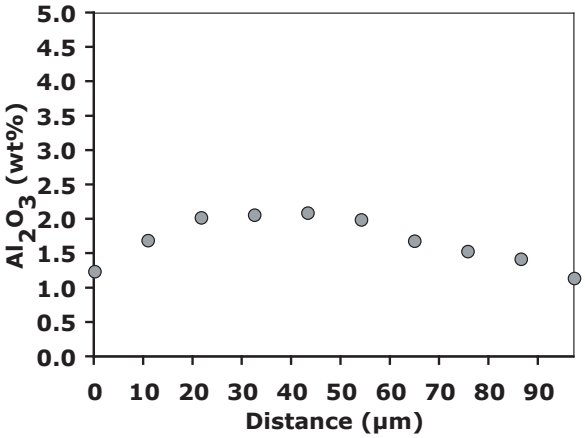


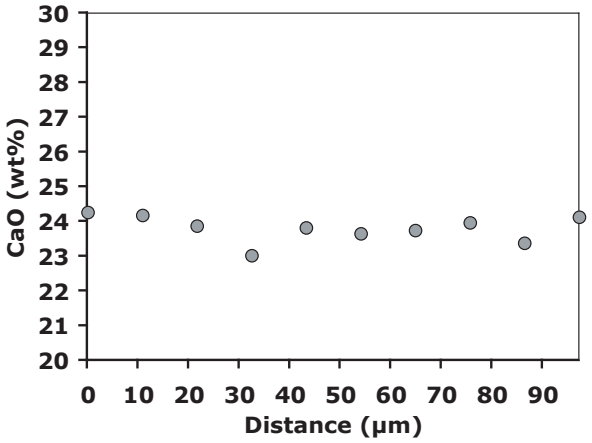


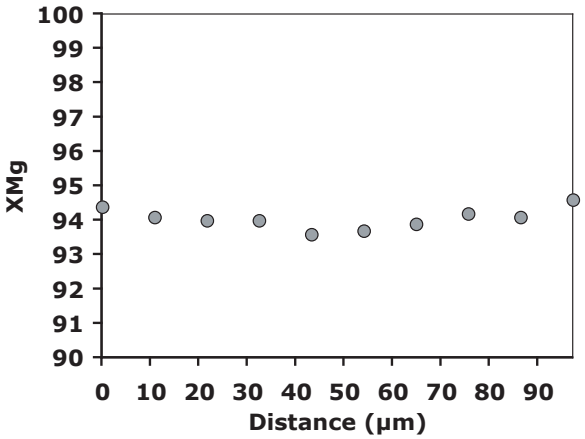


Pindos ophiolite - Dramala complex
Spinel harzburgite PI2 - Clinopyroxene blast
pi2c1cpxc3

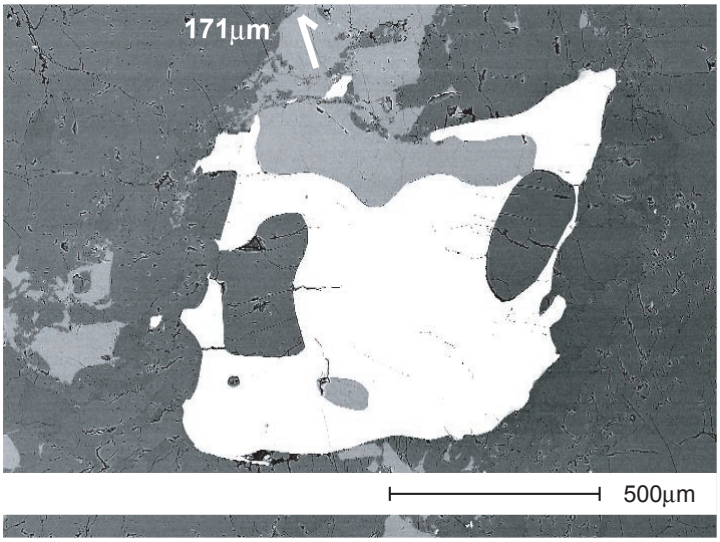


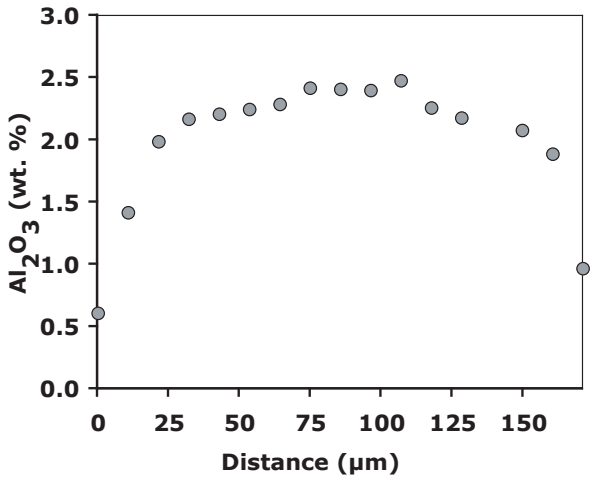


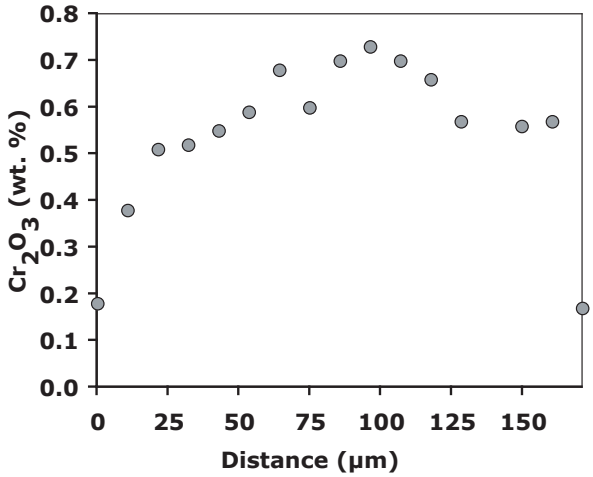


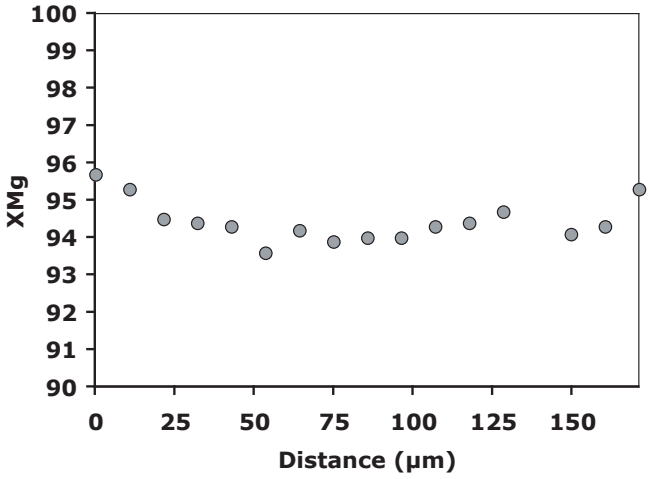


Pindos ophiolite - Dramala complex
Spinel harzburgite Pl2 - Clinopyroxene blast
pi2c4cpxc2

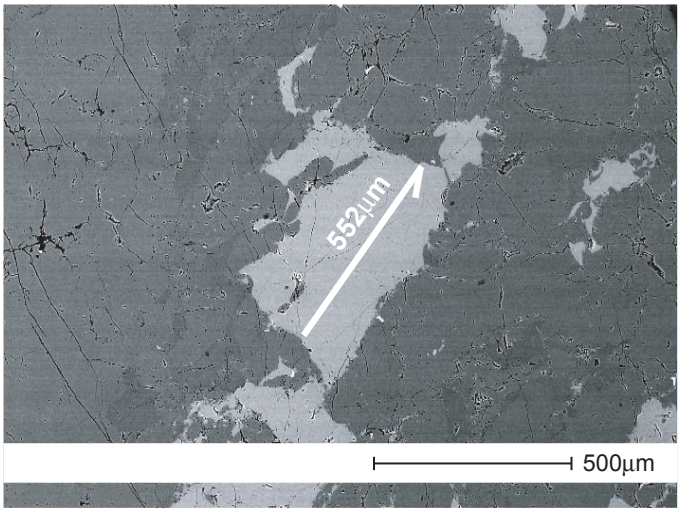


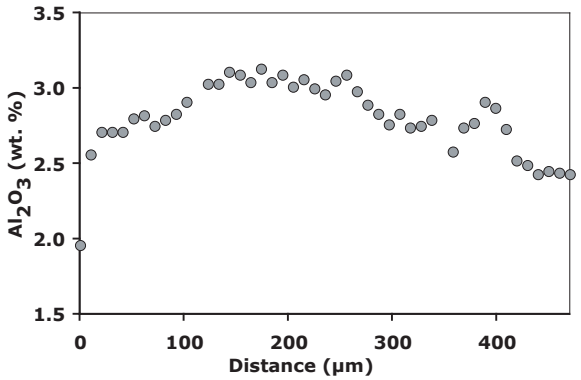


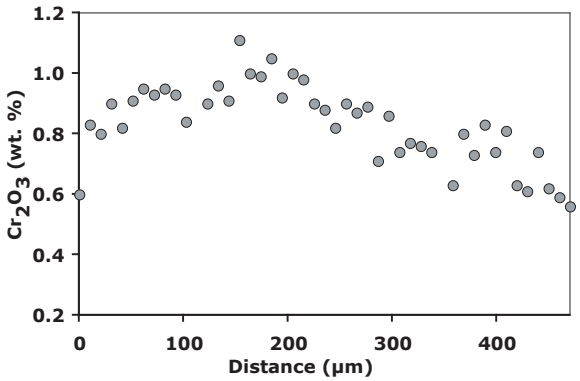


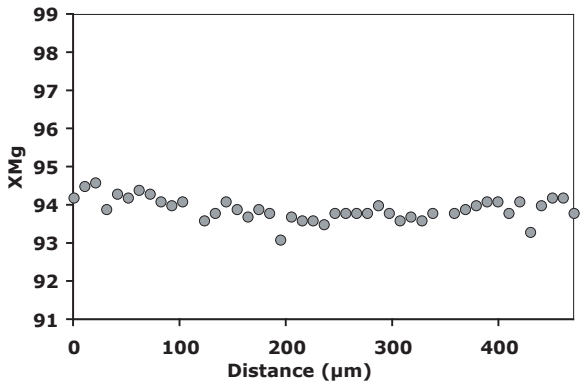


Pindos ophiolite - Dramala complex
Spinel harzburgite PI2 - Clinopyroxene clast
pi2c4cpxc4

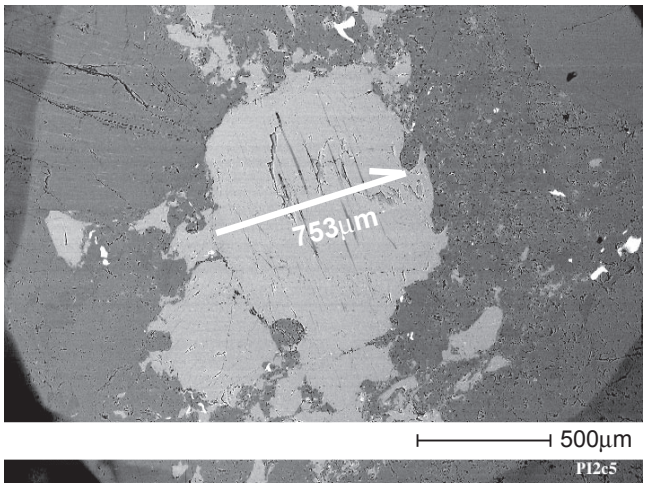


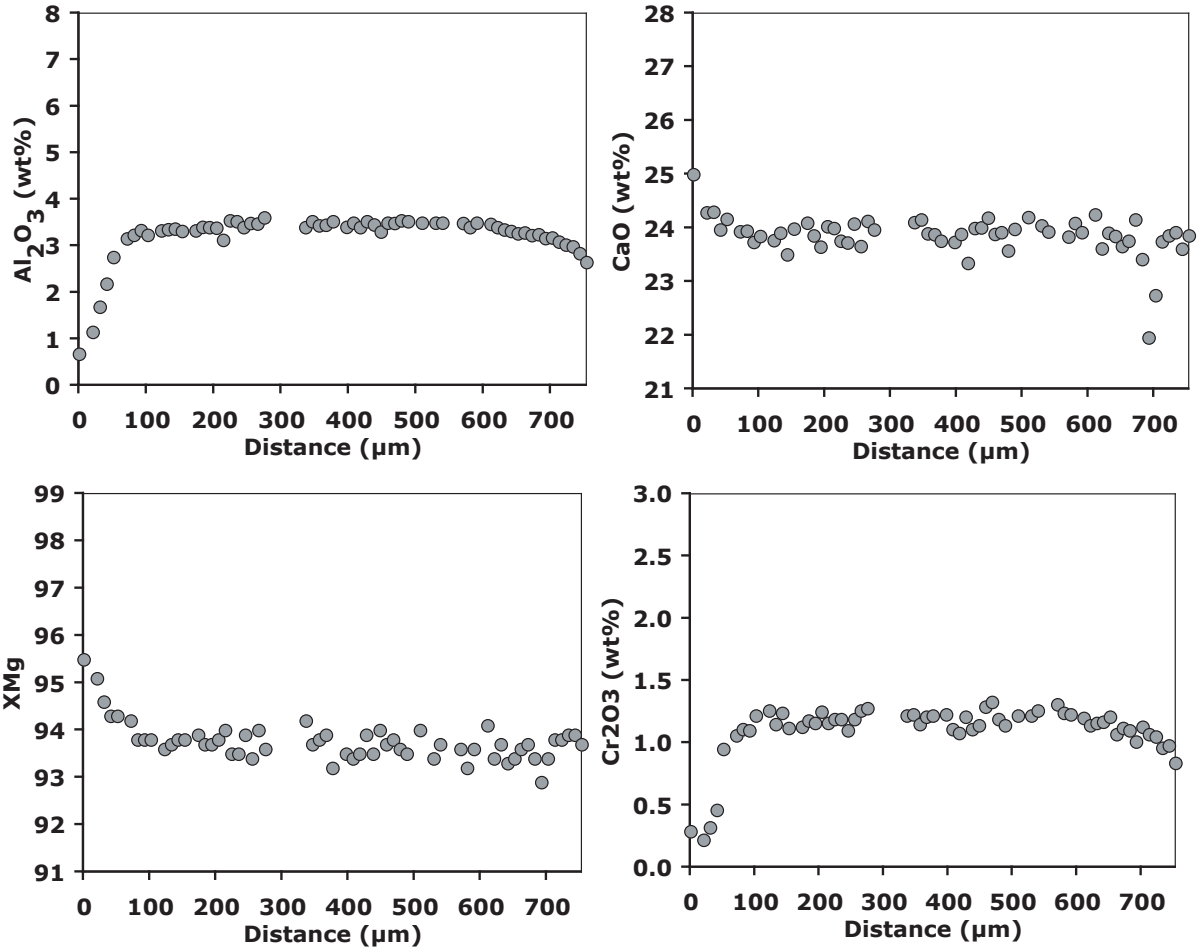




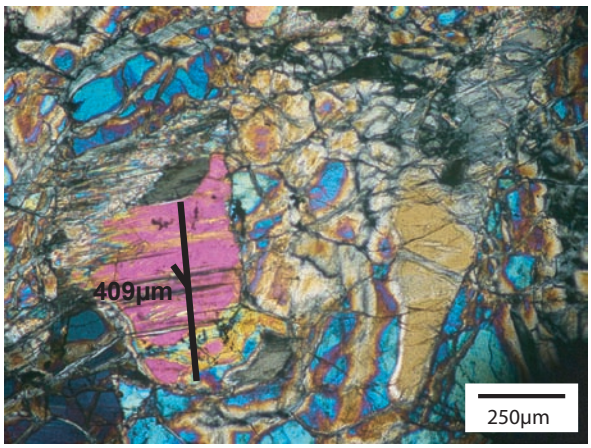


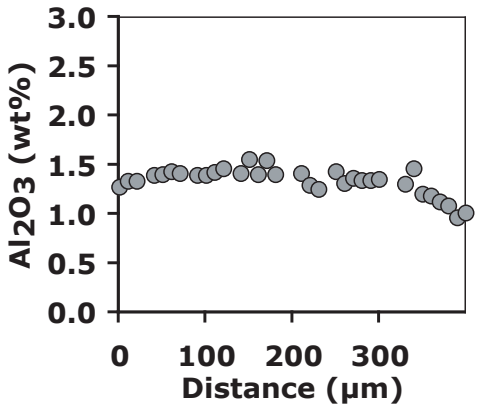
Pindos ophiolite - Dramala complex
Spinel harzburgite PI2 - Clinopyroxene clast
pi2c5cpxc1

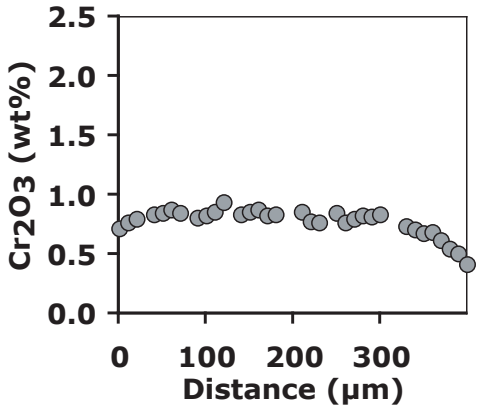




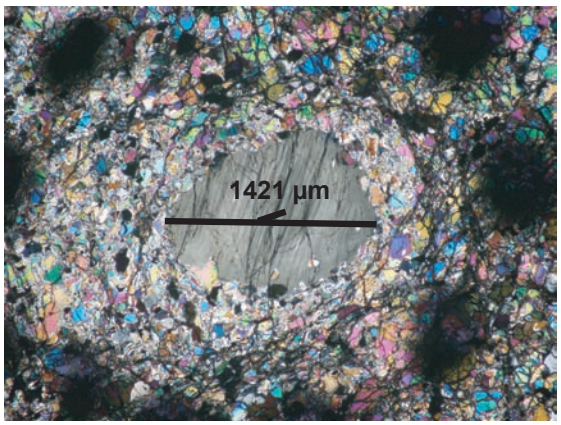
Pindos ophiolite - Dramala complex
Spinel harzburgite Pl6 - Clinoopyroxene clast
pi6cpcc1

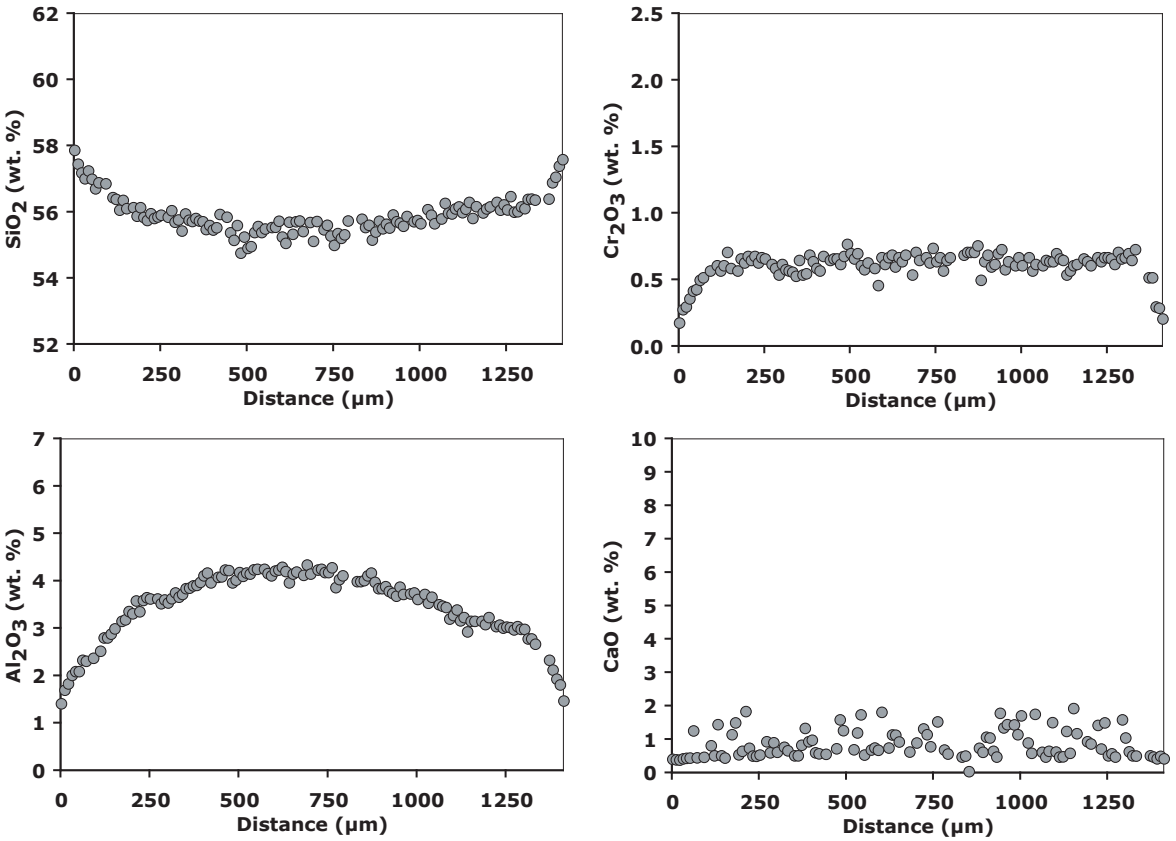




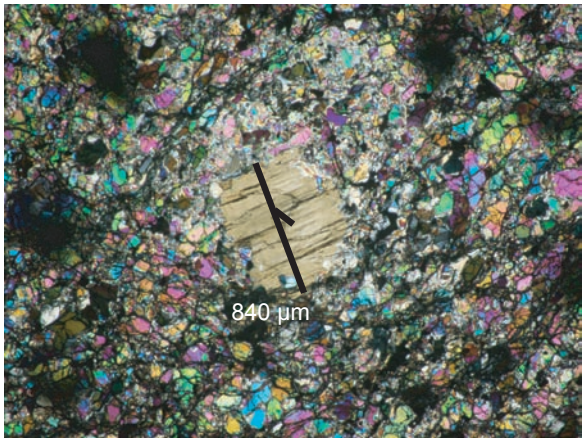


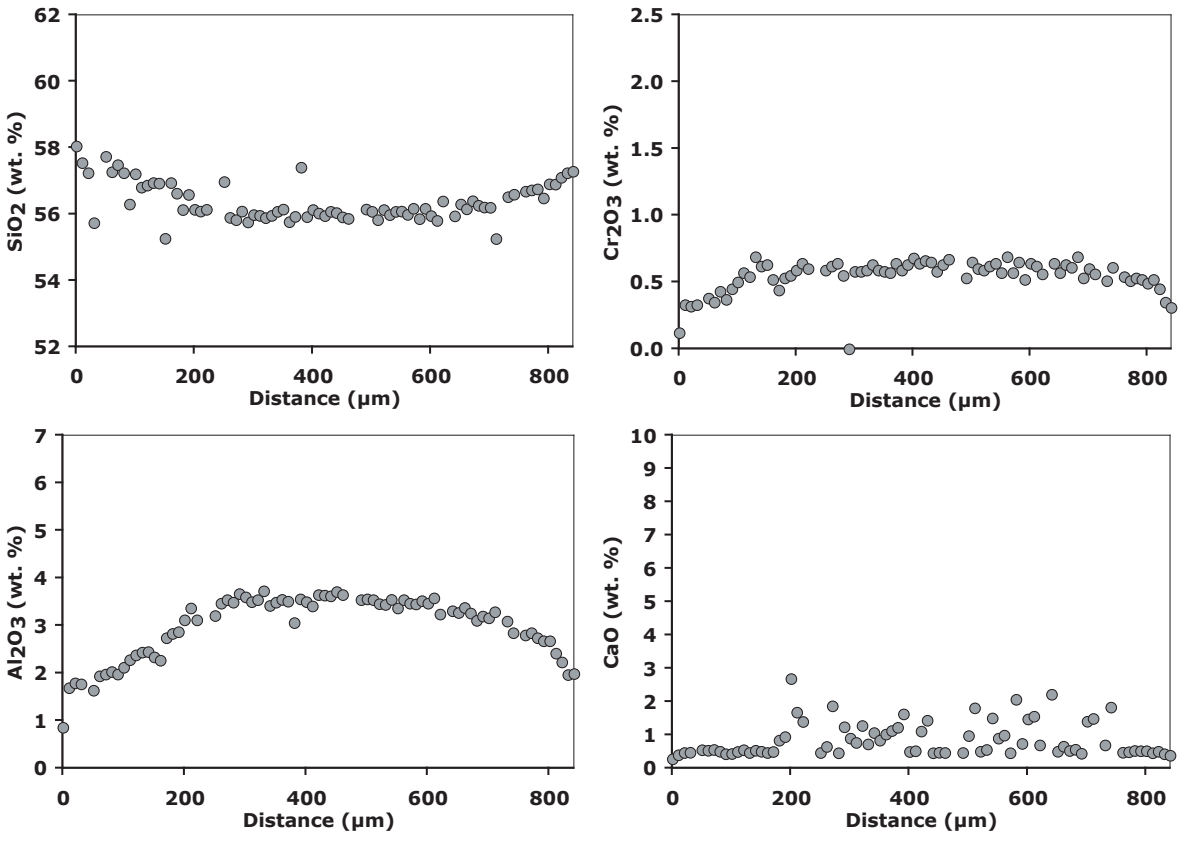
Pindos ophiolite - Dramala complex
Plagioclase-bearing harzburgite PIA109 - Orthopyroxene clast 9c1opxcc1



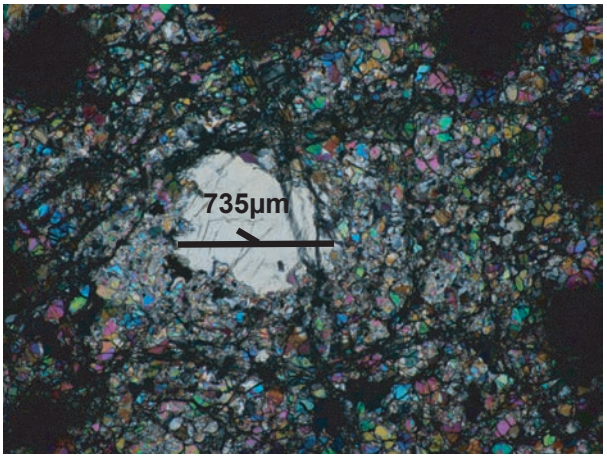


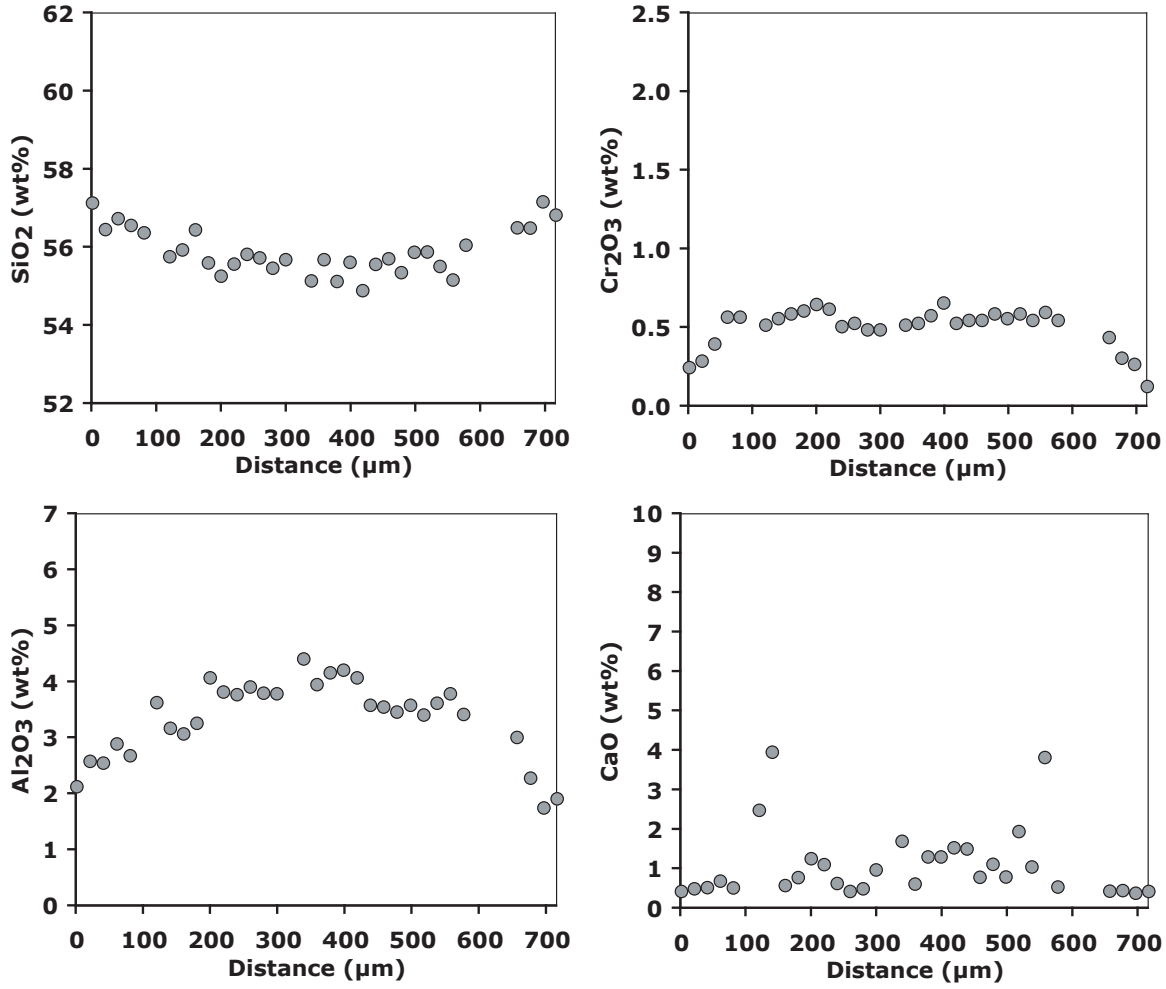
Pindos ophiolite - Dramala complex
Plagioclase-bearing harzburgite PIA109 - Orthopyroxene clast 9c8opxcc1



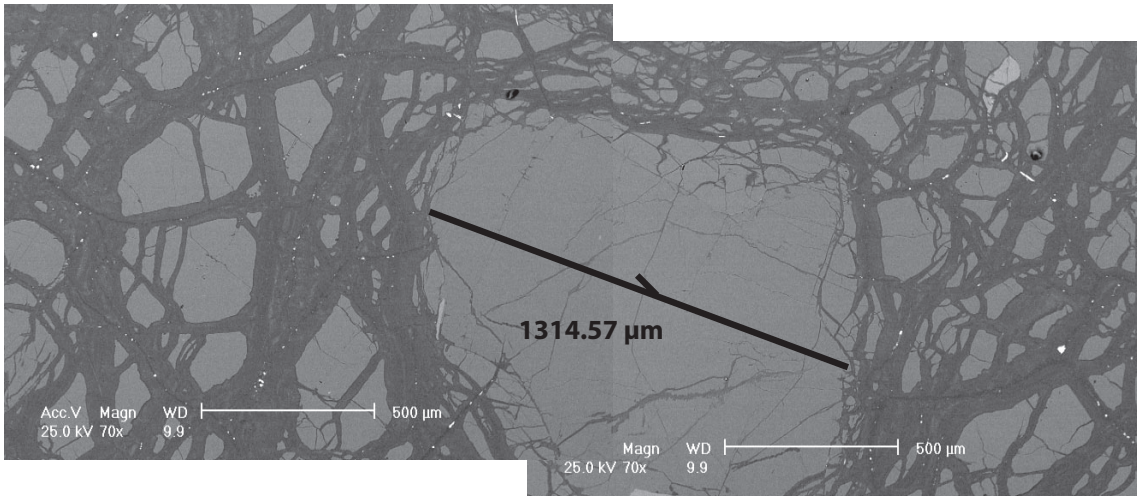


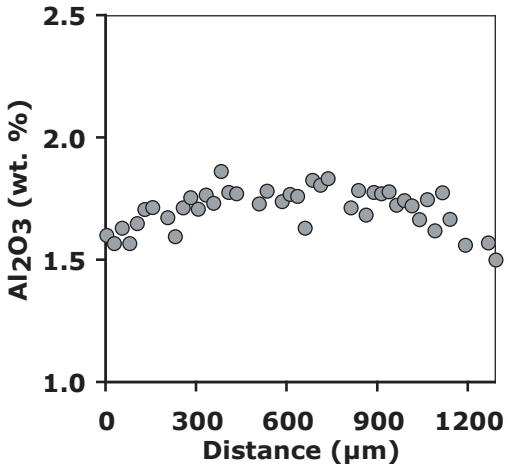
Pindos ophiolite - Dramala complex
Plagioclase-bearing harzburgite PIA109 - Orthopyroxene clast
09siopc2

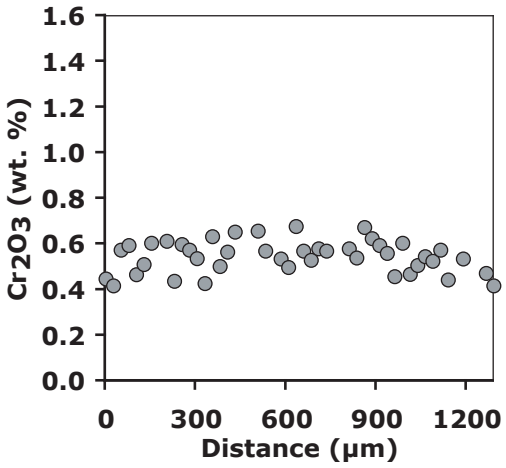


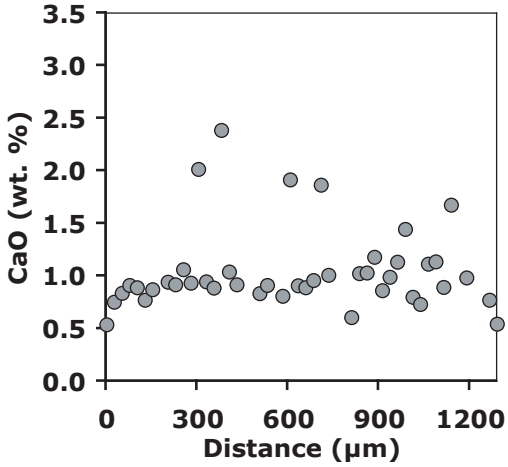


Pindos ophiolite - Dramala complex
Spinel harzburgite PIA44 - Orthopyroxene
p44opcc4

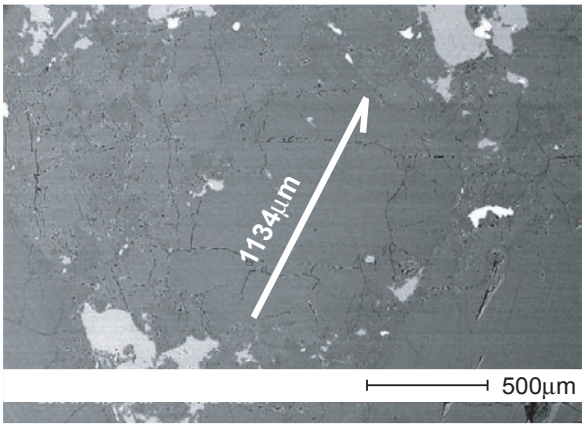


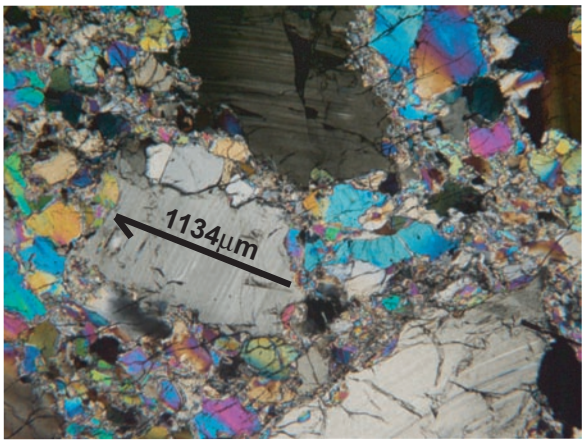


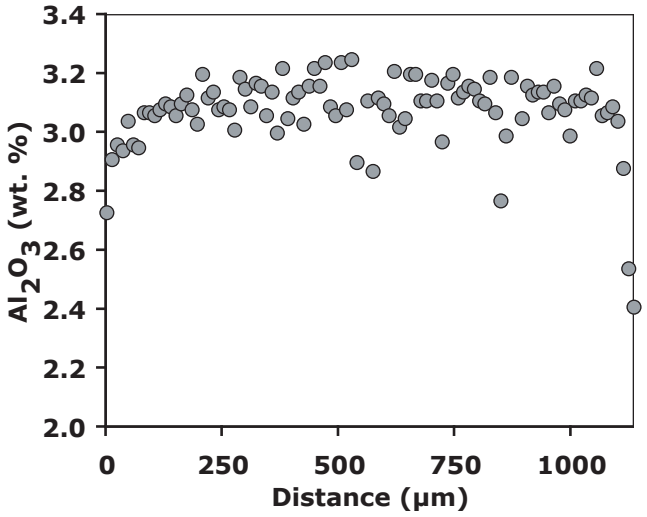


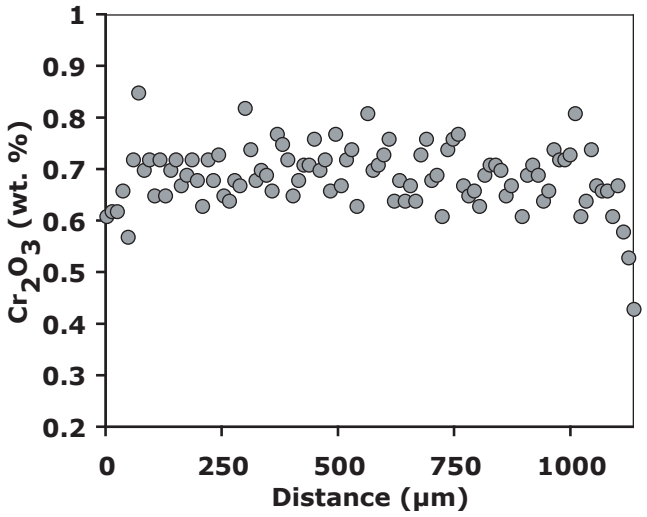


Pindos ophiolite - Dramala complex
Spinel harzburgite PI2 - Orthopyroxene clast
pi2c2opxc2

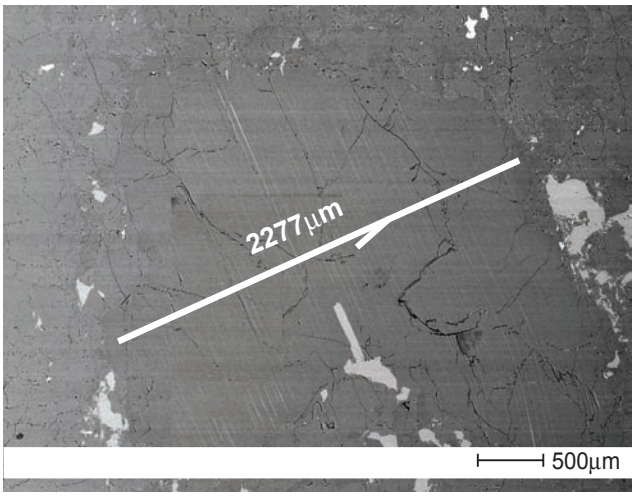


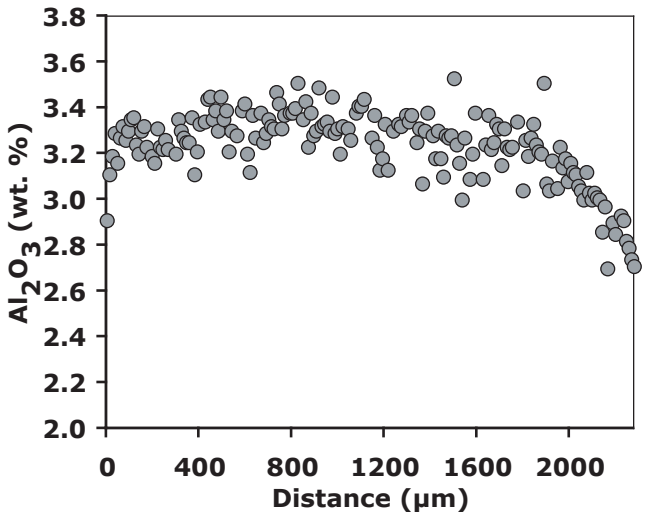


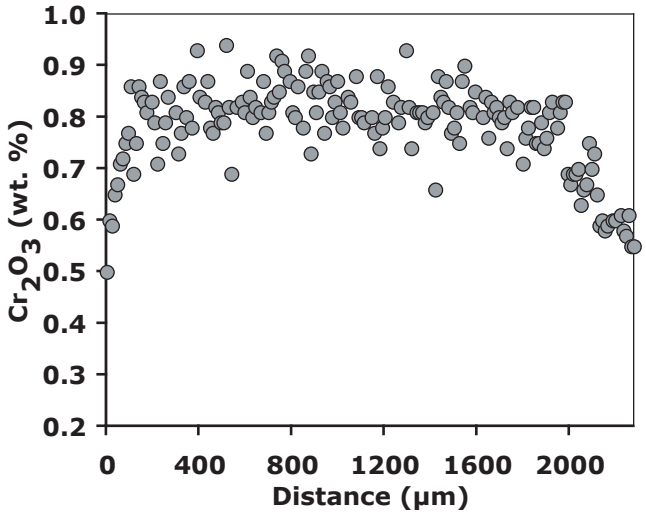




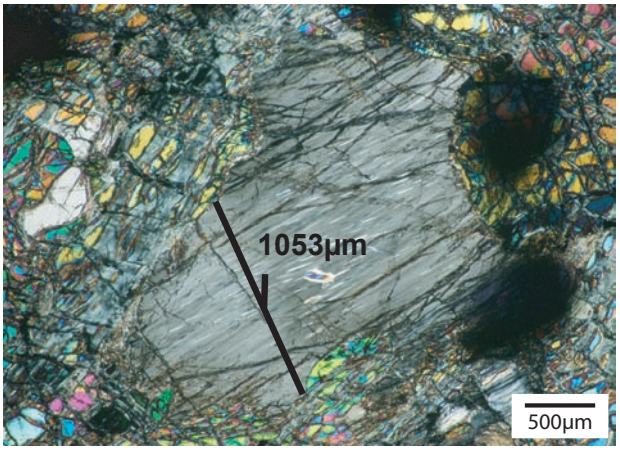
Pindos ophiolite - Dramala complex
Spinel harzburgite PI2 - Orthopyroxene clast
pi2c2opxc3

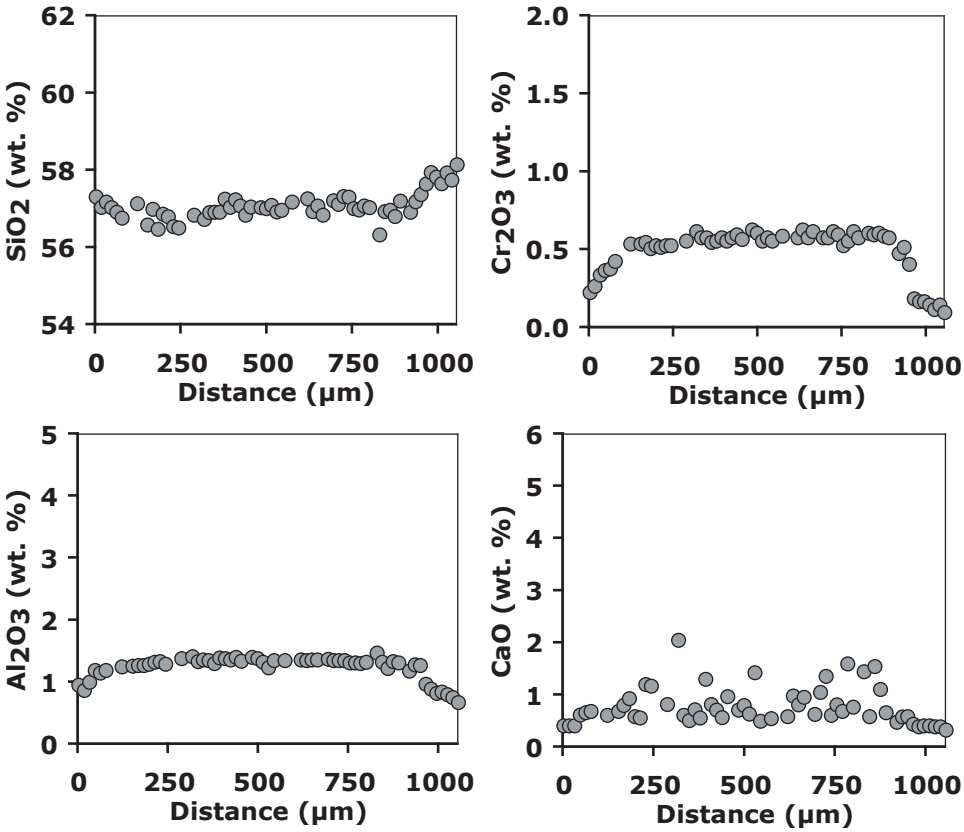




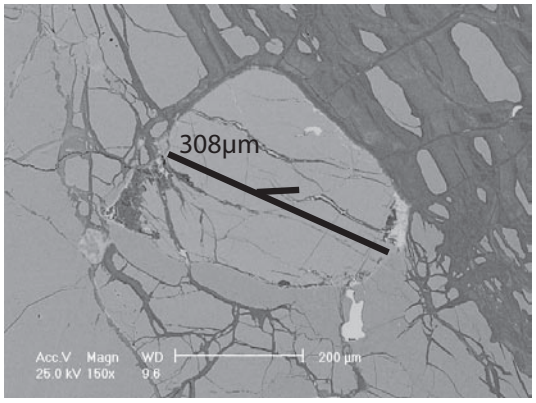


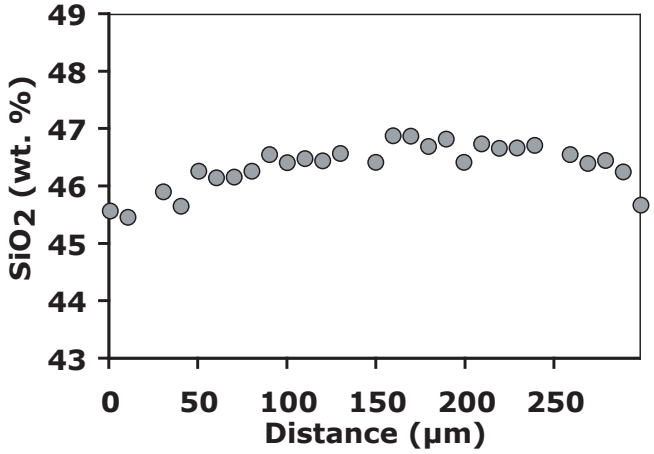
Pindos ophiolite - Dramala complex
Spinel harzburgite PI6 - Orthopyroxene clast
pi6opcc2

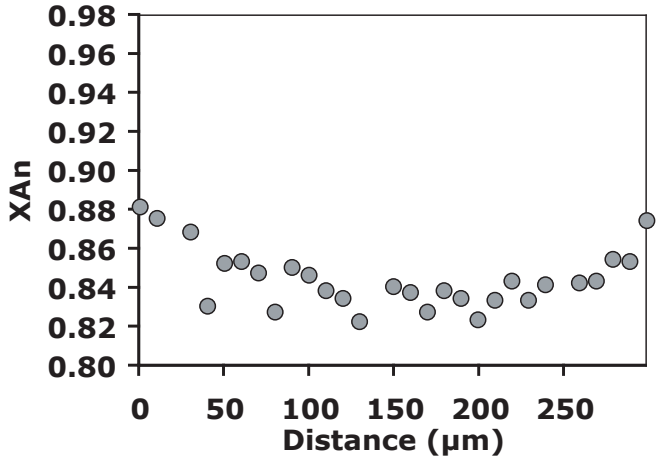




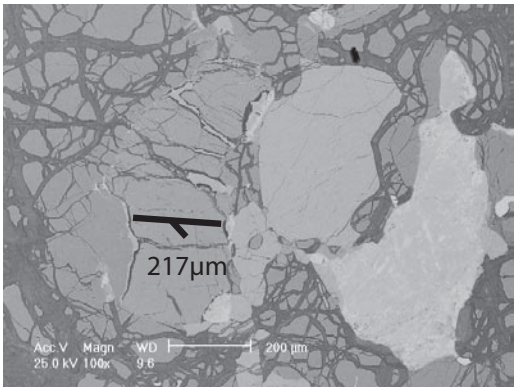
Pindos ophiolite - Dramala complex
Plagioclase-bearing harzburgite PIA120 - Plagioclase 12plc1

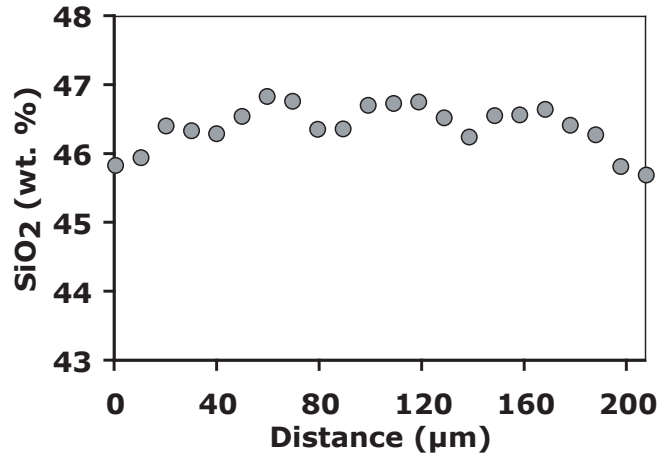


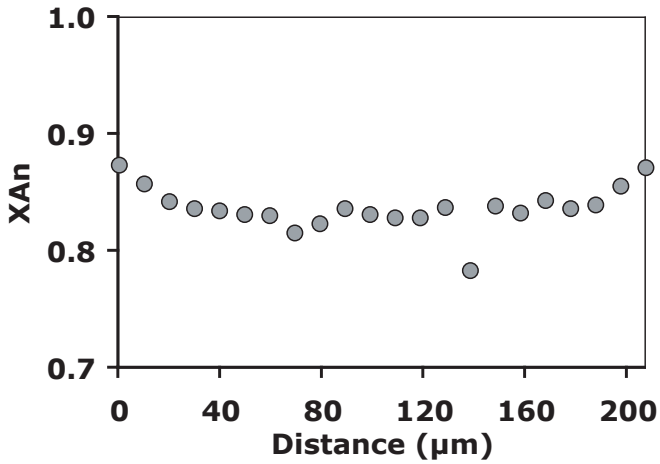




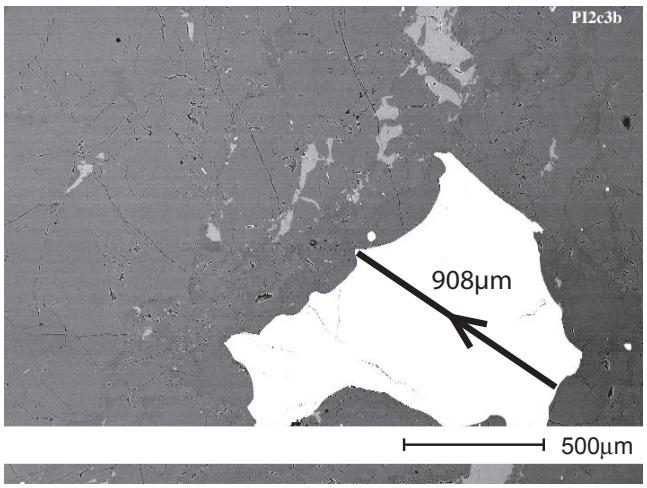
Pindos ophiolite - Dramala complex
Plagioclase-bearing harzburgite PIA120 - Plagioclase 12plc3

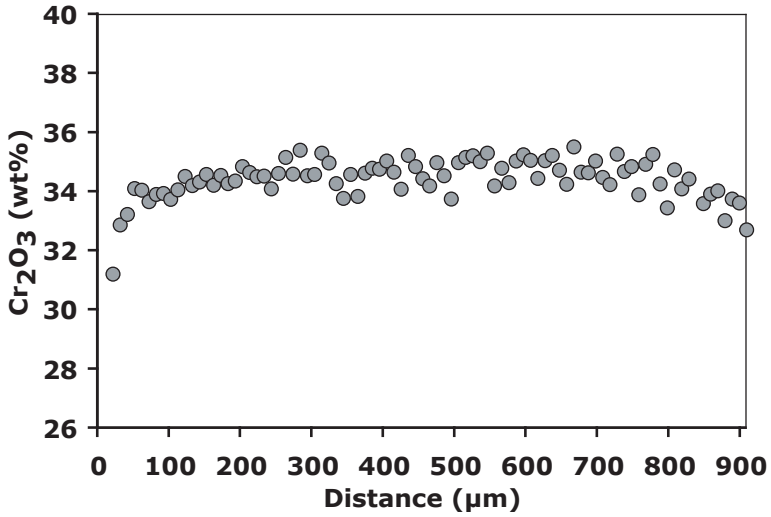


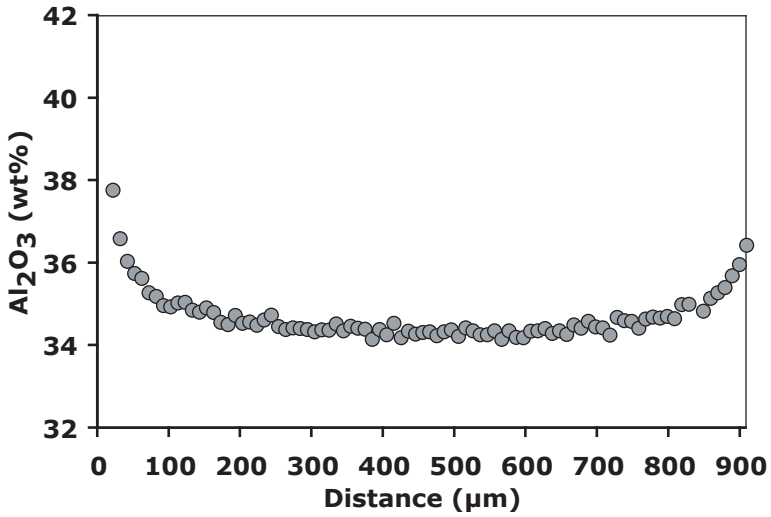




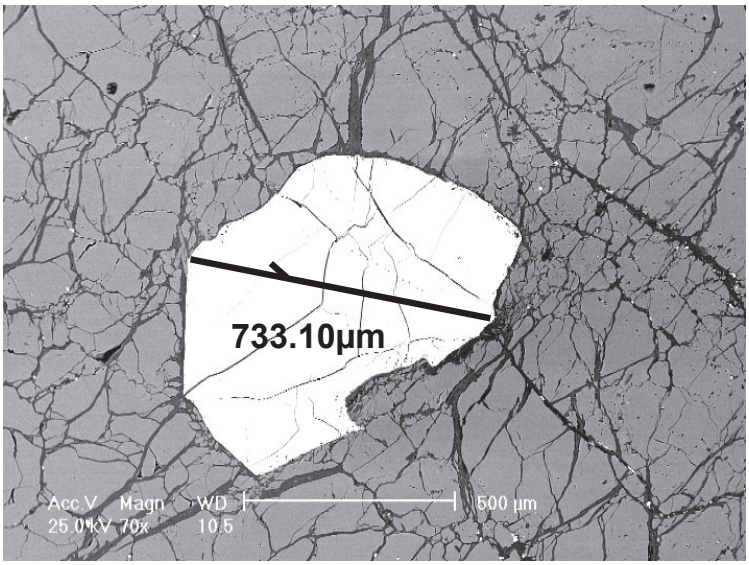
Pindos ophiolite - Dramala complex
Spinel harzburgite PI2 - spinel clast
pi2c316spic1

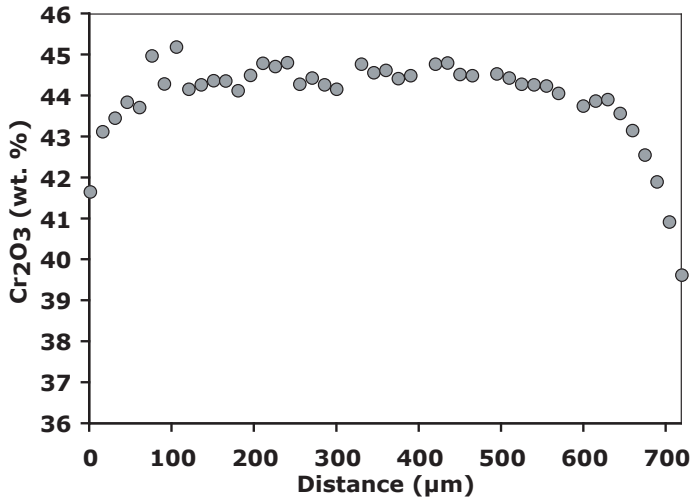


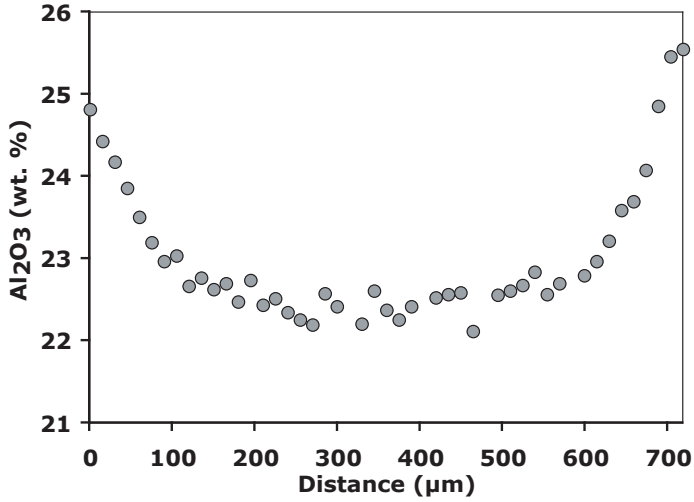




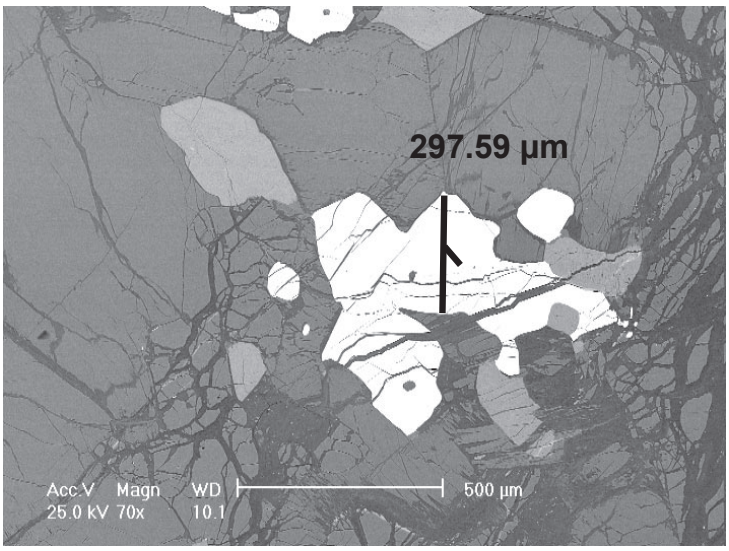
Pindos ophiolite - Dramala complex
Spinel harzburgite PIA27 - Spinel clast
pia27spcc1

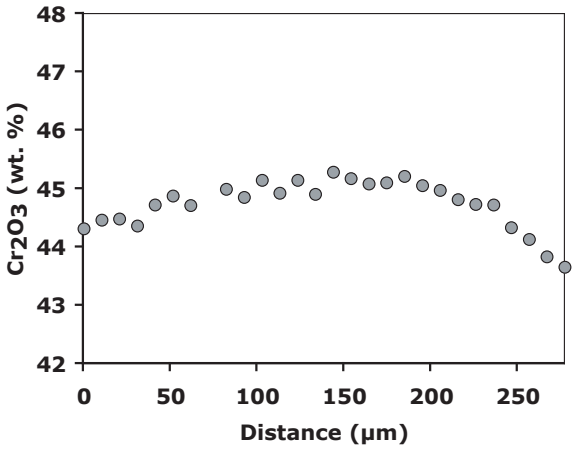


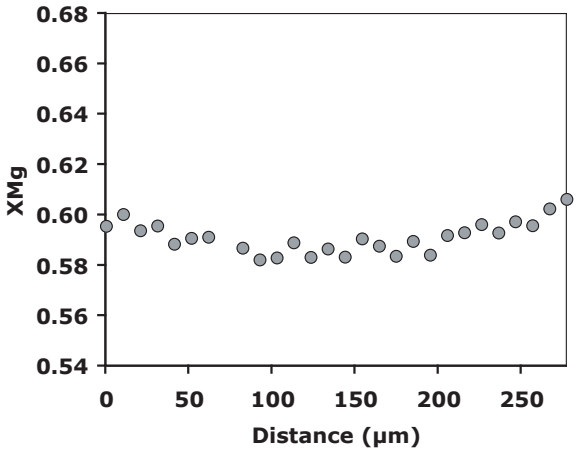


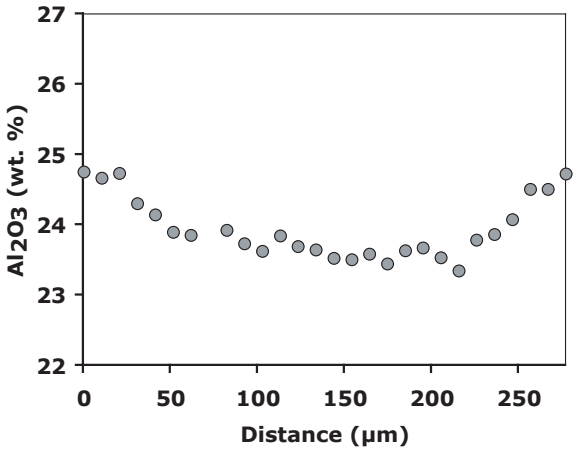


Pindos ophiolite - Dramala complex
Spinel harzburgite PIA44 - Spinel
pia44spcc2

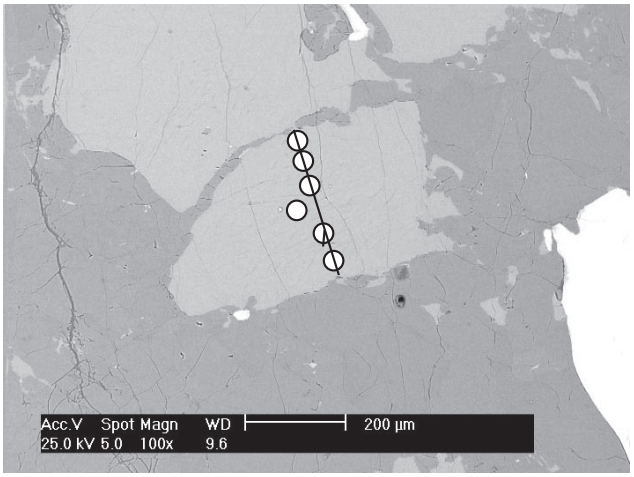


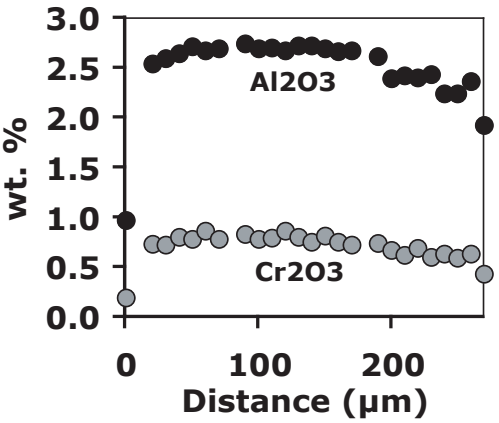


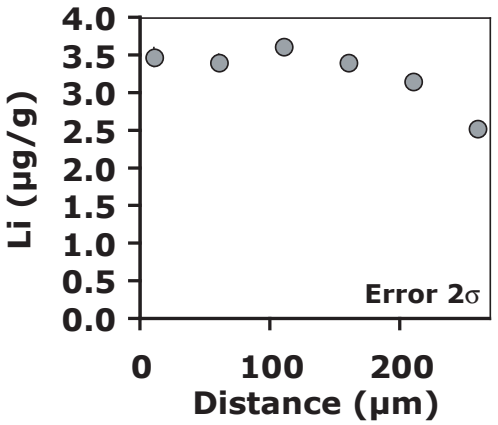


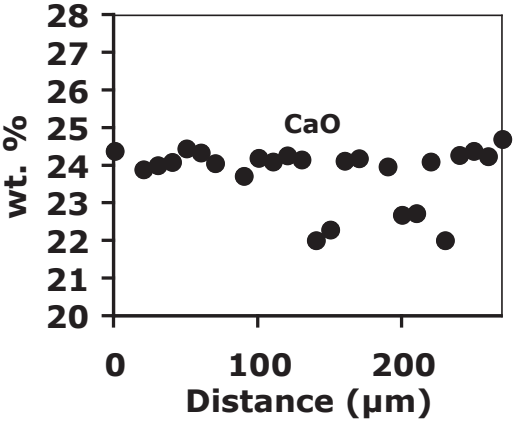


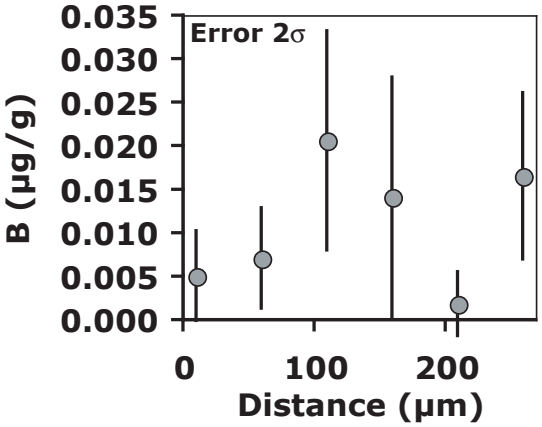
Pindos ophiolite - Dramala complex
Spinel harzburgite PI2 - Clinopyroxene clast
p2c1cpxcc1



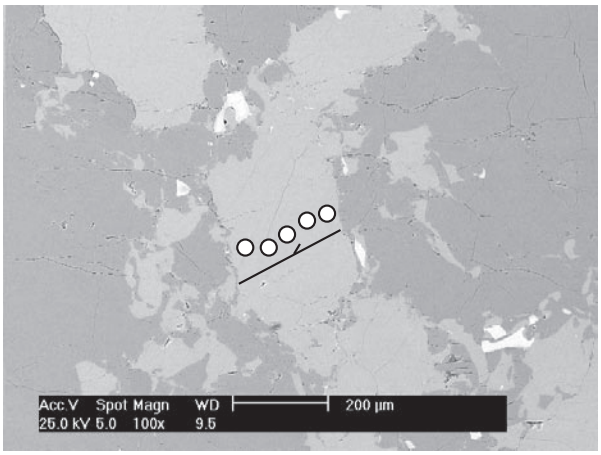


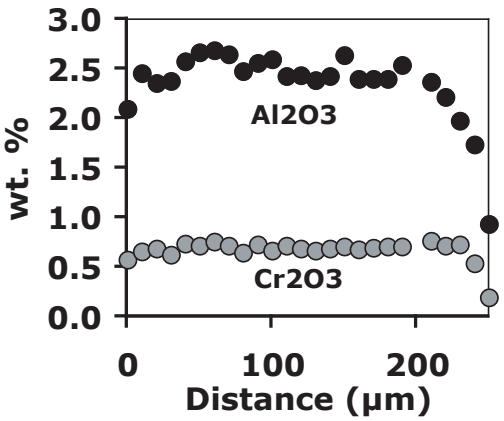


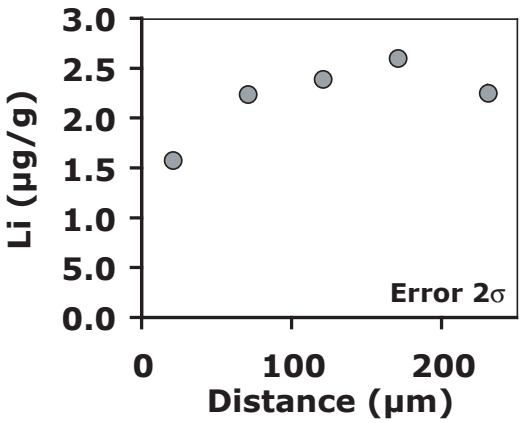


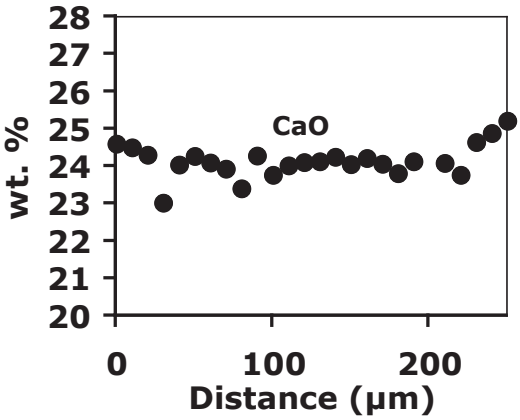


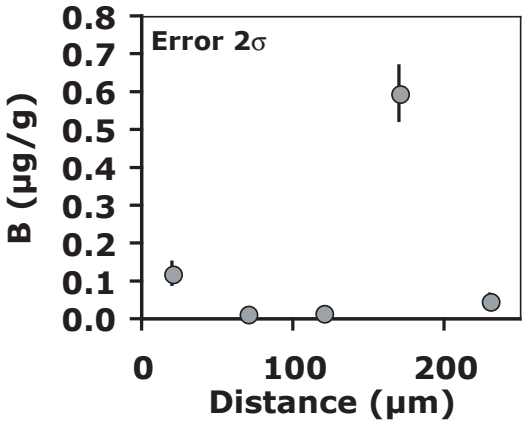
Pindos ophiolite - Dramala complex
Spinel harzburgite PI2 - Clinopyroxene clast
p2c3cpxcc1



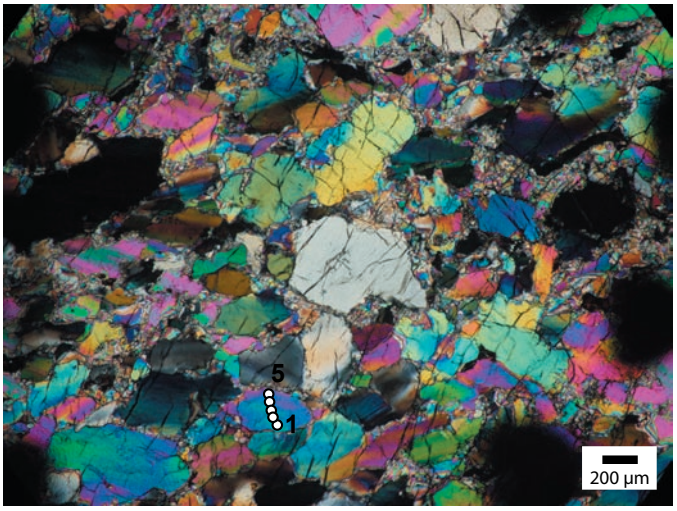


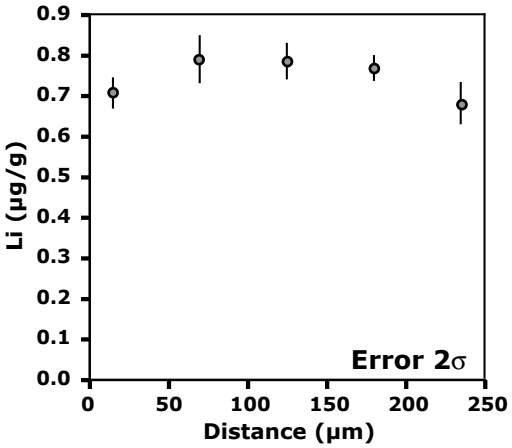


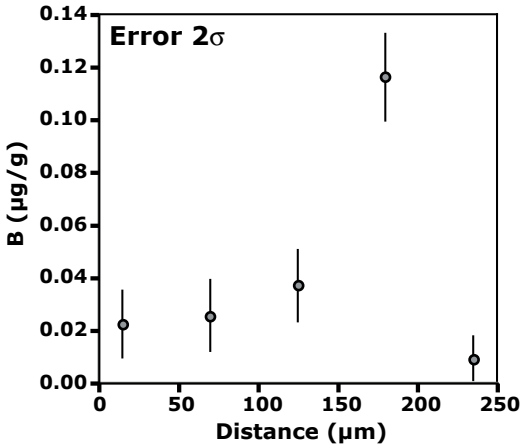




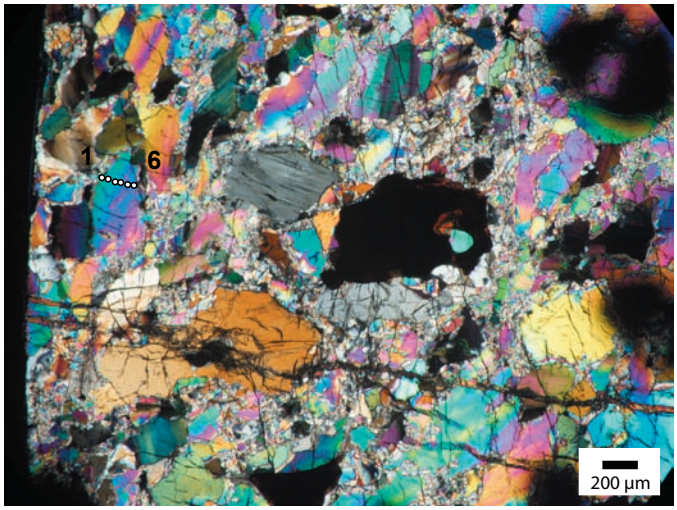
Pindos ophiolite - Dramala complex
Spinel harzburgite Pl2 - Olivine clast
p2olc1

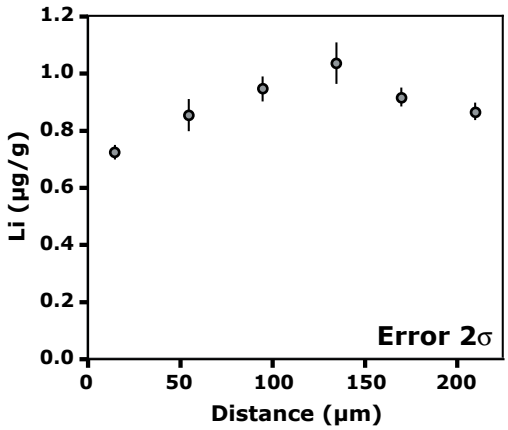


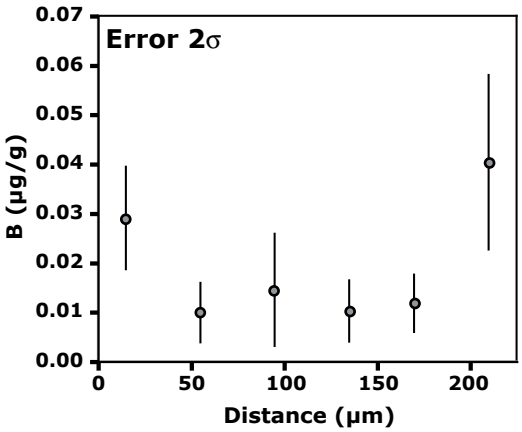




Pindos ophiolite - Dramala complex
Spinel harzburgite Pl2 - Olivine clast
p2olc2

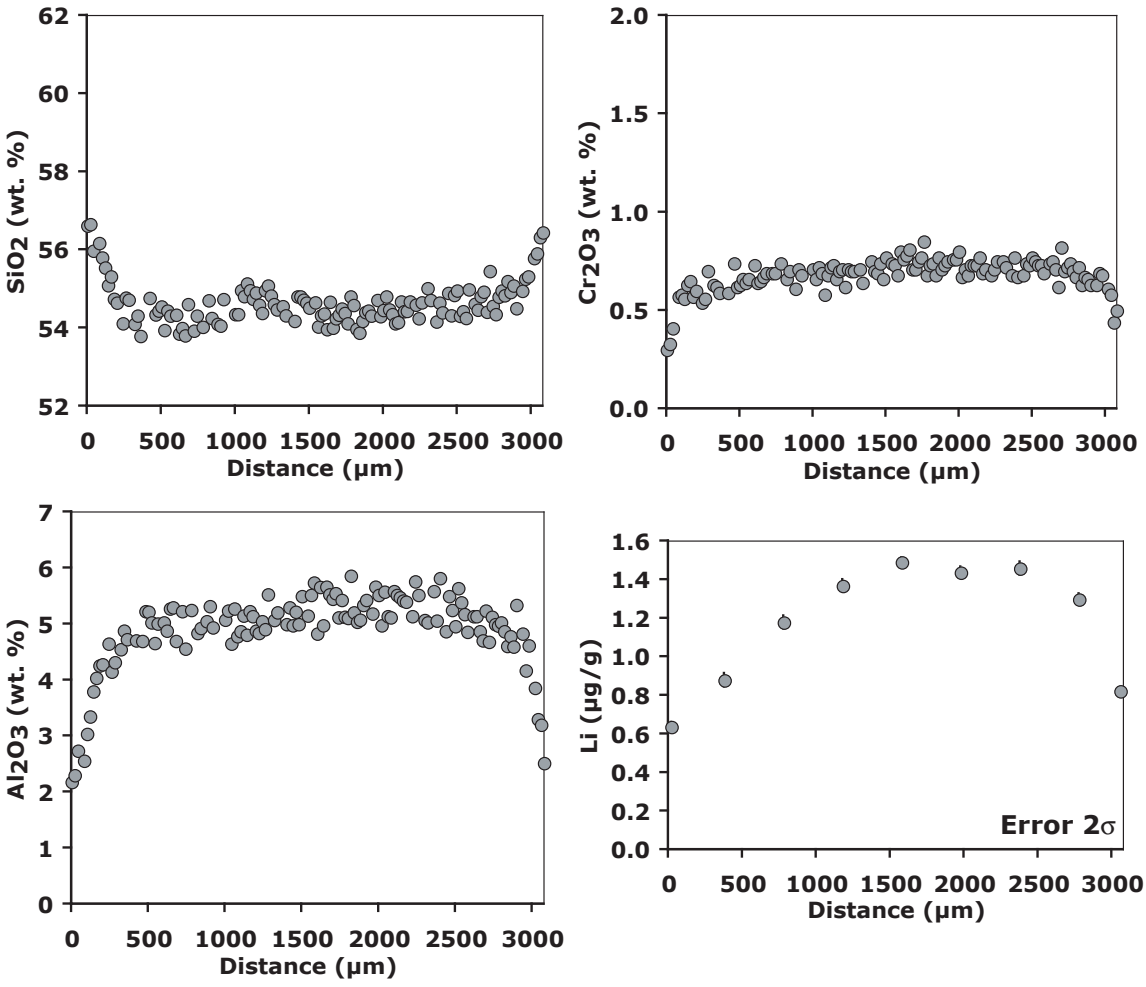




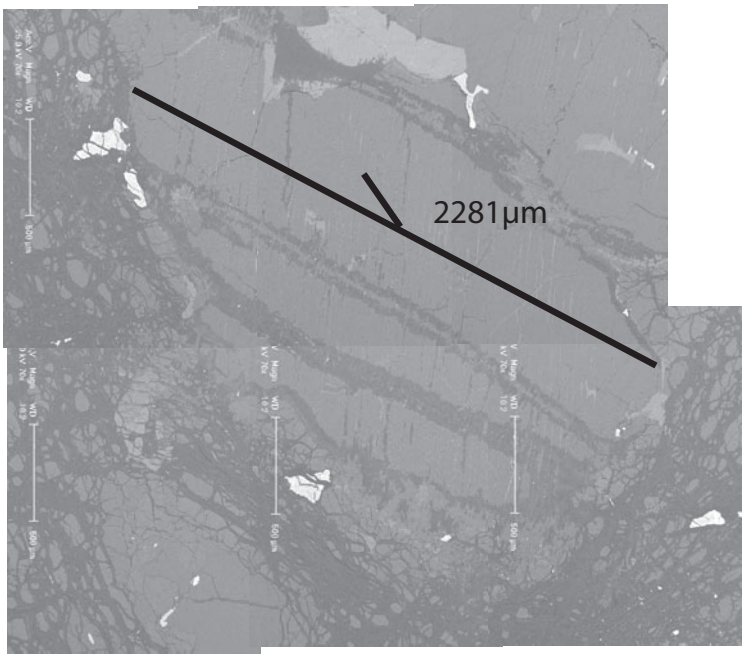


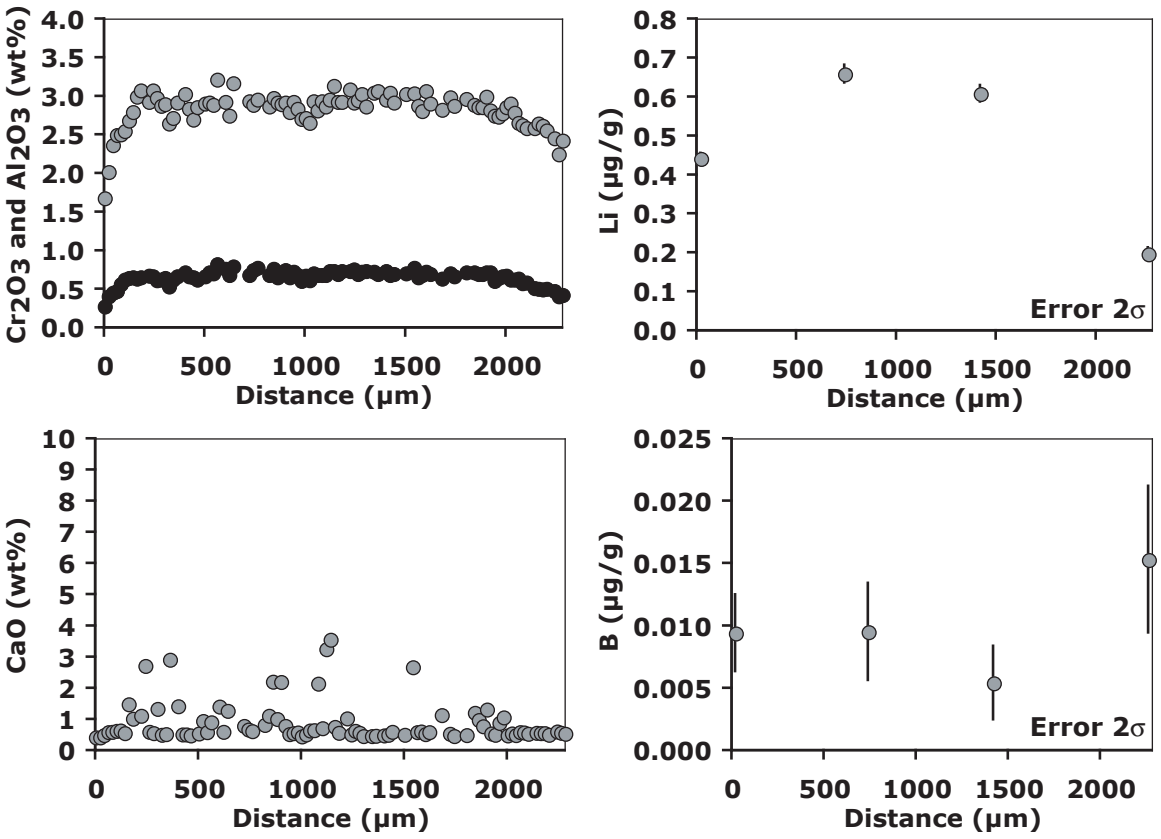
Pindos ophiolite - Dramala complex
Plagioclase-bearing harzburgite PIA109 - Orthopyroxene clast
09siopc3



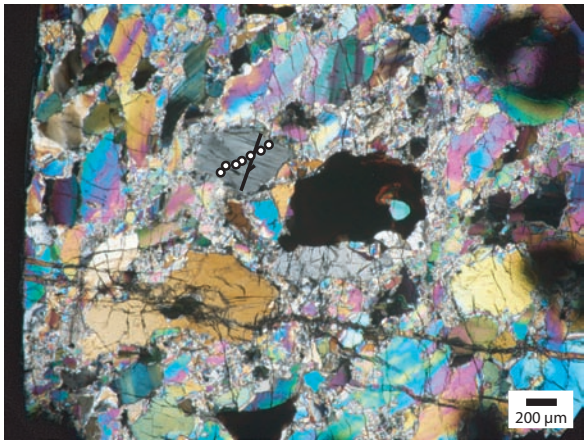


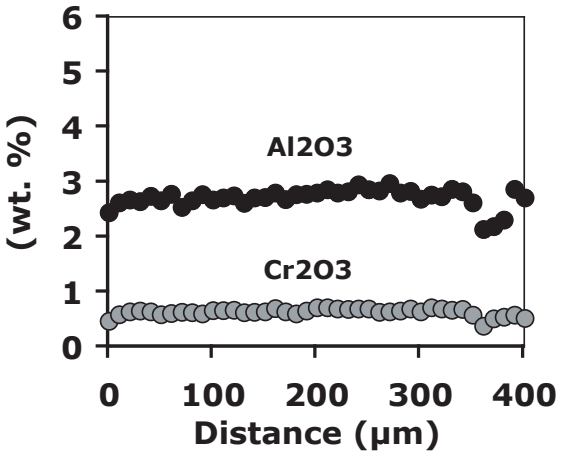
Pindos ophiolite - Dramala complex
Plagioclase-bearing harzburgite PIA120 - Orthopyroxene clast 12opc1

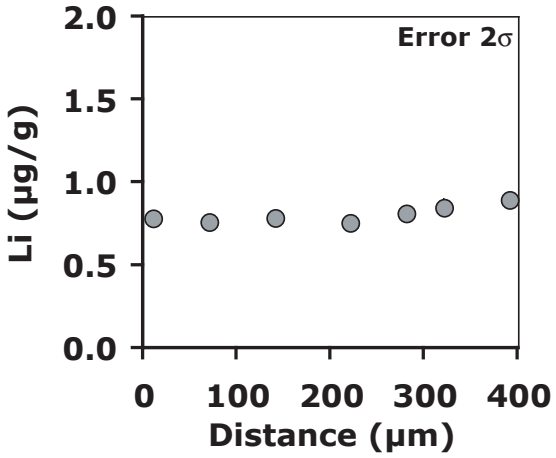


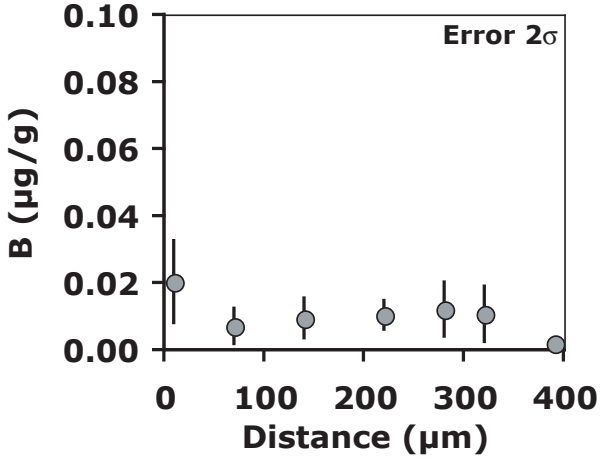


Pindos ophiolite - Dramala complex
Spinel harzburgite PI2 - Orthopyroxene clast
p2c6opxcc1









Secondary ion mass spectrometry (SIMS) light elements (Li, Be, B)

Li, Be and B content of minerals from the Geisspfad ultramafic body measured by SIMS

Sample	Rock	Mineral	Li (µg/g)	Be (µg/g)	B (µg/g)	Li (2σ)	Be (2σ)	B (2σ)
GEI4	Serp	Fo	6.07		0.13	0.08		0.02
		Fo	6.06		0.32	0.08		0.03
		Fo	6.9		0.17	0.1		0.03
		Fo	5.88	0.002	0.35	0.09	0.002	0.02
		Fo	6.80	0.001	0.21	0.09	0.001	0.03
		Fo	6.49		0.16	0.09		0.03
		Fo	5.92	0.001	0.68	0.05	0.001	0.04
		Fo	4.1	0.001	0.60	0.2	0.001	0.04
G11	Serp	Fo	8.8		4.70	0.1		0.09
		Fo	8.5		4.8	0.2		0.1
		Fo	6.52		3.24	0.09		0.07
		Fo	4.57		3.5	0.07		0.1
		Fo	6.39	0.001	3.34	0.05	0.001	0.08
		Fo	6.9		5.6	0.1		0.1
		Fo	5.63	0.001	0.28	0.03	0.001	0.01
		Fo	5.86		0.73	0.05		0.03
		Fo	6.45	0.001	0.24	0.05	0.001	0.02
		Fo	3.81		4.7	0.06		0.1
		Fo	4.56		1.21	0.05		0.06
		Fo	10.1	0.001	7.8	0.1	0.001	0.1
G12	Serp	Fo	3.90		0.24	0.07		0.03
		Fo	3.67		0.29	0.04		0.02
		Fo	3.97		0.28	0.06		0.03
		Fo	3.65		0.14	0.07		0.02
		Fo	3.86	0.001	0.21	0.06	0.001	0.02
		Fo	3.63		0.26	0.05		0.03
G26	Serp	Fo	2.08	0.001	0.11	0.05	0.001	0.02
		Fo	2.30		0.09	0.08		0.02
		Fo	2.7		0.11	0.1		0.03
		Fo	2.68		0.16	0.06		0.03
		Fo	2.39		0.21	0.07		0.02
		Fo	1.48		0.64	0.07		0.07
		Fo	1.66	0.001	0.11	0.06	0.001	0.02
		Fo	2.74		0.18	0.09		0.02
		Fo	2.12		1.50	0.04		0.07
G27	Serp	Fo	5.5	0.001	0.9	0.1	0.001	0.1
		Fo	3.9		1.21	0.1		0.06
		Fo	3.71		2.4	0.09		0.1
		Fo	3.8		1.7	0.1		0.1
		Fo	5.6		0.81	0.1		0.08
G3	Ophi	Fo	4.7		2.9	0.2		0.2
		Fo	3.2		2.22	0.1		0.06
		Fo	3.61	0.002	2.9	0.08	0.002	0.1
		Fo	4.4	0.001	2.29	0.1	0.001	0.09
		Fo	4.70	0.001	3.1	0.05	0.001	0.1
		Fo	2.86		2.0	0.05		0.1
		Fo	5.5		2.79	0.2		0.09

Abbreviations: Fo = forsterite, Srp = serpentinite, Ophi = ophicarbonate.

Li, Be and B content of minerals from the Geisspfad ultramafic body measured by SIMS continued

Sample	Rock	Mineral	Li (µg/g)	Be (µg/g)	B (µg/g)	Li (2σ)	Be (2σ)	B (2σ)
G3	Ophi	Fo	3.5		2.38	0.1		0.09
		Fo	4.3		5.6	0.1		0.1
		Fo	3.5	0.002	3.6	0.1	0.002	0.2
GEI4	Serp	Atg	3.80	0.003	2.9	0.05	0.002	0.1
		Atg	1.24	0.001	1.48	0.04	0.001	0.07
		Atg	0.04	0.002	2.52	0.02	0.002	0.08
		Atg	0.14	0.002	2.62	0.04	0.001	0.09
G11	Serp	Atg	0.08	0.002	2.0	0.01	0.001	0.1
		Atg	0.21	0.007	2.43	0.01	0.002	0.07
		Atg	0.20	0.005	2.7	0.01	0.001	0.1
		Atg	0.11	0.001	1.3	0.01	0.001	0.1
		Atg	0.18	0.004	2.78	0.02	0.002	0.08
		Atg	0.09	0.002	1.92	0.01	0.002	0.08
G12	Serp	Atg	0.08	0.003	3.1	0.01	0.001	0.1
		Atg	0.027	0.002	4.4	0.004	0.001	0.2
		Atg	0.17	0.006	5.0	0.04	0.002	0.1
		Atg	0.020	0.001	1.78	0.004	0.001	0.05
		Atg	0.02	0.001	0.86	0.01	0.001	0.05
		Atg	0.02		0.75	0.01		0.06
G26	Serp	Atg	0.10	0.001	2.3	0.01	0.002	0.1
		Atg	0.08	0.007	2.21	0.01	0.004	0.08
		Atg	0.06	0.004	1.60	0.01	0.003	0.07
		Atg	0.11	0.006	2.24	0.01	0.003	0.05
		Atg	0.13	0.005	3.0	0.02	0.004	0.2
G27	Serp	Atg	0.08	0.002	1.6	0.01	0.003	0.1
		Atg	0.02		1.5	0.01		0.1
		Atg	0.10	0.001	1.64	0.01	0.001	0.09
		Atg	0.02		1.75	0.01		0.08
		Atg	0.02		1.36	0.01		0.09
G3	Ophi	Atg	0.05	0.016	1.8	0.01	0.007	0.1
		Atg	0.03	0.009	1.7	0.01	0.004	0.1
		Atg	0.05	0.018	1.99	0.01	0.007	0.08
		Atg	0.03	0.008	1.50	0.01	0.003	0.06
		Atg	0.02	0.009	2.6	0.01	0.005	0.1
G4	Ophi	Atg	0.01	0.017	3.0	0.01	0.006	0.2
		Atg	0.10	0.030	7.5	0.01	0.006	0.3
		Atg	0.10	0.016	2.6	0.01	0.004	0.1
		Atg	0.08	0.020	2.38	0.02	0.008	0.08
		Atg	0.11	0.023	3.3	0.01	0.006	0.2
GEI9	Ophi	Atg	0.27	0.029	35.3	0.02	0.005	0.9
		Atg	0.26	0.027	9.1	0.02	0.004	0.4
		Atg	0.19	0.021	12.7	0.02	0.003	0.2
		Atg	0.51	0.040	25	0.02	0.006	1
		Atg	0.25	0.019	10.1	0.02	0.003	0.4
		Atg	0.42	0.015	4.8	0.02	0.002	0.1

Abbreviations: Fo = forsterite, Atg = antigorite, Srp = serpentinite, Ophi = ophicarbonate.

Li, Be and B content of minerals from the Geisspfad ultramafic body measured by SIMS continued

Sample	Rock	Mineral	Li (µg/g)	Be (µg/g)	B (µg/g)	Li (2σ)	Be (2σ)	B (2σ)
GEI4	Serp	Tr	1.92	0.088	12.5	0.04	0.008	0.3
		Tr	1.59	0.082	11.5	0.05	0.005	0.2
		Tr	1.86	0.104	9.6	0.06	0.008	0.2
		Tr	1.72	0.071	10.1	0.04	0.006	0.2
		Tr	2.9	0.115	11.6	0.1	0.006	0.2
		Tr	2.01	0.099	12.51	0.07	0.006	0.08
		Tr	2.75	0.12	11.8	0.07	0.01	0.2
G11	Serp	Tr	8.90	0.073	6.5	0.05	0.006	0.1
		Tr	7.16	0.068	4.4	0.05	0.006	0.1
		Tr	11.8	0.072	7.40	0.1	0.007	0.08
		Tr	9.8	0.079	9.5	0.1	0.004	0.1
		Tr	11.6	0.14	18.2	0.1	0.01	0.2
		Tr	6.98	0.069	7.1	0.09	0.009	0.1
G12	Serp	Tr	0.63	0.163	9.2	0.04	0.007	0.2
		Tr	0.40	0.090	8.0	0.02	0.008	0.3
		Tr	0.81	0.19	12.0	0.03	0.01	0.2
		Tr	0.81	0.160	9.5	0.02	0.006	0.1
		Tr	0.56	0.25	9.4	0.01	0.01	0.2
		Tr	0.58	0.22	9.0	0.03	0.01	0.1
G26	Serp	Tr	7.2	0.09	5.1	0.2	0.01	0.2
		Tr	9.1	0.13	6.4	0.1	0.02	0.2
		Tr	10.4	0.15	4.6	0.1	0.02	0.2
		Tr	5.4	0.14	7.3	0.1	0.02	0.2
		Tr	8.9	0.09	5.2	0.1	0.01	0.1
		Tr	4.79	0.09	11.3	0.08	0.01	0.1
		Tr	5.55	0.10	13.6	0.07	0.02	0.3
		Tr	5.0	0.057	5.2	0.1	0.008	0.1
G27	Serp	Tr	5.1	0.13	13.9	0.1	0.02	0.3
		Tr	3.42	0.05	4.2	0.08	0.01	0.1
		Tr	3.19	0.09	7.5	0.08	0.01	0.2
		Tr	3.20	0.07	6.1	0.08	0.02	0.2
		Tr	2.75	0.07	5.9	0.03	0.01	0.2
		Tr	2.10	0.07	4.2	0.07	0.02	0.2
		Tr	3.34	0.16	19.7	0.07	0.02	0.4
		Tr	2.80	0.07	3.8	0.05	0.01	0.1
		Tr	3.3	0.13	12.9	0.1	0.01	0.4
		Tr	1.85	0.06	3.1	0.05	0.01	0.1
G3	Ophi	Tr	2.79	0.17	5.7	0.07	0.02	0.2
		Tr	2.09	0.10	3.4	0.08	0.01	0.1
		Tr	1.85	0.13	4.2	0.07	0.02	0.1
		Tr	2.09	0.13	3.7	0.09	0.02	0.2
		Tr	2.34	0.29	8.2	0.05	0.03	0.3
		Tr	0.70	0.06	1.64	0.06	0.02	0.09
		Tr	2.7	0.20	6.4	0.1	0.03	0.2
		Tr	1.70	0.10	3.2	0.05	0.02	0.2
		Tr	2.36	0.18	5.6	0.07	0.03	0.2
		Tr	1.78	0.12	4.07	0.04	0.02	0.08

Abbreviations: Tr = tremolite, Srp = serpentinite, Ophi = ophicarbonate.

Li, Be and B content of minerals from the Geisspfad ultramafic body measured by SIMS continued

Sample	Rock	Mineral	Li (µg/g)	Be (µg/g)	B (µg/g)	Li (2σ)	Be (2σ)	B (2σ)
G4	Ophi	Tr	0.49	0.054	2.0	0.04	0.008	0.1
		Tr	0.47	0.039	1.63	0.04	0.006	0.08
		Tr	0.71	0.069	3.3	0.04	0.007	0.1
		Tr	0.33	0.049	1.81	0.02	0.009	0.07
		Tr	0.45	0.09	3.6	0.03	0.02	0.1
		Tr	0.54	0.06	2.56	0.04	0.01	0.09
		Tr	0.50	0.05	2.59	0.04	0.01	0.08
		Tr	0.48	0.05	2.1	0.03	0.01	0.1
		Tr	0.30	0.05	1.67	0.03	0.01	0.08
GEI9	Ophi	Tr	0.25	0.107	3.7	0.01	0.006	0.1
		Tr	0.30	0.122	3.64	0.01	0.006	0.05
		Tr	0.37	0.092	4.44	0.03	0.007	0.07
		Tr	0.28	0.100	3.51	0.01	0.009	0.08
		Tr	0.30	0.112	4.1	0.01	0.006	0.1
		Tr	0.19	0.080	2.8	0.02	0.008	0.1
		Tr	0.35	0.091	4.07	0.02	0.006	0.04
G30a	Metabas	Tsch hbl	2.51	2.10	7.7	0.04	0.05	0.2
		Tsch hbl	2.31	1.51	6.8	0.05	0.03	0.1
		Tsch hbl	1.76	1.03	5.1	0.06	0.03	0.1
		Tsch hbl	1.91	1.21	6.1	0.03	0.04	0.1
		Tsch hbl	1.47	1.29	6.9	0.06	0.03	0.2
G34	Metabas	Tsch hbl	9.3	0.59	1.99	0.1	0.02	0.09
		Tsch hbl	8.4	0.66	1.8	0.2	0.02	0.1
		Tsch hbl	10.5	0.73	1.8	0.1	0.02	0.1
		Tsch hbl	11.5	0.75	2.30	0.2	0.02	0.09
		Tsch hbl	9.2	0.55	1.69	0.1	0.03	0.08
G11	Serp	Di	31.6	0.13	0.39	0.3	0.02	0.04
		Di	27.4	0.11	0.15	0.3	0.01	0.03
		Di	30.0	0.16	0.34	0.2	0.02	0.03
G26	Serp	Di	11.8	0.05	0.33	0.1	0.01	0.03
		Di	12.7	0.031	0.08	0.2	0.007	0.02
		Di	7.5	0.025	0.23	0.1	0.008	0.03
		Di	13.3	0.03	0.28	0.3	0.01	0.05
		Di	10.2	0.030	0.05	0.2	0.009	0.01
G27	Serp	Di	1.23	0.027	1.1	0.04	0.008	0.1
		Di	0.71	0.025	0.48	0.05	0.008	0.07
		Di	0.89	0.022	0.52	0.05	0.007	0.05
G4	Ophi	Di	0.65	0.67	1.62	0.03	0.04	0.09
		Di	0.80	0.98	2.2	0.05	0.05	0.1
		Di	0.89	0.44	2.4	0.05	0.03	0.1
		Di	1.37	0.28	1.0	0.08	0.03	0.1
		Di	0.81	0.51	1.4	0.04	0.04	0.1

Abbreviations: Tr = tremolite, Tsch hbl = tschermakitic hornblende, Di = diopside, Srp = serpentinite, Ophi = ophicarbonate, Metabas = metabasite.

Li, Be and B content of minerals from the Dramala spinel harzburgite and plagioclase-bearing harzburgite measured by SIMS

Sample	Rock	Mineral	Li (µg/g)	Be (µg/g)	B (µg/g)	Li (2σ)	Be (2σ)	B (2σ)
PI2	Spl hrz	Opx	1.14		0.07	0.03		0.01
		Opx	1.05		0.01	0.04		0.01
		Opx	0.92		0.05	0.06		0.01
		Opx	0.78		0.002	0.03		0.003
		Opx	1.07		0.01	0.05		0.01
		Opx	0.81	0.001	0.01	0.04	0.001	0.01
		Opx	0.90		0.02	0.05		0.01
		Opx	0.89		0.01	0.03		0.01
		Opx	0.70		0.02	0.05		0.01
		Opx	0.94		0.02	0.03		0.01
		Opx	0.71		0.02	0.03		0.01
		Opx	0.74		0.004	0.02		0.004
		Opx	0.83		0.01	0.03		0.01
		Opx	0.78	0.002	0.01	0.06	0.001	0.01
		Opx	0.75	0.002	0.01	0.04	0.001	0.01
		Opx	0.87		0.008	0.05		0.004
		Opx	0.99		0.02	0.04		0.01
		Opx	0.73		0.01	0.03		0.01
		Opx	0.86		0.01	0.04		0.01
		Opx	1.02		0.04	0.04		0.02
		Opx	0.88		0.06	0.05		0.03
		Opx	0.69		0.39	0.05		0.05
		Opx	0.73		0.01	0.03		0.01
		Opx	0.75		0.01	0.03		0.01
		Opx	0.78		0.01	0.02		0.01
		Opx	0.81		0.01	0.05		0.01
PI6	Spl hrz	Opx	0.10		0.02	0.01		0.01
		Opx	0.29		0.03	0.01		0.01
		Opx	0.29		0.02	0.02		0.01
PIA44	Spl hrz	Opx	0.55	0.001	0.02	0.01	0.001	0.01
		Opx	0.64		0.02	0.02		0.01
		Opx	0.69		0.011	0.02		0.004
		Opx	0.65	0.001	0.01	0.02	0.001	0.01
		Opx	0.60		0.018	0.02		0.004
		Opx	0.62		0.01	0.03		0.01
		Opx	0.64		0.02	0.03		0.01
PIA27	Spl hrz	Opx	0.10		0.04	0.01		0.01
		Opx	0.20		0.03	0.01		0.01
		Opx	0.34		0.04	0.01		0.01
		Opx	0.12		0.16	0.01		0.03
		Opx	0.22		0.10	0.02		0.01
		Opx	0.45		0.17	0.03		0.03
PIA109	Pl-bear hrz	Opx	0.64	0.002	0.008	0.02	0.001	0.003
		Opx	0.94	0.001	0.011	0.02	0.001	0.004
		Opx	1.37		0.008	0.03		0.005
		Opx	1.18	0.003	0.006	0.03	0.002	0.004

Abbreviations: Opx = orthopyroxene, Spl hrz = spinel harzburgite, Pl-bear hrz = plagioclase-bearing harzburgite.

Li, Be and B content of minerals from the Dramala spinel harzburgite and plagioclase-bearing harzburgite measured by SIMS continued

Sample	Rock	Mineral	Li (µg/g)	Be (µg/g)	B (µg/g)	Li (2σ)	Be (2σ)	B (2σ)
PIA109	Pl-bear hrz	Opx	0.88		0.007	0.03		0.004
		Opx	0.64	0.002	0.009	0.02	0.001	0.005
		Opx	1.49	0.002	0.004	0.02	0.001	0.003
		Opx	1.44	0.002	0.006	0.03	0.001	0.005
		Opx	1.46	0.002	0.01	0.03	0.001	0.01
		Opx	1.30		0.003	0.03		0.002
		Opx	0.82		0.006	0.02		0.004
		Opx	0.81		0.007	0.03		0.004
		Opx	0.68		0.005	0.02		0.003
PIA120	Pl-bear hrz	Opx	0.44		0.009	0.01		0.003
		Opx	0.66		0.010	0.02		0.004
		Opx	0.61	0.001	0.005	0.02	0.001	0.003
		Opx	0.20		0.02	0.02		0.01
		Opx	0.26		0.006	0.02		0.004
		Opx	0.26		0.03	0.01		0.01
PI2	Spl hrz	Cpx	3.3		0.00	0.1		0.01
		Cpx	3.3	0.001	0.01	0.1	0.001	0.01
		Cpx	3.25	0.001	0.01	0.08	0.001	0.01
		Cpx	2.20	0.002	0.19	0.08	0.001	0.03
		Cpx	2.49	0.001	0.58	0.06	0.001	0.07
		Cpx	2.15	0.001	0.01	0.07	0.001	0.01
		Cpx	1.51		0.12	0.06		0.03
PI6	Spl hrz	Cpx	0.12		0.012	0.01		0.003
		Cpx	0.11		0.01	0.01		0.01
		Cpx	0.77		0.02	0.03		0.01
		Cpx	1.84	0.002	0.02	0.05	0.001	0.01
		Cpx	0.62	0.003	0.02	0.02	0.001	0.01
PIA44	Spl hrz	Cpx	2.39	0.001	0.01	0.06	0.001	0.01
		Cpx	3.2		0.009	0.1		0.003
		Cpx	3.3	0.001	0.03	0.2	0.001	0.01
		Cpx	2.7		0.03	0.2		0.02
		Cpx	2.39		0.02	0.09		0.01
		Cpx	3.7	0.001	0.05	0.1	0.001	0.02
		Cpx	3.0		0.02	0.4		0.01
		Cpx	3.4		0.015	0.3		0.004
PIA27	Spl hrz	Cpx	0.47	0.001	0.25	0.02	0.001	0.03
		Cpx	0.44		0.26	0.03		0.03
PIA109	Pl-bear hrz	Cpx	3.26		0.001	0.07		0.001
		Cpx	3.71	0.004	0.004	0.05	0.002	0.004
		Cpx	2.83	0.004	0.06	0.04	0.001	0.01
		Cpx	3.02		0.04	0.06		0.01
PIA120	Pl-bear hrz	Cpx	1.75		0.005	0.05		0.004
		Cpx	0.20		0.01	0.01		0.01
PI2	Spl hrz	Ol	0.67		0.02	0.03		0.01
		Ol	0.75	0.001	0.02	0.05	0.001	0.01
		Ol	0.75	0.001	0.04	0.04	0.002	0.01

Abbreviations: Opx = orthopyroxene, Cpx = clinopyroxene, Ol = olivine, Spl hrz = spinel harzburgite, Pl-bear hrz = plagioclase-bearing harzburgite.

Li, Be and B content of minerals from the Dramala spinel harzburgite and plagioclase-bearing harzburgite measured by SIMS continued

Sample	Rock	Mineral	Li (µg/g)	Be (µg/g)	B (µg/g)	Li (2σ)	Be (2σ)	B (2σ)
PI2	Spl hrz	Ol	0.73	0.002	0.11	0.03	0.002	0.02
		Ol	0.65		0.01	0.05		0.01
		Ol	0.82		0.01	0.04		0.01
		Ol	0.62	0.001	0.02	0.05	0.001	0.01
		Ol	0.69		0.03	0.02		0.01
		Ol	0.81		0.01	0.05		0.01
		Ol	0.90	0.001	0.01	0.04	0.001	0.01
		Ol	0.98		0.01	0.07		0.01
		Ol	0.87	0.001	0.01	0.03	0.001	0.01
		Ol	0.82	0.001	0.04	0.03	0.001	0.02
PI6	Spl hrz	Ol	0.56		0.02	0.02		0.01
		Ol	0.65		0.03	0.02		0.01
		Ol	0.83		0.01	0.01		0.01
		Ol	0.86		0.01	0.02		0.01
PIA44	Spl hrz	Ol	0.80		0.02	0.03		0.01
		Ol	0.92		0.04	0.06		0.01
		Ol	0.51		0.03	0.02		0.01
		Ol	0.94		0.01	0.05		0.01
		Ol	0.67		0.009	0.02		0.004
		Ol	0.87		0.01	0.07		0.01
		Ol	0.76		0.010	0.03		0.005
		Ol	0.71		0.006	0.02		0.001
PIA27	Spl hrz	Ol	0.79		0.07	0.04		0.02
		Ol	0.95		0.03	0.06		0.01
		Ol	0.72		0.09	0.04		0.03
PIA109	Pl-bear hrz	Ol	0.94		0.010	0.03		0.005
		Ol	0.72		0.02	0.02		0.01
PIA120	Pl-bear hrz	Ol	1.05		0.01	0.02		0.01
		Ol	0.97		0.007	0.02		0.003
PIA109	Pl-bear hrz	Prg	1.70	0.012	0.04	0.05	0.003	0.01
		Prg	0.89		0.05	0.05		0.02
PIA120	Pl-bear hrz	Prg	0.59	0.003	0.003	0.03	0.001	0.003
		Prg	1.08	0.004	0.02	0.05	0.001	0.01
		Prg	0.62	0.004	0.03	0.02	0.001	0.01
PIA27	Spl hrz	Ed hbl	2.44	0.002	0.08	0.06	0.001	0.01
		Ed hbl	2.14		0.06	0.08		0.02
		Ed hbl	1.94	0.003	0.88	0.05	0.002	0.09
PIA109	Pl-bear hrz	Pl	0.002	0.007	0.004	0.001	0.002	0.002
		Pl	0.001	0.005	0.02	0.001	0.002	0.01
PIA120	Pl-bear hrz	Pl	0.001	0.002	0.005	0.001	0.001	0.003
		Pl	0.001	0.002	0.004	0.001	0.001	0.002
PI6	Spl hrz	Srp	0.48		0.8	0.02		0.2
		Srp	0.08		3.0	0.01		0.7
		Srp	0.20		0.6	0.01		0.1
		Srp	0.32		4.7	0.02		0.9
		Srp	0.48		0.8	0.02		0.2

Abbreviations: Ol = olivine, Prg = pargasite, Ed hbl = edenitic hornblende, Srp = serpentine, Spl hrz = spinel harzburgite, Pl-bear hrz = plagioclase-bearing harzburgite.

Li, Be and B content of minerals from the Dramala spinel harzburgite and plagioclase-bearing harzburgite measured by SIMS continued

Sample	Rock	Mineral	Li (µg/g)	Be (µg/g)	B (µg/g)	Li (2σ)	Be (2σ)	B (2σ)
		Srp	0.08		3.0	0.01		0.7
		Srp	0.20		0.6	0.01		0.1
		Srp	0.32		4.7	0.02		0.9
PIA44	Spl hrz	Srp	0.086		0.12	0.002		0.02
		Srp	0.19		0.07	0.01		0.05
		Srp	0.093		0.09	0.003		0.01
PIA27	Spl hrz	Srp	0.05		22	0.01		1
		Srp	0.07		27.6	0.01		0.8
		Srp	0.27		11.0	0.02		0.1
		Srp	0.27	0.001	6.0	0.01	0.001	0.8
		Srp	0.32		4.6	0.03		0.4
		Srp	0.23	0.001	9	0.01	0.001	1
PIA109	Pl-bear hrz	Srp	0.14		9	0.01		2
		Srp	0.13		10	0.01		1
		Srp	0.12		4	0.01		1
		Srp	0.16		24	0.01		5
PIA120	Pl-bear hrz	Srp	0.78		0.41	0.03		0.03
		Srp	0.010		0.57	0.003		0.03
		Srp	0.002		0.77	0.002		0.07
PIA120	Pl-bear hrz	Chl	2.03		0.07	0.07		0.01
		Chl	3.32		0.27	0.08		0.05
PI6	Spl hrz	Tr	1.6		2.83	0.1		0.06
		Tr	0.09		1.70	0.01		0.07
		Tr	0.06		1.19	0.01		0.04
PIA27	Spl hrz	Tr	0.03	0.001	1.17	0.01	0.001	0.06
		Tr	0.08	0.001	1.5	0.01	0.001	0.2
PI6	Spl hrz	Tlc	3.8		1.5	0.1		0.3
		Tlc	2.91		0.9	0.05		0.1
PIA27	Spl hrz	Tlc	0.15		4.0	0.01		0.6
		Tlc	0.12		0.7	0.01		0.1
		Tlc	0.10		0.77	0.01		0.06
PIA120	Pl-bear hrz	Ntr	0.010		0.007	0.003		0.003
		Ntr	0.12		0.010	0.03		0.004
		Ntr	0.008		0.009	0.003		0.005
PIA120	Pl-bear hrz	Vua	0.03	0.002	0.26	0.01	0.001	0.04
		Vua	0.39		0.22	0.05		0.03
		Vua	0.16	0.002	0.23	0.03	0.001	0.03
PI6	Spl hrz	Pct	5.1		0.10	0.1		0.02
		Pct	11.0		0.8	0.2		0.2
PIA27	Spl hrz	Ath	0.72	0.002	0.40	0.04	0.001	0.06

Abbreviations: Srp = serpentine, Tr = tremolite, Tlc = talc, Ntr = natrolite, Vua = vuagnatite, Pct = pectolite, Ath = anthophyllite., Spl hrz = spinel harzburgite, Pl-bear hrz = plagioclase-bearing harzburgite.

Laser ablation - inductively coupled plasma mass spectrometry (LA-ICPMS)
Li, B and other trace elements

Trace element content of olivine measured by LA-ICPMS in Dramala spinel harzburgite plagioclase-bearing harzburgite

Sample	PI2	PI2	PI2	PI2	PIA91	PIA91	PIA91	PIA91	PI6	PI6	PI6	PI6	PIA44	PIA44	PIA44	PIA27	PIA27	PIA27	PIA120	PIA120
Mineral	**Ol**	**Ol**	**Ol**	**Ol**	**Ol**	**Ol**	**Ol**	**Ol**	**Ol**	**Ol**	**Ol**	**Ol**	**Ol**	**Ol**	**Ol**	**Ol**	**Ol**	**Ol**	**Ol**	**Ol**
(µg/g)																				
Li	1.3	1.1	1.1	1.3	1.0	1.1	1.3	1.3	1.3	1.3	1.2	0.8	1.0	1.3	1.0	0.8	1.3	1.2	1.3	1.6
B	0.25	< 0.14	0.15	0.20	< 0.15	0.13	< 0.18	< 0.16	< 0.18	0.16	< 0.22	< 0.18	< 0.62	< 0.15	0.13	0.32	0.34	< 0.24	< 0.06	< 0.05
P	6	5	5	5	3	3	3	3	3	3	3	3	6	4	4	5	5	6	7	7
Sc	2.6	2.5	2.5	2.7	2.5	2.1	2.2	2.3	2.5	2.5	2.6	2.3	2.9	2.5	2.5	2.1	2.2	2.3	2.0	1.9
V	1.1	1.1	1.0	1.1	1.0	0.7	1.0	1.1	0.7	5.1	0.9	0.7	1.5	1.8	1.0	2.3	1.0	0.8	1.0	1.0
Co	130	128	129	137	140	137	140	146	149	149	147	146	136	138	138	136	144	145	143	142
Ni	2851	2761	2752	2954	3099	2990	3114	3180	3366	3392	3275	3363	3029	2992	3169	3147	3217	3224	2890	2867
Zn	37	41	40	38	45	46	44	47	45	51	44	43	48	42	39	43	47	53	48	48
Ga	< 0.013	< 0.012	< 0.013	< 0.010	< 0.014	< 0.014	< 0.013	< 0.013	< 0.019	0.05	< 0.011	< 0.019	< 0.052	0.03	< 0.012	0.03	0.01	0.02	0.02	< 0.018
Rb	< 0.004	< 0.004	< 0.003	< 0.004	< 0.004	< 0.005	< 0.004	< 0.005	< 0.005	< 0.005	< 0.004	< 0.004	< 0.010	< 0.004	< 0.003	0.016	< 0.003	< 0.006	< 0.005	< 0.004
Sr	0.004	0.004	< 0.002	0.005	0.003	< 0.004	< 0.002	0.013	< 0.003	0.002	< 0.003	< 0.002	< 0.009	< 0.003	0.004	0.010	< 0.003	< 0.005	< 0.003	0.005
Y	0.004	0.008	0.003	0.010	0.003	0.002	< 0.003	< 0.002	< 0.002	< 0.004	< 0.002	< 0.003	< 0.010	< 0.003	< 0.003	0.003	< 0.003	< 0.004	0.014	0.007
Zr	< 0.004	< 0.004	< 0.004	< 0.006	< 0.004	< 0.006	< 0.005	< 0.006	< 0.007	0.006	< 0.004	< 0.006	< 0.012	< 0.005	< 0.006	< 0.005	< 0.007	< 0.008	0.010	0.007
Nb	< 0.003	< 0.002	< 0.003	< 0.003	< 0.003	< 0.002	< 0.005	< 0.002	< 0.005	< 0.005	< 0.004	< 0.005	< 0.012	< 0.003	< 0.002	< 0.003	< 0.004	< 0.006	< 0.003	< 0.002
Sb	0.037	0.021	0.040	0.023	0.020	0.016	0.021	0.014	< 0.015	< 0.012	< 0.015	0.016	< 0.043	0.017	0.020	0.019	0.021	< 0.028	0.025	< 0.015
Cs	< 0.002	< 0.002	< 0.002	< 0.002	< 0.002	< 0.001	< 0.002	< 0.002	< 0.002	< 0.002	< 0.003	< 0.002	< 0.005	< 0.002	< 0.002	0.008	< 0.002	< 0.004	< 0.002	< 0.002
Ba	0.016	< 0.015	< 0.015	0.029	< 0.009	0.021	< 0.018	0.029	< 0.027	< 0.022	< 0.016	0.019	< 0.095	< 0.016	< 0.016	0.021	< 0.016	0.036	< 0.020	< 0.022
La	< 0.003	< 0.002	< 0.002	< 0.004	< 0.003	0.002	< 0.003	< 0.003	< 0.003	< 0.003	< 0.003	< 0.003	< 0.007	< 0.004	< 0.003	< 0.002	< 0.002	< 0.004	< 0.003	< 0.002
Ce	< 0.003	< 0.002	< 0.002	< 0.004	< 0.001	< 0.002	< 0.003	< 0.002	< 0.002	< 0.003	< 0.002	< 0.003	< 0.008	< 0.002	< 0.002	< 0.002	< 0.003	< 0.007	< 0.003	< 0.002
Pr	< 0.001	< 0.002	< 0.002	< 0.002	< 0.001	< 0.001	< 0.002	< 0.002	< 0.003	< 0.003	< 0.003	< 0.002	< 0.006	< 0.002	< 0.002	< 0.002	< 0.002	< 0.003	< 0.002	< 0.002
Nd	< 0.013	< 0.011	< 0.008	< 0.011	< 0.013	< 0.012	< 0.009	< 0.010	< 0.013	< 0.013	< 0.013	< 0.012	< 0.052	< 0.001	< 0.013	< 0.011	< 0.017	< 0.018	< 0.014	< 0.011
Sm	< 0.013	< 0.012	< 0.009	< 0.012	< 0.011	< 0.008	< 0.009	< 0.017	< 0.011	< 0.016	< 0.014	< 0.018	< 0.034	< 0.012	< 0.007	< 0.013	0.009	< 0.017	< 0.015	< 0.010
Eu	< 0.003	< 0.004	< 0.004	< 0.003	< 0.004	< 0.003	< 0.003	< 0.003	< 0.006	< 0.005	< 0.005	< 0.005	< 0.013	< 0.003	< 0.003	< 0.004	< 0.003	< 0.006	< 0.004	< 0.004
Gd	< 0.014	< 0.017	< 0.010	< 0.014	< 0.013	< 0.010	< 0.006	< 0.010	< 0.017	< 0.010	< 0.007	< 0.009	< 0.036	< 0.011	< 0.013	< 0.013	< 0.009	< 0.026	< 0.008	< 0.009
Tb	< 0.002	< 0.001	< 0.002	< 0.002	< 0.002	< 0.001	< 0.001	< 0.003	< 0.003	< 0.002	< 0.002	< 0.002	< 0.004	< 0.002	< 0.002	< 0.001	< 0.002	< 0.002	< 0.002	< 0.003
Dy	< 0.005	< 0.003	< 0.004	< 0.007	< 0.008	< 0.006	< 0.007	< 0.009	< 0.009	0.004	< 0.010	< 0.009	< 0.028	< 0.009	< 0.007	< 0.007	< 0.006	< 0.009	< 0.008	< 0.009
Ho	< 0.001	< 0.002	< 0.001	< 0.002	< 0.002	< 0.002	< 0.002	< 0.001	< 0.002	< 0.002	< 0.002	< 0.003	< 0.006	< 0.002	< 0.001	< 0.002	< 0.002	< 0.003	< 0.002	< 0.002
Er	< 0.005	< 0.004	< 0.006	< 0.006	< 0.008	0.006	< 0.008	< 0.009	< 0.006	< 0.008	< 0.007	< 0.009	< 0.026	< 0.003	< 0.008	< 0.007	< 0.010	< 0.020	< 0.011	0.012
Tm	< 0.001	< 0.001	< 0.002	< 0.002	< 0.001	< 0.001	< 0.001	< 0.003	< 0.003	< 0.003	< 0.002	< 0.002	< 0.007	< 0.002	< 0.001	< 0.002	< 0.002	< 0.002	< 0.002	< 0.002
Yb	< 0.011	< 0.010	< 0.012	< 0.010	< 0.015	0.004	< 0.006	< 0.010	< 0.015	< 0.010	< 0.010	0.011	< 0.042	< 0.007	< 0.012	< 0.014	< 0.009	< 0.017	0.019	< 0.011
Lu	< 0.002	0.003	< 0.001	< 0.001	0.002	< 0.002	< 0.002	< 0.002	< 0.002	< 0.002	< 0.002	< 0.002	< 0.006	< 0.002	< 0.001	< 0.002	< 0.002	< 0.003	0.004	0.004
Hf	< 0.005	< 0.005	< 0.005	< 0.006	< 0.007	< 0.005	< 0.008	< 0.011	< 0.005	< 0.008	< 0.008	< 0.007	< 0.012	< 0.005	< 0.002	< 0.006	< 0.005	< 0.012	< 0.011	< 0.004
Ta	< 0.002	< 0.001	< 0.002	< 0.002	< 0.003	< 0.002	< 0.002	< 0.003	< 0.003	< 0.002	< 0.002	< 0.003	< 0.006	< 0.002	< 0.002	< 0.002	< 0.001	< 0.004	< 0.002	< 0.002
Pb	0.270	0.173	0.165	0.164	0.012	0.013	0.021	0.018	< 0.009	0.012	0.009	0.007	< 0.026	0.015	0.038	0.067	0.058	0.024	0.025	0.021
Th	< 0.001	< 0.003	< 0.002	< 0.002	< 0.001	< 0.002	0.001	0.001	< 0.003	< 0.001	< 0.002	< 0.002	< 0.010	< 0.002	< 0.002	< 0.002	< 0.001	< 0.003	< 0.002	< 0.003
U	< 0.003	< 0.004	< 0.002	< 0.002	< 0.002	< 0.001	< 0.001	< 0.001	< 0.001	< 0.003	< 0.002	< 0.002	< 0.005	< 0.002	< 0.002	< 0.002	< 0.002	< 0.003	< 0.002	< 0.002

Abbreviation: Ol = olivine.

Trace element content of olivine measured by LA-ICPMS in Dramala spinel harzburgite plagioclase-bearing harzburgite continued

Sample	PIA120	PIA120	PIA51	PIA51	PIA51	PIA51	PIA109	PIA109	PIA109	PIA109
Mineral	Ol	Ol	Ol	Ol	Ol	Ol	Ol	Ol	Ol	Ol
(µg/g)										
Li	1.5	1.5	0.8	1.1	1.1	1.2	1.8	1.5	1.6	1.7
B	< 0.09	< 0.30	0.91	0.77	0.55	0.97	< 0.37	< 0.21	< 0.32	< 0.56
P	8	8	3	3	4	3	5	6	6	7
Sc	1.9	1.9	2.3	2.3	2.6	2.4	2.0	6.7	2.0	2.0
V	0.8	0.9	0.9	0.8	1.0	0.7	0.6	28	0.6	0.8
Co	141	139	143	138	148	145	145	128	139	134
Ni	2890	2911	3045	2969	3211	3157	3059	2610	2947	2950
Zn	46	47	45	44	47	45	31	31	29	36
Ga	0.11	< 0.024	< 0.008	< 0.010	0.01	< 0.009	< 0.012	0.53	< 0.015	0.04
Rb	< 0.008	< 0.006	0.004	< 0.003	< 0.004	< 0.004	< 0.008	0.006	< 0.006	< 0.011
Sr	0.033	< 0.004	< 0.003	< 0.003	< 0.003	< 0.002	< 0.004	0.010	< 0.005	0.022
Y	0.015	< 0.006	< 0.003	0.002	< 0.002	< 0.003	0.011	0.156	0.011	0.009
Zr	0.036	< 0.011	0.010	< 0.006	0.005	< 0.005	< 0.012	0.019	0.009	< 0.019
Nb	< 0.004	< 0.006	0.004	< 0.003	< 0.003	< 0.003	< 0.006	< 0.008	< 0.005	< 0.008
Sb	< 0.035	< 0.018	0.013	0.018	0.020	0.018	0.026	0.022	< 0.015	< 0.035
Cs	< 0.006	< 0.003	< 0.002	< 0.002	< 0.002	< 0.002	< 0.003	< 0.004	< 0.003	< 0.004
Ba	< 0.045	< 0.026	< 0.025	< 0.024	< 0.019	< 0.017	< 0.027	< 0.021	< 0.036	< 0.050
La	< 0.004	< 0.004	< 0.002	< 0.003	< 0.002	< 0.002	< 0.004	< 0.005	< 0.003	< 0.010
Ce	< 0.005	< 0.005	< 0.003	< 0.002	< 0.002	< 0.003	< 0.004	< 0.004	< 0.006	< 0.008
Pr	< 0.003	< 0.002	< 0.001	< 0.002	< 0.002	< 0.003	< 0.003	< 0.003	< 0.004	< 0.006
Nd	< 0.020	< 0.023	< 0.009	< 0.005	< 0.014	< 0.010	< 0.016	< 0.015	< 0.020	< 0.014
Sm	< 0.012	< 0.022	< 0.011	< 0.017	< 0.008	< 0.014	< 0.018	< 0.019	< 0.022	< 0.036
Eu	< 0.009	< 0.008	< 0.002	< 0.004	< 0.004	< 0.004	< 0.007	< 0.007	< 0.004	< 0.013
Gd	< 0.044	< 0.019	< 0.006	< 0.009	< 0.013	< 0.014	< 0.020	< 0.030	< 0.020	< 0.030
Tb	< 0.004	< 0.003	< 0.002	< 0.002	< 0.001	0.001	< 0.003	< 0.003	< 0.002	< 0.007
Dy	< 0.018	< 0.013	< 0.007	< 0.005	< 0.006	< 0.006	< 0.013	0.015	< 0.015	< 0.015
Ho	< 0.004	< 0.003	< 0.002	< 0.001	< 0.002	< 0.001	< 0.003	0.005	< 0.002	< 0.005
Er	< 0.019	< 0.018	< 0.005	< 0.007	< 0.004	< 0.006	< 0.015	0.026	< 0.006	< 0.023
Tm	< 0.005	0.003	< 0.002	< 0.001	< 0.002	< 0.002	< 0.003	0.005	< 0.003	< 0.006
Yb	< 0.028	< 0.017	< 0.007	< 0.010	< 0.008	< 0.009	< 0.015	0.096	< 0.015	< 0.033
Lu	0.006	< 0.003	< 0.002	0.002	< 0.002	< 0.002	0.004	0.010	0.003	< 0.006
Hf	0.014	< 0.012	< 0.005	< 0.005	< 0.004	< 0.006	< 0.011	< 0.014	< 0.007	< 0.013
Ta	< 0.003	< 0.003	< 0.003	< 0.002	< 0.002	< 0.002	< 0.004	< 0.003	< 0.002	< 0.006
Pb	0.035	0.013	0.012	0.012	0.017	0.017	< 0.010	< 0.010	< 0.008	< 0.014
Th	< 0.004	< 0.004	< 0.002	< 0.001	< 0.001	< 0.002	< 0.002	< 0.002	< 0.002	< 0.004
U	< 0.005	< 0.004	< 0.001	< 0.001	0.001	0.002	< 0.001	< 0.002	< 0.002	< 0.004

Abbreviation: Ol = olivine.

Trace element content of orthopyroxene measured by LA-ICPMS in Dramala spinel harzburgite and plagioclase-bearing harzburgite

Sample	PI2	PI2	PI2	PI2	PIA91	PIA91	PIA91	PIA91	PI6	PI6	PI6	PI6	PIA44	PIA44	PIA44	PIA44	PIA44	PIA27	PIA27	PIA27
Mineral	**Opx**	**Opx**	**Opx**	**Opx**	**Opx**	**Opx**	**Opx**	**Opx**	**Opx**	**Opx**	**Opx**	**Opx**	**Opx**	**Opx**	**Opx**	**Opx**	**Opx**	**Opx**	**Opx**	**Opx**
(µg/g)																				
Li	1.3	1.4	1.6	1.5	1.3	1.7	1.1	1.8	0.4	0.4	0.3	0.3	1.2	1.0	1.2	1.1	1.3	0.2	0.3	0.2
B	0.21	0.15	0.65	0.23	0.22	< 0.17	< 0.19	< 0.17	< 0.20	< 0.14	0.18	0.21	< 0.20	0.25	0.12	< 0.15	< 0.13	0.21	0.40	0.32
P	5	5	5	5	4	5	4	3	4	3	3	3	5	4	4	4	4	5	5	4
Sc	29.8	26.4	29.0	26.2	26.3	28.2	23.7	21.6	23.5	21.8	20.9	22.3	28.4	29.2	27.9	28.1	27.2	22.3	22.2	20.4
V	124	119	127	119	115	115	91	93	78	75	70	72	106	104	114	105	110	82	96	89
Co	49	50	52	50	64	66	49	50	53	52	49	48	57	52	58	53	54	53	64	62
Ni	628	629	614	627	773	817	575	625	646	659	607	594	722	641	727	671	704	693	849	805
Zn	33	35	35	36	42	42	35	35	36	36	34	33	40	34	43	38	40	39	47	44
Ga	2.0	2.2	2.1	2.2	1.9	1.8	1.3	1.4	1.1	1.1	1.1	1.1	1.4	1.5	1.5	1.4	1.4	1.4	1.6	1.6
Rb	< 0.010	0.005	0.004	< 0.010	0.012	0.006	< 0.010	< 0.003	0.016	0.004	< 0.004	< 0.003	< 0.004	< 0.003	< 0.004	< 0.004	< 0.004	0.004	< 0.003	0.010
Sr	0.008	< 0.003	0.011	0.006	0.004	0.017	0.004	0.004	0.017	0.008	0.003	0.007	< 0.003	< 0.003	0.003	0.007	0.007	< 0.002	0.005	< 0.004
Y	0.265	0.211	0.240	0.264	0.132	0.137	0.094	0.095	0.035	0.035	0.037	0.037	0.081	0.081	0.085	0.087	0.099	0.104	0.090	0.076
Zr	0.006	0.004	0.007	< 0.008	0.008	< 0.007	< 0.008	< 0.005	< 0.008	< 0.007	0.006	< 0.007	< 0.008	0.013	0.010	0.011	< 0.009	0.012	0.007	0.008
Nb	0.007	0.006	0.008	0.006	0.006	< 0.004	< 0.006	0.006	0.006	< 0.005	< 0.005	< 0.004	0.007	0.006	0.006	0.006	0.008	0.005	< 0.005	0.009
Sb	0.040	0.050	0.074	0.025	0.025	< 0.016	< 0.017	0.019	0.014	< 0.012	< 0.010	0.009	0.028	0.032	0.030	0.030	0.014	0.032	0.038	0.045
Cs	< 0.001	< 0.002	< 0.002	< 0.002	< 0.003	< 0.003	< 0.002	< 0.002	0.003	< 0.002	< 0.003	0.002	< 0.002	< 0.002	< 0.002	< 0.002	< 0.002	< 0.003	< 0.002	< 0.002
Ba	< 0.022	< 0.016	< 0.018	< 0.016	< 0.025	< 0.027	< 0.026	< 0.017	< 0.023	< 0.017	< 0.019	< 0.022	< 0.025	< 0.017	< 0.020	< 0.019	< 0.019	< 0.011	< 0.023	< 0.014
La	< 0.003	< 0.002	< 0.002	< 0.002	< 0.003	< 0.004	< 0.003	< 0.003	< 0.004	< 0.003	< 0.002	< 0.003	< 0.003	< 0.002	< 0.002	< 0.003	< 0.003	< 0.003	< 0.003	< 0.003
Ce	< 0.002	< 0.002	< 0.002	< 0.003	< 0.003	< 0.003	< 0.004	< 0.003	< 0.004	< 0.003	< 0.003	< 0.003	< 0.004	< 0.002	< 0.003	< 0.002	< 0.002	< 0.003	< 0.003	< 0.002
Pr	< 0.001	< 0.002	< 0.002	< 0.001	< 0.003	< 0.002	< 0.003	< 0.002	< 0.003	< 0.001	< 0.001	< 0.001	< 0.002	< 0.002	< 0.003	< 0.002	< 0.002	< 0.001	< 0.002	< 0.003
Nd	< 0.007	< 0.008	< 0.009	< 0.008	< 0.012	< 0.012	< 0.021	< 0.010	< 0.012	< 0.011	< 0.011	< 0.010	< 0.011	< 0.013	< 0.011	< 0.017	< 0.014	< 0.009	< 0.014	< 0.009
Sm	< 0.013	< 0.009	< 0.011	< 0.009	< 0.020	< 0.020	< 0.022	< 0.013	< 0.019	< 0.013	< 0.010	< 0.010	< 0.015	< 0.010	< 0.010	< 0.012	< 0.013	< 0.014	< 0.015	< 0.010
Eu	< 0.004	< 0.002	< 0.003	< 0.003	< 0.004	< 0.005	< 0.004	< 0.005	< 0.004	< 0.005	< 0.004	< 0.005	< 0.003	< 0.004	< 0.003	< 0.002	< 0.003	< 0.004	< 0.004	< 0.003
Gd	< 0.011	< 0.011	< 0.009	< 0.010	< 0.015	< 0.014	< 0.021	< 0.008	< 0.010	< 0.017	< 0.009	< 0.009	< 0.011	< 0.009	< 0.013	< 0.014	0.008	< 0.009	< 0.014	< 0.013
Tb	< 0.002	< 0.002	< 0.001	< 0.001	< 0.002	< 0.003	< 0.002	< 0.002	< 0.002	< 0.002	< 0.002	< 0.001	< 0.002	< 0.002	< 0.002	< 0.002	< 0.002	< 0.001	< 0.001	< 0.002
Dy	0.027	0.022	0.017	0.022	< 0.009	0.011	0.014	< 0.009	< 0.008	< 0.010	< 0.006	< 0.006	< 0.001	< 0.008	0.013	< 0.006	0.014	0.007	< 0.008	0.011
Ho	0.011	0.010	0.009	0.008	0.006	0.004	< 0.002	0.004	< 0.002	< 0.001	< 0.002	< 0.002	0.003	0.003	0.005	< 0.002	0.004	0.004	0.002	0.002
Er	0.039	0.039	0.051	0.050	0.023	0.022	0.019	0.022	< 0.010	0.012	0.011	< 0.011	0.019	0.023	0.022	0.020	0.019	0.018	< 0.010	0.026
Tm	0.011	0.009	0.010	0.011	0.008	0.009	0.007	0.008	0.004	< 0.003	0.003	0.002	0.009	0.004	0.003	0.006	0.003	0.006	0.005	0.005
Yb	0.134	0.117	0.126	0.128	0.065	0.071	0.085	0.060	0.027	0.020	0.025	0.050	0.054	0.090	0.055	0.062	0.060	0.069	0.053	0.052
Lu	0.022	0.021	0.023	0.021	0.016	0.017	0.010	0.014	0.008	0.007	0.008	0.005	0.014	0.017	0.012	0.013	0.010	0.015	0.013	0.010
Hf	< 0.006	< 0.005	< 0.006	< 0.004	< 0.008	< 0.008	< 0.009	< 0.006	< 0.004	< 0.008	< 0.005	< 0.007	< 0.009	0.003	< 0.008	< 0.002	< 0.005	< 0.003	< 0.008	< 0.009
Ta	0.003	< 0.002	< 0.002	< 0.002	< 0.002	< 0.003	< 0.002	< 0.001	< 0.002	< 0.002	< 0.002	< 0.002	< 0.002	0.002	< 0.003	< 0.002	< 0.002	< 0.002	< 0.002	< 0.001
Pb	0.458	0.360	0.262	0.232	0.024	0.017	< 0.009	0.010	0.015	0.010	0.014	0.011	0.065	0.080	0.048	0.049	0.036	0.127	0.099	0.086
Th	< 0.001	< 0.001	< 0.002	< 0.002	< 0.002	< 0.004	< 0.004	< 0.001	< 0.002	< 0.001	< 0.002	< 0.002	< 0.001	< 0.002	< 0.002	< 0.002	< 0.003	< 0.002	< 0.003	< 0.003
U	< 0.002	< 0.002	< 0.002	< 0.002	< 0.002	< 0.003	< 0.003	< 0.002	< 0.002	< 0.001	< 0.002	< 0.002	< 0.002	< 0.002	< 0.002	< 0.002	< 0.002	< 0.002	< 0.003	< 0.002

Abbreviation: Opx = orthopyroxene.

Trace element content of orthopyroxene measured by LA-ICPMS in Dramala spinel harzburgite and plagioclase-bearing harzburgite continued

Sample	PIA120	PIA120	PIA120	PIA120	PIA120	PIA120	PIA51	PIA51	PIA51	PIA109	PIA109	PIA109	PIA109	PIA109
Mineral	Opx	Opx	Opx	Opx	Opx	Opx	Opx	Opx	Opx	Opx	Opx	Opx	Opx	Opx
(µg/g)														
Li	1.1	1.0	0.2	0.2	0.1	0.1	1.1	1.5	1.2	1.9	1.4	2.4	2.4	2.4
B	0.33	0.34	0.08	0.09	< 0.05	< 0.12	0.13	< 0.11	0.19	< 0.22	< 0.15	< 0.16	< 0.19	< 0.20
P	6	5	2	1	1	1	3	3	3	5	4	5	4	5
Sc	24.9	23.3	5.3	6.2	4.2	4.5	24.9	23.3	24.3	29.9	30.0	22.9	22.4	28.7
V	132	127	30	32	21	21	86	94	96	152	136	134	133	157
Co	48	50	12	14	12	11	43	49	48	62	45	58	60	65
Ni	553	558	135	155	131	129	510	602	568	725	537	753	768	817
Zn	35	38	8	10	9	9	28	32	32	40	29	42	44	47
Ga	3.5	4.0	0.9	0.9	0.6	0.6	1.4	1.6	1.6	4.4	3.4	4.1	4.2	4.8
Rb	< 0.005	0.004	0.001	0.006	0.029	0.008	< 0.003	< 0.003	< 0.003	< 0.005	0.003	< 0.003	< 0.004	< 0.005
Sr	0.017	0.010	0.002	0.014	0.027	0.005	0.011	0.011	0.008	< 0.006	< 0.003	0.005	0.003	< 0.004
Y	2.120	1.690	0.352	0.378	0.179	0.200	0.104	0.107	0.101	1.242	1.748	1.284	1.153	1.471
Zr	0.727	0.478	0.109	0.118	0.044	0.047	0.010	0.009	0.010	0.105	0.105	0.103	0.077	0.075
Nb	< 0.004	0.004	< 0.001	< 0.001	< 0.001	0.004	0.010	0.010	0.007	< 0.004	0.005	0.006	0.009	0.006
Sb	< 0.025	0.017	0.004	0.006	< 0.005	< 0.007	0.014	< 0.008	0.014	0.021	0.013	0.022	< 0.012	0.024
Cs	< 0.002	0.002	< 0.001	< 0.001	0.002	< 0.002	< 0..03	< 0.002	< 0.001	< 0.003	< 0.001	< 0.002	0.006	0.002
Ba	< 0.015	< 0.015	< 0.004	< 0.004	0.007	< 0.015	< 0.019	< 0.013	< 0.017	< 0.015	< 0.018	< 0.021	< 0.022	< 0.026
La	< 0.003	< 0.002	< 0.001	< 0.001	< 0.001	< 0.002	< 0.002	< 0.003	< 0.003	< 0.003	< 0.002	< 0.002	< 0.003	< 0.004
Ce	0.010	0.003	< 0.001	0.002	0.004	< 0.002	< 0.002	< 0.001	< 0.003	< 0.002	< 0.002	< 0.003	< 0.003	< 0.003
Pr	0.009	< 0.002	< 0.002	0.001	< 0.001	< 0.002	< 0.001	< 0.001	< 0.002	< 0.004	< 0.002	< 0.002	< 0.001	< 0.002
Nd	0.045	0.024	< 0.003	0.009	< 0.005	< 0.008	< 0.009	< 0.011	< 0.012	< 0.011	0.013	0.015	< 0.012	< 0.013
Sm	0.075	0.027	0.003	0.014	< 0.005	< 0.007	< 0.010	< 0.010	< 0.010	< 0.017	0.025	0.017	< 0.018	0.020
Eu	0.016	0.012	0.001	0.004	< 0.002	0.002	< 0.002	< 0.003	< 0.004	0.011	0.008	0.013	0.009	0.012
Gd	0.102	0.038	0.010	0.021	< 0.006	< 0.008	< 0.011	< 0.011	< 0.006	0.034	0.066	0.041	0.050	0.061
Tb	0.037	0.020	0.004	0.007	0.001	0.002	< 0.001	< 0.002	< 0.001	0.020	0.024	0.017	0.019	0.017
Dy	0.304	0.200	0.046	0.045	0.019	0.019	0.005	0.009	0.007	0.157	0.191	0.145	0.140	0.195
Ho	0.079	0.059	0.011	0.015	0.006	0.007	0.003	< 0.002	0.006	0.039	0.071	0.044	0.040	0.055
Er	0.338	0.247	0.054	0.050	0.022	0.041	0.018	0.016	0.011	0.174	0.265	0.163	0.139	0.232
Tm	0.068	0.048	0.009	0.010	0.008	0.006	0.006	0.003	0.004	0.027	0.051	0.035	0.030	0.036
Yb	0.493	0.402	0.095	0.114	0.074	0.073	0.060	0.060	0.052	0.345	0.461	0.272	0.221	0.350
Lu	0.075	0.075	0.015	0.013	0.012	0.012	0.012	0.010	0.011	0.054	0.068	0.043	0.038	0.058
Hf	0.056	0.037	0.006	0.008	0.003	< 0.006	< 0.004	< 0.005	< 0.004	0.011	0.028	0.021	0.016	0.020
Ta	< 0.002	< 0.002	< 0.001	< 0.001	< 0.001	< 0.001	< 0.001	< 0.002	< 0.002	< 0.002	< 0.002	< 0.003	< 0.002	< 0.002
Pb	0.064	0.042	0.008	0.008	0.007	< 0.007	0.020	0.012	0.012	0.009	0.019	0.011	0.012	0.017
Th	< 0.003	< 0.001	< 0.003	< 0.003	< 0.001	< 0.002	< 0.001	< 0.002	< 0.001	< 0.002	< 0.002	< 0.001	< 0.002	< 0.002
U	< 0.002	< 0.002	< 0.001	< 0.001	< 0.001	< 0.002	< 0.001	< 0.001	0.001	< 0.002	< 0.001	< 0.001	< 0.001	< 0.001

Abbreviation: Opx = orthopyroxene.

Trace element content of spinel measured by LA-ICPMS in Dramala spinel harzburgite and plagioclase-bearing harzburgite

Sample	PI2	PI2	PIA91	PIA91	PI6	PI6	PIA44	PIA44	PIA27	PIA27	PIA120	PIA120	PIA51	PIA51
Mineral	Spl	Spl	Spl	Spl	Spl	Spl	Spl	Spl	Spl	Spl	Spl	Spl	Spl	Spl
(µg/g)														
Li	0.5	0.5	0.4	0.4	< 0.1	0.3	0.3	0.2	0.3	0.2	< 0.5	< 0.8	0.4	0.4
B	0.73	0.40	< 0.37	< 0.24	0.29	< 0.31	1.27	< 0.34	0.62	0.40	< 2.0	< 4.60	< 0.28	0.30
P	9	6	5	5	5	4	8	5	5	5	11	18	4	4
Sc	1.8	1.5	1.9	1.7	4.4	4.5	2.4	2.8	2.9	2.5	1.1	1.0	2.2	2.5
V	1270	1107	1465	1465	1883	1896	1547	1591	1318	1279	1408	1277	1309	1375
Co	383	345	397	392	431	419	362	361	353	341	414	410	364	387
Ni	1122	1029	675	727	463	543	642	690	630	550	1128	1189	679	860
Zn	1545	1441	1539	1427	1592	1491	1288	1298	1402	1410	2328	2517	1464	1498
Ga	44	38	30	30	24	25	29	28	26	25	79	88	25	27
Rb	0.012	< 0.006	< 0.010	0.015	< 0.009	< 0.009	< 0.012	< 0.007	< 0.007	< 0.008	< 0.044	< 0.089	0.013	0.013
Sr	< 0.006	0.009	0.022	< 0.007	0.015	0.010	0.022	< 0.007	0.014	0.011	0.069	0.384	0.039	0.036
Y	< 0.007	< 0.004	< 0.006	< 0.003	< 0.005	< 0.008	< 0.011	< 0.004	0.003	< 0.003	< 0.030	0.146	< 0.008	< 0.005
Zr	0.293	0.238	0.282	0.295	0.290	0.352	0.313	0.310	0.346	0.348	0.185	0.132	0.217	0.222
Nb	0.368	0.324	0.406	0.403	0.412	0.490	0.450	0.424	0.492	0.442	0.237	0.214	0.306	0.324
Sb	0.162	0.126	0.034	0.048	< 0.026	0.022	< 0.038	0.085	0.083	0.083	< 0.151	< 0.232	0.071	0.046
Cs	< 0.005	< 0.004	< 0.004	< 0.003	< 0.005	< 0.004	0.019	< 0.005	< 0.004	< 0.007	< 0.025	< 0.030	< 0.005	< 0.004
Ba	< 0.056	< 0.041	< 0.055	< 0.022	< 0.043	< 0.058	< 0.068	0.192	0.026	< 0.027	0.285	< 0.276	< 0.030	< 0.042
La	< 0.004	< 0.008	< 0.008	< 0.005	< 0.004	< 0.005	< 0.010	< 0.007	< 0.005	< 0.004	0.020	< 0.042	< 0.006	< 0.005
Ce	< 0.008	< 0.007	< 0.008	< 0.004	0.009	< 0.006	< 0.012	< 0.008	< 0.006	< 0.003	0.011	< 0.063	0.006	< 0.005
Pr	< 0.004	< 0.004	< 0.005	< 0.004	< 0.005	< 0.005	< 0.008	0.005	< 0.005	< 0.003	0.020	< 0.040	< 0.004	< 0.003
Nd	< 0.036	< 0.020	< 0.022	< 0.014	< 0.027	< 0.023	< 0.043	< 0.024	< 0.018	0.023	< 0.098	< 0.204	< 0.021	< 0.018
Sm	< 0.033	< 0.026	< 0.036	< 0.029	< 0.035	< 0.034	< 0.058	< 0.020	< 0.027	< 0.022	< 0.176	< 0.236	< 0.036	< 0.018
Eu	< 0.007	< 0.008	< 0.006	< 0.008	< 0.006	< 0.009	< 0.018	< 0.009	< 0.010	< 0.011	< 0.026	< 0.071	< 0.007	< 0.010
Gd	< 0.031	< 0.032	< 0.031	< 0.017	< 0.029	< 0.025	< 0.035	< 0.027	< 0.025	< 0.029	< 0.095	< 0.239	< 0.030	< 0.014
Tb	< 0.005	< 0.005	< 0.005	< 0.004	< 0.003	< 0.004	< 0.005	< 0.003	< 0.005	< 0.003	< 0.025	< 0.040	0.004	< 0.004
Dy	< 0.015	< 0.013	< 0.016	< 0.009	< 0.015	< 0.016	< 0.010	< 0.015	< 0.011	< 0.014	< 0.059	< 0.116	< 0.013	< 0.018
Ho	< 0.004	< 0.003	< 0.003	< 0.004	< 0.003	< 0.004	< 0.009	< 0.004	< 0.004	< 0.004	< 0.020	< 0.014	< 0.003	< 0.004
Er	< 0.020	< 0.018	< 0.018	< 0.012	< 0.013	< 0.011	< 0.032	< 0.015	< 0.048	< 0.022	< 0.082	< 0.080	< 0.010	< 0.009
Tm	< 0.004	< 0.003	< 0.005	< 0.003	< 0.003	< 0.004	< 0.004	< 0.004	< 0.003	< 0.004	< 0.020	< 0.033	< 0.003	0.003
Yb	< 0.027	< 0.024	0.020	< 0.023	< 0.029	< 0.021	< 0.045	< 0.018	< 0.030	< 0.020	< 0.094	0.144	< 0.003	0.014
Lu	< 0.003	< 0.003	< 0.005	< 0.004	< 0.004	< 0.004	< 0.007	< 0.004	< 0.002	< 0.004	< 0.011	0.027	< 0.002	< 0.002
Hf	< 0.012	0.009	< 0.017	< 0.012	< 0.010	< 0.015	< 0.0016	< 0.005	< 0.012	< 0.017	< 0.047	< 0.132	< 0.007	< 0.001
Ta	< 0.006	< 0.006	< 0.006	< 0.004	< 0.005	< 0.006	< 0.007	< 0.006	< 0.003	< 0.003	< 0.022	< 0.042	< 0.004	0.002
Pb	1.375	0.440	0.037	0.045	0.040	0.031	0.110	0.131	0.194	0.154	< 0.078	< 0.133	0.042	0.027
Th	< 0.007	< 0.008	< 0.006	< 0.003	< 0.004	< 0.004	< 0.006	< 0.003	< 0.002	< 0.003	< 0.028	< 0.039	< 0.003	0.003
U	< 0.006	< 0.002	< 0.005	< 0.003	< 0.004	< 0.003	< 0.008	< 0.005	< 0.003	< 0.004	< 0.017	< 0.030	0.003	< 0.004

Abbreviation: Spl = spinel.

Trace element content of plagioclase measured by LA-ICPMS in Dramala plagioclase-bearing harzburgite

Sample	**PIA120**	**PIA120**	**PIA120**	**PIA120**	**PIA120**	**PIA109**	**PIA109**	**PIA109**
Mineral	**Pl**	**Pl**	**Pl**	**Pl**	**Pl**	**Pl**	**Pl**	**Pl**
(µg/g)								
Li	< 0.08	< 0.19	< 0.19	< 0.16	< 0.27	< 0.51	< 0.21	< 0.35
B	0.60	1.05	< 0.76	< 0.54	< 1.22	< 1.30	< 1.07	1.37
P	11	12	14	13	15	13	10	11
Sc	0.3	0.3	0.3	0.3	0.2	0.3	0.2	0.5
V	0.4	0.4	0.4	1.8	0.3	0.4	0.2	0.4
Co	0.26	0.06	0.67	0.64	0.37	< 0.15	< 0.07	< 0.09
Ni	10	< 2	21	6	14	< 4	< 2	< 3
Zn	0.5	0.6	0.5	0.7	< 0.7	< 0.7	1.2	0.9
Ga	15	14	14	14	16	11	11	15
Rb	< 0.012	< 0.014	< 0.014	< 0.020	< 0.035	< 0.046	0.044	< 0.029
Sr	14.3	20.6	15.2	17.9	13.2	0.9	2.3	1.3
Y	0.103	0.123	0.122	0.079	0.082	0.119	0.105	0.064
Zr	< 0.013	< 0.030	< 0.023	< 0.015	< 0.043	< 0.026	< 0.031	< 0.037
Nb	< 0.011	< 0.011	< 0.017	< 0.012	< 0.022	< 0.037	< 0.035	< 0.034
Sb	0.061	< 0.052	0.041	0.083	< 0.104	< 0.084	< 0.072	< 0.066
Cs	< 0.004	0.008	< 0.008	< 0.005	< 0.014	< 0.028	< 0.016	< 0.010
Ba	0.160	0.144	< 0.071	0.126	< 0.106	< 0.24	< 0.16	< 0.21
La	< 0.006	0.010	< 0.009	< 0.012	< 0.021	< 0.030	< 0.012	< 0.029
Ce	0.087	0.068	0.094	0.087	0.070	< 0.030	< 0.012	< 0.020
Pr	0.024	0.024	0.017	0.032	0.026	< 0.029	< 0.016	< 0.018
Nd	0.161	0.151	0.180	0.238	< 0.087	< 0.10	< 0.07	< 0.06
Sm	0.080	0.058	< 0.052	< 0.045	< 0.078	< 0.18	0.13	< 0.09
Eu	0.219	0.201	0.264	0.267	0.244	0.087	0.074	0.086
Gd	< 0.029	< 0.046	< 0.065	< 0.038	< 0.088	0.10	< 0.12	< 0.08
Tb	< 0.005	< 0.007	<0.006	< 0.005	< 0.015	< 0.017	< 0.013	< 0.009
Dy	0.034	0.043	0.031	< 0.026	0.029	< 0.073	< 0.060	< 0.061
Ho	0.005	< 0.008	< 0.008	< 0.009	< 0.014	< 0.022	< 0.011	< 0.013
Er	< 0.011	< 0.036	< 0.034	< 0.025	< 0.041	< 0.097	< 0.049	< 0.049
Tm	< 0.003	< 0.005	< 0.007	< 0.008	0.011	< 0.019	< 0.006	< 0.010
Yb	< 0.033	0.044	< 0.043	< 0.058	< 0.100	< 0.102	< 0.072	< 0.057
Lu	< 0.004	< 0.010	< 0.009	< 0.005	< 0.012	< 0.017	< 0.013	< 0.014
Hf	< 0.021	< 0.022	< 0.020	< 0.027	< 0.041	< 0.063	< 0.029	< 0.044
Ta	< 0.003	< 0.009	< 0.005	< 0.009	< 0.021	< 0.035	< 0.020	< 0.011
Pb	0.106	0.062	0.071	0.062	< 0.062	< 0.052	< 0.043	< 0.044
Th	< 0.006	< 0.009	< 0.009	< 0.008	< 0.019	< 0.018	< 0.016	< 0.015
U	0.004	< 0.006	< 0.009	< 0.009	0.010	< 0.008	< 0.013	< 0.017

Abbreviation: Pl = plagioclase.

Trace element content of serpentine, talc, vuagnatite, natrolite and edenetic hornblende measured by LA-ICPMS in Dramala spinel harzburgite and plagioclase-bearing harzburgite

Sample	PIA44	PIA120	PIA120	PIA120	PI6	PIA27	PIA27	PIA120	PIA120	PIA120	PIA120	PIA27	PIA27	PIA27	PIA27
Mineral	Srp	Srp	Srp	Srp	Tlc	Tlc	Tlc	Vua	Vua	Ntr	Ntr	Ed hbl	Ed hbl	Ed hbl	Ed hbl
(µg/g)															
Li	0.1	< 0.04	< 0.08	0.18	1.6	1.8	0.3	0.27	< 0.10	< 0.13	< 0.19	2.7	3.5	1.0	3.2
B	< 0.18	0.80	1.33	< 0.29	0.62	1.00	0.99	0.30	0.34	< 0.66	< 0.52	< 0.62	< 0.74	0.38	0.47
P	4	7	7	6	3	6	5	8	8	6	8	8	7	6	6
Sc	2.0	1.4	1.5	1.7	14.7	13.9	15.5	0.2	0.2	0.2	0.3	113.8	108.4	90.2	93.2
V	0.8	0.7	0.7	4.2	81	80	94	0.2	0.2	0.2	0.3	472	463	433	451
Co	93	93	113	97	31	52	41	0.36	0.28	< 0.04	< 0.04	33	33	35	34
Ni	2182	1981	2140	2167	718	1045	760	1.2	< 0.6	< 1.3	1.4	857	864	856	831
Zn	28	18	19	21	17	25	20	35	18	< 0.35	0.61	12	14	16	16
Ga	0.08	0.32	0.32	1.82	1.0	1.8	2.0	8	8	0.7	0.8	5	4	5	5
Rb	0.009	0.007	0.016	< 0.008	0.182	0.904	0.348	0.015	< 0.008	< 0.016	0.014	3	2	1	2
Sr	0.022	0.411	0.331	0.213	0.068	0.744	0.261	15	15	0.091	0.143	0.235	0.306	0.196	0.241
Y	< 0.004	0.013	0.007	0.018	0.006	0.018	0.016	0.100	0.071	0.016	0.061	2	2	2	1
Zr	< 0.007	0.013	< 0.011	0.019	< 0.008	< 0.008	< 0.006	< 0.013	< 0.010	< 0.018	< 0.019	0.174	0.156	0.144	0.159
Nb	< 0.004	< 0.004	< 0.005	< 0.005	0.005	< 0.005	0.008	< 0.004	< 0.006	< 0.010	< 0.014	0.030	0.020	0.020	0.025
Sb	0.023	< 0.012	< 0.018	< 0.017	< 0.015	0.073	0.091	0.044	0.033	< 0.046	< 0.040	< 0.049	< 0.055	0.060	0.061
Cs	< 0.003	< 0.002	< 0.004	< 0.003	0.013	0.056	0.020	0.004	< 0.003	< 0.007	< 0.006	0.053	0.067	0.018	0.032
Ba	0.035	< 0.022	< 0.030	< 0.020	< 0.020	0.862	0.167	5	7	< 0.099	0.182	0.281	0.245	0.095	0.159
La	< 0.004	< 0.003	< 0.004	< 0.004	< 0.003	< 0.005	< 0.003	< 0.004	0.005	< 0.009	< 0.006	< 0.008	< 0.014	< 0.004	< 0.005
Ce	< 0.003	< 0.002	< 0.005	< 0.003	< 0.003	< 0.005	< 0.003	0.092	0.087	< 0.010	0.016	< 0.009	< 0.010	< 0.004	< 0.005
Pr	< 0.003	< 0.002	< 0.002	0.002	< 0.003	< 0.003	< 0.001	0.028	0.022	< 0.007	0.009	< 0.010	< 0.009	< 0.004	< 0.002
Nd	< 0.017	< 0.010	< 0.016	< 0.018	< 0.015	< 0.020	< 0.013	0.147	0.150	< 0.050	0.068	< 0.046	< 0.035	< 0.016	< 0.011
Sm	< 0.018	< 0.015	< 0.027	< 0.021	< 0.020	< 0.023	< 0.014	0.027	0.036	< 0.048	< 0.042	< 0.053	< 0.077	< 0.018	< 0.016
Eu	< 0.005	< 0.004	< 0.005	< 0.007	0.004	< 0.005	< 0.005	0.293	0.208	< 0.012	0.029	< 0.015	< 0.016	< 0.005	< 0.006
Gd	< 0.014	< 0.014	< 0.020	< 0.015	< 0.012	< 0.026	< 0.021	0.034	0.032	< 0.058	< 0.034	< 0.049	< 0.061	0.026	0.026
Tb	< 0.001	< 0.001	< 0.004	< 0.002	< 0.002	< 0.003	< 0.002	0.006	0.005	< 0.004	< 0.008	0.008	< 0.010	0.009	0.010
Dy	< 0.013	< 0.008	< 0.013	< 0.014	< 0.007	0.009	< 0.007	0.021	< 0.013	0.017	< 0.028	0.171	0.170	0.149	0.146
Ho	< 0.002	< 0.002	< 0.003	< 0.004	< 0.003	< 0.003	0.003	< 0.005	< 0.005	< 0.007	< 0.006	0.058	0.050	0.056	0.055
Er	< 0.006	< 0.009	< 0.012	< 0.013	0.009	< 0.011	< 0.012	< 0.011	< 0.016	< 0.025	< 0.033	0.231	0.271	0.201	0.217
Tm	< 0.003	< 0.002	0.002	< 0.003	< 0.003	< 0.002	< 0.002	< 0.004	< 0.001	< 0.004	< 0.005	0.037	0.052	0.047	0.044
Yb	< 0.011	0.012	< 0.010	< 0.018	< 0.014	0.018	< 0.015	< 0.017	< 0.020	0.031	< 0.043	0.542	0.596	0.465	0.376
Lu	< 0.002	0.002	0.004	< 0.004	< 0.002	0.006	< 0.002	< 0.004	< 0.004	< 0.008	< 0.007	0.077	0.086	0.060	0.066
Hf	< 0.008	< 0.005	< 0.010	< 0.014	< 0.011	< 0.009	< 0.007	< 0.009	< 0.013	< 0.014	< 0.024	< 0.019	< 0.034	0.012	< 0.010
Ta	< 0.004	< 0.001	< 0.003	< 0.004	< 0.004	< 0.002	< 0.003	< 0.005	< 0.003	< 0.005	< 0.008	0.008	< 0.009	< 0.002	< 0.002
Pb	0.017	0.018	0.020	0.019	< 0.007	0.090	0.064	0.046	0.045	< 0.036	0.047	0.253	0.270	0.282	0.300
Th	< 0.003	< 0.002	< 0.004	< 0.003	< 0.002	< 0.005	< 0.003	< 0.004	< 0.003	< 0.005	< 0.007	< 0.013	< 0.011	< 0.003	< 0.004
U	< 0.002	< 0.002	< 0.003	< 0.003	< 0.002	< 0.003	< 0.005	< 0.003	< 0.003	< 0.007	< 0.008	< 0.011	< 0.008	< 0.002	0.003

Abbreviations: Srp = serpentine, Tlc = talc, Vua = vuagnatite, Ntr = natrolite, Ed hbl = edenitic hornblende.

Standard data

ICP-MS results and standards for the serpentinite, ophicarbonate, metabasite and gneiss from the Geisspfad ultramafic body

University of Boston (USA), Terry Plank and Louise Bolge

	std-unknown DNC-1	**std-published DNC-1**	**Deviation from published values**	sample precision					g32a	sample precision					g15
				g32a	g32a	**ave**	%RSD	%RSD	(ppm)RSD	g15	g15	**ave**	%RSD	%RSD	(ppm)RSD
ppm	**run-b**	**Kelley et al. 2003**	**DNC-1**	run-a	run-a	**run-a**	run-a	run-a	run-a	run-a	run-a	**run-a**	run-a	run-a	run-a
Li	**5.083**	5.100	**0.33%**	37.0	35.6	**36.3**	*2.8*	*0.028*	*1.022*	2.94	2.87	**2.90**	*1.8*	*0.018*	0.0535
Be	**0.220**	0.225	**2.08%**	3.15	3.00	**3.07**	*3.3*	*0.033*	*0.103*	0.0008	0.0021	**0.0015**	*63.1*	*0.631*	0.0005
Sc	**29.4**	31.000	**5.11%**	8.04	8.14	**8.09**	*0.8*	*0.008*	*0.068*	9.784	9.190	**9.487**	*4.4*	*0.044*	0.4335
TiO2 (%)	**0.472**	0.480	**1.58%**	0.461	0.460	**0.460**	*0.1*	*0.001*	*0.001*	0.022	0.020	**0.021**	*5.4*	*0.054*	0.0012
V	**143.0**	157.00	**8.91%**	35.5	35.6	**35.6**	*0.1*	*0.001*	*0.042*	51.7	48.0	**49.9**	*5.2*	*0.052*	2.7112
Co	**54.8**	56.00	**2.12%**	80.7	81.6	**81.2**	*0.7*	*0.007*	*0.577*	118.7	112.4	**115.6**	*3.8*	*0.038*	4.5290
Ni	**255**	256.00	**0.29%**	13.0	14.0	**13.5**	*5.0*	*0.050*	*0.652*	2562	2458	**2510**	*2.9*	*0.029*	74.8235
Cu	**98.5**	96.000	**2.62%**	10.0	9.7	**9.8**	*2.2*	*0.022*	*0.220*	124.7	119.0	**121.9**	*3.3*	*0.033*	4.0903
Ga	**12.7**	13.700	**7.06%**	30.4	30.0	**30.2**	*1.1*	*0.011*	*0.345*	1.060	1.120	**1.090**	*3.8*	*0.038*	0.0407
Zn	**66.0**	66.000	**0.02%**	56.3	55.5	**55.9**	*1.0*	*0.010*	*0.576*	53.42	50.00	**51.71**	*4.7*	*0.047*	2.5010
Rb	**3.97**	3.900	**1.91%**	165	161	**163**	*1.4*	*0.014*	*2.245*	0.166	0.161	**0.164**	*2.0*	*0.020*	0.0033
Sr	**142**	144.500	**1.60%**	187	188	**187**	*0.3*	*0.003*	*0.651*	1.703	1.646	**1.675**	*2.4*	*0.024*	0.0408
Y	**17.6**	17.700	**0.81%**	47.3	47.2	**47.2**	*0.2*	*0.002*	*0.075*	0.204	0.201	**0.202**	*1.0*	*0.010*	0.0020
Zr	**38.8**	36.900	**5.08%**	2.1	2.1	**2.1**	*0.9*	*0.009*	*0.018*	0.940	0.886	**0.913**	*4.1*	*0.041*	0.0390
Nb	**1.57**	1.470	**6.58%**	14.6	14.3	**14.4**	*1.0*	*0.010*	*0.147*	0.454	0.434	**0.444**	*3.1*	*0.031*	0.0141
Cs	**0.210**	0.207	**1.58%**	5.50	5.43	**5.46**	*0.8*	*0.008*	*0.045*	0.015	0.015	**0.015**	*0.0*	*0.000*	0.0000
Ba	**104.3**	103.300	**1.01%**	941	939	**940**	*0.2*	*0.002*	*1.941*	0.226	0.207	**0.217**	*6.2*	*0.062*	0.0141
La	**3.523**	3.560	**1.03%**	39.4	39.1	**39.3**	*0.5*	*0.005*	*0.214*	0.1294	0.1270	**0.1282**	*1.3*	*0.013*	0.0017
Ce	**8.302**	8.110	**2.36%**	83.8	83.0	**83.4**	*0.6*	*0.006*	*0.531*	0.2626	0.2590	**0.2608**	*1.0*	*0.010*	0.0026
Pr	**1.089**	1.120	**2.76%**	10.1	10.1	**10.1**	*0.1*	*0.001*	*0.005*	0.0299	0.0286	**0.0292**	*3.3*	*0.033*	0.0010
Nd	**4.819**	4.980	**3.23%**	37.9	37.2	**37.6**	*1.2*	*0.012*	*0.443*	0.1053	0.1066	**0.1059**	*0.9*	*0.009*	0.0009
Sm	**1.374**	1.430	**3.92%**	8.21	8.09	**8.15**	*1.0*	*0.010*	*0.082*	0.0160	0.0201	**0.0180**	*16.1*	*0.161*	0.0026
Eu	**0.582**	0.570	**2.11%**	1.33	1.31	**1.32**	*1.3*	*0.013*	*0.018*	0.0040	0.0035	**0.0038**	*8.6*	*0.086*	0.0003
Gd	**2.055**	2.110	**2.60%**	8.16	8.00	**8.08**	*1.4*	*0.014*	*0.116*	0.0215	0.0226	**0.0221**	*3.5*	*0.035*	0.0008
Tb	**0.389**	0.399	**2.50%**	1.38	1.35	**1.36**	*1.6*	*0.016*	*0.021*	0.0037	0.0036	**0.0037**	*1.9*	*0.019*	0.0001
Dy	**2.661**	2.760	**3.59%**	8.08	7.91	**8.00**	*1.5*	*0.015*	*0.118*	0.0247	0.0251	**0.0249**	*1.1*	*0.011*	0.0003
Ho	**0.622**	0.620	**0.27%**	1.68	1.65	**1.66**	*1.3*	*0.013*	*0.021*	0.0063	0.0062	**0.0063**	*1.4*	*0.014*	0.0001
Er	**1.837**	1.870	**1.75%**	4.72	4.64	**4.68**	*1.1*	*0.011*	*0.052*	0.0219	0.0218	**0.0219**	*0.6*	*0.006*	0.0001
Yb	**1.890**	1.970	**4.04%**	4.18	4.08	**4.13**	*1.6*	*0.016*	*0.068*	0.0342	0.0320	**0.0331**	*4.7*	*0.047*	0.0016
Lu	**0.303**	0.320	**5.32%**	0.590	0.575	**0.582**	*1.7*	*0.017*	*0.010*	0.0066	0.0069	**0.0068**	*2.8*	*0.028*	0.0002
Hf	**0.952**	0.995	**4.36%**	0.193	0.184	**0.189**	*3.3*	*0.033*	*0.006*	0.0225	0.0248	**0.0237**	*7.0*	*0.070*	0.0016
Ta	**0.097**	0.095	**2.42%**	1.17	1.15	**1.16**	*1.4*	*0.014*	*0.016*	0.0421	0.0418	**0.0420**	*0.5*	*0.005*	0.0002
Pb	**6.869**	6.200	**10.79%**	29.6	28.6	**29.1**	*2.5*	*0.025*	*0.743*	0.0764	0.0804	**0.0784**	*3.6*	*0.036*	0.0028
Th	**0.228**	0.240	**4.84%**	15.7	15.1	**15.4**	*2.7*	*0.027*	*0.421*	0.0159	0.0169	**0.0164**	*4.4*	*0.044*	0.0007
U	**0.054**	0.050	**8.45%**	3.06	2.99	**3.03**	*1.5*	*0.015*	*0.046*	0.0035	0.0041	**0.0038**	*10.4*	*0.104*	0.0004

Methods: Samples prepared and analyzed as in Kelley et al. (2003), except for following modifications. Digestions - final sample dilution 1/1000, because of low concentrations.
For most samples, used REE, Rb, Y , Ba, Zr collected in pulse counting mode instead of analog mode. Stds: calibration standards are BIR-1, W-2, MAR-1, using values in Kelley et al (2003)
DNC-1 is a std reference material run as an unknown; compare with values in Kelley et al (2003) or GeoRem. Precision reported as %relative std deviation, for in-run replicates.
Precision high abundance sample (g32a) is typical for our lab - generally < 2-3% RSD for all elements. Precision degrades with decreasing abundance (g15) - to 5% range, but still very good for some elements in ppb range (e.g., Lu)
Note our digestion procedure does not digest chromite or zircon, and this may affect some of the elements (e.g., Zr and Hf and HREE in orthogeniess). Boston University, May 2007. Louise Bolge (chemist and analyst)
Terry Plank (final data reduction).
Kelley, K.A., **Plank, T.**, Ludden, J.N. and H. Staudigel (2003) The composition of altered oceanic crust at ODP sites 801 and 1149. *Geochem. Geophys. Geosyst.* . 4 (6), doi: 10.1029/2002GC000435.

ICP-MS results and standards for the Dramala spinel harzburgite and plagioclase-bearing harzburgite of the Pindos ophiolite

University of Bristol (UK), Horst Marschall

(µg/g)	Li	Be	Rb	Sr	Ba	Y	Ce	Pr	Sm	Eu	Gd	Tb	Dy
Pi2	0.88	<0.0016	<0.011	0.052	0.26	0.133	0.0121	0.0012	0.0013	<0.0003	0.0032	0.0011	0.0144
PiA91	0.97	<0.0016	<0.011	0.105	<0.16	0.073	0.0033	0.0003	<0.0005	<0.0003	<0.0031	0.0006	0.0074
Pi6	0.51	<0.0016	0.031	0.325	<0.16	0.017	0.0040	0.0004	0.0007	<0.0003	<0.0031	0.0001	0.0012
PiA27	0.64	<0.0016	0.164	0.413	0.26	0.042	0.0062	0.0006	0.0011	0.0004	<0.0031	0.0002	0.0030
PiA44	0.76	<0.0016	0.035	0.059	<0.16	0.036	0.0058	0.0007	0.0010	0.0004	<0.0031	0.0001	0.0025
PiA51	0.92	<0.0016	0.027	0.167	<0.16	0.118	0.0062	0.0007	0.0018	0.0009	<0.0031	0.0011	0.0123
PiA109	1.07	<0.0009	0.013	0.084	<0.17	0.954	0.0048	0.0009	0.0240	0.0089	0.0550	0.0159	0.1439
PiA120	0.97	<0.0009	0.072	2.845	<0.17	1.902	0.0204	0.0109	0.0907	0.0317	0.1567	0.0389	0.3161
Det limit 1	0.028	0.0016	0.011	0.043	0.16	0.001	0.0014	0.0001	0.0005	0.0003	0.0031	0.0000	0.0002
Det limit 2	0.005	0.0009	0.003	0.030	0.17	0.000	0.0008	0.0001	0.0002	0.0002	0.0003	0.0000	0.0000
Standard measured values													
PiA51-D	1.06	0.0010	0.029	0.166	0.21	0.121	0.0064	0.0009	0.0021	0.0008	0.0039	0.0011	0.0138
UB-N	21.93	0.2000	3.238	5.906	26.76	2.448	0.7476	0.1109	0.1722	0.0589	0.2607	0.0554	0.4089
PCC1-D	1.11	<0.0016	0.061	0.338	1.04	0.077	0.0597	0.0070	0.0045	0.0010	0.0059	0.0011	0.0086
PCC1 Std 1	1.058	0.0020	0.055	0.299	0.68	0.072	0.0505	0.0065	0.0051	0.0008	0.0054	0.0011	0.0086
PCC1 Std 2	1.039	0.0019	0.049	0.316	0.72	0.072	0.0529	0.0067	0.0048	0.0010	0.0055	0.0010	0.0083
PCC1 Std 3	1.069	0.0025	0.062	0.350	0.79	0.080	0.0582	0.0077	0.0053	0.0011	0.0055	0.0010	0.0087
PCC1 Std 4	1.002	0.0029	0.066	0.355	0.85	0.085	0.0636	0.0079	0.0048	0.0011	0.0068	0.0013	0.0100
PCC1 Std 5	0.757	0.0026	0.055	0.330	0.87	0.072	0.0551	0.0071	0.0045	0.0013	0.0064	0.0012	0.0101
PCC1 min	0.757	0.002	0.049	0.299	0.678	0.072	0.051	0.007	0.005	0.001	0.005	0.001	0.008
PCC1 max	1.069	0.003	0.066	0.355	0.872	0.085	0.064	0.008	0.005	0.001	0.007	0.001	0.010
Standard published values													
UB-N	27	0.2	3.5	7.8	26	2.4	0.8	0.123	0.216	0.081	0.32	0.06	0.42
PCC-1	0.985	0.001	0.058	0.3	0.76	0.077	0.0563	0.0072	0.005	0.001	0.0058	0.0011	0.0089
Deviation from published value UB-N	**18.77%**	**0.00%**	**7.48%**	**24.29%**	**2.92%**	**1.99%**	**6.55%**	**9.85%**	**20.27%**	**27.23%**	**18.53%**	**7.71%**	**2.63%**
Deviation from published value PCC1 D	**13.15%**		**4.72%**	**2.53%**	**36.44%**	**0.16%**	**6.04%**	**3.26%**	**9.42%**	**3.26%**	**2.29%**	**2.42%**	**3.90%**
Deviation from published value PCC1 min	**23.17%**	**85.34%**	**15.69%**	**9.38%**	**10.81%**	**7.14%**	**10.28%**	**9.35%**	**9.76%**	**23.26%**	**7.36%**	**6.53%**	**6.71%**
Deviation from published value PCC1 max	**8.50%**	**190.80%**	**13.37%**	**7.51%**	**14.71%**	**9.91%**	**12.94%**	**9.31%**	**6.54%**	**29.23%**	**17.00%**	**14.85%**	**13.90%**

	Li	Be	Rb	Sr	Ba	Y	Ce	Pr	Sm	Eu	Gd	Tb	Dy
Error UB-N	**18.77%**	**0.00%**	**7.48%**	**24.29%**	**2.92%**	**1.99%**	**6.55%**	**9.85%**	**20.27%**	**27.23%**	**18.53%**	**7.71%**	**2.63%**
Error PCC1 D	**13.15%**		**4.72%**	**2.53%**	**36.44%**	**0.16%**	**6.04%**	**3.26%**	**9.42%**	**3.26%**	**2.29%**	**2.42%**	**3.90%**
Error PCC1 max	**23.17%**	**190.80%**	**15.69%**	**9.38%**	**14.71%**	**9.91%**	**12.94%**	**9.35%**	**9.76%**	**29.23%**	**17.00%**	**14.85%**	**13.90%**

Detection limits are statistical (3 sigma above the background produced by the blank).
Det limit 1 applies to samples Pi2, Pi6, PiA27, PiA44, PiA51, PiA91, UB-N, PCC1.
Det limit 2 applies to samples PiA51-D, PiA109, PiA120
PiA51-D is a repeat of PiA51, which was dissolved in two batches.
PCC1-D is a repeat of PCC1, which was dissolved in two batches.
All values are calculated using PCC1 as a standard, except for Be concentrations, which were calculated with UB-N as the reference.
Reference material PCC1 was analysed five times during the sequence.

ICP-MS results and standards for the Dramala spinel harzburgite and plagioclase-bearing harzburgite of the Pindos ophiolite

University of Bristol (UK), Horst Marschall

(µg/g)	Ho	Er	Tm	Yb	Lu	Pb	Th	U
Pi2	0.0046	0.0205	0.0040	0.0396	0.0079	0.040	0.0018	0.0008
PiA91	0.0024	0.0113	0.0024	0.0247	0.0052	0.052	0.0003	<0.0003
Pi6	0.0005	0.0032	0.0009	0.0116	0.0029	0.117	0.0007	<0.0003
PiA27	0.0013	0.0071	0.0016	0.0188	0.0042	0.117	0.0009	0.0003
PiA44	0.0012	0.0068	0.0017	0.0186	0.0040	0.054	0.0006	<0.0003
PiA51	0.0041	0.0177	0.0036	0.0338	0.0067	0.025	0.0006	<0.0003
PiA109	0.0355	0.1162	0.0186	0.1401	0.0241	0.076	0.0002	0.0002
PiA120	0.0720	0.2237	0.0338	0.2378	0.0389	0.068	0.0001	0.0001
Det limit 1	0.0000	0.0001	0.0001	0.0006	0.0003	0.003	0.0001	0.0003
Det limit 2	0.0000	0.0000	0.0000	0.0002	0.0001	0.004	0.0000	0.0000
Standard measured values								
PiA51-D	0.0043	0.0179	0.0040	0.0351	0.0072	0.133	0.0003	0.0003
UB-N	0.0885	0.2701	0.0390	0.2780	0.0438	(12.95)	0.0421	0.0459
PCC1-D	0.0023	0.0103	0.0021	0.0198	0.0042	n.a.	0.0090	0.0037
PCC1 Std 1	0.0025	0.0102	0.0020	0.0205	0.0045	7.25	0.0108	0.0037
PCC1 Std 2	0.0025	0.0099	0.0021	0.0188	0.0042	7.35	0.0105	0.0036
PCC1 Std 3	0.0025	0.0111	0.0021	0.0207	0.0045	8.15	0.0115	0.0037
PCC1 Std 4	0.0030	0.0124	0.0026	0.0244	0.0052	9.25	0.0133	0.0045
PCC1 Std 5	0.0029	0.0124	0.0025	0.0244	0.0049	9.00	0.0135	0.0048
PCC1 min	0.002	0.010	0.002	0.019	0.004	7.253	0.010	0.004
PCC1 max	0.003	0.012	0.003	0.024	0.005	9.250	0.014	0.005
Standard published values								
UB-N	0.097	0.282	0.043	0.283	0.046	12.8	0.0585	0.0496
PCC-1	0.0026	0.0109	0.0022	0.0211	0.0046	8	0.0115	0.0039
Deviation from published value UB-N	**8.73%**	**4.21%**	**9.31%**	**1.75%**	**4.84%**	**201.17%**	**28.09%**	**7.38%**
Deviation from published value PCC1 D	**9.66%**	**5.51%**	**3.58%**	**5.99%**	**8.17%**		**21.97%**	**4.61%**
Deviation from published value PCC1 min	**5.66%**	**8.93%**	**7.76%**	**11.01%**	**9.25%**	**9.34%**	**9.12%**	**6.45%**
Deviation from published value PCC1 max	**14.36%**	**13.55%**	**18.22%**	**15.83%**	**13.66%**	**15.63%**	**17.73%**	**23.05%**

	Ho	Er	Tm	Yb	Lu	Pb	Th	U
Error UB-N	**8.73%**	**4.21%**	**9.31%**	**1.75%**	**4.84%**	**201.17%**	**28.09%**	**7.38%**
Error PCC1 D	**9.66%**	**5.51%**	**3.58%**	**5.99%**	**8.17%**		**21.97%**	**4.61%**
Error PCC1 max	**14.36%**	**13.55%**	**18.22%**	**15.83%**	**13.66%**	**15.63%**	**17.73%**	**23.05%**

Detection limits are statistical (3 sigma above the background produced by the blank).
Det limit 1 applies to samples Pi2, Pi6, PiA27, PiA44, PiA51, PiA91, UB-N, PCC1.
Det limit 2 applies to samples PiA51-D, PiA109, PiA120
PiA51-D is a repeat of PiA51, which was dissolved in two batches.
PCC1-D is a repeat of PCC1, which was dissolved in two batches.
All values are calculated using PCC1 as a standard, except for Be concentrations, which were calculated with UB-N as the reference.
Reference material PCC1 was analysed five times during the sequence.

ICP-MS Bristol (UK) reference values

	Sample	ANRT UB-N	USGS PCC-1	ANRT UB-N			USGS PCC-1		
	Material	serpentinite	peridotite	serpentinite			peridotite		
	Last Name	Govindaraju 1994	Govindaraju 1994	"Best value"	Reference	Method	"Best value"	Reference	Method
	Major elements (wt % oxides)								
	SiO2	39.43	41.71						
	TiO2	0.11	0.01						
	Al2O3	2.9	0.675						
	Fe2O3(t)	8.34	8.25						
	MnO	0.12	0.12						
	MgO	35.21	43.43						
	CaO	1.2	0.52						
	Na2O	0.1	0.03						
	K2O	0.02	0.007						
	P2O5	0.04	0.002						
	CO2	0.39	0.15						
	H2O+	10.84	4.71						
	H2O-	1.26	0.44						
	LOI	12.06	5.12						
	Total	99.96	100.054						
	Trace elements (µg/g)								
3	Li	27	1.6	27	Govindaraju, 1995	compiled	0.985	Moriguti, 2004	ID-TIMS
4	Be	0.2	0.05	0.2	Govindaraju, 1995	compiled	0.001	Eggins, 1997	ICP-MS
5	B	140	1.7	157	D´Orazio, 1999	ID-ICPMS	1.7	Govindaraju, 1994	compiled
6	C		420				420	Govindaraju, 1994	compiled
7	N		44				44	Govindaraju, 1994	compiled
9	F	95	12	95			12	Govindaraju, 1994	compiled
16	S	200	20	174	Okai, 2001	ICP-AES	13.7	Makishima, 2001	ID-FI-ICPMS
17	Cl	800	71	800			71		
21	Sc	13	8.4	14	Ionov, 2005	ICP-MS	9.0	Eggins, 1997	ICP-MS
23	V	75	31	75			27	Eggins, 1997	ICP-MS
24	Cr	2300	2730	2300			2730		
27	Co	100	112	100			105	Eggins, 1997	ICP-MS
28	Ni	2000	2380	2000			2380		
29	Cu	28	10	28			7.0	Eggins, 1997	ICP-MS
30	Zn	85	42	85			31	Eggins, 1997	ICP-MS
31	Ga	3	0.7	3			0.48	Eggins, 1997	ICP-MS
32	Ge	0.85	0.94	0.85			0.94		
33	As	10	0.056	10			0.056		
34	Se		0.027				0.027		
35	Br		0.44				0.44		
37	Rb	4	0.066	3.5	Ionov, 2005	ICP-MS	0.058	Eggins, 1997	ICP-MS
38	Sr	9	0.4	7.8	Ionov, 2005	ICP-MS	0.33	Eggins, 1997	ICP-MS
39	Y	2.5	0.1	2.40	Robinson, 1999	HR-ICP-MS	0.077	Robinson, 1999	HR-ICP-MS
40	Zr	4	10	3.3	Ionov, 2005	ICP-MS	0.105	Weyer, 2003	ID-ICP-MS
41	Nb	0.05	1	0.08	Ionov, 2005	ICP-MS	0.0085	Weyer, 2003	ICP-MS
42	Mo	0.55	2	0.55			0.032	Eggins, 1997	ICP-MS
44	Ru		0.01				0.01		
45	Rh		0.0014				0.0014		
46	Pd		0.0054				0.0054		
47	Ag		0.008				0.008		
48	Cd		0.019				0.022	Eggins, 1997	ICP-MS
49	In	0.015	0.0037	0.015			0.0037		
50	Sn		1.6				1.24	Eggins, 1997	ICP-MS
51	Sb	0.3	1.28	0.3			1.36	Eggins, 1997	ICP-MS
52	Te		0.0031				0.0031		
53	I		0.185				0.185		
55	Cs	10	0.0055	10			0.0045	Eggins, 1997	ICP-MS
56	Ba	27	1.2	26	Ionov, 2005	ICP-MS	0.76	Eggins, 1997	ICP-MS
57	La	0.35	0.052	0.33	Ionov, 2005	ICP-MS	0.0304	Jain, 2000	ICP-MS
58	Ce	0.8	0.1	0.8	Ionov, 2005	ICP-MS	0.0563	Jain, 2000	ICP-MS
59	Pr	0.12	0.013	0.123	Ionov, 2005	ICP-MS	0.0072	Jain, 2000	ICP-MS
60	Nd	0.6	0.042	0.61	Ionov, 2005	ICP-MS	0.0262	Jain, 2000	ICP-MS
62	Sm	0.2	0.0066	0.216	Ionov, 2005	ICP-MS	0.005	Jain, 2000	ICP-MS
63	Eu	0.08	0.0018	0.081	Ionov, 2005	ICP-MS	0.001	Jain, 2000	ICP-MS
64	Gd	0.3	0.014	0.32	Ionov, 2005	ICP-MS	0.0058	Jain, 2000	ICP-MS
65	Tb	0.06	0.0015	0.06	Ionov, 2005	ICP-MS	0.0011	Jain, 2000	ICP-MS
66	Dy	0.38	0.01	0.42	Ionov, 2005	ICP-MS	0.0089	Jain, 2000	ICP-MS
67	Ho	0.09	0.0025	0.097	Ionov, 2005	ICP-MS	0.0026	Jain, 2000	ICP-MS
68	Er	0.28	0.012	0.282	Ionov, 2005	ICP-MS	0.0109	Jain, 2000	ICP-MS
69	Tm	0.045	0.0027	0.043	Ionov, 2005	ICP-MS	0.0022	Jain, 2000	ICP-MS
70	Yb	0.28	0.024	0.283	Ionov, 2005	ICP-MS	0.0211	Jain, 2000	ICP-MS
71	Lu	0.045	0.0057	0.046	Ionov, 2005	ICP-MS	0.0046	Jain, 2000	ICP-MS
72	Hf	0.1	0.04	0.122	Ionov, 2005	ICP-MS	0.0054	Eggins, 1997	ICP-MS
73	Ta	0.02	0.02	0.015	Ionov, 2005	ICP-MS	0.002	Eggins, 1997	ICP-MS
74	W	20	0.02	20			0.02		
75	Re		0.000058				0.000058		
76	Os		0.007				0.007		
77	Ir		0.0048				0.0048		
78	Pt		0.008				0.008		
79	Au		0.0079				0.0079		
80	Hg		0.006				0.006		
81	Tl	0.06	0.002	0.06			0.002		
82	Pb	13	10	12.8	Ionov, 2005	ICP-MS	8	Eggins, 1997	ICP-MS
83	Bi	0.1	0.008	0.1			0.008		
90	Th	0.07	0.013	0.0585	Pin, 2001	ID-ICP-MS	0.0115	Eggins, 1997	ICP-MS
92	U	0.07	0.0045	0.0496	Pin, 2001	ID-ICP-MS	0.0039	Eggins, 1997	ICP-MS

PGNAA standard analysis

Hungarian Academy of Sciences, Institute of Isotopes, Budapest (H), Katalin Gméling, Tamas Belgya

For details see Gméling et al. (2005), Journal of Radioanalytical and Nuclear Chemistry, 265, 2, 201-212.
These standards (GSJ volcanic rocks) were not analyzed with the samples from the present study.
An internal standard was used and all the elements of the periodic table were measured and compared to the PGNAA library.
These results can give a good estimate of the precision of this technique.

Standard name	B std	B analyzed	B precision	Cl std	Cl analyzed	Cl precision	H2O std	H2O analyzed	H2O precision
JB1A	7.88	8.61	9.3%	171	169.42	0.9%	1.84	1.86	1.1%
JB2	30.2	30.76	1.9%	281	304.46	8.3%	0.25	0.35	40.0%
JB3	18	21.4	18.9%	259	320	23.6%	0.25	0.27	8.0%
JA2	20.7	21.06	1.7%	920	1005.68	9.3%	1.12	1.71	52.7%
JA3	24.8	27.52	11.0%		MAX	23.6%	0.31	0.52	67.7%
JR1	117	131.59	12.5%		MIN	0.9%	1.16	1.41	21.6%
JR2	145	168.4	16.1%				1.41	1.5	6.4%
		MAX	18.9%					MAX	67.7%
		MIN	1.7%					MIN	1.1%

These data were calculated from Gméling et al. (2005).

LA-ICP-MS analyzed standards for the Dramala spinel harzburgite and plagioclase-bearing harzburgite of the Pindos ophiolite

University of Bern (CH), Thomas Pettke and Laure Pelletier

				Measured isotopes																
Sample	**Standard**	**Spot size (µm)**		**Li 7**	**B 11**	**MgO 25**	**Al2O3 27**	**P2O5 31**	**CaO 42**	**Sc 45**	**TiO2 49**	**V 51**	**Co 59**	**Ni 62**	**Zn 66**	**Ga 71**	**Rb 85**	**Sr 88**	**Y 89**	**Zr 90**
				µg/g	**µg/g**	**wt. %**	**wt. %**	**wt. %**	**wt. %**	**µg/g**	**wt. %**	**µg/g**	**µg/g**	**µg/g**	**µg/g**	**µg/g**	**µg/g**	**µg/g**	**µg/g**	**µg/g**
PI2	NIST SRM610	44	std-1	489.614	360.759	0.078	2.043	0.078	11.450	437.574	0.072	444.838	403.449	435.966	458.475	434.744	429.025	495.784	447.144	435.593
	NIST SRM610	44	std-2	479.656	352.087	0.077	2.035	0.079	11.450	444.635	0.073	438.559	406.552	451.833	454.123	441.455	433.173	499.016	452.661	444.217
	NIST SRM610	44	std-3	488.739	352.699	0.079	2.019	0.079	11.450	438.113	0.073	443.882	406.826	448.949	465.342	442.383	436.744	499.612	451.166	439.811
	NIST SRM610	44	std-4	480.507	360.068	0.076	2.059	0.078	11.450	444.094	0.072	439.516	403.173	438.852	447.249	433.818	425.462	495.188	448.632	439.989
PIA91	NIST SRM610	44	std-1	486.223	352.166	0.078	2.052	0.078	11.450	443.191	0.072	443.758	407.412	437.002	451.912	435.514	425.896	495.095	449.942	436.258
	NIST SRM610	44	std-2	482.978	360.632	0.077	2.026	0.079	11.450	439.012	0.073	439.646	402.591	450.796	460.687	440.682	436.296	499.704	449.858	443.540
	NIST SRM610	44	std-3	502.830	368.990	0.081	2.104	0.080	11.450	455.439	0.074	457.025	417.371	452.062	471.880	446.118	438.062	506.851	457.198	448.442
	NIST SRM610	44	std-4	466.382	343.816	0.073	1.974	0.077	11.450	426.779	0.070	426.405	392.642	435.740	440.723	430.095	424.149	487.953	442.604	431.362
PIA27	NIST SRM610	44	std-1	482.667	351.855	0.077	2.038	0.077	11.450	443.865	0.072	441.391	401.846	436.636	458.839	435.550	424.876	496.296	444.751	434.452
	NIST SRM610	44	std-2	486.525	360.927	0.077	2.040	0.080	11.450	438.334	0.073	442.009	408.153	451.146	453.762	440.647	437.317	498.504	455.049	445.348
	NIST SRM610	44	std-3	480.046	354.683	0.079	2.011	0.079	11.450	432.689	0.072	443.496	406.202	438.974	461.054	435.229	436.943	495.725	448.558	440.131
	NIST SRM610	44	std-4	489.136	358.111	0.076	2.067	0.078	11.450	449.512	0.073	439.905	403.798	448.814	451.548	440.968	425.263	499.074	451.242	439.669
PI6	NIST SRM610	44	std-1	492.220	351.488	0.077	2.047	0.079	11.450	441.008	0.073	439.688	408.451	444.232	461.346	443.170	434.288	500.899	452.395	442.204
	NIST SRM610	44	std-2	476.983	361.312	0.077	2.031	0.078	11.450	441.192	0.072	443.712	401.546	443.568	451.248	433.025	427.909	493.903	447.406	437.597
	NIST SRM610	44	std-3	490.382	361.037	0.077	2.106	0.079	11.450	446.377	0.072	441.636	404.570	451.960	440.756	438.459	428.208	505.701	453.229	436.899
	NIST SRM610	44	std-4	478.820	351.763	0.077	1.972	0.078	11.450	435.826	0.072	441.764	405.431	435.843	471.863	437.741	433.994	489.104	446.572	442.899
PIA44	NIST SRM610	44	std-1	483.102	350.759	0.077	2.017	0.077	11.450	439.193	0.071	439.032	400.605	445.533	459.311	434.673	427.311	496.668	445.326	433.865
	NIST SRM610	44	std-2	486.097	362.039	0.078	2.061	0.080	11.450	443.007	0.073	444.367	409.393	442.266	453.288	441.526	434.890	498.132	454.473	445.929
	NIST SRM610	44	std-3	481.746	357.900	0.077	2.054	0.079	11.450	441.436	0.073	440.512	405.582	454.906	454.818	439.542	436.262	501.263	454.947	443.657
	NIST SRM610	44	std-4	487.451	354.900	0.077	2.024	0.078	11.450	440.764	0.072	442.887	404.419	432.888	457.782	436.658	425.937	493.538	444.854	436.146
PIA120	NIST SRM610	44	std-1	487.910	352.132	0.078	2.041	0.078	11.450	440.325	0.073	445.131	406.972	449.200	465.429	446.116	438.566	506.794	460.178	446.758
	NIST SRM610	44	std-2	481.276	360.674	0.076	2.037	0.079	11.450	441.874	0.072	438.269	403.029	438.605	447.167	430.091	423.635	488.010	439.633	433.047
	NIST SRM610	44	std-3	482.047	358.937	0.078	2.045	0.079	11.450	439.598	0.073	439.770	401.691	444.976	451.365	428.969	426.324	489.314	445.115	436.382
	NIST SRM610	44	std-4	487.165	353.859	0.076	2.033	0.078	11.450	442.601	0.072	443.629	408.309	442.825	461.237	447.223	435.875	505.482	454.680	443.416
PIA120	NIST SRM610	44	std-1	488.386	354.729	0.078	2.044	0.078	11.450	444.720	0.073	441.143	407.248	442.311	462.207	441.637	432.879	497.795	451.631	440.380
	NIST SRM610	44	std-2	480.819	358.069	0.076	2.034	0.079	11.450	437.478	0.072	442.257	402.752	445.494	450.398	434.561	429.321	497.005	448.168	439.420
	NIST SRM610	44	std-3	487.920	352.501	0.078	2.034	0.077	11.450	440.014	0.073	444.048	405.886	445.485	464.318	444.050	436.509	504.242	457.403	444.218
	NIST SRM610	44	std-4	481.285	360.295	0.077	2.044	0.079	11.450	442.187	0.072	439.353	404.114	442.310	448.289	432.147	425.691	490.561	442.395	435.579
PIA109	NIST SRM610	44	std-1	482.589	358.842	0.077	2.044	0.079	11.450	441.692	0.072	444.088	407.711	447.624	461.604	442.278	432.653	497.864	451.925	439.744
	NIST SRM610	44	std-2	486.617	353.951	0.078	2.034	0.078	11.450	440.508	0.073	439.313	402.286	440.174	450.995	433.913	429.548	496.937	447.878	440.055
	NIST SRM610	44	std-3	490.458	354.606	0.078	2.053	0.078	11.450	443.358	0.072	439.927	403.825	444.208	461.750	438.137	430.327	501.296	450.218	440.363
	NIST SRM610	44	std-4	478.726	358.199	0.076	2.025	0.079	11.450	438.842	0.073	443.473	406.176	443.592	450.849	438.063	431.873	493.508	449.582	439.438
PIA109	NIST SRM610	44	std-1	483.862	355.394	0.078	2.059	0.080	11.450	443.817	0.073	442.335	406.452	453.782	452.263	443.115	439.261	504.954	459.412	446.945
	NIST SRM610	44	std-2	485.338	357.406	0.076	2.019	0.077	11.450	438.383	0.072	441.066	403.550	434.031	460.335	433.094	422.951	489.855	440.394	432.857
	NIST SRM610	44	std-3	484.319	348.701	0.076	2.026	0.076	11.450	433.515	0.071	439.533	395.145	432.757	455.720	429.324	424.262	493.666	441.209	435.360
	NIST SRM610	44	std-4	484.881	364.100	0.078	2.052	0.081	11.450	448.685	0.074	443.865	414.845	455.028	456.879	446.860	437.929	501.130	458.586	444.438
PIA51	NIST SRM610	44	std-1	479.363	355.008	0.076	2.028	0.079	11.450	440.153	0.073	437.342	399.320	433.551	451.652	430.409	427.576	494.970	448.327	437.231
	NIST SRM610	44	std-2	489.853	357.794	0.078	2.050	0.078	11.450	442.047	0.072	446.053	410.676	454.250	460.945	445.793	434.624	499.832	451.474	442.572
	NIST SRM610	44	std-3	486.823	362.499	0.079	2.072	0.079	11.450	444.552	0.072	434.164	406.142	452.551	448.199	435.697	425.192	495.111	450.677	437.679
	NIST SRM610	44	std-4	482.371	350.295	0.076	2.006	0.078	11.450	437.648	0.072	449.227	403.858	435.249	464.397	440.503	437.009	499.691	449.122	442.124
	standard NIST SRM610 min			466.382	343.816	0.073	1.972	0.076	11.450	426.779	0.070	426.405	392.642	432.757	440.723	428.969	422.951	487.953	439.633	431.362
	standard NIST SRM610 max			502.830	368.990	0.081	2.106	0.081	11.450	455.439	0.074	457.025	417.371	455.028	471.880	447.223	439.261	506.851	460.178	448.442
	published NIST SRM610 average			484.600	356.400	0.077	2.039	0.078	11.450	441.100	0.072	441.700	405.000	443.900	456.300	438.100	431.100	497.400	449.900	439.900
	deviation from published value min			3.76%	3.53%	5.39%	3.29%	2.27%	0.00%	3.25%	2.78%	3.46%	3.05%	2.51%	3.41%	2.08%	1.89%	1.90%	2.28%	1.94%
	deviation from published value max			3.76%	3.53%	4.98%	3.29%	3.85%	0.00%	3.25%	2.78%	3.47%	3.05%	2.51%	3.41%	2.08%	1.89%	1.90%	2.28%	1.94%

	Li	**B**	**MgO**	**Al2O3**	**P2O5**	**CaO**	**Sc**	**TiO2**	**V**	**Co**	**Ni**	**Zn**	**Ga**	**Rb**	**Sr**	**Y**	**Zr**
Error	**3.76%**	**3.53%**	**5.39%**	**3.29%**	**3.85%**	**0.00%**	**3.25%**	**2.78%**	**3.47%**	**3.05%**	**2.51%**	**3.41%**	**2.08%**	**1.89%**	**1.90%**	**2.28%**	**1.94%**

Published NIST SRM610: Pearce et al. (1997), Geostandards Newsletter, 21, 1, 115-144, preferred average used for all elements, except for Ca and Al where overall average was used.

LA-ICP-MS analyzed standards for the Dramala spinel harzburgite and plagioclase-bearing harzburgite of the Pindos ophiolite

University of Bern (CH), Thomas Pettke and Laure Pelletier

				Measured isotopes																
Sample	**Standard**	**Spot size (µm)**		**Nb 93 µg/g**	**Sb 121 µg/g**	**Cs 133 µg/g**	**Ba 137 µg/g**	**La 139 µg/g**	**Ce 140 µg/g**	**Pr 141 µg/g**	**Nd 146 µg/g**	**Sm 147 µg/g**	**Eu 151 µg/g**	**Gd 157 µg/g**	**Tb 159 µg/g**	**Dy 163 µg/g**	**Ho 165 µg/g**	**Er 167 µg/g**	**Tm 169 µg/g**	**Yb 173 µg/g**
PI2	NIST SRM610	44	std-1	415.917	364.783	358.501	422.118	457.827	448.720	427.642	429.464	453.775	463.697	420.265	445.724	428.159	450.699	425.925	422.968	465.817
	NIST SRM610	44	std-2	422.891	372.224	363.303	426.088	456.971	446.878	431.963	432.139	447.221	458.500	419.534	439.875	424.840	448.101	426.075	417.229	457.182
	NIST SRM610	44	std-3	417.929	369.533	364.227	422.966	455.411	449.565	427.516	429.866	447.799	457.849	416.220	436.744	416.616	443.069	419.402	412.370	456.033
	NIST SRM610	44	std-4	420.874	367.465	357.568	425.238	459.398	446.030	432.089	431.736	453.204	464.355	423.589	448.858	436.391	455.735	432.596	427.837	466.968
PIA91	NIST SRM610	44	std-1	417.858	366.666	354.006	423.682	455.505	445.092	431.408	428.589	451.890	465.759	419.923	442.428	429.094	451.547	429.201	423.651	463.817
	NIST SRM610	44	std-2	420.940	370.330	367.777	424.517	459.293	450.503	428.194	433.007	449.112	456.445	419.877	443.171	423.908	447.256	422.803	416.554	459.186
	NIST SRM610	44	std-3	430.199	378.729	370.567	435.202	470.863	463.271	442.970	441.093	463.735	472.534	429.338	453.294	433.428	455.597	433.732	429.307	467.842
	NIST SRM610	44	std-4	408.616	358.290	351.255	413.011	443.955	432.355	416.646	420.526	437.280	449.677	410.469	432.320	419.577	443.210	418.278	410.904	455.167
PIA27	NIST SRM610	44	std-1	415.385	360.189	357.475	421.353	450.142	444.224	431.339	430.588	453.265	463.217	418.590	445.483	426.258	447.393	425.874	417.213	452.894
	NIST SRM610	44	std-2	423.417	376.809	364.324	426.846	464.658	451.376	428.260	431.012	447.735	458.982	421.210	440.117	426.742	451.407	426.126	422.988	470.099
	NIST SRM610	44	std-3	419.199	370.005	365.286	424.590	460.116	453.289	430.269	432.183	453.378	459.597	422.996	444.638	423.447	451.249	428.541	418.836	463.093
	NIST SRM610	44	std-4	419.601	366.995	356.517	423.610	454.684	442.311	429.331	429.418	447.622	462.603	416.804	440.962	429.554	447.551	423.458	421.364	459.908
PI6	NIST SRM610	44	std-1	422.837	372.254	364.877	428.696	464.225	454.664	434.561	438.300	457.333	468.379	423.319	447.242	431.661	453.453	431.259	425.260	466.816
	NIST SRM610	44	std-2	415.966	364.745	356.921	419.506	450.571	440.936	425.037	423.294	443.675	453.828	416.479	438.364	421.347	445.351	420.749	414.943	456.189
	NIST SRM610	44	std-3	417.900	366.036	358.043	427.174	459.241	447.790	431.754	433.114	450.873	467.239	416.745	444.896	431.396	449.386	430.572	421.441	461.584
	NIST SRM610	44	std-4	420.899	370.965	363.758	421.027	455.557	447.810	427.846	428.484	450.128	454.966	423.057	440.707	421.612	449.414	421.435	418.760	461.416
PIA44	NIST SRM610	44	std-1	416.392	362.679	353.093	419.710	451.725	442.354	424.909	424.301	444.856	456.105	410.593	435.889	416.926	439.693	421.721	411.705	449.903
	NIST SRM610	44	std-2	422.407	374.321	368.702	428.482	463.068	453.238	434.684	437.290	456.138	466.089	429.189	449.697	436.056	459.087	430.266	428.474	473.069
	NIST SRM610	44	std-3	423.910	373.653	364.880	429.850	464.542	450.262	435.636	433.803	454.308	467.503	429.828	449.425	432.209	455.498	429.733	426.638	467.381
	NIST SRM610	44	std-4	414.891	363.348	356.923	418.359	450.267	445.342	423.972	427.802	446.696	454.705	409.991	436.188	420.801	443.315	422.277	413.577	455.633
PIA120	NIST SRM610	44	std-1	426.441	373.241	363.930	424.613	455.710	447.082	430.495	430.043	450.001	464.599	420.169	443.615	430.034	446.820	427.137	419.709	461.751
	NIST SRM610	44	std-2	412.363	363.768	357.874	423.588	459.087	448.518	429.106	431.556	450.999	457.603	419.631	441.985	422.969	451.980	424.862	420.491	461.249
	NIST SRM610	44	std-3	417.274	364.644	358.346	421.739	455.388	446.950	427.236	430.369	450.176	457.111	421.098	441.930	421.984	446.840	424.898	419.339	461.969
	NIST SRM610	44	std-4	421.524	372.349	363.451	426.459	459.409	448.649	432.363	431.230	450.824	465.086	418.703	443.670	431.012	451.959	427.102	420.860	461.031
PIA120	NIST SRM610	44	std-1	419.730	370.118	358.493	424.890	458.373	445.503	430.064	426.331	444.178	454.870	413.919	437.504	426.446	445.557	424.178	419.789	455.792
	NIST SRM610	44	std-2	419.070	366.880	363.309	423.310	456.426	450.098	429.536	435.271	456.820	467.328	425.881	448.091	426.554	453.243	427.819	420.410	467.205
	NIST SRM610	44	std-3	424.182	370.672	361.744	422.325	453.583	445.429	429.009	428.047	449.132	463.533	418.597	442.820	427.581	444.178	425.611	417.873	459.539
	NIST SRM610	44	std-4	414.618	366.324	360.055	425.876	461.220	450.172	430.591	433.554	451.867	458.668	421.203	442.780	425.419	454.622	426.388	422.327	463.460
PIA109	NIST SRM610	44	std-1	420.675	373.492	362.581	425.376	458.191	448.111	430.484	430.815	450.279	461.662	422.108	441.419	426.638	447.983	426.176	421.490	458.275
	NIST SRM610	44	std-2	418.127	363.509	359.222	422.824	456.610	447.490	429.117	430.785	450.721	460.539	417.698	444.177	426.362	450.812	425.824	418.713	464.711
	NIST SRM610	44	std-3	420.729	368.441	360.114	423.541	457.305	447.168	429.226	431.509	453.325	460.428	421.534	444.439	427.520	448.878	428.117	421.071	461.077
	NIST SRM610	44	std-4	418.072	368.559	361.685	424.659	457.495	448.431	430.374	430.091	447.681	461.771	418.270	441.165	425.482	449.920	423.890	419.131	461.921
PIA109	NIST SRM610	44	std-1	427.080	380.033	370.391	433.218	471.826	456.970	439.975	441.295	462.576	473.553	430.176	451.173	437.478	461.289	432.552	428.329	473.760
	NIST SRM610	44	std-2	411.723	356.980	351.414	414.984	442.973	438.636	419.631	420.305	438.427	448.665	409.646	434.443	415.546	437.532	419.462	411.890	449.268
	NIST SRM610	44	std-3	419.631	362.771	359.229	422.296	447.580	442.561	424.360	423.335	449.105	454.349	412.830	439.282	415.913	441.052	421.765	410.506	456.511
	NIST SRM610	44	std-4	419.169	374.223	362.570	425.903	467.220	453.036	435.237	438.265	451.895	467.842	426.956	446.312	437.064	457.734	430.226	429.673	466.478
PIA51	NIST SRM610	44	std-1	414.272	362.056	355.242	421.310	451.576	445.831	425.285	424.498	447.270	456.500	418.365	437.353	422.452	444.879	418.291	413.777	456.099
	NIST SRM610	44	std-2	424.529	374.944	366.554	426.890	463.222	449.769	434.315	437.102	453.731	465.701	421.434	448.249	430.550	453.925	433.722	426.433	466.907
	NIST SRM610	44	std-3	416.535	366.466	359.404	424.975	462.942	452.655	434.931	436.533	455.142	470.697	431.464	450.889	433.942	456.448	430.629	427.195	468.313
	NIST SRM610	44	std-4	422.266	370.534	362.395	423.226	451.860	442.945	424.670	425.067	445.857	451.502	408.339	434.706	419.053	442.345	421.363	412.994	454.678
	standard NIST SRM610 min			408.616	356.980	351.255	413.011	442.973	432.355	416.646	420.305	437.280	448.665	408.339	432.320	415.546	437.532	418.278	410.506	449.268
	standard NIST SRM610 max			430.199	380.033	370.567	435.202	471.826	463.271	442.970	441.295	463.735	473.553	431.464	453.294	437.478	461.289	433.732	429.673	473.760
	published NIST SRM610 average			419.400	368.500	360.900	424.100	457.400	447.800	429.800	430.800	450.500	461.100	419.900	442.800	426.500	449.400	426.000	420.100	461.500
	deviation from published value min			2.57%	3.13%	2.67%	2.61%	3.15%	3.45%	3.06%	2.44%	2.93%	2.70%	2.75%	2.37%	2.57%	2.64%	1.81%	2.28%	2.65%
	deviation from published value max			2.57%	3.13%	2.68%	2.62%	3.15%	3.45%	3.06%	2.44%	2.94%	2.70%	2.75%	2.37%	2.57%	2.65%	1.82%	2.28%	2.66%
			Error	**Nb 2.57%**	**Sb 3.13%**	**Cs 2.68%**	**Ba 2.62%**	**La 3.15%**	**Ce 3.45%**	**Pr 3.06%**	**Nd 2.44%**	**Sm 2.94%**	**Eu 2.70%**	**Gd 2.75%**	**Tb 2.37%**	**Dy 2.57%**	**Ho 2.65%**	**Er 1.82%**	**Tm 2.28%**	**Yb 2.66%**

Published NIST SRM610: Pearce et al. (1997), Geostandards Newsletter, 21, 1, 115-144, preferred average used for all elements, except for Ca and Al where overall average was used.

LA-ICP-MS analyzed standards for the Dramala spinel harzburgite and plagioclase-bearing harzburgite of the Pindos ophiolite

University of Bern (CH), Thomas Pettke and Laure Pelletier

				Measured isotopes					
Sample	**Standard**	**Spot size (µm)**		**Lu 175 µg/g**	**Hf 178 µg/g**	**Ta 181 µg/g**	**Pb 208 µg/g**	**Th 232 µg/g**	**U 238 µg/g**
PI2	NIST SRM610	44	std-1	438.268	421.513	383.068	417.403	452.484	460.179
	NIST SRM610	44	std-2	431.134	413.887	370.132	409.194	448.708	454.016
	NIST SRM610	44	std-3	427.943	411.156	372.720	413.941	447.948	460.328
	NIST SRM610	44	std-4	441.453	424.244	380.480	412.659	453.264	453.866
PIA91	NIST SRM610	44	std-1	436.666	419.914	376.021	416.399	450.377	454.645
	NIST SRM610	44	std-2	432.735	415.489	377.178	410.209	450.823	459.550
	NIST SRM610	44	std-3	441.546	423.610	382.978	421.360	459.271	468.874
	NIST SRM610	44	std-4	427.861	411.798	370.235	405.260	441.944	445.348
PIA27	NIST SRM610	44	std-1	431.182	412.102	372.275	412.827	444.466	452.455
	NIST SRM610	44	std-2	438.217	423.295	380.923	413.773	456.742	461.747
	NIST SRM610	44	std-3	433.583	414.563	375.973	416.339	447.523	458.908
	NIST SRM610	44	std-4	435.816	420.836	377.227	410.262	453.682	455.292
PI6	NIST SRM610	44	std-1	441.135	422.746	377.720	416.400	455.887	462.250
	NIST SRM610	44	std-2	428.276	412.663	375.481	410.202	445.324	451.957
	NIST SRM610	44	std-3	435.096	422.083	371.961	407.179	455.887	457.998
	NIST SRM610	44	std-4	434.305	413.325	381.234	419.418	445.324	456.203
PIA44	NIST SRM610	44	std-1	428.200	409.374	369.668	405.651	439.968	448.320
	NIST SRM610	44	std-2	441.182	426.000	383.514	420.932	461.201	465.854
	NIST SRM610	44	std-3	438.386	423.434	380.561	419.071	457.997	460.607
	NIST SRM610	44	std-4	431.023	411.983	372.648	407.542	443.224	453.603
PIA120	NIST SRM610	44	std-1	438.140	419.192	378.689	422.789	452.836	460.468
	NIST SRM610	44	std-2	431.259	416.210	374.512	403.818	448.369	453.735
	NIST SRM610	44	std-3	433.385	420.169	377.081	408.186	448.076	454.969
	NIST SRM610	44	std-4	436.015	415.234	376.119	418.410	453.118	459.229
PIA120	NIST SRM610	44	std-1	431.634	416.507	371.623	411.638	445.772	449.785
	NIST SRM610	44	std-2	437.763	418.893	381.577	414.962	455.435	464.419
	NIST SRM610	44	std-3	436.807	416.839	376.956	420.474	449.825	457.727
	NIST SRM610	44	std-4	432.596	418.561	376.244	406.127	451.376	456.473
PIA109	NIST SRM610	44	std-1	434.719	420.199	375.560	414.881	451.742	455.621
	NIST SRM610	44	std-2	434.682	415.209	377.637	411.721	449.461	458.574
	NIST SRM610	44	std-3	438.397	418.076	377.153	417.516	449.424	455.588
	NIST SRM610	44	std-4	431.016	417.325	376.049	409.090	451.773	458.607
PIA109	NIST SRM610	44	std-1	441.721	428.450	381.631	410.973	456.474	459.889
	NIST SRM610	44	std-2	427.702	406.990	371.582	415.619	444.736	454.319
	NIST SRM610	44	std-3	434.773	408.666	374.200	411.142	438.325	446.688
	NIST SRM610	44	std-4	434.627	426.703	378.993	415.451	462.853	467.485
PIA51	NIST SRM610	44	std-1	428.812	414.796	374.249	405.561	446.610	450.820
	NIST SRM610	44	std-2	440.596	420.607	378.954	421.036	454.589	463.369
	NIST SRM610	44	std-3	441.127	426.450	381.679	409.475	458.312	455.368
	NIST SRM610	44	std-4	428.264	408.939	371.514	417.123	442.889	458.829
	standard NIST SRM610 min			427.702	406.990	369.668	403.818	438.325	445.348
	standard NIST SRM610 max			441.721	428.450	383.514	422.789	462.853	468.874
	published NIST SRM610 average			434.700	417.700	376.600	413.300	450.600	457.100
	deviation from published value min			1.61%	2.56%	1.84%	2.29%	2.72%	2.57%
	deviation from published value max			1.62%	2.57%	1.84%	2.30%	2.72%	2.58%
			Error	**Lu 1.62%**	**Hf 2.57%**	**Ta 1.84%**	**Pb 2.30%**	**Th 2.72%**	**U 2.58%**

Published NIST SRM610: Pearce et al. (1997), Geostandards Newsletter, 21, 1, 115-144, preferred average used for all elements, except for Ca and Al where overall average was used.

Standards used for stable isotope analysis H and O

University of Lausanne (CH), Torsten Venneman, Benita Putlitz and Laure Pelletier

				Measured values	Error
Oxygen isotopes			$\delta^{18}O$ (‰)	$\delta^{18}O$ (‰)	(%)
Standard:	In-house	LS-1 quartz	18.100	18.114	0.08%
				18.117	0.09%

				Measured values	Error
Hydrogen isotopes			δD (‰)	δD (‰)	(%)
Standard:	In-house	KLN-17 kaolinite	-125.00	-126.75	1.40%
				-123.48	1.21%
				-121.20	3.04%
				-121.62	2.70%
				-124.84	0.13%
				-123.79	0.96%
				-124.11	0.72%
				-124.07	0.75%
				-125.81	0.65%
				-125.08	0.06%
				-127.13	1.70%
				-128.03	2.42%
				-129.09	3.27%
	International	NBS-30 biotite	-65.00	-65.00	0.00%
				-67.00	3.08%